Fatigue and restoration of bituminous mixtures during cyclic loading and rest

Frank Ndanusa Williams

Thesis National Number: 2023ENTP0018

A THESIS OF ENTPE
Member of the Université de Lyon

Doctoral school N° 162
Mécanique, Énergétique, Génie Civil, Acoustique (MEGA)

To obtain the graduation of
PhD in Civil Engineering

Defended on Month 21/12/2023 by:
Frank Ndanusa Williams

Fatigue and restoration of bituminous mixtures during cyclic loading and rest

In front of the following examination committee:

CARTER, Alan Professor/ École de technologie supérieure, Canada	Reviewer
TEBALDI, Gabriele Professor II classe/ Università degli Studi di Parma	Reviewer
BABADOPULOS, Lucas Associate professor/ Universidade Federal do Ceará	Examiner
BLANC, Juliette ITPE HDR/ Université Gustave Eiffel	Examiner
DJERAN-MAIGRE, Irini Professor PU/ INSA Lyon	Committee chair
SAUZEAT, Cédric HDR, ENTPE	Supervisor
MANGIAFICO, Salvatore CR, ENTPE	Co-advisor

Numéro national de thèse (NNT) : 2023ENTP0018

THÈSE DE DOCTORAT DE L'ENTPE
Membre de l'Université de Lyon

École Doctorale N° 162
Mécanique, Énergétique, Génie Civil, Acoustique (MEGA)

Spécialité / discipline de doctorat :
Génie Civil

Soutenue publiquement le 21/12/2023, par :
Frank Ndanusa Williams

Fatigue et restauration des mélanges bitumineux pendant les charges cycliques et le repos

Devant le jury composé de :

CARTER, Alan Professeur/ École de technologie supérieure, Canada	Rapporteur
TEBALDI, Gabriele Professeur II classe/ Università degli Studi di Parma	Rapporteur
BABADOPULOS, Lucas Professeur associé/ Universidade Federal do Ceará	Examinateur
BLANC, Juliette ITPE HDR/ Université Gustave Eiffel	Examinatrice
DJERAN-MAIGRE, Irini professeure PU, INSA Lyon	Présidente
SAUZEAT, Cédric HDR, ENTPE	Directeur de thèse
MANGIAFICO Salvatore CR, ENTPE	Co-encadrant

ABSTRACT

This PhD research is within the framework of the work of RILEM (The International Union of Laboratories and Experts in Construction Materials, Systems and Structures) Technical Committee (TC) 278-CHA: Crack-Healing of Asphalt Pavement Materials. The objectives of this study entail firstly, the analysis of DSR test data to evaluate damage and recovery of bituminous binders with data obtained from Politecnico di Torino, Italy and University of Waterloo, Canada. Secondly, the development of ENTPE (Ecole Nationale des Travaux Publics de l'Etat) laboratory test procedure to analyze and evaluate damage and recovery of bituminous mixtures. The Université Gustave Eiffel (France) provided the required bitumen and bituminous mixtures. The study focused on performing repetitive loading and rest tests on binders and mixtures in order characterize damage and recovery of material properties. To successfully undertake this task, different test protocols and analysis methods were carried out on binders and mixtures, with the primary goal to differentiate restoration and reversible phenomena.

All the rheological measurements carried by the two laboratories (Politecnico di Torino, Italy and University of Waterloo, Canada) were performed by means of a DSR from Anton Paar Inc. (Physica MCR 301 and MCR 102 respectively), using an 8-mm parallel plates geometry with a 2-mm gap. The tests performed in this experimental campaign were carried out in strain-control mode. The test involved using the linear amplitude sweep (LAS) test under various loading and rest period durations to effectively determined the recovery behaviour of binder. Therefore, different recovery protocols based on the LAS test were carried out to evaluate the recovery behaviour of the binders. From the result on the binder, Different phenomena occurring during loading and rest were either reversible and not reversible. Therefore, the test protocol does not allow identifying and estimating different phenomena.

A test protocol developed at ENTPE was further improved and carried out on bituminous mixtures. The test procedure is composed of two parts in strain-controlled tension/compression mode on cylindrical samples. In the first part, short complex modulus tests (200 cycles at 10 Hz) at temperatures ranging from 8°C to 14°C and strain amplitudes ranging from 50 to 110µm/m are used to examine the dependency of the mechanical characteristics on strain amplitude and temperature. The aim of the CMT is basically to characterize the linear viscoelastic (LVE) behaviour of the studied bituminous mixtures at undamaged condition. In the second part, five partial fatigue tests (at 10°C) are carried out (each consisting of 100,000 cycles at a 100µm/m strain amplitude and frequency 10 Hz). Each fatigue lag is followed by a

48-hour rest period which consist of short complex modulus tests (100 cycles at 10 Hz) done at predetermined intervals to track the recovery of mechanical parameters. All the two parts of the tests carried out on the mixtures tested.

From the results from mixtures, restoration and unrecovered variations of LVE properties during rest after fatigue loading were successfully isolated, with over 80% of the observed variation of 3D mechanical properties (E* and ν*) during cyclic loading is recovered after 48 hours of rest.

Keywords: Recovery, test protocol, Fatigue, reversible phenomena, restoration

RÉSUMÉ

Cette recherche doctorale s'inscrit dans le cadre des travaux du Comité technique (TC) 278-CHA de RILEM (The International Union of Laboratories and Experts in Construction Materials, Systems and Structures) : Réparation des fissures dans les matériaux de chaussées bitumineuses. Les objectifs de cette étude comprennent tout d'abord l'analyse des données d'essai DSR pour évaluer les dommages et la récupération des liants bitumineux avec des données obtenues par le Politecnico di Torino, Italie et l'Université de Waterloo, Canada. Deuxièmement, le développement de la procédure d'essai en laboratoire de l'ENTPE (Ecole Nationale des Travaux Publics de l'Etat) pour analyser et évaluer l'endommagement et la récupération des mélanges bitumineux. L'Université Gustave Eiffel (France) a fourni le bitume et les mélanges bitumineux nécessaires. L'étude s'est concentrée sur la réalisation d'essais répétitifs de charge et de repos sur les liants et les mélanges afin de caractériser l'endommagement et la récupération des propriétés des matériaux. Pour mener à bien cette tâche, différents protocoles d'essai et méthodes d'analyse ont été appliqués aux liants et aux mélanges, l'objectif principal étant de différencier les phénomènes de restauration et les phénomènes réversibles.

Toutes les mesures rhéologiques effectuées par les deux laboratoires (Politecnico di Torino, Italie et Université de Waterloo, Canada) ont été réalisées au moyen d'un DSR d'Anton Paar Inc. (Physica MCR 301 et MCR 102 respectivement), en utilisant une géométrie de plaques parallèles de 8 mm avec un espace de 2 mm. Les essais réalisés dans le cadre de cette campagne expérimentale ont été effectués en mode de contrôle de la déformation. L'essai a consisté à utiliser le test de balayage d'amplitude linéaire (LAS) sous différentes durées de chargement et de repos afin de déterminer efficacement le comportement de récupération du liant. Par conséquent, différents protocoles de récupération basés sur le test LAS ont été mis en œuvre pour évaluer le comportement de récupération des liants. D'après les résultats obtenus sur le liant, les différents phénomènes survenant pendant la charge et le repos étaient soit réversibles, soit non réversibles. Par conséquent, le protocole d'essai ne permet pas d'identifier et d'estimer les différents phénomènes.

Un protocole d'essai mis au point à l'ENTPE a été amélioré et appliqué aux mélanges bitumineux. La procédure d'essai se compose de deux parties en mode de tension/compression contrôlée sur des échantillons cylindriques. Dans la première partie, des essais courts de module complexe (200 cycles à 10 Hz) à des températures allant de 8°C à 14°C et à des amplitudes de déformation allant de 50 à 110µm/m sont utilisés pour examiner la dépendance des

caractéristiques mécaniques à l'égard de l'amplitude de déformation et de la température. L'objectif de l'essai CMT est essentiellement de caractériser le comportement viscoélastique linéaire (LVE) des mélanges bitumineux étudiés à l'état intact. Dans la deuxième partie, cinq essais de fatigue partielle (à 10°C) sont effectués (chacun consistant en 100.000 cycles à une amplitude de déformation de 100µm/m et à une fréquence de 10 Hz). Chaque période de fatigue est suivie d'une période de repos de 48 heures qui consiste en de courts essais de module complexe (100 cycles à 10 Hz) effectués à des intervalles prédéterminés afin de suivre la récupération des paramètres mécaniques. Les deux parties des essais ont été réalisées sur les mélanges testés.

A partir des résultats des mélanges, la restauration et les variations non récupérées des propriétés LVE pendant le repos après une charge de fatigue ont été isolées avec succès, avec plus de 80% de la variation observée des propriétés mécaniques 3D (E* et ν*) pendant la charge cyclique est récupérée après 48 heures de repos.

Mots-clés : Récupération, protocole d'essai, fatigue, phénomènes réversibles, restauration.

ACKNOWLEDGMENT

I want to take a moment to express my gratitude to everyone who supported during my PhD journey. Your support and encouragement have been of great value and impact to the completion of this thesis.

To my thesis advisors, Professor Cédric Sauzéat and Doctor Salvotore Mangiafico. I wish to extend my heartfelt appreciation and regard to you all for having trusted me and providing me with the crucial direction and assistance over the past three and a half years. It has been a privilege to collaborate with you all. Even though the research was novel to me, you gave me all the necessary assistance to ensure it was smooth and less stressful. Your scientific rigorousness is just a few of the valuable things i have been taught and which will serve as my future instruments for constructing a successful career. Even beyond research, your support, advise and helping hands towards my settling in France was astonishing and it is something I can never forget.

I also want to express my gratitude to the other members of the PhD defense committee for agreeing to examine and review my thesis. I am incredibly grateful that you agreed to take part in my defense, and I understand how difficult it must have been for some of you to travel so far.

I also thank RILEM team, particularly the technical committee (TC) 278-CHA: Crack-Healing of Asphalt Pavement Materials for the material support of this project and for the privilege to undertake this magnificent project. Specifically, I would like to express their sincere gratitude to Ferhat Hammoum (Université Gustave Eiffel) for providing the mixtures. I would also like to express my gratitude to Politecnico di Torino, Italy and University of Waterloo, Canada for providing the data required to analyse the test results on binders.

I would want to express my gratitude to my PhD colleagues, the faculty, the technicians, and the entire ENTPE team. I am grateful for all of the wonderful times we spent conversing, arguing, teaching, learning, eating, sharing coffee, and cooperating.

I wish to thank my family and loved ones. To my ever supportive, caring and understanding wife, you are indeed God sent. To my friends and church family (Winners' family), thank you for sharing with me this moment of my life. Finally, to God Almighty for the grace, wisdom and strength. Thank you, Lord, for seeing me through.

Table of contents

Figures

Figure 5.10. PFRT results obtained for mix 40/60 – 7: φ_E evolution during fatigue lags and recovery periods. The red star indicates the value of φ_E estimated at 100 µm/m at the beginning of the first fatigue lag, purple diamond indicates the value of φ_E estimated at 50 µm/m, green asterisks show values of $\Delta\varphi_{E\ heating}$ and brown triangles indicate values of φ_E estimated at 100 µm/m, after 48 hours of recovery, with non-linearity envelope.

Figure 5.11. PFRT results obtained for mix 40/60 – 7: |v| evolution during fatigue lags and recovery periods. The red star indicates the value of |v*| estimated at 100 µm/m at the beginning of the first fatigue lag, purple diamond indicates the value of |v*| estimated at 50 µm/m, green asterisks show values of $\Delta|v^*_{heating}|$ and brown triangles indicate values of |v*| estimated at 100 µm/m, after 48 hours of recovery, with non-linearity envelope.*

Figure 5.12. PFRT results obtained for mix 40/60 – 7: φ_v evolution during fatigue lags and recovery periods. The red star indicates the value of φ_v estimated at 100 µm/m at the beginning of the first fatigue lag, purple diamond indicates the value of φ_v estimated at 50 µm/m, green asterisks show values of $\Delta\varphi_{v\ heating}$ and brown triangles indicate values of φ_v estimated at 100 µm/m, after 48 hours of recovery, with non-linearity envelope.

Figure 5.13. PFRT results obtained for mix 40/60 - 7: internal and surface temperature evolution during fatigue lags and recovery periods.

Figure 5.14. PFRT results obtained for mix 70/100 - 1: |E| evolution during fatigue lags and recovery periods. The red star indicates the value of |E*| estimated at 100 µm/m at the beginning of the first fatigue lag, purple diamond indicates the value of |E*| estimated at 50 µm/m, green asterisks show values of $\Delta|E^*_{heating}|$ and brown triangles indicate values of |E*| estimated at 100 µm/m, after 48 hours of recovery, with non-linearity envelope.*

Figure 5.15. PFRT results obtained for mix 70/100 – 1: φ_E evolution during fatigue lags and recovery periods. The red star indicates the value of φ_E estimated at 100 µm/m at the beginning of the first fatigue lag, purple diamond indicates the value of φ_E estimated at 50 µm/m, green asterisks show values of $\Delta\varphi_{E\ heating}$ and brown triangles indicate values of φ_E estimated at 100 µm/m, after 48 hours of recovery, with non-linearity envelope.

Figure 5.16. PFRT results obtained for mix PMB - 6: |E| evolution during fatigue lags and recovery periods. The red star indicates the value of |E*| estimated at 100 µm/m at the beginning of the first fatigue lag, purple diamond indicates the value of |E*| estimated at 50 µm/m, green asterisks show values of $\Delta|E^*_{heating}|$ and brown triangles indicate values of |E*| estimated at 100 µm/m, after 48 hours of recovery, with non-linearity envelope.*

Figure 5.29. Quantification of different contributions to φ_v evolution during first and second fatigue lags for mix 40/60 - 7: the envelope line of the first fatigue lag is used for all fatigue lags.

Figure 5.30. Quantification of different absolute and relative contributions to |E| evolutions for mix 40/60 - 7, calculated using the envelope line for the first fatigue lag.*

Figure 5.31. Quantification of different absolute and relative contributions to φ_E evolutions for mix 40/60 - 7, calculated using the envelope line for the first fatigue lag.

Figure 5.32. Quantification of different absolute and relative contributions to |ν| evolutions for mix 40/60 - 7, calculated using the envelope line for the first fatigue lag.*

Figure 5.33. Quantification of different absolute and relative contributions to φ_v evolutions for mix 40/60 - 7, calculated using the envelope line for the first fatigue lag.

Figure 5.34. Relative contribution of non-linearity variations of |E|, φ_E, |ν*| and φ_v with respect to the total variation for each fatigue and rest lag with the void content indicated for mix 40/60 samples.*

Figure 5.35. Relative contribution of non-linearity variations of |E| and φ_E with respect to the total variation for each fatigue and rest lag with the void content indicated for mix 70/100 samples.*

Figure 5.36. Relative contribution of non-linearity variations of |E|, φ_E, |ν*| and φ_v with respect to the total variation for each fatigue and rest lag with the void content indicated for PMB samples.*

Figure 5.37. Relative contribution of unrecovered variations of |E|, φ_E, |ν*| and φ_v with respect to the total variation for each fatigue and rest lag with the void content indicated for mix 40/60 samples.*

Figure 5.38. Relative contribution of unrecovered variations of |E| and φ_E with respect to the total variation for each fatigue and rest lag with the void content indicated for mix 70/100 samples.*

Figure 5.39. Relative contribution of unrecovered variations of |E|, φ_E, |ν*| and φ_v with respect to the total variation for each fatigue and rest lag with the void content indicated for mix PMB samples.*

Figure 5.40. Relative contribution of thixotropy variations of $|E^*|$, φ_E, $|\nu^*|$ and φ_ν with respect to the total variation for each fatigue and rest lag with the void content indicated for mix 40/60 samples.

Figure 5.41. Relative contribution of thixotropy variations of $|E^*|$ and φ_E with respect to the total variation for each fatigue and rest lag with the void content indicated for mix 70/100 samples.

Figure 5.42. Relative contribution of thixotropy variations of $|E^*|$, φ_E, $|\nu^*|$ and φ_ν with respect to the total variation for each fatigue and rest lag with the void content indicated for mix PMB samples.

Figure 5.43. Relative contribution of heating variations of $|E^*|$, φ_E, $|\nu^*|$ and φ_ν with respect to the total variation for each fatigue and rest lag with the void content indicated for mix 40/60 samples.

Figure 5.44. Relative contribution of heating variations of $|E^*|$ and φ_E with respect to the total variation for each fatigue and rest lag with the void content indicated for mix 70/100 samples.

Figure 5.45. Relative contribution of heating variations of $|E^*|$, φ_E, $|\nu^*|$ and φ_ν with respect to the total variation for each fatigue and rest lag with the void content indicated for mix PMB samples.

Figure 5.46. Rate of variation during loading and recovery for $|E^*|$, φ_E, $|\nu^*|$ and φ_ν for each fatigue and rest lag for mix 40/60 - 7.

Figure 5.47. Rate of variation during loading and recovery for $|E^*|$ and φ_E for each fatigue and rest lag for each mix 40/60 sample.

Figure 5.48. Rate of variation during loading and recovery for $|E^*|$ and φ_E for fatigue and rest lag 1 for mix 70/100, mix 40/60 and mix PMB.

Tables

Chapter 1: INTRODUCTION

Transport is a major component of economic activity and a factor that contributes to most other activities, with the global road network spanning 16.3 million kilometres (OECD, 2013). Also from the global road network figure as at 2017, the EU claims about 5 million kilometres, the USA about 4.4 million kilometres and about 3.1 kilometres for China (European Union Road Federation, 2017). Since its early days, transport has been one of the basic components of the civil engineering profession. The construction of highways, bridges, pipelines, tunnels, canals, railroads, ports, harbours and others have influenced the profession from time immemorial and established much of its public image (Sinha et al., 2003). The last century has also undergone an intense urbanization process in both rural and metro cities. It has contributed to the need for quick road building and transport infrastructure. The demand for better roads and services forced researchers, designers and manufacturers to develop creative and cost-effective engineered products to meet growing demand in order to save construction and increase durability (Mohod & Kadam 2016; Dulić & Aladžić, 2016). In fact, transcontinental railways, national highways, canals, petroleum and natural gas pipelines, as well as major public transportation networks, are proof of civil engineers' achievement so far. These achievements have played a major role in the development of the Interstate system , new rail transit lines and major airports in the latter part of the last century (Sinha et al., 2003). According to the World Bank, road networks also hold more than eighty percent of the total passenger-kilometre of a country and more than 50% of its freight tonne-kilometre (Radopoulou & Brilakis, 2016). In particular, there is a great demand for transportation by road among European countries specifically between 1990 and 2005. Predictions were made that freight traffic will increase by more than 60% from 1,706 billion tonne-kilometres in 2005 to 2,824 billion tonne-kilometres in 2030 (Capros et al., 2007; Eurostat, 2009). Even the US Bureau of transit statistics recorded about 193 million registered vehicles used on American roads in 1990 and the amount greatly increased to over 254 million in 2007, with about 136 million of the vehicles been classified as trucks, single-unit 2 axle 6-tire or more (Moghaddam et al., 2011). These statistics invariably indicates the astonishing pressure our roads are encountering and the need for urgent and viable attention.

The most common type of road material used to construct the surface course and, frequently, the base course of pavement structures is bituminous mixture. In road construction, the use of bitumen dated back to the nineteenth century with several attempts been made to use rock asphalt from European deposits for surfacing of road. Therefore, with the advent of coal tar and

bitumen obtained from crude oil, the use of natural products for road construction was gradually replaced (Read & Whiteoak, 2003). Using bitumen as a building material dates back to antiquity. Infact, in comparison to modern bitumen which were highly technological artificial materials, the materials in use then often occurred naturally (Lesueur, 2009). Among the several reasons bitumen is widely used in construction is mainly due to the fact that they are relatively inexpensive and generally provide good durability in paving mixtures. Researcher also discovered the viscoelastic nature of bitumen which makes them outstanding materials for paving roads and streets for a prolonged period despite the daily traffic loads and the climate changes (Wu, 2009; Lesueur, 2009). Even though bituminous materials are widely and overwhelmingly utilised, they are constantly subjected to a wide variety of thermo-mechanical stresses. In fact, improper maintenance over their entire service life can cause premature failure. It usually includes the formation of micro-cracks due to repetitive cycles or loading and gradually leads to the appearance of coalescence macro-cracks (García, 2012). In addition, Lesueur (2009) confirms that after an in-service period of a few years, the flexibility and relaxation capacity of bitumen decreases, the binder becomes brittle causing aggregate segregation, and an extensive damage appears on its surface. It has also been reported that these undesirable effects can occur mainly due to high number of vehicles imposing repetitive higher axle loads on roads, environmental condition and construction errors. These usually cause permanent deformation, fatigue and low temperature cracking, service life of the road pavement is going to be reduced (Oke, 2010; Moghaddam et al., 2011; Tapsoba et al., 2013; Soto, 2015). Researchers have made several attempts at discovering several fatigue resistance mechanisms of bituminous mixtures as potential solutions to these fatigue distresses. (Tapsoba et al., 2013). Interestingly, one of the outcomes obtained from research is the self-healing capability of bituminous materials. This has been known for many years, hence it has been identified as a potential future solution to fatigue distresses (Qiu et al., 2012). The ability of self-healing to increase the lifespan of bituminous pavement has been viewed as a key technique when creating a sustainable infrastructure. Despite all the that have been made towards seeking solution to fatigue distresses and understanding self-healing, we are far from implementing technical solutions based on self-healing because we still do not characterize it correctly and, even less, are able to model it. This has led to several state-of-the-art investigations concerning the self-healing mechanism, model, characterization and enhancement, ranging from bitumen to bituminous pavement (Sun, et al., 2018). Various reversible phenomena other than fatigue has been discovered to occur during laboratory fatigue tests on bituminous mixtures because of cyclic loading applications. This is believed to alter experimental results and thereby leading to

improper conclusions. This is why it is imperative to isolate and quantify these reversible phenomena, therefore isolating real fatigue damage.

The objective of this PhD thesis is to investigate the behaviour of binders and mixtures during fatigue and rest. It entails checking whether different tests (different types of tests, with different durations, loading histories and strain levels involved) performed on corresponding binders and mixtures lead to comparable conclusions. In order to achieve these objectives, tests on binders were carried out by Politecnico di Torino, Italy and University of Waterloo, Canada, while tests on mixtures were performed at ENTPE. Concerning the ENTPE procedure for mixtures, the work allowed further developing the test protocol and the analysis, verifying the repeatability of the results and investigating the variations of Poisson's ratio. All tests were carried out in the framework of RILEM TC 278-CHA, on materials provided by Université Gustave Eiffel. The analysis of data was performed at ENTPE.

There are six chapters presented in this manuscript. Following this introduction, Chapter 2 includes literature review which give detailed backgrounds about an overview, thermomechanical characterization and the self-healing properties of bituminous materials. In Chapter 3, the different tested materials, test procedures and experimental campaigns undertaken are presented. In Chapters 4 presents selected results and analysis/modelling of fatigue/healing tests on bituminous binders using the dynamic shear rheometer which was performed at Torino and Waterloo. Then, Chapters 5 presents various results and analysis of tension-compression tests on bituminous materials performed at ENTPE. Finally, Chapter 6 summarises the conclusions of the results obtained from tests on bitumen and mixtures and drew some perspectives that arose from the entire result.

2.0 Literature Review

2.1 Overview on Bituminous Materials

Bituminous materials are amongst the oldest engineering materials. Their use as binding and waterproofing materials can be dated back to 3000 BC, and later the Romans developed roads in many parts of their empire, marking the first global use of bituminous binders in road paving technology (Widyatmoko, 2016). The term “Bituminous materials” is generally noted to imply all materials consisting of aggregates bound with bitumen (Domone & Illston, 2010). Bituminous mixture is also defined as a composite material made of bitumen and mineral aggregates; the bitumen gives the system cohesion, while the aggregates are thought of as the material's "skeleton" or mineral structure (Corté & Di Benedetto, 2004; Ingham, 2013). According to estimates from the Asphalt Institute and Eurobitume, the globe currently produces 87 million tonnes of bitumen annually for the production of bituminous mixtures. Estimated bitumen-use and application by different sectors are shown in Figure 2.1. Bituminous mixtures has more than 250 documented uses, with paving and roofing applications accounting for the majority of these uses (Chen, 2000).

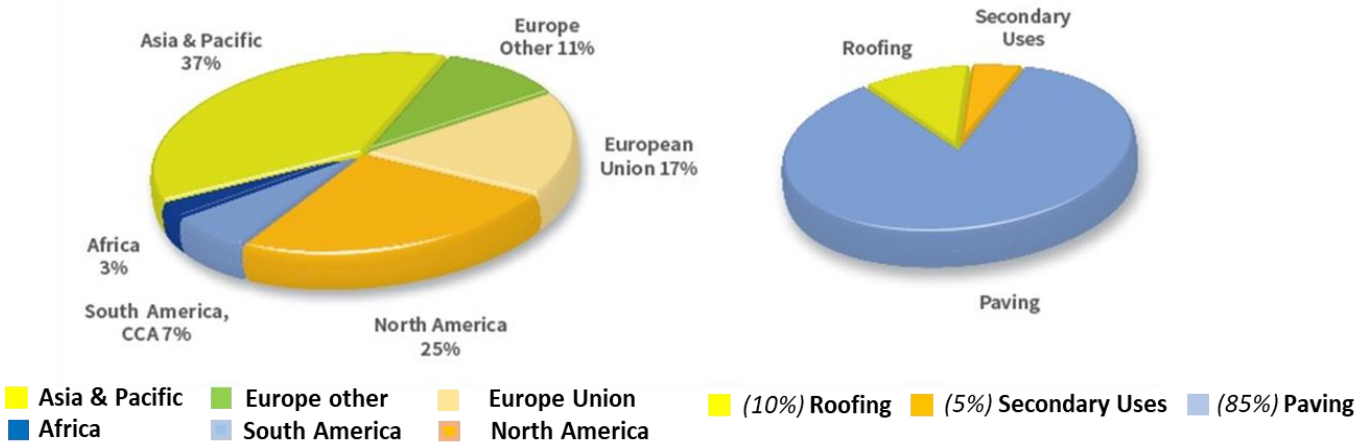

Figure 2.1. Global bitumen use (Source: Asphalt Institute & Eurobitume, 2015).

Currently, it is estimated that over 90% of the roads in Europe are paved with bituminous materials. Also, it has been revealed that the most often utilized paving material in the United States is thought to be bituminous materials. The reason for this increased use of bituminous

materials is not far-fetched, this is because it has been unparalleled in terms of adaptability, toughness, and ease of construction (Eurobitume, 2015).

2.1.1. Aggregates

Aggregates are defined as mineral materials used in the construction industry which can be extracted mechanically from quarries or from natural sources such as alluvial deposits (AFNOR 2005). Aggregates are believed to make up the majority of bituminous mixtures, approximately accounting for about 95% of the mass of bituminous mixtures and 80% to 85% of its volume. Aggregates are often classified as coarse if they are larger than 4.75 mm and as fine if they are less. Also, aggregate particles smaller than 75µm are referred to as filler (Zulkati et al., 2012). They are either rounded or crushed in characteristics, depending on their place of origin and the methods used to extract them. (Corté & Di Benedetto, 2004; Domone & Illston, 2010). The evolution of the passing mass percentage of aggregates with the sieve size is represented by a "grading curve." All fractions are represented in order to maximize aggregate skeleton density; this is shown by the labels "continuous" and "well graded" on the grading curve (Example Figure 3.6). Continuous grading curves are commonly used in the creation of high-modulus bituminous mixtures. Conversely, curves that are "poorly graded" or "gap-graded" exhibit one or more discontinuities. For example, the Stone Mastic Asphalt (SMA) made from the gap-graded aggregates (AFNOR 2006). As already established, aggregates form a network of interparticle connections that forms the skeleton of a bituminous mixture. As a result, the grading curve that maximizes the interparticle interaction network, minimizes the air void content, and yields the densest combination feasible is the ideal one. Nonetheless, bitumen filling all the gaps between aggregate particles will cause bleeding or rutting, thus enough air spaces must be allowed (Lira, Jelagin, & Birgisson, 2013). More recently, a novel approach to optimising aggregate packing has been devised, resulting in the creation of GB5, a bituminous mixture with a minimum air void content based on a gap-graded curve (Olard, 2012).

Road aggregates must adhere to certain geometrical and physical specifications, which includes:

- Shape (AFNOR 2008a; 2012b)
- Angularity (AFNOR 2005)
- Resistance to wear (AFNOR 2011)

- Resistance to fragmentation (AFNOR 2010)
- Assessment of fines (AFNOR 2013a; 2015)

2.1.2. Filler

A filler is defined as that fraction of an inert mineral dust passing the 200-mesh sieve in a bituminous mixture and can perform several functions (Csanyi, 1962). Although the size requirement varies depending on the source, all particles that passes through a 0.063mm sieve are regarded as filler by European paving technologists (AFNOR 2008b). The engineering characteristics of bituminous pavement mixes are significantly influenced by fillers. Traditionally, fillers have included cement, lime, and stone dust. However non-convectional materials have been assessed on the Marshall properties of bituminous paving mixes and have been found to exhibit stability value to be potential fillers (Rahman et al., 2012; Ararsa et al., 2019). The fine packing of the filler, coarse aggregate, and fine aggregate strongly provides a strong foundation for the mixture (Lesueur, 2009; Eisa et al., 2018). It has been poven that the resilient modulus of the bituminous mixtures is increased by the inclusion of mineral filler. However, a surplus of filler is believed to weaken the mixture by requiring more binder to cover the particles, thus, affecting the workability of the mixture (Elliott et al., 1991; Kandhal, et al., 1998; Zulkati et al., 2012). Also, if filler is mixed with less bitumen than it is required to fill its voids, a stiff dry product is obtained which is practically not workable. Overfilling with bitumen, on the contrary, imparts a fluid character to the mixture (Kathem Taeh Alnealy, 2015). The size distribution, particle shape, surface area, surface texture, voids content, mineral composition, and other physiochemical properties vary for several fillers. Therefore, their effect on the properties of bituminous mixtures also varies (Bahia, 2011). To reveal the significance of fillers, fatigue tests were conducted on mastics using a parallel plate DSR to evaluate the effects of fillers on the resistance to fatigue. Result shown in Figure 2.2 depicts the effects for the base binder (no filler) and the 50 % filler (limestone and granite) with fatigue life calculated as the number of cycles to reach a 50% drop in complex modulus. The graph clearly indicate significant improvements in the fatigue performance of bituminous binder after adding the fillers (Faheem et al., 2008).

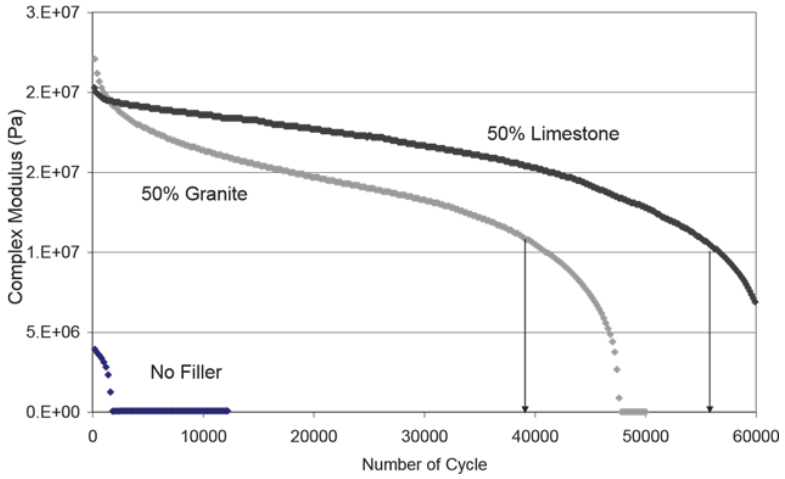

Figure 2.2. Sample Results for Shear Modulus during Fatigue (Faheem et al., 2008).

2.1.3. Bitumen

Bitumen is defined as an organic substance that is either totally or nearly completely soluble in toluene, very viscous or practically solid, virtually non-volatile, sticky, and waterproofing, generated from crude petroleum or present in natural state. It is made up of the thickest layer of crude oil (PIARC, 2019).

2.1.3.1. Sources of Bitumen

Bitumen can be found trapped in rock asphalt or near the surface of the soil as oil seeps also known as natural deposit. However, majority of bitumen are produced using vacuum distillation method from crude oil also known as refinery bitumen (Read & Whiteoak 2003).

2.1.3.2. Manufacture of Bitumen

In order to produce bitumen, lighter crude oil components like gasoline and diesel are essentially removed, leaving the heavier bitumen behind (Read & Whiteoak, 2003). The manufacturing process involves fractional distillation, which is usually carried out in tall steel tower called fractionating or distillation columns as shown in Figure 2.3. It involves dividing crude oil into its constituent parts, or fractions. After being heated to 300 to 350°C, crude oil is distilled at air pressure. After another heating, the atmospheric residue is distilled at 1/10 bar in a vacuum column to extract petrol oil and other distillates like paraffin. "Straight run bitumen," the residue from this second distillation, can be de-asphalted or air-blown as a post-processing method to attain a particular composition prior to storage. Bitumen can be made from several types of crude oil, and the qualities of bitumen vary based on where the crude oil comes from.

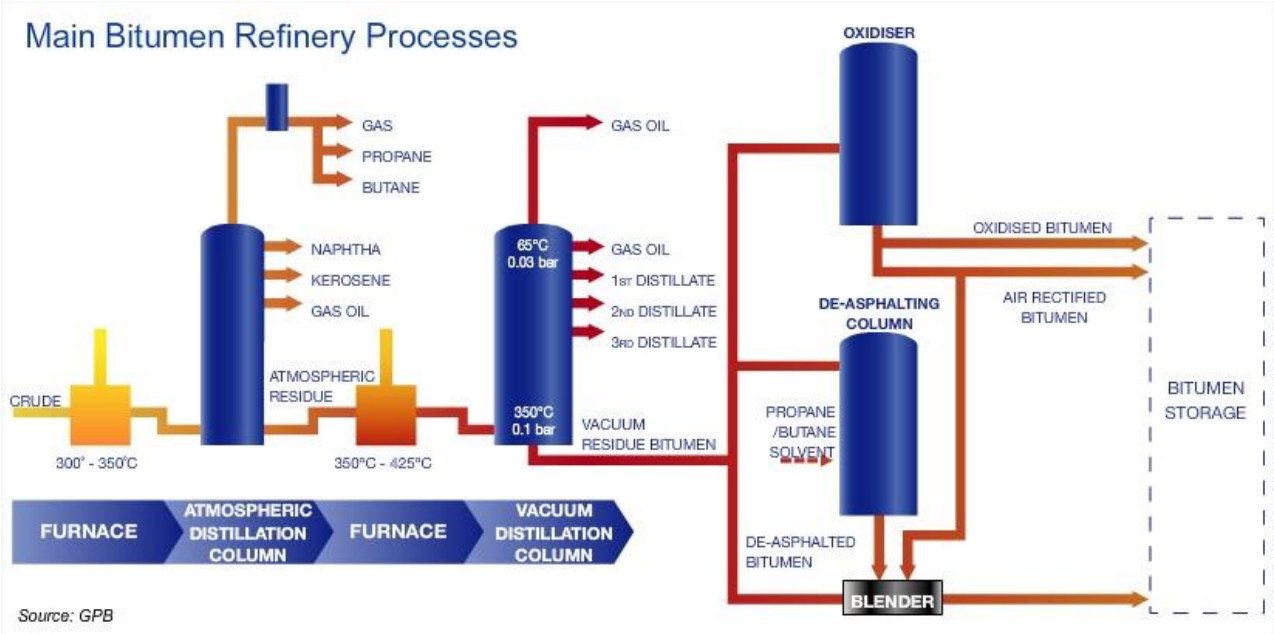

Figure 2.3. Bitumen refining process (Eurobitume website, after Groupement Professionnel des Bitumes, 2005).

2.1.3.3. Types of Bitumen

Bitumen according to Domone and Illston (2010) can be classified into the following grade types:

- Penetration Grade Bitumen: This is the bitumen produced at various viscosities. Based on its hardness, the bitumen is characterized using the penetration test.
- Oxidized Bitumen: This is the bitumen further treated by the introduction of processed air. By maintaining a controlled temperature, the air is introduced under pressure into soft bitumen.
- Cutback Bitumen: These are a grade of bitumen that comes under penetration grade bitumen. This type of bitumen has a temporarily reduced viscosity by the introduction of a volatile oil.
- Bitumen Emulsion: This is the combination of bitumen. As well known, bitumen is a petroleum product and it doesn't mix with water as is naturally sticky, so it is difficult to break down into tiny droplets. An emulsifier is employed to solve this issue.

2.1.3.4. Bitumen composition

Asphaltenes, saturates, aromatics and resins are the typical chemical families into which the constituent or fractions of bitumen are divided according to a separation process known as

SARA as shown in Figure 2.4. According to Read and Whiteoak (2003), these fractions have different distinct properties and their concentration can vary significantly between bitumen:

- **Asphaltenes:** They make up between 5 and 25 percent of the total bitumen and have particles that are 2 to 5 mm in size. These are also insoluble black or brown amorphous solids composed primarily of carbon and hydrogen, with traces of nitrogen, sulfur, and oxygen atoms as well.
- **Resins:** They make up 13 to 25 percent of all the bitumen. These are soluble in n-heptane. They are dark brown in colour, solid or semi-solid polar in nature. Their high polarity confers adhesiveness to the bitumen.
- **Aromatics:** They constitute 40 to 65% of the total bitumen and are dark brown viscous liquids. They consist of non-polar carbon chains in which the unsaturated ring systems (aromatics) dominate and they have a high dissolving ability for other high molecular weight hydrocarbons.
- **Saturates:** This fraction forms 5 to 20% of the bitumen. They are non-polar viscous oils which are straw or white in colour. Saturates consist of straight and branch chain aliphatic hydrocarbons. The average molecular weight range is similar to that of aromatics and the components include both waxy and non-waxy saturates.

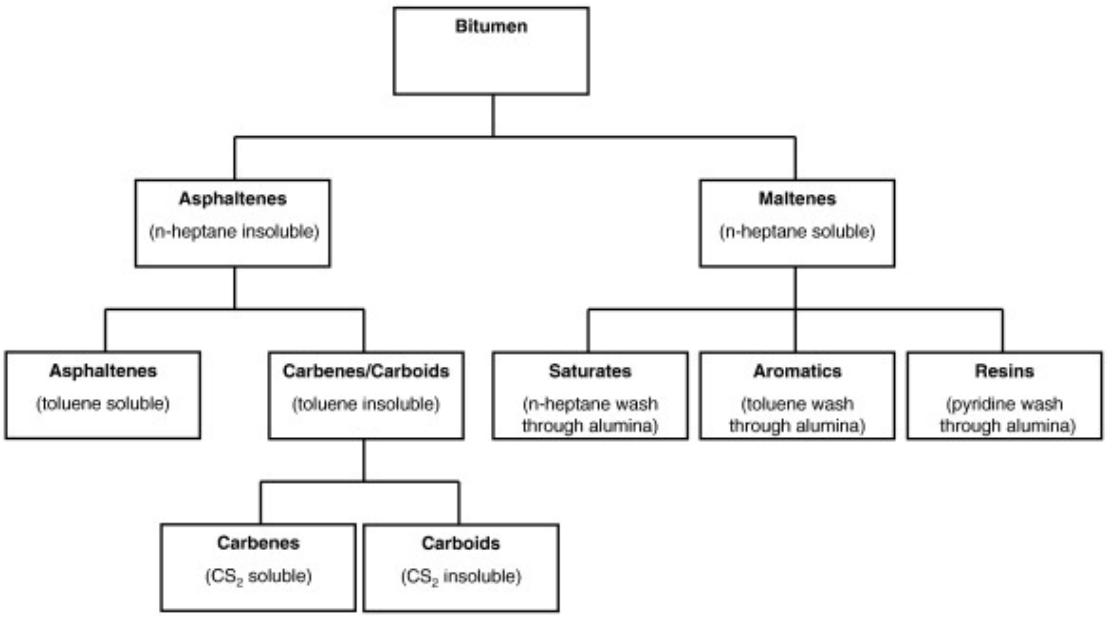

Figure 2.4. Schematic representation of the analysis for broad chemical composition of bitumen (Speight, 2020).

2.1.3.5. Bitumen structure

The most widely accepted structural description of bitumen, the colloidal model fits this category quite well, despite the fact that SARA fractions are only characterised by their process of separation, with overlap across groups (Read & Whiteoak, 2003; Lesueur, 2009; Porto et al., 2022). As shown in Figure 2.5, the liquid viscous matrix is made up of maltenes, whereas the solid micelles are formed by asphaltenes. This description leads to the emergence of two possible microstructures:

- A disjointed, **sol-type** structure with a low concentration of asphaltenes.
- An interior structure created by a **gel-like** structure with a high concentration of asphaltenes, usually in air-blown bitumen.

This description, however, turned out to be rather inaccurate because a gel structure would produce yield stress or a plateau of modulus vs temperature and frequency, neither of which have ever been seen for paving grade bitumen (Lesueur, 2009). The temperature of bitumen has a significant impact on its composition. It is generally known that there is a drastic shift in structure at the glass transition temperature, which ranges from -40 to -10°C (Polacco et al., 2008).

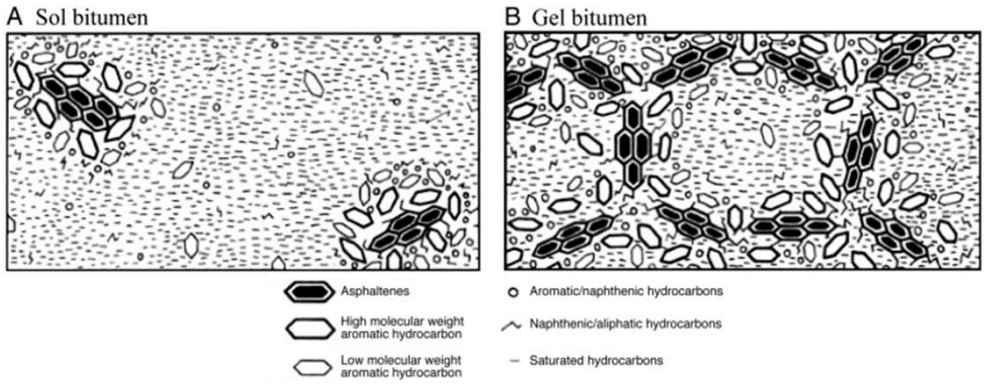

Figure 2.5. Schematic representation of SOL and GEL type bitumens (Read and Whiteoak, 2003).

2.1.3.6. Standard specification tests for bitumen

It is imperative to have various tests on bitumen to characterise different grades since a wide variety of them are manufactured. The characteristics of bituminous materials can be evaluated using a variety of tests. Usually, before bitumen is commercialised in Europe, it is often categorised based on penetration which is called the penetration test (AFNOR 2018a). The

penetration test involves taking a loaded needle penetration depth, measured in pen in 10-1 mm into a bitumen cup at 25 °C. Based on this test, bitumen is categorised into Penetration Grade groups, such as 35/50, 50/70, or 160/220 etc. according to the penetration value. The superpave Performance Grade (PG), which denotes service temperatures for a bituminous mixture containing bitumen, is the most widely used categorization system in North America (AASHTO M320, 2009; AASHTO PP6, 1994). Based on rheological (or mechanical) experiments conducted at various temperatures, these service temperatures have been established (AASHTO T313, 2012; AASHTO T314, 2012; AASHTO T315, 2012; Bhahia & Anderson, 1995). Thus, the stated service temperatures are a little bit of the temperatures at which a subjective consistency metric is determined.

2.1.3.7. Polymer-modified Bitumen (PmB)

The second half of the 20th century have witnessed an increase in traffic worldwide, which have compelled paving experts to improve the mechanical properties and endurance capacity of bituminous materials. A typical PmB is a mixture of pure bitumen and polymer (usually 3 to 7% of total weight), which can be made up of plastomers (like ethylene-vinyl acetate, or EVA) or elastomers (like styrene-butadiene-styrene, or SBS), or a combination of these (Polacco et al. 2015). It is commonly belived that bitumen with high temperature thermomechanical performance and age resistance can be enhanced by polymer modification (McNally 2011; Singh & Kumar 2019). Elastic recovery determination is one of the new tests used to define PmB (AFNOR 2017b). It involves utilising a ductilometer device to measure the percentage of recovered deformation of a standardised bitumen sample that has been stretched and then precisely cut.

2.2. Flexible pavement: An overview

According to Mohod and Kadam (2016) pavements are important characteristics of the urban communication network, which provide an effective means of transport. Pavement are either flexible or rigid with flexible pavements bearing such a name because the entire structure is under load with the elastic deflection. The structure of flexible pavement consists of the bitumen bound materials, thus they are more elastic than rigid and more deformable. On the other hand, rigid pavements consist of cement-based Portland materials which pass the load over a wider

placenta region and it is characterised by lower compression streams and lower deformations. Flexible pavements are preferred over cement concrete roads (rigid pavements) because of their rigidity, jointlessness, quick serviceability and good riding quality. Although, the biggest advantage of using rigid pavement is its high strength and high bearing capacity (Dulić & Aladžić, 2016).

2.2.1. Typical structure of flexible pavement

In general, three types of structures are utilised: pavements that are semi-rigid, flexible, and stiff. A thick layer of reinforced or slab concrete makes up a stiff pavement, and it is this layer that distributes traffic loads to the subgrade on its own. Flexible pavement, on the other hand, is a collection of many bound and unbound layers as shown in Figure 2.6. The compacted mineral subgrade layer is supported by the natural subgrade. Either unbound or hydraulic binder-treated aggregates make up the subbase course. High modulus and good fatigue resistance are expected in bituminous mixtures used as base course in roads and highways. The final course consists of an optional binder course and a bituminous wearing course at the surface that ensures user safety and comfort in addition to particular water sealing qualities. Combining rigid and flexible pavements, a semi-rigid pavement usually consists of a bituminous wearing course overlaid on top of a concrete base course.

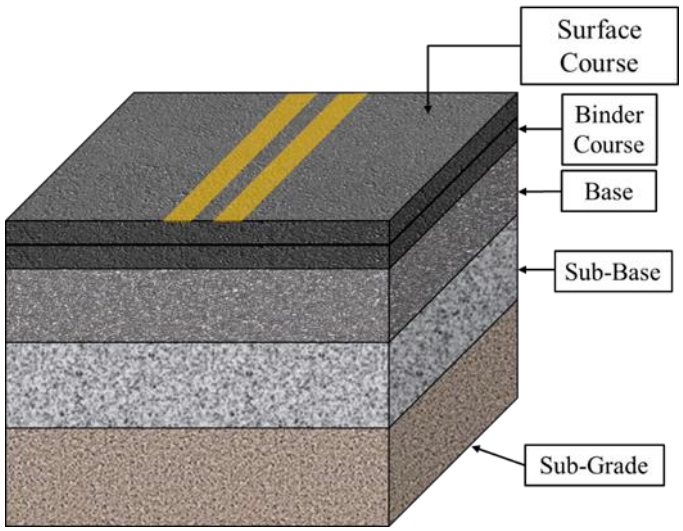

Figure 2.6. Basic components of Flexible Pavements (adapted from Freire, 2020).

2.2.2. Effects of mechanical loading on flexible pavement

The two primary sources of thermomechanical load applied to pavement structure are traffic load and temperature fluctuations. The traffic load acting on the pavement is usually distributed to a wider area, and the stress decreases with the depth as shown in Figure 2.7. Taking advantage of this stress distribution characteristic, flexible pavements normally has many layers, even though characterising the precise distribution of stress and strain is difficult (Di Benedetto and Corté 2005). However, the layered system of flexible pavement gives it suitable quality to sustain maximum compressive stress, in addition to wear and tear. Since the lower layers will experience lesser magnitude of stress, low-quality material can be used (Mathew & Rao, 2007). The elastic layered theory underpins that traffic loads behave on a road pavement structure. (Di Benedetto & Corte, 2004). This theory requires all layers must have the Poisson's ratio and Young modulus, as well as the interface conditions either completely sliding or perfectly bound.

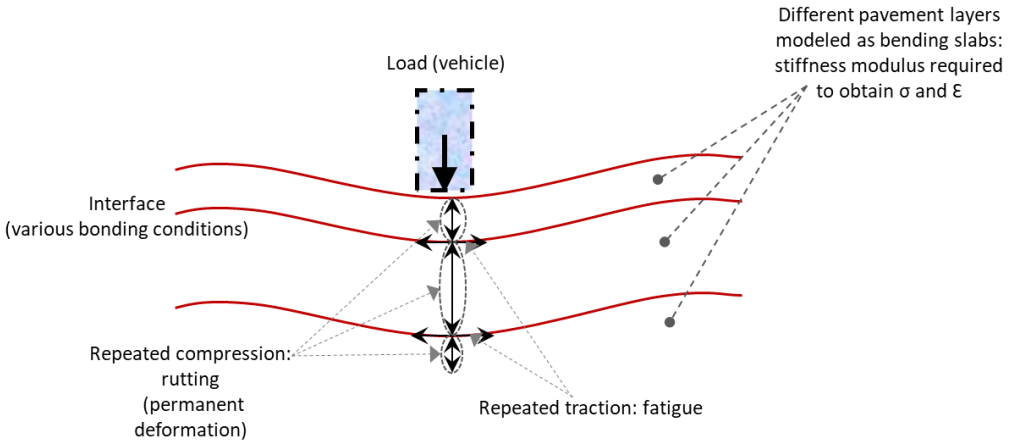

Figure 2.7. Diagram showing how traffic loads affect road pavement structure [(adapted from (Di Benedetto, 1998)].

2.2.3. Effect of climate on flexible pavement

Significant temperature changes inside the pavement structure are caused by the climate as shown in Figure 2.8. It cannot be overemphasized the significant absorption of solar radiation and thermal contraction bituminous layers undergo, thereby oscillating tens of degrees Celsius on a regular basis (Rababaah, 2005). These experiences eventually induce strains on flexible pavement. The following conclusions can be drawn on the effect of weather conditions on flexible pavement (Mangiafico, 2014; Hozayen & Fouad, 2015):

- Sensible changes in the material qualities of flexible pavement are caused by temperature differences. Specifically, stiffness rises with falling temperatures and falls with rising temperatures.
- When temperatures fluctuate, flexible pavement experience thermal expansion and contraction.
- Thermally induced fatigue can also result from repeated strain caused by thermal contraction and expansion.
- Freeze-thaw cycles brought on by temperature fluctuations can then gradually erode the performance and integrity of the material.

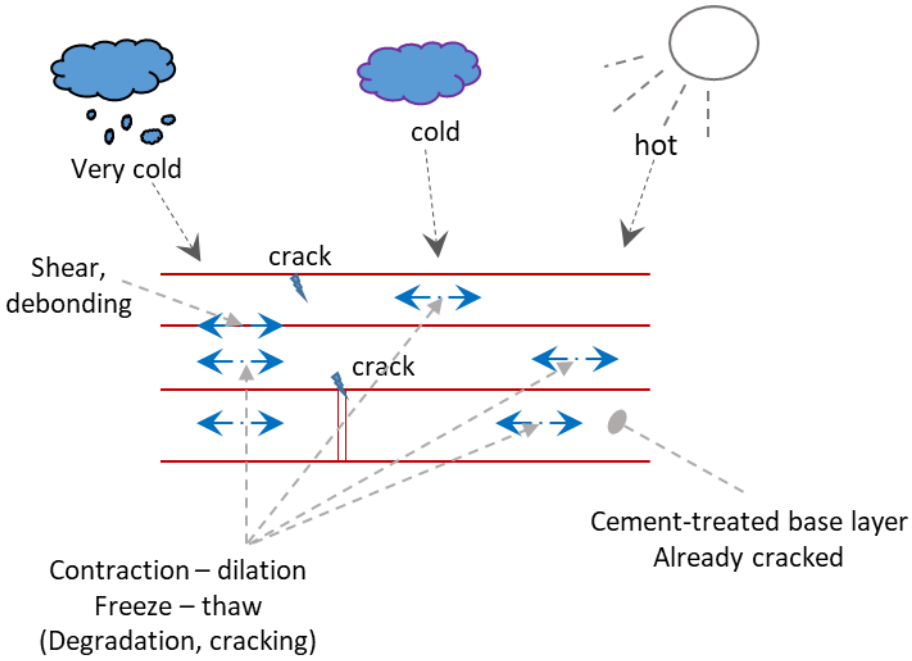

Figure 2.8. Schematic representation of thermal loads and corresponding pavement response [(adapted from Di Benedetto, 1998)].

2.2.4. Effect of fatigue and cracking in flexible pavements

Fatigue is a common type of distress in flexible pavement. It is usually called crocodile crack and sometimes called alligator crack as well schematized in Figure 2.9 (Miller & Bellinger 2014). In general, fatigue cracking is a loading failure, but multiple variables may lead to it. It is also a sign of failure of the sub-base, bad drainage, or frequent overloads. Cracking fatigue is the most common asphalt pavement discomfort caused by surface failure due to traffic loading. Fatigue cracking can, however, be greatly affected by environmental and other

impacts, although the direct cause remains traffic loading. Overloading also occurs because the foundation or subbase does not sustain the surface layer properly and can therefore not withstand loads that it would usually experience. Initially, fatigue cracking expresses itself as longitudinal cracking in the flexible pavement's top layer. These cracks are usually thin and sparsely spaced. If more development of this crack is permitted, these longitudinal cracks are joined to form sharp sided, prismatic fragments by transverse cracks. The scales on the back of a crocodile or alligator mimic this interlaced cracking pattern, hence the term, crocodile cracking.

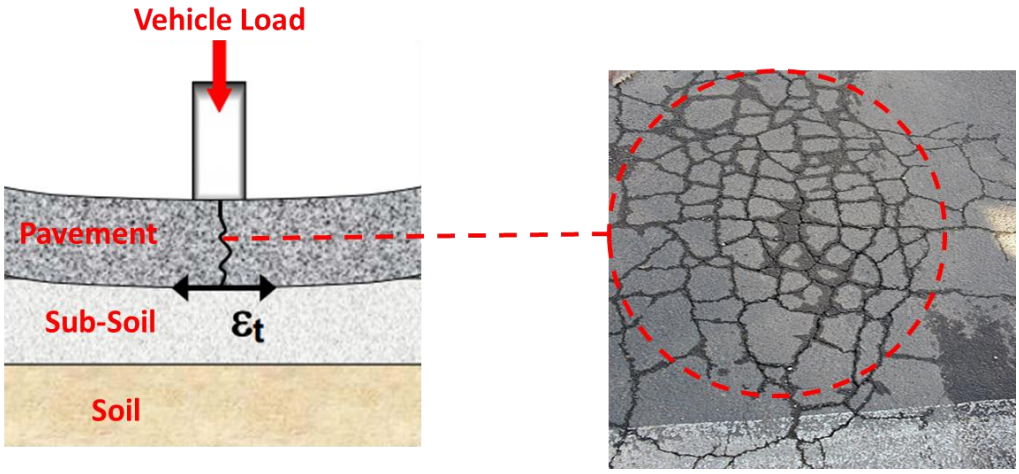

Figure 2.9. Example of fatigue cracking in flexible pavements.

2.3. The domains of thermo-mechanical behaviour of bituminous materials

2.3.1. Behaviour of bitumen

The behaviour of bitumen under cyclic loading is primarily determined by three factors:

- Temperature (T) - Temperature establishes the microstructure of bitumen. When bitumen is at its transition glass temperature (Tg = -20°C), it is in an elastic state. Beyond the point at which wax crystalises (about 90°C), bitumen exhibits a solely viscous condition. However, bitumen exhibits viscoelastic mechanical behaviour at intermediate temperatures.
- Strain amplitude (ε) – When bitumen is subjected to small amplitude strain ("small strain" domain) for a relatively low number of cycles, it can be assumed as a linear viscoelastic material. This is believed to be non-linearity.

- Number of loading cycles (N) - Depending on the loading mode, repeated cycles may result in irreversible deformation or fatigue cracking.

The behaviour of bitumen is complicated and contingent upon the above variables working together. The various mechanical behaviours that bitumen can exhibit in relation to temperature and strain amplitude values are shown in Figure 2.10 (Di Benedetto et al., 2007; Olard et al., 2005). Figure 2.11 also shows typical mechanical behaviour domains depending on Ɛ and T for bitumen (for a given number of cycles N).

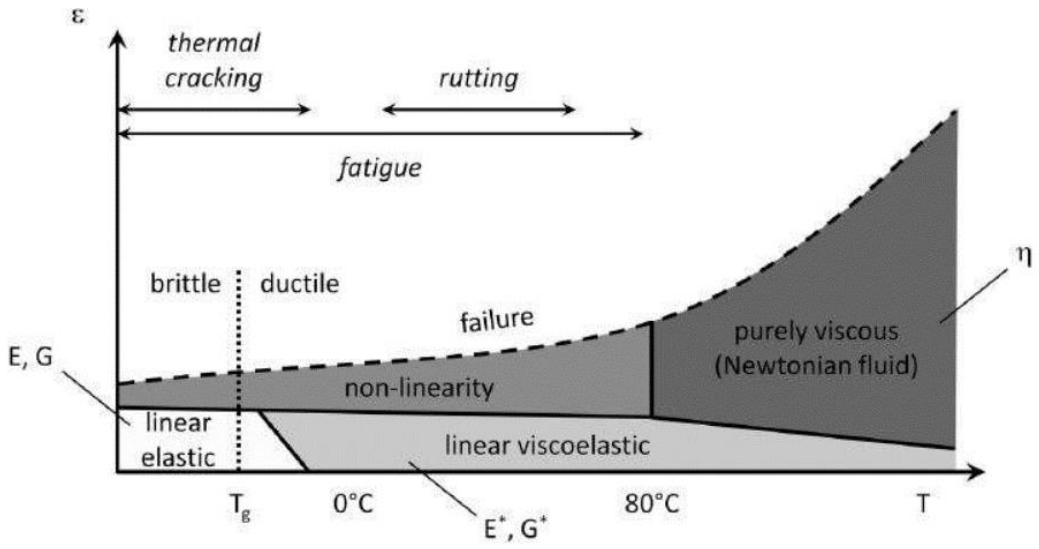

Figure 2.10. Mechanical conducts of bitumen in relation to the temperature and strain amplitude [(adapted from (Olard et al., 200 5)].

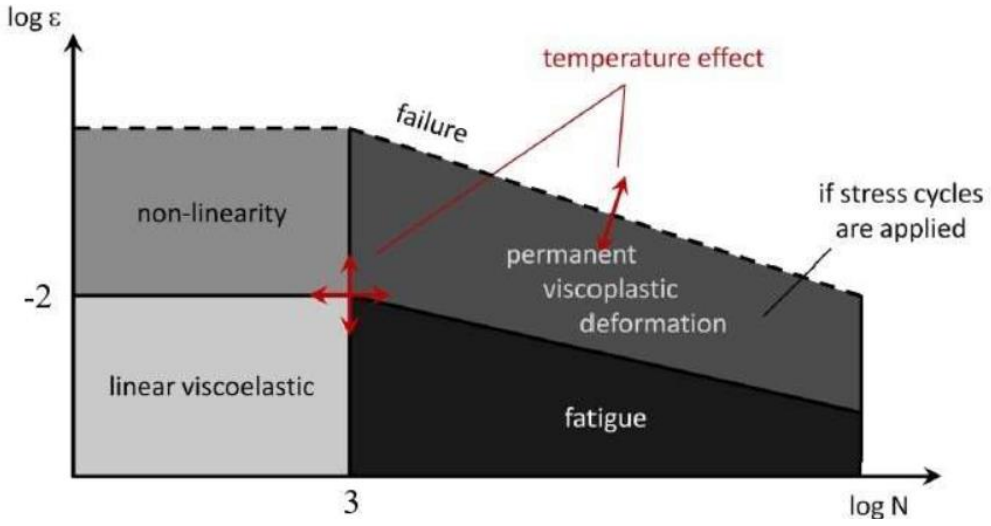

Figure 2.11. Mechanical conducts of bitumen in relation to the number of loading cycles and strain amplitude [adapted from (Mangiafico, 2014)].

The threshold value, called "linear viscoelastic limit", depending on the material and on the test temperature, is approximately equal to 1% for bitumen (Airey, 2003). Finally, if repeated stress cycles not centered on zero are applied to the material, accumulation of permanent viscoplastic deformation occurs as shown in Figure 2.11.

2.3.2. Behaviour of bituminous mixtures

Figure 2.12 shows typical mechanical behaviour domains of bituminous mixtures depending on strain, Ɛ and number of cycles, N (for a given temperature T). They also exhibit similar behaviour to the bitumen domain. Different types of behaviour are usually observed for bituminous mixtures according to the amplitude of the applied strain and the quantity of loading cycles. Within the small strain domain ($\varepsilon<100\mu m/m$) and for limited number of cycles, bituminous materials present an LVE behaviour (Yusoff et al., 2011). This invariably implies that the material's response to a number of elementary loadings is the addition of each of the elementary responses (Corte & Di Benedetto, 2004).

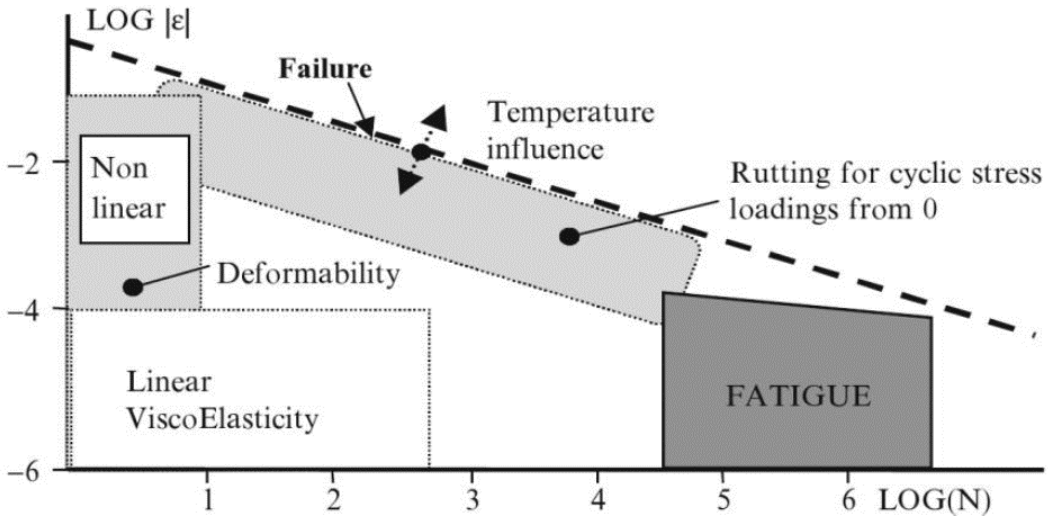

Figure 2.12. Mechanical conducts of bituminous mixtures in relation to the number of loading cycles and strain amplitude [adapted from (Sauzeat & Di Benedetto, 2015)].

2.4. Linear viscoelastic behaviour of bituminous materials

2.4.1. General definitions

Viscoelasticity is a time-dependent material behaviour that is typical of materials that, when deformed, exhibit both elastic and viscous properties. When a stress is applied, viscous materials like honey resist shear flow and strain linearly with time. Also, stretching elastic materials causes them to strain, yet if the stress is removed, they quickly return to their original shape. Viscoelastic materials display time-dependent strain because they combine features of each of these characteristics (Meyers & Chawla, 1999; Stephens et al., 2001). The basic response of the viscoelastic material is as sketched in the Figure 2.13. Therefore, the following are usually noted:

- the loading and unloading curves do not coincide
- there is a dependence on the rate of straining dε /dt, the faster the stretching, the larger the stress required
- there may or may not be some permanent deformation upon complete unloading.

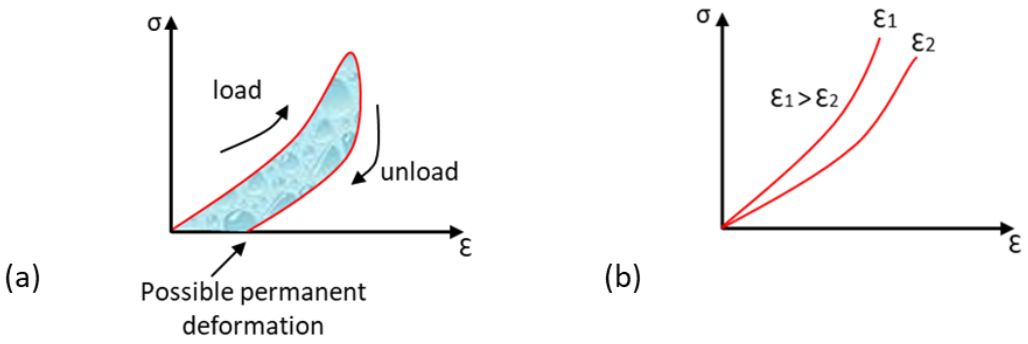

Figure 2.13. Response of a Viscoelastic material in the Tension test; (a) loading and unloading with possible permanent deformation (non-zero strain at zero stress), (b) different rates of stretching.

It can be noticed that the effect of rate of stretching that the viscoelastic material undergoes depends on time. This is totally a contrast with the elastic material, whose constitutive equation is independent of time, for example it makes no difference whether an elastic material is loaded to some given stress level for one second or one day, or loaded slowly or quickly; the resulting strain will be the same. The area beneath the stress-strain curve is the energy per unit volume; during loading, it is the energy stored in a material, during unloading it is the energy recovered.

2.4.2. Creep, recovery and relaxation

The creep-recovery involves loading a material at constant stress, holding that stress for some length of time and then removing the load. The response of a typical viscoelastic material to this test is shown in Figure 2.14. The stress σ(t) is then a Heaviside function, delayed of t_0 as described in Equation 2.3, considering the unloaded material subjected to an instantaneous stress step of σ_0 at t_0. As shown in Equation 2.4, the creep compliance function J (t_0, t, σ_0) is the strain response ε(t) divided by stress amplitude.

$$\sigma(t) = \sigma_0 Y(t - t_0) = \sigma_0 Y_{to}(t) \quad 2.3$$

$$\varepsilon(t) = \sigma_0 J(t_0, t, \sigma_0) \quad 2.4$$

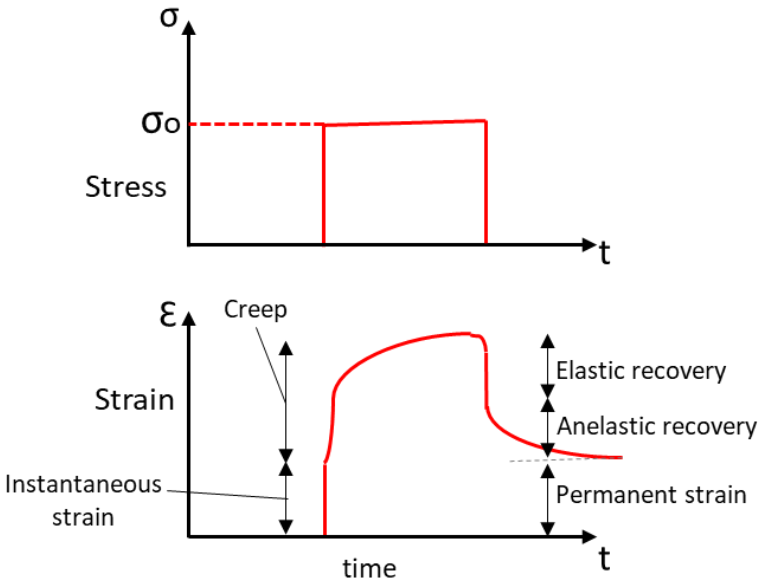

Figure 2.14. Strain response to the creep-recovery

Also, the stress relaxation test involves straining a material at constant strain and then holding that strain as indicated in Figure 2.15. As shown, Equations 2.5 and 2.6 both define the stress relaxation function R (t_0, t, ε_0) as the stress response to a strain step function of ε_0 at t_0, divided by the amplitude.

$$\varepsilon(t) = \varepsilon_0 Y_{t0}(t) \quad 2.5$$

$$\sigma(t) = \varepsilon_0 R(t_0, t, \varepsilon_0) \quad 2.6$$

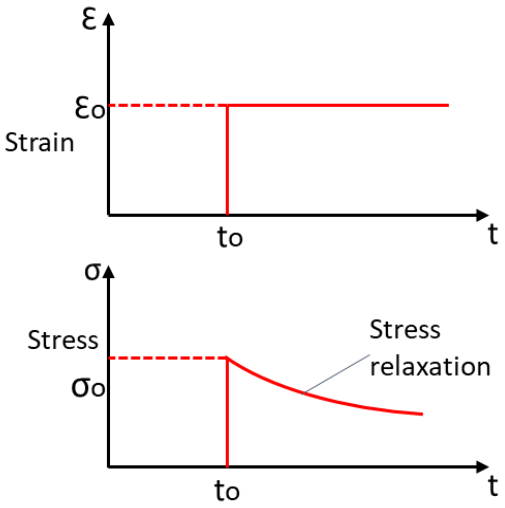

Figure 2.15. Stress response to the stress-relaxation

2.4.3. Laplace-Carson transform

The Laplace transform is an integral transform named after its inventor Pierre-Simon Laplace. It transforms a function of a real variable (often time) to a function of a complex variable (complex frequency). The transform has many applications in science and engineering. The Laplace transform of a function $f(t)$, defined for all real numbers $t \geq 0$, is the function $F(s)$, which is a unilateral transform defined by

$$F(s) = \int_0^\infty e^{-st} f(t) dt \qquad 2.7$$

Where s is the complex number frequency parameter

S = σ + iω, with real numbers σ and ω.

It can also be written as

$$F(s) = L[f(t)] \qquad 2.8$$

The Laplace-Carson transforms of strain (Ɛ), stress (σ), creep function (J) and relaxation function (R) becomes;

$$\varepsilon(s) = J(s)\sigma(s) \qquad 2.9$$

$$\sigma(s) = R(s)\mathcal{E}(s) \quad 2.10$$

2.4.4. Time-Temperature Superposition Principle

Complex modulus is dependent on temperature and frequency, assuming that the theory of LVE behaviour for bituminous materials, consists of remaining within their linear domain is true. (Mangiafico, 2014). It is observed with several LVE materials that complex modulus values plotted on Cole-Cole or black diagrams tend to form a unique curve which is usually independent of temperature and frequency. According to Corte and Di Benedetto (2005), this material behaviour is known as “thermorheologically simple”. The influence of both temperature and frequency can be reduced for these kinds of materials to a single variable, with the equivalent frequency being the most often selected one which is called the "Time Temperature Superposition Principle" (TTSP). Therefore, the "Time Temperature Superposition Principle" (TTSP) is said to be represented by the following for materials with this property:

$$E^*(f, T) = E^*[g(f)T] \quad 2.11$$

Then

F, h (T_1) = f_2 h (T_2) and T1 g (f_2)

The reference temperature and the temperature of the isotherm to shift determine this shift factor. The mathematical procedure to obtain f_{eq} through the shifting procedure is represented by;

$$f_{eq} = f_i \frac{f(Ti)}{f(Tref)} = f_i\, a_t\,(T_i, T_{ref}) \quad 2.12$$

2.4.5. Complex Modulus and Poisson’s ratio

An LVE is usually subjected to a sinusoidal stress with the frequency, f , which can be represented in the form;

$$\sigma(t) = \sigma_0 \sin(\omega t) \quad 2.14$$

with $\omega = 2\pi f$

Where there is further deformation, the resulting deformation will also be sinusoidal and represented by;

$$\varepsilon(t) = \varepsilon_0 \sin(\omega t - \varphi) \quad 2.15$$

where φ, called phase angle, is the phase lag between the two sinusoidal signals

By using complex notations ($i^2 = -1$), σ* and ε* can be defined, respectively, as

$$\sigma(t) = \sigma_0 e^{i\omega t} \quad 2.16$$

$$\varepsilon(t) = \varepsilon_0 e^{i\omega t - \varphi} \quad 2.17$$

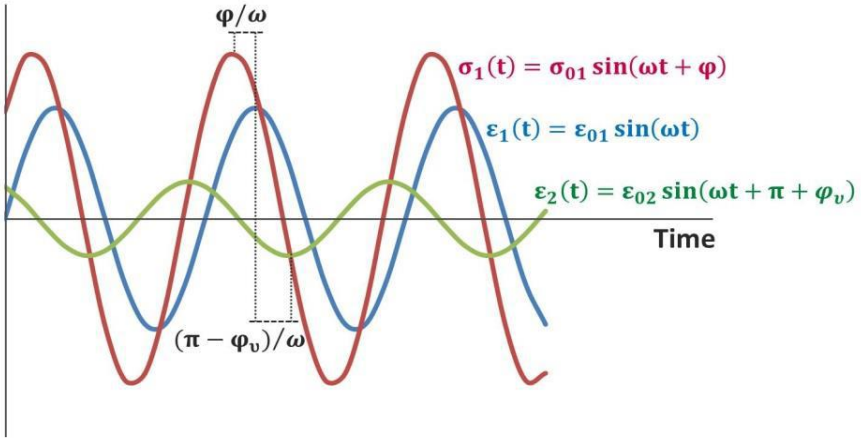

Figure 2.16. Diagrammatic representation of the measurements obtained on an LVE material under sinusoidal loading.

Substituting in equation

$$\sigma(t) = \tilde{R}(i\omega)\varepsilon(t) \quad 2.18$$

therefore

$$\tilde{R}(i\omega) = \frac{\sigma(t)}{\varepsilon(t)} = E(\omega) \quad 2.19$$

The complex modulus (E*) of the LVE materials is defined as the Laplace-Carson transform of the relaxation function ($\tilde{R}$) at a point "jω", as shown in equation

$$E(\omega)= \frac{\sigma_0 e^{i\omega t}}{\varepsilon 0 e^{i\omega t-\varphi}} = |E|e^{i\varphi} \quad 2.20$$

Since E* is complex, its real and imaginary parts, respectively E1 and E2, can be isolated as follows

$$E=E1+i\,E2=|E^*|\cos\varphi + i|E|\sin\varphi \quad 2.21$$

E1, also known as the "storage modulus," denotes the portion of energy that can be recovered from the material when it is loaded. It is the LVE behavior's elastic component. E2, also referred to as the "loss modulus," is the amount of energy lost as a result of internal friction. It is the viscous, irreversible element of the LVE behaviour. The LVE behaviour is then characterised by the phase angle φ in the same way as the E* norm. The material exhibits perfect elastic behaviour when φ=0, and pure viscous behaviour when φ=90°. The material exhibits LVE behaviour for intermediate values. In a similar way to |E|, shear complex modulus G* can be defined as

$$G^*(\omega)= \frac{\tau 0 e^{i\omega t}}{\Upsilon 0 e^{i\omega t-\varphi}} = |G*|e^{i\varphi} = G_1 + i\,G_2 = |G*|\cos\varphi + i\,|G*|\sin\varphi \quad 2.22$$

where $\tau(t)=\tau_0 e^{i\omega t}$ is a sinusoidal shear strain of amplitude τ0 and $\gamma(t)=\gamma_0 e^{i\omega t}$ is a sinusoidal shear strain of amplitude γ_0.

For bituminous materials, the isotropy hypothesis states that E* and G* are related as

$$G^* = \frac{E^*}{2(1+\nu^*)} \quad 2.23$$

where ν* is the complex Poisson's ratio. Given a radial strain $\varepsilon_2(t)=\varepsilon_{02}\sin(\omega t-\varphi+\pi+\varphi_\nu)$, observed during axial loading of the material, ν* is defined as

$$\nu^* = -\frac{\varepsilon_2^*}{\varepsilon_1^*} = \frac{\varepsilon_{02} e^{i\omega t-\pi+\varphi+\varphi_\nu}}{\varepsilon_{01} e^{i\omega t-\varphi}} = |\nu^*|e^{i\varphi_\nu} = \nu_1 + i\,\nu_2 = |\nu^*|Cos\varphi_\nu + i|\nu^*|Sin\varphi_\nu \quad 2.24$$

where φ_ν is the phase angle of Poisson's ratio. Experimentally, measurements have shown that Poisson's ratio is not constant but it depends on frequency and temperature. The values of φν indicates for bituminous mixtures are close to 0°, that is radial and axial strains are approximately in phase opposition. It also shows that values of φν are negative, corresponding to a radial strain slightly late with respect to axial strain (Di Benedetto et al., 2007).

According to Mangiafico (2014) different graphical representations are used to show the variation of complex modulus E* (and its components |E*|, E_1, E_2 and φ) with frequency and temperature. The most common types of plot are:

- Isothermal curves: These curves are obtained by plotting the values of the norm of complex modulus |E*| against corresponding test frequencies, for each test temperature. Both axes are commonly in logarithmic scale.

- Isochronal curves: These curves are complementary to isothermal curves. They are obtained by plotting values of |E*| against corresponding test temperatures, for each test frequency. The graph is generally plotted on a semi-logarithmic scale (log |E*| versus temperature).

- Cole-Cole plot: This graph is obtained by plotting E_1 and E_2 values in the complex plane (imaginary part against real part). Since axes are commonly in linear scale, the large variation of E1 and E2 is not entirely evident. In particular, Cole-Cole plots are useful to highlight the behavior of bituminous materials at low temperature/high frequency.

- Black diagram: This graph is obtained by plotting |E*| values against corresponding φ values, in the so-called "Black space". It is a usually plotted on a semi-logarithmic scale (log |E*| versus φ). For this reason, Black diagrams are useful to highlight bituminous material behavior at high temperature/low frequency.

  All these graphs can be plotted, following a similar approach, for G* and ν*.

2.4.6. Energy Dissipation

Linear elastic materials are usually loaded and due to this, the energy stored in the material during strain accumulation is completely returned during unloading. As shown in the Figure 2.17, there is no coincidence in the stress-strain curve during loading and unloading.

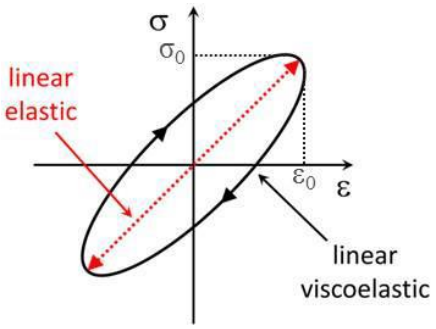

Figure 2.17. Hysteresis: Sinusoidal loading of elastic and LVE materials. (Mangiafico, 2014).

The region inside the stress-strain curve represents the energy dissipated per unit of volume during a loading cycle (W). When an LVE material is subjected to sinusoidal loading, "W" can be expressed as follows:

$$W_{cycle} = \pi \varepsilon_0 \sigma_0 \sin\varphi \qquad 2.25$$

2.4.7. Models of discrete creep behaviour

It has been established that viscoelasticity is derived from the words "viscous" + "elastic"; a viscoelastic material exhibits both viscous and elastic behaviour, that is, a bit like a fluid and a bit like a solid. One can build up a model of linear viscoelasticity by considering combinations of the linear elastic spring and the linear viscous dash-pot. These are known as rheological models or mechanical models.

- **Linear Elastic Spring:** This is the simplest way to create a model of a material is to suppose that it consists of nothing but a linear spring of stiffness “E” as shown in Figure 2.18.

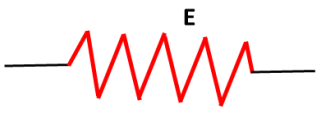

Figure 2.18. The linear elastic spring

The linear elastic spring exhibits proportionate stress and strain, which is represented as follows;

$$\sigma(t) = E\varepsilon(t)$$
$$E^*(\omega) = E \qquad 2.26$$

- **Linear Viscous Dash-pot:** This represent materials which respond like a viscous dash-pot; the dash-pot actually is a piston cylinder arrangement, filled with a viscous fluid, a strain is achieved by dragging the piston through the fluid as shown in Figure 2.19.

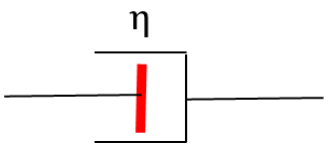

Figure 2.19. The linear Dashpot

By definition, the dash-pot responds with a strain rate proportional to stress:

$$\dot{\epsilon} = \frac{1}{\eta}\delta \qquad 2.27$$

The creep (J) and relaxation (R) function as adapted from Tapsoba (2012) is given by:

$J(t) = {}^{t}/_{\eta}$

$R(t) = \eta\delta(t)$

The complex modulus equation is given by:

$$E^* = j\omega\eta \qquad 2.28$$

Where ŋ is the viscosity of the material. This is the typical response of many fluids; the larger the stress, the faster the straining (as can be seen by pushing your hand through water at different speeds).

- **Maxwell model:** The Maxwell model can be represented by a purely viscous damper and a purely elastic spring connected in series, as shown in Figure 2.20. Two elements' creep compliance functions add up when they are connected in sequence. For the complex moduli, the creep compliance and the stress relaxation functions of the

Maxwell models are given by Equations 2.29. A relaxation time τ is introduced in Equation 2.30.

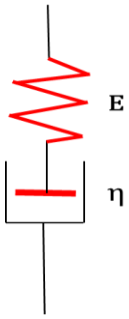

Figure 2.20. The linear Maxwell model

$$J(t) = \frac{1}{E} + \frac{t}{\eta}$$

$$R(t) = E\, e^{-\frac{t}{\tau}}$$

$$E^*(\omega) = E\frac{i\omega\tau}{1+i\omega\tau} = \frac{E2\omega2\eta2 + iE2\omega\eta}{E2 + \omega2\eta2} \qquad 2.29$$

Where i: complex number defined by $i^2 = -1$.

$$\tau = \frac{\eta}{E} \qquad 2.30$$

where τ is the relaxation time.

- **Kelvin–Voigt model:** The Kelvin–Voigt model, also known as the Voigt model, consists of a Newtonian damper and Hookean elastic spring connected in parallel as shown in Figure 2.21. However, when they work together in parallel, their relaxing effects are increased. Therefore, the complex moduli, the creep compliance and the stress relaxation functions of the KV models are given by Equations 2.31. A relaxation time τ is also introduced in equation 2.32.

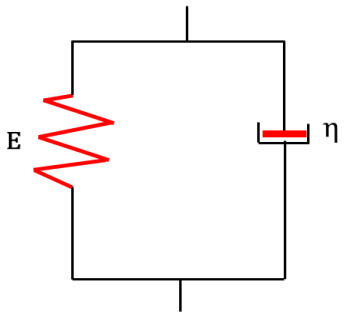

Figure 2.21. The Kelvin-Voigt model

$J(t) = \frac{1}{E}(1 - e^{-\frac{t}{\tau}})$

$R(t) = E + \eta\sigma(t)$,

$$E^*(\omega) = R^*(i\omega) = E + i\omega\eta = E(1 + i\omega\tau) \quad 2.31$$

with σ Dirac function

$$\tau = \frac{\eta}{E} \quad 2.32$$

where τ is the relaxation time.

- **Generalised Maxwell Model:** A number of Maxwell or Kelvin-Voigt components can be combined to create more intricate models. The spring E_0 and dashpot η_∞ are added to the n Maxwell elements that are all parallel in the generalised Maxwell model as shown in Figure 2.22. For all types of LVE materials, this model, also known as the Prony series if = 0, is frequently employed. Along with the changeable number of elements, each Maxwell element has a unique relaxation period that makes it possible to accommodate intricate experimental stress relaxation curves.

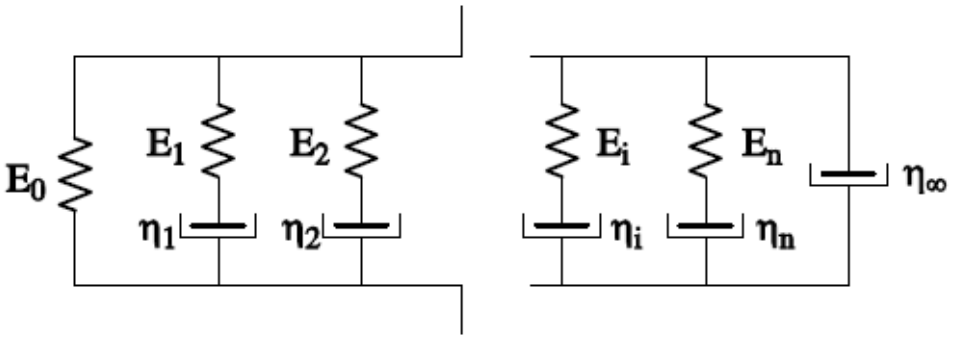

Figure 2.22. The generalised Maxwell Model.

$$R(t) = E_0 + \eta_\omega \delta(t) + \sum_{i=1}^{n} Ei\, e^{-}\frac{t}{\tau i}$$

$$E^*(\omega) = E_0 + i\omega\eta_\omega + \sum_{i=1}^{n} E\frac{i\omega\tau}{1+i\omega\tau} \qquad 2.33$$

- **Generalised Kelvin-Voigt Model:** The generalised Kelvin-Voigt model is made up of n KV elements that are all connected in series with a spring and a dashpot as shown in Figure 2.23.

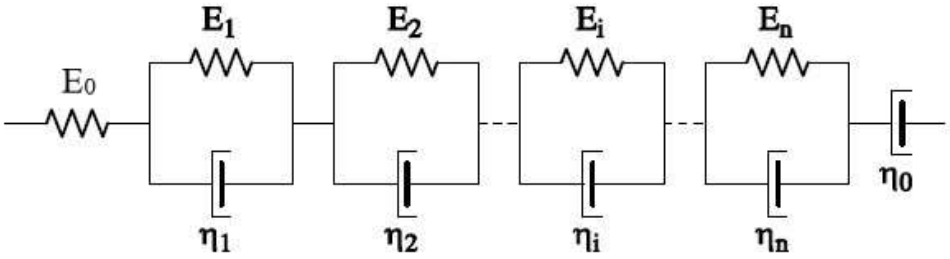

Figure 2.23. The generalised Kelvin-Voigt Model.

$$J(t) = \frac{1}{E_0} + \frac{t}{\eta_0} + \sum_{i=1}^{n} \frac{1}{E_i}(1 - e^{-\frac{t}{\tau_i}})$$

$$E^*(\omega) = \frac{1}{\frac{1}{E_0} + \frac{i}{i\omega\eta_0} + \sum_{i=0}^{n} \frac{1}{E_i(1+i\omega\tau_i)}} \qquad 2.34$$

With $\tau_i = \frac{\eta j}{Ej}$.

If n tends to infinity, a continuous spectrum can also be introduced.

2.4.8. Models of parabolic creep behaviour

It can be assumed that continuity of the relaxation spectrum if the number of Maxwell (or KV) elements is almost limitless. Since H(τ) is the distribution function of the continuous relaxation spectrum (Di Benedetto and Corté 2005). Any type of LVE behaviour can be described using this formalism.

$$E*(\omega) = \int_{\ln\tau=-\infty}^{\ln\tau=+\infty} H(\tau)\frac{i\omega\tau}{1+i\omega\tau}dln\,\tau \qquad 2.35$$

One illustration of a continuous relaxation spectrum is the parabolic element as shown in Figure 2.24. Equation 2.36 indicates the creep compliance function, while equation 2.37 expresses the complex modulus, with a positive τ and 0 < h < 1, and where Γ is the gamma function as represented in 2.37.

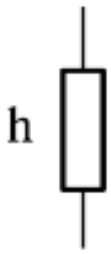

Figure 2.24. The parabolic element

$$J(t) = (\frac{t}{\tau})^h \qquad 2.36$$

$$E^*(\omega) = \frac{(i\omega\tau)^h}{\Gamma(1+h)} \qquad 2.37$$

$$\Gamma(h) = \int_0^{+\infty} x^{h-1}e^{-1} \qquad 2.38$$

- **Huet Model:** Huet first suggested the use of parabolic components to successfully describe the LVE behaviour of bituminous materials (Huet 1963). Two parabolic components and one spring are used in series in the so-called Huet model as shown in Figure 2.25. The creep compliance function as indicated in equation 2.39 and the complex modulus as shown in equation 2.40 are rearranged to have a simplified expression as a function of τ defined in Equation 2.41.

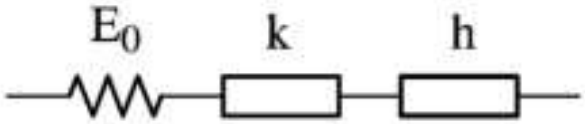

Figure 2.25. The Huet model.

$$J(t) = \frac{1}{E_0} + (\frac{t}{\tau_k})^k + (\frac{t}{\tau_h})^h$$

$$J(t) = \frac{1}{E_0}\left(1 + \delta\frac{(\frac{t}{\tau})^k}{\Gamma(1+k)} + \frac{(\frac{t}{\tau})^h}{\Gamma(1+h)}\right) \qquad 2.39$$

$$E*(\omega) = \frac{E_0}{1 + \delta(i\omega\tau)^{-k} + (i\omega\tau)^{-h}} \qquad 2.40$$

$$\tau = \tau_k\delta^{-\frac{1}{k}}(E_0\Gamma(1+k)^{\frac{1}{k}} = \tau_h(E_0\Gamma(1+h))^{\frac{1}{h}} \qquad 2.41$$

As long as the material only τ depends on temperature and is proportionate to the shift factor, such a model is appropriate for materials that follow the TTSP:

$$\tau(T) = \tau_0 a_T(T, T_{ref}) \qquad 2.42$$

- **Huet-Sayegh model:** The Huet model has proven to be useful for bituminous materials, but it was shown to be inaccurate in simulating mixture behaviour at high temperatures or low frequencies (Huet 1963). Because of the granular structure, mixtures have an

asymptotic elastic modulus E_{00}, also known as a static modulus, in contrast to bitumens, which tend to become totally viscous. Sayegh introduced the Huet-Sayegh model as an upgrade to the Huet model (Sayegh 1965), which incorporates an additional spring in tandem with the original model as shown in Figure 2.26. Both the creep and relaxation functions lack a straightforward analytical expression, however the complex modulus in equation 2.43.

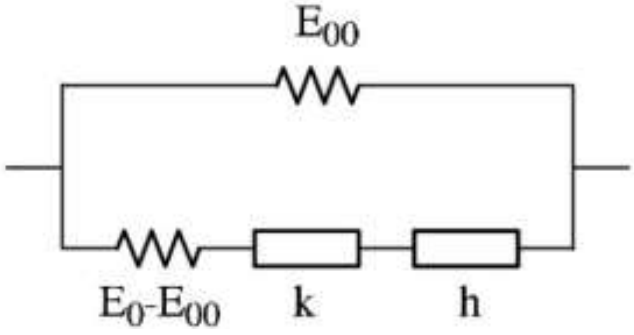

Figure 2.26. The Huet-Sayegh model

$$E^*(\omega) = E_{00} + \frac{E_0 - E_{00}}{1 + \delta(i\omega\tau)^{-k} + (i\omega\tau)^{-h}} \qquad 2.43$$

- **2 Springs, 2 Parabolic & 1 Dashpot (2S2P1D):** According to Olard and Di Benedetto (2003) this model was introduced to avoid the drawbacks with the generalization of the Huet-Sayegh model valid for both the bituminous binders and mixtures. This general model is based on a simple combination of physical elements (spring, dashpot and parabolic element) as shown in Figure 2.27. Like the Huet-Sayegh model, the introduced model has a continuous spectrum (i.e. can be represented by an infinity of Kelvin-Voïgt elements in series or Maxwell elements in parallel).

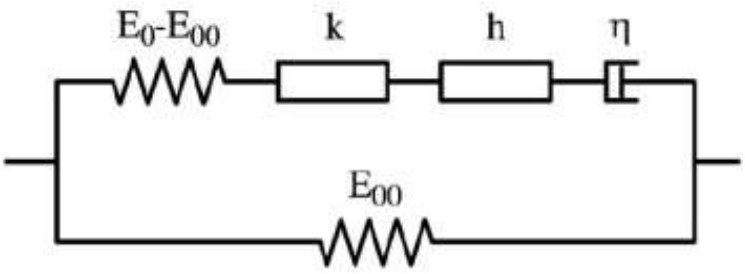

Figure 2.27. Representation of the introduced general model "2S2P1D" for both bituminous binders and mixes, h and k are two parabolic creep elements.

At a given temperature, the introduced model has 7 constants and its complex modulus is given by the following expression:

$$E^*(\omega) = E_{00} + E_{00} + \frac{E_0 + E_{00}}{1 + \delta(i\omega\tau)^{-k} + (i\omega\tau)^{-h} + (\beta i\omega\tau)^{-1}} \quad 2.44$$

With,

$$\beta = (E_0 - E_{00})\eta\tau \quad 2.45$$

However, the analogical structure of the 2S2P1D model allows for the inclusion of physical parameters (such as E_0, E_{00}, τ, and η) and Figure 2.28 shows the impact of each constant on the complex modulus curve.

Figure 2.28 shows the influence of six of the 2S2P1D parameter (E_{00}, E_0, k, h, δ and τ) on a general Cole-Cole curve of a bituminous material.

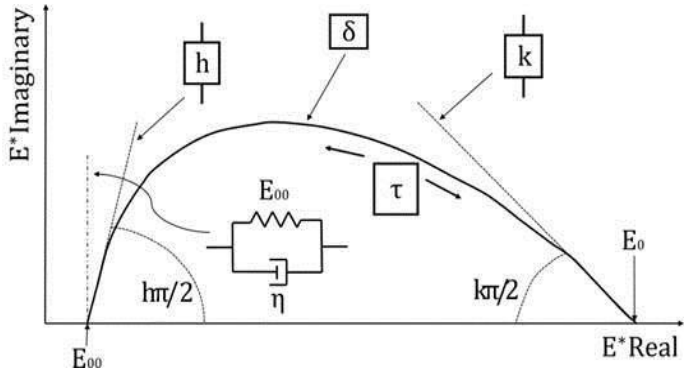

Figure 2.28. Influence of 2S2P1D parameters associated with constitutive elements of the model on a general Cole-Cole curve of bituminous materials.

2.5. Fatigue of bituminous Materials

Fatigue of bituminous materials is one of the main causes of pavement degradation. Fatigue phenomenon has been extensively studied in Europe (RILEM) and in the United States (SHRP) (Perraton et al., 2003). The overall phenomena of fatigue as well as the key elements pertaining to the fatigue of bituminous materials are introduced in this section.

2.5.1. General description of fatigue

Fatigue cracking is known to result from repeated loading cycles induced by traffic, starting with the appearance of micro-cracks followed by their coalescence into macro-cracks (Di Benedetto et al., 2004; Lee, 2005; Moreno-Navarro et al., 2018; Li et al., 2019). Fatigue in elastic solid materials is only linked to permanent damage because of the repeated cycles that cause matter displacement and tiny fractures to grow until they become obvious cracks. However, internal faults that already exist cause the cracks to spread in composite materials (Ewing and Humphrey 1903). In general, the full explanation of the microscopic processes involved in cyclic loading is too intricate to accurately correlate with the macroscopic characteristics that are seen (Murakami 2012). Two methods for interpreting fatigue damage were developed, they are; Continuum damage mechanics (Kachanov 1958; 1986) and fracture mechanics (Griffith 1921; Clark 1971). The idea of dispersed damage, which is typically connected to the loss of resistive cross-section area, is introduced by continuum mechanics. Throughout the test, the apparent stiffness is observed to assess the progression of damage. However, the goal of fracture mechanics is to establish a connection between the fatigue behaviour and fracture properties by examining the propagation of cracks in a variety of geometries, which is mostly connected to bending beams (Hartman and Gilchrist 2004).

2.5.2. Characterization of fatigue of bituminous mixtures

Using one of these two methods of interpreting fatigue is usually sophisticated and complex. This is why it is still a research topic for researchers and professionals in the industry. This is why analysing the fatigue life of material specimens subjected to continuous cyclic loading is the classical method used to characterise fatigue. The fatigue life is mostly determined by the stress or strain amplitude level of the loading.

2.5.2.1. Laboratory tests

Laboratory procedures to reproduce and characterize fatigue of bituminous materials are based on accelerated cyclic loading. It has been emphasized that various methods are usually applied in the laboratory to characterize fatigue of bituminous mixtures with either homogenous and non-homogenous tests (Bodin et al., 2006; Medani & Molenaar, 2000). Homogeneous tests basically have the advantage of enabling direct access to material behavior without any hypothesis which is not the case for non-homogeneous tests (Tapsoba et al., 2013). Sinusoidal

loading is usually applied to determine the fatigue properties of bituminous mixture. As shown in Figure 2.29, It is possible to control either constant axial strain amplitude (controlled-strain mode) or constant axial stress amplitude (controlled-stress mode).

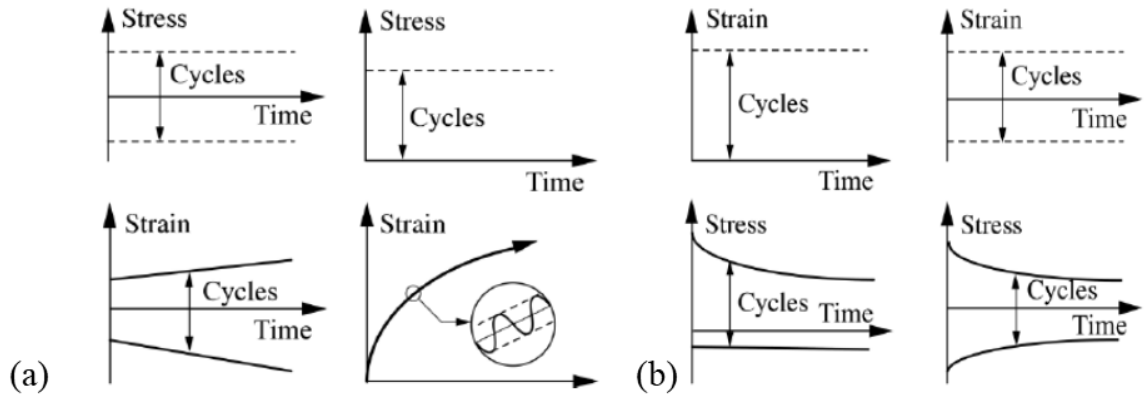

Figure 2.29. Strain and stress evolution during fatigue tests performed in (a). strain control mode and (b). stress control mode [as adapted from (Mangiafico, 2014)].

Characterising the fatigue of bituminous mixtures are usually expressed as relationships between the initial axial strain (or axial stress) and number of load repetitions to failure, determined from tests performed at several axial strain (or stress) levels (Tapsoba et al., 2013). Fatigue behaviour can be characterized by the slope and the relative level of axial strain or axial stress versus the number of load repetitions to failure (Medani & Molenaar, 2000).

- **Evolution of the norm of complex modulus and phase angle**

A typical result by Tapsoba et al. (2013) shows the norm of complex modulus |E*| and phase angle φ plotted as a function of the number of cycles in Figure 2.30. During the fatigue test, three stages were deducted and which affirms with other researchers view such as (Di Benedetto et al., 2004; Lundstrom et al., 2004; Di Benedetto et al., 2011; Moreno-Navarro & Rubio-Gamez, 2016; Mangiafico et al., 2016; Babadopulos et al., 2019), these are:

- Phase I: A rapid decrease of the norm of complex modulus as well as an increase in the phase angle is usually observed. This have been attributed to several reversible phenomena such as heating, thixotropy, non-linearity and irreversible phenomenon known as fatigue damage.

- Phase II: This has been attributed to the development of micro-cracks which is believed to be fatigue. Therefore, decrease in |E*| and increase in φ is quasi-linear.
- Phase III: This is also known as the failure stage which is attributed the development of macro-cracks. At this stage also, homogeneity is believed to be lost.

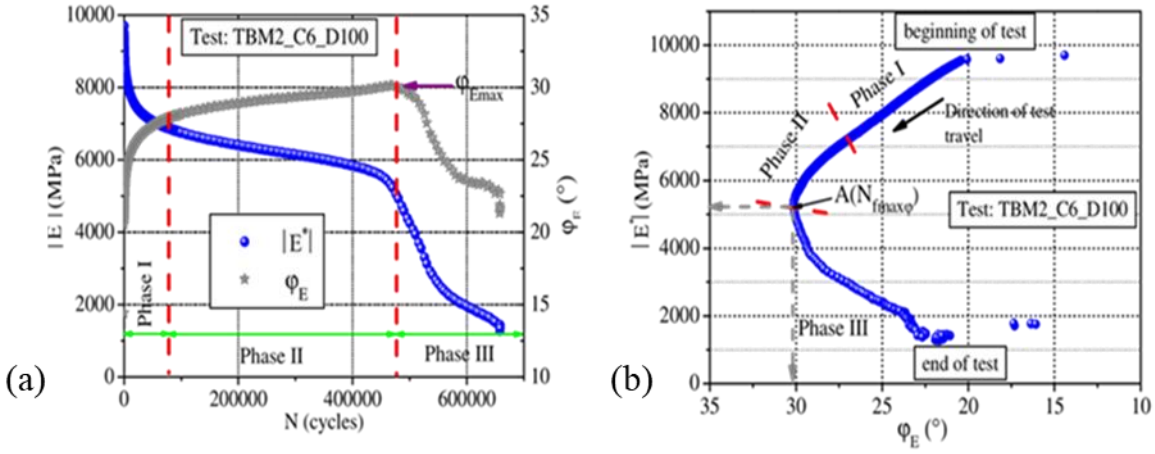

Figure 2.30. (a). Evolution of complex modulus (norm and phase angle (b). Black's space result [for a test sample TBM2_C6_D100 [adapted from (Tapsoba et al., 2013)].

- **Evolution of the norm of Poisson's ratio and radial strain**

Also, Tapsoba et al. (2013) presents result of evolution of the norm of Poisson's ratio and midvalue of radial strain according to the number of cycles as shown in Figure 2.31. Three phases were also deducted as thus:

- Phase I: It was noted that there was an increase in Poisson's ratio while there was a decrease in midvalue of radial strain.
- Phase II: This phase was characterized by a slow decrease in Poisson's ratio and a continuous decrease in midvalue of radial strain.
- Phase III: A quick decrease in Poisson's ratio is attributed to this phase. There also a slow increase in midvalue of radial strain.

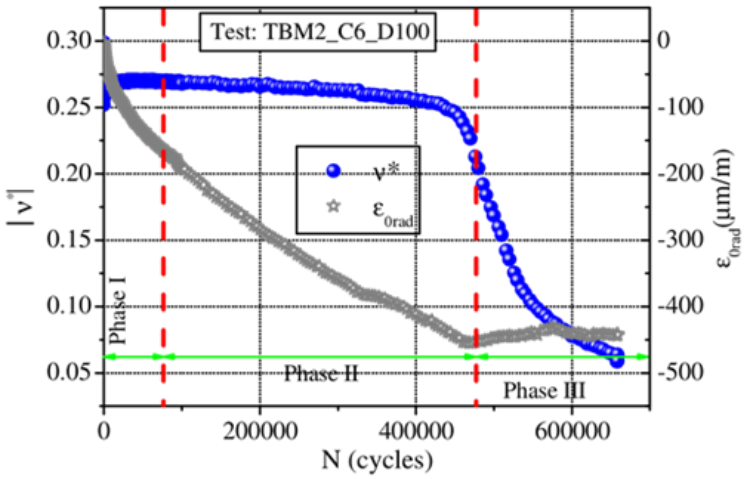

Figure 2.31. Evolution of the norm of Poisson's ratio and midvalue of radial strain [for a test sample TBM2_C6_D100 [adapted from (Tapsoba et al., 2013)].

- **Dissipated energy and temperature**

Dissipated energy per cycle and temperature as a function of the number of cycles is represented in Figure 2.32 as carried out by (Tapsoba et al., 2013). Three phases were deducted from the result of fatigue test as thus;

- Phase I: A rapid increase in temperature is observed in this phase which leads to a decrease in energy dissipated.
- Phase II: A gradual decrease in temperature in noted with a corresponding decrease noted in the energy dissipated.
- Phase III: In this phase, there is a rapid decrease in temperature as well as a corresponding decrease in energy dissipated.

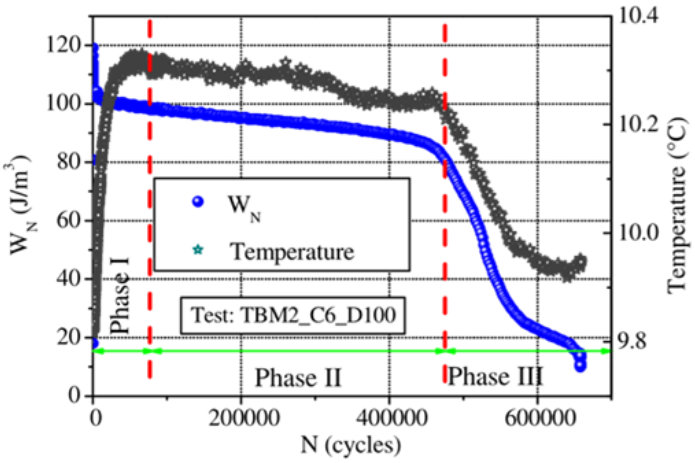

Figure 2.32. Dissipated energy and temperature as a function of the number of cycles [for a test sample TBM2_C6_D100 [adapted from (Tapsoba et al., 2013)].

2.5.2.2. In-situ tests

In situ testing are often performed at full scale, either by using accelerated pavement facilities or applying controlled traffic loads to instrumented pavement portions (Highway research board, 1962). Over simulated laboratory test programs, full-scale test facilities have some advantages that are unique to them. In comparison to what can be directly replicated using scaled models, the influences of size, manufacturing, environment, substructure, and loads represent the on-site conditions far more accurately. But since temperature and moisture cannot be regulated in full-scale test facilities, which are often in outdoor ambient conditions, there will always be discrepancies between laboratory and in-situ test data (Hartman et al., 2001).

2.5.3. Criteria for Fatigue Life

The criterion for defining failure in cyclic tests is a topic that many researchers have discussed in the literature. It is believed that bituminous mixtures do not necessarily have to reach physical failure before they are classified under failure criteria. Thus, six fatigue life criteria have been classified in four categories.

- Classical criteria based on Modulus decrease: The most classical fatigue criterion ($N_{f50\%}$) is defined by (EN 12697-24, AFNOR 2012e) as the number of cycles corresponding to a complex modulus decrease of half (50%) of its initial value. Also, the criterion $N_{f30\%}$ is defined as the number of cycles corresponding to a modulus

decrease of 30% of its initial value. This criterion is criticized by the majority of the researchers, since the choice of the percentage of complex modulus reduction is arbitrary and it does not consider biasing effects occurring during fatigue tests (Di Benedetto et al., 2004)

- Criterion from Phase angle evolution: This is based on the maximum phase angle criterion ($N_{fmax\ \varphi}$) which is also called second inflection point which is used for the analysis of fatigue failure. When the highest value of phase angle is obtained, it is considered that failure is reached. $N_{fmax\ \varphi}$ is the number of cycles corresponding to this highest value of phase angle. It is thought to be a sign of a shift in the material's mechanical behaviour brought on by the accumulation of fatigue damage.

- Criteria obtained from the analysis of specimen homogeneity: This is based on an indication of the homogeneity of axial strain and stress fields. Usually in phases I and II, differences remain small while in phase III, the differences become great which is believed to be due to macrocracking or non-homogeneity.
- Criteria from dissipated viscous energy curve: This criterion as defined by Pronk and Hopman (1990) is based on the change in evolution of the total dissipated energy up to number of cycle N divided by the dissipated energy at cycle N. The dissipated energy ratio (DER) is given by:

$$DER = \sum_{i=1}^{N} \frac{Wi}{WN} \qquad 2.45$$

The parameter DER (Dissipated Energy Ratio) presents an abrupt slope variation when the material reaches to failure.

2.6. Reversible phenomena observed during fatigue test on bituminous mixtures

During these tests, some phenomena related to the intrinsic thermomechanical characteristics of the materials are known to occur producing important variation of material properties which are completely reversible and their effect must not be confused with fatigue damage. These phenomena are mainly thixotropy, self-healing, heating and non-linearity. These phenomena can significantly bias the estimation of fatigue properties of materials unless properly identified and quantified (Babadopulos et al., 2011, 2019; Ayar et al., 2016; Baaj et al., 2018; Williams

et al., 2001; Moreno-Navarro et al., 2015; Santagata et al., 2013; Mangiafico et al., 2015). The different phases that is believed to occur during fatigue testing has been divided into three stages as shown in Figure 2.33, namely: (i) accumulation of permanent deformation; (2) reversible deterioration and initiation of irreversible damage (micro-cracks); (3) coalescence of micro-cracks which leads to the localization and propagation of macro-cracks (Moreno-Navarro & Rubio-Gamez, 2016).

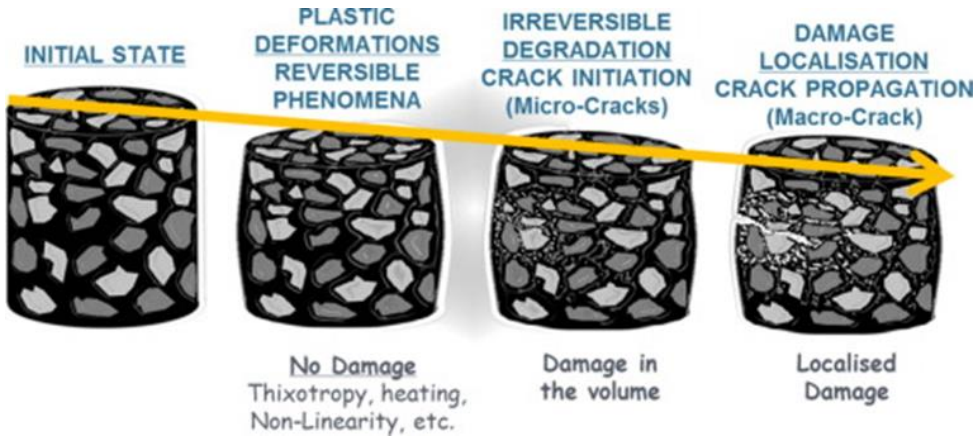

Figure 2.33. Different phases during fatigue processes in bituminous mixtures (Moreno-Navarro & Rubio-Gamez, 2016).

More specifically, these fatigue tests on bituminous mixtures is usually associated to the norm of the complex modulus (sometimes called “dynamic modulus”) decreases with the number of cycles. The decrease of the norm of the complex modulus, and more generally the change in the complex modulus (including norm and phase angle), is explained to be due these reversible phenomena (Di Benedetto et al, 2011; Isailović et al., 2017; Riahi et al. 2017). Ultimately, these reversible phenomena can be significant but as outlined in various standards for fatigue test ASTM 7460 and EN 12697-24, reversible phenomena are not considered when analyzing fatigue results but have shown to be important (Babadopulos et al, 2019). These phenomena are explained in this section along with a technique to distinguish and measure their impact from actual damage.

2.6.1. Non-linearity

Nonlinearity is believed to be an instantaneous and reversible phenomenon that makes stiffness dependent on the levels of loading (like the amplitude of strain in sinusoidal loading). If variations in strain amplitude happen, intrinsic changes in stiffness occur due to nonlinearity (Taylor et al., 2011; Nguyen et al., 2013; Mangiafico et al., 2015; Mangiafico et al., 2016; Nguyen et al., 2019; Babadopulos et al, 2019). Figure 2.34 shows a typical Strain Amplitude Sweep (SAS) tests which shows nonlinearity effect, where an instantaneous decrease in |G*| and also characterized by subsequent increase in φ when strain amplitude increases (Babadopulos et al, 2019). Also, mixture behaviour can show sensible non-linearity for relatively low strain levels applied on samples. Since this effect could be confused with damage accumulation, non-linearity should be considered when performing fatigue tests on bituminous mixtures (Di Benedetto et al., 2011; Doubbaneh, 1995; Gauthier, Bodin, Chailleux, & Gallet, 2010; Nguyen, 2011). Researchers have proven that non-linearity measured during strain sweeps is a separate phenomenon, different from heating, thixotropy and cracking. Also, the amount of non-linearity measured for a given strain amplitude was found very dependant on the number of cycles of solicitation applied to the specimen (Ba_kowski et al., 2009, Mangiafico et al., 2016; Williams et al., 2023).

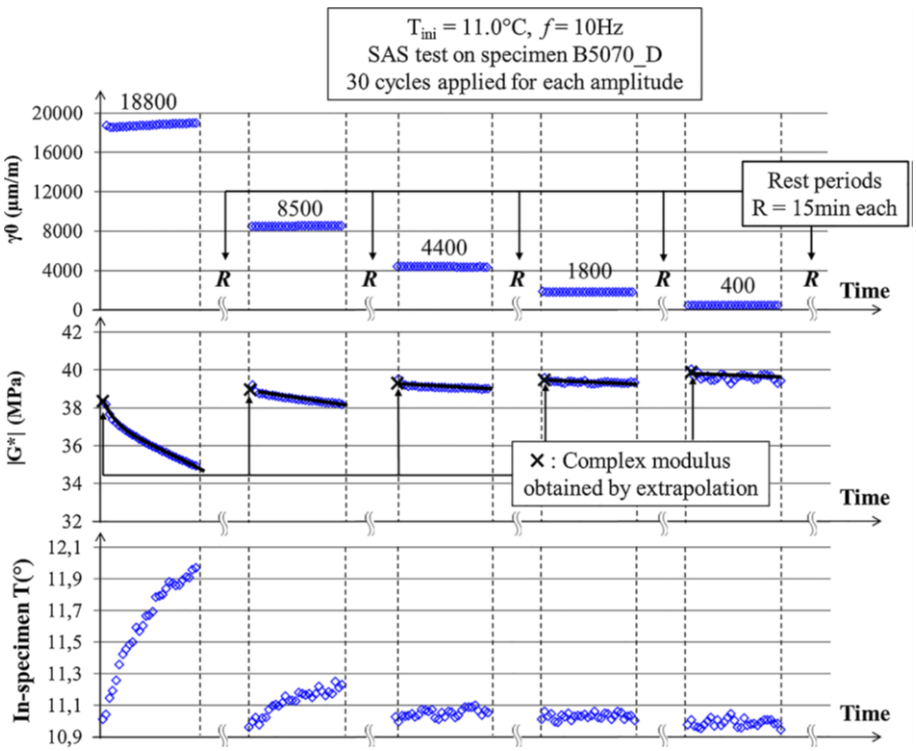

Figure 2.34. Typical SAS test results on a 50/70 pure bitumen showing the effect of non-linearity (Babadopulos et al. 2019)

2.6.2. Self-Heating

Self-heating is considered a consequence of the dissipative viscoelastic behavior of the material, which is thermo-sensitive. The material dissipates mechanical energy in its volume when loaded. That dissipated energy turns into heat and produces a temperature increase in the material. As a consequence, stiffness decreases. If the material is allowed to cool back to the original temperature, the original stiffness is recovered (Babadopulos et al., 2019; Di Benedetto et al., 2004, 2011). Figure 2.35 shows partial fatigue test (PFT) where self-heating is observed as the consequence of viscous energy dissipation during cyclic loading (Mangiafico et al., 2015). The influence of self-heating on test results is believed to be not negligible and should be a consideration in complex modulus variation analyses. This is because in most works on binders, self-heating is usually neglected with an average temperature adopted as the sample temperature which does not represent the temperature field in the material (Di Benedetto et al., 2011; Riahi et al., 2017). In a research carried out by Riahi et al (2017), it affirmed that sample temperature increased by up to 10°C due to self-heating, which causes a complex modulus to lose nearly half of its initial value. However, this decrease was completely recovered during the rest period. Several researchers have reiterated the presence of self-heating in bituminous materials when subjected to repeated loading with sufficiently long rest periods been maintained (Bonnaure, Huibers, & Boonders, 1982; Deacon & Monismith, 1967; Raithby & Sterling, 1970; Hsu & Tseng, 1996; Smith & Hesp, 2000).

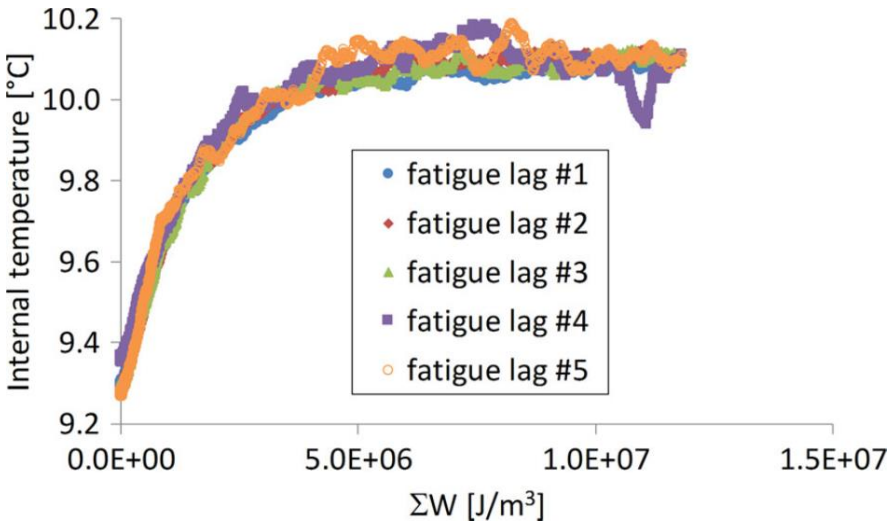

Figure 2.35. Typical PFT results for mix 35/50 B + 20% RAP showing the effect of self-heating during fatigue lags (Mangiafico et al., 2015).

2.6.3. Thixotropy

Thixotropy is thought to be a phenomenon that happens in some fluids, like colloids (of which bitumen is an example), and shows a gradual decrease in viscosity (or stiffness) under continuous loading. This fluctuation continues until the viscosity (or stiffness) reaches equilibrium. When loading is stopped (rest period applied to the material) the original viscosity (or stiffness) is recovered after some time, i.e. the phenomenon is reversible. The thixotropic stiffness decrease process is called breakdown, while the thixotropic stiffness recovery is called build-up of microstructure (Mouillet et al., 2012; Mazzoni et al., 2016; Babadopulos et al., 2019; Larson & Wei, 2019). It has been recognized as a very complex phenomenon, to such an extent that researchers have been unable to agree on a consensus definition (Barnes, 1997; Mewis & Wagner, 2009). Methods for characterizing thixotropy for fluids are relatively well known but the situation is thought to be more difficult for viscoelastic materials. For bituminous binders, it is believed to correspond to a decrease of material stiffness under cyclic loading by modification of its internal structure and to a recovery of this stiffness after rest (Mouillet et al., 2012). The loading amplitude determines how big the breakdown gets. Thus, the change in the steady state of the material reaction with time as a function of the loading amplitude is referred to as thixotropy. The determining experiment for thixotropy is a step-down in shear rate as shown in Figure 2.36 and 2.37. However, Figure 2.37 shows thixotropic material response to shear rate step tests. As observed, the transient shear stress is tracked after a sudden reduction in shear rate from $\dot{\gamma}$ to $\dot{\gamma}_e$ (Figure 2.37a). Normal viscoelastic fluids, irrespective of being in the linear or nonlinear region, would react to such shear history by a monotonic decrease of the stress to a new plateau value (Figure 2.37b). During the stress relaxation the microstructure should recover to its new steady state level. In contrast, under similar conditions the shear stress in an inelastic thixotropic material would drop instantaneously to a lower value, subsequently to increase gradually to its new steady state (Figure 2.37c). The most general response would be a combination of the two types, i.e. an instantaneous drop in stress followed by a relatively fast relaxation and finally a slow, gradual increase in viscosity (Figure 2.37d).

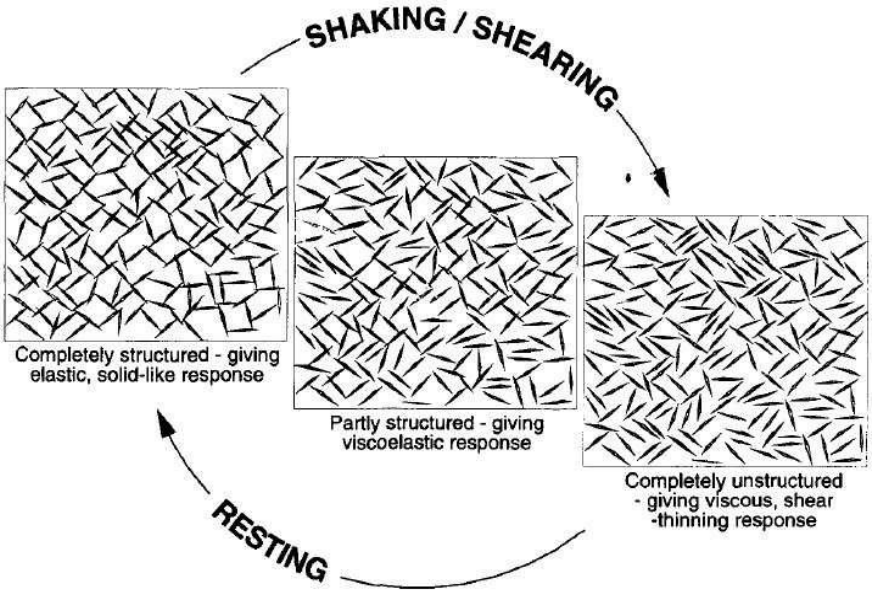

Figure 2.36. Diagram showing how a thixotropic substance breaks down and builds up (Barnes 1997).

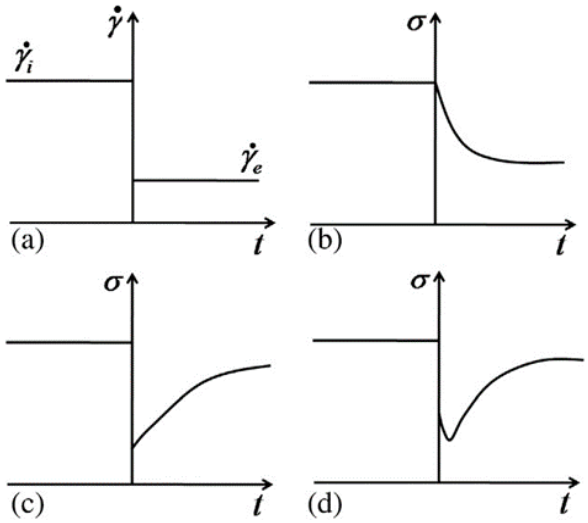

Figure 2.37. Various types of response to a sudden reduction in shear rate (a): b) viscoelastic; c) inelastic thixotropic; d) most general (Mewis & Wagner, 2009).

2.6.4. General framework for the separation and quantification of reversible phenomena during load and rest periods

At ENTPE/University of Lyon, a general framework for separating and quantifying experimental results from cyclic loading and fatigue tests has been developed (Nguyen, 2011; Di Benedetto et al., 2011; Mangiafico, 2014; Williams et al., 2023). The framework considers the several reversible phenomena that causes complex modulus variations during fatigue test, such as nonlinearity, self-heating, thixotropy and damage. This approach was first proposed by Nguyen (Nguyen, 2011; Di Benedetto et al., 2011) and then other researchers continued to develop it (Mangiafico, 2014; Babadopulos et al., 2019; Williams et al., 2023). These experiments started with the application of 10,000 cycles (1000 seconds) at varying strains and rest period of 6 hours in between. The variations in the observed phase angle and the measured norm of complex modulus ($E(\varepsilon_0,T,N)$ as a function of temperature, number of cycles, and strain amplitude) can be attributed to the following reversible phenomena:

- Nonlinearity: The instantaneous and reversible change in complex modulus resulting from nonlinearity is referred to as $\Delta E_{Nonlinearity}$. It is calculated as:
  $\Delta E_{Nonlinearity} = E(\varepsilon_{01},T_0,1) - E(0,T_0,1)$.

- Self-heating: The temperature-induced change in complex modulus is reversible. Here, $\Delta E_{Heating}$ denotes the change in the complex modulus norm (at a specific cycle N) brought on by self-heating.
  $\Delta E_{Heating} = E(\varepsilon_{01},T,N) - E(\varepsilon_{01},T_0,N)$.

- Thixotropy: When the material microstructure is reorganising during loading and rest, this phenomenon's impact on the complex modulus is seen. Here, $\Delta E_{Thixotropy}$ is the complex modulus norm variation caused by thixotropy.
  $\Delta E_{Thixotropy} = E(\varepsilon_{01},T,N) - E_{rev}(\varepsilon_{01},T,N)$.
  Where $E_{rev}(\varepsilon_{01},T,N)$ is the recovered variation after rest.

- Damage: This is the irreversible part of the phenomenon. It is regarded as the real fatigue damage. Here, $\Delta E_{Fatigue}$ notes the change in the complex modulus norm caused by damage.
  $\Delta E_{Fatigue} = E_{rev}(\varepsilon 01,T,N) - E(\varepsilon_{01},T,1)$.

- Since both thixotropy and fatigue alter stiffness as loading cycles are repeated, they are together referred to as cyclic effects. Here, $\Delta E_{\text{cyclic effect}}$ is the complex modulus norm variation caused by cyclic effect.

  $\Delta E_{\text{Cyclic Effects}} = \Delta E_{\text{Fatigue}} + \Delta E_{\text{Thixotropy}}$

Phase angle evolution can be examined using the same framework.

$$\varphi(\varepsilon_0, T, N) = \varphi(\varepsilon_0, T, 1) + \Delta\varphi_{nonlinearity} + \Delta\varphi_{heating} + \Delta\varphi_{thixotropy} + \Delta\varphi_{fatigue}$$

From the work of Nguyen, the changes in complex modulus estimated during fatigue loading and during rest is presented schematically in Figure 2.38.

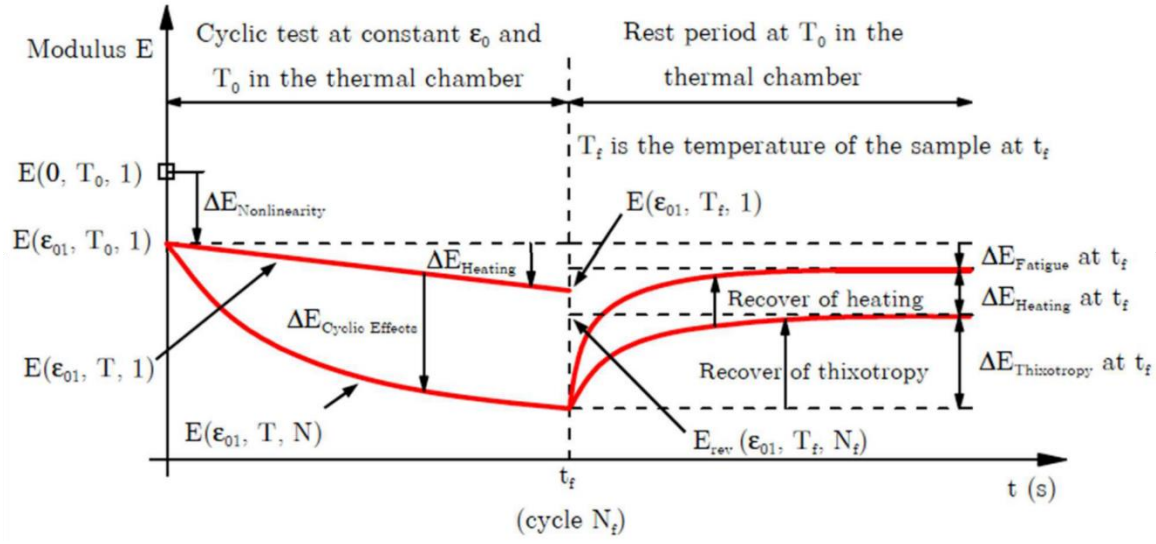

Figure 2.38. Scheme illustrating the contributions made by the various reversible phenomena to the complex modulus norm that was measured throughout the loading and rest test (Nguyen, 2011).

Using the same framework, Figure 2.39 displays experimental data for norm of complex modulus and phase angle from loading and rest period tests by Mangiafico, 2014. As an improvement, these experiments were conducted by applying 100,000 cycles at 100μm/m and rest period for 24 hours in between. From the results obtained from Nguyen (2011) and Mangiafico (2014), It can be seen that damage is linked to unrecovered variations in the complex modulus, which is thought to be the phenomena that is associated with damage. This

implies that majority of the occurrence during fatigue test is associated to reversible phenomena. This validates the need to ensure these phenomena are included during fatigue analysis of bituminous mixes due to the minor relative value of unrecovered variation< in relation to the total modulus variation during loading and rest tests.

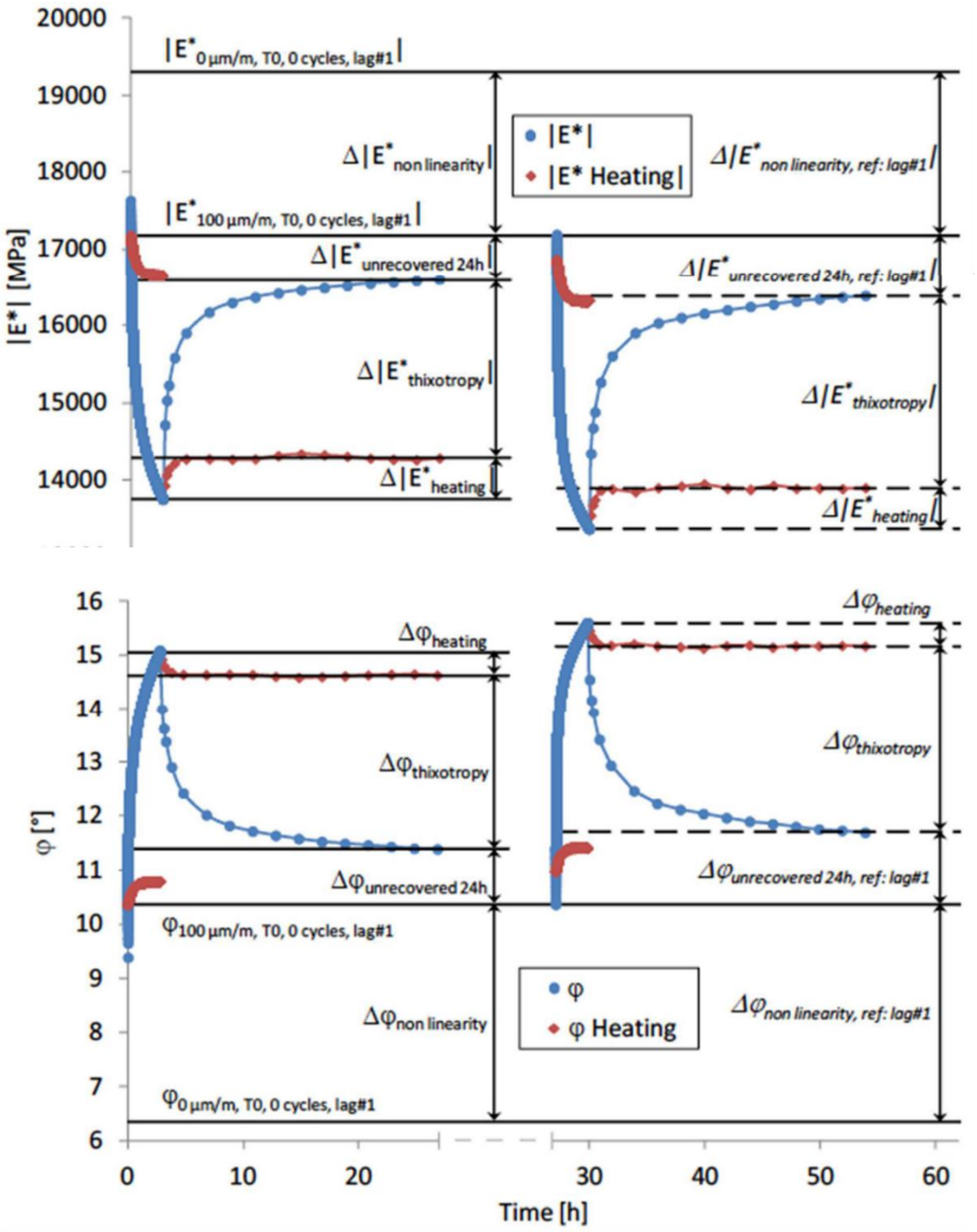

Figure 2.39. Scheme illustrating the contributions made by the various reversible phenomena to norm of complex modulus and phase angle measured throughout the loading and rest test (Mangiafico, 2014).

While this framework is a useful tool for the determination and quantification of the various reversible phenomena, the following is considered in the PhD study in order to improve on the framework and to better assess the restoration of material properties, these are;

- Considering longer rest periods, in the last, 24 hours is the maximum that has been carried out so far.
- Evaluating the 3D properties (complex Poisson's ratio) could prove interesting since it has never been considered.
- Evaluating the repeatability of the framework by carrying out and comparing the results with several repetitions on different samples and different bituminous mixture.

2.7. Self-Healing

It is commonly attributed to bituminous materials undergoing repeatedly loaded and eventual rest for an adequate amount of time, thereby recovering their LVE properties. (Inozemtcev & Korolev, 2020; Hung et al., 2018; Sun et al., 2018; Ayar et al., 2016 ; Zhong & Post, 2015; Agzenai et al., 2015; Bhasin et al., 2008 ; Kim et al., 2003). It is common to refer to this occurrence as "self-healing" (Phillips, 1999; Pronk, 1997). Self-healing materials have been developed since the 1990s and are currently used in various applications (Ayar et al., 2016). The self-healing capability of bituminous materials has been known for many years with several researches utilizing rest intervals in laboratory fatigue tests to investigate the self-healing phenomena. Three strategies have been used to maintain rest intervals throughout a fatigue test namely; intermittent cyclic loading, discontinuous loading and the field-based loading test (Qiu et al., 2012). However, numerous studies have focused the assessment of mechanical property recovery during rest periods and its influence on fatigue life, since fatigue damage is often measured in terms of material properties deterioration.

However, it has been noted that self-healing refers to the true recovery of LVE qualities following the occurrence of actual damage, like material breakage. Therefore, materials that did not experience crack are not covered by the idea of self-healing. In this instance, a number of transitory events might be responsible for the observed recovery of LVE features during rest periods. In an effort to clarify some of the concepts related to self-healing, RILEM "Réunion Internationale des Laboratoires et Experts des Matériaux, systèmes de construction et ouvrages" Technical Committee on Crack-Healing of Asphalt Pavement Materials (TC 278-CHA) in collaboration with Leegwater et al. (2020) recently proposed a scheme as shown in Figure 2.40

and some definitions in order to provide vocabulary for the analysis of this complex phenomenon in particular,

- Recovery: This is the component of restoration that can be attributed to changes in response resulting from cyclic loading, more specifically heating and thixotropy.
- Restoration: This is intended as the total observed change in mechanical properties after a period of rest.
- Self-healing: This is regarded as the component of the restoration that can be attributed to the closure and repair of (micro) cracks;
- Damage: This is regarded as the loss of original mechanical properties due to the initiation, coalescence and propagation of micro-cracks within the material.

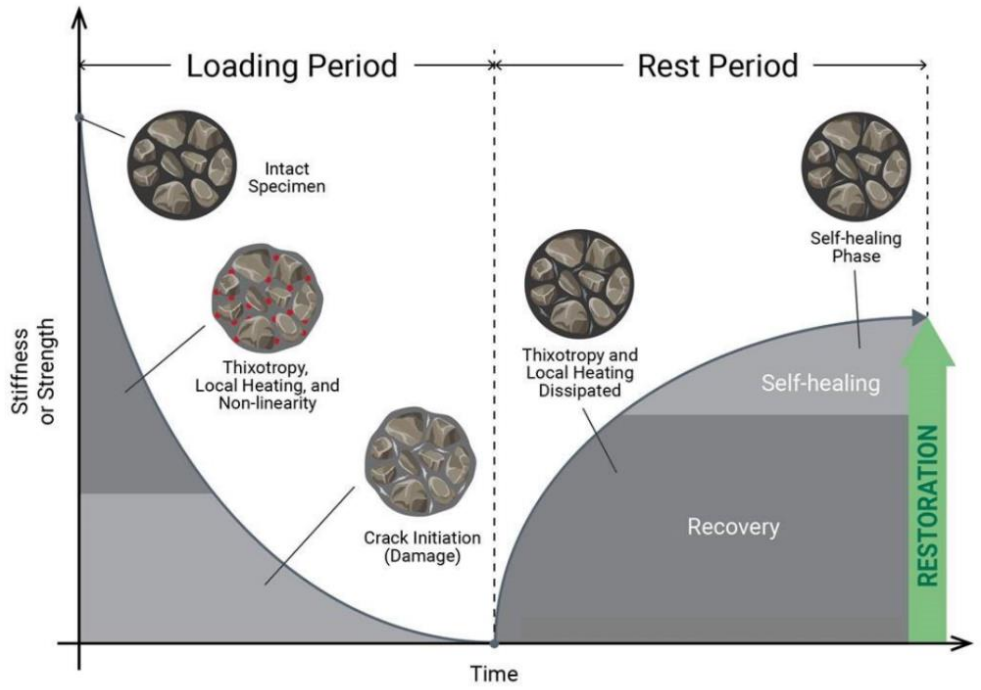

Figure 2.40. Schematic overview of contributions to the restoration of performance of different Phenomena (Leegwater et al., 2020).

Consequently, Sun et al. (2018) reiterates that self-healing is totally different from the viscoelastic responses including the non-linearity, self-heating, thixotropy and steric hardening although they present similar mechanical recovery during unloading. A number of outstanding studies have been conducted to quantify the impact of thixotropy, plastic deformation, steric hardening, and non-linearity on the ability to heal. To differentiate these occurrences and measure their contributions to recovering characteristics, more research is still desperately

needed. In the future, the impact of important test parameters including test temperature, strain, and frequency will also be assessed.

2.7.1. Self-Healing mechanism and models of bituminous materials

The process of self-healing is incredibly intricate and complex. As a result, numerous researches stressed the significance of understanding the bituminous-level healing mechanism using a variety of physicochemical techniques. Four different potential self-healing mechanisms are presented in this section, along with matching models of asphalt materials.

2.7.1.1. Molecular diffusion healing mechanisms

This was Inspired by self-healing polymeric systems that explain recovery behaviour based on polymer chain dynamics (Wool & O'connor, 1981; Kim et al., 2003). Based on the molecular interdiffusion principle, it separates the healing process of fracture in bituminous materials into five major stages as shown in Figure 2.41 and demonstrates how the process varies with time and temperature (Bhasin et al., 2008).

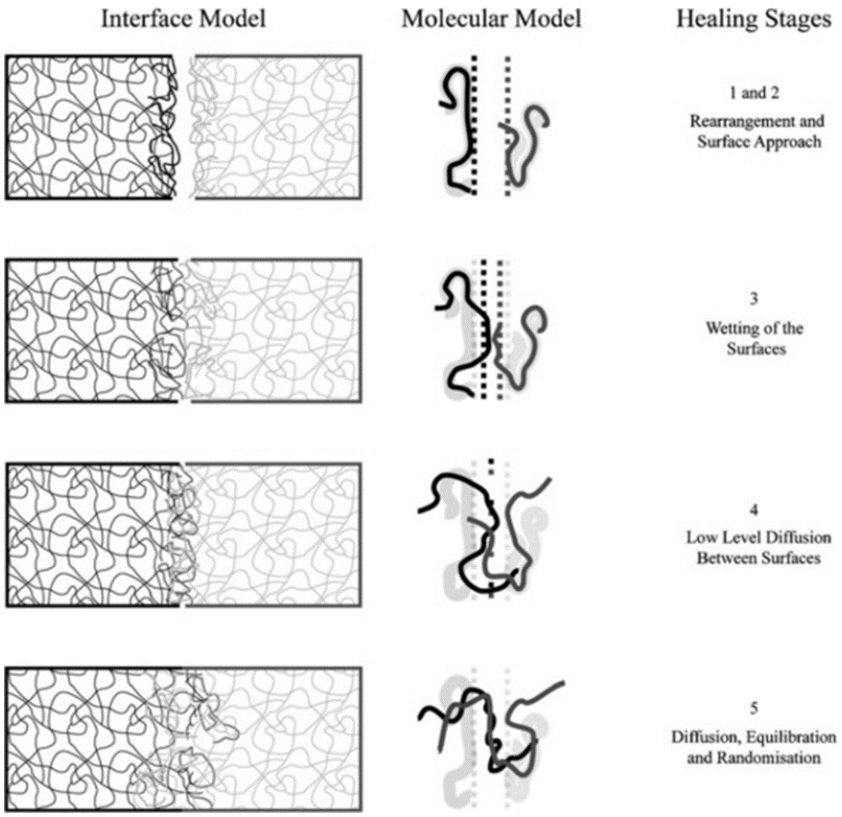

Figure 2.41. Inter-diffusion mechanisms for self-healing

2.7.1.2. Surface energy healing

Schapery and Lytton introduced the surface energy healing hypothesis for bituminous materials, which links the surface energies of the material with healing efficiency (Schapery, 1989; Lytton et al., 1993; Little et al., 2001). Based on this relationship, a healing rate function was constructed. Due to the wide space between the faces, molecular interdiffusion may not happen in a recently formed open fracture in bituminous. Despite this, self-healing is capable of happening when there is enough rest and energy where apparent fissures will eventually disappear (Sun et al., 2018).

2.7.1.3. Capillary flow healing theory

By modifying the Lucas-Washburn equation, a capillary flow-based healing theory can characterise the mesocrack healing or even macrocrack healing efficiency because the aforementioned theories are unable to describe the healing of open fractures in asphalt pavement (Garcia et al., 2015).

2.7.1.4. Phase field healing Model

Utilising phase field theory, Kringos and Skarpas (2011) created a different model and suggested that bitumen is multiphase, which would serve as the foundation for the healing model through studies utilising an atomic force microscope (AFM). It illustrates how a phase transition causes a fracture to emerge and fade.

However, even with these models, there are still certain restrictions. For example, in the thermal cycling experiment, it is challenging to determine the precise physical characteristics of the separated phases (Sun et al., 2018).

2.7.2. Self-healing bituminous mixture enhancement technology

These abilities are based on using various self-healing techniques or additives to modify the self-healing properties of bituminous materials. These techniques are meant increase the longevity and sustainability of asphalt pavement. They are novel self-healing technologies as shown in Figure 2.42.

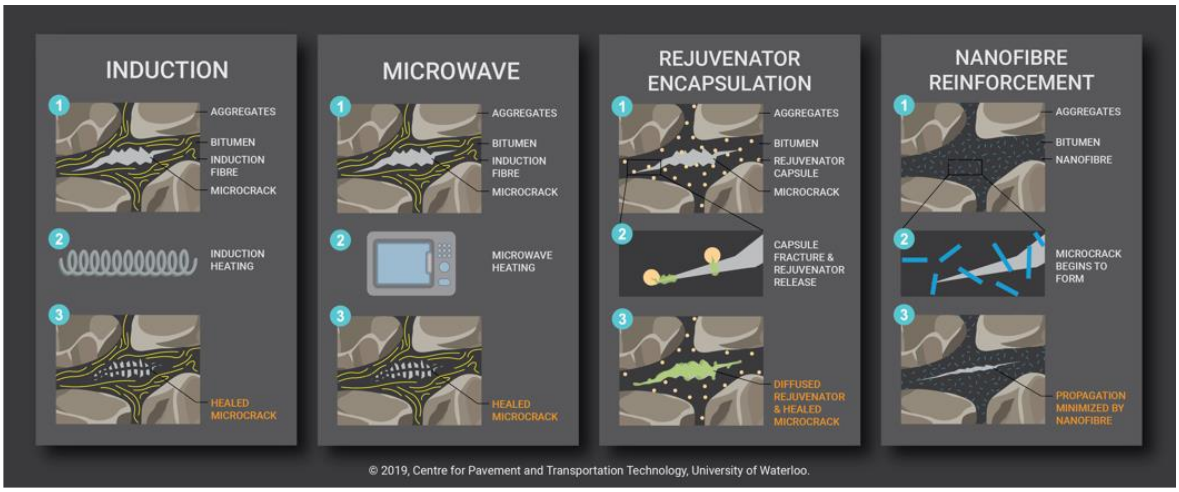

Figure 2.42. Different approaches to enhance self-healing performance to bituminous materials (Leegwater et al., 2020).

- **Induction heating:** This method involves incorporating electrically conductive fibres into bitumen and utilizing an alternating magnetic field generator near the road surface to inductively heat the conductive particles, which then heat the bitumen around them. The resistance of the fibres to induced eddy currents, which are concentrated near the surface of the fibres, generates heat. Cracks in asphalt mixtures can be totally closed and the lifetime of asphalt specimens damaged by cyclic loading can be extended by at least 30% when heating is at its peak (Tabaković & Schlangen, 2016; Liu et al., 2010).

- **Microwave radiation heating:** Bituminous materials are subjected to alternating electromagnetic fields of the order of Megahertz in this process. The water and bitumen in the asphalt mixture are affected by microwave heating. As a result of the alternating magnetic field, the polar molecules shift their orientation, resulting in internal friction and an increase in the temperature of the material. Although it has not been thoroughly investigated, recent research has demonstrated that this approach has the ability to cure asphalt mixtures and polymeric composite materials (Tabaković et al., 2019; Wang et al., 2022).

- **Rejuvenator encapsulation:** Capsule rejuvenators, such as capsules containing non-volatile bitumen solvents with excellent heat stability, such as sunflower oil, are applied on asphalt pavements When the road reaches a particular degree of deterioration, fissures allow water to infiltrate the asphalt, allowing water to access the microcapsules and destroying their shell. Solvents are released from the capsules, which disperse

through the bitumen and lower viscosity locally. Unlike induction heating, encapsulated rejuvenators have the advantage of not requiring an external stimulation to speed up self-healing. At room temperature, capsules can withstand mixing and compaction and speed up the natural self-healing mechanism of asphaltic materials (Garcia et al., 2015; Xu et al., 2021; Zain et al., 2022).

- **Nanofibre reinforcement:** In the last two decades, self-healing nanofibres have gained a lot of attention due to their novel uses, new synthetic techniques, and understanding of nanoscale mechanisms, as well as the discovery of nanomaterials. Large surface area, rich functional groups, and unique features are provided by nanomaterials and nanostructures in polymers, which aid in the healing process (Yoo et al., 2018; Zhai et al., 2020; Xia et al., 2021).

These variety of newly produced revolutionary self-healing enhanced system materials fall into two categories: liquid-based and solid-based self-healing systems (Qiu, 2012). Even though these potential self-healing enhanced systems provide prospecting inspirations for the self-healing enhancement of bituminous materials, at the very least, they must still be well compatible with bitumen and not compromise any of its other qualities.

2.7.3. Characterisation of self-healing

Currently, there is no European standard, but only few laboratory test procedures are used in a few laboratories around the world. Hence, researchers have developed different methods to characterize the healing capability of bituminous materials (Ayar et al., 2016; Mangiafico et al., 2016; Zeiada et al., 2014).

2.7.3.1. Characterisation of self-healing of binders

- **Ductility test:** In this bitumen test as carried out by Qiu et al. (2012), the specimen is cut in the centre (two halves) using a sharp knife, the two parts are put on a glass and left to heal. A small force was applied for 10 seconds to retain the samples in full contact. The samples are allowed to heal for a period of 4 hours at a temperature of about 20 to 22°C before being re-tested for healing as a ratio of self-healed sample length at break

to reference sample length at break. Standard bitumen was found to have recovered to 70% of its previous ductility. The amount of modified bitumen recovered ranged from 15% to 90%.

- **DSR test:** Researcher have successfully evaluated healing mechanism are also possible with the use of a dynamic shear rheometer. Fatigue tests with rest periods have been used in several investigations to characterize healing of binder. The binder's recovery during the rest interval is often measured using a pre-determined healing parameter. There are some differences in the test protocol/test conditions and modeling/analysis procedures used for healing assessment among these test methods. One of the most extensively utilized fatigue test methods for determining bitumen healing is the time sweep test. Healing is enabled in this test by interrupting the loading with one or more rest periods. The extent of healing is measured by the lengthening of fatigue life and the recovery of modulus (Santagata et al., 2013; Shan et al., 2011; Bhasin et al., 2008).

- **Binder Bond Strength (BBS) test:** The BBS test is used to assess the bonding healing behaviour between the bituminous binder interfaces. Multiple fracture-healing cycles for the samples are employed to analyze the healing, and the amount of healing is assessed using the recovered bond strength. It was revealed that bond strength recovery ranged from 10% to 100% and was dependent on healing time and temperature (Huang et al., 2016; Shen et al., 2016; Li et al., 2019; Lv et al., 2020; Zhou et al., 2020).

2.7.3.2. Characterisation of self-healing of mixtures

- **Beam test:** To assess the ability of bituminous mixtures to heal, several studies have applied this loading condition using the two-point, three-point and four-point beam bending tests (Qiu, 2012; Shen and Carpenter, 2007). In these fatigue-based tests, every loading cycle with an intermittent loading condition is followed by a long rest interval (Shen and Carpenter, 2007; Zeiada, 2012). Since there is a rest between load applications of the subsequent axles of passing cars in real-life scenarios, an intermittent loading condition (used in Two-Point Bending, Three-Point Bending Test, Four-Point Bending tests) seems to offer a more realistic test. However, majority of fatigue-healing studies are used to evaluate healing in four-point bending tests (Dave & Koktan, 2011).

Based on several positive outcomes, these tests have continued to be used for the evaluation of healing capability in bituminous mixtures (Qiu, 2012).

- **Tension-Compression test:** A hydraulic press that has a load cell to measure axial stress is used to perform tension/compression tests. One can conduct axial stress-controlled or axial strain-controlled tests using the electronic control system. Usually, a cylindrical specimen is used, with a height ranging from 120 to 160 mm, and a diameter from 75 to 80 mm (Gudmarsson et al., 2014; Sauzeat & Di Benedetto, 2015). Uniaxial Tension/Compression (T/C) testing improves on fatigue characterization of asphalt mixes and offers more homogeneous stress conditions than beam testing (Boussabnia et al., 2020). Researchers have used the T/C test to analyze the structural behaviour of pavements and its evolution with time and to investigate the thermomechanical properties of bituminous mixture which are either complex modulus test or fatigue tests (Di Benedetto et al., 2011; Tapsoba et al., 2014; Sauzeat & Di Benedetto, 2015; Mangiafico et al., 2016). The T/C have also been recently used to evaluate the healing of damage by several researchers where samples were tested by applied intermittent loading with rest periods (Cordier et al., 2008; Williams et al., 2001; Mangiafico et al., 2015).

- **Indirect Tensile test:** Another type of test used to assess fatigue and healing in bituminous mixtures is the indirect tensile test (Qiu, 2012; Shen and Carpenter, 2007). This is also an interrupted loading (group-rest healing) test which entails a short healing test in which several duration of rest periods is imposed at different damage levels in order to determine a modulus or energy recovery as a function of rest period and damage level (Zeiada, 2012). In this test, some researchers have tried to use a lower load during the rest interval in order to make data collection easier (Shen and Carpenter, 2007). The indirect tensile test could include a long loading period followed by a healing phase in which the applied load level is lowered by 5% (Qiu, 2012).

- **Semi-Circular bond test:** In semi-circular bend test, Fracture-healing-fracture experiments are performed using notched semi-circular specimens of bituminous mixes in this manner (Bhasin et al., 2008; Qiu et al., 2011). Lately, researchers have modified the semi-circular bend test in order to better assess the healing capability of bituminous mixtures (Qiu, 2012). In addition to assessing healing capability of mixtures with an

environmental scanning electron microscope, Kringos et al (2013) also employed a test akin to this one. The findings showed that healing is a phenomenon that is both driven by viscosity and accelerated by heat.

2.7.4. Factors affecting self-Healing capabilities

Some researchers have found that the characteristics of the bitumen play an important role in the healing capability of asphalt pavements (Luo, 2012; Qiu, 2012). The ability of bituminous materials to heal is greatly reliant on a variety of factors. While some of these materials accelerate self-healing, others are thought to reduce the ability of the material to heal (Varma et al., 2021).

2.7.4.1. Intrinsic factors

An inherent characteristic of bitumen is the capability for self-healing. This is primary dependent on the several physically-based properties such as the material constituent, aging and the effect of modifiers (Sun et al., 2018).

- **Effect of Machanical properties:** Material factors like viscosity, grade pentration, volumetric and gradational characteristics, effect of age and effect of modifiers have been identified by various researchers affecting self-healing capabilities of bituminous materials (Hsu & Tseng, 1996; Lee et al., 2000; Abo-Qudais & Suleiman, 2005).

- **Effect of age:** It has been found that aging is a key process that influences how well bituminous materials heal. The ability of the binder to heal specifically diminished with age. It was discovered that aging reduced the capacity for healing, causing cracks to appear (Zhang et al., 2012). According to bituminous binder SARA fractions at various aging conditions, resin and asphaltene fractions increased with enhanced oxidative aging while saturates and aromatics fractions declined.

- **Effect of modifiers:** Applying modifiers have shown to increase the ability of bituminous mixes to heal. When compared to other mixes like gilsonite and styrene butadiene rubber (SBR) polymer, the SBS polymer modified bituminous mixture had the highest healing capability (Lee et al., 2000; Canestrari et al., 2015; Huang & Huang,

2016). A DSR fatigue-based test investigation revealed that polymer modified bitumen had a higher healing rate than neat bitumen (Shen et al., 2010).

2.7.4.2. Extrinsic factors

The following are believed to extrinsically affect the healing capabilities of bituminous materials;

- **Effect of Temperature:** The ability of bituminous materials to heal is conceived to be influenced by changes in the temperature of pavement over the course of its useful life. Infact, it is claimed that healing happens quickly at high enough temperatures thereby extending fatigue life (Bhasin et al., 2009; Shen et al., 2010)

- **Effect of Loading:** Self-healing is a time-dependent process; thus, it is conceived that if the loading or frequency provided to a bituminous material is too high in order for significant cracks to emerge quickly, healing may never take place (Varma et al., 2021). The loading amplitude and frequency are shown to affect the fatigue and healing behavior of asphalt mixtures. In particular, healing is likely to occur when the loading is carried out at low strain levels and vice versa (Khavandi Khiavi & Rasouli, 2018; Xiang et al., 2019; Botella et al., 2020).

- **Effect of Rest period:** During the rest periods, bituminous materials have been reported to regain their qualities. However, reversible phenomena like thixotropy have been discovered to be responsible for this recovery (Hsu & Tseng, 1996; Soltani & Anderson, 2005; Mangiafico et al., 2016; Moreno-Navarro & Rubio-Gamez, 2016).

- **Effect of moisture:** It has been severally demonstrated that moisture has a detrimental impact on the healing of bituminous materials because moisture has a stronger affinity for aggregates than bitumen, potentially impeding the process of healing (Sun, et al., 2018; Varma et al., 2021). Moisture has a detrimental influence on the strength of the connection between the binder and the aggregate because its presence reduces the adhesion of the binder and the aggregate and impairs the healing of adhesive bonds. Moisture conditioning decreases cohesion, raises the activation energy of the binder, and lessens time-dependent and fast healing as a result (Mannan et al., 2017).

CHAPTER 3: EXPERIMENTAL CAMPAIGNS

As earlier noted, the aim of the thesis is to study the fatigue properties and self-healing of bituminous mixes and binders. This section provides a description of the materials examined such as the various composition and sources of the various materials used for the proposed test. It also follows a description of the experimental procedures conducted on bitumen and mixtures in order to describe their fatigue properties and self-healing capabilities. The experimental devices used allow for the behaviour of the various materials to be studied at various loading frequencies and temperatures.

The Study is within the framework of the work of RILEM (The International Union of Laboratories and Experts in Construction Materials, Systems and Structures) Technical Committee (TC) 278-CHA: Crack-Healing of Asphalt Pavement Materials. The RILEM TCs are the heart of the scientific activities of the association (RILEM). They are the main forum where RILEM members meet, discuss and exchange expertise, ideas and knowledge, thereby ensuring scientific knowledge are effectively and efficiently enhanced and promoted. The TC is essentially a group of international experts working together in a particular field in order to assemble and evaluate research data, harmonise testing methods and promote their conclusions by publishing recommendations, technical reports or state-of-the-art reports for test methods or construction practice.

The main focus of this technical committee (278-CHA: Crack-Healing of Asphalt Pavement Materials) is characterization, analysis and modelling of fatigue and healing on bituminous binders and mixtures, with several participating institutions as shown in Tables 3.1 and 3.2. Université Gustave Eiffel (France) provided the required bitumen and bituminous mixtures. The scientific focus of the study is to perform repetitive loading and rest tests on binders and mixtures in order characterize damage and recovery of material properties. To successfully undertake this task, different test protocols and analysis methods were carried out on binders and mixtures, with the main objective to differentiate healing and reversible phenomena. The scope of my PhD thesis is within this RILEM framework and it is divided into two distinct parts (Table 3.3). Firstly, it entails carrying out rheological analysis on binders with data obtained from University of Waterloo (Canada) and Politecnico di Torino (Italy) as shown in Tables 3.1 and 3.3. Secondly, it entails carrying out tension/compression test on several bituminous mixtures. Details about the performed tests and analyses performed within the PhD work are provided in the different sections of this chapter.

Table 3.1. Analyses and modelling of binders by various laboratories.

Institution	Activity
Politecnico di Torino, Italy	ViscoElastic Continuum Damage
Université de Lyon/ENTPE, France	Rheological analysis of G* variation
University of Waterloo, Canada	Fracture Energy Analysis using pure LAS (PLAS)
University of New Hampshire	« Modified VECD »

Table 3.2. Participants and used protocol by each Laboratory for mixtures

Protocol	Description	Laboratory
Tension/ compression	Cyclic loading @ 10°C, Strain-controlled mode with multiple rest periods (48h).	Université de Lyon/ENTPE, France
Torsion	Cyclic loading @ 10°C, stress-controlled mode with short rest period (60 min.).	Université de Limoges, France
Tension/ compression	Cyclic loading @ 10°C, strain-controlled mode with single rest period (8h).	University of Waterloo, Canada
Dynamic High-frequency healing with rest period	Ultrasonic test along indirect tensile test.	University of Waterloo, Canada

Table 3.3. Details of PhD work within the RILEM framework

Binders	Tests on binders	Tests on mixtures
40/60	NO	✓
70/100	✓	✓
PMB	✓	✓
	See table 3.5	**See tables 3.6 and 3.7**

3.1. Campaign on binders performed at Politecnico di torino (Italy) & University of Waterloo (Canada).

This section describes the details of the tested materials for binders used, how the samples were prepared for test, experimental set-ups used in this work: The Dynamic Shear Rheometer (DSR) set-up, used for testing binder and the different protocol used for testing the binders. As earlier reiterated, tests on bitumen were carried out by University of Waterloo in Canada and Politecnico di Torino in Italy.

3.1.1. Tested binders

Three binders were selected to be used in the study (Table 3.4): two neat binders (40/60 penetration grade and 70/100 penetration grade) and an SBS-modified binder. The reason for this choice was to investigate the influence of binder grade and polymer modification.

While all three binders were used to produce the mixtures for the study (Table 3.3), the test campaign on binders was limited to the 70/100 and the modified binder, for time constraint.

Table 3.4. Bitumen semi-empirical properties and classification

Binder type	Neat	Neat	SBS modified
Penetration (10^{-1} mm)	80	49	>60
Softening point (°C)	45.8		35 - 45
Penetration grade	70/100	40/60	

3.1.2. Sample preparation for binders

The binders are firstly heated up to 130 °C (for the 70/100 binder) and 150 °C (for polymer-modified binder) for about 30 minutes which is sufficient to be properly ensure the binders are annealed. Then bar shaped beams of material are formed and left to cool at room temperature for 15 minutes. Afterwards, the bars are stored in a commercial freezer (T = -20 °C) as shown in figure 3.1(a) to limit aging. The required sample is obtained for the test after leaving it for 15 minutes at room temperature. The sample was taken by cutting the beam by means of a heated spatula into a silicon mold as shown in figure 3.1(b). The bitumen is melted for up to 130°C (for neat binder) and 150°C (for polymer-modified binder), and then homogeneously mixed with a thin rod in silicon mold, with figure 3.1(c) showing the already mixed bitumen. The material is left to rest for 10 minutes at room temperature, then for 5 minutes at -5°C covered with aluminum foil. This allows demolding of sample before being set up between the parallel plates of the DSR.

(a).

(b).

(c).

Figure 3.1. Material preparations (a). Material storage in freezer (b). Sample been prepared after been left at room temperature (c). Melted and homogeneously mixed sample.

3.1.3. Equipment and test set-up on binders

For all the tests, the two laboratories (Politecnico and Waterloo) used the different models of DSR. A Physica MCR 301 and MCR 102 from Anton Paar Inc. was used by Politecnico and Waterloo respectively. Generally, the DSR consist an air bearing stress-controlled device which can also operate in strain-controlled mode through a feedback-controlled loop. The DSR is equipped with a permanent magnet synchronous drive (minimum torque = 0.1 μN m, torque resolution <0.1 μN m) and an optical incremental encoder for measurement of angular rotation (resolution <1 μrad). An 8 mm parallel plate configuration was used with a 2 mm gap between the plates. One of the plates is fixed while the other one moves, thus imposing a shear loading to the sample. The rotation angle of the moving plate and the applied torque are continuously measured. All tests performed in this experimental campaign were carried out in strain-control mode.

The test set-up on DSR begins with preheating the system at 45°C (for neat binder) and 50°C (for modified binder) to ensure adequate adhesion of the binder as shown in figure 3.2(a). As shown in figure 3.2(b), the upper plate is lowered to trimming position, with a gap between plates of 2.1 mm. The excess material is scraped off the contour of the sample (trimming operation), the upper plate is finally lowered to 2 mm to form the bulge as stipulated in AASHTO T 315-12. Then, a thermal conditioning time of 30 minutes is allowed at the testing temperature of 20°C.

(a). (b).

Figure 3.2. Testing set-up (a). System preheated for adhesion (b). Trimmed sample at 2.1 mm.

3.1.4. Preliminary frequency sweep test

Frequency sweep tests generally serve the purpose of describing the LVE behavior of binders in their small strain domain. The frequency sweep test is performed at a fixed temperature by applying a sinusoidal shear loading at constant amplitude over a range of loading frequencies. in this study, a frequency sweep test was systematically performed on all samples before carrying out any of the other tests described in the following sections.

For the frequency sweep tests a strain amplitude of 0.1% was applied at 20°C, over a range of frequencies from 0.2–30 Hz (0.2, 0.4, 0.6, 0.8, 1.0, 2.0, 4.0, 6.0, 8.0, 10, 20 and 30 Hz, specifically) with no rest periods between different frequencies.

Norm and phase angle of complex shear modulus (|G*| and σ respectively) were determined for each loading frequency in stationary conditions (data obtained during transient response phases were discarded). Because of the limitations of the DSR software it was not possible to obtain detailed data on the number of cycles for each frequency. Hence, the values obtained from the DSR are average values of a low number of cycles, but the exact number of cycles applied and the number of data points acquired per cycle are not known.

3.1.5. Summary of repeated loading and rest tests on binders

In order to evaluate the responses of the materials under repeated loading and rest, different types of tests were performed, all at 20°C. The base test type chosen to determine the effect of

repeated loading was a continuous Linear Amplitude Sweep (LAS) test. The restoration of material properties during rest was evaluated by interrupting LAS tests with rest periods of different durations (0, 5 and 30 minutes) and restarting them. The different rest period durations were chosen and tried in order to determine the differences between instantaneous and time-dependent recovery variations. These tests are hereafter called LASH (Linear Amplitude Sweep Healing). The value of strain amplitude of the interruption of the test was chosen according to results of the LAS tests, in particular with respect to the strain amplitude corresponding to the peak of the registered stress amplitude. LASH tests were therefore performed with the interruption at this strain amplitude ("peak") or at half of this value ("half-peak"). The application of rest periods at "half-peak" and at "peak" allowed defining both the pre-failure and post-failure healing properties of the binders. Finally, some LAS tests were also performed by adding an additional 30-minutes conditioning period before the actual test, in order to evaluate the effects of steric hardening over this time length, equal to the longest rest period applied for LASH tests. The tests with this additional pre-test rest periods are hereafter referred to as "LAS 30 min. steric".

Table 3.5 summarizes the various tests carried out by the different laboratories, with an indication of the laboratory that performed them (T for Politecnico di Torino, W for University of Waterloo). In fact, tests on the 70/100 binder were performed by both laboratories while tests on the PMB were carried out only by University of Waterloo.

Table 3.5. Details of tests carried out by the different laboratories.

	Loading Interruption	Rest duration	Pre-test and rest periods	Pre-test duration	Binders	
					70/100	PMB
LAS	-	-	0.1% γ_0 cont. oscill.	30 minutes	W & T	W
LASH Peak 0 min.	7.70%	0 minute	0.1% γ_0 cont. oscill.	30 minutes	W & T	W
LASH Peak 5min.	7.70%	5 minutes	0.1% γ_0 cont. oscill.	30 minutes	W & T	W
LASH Peak 30 min.	7.70%	30 minutes	0.1% γ_0 cont. oscill.	30 minutes	W & T	W
LASH Half Peak 0 min.	3.85%	0 minute	0.1% γ_0 cont. oscill.	30 minutes	W & T	W
LASH Half Peak 5 min.	3.85%	5 minutes	0.1% γ_0 cont. oscill.	30 minutes	W & T	W
LASH Half Peak 30 min.	3.85%	30 minutes	0.1% γ_0 cont. oscill.	30 minutes	W & T	W
LASH Peak 5 min. "real rest"	7.70%	5 minutes	0.0001% γ_0 cont. oscill.	30 minutes	W & T	W
LASH Peak 30 min. "real rest"	7.70%	30 minutes	0.0001% γ_0 cont. oscill.	30 minutes	W & T	W
LAS-SH	-	30 minutes	0.1% γ_0 cont. oscill.	60 minutes	W	W

W – University of Waterloo **T – Politecnico di Torino**

3.1.6. Linear amplitude sweep (LAS) test

The standard LAS test is stipulated by AASHTO TP101-12 (2018). As already mentioned, the continuous LAS tests were conducted at the temperature of 20°C and the loading frequency applied was 10 Hz. Before the actual test, a 30-minute conditioning period is maintained, consisting of a 0.1% shear amplitude continuous oscillation, during which data are recorded every about 2 seconds (shear strain and shear stress amplitudes, norm and phase angle of complex shear modulus). The test specifically consisted of an oscillatory strain amplitude sweep in strain-control mode, during which the strain amplitude is increased from 0.1% to 30%. Loading is increased linearly over the course of 3,100 cycles of loading with an average 0.00968%/cycle strain amplitude increase rate. The data provided by the DSR software at the end of the test report one point every 10 load cycles (1 s), with values of shear strain and shear stress amplitudes, norm and phase angle of complex shear modulus, rotation angle and torque. Figure 3.3 shows an example of the shear strain amplitude loading sequence applied during a LAS test, with the pre-test period followed by the linear shear strain amplitude increase.

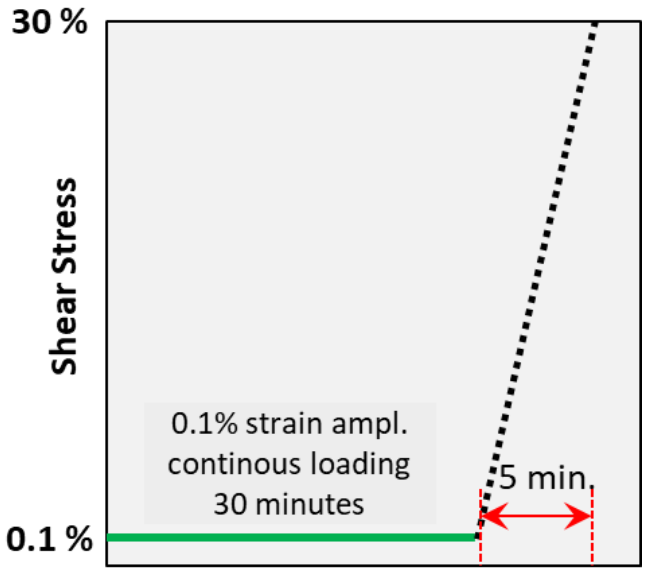

Figure 3.3. Shear strain amplitude loading sequence applied during a LAS test

3.1.7. Linear Amplitude Sweep Healing (LASH) Test

As already explained, LASH tests consisted in LAS tests interrupted by a rest period, after which the loading is reapplied from the initial strain amplitude value. Hereafter, the first loading

sequence (from 0.1% shear strain amplitude to the interruption) is called “first loading”, the second loading sequence following the interruption (from 0.1% to 30% shear strain amplitude) is called “second loading”. From the results of the LAS tests (showed in section 4.1), two different values of strain amplitude were chosen to interrupt the test 7.70% (“peak”) and 3.85% (“half-peak”), corresponding respectively to the peak of the registered stress amplitude during LAS tests and to half of the same value. Three different durations of the rest period were chosen (0, 5 and 30 minutes). All LASH tests were carried out at a frequency of 10 Hz and the temperature of 20°C. As for LAS tests, a 30-minute conditioning period (“pre-test”) was maintained. Both the pre-test and the rest periods (before and during the LASH tests, respectively) consisted of 0.1% shear amplitude continuous oscillations, during which data are recorded every 2s. The LASH test at peak also included having a real rest for 5 minutes and 30 minutes at 0.0001% shear amplitude continuous oscillations. This was carried to make comparisons with the rest periods of 0.1% shear amplitude continuous oscillations. Figure 3.4 shows an example of the shear strain amplitude loading sequence applied during a “LASH Peak 30 min.” test, with the pre-test period followed by the linear shear strain amplitude increase from 0.1% to 7.70% (first loading), a 30-minute rest period and again the shear strain amplitude increase from 0.1% to 30% (second loading).

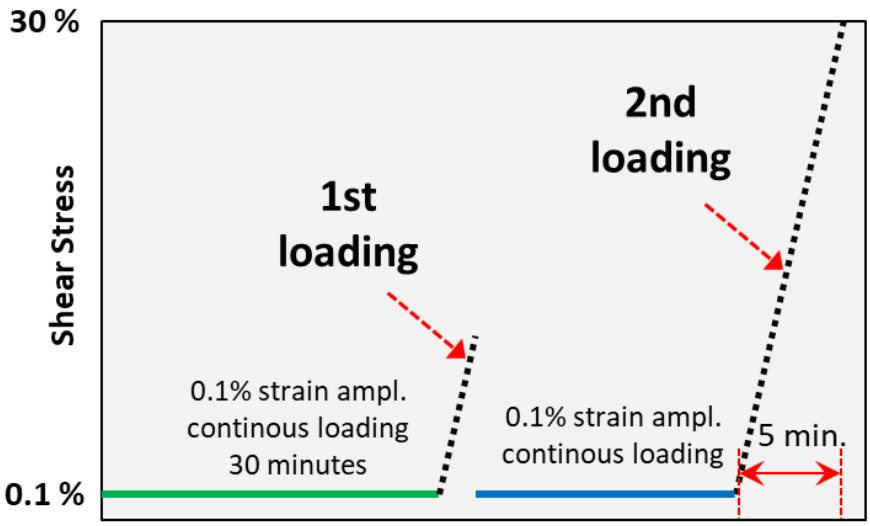

Figure 3. 4. Shear strain amplitude loading sequence applied during a LASH Peak 30 min. test.

3.1.8. Linear Amplitude Sweep - Steric Hardening (LAS-SH) Test

This test consisted in a LAS test with a longer initial pre-test period (0.1 % shear strain amplitude continuous oscillation) of 60 minutes instead of 30 minutes. The rest of the test is identical to the standard LAS test described in section 3.1.5, with a shear strain amplitude sweep during which strain amplitude increases linearly from 0.1 % to 30 %. The whole procedure is carried out at 20°C and at the loading frequency of 10 Hz. Figure 3.5 shows an example of the shear strain amplitude loading sequence applied.

This test procedure was conceived to highlight the effect of steric hardening during the pre-test and to evaluate potential differences in the trends of evolution of material properties during loading.

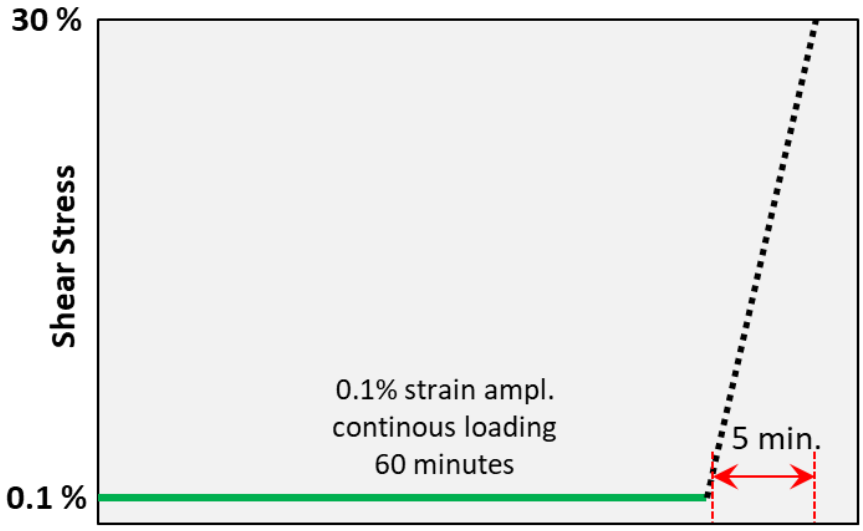

Figure 3.5. Shear strain amplitude loading sequence applied during a LAS-SH test.

3.2. Campaign on mixtures performed at ENTPE

This section describes the details of the tested mixtures, how the samples were prepared for test, experimental set-ups used in this work: The MTS LandMark hydraulic press used for testing mixtures and the protocol used for testing the mixtures.

3.2.1. Tested materials for mixtures

In this campaign, 3 different mixes with three selected binders were used, which are 70/100, 40/60 and SBS PMB. The 70/100 penetration grade and the SBS PMB binders are the same as the one used in the campaign on binders described in Section 3.1. Table 3.7 summarizes penetration and softening point of the three binders as well as the main details of the production of the three corresponding mixtures (binder content, mixing temperature, compacity and density).

The material tested is a Stone Mastic Asphalt (SMA)-type bituminous mixture which meets the requirement specified by European standards (EN 13108-20 and EN 13108-21). The same binder content (6.60% of total mixture mass) and grading curve (shown in Figure 3.6) were used for all mixtures. The maximum specific gravity (MVR) obtained for all the bituminous mixtures was 2.558. Aggregates proportions are listed in Table 3.6.

Table 3.6**.** Bituminous mixture aggregates proportions

Quarry	***Gradation (mm)***	***Mass proportion (%)***	***Specific density***
Noubleau	10/14	17.00	2.89
Noubleau	6/10	35.30	2.87
Noubleau	4/6	14.80	2.91
Noubleau	2/4	6.60	2.86
Noubleau	0/2	18.00	2.86
Airvault	Filler	8.30	2.67

Table 3.7. Binder and mixture composition

Binder	***70/100***	***40/60***	***PmB***
Penetration (10^{-1} mm)	80	49	35 - 45
Softening point (°C)	45.8	53.6	> 60
Mixture	***Mix 70/100***	***Mix 40/60***	***Mix PmB***
Binder content (%)	6.6	6.6	6.6
Temperature of fabrication (°C)	150	160	170
Compacity (mean value) (%)	95	95	94
Maximum specific gravity	2.558	2.558	2.558

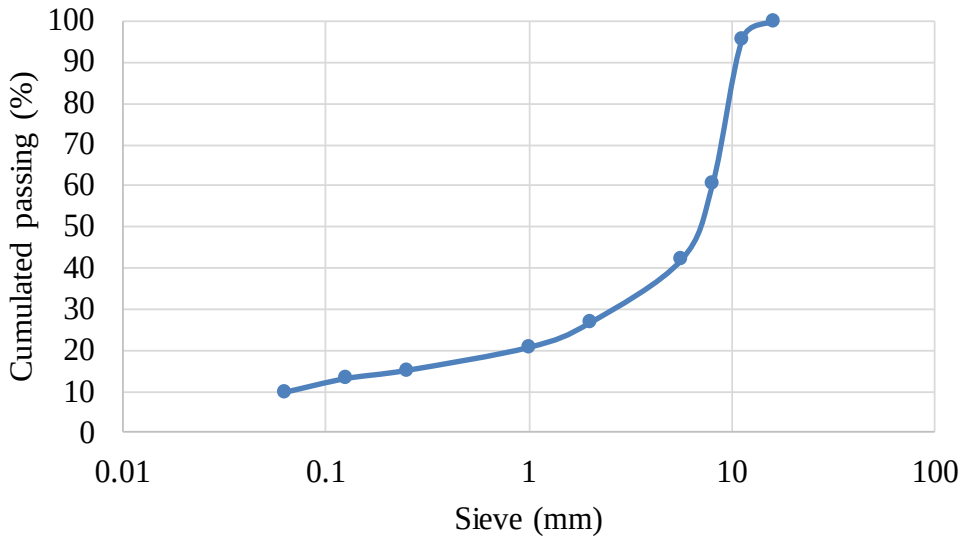

Figure 3.6. Bituminous mixture gradation curve.

3.2.2. Sample preparation

After mixing, the materials were compacted into slabs of 395 mm x 595 mm x 150 mm using a wheel compactor (EN 12697-33+A1, 2007). The same compaction effort and plan was applied to all slabs. The slabs were cut into different parts using a circular saw and cored using a core drill, in order to obtain specimens with the desired geometry (150 mm height and 75 mm diameter cylinders), with a total number of 15 specimens cored from the slabs as shown in

figure 3.7. Mixture production, compaction and sample preparation were performed by the MIT ("Matériaux pour Infrastructures de Transport") laboratory of Université Gustave Eiffel.

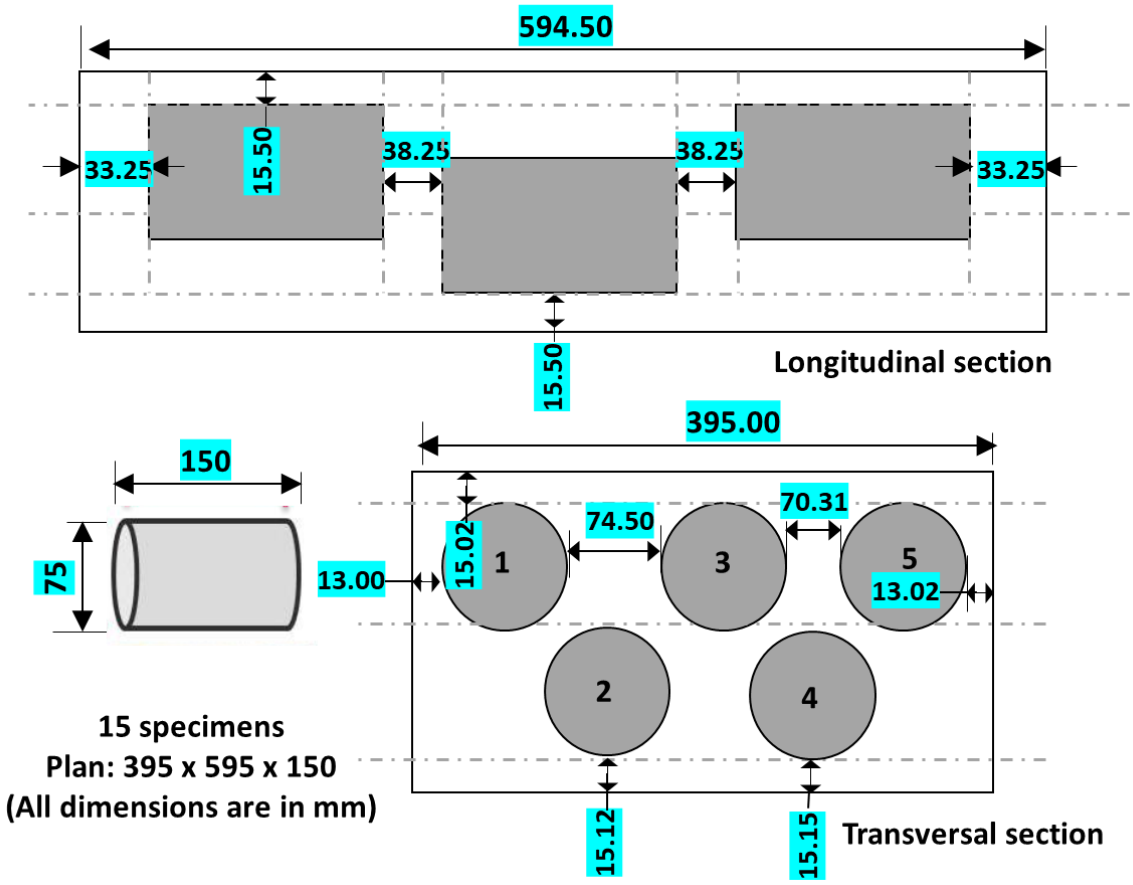

Figure 3.7. Coring scheme for cylindrical specimen.

For this research, 8 samples per mixture were selected for testing, with air void content varying from 3% to 10%. The content of air voids (MVA) for each specimen used in this research was determined as in Equation 3.1. By dividing the specimen weight ($W_{Specimen}$) by the volume of a cylinder of the same dimensions ($V_{Cylinder}$) as the specimen, geometrical MVA is classically obtained.

$$MVA = \frac{W_{Specimen}}{V_{Cylinder}} = \frac{4 \cdot W_{Cylinder}}{\pi \cdot h \cdot D^2} \quad 3.1$$

Table 3.8 presents the air voids contents of the specimens selected for testing for the three mixtures produced, as well as their averages and standard deviations.

Table 3.8. Air voids contents, averages and standard deviations of specimens from for Mix 40/60, Mix 70/100 and Mix PmB.

Specimen slab Mix 40/60	Air voids (%)	Specimen slab Mix 70/100	Air voids (%)	Specimen slab Mix PMB	Air voids (%)
1	10.10	1	2.60	1	3.40
2	9.02	2	2.04	2	3.60
3	7.03	3	1.87	3	3.35
4	8.90	4	1.79	4	3.54
5	8.50	5	7.30	5	6.20
6	6.50	6	7.10	6	6.60
7	5.29	7	7.24	7	7.05
8	2.84	8	6.00	8	6.89
Average	**7.27**		**4.49**		**5.08**
Standard Deviation	**2.22**		**2.46**		**1.62**

3.2.3. Equipment and test set-up on mixtures

The cylindrical samples were glued with a two-component epoxy glue to aluminum caps at the top and bottom ends in order to install them in the hydraulic press used for tests. The caps were cleaned with a tissue soaked in acetone to remove bitumen and grease residues, and then scrubbed with sandpaper to remove any remaining impurities and glue residue from prior uses before being glued. This is followed by gluing the cap on a bench and the second cap was glued directly at the hydraulic press.

An MTS LandMark hydraulic press (as shown in figure 3.8) equipped with a 250 kN capacity load cell was used to carry out the tests. The applied axial stress on the tested material was determined from axial force measured by the load cell of the press. Axial stress was determined from axial load F using the sample's initial diameter D as the input:

$$\sigma = \frac{F}{\pi\left(\frac{D}{2}\right)^2} \qquad 3.2$$

Where, D is the sample's diameter and F is the force as determined by the load cell.
On-specimen axial strain on bituminous mixtures cylinder specimens was measured using three extensometers positioned around the sample at a 120° angle in the central part of the sample (as shown in Figure 3.8). Gauge length used is 75mm. In order to disregard border effects, extensometers were positioned in the middle of the sample. Six springs were used to hold them in place on the sample. The axial strain (ε_{1_i}) measured by each extensometer (i = [1,2,3]) is obtained as:

$$\varepsilon_{1_i} = \frac{\Delta L_i}{L} \qquad 3.3$$

Where, ΔL_i is the displacement measured by each extensometer and L is the measuring span of the extensometer.

Therefore, the average of the three extensometers, ε_1, was retained as value of axial strain and used to control tests:

$$\varepsilon_1 = \frac{\sum_{i=1}^{3} \varepsilon_{1_i}}{3} \qquad 3.4$$

To determine radial strain, two non-contact sensors (Micro-Epsilon eddy current sensors with a range of 0-0.5 mm) were placed on the specimen diameter and used to measure radial displacement. As seen in Figure 3.9, radial strain was measured using two non-contact transducers positioned at the opposite sides of the sample (at 180°). Alternating current circulation in the transducer head coil generates an alternating magnetic field which induces eddy currents in an aluminum target tape glued to the surface of the sample. The aluminum target generates then a resisting magnetic field and the interaction between both fields depends on the distance between the target and the head of the transducer. During cyclic loading, the magnetic field sensed by the electronics in the transducer varies as the sample deforms radially. These variations are then translated into variations of the distance between the sensor head and

the sample. Radial strain (ε_3) was calculated from the two displacement measures (Δl_{3_i} with i = [1,2]) as:

$$\varepsilon_3 = \frac{\Delta_{3\_1} + \Delta_{3\_2}}{D} \qquad 3.5$$

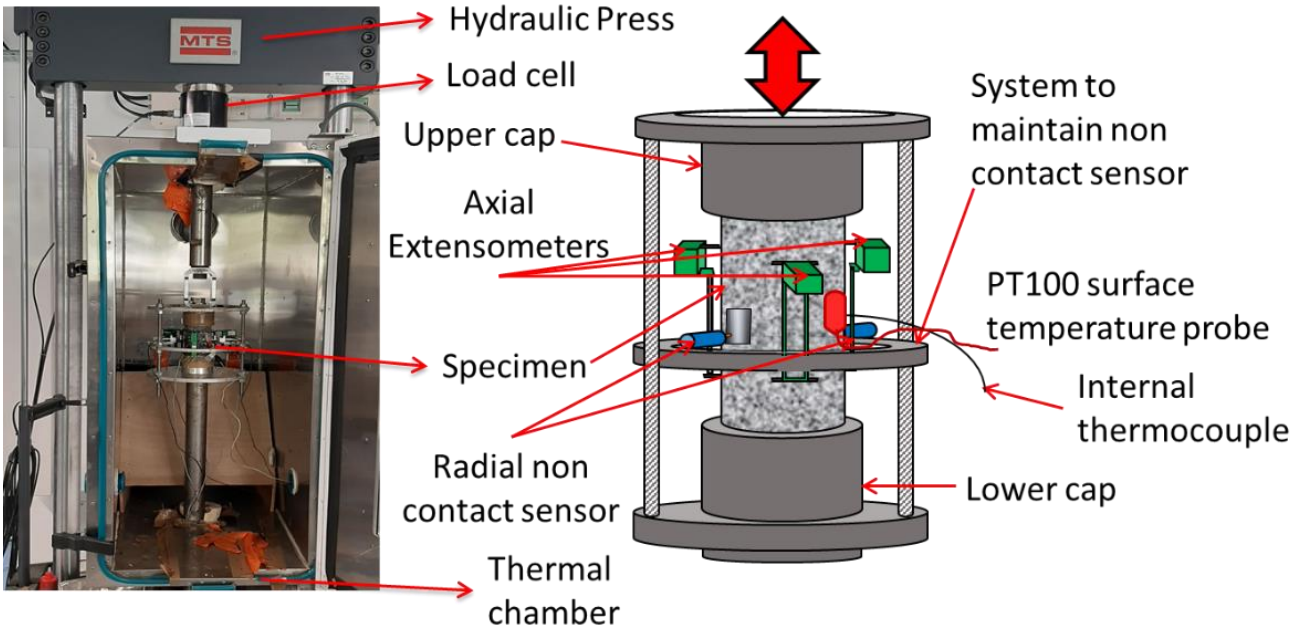

Figure 3.8. Tension-compression test apparatus showing detailed scheme of measurement devices (carried out at ENTPE laboratory, Vaulx-en-Velin, France).

As shown in figure 3.9, a temperature probe was placed on the sample's surface in order to measure the external surface temperature. Internal temperature was also measured using a 1 mm diameter thermocouple inserted inside the sample by a carefully and properly drilled hole (1.7 mm in diameter and 30 mm deep). The hole is then filled with bitumen to ensure the material's continuity (as shown in figure 3.9). With the aid of a thermal chamber, sample conditioning and temperature control was successfully carried out. The imposed temperature in the chamber and the actual internal and external sample temperature readings were found to differ by only roughly 0.4°C and 0.7°C, respectively. For the analysis, the recorded internal temperature was considered.

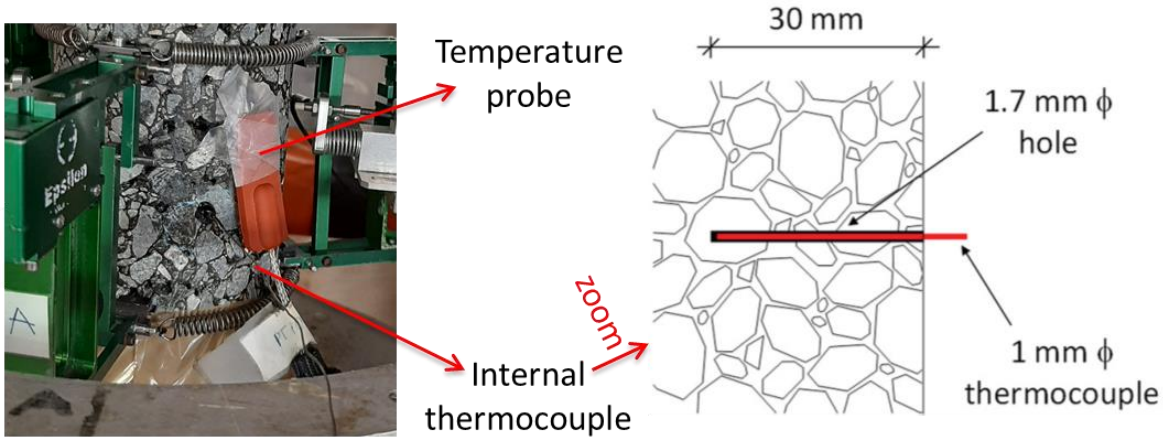

Figure 3.9. Picture showing temperature probe and internal thermocouple with a scheme of internal thermocouple (carried out at ENTPE laboratory, Vaulx-en-Velin, France).

3.3. Test procedures for mixtures

This section describes the test protocol carried out on the mixtures. The test protocol is composed of two parts, respectively complex modulus tests and fatigue and rest periods, carried out consecutively on the same sample.

3.3.1. Complex Modulus test

The objective of the complex modulus test is to monitor the viscoelastic characteristics of the bituminous mixtures in undamaged conditions at temperatures, loading frequencies, and strain levels that are equivalent to (or nearly equal to) those typically used for fatigue tests (10°C, 10 Hz, and 100 m/m, respectively). As illustrated in Figure 3.10, this test protocol comprises performing short Complex Modulus Tests (CMTs) at four different temperatures (8°C, 10°C, 12°C, and 14°C) with variable strain amplitude. Four CMTs are carried out for each temperature with ultimate targeted strain amplitudes of 50, 75, 100, and 110 m/m. Every CMT consists of 200 loading cycles, which are divided into five sequential sequences of 40 loading cycles each, at step-wise increasing strain amplitude. The number of cycles was chosen to in order not to induce significant fatigue due to repeated loading. These tests enable evaluation of the viscoelastic behaviour of the materials' dependence on strain. Following each CMT, there is a 900-second rest interval in which no strain is applied. During each temperature change, a thermal conditioning period of 6 hours is maintained under stress control (no stress is imposed). This is done to ensure that the temperature is uniform in the whole sample.

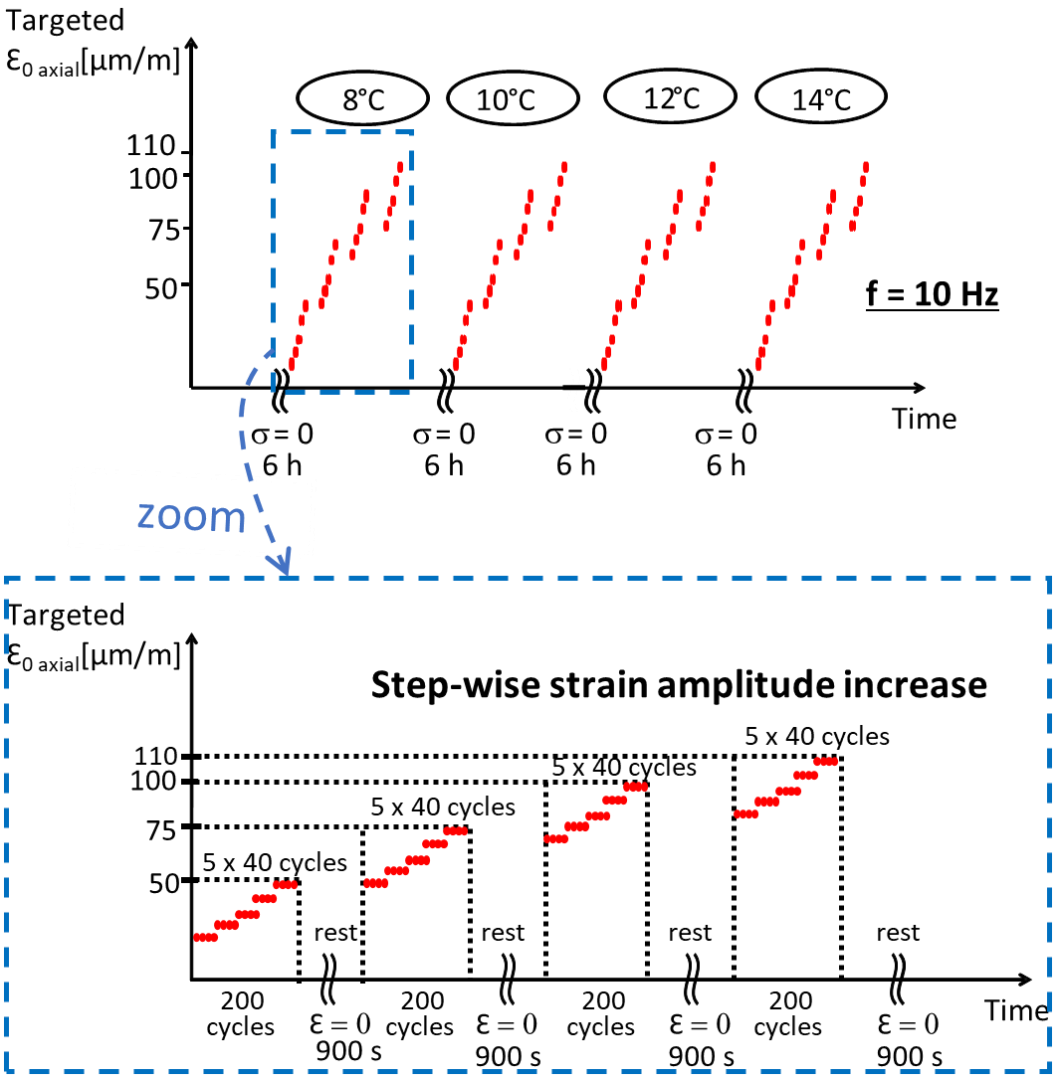

Figure 3. 10. Procedure of the preliminary CMTs test protocol: CMT at varying temperatures and strain amplitudes.

3.3.2. Fatigue and rest test

In the second part of the test protocol as shown in figure 3.11 partial fatigue with rest periods tests (PFRT) are performed. For every material, the same sample used for CMTs is used also for PFRTs. In the protocol, five 100,000 cycle fatigue lags at a frequency of 10 Hz are imposed, followed by a last fatigue lag until failure. The first 48 cycles of each fatigue lag are applied at step-wise increasing strain amplitude of 12 cycles at 65, 80, 85 and 90 μm/m, while the remaining 99,952 cycles are applied with a constant targeted strain amplitude of 100 μm/m. Afte00r each fatigue lag, a 48-hour rest time is maintained (in strain-control, with no strain

imposed). During rest period, 22 short complex modulus tests of 100 cycles each are conducted at 10 Hz at predetermined intervals (after the end respectively, 10, 20 and 30 minutes and 1, 2, 4, 6, 8, 10, 12, 14, 16, 18, 20, 22, 24, 28, 32, 36, 40, 44 and 48 hours of each fatigue lag). Each of these short complex modulus tests consists of five sequences of 20 loading cycles each, with the final strain amplitude of 100 µm/m being the desired value (20 cycles at 65, 80, 85, and 90 µm/m). These short complex modulus tests have the purpose of observing the recovery of the viscoelastic properties during rest. The sample is conditioned at a test temperature of 10°C (under stress control, with no stress imposed) for 6 hours prior to the first fatigue lag. The temperature within the thermal chamber is kept at 10°C during the entire operation. As previously explained, after the fifth period of rest, a final fatigue loading lag is conducted until the sample fails (with the same number of initial cycles of rising strain amplitude as for the previous fatigue lags).

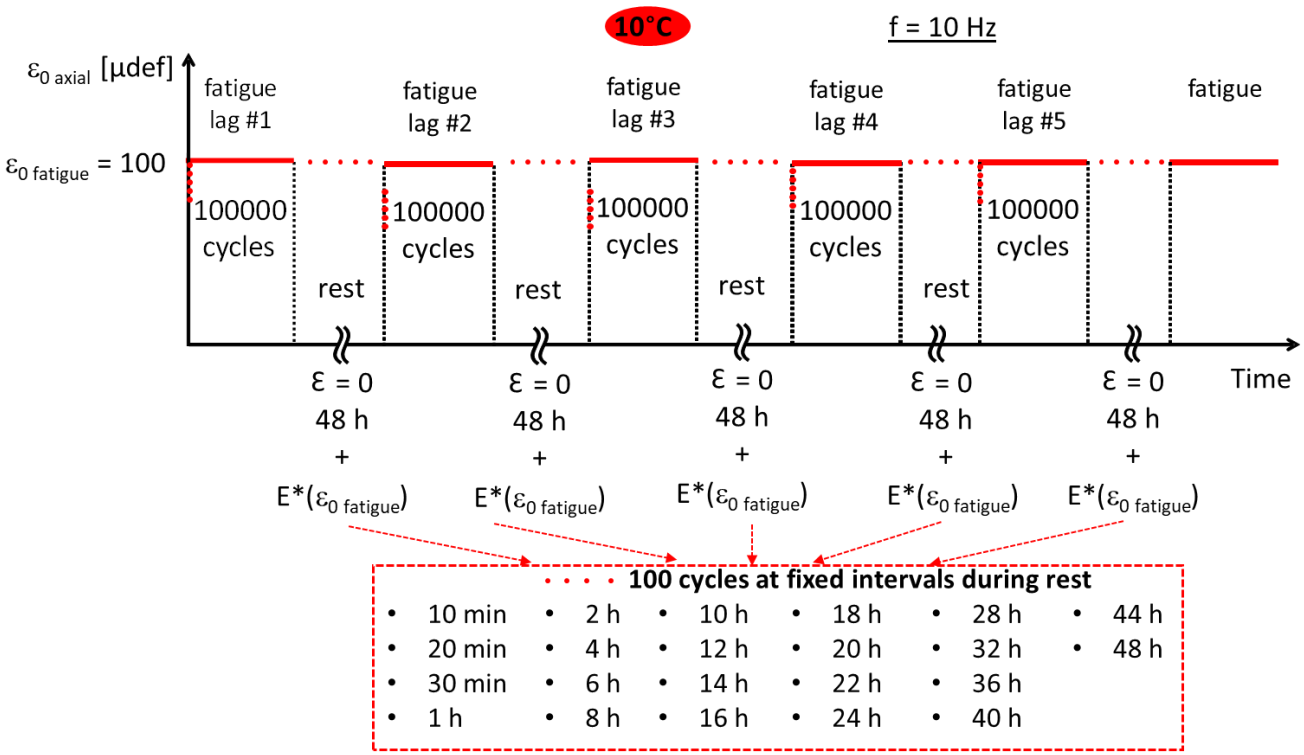

Figure 3.11. Procedure of the second part of the test protocol: Partial Fatigue and Rest Tests (PFRT).

3.3.3. Example of mechanical parameters during tension-compression tests on bituminous mixtures.

Figure 3.12 shows an example of axial stress, axial strain and radial strain signals obtained during a sinusoidal tension-compression test (fatigue test on Mix PmB – 6).

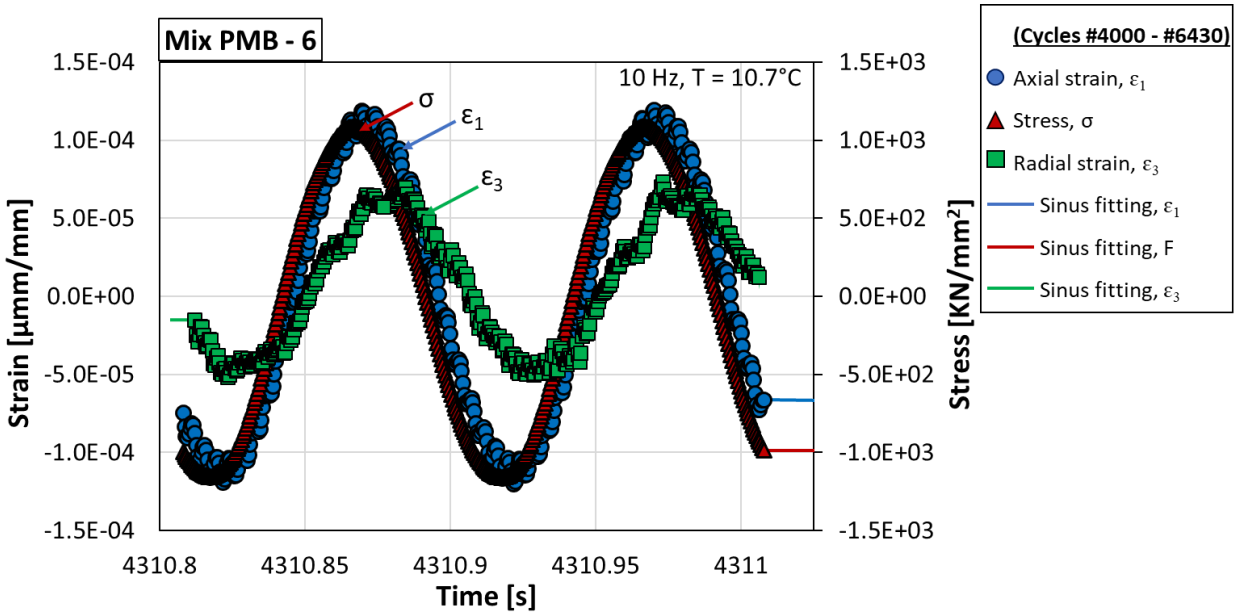

Figure 3.11. Example of sinusoidal signals and fitting (axial stress, axial strain and radial strain) during a T-C test (example from fatigue test on Mix PmB – 6).

The consecutive cycles (100,000 cycles) are combined to treat the data. Complex modulus is rigorously defined only in the scenario of a perfectly linear viscoelastic response (no strain dependency), with stress and strain signals being precisely sinusoidal. Sinusoidal functions for axial stress, axial and radial strains (combined data from cycles i and i+1) are fitted using least squares method for each cycle i. Following that, mechanical propertied are determined as explained in Section 2.4.2.2. The parameters that were tracked during tension-compression testing on the various bituminous mixes are shown in Table 3.8.

Table 3.9. Mechanical Parameters monitored during sinusoidal tension-compression cyclic tests on cylindrical bituminous samples.

Parameter	**Symbol**	**Measure unit**
Frequency	f	[Hz]
Axial stress amplitude	σ	[MPa]
Axial stress average value	$\sigma_{average}$	[MPa]
Axial strain amplitude	ε_1	[μm/m]
Axial strain average value	ε_0	[μm/m]
Radial strain amplitude	ε_3	[μm/m]
Radial strain average value	$\varepsilon_{average}$	[μm/m]
Surface temperature	T_1	[°C]
Internal temperature	T_2	[°C]
Complex modulus norm	$\|E^*\|$	[MPa]
Complex modulus phase angle	φ_E	[°]
Real component of the complex modulus	E_1	[MPa]
Imaginary component of the complex modulus	E_2	[MPa]
Complex Poisson's ratio norm	$\|\nu^*\|$	-
Complex Poisson's ratio phase angle	φ_ν	[°]
Dissipated energy per cycle	W	[J m^{-3}]

Chapter 4: ANALYSIS OF DSR TESTS DATA FROM RILEM TC 278 CHA

The essence of this chapter is to analyse fatigue and rest test results on bituminous binders in order to describe their fatigue properties and restoration capabilities, with data obtained from Politecnico di Torino, Italy and University of Waterloo, Canada. As earlier reiterated, all the rheological measurements carried by the two laboratories were performed by means of a DSR from Anton Paar Inc. (Physica MCR 301), using an 8-mm parallel plates geometry with a 2-mm gap. At least two replicates were performed for each test, and average results were considered in the analyses. However, the result of a 70/100 binder replicate from Politecnico de Torino and of a PMB binder replicate from Waterloo are presented as typical examples in this chapter. The results obtained from all replicates on the two binders carried out by the two laboratories are presented in the appendix.

4.1. LVE properties of binders in undamaged conditions

In general, frequency sweeps tests are used to describe the time-dependent behaviour of binders in the small strain domain, in undamaged condition. In the frequency sweep test, measurements are made over a range of oscillation frequencies from 0.2–30 Hz at a constant oscillation amplitude of 0.1% strain and temperature of 20°C. The frequency sweep tests at various frequencies could identify the linear viscoelastic response of the binders. Results of this preliminary characterisation are displayed in diagrams in Figure 4.1 and Figure 4.2, where the norm of the complex modulus is plotted as a function of the phase angle and the Imaginary (G*) - Real (G*) curve is also plotted. The Figure 4.1 results shows the frequency sweep for the pure 70/100 binders while Figure 4.2 shows the results obtained for the modified binders. The continuous smooth curves obtained for all the tests indicate that their behaviour are thermo–rheological simple.

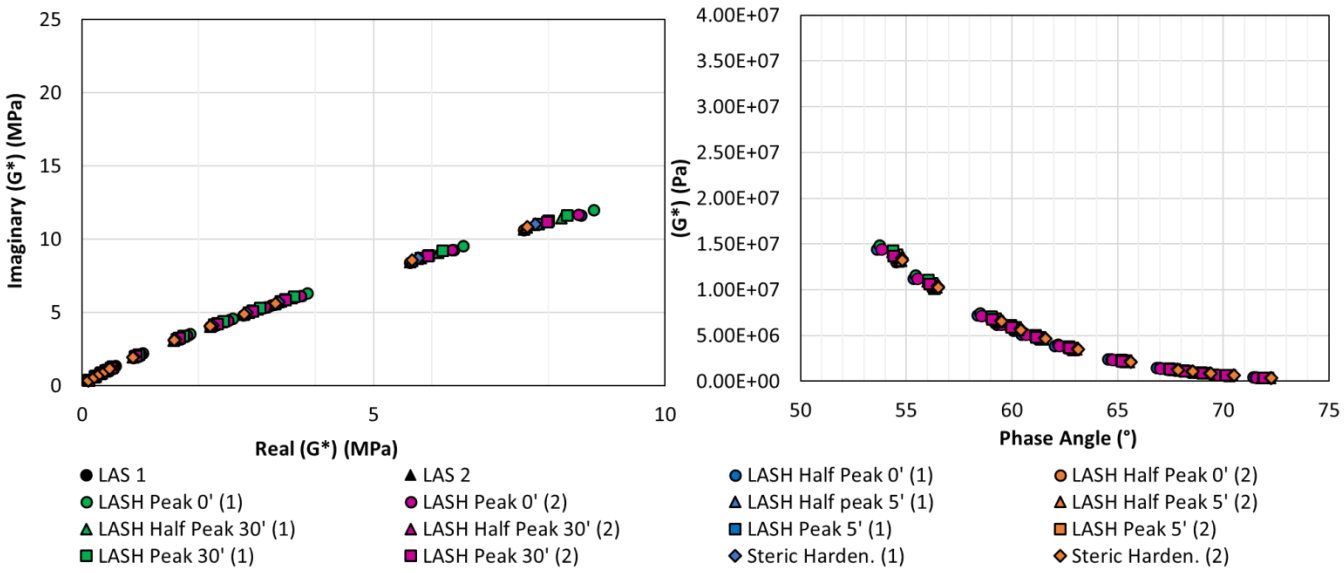

Figure 4.1. Imaginary (G*) vs Real (G*) and (G*) versus φ for the 70/100 binders [Data from Waterloo].

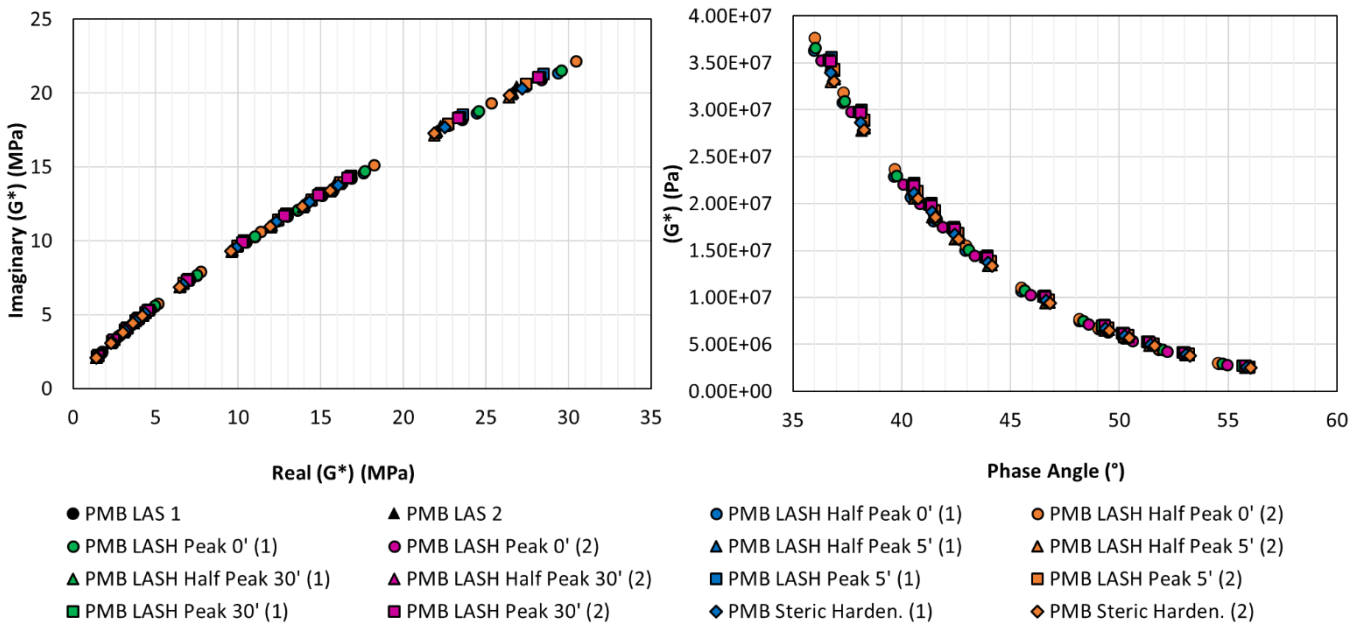

Figure 4.2. Imaginary (G*) - Real (G*) and (G*) - φ for polymer-modified binders [Data from Waterloo].

4.2. Result of LAS test

The LAS test is a type of cyclic fatigue test which was conducted in this study to evaluate the damage resistance of the tested binders. The detailed procedure of the LAS test is described in section 3.1.5. The 70/100 and PMB binders were tested at the temperature of 20°C. According to Sabouri and Kim (2014), in order to prevent the consequences of viscoplasticity, this temperature falls within the range recommended. The test consists in a linear oscillatory strain sweep with strain amplitudes ranging from 0.1% to 30%. The LAS test results of the neat binder (from Politecnico di Torino) and the PMB (from University of Waterloo) are shown in Figure 4.3 and Figure 4.4. In each figure, "LAS 1" and "LAS 2" identify the results obtained on different repetitions on distinct samples of the same binder and as observed, both binders showed good repeatability of the test for the tested binders. Using the LAS test, various damage level and rest period durations were determined as shown in Figure 4.4. From the peak stress as shown by τ_{max}, the strain amplitude corresponding to the peak and half peak of strain as threshold values for LASH test was chosen (as indicated in section 3.1.6). This trend of results corresponds with the trend of LAS results obtained by several authors namely; (Xie et al., 2017; Wang et al., 2015; Miglietta et al., 2021 & Miglietta et al., 2022).

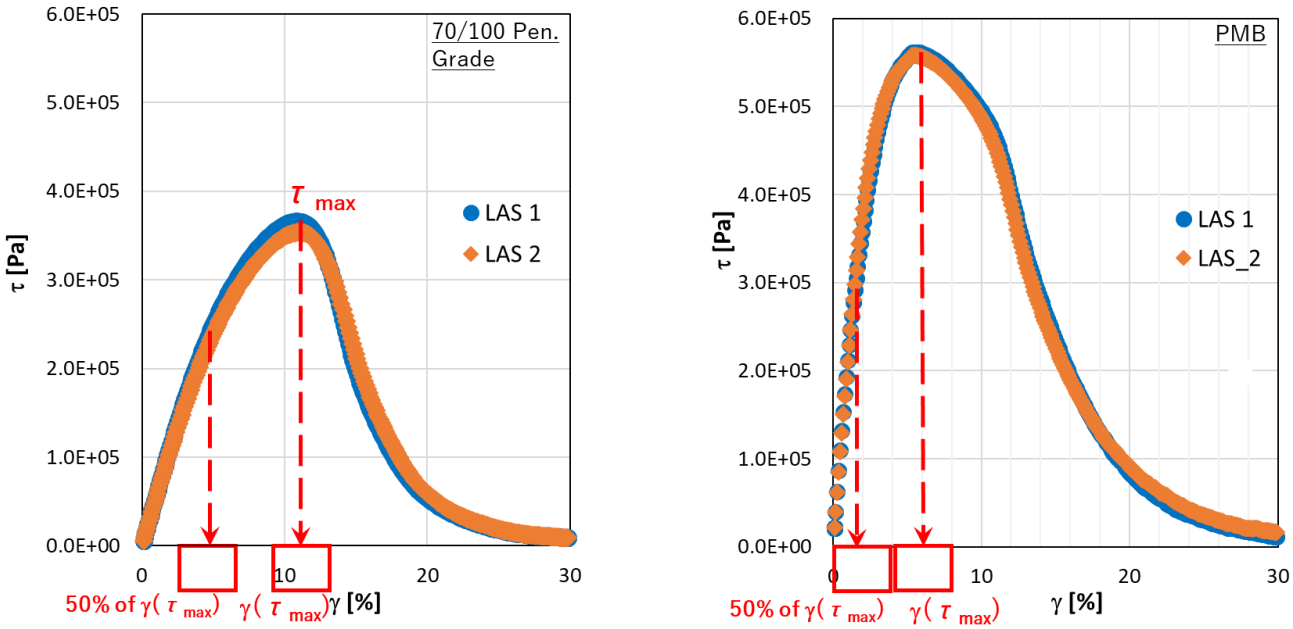

Figure 4.3. Typical LAS tests result in stress – strain curve showing the peak and half peak stresses with increasing peak strain for 70/100 binder [Data from Torino] and PMB binder [Data from Waterloo].

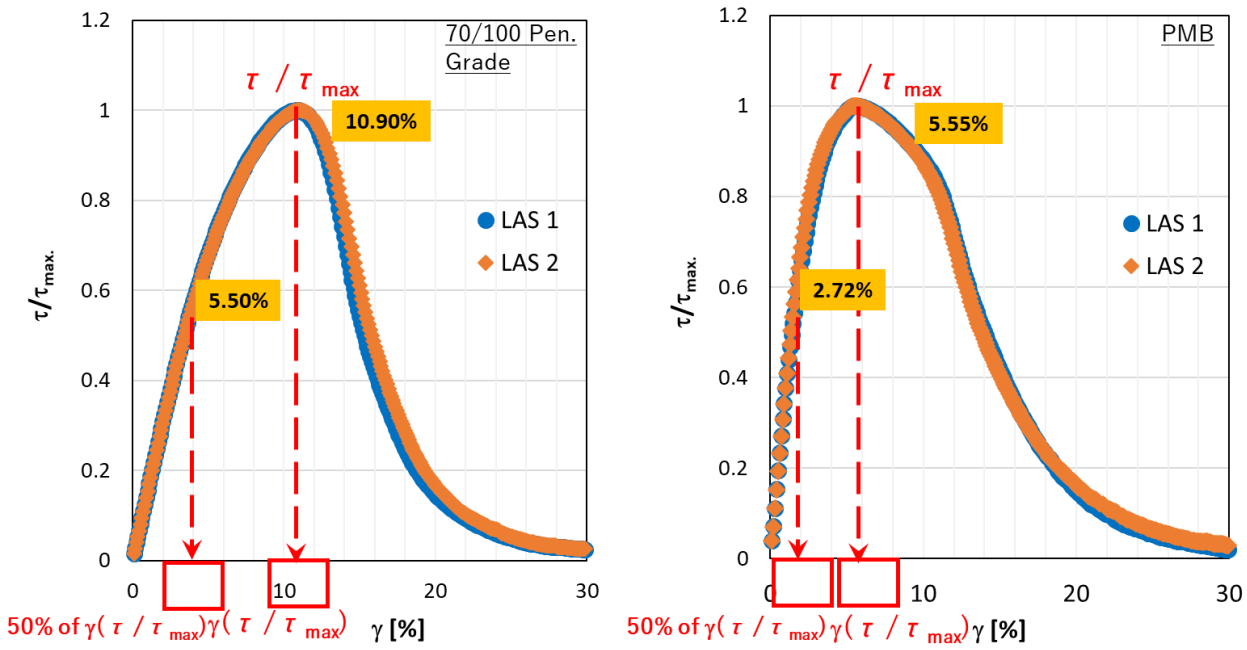

Figure 4.4. Typical LAS tests result in normalised curve showing the peak and half peak stresses with increasing peak strain for 70/100 binder [Data from Torino] and the PMB binder [Data from Waterloo].

Finally, from the results of the LAS test as shown in figures 4.3 and 4.4, it is observed that higher peak stress amplitude at lower corresponding strain amplitude was found for the modified binder. This result presumably illustrates the rationale of selecting the two different binders.

4.3. Results of LASH test

The two main fundamental elements that are required to design a standard healing test protocol for binders are the selection of the damage level at which rest periods should be applied and the length of the rest period (Xie et al., 2017). Figure 4.5 presents an example of results obtained from a LASH test at peak with a 5-minute rest for the 70/100 binder with data from University of Waterloo.

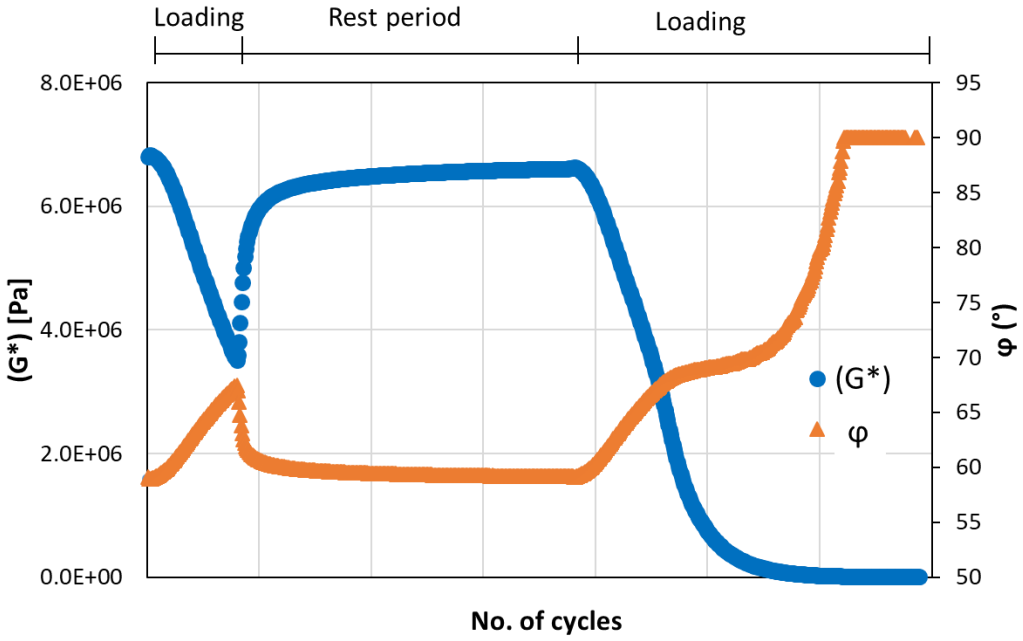

Figure 4.5. Example of results obtained from LASH tests at peak stress for 70/100 binder [Data from Waterloo].

The rest period durations of 0 min, 5 min and 30 min were applied. The LASH test specifically entailed imposing loading determined from the LAS test results, followed by rest periods at the same LAS test temperature (20°C). Finally, the LAS loading sequence is reapplied with the

same rate of increase in strain as the LAS test. However, in the rest of this section, the results obtained from LASH tests are analyzed in order to determine the effects of the different loading histories (strain amplitude before rest and after rest duration) and binder type on test results.

4.3.1. Effect of rest periods and loading history

Results of the LASH test at half peak with respect to stress-strain curve are shown in Figure 4.6 for the 70/100 binder with data from Politecnico di Torino, Italy. From the results, it can be seen that the curves of the first and second loading coincide, indicating that the binders did not experience damage from the application of the first loading before the rest period (half-peak at 0 min., 5 min. and 30 min.). By comparing the results obtained for the 0-minute, 5 minutes and 30 minutes rest periods imposed, it is difficult to say whether the difference is due to steric hardening or simply sample variation. It is clear that the variation of the material properties observed during first loading is obviously not damage and is not time-related either. It is then reasonable to attribute these variations to non-linear viscoelasticity.

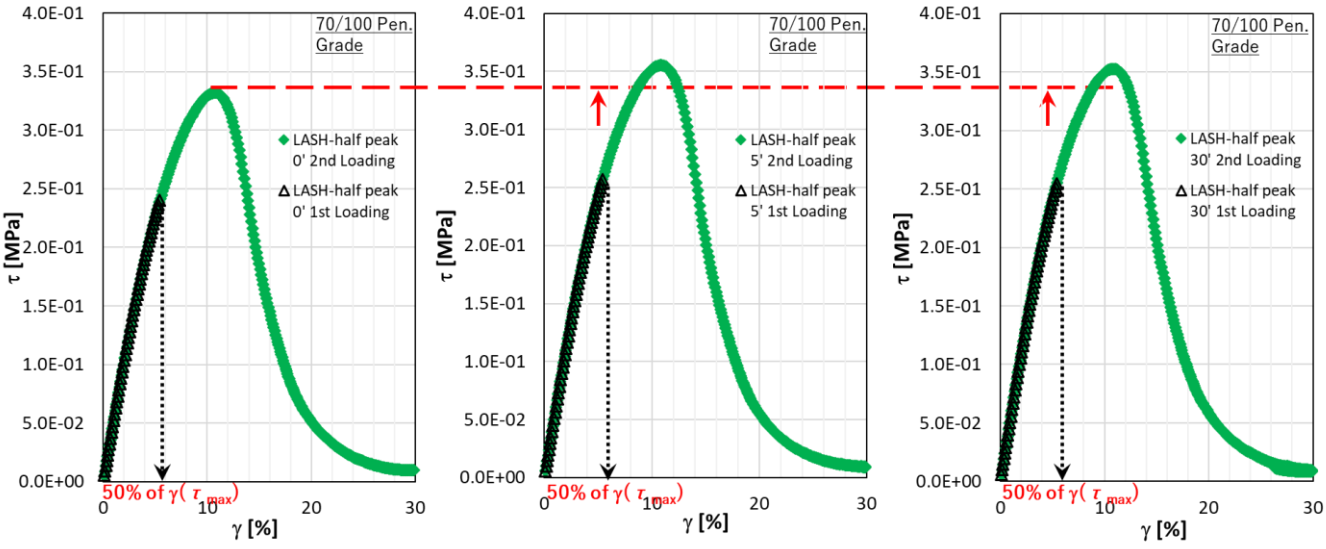

Figure 4.6. LASH test results at half peak for stress - strain curve for 70/100 binder showing the effect of rest periods at 0 min., 5 min. and 30 min. [Data from Torino].

Figure 4.7 shows the same representation of result obtained in figure 4.6 but in |G*| – strain, φ-strain and their equivalent normalized curves for 70/100 binder. At 0 minute, there was 0.11

MPa and 2% loss in complex modulus with 0.39° gain in phase but there was full recovery at 5 minutes and 30 minutes. Consequently, from the result presented in Figure 4.7, it can be seen that when the rest period is introduced at "half-peak", negligible damage is visible even at 0 minute. This also confirms what was noticed in figure 4.6 for the LASH test at half peak with respect to stress-strain curve.

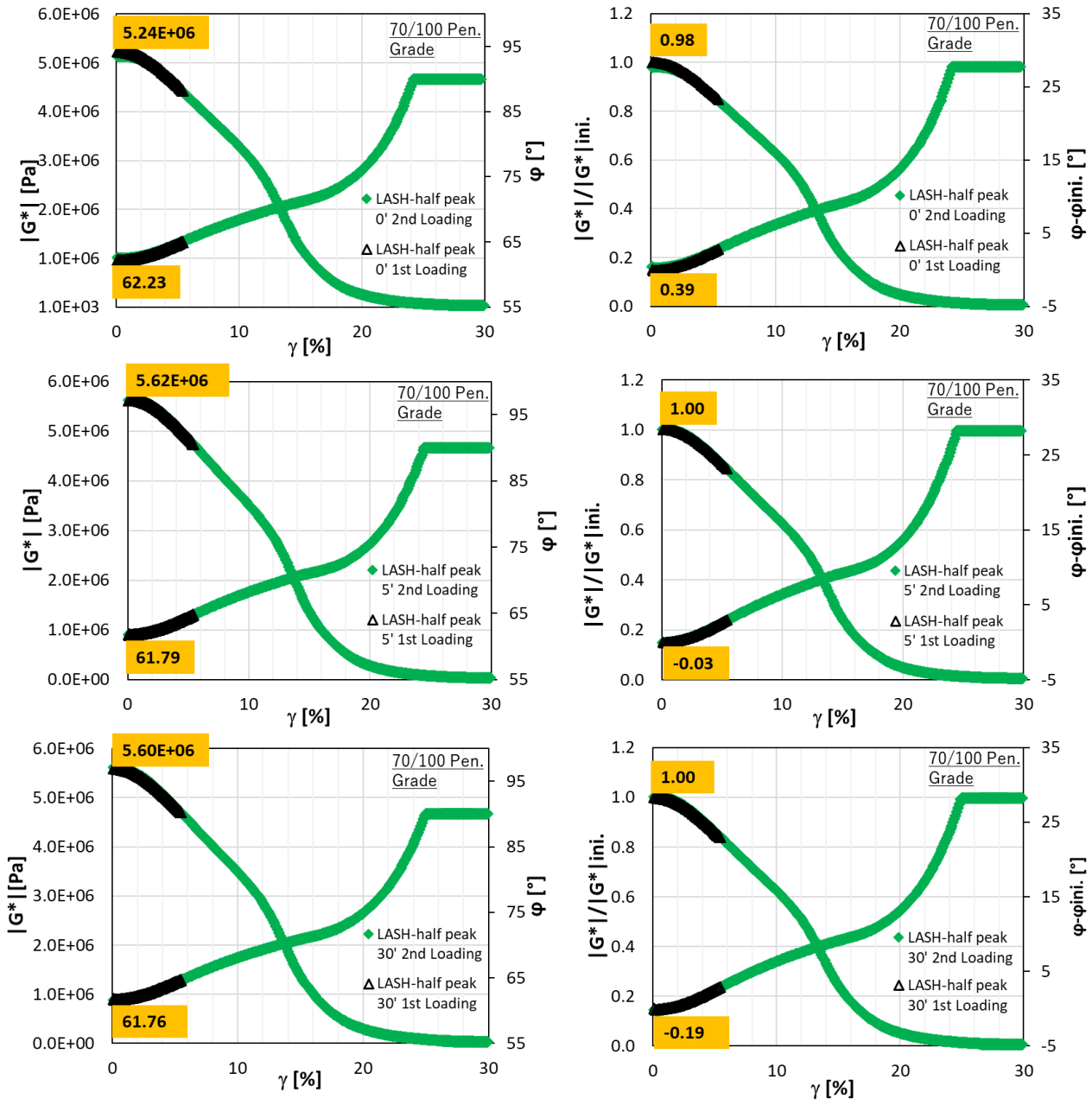

Figure 4.7. LASH stress half peak result of |G*| vs strain, φ vs strain and normalised curve for 70/100 binder showing the effect of rest periods at 0 min., 5 min. and 30 min. [Data from Torino].

Figure 4.8 shows recovery at half peak during the rest period durations with respect to stress – strain curve for the PMB binder with data from Waterloo. Generally, results indicate similar trend of recovery behaviour with the 70/100 binder signifying that the binders did not experience damage from the application of the first loading before the rest period (half-peak at 0 min., 5 min. and 30 min.). These variations could also be attributed to non-linear viscoelasticity.

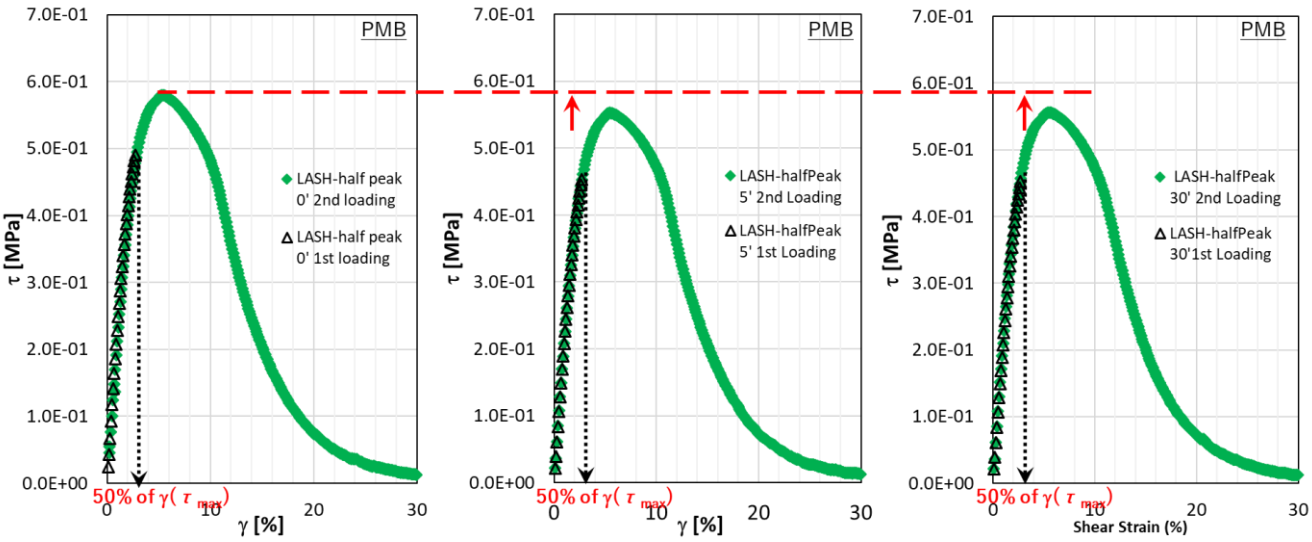

Figure 4.8. LASH test results at half peak for stress - strain curve for PMB binder showing the effect of rest periods at 0 min., 5 min. and 30 min. [Data from Waterloo].

Figure 4.9 shows the recovery during the rest periods with respect to |G*| – strain, φ - strain and the normalized curves for the PMB binder. The observed result of the 0-minute tests can be attributed to strain control issues immediately after the first loading, leading to incorrect data in the initial part of the second loading curves. However, for the other tests, it can be noted that the binders did not experience damage due to the first loading before the rest period (half-peak at 5 minutes and 30 minutes). Finally, for rest times of 5 minutes and 30 minutes there seem to be total recovery and no difference between these rest durations as seen by the 99% and 100% recovery obtained from the normalized curves. Also, this variation is not (fatigue) damage and is not (or too little) time-related, it is also obviously non-linearity.

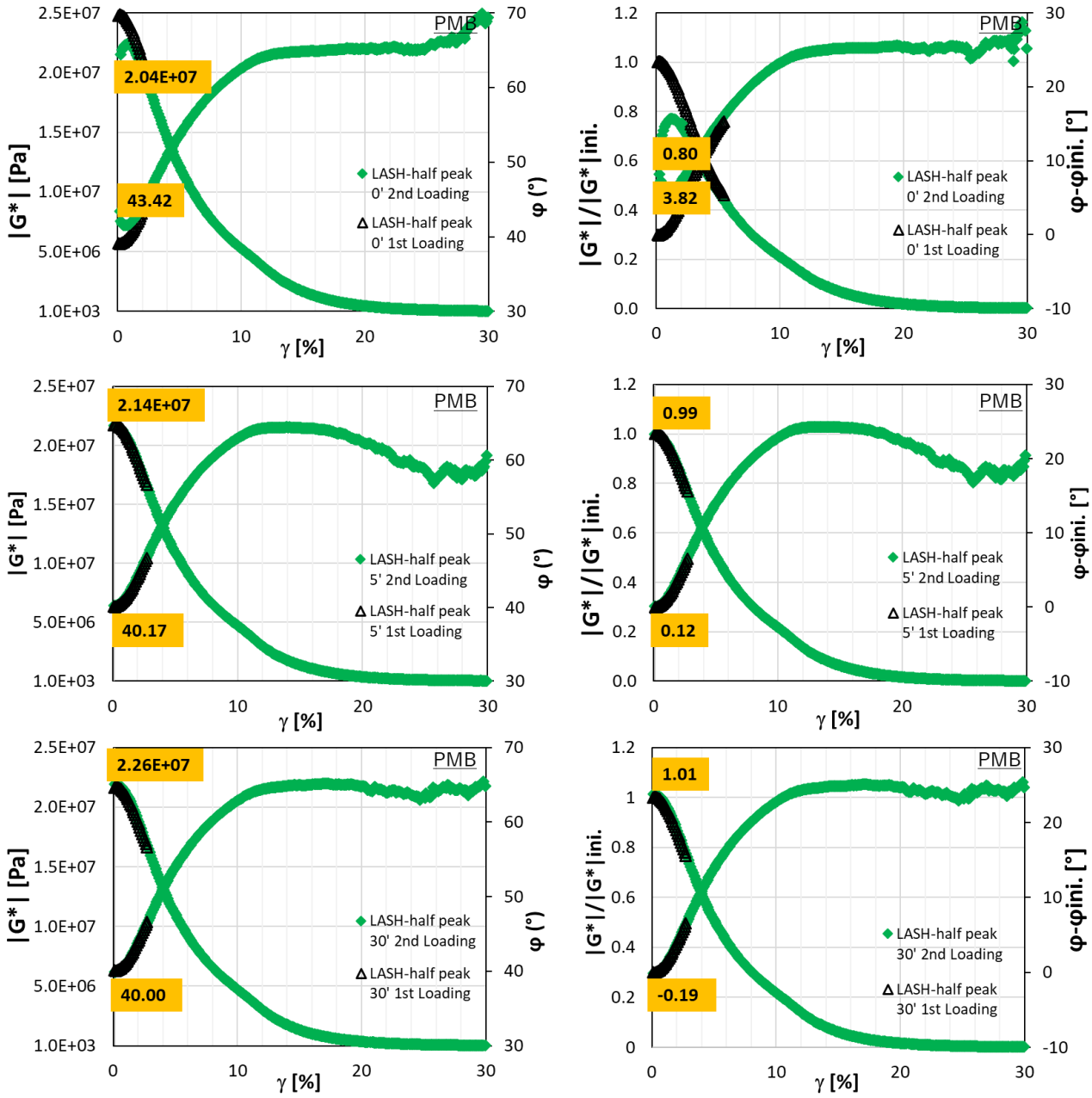

Figure 4.9. LASH stress half peak result of |G*| vs strain, φ vs strain and normalised curve for 70/100 binder showing the effect of rest periods at 0 min., 5 min. and 30 min. [Data from Waterloo].

Results of the LASH test at peak with respect to stress-strain curve are shown in Figure 4.10 for the 70/100 binder with data from Politecnico di Torino. As observed, relative damage after first loading was more important for LASH peak than with LASH half peak. Even though damage experienced by the material is reversible during rest, there appear to be differences in recovery at the second loading at the various rest times (that is 0 minute, 5 minutes and 30 minutes). It can be clearly seen from the result that after 30 minutes, there is slight increase of

the peak stress amplitude than at 5 minutes and 0 minute, implying the effect of rest duration. This suggests that the differences observed during different rest times could be attributed to time-dependent recovery. However, even though recovery is observed, it is still impossible to distinguish the various phenomena responsible for it. Although these results appear to agree with most of the literature on recovery of bitumen, considering recovery as the combination of an instantaneous and a time-dependent strength gain, the nature of the tests performed, implying high strain levels and rapid variations of strain amplitude, prevents distinguishing clearly between actual healing and recovery of reversible phenomena. These observations suggest that the LASH test protocol is not effective to investigate the behaviour of bituminous materials during fatigue and rest.

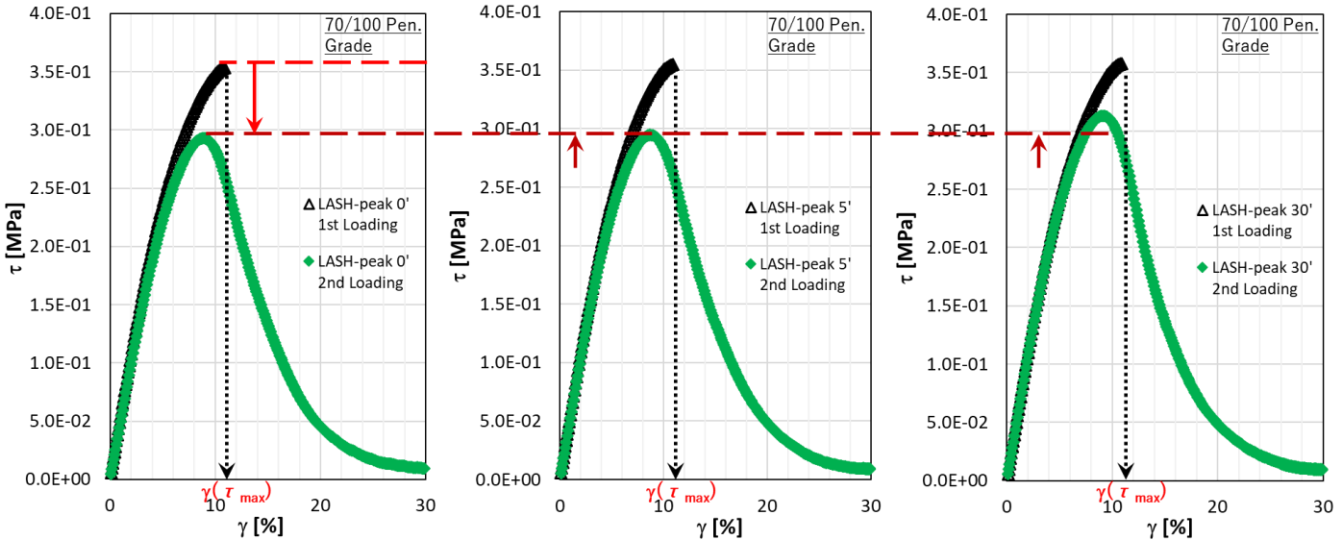

Figure 4.10. LASH test results at peak for stress - strain curve for 70/100 binder showing the effect of rest periods at 0 min., 5 min. and 30 min. [Data from Torino].

Figure 4.11 shows the same representation of the results obtained in figure 4.10 but in |G*| - strain, φ - strain and their equivalent normalized curves for 70/100 binder. The result further confirms the occurrence in figure 4.10. When considered independently, at 0 minute, there was 0.55 MPa and 11% loss in complex modulus with 1.26° gain in phase angle, at 5 minutes of rest, there was 0.33 MPa and 4% loss in complex modulus with 0.11° gain in phase angle and at 30 minutes rest, full recovery was attained with 0.55 MPa and 2% loss in complex modulus with -0.17° gain in phase angle. This also suggests that the differences observed during different rest time durations could be attributed to time-dependent recovery.

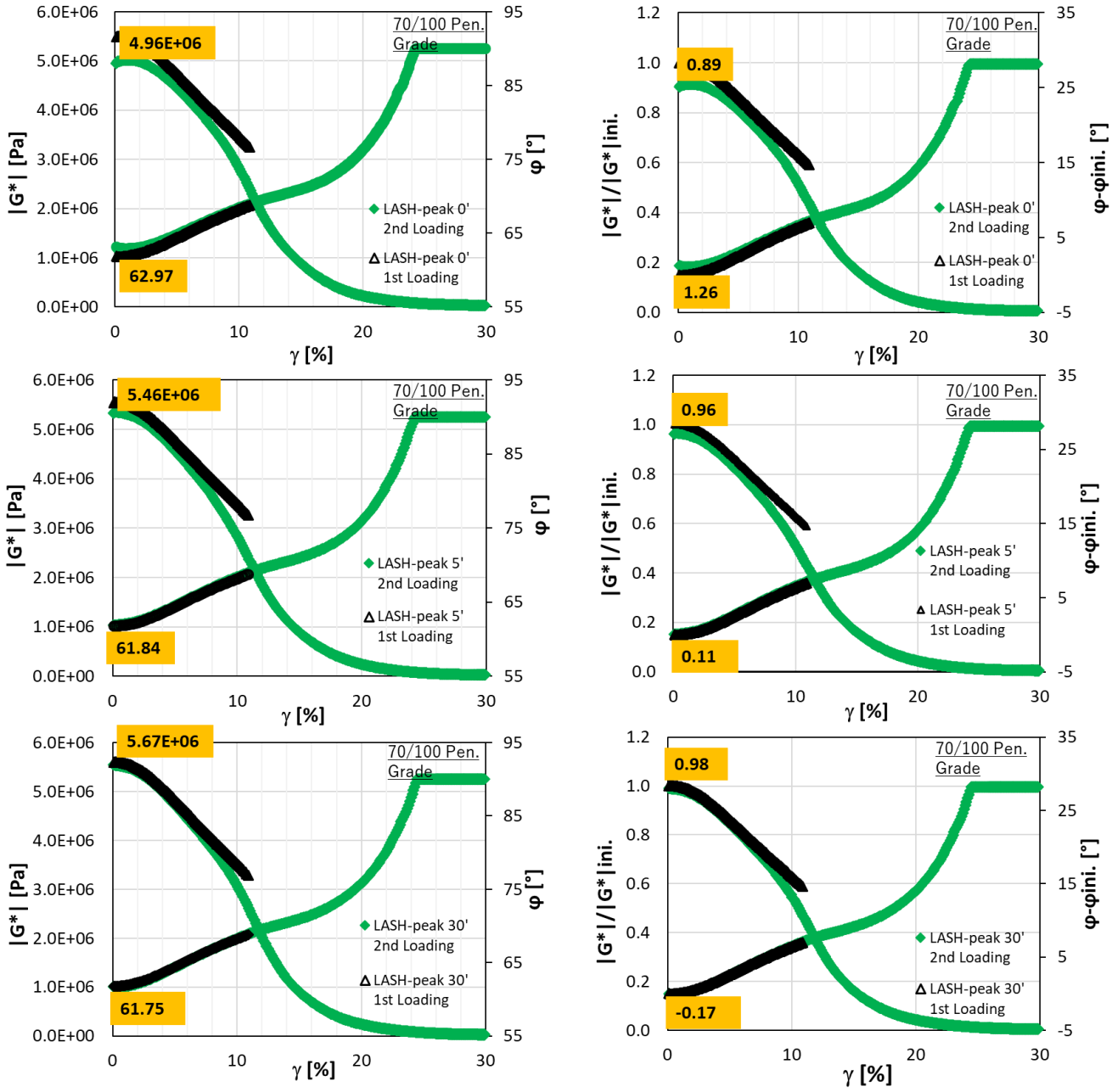

Figure 4.11. LASH stress peak result of |G*| vs strain, φ vs strain and normalised curve for 70/100 binder showing the effect of rest periods at 0 min., 5 min. and 30 min. [Data from Torino].

Figure 4.12 shows recovery at peak during the rest periods with respect to stress – strain curve for the PMB binder with data from Waterloo. The results are still similar to those of the half peak tests where the PMB binders did not experience damage due to the first loading before the rest period (peak at 0 min., 5 min. and 30 min.). Results demonstrates that no difference exist

for the PMB binder even at this level of damage. This also confirms higher recovery for PMB than for 70/100 binder.

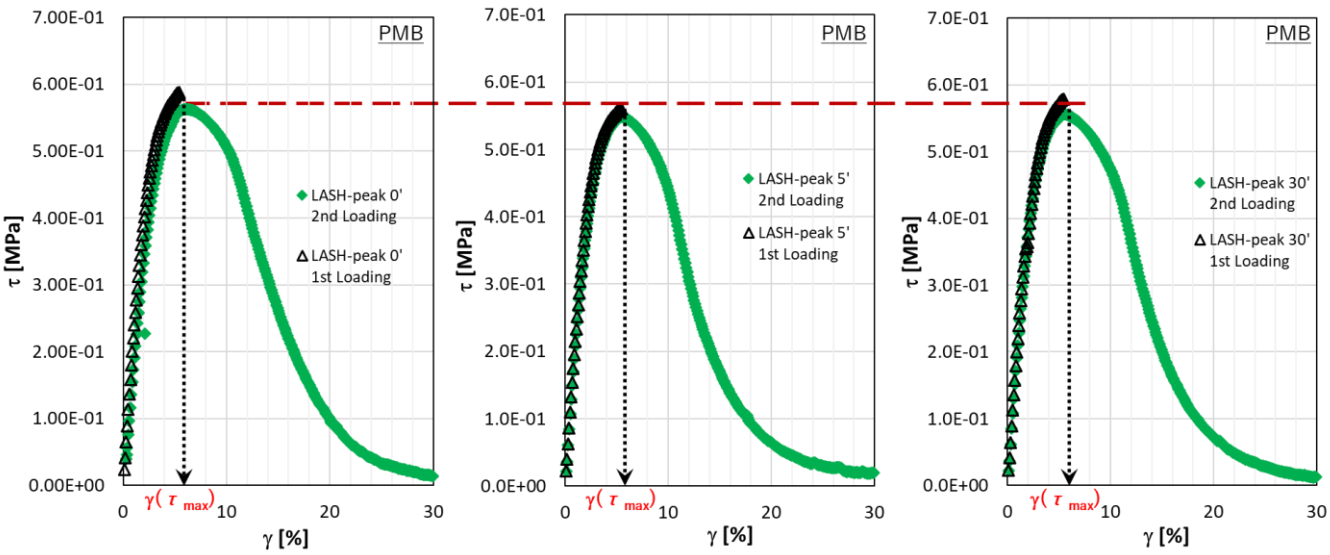

Figure 4.12. LASH test results at peak for stress - strain curve for the PMB binder showing the effect of rest periods at 0 min., 5 min. and 30 min. [Data from Waterloo].

Figure 4.13 shows the same representation of the results in figure 4.12 but in |G*| - strain, φ - strain and their equivalent normalized curves for PMB binder. At 0 minute, similar to the experience with the half peak, the DSR had strain control issues immediately after the first loading, hence, data obtained were incorrect. However, as noted in the subsequent rest times, it can be seen that the curves of the first and second loading coincide, indicating that the binders did not experience damage from the application of the first loading before the rest period (peak at 5 min. and 30 min.) was induced. It can be seen that when the rest period is introduced at "peak", negligible damage is visible even at 5 and 30 minutes. Since there is obviously no damage in the materials, then the variations observed are also obviously attributable to non-linearity.

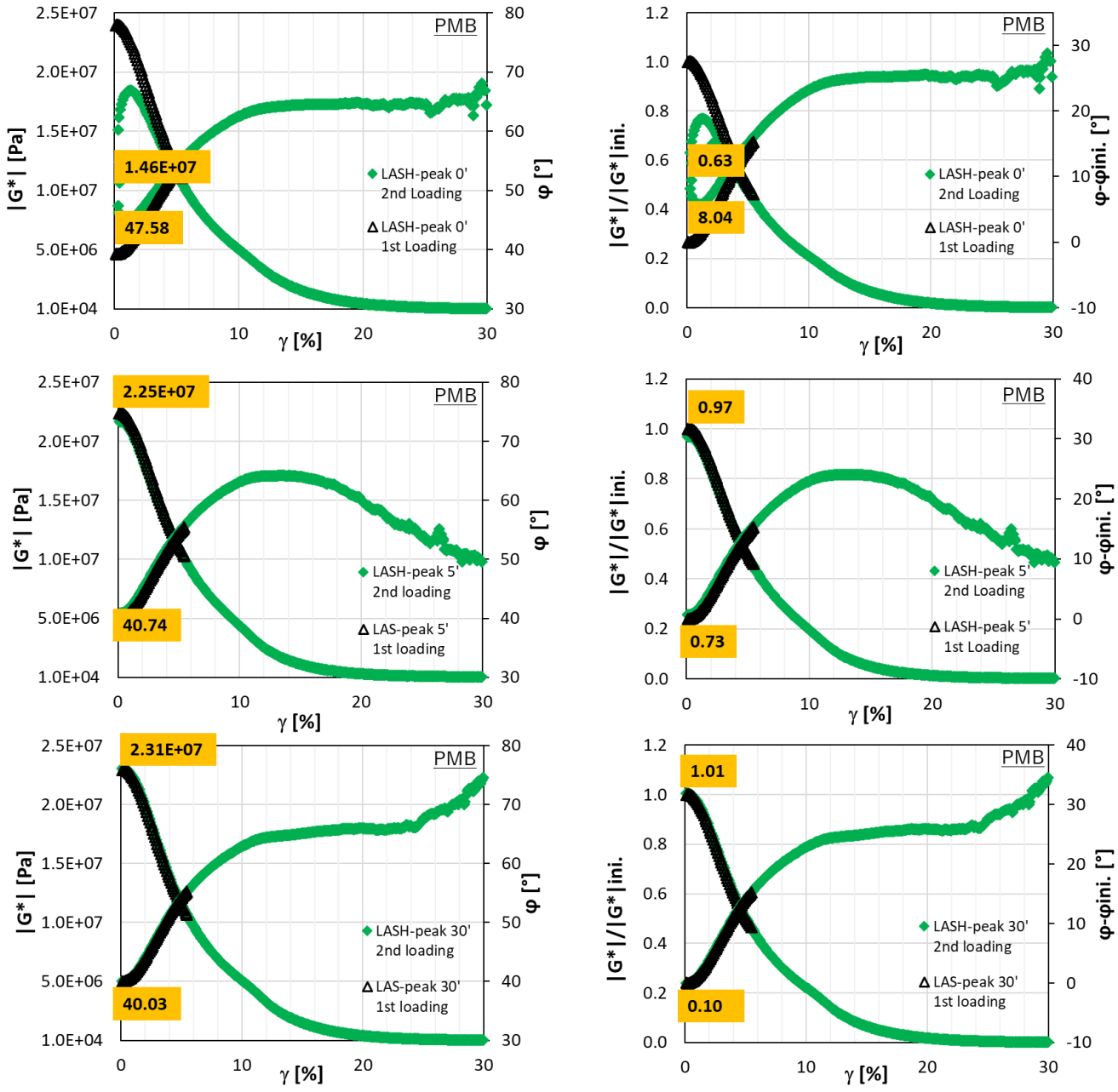

Figure 4.13. LASH stress peak result of |G*| vs strain, φ vs strain and normalised curve for the PMB binder showing the effect of rest periods at 0 min., 5 min. and 30 min. [Data from Waterloo].

From the results presented in this section, it can be seen that when the rest period is introduced at "half-peak" negligible damage is visible even at 0 minutes, while higher differences between the first and second loading at 0 minutes can be observed when rest periods are introduced at "peak". Even though it is clear there is no damage, it can be clearly seen that the properties of the materials are changing during first loading. From half-peak LASH tests, all the variation of material properties observed during the first loading is instantaneously recovered which

signifies non-linearity with no damage. However, for the 70/100 binder, from peak LASH tests during second loading the initial norm and phase angle is different with the initial norm and phase angle at the beginning of 1st loading, in the case of 0-minute rest but this difference is completely recovered after 30-minute rest (for 70/100 binder). The PMB binder did not show important differences with the various rest period durations applied. The only clear conclusion from these tests is the difference between the behaviour of neat and modified binder, but no clear information was drawn on fatigue damage and healing properties. LAS (and LASH) tests are not adapted, because of the high strain amplitude levels and the rapid strain amplitude variations.

4.3.2. Results of steric hardening tests

As earlier reiterated, the steric hardening test is conducted by performing the standard LAS test after an additional rest period of 30 minutes is applied after the pre-test period of 30 minutes, making the 0.1% strain amplitude continuous loading a total of 60 minutes before the loading phase is applied. Figure 4.14 shows typical results obtained from a steric hardening test on the PMB binder. By plotting measured values of complex modulus and phase angle as functions of time, the two stages of the rest sequence (pre-test and steric hardening) can be distinguished.

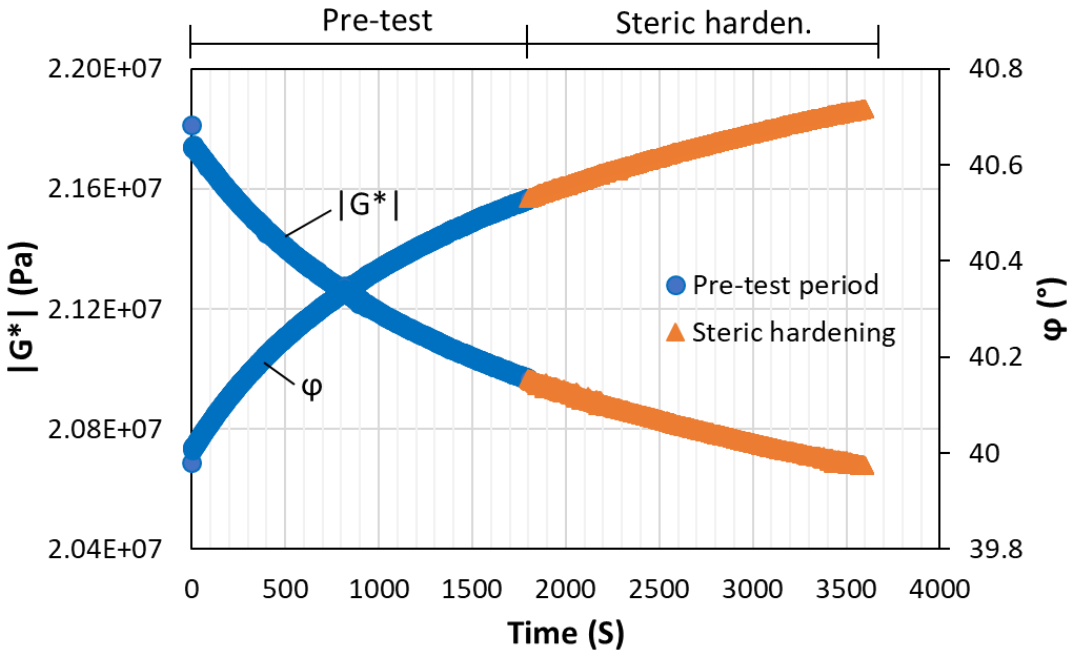

Figure 4.14. Example of steric hardening test results for the PMB binder [Data from Waterloo].

The results in Figure 4.15 shows the effect of steric hardening during LAS tests with respect to stress – strain curve for the 70/100 and PMB binders. Insignificant difference is noticed between the LAS-SH and LAS results for both binders. Results indicates no occurrence of physical and/or steric hardening during the recovery phase when an extended rest period is applied at 30 minutes.

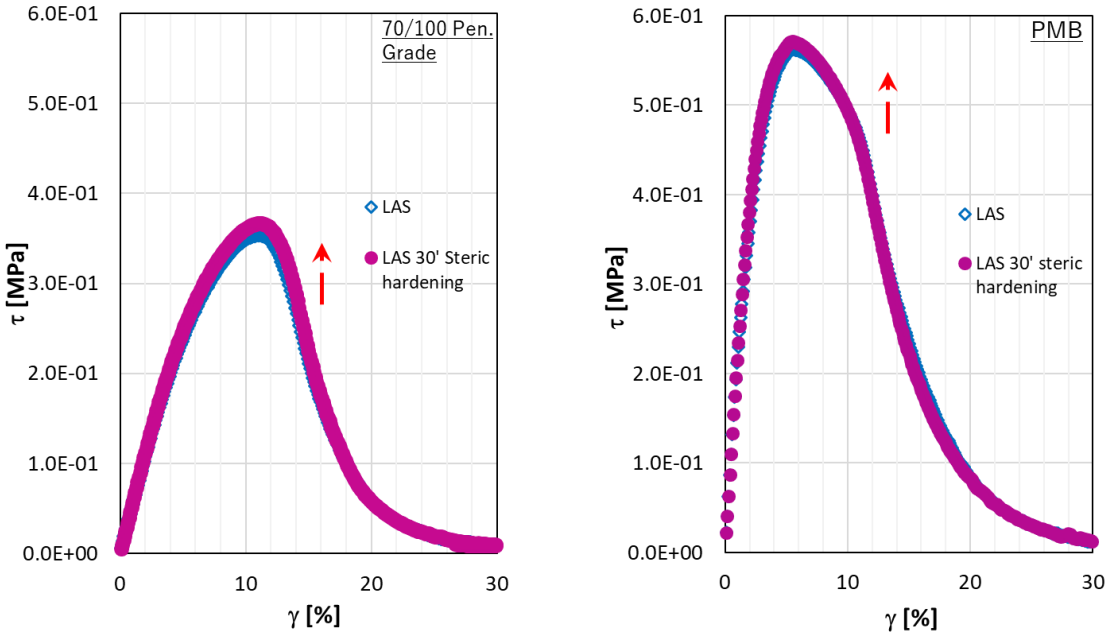

Figure 4.15. LAS test and LAS-SH tests result for stress - strain curve for 70/100 binder. [Data from Torino] and PMB binder [Data from Waterloo].

Figure 4.16 shows the effect of steric hardening during LAS tests with respect to |G*| – strain, φ - strain and their equivalent normalized curves for 70/100 and PMB binders. The LAS test result is used as reference in calculating and making comparison with the LAS-SH result. It can also be noted that there is a slight insignificant increase in complex modulus (0.17 MPa with 3% for the 70/100 binder and 0.013 MPa with 1% for the PMB) and decrease in phase angle (0.08° for the 70/100 binder and 0.23° for the PMB) when the LAS-SH tests are compared with LAS tests. The results show that the effect of the additional 30 minutes rest before tests for both binder types are insignificant with respect to the evolution of material properties during the LAS tests.

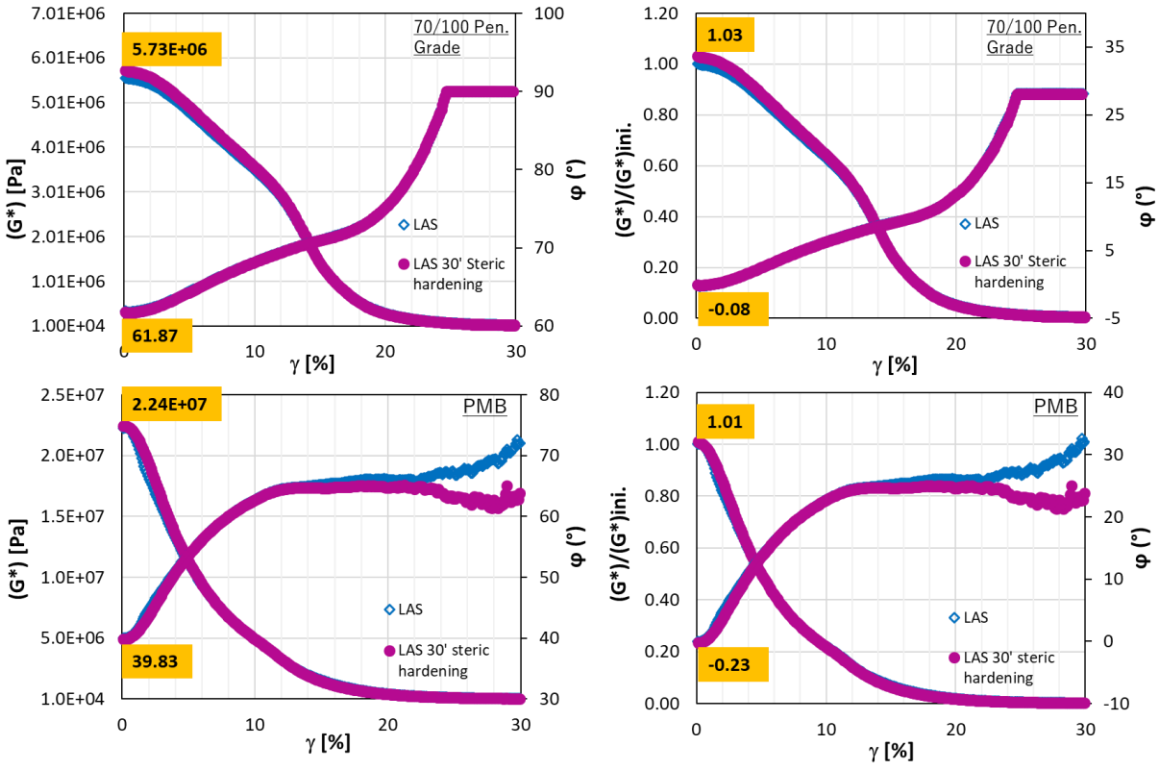

Figure 4.16. LAS test and LAS-SH tests result for |G*| - strain and normalized curves for 70/100 binder [Data from Torino] and PMB binder [Data from Waterloo].

Finally, from the test results, it can be observed that the effect of steric hardening applied at 30 minutes was insignificant for the binders (70/100 and PMB) tested. As noted, the change of complex modulus and phase angle was small and no significant difference between LAS curves were observed.

4.4. Evaluation of energy dissipation

In the energy dissipation-based approach, the total energy dissipated by the material during the loading is used to assess the damage and recovery. Such analysis methods are used for bitumen, mastic, and mixtures. Hence, using the concept of dissipated energy properly is essential in interpreting damage and recovery. The energy dissipation per loading cycle, W_i is expressed as follows:

$$W_0 = \pi \tau_0 \Upsilon_0 sin\varphi \qquad 4.1$$

where W_0, is dissipated energy in cycle i; τ_0, is stress amplitude in cycle 0; Υ_0, is strain amplitude in cycle 0; φ is phase angle.

However, this method is an estimation and does not represent the true state of energy dissipated since the calculations are based on the hypothesis of linear viscoelastic beahviour. Considering the strain amplitudes applied during the protocol, this hypothesis is not valid for most of the duration of the tests. The evolution of W_i the LAS tests is shown in Figure 4.17 for the 70/100 and PMB binders. It also shows a similar trend of result with the LAS test results in the stress-strain curve. The results in Figure 4.17 for neat and modified binders shows good repeatability of the test for the tested binders. From the result, it shows that the strain amplitude corresponding to peak of energy dissipation is higher than strain amplitude corresponding to peak of stress amplitude, for both binders.

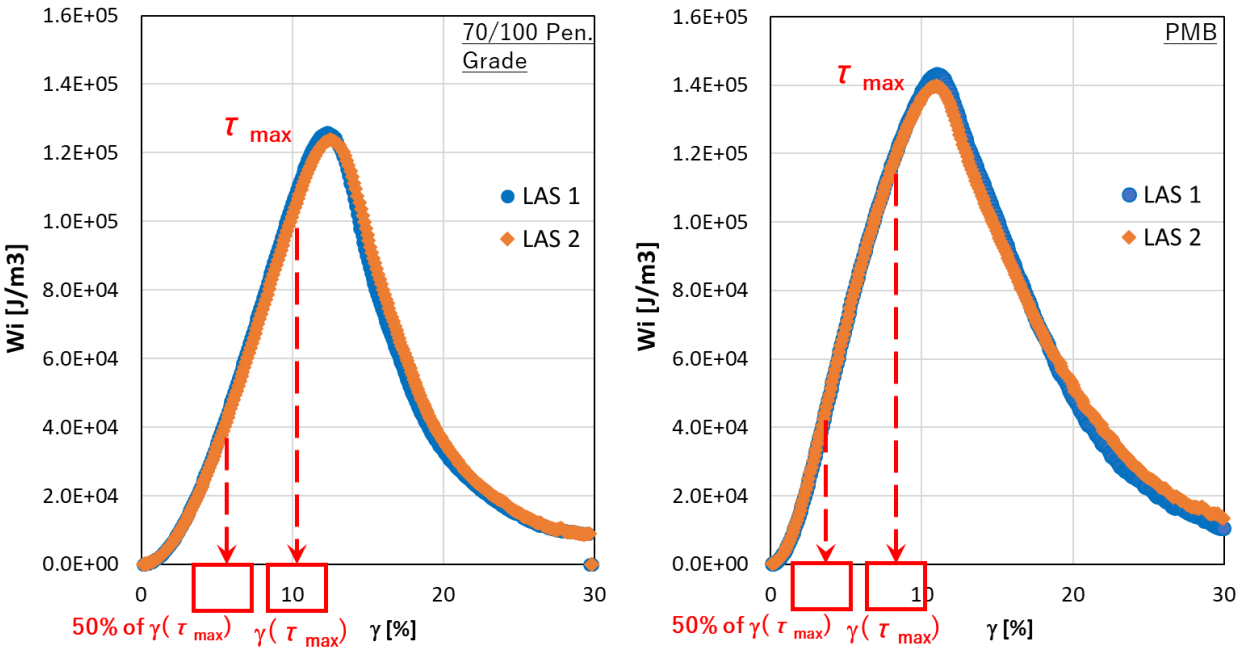

Figure 4.17. Typical LAS tests result in energy dissipation – strain curve for 70/100 binder showing traces of peak and half peak stresses with increasing peak strain. [Data from Torino].

Figure 4.18 shows the LASH tests for energy dissipation - strain curve for 70/100 binder carried out at half peak stress at rest periods of 0 minute, 5 minutes and 30 minutes. The energy approach confirms what was observed previously for these tests. As observed, results confirm that the binders did not experience damage during the first loading before the rest period (half-

peak at 0 min., 5 min. and 30 min.) was induced. Comparing the results obtained for the 0-minute, 5 minutes and 30 minutes rest periods imposed, it shows differences in energy dissipation at the various rest duration, varying the existence of instantaneous and time-dependent variations. This affirms the earlier results obtained for recovery at half peak during the rest periods with respect to stress – strain curve for the PMB binder.

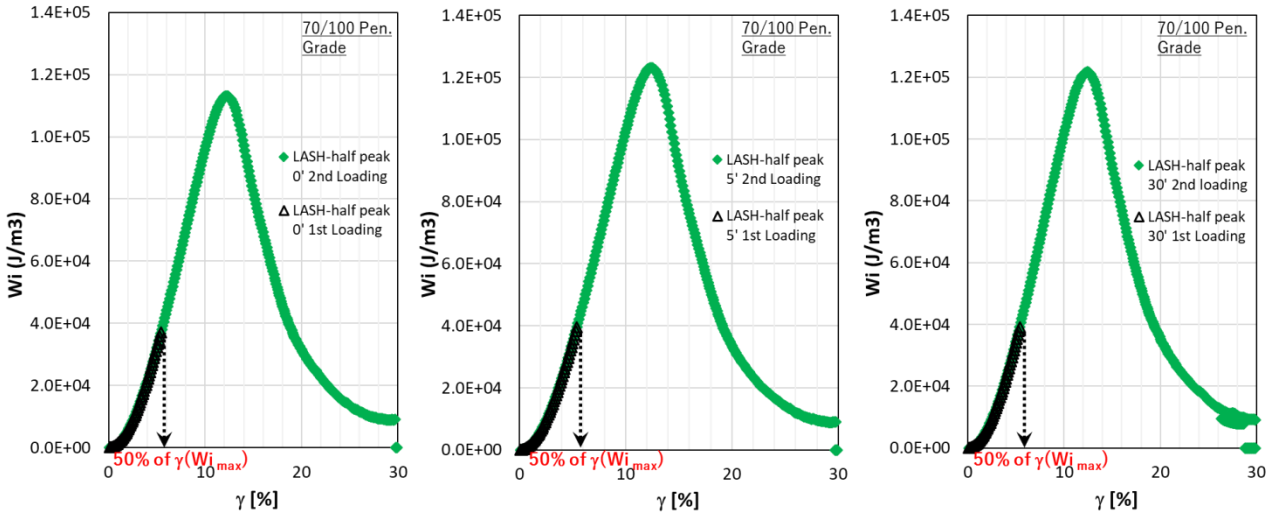

Figure 4.18. LASH test results at half peak for energy dissipation - strain curve for 70/100 binder showing the effect of rest periods at 0 min., 5 min. and 30 min. [Data from Torino].

Then Figure 4.19 shows the LASH tests for energy dissipation - strain curve for the PMB binder carried out at half peak stress at rest periods of 0 minute, 5 minutes and 30 minutes. The energy dissipation confirms that the binders did not experience damage due to the first loading before the rest period (half-peak at 0 min., 5 min. and 30 min.). Results show no difference in energy dissipation at the various rest periods.

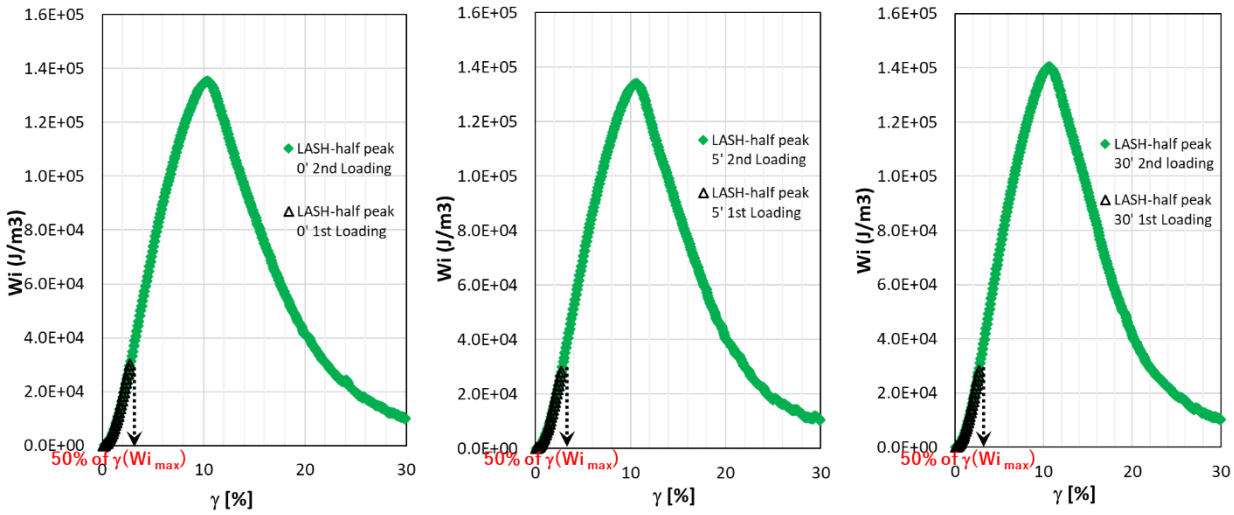

Figure 4.19. LASH test results at half peak for energy dissipation - strain curve for the PMB binder showing the effect of rest periods at 0 min., 5 min. and 30 min. [Data from Waterloo].

Figure 4.20 shows the energy dissipation-strain curve for LASH tests on 70/100 binder carried out at peak at rest periods of 0 minute, 5 minutes and 30 minutes. As observed, this approach shows that the peak value of Wi and the strain for which it occured seem to be influenced by the first loading. This implies that the first loading before rest induced substantial effects on material behaviour. Partial recovery is observed after 30 minutes of rest, suggesting some time-dependent effects. However, it is also not clear how the various reversible phenomena can be distinguished.

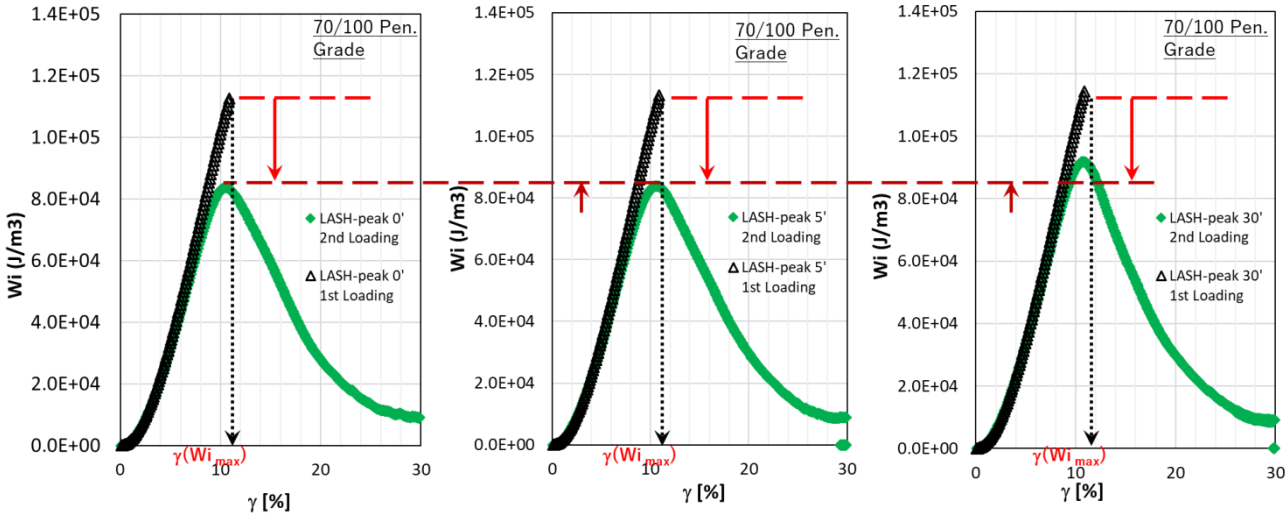

Figure 4.20. LASH test results at peak for energy dissipation - strain curve for 70/100 binder showing the effect of rest periods at 0 min., 5 min. and 30 min. [Data from Torino].

Figure 4.21 shows the LASH tests for energy dissipation - strain curve for the PMB binder carried out at peak at rest periods of 0 minute, 5 minutes and 30 minutes. In this instance, result shows that W_i curves do not seem to be influenced by the first loading. Hence, the binder recovered fully at all the rest periods considered (0 minute, 5 minutes and 30 minutes). It can also be noted that comparing the results obtained for the 0-minute, 5 minutes and 30 minutes rest periods imposed, no difference between instantaneous and time-dependent variations of energy dissipation exist. For this binder, the energy approach validates conclusions obtained when τ, $|G^*|$ and φ were considered.

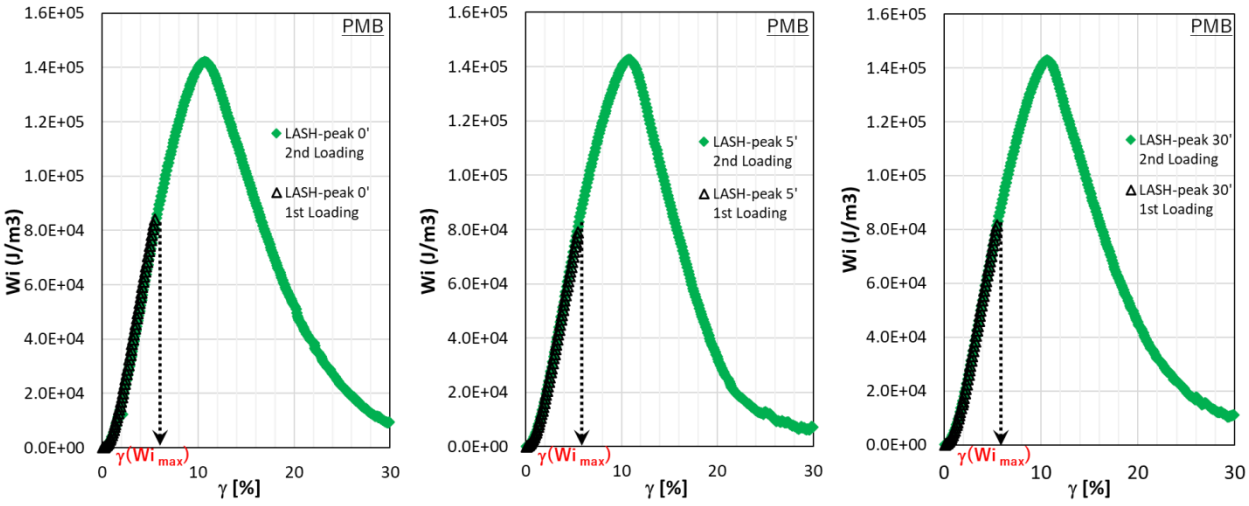

Figure 4.21. LASH test results at peak for energy dissipation - strain curve for the PMB binder showing the effect of rest periods at 0 min., 5 min. and 30 min. [Data from Waterloo].

It is observed, that for both binders, the strain amplitude corresponding to the peak of energy dissipation is greater than the strain amplitude corresponding to the peak of stress amplitude. However, this observation could be misleading since this method is an estimation and does not represent the true state of energy dissipated. The 70/100 binder, an evident decrease of the peak of energy dissipation during second loading is observed with only partial recovery for 30-minutes rest periods occurring.

4.5. Analysis of the recovery parameters

This section shows comparison of the various recovery parameters measured after the various rest periods (0 minute, 5 minutes and 30 minutes), which are summarized in bar charts for half peak and peak stresses for the 70/100 and PMB binders. The percentage recovery is determined from the following equations 4.2 - 4.4;

$$\% \text{ recovery} = \frac{\tau_{max.}\ 2nd\ loading}{\tau_{max.}\ 1st\ loading} \quad 4.2$$

For peak shear stress,

$$\% \text{ recovery} = \frac{|G*|\ 2nd\ loading}{|G*|\ 1st\ loading} \quad 4.3$$

For initial complex modulus (at the beginning of 1st and 2nd loading),

$$\% \text{ recovery} = \frac{Wi_{max.}\ 2nd\ loading}{Wi_{max.}\ 1st\ loading} \quad 4.4$$

For peak energy dissipation.

Figure 4.22 shows the summary of total recovery based on norm of complex modulus at the beginning of the 2nd loading period, peak shear stress and peak dissipated energy at half peak stress for 70/100 binder. As shown in the figure, recovery calculated based on complex modulus showed the highest amount of recovery compared to the other parameters (i.e. shear stress and dissipated energy). Also, similar recoveries are estimated for dissipated energy and shear stress. The recovery after 30 minutes of rest for half peak seem to achieve total recovery (or close) for all the considered parameters. Results show good repeatability at the various time durations. Regardless of approach, test results show time-dependent recovery. Finally, the different approaches show differences in recovery.

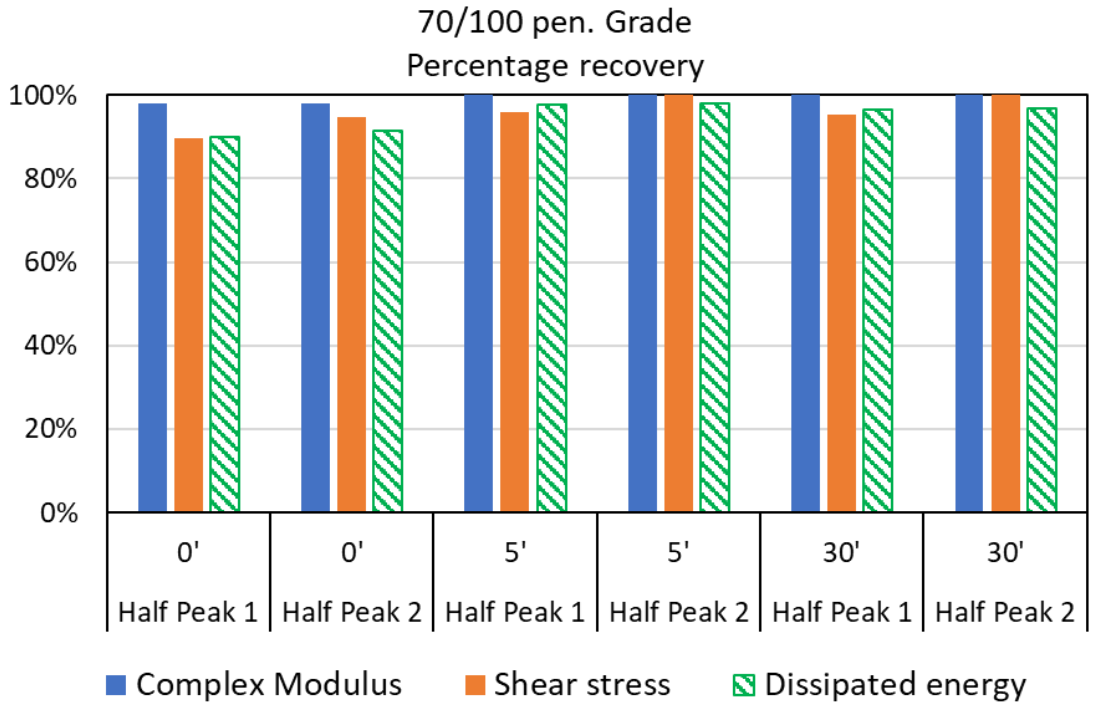

Figure 4.22. Summary of total recovery based on complex modulus, shear stress and dissipated energy at half peak stress for 70/100 binder [Data from Torino].

Figure 4.23 shows the summary of total recovery based on complex modulus, shear stress and dissipated energy at peak stress for 70/100 binder. As noticed in the figure, complex modulus also recorded the highest amount of recovery compared to the other parameters (i.e. shear stress and dissipated energy). On the other hand, dissipated energy recorded the least amount of recovery as observed. From the chart, it shows that the percentage recovery using the energy dissipation approach become less sensitive to rest period duration when there was higher level of damage. As shown, only the recovery based on the complex modulus indicates complete recovery. The results at the level of damage also show good repeatability from the various repetitions. However, the different approaches utilized show differences in recovery.

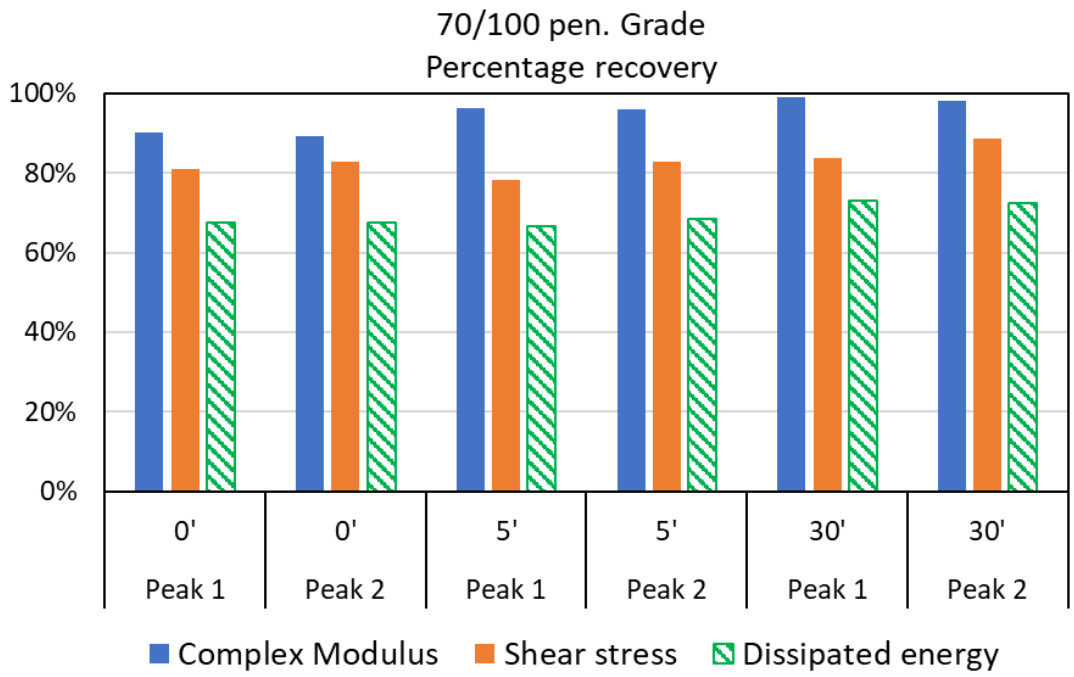

Figure 4.23. Summary of total recovery based on complex modulus, shear stress and dissipated energy at peak stress for 70/100 binder. [Data from Torino].

The results obtained highlights the complexity of correctly defining and characterizing recovery of the mechanical properties of bituminous binders using the LASH test protocol. Results from the different approaches considered confirm that the LASH protocol does not allow drawing clear conclusions based on qualitative and quantitative estimations of the various phenomena. Basically, until a direct observation is made, it is impossible to prove it. Finally, the differences in estimations of recovery according to the considered properties (G*, τ, Wi) show the limitation and ineffectiveness of the test protocol at identifying and estimating the different reversible phenomena.

4.6. Partial conclusion on DSR test for binders

Based on the DSR test for binders, the following conclusions were drawn from obtained experimental results and performed analyses:

- For the half-peak LASH tests, it was observed that all the variation of material properties observed during the first loading is instantaneously recovered. This occurrence validates the existence of non-linearity with no damage.

- Time-dependent recovery was observed for tested binders especially at peak. However, higher recovery was observed for PMB than for 70/100 binder.
- It was also observed that the effect of steric hardening at 30 minutes was insignificant with both binders tested. The change of G* was small and no significant difference between the LAS curves were observed.
- The different approaches (complex modulus, shear stress and dissipated energy) were used to assess the damage and recovery of the different binders tested. However, among all the approaches considered, complex modulus seems to record the highest amount of recovery compared to the other parameters (i.e. shear stress and dissipated energy). Also, using the dissipated energy approach, it recorded the least amount of recovery especially with the peak stress. Also, the percentage recovery using the energy dissipation approach seems to be less sensitive to rest period duration when there was higher level of damage. Consequently, results obtained shows the complexity of correctly defining and characterizing recovery of the mechanical properties of bituminous binders using the LASH test.
- The performed test protocol (LASH test), with and without rest periods, can clearly distinguish different binders (in our case, a straight-run and a PMB), but it is not possible to distinguish the different and complex phenomena responsible for the response of the observed variations of material properties during loading and rest (damage, recovery, restoration). This is clearly observed for the different estimations of recovery according to considered property (G*, τ, Wi) where the different phenomena occurring during loading and rest were limited to just reversible and not reversible.

Chapter 5: TENSION-COMPRESSION TESTS ON BITUMINOUS MIXTURES PERFORMED AT ENTPE: RESULTS AND ANALYSIS

This chapter presents the results of the tests carried out on the mixtures, following a test procedure developed at ENTPE. The developed procedure is composed of two parts, which is carried out on the same sample. The first part of the test consists of complex modulus tests (CMT) carried out in order to characterize the linear viscoelastic (LVE) behaviour of the studied bituminous mixtures in undamaged conditions. Details of the CMT are described in section 3.3.1. The second part of the test consists in fatigue and rest (PFRT) with a final fatigue test carried out afterwards sequences aiming to characterise the variation of mechanical properties of the materials during loading and rest. However, the results of the final fatigue were not used for analysis in the dissertation. Details of the fatigue and rest test periods are described in section 3.3.2.

Eight samples were tested for each of the three mixtures (mix 70/100, mix 40/60 and mix PMB), for a total of twenty-four samples tested. Three of the eight tests performed on both mix 70/100 and mix 40/60 and four of those carried out on mix PMB were interrupted due to experimental problems. Details of the various tests carried out on the all samples are shown in Table 5.1. As an example, the result for mix 40/60 – 7 is presented in this chapter as an example for the CMT and fatigue and rest tests. The remaining results on the other mixtures are presented in the appendix.

Table 5.1. Details of the various tests carried out on the various samples

Sample	**CMT**	**Fatigue & Rest test**					
		Fatigue 1 & Rest 1	Fatigue 2 & Rest 2	Fatigue 3 & Rest 3	Fatigue 4 & Rest 4	Fatigue 5 & Rest 5	Fatigue 6
Mix 70/100 - 1	X	X	Failure during fatigue 2				
Mix 70/100 - 2	Sample unusable						
Mix 70/100 - 3	X	X	X	Failure during fatigue 3			
Mix 70/100 - 4	X	X	Failure during fatigue 2				
Mix 70/100 - 5	X	X	X	X	X	Failure during fatigue 4	
Mix 70/100 - 6	Sample unusable						
Mix 70/100 - 7	Sample unusable						
Mix 70/100 - 8	X	X	X	Failure during fatigue 3			
Mix 40/60 - 1	X	Test interrupted due to water supply cut					
Mix 40/60 - 2	X	Test interrupted due to water supply cut					
Mix 40/60 - 3	X	Test interrupted due to water supply cut					
Mix 40/60 - 4	X	X	X	X	X	X	X
Mix 40/60 - 5	X	X	X	X	X	X	X
Mix 40/60 - 6	X	X	X	X	X	X	X
Mix 40/60 - 7	X	X	X	X	X	X	X
Mix 40/60 - 8	X	X	X	X	X	X	X
Mix PMB - 1	X	X	X	Test interrupted by press			
Mix PMB - 2	X	X	X	X	X	X	X
Mix PMB - 3	X	Test interrupted due to water supply cut					
Mix PMB - 4	X	Test interrupted due to temperature chamber					
Mix PMB - 5	X	X	X	X	X	X	X
Mix PMB - 6	X	X	X	X	X	X	X
Mix PMB - 7	X	Test interrupted due to temperature chamber					
Mix PMB - 8	Sample not tested due to temperature chamber						

5.1. Evolution of 3D LVE properties (E*eq. and ν*eq.) with strain amplitude and temperature in undamaged condition.

According to the definition of viscoelasticity, complex modulus can be defined only if the behaviour of the material is linear viscoelastic, that is independent from strain amplitude. The results obtained show a variation of material stiffness with applied strain level. Stress and strain signals were treated cycle by cycle and could be fitted with sinusoidal functions with satisfactory quality. For this reason, an equivalent complex modulus and equivalent Poisson ratio could be determined for each loading cycle at varying strain levels. For more details, the reader can refer to (Mangiafico, 2014; Mangiafico et al., 2016; Williams et al., 2023). However, for simplicity "equivalent" for |E*| and |ν*| values were not mentioned throughout the whole chapter (and in conclusions).

The phenomenon of nonlinearity is believed to be the reliance of the material's stiffness on the loading level (also known as stress or strain dependence). Even at relatively small strain amplitudes, nonlinearity is likely to occur. When a material exhibits nonlinearity and is subjected to sinusoidal strain input, the stress output is anticipated to differ from the linear viscoelastic predicted response. This means that the loading level will affect both the ratio of stress amplitude to strain amplitude and their phase difference. This dependence on loading level is the objective of the investigation presented in this section. Amplitude sweeps, or tests with a few loading cycles at various stress or strain amplitude levels, are the most often used technique to look at nonlinearity in bituminous materials. However, the test is referred to as a strain amplitude sweep if the loading is controlled in the strain amplitude.

This section shows the CMT test results performed during the first part of the test protocol for mix 40/60 - 7 as an example. The results obtained for all tested samples are reported in the appendix. In particular, norm |E*| and phase angle φ_E of complex modulus and norm |ν*| and phase angle φ_ν of Poisson's ratio are plotted against strain amplitude ε_0. As observed, during the first part of all CMTs, strain level gradually increases to the imposed value as described in the test protocol in chapter 3. The results confirm the existence of nonlinear behaviour for bituminous mixtures even for small strain amplitudes as small. Therefore, the assumption of LVE behaviour can be accepted only as a first approximation. Depending on test temperature, complex modulus and Poisson's ratio follow a linear trend with strain level. The first and last cycles applied for each strain level were not considered and not plotted in the figures. Therefore, cycles 2 to 39 for each strain of each CMT were satisfactorily fitted with linear regression equations in order to obtain envelope lines of |E*|, φ_E, ν and φ_ν with ε_0 (indicated in figures 5.1

– 5.4) as functions of strain level, with strain points highlighted at 50 µm/m, 75 µm/m, 100 µm/m and 110 µm/m. The result obtained reinforces the existence nonlinearity, which has been defined as strain dependence of complex modulus (i.e. the higher the strain amplitude, the lower the norm of complex modulus and phase angle of Poisson's ratio with the higher the phase angle and Poisson's ratio). The linear regressions, hereafter named "non-linearity envelopes", obtained for each of the four test temperatures provide an estimation of the variation of $|E^*|$, φ_E, ν and φ_ν with ε_0. Consequently, the non-linearity coefficients corresponding to the variation of the desired LVE parameter with strain level and extrapolated values at 0 µm/m obtained for every temperature for $|E^*|$, φ_E, ν and φ_ν are expressed in equations 5.1 – 5.4:

$$|E^*| = S_E\,\varepsilon_0 + |E_0^*| \quad 5.1$$

$$\varphi_E = S_\varphi\,\varepsilon_0 + \varphi_{E0} \quad 5.2$$

$$|\nu^*| = S_\nu\,\varepsilon_0 + |\nu_0^*| \quad 5.3$$

$$\varphi_\nu = S_{\varphi\nu}\,\varepsilon_0 + \varphi_{\nu 0} \quad 5.4$$

where, S_E, S_φ, S_ν and $S_{\varphi\nu}$ are expressions of the non-linearity coefficients for $|E^*|$, φ_E, ν and φ_ν. Virtual 0 µm/m values of $|E_0^*|$, φ_{E0}, $|\nu_0^*|$ and $\varphi_{\nu 0}$ and ε_0 is the applied strain amplitude.

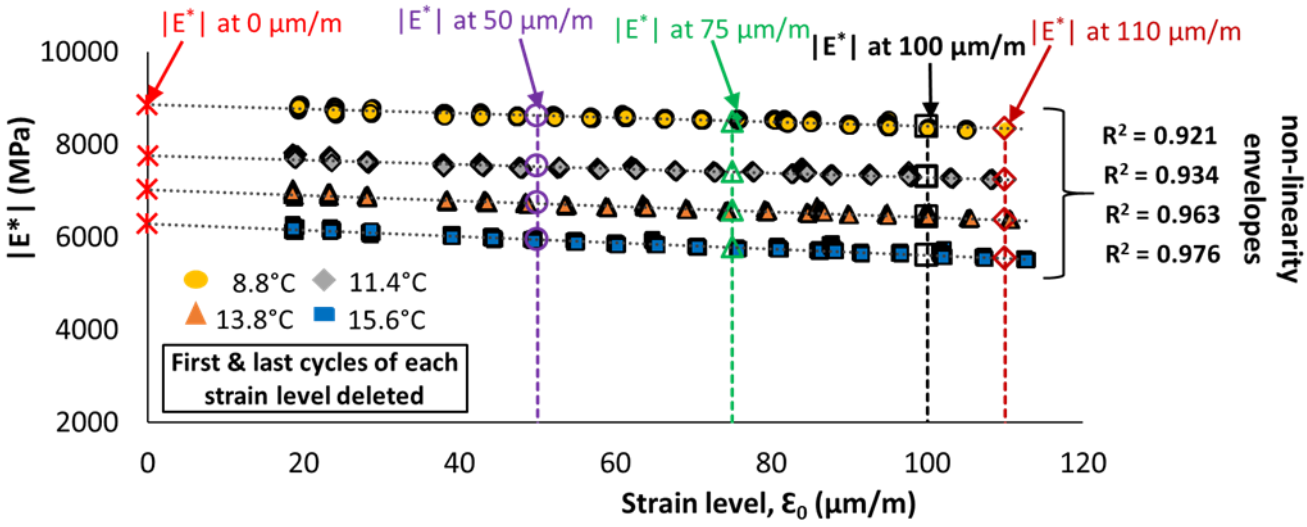

Figure 5.1. CMT results obtained for mix 40/60 - 7: $|E^*|$ against applied strain amplitude at different temperatures.

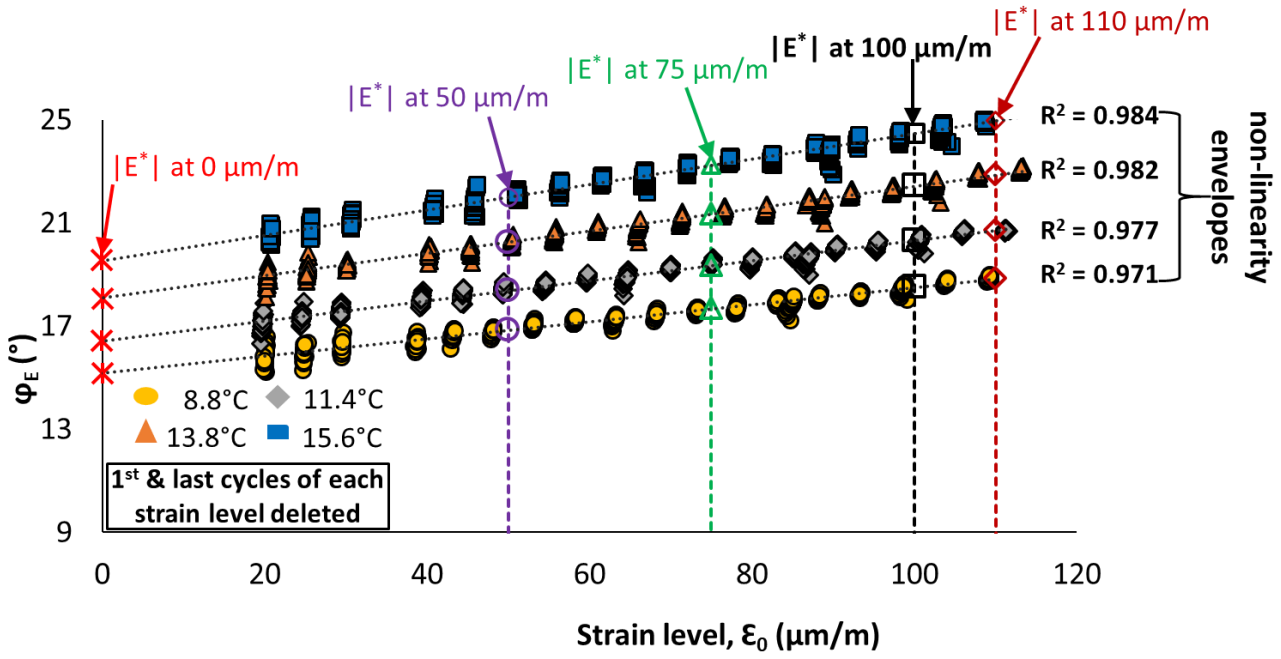

Figure 5.2. CMT results obtained for mix 40/60 - 7: φ_E against applied strain amplitude at different temperatures.

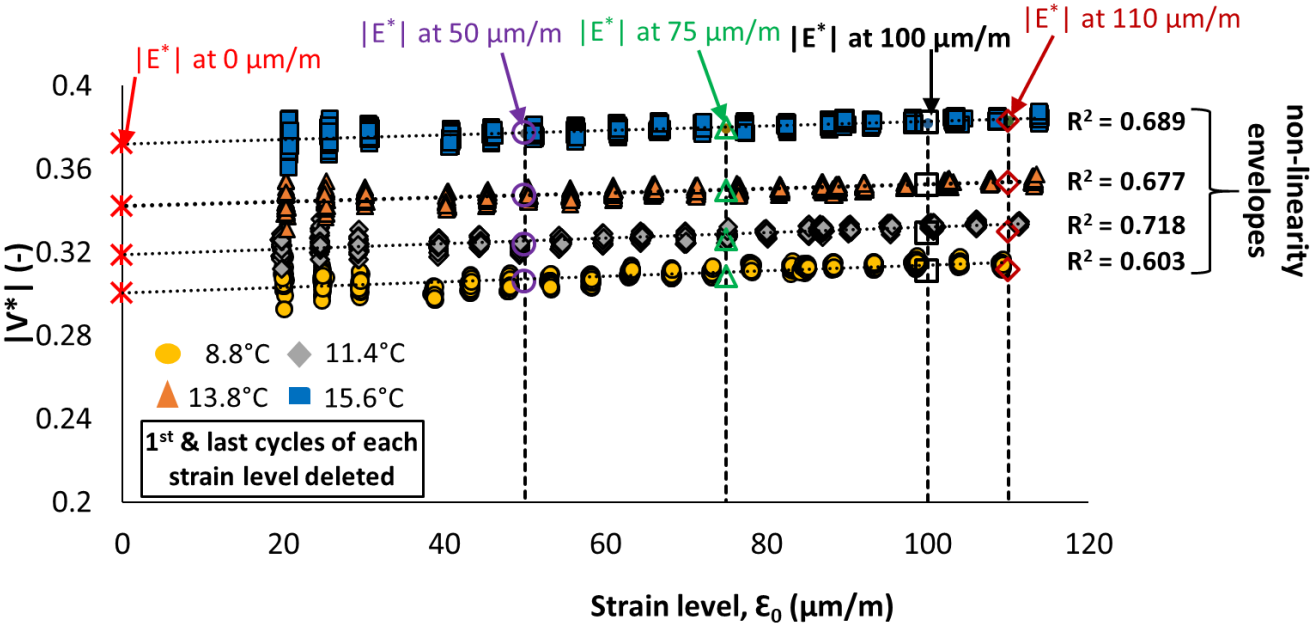

Figure 5.3. CMT results obtained for mix 40/60 - 7: |v*| against applied strain amplitude at different temperatures.

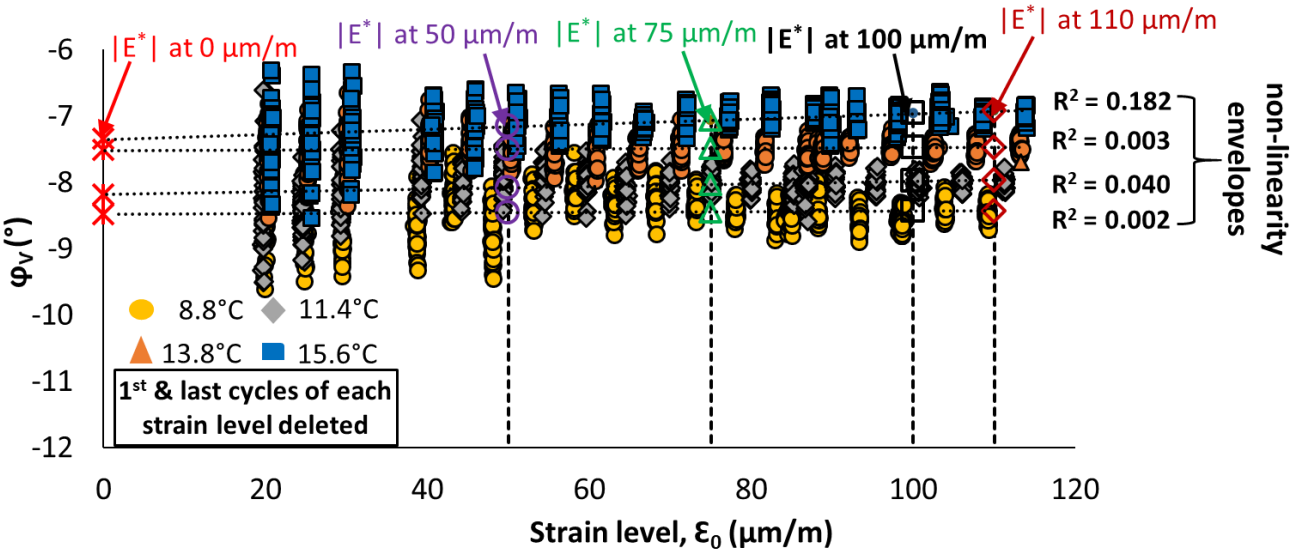

Figure 5.4. CMT results obtained for mix 40/60 - 7: φ_v against applied strain amplitude at different temperatures.

Figures 5.5 – 5.9 shows values of |E*|, φ_E, |v*| and φ_v calculated using envelopes (regression equations) plotted as functions of temperature, for values of strain amplitude equal to 50 µm/m, 75 µm/m, 100 µm/m and 110 µm/m. This is used to determine temperature-dependent mechanical properties of materials from known properties at reference temperatures. The result shows that with increase with loading rate but decrease when the temperature is increased Additionally, virtual values for 0 µm/m strain amplitude were calculated and plotted. For each strain amplitude, linear expressions were performed providing equations (equations 5.5 – 5.8) relating mechanical properties to temperature.

$$|E^*| = b_E + |E^*0°C| \quad 5.5$$

$$\varphi_E = b_{\varphi E} + |\varphi_E^*0°C| \quad 5.6$$

$$|v^*| = b_v + |v^*0°C| \quad 5.7$$

$$\varphi_v = b\,\varphi_v + |\varphi_v^*0°C| \quad 5.8$$

where b_E, $b_{\varphi E}$, b_v and $b_{\varphi v}$ are coefficients expressing the variation of mechanical properties (|E*|, φ_E, v and φ_v) with temperature in undamaged conditions ($|E_0^*|$, φ_{E0}, $|v_0^*|$ and φ_{v0}). The coefficient b_E, $b_{\varphi E}$, b_v and $b_{\varphi v}$ obtained at 100 µm/m were used in the analysis of the fatigue tests carried out during the second part of the test protocol, to estimate the influence of self-heating phenomenon during fatigue loading (and corresponding cooling of the sample during rest periods).

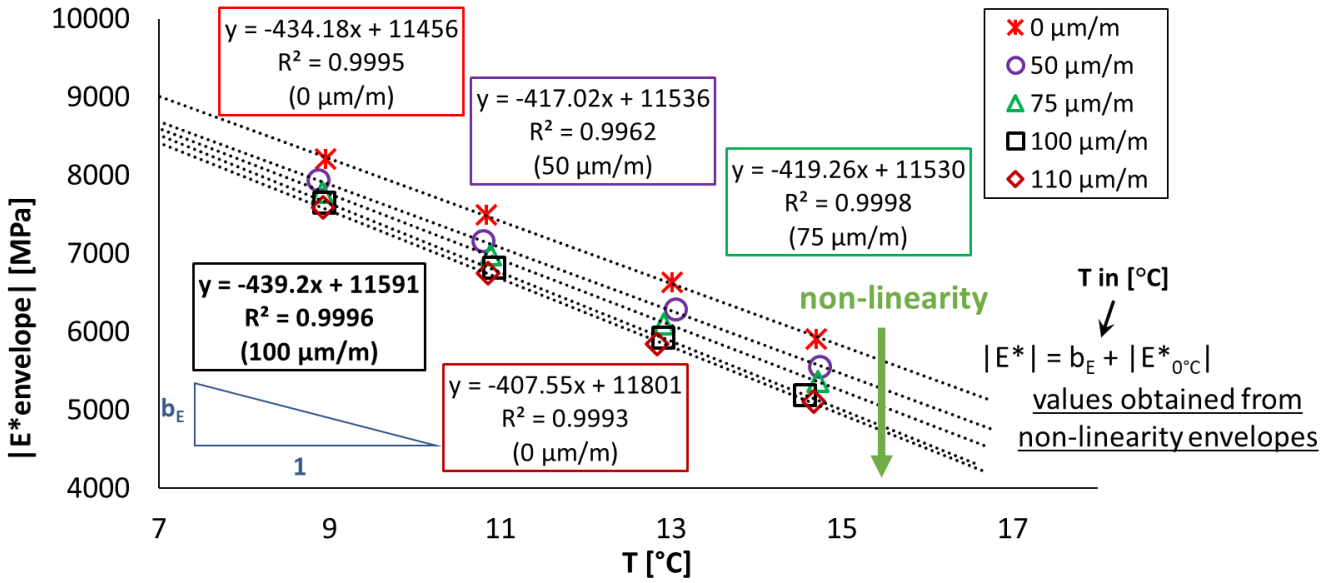

Figure 5.5. CMT results obtained for mix 40/60 - 7: Regression of estimated values of |E*| (from Figure 5.1) as a function of temperature.

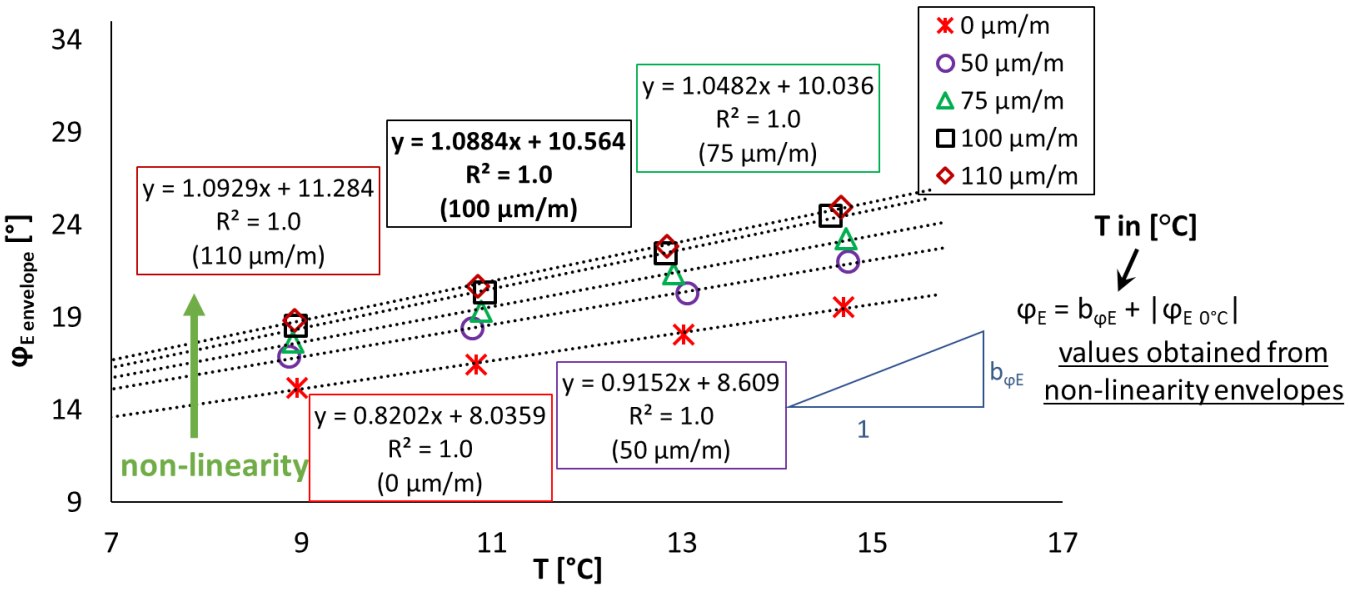

Figure 5.6. CMT results obtained for mix 40/60 - 7: Regression of estimated values of φ_E (from Figure 5.2) as a function of temperature.

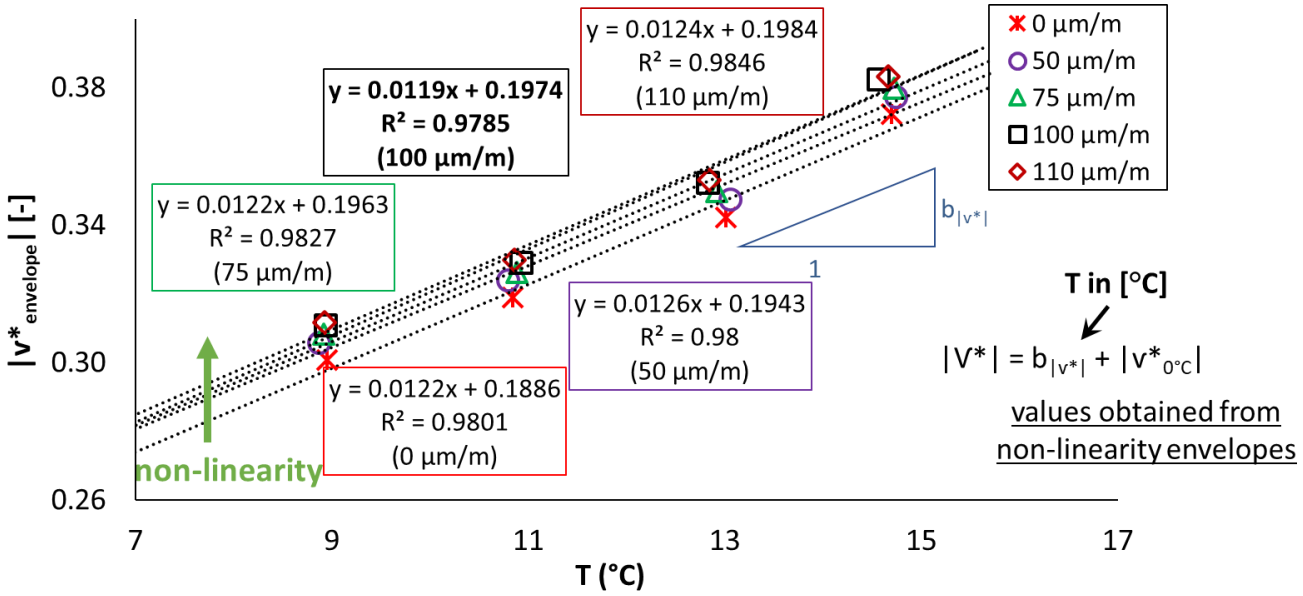

Figure 5.7. CMT results obtained for mix 40/60 - 7: Regression of estimated values of |v*| (from Figure 5.3) as a function of temperature.

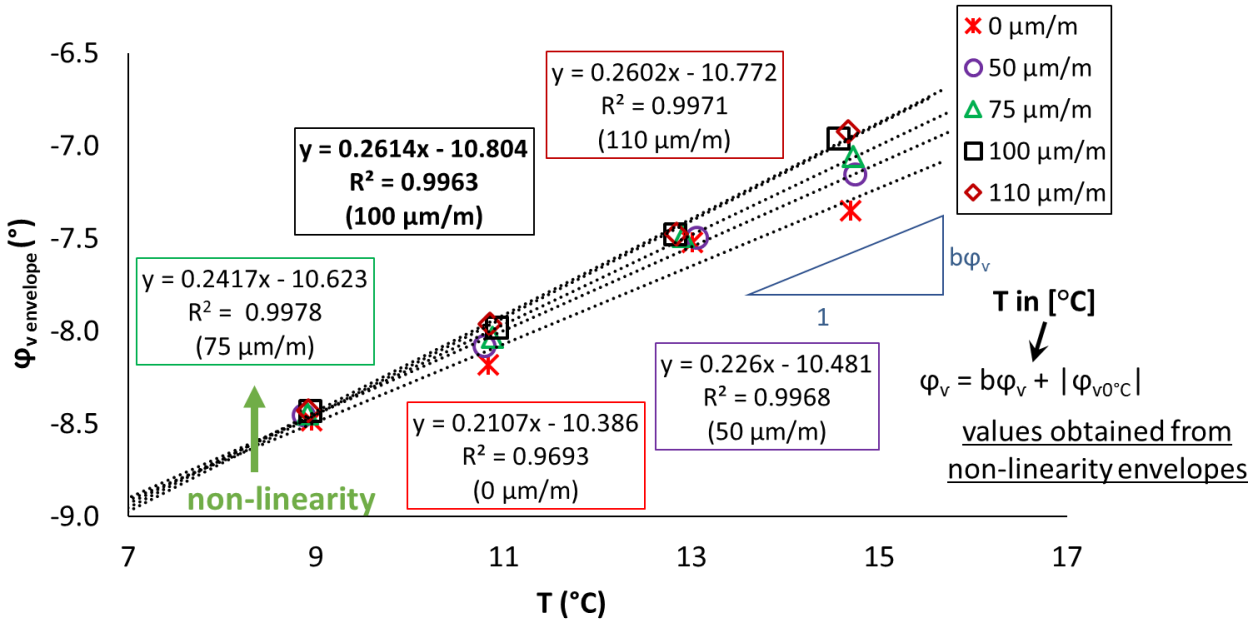

Figure 5.8. CMT results obtained for mix 40/60 - 7: Regression of estimated values of φ_v (from Figure 5.4) as a function of temperature.

This experimental approach was chosen over using any of the available viscoelastic models because this approach allows obtaining precise data for the tested specimen. Also, viscoelastic models simulate over long range of results which usually leads to getting estimated values.

Since the temperature utilised is relatively close and similar to the level used in fatigue tests (10°C), using the experimental approach becomes imperative for precise results to be obtained. Consequently, Complex modulus tests in undamaged conditions allowed studying the variation of |E*|, φE, |ν*| and φν with strain amplitude and temperature. Regression equations were successfully fitted and coefficients bE, bφ, bν and bφν were successfully determined to estimate the influence of non-linearity and self-heating phenomena during cyclic loading tests for |E*|, φE, |ν*| and φν, respectively.

5.2. Evolution of 3D mechanical properties (E*eq. and ν*eq.) during cyclic loading and rest periods

5.2.1. Effect of rest periods.

This is carried out as a basis to quantitatively estimate different reversible phenomenon and unrecovered LVE parameter variation during cyclic loading and rest periods. Figures 5.9, 5.10, 5.11 and 5.12 show the results of the PFRT performed for mix 40/60 - 7 during the second part of the test protocol. In Figures 5.9, 5.10, 5.11 and 5.12, |E*|, φ_E, |ν*| and φ_ν obtained during the various fatigue and rest periods with a final fatigue afterwards are presented. In particular, for each figure, figures (a) shows |E*|, φ_E, |ν*| and φ_ν as a function of time during the first fatigue lag and rest period, (b) show the results of the first fatigue lag and the following rest period plotted against time and strain amplitude and (c) |E*|, φ_E, |ν*| and φ_ν as a function of time during the five fatigue lags and rest periods., respectively, in order to present the analysis performed. Grey circles represent data obtained during the first 48 cycles of each fatigue lag, at varying strain amplitude, blue circles represent data obtained during the remaining 99,952 cycles of each fatigue lag and orange circles represent data obtained during the short complex modulus tests performed within the 48h rest periods, at different times. Values of |E*|, φ_E, |ν*| and φ_ν obtained during cycles 2-48 of each fatigue lag were fitted with non-linearity envelope by linear regression, in order to estimate their variation at the beginning of the fatigue lag due to non-linearity. The red star indicates the value of |E*| estimated at 100 µm/m at the beginning of the first fatigue lag, while the purple diamond indicate the value of |E*| estimated at 50 µm/m, then the green asterisks show values of Δ|E*heating| (E* corrected from self-heating during rest periods and then the brown triangles indicate values of |E*| estimated at 100 µm/m for each short complex modulus test during rest periods

Figure 5.13 shows temperature measurements for mix 40/60 - 7 while temperature data measured during tests on all mixtures are shown in Appendix. Surface and internal temperature of samples were continuously recorded in order to monitor the self-heating phenomenon. Surface and internal temperatures of the sample increase rapidly during loading. The increase of internal temperature is obviously more important than the one of surface temperature due to heat dispersion in the thermal chamber. Average temperature values recording during the 100 cycles (that is from 1 to 100 cycles) were considered for complex modulus tests during rest periods. Specifically, internal temperature was found to increase by approximately 0.9 - 1.2 °C during fatigue lags and to rapidly (less than 2 hours) return to its initial value during rest periods. For each i-th fatigue lag, the corresponding variations of E* and ν* due to self-heating (increase during loading, decrease during rest), $\Delta|E^*_{\text{heating, lag i}}|$, $\Delta\varphi_{E\text{heating, lag i}}$, $\Delta|\nu^*|_{\text{heating, lag i}}$ and $\Delta\varphi_{\nu\ \text{heating, lag i}}$ were estimated using the coefficients b_E, $b_{\varphi E}$, b_ν and $b_{\varphi\nu}$ of Equations 5.1, 5.2, 5.3 and 5.4 as functions of the variation of internal temperature ΔT. However, detailed explanation, with equations are indicated in section 5.2.2.

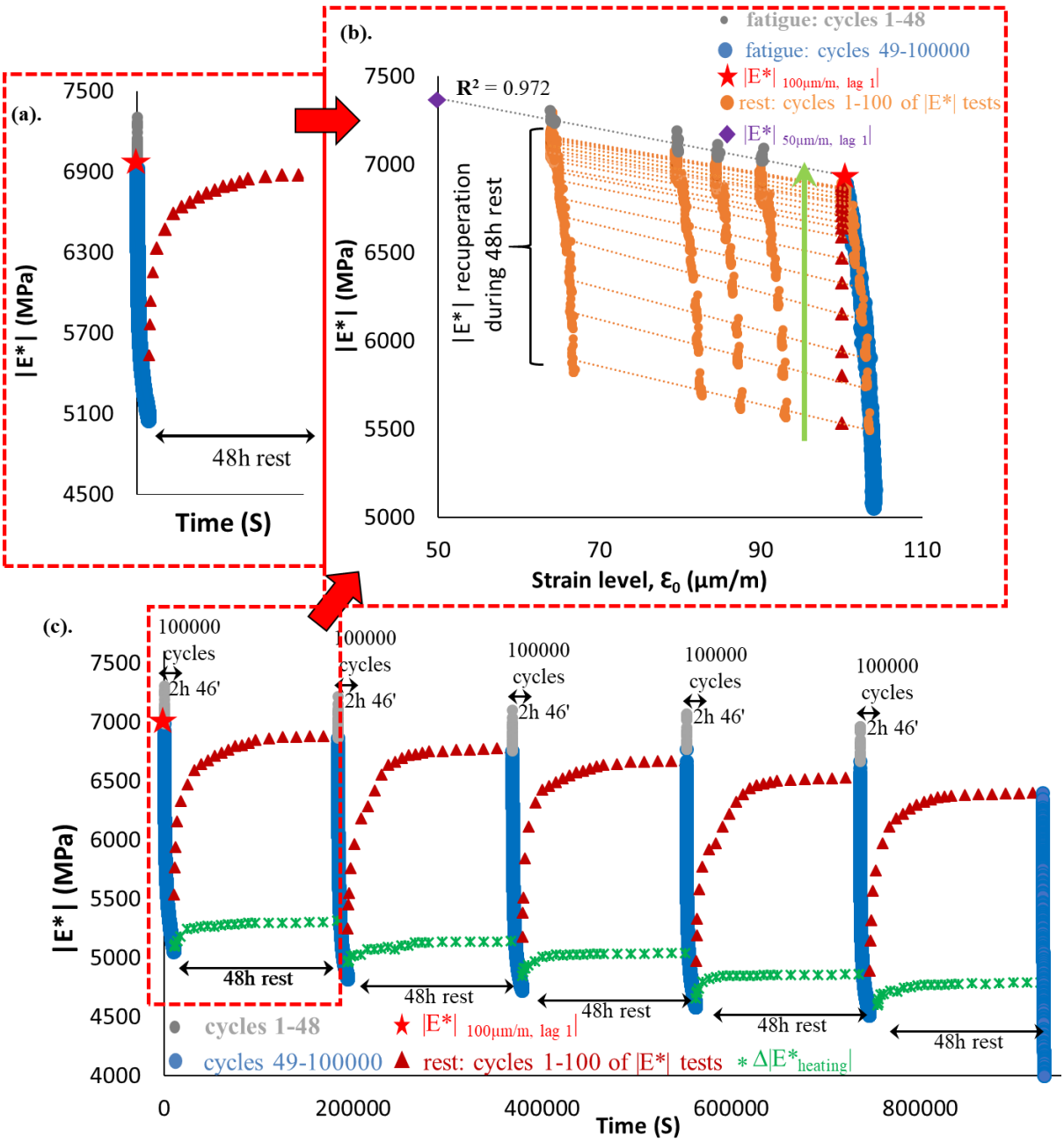

Figure 5.9. PFRT results obtained for mix 40/60 – 7: |E*| evolution during fatigue lags and recovery periods. The red star indicates the value of |E*| estimated at 100 µm/m at the beginning of the first fatigue lag, purple diamond indicates the value of |E*| estimated at 50 µm/m, green asterisks show values of $\Delta|E^*_{heating}|$ and brown triangles indicate values of |E*| estimated at 100 µm/m, after 48 hours of recovery, with non-linearity envelope.

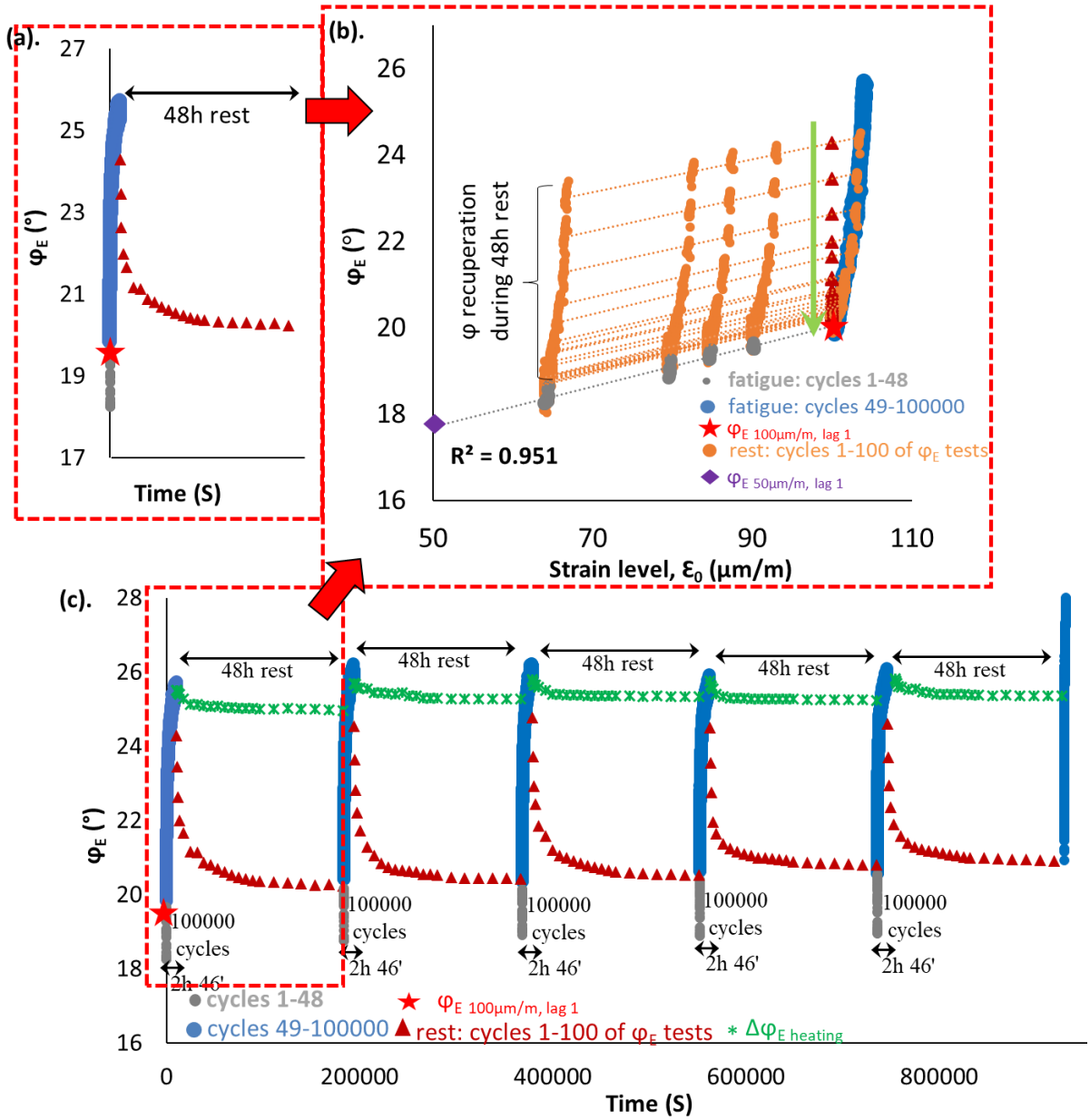

Figure 5.10. PFRT results obtained for mix 40/60 – 7: φ_E evolution during fatigue lags and recovery periods. The red star indicates the value of φ_E estimated at 100 µm/m at the beginning of the first fatigue lag, purple diamond indicates the value of φ_E estimated at 50 µm/m, green asterisks show values of $\Delta \varphi_{E\ heating}$ and brown triangles indicate values of φ_E estimated at 100 µm/m, after 48 hours of recovery, with non-linearity envelope.

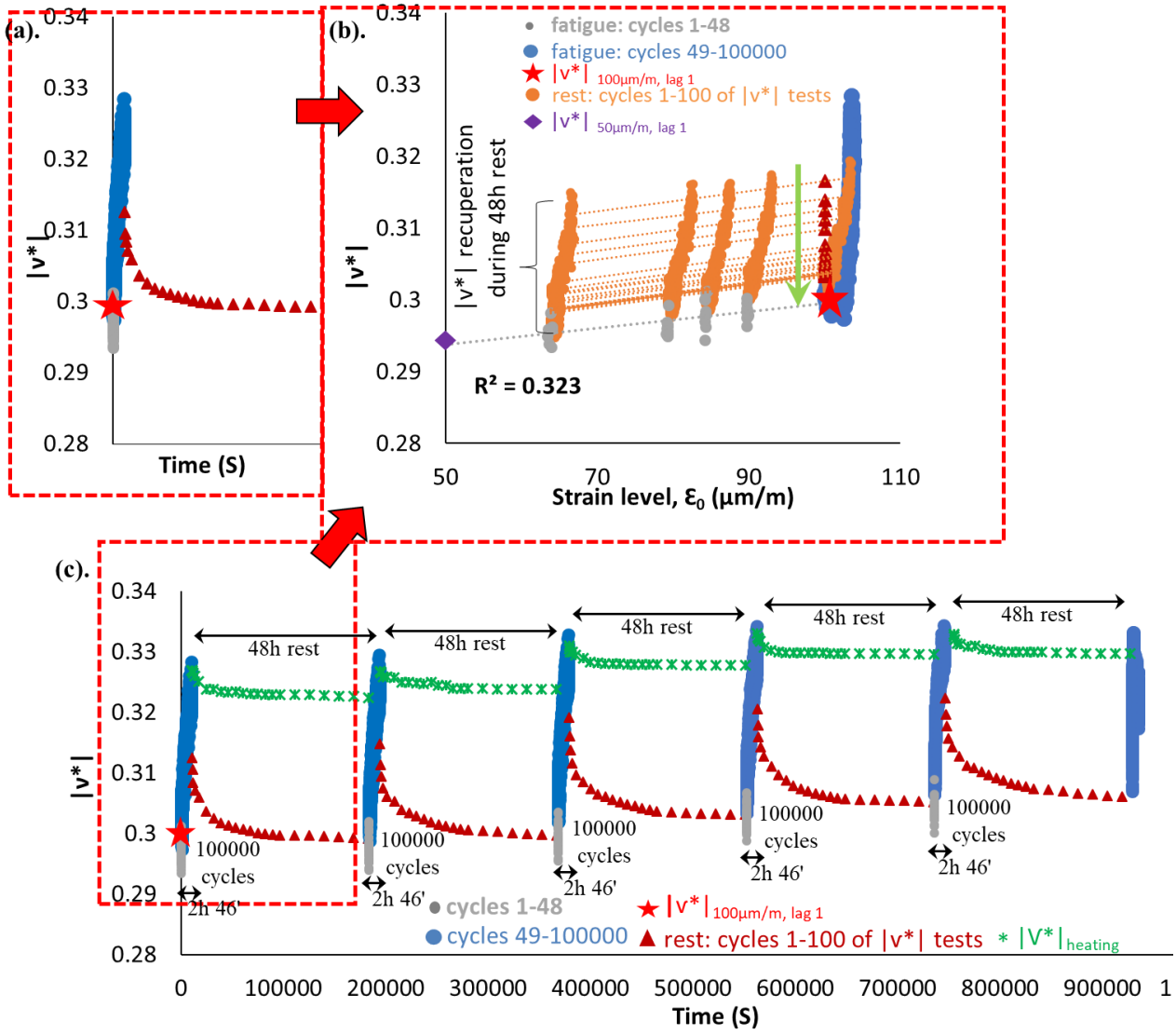

Figure 5.11. PFRT results obtained for mix 40/60 – 7: |v*| evolution during fatigue lags and recovery periods. The red star indicates the value of |v*| estimated at 100 µm/m at the beginning of the first fatigue lag, purple diamond indicates the value of |v*| estimated at 50 µm/m, green asterisks show values of $\Delta|v^*_{heating}|$ and brown triangles indicate values of |v*| estimated at 100 µm/m, after 48 hours of recovery, with non-linearity envelope.

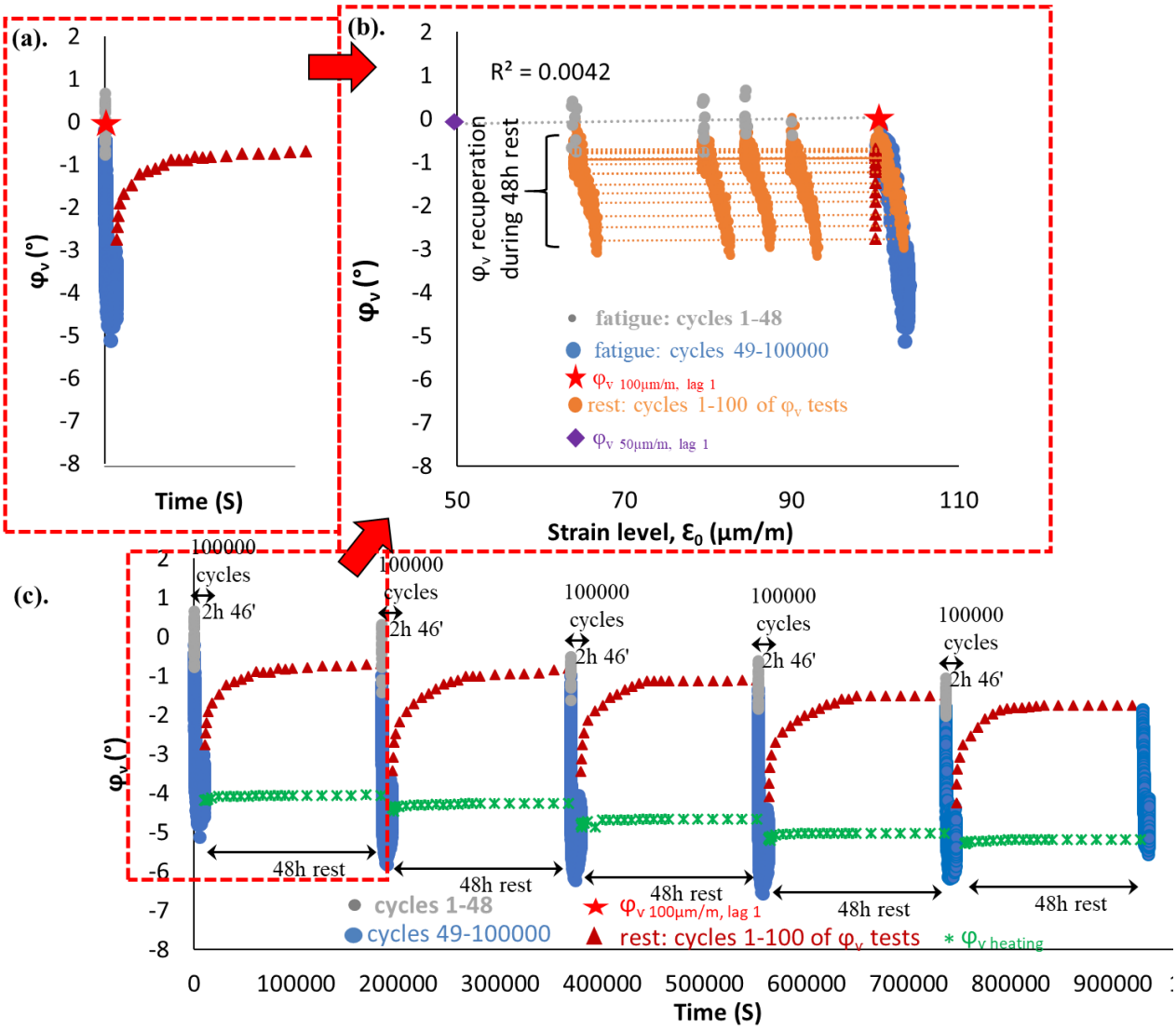

Figure 5.12. PFRT results obtained for mix 40/60 – 7: φ_v evolution during fatigue lags and recovery periods. The red star indicates the value of φ_v estimated at 100 µm/m at the beginning of the first fatigue lag, purple diamond indicates the value of φ_v estimated at 50 µm/m, green asterisks show values of $\Delta\varphi_{v\ heating}$ and brown triangles indicate values of φ_v estimated at 100 µm/m, after 48 hours of recovery, with non-linearity envelope.

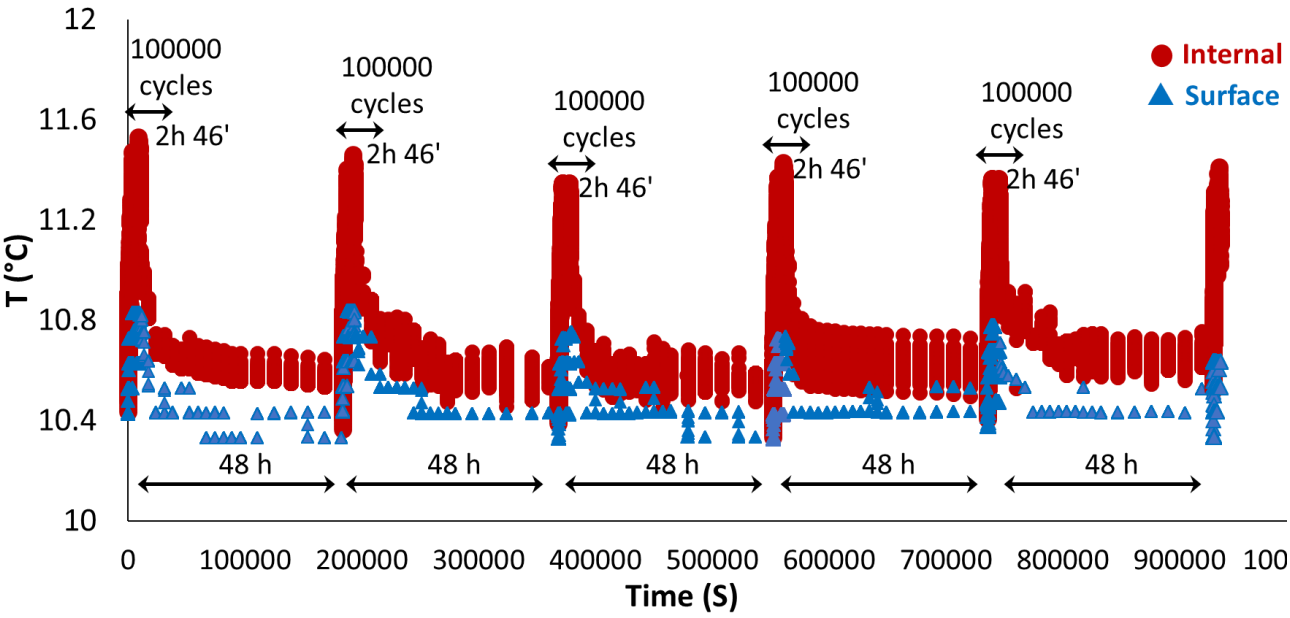

Figure 5.13. PFRT results obtained for mix 40/60 - 7: internal and surface temperature evolution during fatigue lags and recovery periods.

From figures 5.9 – 5.12, the following observations can be made on $|E^*|$, φ_E, $|\nu^*|$ and φ_ν evolution:

- Variations of $|E^*|$, φ_E, $|\nu^*|$ and φ_ν during each fatigue period are almost entirely recovered during rest periods which is shown by the orange circles representing data obtained during the short complex modulus tests performed within the 48h rest periods.
- $|\nu^*|$ and φ_ν slightly increase and decrease, respectively, during loading periods. The relative changes of $|\nu^*|$ and φ_ν seem to be less important than those of $|E^*|$ and φ_E. For example, during each loading period, $|E^*|$ decrease is about 40% of the initial modulus and the increase in φ_E is about 7°. Meanwhile, the increase of $|\nu^*|$ is only 10% and the decrease in φ_ν is around 4°.
- Data obtained during the first 48 cycles of each fatigue lag, which is considered the effect of nonlinearity of $|E^*|$, φ_E, $|\nu^*|$ and φ_ν for the various fatigue lags, appear to contribute small effects of the total $|E^*|$, φ_E, $|\nu^*|$ and φ_ν variations during each fatigue lag.
- The effects of self-heating on $|E^*|$, φ_E, $|\nu^*|$ and φ_ν variations during fatigue tests, which is represented by the green asterisks also contribute small effects of the total $|E^*|$, φ_E, $|\nu^*|$ and φ_ν variations during each fatigue lag.

- The effects of thixotropy on |E*|, φ_E, |ν*| and φ_ν variations during fatigue tests, which is represented by the blue circles shows data obtained during the remaining 99,952 cycles of each fatigue lag, seem to be significant and very important for |E*|, φ_E, |ν*| and φ_ν. However, this effect appears to be more important for |E*| and φ_E than for |ν*| and $\varphi_{\nu.}$

Also, Figure 5.14 – 5.17 shows results of PFRT results of |E*| and φ_E obtained for mix 70/100 - 1 and mix PMB - 6 as examples with other results presented in the appendix. As shown in Figure 5.14 and 5.15, mix 70/100 - 1 experienced premature failure during fatigue lag 2 but very rapid recovery while mix PMB – 6 went through all the fatigue lags. As observed, the three considered mixtures show different relative proportions of these reversible phenomenon effects. The unrecovered variations of |E*| and φ_E are although small for all materials but most for mix 70/100 - 1.

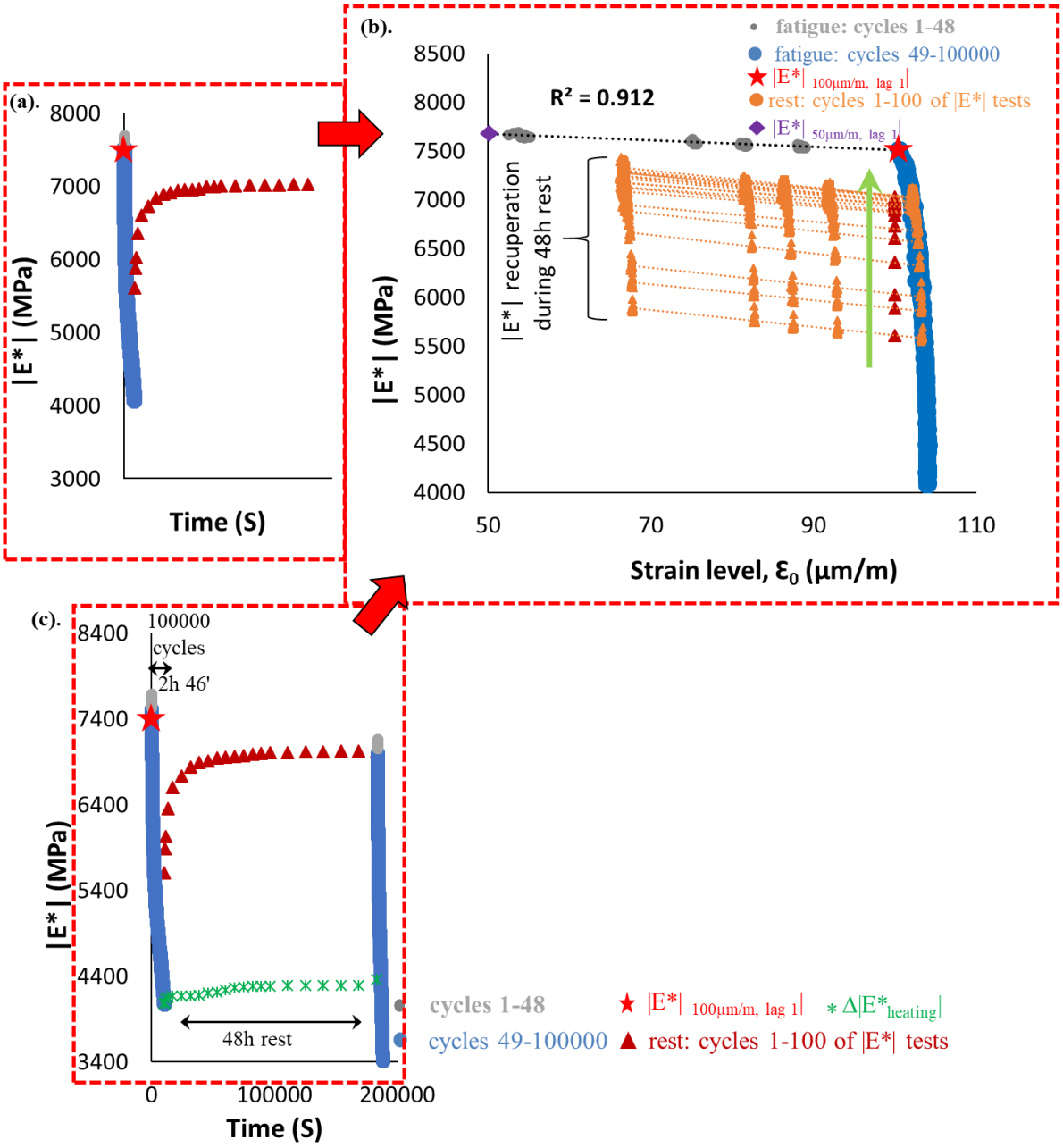

Figure 5.14. PFRT results obtained for mix 70/100 - 1: |E*| evolution during fatigue lags and recovery periods. The red star indicates the value of |E*| estimated at 100 µm/m at the beginning of the first fatigue lag, purple diamond indicate the value of |E*| estimated at 50 µm/m, green asterisks show values of Δ|E*heating| (E* corrected from self-heating during rest periods, explained afterwards in this chapter) and brown triangles indicate values of |E*| estimated at 100 µm/m, after 48 hours of recovery, with non-linearity envelope.

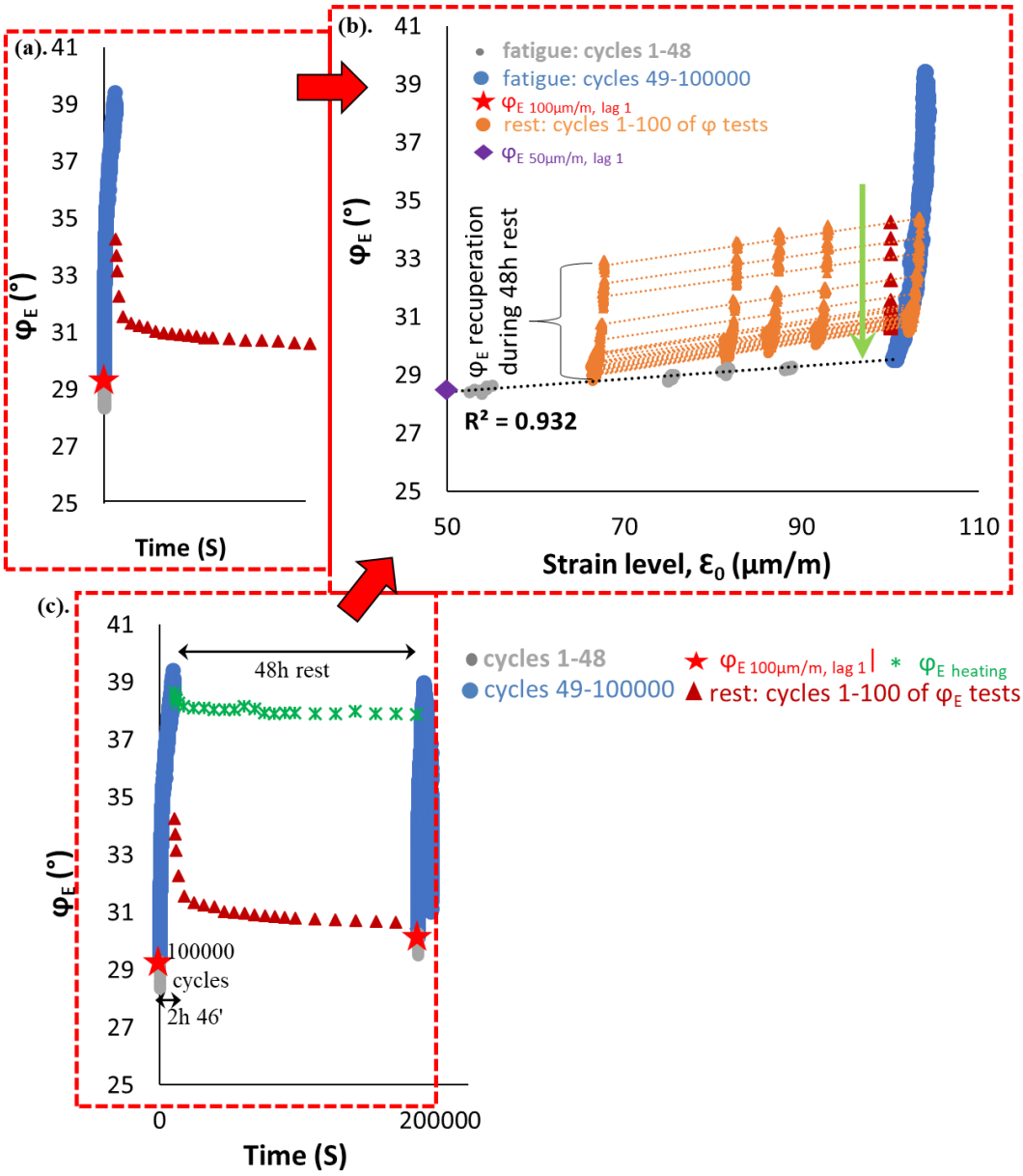

Figure 5.15. PFRT results obtained for mix 70/100 – 1: (a) φ_E evolution during fatigue lags and recovery periods. The red star indicates the value of φ_E estimated at 100 µm/m at the beginning of the first fatigue lag, purple diamond indicates the value of φ_E estimated at 50 µm/m, green asterisks show values of $\Delta\ \varphi_{E\ heating}$ (φ_E corrected from self-heating during rest periods, explained afterwards in this chapter) and brown triangles indicate values of φ_E estimated at 100 µm/m, after 48 hours of recovery, with non-linearity envelope.

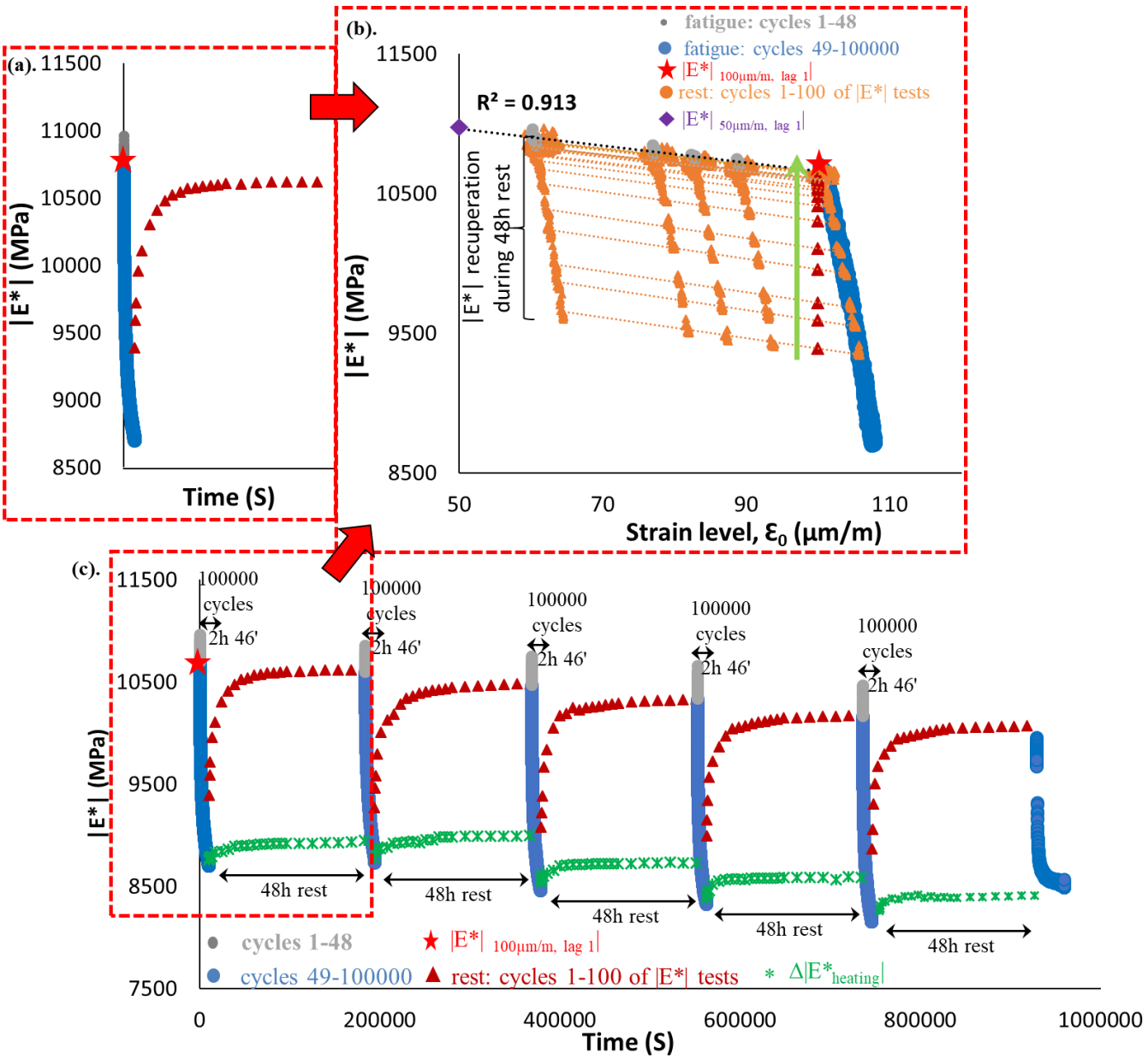

Figure 5.16. PFRT results obtained for mix PMB - 6: (a) |E*| evolution during fatigue lags and recovery periods. The red star indicates the value of |E*| estimated at 100 µm/m at the beginning of the first fatigue lag, purple diamond indicate the value of |E*| estimated at 50 µm/m, green asterisks show values of Δ|E*heating| (E* corrected from self-heating during rest periods, explained afterwards in this chapter) and brown triangles indicate values of |E*| estimated at 100 µm/m, after 48 hours of recovery, with non-linearity envelope.

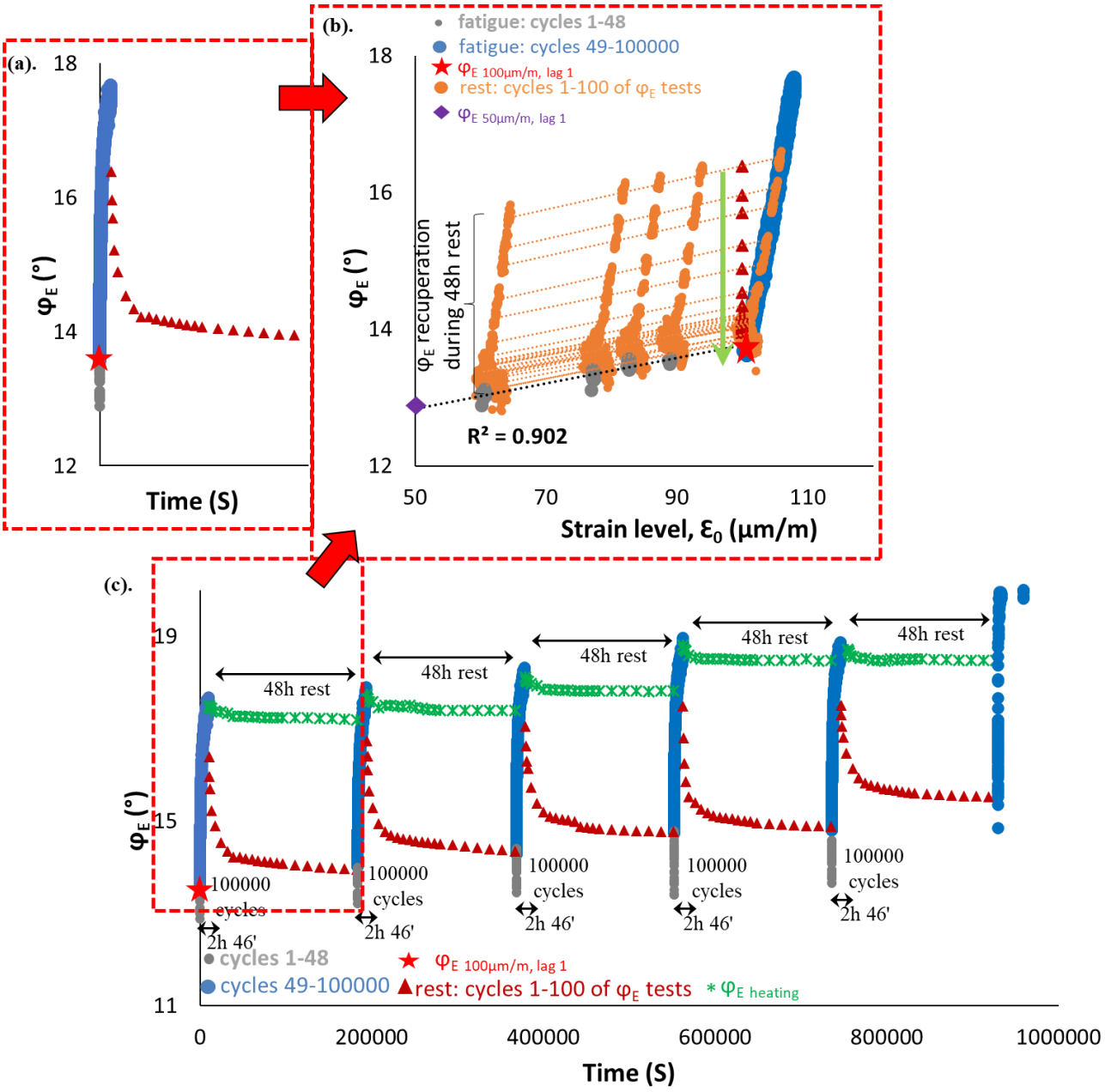

Figure 5.17. PFRT results obtained for mix PMB - 6: (a) φ_E evolution during fatigue lags and recovery periods. The red star indicates the value of φ_E estimated at 100 µm/m at the beginning of the first fatigue lag, purple diamond indicates the value of φ_E estimated at 50 µm/m, green asterisks show values of $\Delta\ \varphi_{E\ heating}$ (φ_E corrected from self-heating during rest periods, explained afterwards in this chapter) and brown triangles indicate values of φ_E estimated at 100 µm/m, after 48 hours of recovery, with non-linearity envelope.

5.2.2. Quantification of different reversible phenomena to 3D properties (E*eq. and ν*eq.) for each fatigue lag

The estimations of the contributions of the different phenomena (non-linearity, self-heating, thixotropy and unrecovered variation) to the variations of $|E^*|$, φ_E, $|\nu^*|$ and φ_ν of mix 40/60 - 7 during the first and second fatigue lags are graphically shown in Figures 5.18 to figure 5.21. The complete representation of the results obtained during all fatigue and rest periods for this test and all the other samples and mixtures can be found in the appendix.

The envelopes of the each i-th fatigue lag were used to estimate $|E^*|$, φ_E, $|\nu^*|$ and φ_ν values corresponding to 50 µm/m and 100 µm/m strain amplitude ($|E^*_{50\mu m/m,\ lag\ i}|$, $|E^*_{100\mu m/m,\ lag\ i}|$, $\varphi_{E50\mu m/m,\ lag\ i}|$, $\varphi_{E100\mu m/m,\ lag\ 1,}$ $|\nu^*_{50\mu m/m,\ lag\ i}|$, $|\nu^*_{100\mu m/m,\ lag\ i|}$ and $\varphi_{\nu 50\mu m/m,\ lag\ i}$, $\varphi_{\nu 100\mu m/m,\ lag\ i}$).
For any i-th fatigue lag, the influence of non-linearity, $\Delta|E^*_{nonlinearity}|$, $\Delta\varphi_{Enonlinearity}$, $\Delta|\nu^*_{nonlinearity}|$ and $\Delta\varphi_{\nu nonlinearity}$ was calculated as the difference between these values:

$$\Delta|E^*_{nonlinearity}| = |E^*_{50\mu m/m,\ lag\ i}| - |E^*_{100\mu m/m,\ lag\ i}| \quad 5.9$$

$$\Delta\varphi_{Enonlinearity} = \varphi_{E50\mu m/m,\ lag\ i} - \varphi_{E100\mu m/m,\ lag\ i} \quad 5.10$$

$$\Delta|\nu^*_{nonlinearity}| = |\nu^*_{50\mu m/m,\ lag\ i}| - |\nu^*_{100\mu m/m,\ lag\ i}| \quad 5.11$$

$$\Delta\varphi_{\nu nonlinearity} = \varphi_{\nu 50\mu m/m,\ lag\ i} - \varphi_{\nu 100\mu m/m,\ lag\ i} \quad 5.12$$

For each i-th fatigue lag and corresponding 48-hour rest period, it was possible to estimate the unrecovered variations of $|E^*|$, φ_E, $|\nu^*|$ and φ_ν, $\Delta|E^*_{unrecovered\ 48\ h,\ lag\ i}|$, $\Delta\varphi_{Eunrecovered\ 48\ h,\ lag\ i}$, $\Delta|\nu^*_{unrecovered}|$ and $\Delta\varphi_{\nu unrecovered}$ respectively, at the end of the rest period with respect to $|E^*_{100\mu m/m,\ lag\ i}|$, $\varphi_{E100\mu m/m,\ lag\ i}$, $|\nu^*_{100\mu m/m,\ lag\ i|}$ and $\varphi_{\nu 100\mu m/m,\ lag\ i}$ (the values of $|E^*|$, φ_E, $|\nu^*|$ and φ_ν estimated at 100 µm/m at the beginning of the first fatigue lag), considered as the undamaged condition:

$$\Delta|E^*_{unrecovered\ 48\ h,\ lag\ i}| = |E^*_{100\mu m/m,\ 48\ h,\ rest\ i}| - |E^*_{100\mu m/m,\ lag\ i}| \quad 5.13$$

$$\Delta\varphi_{Eunrecovered\ 48\ h,\ lag\ i} = \varphi_{E100\mu m/m,\ 48\ h,\ rest\ i} - \varphi_{E100\mu m/m,\ lag\ i} \quad 5.14$$

$$\Delta|\nu^*_{unrecovered\ 48\ h,\ lag\ i}| = |\nu^*_{100\mu m/m,\ 48\ h,\ rest\ i}| - |\nu^*_{100\mu m/m,\ lag\ i}| \quad 5.15$$

$$\Delta\varphi_{\nu unrecovered\ 48\ h,\ lag\ i} = \varphi_{\nu 100\mu m/m,\ 48\ h,\ rest\ i} - \varphi_{\nu 100\mu m/m,\ lag\ i} \quad 5.16$$

where $|E^*_{100\mu m/m,\ 48\ h,\ rest\ i}|$, $\varphi_{E100\mu m/m,\ 48\ h,\ rest\ i,}$ $|\nu^*_{100\mu m/m,\ 48\ h,\ rest\ i}|$ and $\varphi_{\nu 100\mu m/m,\ 48\ h,\ rest\ i}$ are the values of $|E^*|$, φ_E, $|\nu^*|$ and φ_ν, respectively, estimated at 100µm/m (using the non-linearity envelopes,

as shown in Figure 5.9 to 5.12) during the last short complex modulus test, after 48 hours, of each i-th rest period.

The effect due to self-heating were estimated from temperature variations using coefficients estimated in section 5.1 (figures 5.5 to 5.9). Therefore, for any i-th fatigue lag, ΔTlag i was evaluated for the cooling of the sample during rest (respectively $\Delta|E^*_{heating}|$, $\Delta\varphi_{Eheating}$, $\Delta|v^*_{heating}|$ and $\Delta\varphi_{vheating}$) as the difference between the temperature at the end of the fatigue lag (100,000th cycle) and the temperature during the last complex modulus and phase angle test at the end of the 48-hour rest period:

$$\Delta|E^*_{heating}| = -\, b_E\, \Delta T_{lag\ i} \quad 5.17$$

$$\Delta\varphi_{Eheating} = -\, b_\varphi\, \Delta T_{lag\ i} \quad 5.18$$

$$\Delta|v^*_{heating}| = -\, b_v\, \Delta T_{lag\ i} \quad 5.19$$

$$\Delta\varphi_{vheating} = -\, b\varphi_v\, \Delta T_{lag\ i} \quad 5.20$$

During any i-th fatigue lag, the influence of thixotropy on |E*|, φ_E, |v*| and φ_v variations (respectively $\Delta|E^*_{thixotropy}|$, $\Delta\varphi_{Ethixotropy}$, $\Delta|v^*_{thixotropy}|$ and $\Delta\varphi_{vthixotropy}$) was considered as the remaining part of the recovered variation of |E*|, φ_E, |v*| and φ_v. As a result, Equations 5.21, 5.22, 5.23 and 5.24 are used to calculate $\Delta|E^*_{thixotropy}|$, $\Delta\varphi_{Ethixotropy}$, $\Delta|v^*_{thixotropy}|$ and $\Delta\varphi_{vthixotropy}$:

$$\Delta|E^*_{thixotropy}| = |E^*_{100{,}000\ cycles,\ lag\ i}| - |E^*_{100\mu m/m,\ 48\ h,\ rest}| - \Delta|E^*_{heating}| \quad 5.21$$

$$\Delta\varphi_{Ethixotropy} = \varphi_{E100{,}000\ cycles,\ lag\ i} - \varphi_{E\ 4100\mu m/m,\ 8\ h,\ rest} - \Delta\varphi_{Eheating} \quad 5.22$$

$$\Delta|v^*_{thixotropy}| = |v^*_{100{,}000\ cycles,\ lag\ i}| - |v^*_{100\mu m/m,\ 48\ h,\ rest}| - |v^*_{heating}| \quad 5.23$$

$$\Delta\varphi_{vthixotropy} = \varphi_{v100{,}000\ cycles,\ lag\ i} - \varphi_{v\ 100\mu m/m\ 48\ h,\ rest} - \varphi_{vheating} \quad 5.24$$

where $|E^*_{100000\ cycles,\ lag\ i}|$, $\varphi_{E100{,}000\ cycles,\ lag\ I}$, $|v^*_{thixotropy}|$ and $\varphi_{vthixotropy}$ are the last values of |E*|, φ_E, |v*| and φ_v obtained at the end of any i-th fatigue lag (100,000th cycle).

Also, the difference between envelopes obtained during any i-th fatigue lag and the envelopes of the first fatigue lag (considered as the undamaged condition) were calculated as in Equations 5.21, 5.22, 5.23 and 5.24:

$$|E^*_{envel.diff.,\ lag\ i|} = |E^*_{100{,}000\ cycles,\ lag\ i}| - |E^*_{100{,}000\ cycles,\ lag\ 1}| \quad 5.25$$

$$\varphi_{Eenvel.diff.,\ lag\ i} = \varphi_{E100{,}000\ cycles,\ lag\ i} - \varphi_{E100{,}000\ cycles,\ lag\ 1} \quad 5.26$$

$$|v^*_{envel.diff.,\ lag\ i|} = v_{100{,}000\ cycles,\ lag\ i} - v_{100{,}000\ cycles,\ lag\ 1} \quad 5.27$$

$$\varphi_{venvel.diff.} = \varphi_{v100,000\ cycles,\ lag\ i} - \varphi_{v100,000\ cycles,\ lag\ 1} \quad 5.28$$

Each fatigue (and rest) lag is considered separately, according to its envelope. $|E^*|$, φ_E, ν and φ_v total variations (respectively, $\Delta|E^*_{total}|$, $\Delta\varphi_{total}$, $\Delta\nu_{total}$ and $\Delta\varphi_{vtotal}$) are calculated as in, respectively, Equations 5.25, 5.26, 5.27 and 5.28:

$$\Delta|E^*_{total,\ lag\ i}| = |E^*_{100,000\ cycles,\ lag\ i}| - |E^*_{50\mu m/m,\ lag\ i}| \quad 5.29$$

$$\Delta\varphi_{Etotal,\ lag\ i} = \varphi_{E100,000\ cycles,\ lag\ i} - \varphi_{E50\mu m/m,\ lag\ i} \quad 5.30$$

$$\Delta|\nu^*_{total,\ lag\ i}| = |\nu^*_{100,000\ cycles,\ lag\ i}| - |\nu^*_{50\mu m/m,\ lag\ i}| \quad 5.31$$

$$\Delta\varphi_{vtotal,\ lag\ i} = \varphi_{v100,000\ cycles,\ lag\ i} - \varphi_{v50\mu m/m,\ lag\ 1} \quad 5.32$$

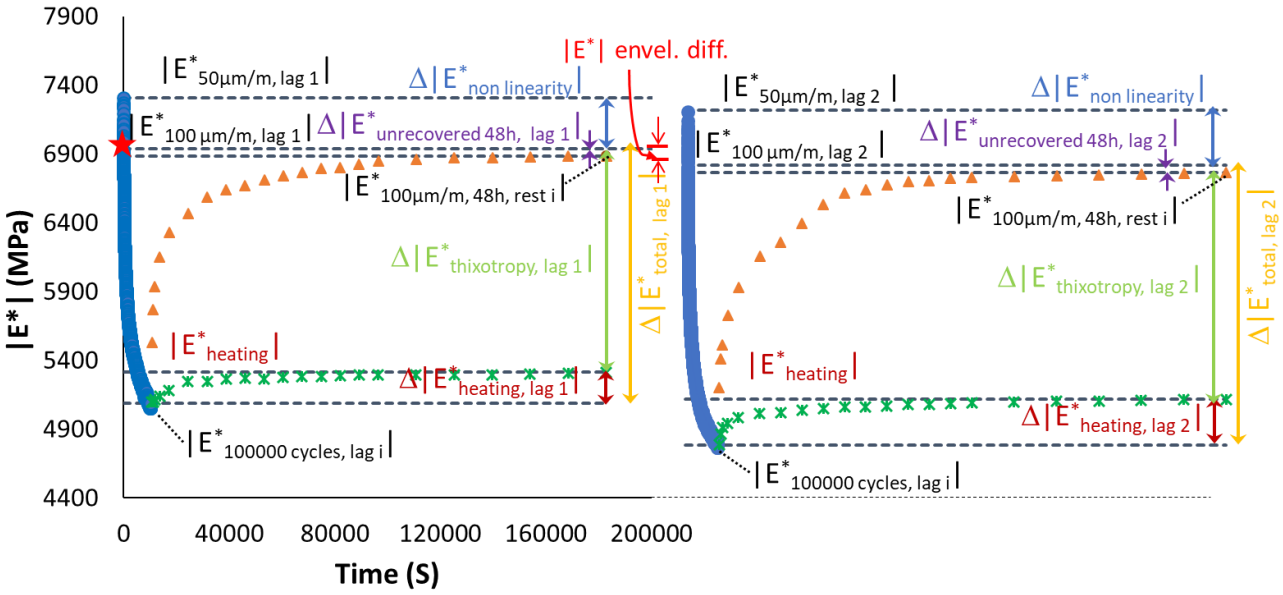

Figure 5.18. Quantification of different contributions to |E*| evolution, for the first two fatigue lags for mix 40/60 - 7: different envelope line is used for each fatigue lag.

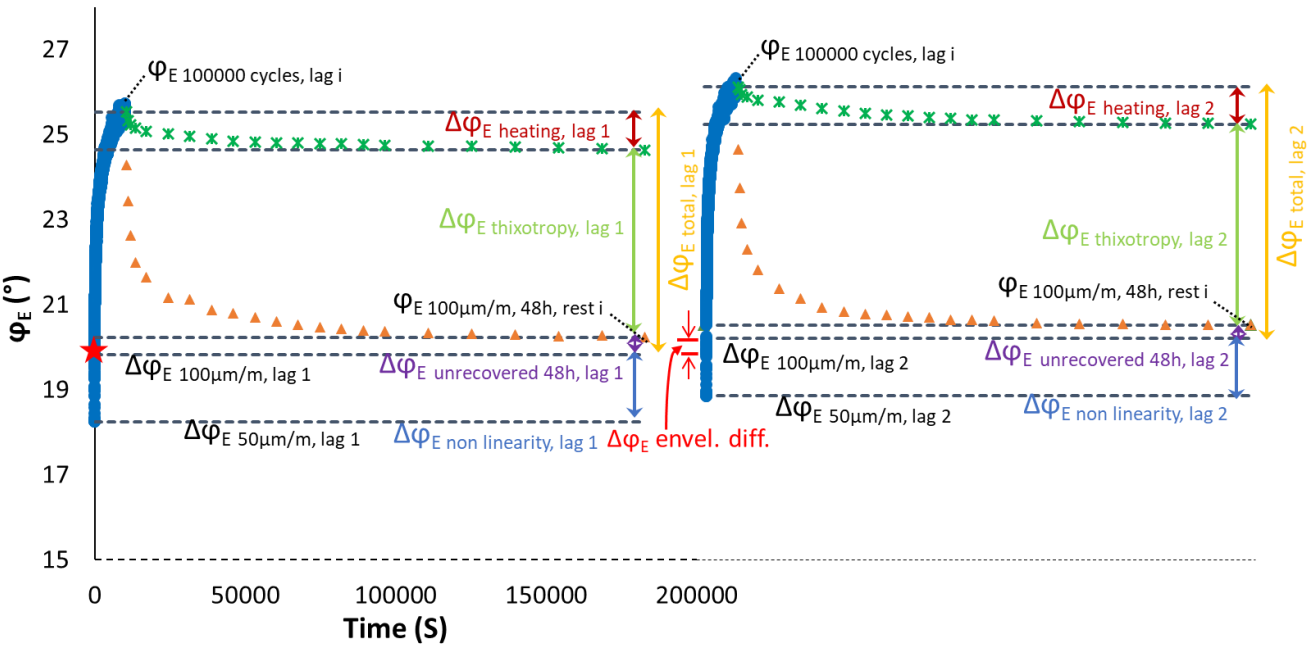

Figure 5.19. Quantification of different contributions φ_E evolution, for the first two fatigue lags for mix 40/60 - 7: different envelope line is used for each fatigue lag.

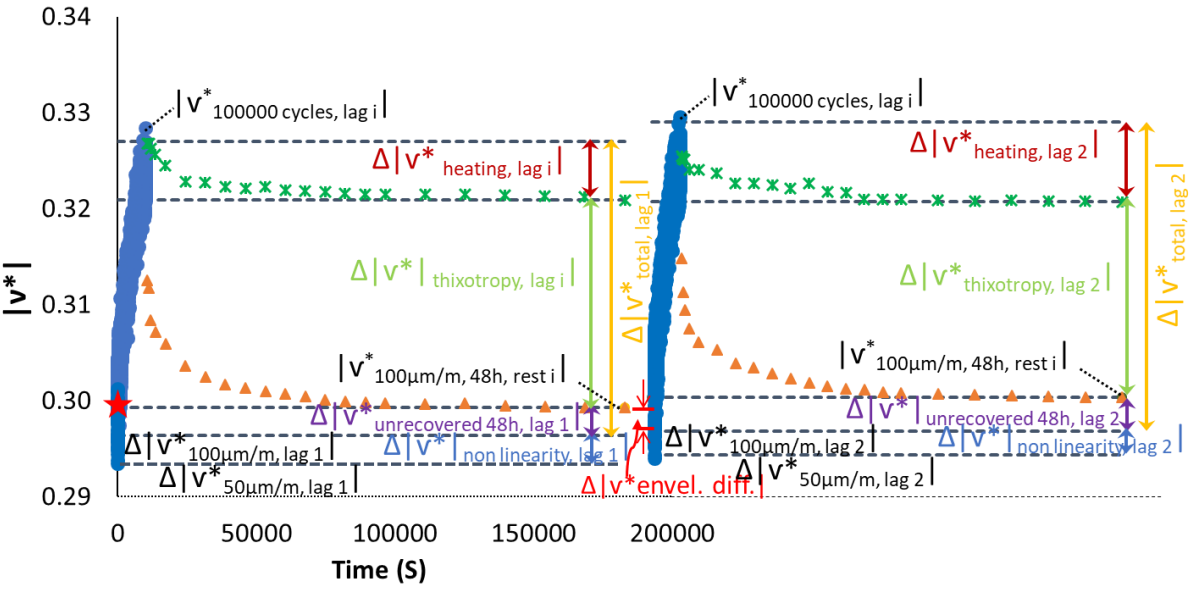

Figure 5.20. Quantification of different contributions to |v*| evolution, for the first two fatigue lags for mix 40/60 - 7: different envelope line is used for each fatigue lag.

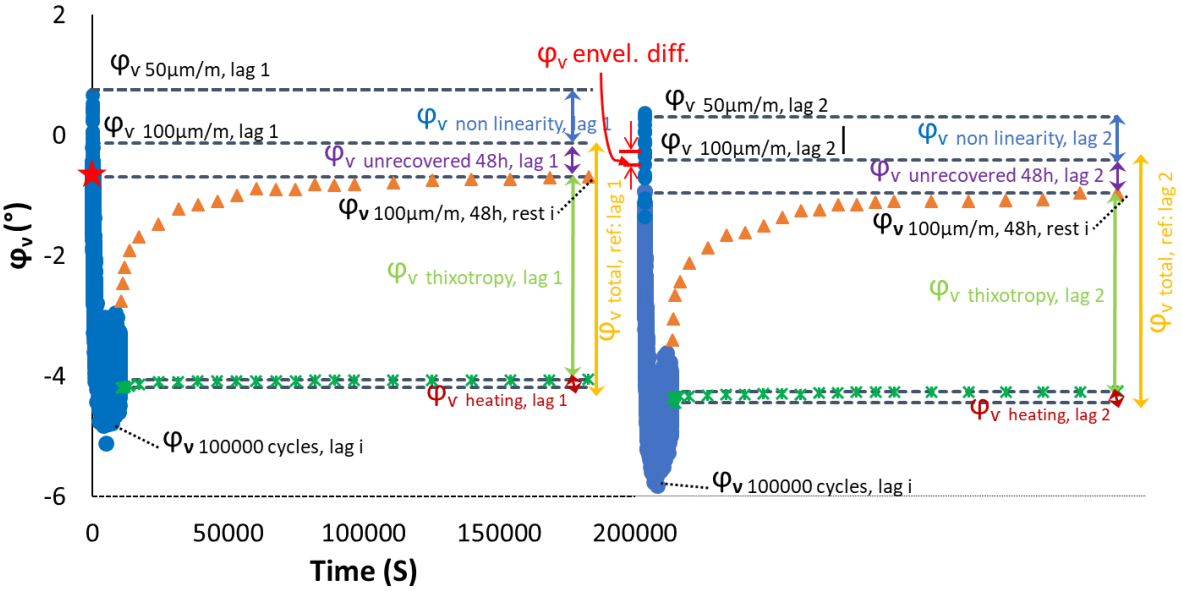

Figure 5.21. Quantification of different contributions to φ_v evolution, for the first two fatigue lags for mix 40/60 - 7: different envelope line is used for each fatigue lag.

Figure 5.22 to figure 5.25 shows histograms of relative and absolute (with respect to $\Delta|E^*_{total}|$, $\Delta\varphi_{E\ total}$, $\Delta|v^*_{total}|$ and $\Delta\varphi_{v\ total}$) importance of biasing effects and unrecovered $|E^*|$, φ_E, $|v^*|$ and φ_v variations during the five fatigue lags, for mix 40/60 - 7. Similar histograms for all the other mixtures are also presented in the appendix.

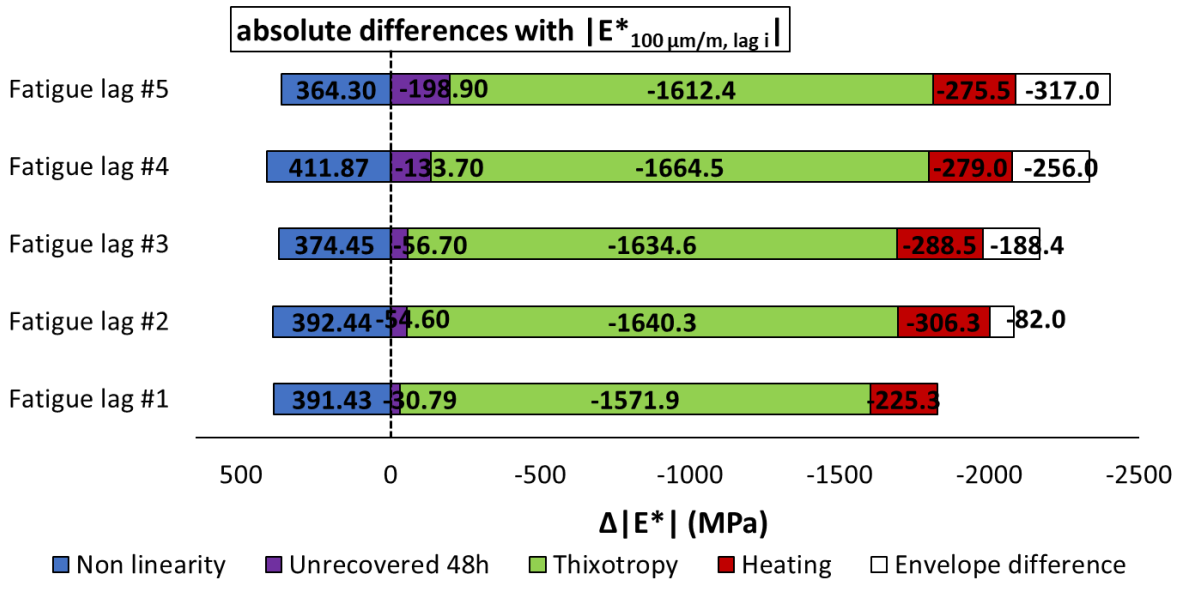

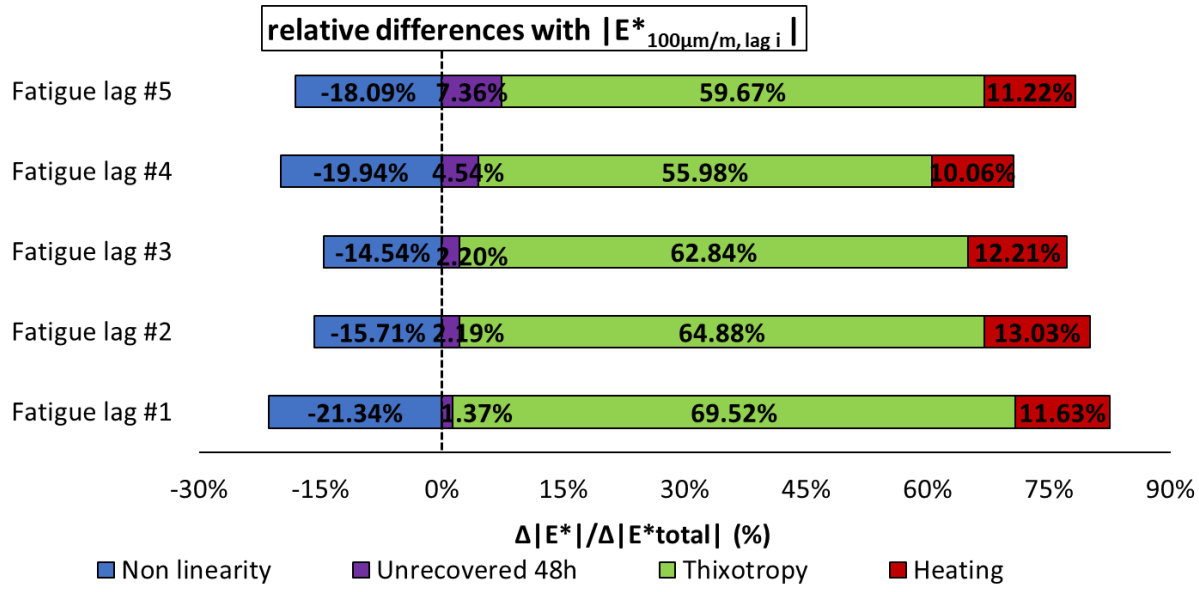

Figure 5.22. Quantification of different absolute and relative contributions to |E*| evolutions for mix 40/60 - 7, calculated using a different envelope line for each fatigue lag.

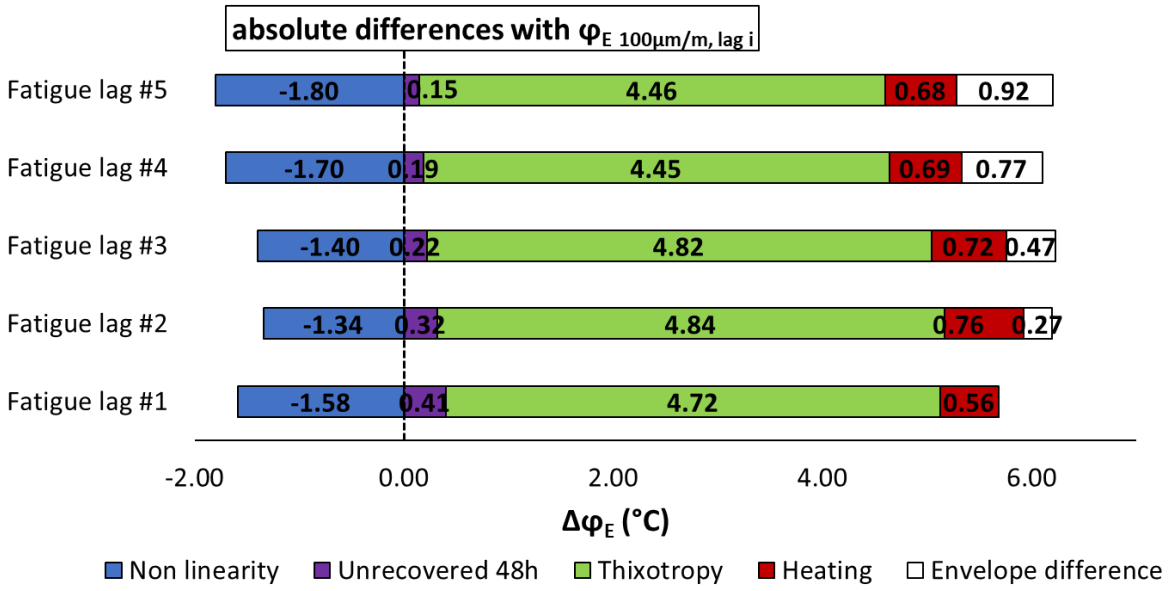

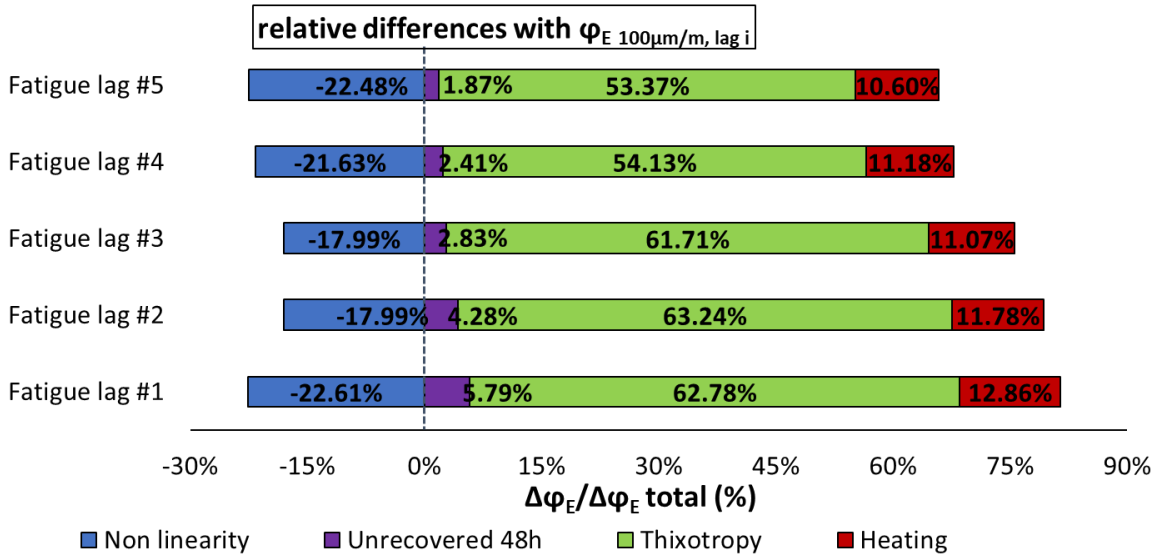

Figure 5.23. Quantification of different absolute and relative contributions to φ_E evolutions for mix 40/60 - 7, calculated using a different envelope line for each fatigue lag.

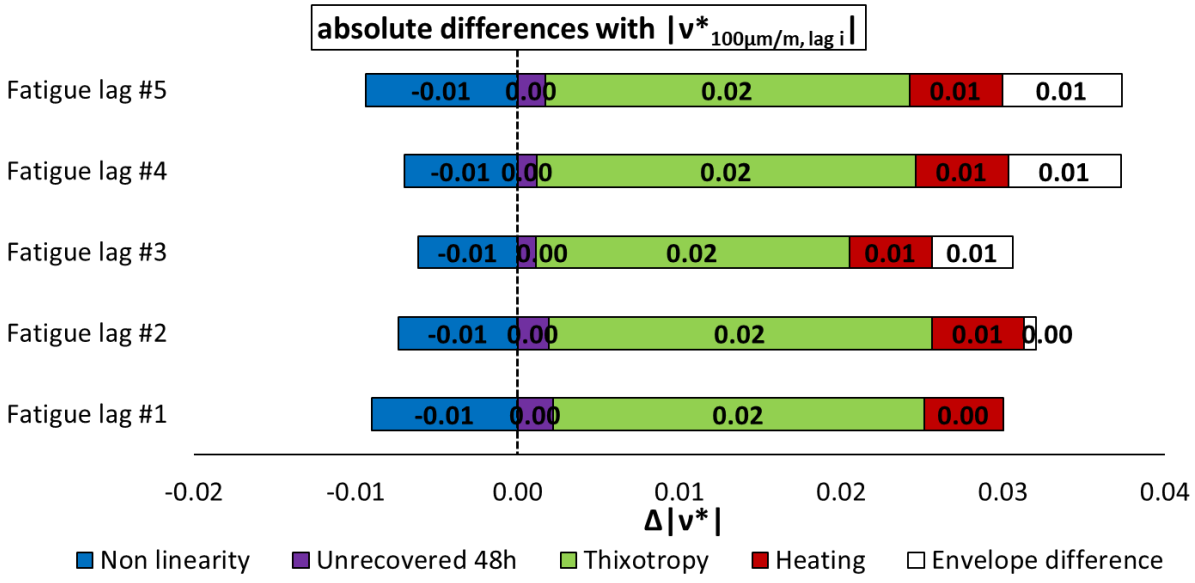

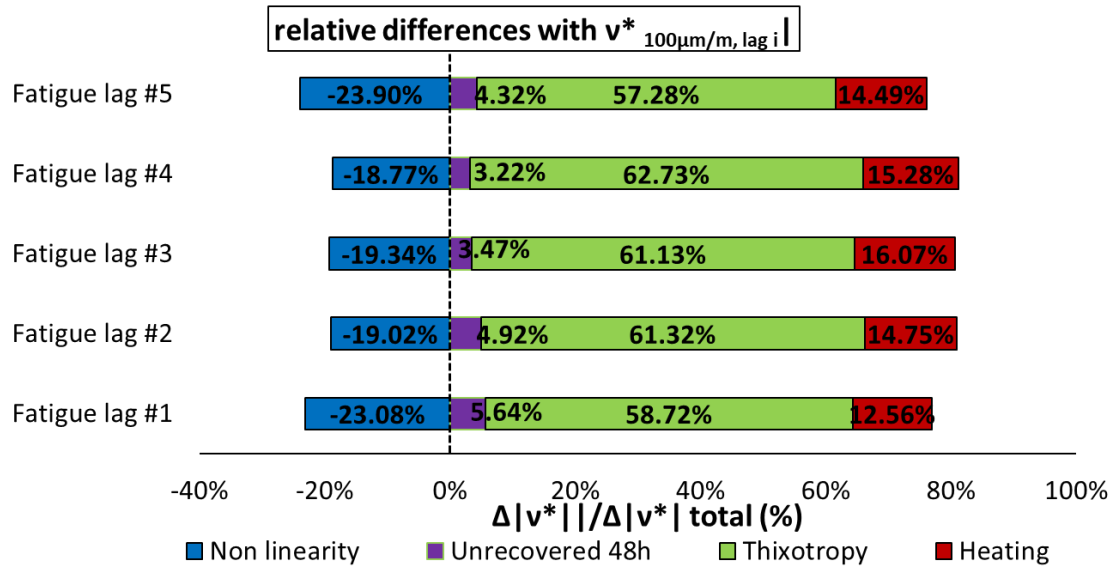

Figure 5.24. Quantification of different absolute and relative contributions to |v*| evolutions for mix 40/60 - 7, calculated using a different envelope line for each fatigue lag.

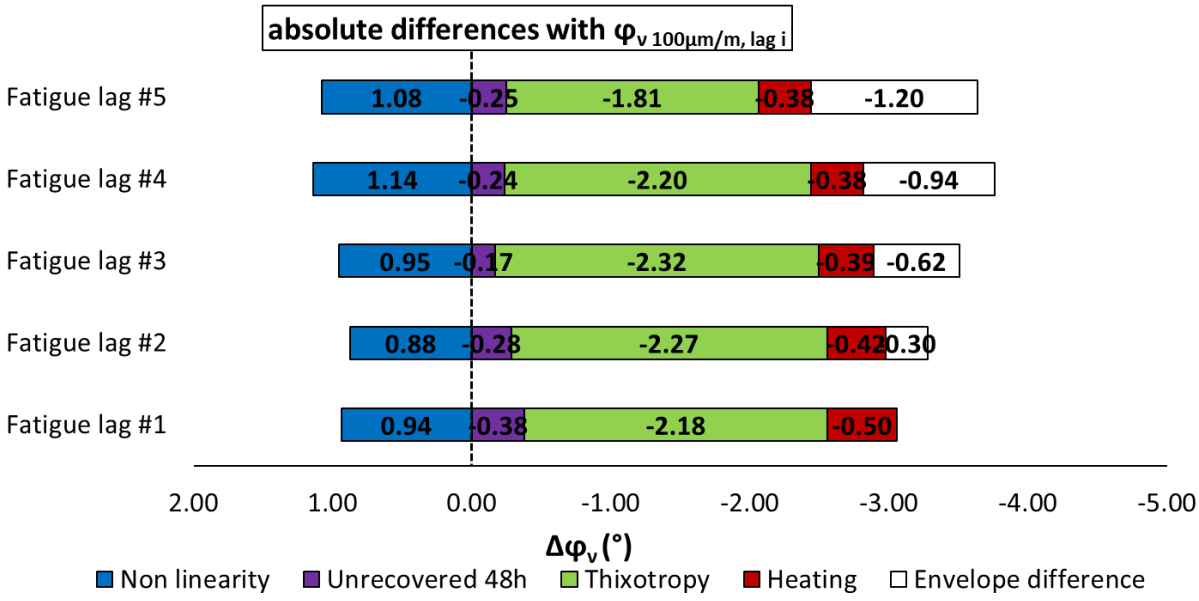

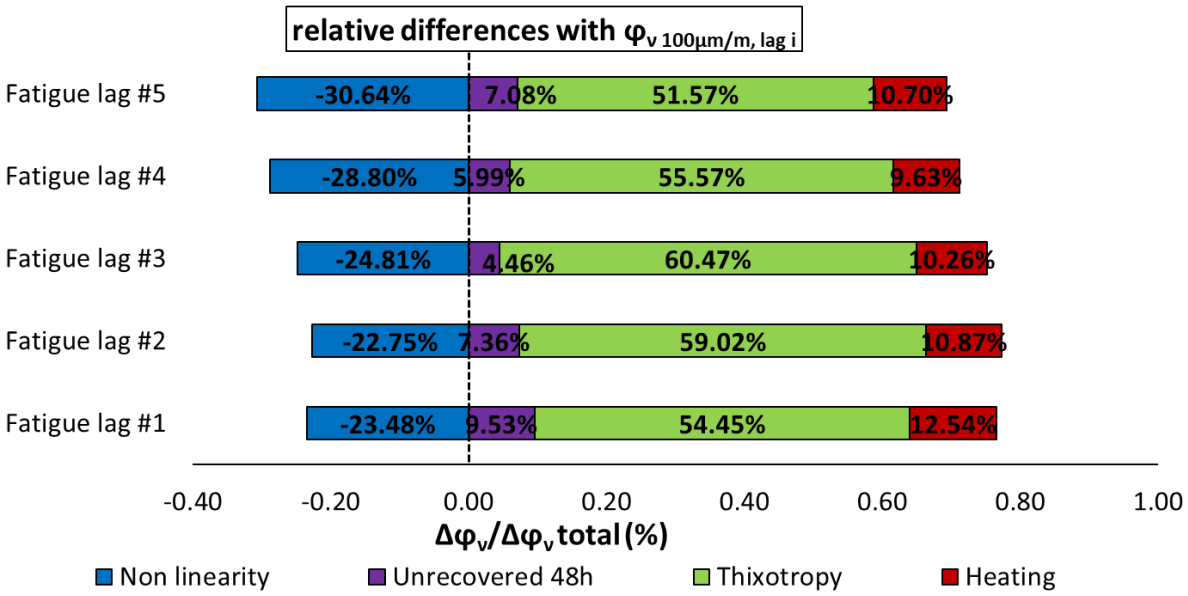

Figure 5.25. Quantification of different absolute and relative contributions to φ_v evolutions for mix 40/60 - 7, calculated using a different envelope line for each fatigue lag.

A second approach was also followed to estimate the reversible and unrecovered variations of $|E^*|$, φ_E, $|\nu^*|$ and φ_v. It consists in holding the non-linearity envelope line of the first fatigue lag as a reference for the calculation of biasing effects occurring in all fatigue lags. Envelopes of second, third, fourth and fifth fatigue lags are therefore neglected.

Non-linearity effects are therefore considered constant throughout the whole test since they are calculated only with respect to lag 1. Thus, contributions of non-linearity ($\Delta|E^*_{\text{nonlinearity, ref: lag 1}}|$, $\Delta\varphi_{\text{nonlinearity, ref: lag 1}}$, $\Delta\nu_{\text{nonlinearity, ref: lag 1}}$ and $\Delta\varphi_{\text{vnonlinearity, ref: lag 1}}$) to variations of complex modulus and complex poisson's ratio are:

$$\Delta|E^*_{\text{nonlinearity, ref: lag 1}}| = |E^*_{50\mu m/m,\ \text{lag 1}}| - |E^*_{100\mu m/m,\ \text{lag 1}}| \quad 5.33$$

$$\varphi_{E\ \text{nonlinearity, ref: lag 1}} = \varphi_{E\ 50\mu m/m,\ \text{lag 1}} - \varphi_{E\ 100\mu m/m,\ \text{lag 1}} \quad 5.34$$

$$|\nu^*_{\text{nonlinearity, ref: lag 1}}| = |\nu^*_{50\mu m/m,\ \text{lag 1}}| - |\nu^*_{100\mu m/m,\ \text{lag 1}}| \quad 5.35$$

$$\varphi_{v\ \text{nonlinearity, ref: lag 1}} = \varphi_{v\ 50\mu m/m,\ \text{lag 1}} - \varphi_{v\ 100\mu m/m,\ \text{lag 1}} \quad 5.36$$

Unrecovered variations ($\Delta|E^*_{\text{unrecovered 48 h, ref:lag 1}}|$, $\Delta\varphi_{E\ \text{unrecovered 48 h, ref: lag1}}$, $\Delta|\nu^*_{\text{unrecovered 48 h, ref: lag1}}|$ and $\Delta\varphi_{\text{vunrecovered 48 h,ref:lag001}}$) are calculated as;

$$\Delta|E^*_{\text{unrecovered 48 h,ref.: lag 1}}| = |E^*_{100\mu m/m,\ 48\ h,\text{lag i}}| - |E^*_{100\mu m/m,\ \text{lag 1}}| \quad 5.37$$

$$\varphi_{E\ \text{unrecovered 48 h,ref.: lag 1}} = \varphi_{E\ 100\mu m/m,\ 48\ h\ \text{lag i}} - \varphi_{E100\mu m/m,\ \text{lag 1}} \quad 5.38$$

$$|v^*_{\text{unrecovered 48 h,ref.: lag 1}}| = |v^*_{100\mu m/m,\ 48\ h\ \text{lag i}}| - |v^*_{100\mu m/m,\ \text{lag 1}}| \quad 5.39$$

$$\varphi_{v\ \text{unrecovered 48 h,ref.: lag 1}} = \varphi_{v\ 100\mu m/m,\ 48\ h\ \text{lag i}} - \varphi_{v100\mu m/m,\ \text{lag 1}} \quad 5.40$$

The contributions heating and thixotropy are calculated as in the previous approach.

Figure 5.26 to figure 5.29 shows a typical example of such calculations for $|E^*|$, φ_E, $|v^*|$ and φ_v variations estimated using the envelope line of the first fatigue lag for all the fatigue lags. Total variations are calculated as;

$$\Delta|E^*_{\text{total, ref: lag 1}}| = |E^*_{100{,}000\ \text{cycles, lag i}}| - |E^*_{50\mu m/m,\ \text{lag 1}}| \quad 5.41$$

$$\Delta\varphi_{E\ \text{total, ref: lag 1}} = \varphi_{E100{,}000\ \text{cycles, lag i}} - \varphi_{E50\mu m/m,\ \text{lag 1}} \quad 5.42$$

$$\Delta|v^*_{\text{total, ref: lag 1}}| = |v^*_{100{,}000\ \text{cycles, lag i}}| - |v^*_{50\mu m/m,\ \text{lag 1}}| \quad 5.43$$

$$\Delta\varphi_{v\ \text{total, ref: lag 1}} = \varphi_{v100{,}000\ \text{cycles, lag i}} - \varphi_{v50\mu m/m,\ \text{lag 1}} \quad 5.44$$

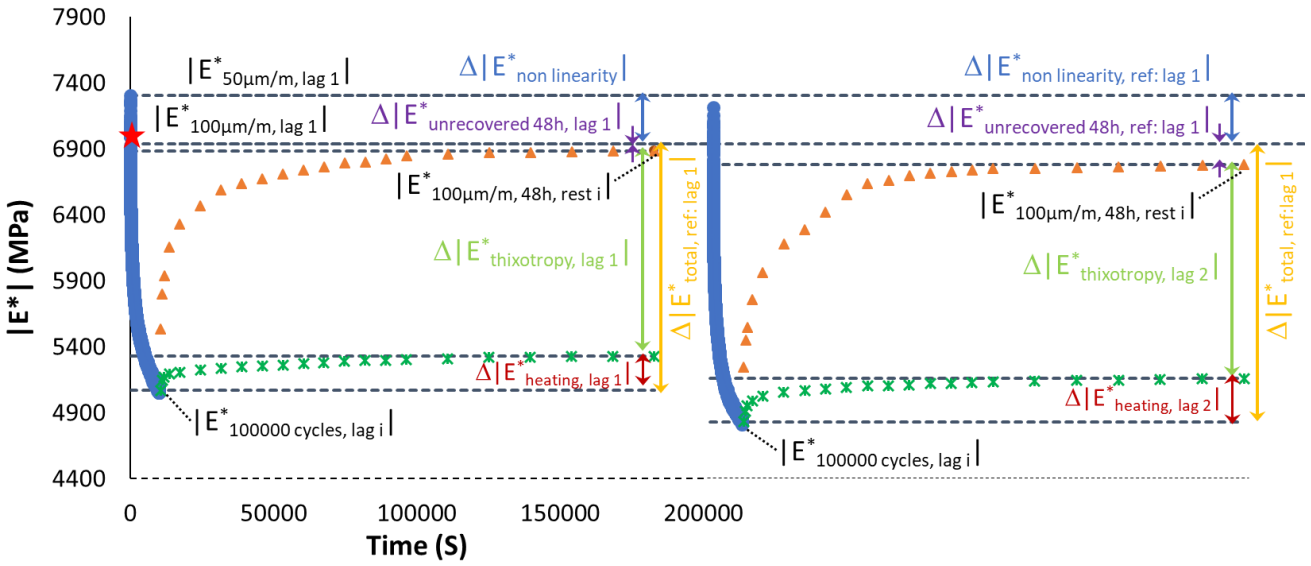

Figure 5.26. Quantification of different contributions to |E*| evolution during first and second fatigue lags for mix 40/60 - 7: the envelope line of the first fatigue lag is used for all fatigue lags.

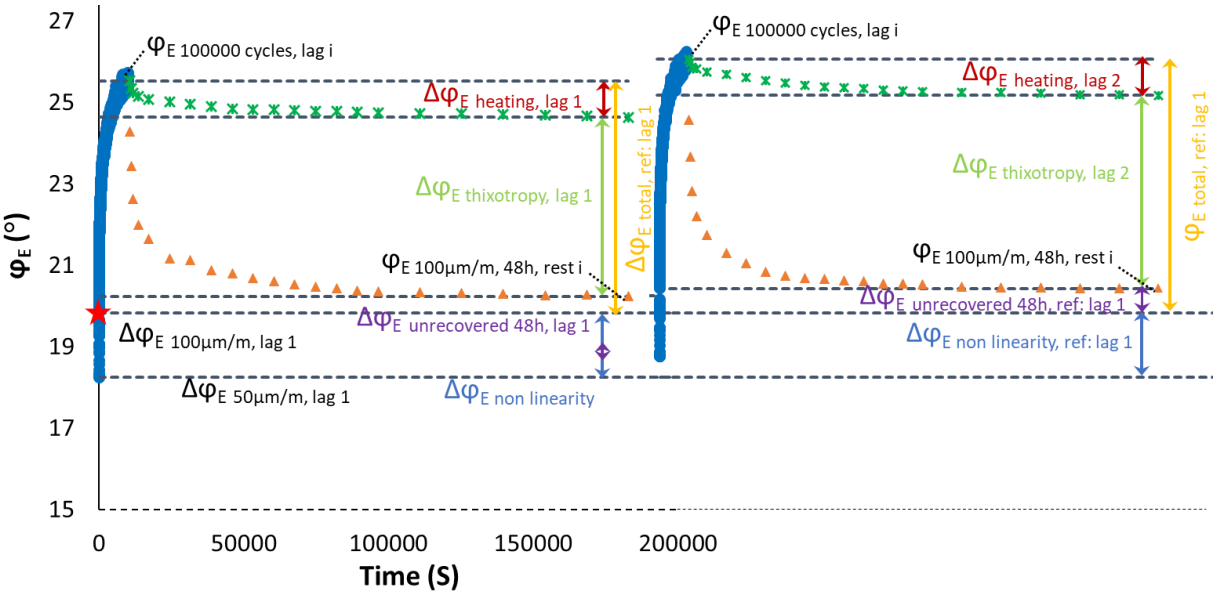

Figure 5.27. Quantification of different contributions to φ_E evolution during first and second fatigue lags for mix 40/60 - 7: the envelope line of the first fatigue lag is used for all fatigue lags.

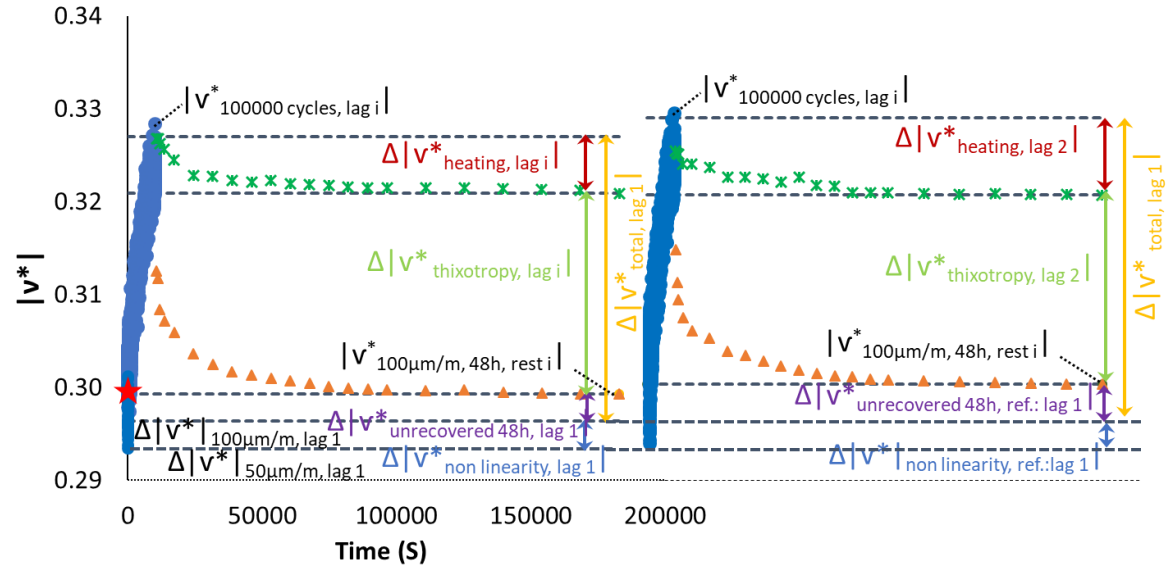

Figure 5.28. Quantification of different contributions to |v*| evolution during first and second fatigue lags for mix 40/60 - 7: the envelope line of the first fatigue lag is used for all fatigue lags.

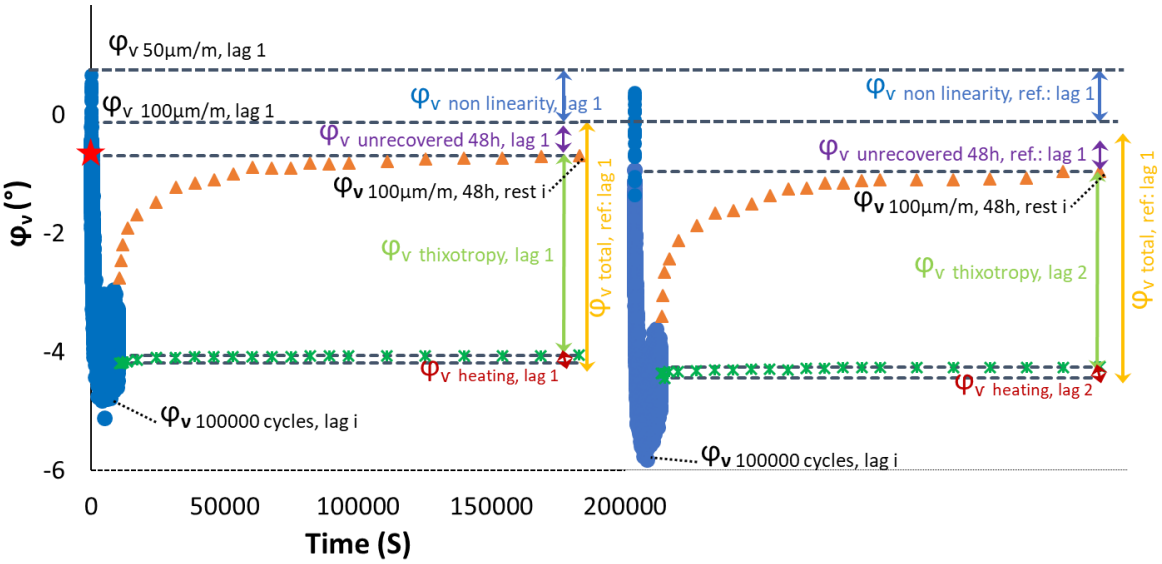

Figure 5.29. Quantification of different contributions to φ_v evolution during first and second fatigue lags for mix 40/60 - 7: the envelope line of the first fatigue lag is used for all fatigue lags.

Figure 5.30 to figure 5.33 shows histograms of absolute and relative (with respect to $\Delta|E^*_{total,\ ref:lag\ 1}|$, $\Delta\varphi_{total,ref:lag\ 1}$, $\Delta v_{total,ref:lag\ 1}$ and $\Delta\varphi_{vtotal,ref:lag\ 1}$) contributions of reversible phenomena and unrecovered $|E^*|$, φ_E, $|v^*|$ and φ_v variations during fatigue lags, estimated with respect to the non-linearity envelope line of the first lag, for mix 40/60 - 7. Similar histograms for all the other mixtures are also presented in the appendix.

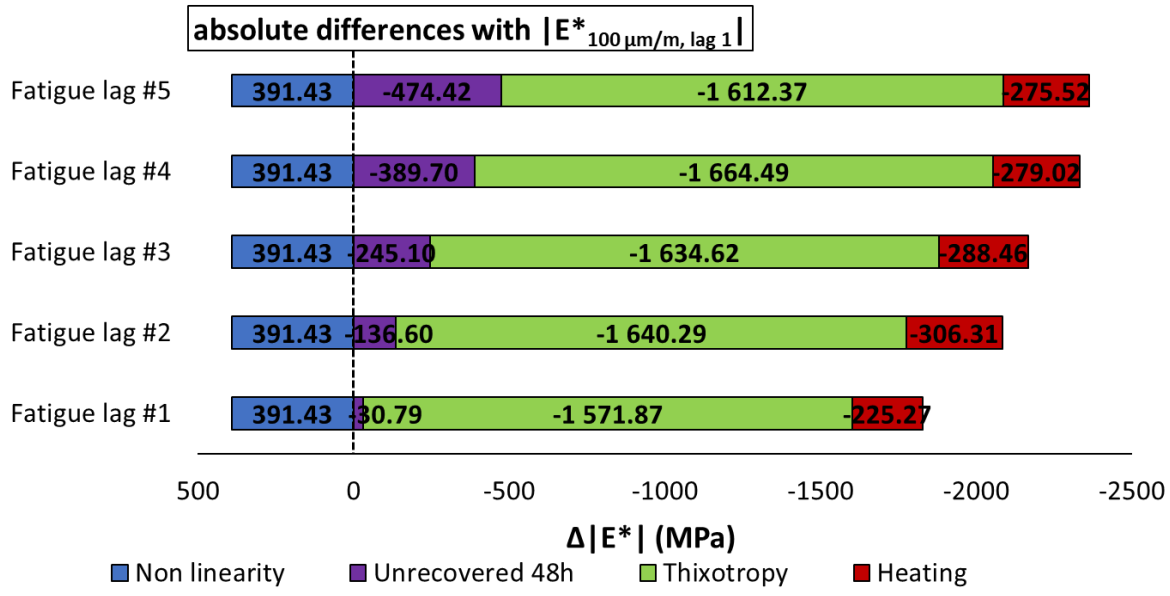

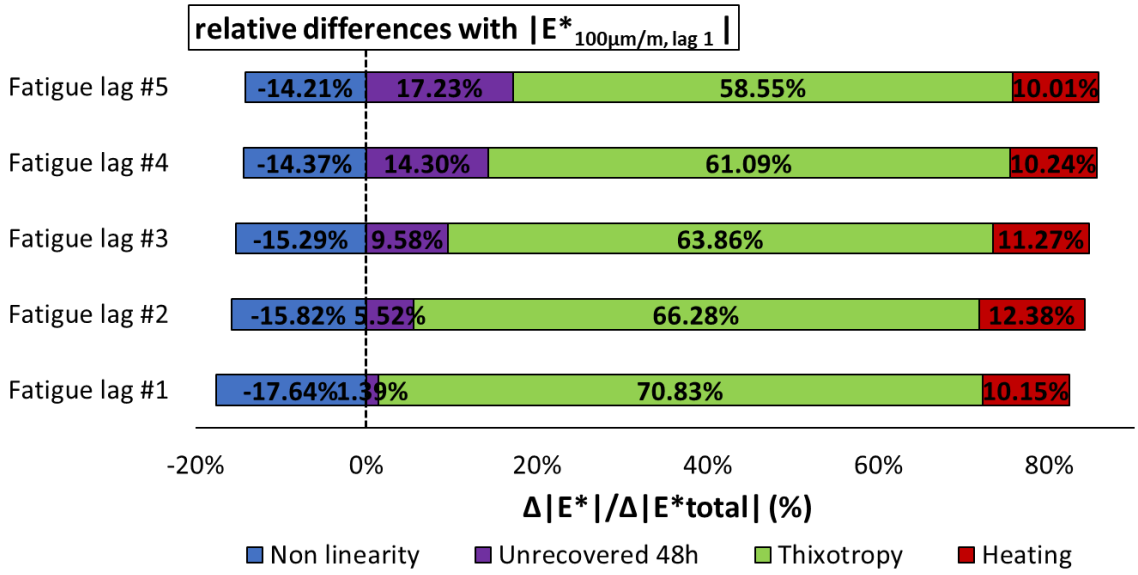

Figure 5.30. Quantification of different absolute and relative contributions to |E*| evolutions for mix 40/60 - 7, calculated using the envelope line for the first fatigue lag.

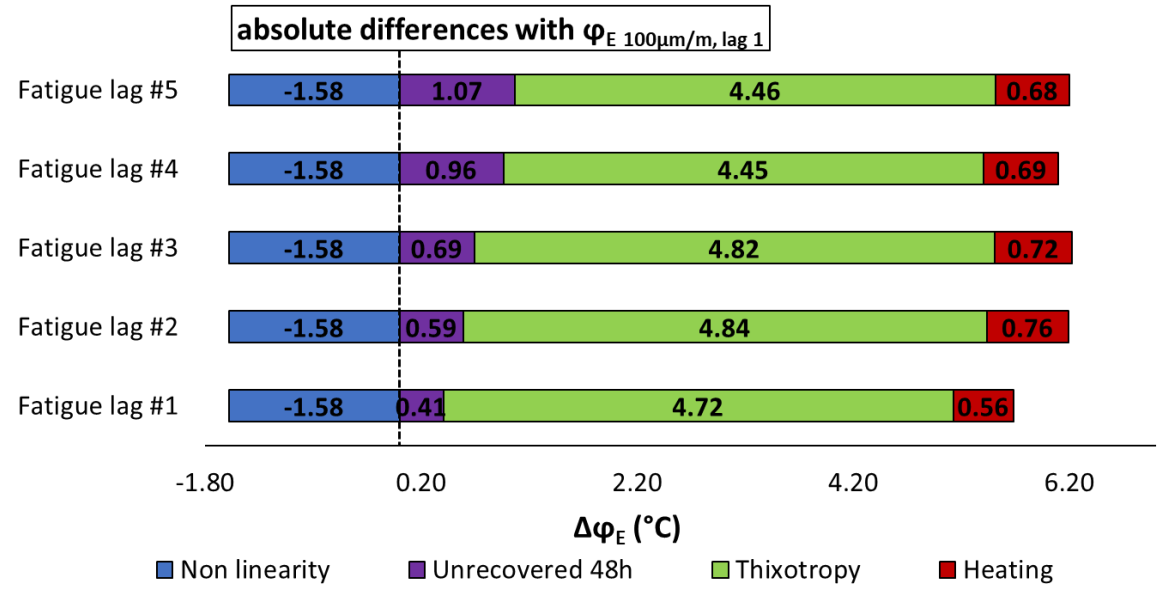

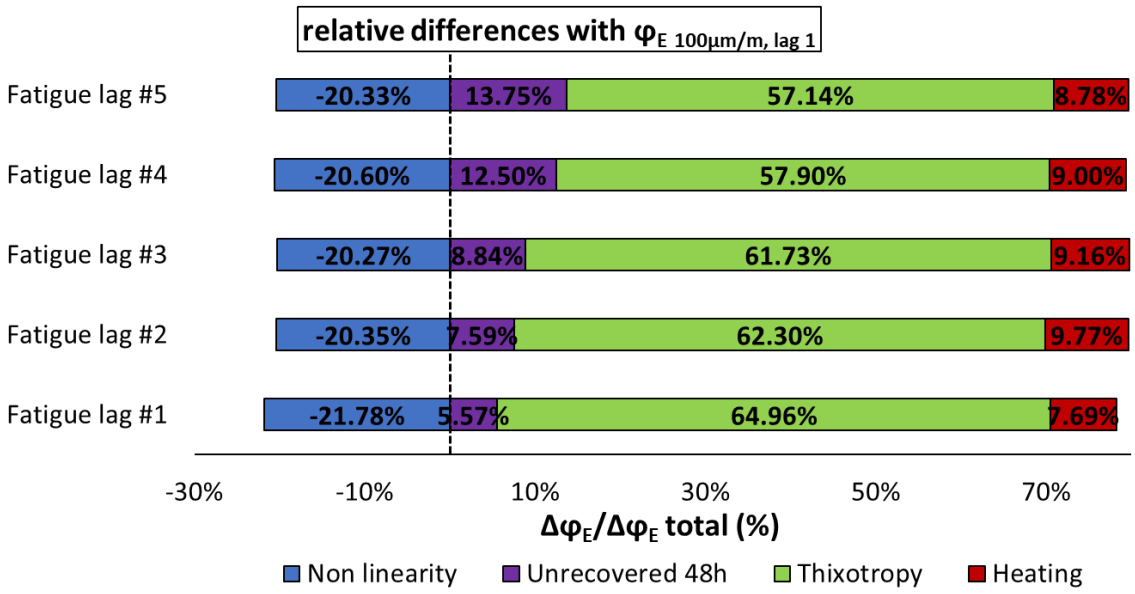

Figure 5.31. Quantification of different absolute and relative contributions to φ_E evolutions for mix 40/60 - 7, calculated using the envelope line for the first fatigue lag.

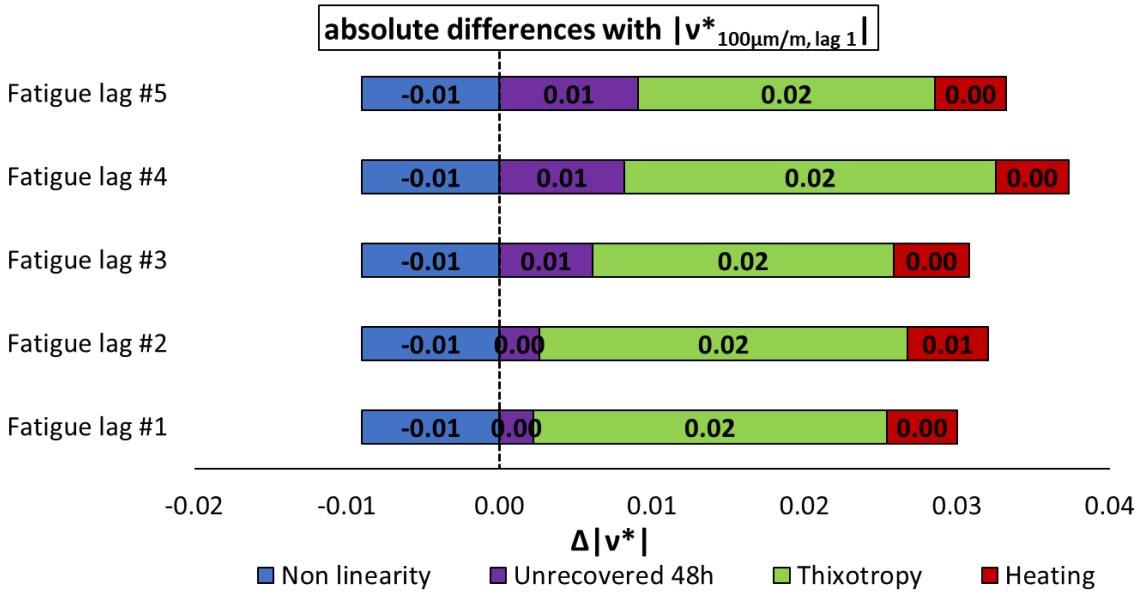

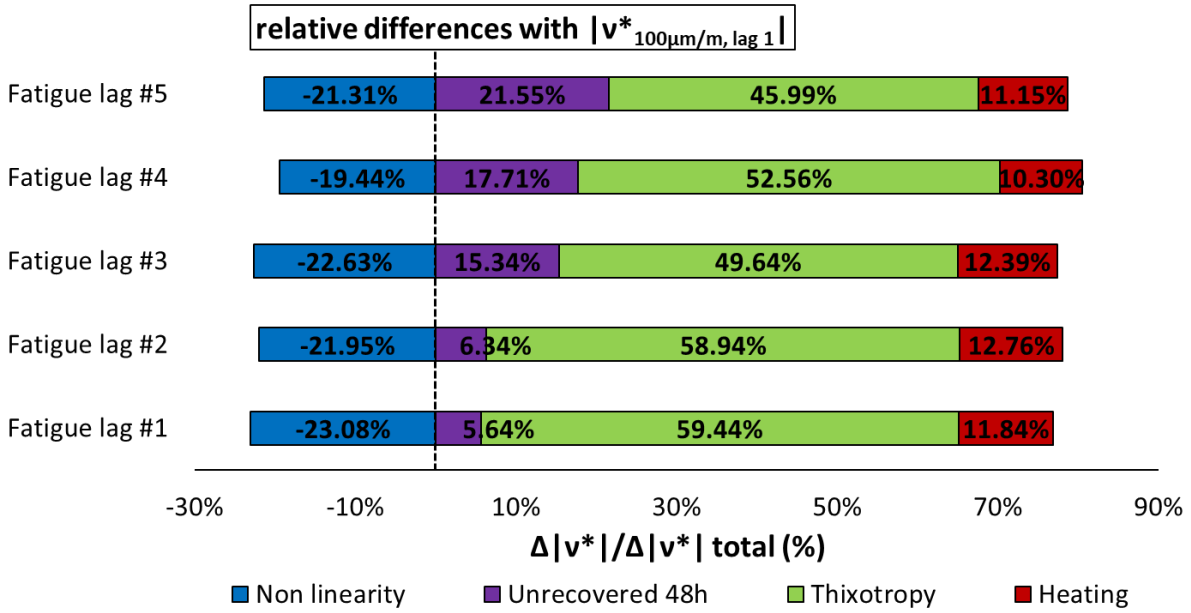

Figure 5.32. Quantification of different absolute and relative contributions to |v*| evolutions for mix 40/60 - 7, calculated using the envelope line for the first fatigue lag.

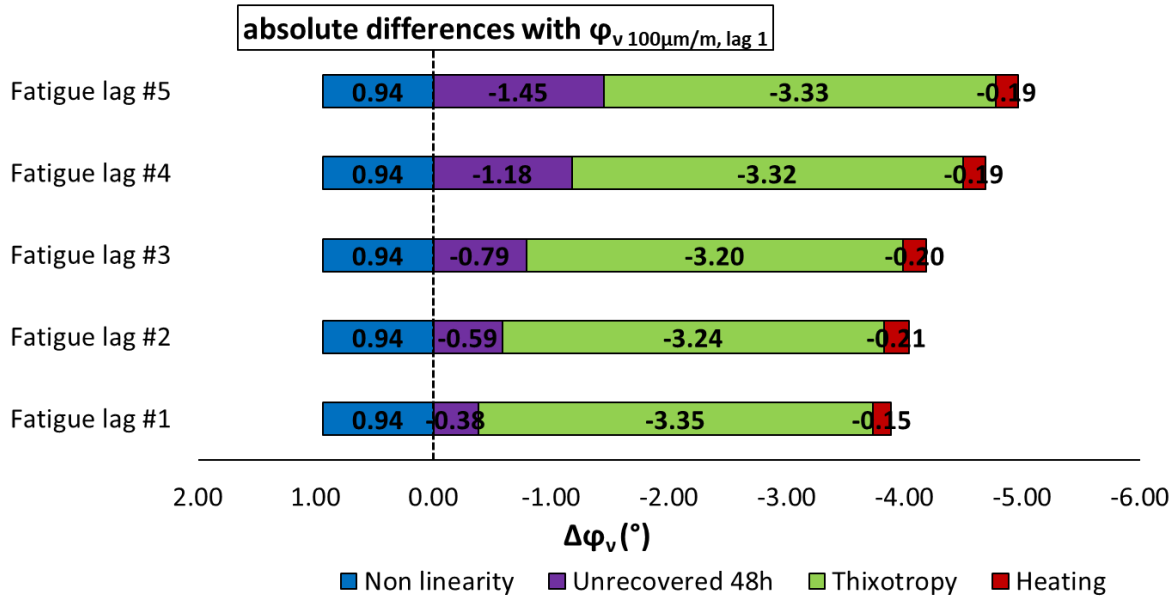

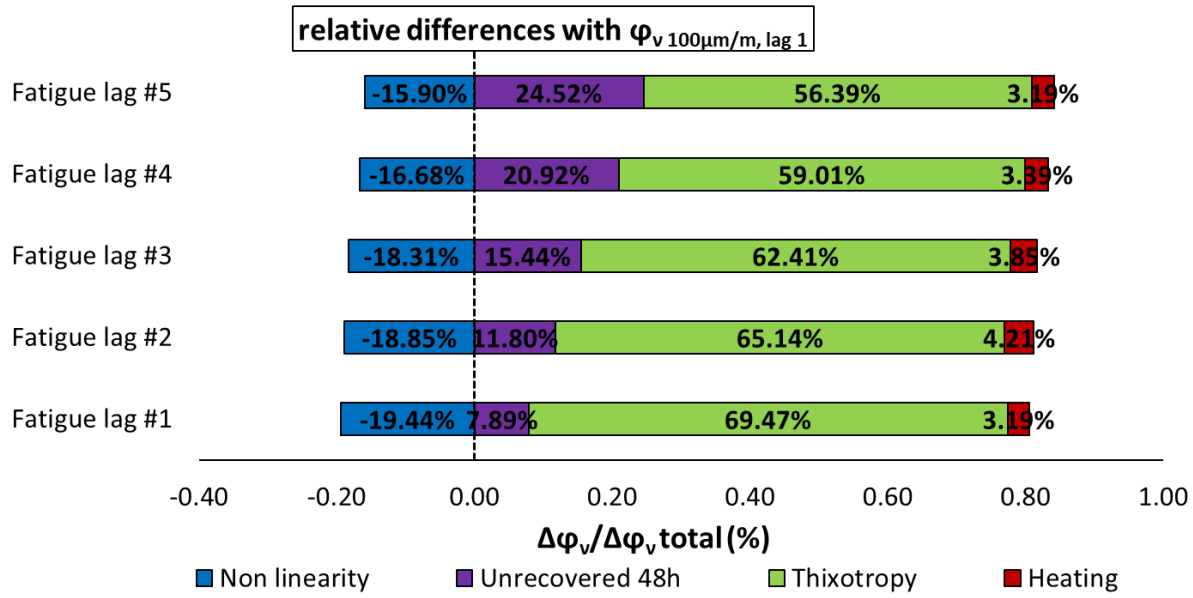

Figure 5.33. Quantification of different absolute and relative contributions to φ_v evolutions for mix 40/60 - 7, calculated using the envelope line for the first fatigue lag.

Based on the various approaches for the quantification of different reversible phenomena to 3D properties for each fatigue lag, the following observations can be made on |E*|, φE, |ν*| and φν evolution:

- When each fatigue lag is considered separately, measuring |E*|, φ_E, |ν*| and φ_ν variations using the different non-linearity envelopes for each fatigue lag, the effects of non-linearity appear to be although small and quite similar for |E*|, φ_E, |ν*| and φ_ν. In particular, the effect due to non-linearity ranged from 15% to 20%.
- The effects of unrecovered variations on |E*|, φ_E, |ν*| and φ_ν during fatigue tests appear small effects because there appear to be almost total recovery. Specifically, when the i-th lag is considered, unrecovered variations are always lower than 15% but when the first lag is considered, they are between 14% and 24%, depending on the considered property. This result emphasizes the need to distinguish between the restoration of the various reversible phenomena and the restoration of actual damage. This outcome

validates the need to carefully consider the analysis of traditional fatigue tests and, in the end, to reconsider the practices currently used in these tests.

- The effects of self-heating on |E*|, φ_E and φ_v variations during fatigue tests are smaller than the effects of non-linearity and thixotropy. However, the effects of self-heating on |ν*| variations seem to be more important that the effects of non-linearity but less than the effect of thixotropy. The effect of self-heating on φ_v variations seem to be insignificant and almost constant. Specifically, for |E*| and φ_E self-heating appears to account for about 8% to 13% of total |E*| and φ_E variations, about 15% for |ν*| and 4% for and φ_v during each fatigue lag. Approximately the same relative influences are found when overall variations during the entire test are considered.
- The effects of thixotropy on |E*|, φ_E, |ν*| and φ_v variations during fatigue tests appear to be substantially. They seem almost the same for all the measuring variations. Among reversible phenomena explaining the recovery of |E*|, φ_E, |ν*| and φ_v during rest periods, thixotropy appears to be the most important (always higher than 55% of the total restoration during rest).

5.2.3. Repeatability on the test on different samples of the same materials

This section presents an evaluation of the repeatability of the test protocol by comparing results obtained on different samples of the same material. This is essential since results were collected under similar conditions such as same method, equipment, environmental conditions and location. Consequently, the evaluation of the repeatability for the relative contributions of the various variations with respect to |E*|, φ_E, |ν*| and φ_v throughout the whole test for the tested samples is calculated using standard deviation. Figure 5.34 – Figure 5.36 presents comparison of the relative contributions of the non-linearity variation of |E*|, φ_E, |ν*| and φ_v throughout the whole test for the tested samples for mix 40/60, mix 70/100 and mix PMB. Mean and standard

deviations are shown for each fatigue lag, respectively as a point (black dash) and error bars. Values were calculated using different envelopes for each fatigue lag, therefore by considering each fatigue (and rest) lag separately, with its own envelope. The results obtained for the relative contribution of the non-linearity effect of the various samples of the same mixture appear be quite repeatable for mix 40/60, while a higher scatter is observed for mix PMB and, above all, for mix 70/100, although for this mix most of the samples experienced premature failure as represented in the appendix. However, mix PMB – 5 had issues with the non-contactless sensor and the radial strain could not be recorded. Also, variations of $|v^*|$ and φ_v for mix 70/100 showed bizarre results which could not be analysed as shown in the appendix. The influence of non-linearity on $|E^*|$, φ_E, $|v^*|$ and φ_v variations appear somehow similar for all the tested mixtures, ranging approximately from 5% to 20% for $|E^*|$ and φ_E (generally slightly higher for φ_E than for $|E^*|$) and about 20% to 30% for $|v^*|$ and φ_v (with the exception of sample 5 of mix 70/100, for which almost 40% was achieved). Specifically, the difference between the estimations based on $|E^*|$ and those based on φ_E, $|v^*|$ and φ_v is more pronounced for mix PMB. In the plots (for $|E^*|$, φ_E, $|v^*|$ and φ_v), most of the points fall within the standard deviation, indicated by error bars for all the tested mixtures except on φ_E for mix 70/100 - 5. The few points outside error bars do not belong to any particular sample. From these observations, the test procedure appears to provide repeatable results for the same material, despite the significant variations found between air void content of the different samples of the same mixture (from 2.8% to 8.9% for mix 40/60, 1.8% to 7.3% for mix 70/100 and 2.6% to 6.6% for mix PMB). Moreover, no clear tendency is observed between the non-linearity variation of $|E^*|$, φ_E, $|v^*|$ and φ_v and air void content.

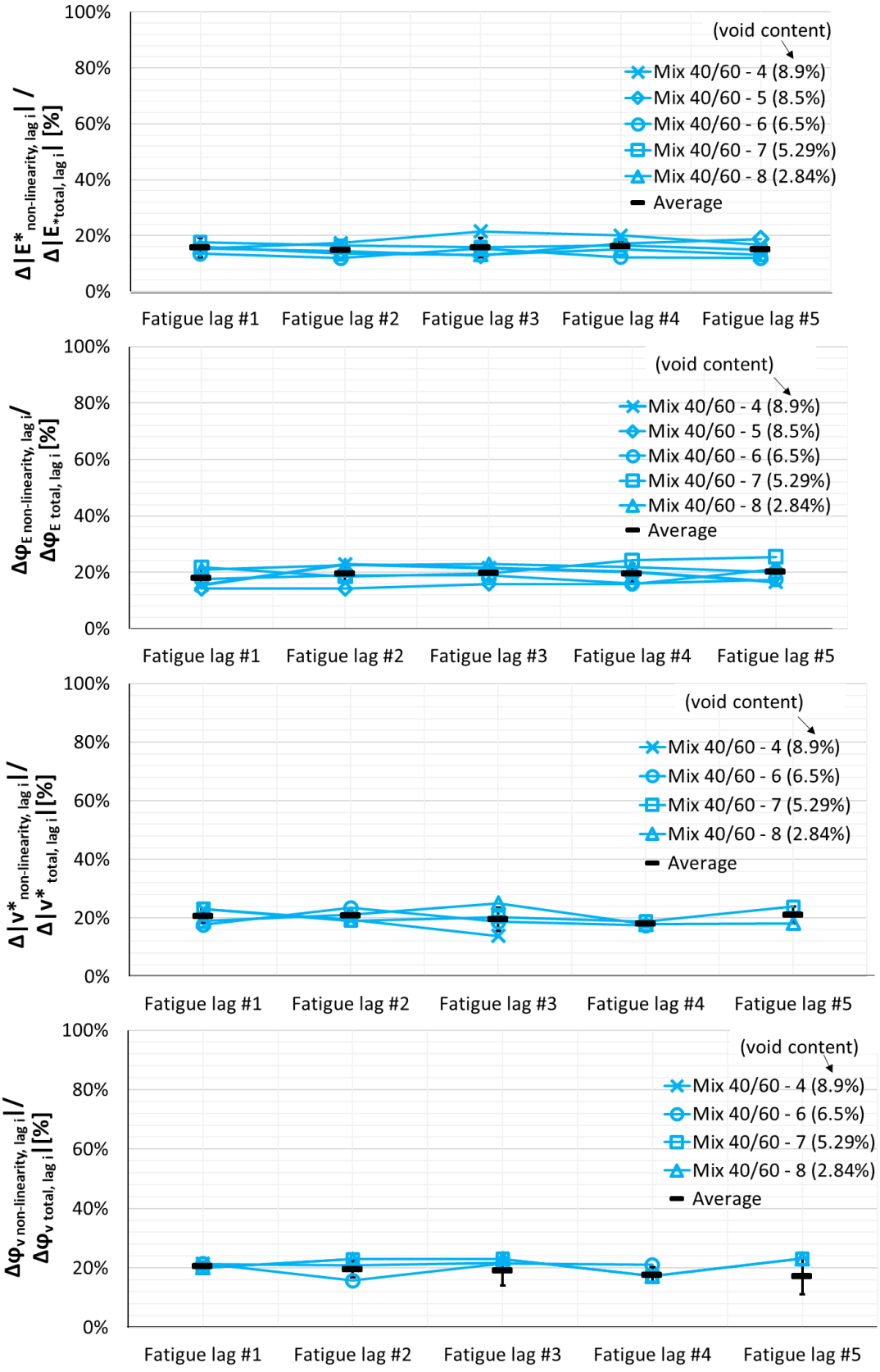

Figure 5.34. Relative contribution of non-linearity variations of |E*|, φ_E, |v*| and φ_v with respect to the total variation for each fatigue and rest lag with the void content indicated for mix 40/60.

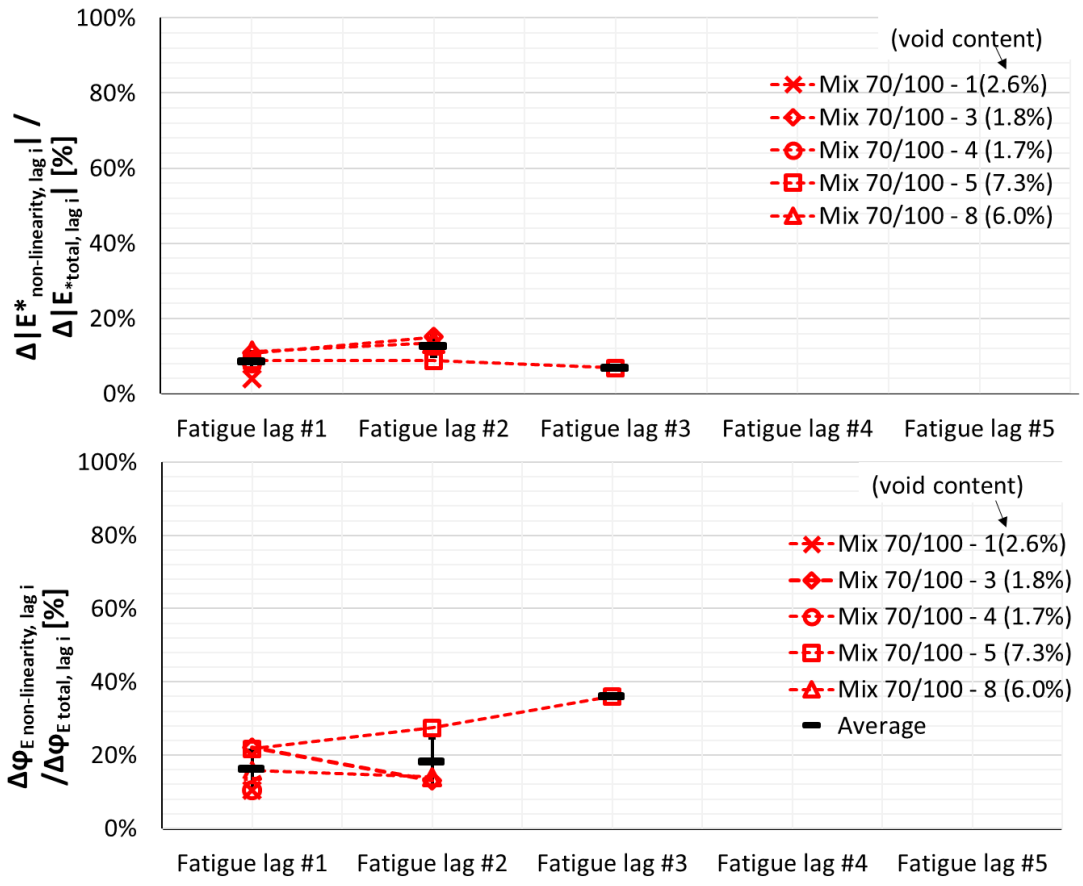

Figure 5.35. Relative contribution of non-linearity variations of |E*| and φ_E with respect to the total variation for each fatigue and rest lag with the void content indicated for mix 70/100 samples.

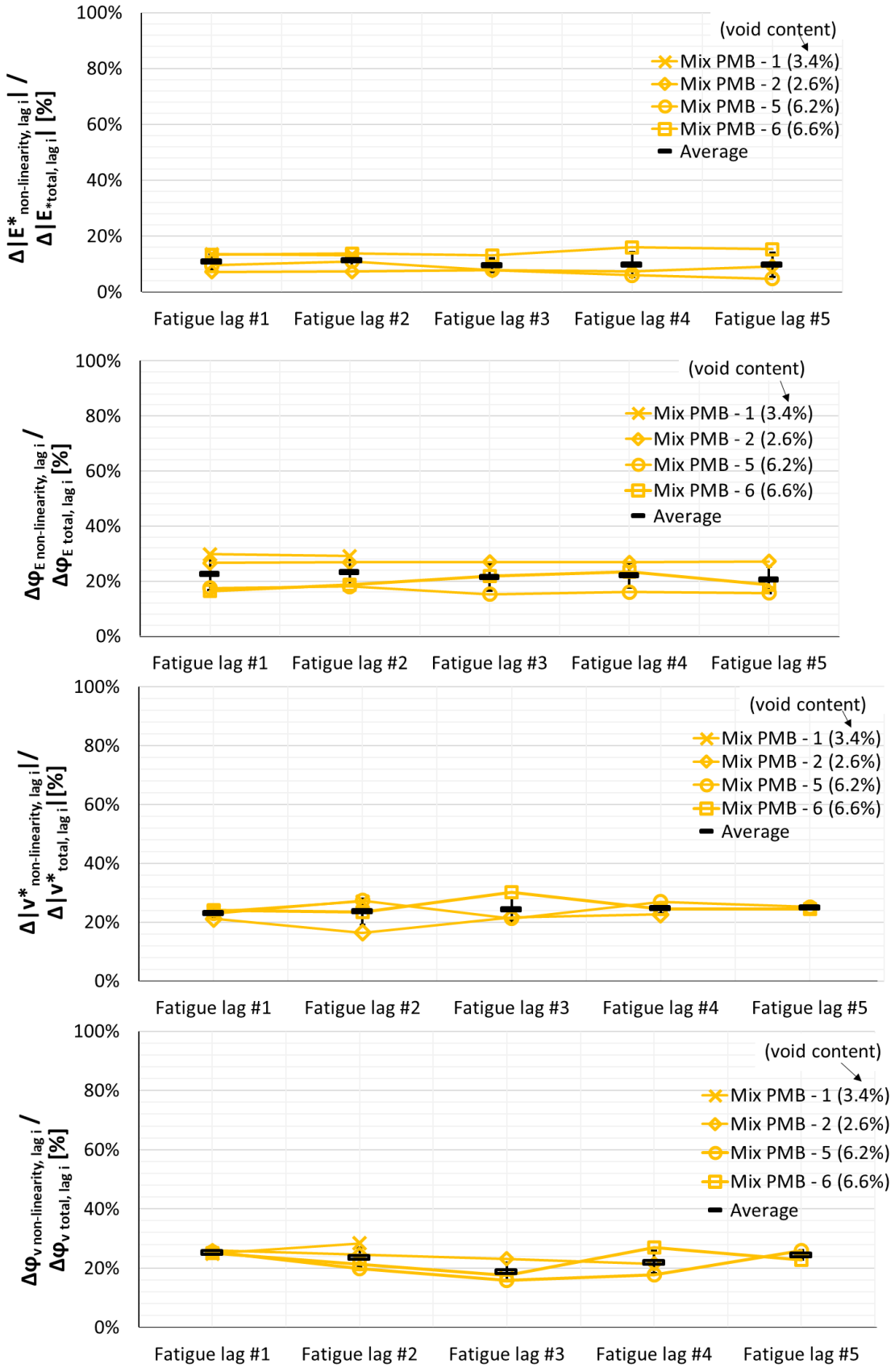

Figure 5.36. Relative contribution of non-linearity variations of |E*|, φ_E, |v*| and φ_v with respect to the total variation for each fatigue and rest lag with the void content indicated for mix PMB samples.

Figure 5.37 – Figure 5.39 shows comparison of the relative contributions of the unrecovered variations of |E*|, φ_E, |v*| and φ_v throughout the whole test for the tested mixtures (mix 40/60, mix 70/100 and mix PMB). Values were calculated using the envelope line for the first fatigue lag, therefore by considering each fatigue (and rest) lag separately, with its own envelope. The tested samples of the considered mixtures show relatively the same proportions of unrecovered effect except for mix 70/100 where most of the samples experienced significant variations. The influence of unrecovered variations of |E*|, φ_E, |v*| and φ_v for mix 40/60, mix 70/100 and mix PMB vary with the fatigue lags, approximately, not exceeding 15% for |E*| and φ_E, and 20% for |v*| and φ_v, with Mix 70/100 showing the highest unrecovered variations, approximately 20% for |E*| and about 40% for φ_E. Also, higher scatter is observed for mix PMB than for mix 40/60. In all plots (for |E*|, φ_E, |v*| and φ_v) for all samples of the same mixture, most of the points fall within the standard deviation, indicated by error bars. The few points outside error bars do not belong to any particular sample of the same mixture. From these observations, together with the relative value of standard deviation calculated, the test procedure appears to provide repeatable results for the same material. Therefore, significant variations were found between air void content of the tested samples of the various mixtures. Hence, no clear tendency is observed between the unrecovered variation of |E*|, φ_E, |v*| and φ_v and air void content.

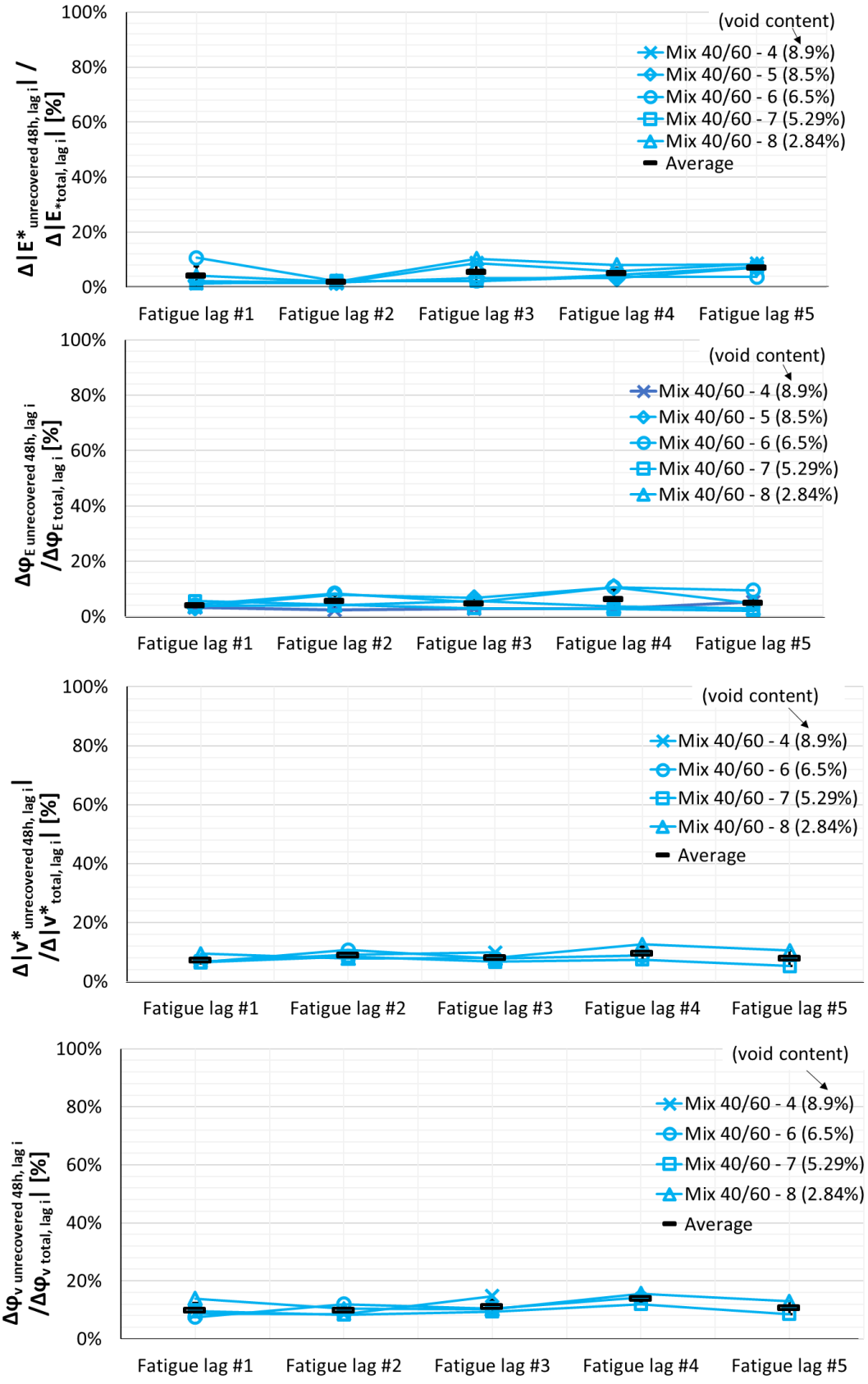

Figure 5.37. Relative contribution of unrecovered variations of |E*|, φ_E, |v*| and φ_v with respect to the total variation for each fatigue and rest lag with the void content indicated for mix 40/60 samples.

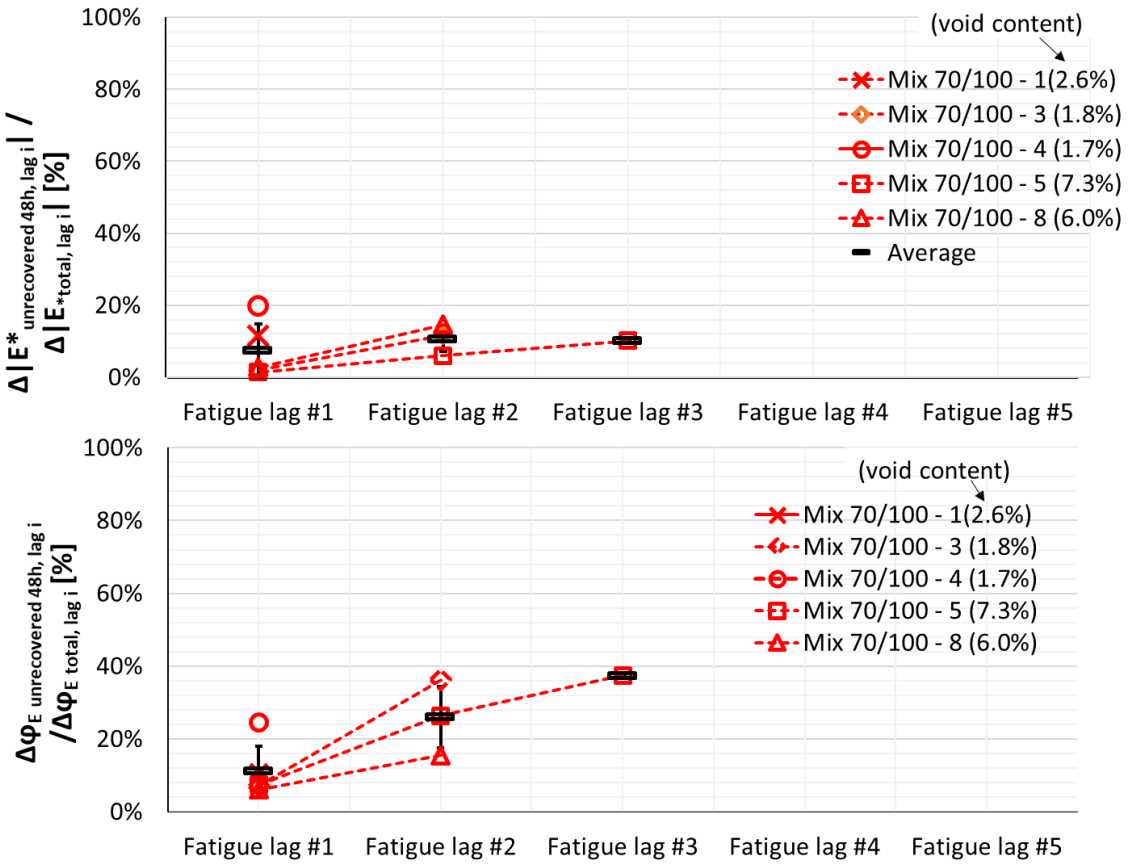

Figure 5.38. Relative contribution of unrecovered variations of |E*| and φ_E with respect to the total variation for each fatigue and rest lag with the void content indicated for mix 70/100 samples.

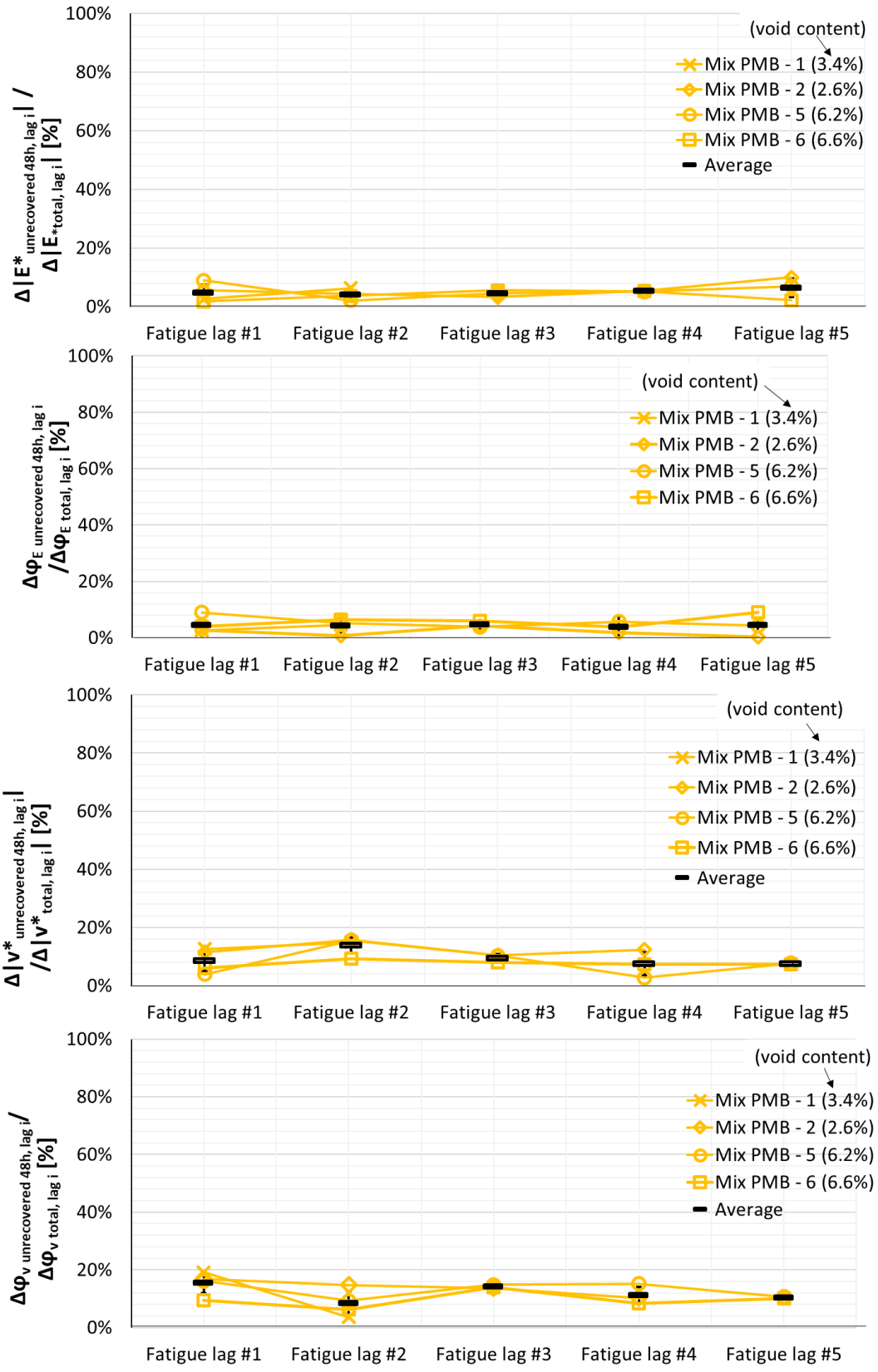

Figure 5.39. Relative contribution of unrecovered variations of |E*|, φ_E, |v*| and φ_v with respect to the total variation for each fatigue and rest lag with the void content indicated for mix PMB samples.

Figure 5.40 – Figure 5.42 shows the comparison of the relative contributions of the thixotropy variation of $|E^*|$, φ_E, $|v^*|$ and φ_v throughout the whole test for the tested samples for mix 40/60, mix 70/100 and mix PMB. Values were calculated using the envelope line for the first fatigue lag, therefore by considering each fatigue (and rest) lag separately, with its own envelope. Variability of results among samples of same mixture appear to be higher than for the other effects considered so far (non-linearity and unrecovered variations). The contribution of thixotropy appears more important for mix PMB than for mix 40/60. As a general remark, it can be noted that the estimations based on $|E^*|$ and φ_E are higher than the estimations based on $|v^*|$ and φ_v. Moreover, for mix PMB, a slight difference is found between estimations based on $|E^*|$ and φ_E, with the former ones being higher than the latter ones. For mix 40/60, higher variability is observed for estimations based on $|E^*|$ than for estimations based on φ_E, $|v^*|$ and φ_v.

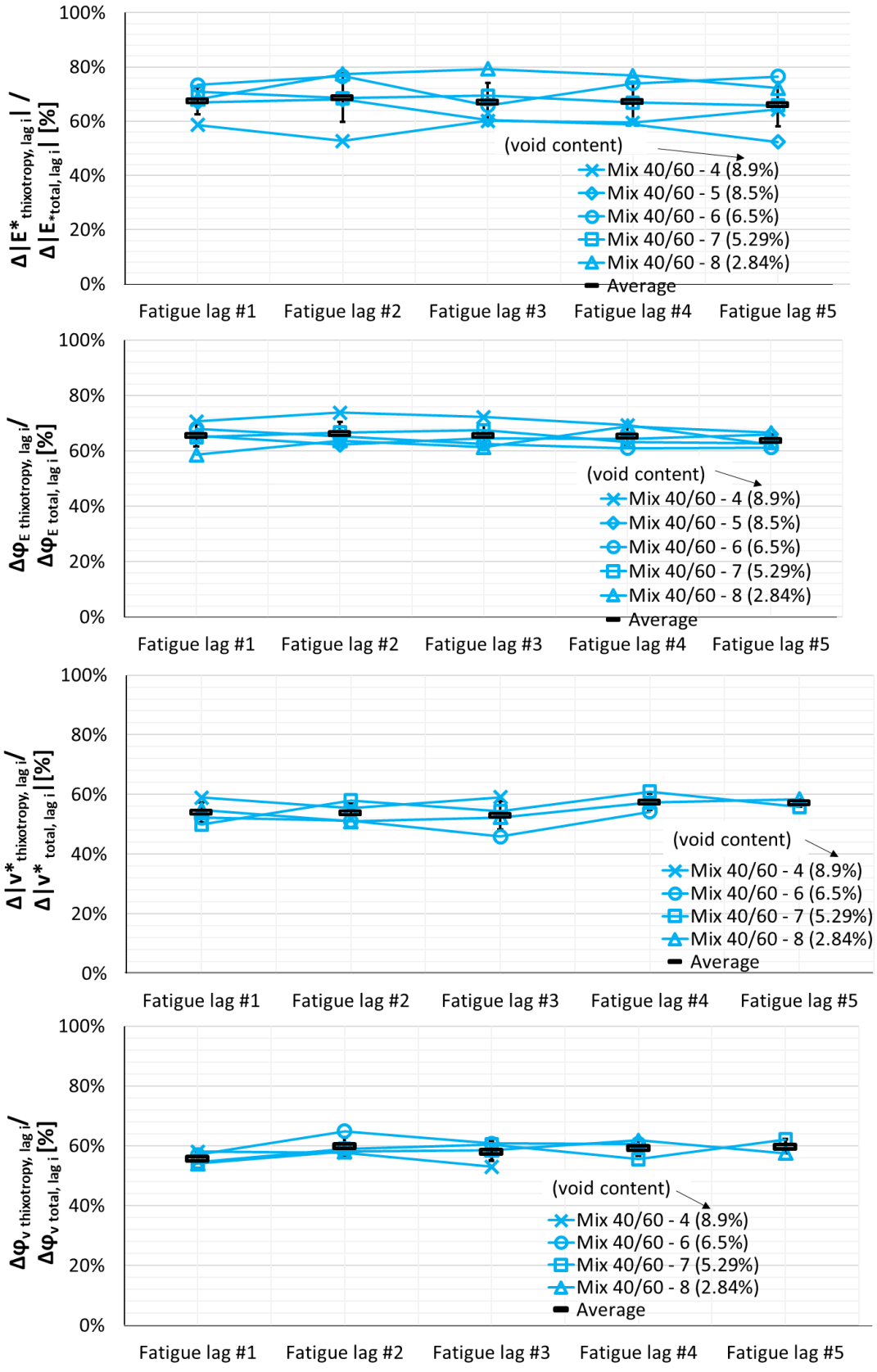

Figure 5.40. Relative contribution of thixotropy variations of |E*|, φ_E, |v*| and φ_v with respect to the total variation for each fatigue and rest lag with the void content indicated for mix 40/60 samples.

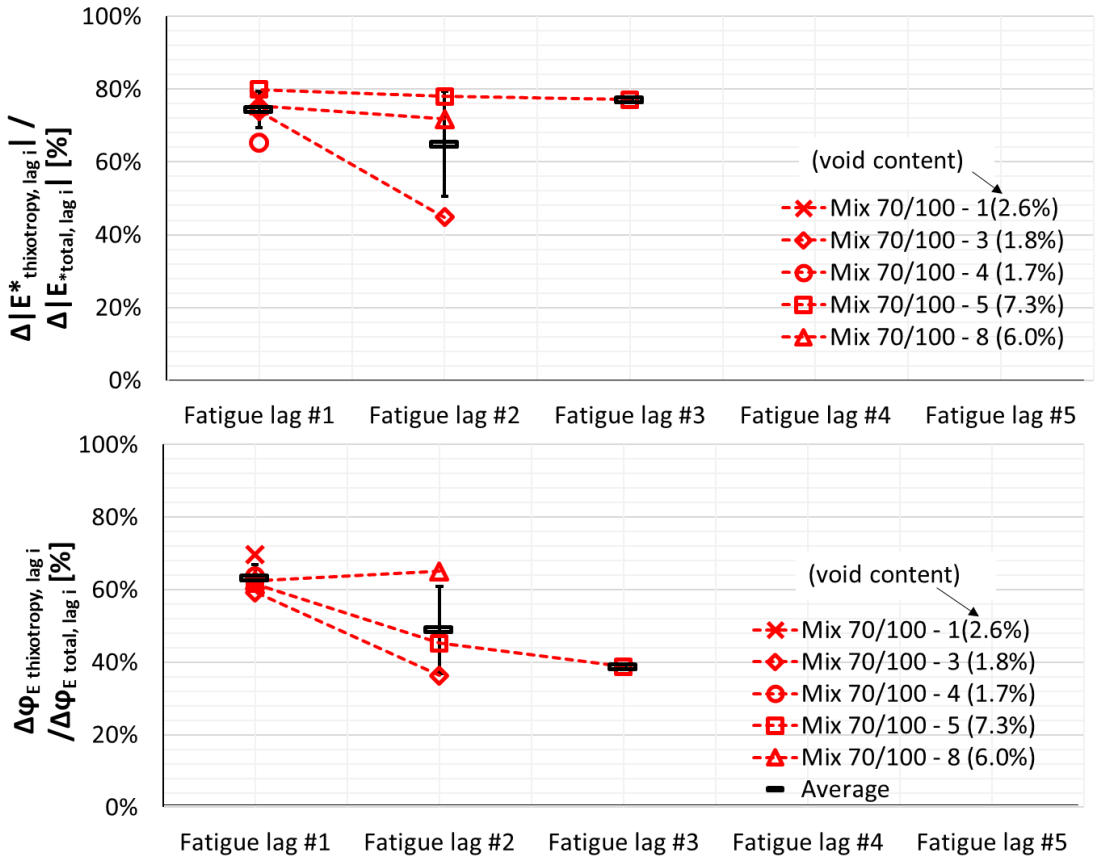

Figure 5.41. Relative contribution of thixotropy variations of |E*| and φ_E with respect to the total variation for each fatigue and rest lag with the void content indicated for mix 70/100 samples.

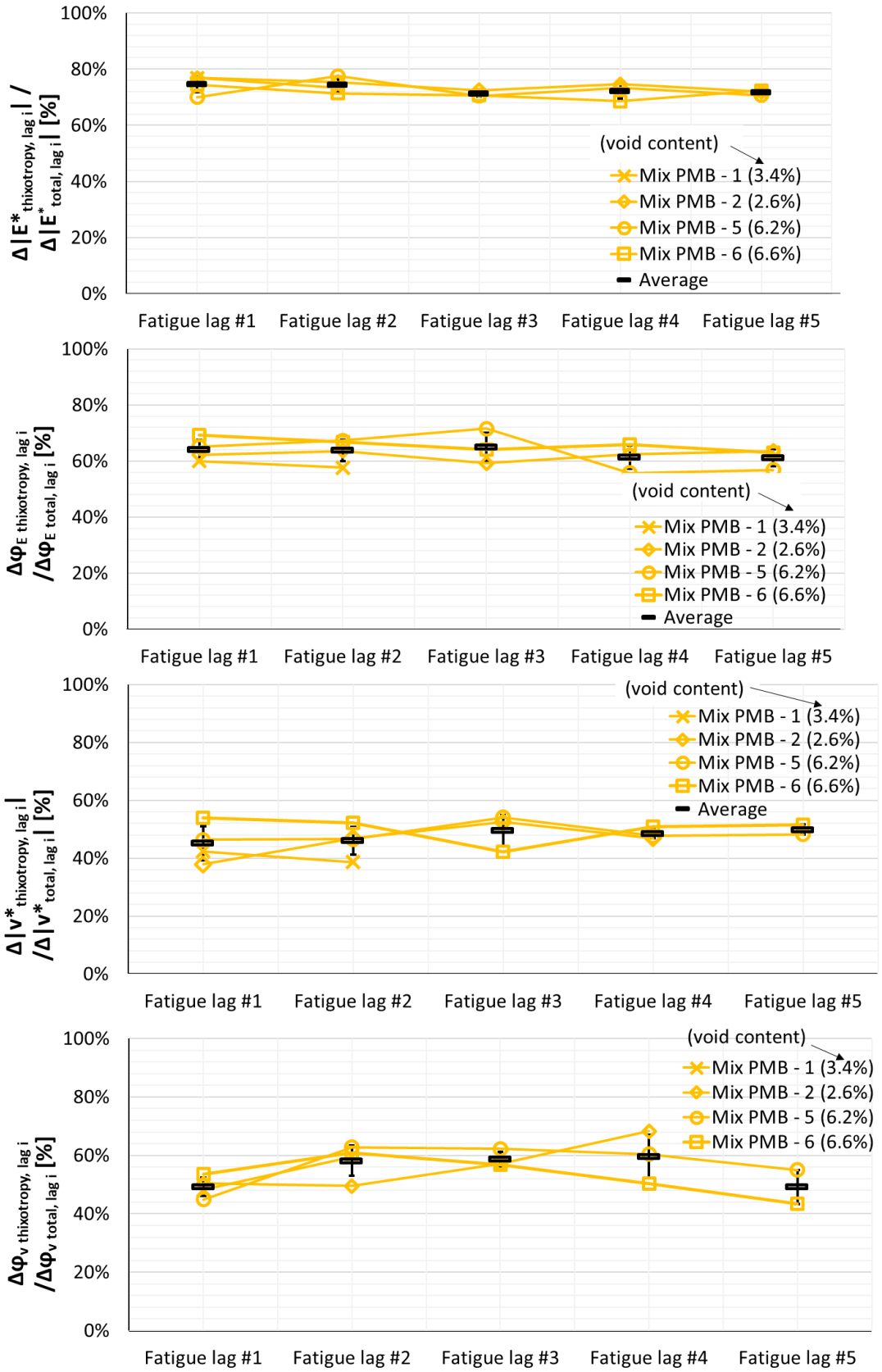

Figure 5.42. Relative contribution of thixotropy variations of |E*|, φ_E, |v*| and φ_v with respect to the total variation for each fatigue and rest lag with the void content indicated for mix PMB samples.

Figure 5.43 – Figure 5.45 shows the comparison of the relative contributions of the heating variation of |E*|, φ_E, |v*| and φ_v throughout the whole test for the tested samples (mix 40/60, mix 70/100 and mix PMB). Values were calculated using the envelope line for the first fatigue lag, therefore by considering each fatigue (and rest) lag separately, with its own envelope. The samples of each considered mixture show relatively the same proportion with respect to heating effect. The influence of heating variations for |E*|, φ_E, |v*| and φ_v does not vary substantially with fatigue lags, approximately ranging from 8% to 14% for mix 40/60 and 8% to 10% mix PMB, while mix 70/100 showed relatively more contribution to the variation of heating, approximately ranging from 10% to 20%. In both plots (for |E*|, φ_E, |v*| and φ_v), most of the points fall within the standard deviation, indicated by error bars. The few points outside error bars do not belong to any particular sample. From these observations, together with the relative low value of standard deviation calculated, the test procedure appears to provide repeatable results for the same material. Moreover, significant variations were found between air void content of the e tested samples of the various mixtures. No clear tendency is observed between the unrecovered variation of |E*|, φ_E, |v*| and φ_v and air void content. Results seem to indicate that self-heating appears to contribute to |E*|, φ_E, |v*| and φ_v variations substantially less than thixotropy, non-linearity and unrecovered variations.

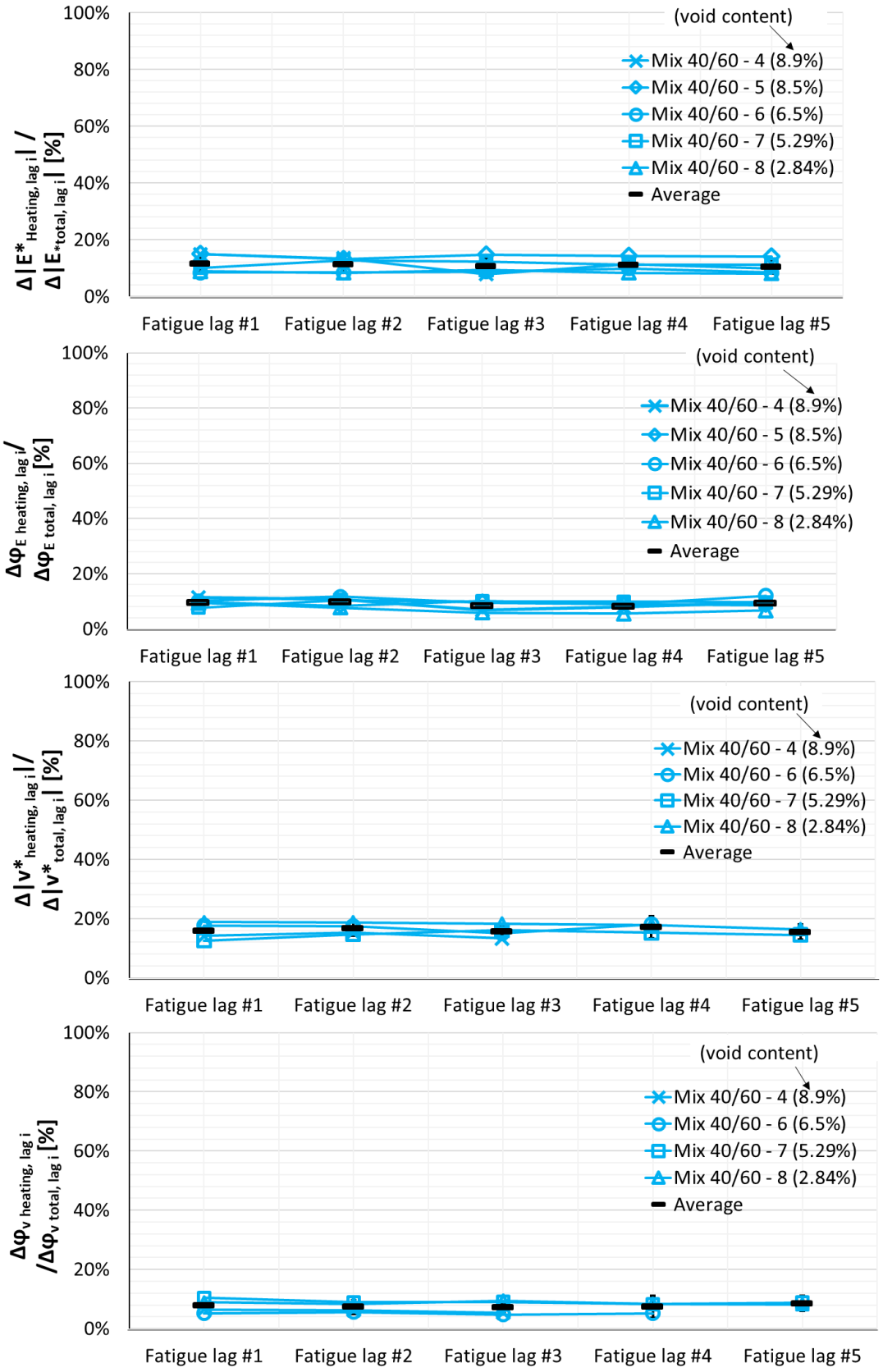

Figure 5.43. Relative contribution of heating variations of |E*|, φ_E, |v*| and φ_v with respect to the total variation for each fatigue and rest lag with the void content indicated for mix 40/60 samples.

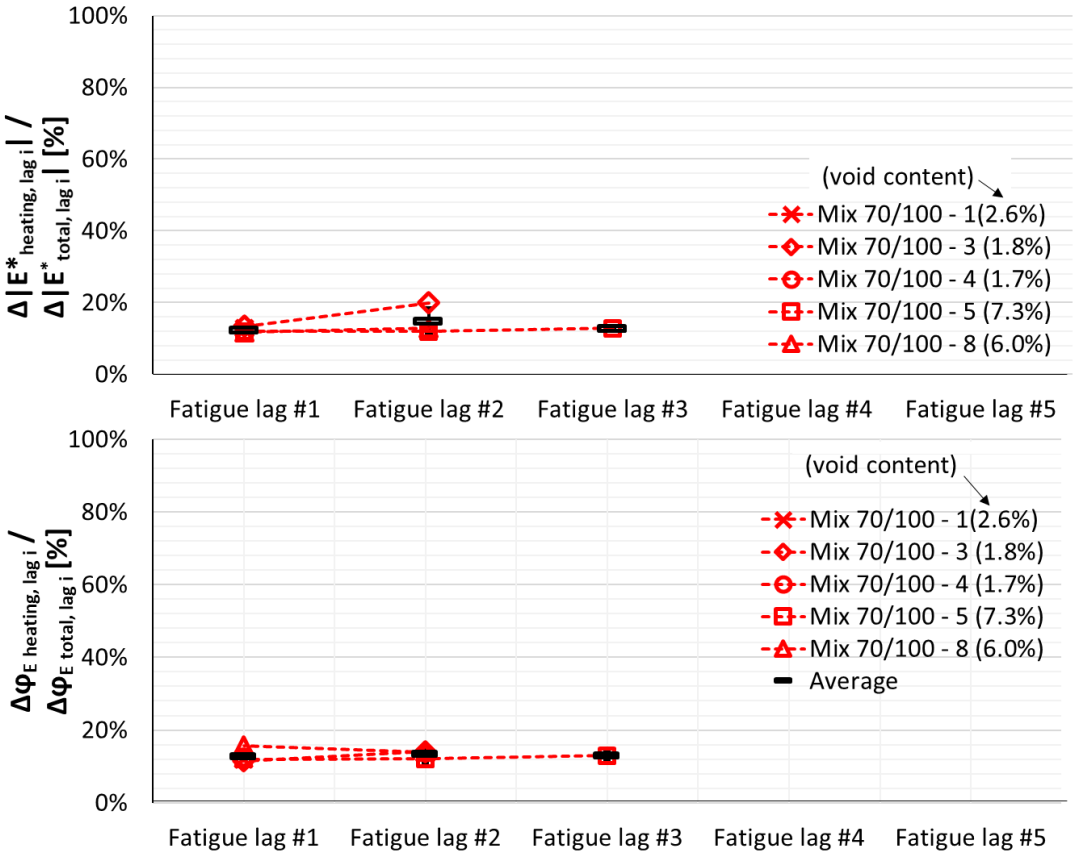

Figure 5.44. Relative contribution of heating variations of $|E^*|$, φ_E, $|\nu^*|$ and φ_ν with respect to the total variation for each fatigue and rest lag with the void content indicated for mix 70/100 samples.

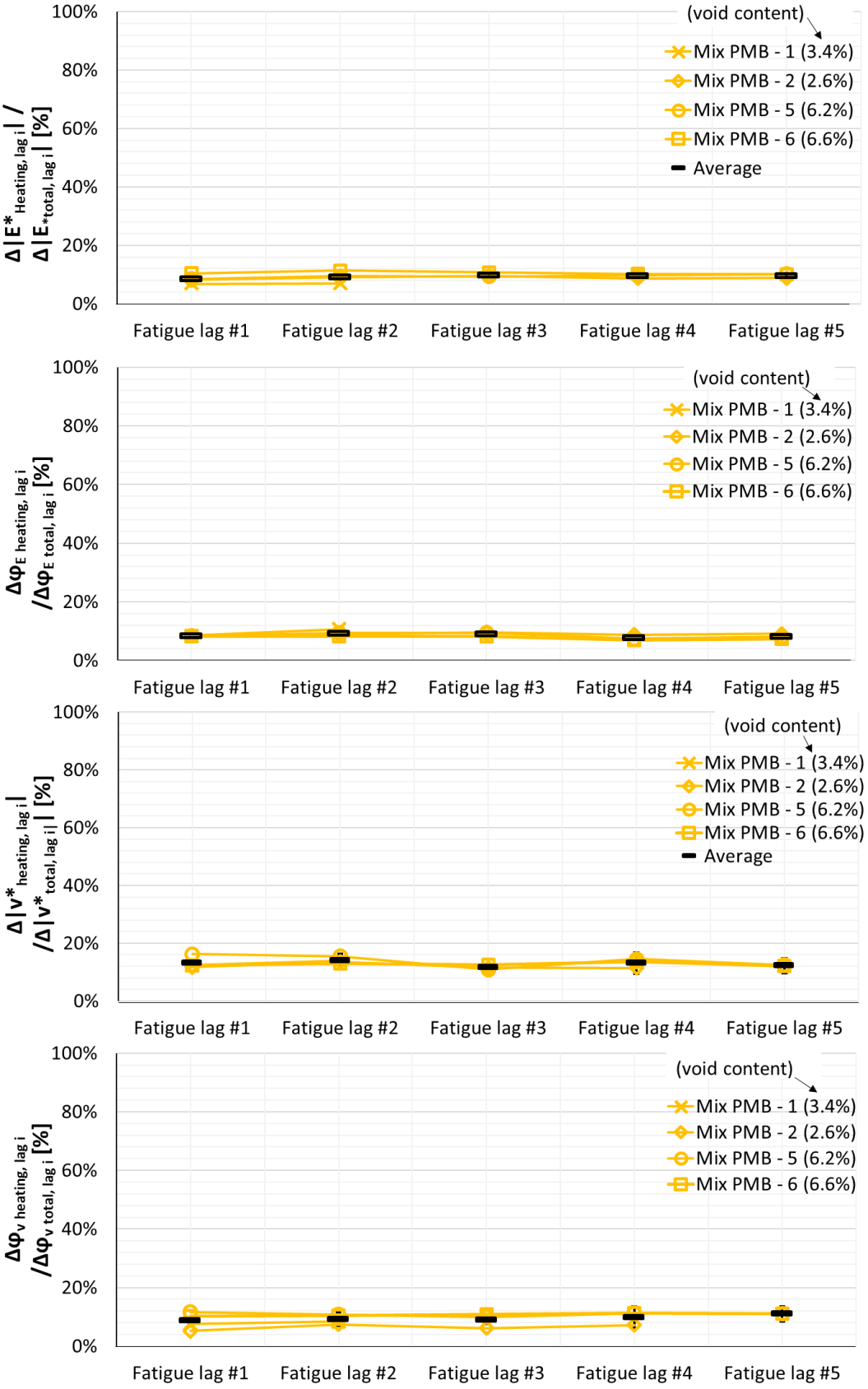

Figure 5.45. Relative contribution of heating variations of |E*|, φ_E, |v*| and φ_v with respect to the total variation for each fatigue and rest lag with the void content indicated for mix PMB samples.

Finally, the comparison of the data obtained on the various tested samples of the same mixtures for at least 3 successfully tested samples for each mixture, indicates that the test protocol appears to provide repeatable results. This can be noticed in the plots in Figures 5.34 - 5.37 (for |E*|, φE, |v*| and φv). This is also indicated by the error bars for all the tested mixtures, where most of the points fall within the standard deviation. The result obtained validates the fact that results collected under similar conditions would result in repeatable test procedures.

5.2.4. Analysis of rate of variation of mechanical properties during loading and recovery

It is interesting to compare the rate or speed at the variations of mechanical properties during loading and rest occur in each fatigue lag, within samples and amongst the different mixtures. This is intended to show if there is a relationship between the rate of variation of mechanical properties during loading and recovery. It also gives perspective to the probable existence to any variance and influence in the rate of speed during loading and recovery in each fatigue lag. The section gives a descriptive analysis of the rate of loading and recovery of the tested samples. The rate was obtained from the following ratios:

$$\text{Rate} = \frac{\Delta|E*|}{\Delta t},\ \frac{\Delta\varphi_E}{\Delta t},\ \frac{\Delta|v*|}{\Delta t} \text{ and } \frac{\Delta\varphi_v}{\Delta t} \qquad 5.45$$

where $\Delta|E^*|$, $\Delta\varphi_E$, $\Delta|v^*|$ and $\Delta\varphi_E$ are the changes in norm of complex modulus and phase angle of complex modulus, respectively, while Δt is a defined time interval. The time intervals used for the analysis during fatigue loading was 10 - 20 seconds, 100 - 110 seconds, 200 - 210 seconds, 500 – 500 seconds, 1000 – 1010 seconds, 2000 – 2010 seconds, 4000 – 4010 seconds, 6000 – 6010 seconds, 8000 – 8010 seconds, 9000 – 9010 seconds and 9990 – 10000 seconds. Also, the time intervals used for the analysis during rest periods was 10, 20 and 30 minutes and 1, 2, 4, 6, 8, 10, 12, 14, 16, 18, 20, 22, 24, 28, 32, 36, 40, 44 and 48 hours.

Figure 5.46 shows rates of variation during loading and recovery for |E*|, φ_E, |v*| and φ_v for each fatigue and rest lag for mix 40/60 - 7. Other results for the rates of variation during loading and recovery |v*| and φ_v performed on other mixtures are represented in the appendix. It can be observed that following the completion of loading, the |E*|, φ_E, |v*| and φ_v rapidly increased and decreased respectively throughout the rest period. The majority of the recovery for the duration of the rest period occurs within the first four hours of recovery; after that, this increase and decrease (with respect to |E*|, φ_E, |v*| and φ_v respectively) becomes considerably more moderate. The recovery of mechanical properties occurred at a significantly slower rate towards

the end of each rest session. At the same time, the rate of variation during fatigue loading was significantly higher at the beginning of each loading session (approximately for the first 10,000 cycles) than at the end. Additionally, while the rate of variation observed during the various rest periods is almost identical, in trend and amplitude. However, slight variations are observed among the curves of the fatigue loadings, with fatigue lag 1 invariably showing the slowest variations and fatigue lag 5 indicating the fastest. Nonetheless, the other fatigue lags cannot be ranked in their corresponding order.

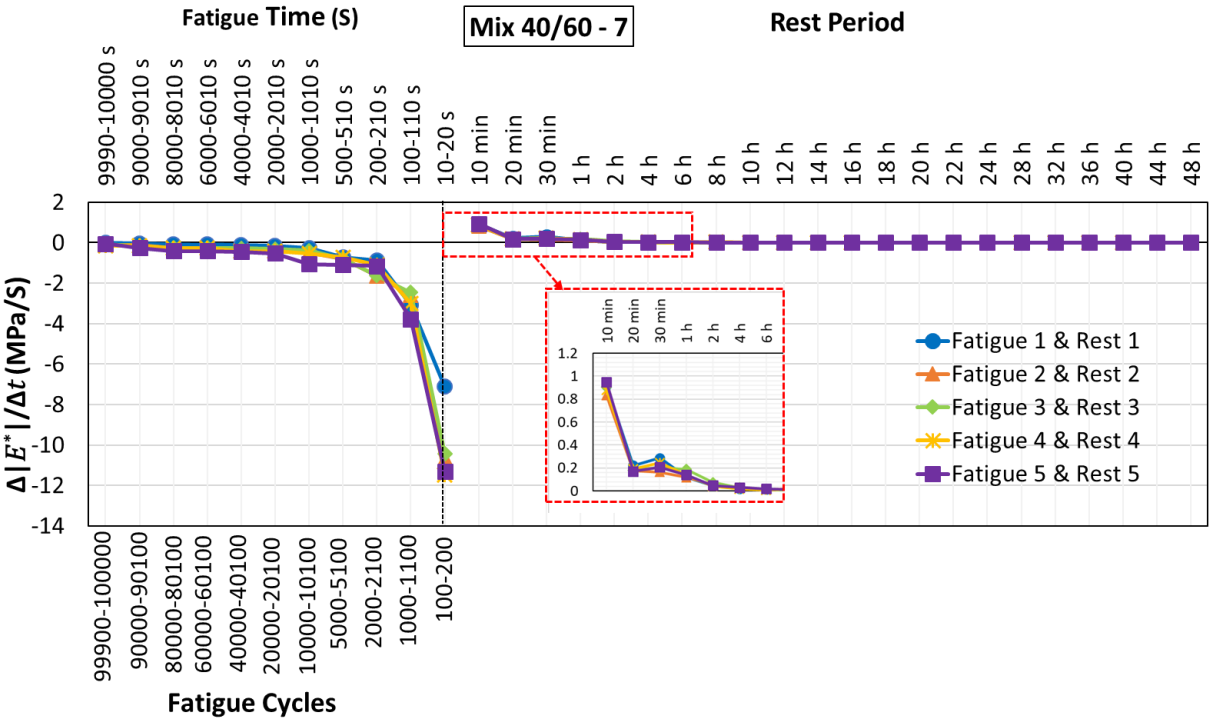

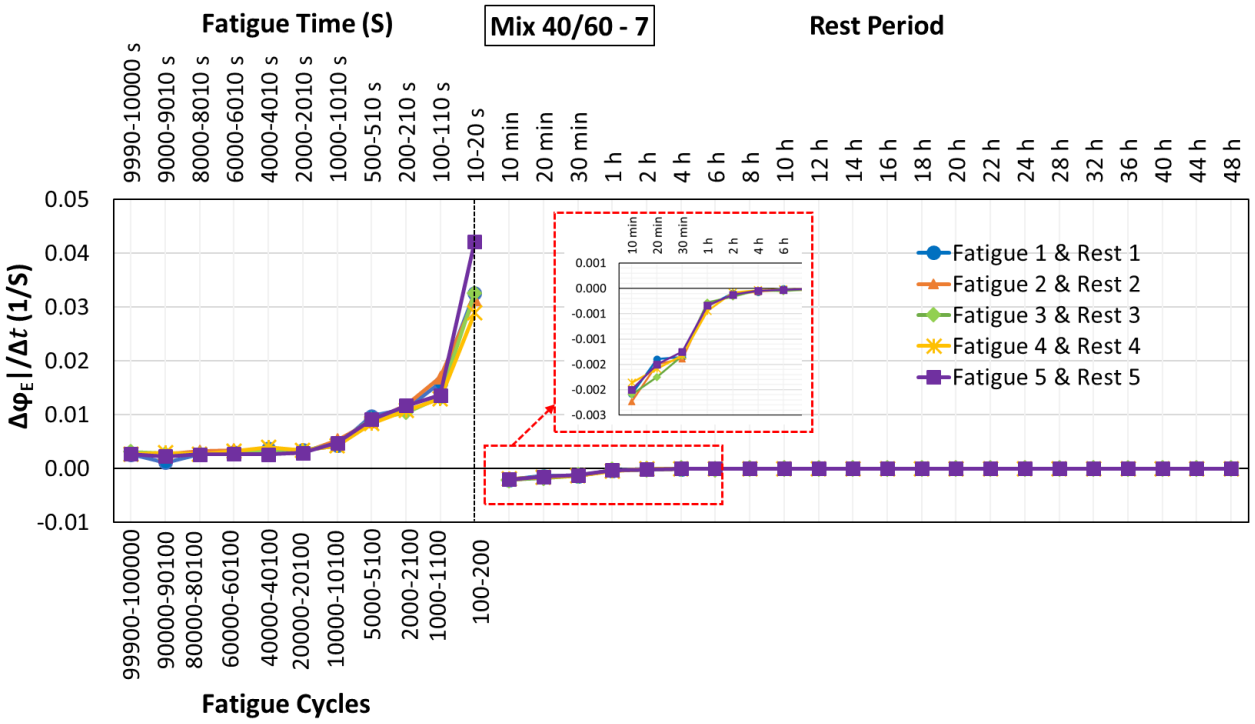
Fatigue Time (S)
Mix 40/60 - 7
Rest Period
9990-10000 s
9000-9010 s
8000-8010 s
6000-6010 s
4000-4010 s
2000-2010 s
1000-1010 s
500-510 s
200-210 s
100-110 s
10-20 s
10 min
20 min
30 min
1 h
2 h
4 h
6 h
8 h
10 h
12 h
14 h
16 h
18 h
20 h
22 h
24 h
28 h
32 h
36 h
40 h
44 h
48 h
0.05
0.04
0.03
0.02
0.01
0.00
-0.01
Δφ_E|/Δt (1/S)
Fatigue 1 & Rest 1
Fatigue 2 & Rest 2
Fatigue 3 & Rest 3
Fatigue 4 & Rest 4
Fatigue 5 & Rest 5
99900-100000
90000-90100
80000-80100
60000-60100
40000-40100
20000-20100
10000-10100
5000-5100
2000-2100
1000-1100
100-200
Fatigue Cycles

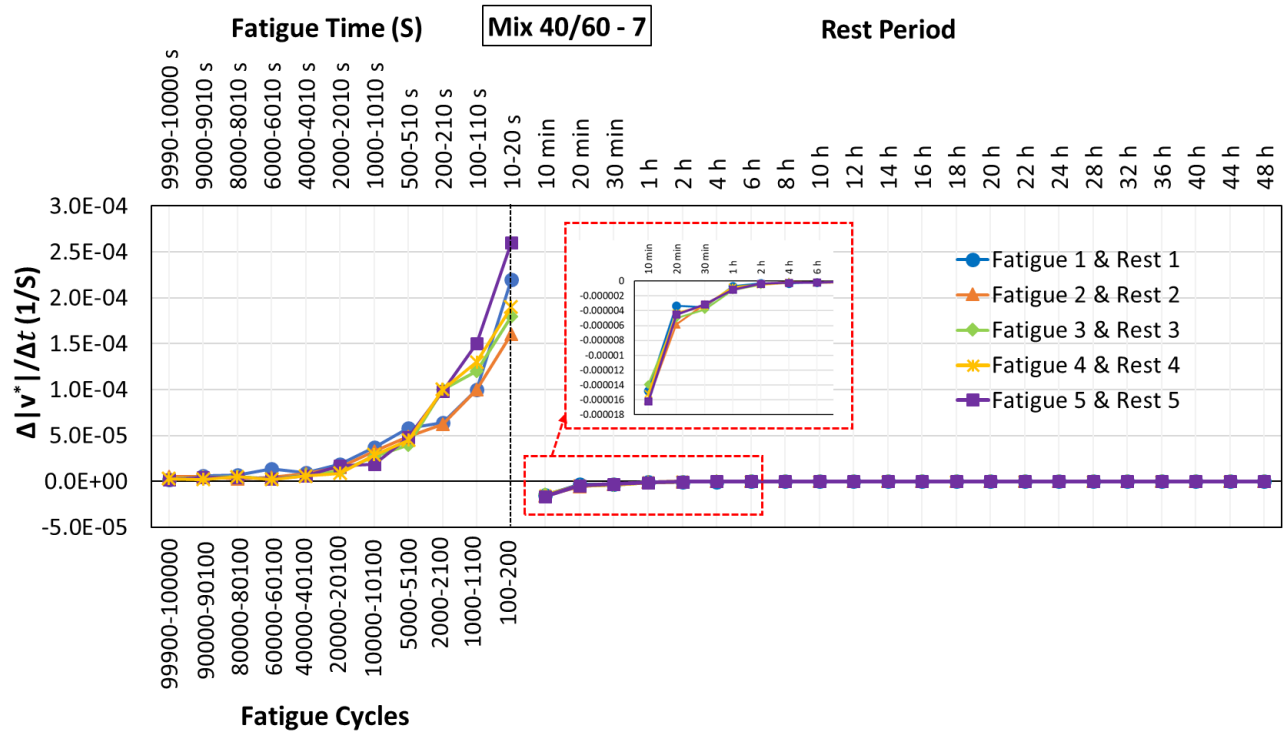
Fatigue Time (S)
Mix 40/60 - 7
Rest Period
9990-10000 s
9000-9010 s
8000-8010 s
6000-6010 s
4000-4010 s
2000-2010 s
1000-1010 s
500-510 s
200-210 s
100-110 s
10-20 s
10 min
20 min
30 min
1 h
2 h
4 h
6 h
8 h
10 h
12 h
14 h
16 h
18 h
20 h
22 h
24 h
28 h
32 h
36 h
40 h
44 h
48 h
3.0E-04
2.5E-04
2.0E-04
1.5E-04
1.0E-04
5.0E-05
0.0E+00
-5.0E-05
Δ|v*|/Δt (1/S)
Fatigue 1 & Rest 1
Fatigue 2 & Rest 2
Fatigue 3 & Rest 3
Fatigue 4 & Rest 4
Fatigue 5 & Rest 5
99900-100000
90000-90100
80000-80100
60000-60100
40000-40100
20000-20100
10000-10100
5000-5100
2000-2100
1000-1100
100-200
Fatigue Cycles

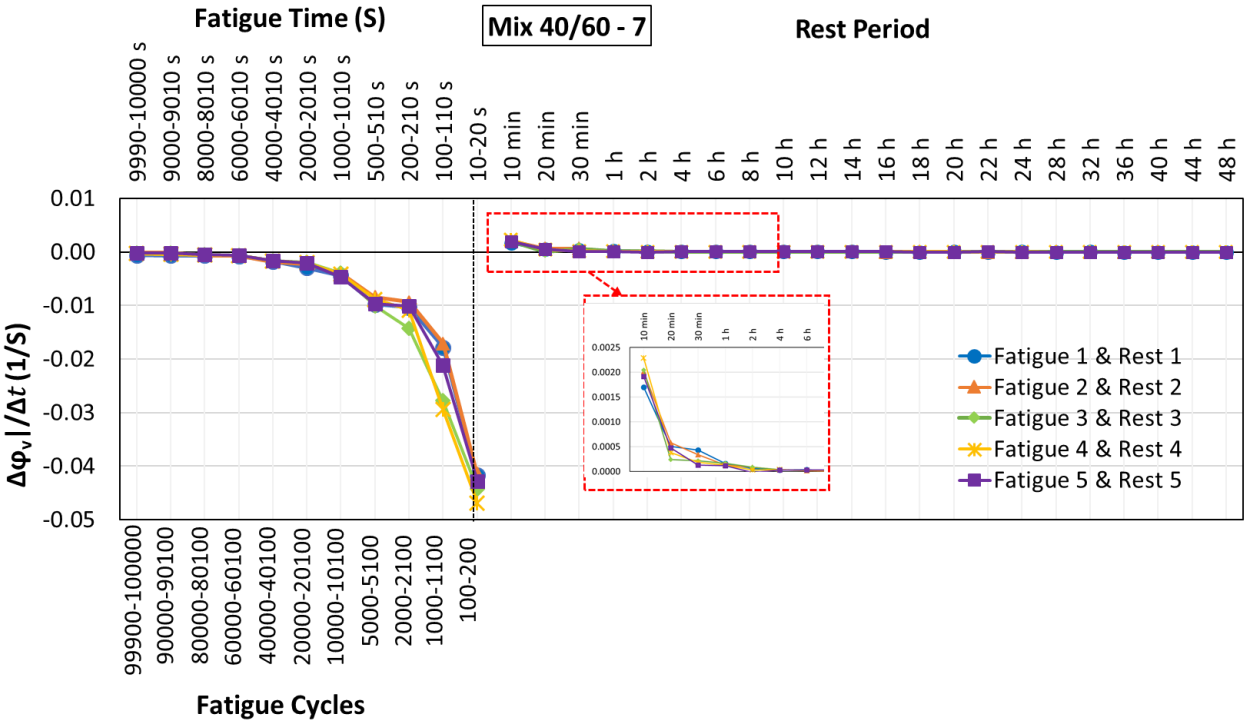

Figure 5.46. Rate of variation during loading and recovery for |E*|, $\varphi_{E,}$ |v*| and φ_v for each fatigue and rest lag for mix 40/60 - 7.

The rate of variation during loading and recovery for each lag of all samples for each mixture was analysed and compared. Plots for mix 40/60 are shown in Figure 5.47 while those of the other two mixtures are in the appendix. The legend is structured with all lags indicated within brackets for all samples (in different colors). For example, "Mix 40/60 – 7(4) 5.3%", plotted in yellow, representing results obtained during lag 4 for sample 7 of mix 40/60, having a voids content of 5.3%. Results obtained for samples 1 and 8 of mix 40/60 (Mix 40/60 – 1, Mix 40/60 – 8) show the lowest and highest, respectively, variation rates of |E*| and φ_E during fatigue loading while similar recovery rate during rest were observed for all samples, both for |E*| and φ_E.

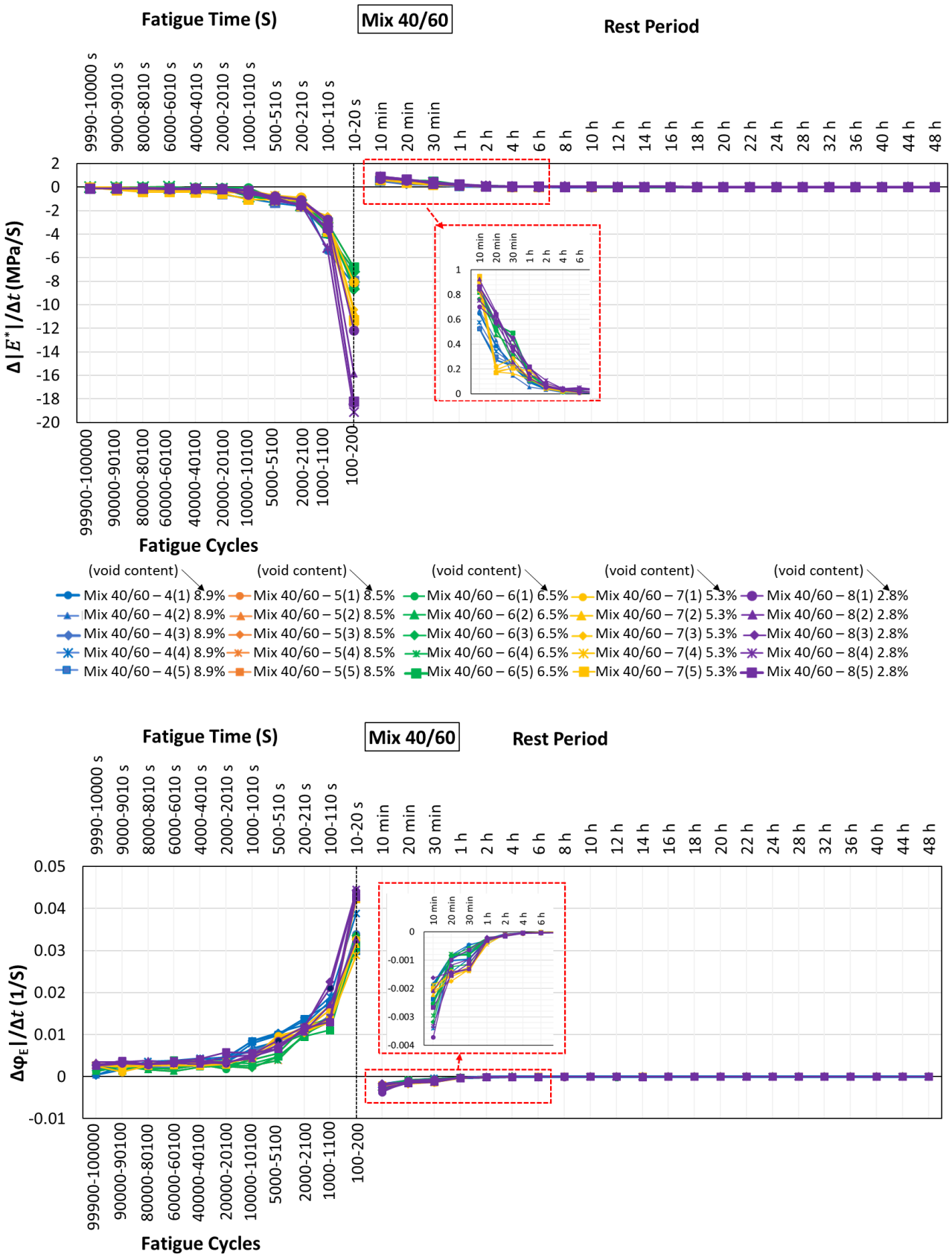

Figure 5.47. Rate of variation during loading and recovery for |E*| and φ_E for each fatigue and rest lag for each mix 40/60 sample.

Figures 5.48 - 5.52 present the rates of variation during each fatigue and rest lag (#1 to #5) for all samples of the tested mixtures (mix 70/100, mix 40/60 and mix PMB). While no precise ranking can be identified among materials with respect to the rate of variation of |E*| and φ_E during fatigue loading, some differences can be observed for the results obtained during rest, with mix 70/100 showing the highest rates of recovery for the first rest period. As already mentioned, samples of mix 70/100 failed generally well before samples of other mixtures: of the five samples successfully tested, two reached rest period #2, one reached rest period #3 and none reached rest period #4.

No substantial overall differences could be found between mix 40/60 and mix PMB (no clear ranking between the two materials). If the analysis is limited to these two materials, starting from fatigue and rest lag #2, sample 5 and sample 6 of mix PMB are generally among the ones with, respectively, the highest and the lowest recovery rates, despite their similar void content (6.2% and 6.6%, respectively).

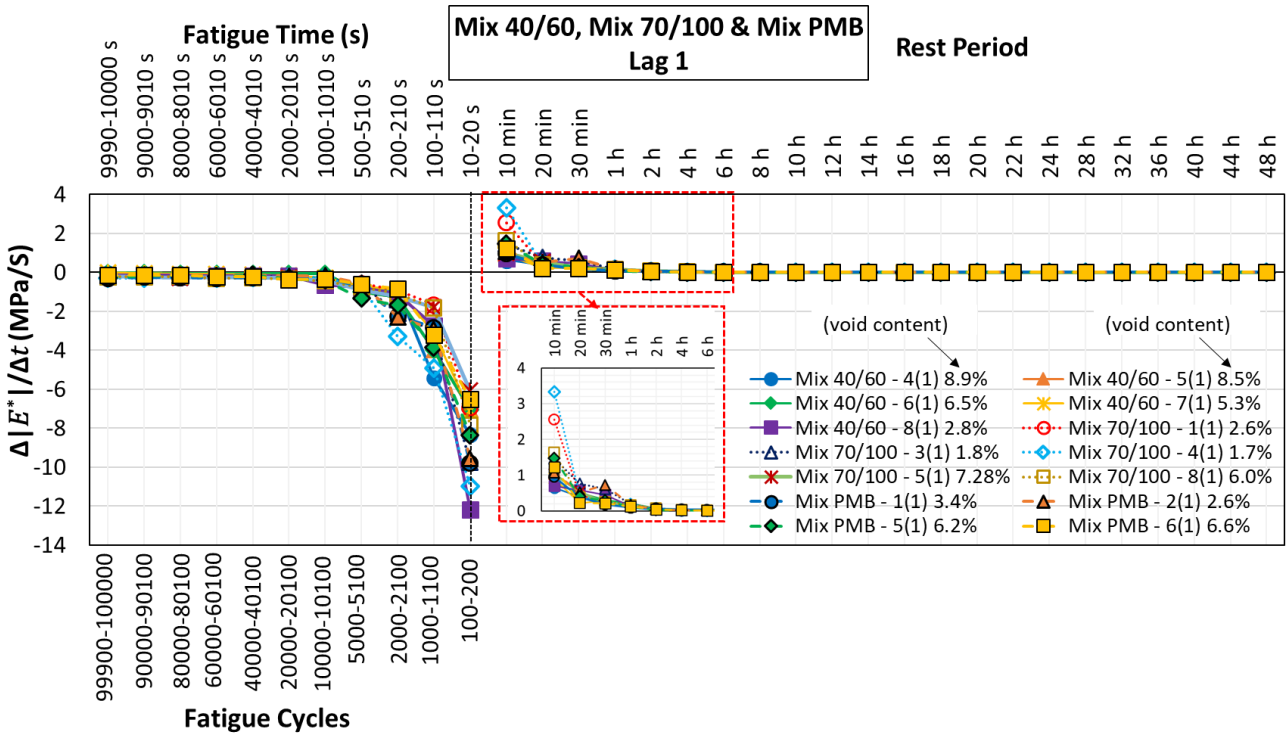

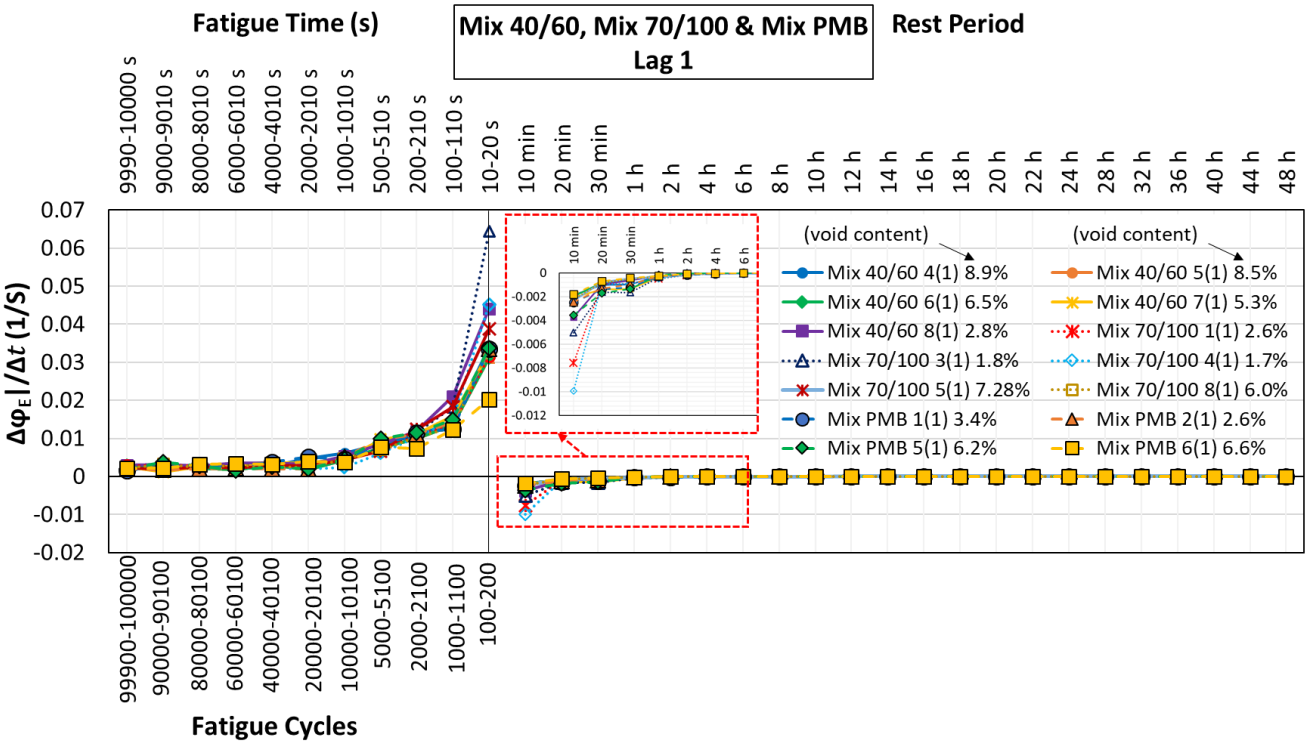

Figure 5.48. Rate of variation during loading and recovery for |E*| and φ_E for fatigue and rest lag 1 for mix 70/100, mix 40/60 and mix PMB.

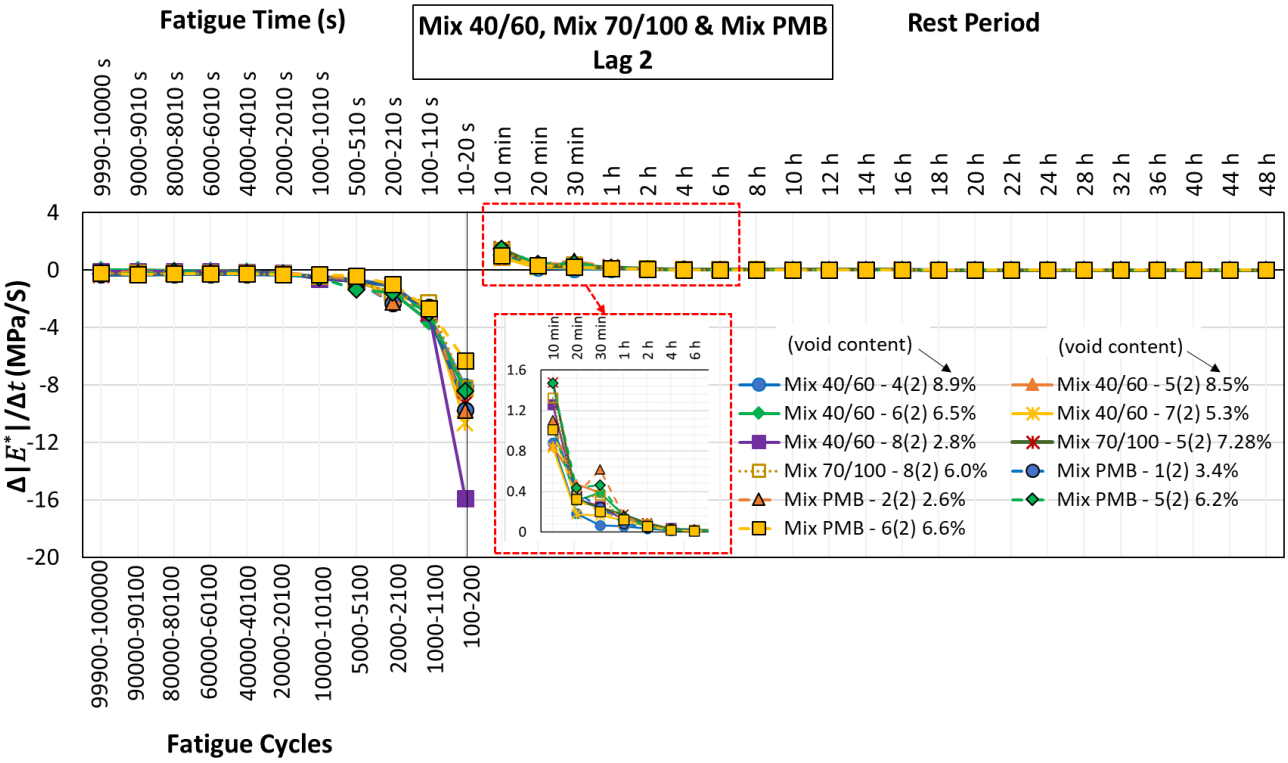

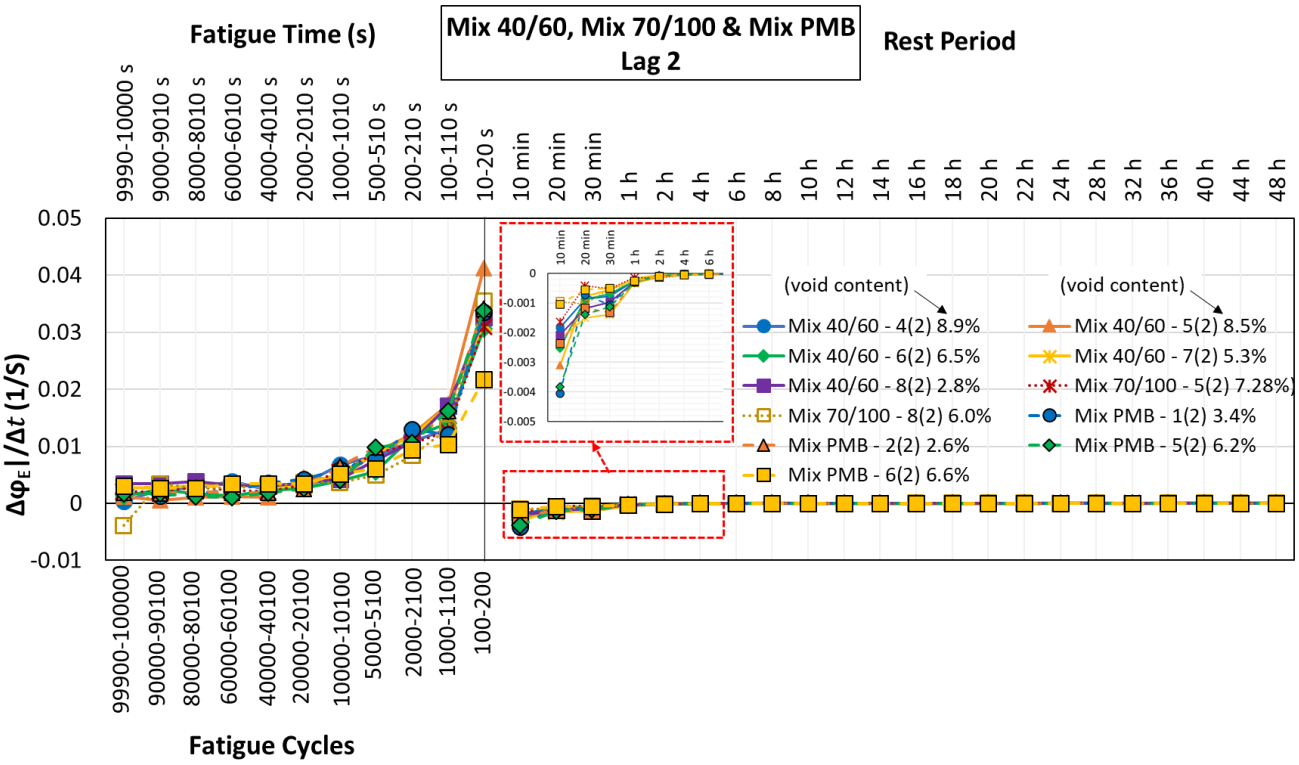

Figure 5.49. Rate of variation during loading and recovery for |E*| and φ_E for fatigue and rest lag 2 for mix 70/100, mix 40/60 and mix PMB.

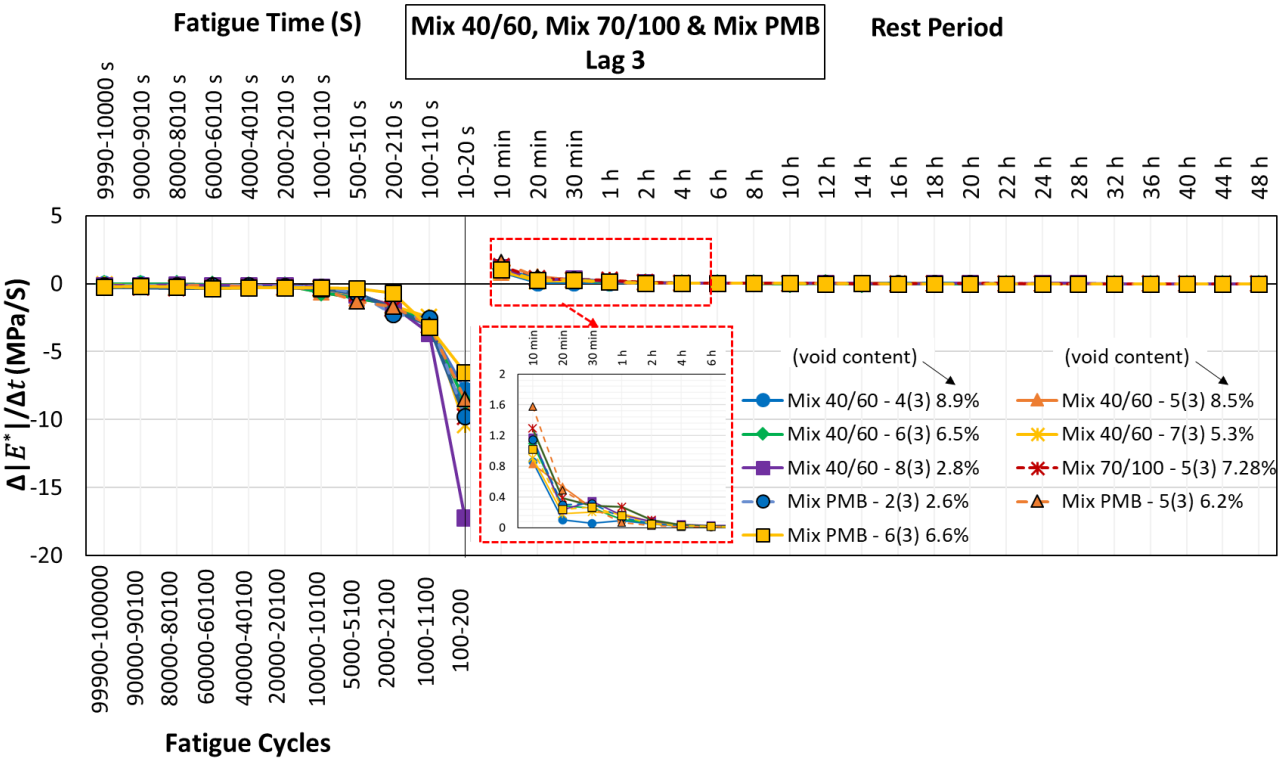

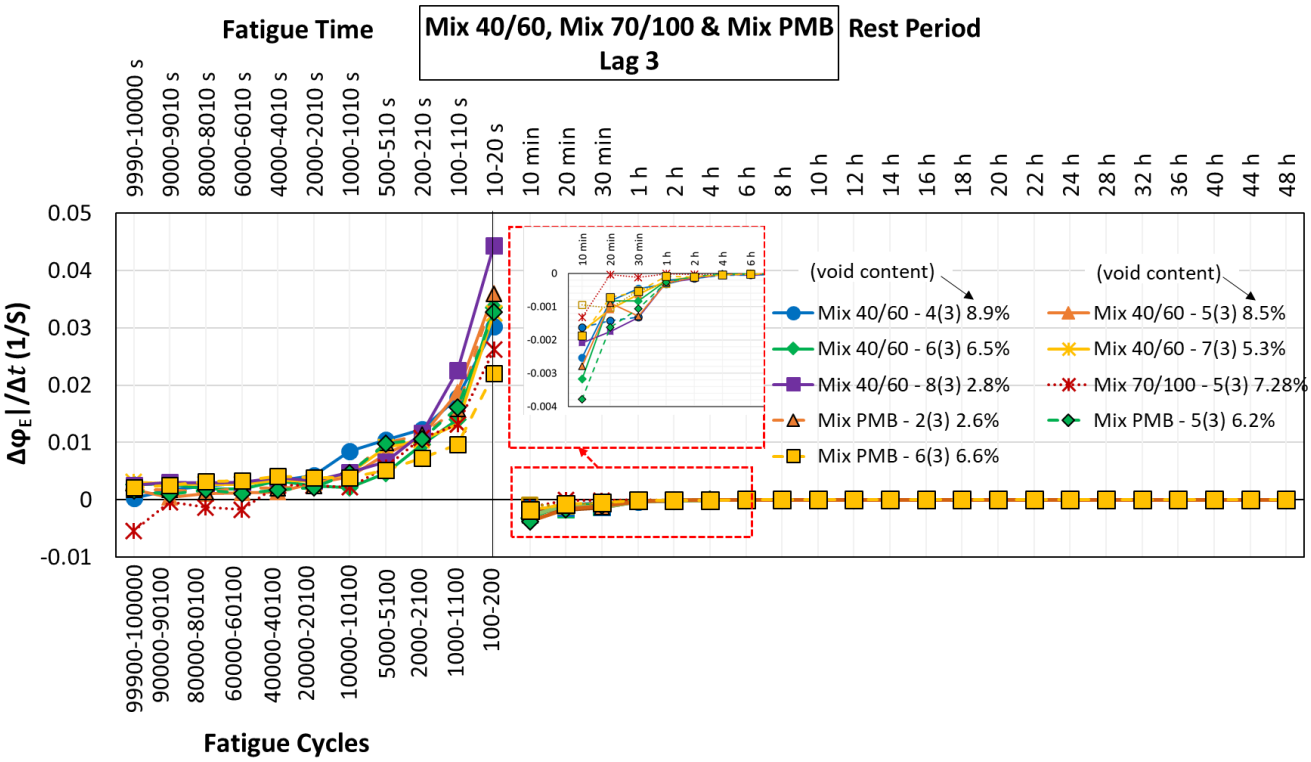

Figure 5.50. Rate of variation during loading and recovery for |E*| and φ_E for fatigue and rest lag 3 for mix 70/100, mix 40/60 and mix PMB.

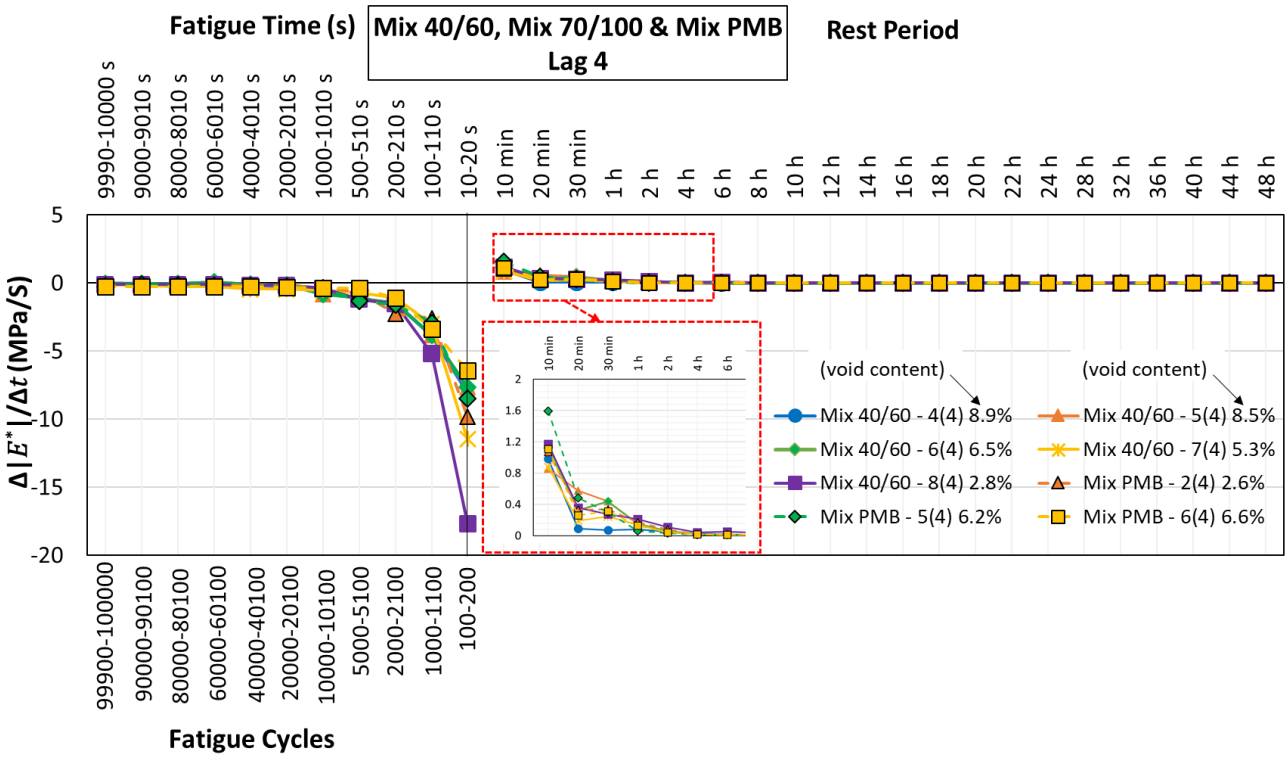

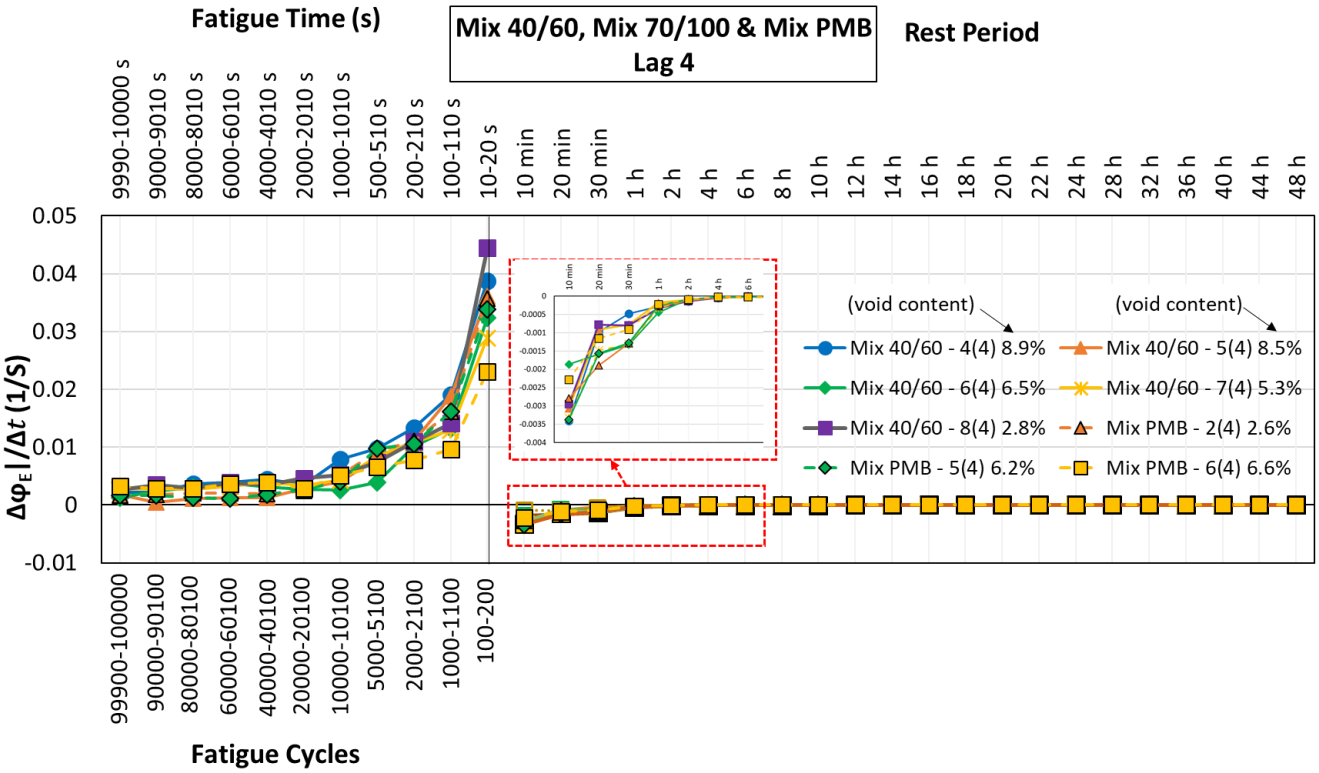

Figure 5.51. Rate of variation during loading and recovery for |E*| and φ for fatigue and rest lag 4 for mix 70/100, mix 40/60 and mix PMB.

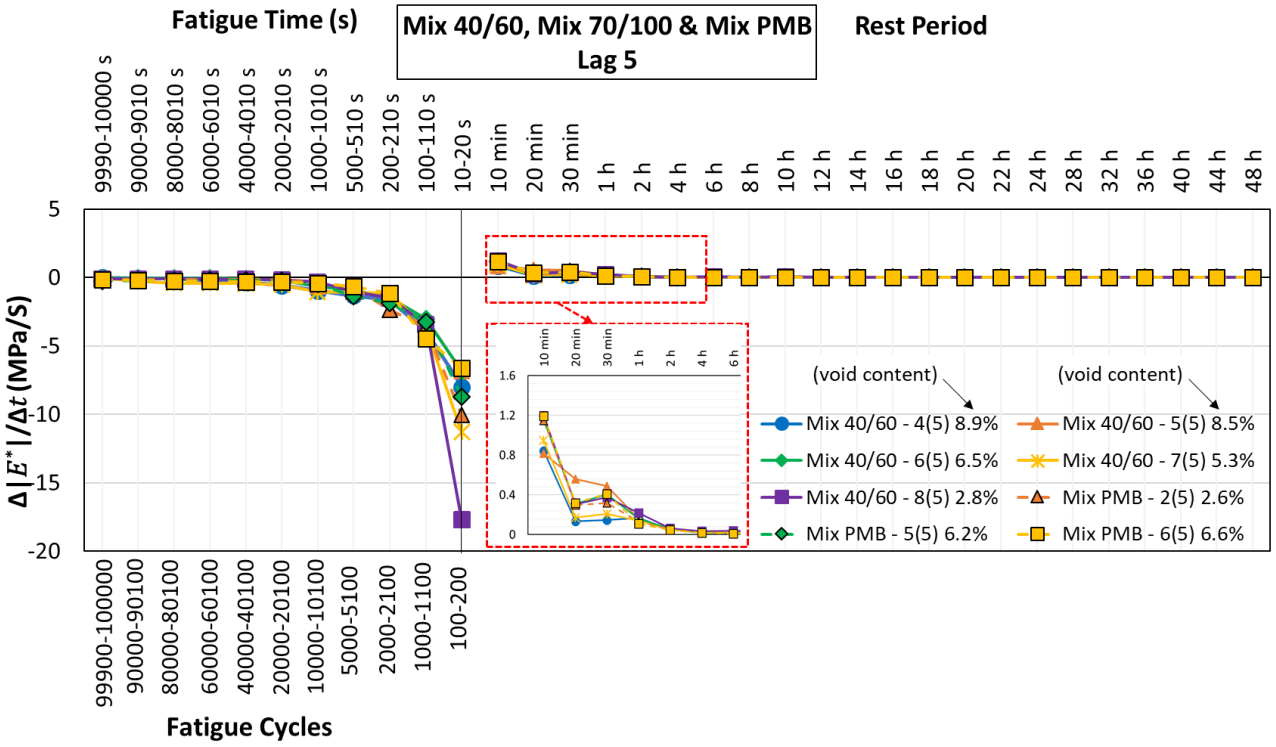

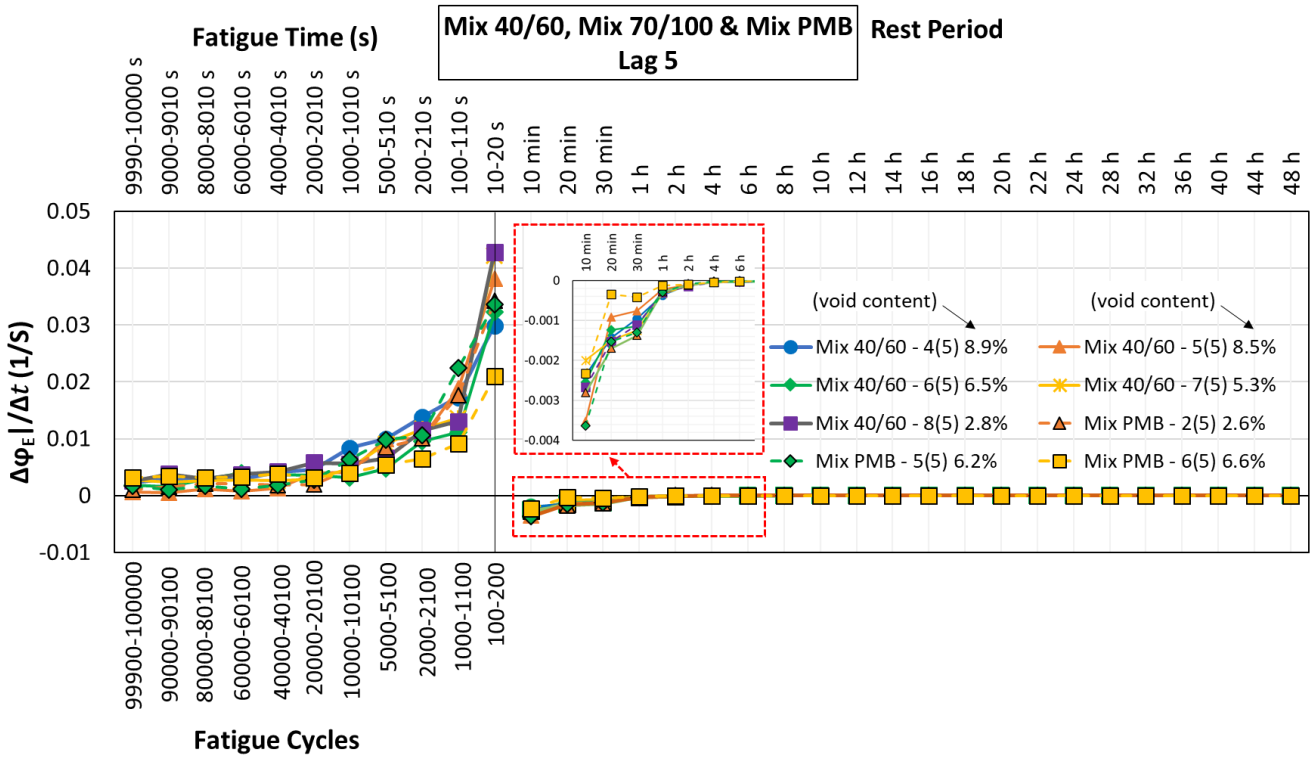

Figure 5.52. Rate of variation during loading and recovery for |E*| and φ_E for fatigue and rest lag 5 for mix 70/100, mix 40/60 and mix PMB.

Generally, most of the variation during loading occurs within the first 1000 seconds approximately (approximately for the first 10,000 cycles) than at the end, while most of the variation during recovery occurs within the first four hours. With this obvious occurrence, it can be concluded that the rates of variation during loading and recovery for the various fatigue and rest periods show similar trends as shown in Figures 5.48 – 5.52. Interestingly, the rate of variation observed during the various loading and rest periods are invariably similar in trend. This implies that the rate of loadings and recoveries obtained for each fatigue and rest period are extremely comparable in pace and amplitude. These results indicate that the approach is probably not a clear method to distinguish between materials.

5.2.5. Analysis of energy dissipation

Different approaches are usually used to characterise fatigue resistance in mixtures including the dissipated energy approach. Energy dissipation analysis have been successfully applied in evaluating the fatigue performance of bituminous materials. This is because fatigue damage is usually related to energy dissipation, hence, using the concept of dissipated energy properly is

essential for interpreting the variation of mechanical properties during loading and recovery. This section sets out to investigate the energy dissipation features of the tested materials under fatigue loading and rest. Therefore, the feasibility and effectiveness of energy dissipation under fatigue loading and rest were evaluated graphically. Based on these, one hypothesis that comes from this study it that there is a possibility for the dissipated energy to be used to assess rate of variation during loading and energy dissipation.

Since viscous energy dissipation during cyclic loading leads to self-heating, the amounts of dissipated energy per cycle (W_N) and cumulated dissipated energy (ΣW) were monitored. The formula for cumulative dissipated energy (ΣW) was as follows:

$$\Sigma W = \pi \varepsilon_A \sigma_A \sin\varphi$$

where ε_A and σ_A are, respectively, strain and stress amplitudes at cycle N.

The rate of energy dissipation depends on factors such as loading frequency, temperature, and environmental conditions. Plotting internal temperature against cumulated dissipated energy was done to further confirm the relationship between energy dissipation and self-heating with typical Figure 5.53 providing an example for mix 40/60 - 7. As observed, an increase in internal temperature seems to perfectly correspond with cumulated dissipated energy for all the five fatigue lags.

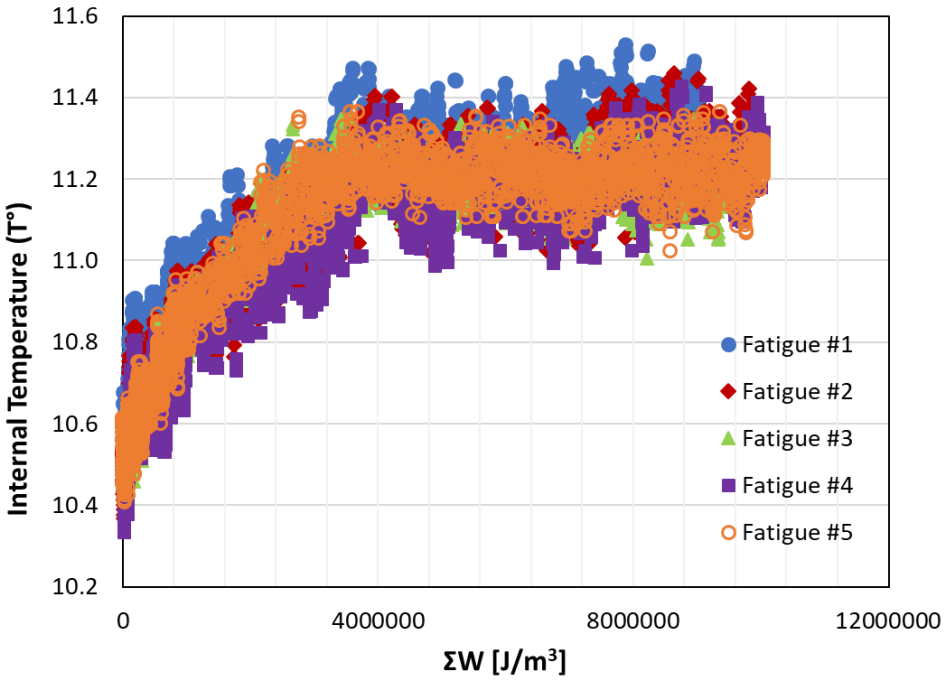

Figure 5.53. Internal temperature against cumulated dissipated energy (ΣW) during fatigue lags for mix 40/60 - 7.

Comparison of the energy dissipation for all the mixtures for the various fatigue lags was carried out by plotting the cumulated dissipated energy against the number of cycles. The result in Figure 5.54 shows energy dissipation tends to increase with the progression of fatigue cycles with mix 70/100 appearing to dissipate the most and mix PMB the least.

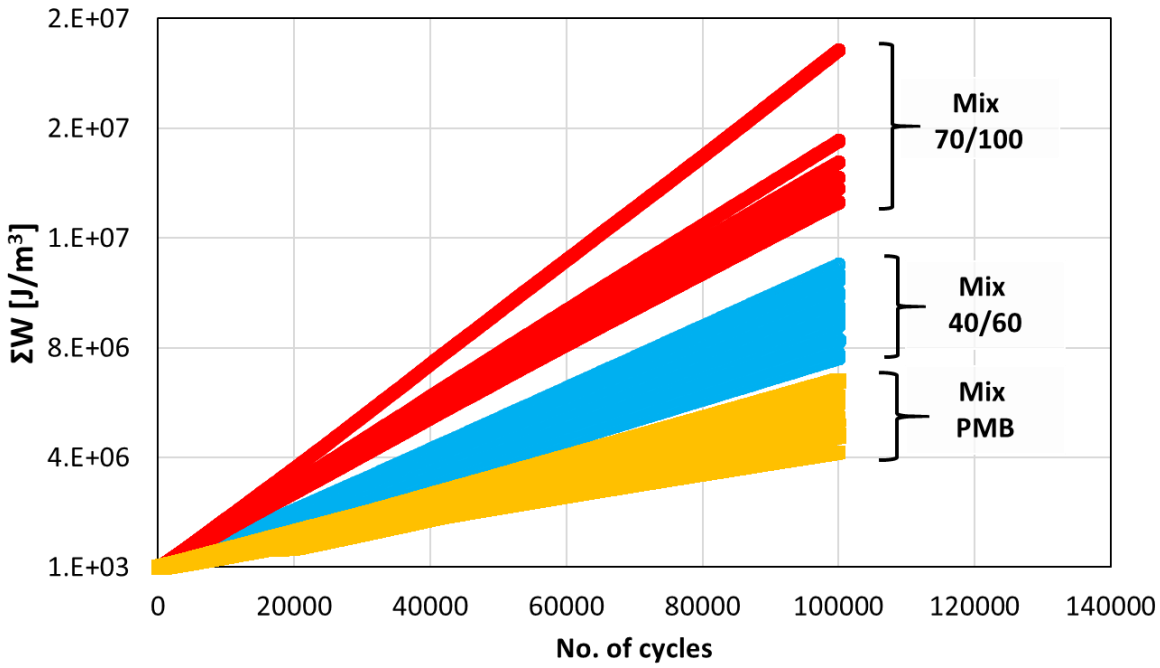

Figure 5.54. Cumulated dissipated energy (ΣW) against number of cycles during fatigue lags for all the mixtures.

Based on the Figures 5.53 and 5.54, the potential relation between the rates of variation of mechanical properties and energy dissipation during fatigue loading and rest for the different bituminous mixtures tested was investigated. This is essential because energy dissipation during the rate of variation during loading is often considered in literature when studying the fatigue behaviour of bituminous materials.

Rates of variation of |E*| and φ_E during fatigue loading and rest are plotted against dissipated energy as shown in Figures 5.55 and 5.56 for mix 70/100, mix 40/60 and mix PMB for all the fatigue lags and rest with results for complex Poisson presented in the appendix. Among all the tested mixtures, results of mix 70/100 appear to follow a distinct path during fatigue loading, with respect to the other two mixtures, regardless of the material property used for the estimation (|E*| and φ_E). Also, for the rates of recovery during, mix 70/100 appear to be distinct.

No clear differences between the overall trends of the other two materials (mix 40/60 and mix PMB) could be observed for rates of recovery during rest. Also, no correlation seems to exist between rate of variation and energy dissipation.

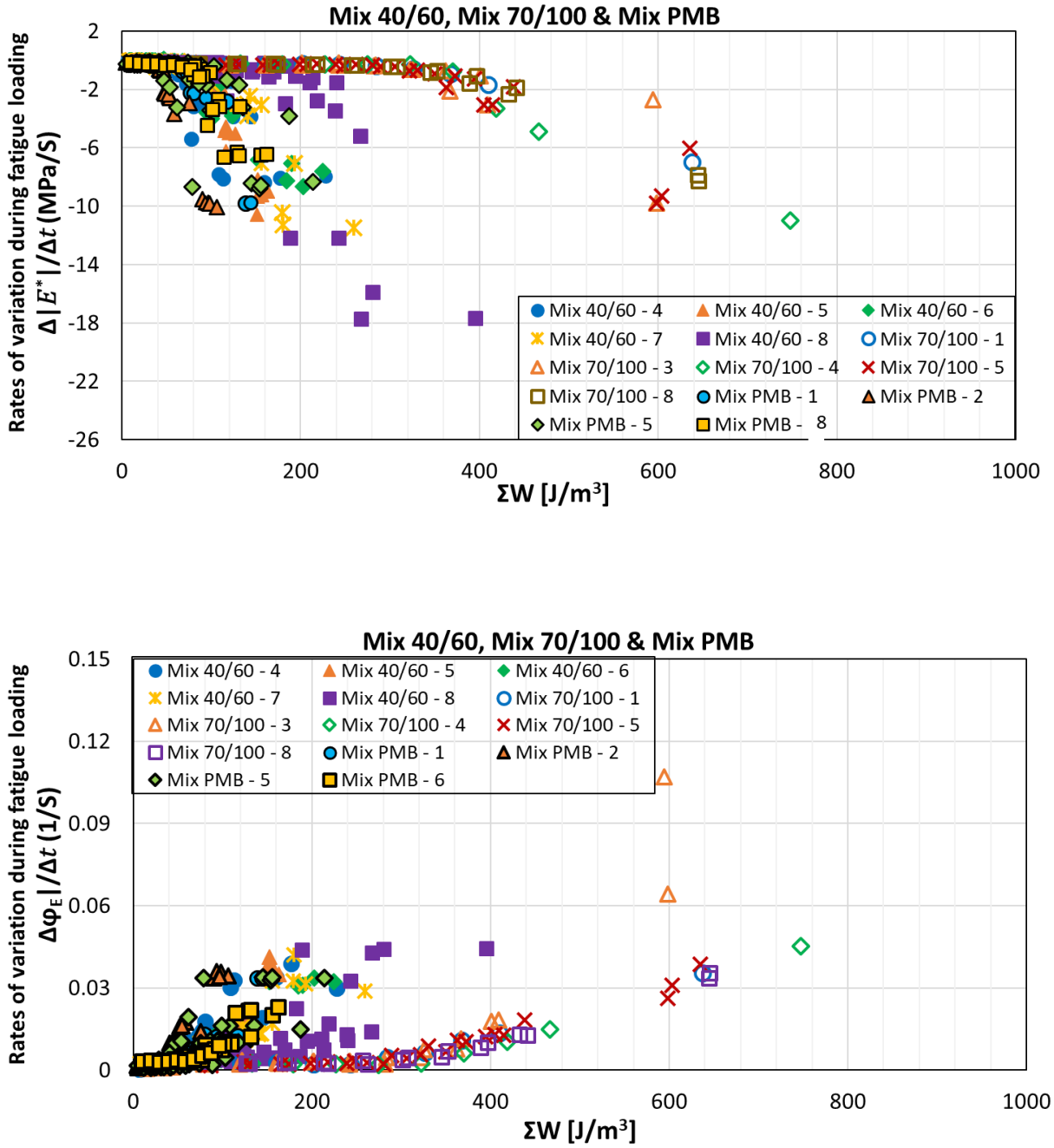

Figure 5.55. Rate of variation during loading and energy dissipation for |E*| and φ_E of all fatigue and rest lags for mix 70/100, mix 40/60 and mix PMB.

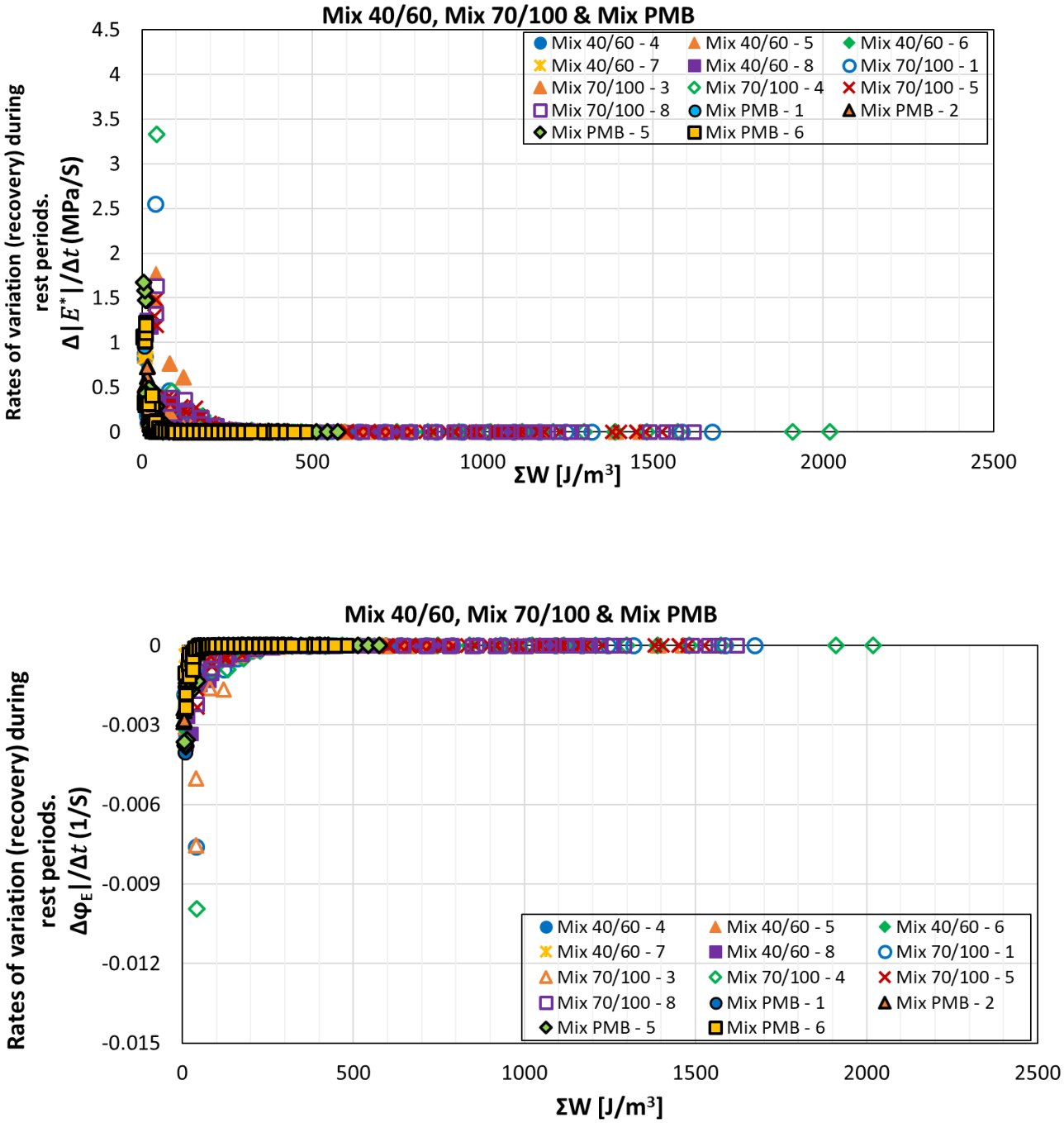

Figure 5.56. Rate of variation during recovery and energy dissipation for |E*| and φ_E of all fatigue and rest lags for mix 70/100, mix 40/60 and mix PMB.

This section investigated the energy dissipation against various parameters such as temperature, number of loading and the rate variation during loading and rest periods for the tested mixtures. The feasibility and effectiveness of the fatigue and recovery derived from dissipated energy were evaluated. It could be noted that energy dissipation and property evolution of the tested mixtures depended on temperature and the amplitude of applied fatigue loads. In particular, the

Mix PMB showed the lowest amount of relative energy dissipation followed by Mix 40/60. This could be found to be due to high fatigue resistance of the Mix PMB. However, dissipated energy and the rate of loading and recovery during rest shows no relationship. Among all the tested mixtures, results of mix 70/100 appear to follow a distinct path during fatigue loading, with respect to the other two mixtures, regardless of the material property used for the estimation. No clear differences between the overall trends of the three materials could be observed for rates of recovery during rest.

5.3. Partial conclusion on the partial fatigue and rest test

The following conclusions were drawn based on the results obtained for PFRT carried out the tested materials:

- Restoration and unrecovered variations of LVE properties during rest after fatigue loading were successfully isolated. The effects and relative importance of the different reversible phenomena (non-linearity, self-heating, thixotropy) on the restoration of material properties were identified and quantified.
- The majority of the $|E^*|$, φ_E, $|\nu^*|$ and φ_ν variations recorded during 100,000 cycles is regained after the 48-hour rest. At the end of each rest period, when the i-th lag is considered, unrecovered variations are always lower than 15% but when the first lag is considered, they are between 14% and 24%, depending on the considered property. This result emphasizes the need to distinguish between the recovery of the various reversible phenomena and the restoration of actual damage.
- Estimating $|E^*|$, φ_E, $|\nu^*|$ and φ_ν variations using the different non-linearity envelopes for each fatigue lag, the effects of non-linearity appear to be small and quite similar for $|E^*|$, φ_E, $|\nu^*|$ and φ_ν variations. In particular, the effect due to non-linearity ranged from 15% to 20%.
- Among the various reversible phenomena explaining the recovery of $|E^*|$, φ_E, $|\nu^*|$ and φ_ν during rest periods, thixotropy appears to be the most important (always higher than 55% of the total restoration during rest).
- The effects of self-heating on $|E^*|$, φ_E, $|\nu^*|$ and φ_ν variations during fatigue tests are has less of an impact compared to non-linearity and thixotropy. Specifically, the effect due to self-heating ranged from 4% to 15% during each fatigue lag, depending on the material with φ_ν variations having the least ranging from 4% to 7%.

- The test protocol seems to produce repeatable results based on the comparison of the data collected on the tested samples. This can be noticed in the plots (for $|E^*|$, φ_E, $|\nu^*|$ and φ_ν) indicated by error bars for all the tested mixtures, where most of the points fall within the standard deviation. Furthermore, the relative importance of $|E^*|$, φ_E, $|\nu^*|$ and φ_ν variations due to the various reversible phenomena does not appear to be related to the void content of the tested samples.
- The rate of variation during fatigue loading (for $|E^*|$, φ_E, $|\nu^*|$ and φ_ν) was significantly higher at the beginning of each loading session (approximately for the first 10,000 cycles) than at the end. In addition, majority of the recovery for the duration of the rest period occurs within the first four hours of recovery; after that, this increase and decrease (with respect to $|E^*|$, φ_E, $|\nu^*|$ and φ_ν respectively) becomes considerably more moderate.

- The rates of variation during loading and recovery for the various fatigue and rest periods for (for $|E^*|$, φ_E, $|\nu^*|$ and φ_ν) show similar trends. In general, the rate of loadings and recoveries obtained for each fatigue and rest period are extremely comparable in pace and amplitude.
- Dissipated energy and the rate of loading show no relationship but energy dissipation tends to increase with the progression of fatigue cycles. Among all the tested mixtures, results of mix 70/100 appear to follow a distinct path during fatigue loading, with respect to the other two mixtures, regardless of the material property used for the estimation. No clear differences between the overall trends of the three materials could be observed for rates of recovery during rest.

Chapter 6: CONCLUSIONS AND PERSPECTIVES

The thesis has been carried out within the framework of the work of RILEM (The International Union of Laboratories and Experts in Construction Materials, Systems and Structures) Technical Committee (TC) 278-CHA: Crack-Healing of Asphalt Pavement Materials. The objective of the study was the characterization of fatigue and restoration in bituminous binders and mixtures. Test on binders were performed by Politecnico di Torino (Italy) and University of Waterloo (Canada), while tests on mixtures were carried out at ENTPE, together with the analysis on all data. All the required materials were provided by Université Gustave Eiffel (France). In order to achieve the objective, repetitive loading and rest tests on binders and mixtures were performed using different test protocols, with the purpose to differentiate damage and restoration of material properties and, within the restoration, to isolate the recovery of properties due to reversible phenomena. Tests on binders were carried out a DSR (different models in the two laboratories) in strain-control mode. The applied test protocols were Linear Amplitude Sweep (LAS) tests with and without rest periods, with various loading amplitudes, loading histories and rest period durations. For mixtures, a test protocol developed at ENTPE was further improved and the analysis of results refined, applying longer rest periods (48 hours), improving the estimation of materials properties during rest periods and studying the evolution of complex Poisson's ratio during fatigue and rest. The following conclusions were drawn from obtained experimental results and performed analyses.

Regarding DSR test for binders:

- For the half-peak LASH tests, it was observed that all the variation of material properties observed during the first loading is instantaneously recovered. This is clearly observed for both binders where the second loading is always superposed with the first loading, practically independently from the duration of the rest period (0, 5 or 30 minute), indicating that only non-linear viscoelasticity with no damage is observed during the first loading.
- Time-dependent recovery was observed for tested binders especially at peak. Higher recovery was observed for PMB than for 70/100 binder. This is clearly seen in stress amplitude-strain amplitude curves of second loading, which are almost superposed with first loading for PMB binder for practically all rest period duration (indicating practically no damage from first loading), while for 70/100 binder the curves of the

second loading are different from those of the first loading, even after 30 minutes (slight increase but not complete recovery).

- It was also observed that the effect of steric hardening at 30 minutes was insignificant with both binders tested. The change of G* was small and no significant differences between the LAS curves were observed.
- Different properties (complex modulus, peak shear amplitude stress and dissipated energy) were considered to assess the damage and recovery of the different binders tested. However, among all the approaches considered, complex modulus shows the highest amount of recovery while the dissipated energy approach shows the least. Also, the percentage recovery using the energy dissipation approach seems to be less sensitive to rest period duration. Consequently, the results obtained show the complexity of correctly defining and characterizing recovery of the mechanical properties of bituminous binders using the LASH test.
- The performed test protocol (LASH test), with and without rest periods, can clearly distinguish different binders (in our case, a straight-run and a PMB), but it is not possible to distinguish the different and complex phenomena responsible for the response of the observed variations of material properties during loading and rest (damage, recovery, restoration). This is clearly observed for the different estimations of recovery according to considered property (G*, τ, Wi) where the different phenomena occurring during loading and rest were limited to just reversible and not reversible.

Regarding complex modulus and partial fatigue test for mixtures:

- Restoration and unrecovered variations of LVE properties during rest after fatigue loading were successfully isolated. The effects and relative importance of the different reversible phenomena (non-linearity, self-heating, thixotropy) on the restoration of material properties were identified and quantified.
- The majority of the E*|, φ_E, |ν*| and φ_ν variations recorded during 100,000 cycles is regained after the 48-hour rest. At the end of each rest period, when the i-th lag is considered, unrecovered variations are always lower than 15% but when the first lag is considered, they are between 14% and 24%, depending on the considered property. This result emphasizes the need to distinguish between the recovery of the various reversible phenomena and the restoration of actual damage.

- Estimating |E*|, φ_E, |ν*| and φ_ν variations using the different non-linearity envelopes for each fatigue lag, the effects of non-linearity appear to be small and quite similar for |E*|, φ_E, |ν*| and φ_ν variations. In particular, the effect due to non-linearity ranged from 15% to 20%.
- Among the various reversible phenomena explaining the recovery of |E*|, φ_E, |ν*| and φ_ν during rest periods, thixotropy appears to be the most important (always higher than 55% of the total restoration during rest).
- The effects of self-heating on |E*|, φ_E, |ν*| and φ_ν variations during fatigue tests are has less of an impact compared to non-linearity and thixotropy. Specifically, the effect due to self-heating ranged from 4% to 15% during each fatigue lag, depending on the material with φv variations having the least ranging from 4% to 7%.
- The test protocol seems to produce repeatable results based on the comparison of the data collected on the tested samples. This can be noticed in the plots (for |E*|, φ_E, |ν*| and φ_ν) indicated by error bars for all the tested mixtures, where most of the points fall within the standard deviation. Furthermore, the relative importance of |E*|, φ_E, |ν*| and φ_ν variations due to the various reversible phenomena does not appear to be related to the void content of the tested samples.
- The rate of variation during fatigue loading (for |E*|, φ_E, |ν*| and φ_ν) was significantly higher at the beginning of each loading session (approximately for the first 10,000 cycles) than at the end. In addition, majority of the recovery for the duration of the rest period occurs within the first four hours of recovery; after that, this increase and decrease (with respect to |E*|, φ_E, |ν*| and φ_ν respectively) becomes considerably more moderate.
- The rates of variation during loading and recovery for the various fatigue and rest periods for (for |E*|, φ_E, |ν*| and φ_ν) show similar trends. In general, the rate of loadings and recoveries obtained for each fatigue and rest period are extremely comparable in pace and amplitude.
- Dissipated energy and the rate of loading show no relationship but energy dissipation tends to increase with the progression of fatigue cycles. Among all the tested mixtures, results of mix 70/100 appear to follow a distinct path during fatigue loading, with respect to the other two mixtures, regardless of the material property used for the estimation. No clear differences between the overall trends of the three materials could be observed for rates of recovery during rest.

Finally, the following general conclusions can be drawn from the campaigns on binders and mixtures with corresponding materials:

- It is important to note that the two test protocols are quite different in their conception with important differences in strain amplitudes among the two protocols. For the DSR test, strain amplitude is increased from 0.1% to 30% (largely beyond the linear viscoelastic limit of bituminous binders), while a constant targeted strain amplitude of 100 µm/m (usually considered equal to close to the linear viscoelastic limit of mixtures, roughly) is applied with T/C test on mixtures. This important difference can explain the discrepancies observed. The high strain amplitudes applied during LASH tests on binders must be considered in the evaluation and the pertinence of the results of these tests.
- Although the observations made on the 70/100 and PMB binders from the DSR tests and on the two corresponding mixtures from the T/C tests appear to point in the same direction, the conclusions are not clear because of the aforementioned nature of the LASH protocol and the difference between the tests on binders and mixtures. In particular, the 70/100 binder showed incomplete restoration of material properties in the LASH tests, while PMB binder recovered completely. The 70/100 mixture showed the highest unrecovered variations and among the tested mixtures and generally failed without withstanding the five partial fatigue tests, while the PMB mixture showed the lowest unrecovered variations and generally withstood all the fatigue lags.

This investigation gave rise to several perspectives:

- The dissertation did not treat all the results on the final fatigue, until cracking of the mixture tests. These data could provide interesting results concerning the fatigue resistance of materials and the effect of rest periods. Moreover, this analysis might allow distinguishing further the behavior of mixtures containing different base binders.

- The influence of other external elements, such as loading mode, ageing, temperature and moisture should be considered for future study.

- Making sense of self-healing mechanisms may be possible through a multiscale analysis of the complex physicochemical interaction between pure bitumen and additional inclusions (such as filler, aggregate, polymer, or other modifiers).
- Additional perspective on the analysis on 3D behaviour of mixtures, using Poisson's ratio results and also volume changes of the materials during loading and rest should also be considered for further study.

References

AASHTO M320. (2009). Standard Specification for Performance-Graded Asphalt Binder. American association of state Highway and Transportation officials.

AASHTO PP6. (1994). Standard practice for grading or verifying the performance grade of an asphalt binder. American association of state highway and transportation officials.

AASHTO T313. (2012). Standard Method of Test for Determining the Flexural Creep Stiffness of asphalt binder using the bending beam rheometer (BBR). American association of state highway and transportation officials.

AASHTO T314. (2012). Standard Method of Test for Determining the Fracture Properties of asphalt binder in direct tension (DT). American association of state highway and transportation officials.

AASHTO T315. (2012). Standard Method of Test for Determining the Rheological Properties of asphalt binder using a Dynamic Shear Rheometer (DSR). American association of state highway and transportation officials.

Abo-Qudais, S., & Suleiman, A. (2005). Monitoring fatigue famage and crack healing by ultrasound wave velocity. *Nondestructive Testing and Evaluation*, *20*(2), 125–145. https://doi.org/10.1080/10589750500206774

AFNOR. 2005. 'NF EN 933-5 July 2005 Tests for Geometrical Properties of Aggregates - Determination of Percentage of Crushed and Broken Surfaces in Coarse Aggegate Particles'.

AFNOR. 2006. 'NF EN 13108-5 December 2006 Bituminous Mixtures - Material Specifications Part 5: Stone Mastic Asphalt'.

AFNOR. 2008a. 'NF EN 933-4 June 2008 Tests for Geometrical Properties of Aggregates - Determination of Particle Shape - Shape Index'.

AFNOR. 2008b. 'NF EN 12620 June 2008 Aggregates for Concrete'.

AFNOR. 2010. 'NF EN 1097-2 June 2010 Tests for Mechanical and Physical Properties of Aggregates - Methods for the Determination of Resistance to Fragmentation'.

AFNOR. 2011. 'NF EN 1097-1 August 2011 Tests for Mechanical and Physical Properties of Aggregates - Determination of Resistance to Wear (Micro-Deval)'.

AFNOR. 2012b. 'NF EN 933-3 March 2012 Tests for Geometrical Properties of Aggregates - Determination of Particle Shape - Flawkiness Index'.

AFNOR. 2012e. 'NF EN 14770 August 2012 - Bitumen and Bituminous Binders - Determination of Complex Shear Modulus and Phase Angle'.

AFNOR. 2013a. ‘NF EN 933-9 June 2013 Tests for Geometrical Properties of Aggregates - Assessment of Fines - Methylene Blue Test’.

AFNOR. 2015. ‘NF EN 933-8 July 2015 Tests for Geometrical Properties of Aggregates - Assessment of Fines -Sand Equivalent Test’.

AFNOR. 2017b. ‘NF EN 13398 December 2017 Bitumen and Bituminous Binders - Determination of Elsatic Recovery Modified Bitumen’.

AFNOR. 2018a. ‘NF EN 1426 January 2018 Bitumen and Bituminous Binders - Determination of Needle Penetration’.

Agzenai, Y., Pozuelo, J., Sanz, J., Perez, I., & Baselga, J. (2015). Advanced Self-Healing Asphalt Composites in the Pavement Performance Field: Mechanisms at the Nano Level and New Repairing Methodologies. *Recent Patents on Nanotechnology*, *9*(1), 43–50. https://doi.org/10.2174/1872208309666141205125017

Airey, G. D. (2003). Rheological properties of styrene butadiene styrene polymer modified road bitumens. *Fuel*. https://doi.org/10.1016/S0016-2361(03)00146-7

Ararsa, W., Quezon, E. T., Bedada, A., Mekonnen, E., & Gudissa, D. (2019). Laboratory Investigation on the Likely Usage of Sub-base Course Dust: An Alternative Filler Material Ingredient for Marshall Design Mix. *SSRN Electronic Journal*, *7*(4), 157–166. https://doi.org/10.2139/ssrn.3491000

Asphalt Institute (2015). *Asphalt Mix Design Methods (Metodos de Diseño de Concreto Asfaltico)*.

ASTM 7460 (2010). American Society for Testing and Materials. Standard test method for determining fatigue failure of compacted asphalt concrete subjected to repeated flexural bending.

Ayar, P., Moreno-Navarro, F., & Rubio-Gámez, M. C. (2016). The healing capability of asphalt pavements: A state of the art review. *Journal of Cleaner Production*, *113*, 28–40. https://doi.org/10.1016/j.jclepro.2015.12.034

Ba_kowski, W., Soenen, H., Sybilski, D., Gajewski, M., & Gauthier, G. (2009). Binder fatigue properties and the results of the Rilem Round Robin Test. *Advanced Testing and Characterization of Bituminous Materials, August 2015*. https://doi.org/10.1201/9780203092989.ch118

Babadopulos, L. F. d. A. L., Orozco, G., Sauzéat, C., & Di Benedetto, H. (2019). Reversible phenomena and fatigue damage during cyclic loading and rest periods on bitumen. *International Journal of Fatigue*, *124*(December 2018), 303–314. https://doi.org/10.1016/j.ijfatigue.2019.03.008

Bahia, H. U., Zhai, H., Onnetti, K., & Kose, S. (1999). Non-Linear Viscoelastic and Fatigue Properties of Asphalt Binders. Journal of the Association of Asphalt Paving Technologists, 68, 1–34.

Barnes, Howard A. 1997. 'Thixotropy—a Review'. Journal of Non-Newtonian Fluid Mechanics 70 (1–2): 1–33. https://doi.org/10.1016/S0377-0257(97)00004-9.

Bhasin, A., Parthasarthy, A. S., & Little, D. N. (2009). *Laboratory investigation of a novel method to accelerate healing in asphalt mixtures using thermal treatment*. *7*(2), 36.

Bhasin, A., Little, D. N., Bommavaram, R., & Vasconcelos, K. (2008). A framework to quantify the effect of healing in bituminous materials using material properties. *Road Materials and Pavement Design*, *9*(SPECIAL ISSUE), 219–242. https://doi.org/10.3166/RMPD.9HS.219-242

Bodin, D., De La Roche, C., & Pijaudier-Cabot, G. (2006). Size effect regarding fatigue evaluation of asphalt mixtures: Laboratory cantilever bending tests. *Road Materials and Pavement Design*, *7*, 181–200. https://doi.org/10.1080/14680629.2006.9690064

Bonnaure, F. P., Huibers, A. H. J. J., & Boonders, A. (1982). A laboratory investigation of the influence of rest periods on fatigue characteristics of bituminous mixes. Journal of the Association of Asphalt Paving Technologists, 51, 104-128.

Botella, R., Pérez-Jiménez, F. E., López-Montero, T., & Miró, R. (2020). Cyclic testing setups to highlight the importance of heating and other reversible phenomena on asphalt mixtures. International Journal of Fatigue, 134(January), 105514. https://doi.org/10.1016/j.ijfatigue.2020.105514

Canestrari, F., Virgili, A., Graziani, A., & Stimilli, A. (2015). Modeling and assessment of self-healing and thixotropy properties for modified binders. International Journal of Fatigue, 70, 351–360. https://doi.org/10.1016/j.ijfatigue.2014.08.004

Capros, P., Mantzos, L., Papandreou, V., & Tasios, N. (2007). European Energy and Transport - Trends to 2030 - update 2007. In *Transport*.

Chen, E. Y. H. (2000). A global perspective. In *Hong Kong Journal of Psychiatry* (Vol. 10, Issue 2).

Clark, W. G. (1971). 'Fracture Mechanics in Fatigue: Paper Presents a Review of the Current State of the Art of Fracture-Mechanics Approach to Fatigue'. Experimental Mechanics 11 (9): 421– 428. https://doi.org/10.1007/BF02327647.

Cook, R. D. (2018). Principal components, sufficient dimension reduction, and envelopes. Annu. Rev. Statist. Appl. 5, 533–59.

Cordier, P., Tournilhac, F., Soulié-Ziakovic, C., & Leibler, L. (2008). Self-healing and

thermoreversible rubber from supramolecular assembly. Nature. https://doi.org/10.1038/nature06669.

Corté, J.-F., & Di Benedetto H. (2005). Matériaux routiers bitumineux 1: Description et propriétés des constituants [Bituminous paving materials 1: Description and constituent properties]. Paris: Hermes-Lavoisier. [in French]

Csanyi, L. H. (1962). Functions of fillers in bituminous mixes. *Symposium on mineral fillers for bituminous mixtures*. Highway Research Board.

Dave, E. V, & Koktan, P. (2011). Synthesis of Performance Testing of Asphalt Concretes. Minnesota Department of Transportation, Report No.(2011–22).

Deacon, J. A., & Monismith, C. L. (1967). Laboratory flexural-fatigue testing of asphalt concrete with emphasis on compound loading tests. Highway Research Records, 158, 1-31.

Di Benedetto, H., De La Roche, C., Baaj, H., Pronk, A., & Lundström, R. (2004). Fatigue of bituminous mixtures. *Materials and Structures/Materiaux et Constructions*, *37*(267), 202–216. https://doi.org/10.1007/bf02481620

Di Benedetto, Hervé, Delaporte, B., & Sauzéat, C. (2007). Three-dimensional linear behavior of bituminous materials: Experiments and modeling. *International Journal of Geomechanics*, *7*(2), 149–157. https://doi.org/10.1061/(ASCE)1532-3641(2007)7:2(149)

Di Benedetto, Hervé, Nguyen, Q. T., & Sauzéat, C. (2011). Nonlinearity, heating, fatigue and thixotropy during cyclic loading of asphalt mixtures. *Road Materials and Pavement Design*, *12*(1), 129–158. https://doi.org/10.1080/14680629.2011.9690356

Domone, P. L. J., & Illston, J. M. (2010, January 1). Construction Materials. http://books.google.ie/books?id=6G3XswEACAAJ&dq=Domone+%26+Illston,+2010&hl=&cd=3&source=gbs_api

Eisa, M. S., Basiouny, M. E., & Youssef, A. M. (2018). Effect of using various waste materials as mineral filler on the properties of asphalt mix. *Innovative Infrastructure Solutions*, *3*(1). https://doi.org/10.1007/s41062-018-0129-4

Elliott, R., Jr, M. F., Ghanim, M., & Tu, Y. (1991). Effect of aggregate gradation variation on asphalt concrete mix properties. *Transportation Research …*, *1317*, 52–60. http://trid.trb.org/view.aspx?id=365390

EN 12697-24 (2012). Bituminous mixtures. Test methods for hot mix asphalt. Part 24: Resistance to fatigue. European Standard.

European Union Road Federation (ERF). (2017). Road Statistics - Yearbook 2017. *European Road Federation*, 93. http://erf.be/images/2017/Statistics/Road_statistics_2017.pdf

Ewing, J. A., and Humphrey, J. C. W. (1903). 'The Fracture of Metals under Repeated Alternations of stress'. Proceedings of the Royal Society of London 71: 467–76. https://doi.org/10.1098/rspl.1902.0065.

Faheem, A., Wen, H., Stephenson, L., & Bahia, H. (2008). Effect of mineral filler on damage resistance characteristics of asphalt binders. *Asphalt Paving Technology: Association of Asphalt Paving Technologists-Proceedings of the Technical Sessions*, *77*(January 2008), 885–907.

Freire, R. (2020). *Linear Viscoelastic Behaviour of Geogrids Interface within Bituminous Mixtures*. [Doctoral dissertation].

García, Á. (2012). Self-healing of open cracks in asphalt mastic. *Fuel*, *93*, 264–272. https://doi.org/10.1016/j.fuel.2011.09.009

Garcia, A., Jelfs, J., & Austin, C. J. (2015). Internal asphalt mixture rejuvenation using capsules. *Construction and Building Materials*, *101*, 309–316. https://doi.org/10.1016/j.conbuildmat.2015.10.062

García, A., Norambuena-Contreras, J., Bueno, M. & Partl, M. N. (2015). Single and multiple healing of porous and dense asphalt concrete. Journal of Intelligent Material Systems and Structures published online 24 March 20142015;26(4):425–33. DOI: 10.1177/1045389X14529029.

Griffith, A. A. (1921). The Phenomena of Rupture and Flow in Solids'. Philosophical Transactions of the Royal Society of London. Series A, Containing Papers of a Mathematical or Physical Character 221 (582–593): 163–98. https://doi.org/10.1098/rsta.1921.0006.

Gudmarsson, A., Ryden, N., Di Benedetto, H., Sauzéat, C., Tapsoba, N., & Birgisson, B. (2014). Comparing Linear Viscoelastic Properties of Asphalt Concrete Measured by Laboratory Seismic and Tension–Compression Tests. Journal of Nondestructive Evaluation, 33(4), 571–582. https://doi.org/10.1007/s10921-014-0253-9

Hartman, A. M., & Gilchrist, M. D. (2004). Evaluating Four-Point Bend Fatigue of Asphalt Mix Using image analysis. Journal of Materials in Civil Engineering 16 (1): 60–68. https://doi.org/10.1061/(ASCE)0899-1561(2004)16:1(60).337–357. https://doi.org/10.1080/14680629.2001.9689907

Hartman, A. M., Gilchrist, M. D., Owende, P. M. O., Ward, S. M., & Clancy, F. (2001). In-situ Accelerated Testing of Bituminous Mixtures. *Road Materials and Pavement Design*, *2*(4), 337–357. https://doi.org/10.1080/14680629.2001.9689907

Highway research board. (1962). The AASHO road test Report 5- Pavement Research. HRB

Special Report 61E. *Highway Research Board Special Report, Special Re(61 E)*, 1–352.

Howard A. Barnes. (1997). Thixotropy - a review. *Journal Non-Newtonian Fluid Mech., 70 (1997) 1-33*, *12*(2), 251–264. https://doi.org/10.1002/bbb.1835

Hsu, T.-W., & Tseng, K.-H. (1996). Effect of rest periods on fatigue response of asphalt concrete mixtures. Journal of Transportation Engineering, 122, 316-322. DOI: 10.1061/(ASCE)0733-947X(1996)122:4(316)

Huang, M., & Huang, W. (2016). Laboratory investigation on fatigue performance of modified asphalt concretes considering healing. Construction and Building Materials, 113, 68–76. https://doi.org/10.1016/j.conbuildmat.2016.02.083

Huang, W., Lv, Q., & Xiao, F. (2016). Investigation of using binder bond strength test to evaluate adhesion and self-healing properties of modified asphalt binders. Construction and Building Materials, 113, 49–56. https://doi.org/10.1016/j.conbuildmat.2016.03.047

Huet, C. (1963). Etude Par Une Méthode d'impédance Du Comportement Viscoélastique Des Matériaux Hydrocarbonés. Laboratoire Central des Ponts et Chaussées.

Hung, C. C., Su, Y. F., & Su, Y. M. (2018). Mechanical properties and self-healing evaluation of strain-hardening cementitious composites with high volumes of hybrid pozzolan materials. *Composites Part B: Engineering*, *133*, 15–25. https://doi.org/10.1016/j.compositesb.2017.09.005

Ingham, J. P. (2013). Bituminous mixtures. *Geomaterials Under the Microscope*, 171–174. https://doi.org/10.1201/b15140-11

Inozemtcev, S., & Korolev, E. (2020). Review of Road Materials Self-healing: Problems and Perspective. *IOP Conference Series: Materials Science and Engineering*, *855*(1). https://doi.org/10.1088/1757-899X/855/1/012010

Isailović, I., Wistuba, M. P., & Falchetto, A. C. (2017, June 23). Experimental study on asphalt mixture recovery. Materials and Structures, 50(4). https://doi.org/10.1617/s11527-017-1064-0

Kachanov, L. M. (1958). Time of the Rupture Process under Creep Conditions'. Izvestiia Akademii Nauk SSSR 8: 26–31.

Kachanov, L. M. (1986). Introduction to Continuum Damage Mechanics. Dordrecht: Springer Netherlands. http://public.ebookcentral.proquest.com/choice/publicfullrecord.aspx?p=3106040.

Kandhal, P. S., Lynn, C. Y., & Parker, F. (1998). Characterization tests for mineral fillers related to performance of asphalt paving mixtures. *Transportation Research Record*, *1638*, 101–110. https://doi.org/10.3141/1638-12

Kathem Taeh Alnealy, D. S. (2015). Effect of Using Waste Material as Filler in Bituminous Mix Design. *American Journal of Civil Engineering*, *3*(3), 88. https://doi.org/10.11648/j.ajce.20150303.16

Khavandi Khiavi, A., & Rasouli, R. (2018). Laboratory evaluation of loading frequency effects on HMA self-healing. Construction and Building Materials, 162, 1–8. https://doi.org/10.1016/j.conbuildmat.2017.11.169

Kim, Y. R., Little, D. N., & Lytton, R. L. (2003). Fatigue and healing characterization of asphalt mixtures. *Journal of Materials in Civil Engineering*, *15*(1), 75–83. https://doi.org/10.1061/(ASCE)0899-1561(2003)15:1(75)

Kringos, N., & Skarpas, A. (2011). Towards an understanding of the self- healing capacity of asphaltic mixtures. *HERON Vol. 56 (2011) No. 1 / 2 45*.

Kringos, N., Birgisson, B., Frost, D., & Wang, L. (2013, May 26). Multi-Scale Modeling and Characterization of Infrastructure Materials. Springer Science & Business Media. http://books.google.ie/books?id=AcBEAAAAQBAJ&printsec=frontcover&dq=Gaskin,+J.,+2013.+On+Bitumen+Microstructure+and+the+Effects+of+Crack+Healing+(PhD+dissertation).+University+of+Nottingham,+Nottingham,+UK.&hl=&cd=1&source=gbs_api

Larson, R. G., & Wei, Y. (2019). A review of thixotropy and its rheological modeling. *Journal of Rheology*, *63*(3), 477–501. https://doi.org/10.1122/1.5055031

Lee, H. J., Daniel, J. S., & Kim, Y. R. (2000). Laboratory Performance Evaluation of Modified Asphalt Mixtures for Inchon Airport Pavements. International Journal of Pavement Engineering, 1(2), 151–169. https://doi.org/10.1080/10298430008901703

Lee, Y. L. (2005). Fatigue Damage Theories. *Fatigue Testing and Analysis*, 57–76. https://doi.org/10.1016/B978-075067719-6/50003-8

Leegwater, G., Tabokovi, A., Baglieri, O., & Hammoum, F. (2020). *Terms and definitions on crack-healing and restoration of mechanical properties in bituminous materials*. 1–6.

Lesueur, D. (2009). The colloidal structure of bitumen: Consequences on the rheology and on the mechanisms of bitumen modification. *Advances in Colloid and Interface Science*, *145*(1–2), 42–82. https://doi.org/10.1016/j.cis.2008.08.011

Li, K., Huang, M., Zhong, H., & Li, B. (2019). Comprehensive evaluation of fatigue performance of modified asphalt mixtures in different fatigue tests. *Applied Sciences (Switzerland)*, *9*(9), 1–10. https://doi.org/10.3390/app9091850

Lira, B., Jelagin, D., & Birgisson, B. (2013). Gradation-based framework for asphalt mixture. Materials and Structures, 46(8), 1401–1414. https://doi.org/10.1617/s11527-012-9982-3

Little, D. N., Lytton, R. L., Williams, D. & Chen, C. W. (2001). Microdamage healing in asphalt

and asphalt concrete. Microdamage and microdamage healing, project summary report, vol. I.

Liu, Q., Schlangen, E., García, Á., & Ven, M. Van De. (2010). Induction heating of electrically conductive porous asphalt concrete. *Construction and Building Materials*, *24*(7), 1207–1213. https://doi.org/10.1016/j.conbuildmat.2009.12.019

Lundstrom, R., Benedetto, H. Di, & Isacsson, U. (2004). *Influence of Asphalt Mixture Stiffness on Fatigue Failure*. *16*(December), 516–525. https://doi.org/10.1061/(ASCE)0899-1561(2004)16

Lv, Q., Huang, W., Zheng, M., Hao, G., Yan, C., & Sun, L. (2020). Investigating the asphalt binder / mastic bonding healing behavior using bitumen bonding strength test and X-ray Computed Tomography scan. Construction and Building Materials, 257, 119504. https://doi.org/10.1016/j.conbuildmat.2020.119504

Lytton, R. L., Uzan, J., Fernando, E. G, Roque, R., Hiltunen, D. & Stoffels, S, M. (1993). Development and validation of performance prediction models and specifications for asphalt binders;and paving mixes. Washington, DC: Strategic Highway Research Program.

Mangiafico, S., Sauzéat, C., Di Benedetto, H., Pouget, S., Olard, F., & Planque, L. (2015). Quantification of biasing effects during fatigue tests on asphalt mixes: Non-linearity, self-heating and thixotropy. *Road Materials and Pavement Design*, *16*(Supplement 2), 143–180. https://doi.org/10.1080/14680629.2015.1077000.

Mangiafico, Salvatore. (2014). *Linear viscoelastic properties and fatigue of bituminous mixtures produced with Reclaimed Asphalt Pavement and corresponding binder blends*. 312.

Mangiafico, S., Sauzéat, C., Benedetto, H. Di, Pouget, S., & Olard, F. (2016). Fatigue Tests on Bituminous Mixtures. 6th Eurasphalt & Eurobitume Congress, Prague, Czech Republic, 1-3 June 2016. https://doi.org/10.14311/EE.2016.138

Mannan, U. A., Ahmad, M., & Tarefder, R. A. (2017). Influence of moisture conditioning on healing of asphalt binders. Construction and Building Materials, 146, 360–369. https://doi.org/10.1016/j.conbuildmat.2017.04.087.

Mathew, T. V., & Rao, K. K. (2006). Introduction to Transportation engineering. Civil Engineering–Transportation Engineering. IIT Bombay, NPTEL ONLINE, http://www. cdeep. iitb. ac. in/nptel/Civil% 20Engineering.

Mazzoni, G., Stimilli, A., & Canestrari, F. (2016). Self-healing capability and thixotropy of bituminous mastics. *International Journal of Fatigue*, *92*, 8–17.

https://doi.org/10.1016/j.ijfatigue.2016.06.028

McNally, Tony, ed. 2011. Polymer Modified Bitumen: Properties and Characterisation. Woodhead Publishing in Materials. Oxford ; Philadelphia: Woodhead Publishing Ltd.

Medani, T. O., & Molenaar, A. A. A. (2000). Estimation of fatigue characteristics of asphaltic mixes using simple tests. In *Heron* (Vol. 45, Issue 3, pp. 155–165).

Mewis, J., & Wagner, N. J. (2009). Thixotropy. *Advances in Colloid and Interface Science*, *147–148*(C), 214–227. https://doi.org/10.1016/j.cis.2008.09.005

Meyers, M. A., & Chawla, K. K. (2008). Mechanical behavior of materials. Cambridge university press.

Miglietta, F., Tsantilis, L., Baglieri, O., & Santagata, E. (2021). A new approach for the evaluation of time–temperature superposition effects on the self-healing of bituminous binders. *Construction and Building Materials*, *287*, 122987. https://doi.org/10.1016/j.conbuildmat.2021.122987

Miglietta, F., Tsantilis, L., Baglieri, O., & Santagata, E. (2022). Investigating the effect of temperature on self-healing properties of neat and polymer-modified bituminous binders. *Road Materials and Pavement Design*, *23*(S1), 2–15. https://doi.org/10.1080/14680629.2021.1982752

Miller, J. S., and W. Y. Bellinger. (2014). 'Distress Identification Manual for the Long-Term Pavement Performance Program (Fifth Revised Edition)'. FHWA-HRT-13-092.

Moghaddam, T. B., Karim, M. R., & Abdelaziz, M. (2011). A review on fatigue and rutting performance of asphalt mixes. *Scientific Research and Essays*, *6*(4), 670–682. https://doi.org/10.5897/SRE10.946

Mohod, M. V., & Kadam, K. N. (2016). A Comparative Study on Rigid and Flexible Pavement: A Review. *IOSR Journal of Mechanical and Civil Engineering*, *13*(3), 84–88. https://doi.org/10.9790/1684-1303078488

Moreno-Navarro, F. &, & Rubio-Gamez, M. C. (2016). A review of fatigue damage in bituminous mixtures : Understanding the phenomenon from a new perspective. *Construction and Building Materials*, *113*, 927–938. https://doi.org/10.1016/j.conbuildmat.2016.03.126

Mouillet, V., De la Roche, C., Chailleux, E., & Coussot, P. (2012). Thixotropic Behavior of Paving-Grade Bitumens under Dynamic Shear. *Journal of Materials in Civil Engineering*, *24*(1), 23–31. https://doi.org/10.1061/(ASCE)MT.1943-5533.0000354

Murakami, S. (2012). Continuum Damage Mechanics. Vol. 185. Solid Mechanics and Its applications. Dordrecht: Springer Netherlands. https://doi.org/10.1007/978-94-007-26666.

Nguyen, Q. T., Di Benedetto, H., Sauzéat, C., & Tapsoba, N. (2013). Time Temperature Superposition Principle Validation for Bituminous Mixes in the Linear and Nonlinear Domains. *Journal of Materials in Civil Engineering*, *25*(9), 1181–1188. https://doi.org/10.1061/(asce)mt.1943-5533.0000658

Nguyen, Q. T., Nguyen, M. L., Benedetto, H. Di, Sauzéat, C., Chailleux, E., & Hoang, T. T. N. (2019). Nonlinearity of bituminous materials for small amplitude cyclic loadings. *Road Materials and Pavement Design*, *20*(7), 1571–1585. https://doi.org/10.1080/14680629.2018.1465452

OCDE (2013), Environment at a Glance 2013 : OECD Indicators, Éditions OCDE, Paris, https://doi.org/10.1787/9789264185715-en.

Olard, F., Di Benedetto, H., Dony, A., & Vaniscote, J. C. (2005). Properties of bituminous mixtures at low temperatures and relations with binder characteristics. *Materials and Structures/Materiaux et Constructions*, *38*(275), 121–126. https://doi.org/10.1617/14132

Perraton, D., Baaj, H., Di Benedetto, H., & Paradis, M. (2003). Évaluation De La Résistance À La Fatigue Des Enrobés Bitumineux Fondée Sur L'Évolution De L'Endommagement Du Matériau En Cours D'Essia : Aspects Fondamentaux Et Application À L'Enrobé À Matrice De Pierre. *Canadian Journal of Civil Engineering*, *30*(5), 902–913. https://doi.org/10.1139/l03-067

Phillips, M. C. (1999). Multi-step models for fatigue and healing, and binder propertiesinvolved in healing. Luxembourg: Eurobitume workshop on performance relatedproperties for bituminous binders.

PIARC. (2019). 'Road Dictionary'. In . https://www.piarc.org/en/activities/Road-Dictionary-Terminology-Road-Transport.

Polacco, G., Kříž, P., Filippi, S., Stastna, J., Biondi, D., & Zanzotto, L. (2008). Rheological properties of asphalt/SBS/clay blends. *European Polymer Journal*, *44*(11), 3512–3521. https://doi.org/10.1016/j.eurpolymj.2008.08.032

Porto, M., Angelico, R., Caputo, P., Abe, A. A., Teltayev, B., & Rossi, C. O. (2022). The Structure of Bitumen: Conceptual Models and Experimental Evidences. *Materials*, *15*(3). https://doi.org/10.3390/ma15030905

Pronk, A. C. (1995). Evaluation of the Dissipated Energy Concept for the Interpretation of Fatigue Measurements in the Crack Initiation Phase. P-DWW. https://books.google.fr/books?id=aDMbcgAACAAJ.

Qiu, J., van de Ven, M., Wu, S., Yu, J., & Molenaar, A. (2012). Evaluating Self Healing Capability of Bituminous Mastics. *Experimental Mechanics*, *52*(8), 1163–1171.

https://doi.org/10.1007/s11340-011-9573-1

Qiu, J., 2012. Self Healing of Asphalt Mixtures towards a Better Understanding of the Mechanism (PhD dissertation). Delft University of Technology, Delft, The Netherlands.

Qiu, J., Van De Ven, M. F. C., Wu, S. P., Yu, J. Y., Molenaar, A. A. A., (2011). Investigating self healing behaviour of pure bitumen using dynamic shear rheometer. Fuel 90, 2710e2720. http://dx.doi.org/10.1016/j.fuel.2011.03.016.

Rababaah, H. (2005). Asphalt Pavement Crack Classification : A Comparative Study of Three AI Approaches: Multilayer Perceptron, Genetic Algorithms and Self-Organizing Maps.

Radopoulou, S. C., & Brilakis, I. (2016). Improving Road Asset Condition Monitoring. *Transportation Research Procedia*, *14*(0), 3004–3012. https://doi.org/10.1016/j.trpro.2016.05.436

Rahman, A., Ali, S. A., Adhikary, S. K., & Hossain, Q. S. (2012). Effect Of Fillers On Bituminous Paving Mixes: An Experimental Study. *Journal of Engineering Science*, *3*(1), 121–127.

Raithby, K. D., & Sterling, A. B. (1970). The effect of rest periods on the fatigue performance of a hot-rolled asphalt under reversed axial loading. Journal of the Association of Asphalt Paving Technologists, 39, 134-152.

Read, J., & Whiteoak, D. (2003). The Shell bitumen handbook. In *Read, J., & Whiteoak, D. (2003). The Shell bitumen handbook. Thomas Telford.* https://doi.org/10.1680/sbh.32200

Riahi, E., Allou, F., Botella, R., Dubois, F., Absi, J., & Petit, C. (2017, November). Quantification of self-heating and its effects under cyclic tests on a bituminous binder. International Journal of Fatigue, 104, 334–341. https://doi.org/10.1016/j.ijfatigue.2017.07.016

Santagata, E., Baglieri, O., Tsantilis, L., & Dalmazzo, D. (2013). Evaluation of self healing properties of bituminous binders taking into account steric hardening effects. Construction and Building Materials, 41(May), 60–67. https://doi.org/10.1016/j.conbuildmat.2012.11.118

Sauzeat, C., & Di Benedetto, H. (2015). Tridimensional linear viscoelastic behavior of bituminous materials. In *Advances in Asphalt Materials: Road and Pavement Construction*. Elsevier Ltd. https://doi.org/10.1016/B978-0-08-100269-8.00003-9

Sayegh, G. (1965). 'Variation Des Modules de Quelques Bitumes Purs et Bétons Bitumineux'. PhD Thesis, Université de Paris.

Schapery, R. A. (1989). On the mechanics of crack closing and bonding in linear viscoelastic media. International journal of fracture; 39(1–3):163–89.

Shan, L., Tan, Y., Underwood, B. S., & Kim, Y. R. (2011). Thixotropic Characteristics of Asphalt Binder. Journal of Materials in Civil Engineering, 23(12), 1681–1686. https://doi.org/10.1061/(asce)mt.1943-5533.0000328.

Shen, S. & Carpenter, S. H. (2007). Dissipated Energy Concepts for HMA Performance: Fatigue and Healing (COE report no. 29). Center of Excellence for Airport Technology, Department of Civil and Environmental Engineering, University of Illinois at Urbana-Champaign, Champaign-Urbana Metropolitan Area, Illinois, USA.

Shen, S., Chiu, H.-M., & Huang, H. (2010). Characterization of Fatigue and Healing in Asphalt Binders. Journal of Materials in Civil Engineering, 22(9), 846–852. https://doi.org/10.1061/(asce)mt.1943-5533.0000080.

Shen, S., Lu, X., Liu, L., & Zhang, C. (2016). Investigation of the influence of crack width on healing properties of asphalt binders at multi-scale levels. Construction and Building Materials, 126, 197–205. https://doi.org/10.1016/j.conbuildmat.2016.08.107.

Sinha, K. C., Bullock, D., Hendrickson, C. T., Levinson, H. S., Lyles, R. W., Radwan, A. E., & Li, Z. (2003). Development of Transportation Engineering Research, Education, and Practice in a Changing Civil Engineering World. *Perspectives in Civil Engineering: Commemorating the 150th Anniversary of the American Society of Civil Engineers*, *August*, 193–205.

Smith, B. J., & Hesp, S. A. M. (2000). Crack pinning in asphalt mastic and concrete: effect of rest periods and polymer modifiers on the fatigue life. In Proceedings of the 2nd Eurasphalt and Eurobitume Congress, Volume 2 (pp. 539-546). Breukelen: Foundation Eurasphalt.

Soltani, A., & Anderson, D. A. (2005). New test protocol to measure fatigue damage in asphalt mixtures. Road Materials and Pavement Design, 6(4), 485–514. https://doi.org/10.1080/14680629.2005.9690017

Speight, J. G. (2020). Asphaltenes and the Structure of Petroleum. *Petroleum Chemistry And Refining*, *59*(5), 117–134. https://doi.org/10.1201/9781482229349-11

Stephens, R., Fatemi, A., Stephens, R. R., & Fuchs, H. O. (2001). Fatigue design methods. *Metal Fatigue in Engineering*, 14. https://www.efatigue.com/training/Chapter_2.pdf

Sun, D., Sun, G., Zhu, X., Guarin, A., Li, B., Dai, Z., & Ling, J. (2018). A comprehensive review on self-healing of asphalt materials: Mechanism, model, characterization and enhancement. *Advances in Colloid and Interface Science*, *256*, 65–93. https://doi.org/10.1016/j.cis.2018.05.003

Tabaković, A., O'Prey, D., McKenna, D., & Woodward, D. (2019). Microwave self-healing

technology as airfield porous asphalt friction course repair and maintenance system. *Case Studies in Construction Materials*, *10*, e00233. https://doi.org/10.1016/j.cscm.2019.e00233

Tabaković, A., & Schlangen, E. (2016). Self-healing technology for asphalt pavements. *Advances in Polymer Science*, *273*, 285–306. https://doi.org/10.1007/12_2015_335

Tapsoba, N., Sauzéat, C., & Di Benedetto, H. (2013). Analysis of fatigue test for bituminous mixtures. *Journal of Materials in Civil Engineering*, *25*(6), 701–710. https://doi.org/10.1061/(ASCE)MT.1943-5533.0000636

Taylor, P., Gauthier, G., Bodin, D., Chailleux, E., & Gallet, T. (2011). *Road Materials and Pavement Design Non Linearity in Bituminous Materials during Cyclic Tests Non Linearity in Bituminous Materials during Cyclic Tests*. *0629*(December 2012), 37–41. https://doi.org/10.3166/RMPD.11HS.379-410.

Varma, R., Balieu, R., & Kringos, N. (2021). Indices-Based Healing Quantification for Bituminous Materials. Journal of Materials in Civil Engineering, 33(11), 04021294. https://doi.org/10.1061/(asce)mt.1943-5533.0003924

Wang, C., Castorena, C., Zhang, J., & Kim, Y. R. (2015). Unified failure criterion for asphalt binder under cyclic fatigue loading. *Asphalt Paving Technology: Association of Asphalt Paving Technologists-Proceedings of the Technical Sessions*, *84*, 269–300. https://doi.org/10.1080/14680629.2015.1077010

Wang, F., Zhu, H., Shu, B., Li, Y., Gu, D., Gao, Y., Chen, A., Feng, J., Wu, S., Liu, Q., & Li, C. (2022). Microwave heating mechanism and self-healing performance of asphalt mixture with basalt and limestone aggregates. *Construction and Building Materials*, *342*(PA), 127973. https://doi.org/10.1016/j.conbuildmat.2022.127973

Widyatmoko, I. (2016). Sustainability of bituminous materials. In *Sustainability of Construction Materials* (Second Edi). Elsevier Ltd. https://doi.org/10.1016/b978-0-08-100370-1.00014-7

Williams, D., Little, D. N., Lytton, R. L., Kim, Y. R. (2001). Microdamage healing in asphalt and asphalt concrete, volume II: Laboratory and field testing to assess and evaluate microdamage and microdamage healing. 1, 6–8. https://doi.org/10.16309/j.cnki.issn.1007-1776.2003.03.004

Williams, F. N., Mangiafico, S., & Sauzeat, C. (2023). Experimental evaluation of fatigue and recovery properties of a bituminous mixture during cyclic loading and rest tests. *Road Materials and Pavement Design*. https://doi.org/10.1080/14680629.2023.2191740

Wool, R. P., and K. M. O'Connor. 1981. 'A Theory Crack Healing in Polymers'. Journal of

Applied physics 52 (10): 5953–63. https://doi.org/10.1063/1.328526.

Wu, J. (2009). *The influence of mineral aggregrates and binder volumetrics on bitumen ageing* (Doctoral dissertation, University of Nottingham).Xia, W., Fan, S., Li, C., Xu, T., & Ph, D. (2021). *Effects of Different Nanofibers on Self-Healing Properties of Composite Modified Emulsified Asphalt*. *33*(2009), 1–10. https://doi.org/10.1061/(ASCE)MT.1943-5533.0003796

Xia, W., Fan, S., Li, C., Xu, T., & Ph, D. (2021). Effects of Different Nanofibers on Self-Healing Properties of Composite Modified Emulsified Asphalt. 33(2009), 1–10. https://doi.org/10.1061/(ASCE)MT.1943-5533.0003796.

Xie, W., Castorena, C., Wang, C., & Richard Kim, Y. (2017). A framework to characterize the healing potential of asphalt binder using the linear amplitude sweep test. *Construction and Building Materials*, *154*, 771–779. https://doi.org/10.1016/j.conbuildmat.2017.08.021

Xu, S., Liu, X., Tabakovi, A., Lin, P., Zhang, Y., Nahar, S., Lommerts, B. J., & Schlangen, E. (2021). *The role of rejuvenators in embedded damage healing for asphalt pavement*. *202*. https://doi.org/10.1016/j.matdes.2021.109564

Yoo, D. Y., Kim, S., Kim, M. J., Kim, D., & Shin, H. O. (2018, January). Self-healing capability of asphalt concrete with carbon-based materials. Journal of Materials Research and Technology, 8(1), 827–839. https://doi.org/10.1016/j.jmrt.2018.07.001

Zain, A., Abadeen, U., Hussain, A., Kumar, V. S., Murali, G., Vatin, N. I., & Riaz, H. (2022). *Comprehensive Self-Healing Evaluation of Asphalt Concrete Containing Encapsulated Rejuvenator*. 1–17.

Zeiada, W., (2012). Endurance Limit for HMA Based on Healing Phenomenon Using Viscoelastic Continuum Damage Analysis (PhD dissertation). Arizona State University, Tempe, Arizona, USA.

Zeiada, W. A., Souliman, M. I., Kaloush, K. E., & Mamlouk, M. (2014). Endurance limit for HMA based on healing concept using uniaxial tension-compression fatigue test. Journal of Materials in Civil Engineering, 26(8). https://doi.org/10.1061/(ASCE)MT.1943-5533.0000917

Zhai, L., Narkar, A., & Ahn, K. (2020). Nano Today Self-healing polymers with nanomaterials and nanostructures. *Nano Today*, *30*, 100826. https://doi.org/10.1016/j.nantod.2019.100826

Zhong, N., & Post, W. (2015). Self-repair of structural and functional composites with intrinsically self-healing polymer matrices: A review. *Composites Part A: Applied*

Science and Manufacturing, *69*, 226–239. https://doi.org/10.1016/j.compositesa.2014.11.028.

Zhou, L., Huang, W., Zhang, Y., Lv, Q., Yan, C., & Jiao, Y. (2020). Evaluation of the adhesion and healing properties of modified asphalt binders. Construction and Building Materials, 251, 119026. https://doi.org/10.1016/j.conbuildmat.2020.119026.

Zulkati, A., Diew, W. Y., & Delai, D. S. (2012). Effects of fillers on properties of asphalt-concrete mixture. *Journal of Transportation Engineering*, *138*(7), 902–910. https://doi.org/10.1061/(ASCE)TE.1943-5436.0000395

APPENDIX –

Analysis of DSR tests data from RILEM TC 278 CHA

&

Tension-Compression Tests on Bituminous Mixtures Performed at ENTPE

1. **Analysis of DSR Tests data from RILEM TC 278 CHA**

1.1. LVE properties of binders in undamaged conditions

1.1.1. Imaginary (G*) vs Real (G*) and (G*) versus φ for the 70/100 binders [Data from Torino].

1.2. Result of LAS test

1.2.1. Typical LAS tests result in stress – strain curve for 70/100 binder showing the peak and half peak stresses with increasing peak strain. [Data from Waterloo].

1.2.2. Typical LAS tests result in complex modulus – strain curve, complex modulus – No. of cycles & Normalised curve for 70/100 binder [Data from Waterloo].

1.2.3. Typical LAS tests result in complex modulus – strain curve, complex modulus – No. of cycles & Normalised curve for 70/100 binder [Data from Torino].

1.3. Results of LASH test

1.3.1. Comparing Strain at 0.1% and 0.0001% during pre-test for 70/100 binder [Data from Waterloo].

1.3.2. Comparing Strain at 0.1% and 0.0001% during pre-test for the PMB binder [Data from Waterloo].

1.3.3. Comparing Strain at 0.1% and 0.0001% during 5 min. rest for the 70/100 binder [Data from Waterloo].

1.3.4. Comparing Strain at 0.1% and 0.0001% during 30 min. rest for the 70/100 binder [Data from Waterloo].

1.4. Effect of rest periods and loading history

1.4.1. LASH test results at half peak for stress - strain curve for 70/100 binder showing the effect of rest periods [Data from Torino].

1.4.2. LASH test results at half peak for stress - strain curve for 70/100 binder showing the effect of rest periods [Data from Waterloo].

1.4.3. LASH test results at half peak for stress - strain curve for PMB showing the effect of rest periods [Data from Waterloo].

1.4.4. LASH test results at peak for stress - strain curve for 70/100 binder showing the effect of rest periods. [Data from Torino].

1.4.5. LASH test results at peak for stress - strain curve for 70/100 binder showing the effect of rest periods [Data from Waterloo].

1.4.6. LASH test results at peak for stress - strain curve for PMB showing the effect of rest periods [Data from Waterloo].

1.4.7. LASH stress half peak result of |G*| vs strain and φ vs strain for 70/100 binder showing the effect of rest periods [Data from Torino].

1.4.8. LASH stress half peak result of |G*| vs strain and φ vs strain for 70/100 binder showing the effect of rest periods [Data from Waterloo].

1.4.9. LASH test results at half peak result of |G*| vs strain and φ vs strain for PMB showing the effect of rest periods [Data from Waterloo].

1.4.10. LASH test results at peak result of |G*| vs strain and φ vs strain for 70/100 binder showing the effect of rest periods [Data from Torino].

1.4.11. LASH test results at peak result of |G*| vs strain and φ vs strain for 70/100 binder showing the effect of rest periods at 0 min., 5 min. and 30 min. [Data from Waterloo].

2.1.19. CMT results obtained for Mix PMB - 1: |E*|, φ_E, |ν*| and φ_ν against applied strain amplitude at different temperatures.
2.1.20. CMT results obtained for Mix PMB - 1: Regression of estimated values of |E*| φ_E, |ν*| and φ_ν as a function of temperature.
2.1.21. CMT results obtained for Mix PMB - 2: |E*| and φ_E against applied strain amplitude at different temperatures.
2.1.22. CMT results obtained for Mix PMB - 2: Regression of estimated values of |E*| and φ_E as a function of temperature.
2.1.23. CMT results obtained for Mix PMB - 5: |E*| φ_E, |ν*| and φ_ν against applied strain amplitude at different temperatures.
Figure 2.1.24. CMT results obtained for Mix PMB - 5: Regression of estimated values of |E*| φ_E, |ν*| and φ_ν as a function of temperature.
2.1.25. CMT results obtained for Mix PMB - 6: |E*| φ_E, |ν*| and φ_ν against applied strain amplitude at different temperatures.
Figure 2.1.26. CMT results obtained for Mix PMB - 6: Regression of estimated values of |E*| φ_E, |ν*| and φ_ν as a function of temperature.

3. Evolution of 3D mechanical properties (E*eq. and ν*eq.) during cyclic loading and rest periods.

3.1. PFRT results

3.1.1. PFRT results obtained for mix 70/100 - 1: (a) |E*| as a function of time during the first fatigue lag and rest period (b) |E*| as a function of applied strain amplitude during the first fatigue lags and the short complex modulus tests performed within its following rest periods; (c) |E*| as a function of time during the five fatigue lags and rest periods [Red stars indicate values of |E*| estimated at 100 µm/m at the beginning of fatigue lag, green asterisk shows values of $\Delta|E^*_{heating}|$ as influence of self-heating and brown triangles indicate values of |E*| estimated at 100 µm/m for each short complex modulus test during rest (all these values were obtained using non-linearity envelopes, as shown in Figure (b) for the first fatigue lag and rest period)].

3.1.2. PFRT results obtained for mix 70/100 – 1: (a) φ_E as a function of time during the first fatigue lag and rest period (b) φ_E as a function of applied strain amplitude during the first fatigue lags and the short complex modulus tests performed within its following rest periods; (c) φ_E as a function of time during the five fatigue lags and rest periods (Red stars indicate values of φ_E estimated at 100 µm/m at the beginning of fatigue lag, green asterisk shows values of $\Delta\varphi_{E\ heating}$ as influence of self-heating and brown triangles indicate values of φ_E estimated at 100 µm/m for each short complex modulus test during rest (all these values were obtained using non-linearity envelopes, as shown in (b) for the first fatigue lag and rest period).

3.1.3. PFRT results obtained for mix 70/100: |ν*| and φ_ν as a function of time during the first fatigue lags and rest periods (red. stars indicate values of |ν*| and φ_ν estimated at 100 µm/m at the beginning of fatigue lag, brown triangles indicate values of |ν*| and φ_ν estimated at 100 µm/m for each short complex modulus test during rest.

3.1.4. PFRT results obtained for Mix 70/100 – 1: internal and surface temperature evolution during fatigue lags and recovery periods.

3.1.5. Quantification of different contributions to |E*| and φ_E evolution, for the first two fatigue lags for Mix 70/100 – 1: different envelope line is used for each fatigue lag

3.1.6. Quantification of different absolute and relative contributions to |E*| and φ_E evolutions for AZALT 6, calculated using a different envelope line for each fatigue lag.

3.1.7. PFRT results obtained for mix 70/100 - 3: (a) |E*| as a function of time during the first fatigue lag and rest period (b) |E*| as a function of applied strain amplitude during the first fatigue lags and the short complex modulus tests performed within its following rest periods; (c) |E*| as a function of time during the two fatigue lags and rest periods [Red stars indicate values of |E*| estimated at 100 µm/m at the beginning of fatigue lag, green asterisk shows values of $\Delta|E^*_{heating}|$ as influence of self-heating and brown triangles indicate values of |E*| estimated at 100 µm/m for each short complex modulus test during rest (all these values were obtained using non-linearity envelopes, as shown in Figure (b) for the first fatigue lag and rest period)].

3.1.8. PFRT results obtained for mix 70/100 - 3: (a) |E*| as a function of time during the second fatigue lag and rest period (b) |E*| as a function of applied strain amplitude during the second fatigue lags and the short complex modulus tests performed within its following rest periods; (c) |E*| as a function of time during the two fatigue lags and rest periods [Red stars indicate values of |E*| estimated at 100 µm/m at the beginning of fatigue lag, green asterisk shows values of $\Delta|E^*_{heating}|$ as influence of self-heating and brown triangles indicate values of |E*| estimated at 100 µm/m for each short complex modulus test during rest (all these values were obtained using non-linearity envelopes, as shown in Figure (b) for the first fatigue lag and rest period)].

3.1.9. PFRT results obtained for mix 70/100 – 3: (a) φ_E as a function of time during the first fatigue lag and rest period (b) φ_E as a function of applied strain amplitude during the first fatigue lags and the short complex modulus tests performed within its following rest periods; (c) φ_E as a function of time during the two fatigue lags and rest periods (Red stars indicate values of φ_E estimated at 100 µm/m at the beginning of fatigue lag, green asterisk shows values of $\Delta\varphi_{E\ heating}$ as influence of self-heating and brown triangles indicate values of φ_E estimated at 100 µm/m for each short complex modulus test during rest (all these values were obtained using non-linearity envelopes, as shown in (b) for the first fatigue lag and rest period).

3.1.10. PFRT results obtained for mix 70/100 – 3: (a) φ_E as a function of time during the second fatigue lag and rest period (b) φ_E as a function of applied strain amplitude during the second fatigue lags and the short complex modulus tests performed within its following rest periods; (c) φ_E as a function of time during the two fatigue lags and rest periods (Red stars indicate values of φ_E estimated at 100 µm/m at the beginning of fatigue lag, green asterisk shows values of $\Delta\varphi_{E\ heating}$ as influence of self-heating and brown triangles indicate values of φ_E estimated at 100 µm/m for each short complex modulus test during rest (all these values were obtained using non-linearity envelopes, as shown in (b) for the first fatigue lag and rest period).

3.1.11. PFRT results obtained for mix 70/100 – 3: $|\nu^*|$ and φ_ν as a function of applied strain amplitude during the first fatigue lags.

3.12. PFRT results obtained for mix 70/100 – 3: internal and surface temperature evolution during fatigue lags and recovery periods.

3.1.13. Quantification of different contributions $|E^*|$ and φ_E evolution, for the first two fatigue lags for mix 70/100 - 3: different envelope line is used for each fatigue lag.
Figure 3.1.14. Quantification of different absolute and relative contributions to $|E^*|$ and φ_E evolutions for mix 70/100 - 3, calculated using a different envelope line for each fatigue lag.

Figure 3.1.15. Quantification of different contributions to $|E^*|$ and φ_E evolution during first and second fatigue lags for mix 70/100 - 3: the envelope line of the first fatigue lag is used for all fatigue lags.

Figure 3.1.16. Quantification of different absolute and relative contributions to $|E^*|$ and φ_E evolutions for mix 70/100 - 3, calculated using the envelope line for the first fatigue lag. 338
3.1.17. PFRT results obtained for mix 70/100 - 4: (a) $|E^*|$ as a function of time during the first fatigue lag and rest period (b) $|E^*|$ as a function of applied strain amplitude during the first fatigue lags and the short complex modulus tests performed within its following rest periods; (c) $|E^*|$ as a function of time during the two fatigue lags and rest periods [Red stars indicate values of $|E^*|$ estimated at 100 µm/m at the beginning of fatigue lag, green asterisk shows values of $\Delta|E^*_{heating}|$ as influence of self-heating and brown triangles indicate values of $|E^*|$ estimated at 100 µm/m for each short complex modulus test during rest (all these values were obtained using non-linearity envelopes, as shown in Figure (b) for the first fatigue lag and rest period)].

3.1.18. PFRT results obtained for mix 70/100 – 4: (a) φ_E as a function of time during the first fatigue lag and rest period (b) φ_E as a function of applied strain amplitude during the first fatigue lags and the short complex modulus tests performed within its following rest periods; (c) φ_E as a function of time during the two fatigue lags and rest periods (Red stars indicate values of φ_E estimated at 100 µm/m at the beginning of fatigue lag, green asterisk shows values of $\Delta\varphi_{E\ heating}$ as influence of self-heating and brown triangles indicate values of φ_E estimated at 100 µm/m for each short complex modulus test during rest (all these values were obtained using non-linearity envelopes, as shown in (b) for the first fatigue lag and rest period).

3.1.19. PFRT results obtained for mix 70/100 - 4: internal and surface temperature evolution during fatigue lags and recovery periods.

Figure 3.1.20. Quantification of different contributions $|E^*|$ and φ_E evolution, for the first two fatigue lags for mix 70/100 - 4: different envelope line is used for each fatigue lag.
3.1.21. Quantification of different absolute and relative contributions to $|E^*|$ and φ_E evolutions for mix 70/100 - 4, calculated using a different envelope line for each fatigue lag.
3.1.22. PFRT results obtained for mix 70/100 - 5: (a) $|E^*|$ as a function of time during the first fatigue lag and rest period (b) $|E^*|$ as a function of applied strain amplitude during the first

fatigue lags and the short complex modulus tests performed within its following rest periods; (c) |E*| as a function of time during the three fatigue lags and rest periods [Red stars indicate values of |E*| estimated at 100 µm/m at the beginning of fatigue lag, green asterisk shows values of $\Delta|E^*_{heating}|$ as influence of self-heating and brown triangles indicate values of |E*| estimated at 100 µm/m for each short complex modulus test during rest (all these values were obtained using non-linearity envelopes, as shown in Figure (b) for the first fatigue lag and rest period)].

3.1.23. PFRT results obtained for mix 70/100 - 5: (a) |E*| as a function of time during the second fatigue lag and rest period (b) |E*| as a function of applied strain amplitude during the second fatigue lags and the short complex modulus tests performed within its following rest periods; (c) |E*| as a function of time during the three fatigue lags and rest periods [Red stars indicate values of |E*| estimated at 100 µm/m at the beginning of fatigue lag, green asterisk shows values of $\Delta|E^*_{heating}|$ as influence of self-heating and brown triangles indicate values of |E*| estimated at 100 µm/m for each short complex modulus test during rest (all these values were obtained using non-linearity envelopes, as shown in Figure (b) for the first fatigue lag and rest period)].

3.1.24. PFRT results obtained for mix 70/100 - 5: (a) |E*| as a function of time during the thirdfatigue lag and rest period (b) |E*| as a function of applied strain amplitude during the third fatigue lags and the short complex modulus tests performed within its following rest periods; (c) |E*| as a function of time during the three fatigue lags and rest periods [Red stars indicate values of |E*| estimated at 100 µm/m at the beginning of fatigue lag, green asterisk shows values of $\Delta|E^*_{heating}|$ as influence of self-heating and brown triangles indicate values of |E*| estimated at 100 µm/m for each short complex modulus test during rest (all these values were obtained using non-linearity envelopes, as shown in Figure (b) for the first fatigue lag and rest period)].

3.1.25. PFRT results obtained for mix 70/100 – 5: (a) φ_E as a function of time during the first fatigue lag and rest period (b) φ_E as a function of applied strain amplitude during the first fatigue lags and the short complex modulus tests performed within its following rest periods; (c) φ_E as a function of time during the three fatigue lags and rest periods (Red stars indicate values of φ_E estimated at 100 µm/m at the beginning of fatigue lag, green asterisk shows values of $\Delta\varphi_{E\ heating}$ as influence of self-heating and brown triangles indicate values of φ_E estimated at 100 µm/m for each short complex modulus test during rest (all these values were obtained using non-linearity envelopes, as shown in (b) for the first fatigue lag and rest period).

3.1.26. PFRT results obtained for mix 70/100 – 5: (a) φ_E as a function of time during the secondfatigue lag and rest period (b) φ_E as a function of applied strain amplitude during the second fatigue lags and the short complex modulus tests performed within its following rest periods; (c) φ_E as a function of time during the three fatigue lags and rest periods (Red stars indicate values of φ_E estimated at 100 µm/m at the beginning of fatigue lag, green asterisk shows values of $\Delta\varphi_{E\ heating}$ as influence of self-heating and brown triangles indicate values of φ_E estimated at 100 µm/m for each short complex modulus test during rest (all these values were obtained using non-linearity envelopes, as shown in (b) for the first fatigue lag and rest period).

3.1.27. PFRT results obtained for mix 70/100 – 5: (a) φ_E as a function of time during the third fatigue lag and rest period (b) φ_E as a function of applied strain amplitude during the thirdfatigue lags and the short complex modulus tests performed within its following rest periods; (c) φ_E as a function of time during the three fatigue lags and rest periods (Red stars indicate values of φ_E estimated at 100 µm/m at the beginning of fatigue lag, green asterisk shows values of $\Delta\varphi_{E\ heating}$ as influence of self-heating and brown triangles indicate values of φ_E estimated at 100 µm/m for each short complex modulus test during rest (all these values were obtained using non-linearity envelopes, as shown in (b) for the first fatigue lag and rest period).

3.1.28. PFRT results obtained for mix 70/100 – 5: $|\nu^*|$ and φ_ν as a function of time amplitude during the first fatigue lags.

3.1.29. PFRT results obtained for mix 70/100 – 5: internal and surface temperature evolution during fatigue lags and recovery periods.

3.1.30. Quantification of different contributions $|E^*|$ and φ_E evolution, for the first two fatigue lags for mix 70/100 – 5: different envelope line is used for each fatigue lag.

3.1.31. Quantification of different absolute and relative contributions to $|E^*|$ and φ_E evolutions for mix 70/100 – 5, calculated using a different envelope line for each fatigue lag.

3.1.32. Quantification of different contributions to $|E^*|$ and φ_E evolution during first and second fatigue lags for mix 70/100 – 5: the envelope line of the first fatigue lag is used for all fatigue lags.

3.1.33. Quantification of different absolute and relative contributions to $|E^*|$ and φ_E evolutions for mix 70/100 – 5, calculated using the envelope line for the first fatigue lag.

3.1.34. PFRT results obtained for mix 70/100 - 8: (a) $|E^*|$ as a function of time during the first fatigue lag and rest period (b) $|E^*|$ as a function of applied strain amplitude during the firstfatigue lags and the short complex modulus tests performed within its following rest periods; (c) $|E^*|$ as a function of time during the two fatigue lags and rest periods [Red stars indicate values of $|E^*|$ estimated at 100 µm/m at the beginning of fatigue lag, green asterisk shows values of $\Delta|E^*_{heating}|$ as influence of self-heating and brown triangles indicate values of $|E^*|$ estimated at 100 µm/m for each short complex modulus test during rest (all these values were obtained using non-linearity envelopes, as shown in Figure (b) for the first fatigue lag and rest period)].

3.1.35. PFRT results obtained for mix 70/100 - 8: (a) $|E^*|$ as a function of time during the second fatigue lag and rest period (b) $|E^*|$ as a function of applied strain amplitude during the second fatigue lags and the short complex modulus tests performed within its following rest periods; (c) $|E^*|$ as a function of time during the two fatigue lags and rest periods [Red stars indicate values of $|E^*|$ estimated at 100 µm/m at the beginning of fatigue lag, green asterisk shows values of $\Delta|E^*_{heating}|$ as influence of self-heating and brown triangles indicate values of $|E^*|$ estimated

at 100 μm/m for each short complex modulus test during rest (all these values were obtained using non-linearity envelopes, as shown in Figure (b) for the first fatigue lag and rest period)].

3.1.36. PFRT results obtained for mix 70/100 – 8: (a) φ_E as a function of time during the first fatigue lag and rest period (b) φ_E as a function of applied strain amplitude during the first fatigue lags and the short complex modulus tests performed within its following rest periods; (c) φ_E as a function of time during the two fatigue lags and rest periods (Red stars indicate values of φ_E estimated at 100 μm/m at the beginning of fatigue lag, green asterisk shows values of $\Delta\varphi_{E\ heating}$ as influence of self-heating and brown triangles indicate values of φ_E estimated at 100 μm/m for each short complex modulus test during rest (all these values were obtained using non-linearity envelopes, as shown in (b) for the first fatigue lag and rest period).

3.1.37. PFRT results obtained for mix 70/100 – 8: (a) φ_E as a function of time during the second fatigue lag and rest period (b) φ_E as a function of applied strain amplitude during the second fatigue lags and the short complex modulus tests performed within its following rest periods; (c) φ_E as a function of time during the two fatigue lags and rest periods (Red stars indicate values of φ_E estimated at 100 μm/m at the beginning of fatigue lag, green asterisk shows values of $\Delta\varphi_{E\ heating}$ as influence of self-heating and brown triangles indicate values of φ_E estimated at 100 μm/m for each short complex modulus test during rest (all these values were obtained using non-linearity envelopes, as shown in (b) for the first fatigue lag and rest period).

3.1.38. PFRT results obtained for mix 70/100 – 8: internal and surface temperature evolution during fatigue lags and recovery periods

3.1.39. Quantification of different contributions |E*| and φ_E evolution, for the first two fatigue lags for mix 70/100 – 8: different envelope line is used for each fatigue lag.

3.1.40. Quantification of different absolute and relative contributions to |E*| and ϕ_E evolutions for mix 70/100 – 8, calculated using a different envelope line for each fatigue lag.

3.1.41. Quantification of different contributions to |E*| and φ_E evolution during first and second fatigue lags for mix 70/100 – 8: the envelope line of the first fatigue lag is used for all fatigue lags.

Figure 3.1.42. Quantification of different absolute and relative contributions to |E*| and φ_E evolutions for mix 70/100 – 8, calculated using the envelope line for the first fatigue lag.

3.1.43. PFRT results obtained for mix 40/60 – 4: (a) |E*| as a function of time during the first fatigue lag and rest period (b) |E*| as a function of applied strain amplitude during the first fatigue lags and the short complex modulus tests performed within its following rest periods; (c) |E*| as a function of time during the five fatigue lags and rest periods [Red stars indicate values of |E*| estimated at 100 μm/m at the beginning of fatigue lag, green asterisk shows values of $\Delta|E^*_{heating}|$ as influence of self-heating and brown triangles indicate values of |E*| estimated at 100 μm/m for each short complex modulus test during rest (all these values were obtained using non-linearity envelopes, as shown in (b) for the first fatigue lag and rest period)].

3.1.44. PFRT results obtained for mix 40/60 – 4: (a) |E*| as a function of time during the second fatigue lag and rest period (b) |E*| as a function of applied strain amplitude during the second fatigue lags and the short complex modulus tests performed within its following rest periods; (c) |E*| as a function of time during the five fatigue lags and rest periods [Red stars indicate values of |E*| estimated at 100 µm/m at the beginning of fatigue lag, green asterisk shows values of $\Delta|E^*_{heating}|$ as influence of self-heating and brown triangles indicate values of |E*| estimated at 100 µm/m for each short complex modulus test during rest (all these values were obtained using non-linearity envelopes, as shown in (b) for the first fatigue lag and rest period)].

3.1.45. PFRT results obtained for mix 40/60 – 4: (a) |E*| as a function of time during the third fatigue lag and rest period (b) |E*| as a function of applied strain amplitude during the third fatigue lags and the short complex modulus tests performed within its following rest periods; (c) |E*| as a function of time during the five fatigue lags and rest periods [Red stars indicate values of |E*| estimated at 100 µm/m at the beginning of fatigue lag, green asterisk shows values of $\Delta|E^*_{heating}|$ as influence of self-heating and brown triangles indicate values of |E*| estimated at 100 µm/m for each short complex modulus test during rest (all these values were obtained using non-linearity envelopes, as shown in (b) for the first fatigue lag and rest period)].

3.1.46. PFRT results obtained for mix 40/60 – 4: (a) |E*| as a function of time during the fourth fatigue lag and rest period (b) |E*| as a function of applied strain amplitude during the fourth fatigue lags and the short complex modulus tests performed within its following rest periods; (c) |E*| as a function of time during the five fatigue lags and rest periods [Red stars indicate values of |E*| estimated at 100 µm/m at the beginning of fatigue lag, green asterisk shows values of $\Delta|E^*_{heating}|$ as influence of self-heating and brown triangles indicate values of |E*| estimated at 100 µm/m for each short complex modulus test during rest (all these values were obtained using non-linearity envelopes, as shown in (b) for the first fatigue lag and rest period)].

3.1.47. PFRT results obtained for mix 40/60 – 4: (a) |E*| as a function of time during the fifth fatigue lag and rest period (b) |E*| as a function of applied strain amplitude during the fifth fatigue lags and the short complex modulus tests performed within its following rest periods; (c) |E*| as a function of time during the five fatigue lags and rest periods [Red stars indicate values of |E*| estimated at 100 µm/m at the beginning of fatigue lag, green asterisk shows values of $\Delta|E^*_{heating}|$ as influence of self-heating and brown triangles indicate values of |E*| estimated at 100 µm/m for each short complex modulus test during rest (all these values were obtained using non-linearity envelopes, as shown in (b) for the first fatigue lag and rest period)].

3.1.48. PFRT results obtained for mix 40/60 – 4: (a) φ_E as a function of time during the first fatigue lag and rest period (b) φ_E as a function of applied strain amplitude during the first fatigue lags and the short complex modulus tests performed within its following rest periods; (c) φ_E as a function of time during the five fatigue lags and rest periods (Red stars indicate values of φ_E estimated at 100 µm/m at the beginning of fatigue lag, green asterisk shows values of $\Delta\varphi_{E\ heating}$ as influence of self-heating and brown triangles indicate values of φ_E estimated at 100 µm/m for each short complex modulus test during rest (all these values were obtained using non-linearity envelopes, as shown in (b) for the first fatigue lag and rest period).

3.1.49. PFRT results obtained for mix 40/60 – 4: (a) φ_E as a function of time during the second fatigue lag and rest period (b) φ_E as a function of applied strain amplitude during the second fatigue lags and the short complex modulus tests performed within its following rest periods; (c) φ_E as a function of time during the five fatigue lags and rest periods (Red stars indicate values of φ_E estimated at 100 µm/m at the beginning of fatigue lag, green asterisk shows values of $\Delta\varphi_{E\ heating}$ as influence of self-heating and brown triangles indicate values of φ_E estimated at 100 µm/m for each short complex modulus test during rest (all these values were obtained using non-linearity envelopes, as shown in (b) for the first fatigue lag and rest period).

3.1.50. PFRT results obtained for mix 40/60 – 4: (a) φ_E as a function of time during the third fatigue lag and rest period (b) φ_E as a function of applied strain amplitude during the third fatigue lags and the short complex modulus tests performed within its following rest periods; (c) φ_E as a function of time during the five fatigue lags and rest periods (Red stars indicate values of φ_E estimated at 100 µm/m at the beginning of fatigue lag, green asterisk shows values of $\Delta\varphi_{E\ heating}$ as influence of self-heating and brown triangles indicate values of φ_E estimated at 100 µm/m for each short complex modulus test during rest (all these values were obtained using non-linearity envelopes, as shown in (b) for the first fatigue lag and rest period).

3.1.51. PFRT results obtained for mix 40/60 – 4: (a) φ_E as a function of time during the fourth fatigue lag and rest period (b) φ_E as a function of applied strain amplitude during the fourth fatigue lags and the short complex modulus tests performed within its following rest periods; (c) φ_E as a function of time during the five fatigue lags and rest periods (Red stars indicate values of φ_E estimated at 100 µm/m at the beginning of fatigue lag, green asterisk shows values of $\Delta\varphi_{E\ heating}$ as influence of self-heating and brown triangles indicate values of φ_E estimated at 100 µm/m for each short complex modulus test during rest (all these values were obtained using non-linearity envelopes, as shown in (b) for the first fatigue lag and rest period).

3.1.52. PFRT results obtained for mix 40/60 – 4: (a) φ_E as a function of time during the fifth fatigue lag and rest period (b) φ_E as a function of applied strain amplitude during the fifth fatigue lags and the short complex modulus tests performed within its following rest periods; (c) φ_E as a function of time during the five fatigue lags and rest periods (Red stars indicate values of φ_E estimated at 100 µm/m at the beginning of fatigue lag, green asterisk shows values of $\Delta\varphi_{E\ heating}$ as influence of self-heating and brown triangles indicate values of φ_E estimated at 100 µm/m for each short complex modulus test during rest (all these values were obtained using non-linearity envelopes, as shown in (b) for the first fatigue lag and rest period).

3.1.53. PFRT results obtained for mix 40/60 – 4: (a) $|v^*|$ as a function of time during the fifth fatigue lag and rest period (b) $|v^*|$ as a function of applied strain amplitude during the fifth fatigue lags and the short complex modulus tests performed within its following rest periods; (c) $|v^*|$ as a function of time during the five fatigue lags and rest periods (Red stars indicate values of $|v^*|$ estimated at 100 µm/m at the beginning of fatigue lag, green asterisk shows values of $\Delta|v^*|_{heating}$ as influence of self-heating and brown triangles indicate values of $|v^*|$ estimated

at 100 µm/m for each short complex modulus test during rest (all these values were obtained using non-linearity envelopes, as shown in (b) for the first fatigue lag and rest period).

3.1.54. PFRT results obtained for mix 40/60 – 4: (a) φ_v as a function of time during the fifth fatigue lag and rest period (b) |v*| as a function of applied strain amplitude during the fifth fatigue lags and the short complex modulus tests performed within its following rest periods; (c) φ_v as a function of time during the five fatigue lags and rest periods (Red stars indicate values of φ_v estimated at 100 µm/m at the beginning of fatigue lag, green asterisk shows values of $\varphi_{v\ heating}$ as influence of self-heating and brown triangles indicate values of φ_v estimated at 100 µm/m for each short complex modulus test during rest (all these values were obtained using non-linearity envelopes, as shown in (b) for the first fatigue lag and rest period).

Figure 3.1.55. PFRT results obtained for mix 40/60 – 4: internal and surface temperature evolution during fatigue lags and recovery periods.

Figure 3.1.56. Quantification of different contributions |E*|, φ_E, |v*| and φ_v evolution, for all fatigue lags for mix 40/60 – 4: different envelope line is used for each fatigue lag.

Figure 3.1.57. Quantification of different absolute and relative contributions to |E*|, φ_E, |v*| and φ_v evolutions for mix 40/60 – 4, calculated using a different envelope line for each fatigue lag.

Figure 3.1.58. Quantification of different contributions to |E*|, φ_E, |v*| and φ_v evolution during first and second fatigue lags for mix 40/60 – 4: the envelope line of the first fatigue lag is used for all fatigue lags.

3.1.59. Quantification of different absolute and relative contributions to |E*|, φ_E, |v*| and φ_v evolutions for mix 40/60 – 4, calculated using the envelope line for the first fatigue lag. 388
3.1.60. PFRT results obtained for mix 40/60 – 5: (a) |E*| as a function of time during the first fatigue lag and rest period (b) |E*| as a function of applied strain amplitude during the first fatigue lags and the short complex modulus tests performed within its following rest periods; (c) |E*| as a function of time during the five fatigue lags and rest periods [Red stars indicate values of |E*| estimated at 100 µm/m at the beginning of fatigue lag, green asterisk shows values of $\Delta|E^*_{heating}|$ as influence of self-heating and brown triangles indicate values of |E*| estimated at 100 µm/m for each short complex modulus test during rest (all these values were obtained using non-linearity envelopes, as shown in (b) for the first fatigue lag and rest period)].

3.1.61. PFRT results obtained for mix 40/60 – 5: (a) |E*| as a function of time during the second fatigue lag and rest period (b) |E*| as a function of applied strain amplitude during the second fatigue lags and the short complex modulus tests performed within its following rest periods; (c) |E*| as a function of time during the five fatigue lags and rest periods [Red stars indicate values of |E*| estimated at 100 µm/m at the beginning of fatigue lag, green asterisk shows values of $\Delta|E^*_{heating}|$ as influence of self-heating and brown triangles indicate values of |E*| estimated at 100 µm/m for each short complex modulus test during rest (all these values were obtained using non-linearity envelopes, as shown in (b) for the first fatigue lag and rest period)].

3.1.62. PFRT results obtained for mix 40/60 – 5: (a) |E*| as a function of time during the third fatigue lag and rest period (b) |E*| as a function of applied strain amplitude during the third fatigue lags and the short complex modulus tests performed within its following rest periods; (c) |E*| as a function of time during the five fatigue lags and rest periods [Red stars indicate values of |E*| estimated at 100 µm/m at the beginning of fatigue lag, green asterisk shows values of $\Delta|E^*_{heating}|$ as influence of self-heating and brown triangles indicate values of |E*| estimated at 100 µm/m for each short complex modulus test during rest (all these values were obtained using non-linearity envelopes, as shown in (b) for the first fatigue lag and rest period)].

3.1.63. PFRT results obtained for mix 40/60 – 5: (a) |E*| as a function of time during the fourth fatigue lag and rest period (b) |E*| as a function of applied strain amplitude during the fourth fatigue lags and the short complex modulus tests performed within its following rest periods; (c) |E*| as a function of time during the five fatigue lags and rest periods [Red stars indicate values of |E*| estimated at 100 µm/m at the beginning of fatigue lag, green asterisk shows values of $\Delta|E^*_{heating}|$ as influence of self-heating and brown triangles indicate values of |E*| estimated at 100 µm/m for each short complex modulus test during rest (all these values were obtained using non-linearity envelopes, as shown in (b) for the first fatigue lag and rest period)].

3.1.64. PFRT results obtained for mix 40/60 – 5: (a) |E*| as a function of time during the fifth fatigue lag and rest period (b) |E*| as a function of applied strain amplitude during the fifth fatigue lags and the short complex modulus tests performed within its following rest periods; (c) |E*| as a function of time during the five fatigue lags and rest periods [Red stars indicate values of |E*| estimated at 100 µm/m at the beginning of fatigue lag, green asterisk shows values of $\Delta|E^*_{heating}|$ as influence of self-heating and brown triangles indicate values of |E*| estimated at 100 µm/m for each short complex modulus test during rest (all these values were obtained using non-linearity envelopes, as shown in (b) for the first fatigue lag and rest period)].

3.1.65. PFRT results obtained for mix 40/60 – 5: (a) φ_E as a function of time during the first fatigue lag and rest period (b) φ_E as a function of applied strain amplitude during the first fatigue lags and the short complex modulus tests performed within its following rest periods; (c) φ_E as a function of time during the five fatigue lags and rest periods (Red stars indicate values of φ_E estimated at 100 µm/m at the beginning of fatigue lag, green asterisk shows values of $\Delta\varphi_{E\ heating}$ as influence of self-heating and brown triangles indicate values of φ_E estimated at 100 µm/m for each short complex modulus test during rest (all these values were obtained using non-linearity envelopes, as shown in (b) for the first fatigue lag and rest period).

3.1.66. PFRT results obtained for mix 40/60 – 5: (a) φ_E as a function of time during the second fatigue lag and rest period (b) φ_E as a function of applied strain amplitude during the second fatigue lags and the short complex modulus tests performed within its following rest periods; (c) φ_E as a function of time during the five fatigue lags and rest periods (Red stars indicate values of φ_E estimated at 100 µm/m at the beginning of fatigue lag, green asterisk shows values of $\Delta\varphi_{E\ heating}$ as influence of self-heating and brown triangles indicate values of φ_E estimated at

100 µm/m for each short complex modulus test during rest (all these values were obtained using non-linearity envelopes, as shown in (b) for the first fatigue lag and rest period).

3.1.67. PFRT results obtained for mix 40/60 – 5: (a) φ_E as a function of time during the third fatigue lag and rest period (b) φ_E as a function of applied strain amplitude during the third fatigue lags and the short complex modulus tests performed within its following rest periods; (c) φ_E as a function of time during the five fatigue lags and rest periods (Red stars indicate values of φ_E estimated at 100 µm/m at the beginning of fatigue lag, green asterisk shows values of $\Delta\varphi_{E\ heating}$ as influence of self-heating and brown triangles indicate values of φ_E estimated at 100 µm/m for each short complex modulus test during rest (all these values were obtained using non-linearity envelopes, as shown in (b) for the first fatigue lag and rest period).

3.1.68. PFRT results obtained for mix 40/60 – 5: (a) φ_E as a function of time during the fourth fatigue lag and rest period (b) φ_E as a function of applied strain amplitude during the fourth fatigue lags and the short complex modulus tests performed within its following rest periods; (c) φ_E as a function of time during the five fatigue lags and rest periods (Red stars indicate values of φ_E estimated at 100 µm/m at the beginning of fatigue lag, green asterisk shows values of $\Delta\varphi_{E\ heating}$ as influence of self-heating and brown triangles indicate values of φ_E estimated at 100 µm/m for each short complex modulus test during rest (all these values were obtained using non-linearity envelopes, as shown in (b) for the first fatigue lag and rest period).

3.1.69. PFRT results obtained for mix 40/60 – 5: (a) φ_E as a function of time during the fifth fatigue lag and rest period (b) φ_E as a function of applied strain amplitude during the fifth fatigue lags and the short complex modulus tests performed within its following rest periods; (c) φ_E as a function of time during the five fatigue lags and rest periods (Red stars indicate values of φ_E estimated at 100 µm/m at the beginning of fatigue lag, green asterisk shows values of $\Delta\varphi_{E\ heating}$ as influence of self-heating and brown triangles indicate values of φ_E estimated at 100 µm/m for each short complex modulus test during rest (all these values were obtained using non-linearity envelopes, as shown in (b) for the first fatigue lag and rest period).

3.1.70. PFRT results obtained for mix 40/60 – 5: internal and surface temperature evolution during fatigue lags and recovery periods.

3.1.71. Quantification of different contributions E*| and φ_E evolution, for the five fatigue lags for mix 40/60 – 5: different envelope line is used for each fatigue lag.

3.1.72. Quantification of different absolute and relative contributions to |E*| and ϕ_E evolutions for mix 40/60 – 5, calculated using a different envelope line for each fatigue lag.

3.1.73. Quantification of different contributions to |E*| and φ_E evolution during five fatigue lags for mix 40/60 – 5: the envelope line of the first fatigue lag is used for all fatigue lags.

.

3.1.74. Quantification of different absolute and relative contributions to |E*| and φ_E evolutions for mix 40/60 – 5, calculated using the envelope line for the first fatigue lag.

3.1.75. PFRT results obtained for mix 40/60 – 6: (a) |E*| as a function of time during the first fatigue lag and rest period (b) |E*| as a function of applied strain amplitude during the first fatigue lags and the short complex modulus tests performed within its following rest periods; (c) |E*| as a function of time during the five fatigue lags and rest periods [Red stars indicate values of |E*| estimated at 100 µm/m at the beginning of fatigue lag, green asterisk shows values of $\Delta|E^*_{heating}|$ as influence of self-heating and brown triangles indicate values of |E*| estimated at 100 µm/m for each short complex modulus test during rest (all these values were obtained using non-linearity envelopes, as shown in (b) for the first fatigue lag and rest period)].

3.1.76. PFRT results obtained for mix 40/60 – 6: (a) |E*| as a function of time during the second fatigue lag and rest period (b) |E*| as a function of applied strain amplitude during the second fatigue lags and the short complex modulus tests performed within its following rest periods; (c) |E*| as a function of time during the five fatigue lags and rest periods [Red stars indicate values of |E*| estimated at 100 µm/m at the beginning of fatigue lag, green asterisk shows values of $\Delta|E^*_{heating}|$ as influence of self-heating and brown triangles indicate values of |E*| estimated at 100 µm/m for each short complex modulus test during rest (all these values were obtained using non-linearity envelopes, as shown in (b) for the first fatigue lag and rest period)].

3.1.77. PFRT results obtained for mix 40/60 – 6: (a) |E*| as a function of time during the third fatigue lag and rest period (b) |E*| as a function of applied strain amplitude during the third fatigue lags and the short complex modulus tests performed within its following rest periods; (c) |E*| as a function of time during the five fatigue lags and rest periods [Red stars indicate values of |E*| estimated at 100 µm/m at the beginning of fatigue lag, green asterisk shows values of Δ|E*heating| as influence of self-heating and brown triangles indicate values of |E*| estimated at 100 µm/m for each short complex modulus test during rest (all these values were obtained using non-linearity envelopes, as shown in (b) for the first fatigue lag and rest period)].

3.1.78. PFRT results obtained for mix 40/60 – 6: (a) |E*| as a function of time during the fourth fatigue lag and rest period (b) |E*| as a function of applied strain amplitude during the fourth fatigue lags and the short complex modulus tests performed within its following rest periods; (c) |E*| as a function of time during the five fatigue lags and rest periods [Red stars indicate values of |E*| estimated at 100 µm/m at the beginning of fatigue lag, green asterisk shows values of $\Delta|E^*_{heating}|$ as influence of self-heating and brown triangles indicate values of |E*| estimated at 100 µm/m for each short complex modulus test during rest (all these values were obtained using non-linearity envelopes, as shown in (b) for the first fatigue lag and rest period)].

3.1.79. PFRT results obtained for mix 40/60 – 6: (a) |E*| as a function of time during the fifth fatigue lag and rest period (b) |E*| as a function of applied strain amplitude during the fifth fatigue lags and the short complex modulus tests performed within its following rest periods; (c) |E*| as a function of time during the five fatigue lags and rest periods [Red stars indicate values of |E*| estimated at 100 µm/m at the beginning of fatigue lag, green asterisk shows values of $\Delta|E^*_{heating}|$ as influence of self-heating and brown triangles indicate values of |E*| estimated

at 100 μm/m for each short complex modulus test during rest (all these values were obtained using non-linearity envelopes, as shown in (b) for the first fatigue lag and rest period)].

3.1.80. PFRT results obtained for mix 40/60 – 6: (a) φ_E as a function of time during the first fatigue lag and rest period (b) φ_E as a function of applied strain amplitude during the first fatigue lags and the short complex modulus tests performed within its following rest periods; (c) φ_E as a function of time during the five fatigue lags and rest periods (Red stars indicate values of φ_E estimated at 100 μm/m at the beginning of fatigue lag, green asterisk shows values of $\Delta\varphi_{E\ heating}$ as influence of self-heating and brown triangles indicate values of φ_E estimated at 100 μm/m for each short complex modulus test during rest (all these values were obtained using non-linearity envelopes, as shown in (b) for the first fatigue lag and rest period).

3.1.81. PFRT results obtained for mix 40/60 – 6: (a) φ_E as a function of time during the second fatigue lag and rest period (b) φ_E as a function of applied strain amplitude during the second fatigue lags and the short complex modulus tests performed within its following rest periods; (c) φ_E as a function of time during the five fatigue lags and rest periods (Red stars indicate values of φ_E estimated at 100 μm/m at the beginning of fatigue lag, green asterisk shows values of $\Delta\varphi_{E\ heating}$ as influence of self-heating and brown triangles indicate values of φ_E estimated at 100 μm/m for each short complex modulus test during rest (all these values were obtained using non-linearity envelopes, as shown in (b) for the first fatigue lag and rest period).

3.1.82. PFRT results obtained for mix 40/60 – 6: (a) φE as a function of time during the third fatigue lag and rest period (b) φE as a function of applied strain amplitude during the third fatigue lags and the short complex modulus tests performed within its following rest periods; (c) φE as a function of time during the five fatigue lags and rest periods (Red stars indicate values of φE estimated at 100 μm/m at the beginning of fatigue lag, green asterisk shows values of ΔφE heating as influence of self-heating and brown triangles indicate values of φE estimated at 100 μm/m for each short complex modulus test during rest (all these values were obtained using non-linearity envelopes, as shown in (b) for the first fatigue lag and rest period).

3.1.83. PFRT results obtained for mix 40/60 – 6: (a) φ_E as a function of time during the fourth fatigue lag and rest period (b) φ_E as a function of applied strain amplitude during the fourth fatigue lags and the short complex modulus tests performed within its following rest periods; (c) φ_E as a function of time during the five fatigue lags and rest periods (Red stars indicate values of φ_E estimated at 100 μm/m at the beginning of fatigue lag, green asterisk shows values of $\Delta\varphi_{E\ heating}$ as influence of self-heating and brown triangles indicate values of φ_E estimated at 100 μm/m for each short complex modulus test during rest (all these values were obtained using non-linearity envelopes, as shown in (b) for the first fatigue lag and rest period).

3.1.84. PFRT results obtained for mix 40/60 – 6: (a) φ_E as a function of time during the fifth fatigue lag and rest period (b) φ_E as a function of applied strain amplitude during the fifth fatigue lags and the short complex modulus tests performed within its following rest periods; (c) φ_E as a function of time during the five fatigue lags and rest periods (Red stars indicate values of φ_E estimated at 100 μm/m at the beginning of fatigue lag, green asterisk shows values of $\Delta\varphi_{E\ heating}$

as influence of self-heating and brown triangles indicate values of φ_E estimated at 100 µm/m for each short complex modulus test during rest (all these values were obtained using non-linearity envelopes, as shown in (b) for the first fatigue lag and rest period).

3.1.85. PFRT results obtained for mix 40/60 – 6: (a) |v*| as a function of time during the first fatigue lag and rest period (b) |v*| as a function of applied strain amplitude during the first fatigue lags and the short complex modulus tests performed within its following rest periods; (c) |v*| as a function of time during the five fatigue lags and rest periods [Red stars indicate values of |v*| estimated at 100 µm/m at the beginning of fatigue lag, green asterisk shows values of $\Delta|v^*_{heating}|$ as influence of self-heating and brown triangles indicate values of |v*| estimated at 100 µm/m for each short complex modulus test during rest (all these values were obtained using non-linearity envelopes, as shown in (b) for the first fatigue lag and rest period)].

3.1.86. PFRT results obtained for mix 40/60 – 6: (a) φ_V as a function of time during the first fatigue lag and rest period (b) φ_V as a function of applied strain amplitude during the first fatigue lags and the short complex modulus tests performed within its following rest periods; (c) φ_V as a function of time during the five fatigue lags and rest periods (Red stars indicate values of φ_V estimated at 100 µm/m at the beginning of fatigue lag, green asterisk shows values of $\Delta\varphi_{E\ heating}$ as influence of self-heating and brown triangles indicate values of φ_V estimated at 100 µm/m for each short complex modulus test during rest (all these values were obtained using non-linearity envelopes, as shown in (b) for the first fatigue lag and rest period).

3.1.87. PFRT results obtained for mix 40/60 – 6: internal and surface temperature evolution during fatigue lags and recovery periods.

3.1.88. Quantification of different contributions |E*|, φ_E, |v*| and φ_v evolution, for the first two fatigue lags for mix 40/60 – 6: different envelope line is used for each fatigue lag.

3.1.89. Quantification of different absolute and relative contributions to |E*|, φ_E, |v*| and φ_v evolutions for mix 40/60 – 6, calculated using a different envelope line for each fatigue lag.

3.1.90. Quantification of different contributions to |E*|, φ_E, |v*| and φ_v evolution during five fatigue lags for mix 40/60 – 6: the envelope line of the first fatigue lag is used for all fatigue lags.

3.1.91. Quantification of different absolute and relative contributions to |E*|, φ_E, |v*| and φ_v evolutions for mix 40/60 – 6, calculated using the envelope line for the first fatigue lag. 432
3.1.92. PFRT results obtained for mix 40/60 – 8: (a) |E*| as a function of time during the first fatigue lag and rest period (b) |E*| as a function of applied strain amplitude during the first fatigue lags and the short complex modulus tests performed within its following rest periods; (c) |E*| as a function of time during the five fatigue lags and rest periods [Red stars indicate values of |E*| estimated at 100 µm/m at the beginning of fatigue lag, green asterisk shows values of $\Delta|E^*_{heating}|$ as influence of self-heating and brown triangles indicate values of |E*| estimated

at 100 µm/m for each short complex modulus test during rest (all these values were obtained using non-linearity envelopes, as shown in (b) for the first fatigue lag and rest period)].

3.1.93. PFRT results obtained for mix 40/60 – 8: (a) |E*| as a function of time during the second fatigue lag and rest period (b) |E*| as a function of applied strain amplitude during the second fatigue lags and the short complex modulus tests performed within its following rest periods; (c) |E*| as a function of time during the five fatigue lags and rest periods [Red stars indicate values of |E*| estimated at 100 µm/m at the beginning of fatigue lag, green asterisk shows values of $\Delta|E^*_{heating}|$ as influence of self-heating and brown triangles indicate values of |E*| estimated at 100 µm/m for each short complex modulus test during rest (all these values were obtained using non-linearity envelopes, as shown in (b) for the first fatigue lag and rest period)].

3.1.94. PFRT results obtained for mix 40/60 – 8: (a) |E*| as a function of time during the third fatigue lag and rest period (b) |E*| as a function of applied strain amplitude during the thirdfatigue lags and the short complex modulus tests performed within its following rest periods; (c) |E*| as a function of time during the five fatigue lags and rest periods [Red stars indicate values of |E*| estimated at 100 µm/m at the beginning of fatigue lag, green asterisk shows values of $\Delta|E^*_{heating}|$ as influence of self-heating and brown triangles indicate values of |E*| estimated at 100 µm/m for each short complex modulus test during rest (all these values were obtained using non-linearity envelopes, as shown in (b) for the first fatigue lag and rest period)].

3.1.95. PFRT results obtained for mix 40/60 – 8: (a) |E*| as a function of time during the fourth fatigue lag and rest period (b) |E*| as a function of applied strain amplitude during the fourth fatigue lags and the short complex modulus tests performed within its following rest periods; (c) |E*| as a function of time during the five fatigue lags and rest periods [Red stars indicate values of |E*| estimated at 100 µm/m at the beginning of fatigue lag, green asterisk shows values of $\Delta|E^*_{heating}|$ as influence of self-heating and brown triangles indicate values of |E*| estimated at 100 µm/m for each short complex modulus test during rest (all these values were obtained using non-linearity envelopes, as shown in (b) for the first fatigue lag and rest period)].

3.1.96. PFRT results obtained for mix 40/60 – 8: (a) |E*| as a function of time during the first fatigue lag and rest period (b) |E*| as a function of applied strain amplitude during the first fatigue lags and the short complex modulus tests performed within its following rest periods; (c) |E*| as a function of time during the five fatigue lags and rest periods [Red stars indicate values of |E*| estimated at 100 µm/m at the beginning of fatigue lag, green asterisk shows values of $\Delta|E^*_{heating}|$ as influence of self-heating and brown triangles indicate values of |E*| estimated at 100 µm/m for each short complex modulus test during rest (all these values were obtained using non-linearity envelopes, as shown in (b) for the first fatigue lag and rest period)].

3.1.97. PFRT results obtained for mix 40/60 – 8: (a) φ_E as a function of time during the first fatigue lag and rest period (b) φ_E as a function of applied strain amplitude during the first fatigue lags and the short complex modulus tests performed within its following rest periods; (c) φ_E as a function of time during the five fatigue lags and rest periods (Red stars indicate values of φ_E

estimated at 100 µm/m at the beginning of fatigue lag, green asterisk shows values of $\Delta\varphi_{E\ heating}$ as influence of self-heating and brown triangles indicate values of φ_E estimated at 100 µm/m for each short complex modulus test during rest (all these values were obtained using non-linearity envelopes, as shown in (b) for the first fatigue lag and rest period).

3.1.98. PFRT results obtained for mix 40/60 – 8: (a) φ_E as a function of time during the first fatigue lag and rest period (b) φ_E as a function of applied strain amplitude during the first fatigue lags and the short complex modulus tests performed within its following rest periods; (c) φ_E as a function of time during the five fatigue lags and rest periods (Red stars indicate values of φ_E estimated at 100 µm/m at the beginning of fatigue lag, green asterisk shows values of $\Delta\varphi_{E\ heating}$ as influence of self-heating and brown triangles indicate values of φ_E estimated at 100 µm/m for each short complex modulus test during rest (all these values were obtained using non-linearity envelopes, as shown in (b) for the first fatigue lag and rest period).

3.1.99. PFRT results obtained for mix 40/60 – 8: (a) φ_E as a function of time during the third fatigue lag and rest period (b) φ_E as a function of applied strain amplitude during the third fatigue lags and the short complex modulus tests performed within its following rest periods; (c) φ_E as a function of time during the five fatigue lags and rest periods (Red stars indicate values of φ_E estimated at 100 µm/m at the beginning of fatigue lag, green asterisk shows values of $\Delta\varphi_{E\ heating}$ as influence of self-heating and brown triangles indicate values of φ_E estimated at 100 µm/m for each short complex modulus test during rest (all these values were obtained using non-linearity envelopes, as shown in (b) for the first fatigue lag and rest period).

3.1.100. PFRT results obtained for mix 40/60 – 8: (a) φ_E as a function of time during the fourth fatigue lag and rest period (b) φ_E as a function of applied strain amplitude during the fourth fatigue lags and the short complex modulus tests performed within its following rest periods; (c) φ_E as a function of time during the five fatigue lags and rest periods (Red stars indicate values of φ_E estimated at 100 µm/m at the beginning of fatigue lag, green asterisk shows values of $\Delta\varphi_{E\ heating}$ as influence of self-heating and brown triangles indicate values of φ_E estimated at 100 µm/m for each short complex modulus test during rest (all these values were obtained using non-linearity envelopes, as shown in (b) for the first fatigue lag and rest period).

3.1.101. PFRT results obtained for mix 40/60 – 8: (a) φ_E as a function of time during the fifth fatigue lag and rest period (b) φ_E as a function of applied strain amplitude during the fifth fatigue lags and the short complex modulus tests performed within its following rest periods; (c) φ_E as a function of time during the five fatigue lags and rest periods (Red stars indicate values of φ_E estimated at 100 µm/m at the beginning of fatigue lag, green asterisk shows values of $\Delta\varphi_{E\ heating}$ as influence of self-heating and brown triangles indicate values of φ_E estimated at 100 µm/m for each short complex modulus test during rest (all these values were obtained using non-linearity envelopes, as shown in (b) for the first fatigue lag and rest period).

3.1.102. PFRT results obtained for mix 40/60 – 8: (a) |v*| as a function of time during the first fatigue lag and rest period (b) |v*| as a function of applied strain amplitude during the first fatigue lags and the short complex modulus tests performed within its following rest periods;

(c) |v*| as a function of time during the five fatigue lags and rest periods [Red stars indicate values of |E*| estimated at 100 µm/m at the beginning of fatigue lag, green asterisk shows values of $\Delta|E^*_{heating}|$ as influence of self-heating and brown triangles indicate values of |v*| estimated at 100 µm/m for each short complex modulus test during rest (all these values were obtained using non-linearity envelopes, as shown in (b) for the first fatigue lag and rest period)].

3.1.103. PFRT results obtained for mix 40/60 – 8: (a) φ_E as a function of time during the first fatigue lag and rest period (b) φ_E as a function of applied strain amplitude during the first fatigue lags and the short complex modulus tests performed within its following rest periods; (c) φ_E as a function of time during the five fatigue lags and rest periods (Red stars indicate values of φ_E estimated at 100 µm/m at the beginning of fatigue lag, green asterisk shows values of $\Delta\varphi_{E\ heating}$ as influence of self-heating and brown triangles indicate values of φ_E estimated at 100 µm/m for each short complex modulus test during rest (all these values were obtained using non-linearity envelopes, as shown in (b) for the first fatigue lag and rest period).

3.1.104. PFRT results obtained for mix 40/60 – 8: internal and surface temperature evolution during fatigue lags and recovery periods.

3.1.105. Quantification of different contributions |E*|, φ_E, |v*| and φ_v evolution, for the first two fatigue lags for mix 40/60 – 8: different envelope line is used for each fatigue lag. 449
3.1.106. Quantification of different absolute and relative contributions to |E*|, φ_E, |v*| and φ_v evolutions for mix 40/60 – 8, calculated using a different envelope line for each fatigue lag.

3.1.107. Quantification of different contributions to |E*|, φ_E, |v*| and φ_v evolution during five fatigue lags for mix 40/60 – 8: the envelope line of the first fatigue lag is used for all fatigue lags.

3.1.108. Quantification of different absolute and relative contributions to |E*|, φ_E, |v*| and φ_v evolutions for mix 40/60 – 8, calculated using the envelope line for the first fatigue lag. 459
3.1.109. PFRT results obtained for mix PMB - 1: (a) |E*| as a function of time during the first fatigue lag and rest period (b) |E*| as a function of applied strain amplitude during the first fatigue lags and the short complex modulus tests performed within its following rest periods; (c) |E*| as a function of time during the two fatigue lags and rest periods [Red stars indicate values of |E*| estimated at 100 µm/m at the beginning of fatigue lag, green asterisk shows values of $\Delta|E^*_{heating}|$ as influence of self-heating and brown triangles indicate values of |E*| estimated at 100 µm/m for each short complex modulus test during rest (all these values were obtained using non-linearity envelopes, as shown in Figure 5.9(b) for the first fatigue lag and rest period)].

3.1.110. PFRT results obtained for mix PMB - 1: (a) |E*| as a function of time during the second fatigue lag and rest period (b) |E*| as a function of applied strain amplitude during the second fatigue lags and the short complex modulus tests performed within its following rest periods; (c) |E*| as a function of time during the two fatigue lags and rest periods [Red stars indicate values of |E*| estimated at 100 µm/m at the beginning of fatigue lag, green asterisk shows values

of $\Delta|E^*_{heating}|$ as influence of self-heating and brown triangles indicate values of |E*| estimated at 100 µm/m for each short complex modulus test during rest (all these values were obtained using non-linearity envelopes, as shown in Figure 5.9(b) for the first fatigue lag and rest period)].

3.1.111. PFRT results obtained for mix PMB - 1: (a) φ_E as a function of time during the first fatigue lag and rest period (b) φ_E as a function of applied strain amplitude during the first fatigue lags and the short complex modulus tests performed within its following rest periods; (c) φ_E as a function of time during the five fatigue lags and rest periods (Red stars indicate values of φ_E estimated at 100 µm/m at the beginning of fatigue lag, green asterisk shows values of $\Delta\varphi_{E\ heating}$ as influence of self-heating and brown triangles indicate values of φ_E estimated at 100 µm/m for each short complex modulus test during rest (all these values were obtained using non-linearity envelopes, as shown in (b) for the first fatigue lag and rest period).

3.1.112. PFRT results obtained for mix PMB - 1: (a) φ_E as a function of time during the second fatigue lag and rest period (b) φ_E as a function of applied strain amplitude during the second fatigue lags and the short complex modulus tests performed within its following rest periods; (c) φ_E as a function of time during the five fatigue lags and rest periods (Red stars indicate values of φ_E estimated at 100 µm/m at the beginning of fatigue lag, green asterisk shows values of $\Delta\varphi_{E\ heating}$ as influence of self-heating and brown triangles indicate values of φ_E estimated at 100 µm/m for each short complex modulus test during rest (all these values were obtained using non-linearity envelopes, as shown in (b) for the first fatigue lag and rest period).

3.1.113. PFRT results obtained for mix PMB - 1: (a) |v*| as a function of time during the first fatigue lag and rest period (b) |v*| as a function of applied strain amplitude during the first fatigue lags and the short complex modulus tests performed within its following rest periods; (c) |v*| as a function of time during the two fatigue lags and rest periods [Red stars indicate values of |E*| estimated at 100 µm/m at the beginning of fatigue lag, green asterisk shows values of $\Delta|v^*_{heating}|$ as influence of self-heating and brown triangles indicate values of |v*| estimated at 100 µm/m for each short complex modulus test during rest (all these values were obtained using non-linearity envelopes, as shown in Figure 5.9(b) for the first fatigue lag and rest period)].

3.1.114. PFRT results obtained for mix PMB - 1: (a) φ_V as a function of time during the first fatigue lag and rest period (b) φ_V as a function of applied strain amplitude during the first fatigue lags and the short complex modulus tests performed within its following rest periods; (c) φ_V as a function of time during the five fatigue lags and rest periods (Red stars indicate values of φ_V estimated at 100 µm/m at the beginning of fatigue lag, green asterisk shows values of $\Delta\varphi_{V\ heating}$ as influence of self-heating and brown triangles indicate values of φ_V estimated at 100 µm/m for each short complex modulus test during rest (all these values were obtained using non-linearity envelopes, as shown in (b) for the first fatigue lag and rest period).

3.1.115. PFRT results obtained for PMB - 1: internal and surface temperature evolution during fatigue lags and recovery periods.

3.1.116. Quantification of different contributions |E*|, φ_E, |v*| and φ_v evolution, for the first two fatigue lags for mix PMB - 1: different envelope line is used for each fatigue lag.

3.1.117. Quantification of different absolute and relative contributions to |E*|, φ_E, |v*| and φ_v evolutions for mix PMB -1, calculated using a different envelope line for each fatigue lag.

3.1.118. Quantification of different contributions to |E*|, φ_E, |v*| and φ_v evolution during five fatigue lags for mix PMB -1: the envelope line of the first fatigue lag is used for all fatigue lags.

471

Figure 3.1.119. Quantification of different absolute and relative contributions to |E*|, φ_E, |v*| and φ_v evolutions for mix PMB -1, calculated using the envelope line for the first fatigue lag.

3.1.120. PFRT results obtained for mix PMB - 2: (a) |E*| as a function of time during the first fatigue lag and rest period (b) |E*| as a function of applied strain amplitude during the first fatigue lags and the short complex modulus tests performed within its following rest periods; (c) |E*| as a function of time during the five fatigue lags and rest periods [Red stars indicate values of |E*| estimated at 100 μm/m at the beginning of fatigue lag, green asterisk shows values of $\Delta|E^*_{heating}|$ as influence of self-heating and brown triangles indicate values of |E*| estimated at 100 μm/m for each short complex modulus test during rest (all these values were obtained using non-linearity envelopes, as shown in (b) for the first fatigue lag and rest period)].

3.1.121. PFRT results obtained for mix PMB - 2: (a) |E*| as a function of time during the second fatigue lag and rest period (b) |E*| as a function of applied strain amplitude during the second fatigue lags and the short complex modulus tests performed within its following rest periods; (c) |E*| as a function of time during the five fatigue lags and rest periods [Red stars indicate values of |E*| estimated at 100 μm/m at the beginning of fatigue lag, green asterisk shows values of $\Delta|E^*_{heating}|$ as influence of self-heating and brown triangles indicate values of |E*| estimated at 100 μm/m for each short complex modulus test during rest (all these values were obtained using non-linearity envelopes, as shown in (b) for the first fatigue lag and rest period)].

3.1.122. PFRT results obtained for mix PMB - 2: (a) |E*| as a function of time during the third fatigue lag and rest period (b) |E*| as a function of applied strain amplitude during the third fatigue lags and the short complex modulus tests performed within its following rest periods; (c) |E*| as a function of time during the five fatigue lags and rest periods [Red stars indicate values of |E*| estimated at 100 μm/m at the beginning of fatigue lag, green asterisk shows values of $\Delta|E^*_{heating}|$ as influence of self-heating and brown triangles indicate values of |E*| estimated at 100 μm/m for each short complex modulus test during rest (all these values were obtained using non-linearity envelopes, as shown in (b) for the first fatigue lag and rest period)].

3.1.123. PFRT results obtained for mix PMB - 2: (a) |E*| as a function of time during the fourth fatigue lag and rest period (b) |E*| as a function of applied strain amplitude during the fourth fatigue lags and the short complex modulus tests performed within its following rest periods; (c) |E*| as a function of time during the five fatigue lags and rest periods [Red stars indicate values of |E*| estimated at 100 μm/m at the beginning of fatigue lag, green asterisk shows values

of $\Delta|E^*_{heating}|$ as influence of self-heating and brown triangles indicate values of |E*| estimated at 100 μm/m for each short complex modulus test during rest (all these values were obtained using non-linearity envelopes, as shown in (b) for the first fatigue lag and rest period)].

3.1.124. PFRT results obtained for mix PMB - 2: (a) |E*| as a function of time during the fifth fatigue lag and rest period (b) |E*| as a function of applied strain amplitude during the fifth fatigue lags and the short complex modulus tests performed within its following rest periods; (c) |E*| as a function of time during the five fatigue lags and rest periods [Red stars indicate values of |E*| estimated at 100 μm/m at the beginning of fatigue lag, green asterisk shows values of $\Delta|E^*_{heating}|$ as influence of self-heating and brown triangles indicate values of |E*| estimated at 100 μm/m for each short complex modulus test during rest (all these values were obtained using non-linearity envelopes, as shown in (b) for the first fatigue lag and rest period)].

3.1.125. PFRT results obtained for mix PMB – 2: (a) φ_E as a function of time during the first fatigue lag and rest period (b) φ_E as a function of applied strain amplitude during the first fatigue lags and the short complex modulus tests performed within its following rest periods; (c) φ_E as a function of time during the five fatigue lags and rest periods (Red stars indicate values of φ_E estimated at 100 μm/m at the beginning of fatigue lag, green asterisk shows values of $\Delta\varphi_{E\ heating}$ as influence of self-heating and brown triangles indicate values of φ_E estimated at 100 μm/m for each short complex modulus test during rest (all these values were obtained using non-linearity envelopes, as shown in (b) for the first fatigue lag and rest period).

3.1.126. PFRT results obtained for mix PMB – 2: (a) φ_E as a function of time during the second fatigue lag and rest period (b) φ_E as a function of applied strain amplitude during the second fatigue lags and the short complex modulus tests performed within its following rest periods; (c) φ_E as a function of time during the five fatigue lags and rest periods (Red stars indicate values of φ_E estimated at 100 μm/m at the beginning of fatigue lag, green asterisk shows values of $\Delta\varphi_{E\ heating}$ as influence of self-heating and brown triangles indicate values of φ_E estimated at 100 μm/m for each short complex modulus test during rest (all these values were obtained using non-linearity envelopes, as shown in (b) for the first fatigue lag and rest period).

3.1.127. PFRT results obtained for mix PMB – 2: (a) φ_E as a function of time during the third fatigue lag and rest period (b) φ_E as a function of applied strain amplitude during the third fatigue lags and the short complex modulus tests performed within its following rest periods; (c) φ_E as a function of time during the five fatigue lags and rest periods (Red stars indicate values of φ_E estimated at 100 μm/m at the beginning of fatigue lag, green asterisk shows values of $\Delta\varphi_{E\ heating}$ as influence of self-heating and brown triangles indicate values of φ_E estimated at 100 μm/m for each short complex modulus test during rest (all these values were obtained using non-linearity envelopes, as shown in (b) for the first fatigue lag and rest period).

3.1.128. PFRT results obtained for mix PMB – 2: (a) φ_E as a function of time during the fourth fatigue lag and rest period (b) φ_E as a function of applied strain amplitude during the fourth fatigue lags and the short complex modulus tests performed within its following rest periods; (c) φ_E as a function of time during the five fatigue lags and rest periods (Red stars indicate

values of φ_E estimated at 100 µm/m at the beginning of fatigue lag, green asterisk shows values of $\Delta\varphi_{E\ heating}$ as influence of self-heating and brown triangles indicate values of φ_E estimated at 100 µm/m for each short complex modulus test during rest (all these values were obtained using non-linearity envelopes, as shown in (b) for the first fatigue lag and rest period).

3.1.129. PFRT results obtained for mix PMB – 2: (a) φ_E as a function of time during the fifth fatigue lag and rest period (b) φ_E as a function of applied strain amplitude during the fifth fatigue lags and the short complex modulus tests performed within its following rest periods; (c) φ_E as a function of time during the five fatigue lags and rest periods (Red stars indicate values of φ_E estimated at 100 µm/m at the beginning of fatigue lag, green asterisk shows values of $\Delta\varphi_{E\ heating}$ as influence of self-heating and brown triangles indicate values of φ_E estimated at 100 µm/m for each short complex modulus test during rest (all these values were obtained using non-linearity envelopes, as shown in (b) for the first fatigue lag and rest period).

3.1.130. PFRT results obtained for mix PMB - 2: (a) |v*| as a function of time during the first fatigue lag and rest period (b) |v*| as a function of applied strain amplitude during the first fatigue lags and the short complex modulus tests performed within its following rest periods; (c) |v*| as a function of time during the five fatigue lags and rest periods [Red stars indicate values of |E*| estimated at 100 µm/m at the beginning of fatigue lag, green asterisk shows values of $\Delta|v^*_{heating}|$ as influence of self-heating and brown triangles indicate values of |v*| estimated at 100 µm/m for each short complex modulus test during rest (all these values were obtained using non-linearity envelopes, as shown in (b) for the first fatigue lag and rest period)].

3.1.131. PFRT results obtained for mix PMB – 2: (a) φ_v as a function of time during the first fatigue lag and rest period (b) φ_v as a function of applied strain amplitude during the first fatigue lags and the short complex modulus tests performed within its following rest periods; (c) φ_v as a function of time during the five fatigue lags and rest periods (Red stars indicate values of φ_v estimated at 100 µm/m at the beginning of fatigue lag, green asterisk shows values of $\Delta\varphi_{v\ heating}$ as influence of self-heating and brown triangles indicate values of φ_v estimated at 100 µm/m for each short complex modulus test during rest (all these values were obtained using non-linearity envelopes, as shown in (b) for the first fatigue lag and rest period).

3.1.132. PFRT results obtained for mix PMB – 2: internal and surface temperature evolution during fatigue lags and recovery periods.

3.1.133. Quantification of different contributions |E*| and φ_E evolution, for the five fatigue lags for mix PMB – 2: different envelope line is used for each fatigue lag.

3.1.133. Quantification of different contributions |E*|, φ_E, |v*| and φ_v evolution, for the five fatigue lags for mix PMB – 2: different envelope line is used for each fatigue lag.

3.1.134. Quantification of different absolute and relative contributions to |E*|, φ_E, |v*| and φ_v evolutions for mix PMB – 2, calculated using a different envelope line for each fatigue lag.

3.1.135. Quantification of different contributions to |E*|, φ_E, |ν*| and φ_ν evolution during five fatigue lags for mix PMB – 2: the envelope line of the first fatigue lag is used for all fatigue lags.

3.1.136. Quantification of different absolute and relative contributions to |E*|, φ_E, |ν*| and φ_ν evolutions for mix PMB – 2, calculated using the envelope line for the first fatigue lag.

3.1.137. PFRT results obtained for mix PMB – 5: (a) |E*| as a function of time during the first fatigue lag and rest period (b) |E*| as a function of applied strain amplitude during the first fatigue lags and the short complex modulus tests performed within its following rest periods; (c) |E*| as a function of time during the five fatigue lags and rest periods [Red stars indicate values of |E*| estimated at 100 μm/m at the beginning of fatigue lag, green asterisk shows values of $\Delta|E^*_{heating}|$ as influence of self-heating and brown triangles indicate values of |E*| estimated at 100 μm/m for each short complex modulus test during rest (all these values were obtained using non-linearity envelopes, as shown in (b) for the first fatigue lag and rest period)].

3.1.138. PFRT results obtained for mix PMB – 5: (a) |E*| as a function of time during the second fatigue lag and rest period (b) |E*| as a function of applied strain amplitude during the second fatigue lags and the short complex modulus tests performed within its following rest periods; (c) |E*| as a function of time during the five fatigue lags and rest periods [Red stars indicate values of |E*| estimated at 100 μm/m at the beginning of fatigue lag, green asterisk shows values of $\Delta|E^*_{heating}|$ as influence of self-heating and brown triangles indicate values of |E*| estimated at 100 μm/m for each short complex modulus test during rest (all these values were obtained using non-linearity envelopes, as shown in (b) for the first fatigue lag and rest period)].

3.1.139. PFRT results obtained for mix PMB – 5: (a) |E*| as a function of time during the third fatigue lag and rest period (b) |E*| as a function of applied strain amplitude during the third fatigue lags and the short complex modulus tests performed within its following rest periods; (c) |E*| as a function of time during the five fatigue lags and rest periods [Red stars indicate values of |E*| estimated at 100 μm/m at the beginning of fatigue lag, green asterisk shows values of $\Delta|E^*_{heating}|$ as influence of self-heating and brown triangles indicate values of |E*| estimated at 100 μm/m for each short complex modulus test during rest (all these values were obtained using non-linearity envelopes, as shown in (b) for the first fatigue lag and rest period)].

3.1.140. PFRT results obtained for mix PMB – 5: (a) |E*| as a function of time during the fourth fatigue lag and rest period (b) |E*| as a function of applied strain amplitude during the fourth fatigue lags and the short complex modulus tests performed within its following rest periods; (c) |E*| as a function of time during the five fatigue lags and rest periods [Red stars indicate values of |E*| estimated at 100 μm/m at the beginning of fatigue lag, green asterisk shows values of $\Delta|E^*_{heating}|$ as influence of self-heating and brown triangles indicate values of |E*| estimated at 100 μm/m for each short complex modulus test during rest (all these values were obtained using non-linearity envelopes, as shown in (b) for the first fatigue lag and rest period)].

3.1.141. PFRT results obtained for mix PMB – 5: (a) |E*| as a function of time during the fifth fatigue lag and rest period (b) |E*| as a function of applied strain amplitude during the fifth fatigue lags and the short complex modulus tests performed within its following rest periods; (c) |E*| as a function of time during the five fatigue lags and rest periods [Red stars indicate values of |E*| estimated at 100 μm/m at the beginning of fatigue lag, green asterisk shows values of $\Delta|E^*_{heating}|$ as influence of self-heating and brown triangles indicate values of |E*| estimated at 100 μm/m for each short complex modulus test during rest (all these values were obtained using non-linearity envelopes, as shown in (b) for the first fatigue lag and rest period)].

3.1.142. PFRT results obtained for mix PMB – 5: (a) φ_E as a function of time during the first fatigue lag and rest period (b) φ_E as a function of applied strain amplitude during the first fatigue lags and the short complex modulus tests performed within its following rest periods; (c) φ_E as a function of time during the five fatigue lags and rest periods (Red stars indicate values of φ_E estimated at 100 μm/m at the beginning of fatigue lag, green asterisk shows values of $\Delta\varphi_{E\ heating}$ as influence of self-heating and brown triangles indicate values of φ_E estimated at 100 μm/m for each short complex modulus test during rest (all these values were obtained using non-linearity envelopes, as shown in (b) for the first fatigue lag and rest period).

3.1.143. PFRT results obtained for mix PMB – 5: (a) φ_E as a function of time during the second fatigue lag and rest period (b) φ_E as a function of applied strain amplitude during the second fatigue lags and the short complex modulus tests performed within its following rest periods; (c) φ_E as a function of time during the five fatigue lags and rest periods (Red stars indicate values of φ_E estimated at 100 μm/m at the beginning of fatigue lag, green asterisk shows values of $\Delta\varphi_{E\ heating}$ as influence of self-heating and brown triangles indicate values of φ_E estimated at 100 μm/m for each short complex modulus test during rest (all these values were obtained using non-linearity envelopes, as shown in (b) for the first fatigue lag and rest period).

3.1.144. PFRT results obtained for mix PMB – 5: (a) φ_E as a function of time during the third fatigue lag and rest period (b) φ_E as a function of applied strain amplitude during the third fatigue lags and the short complex modulus tests performed within its following rest periods; (c) φ_E as a function of time during the five fatigue lags and rest periods (Red stars indicate values of φ_E estimated at 100 μm/m at the beginning of fatigue lag, green asterisk shows values of $\Delta\varphi_{E\ heating}$ as influence of self-heating and brown triangles indicate values of φ_E estimated at 100 μm/m for each short complex modulus test during rest (all these values were obtained using non-linearity envelopes, as shown in (b) for the first fatigue lag and rest period).

3.1.145. PFRT results obtained for mix PMB – 5: (a) φ_E as a function of time during the fourth fatigue lag and rest period (b) φ_E as a function of applied strain amplitude during the fourth fatigue lags and the short complex modulus tests performed within its following rest periods; (c) φ_E as a function of time during the five fatigue lags and rest periods (Red stars indicate values of φ_E estimated at 100 μm/m at the beginning of fatigue lag, green asterisk shows values of $\Delta\varphi_{E\ heating}$ as influence of self-heating and brown triangles indicate values of φ_E estimated at 100 μm/m for each short complex modulus test during rest (all these values were obtained using non-linearity envelopes, as shown in (b) for the first fatigue lag and rest period).

3.1.146. PFRT results obtained for mix PMB – 5: (a) φ_E as a function of time during the fifth fatigue lag and rest period (b) φ_E as a function of applied strain amplitude during the fifth fatigue lags and the short complex modulus tests performed within its following rest periods; (c) φ_E as a function of time during the five fatigue lags and rest periods (Red stars indicate values of φ_E estimated at 100 µm/m at the beginning of fatigue lag, green asterisk shows values of $\Delta\varphi_{E\ heating}$ as influence of self-heating and brown triangles indicate values of φ_E estimated at 100 µm/m for each short complex modulus test during rest (all these values were obtained using non-linearity envelopes, as shown in (b) for the first fatigue lag and rest period).

3.1.147. PFRT results obtained for mix PMB – 5: (a) |v*| as a function of time during the first fatigue lag and rest period (b) |v*| as a function of applied strain amplitude during the first fatigue lags and the short complex modulus tests performed within its following rest periods; (c) |v*| as a function of time during the five fatigue lags and rest periods [Red stars indicate values of |v*| estimated at 100 µm/m at the beginning of fatigue lag, green asterisk shows values of $\Delta|v^*_{heating}|$ as influence of self-heating and brown triangles indicate values of |v*| estimated at 100 µm/m for each short complex modulus test during rest (all these values were obtained using non-linearity envelopes, as shown in (b) for the first fatigue lag and rest period)].

3.1.148. PFRT results obtained for mix PMB – 5: (a) φ_v as a function of time during the first fatigue lag and rest period (b) φ_v as a function of applied strain amplitude during the first fatigue lags and the short complex modulus tests performed within its following rest periods; (c) φ_v as a function of time during the five fatigue lags and rest periods (Red stars indicate values of φ_v estimated at 100 µm/m at the beginning of fatigue lag, green asterisk shows values of $\Delta\varphi_{v\ heating}$ as influence of self-heating and brown triangles indicate values of φ_v estimated at 100 µm/m for each short complex modulus test during rest (all these values were obtained using non-linearity envelopes, as shown in (b) for the first fatigue lag and rest period).

3.1.149. PFRT results obtained for mix PMB – 5: internal and surface temperature evolution during fatigue lags and recovery periods.

Figure 3.1.150. Quantification of different contributions |E*|, φ_E, |v*| and φ_v evolution, for the five fatigue lags for mix PMB – 5: different envelope line is used for each fatigue lag.
3.1.151. Quantification of different absolute and relative contributions to |E*|, φ_E, |v*| and φ_v evolutions for mix PMB – 5, calculated using a different envelope line for each fatigue lag.

3.1.152. Quantification of different contributions to |E*|, φ_E, |v*| and φ_v evolution during five fatigue lags for mix PMB – 5: the envelope line of the first fatigue lag is used for all fatigue lags.
3.1.153. Quantification of different absolute and relative contributions to |E*|, φ_E, |v*| and φ_v evolutions for mix PMB – 5, calculated using the envelope line for the first fatigue lag.
3.1.154. PFRT results obtained for mix PMB – 6: (a) |E*| as a function of time during the first fatigue lag and rest period (b) |E*| as a function of applied strain amplitude during the first fatigue lags and the short complex modulus tests performed within its following rest periods;

(c) |E*| as a function of time during the five fatigue lags and rest periods [Red stars indicate values of |E*| estimated at 100 μm/m at the beginning of fatigue lag, green asterisk shows values of $\Delta|E^*_{heating}|$ as influence of self-heating and brown triangles indicate values of |E*| estimated at 100 μm/m for each short complex modulus test during rest (all these values were obtained using non-linearity envelopes, as shown in (b) for the first fatigue lag and rest period)].

3.1.155. PFRT results obtained for mix PMB – 6: (a) |E*| as a function of time during the second fatigue lag and rest period (b) |E*| as a function of applied strain amplitude during the second fatigue lags and the short complex modulus tests performed within its following rest periods; (c) |E*| as a function of time during the five fatigue lags and rest periods [Red stars indicate values of |E*| estimated at 100 μm/m at the beginning of fatigue lag, green asterisk shows values of $\Delta|E^*_{heating}|$ as influence of self-heating and brown triangles indicate values of |E*| estimated at 100 μm/m for each short complex modulus test during rest (all these values were obtained using non-linearity envelopes, as shown in (b) for the first fatigue lag and rest period)].

3.1.156. PFRT results obtained for mix PMB – 6: (a) |E*| as a function of time during the third fatigue lag and rest period (b) |E*| as a function of applied strain amplitude during the third fatigue lags and the short complex modulus tests performed within its following rest periods; (c) |E*| as a function of time during the five fatigue lags and rest periods [Red stars indicate values of |E*| estimated at 100 μm/m at the beginning of fatigue lag, green asterisk shows values of $\Delta|E^*_{heating}|$ as influence of self-heating and brown triangles indicate values of |E*| estimated at 100 μm/m for each short complex modulus test during rest (all these values were obtained using non-linearity envelopes, as shown in (b) for the first fatigue lag and rest period)].

3.1.157. PFRT results obtained for mix PMB – 6: (a) |E*| as a function of time during the fourth fatigue lag and rest period (b) |E*| as a function of applied strain amplitude during the fourth fatigue lags and the short complex modulus tests performed within its following rest periods; (c) |E*| as a function of time during the five fatigue lags and rest periods [Red stars indicate values of |E*| estimated at 100 μm/m at the beginning of fatigue lag, green asterisk shows values of $\Delta|E^*_{heating}|$ as influence of self-heating and brown triangles indicate values of |E*| estimated at 100 μm/m for each short complex modulus test during rest (all these values were obtained using non-linearity envelopes, as shown in (b) for the first fatigue lag and rest period)].

3.1.158. PFRT results obtained for mix PMB – 6: (a) |E*| as a function of time during the fifth fatigue lag and rest period (b) |E*| as a function of applied strain amplitude during the fifth fatigue lags and the short complex modulus tests performed within its following rest periods; (c) |E*| as a function of time during the five fatigue lags and rest periods [Red stars indicate values of |E*| estimated at 100 μm/m at the beginning of fatigue lag, green asterisk shows values of $\Delta|E^*_{heating}|$ as influence of self-heating and brown triangles indicate values of |E*| estimated at 100 μm/m for each short complex modulus test during rest (all these values were obtained using non-linearity envelopes, as shown in (b) for the first fatigue lag and rest period)].

3.1.159. PFRT results obtained for mix PMB – 6: (a) φ_E as a function of time during the first fatigue lag and rest period (b) φ_E as a function of applied strain amplitude during the first fatigue

lags and the short complex modulus tests performed within its following rest periods; (c) φ_E as a function of time during the five fatigue lags and rest periods (Red stars indicate values of φ_E estimated at 100 μm/m at the beginning of fatigue lag, green asterisk shows values of $\Delta\varphi_{E\ heating}$ as influence of self-heating and brown triangles indicate values of φ_E estimated at 100 μm/m for each short complex modulus test during rest (all these values were obtained using non-linearity envelopes, as shown in (b) for the first fatigue lag and rest period).

3.1.160. PFRT results obtained for mix PMB – 6: (a) φ_E as a function of time during the second fatigue lag and rest period (b) φ_E as a function of applied strain amplitude during the first fatigue lags and the short complex modulus tests performed within its following rest periods; (c) φ_E as a function of time during the five fatigue lags and rest periods (Red stars indicate values of φ_E estimated at 100 μm/m at the beginning of fatigue lag, green asterisk shows values of $\Delta\varphi_{E\ heating}$ as influence of self-heating and brown triangles indicate values of φ_E estimated at 100 μm/m for each short complex modulus test during rest (all these values were obtained using non-linearity envelopes, as shown in (b) for the first fatigue lag and rest period).

3.1.161. PFRT results obtained for mix PMB – 6: (a) φ_E as a function of time during the third fatigue lag and rest period (b) φ_E as a function of applied strain amplitude during the third fatigue lags and the short complex modulus tests performed within its following rest periods; (c) φ_E as a function of time during the five fatigue lags and rest periods (Red stars indicate values of φ_E estimated at 100 μm/m at the beginning of fatigue lag, green asterisk shows values of $\Delta\varphi_{E\ heating}$ as influence of self-heating and brown triangles indicate values of φ_E estimated at 100 μm/m for each short complex modulus test during rest (all these values were obtained using non-linearity envelopes, as shown in (b) for the first fatigue lag and rest period).

3.1.162. PFRT results obtained for mix PMB – 6: (a) φ_E as a function of time during the fourth fatigue lag and rest period (b) φ_E as a function of applied strain amplitude during the fourth fatigue lags and the short complex modulus tests performed within its following rest periods; (c) φ_E as a function of time during the five fatigue lags and rest periods (Red stars indicate values of φ_E estimated at 100 μm/m at the beginning of fatigue lag, green asterisk shows values of $\Delta\varphi_{E\ heating}$ as influence of self-heating and brown triangles indicate values of φ_E estimated at 100 μm/m for each short complex modulus test during rest (all these values were obtained using non-linearity envelopes, as shown in (b) for the first fatigue lag and rest period).

3.1.163. PFRT results obtained for mix PMB – 6: (a) φ_E as a function of time during the fifth fatigue lag and rest period (b) φ_E as a function of applied strain amplitude during the fifth fatigue lags and the short complex modulus tests performed within its following rest periods; (c) φ_E as a function of time during the five fatigue lags and rest periods (Red stars indicate values of φ_E estimated at 100 μm/m at the beginning of fatigue lag, green asterisk shows values of $\Delta\varphi_{E\ heating}$ as influence of self-heating and brown triangles indicate values of φ_E estimated at 100 μm/m for each short complex modulus test during rest (all these values were obtained using non-linearity envelopes, as shown in (b) for the first fatigue lag and rest period).

3.1.164. PFRT results obtained for mix PMB – 6: internal and surface temperature evolution during fatigue lags and recovery periods.

3.1.165. Quantification of different contributions to |E*|, φ_E, |v*| and φ_v evolution during five fatigue lags for mix PMB – 6: the envelope line of the first fatigue lag is used for all fatigue lags.
3.1.167. Quantification of different absolute and relative contributions to |E*|, φ_E, |v*| and φ_v evolutions for mix PMB – 6 calculated using a different envelope line for each fatigue lag. 537
3.1.168. Quantification of different contributions to |E*|, ϕ_E and |v*| evolution during five fatigue lags for mix PMB – 6: the envelope line of the first fatigue lag is used for all fatigue lag

3.1.169. Quantification of different absolute and relative contributions to |E*|, φ_E, |v*| and φ_v evolutions for mix PMB – 6, calculated using the envelope line for the first fatigue lag. 2
3.2. Comparing the relative contributions
3.2.1. Comparing the relative contributions of unrecovered variations of |E*| and φ_E with respect to the total variation of |E*| and φ_E for each fatigue and rest lag for all the tested samples, calculated using the envelope line for the first fatigue lag.
3.3. Analysis of rate of variation of mechanical properties during loading and recovery.
3.3.1. Rate of variation during loading and recovery for for |E*|, φ_E, |v*| and φ_v for each fatigue and rest lag for mix 40/60 - 4.
3.3.2. Rate of variation during loading and recovery for |E*| and φ_E for each fatigue and rest lag for mix 40/60 - 5
3.3.3. Rate of variation during loading and recovery for |E*|, φ_E, |v*| and φ_v for each fatigue and rest lag for mix 40/60 - 6.
3.3.4. Rate of variation during loading and recovery for |E*| and φ_E for each fatigue and rest lag for mix 40/60 - 8.
3.3.5. Rate of variation during loading and recovery for |E*| and φ_E for each fatigue and rest lag for mix 70/100 - 1. 11
3.3.6. Rate of variation during loading and recovery for |E*| and φ_E for each fatigue and rest lag for mix 70/100 - 3.
3.3.7. Rate of variation during loading and recovery for |E*| and φ_E for each fatigue and rest lag for mix 70/100 - 4.
133.3.8. Rate of variation during loading and recovery for |E*| and φ_E for each fatigue and rest lag for mix 70/100 - 5.
3.3.9. Rate of variation during loading and recovery for |E*| and φ_E for each fatigue and rest lag for mix 70/100 – 8.
3.3.10. Rate of variation during loading and recovery for |E*|, φ_E, |v*| and φ_v for each fatigue and rest lag for mix PMB – 1.
3.3.11. Rate of variation during loading and recovery for |E*| and φ_E for each fatigue and rest lag for mix PMB – 2.
3.3.12. Rate of variation during loading and recovery for |E*| and φ_E for each fatigue and rest lag for mix PMB – 5.
3.3.13. Rate of variation during loading and recovery for |E*|, φE, |v*| and φv for each fatigue and rest lag for mix PMB – 6.
3.4. Analysis of energy dissipation

3.4.1. Rate of variation during loading and energy dissipation for |E*| and φ_E for fatigue and rest lag 1 for mix 70/100, mix 40/60 and mix PMB.

3.4.2. Rate of variation during loading and energy dissipation for |E*| and φ_E for fatigue and rest lag 2 for mix 70/100, mix 40/60 and mix PMB.

3.4.3. Rate of variation during loading and energy dissipation for |E*| and φ_E for fatigue and rest lag 3 for mix 70/100, mix 40/60 and mix PMB.

3.4.4. Rate of variation during loading and energy dissipation for |E*| and φ_E for fatigue and rest lag 4 for mix 70/100, mix 40/60 and mix PMB.

3.4.5. Rate of variation during loading and energy dissipation for |E*| and φ_E for fatigue and rest lag 5 for mix 70/100, mix 40/60 and mix PMB.

3.4.6. Rate of variation during loading and energy dissipation for |v*| and φ_v of all fatigue and rest lags for mix 70/100, mix 40/60 and mix PMB.

1. Analysis of DSR Tests data from RILEM TC 278 CHA

1.1. LVE properties of binders in undamaged conditions

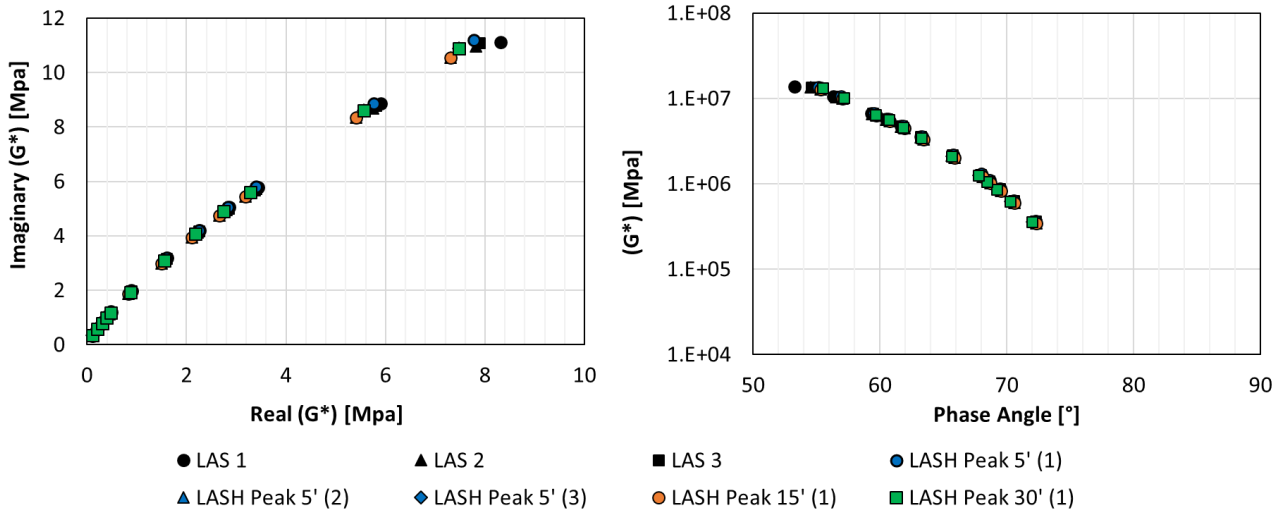

1.1.1. Imaginary (G*) vs Real (G*) and (G*) versus φ for the 70/100 binders [Data from Torino].

1.2.Result of LAS test

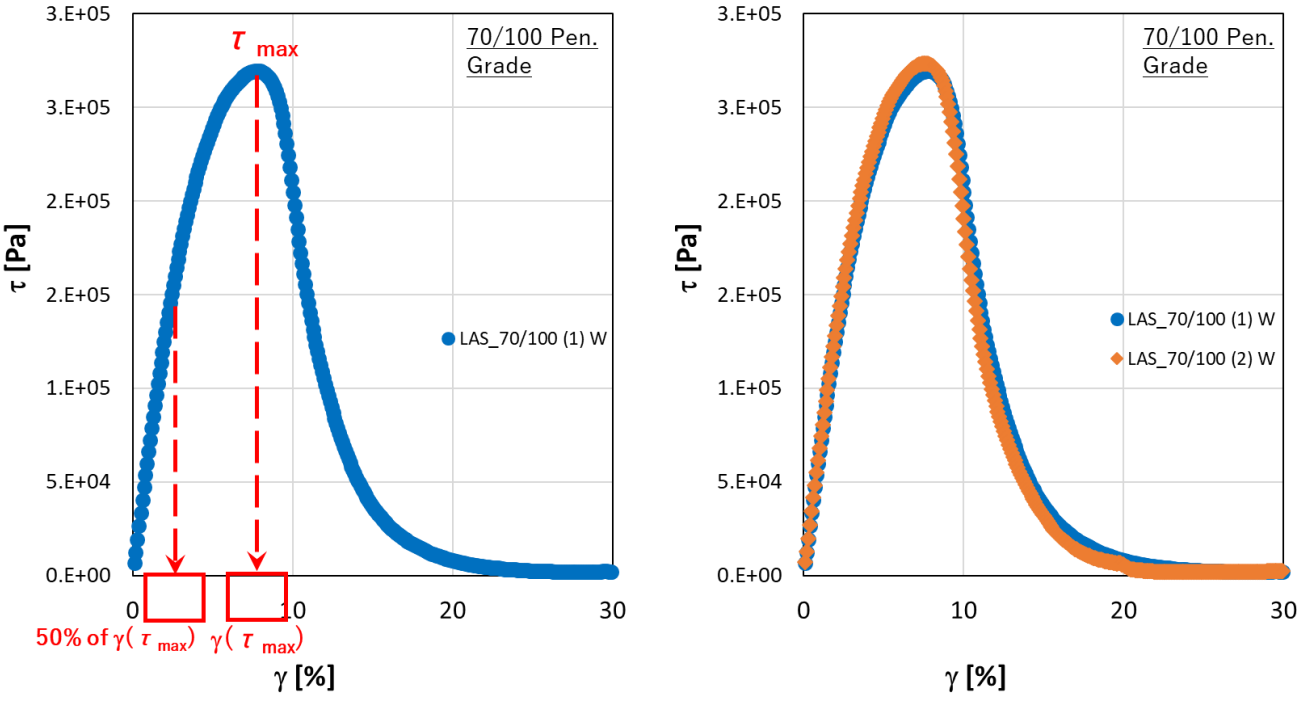

1.2.1. Typical LAS tests result in stress – strain curve for 70/100 binder showing the peak and half peak stresses with increasing peak strain. [Data from Waterloo].

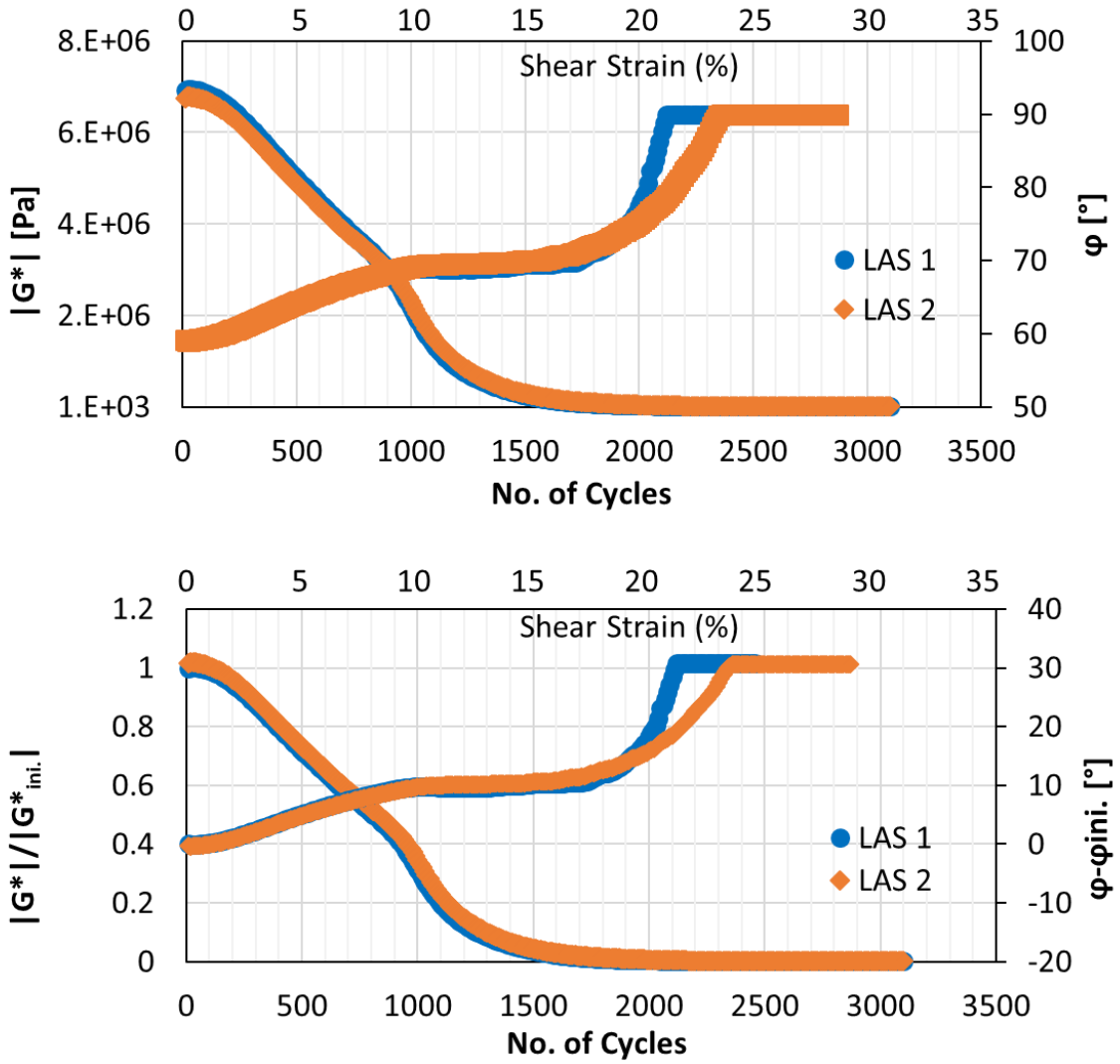

1.2.2. Typical LAS tests result in complex modulus – strain curve, complex modulus – No. of cycles & Normalised curve for 70/100 binder [Data from Waterloo].

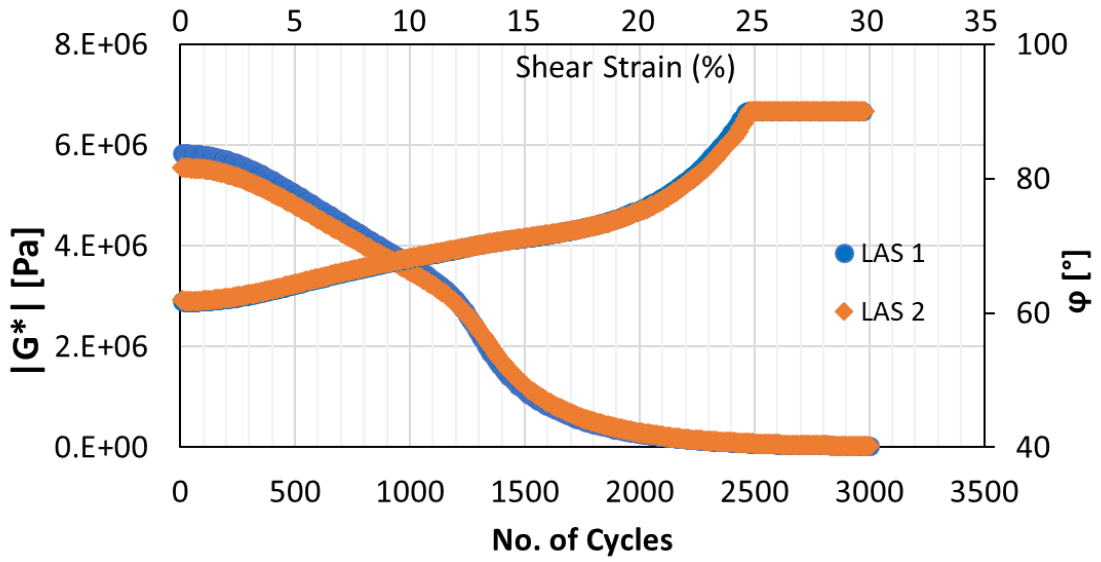

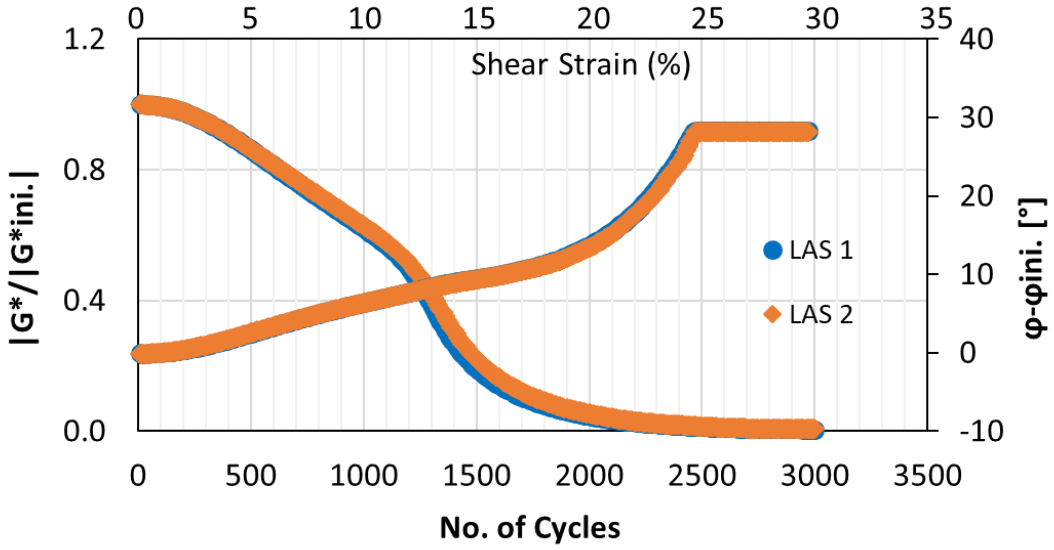

1.2.3. Typical LAS tests result in complex modulus – strain curve, complex modulus – No. of cycles & Normalised curve for 70/100 binder [Data from Torino].

1.3. Results of LASH test

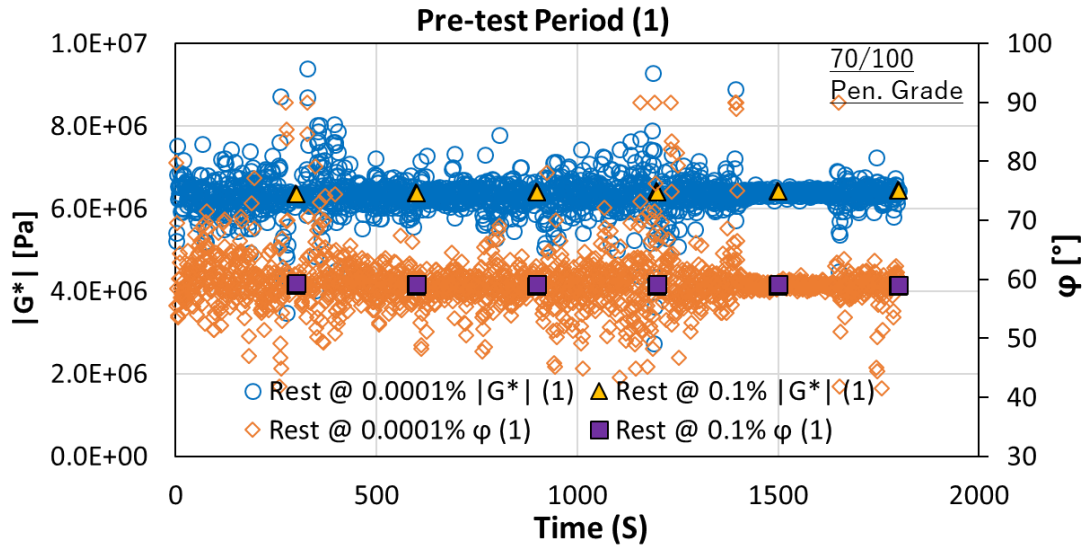

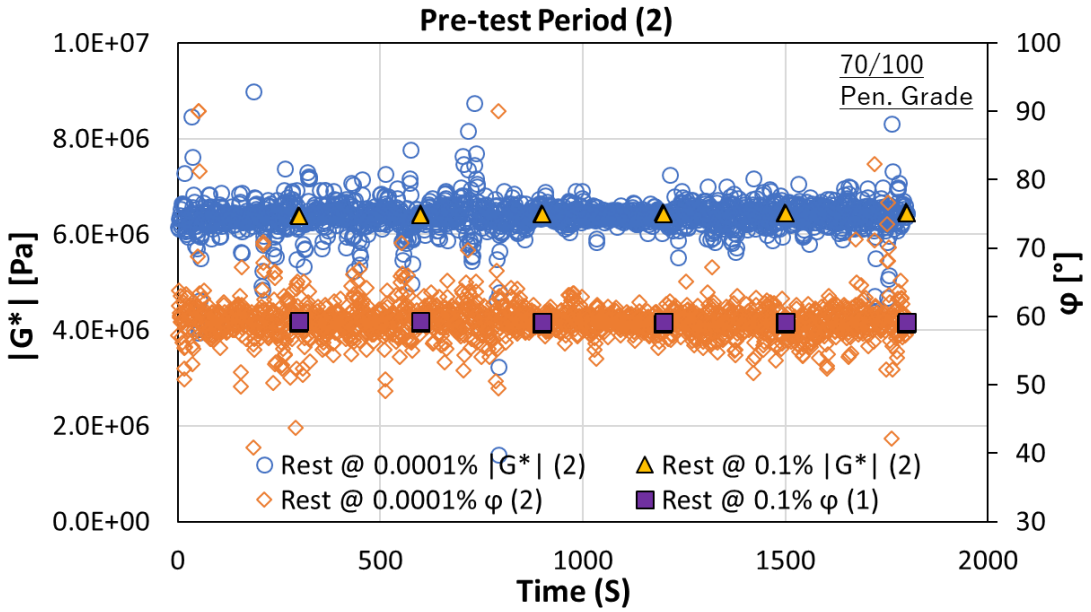

1.3.1. Comparing Strain at 0.1% and 0.0001% during pre-test for 70/100 binder [Data from Waterloo].

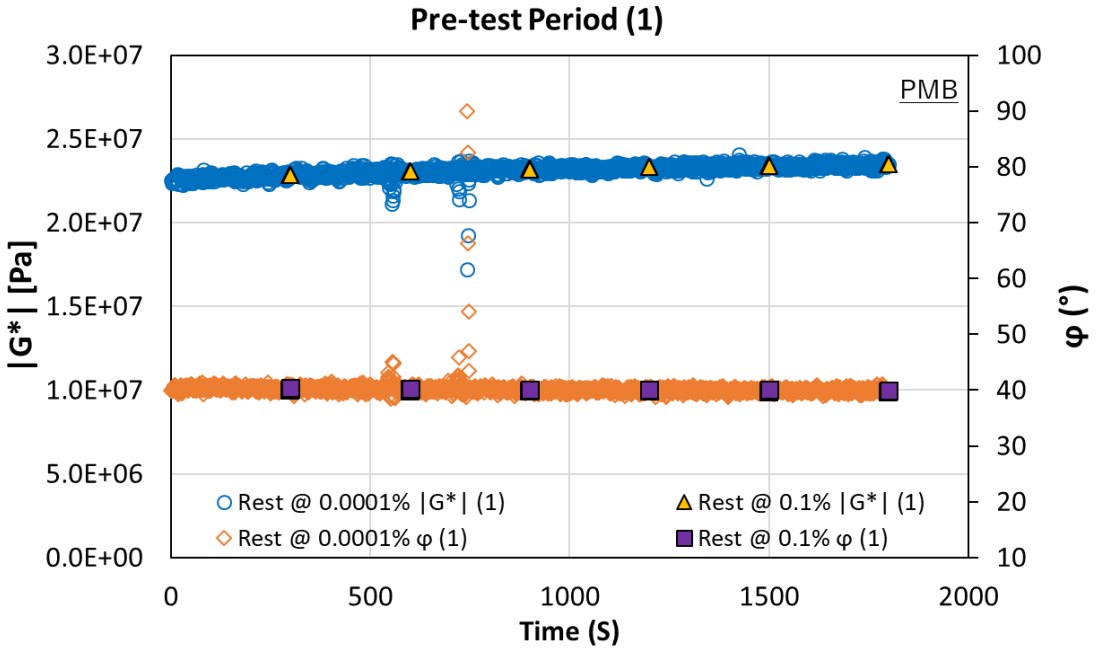

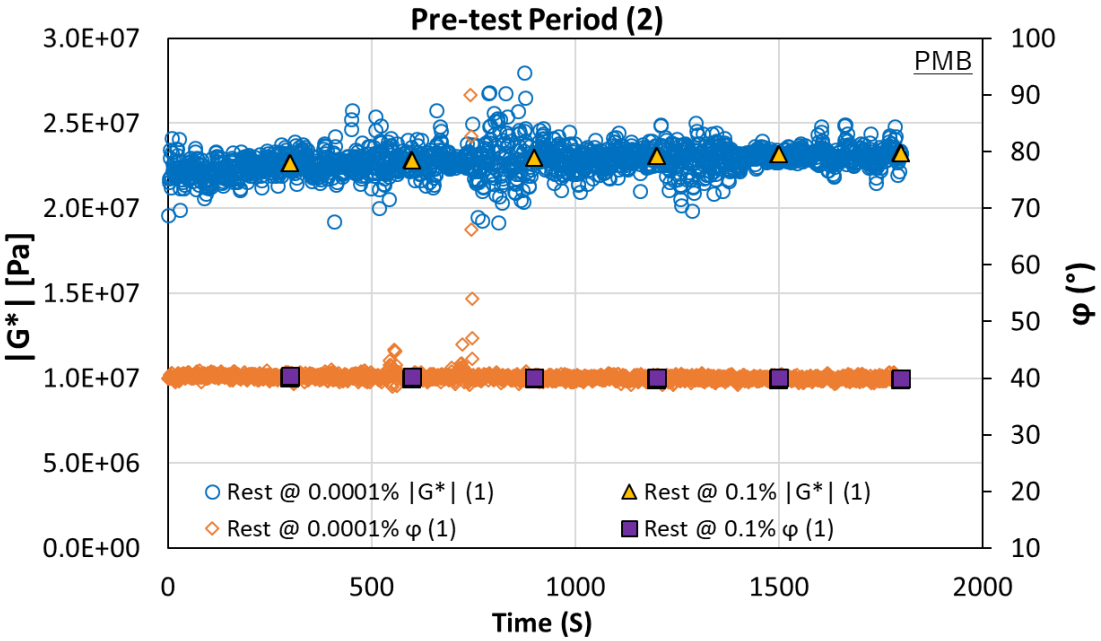

1.3.2. Comparing Strain at 0.1% and 0.0001% during pre-test for the PMB binder [Data from Waterloo].

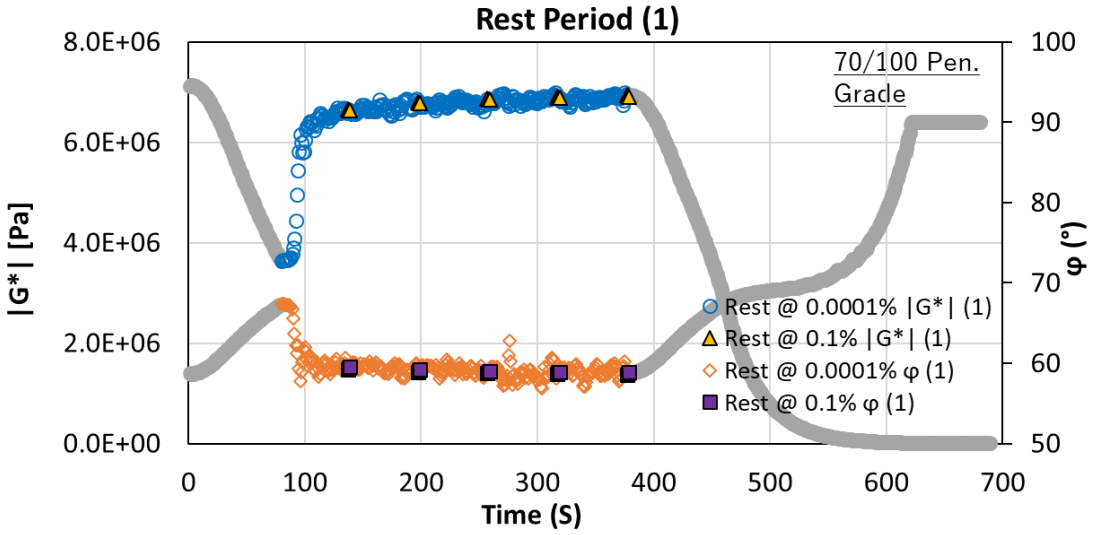

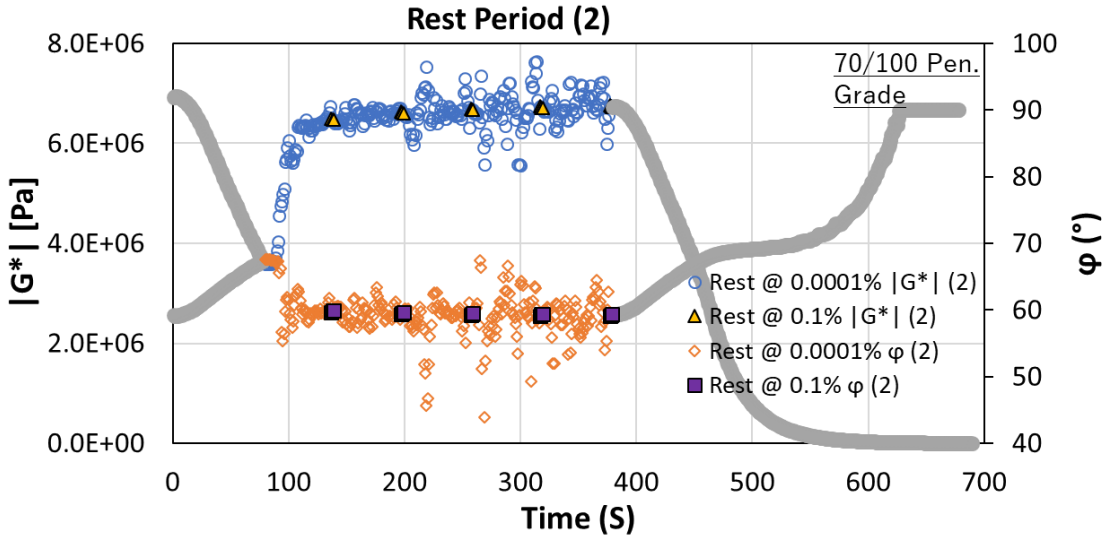

1.3.3. Comparing Strain at 0.1% and 0.0001% during 5 min. rest for the 70/100 binder [Data from Waterloo].

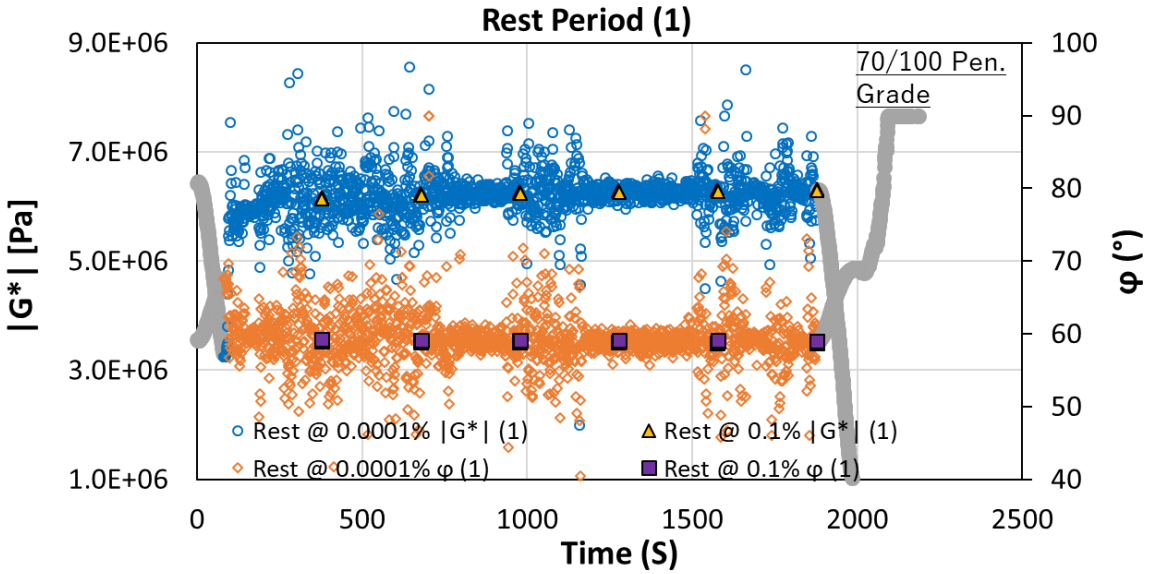

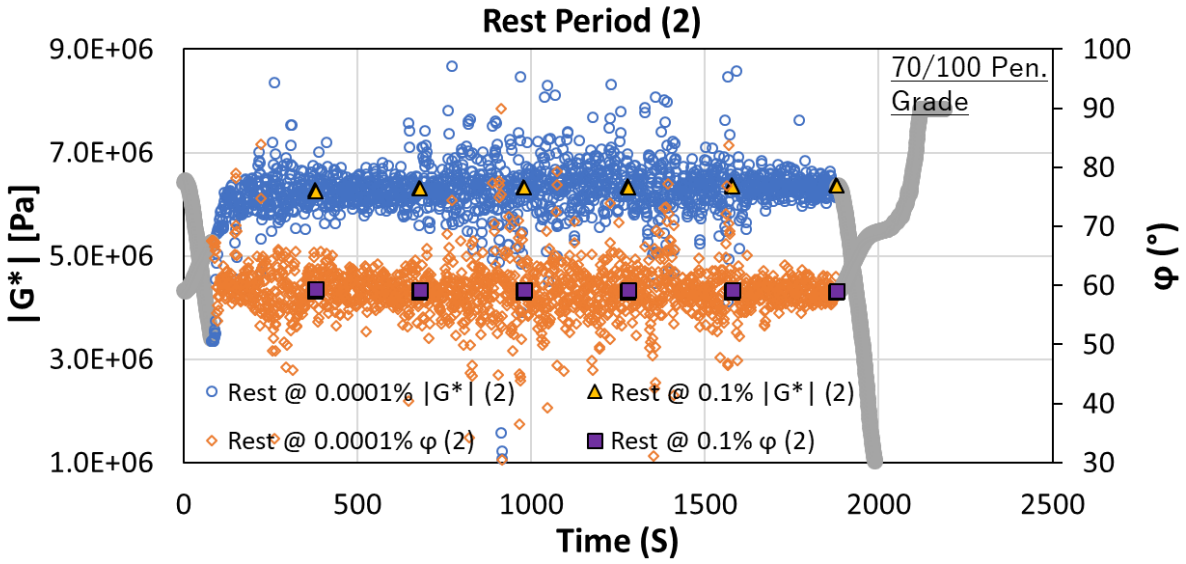

1.3.4. Comparing Strain at 0.1% and 0.0001% during 30 min. rest for the 70/100 binder [Data from Waterloo].

1.4. Effect of rest periods and loading history

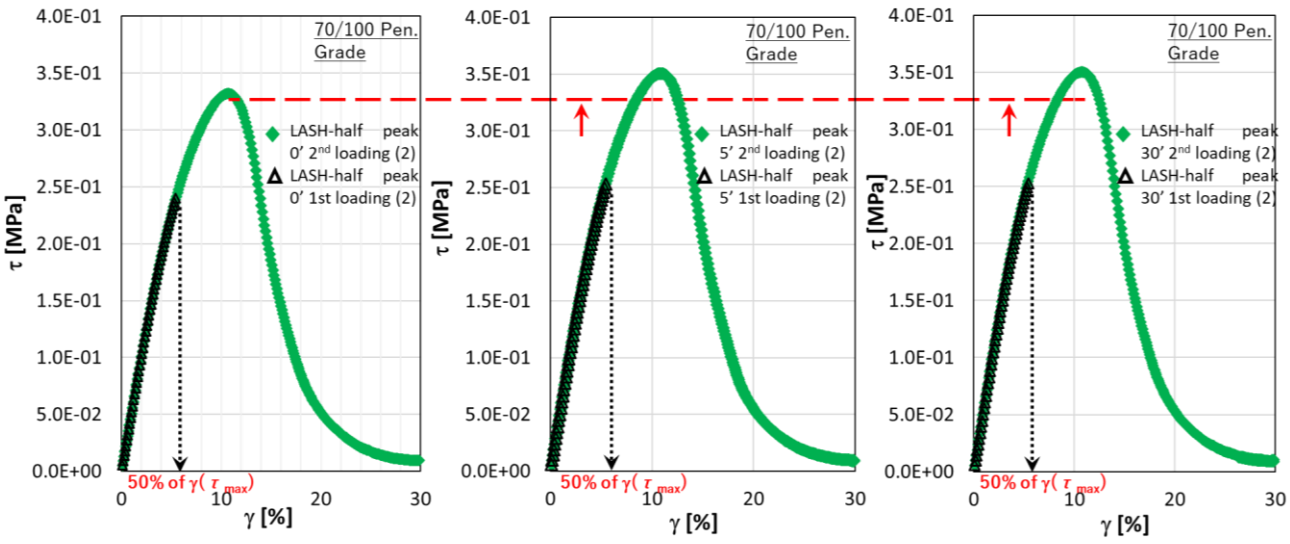

1.4.1. LASH test results at half peak for stress - strain curve for 70/100 binder showing the effect of rest periods [Data from Torino].

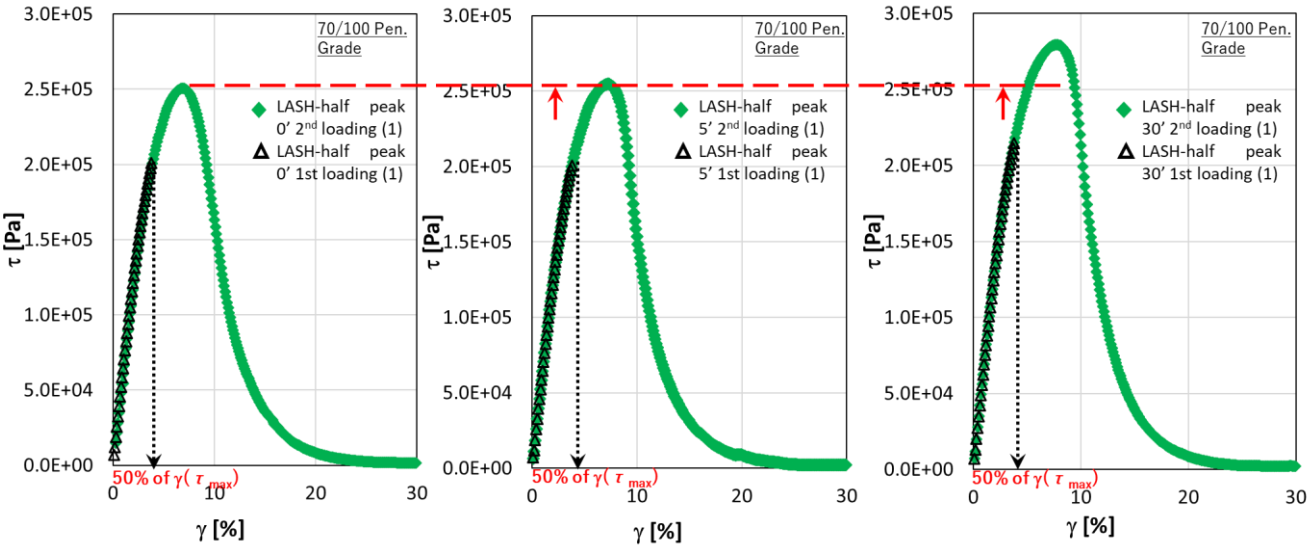

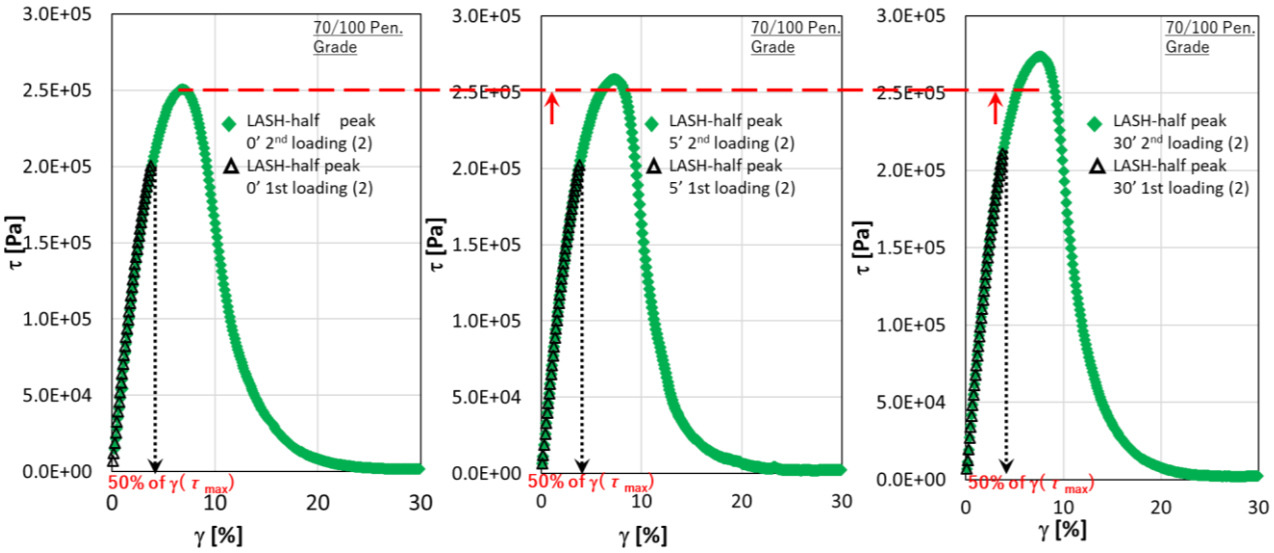

1.4.2. LASH test results at half peak for stress - strain curve for 70/100 binder showing the effect of rest periods [Data from Waterloo].

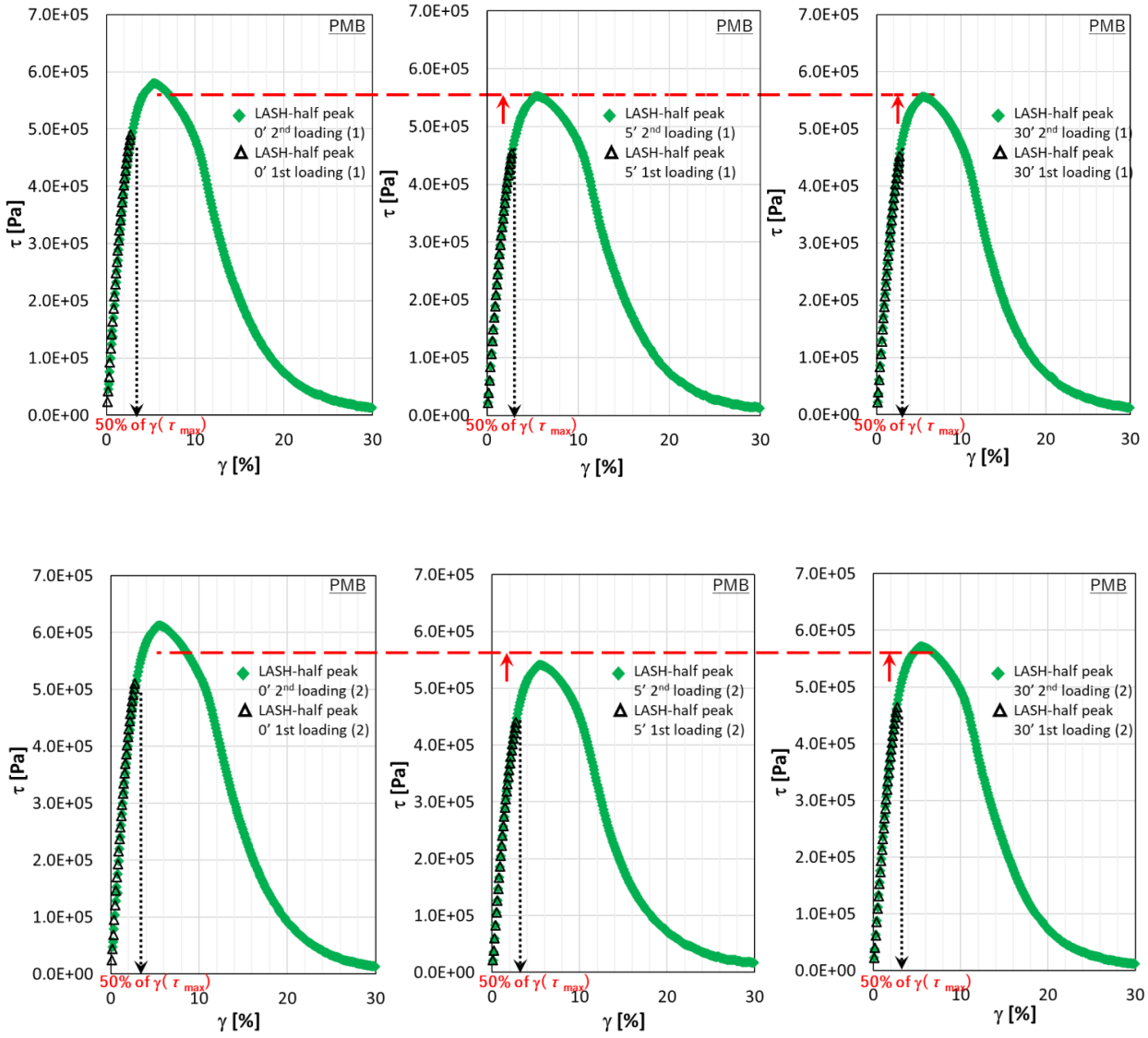

1.4.3. LASH test results at half peak for stress - strain curve for PMB showing the effect of rest periods [Data from Waterloo].

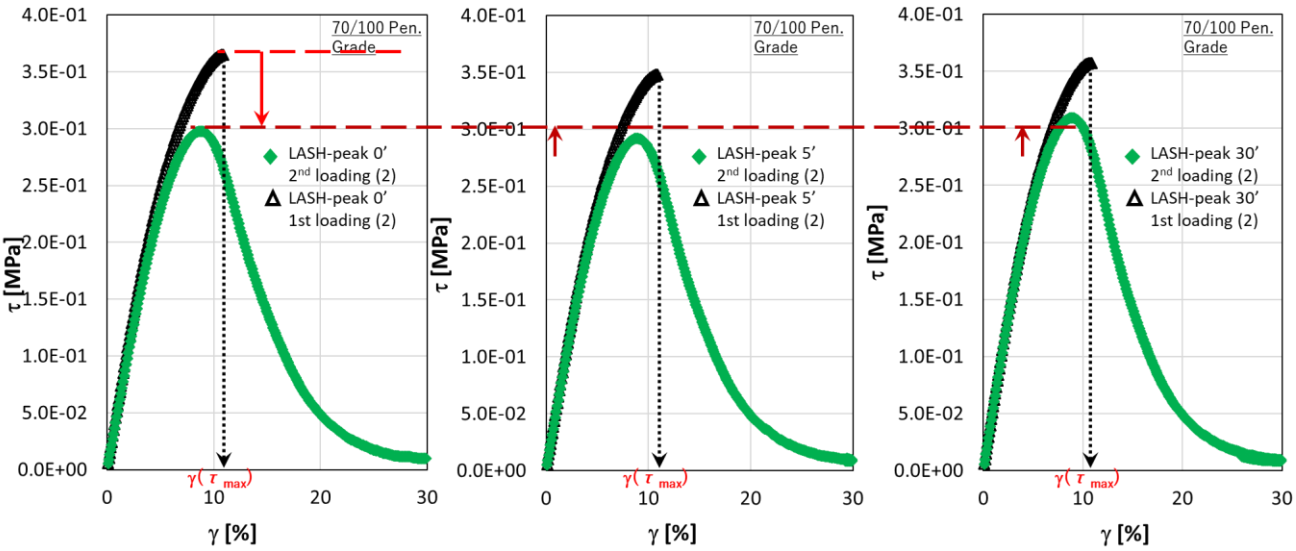

1.4.4. LASH test results at peak for stress - strain curve for 70/100 binder showing the effect of rest periods. [Data from Torino].

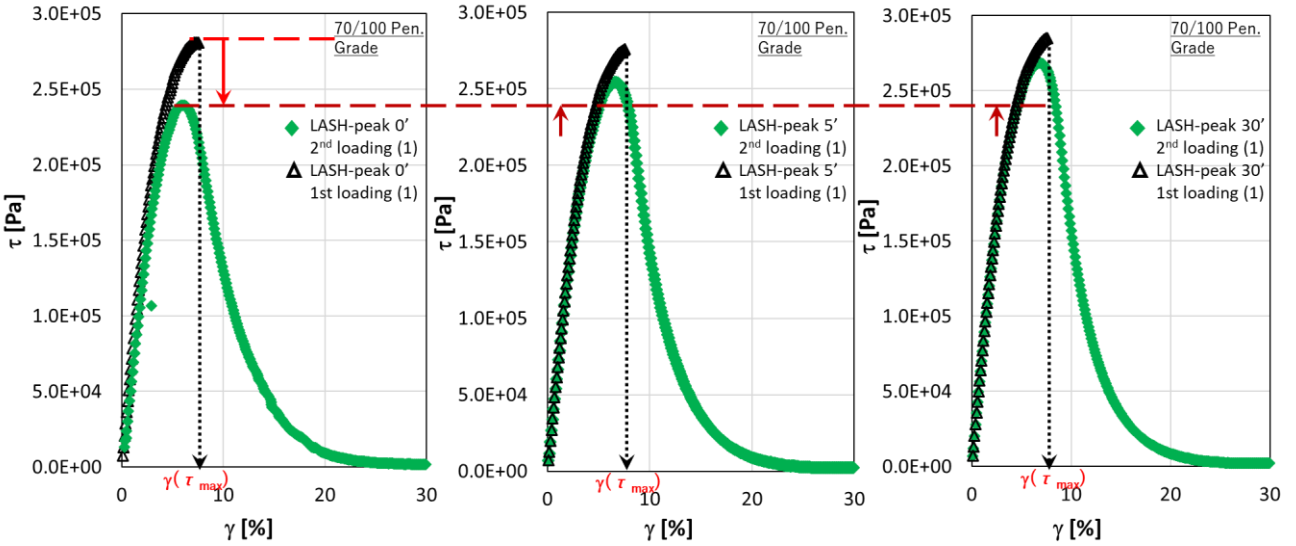

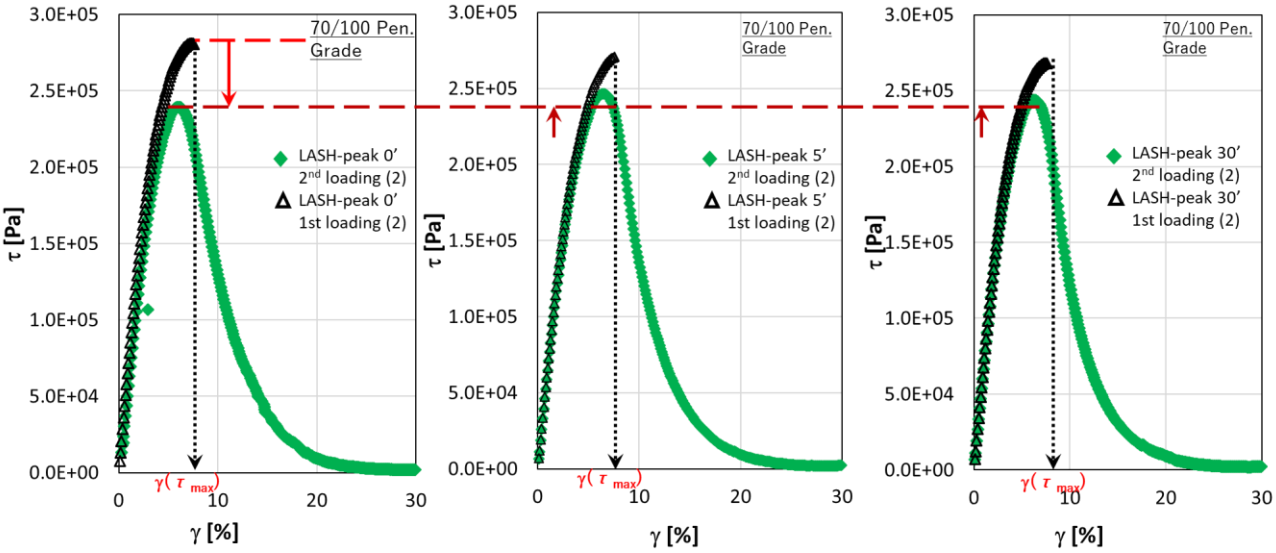

1.4.5. LASH test results at peak for stress - strain curve for 70/100 binder showing the effect of rest periods [Data from Waterloo].

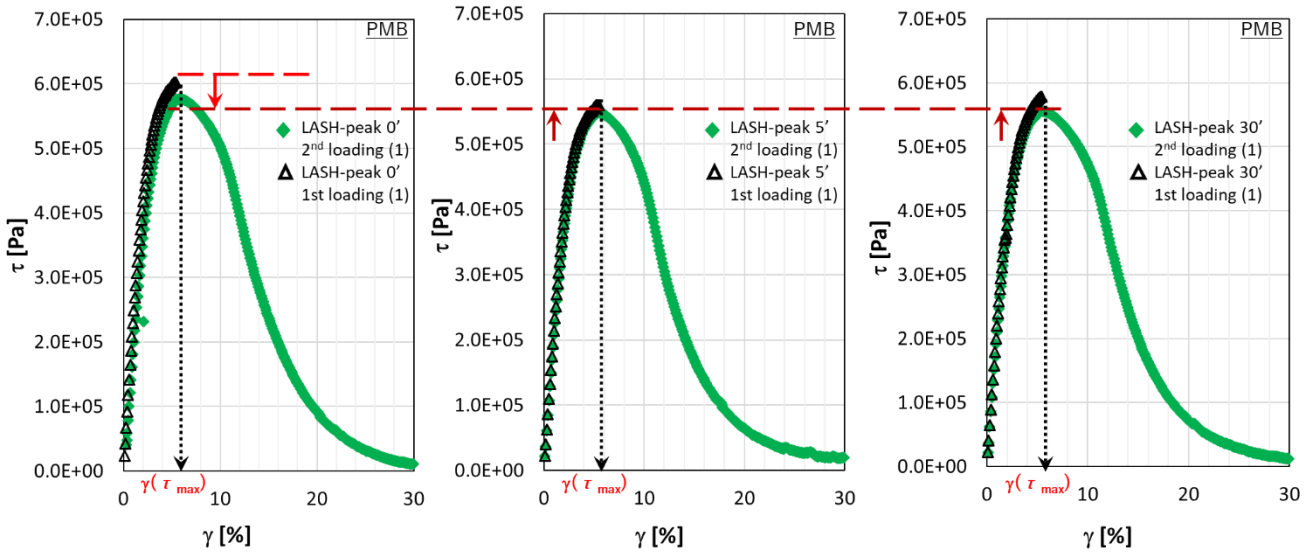

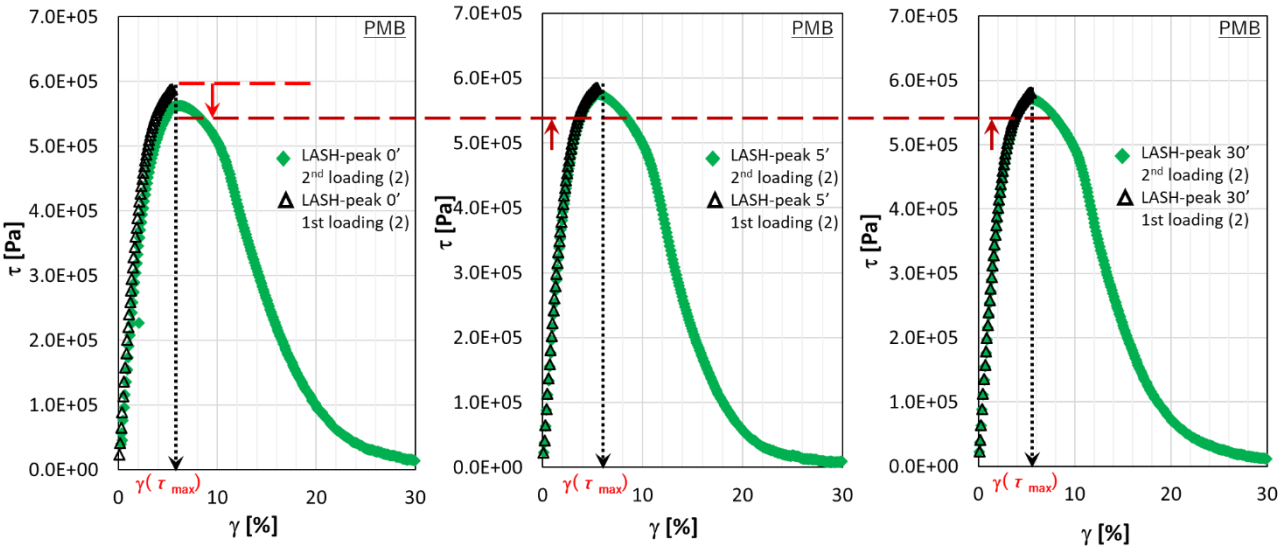

1.4.6. LASH test results at peak for stress - strain curve for PMB showing the effect of rest periods [Data from Waterloo].

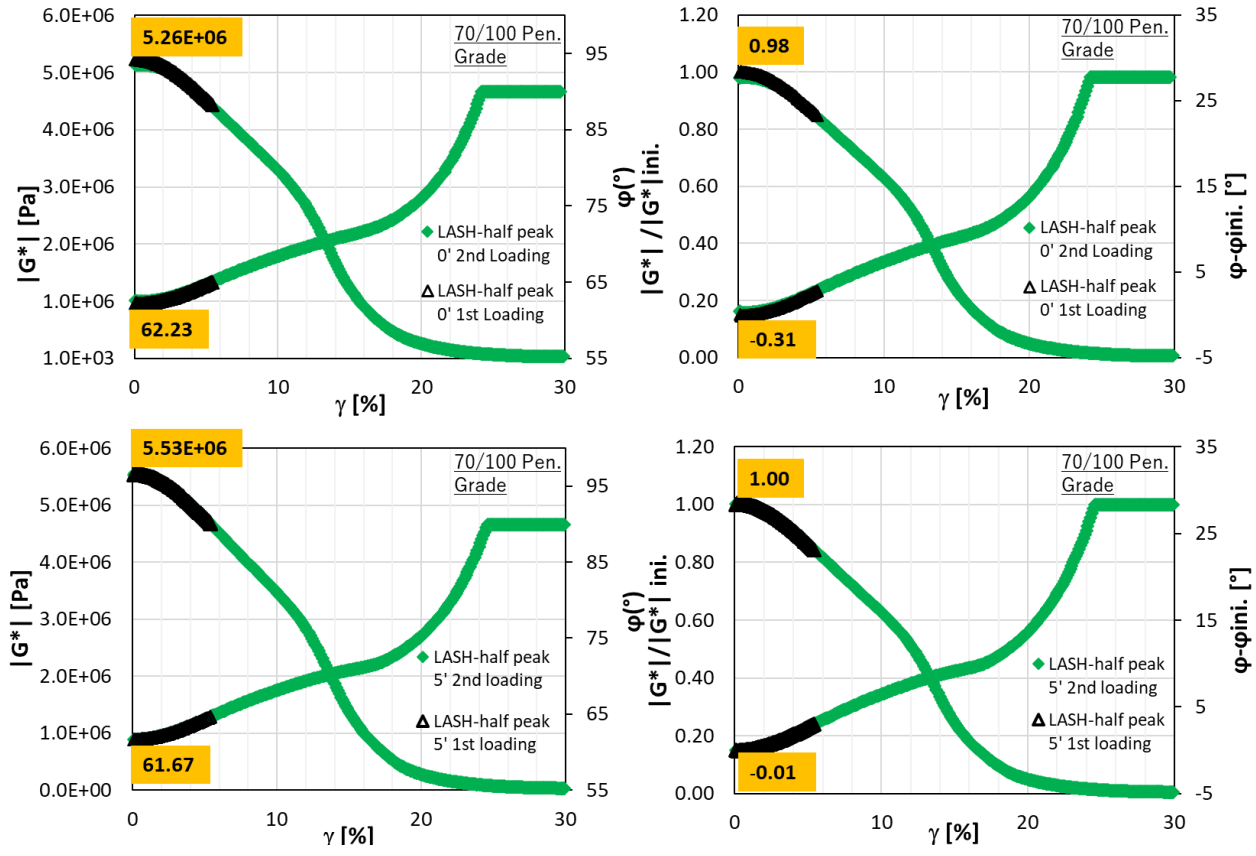

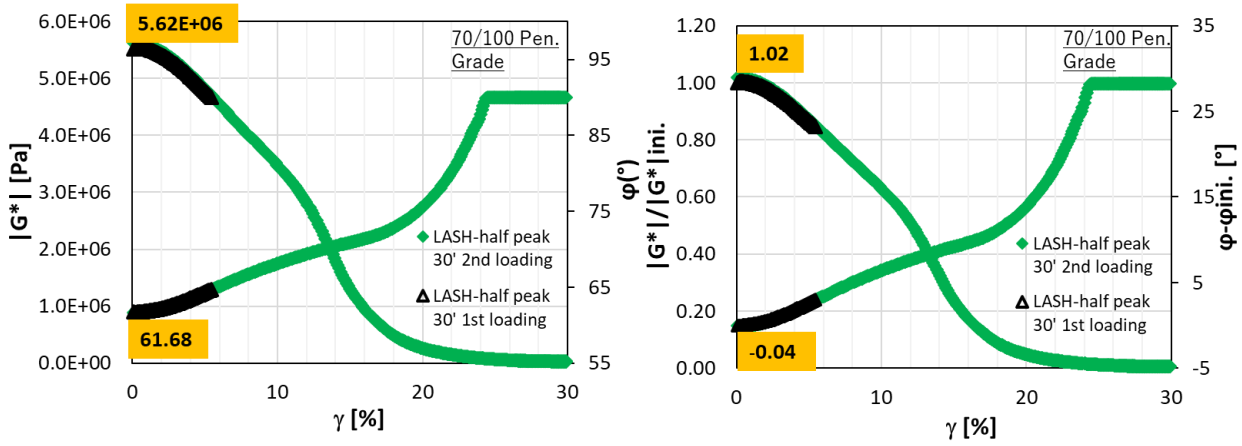

1.4.7. LASH stress half peak result of |G*| vs strain and φ vs strain for 70/100 binder showing the effect of rest periods [Data from Torino].

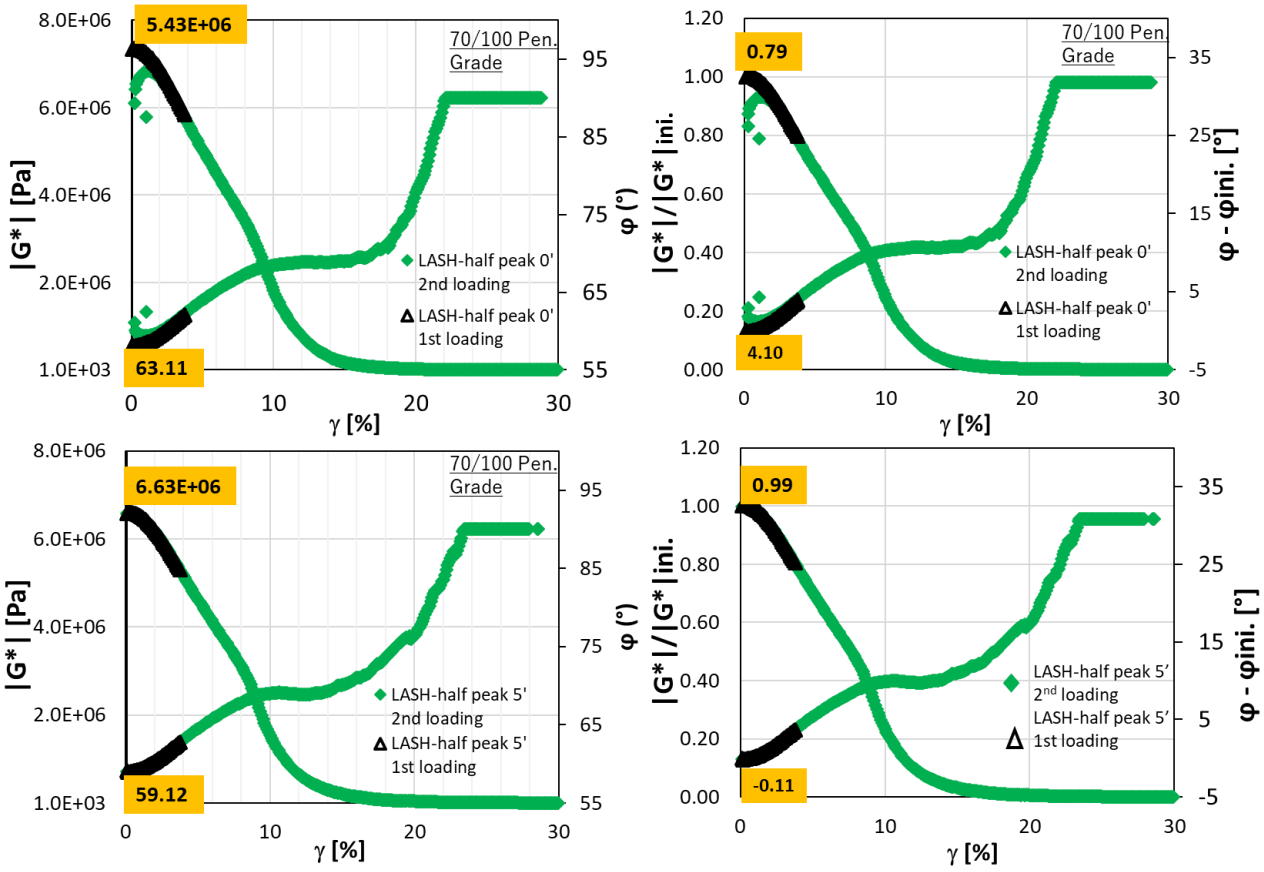

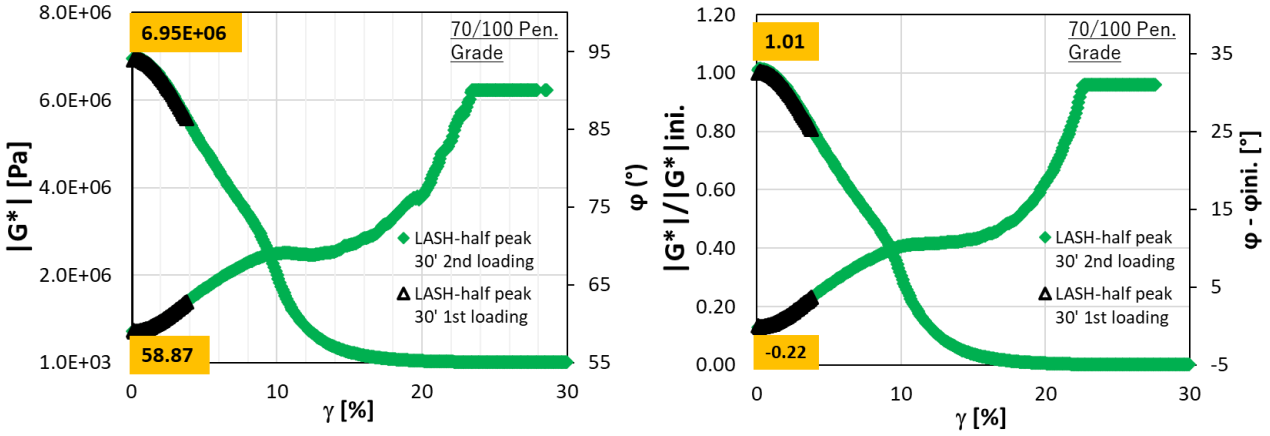

1.4.8. LASH stress half peak result of |G*| vs strain and φ vs strain for 70/100 binder showing the effect of rest periods [Data from Waterloo].

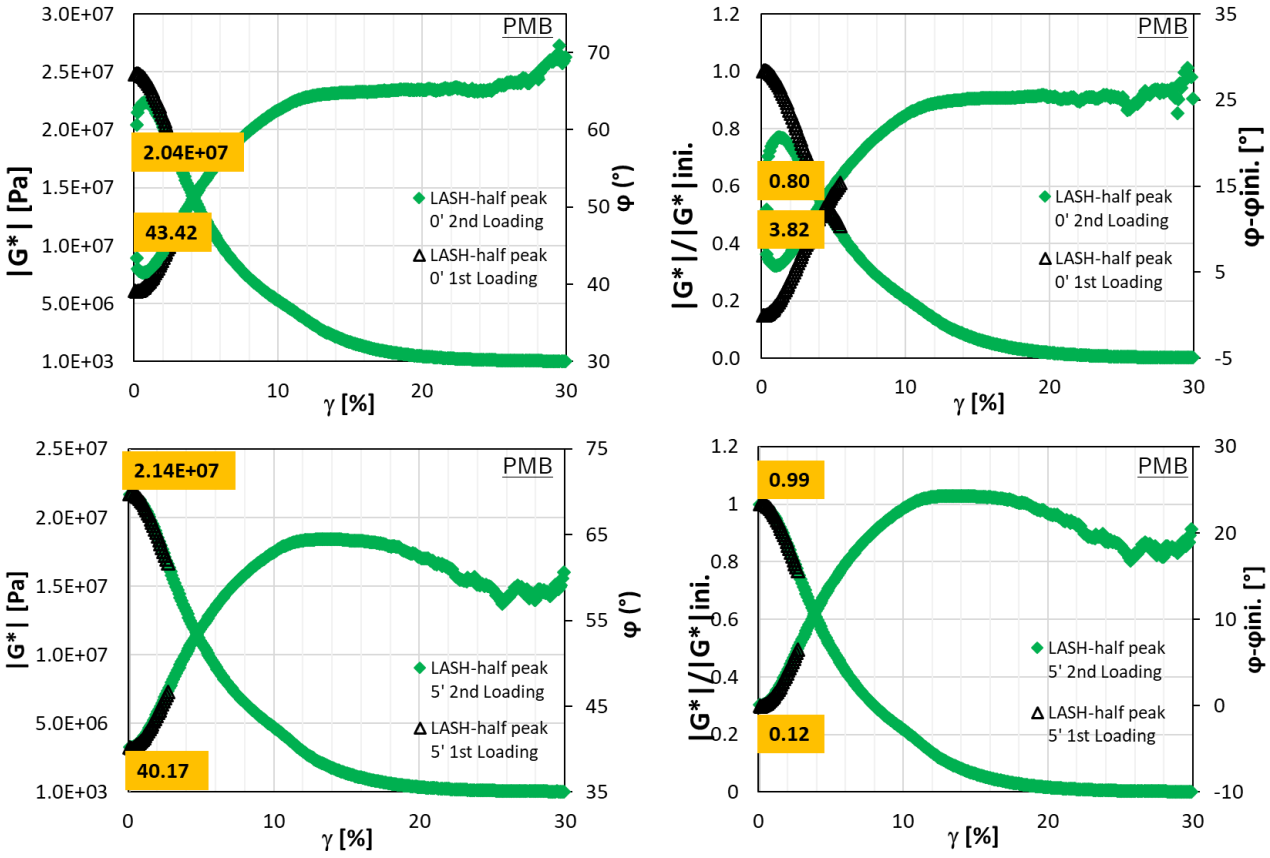

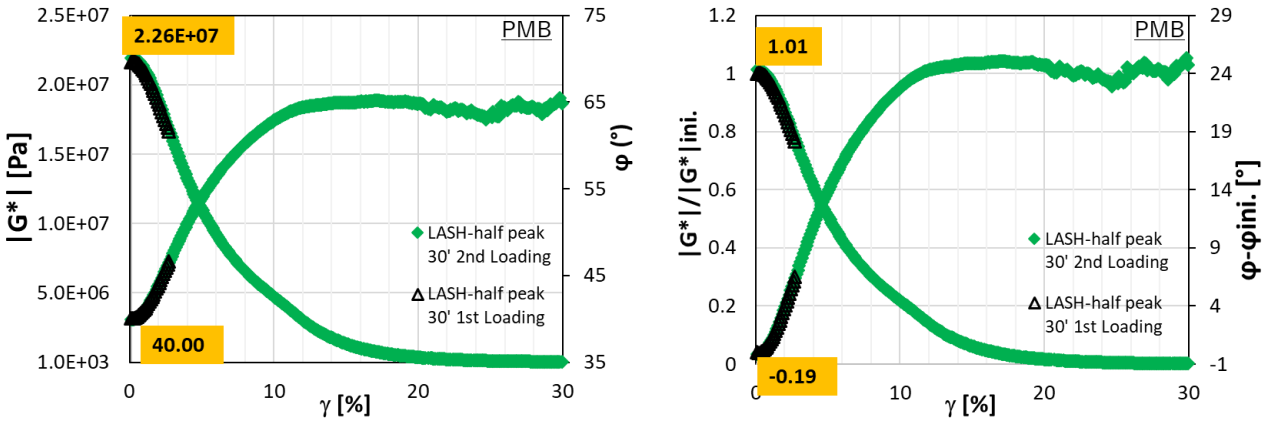

1.4.9. LASH test results at half peak result of |G*| vs strain and φ vs strain for PMB showing the effect of rest periods [Data from Waterloo].

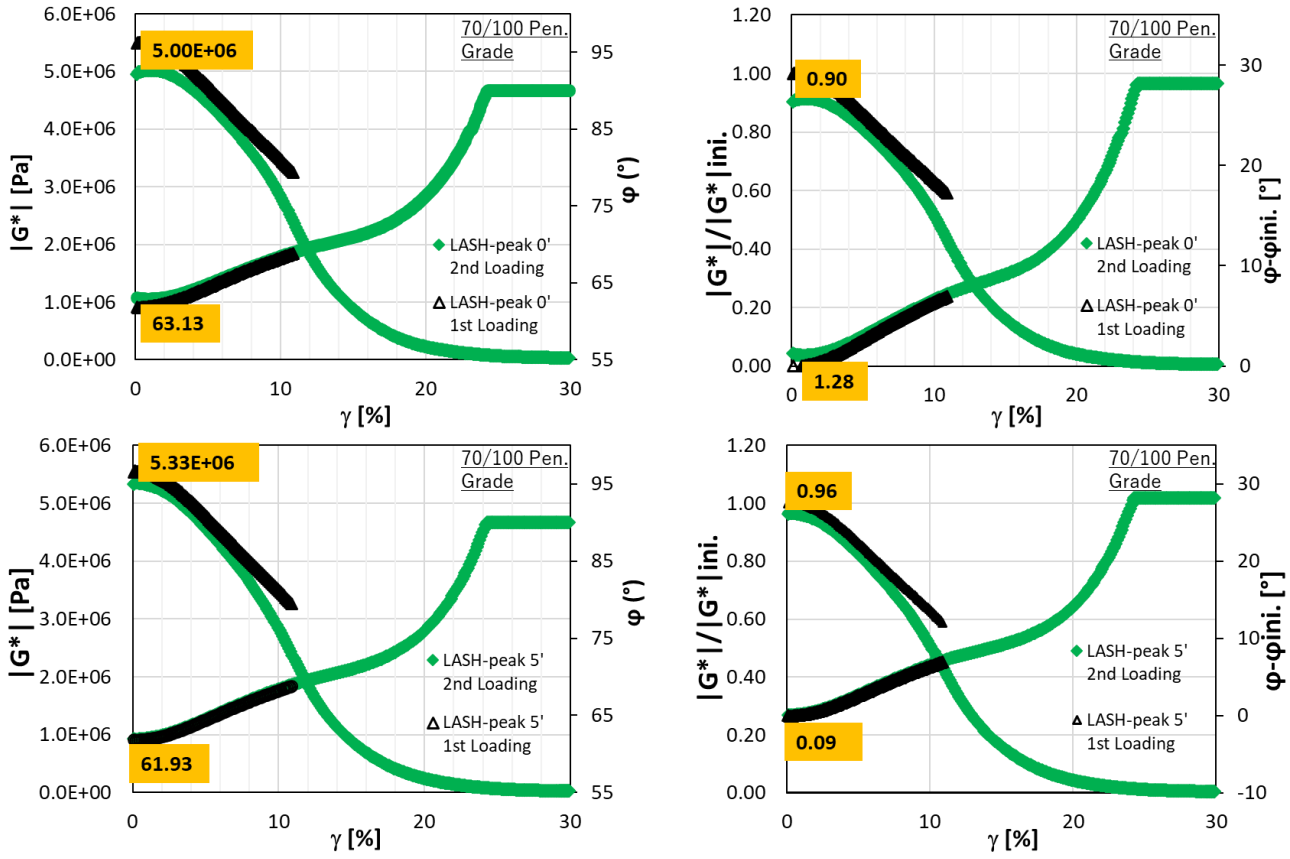

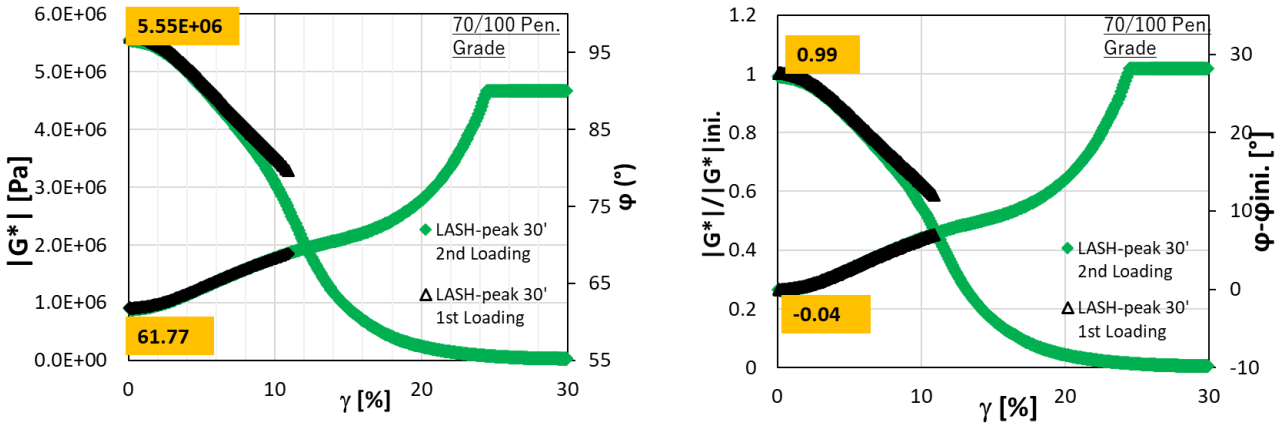

1.4.10. LASH test results at peak result of |G*| vs strain and φ vs strain for 70/100 binder showing the effect of rest periods [Data from Torino].

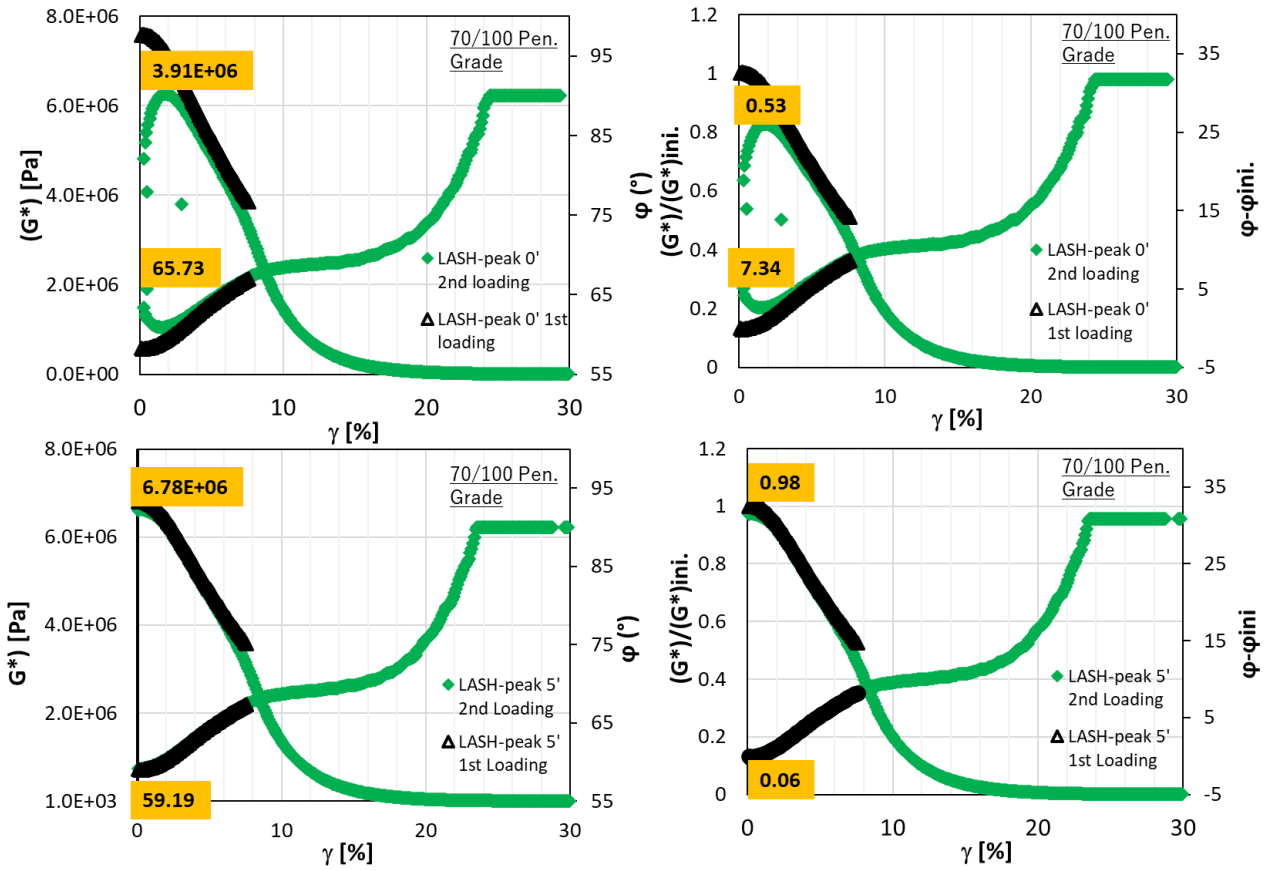

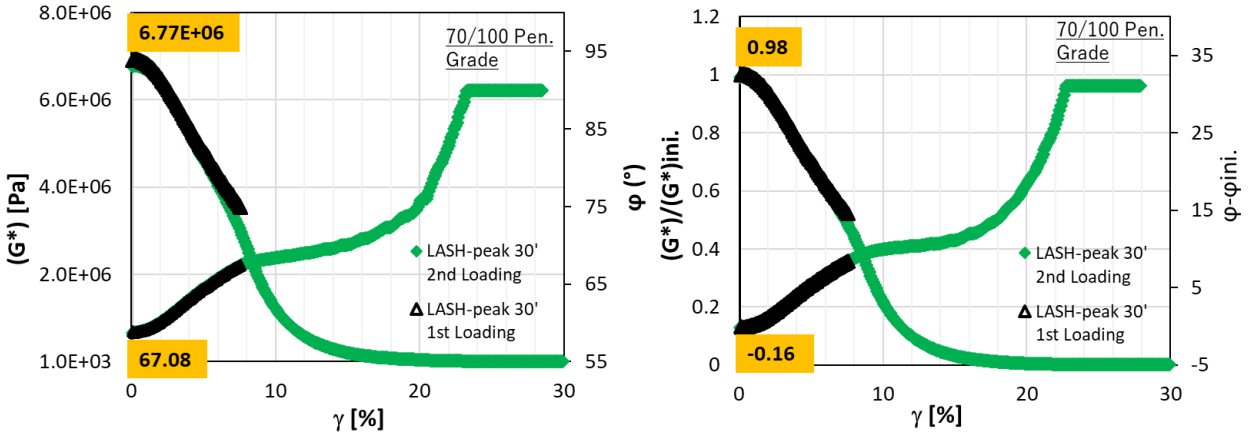

1.4.11. LASH test results at peak result of |G*| vs strain and φ vs strain for 70/100 binder showing the effect of rest periods at 0 min., 5 min. and 30 min. [Data from Waterloo].

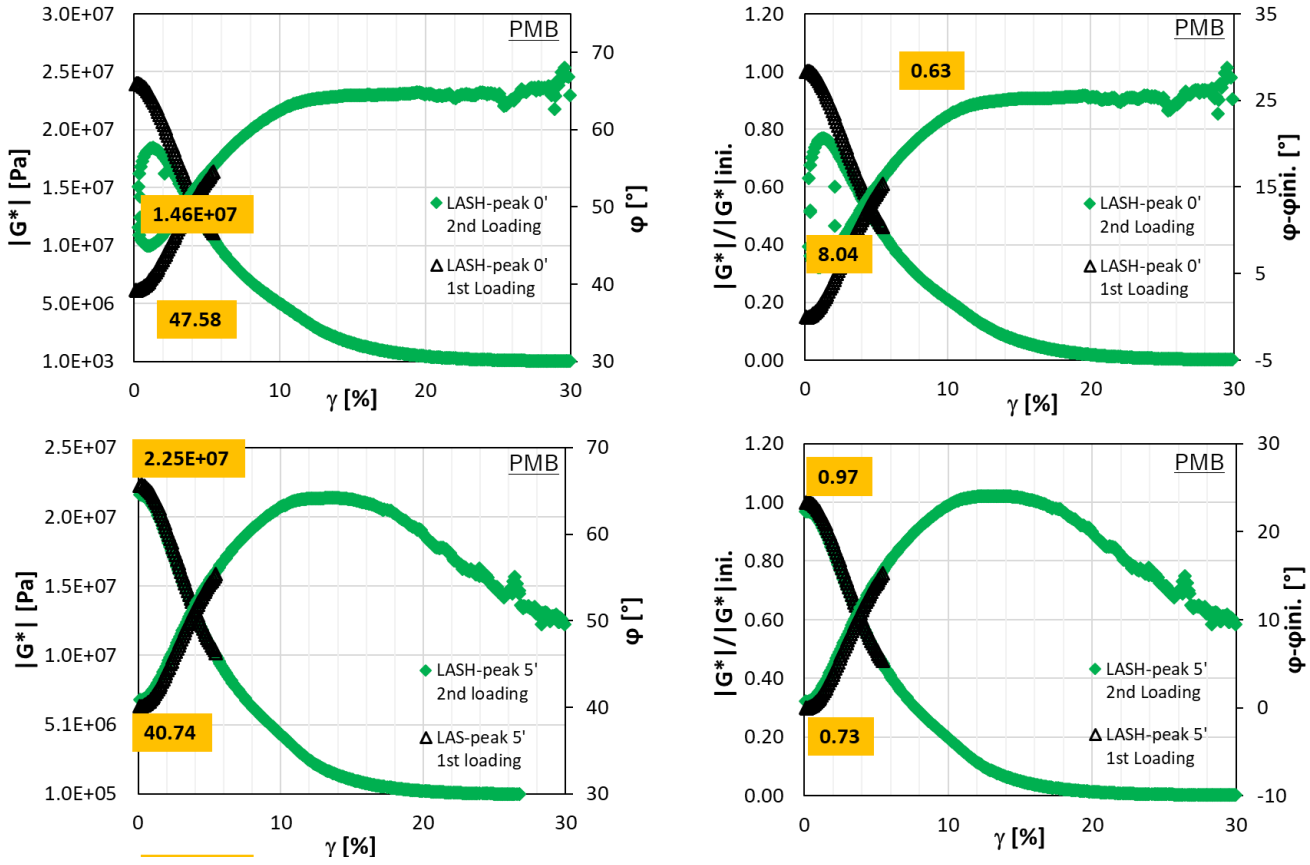

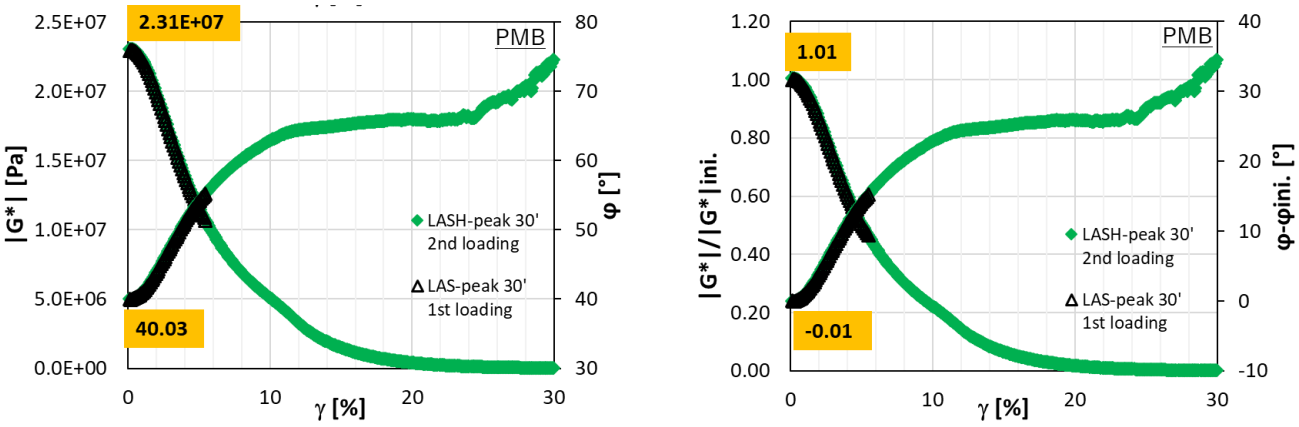

1.4.12. LASH test results at peak result of |G*| vs strain and φ vs strain for PMB showing the effect of rest periods at 0 min., 5 min. and 30 min. [Data from Waterloo].

1.5. Results of steric hardening tests

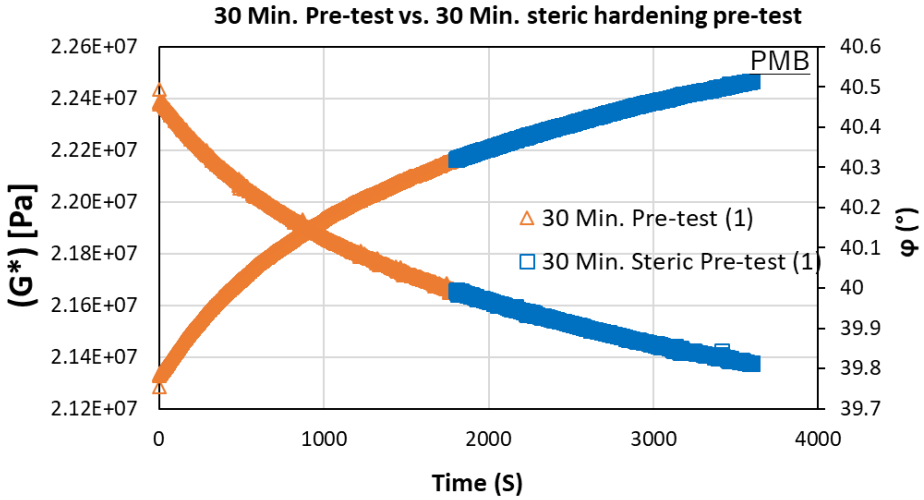

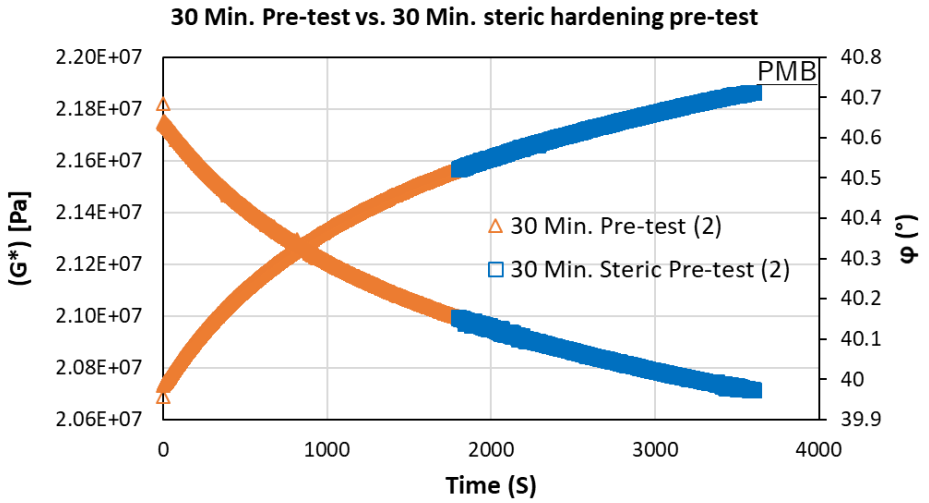

1.5.1. Typical steric hardening test results for PMB [Data from Waterloo].

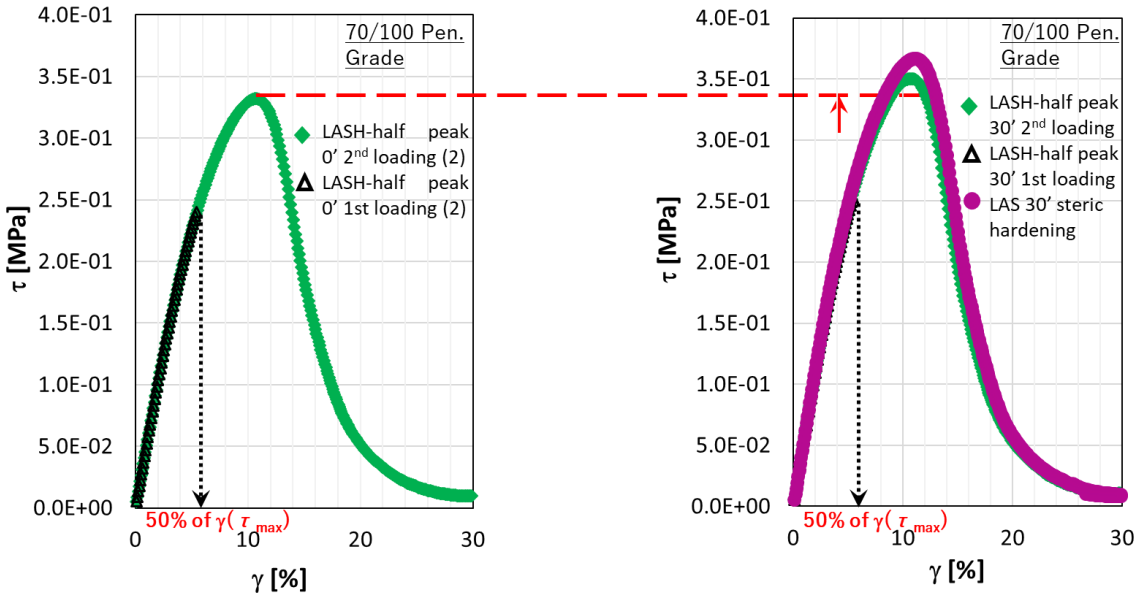

1.5.2. LASH test and LAS-SH tests result at half peak for stress - strain curve for 70/100 binder. [Data from Torino].

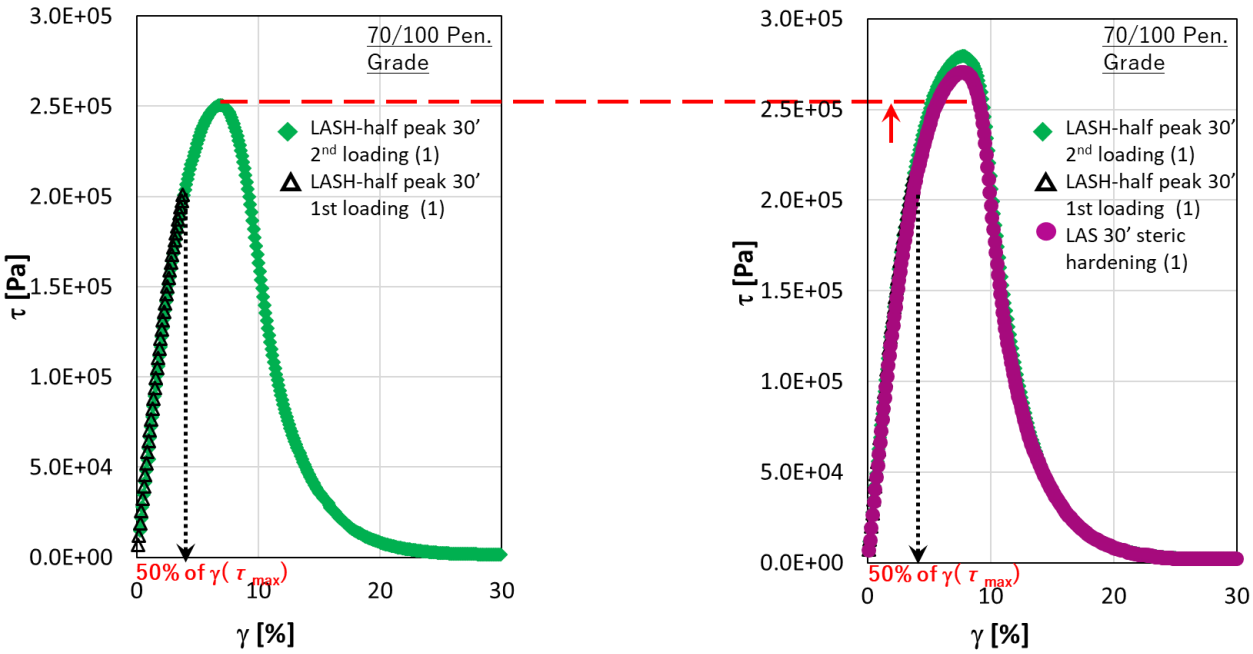

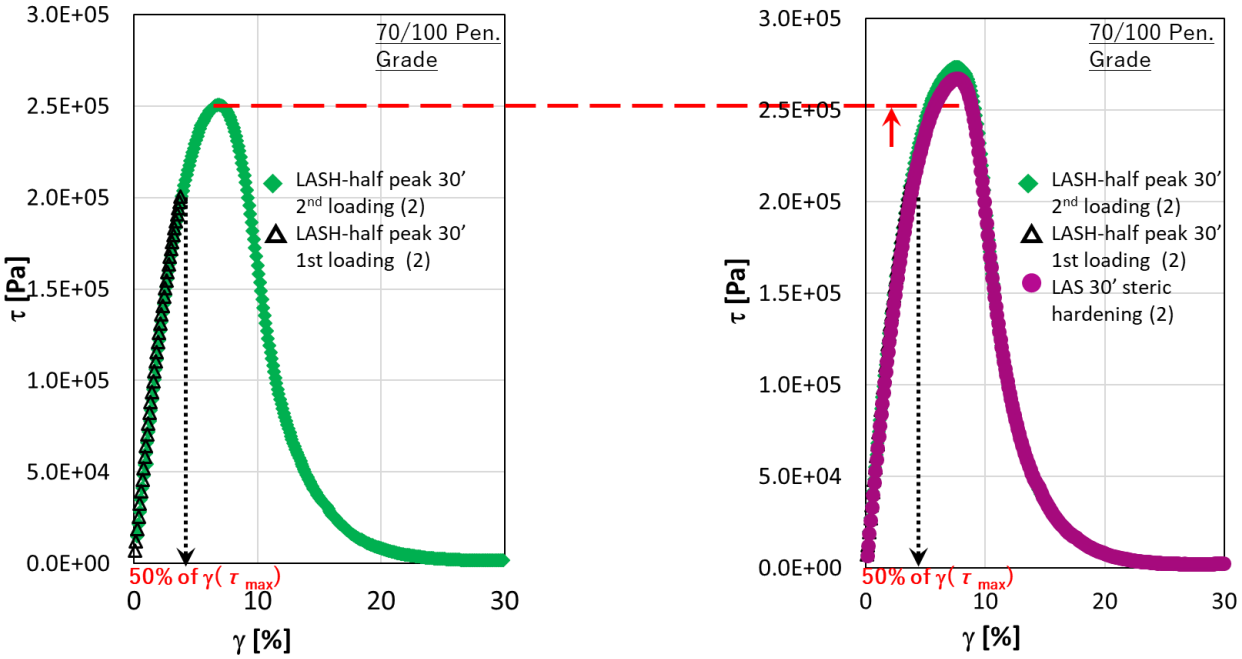

1.5.3. LASH test and LAS-SH tests result at half peak for stress - strain curve for 70/100 binder. [Data from Waterloo].

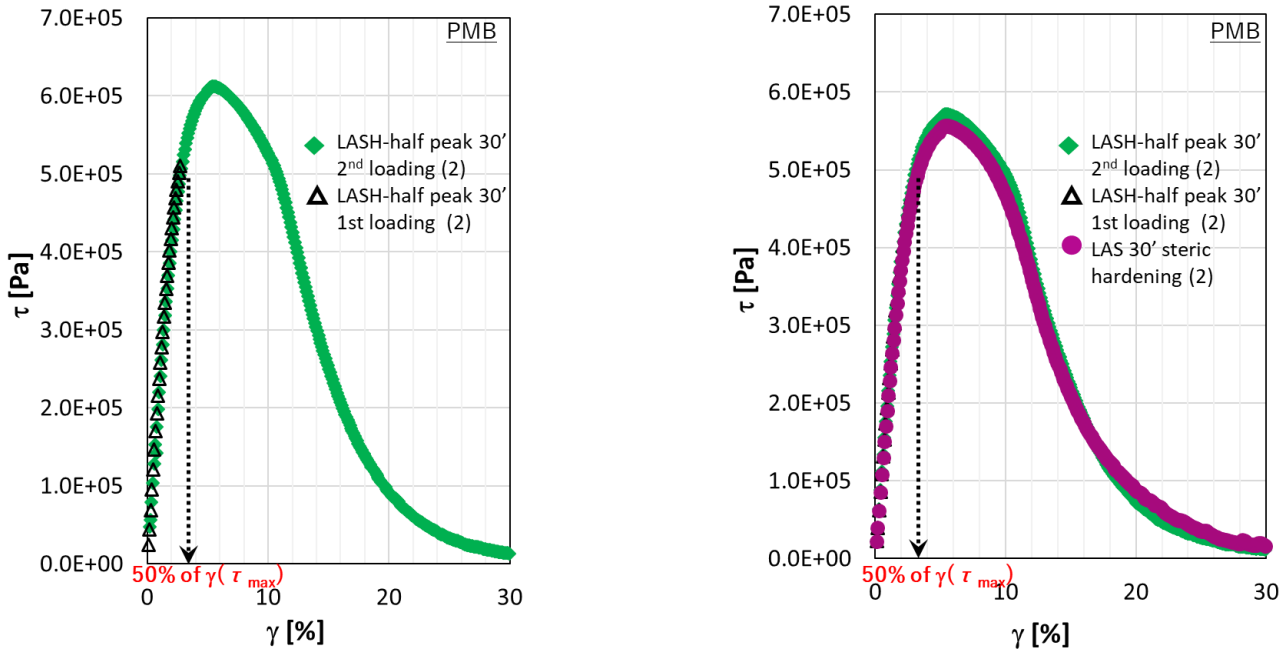

1.5.4. LASH test and LAS-SH tests result at half peak for stress - strain curve for PMB [Data from Waterloo].

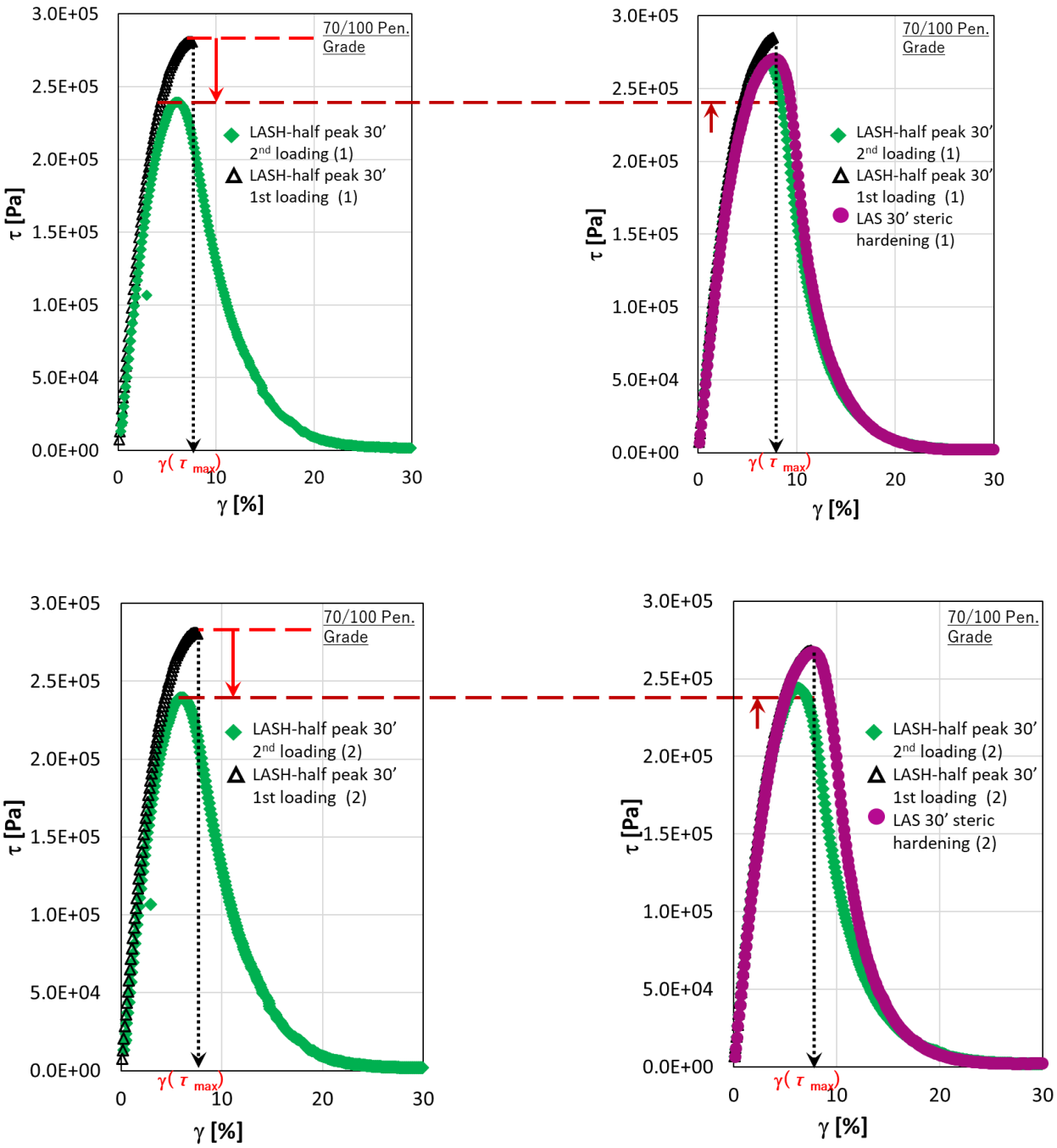

1.5.5. LASH test and LAS-SH tests result at peak for stress - strain curve for 70/100 binder. [Data from Waterloo].

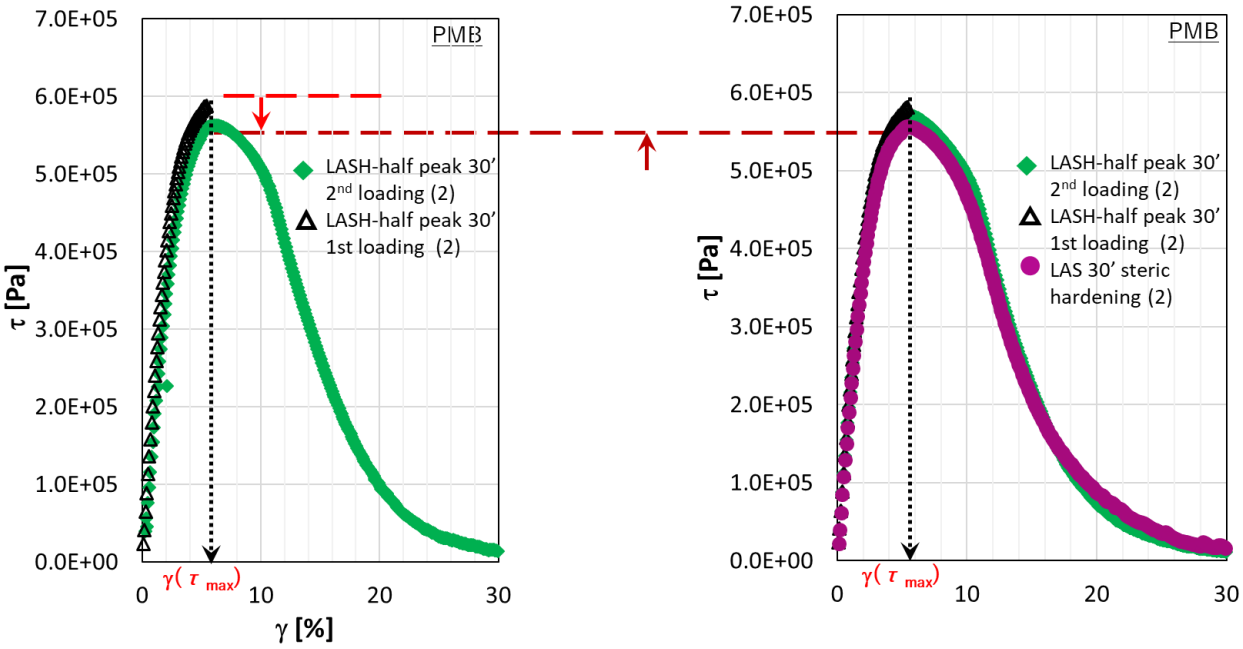

1.5.6. LASH test and LAS-SH tests result at peak for stress - strain curve for PMB [Data from Waterloo].

1.6. Evaluation of Energy dissipation

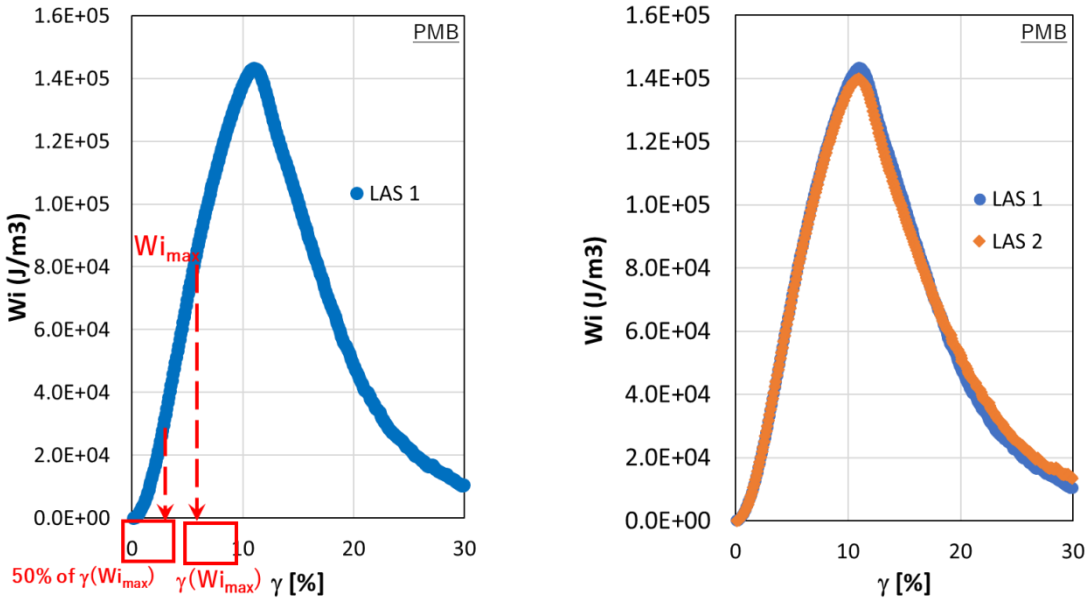

1.6.1. Typical LAS tests result in energy dissipation [Data from Waterloo].

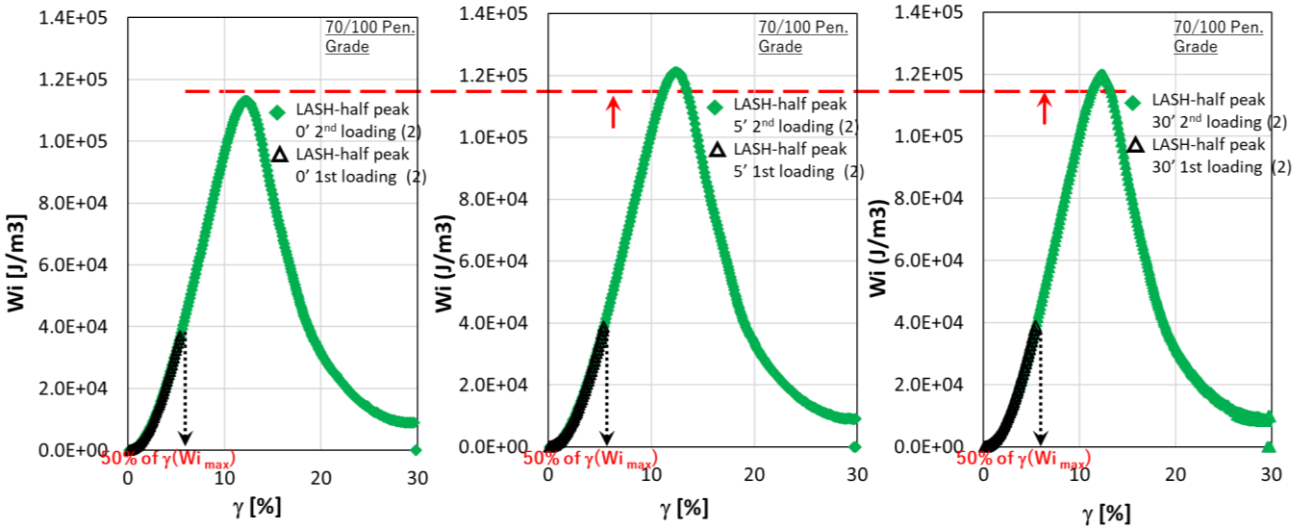

1.6.2. LASH test results at half peak for energy dissipation [Data from Torino].

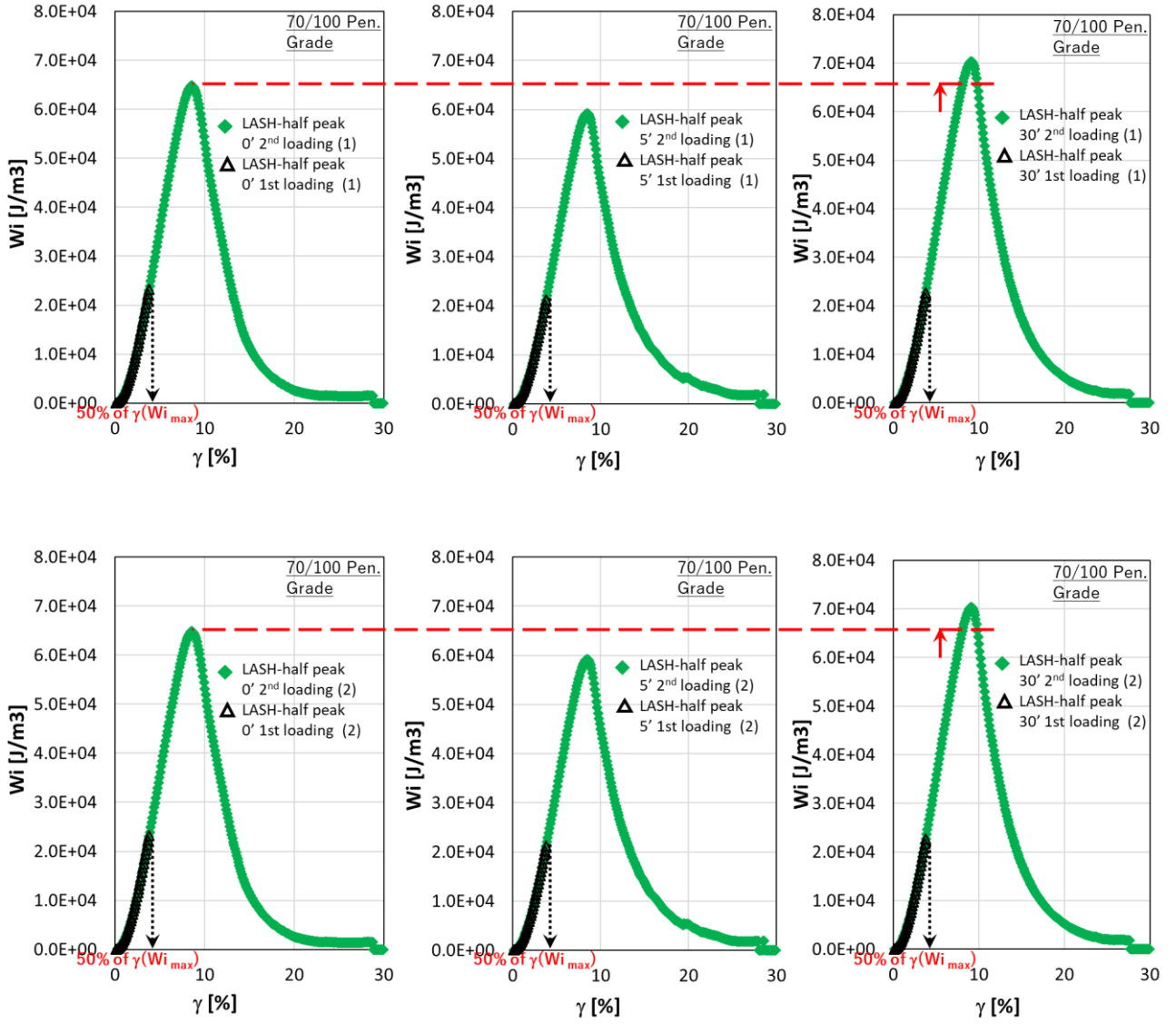

Figure 1.6.3. LASH test results at half peak for energy dissipation - strain curve for 70/100 binder showing the effect of rest periods at 0 min., 5 min. and 30 min. [Data from Waterloo].

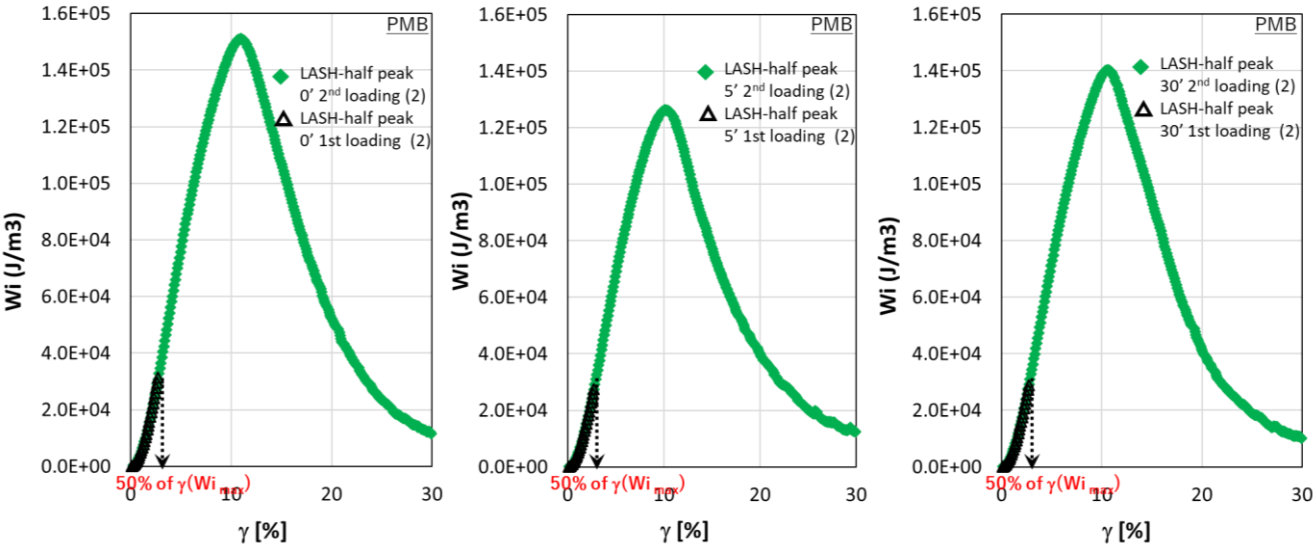

1.6.4. LASH test results at half peak for energy dissipation for PMB [Data from Waterloo].

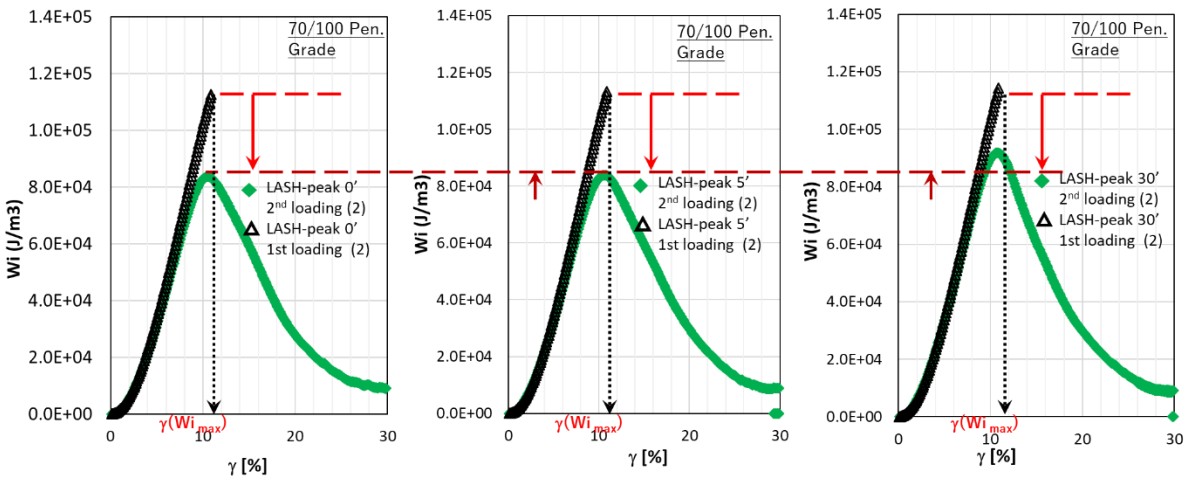

Figure 1.6.5. LASH test results at peak for energy dissipation - strain curve for 70/100 binder [Data from Torino].

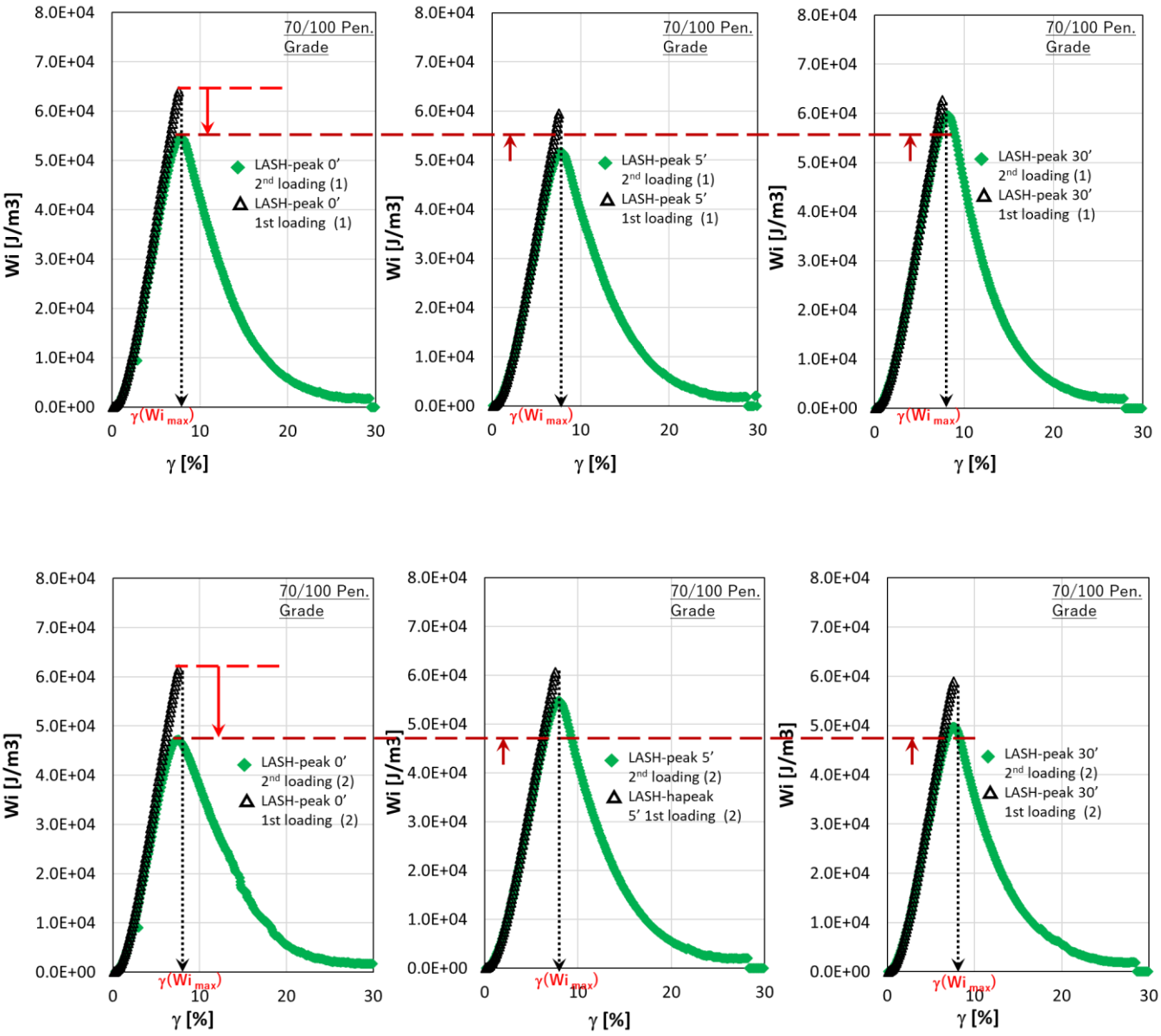

Figure 1.6.6. LASH test results at peak for energy dissipation - strain curve for 70/100 binder [Data from Waterloo].

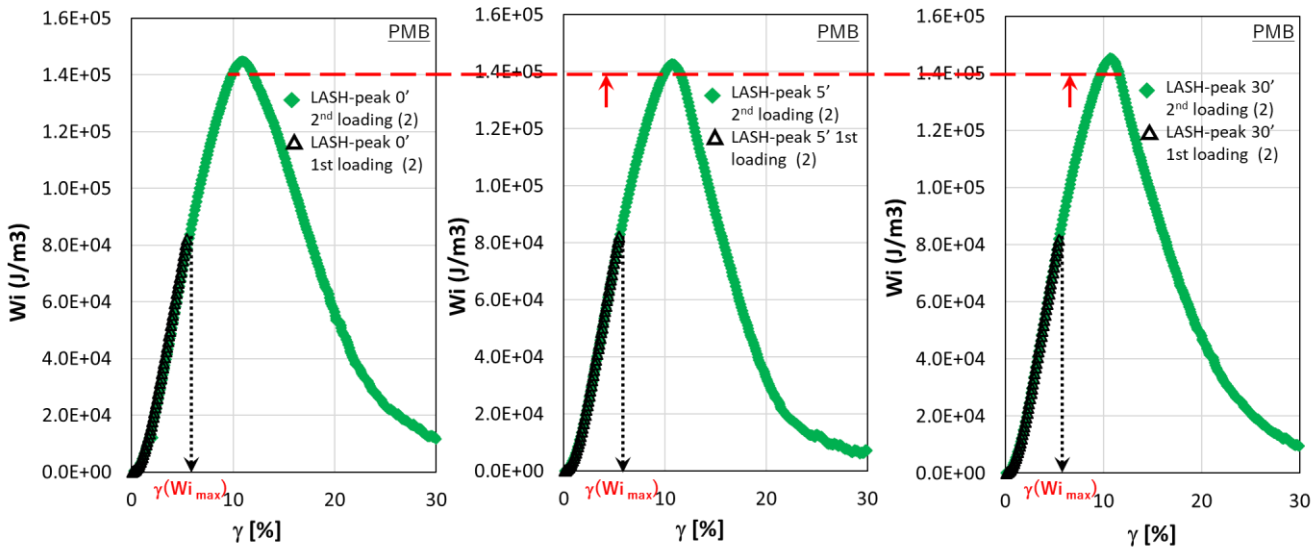

Figure 1.6.7. LASH test results at peak for energy dissipation - strain curve for PMB [Data from Waterloo].

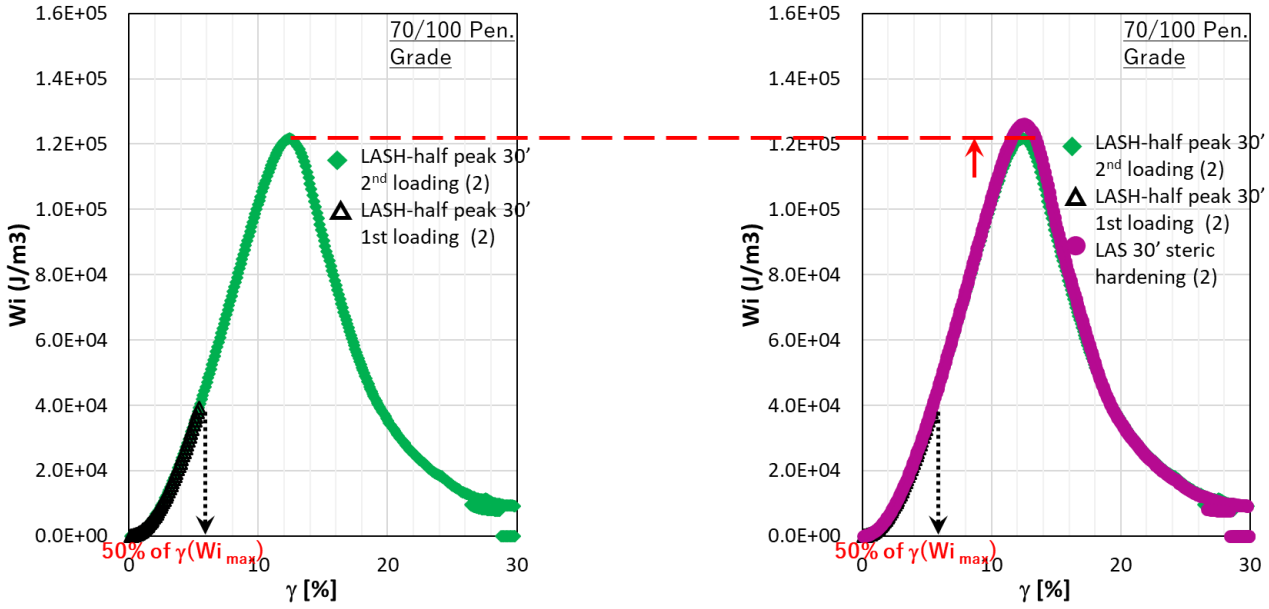

Figure 1.6.8. LASH test and steric hardening results at half-peak for energy dissipation - strain curve for 70/100 binder. [Data from Torino].

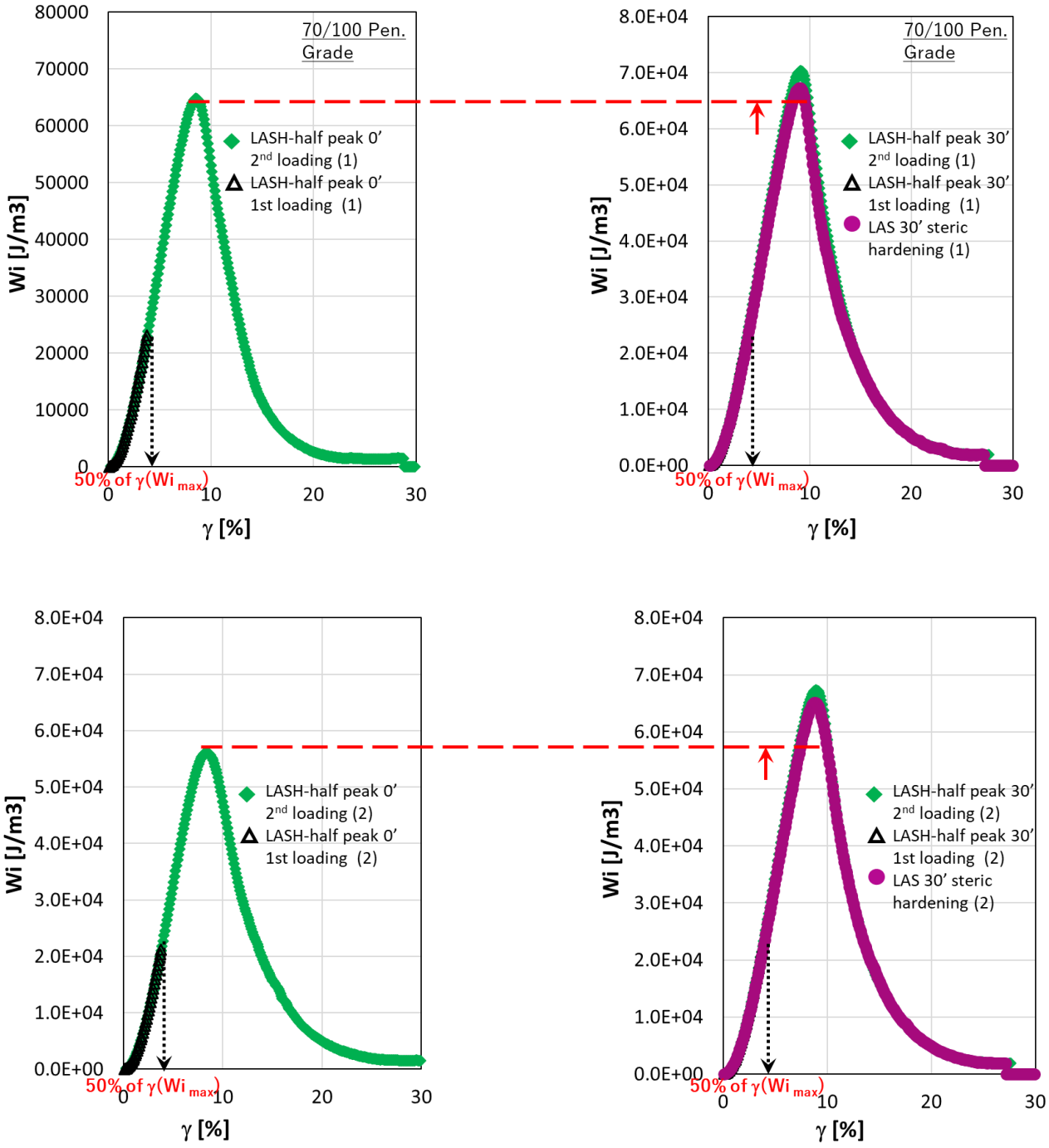

Figure 1.6.9. LASH test and steric hardening results at half-peak for energy dissipation - strain curve for 70/100 binder. [Data from Waterloo].

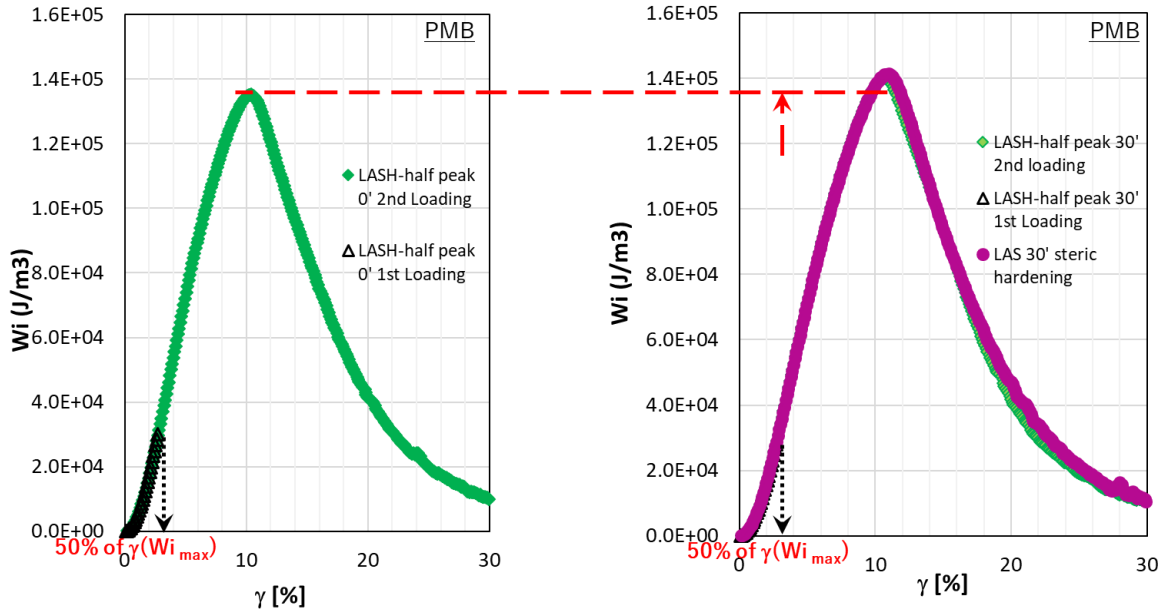

Figure 1.6.10. LASH test and steric hardening results at half-peak for energy dissipation - strain curve for PMB. [Data from Waterloo].

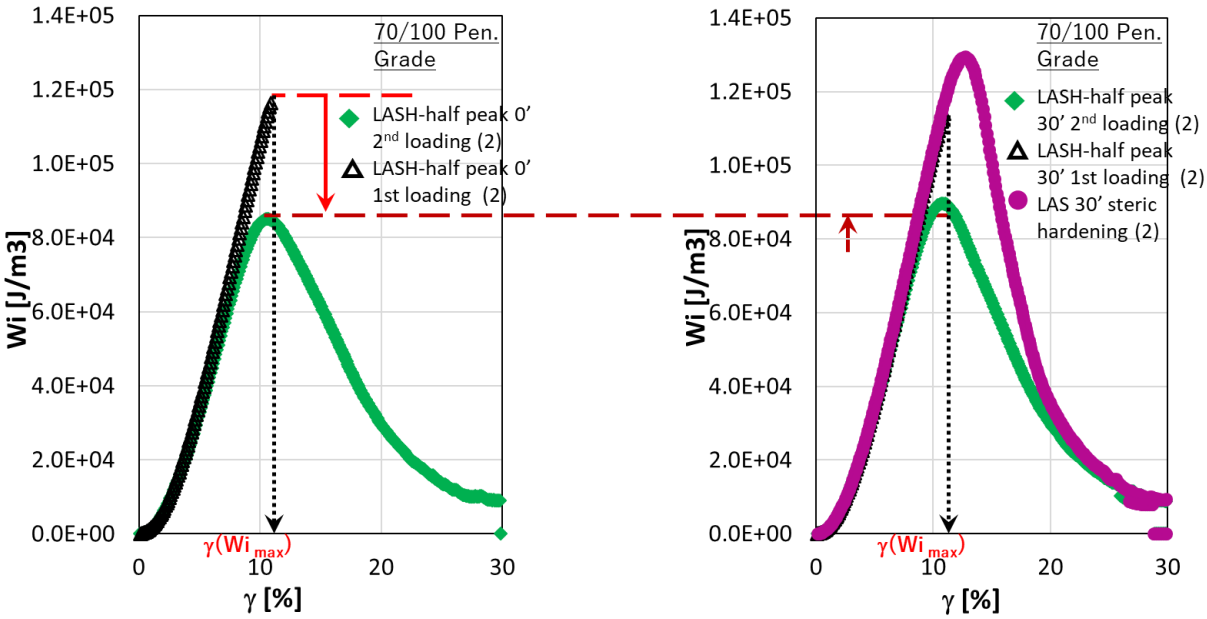

Figure 1.6.11. LASH test and steric hardening results at peak for energy dissipation - strain curve for 70/100 binder. [Data from Torino].

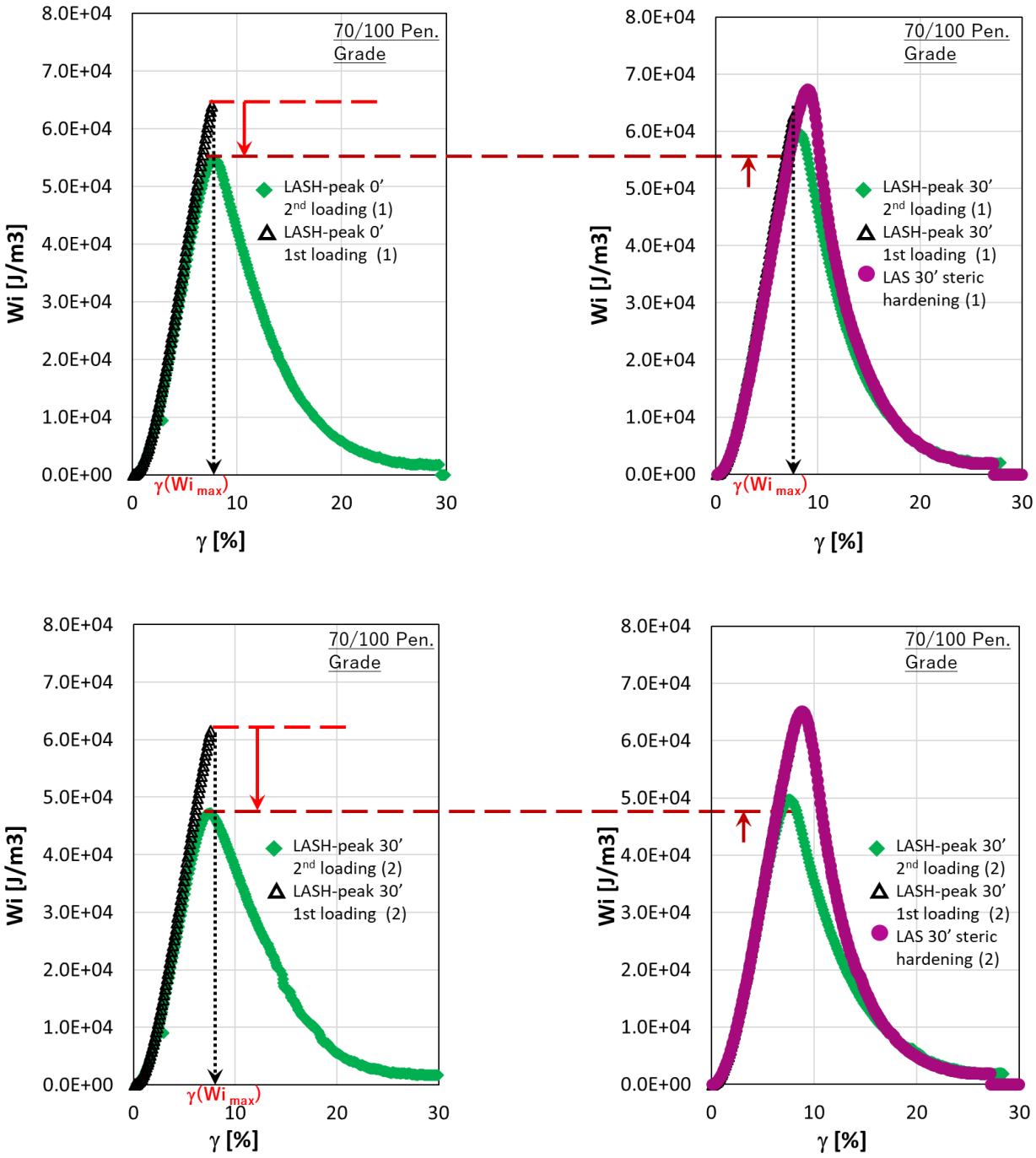

Figure 1.6.12. LASH test and steric hardening results at peak for energy dissipation - strain curve for 70/100 binder. [Data from Waterloo].

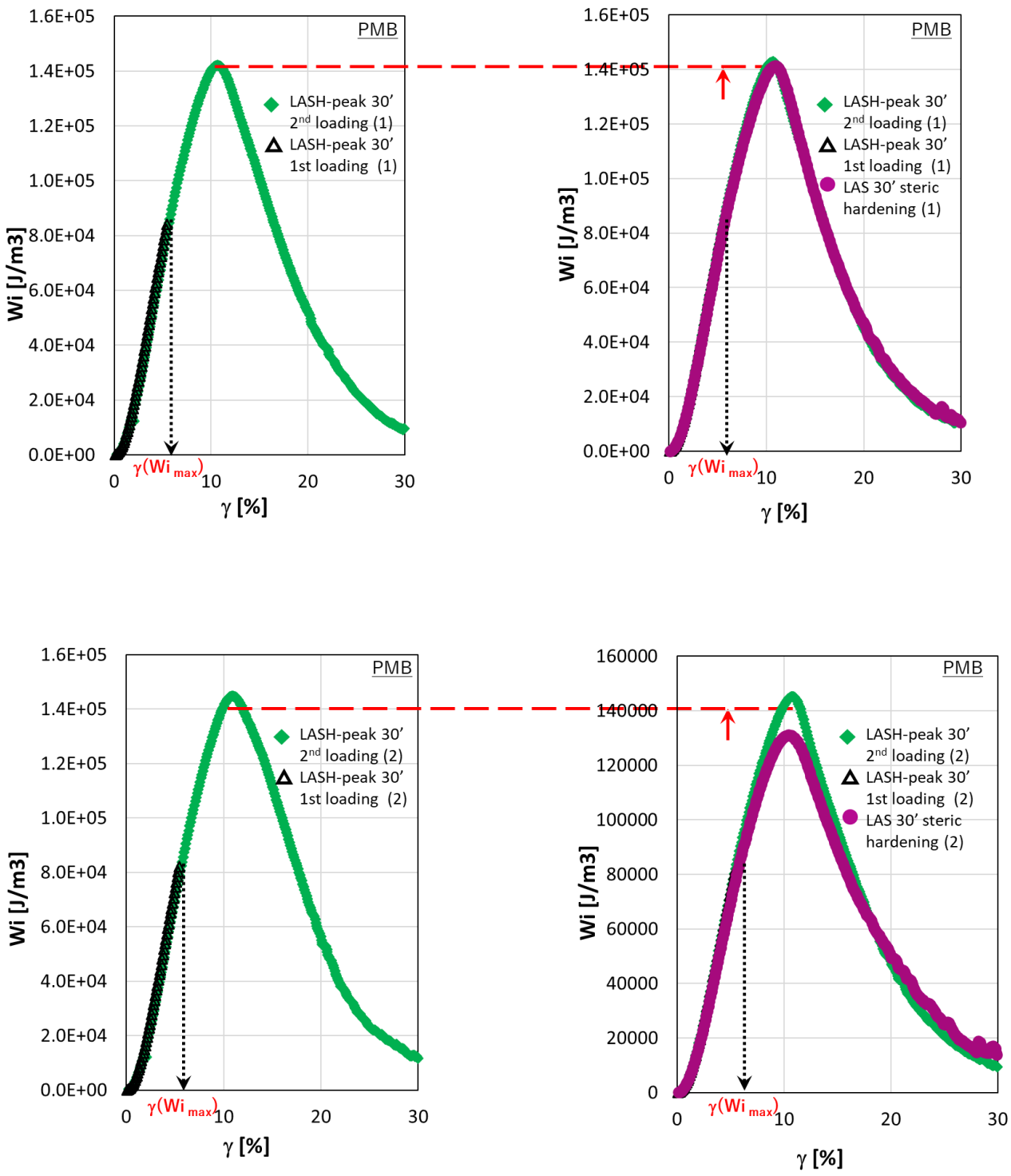

1.6.13. LASH test and steric hardening results at peak for energy dissipation - strain curve for PMB. [Data from Waterloo].

1.7. Analysis of the recovery parameters

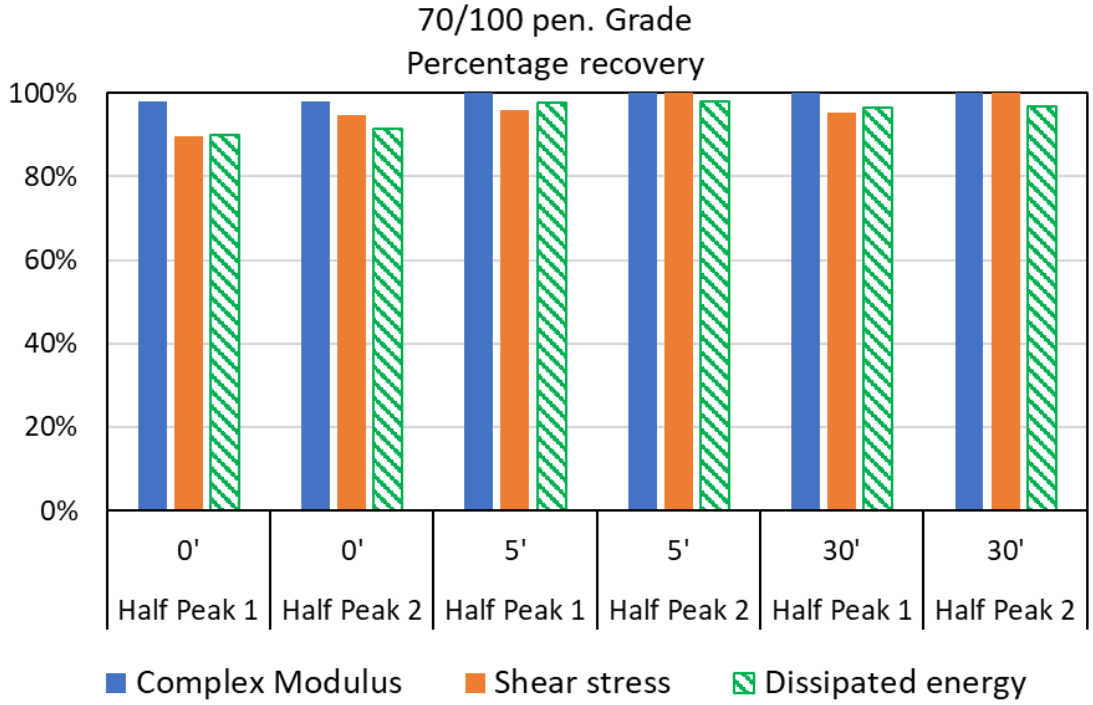

Figure 1.7.1. Summary of total recovery based on complex modulus, shear stress and dissipated energy at half peak stress for 70/100 binder [Data from Torino].

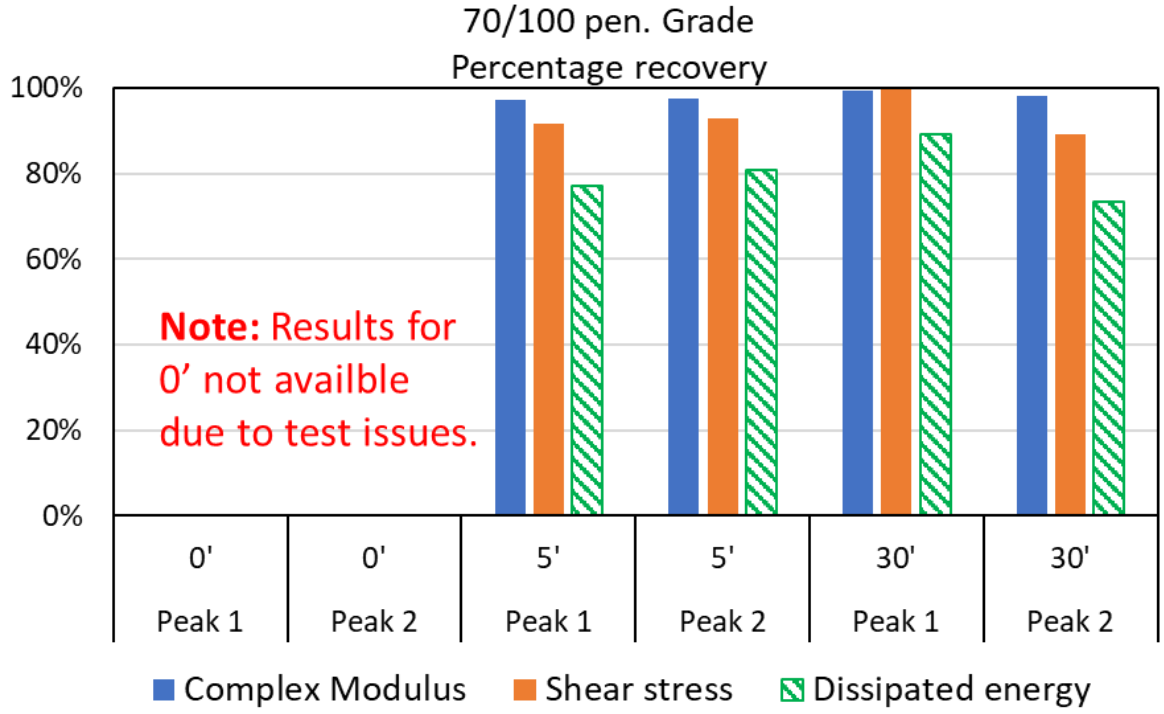

Figure 1.7.2. Summary of total recovery based on complex modulus, shear stress and dissipated energy at peak stress for 70/100 binder. [Data from Waterloo].

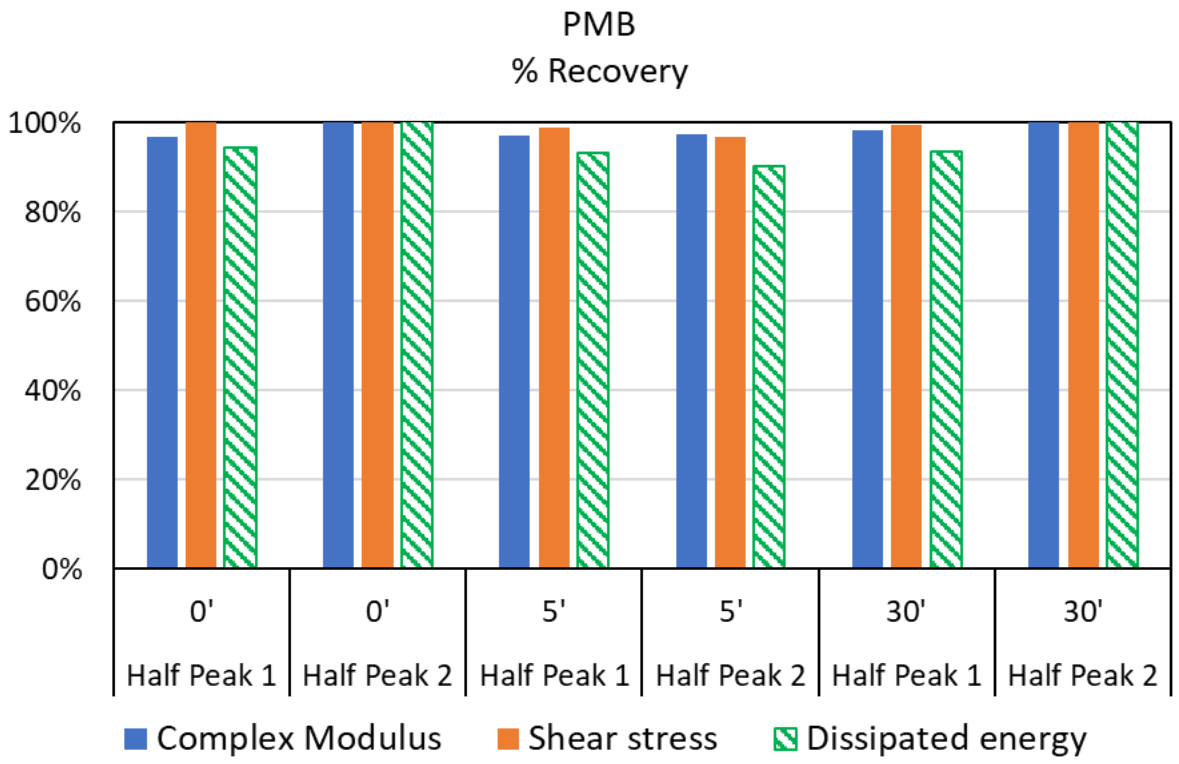

Figure 1.7.3. Summary of total recovery based on complex modulus, shear stress and dissipated energy at half peak stress for PMB. [Data from Waterloo].

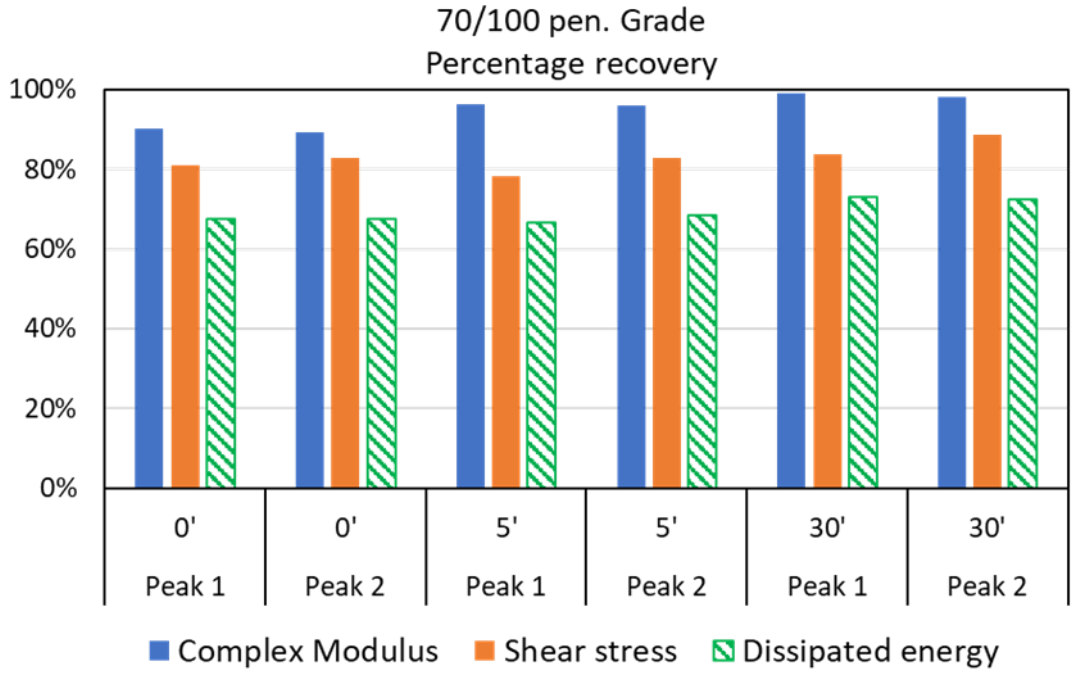

Figure 1.7.4. Summary of total recovery based on complex modulus, shear stress and dissipated energy at peak stress for 70/100 binder. [Data from Torino].

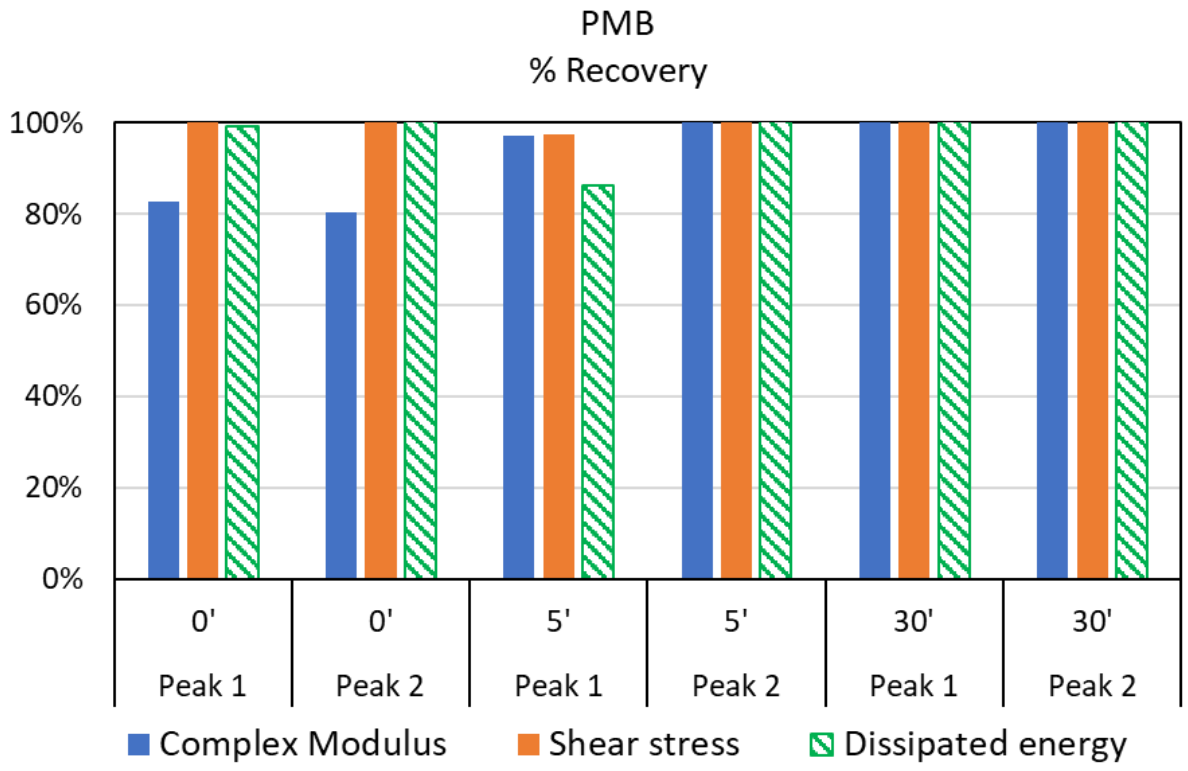

Figure 1.7.5. Summary of total recovery based on complex modulus, shear stress and dissipated energy at peak stress for PMB. [Data from Waterloo].

2. Tension-Compression tests on Bituminous mixtures performed at ENTPE

2.1. Evolution of 3D LVE properties with strain amplitude and temperature

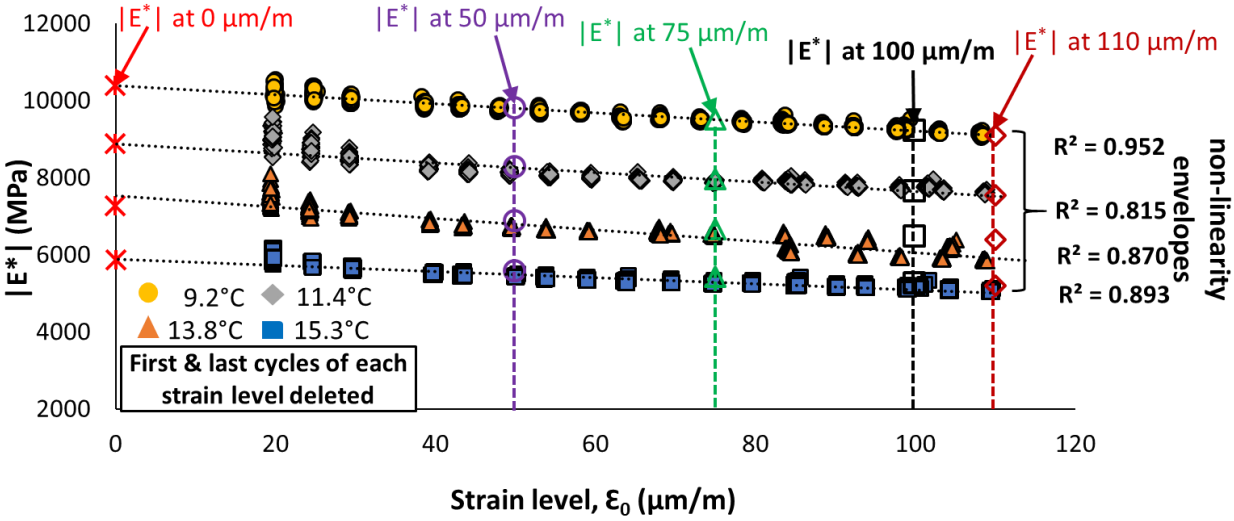

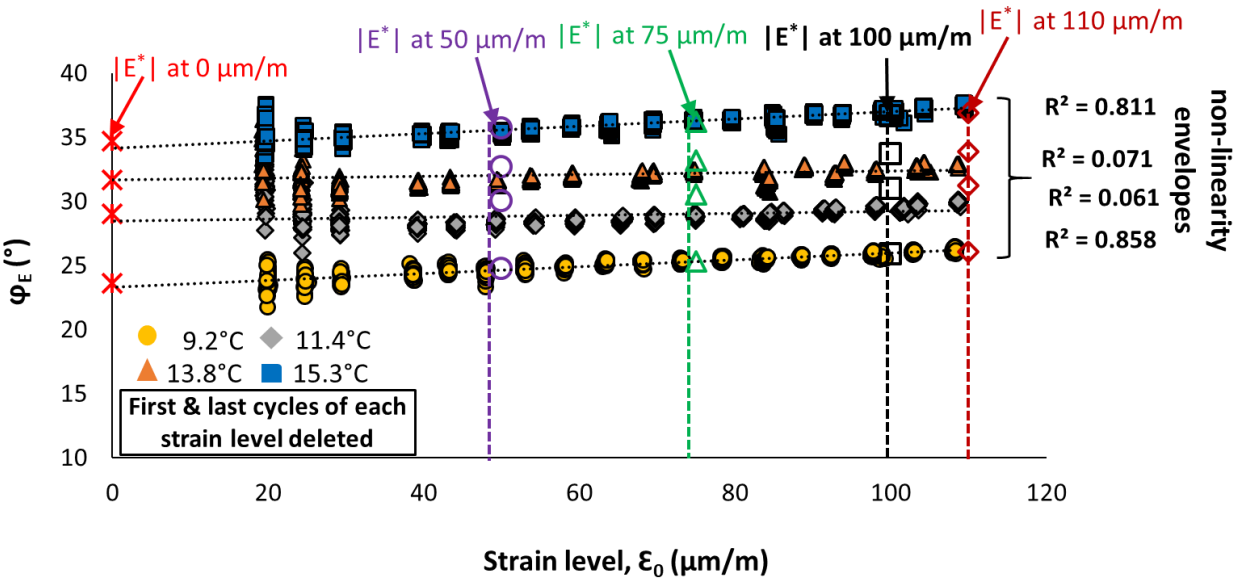
|E*| at 0 µm/m
|E*| at 50 µm/m
|E*| at 75 µm/m
|E*| at 100 µm/m
|E*| at 110 µm/m
φE (°)
Strain level, ε0 (µm/m)
9.2°C
11.4°C
13.8°C
15.3°C
First & last cycles of each strain level deleted
R² = 0.811
R² = 0.071
R² = 0.061
R² = 0.858
non-linearity envelopes

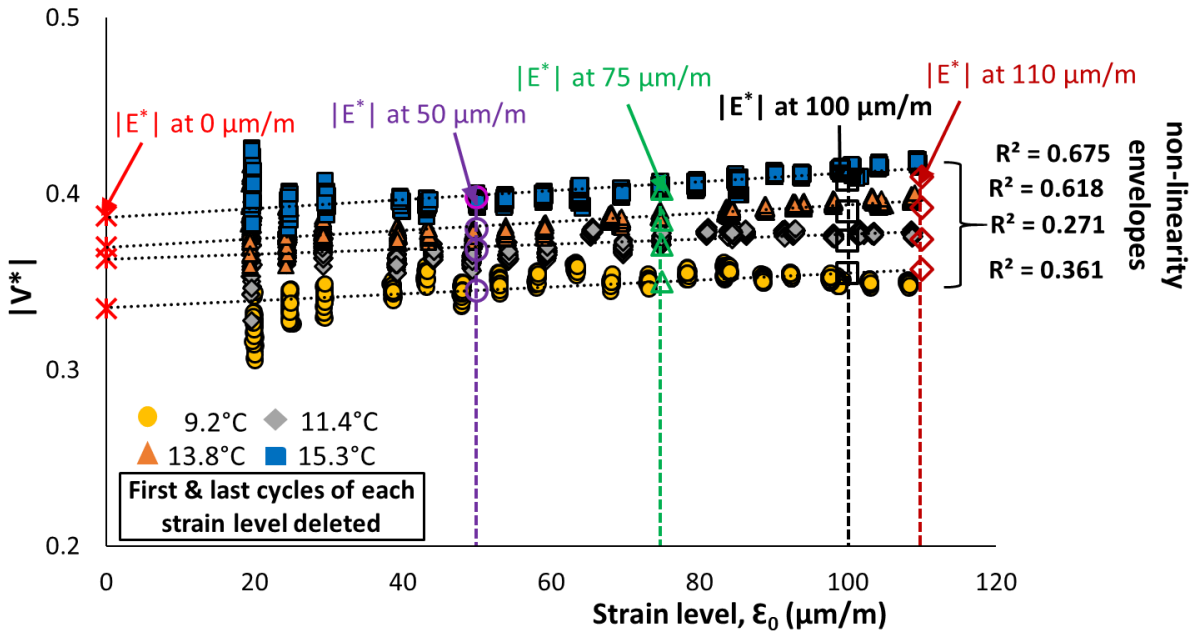
|E*| at 0 µm/m
|E*| at 50 µm/m
|E*| at 75 µm/m
|E*| at 100 µm/m
|E*| at 110 µm/m
|E*|
Strain level, ε0 (µm/m)
9.2°C
11.4°C
13.8°C
15.3°C
First & last cycles of each strain level deleted
R² = 0.675
R² = 0.618
R² = 0.271
R² = 0.361
non-linearity envelopes

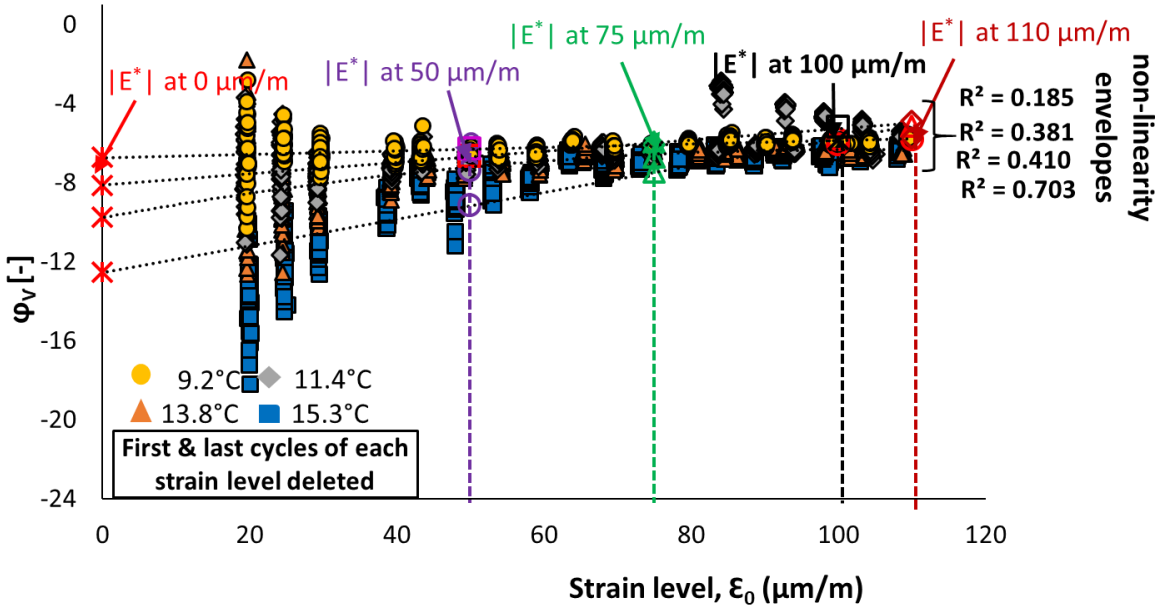

2.1.1. CMT results obtained for Mix 70/100 - 1: |E*|, φ_E, |v*| and φ_v against applied strain amplitude at different temperatures.

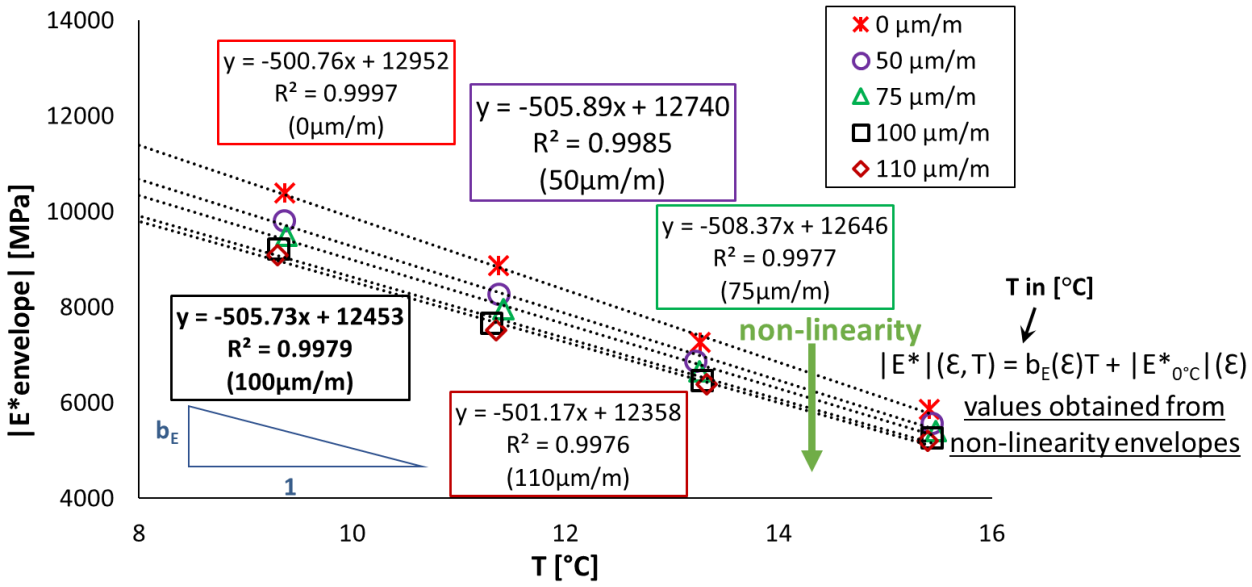

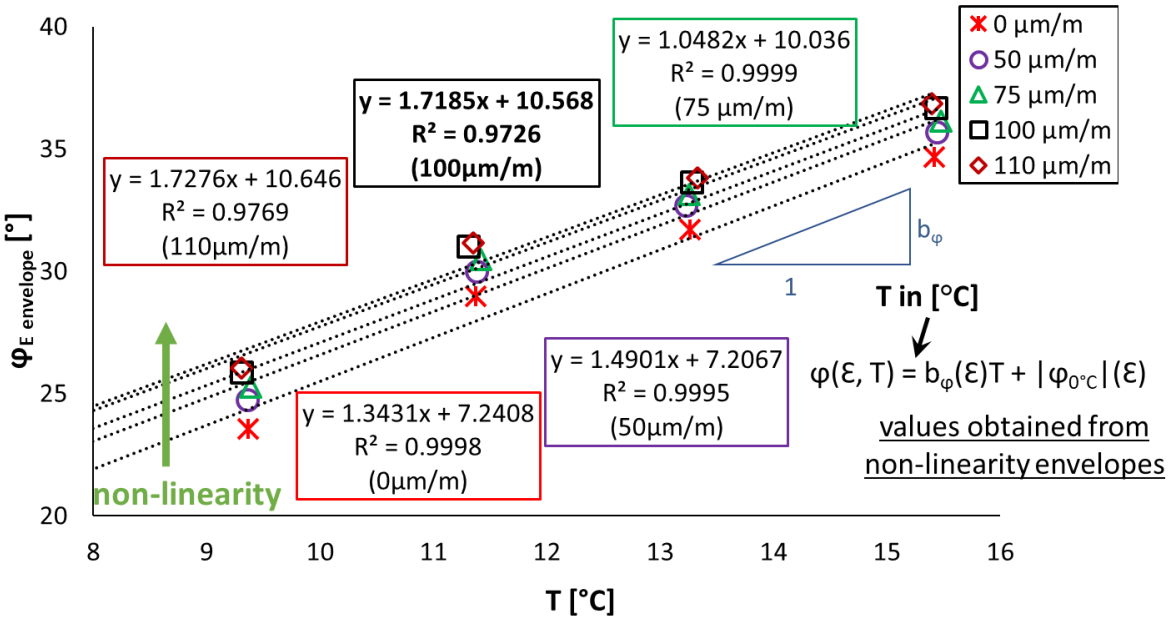
40
35
30
25
20
8
9
10
11
12
13
14
15
16
φE envelope [°]
T [°C]
y = 1.7276x + 10.646
R² = 0.9769
(110µm/m)
y = 1.7185x + 10.568
R² = 0.9726
(100µm/m)
y = 1.0482x + 10.036
R² = 0.9999
(75 µm/m)
y = 1.4901x + 7.2067
R² = 0.9995
(50µm/m)
y = 1.3431x + 7.2408
R² = 0.9998
(0µm/m)
0 µm/m
50 µm/m
75 µm/m
100 µm/m
110 µm/m
bφ
1
T in [°C]
φ(Ɛ, T) = bφ(Ɛ)T + |φ0°C|(Ɛ)
values obtained from
non-linearity envelopes
non-linearity

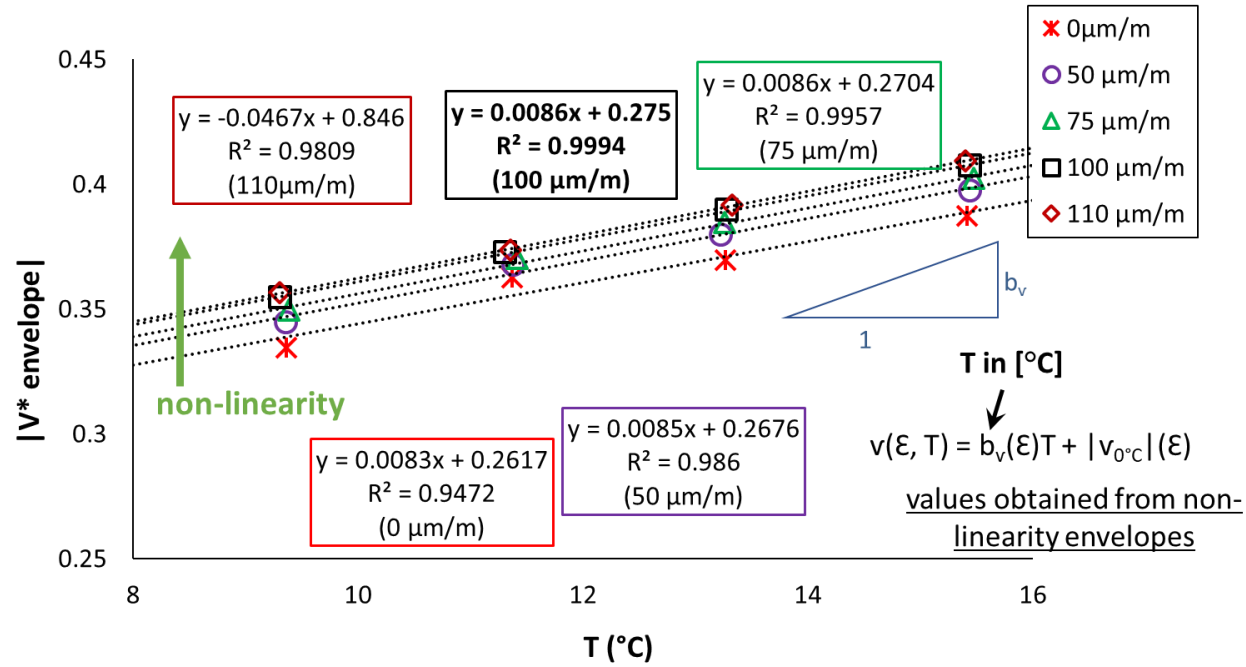
0.45
0.4
0.35
0.3
0.25
8
10
12
14
16
|V* envelope|
T (°C)
y = -0.0467x + 0.846
R² = 0.9809
(110µm/m)
y = 0.0086x + 0.275
R² = 0.9994
(100 µm/m)
y = 0.0086x + 0.2704
R² = 0.9957
(75 µm/m)
y = 0.0085x + 0.2676
R² = 0.986
(50 µm/m)
y = 0.0083x + 0.2617
R² = 0.9472
(0 µm/m)
0µm/m
50 µm/m
75 µm/m
100 µm/m
110 µm/m
bv
1
T in [°C]
v(Ɛ, T) = bv(Ɛ)T + |v0°C|(Ɛ)
values obtained from non-
linearity envelopes
non-linearity

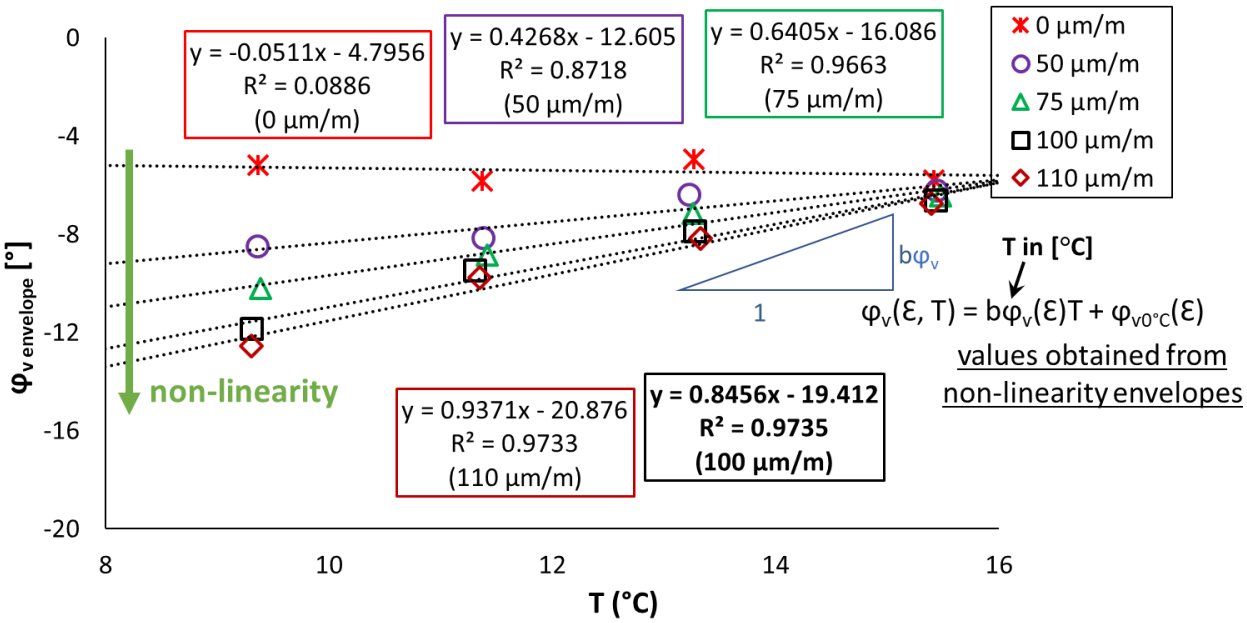

2.1.2. CMT results obtained for Mix 70/100 - 1: Regression of estimated values of |E*|, φ_E, |ν*| and φ_ν as a function of temperature.

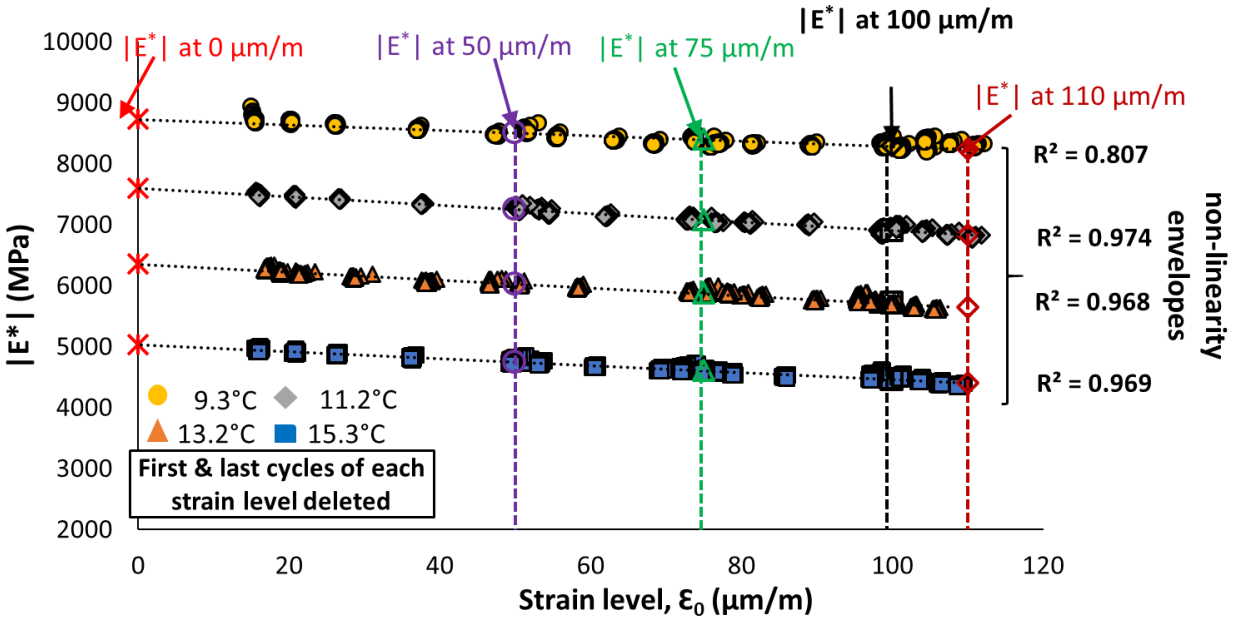

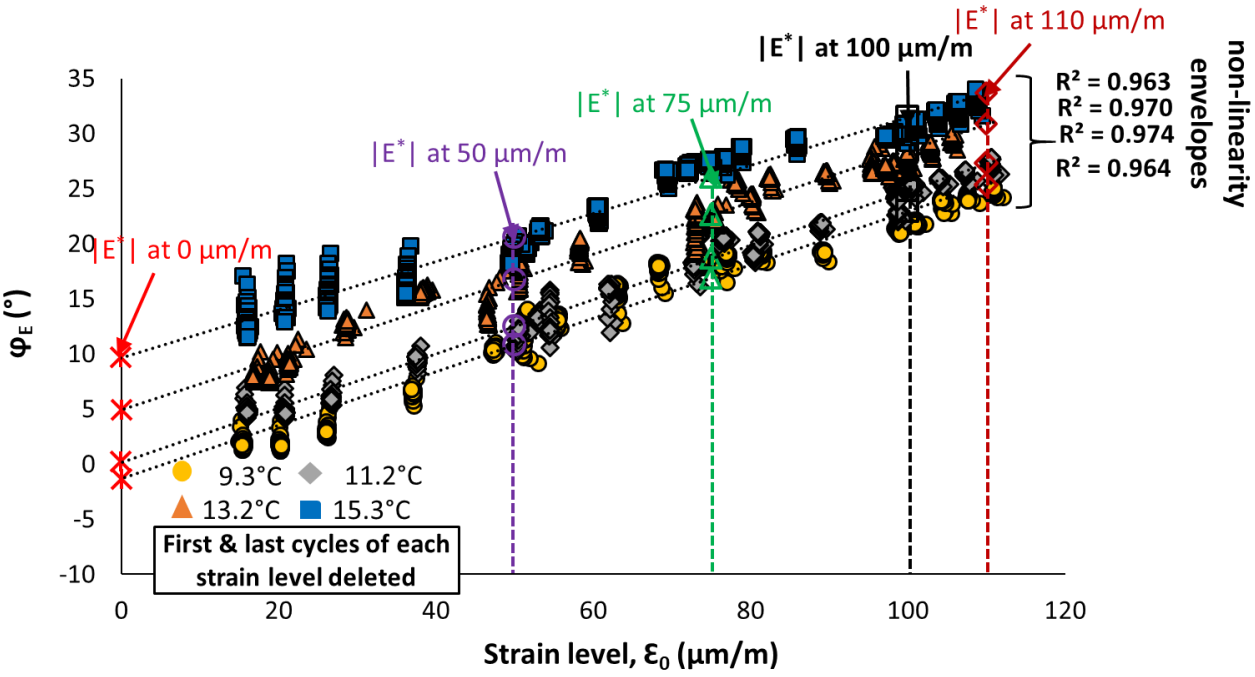

2.1.3. CMT results obtained for Mix 70/100 - 3: |E*|and φ_E against applied strain amplitude at different temperatures.

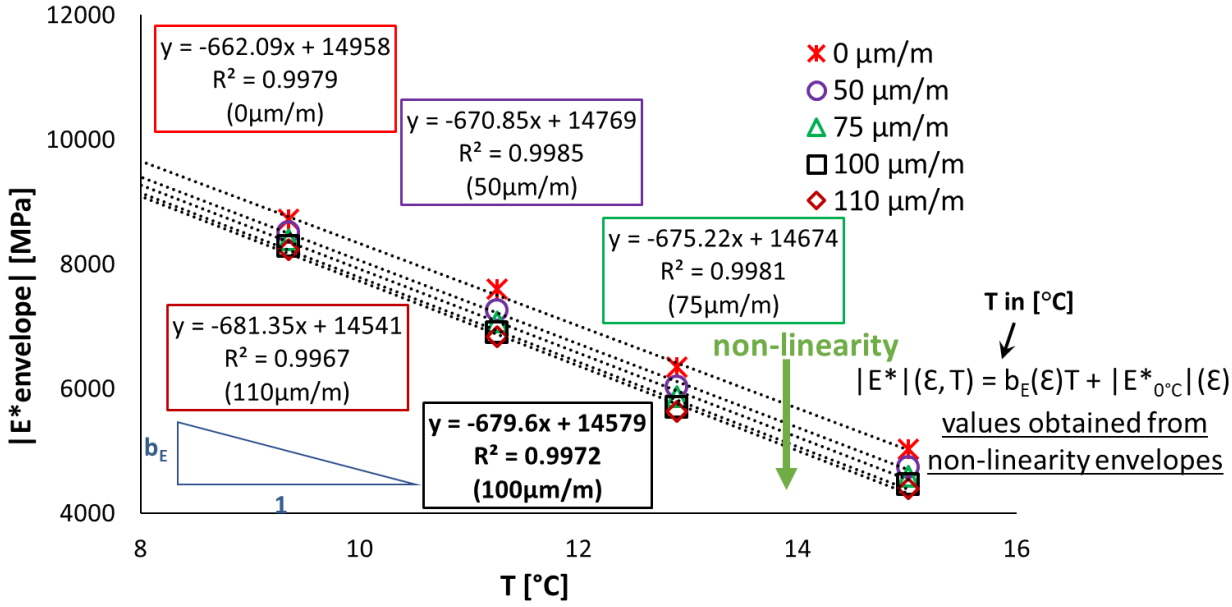

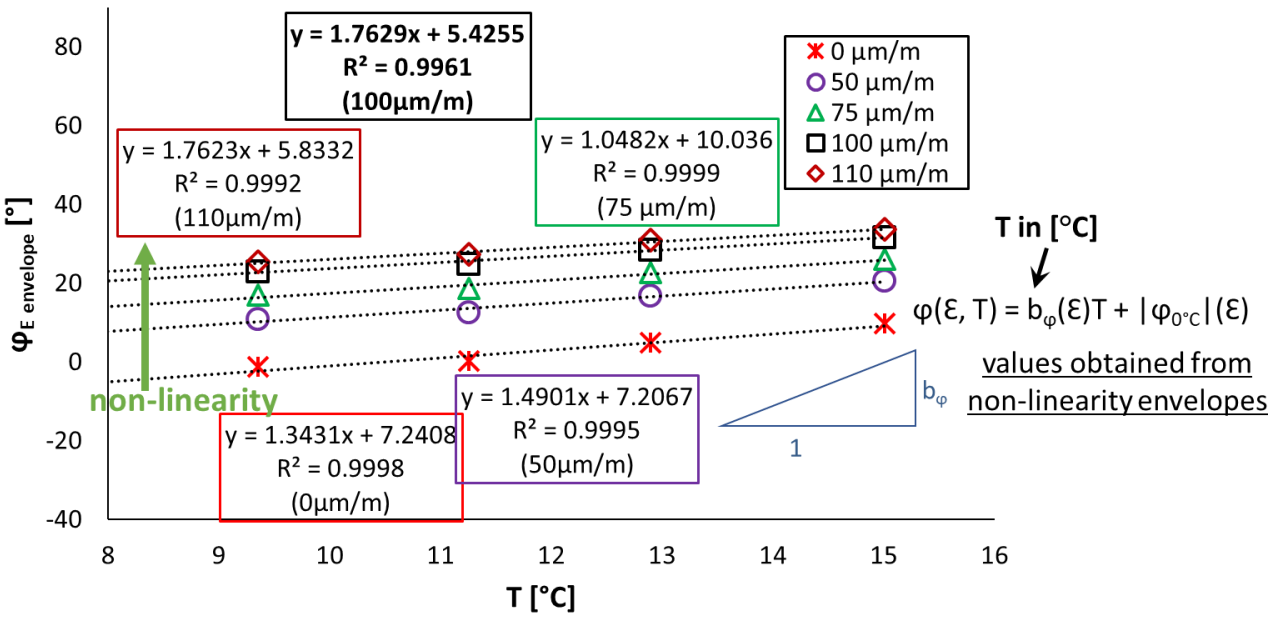

2.1.4. CMT results obtained for Mix 70/100 - 3: Regression of estimated values of |E*| and φ_E as a function of temperature.

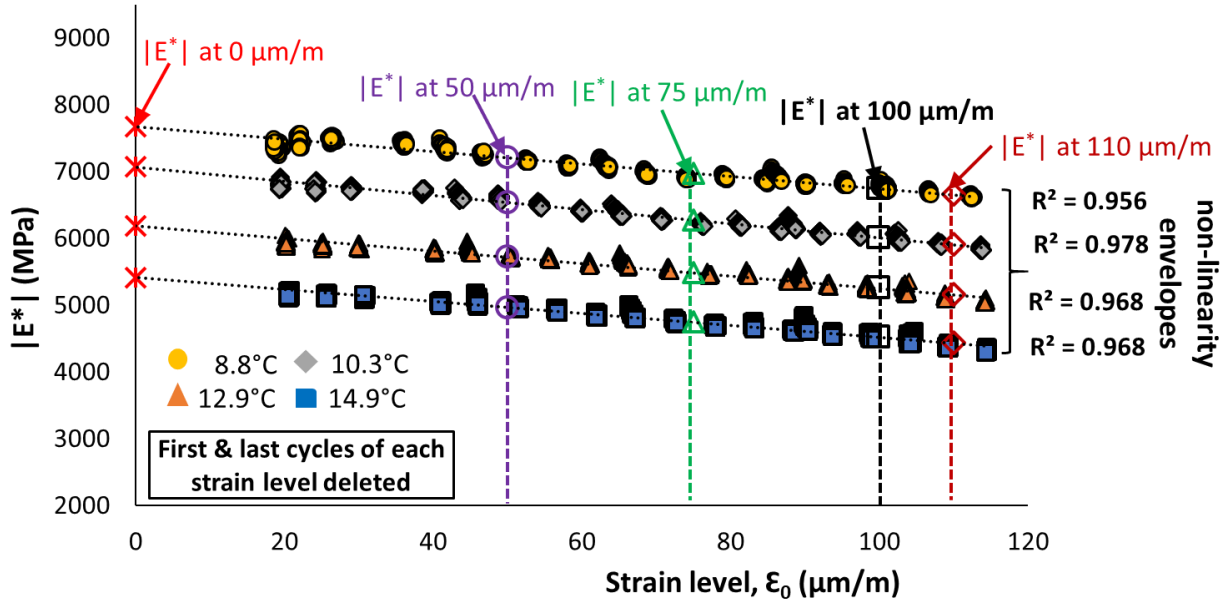

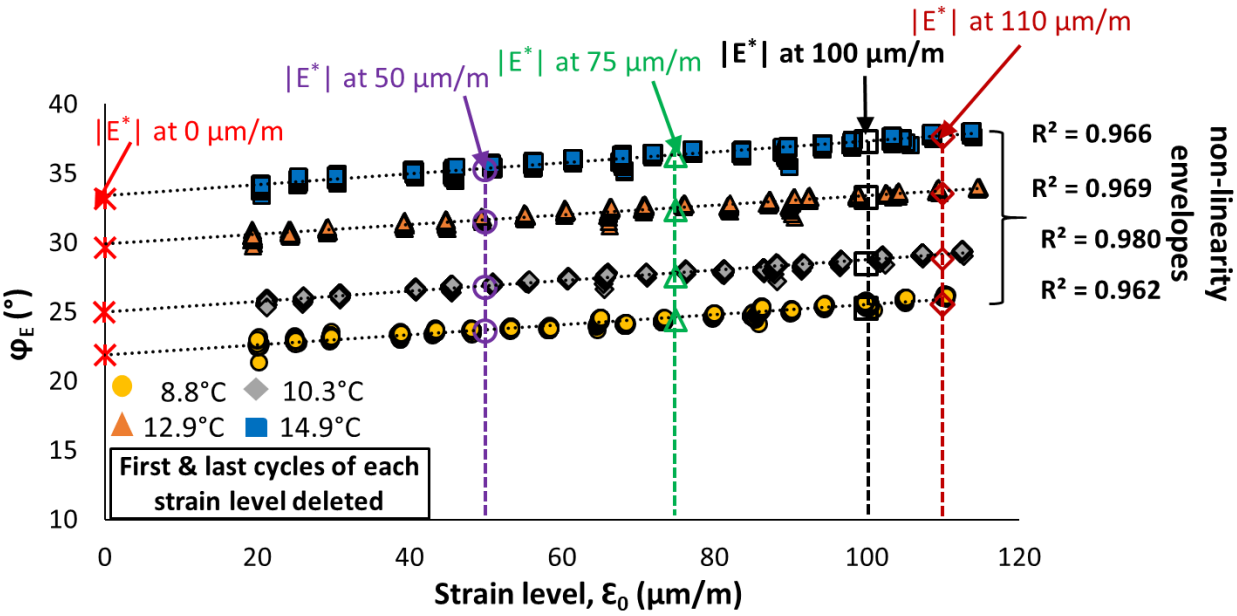
|E*| at 110 µm/m
|E*| at 50 µm/m
|E*| at 75 µm/m
|E*| at 100 µm/m
|E*| at 0 µm/m
R² = 0.966
R² = 0.969
R² = 0.980
R² = 0.962
non-linearity envelopes
8.8°C
10.3°C
12.9°C
14.9°C
First & last cycles of each strain level deleted
φE (°)
Strain level, ε0 (µm/m)

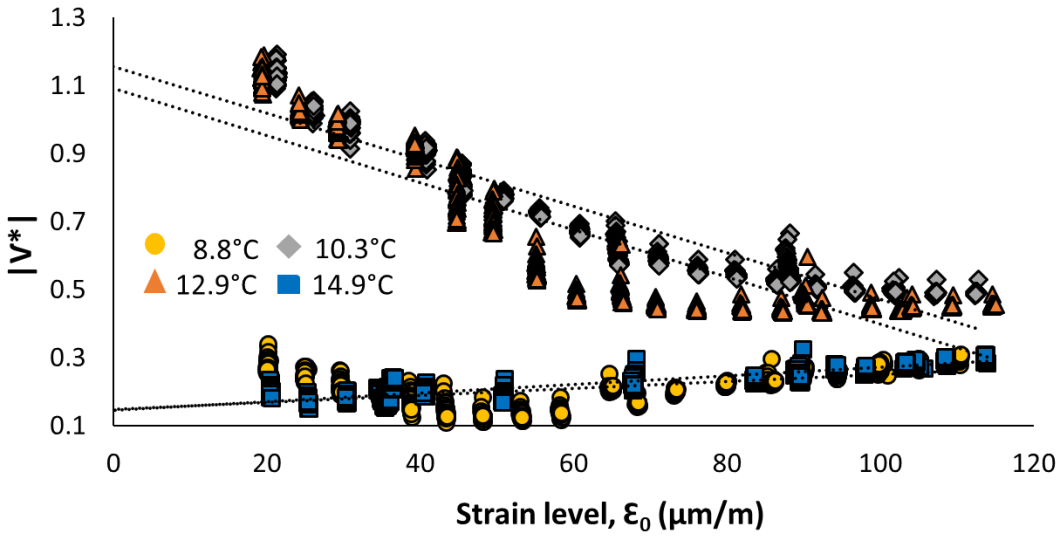
|V*|
8.8°C
10.3°C
12.9°C
14.9°C
Strain level, ε0 (µm/m)

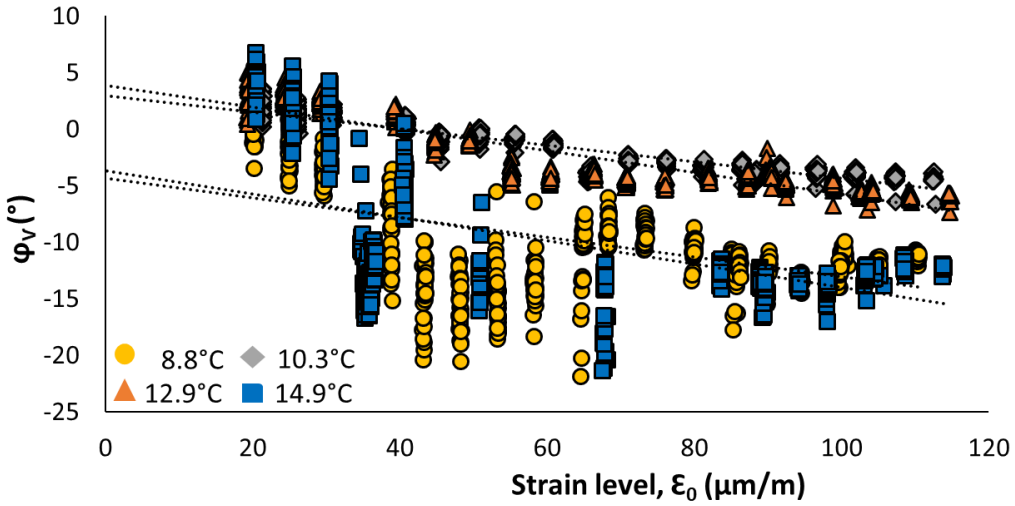

2.1.5. CMT results obtained for Mix 70/100 - 4: |E*|, φ_E, |ν*| and φν against applied strain amplitude at different temperatures.

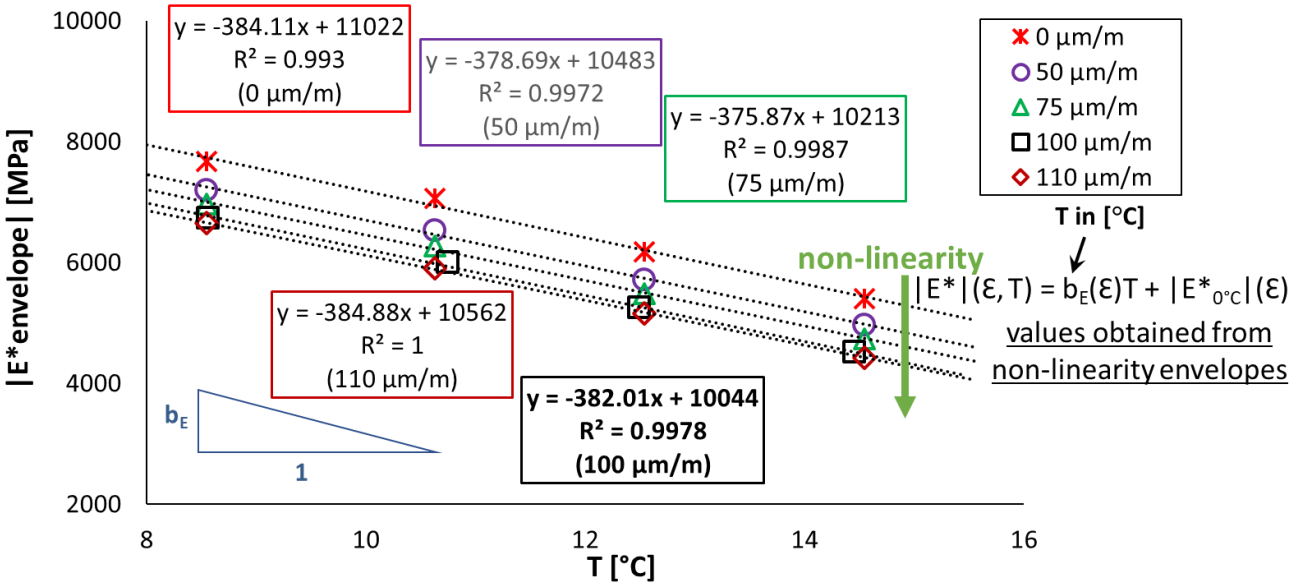

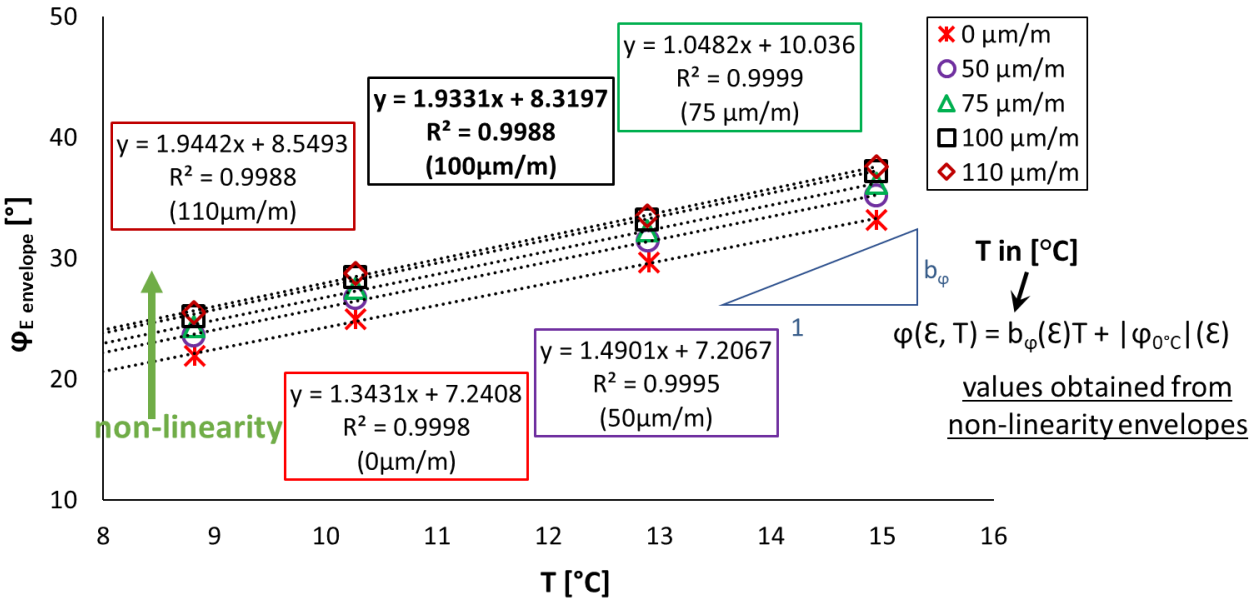

Figure 2.1.6. CMT results obtained for Mix 70/100 - 4: Regression of estimated values of |E*| and φ_E as a function of temperature.

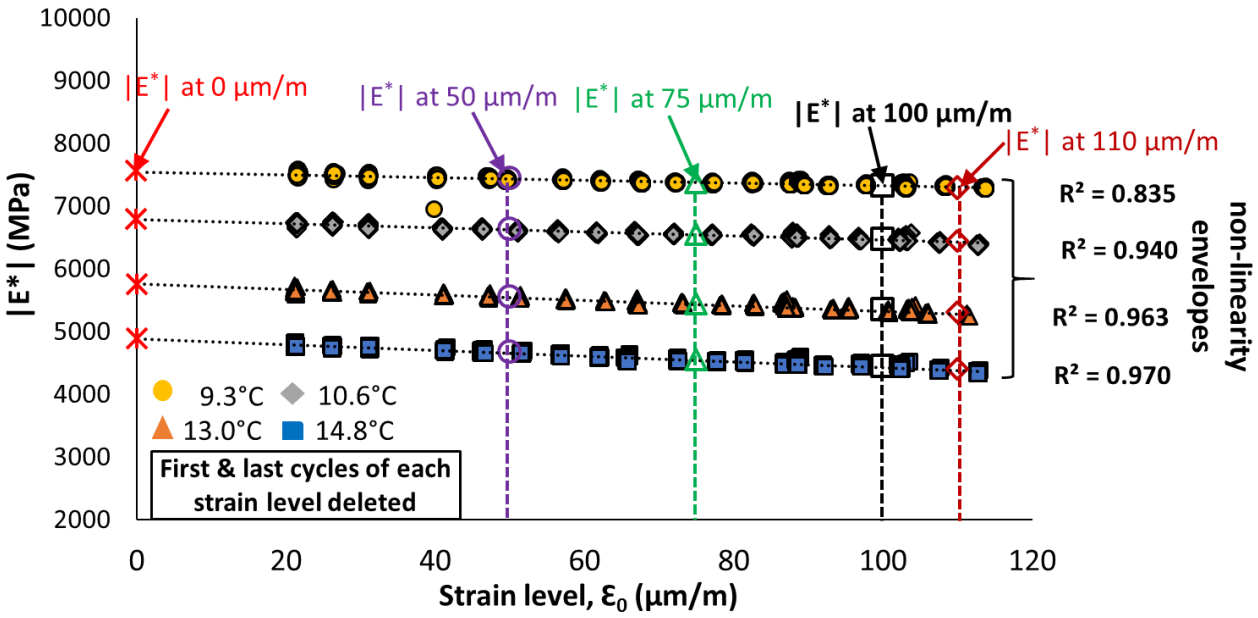

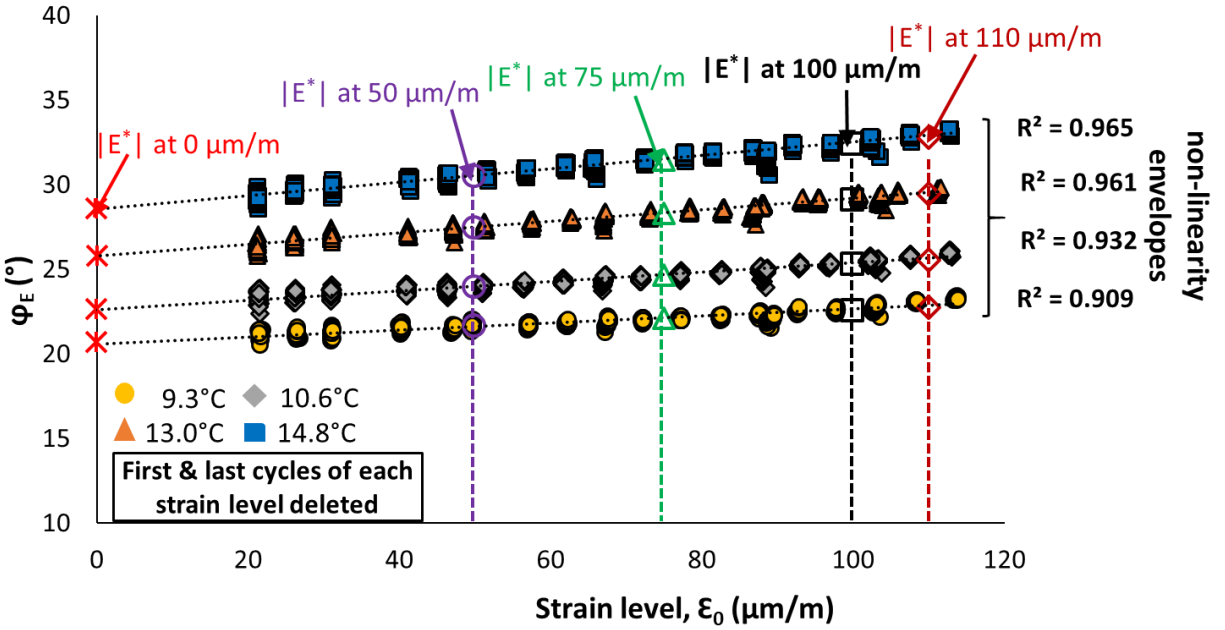
|E*| at 0 µm/m
|E*| at 50 µm/m
|E*| at 75 µm/m
|E*| at 100 µm/m
|E*| at 110 µm/m
φE (°)
40
35
30
25
20
15
10
0
20
40
60
80
100
120
Strain level, ε0 (µm/m)
9.3°C
10.6°C
13.0°C
14.8°C
First & last cycles of each strain level deleted
R² = 0.965
R² = 0.961
R² = 0.932
R² = 0.909
non-linearity envelopes

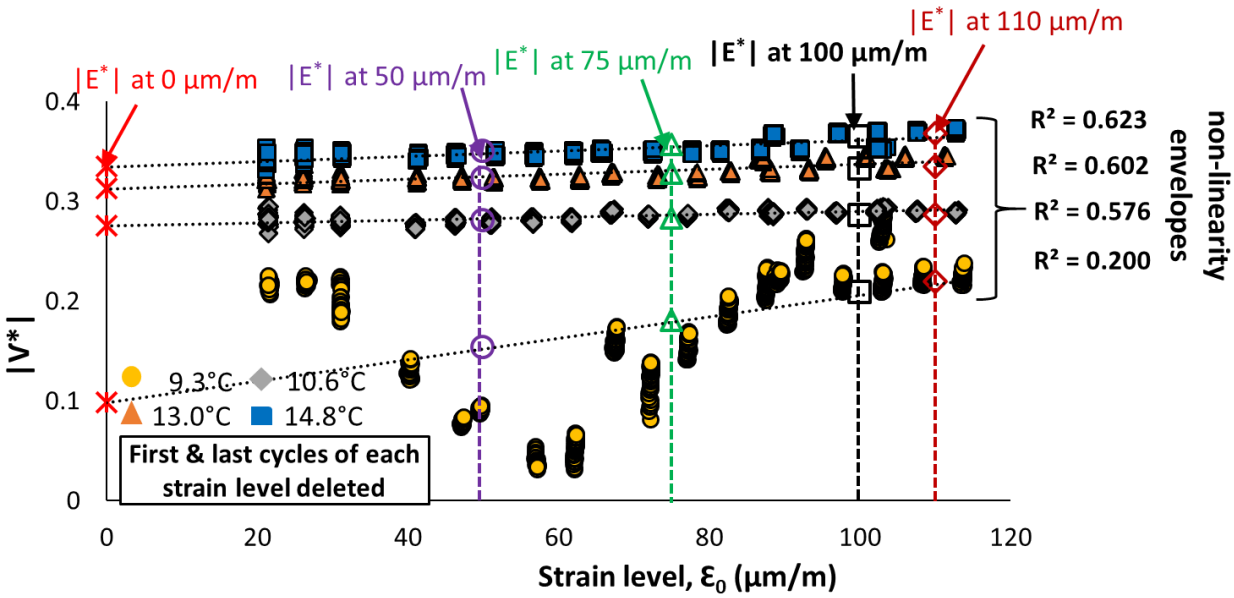
|E*| at 0 µm/m
|E*| at 50 µm/m
|E*| at 75 µm/m
|E*| at 100 µm/m
|E*| at 110 µm/m
|V*|
0.4
0.3
0.2
0.1
0
0
20
40
60
80
100
120
Strain level, ε0 (µm/m)
9.3°C
10.6°C
13.0°C
14.8°C
First & last cycles of each strain level deleted
R² = 0.623
R² = 0.602
R² = 0.576
R² = 0.200
non-linearity envelopes

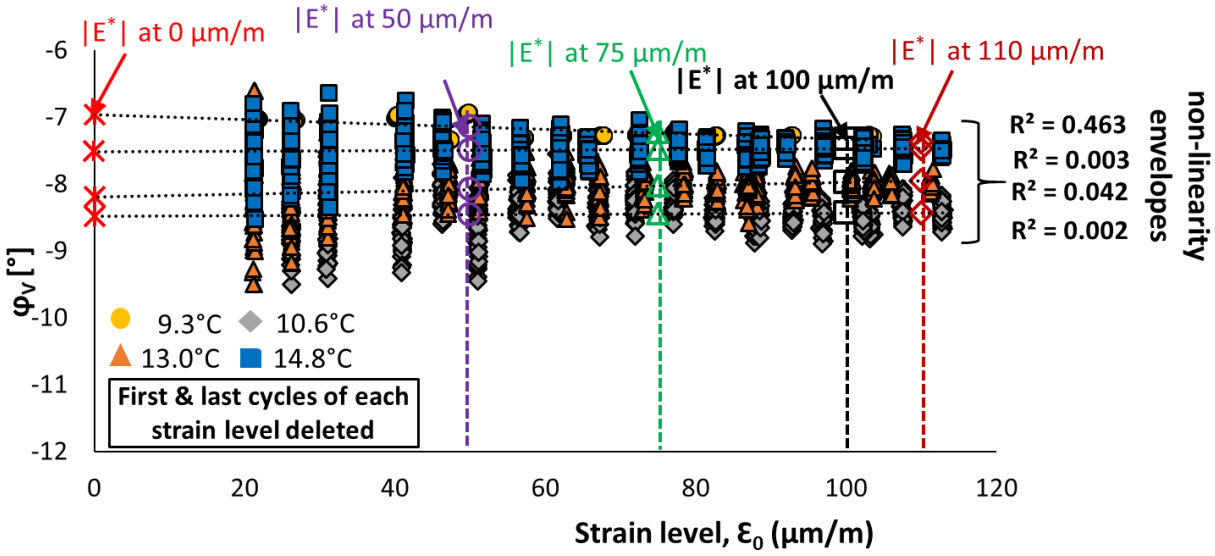

Figure 2.1.7. CMT results obtained for Mix 70/100 - 5: |E*|, φ_E, |ν*| and φ_ν against applied strain amplitude at different temperatures.

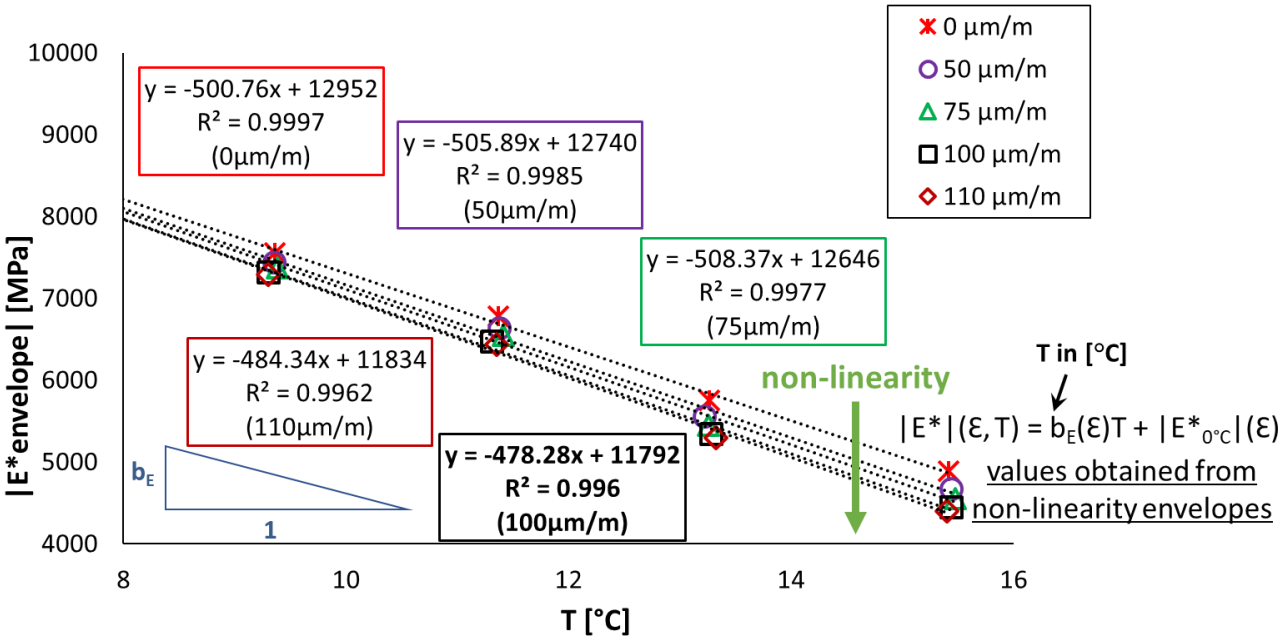

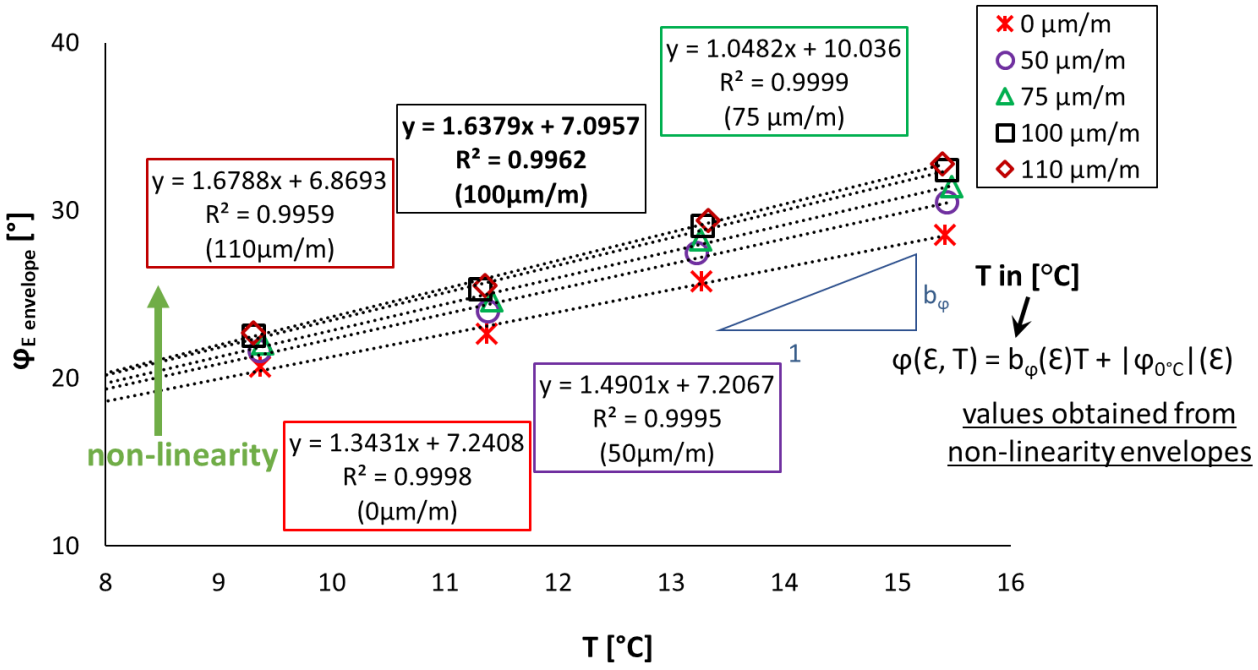
40
30
20
10
8
9
10
11
12
13
14
15
16
T [°C]
φE envelope [°]
y = 1.6788x + 6.8693
R² = 0.9959
(110µm/m)
y = 1.6379x + 7.0957
R² = 0.9962
(100µm/m)
y = 1.0482x + 10.036
R² = 0.9999
(75 µm/m)
y = 1.4901x + 7.2067
R² = 0.9995
(50µm/m)
y = 1.3431x + 7.2408
R² = 0.9998
(0µm/m)
non-linearity
bφ
1
0 µm/m
50 µm/m
75 µm/m
100 µm/m
110 µm/m
T in [°C]
φ(Ɛ, T) = bφ(Ɛ)T + |φ0°C|(Ɛ)
values obtained from
non-linearity envelopes

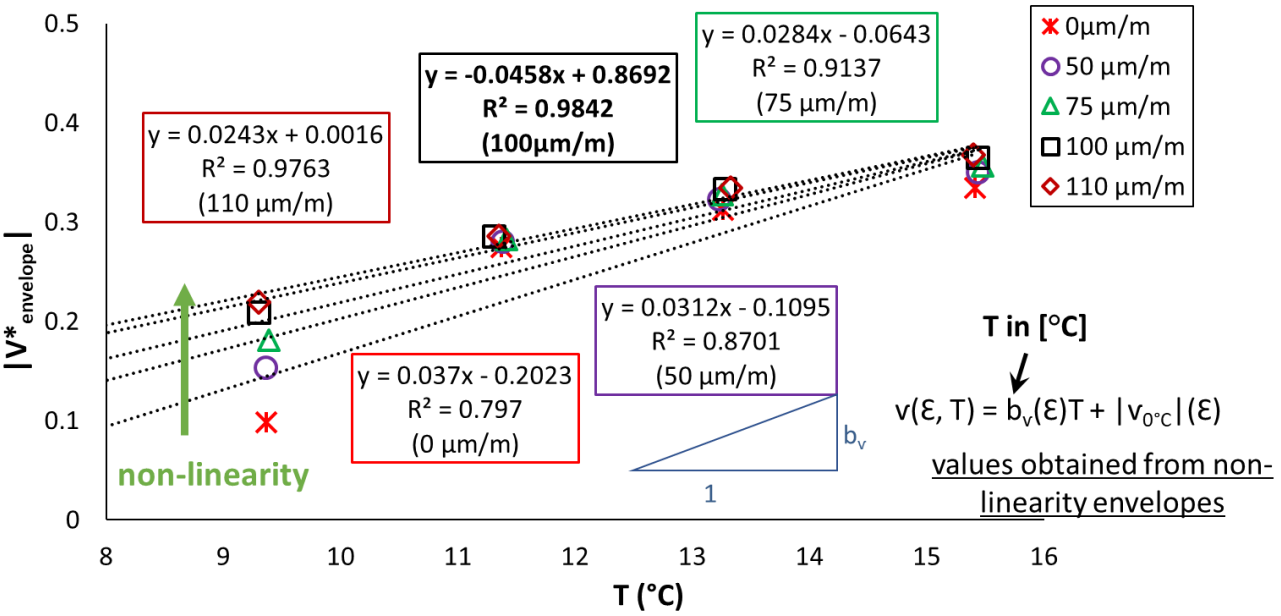
0.5
0.4
0.3
0.2
0.1
0
8
9
10
11
12
13
14
15
16
T (°C)
|V* envelope|
y = 0.0243x + 0.0016
R² = 0.9763
(110 µm/m)
y = -0.0458x + 0.8692
R² = 0.9842
(100µm/m)
y = 0.0284x - 0.0643
R² = 0.9137
(75 µm/m)
y = 0.037x - 0.2023
R² = 0.797
(0 µm/m)
y = 0.0312x - 0.1095
R² = 0.8701
(50 µm/m)
non-linearity
bv
1
0µm/m
50 µm/m
75 µm/m
100 µm/m
110 µm/m
T in [°C]
v(Ɛ, T) = bv(Ɛ)T + |v0°C|(Ɛ)
values obtained from non-
linearity envelopes

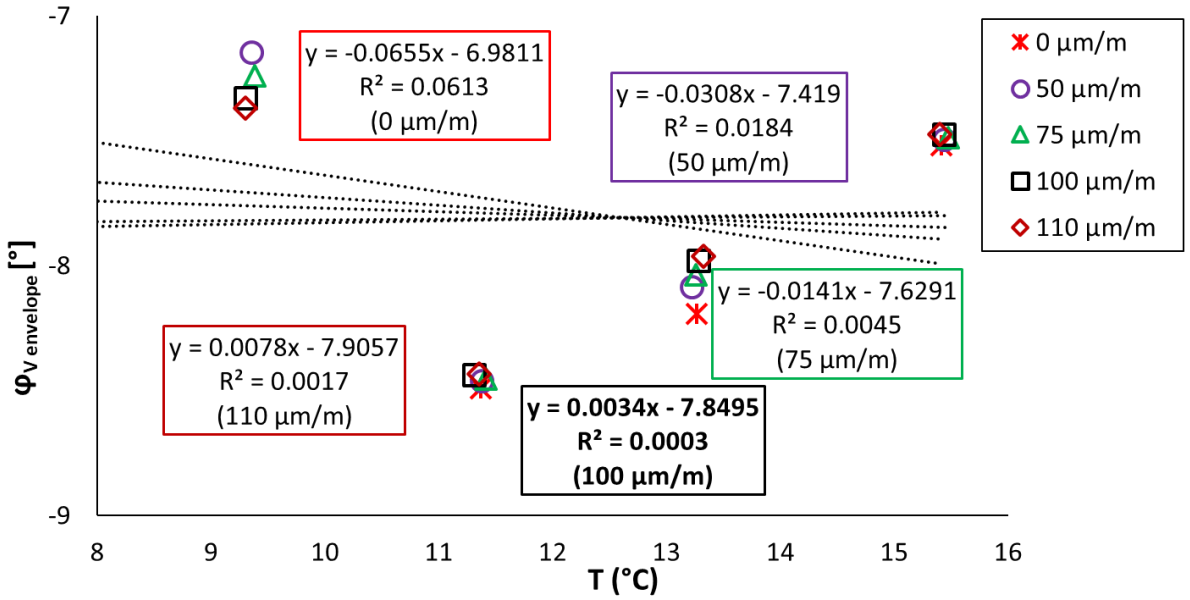

Figure 2.1.8. CMT results obtained for Mix 70/100 - 5: Regression of estimated values of |E*|, φ_E, |ν*| and φ_ν as a function of temperature.

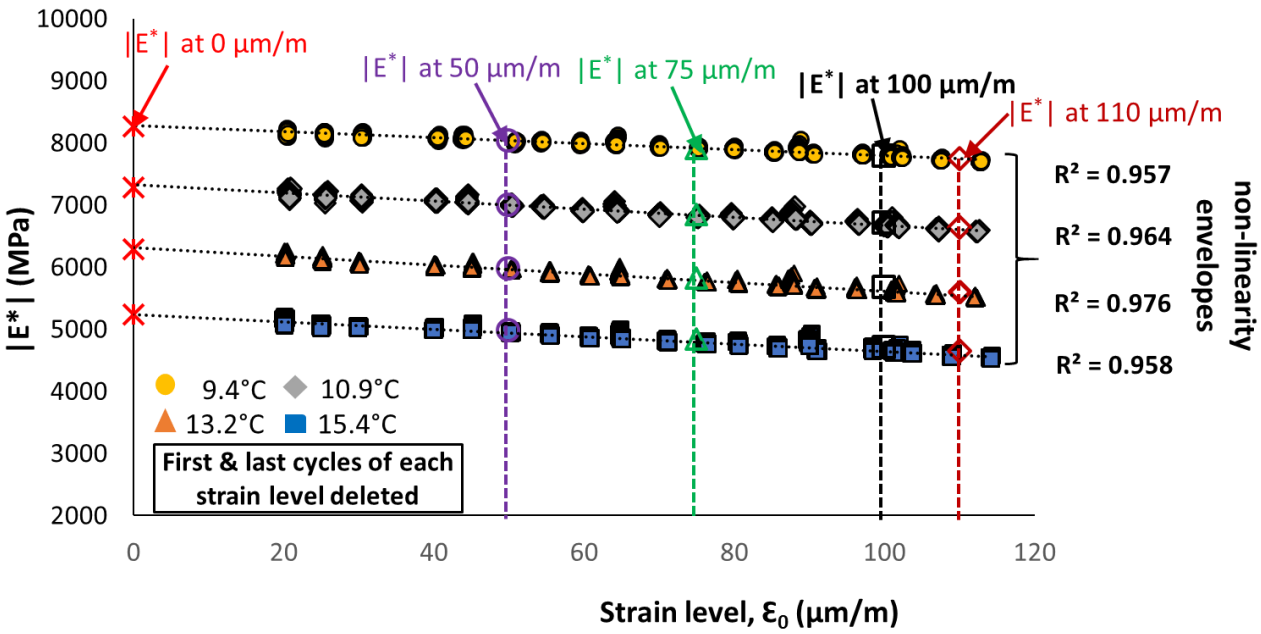

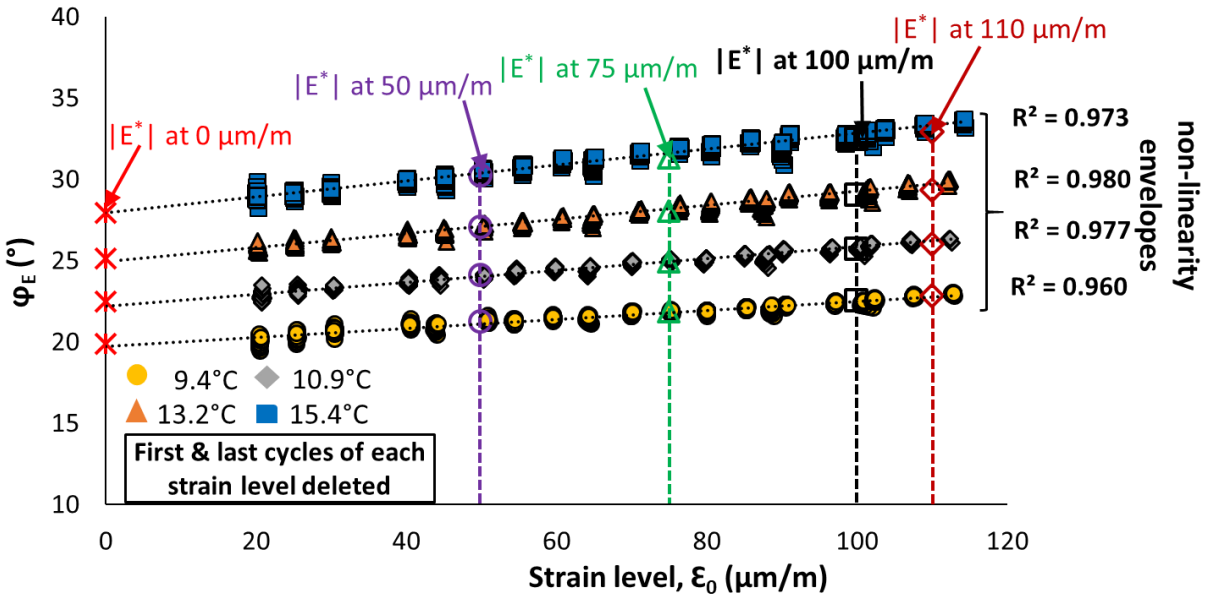
|E*| at 0 µm/m
|E*| at 50 µm/m
|E*| at 75 µm/m
|E*| at 100 µm/m
|E*| at 110 µm/m
φE (°)
Strain level, ε0 (µm/m)
9.4°C
10.9°C
13.2°C
15.4°C
First & last cycles of each strain level deleted
R² = 0.973
R² = 0.980
R² = 0.977
R² = 0.960
non-linearity envelopes

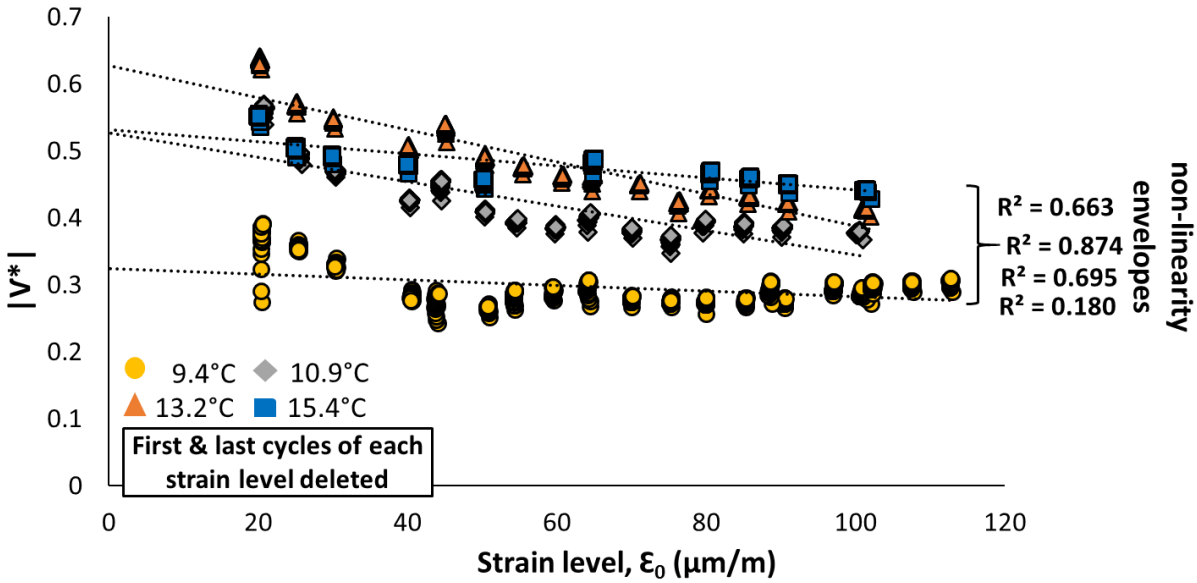
|E*|
Strain level, ε0 (µm/m)
9.4°C
10.9°C
13.2°C
15.4°C
First & last cycles of each strain level deleted
R² = 0.663
R² = 0.874
R² = 0.695
R² = 0.180
non-linearity envelopes

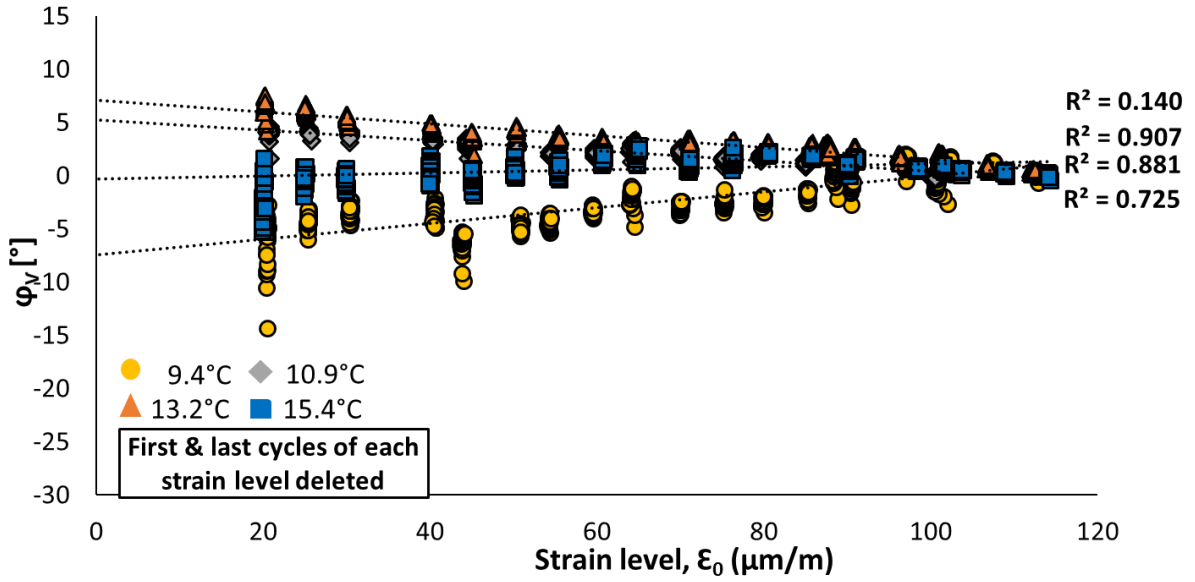

2.1.9. CMT results obtained for Mix 70/100 - 8: |E*|, φ_E, |ν*| and φ_ν against applied strain amplitude at different temperatures.

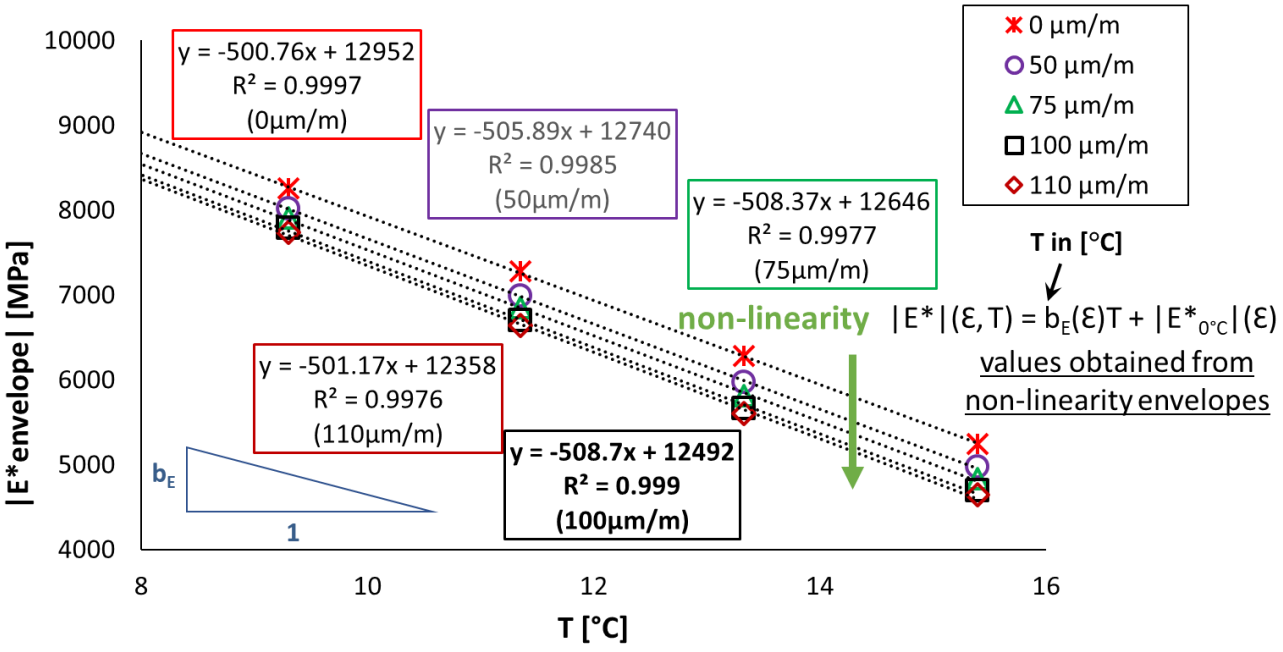

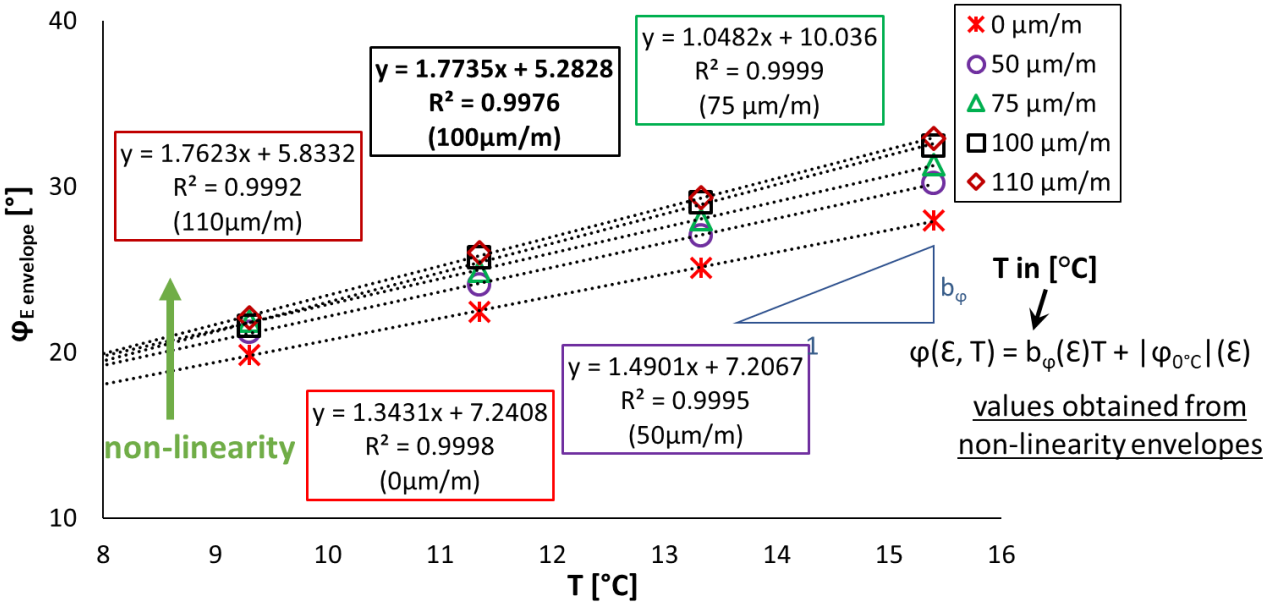

2.1.10. CMT results obtained for Mix 70/100 - 8: Regression of estimated values of |E*| and φ_E as a function of temperature.

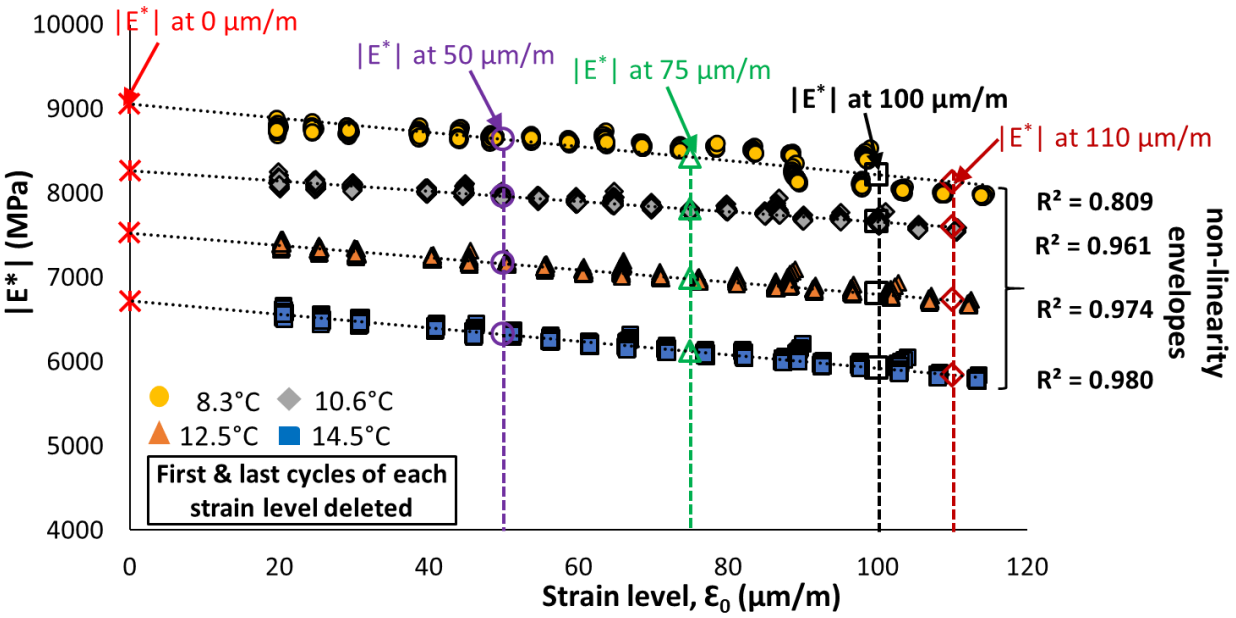

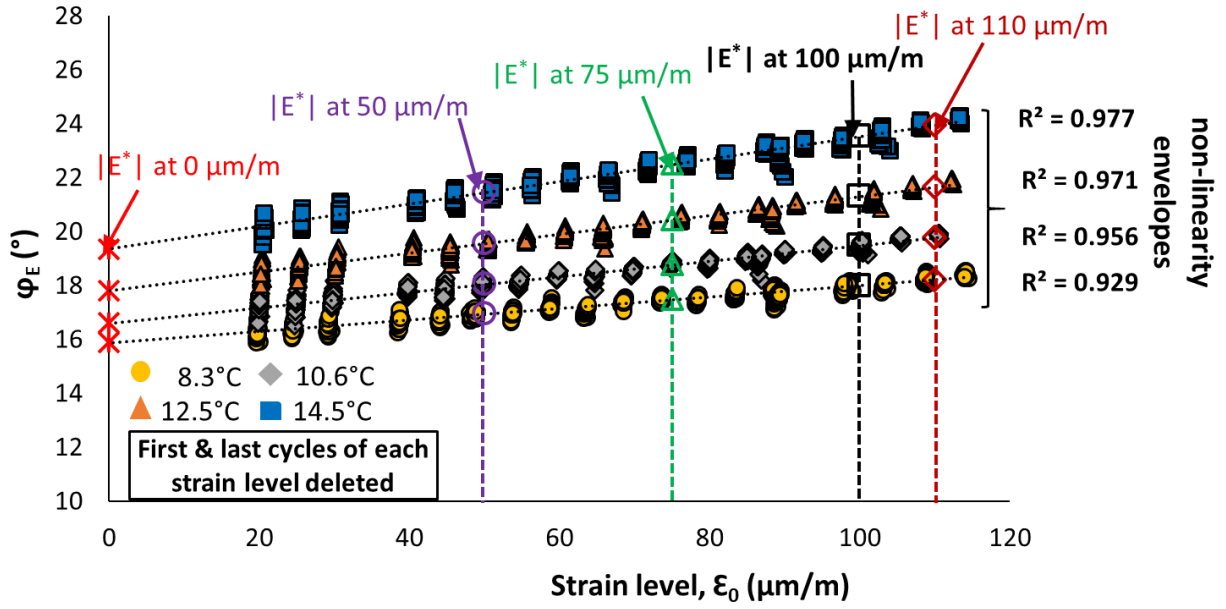
|E*| at 0 µm/m
|E*| at 50 µm/m
|E*| at 75 µm/m
|E*| at 100 µm/m
|E*| at 110 µm/m
R² = 0.977
R² = 0.971
R² = 0.956
R² = 0.929
non-linearity envelopes
8.3°C
10.6°C
12.5°C
14.5°C
First & last cycles of each strain level deleted
φE (°)
Strain level, ε0 (µm/m)

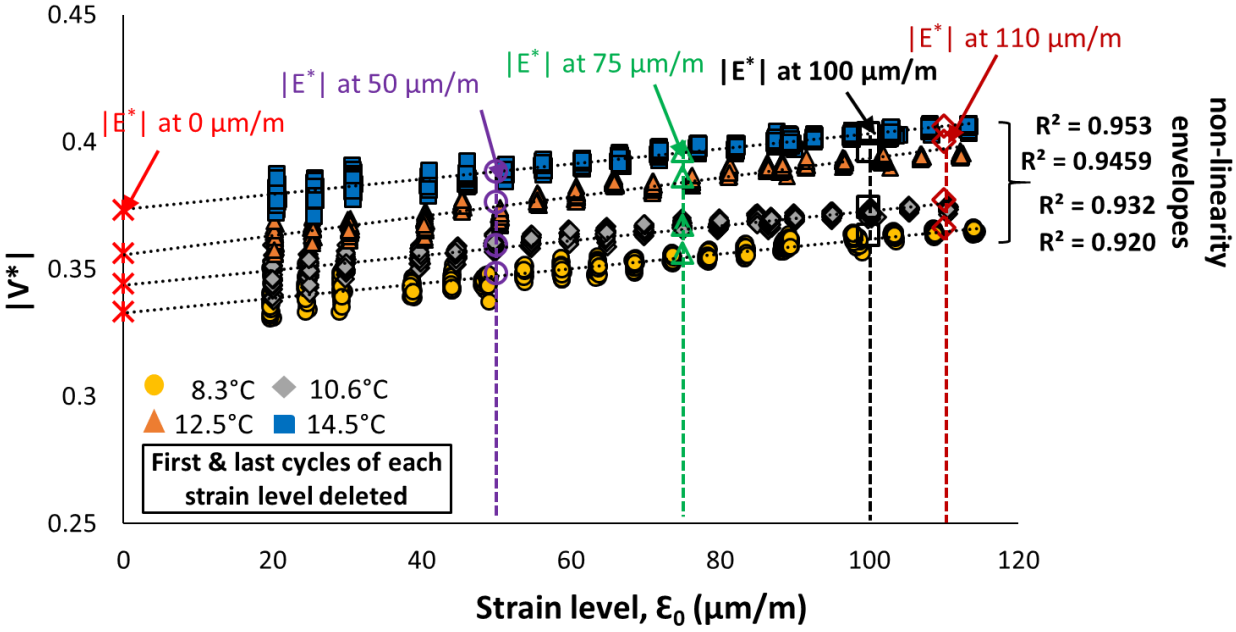
|E*| at 0 µm/m
|E*| at 50 µm/m
|E*| at 75 µm/m
|E*| at 100 µm/m
|E*| at 110 µm/m
R² = 0.953
R² = 0.9459
R² = 0.932
R² = 0.920
non-linearity envelopes
8.3°C
10.6°C
12.5°C
14.5°C
First & last cycles of each strain level deleted
|V*|
Strain level, ε0 (µm/m)

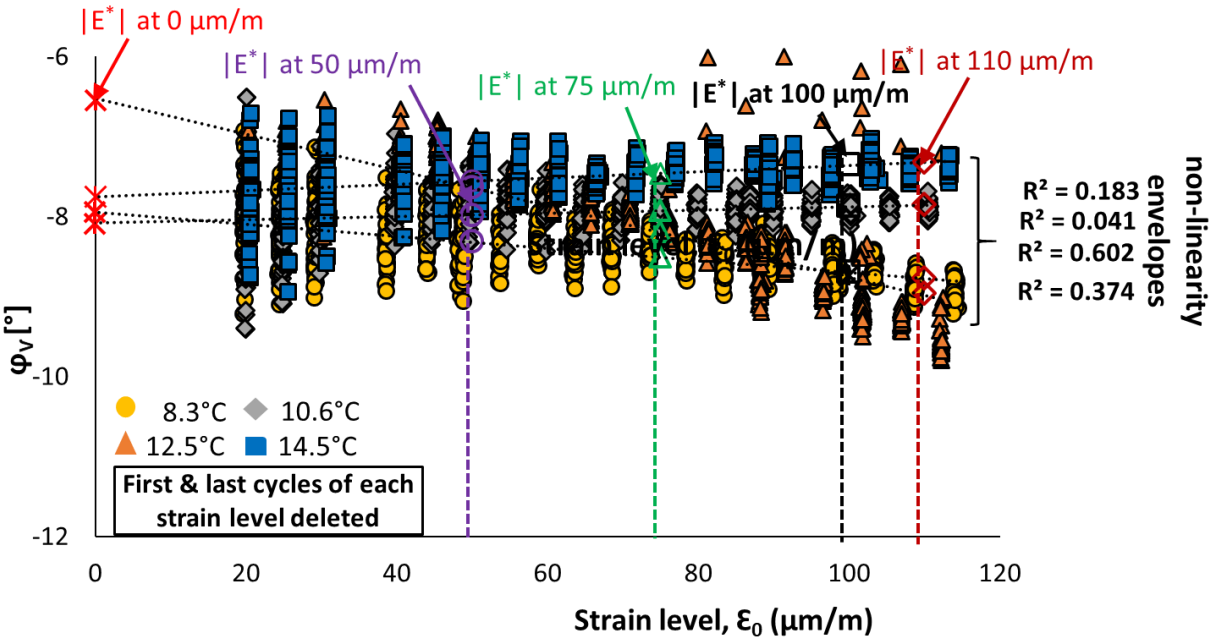

2.1.11. CMT results obtained for Mix 40/60 - 4: $|E^*|$, φ_E, $|\nu^*|$ and φ_ν as a function of temperature.

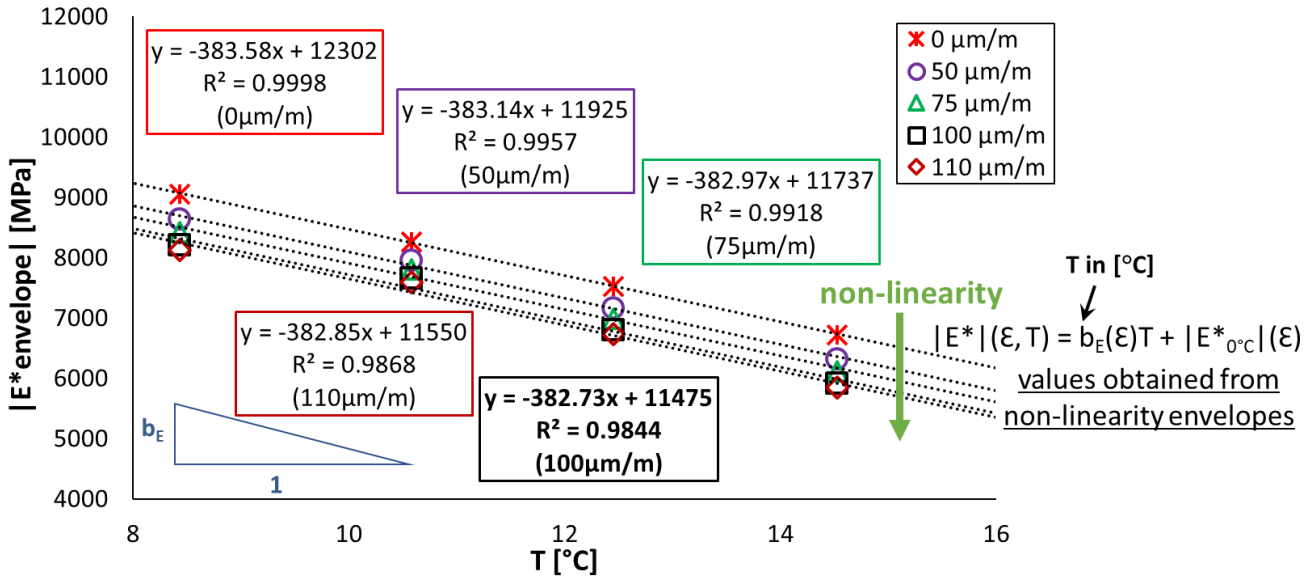

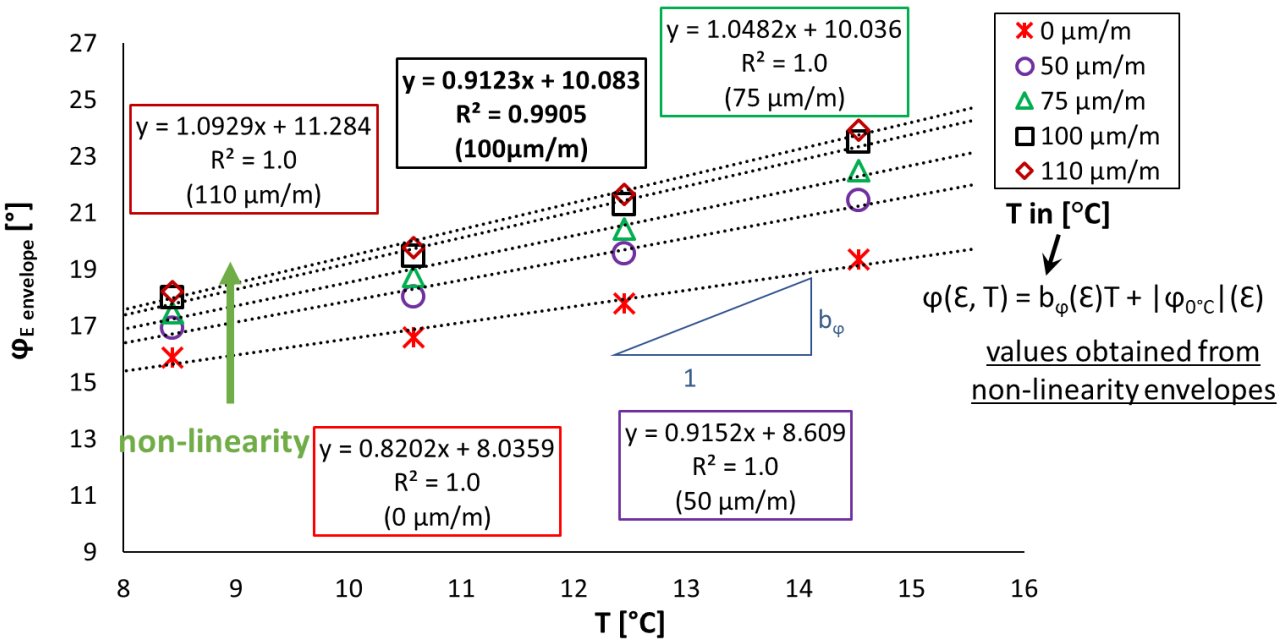
y = 1.0929x + 11.284
R² = 1.0
(110 µm/m)
y = 0.9123x + 10.083
R² = 0.9905
(100µm/m)
y = 1.0482x + 10.036
R² = 1.0
(75 µm/m)
0 µm/m
50 µm/m
75 µm/m
100 µm/m
110 µm/m
T in [°C]
φ(Ɛ, T) = b_φ(Ɛ)T + |φ_0°C|(Ɛ)
values obtained from non-linearity envelopes
b_φ
1
non-linearity
y = 0.8202x + 8.0359
R² = 1.0
(0 µm/m)
y = 0.9152x + 8.609
R² = 1.0
(50 µm/m)
φ_E envelope [°]
T [°C]

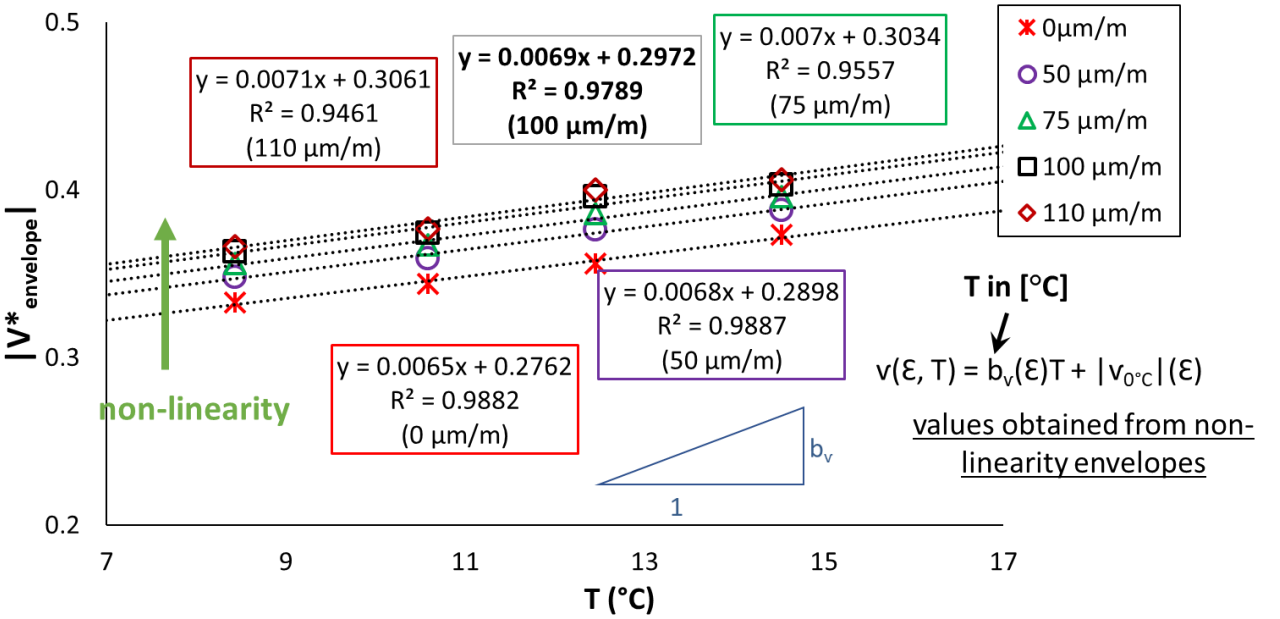
y = 0.0071x + 0.3061
R² = 0.9461
(110 µm/m)
y = 0.0069x + 0.2972
R² = 0.9789
(100 µm/m)
y = 0.007x + 0.3034
R² = 0.9557
(75 µm/m)
0µm/m
50 µm/m
75 µm/m
100 µm/m
110 µm/m
T in [°C]
v(Ɛ, T) = b_v(Ɛ)T + |v_0°C|(Ɛ)
values obtained from non-linearity envelopes
b_v
1
non-linearity
y = 0.0068x + 0.2898
R² = 0.9887
(50 µm/m)
y = 0.0065x + 0.2762
R² = 0.9882
(0 µm/m)
|V*_envelope|
T (°C)

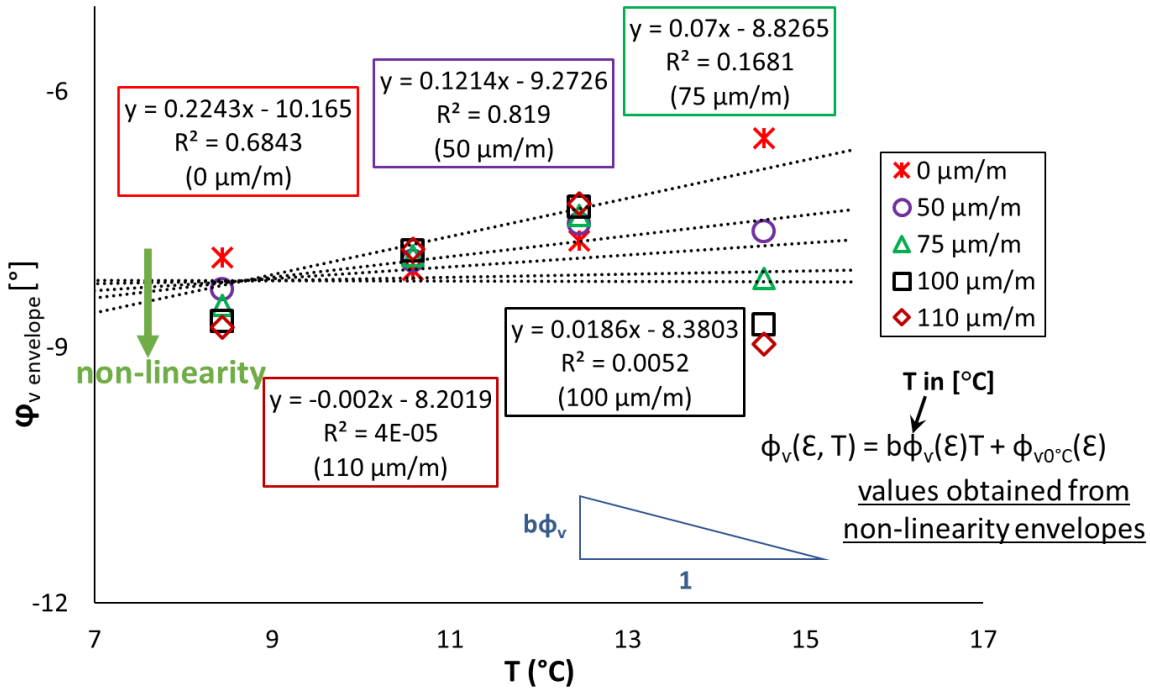

2.1.12. CMT results obtained for Mix 40/60 - 4: Regression of estimated values of |E*|, φ_E, |ν*| and φ_ν as a function of temperature.

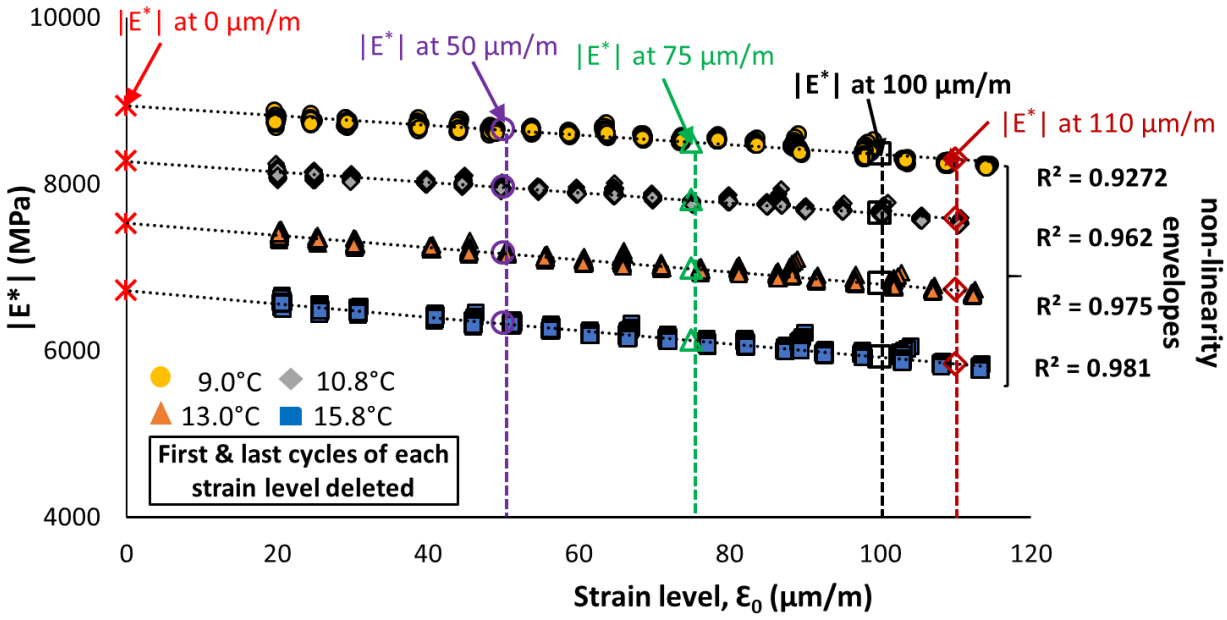

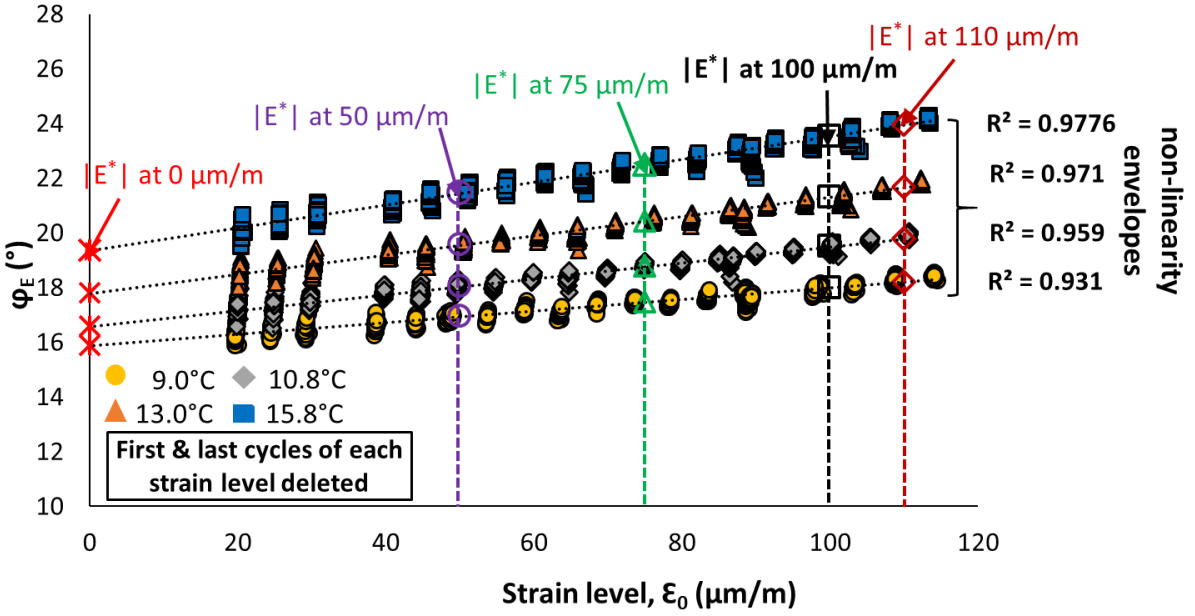
|E*| at 0 µm/m
|E*| at 50 µm/m
|E*| at 75 µm/m
|E*| at 100 µm/m
|E*| at 110 µm/m
R² = 0.9776
R² = 0.971
R² = 0.959
R² = 0.931
non-linearity envelopes
9.0°C
10.8°C
13.0°C
15.8°C
First & last cycles of each strain level deleted
φE (°)
Strain level, ε0 (µm/m)

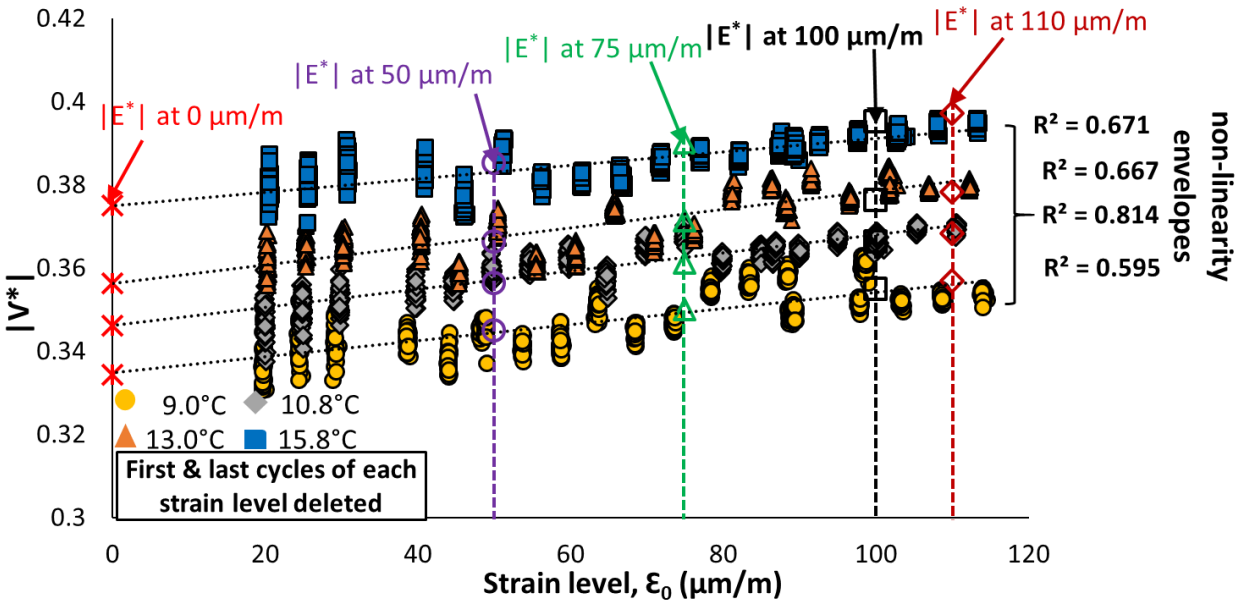
|E*| at 0 µm/m
|E*| at 50 µm/m
|E*| at 75 µm/m
|E*| at 100 µm/m
|E*| at 110 µm/m
R² = 0.671
R² = 0.667
R² = 0.814
R² = 0.595
non-linearity envelopes
9.0°C
10.8°C
13.0°C
15.8°C
First & last cycles of each strain level deleted
|V*|
Strain level, ε0 (µm/m)

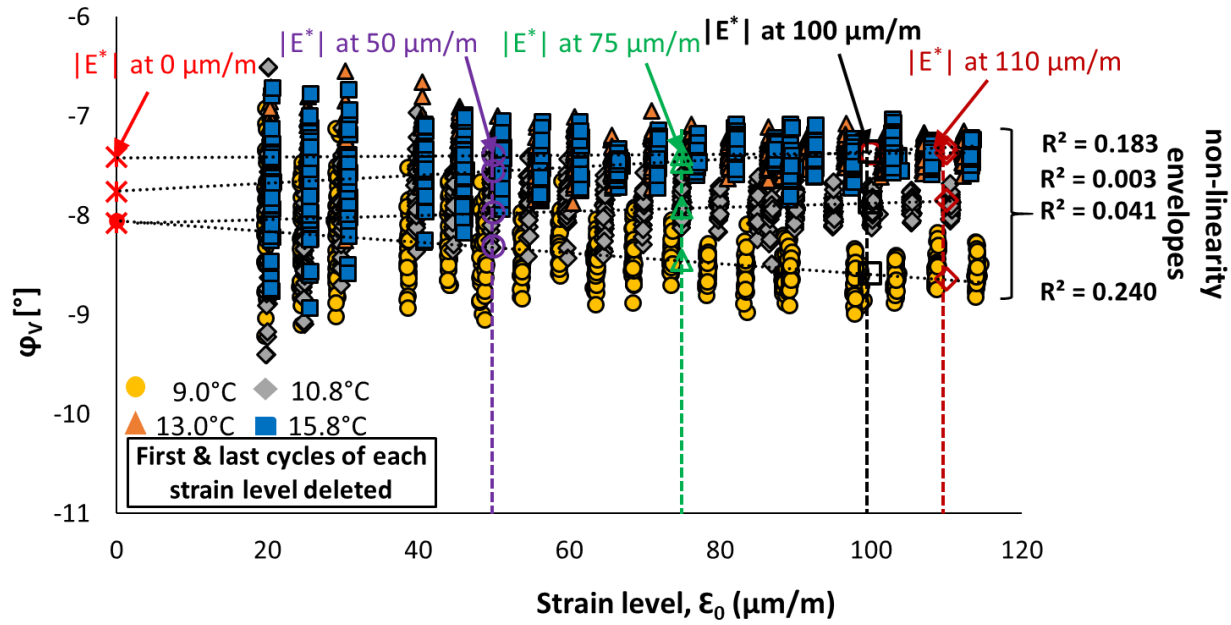

2.1.13. CMT results obtained for Mix 40/60 - 5: |E*|, φ_E, |ν*| and φ_ν against applied strain amplitude at different temperatures.

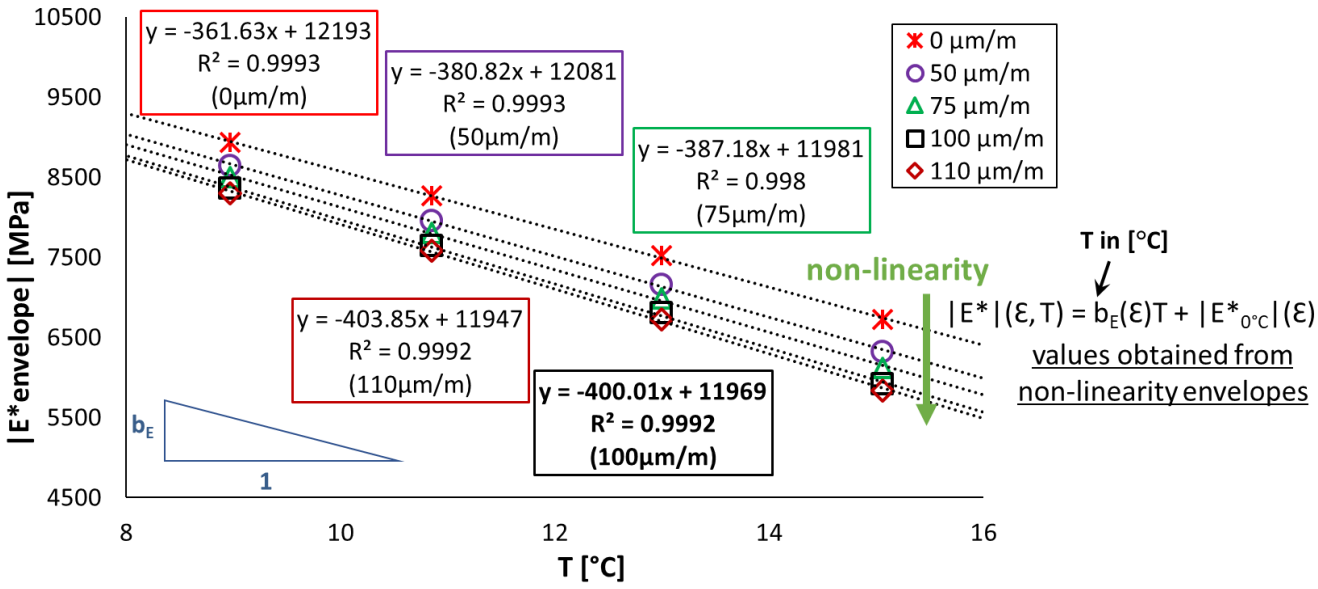

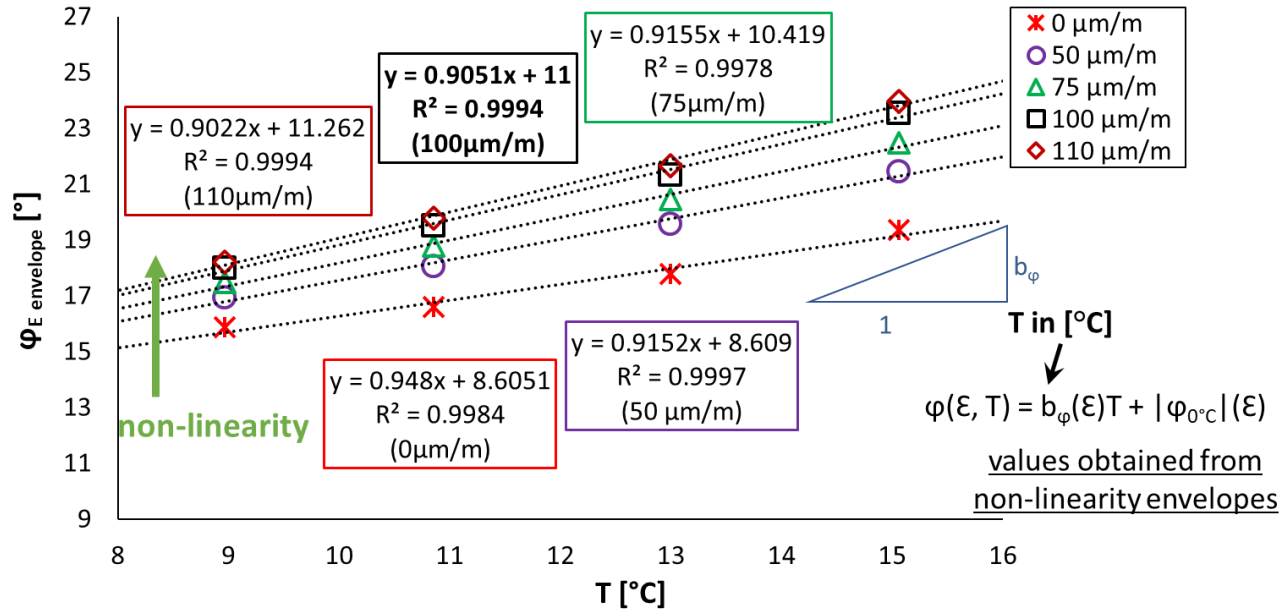
y = 0.9022x + 11.262
R² = 0.9994
(110µm/m)
y = 0.9051x + 11
R² = 0.9994
(100µm/m)
y = 0.9155x + 10.419
R² = 0.9978
(75µm/m)
y = 0.948x + 8.6051
R² = 0.9984
(0µm/m)
y = 0.9152x + 8.609
R² = 0.9997
(50 µm/m)
0 µm/m
50 µm/m
75 µm/m
100 µm/m
110 µm/m
non-linearity
b_φ
1
T in [°C]
$\varphi(\varepsilon, T) = b_\varphi(\varepsilon)T + |\varphi_{0°C}|(\varepsilon)$
values obtained from non-linearity envelopes
$\varphi_{E\ envelope}$ [°]
T [°C]

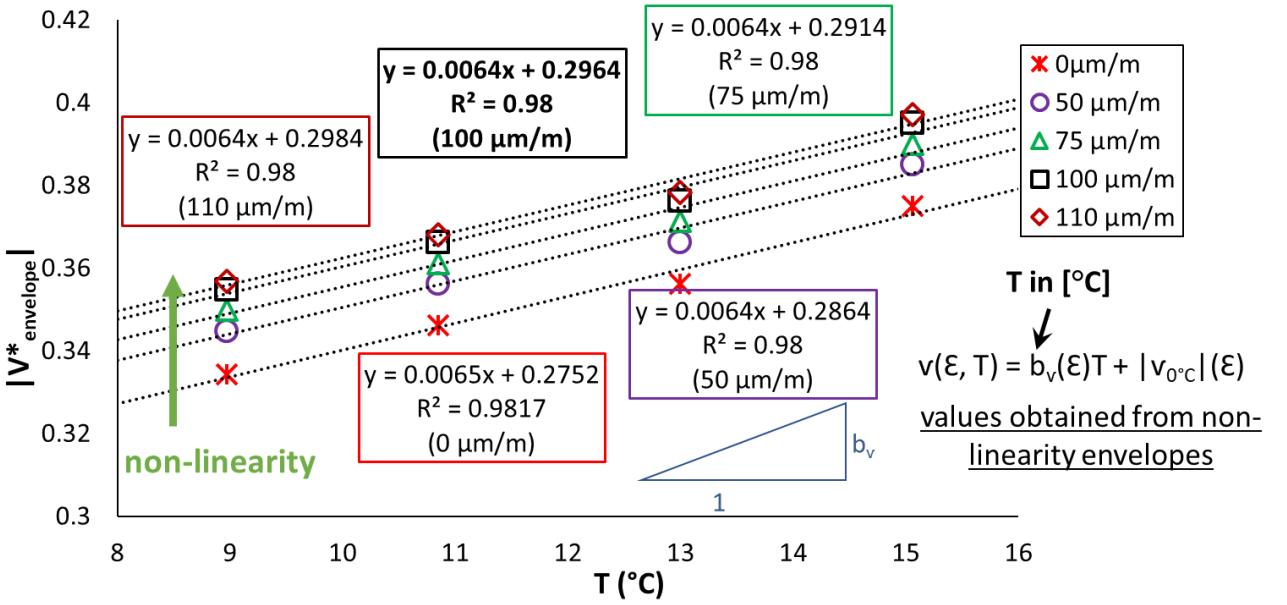
y = 0.0064x + 0.2984
R² = 0.98
(110 µm/m)
y = 0.0064x + 0.2964
R² = 0.98
(100 µm/m)
y = 0.0064x + 0.2914
R² = 0.98
(75 µm/m)
y = 0.0065x + 0.2752
R² = 0.9817
(0 µm/m)
y = 0.0064x + 0.2864
R² = 0.98
(50 µm/m)
0µm/m
50 µm/m
75 µm/m
100 µm/m
110 µm/m
non-linearity
b_v
1
T in [°C]
$v(\varepsilon, T) = b_v(\varepsilon)T + |v_{0°C}|(\varepsilon)$
values obtained from non-linearity envelopes
$|V^*_{envelope}|$
T (°C)

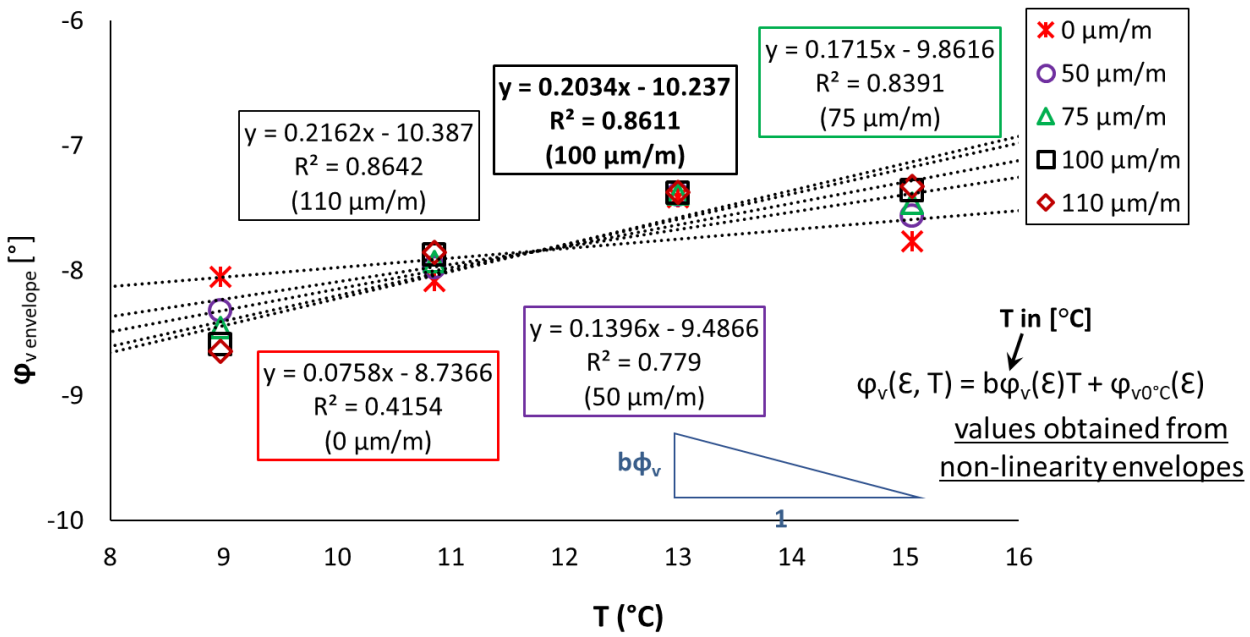

2.1.14. CMT results obtained for Mix 40/60 - 5: Regression of estimated values of |E*|, φ_E, |ν*| and φ_ν as a function of temperature.

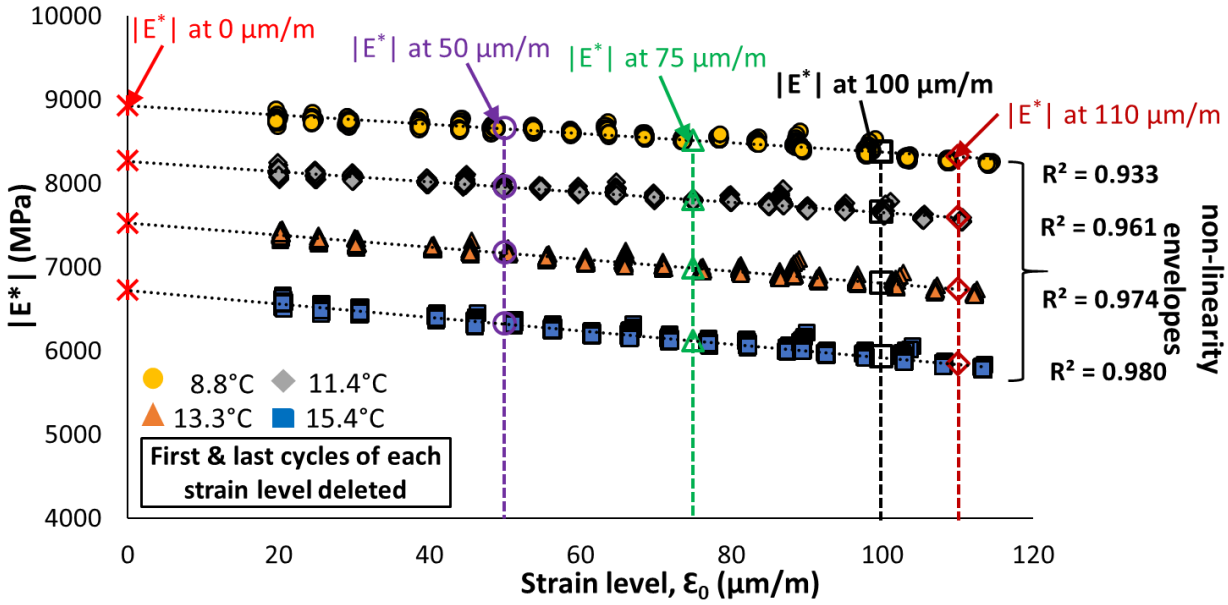

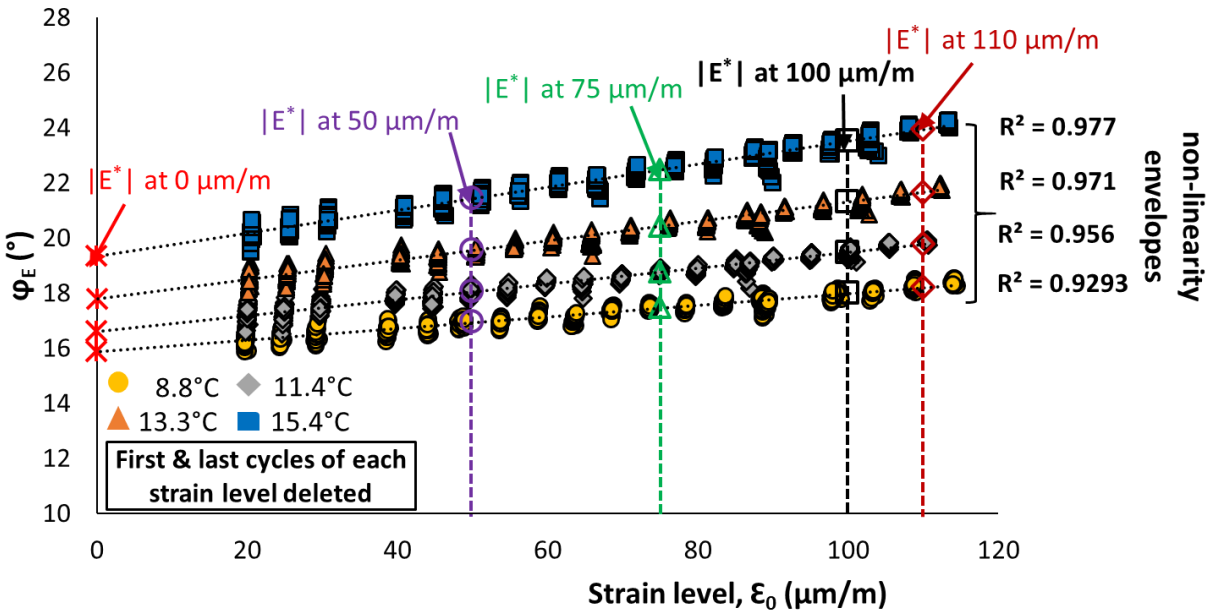
|E*| at 110 µm/m
|E*| at 100 µm/m
|E*| at 75 µm/m
|E*| at 50 µm/m
|E*| at 0 µm/m
R² = 0.977
R² = 0.971
R² = 0.956
R² = 0.9293
non-linearity envelopes
8.8°C
11.4°C
13.3°C
15.4°C
First & last cycles of each strain level deleted
φE (°)
Strain level, ε0 (µm/m)

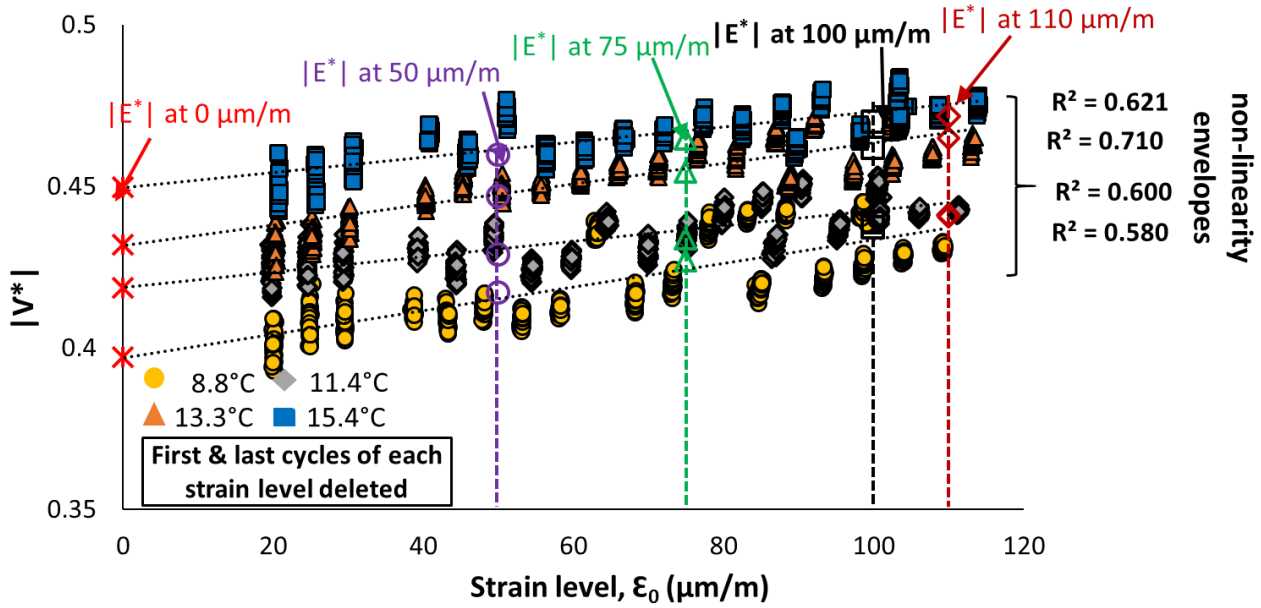
|E*| at 110 µm/m
|E*| at 100 µm/m
|E*| at 75 µm/m
|E*| at 50 µm/m
|E*| at 0 µm/m
R² = 0.621
R² = 0.710
R² = 0.600
R² = 0.580
non-linearity envelopes
8.8°C
11.4°C
13.3°C
15.4°C
First & last cycles of each strain level deleted
|V*|
Strain level, ε0 (µm/m)

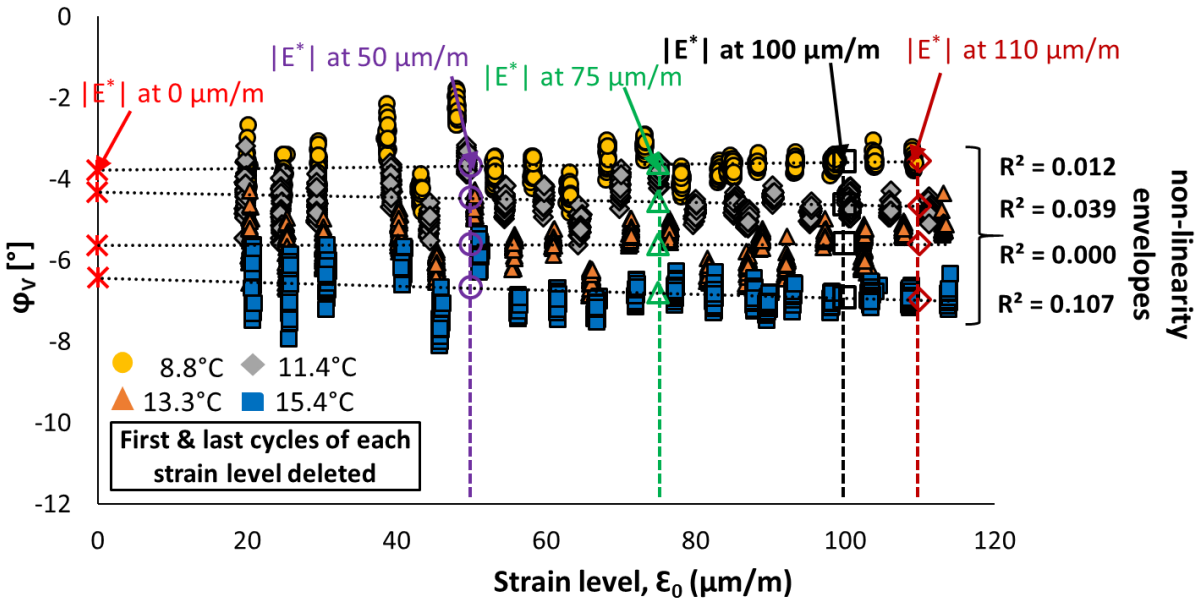

2.1.15. CMT results obtained for Mix 40/60 - 6: |E*|, φ_E, |ν*| and φ_ν against applied strain amplitude at different temperatures.

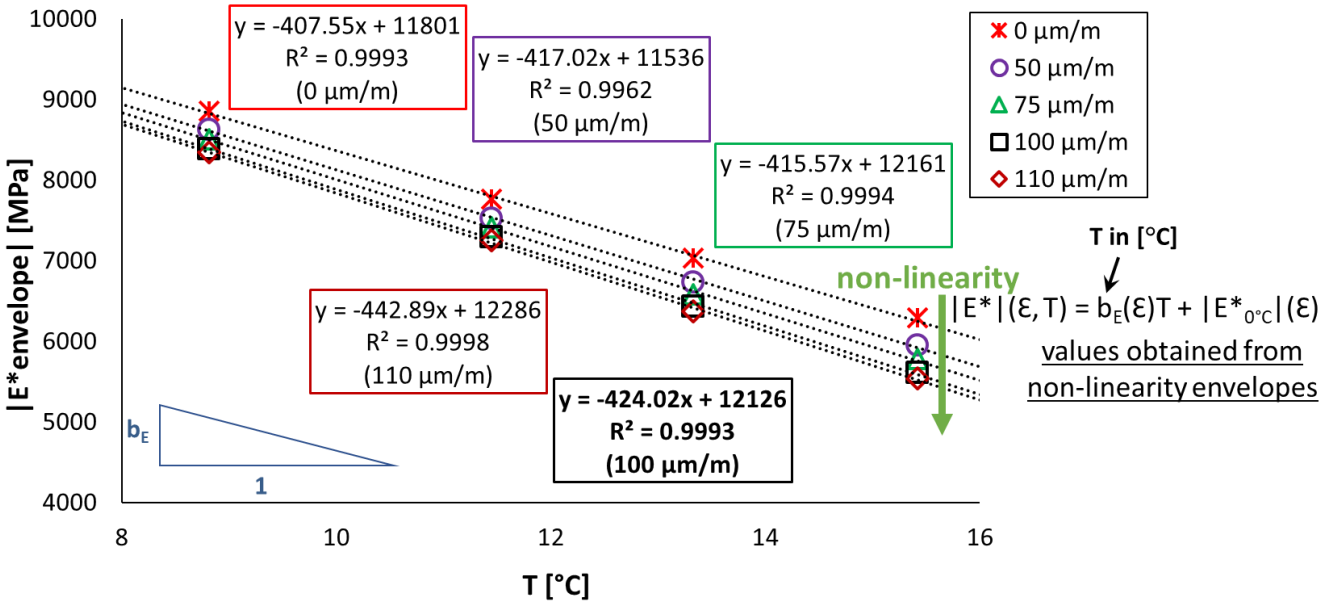

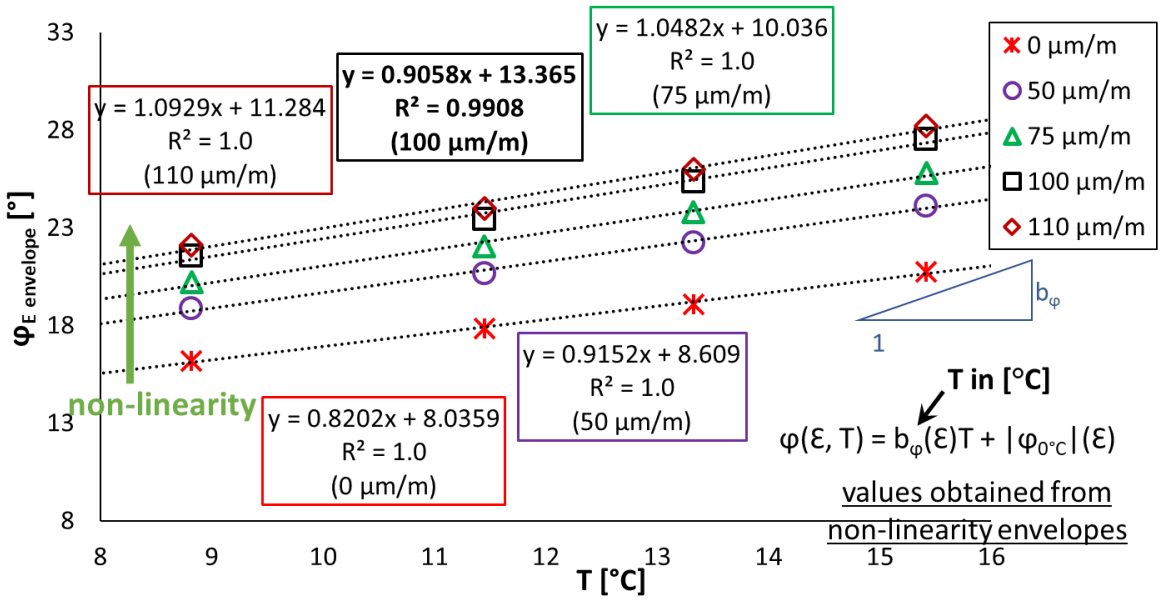
y = 1.0929x + 11.284
R² = 1.0
(110 µm/m)
y = 0.9058x + 13.365
R² = 0.9908
(100 µm/m)
y = 1.0482x + 10.036
R² = 1.0
(75 µm/m)
y = 0.9152x + 8.609
R² = 1.0
(50 µm/m)
y = 0.8202x + 8.0359
R² = 1.0
(0 µm/m)
0 µm/m
50 µm/m
75 µm/m
100 µm/m
110 µm/m
non-linearity
T in [°C]
φ(Ɛ, T) = b_φ(Ɛ)T + |φ_0°C|(Ɛ)
values obtained from non-linearity envelopes
T [°C]
φE envelope [°]

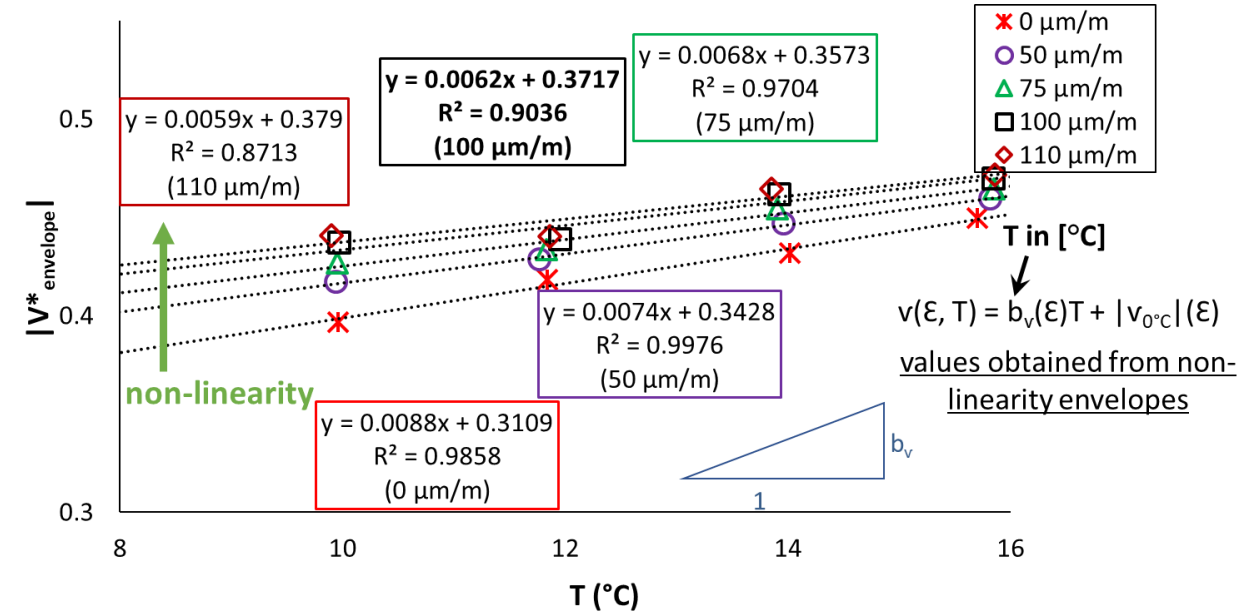
y = 0.0059x + 0.379
R² = 0.8713
(110 µm/m)
y = 0.0062x + 0.3717
R² = 0.9036
(100 µm/m)
y = 0.0068x + 0.3573
R² = 0.9704
(75 µm/m)
y = 0.0074x + 0.3428
R² = 0.9976
(50 µm/m)
y = 0.0088x + 0.3109
R² = 0.9858
(0 µm/m)
0 µm/m
50 µm/m
75 µm/m
100 µm/m
110 µm/m
non-linearity
T in [°C]
v(Ɛ, T) = b_v(Ɛ)T + |v_0°C|(Ɛ)
values obtained from non-linearity envelopes
T (°C)
|V* envelope|

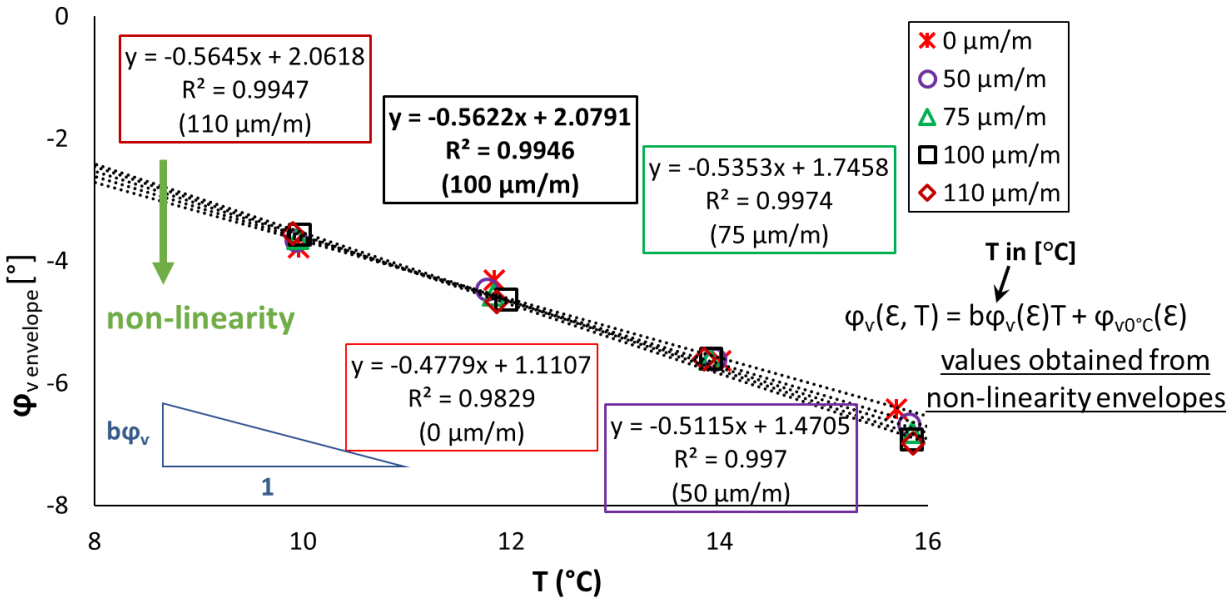

Figure 2.1.16. CMT results obtained for Mix 40/60 - 6: Regression of estimated values of |E*|, φ_E, |ν*| and φ_v against applied strain amplitude at different temperatures.

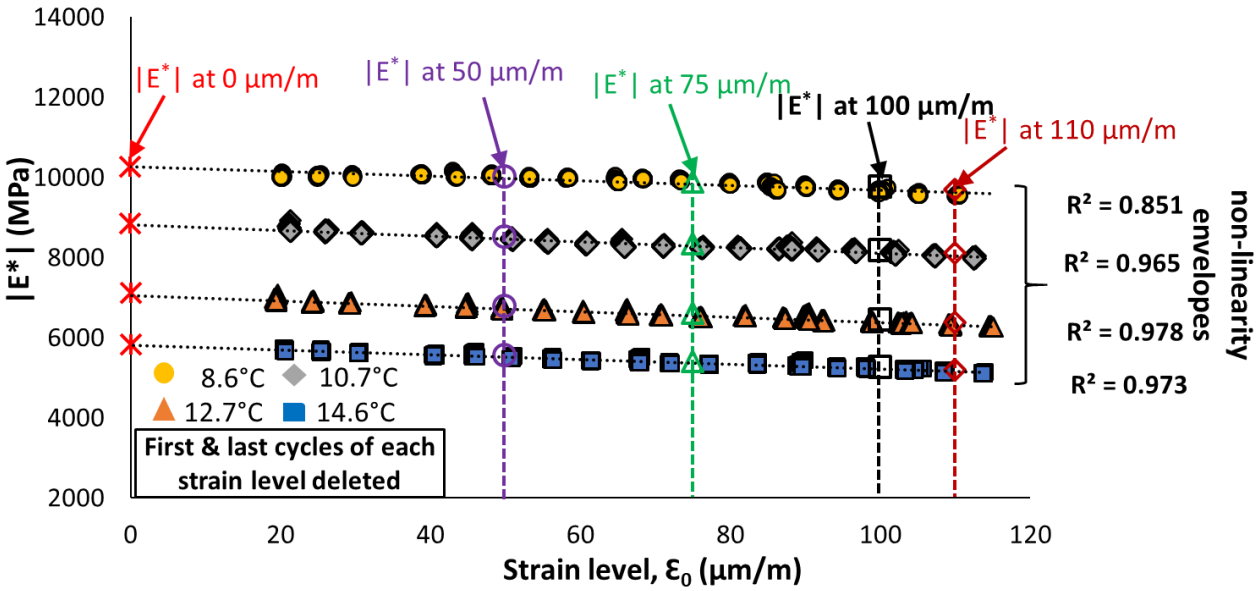

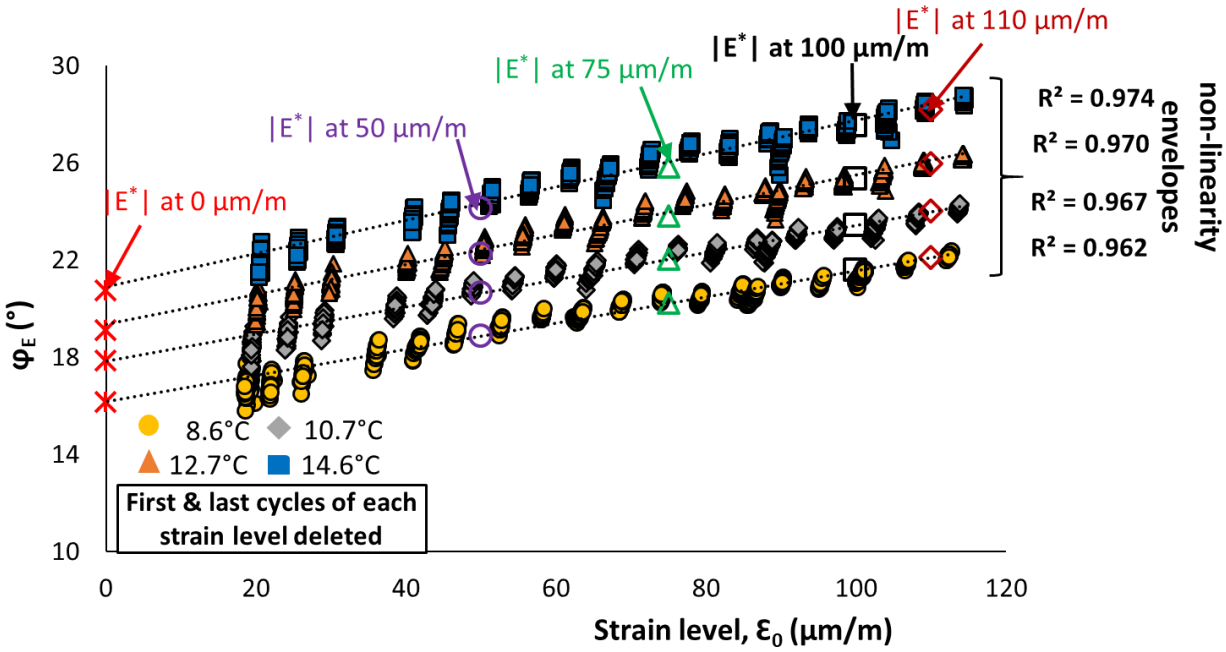
|E*| at 110 µm/m
|E*| at 100 µm/m
|E*| at 75 µm/m
|E*| at 50 µm/m
|E*| at 0 µm/m
R² = 0.974
R² = 0.970
R² = 0.967
R² = 0.962
non-linearity envelopes
φE (°)
8.6°C
10.7°C
12.7°C
14.6°C
First & last cycles of each strain level deleted
Strain level, ε0 (µm/m)

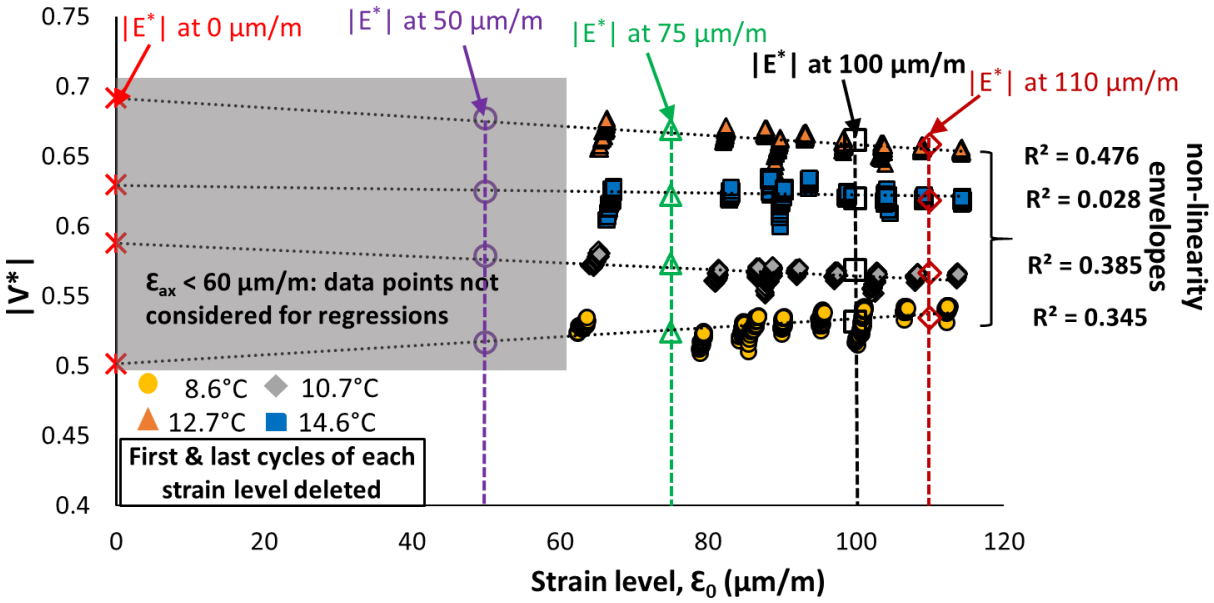
|E*| at 0 µm/m
|E*| at 50 µm/m
|E*| at 75 µm/m
|E*| at 100 µm/m
|E*| at 110 µm/m
R² = 0.476
R² = 0.028
R² = 0.385
R² = 0.345
non-linearity envelopes
|V*|
εax < 60 µm/m: data points not considered for regressions
8.6°C
10.7°C
12.7°C
14.6°C
First & last cycles of each strain level deleted
Strain level, ε0 (µm/m)

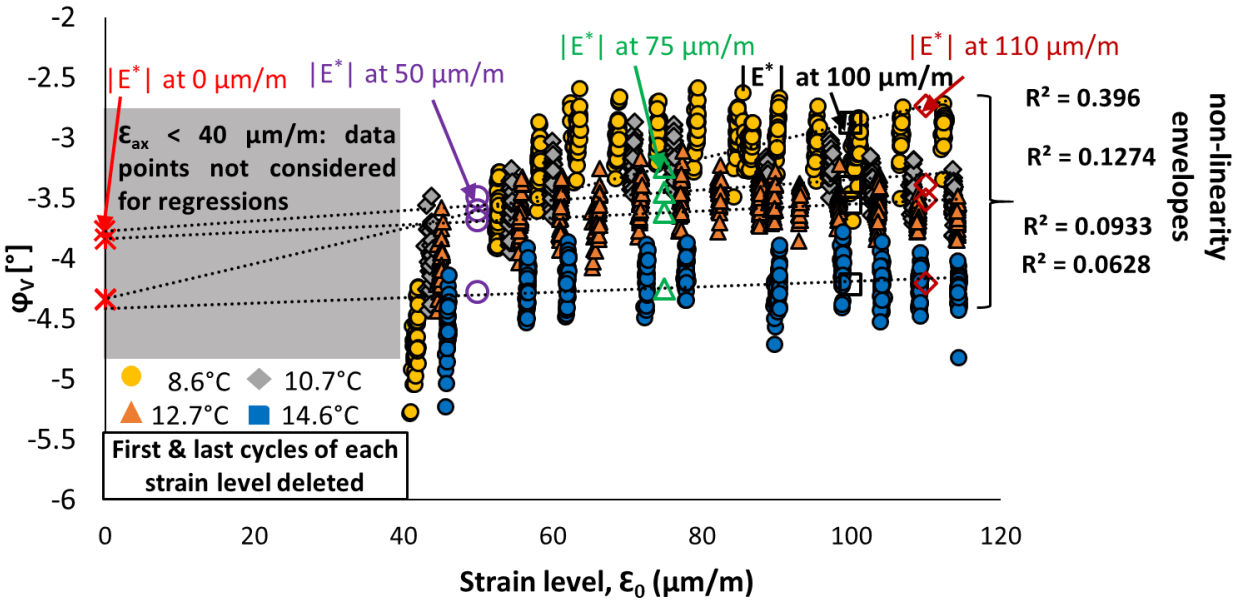

Figure 2.1.17. CMT results obtained for Mix 40/60 - 8: |E*|, φ_E, |ν*| and φ_ν against applied strain amplitude at different temperatures.

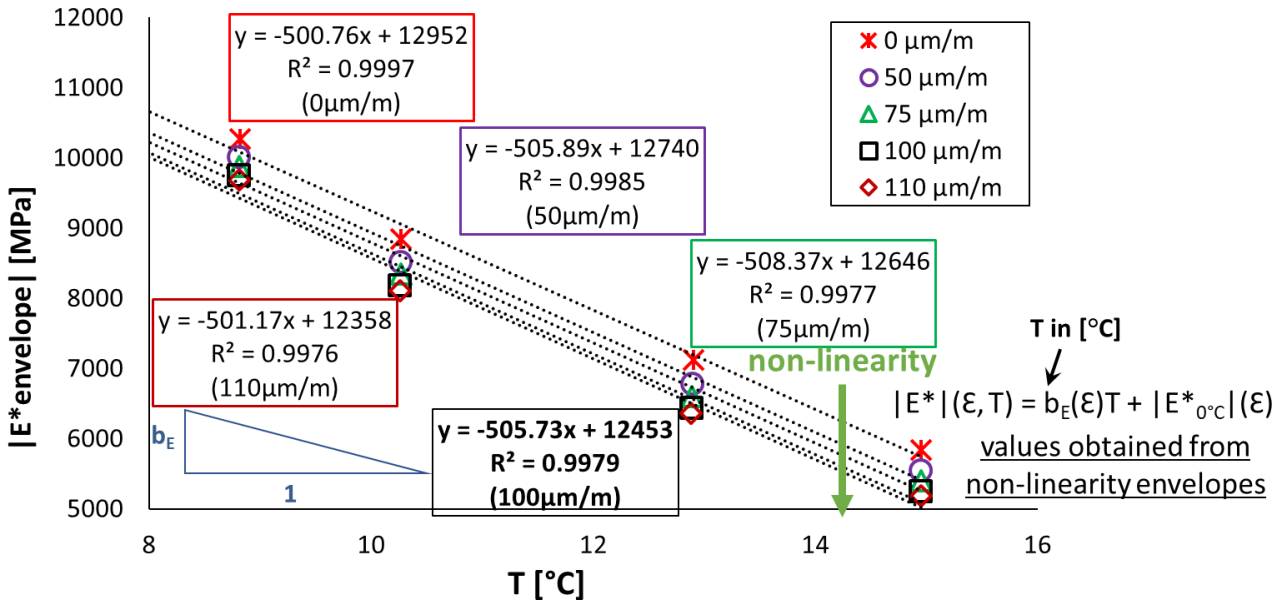

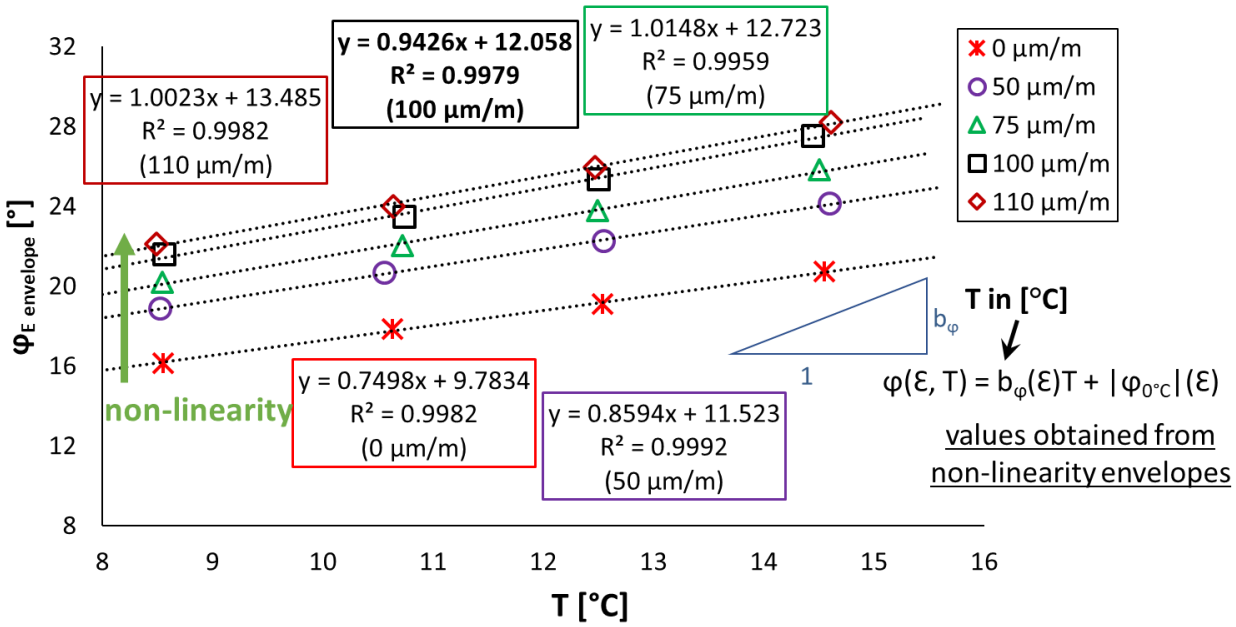
y = 1.0023x + 13.485
R² = 0.9982
(110 µm/m)
y = 0.9426x + 12.058
R² = 0.9979
(100 µm/m)
y = 1.0148x + 12.723
R² = 0.9959
(75 µm/m)
0 µm/m
50 µm/m
75 µm/m
100 µm/m
110 µm/m
non-linearity
y = 0.7498x + 9.7834
R² = 0.9982
(0 µm/m)
y = 0.8594x + 11.523
R² = 0.9992
(50 µm/m)
T in [°C]
φ(Ɛ, T) = b_φ(Ɛ)T + |φ_0°C|(Ɛ)
values obtained from non-linearity envelopes
φ E envelope [°]
T [°C]

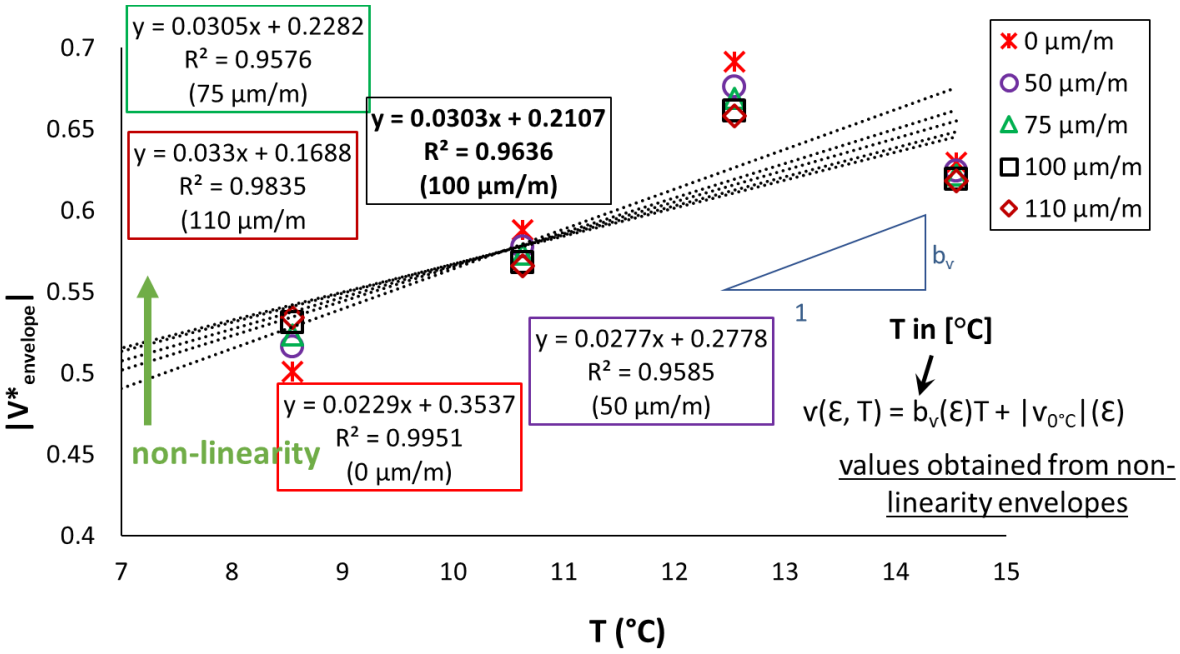
y = 0.0305x + 0.2282
R² = 0.9576
(75 µm/m)
y = 0.0303x + 0.2107
R² = 0.9636
(100 µm/m)
y = 0.033x + 0.1688
R² = 0.9835
(110 µm/m
0 µm/m
50 µm/m
75 µm/m
100 µm/m
110 µm/m
non-linearity
y = 0.0277x + 0.2778
R² = 0.9585
(50 µm/m)
y = 0.0229x + 0.3537
R² = 0.9951
(0 µm/m)
T in [°C]
v(Ɛ, T) = b_v(Ɛ)T + |v_0°C|(Ɛ)
values obtained from non-linearity envelopes
|V* envelope|
T (°C)

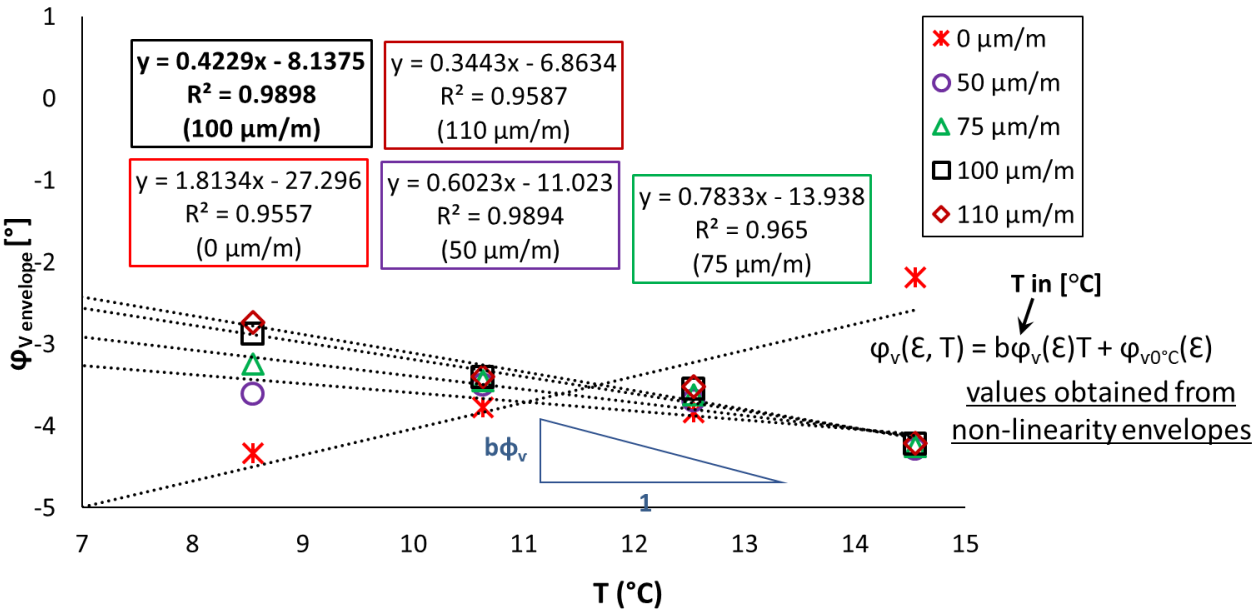

Figure 2.1.18. CMT results obtained for Mix 40/60 - 8: Regression of estimated values of |E*|, φ_E, |ν*| and φ_ν against applied strain amplitude at different temperatures.

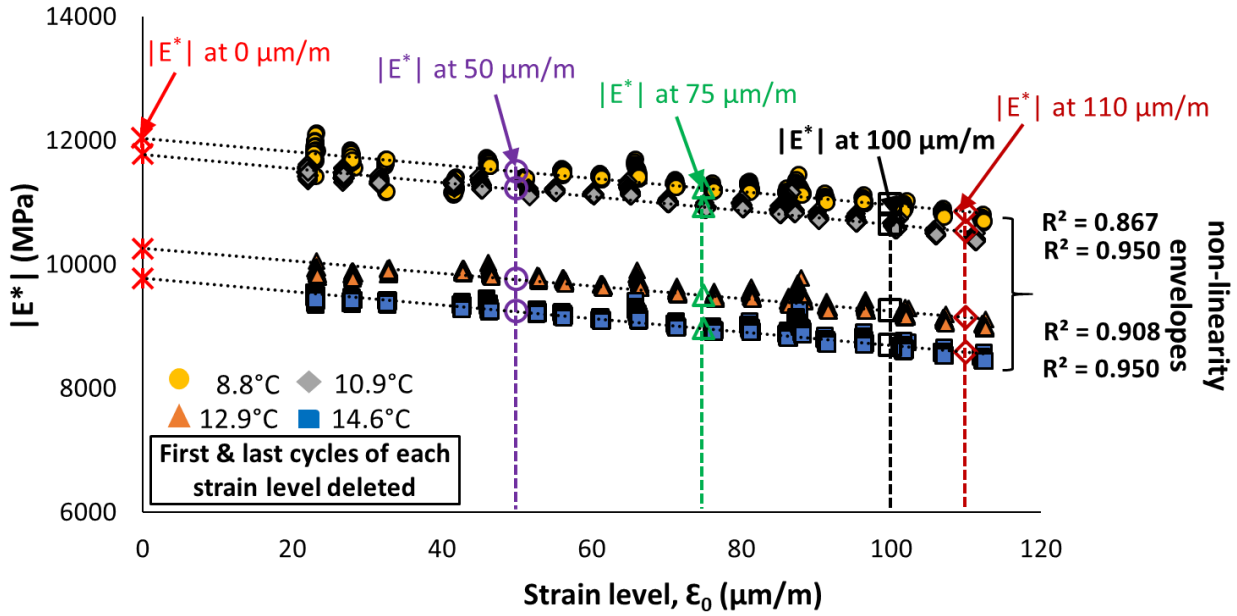

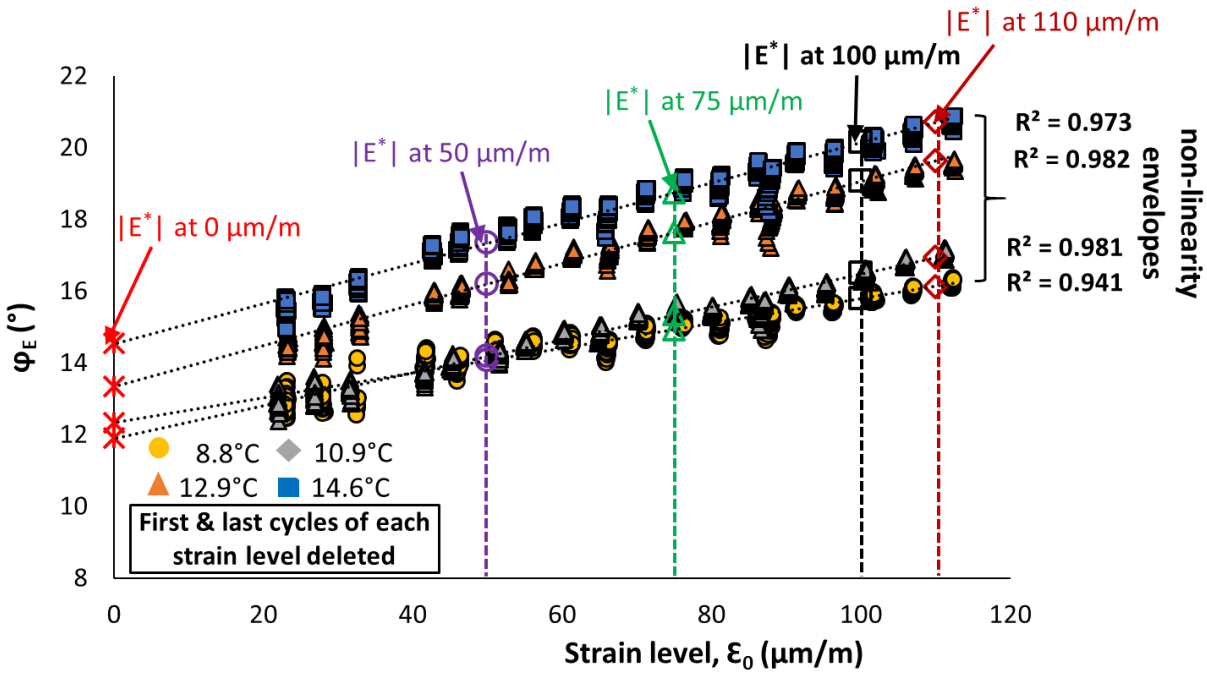
|E*| at 110 µm/m
|E*| at 100 µm/m
|E*| at 75 µm/m
|E*| at 50 µm/m
|E*| at 0 µm/m
R² = 0.973
R² = 0.982
R² = 0.981
R² = 0.941
non-linearity envelopes
φE (°)
8.8°C
10.9°C
12.9°C
14.6°C
First & last cycles of each strain level deleted
Strain level, ε0 (µm/m)

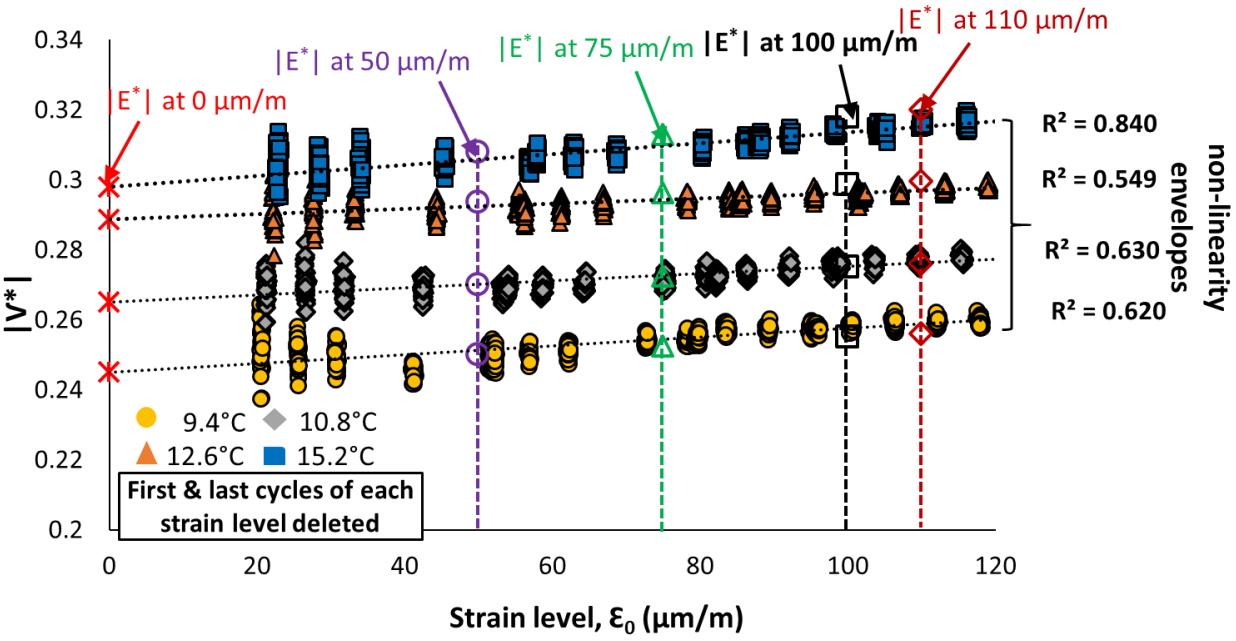
|E*| at 110 µm/m
|E*| at 100 µm/m
|E*| at 75 µm/m
|E*| at 50 µm/m
|E*| at 0 µm/m
R² = 0.840
R² = 0.549
R² = 0.630
R² = 0.620
non-linearity envelopes
|V*|
9.4°C
10.8°C
12.6°C
15.2°C
First & last cycles of each strain level deleted
Strain level, ε0 (µm/m)

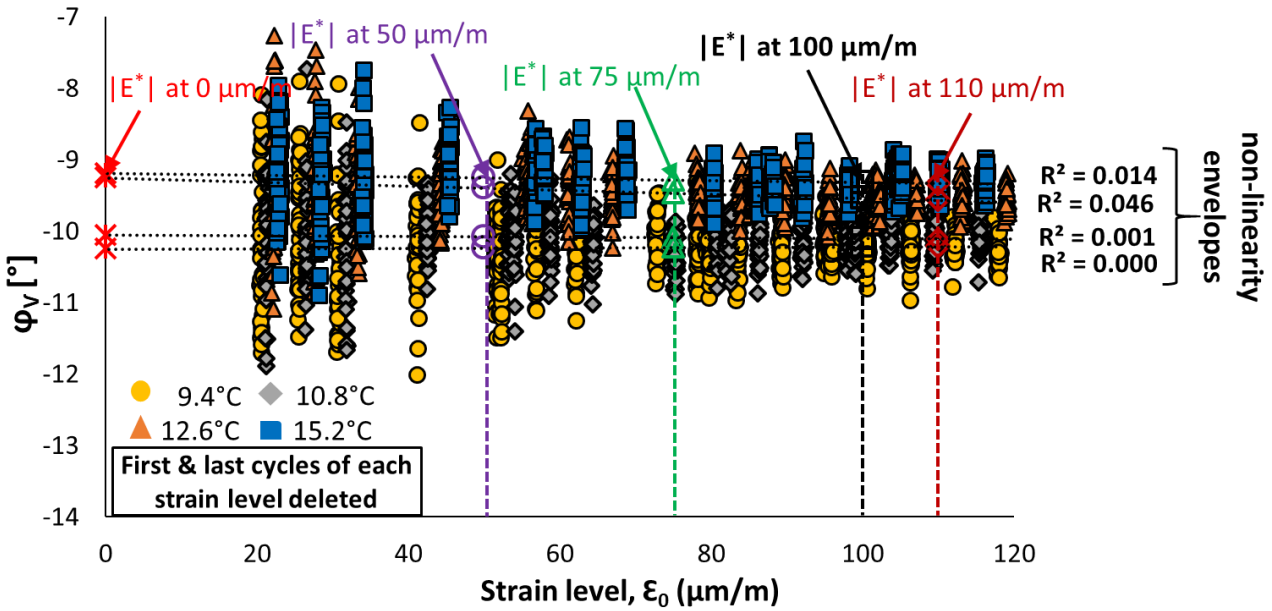

2.1.19. CMT results obtained for Mix PMB - 1: |E*|, φ_E, |v*| and φ_v against applied strain amplitude at different temperatures.

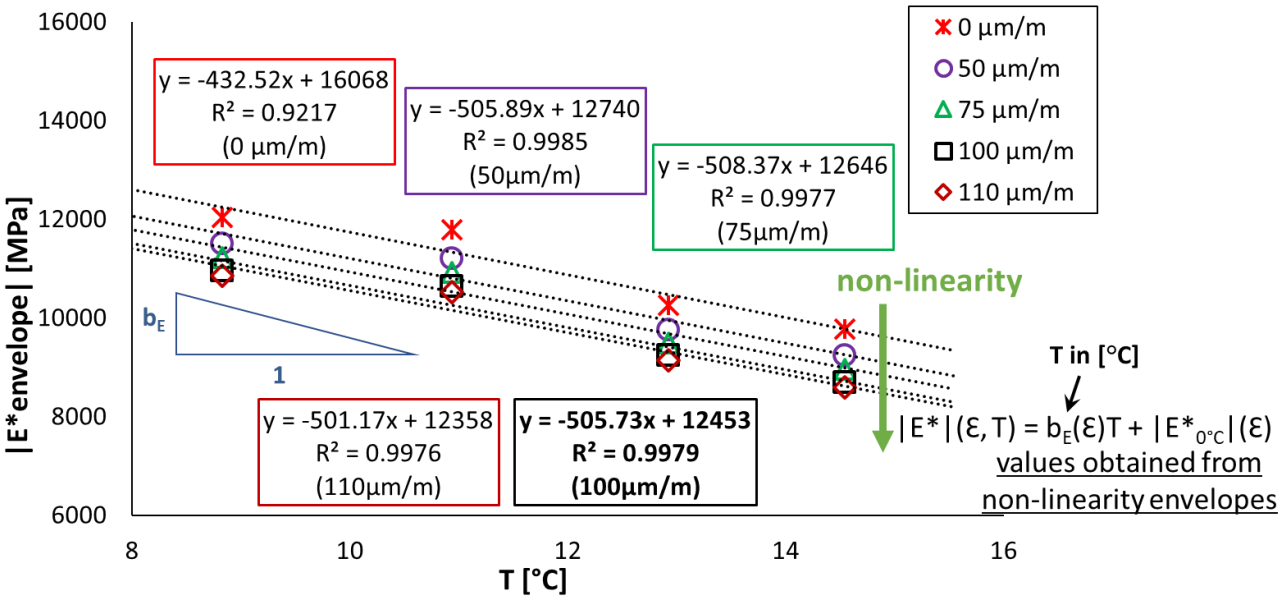

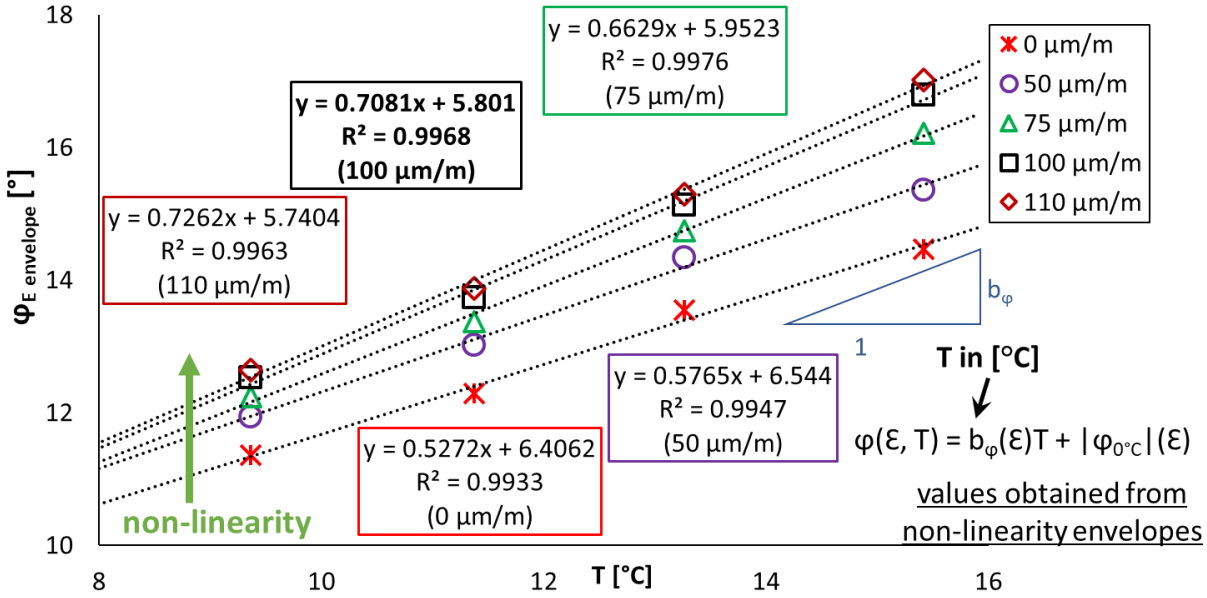
y = 0.6629x + 5.9523
R² = 0.9976
(75 µm/m)
y = 0.7081x + 5.801
R² = 0.9968
(100 µm/m)
y = 0.7262x + 5.7404
R² = 0.9963
(110 µm/m)
y = 0.5765x + 6.544
R² = 0.9947
(50 µm/m)
y = 0.5272x + 6.4062
R² = 0.9933
(0 µm/m)
0 µm/m
50 µm/m
75 µm/m
100 µm/m
110 µm/m
non-linearity
T in [°C]
φ(Ɛ, T) = b_φ(Ɛ)T + |φ_0°C|(Ɛ)
values obtained from non-linearity envelopes
φ E envelope [°]
T [°C]

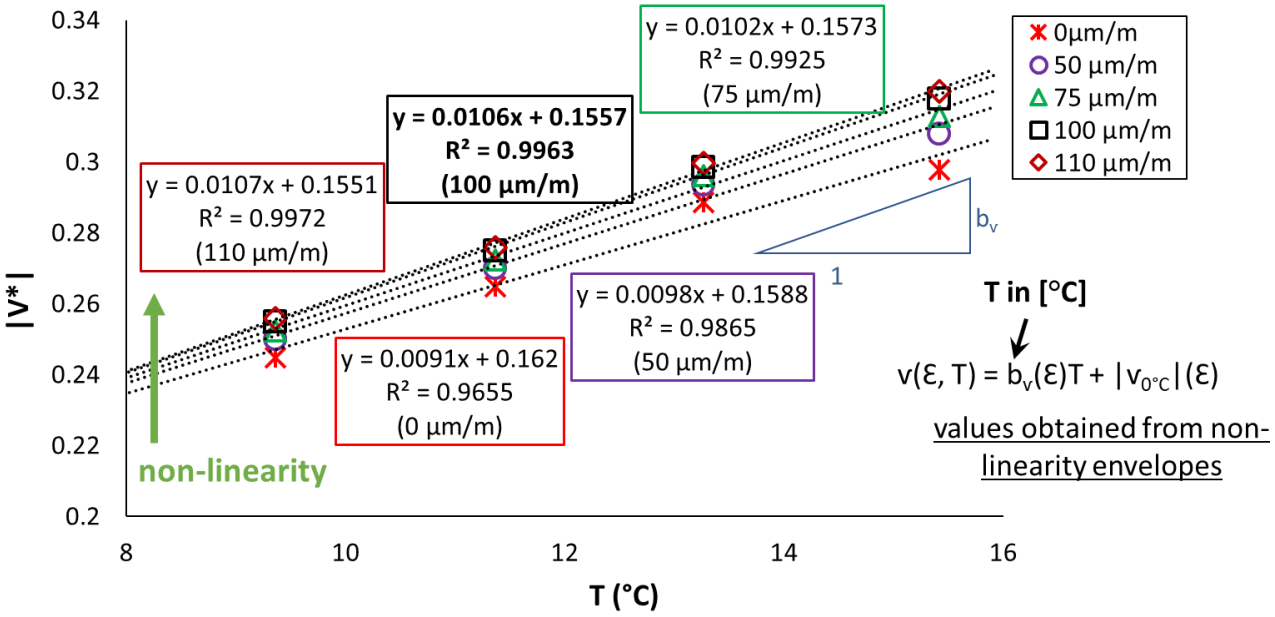
y = 0.0102x + 0.1573
R² = 0.9925
(75 µm/m)
y = 0.0106x + 0.1557
R² = 0.9963
(100 µm/m)
y = 0.0107x + 0.1551
R² = 0.9972
(110 µm/m)
y = 0.0098x + 0.1588
R² = 0.9865
(50 µm/m)
y = 0.0091x + 0.162
R² = 0.9655
(0 µm/m)
0µm/m
50 µm/m
75 µm/m
100 µm/m
110 µm/m
non-linearity
T in [°C]
v(Ɛ, T) = b_v(Ɛ)T + |v_0°C|(Ɛ)
values obtained from non-linearity envelopes
|V*|
T (°C)

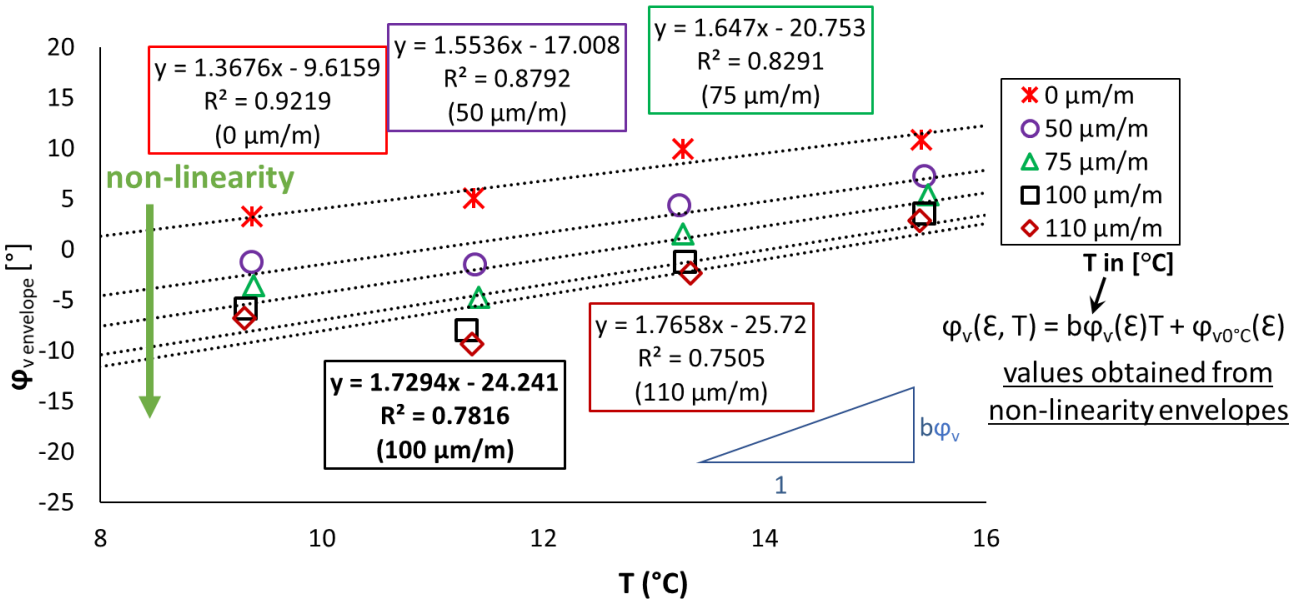

2.1.20. CMT results obtained for Mix PMB - 1: Regression of estimated values of |E*| φ_E, |ν*| and φ_ν as a function of temperature.

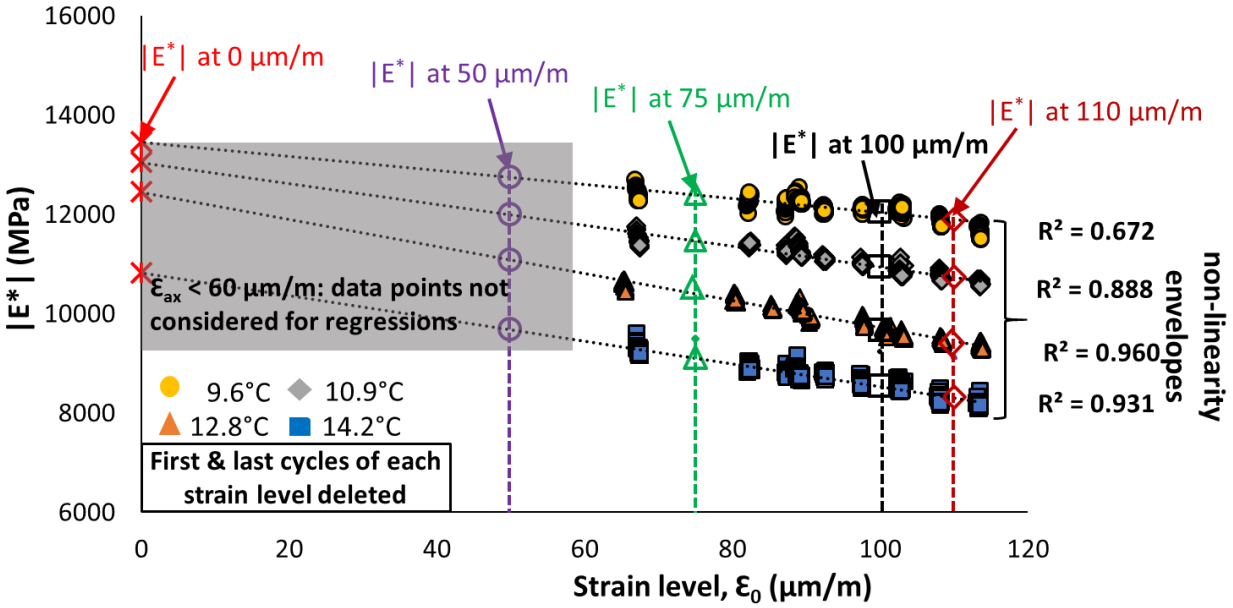

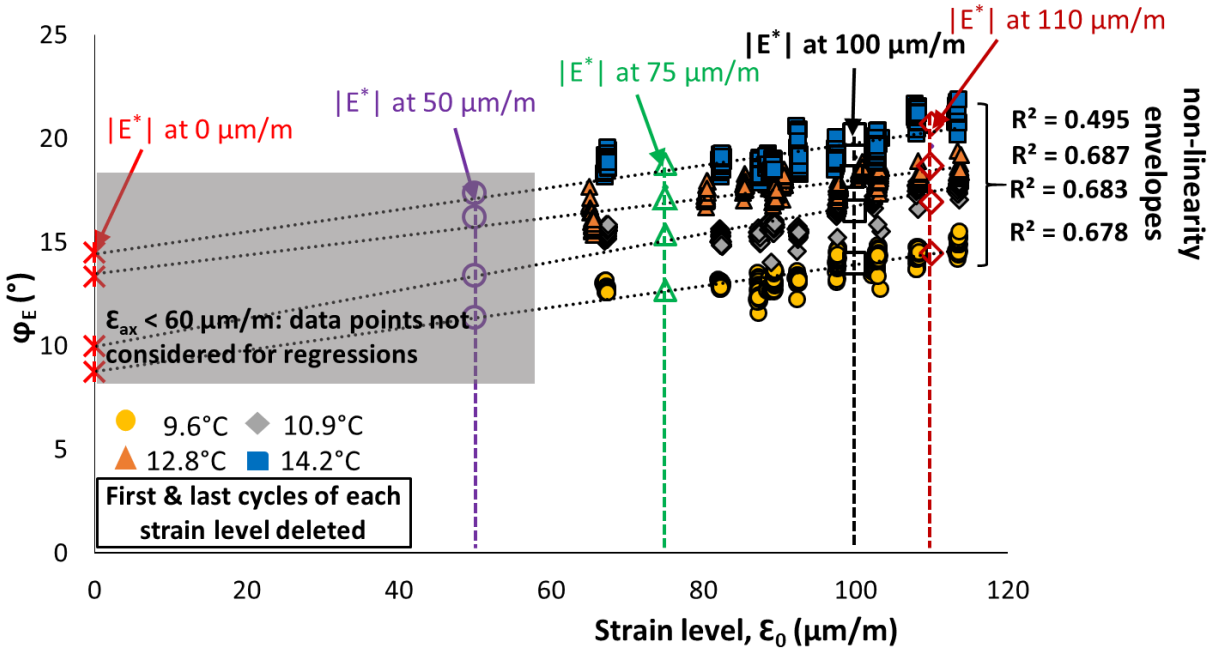

2.1.21. CMT results obtained for Mix PMB - 2: |E*| and φ_E against applied strain amplitude at different temperatures.

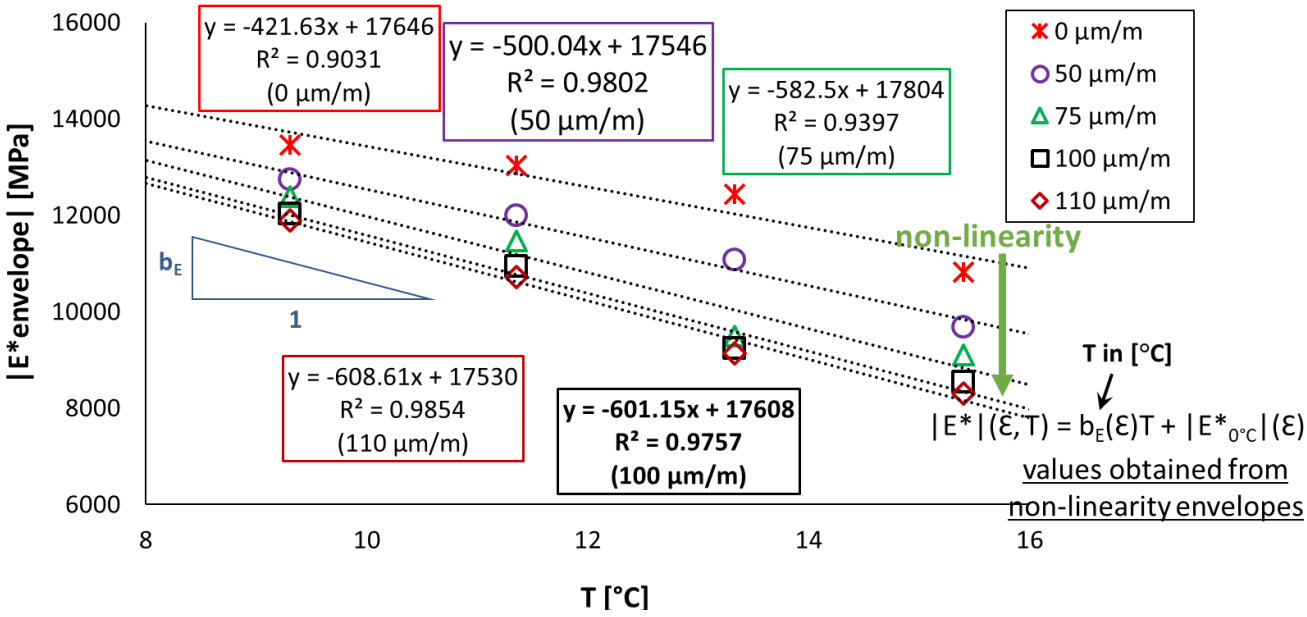

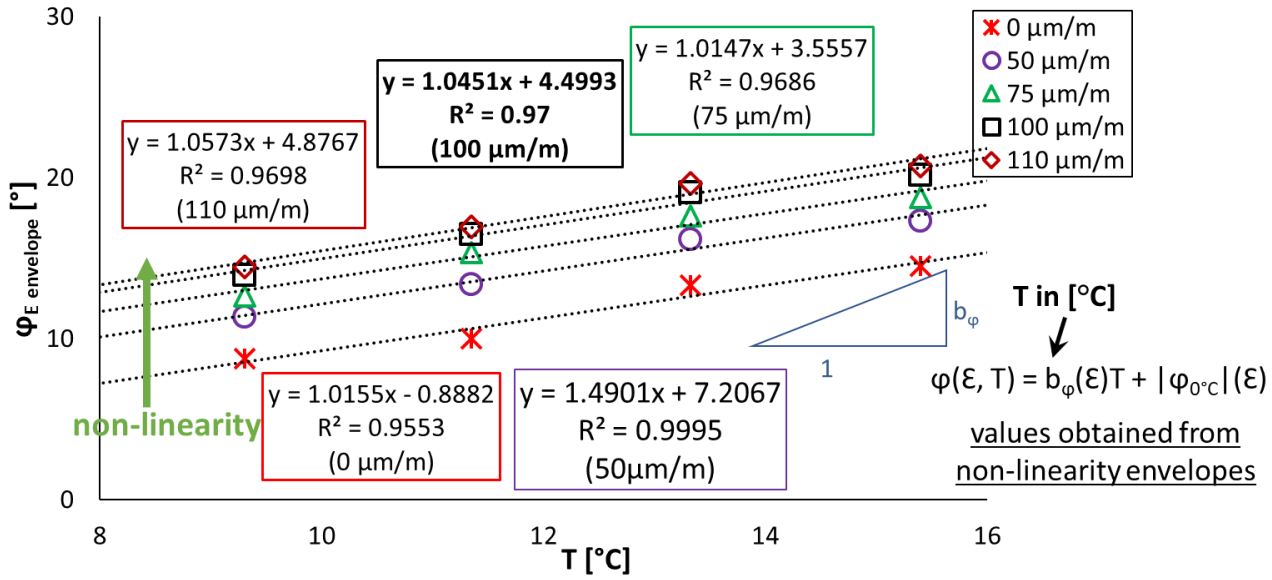

2.1.22. CMT results obtained for Mix PMB - 2: Regression of estimated values of |E*| and φ_E as a function of temperature.

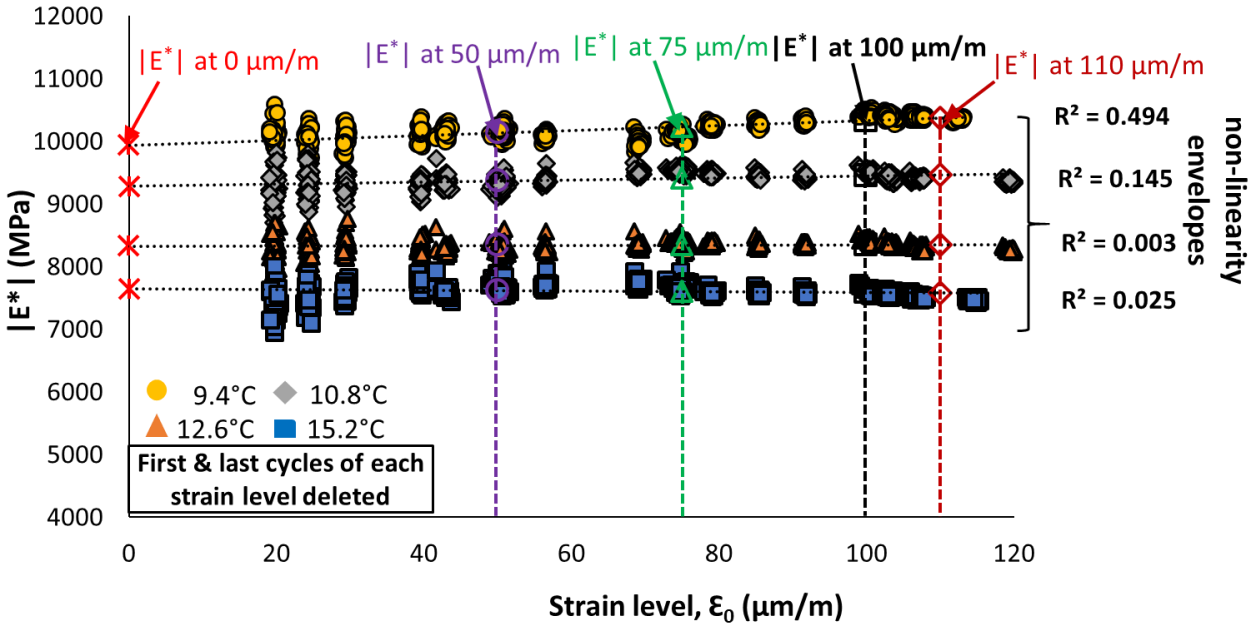

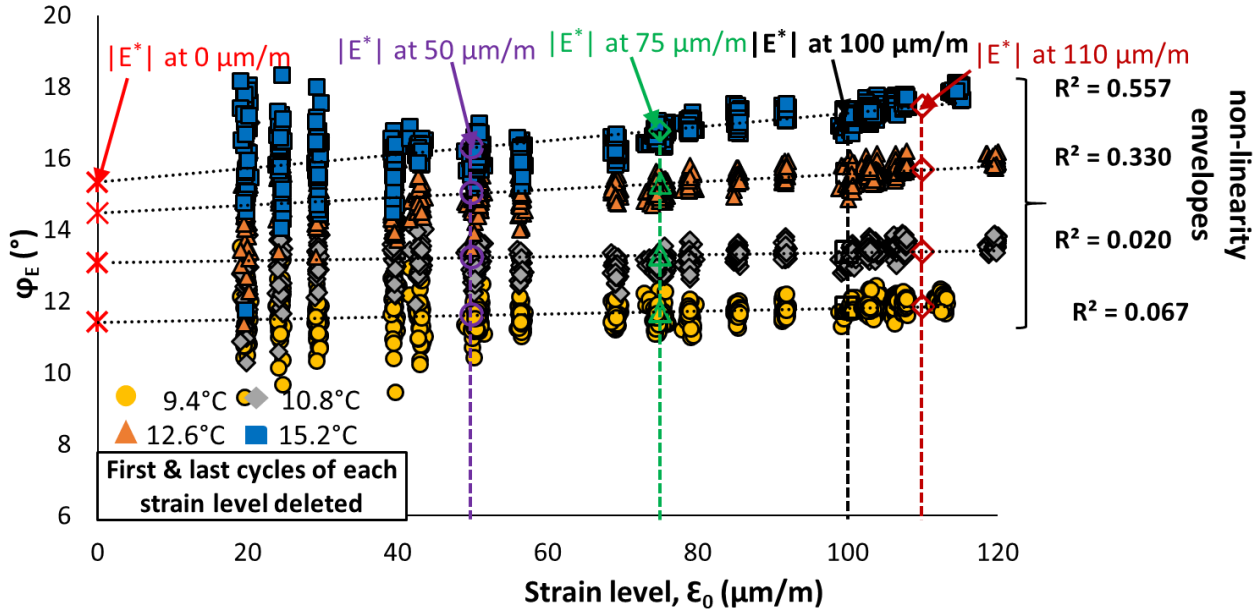
|E*| at 0 µm/m
|E*| at 50 µm/m
|E*| at 75 µm/m
|E*| at 100 µm/m
|E*| at 110 µm/m
R² = 0.557
R² = 0.330
R² = 0.020
R² = 0.067
non-linearity envelopes
9.4°C
10.8°C
12.6°C
15.2°C
First & last cycles of each strain level deleted
φE (°)
Strain level, ε0 (µm/m)

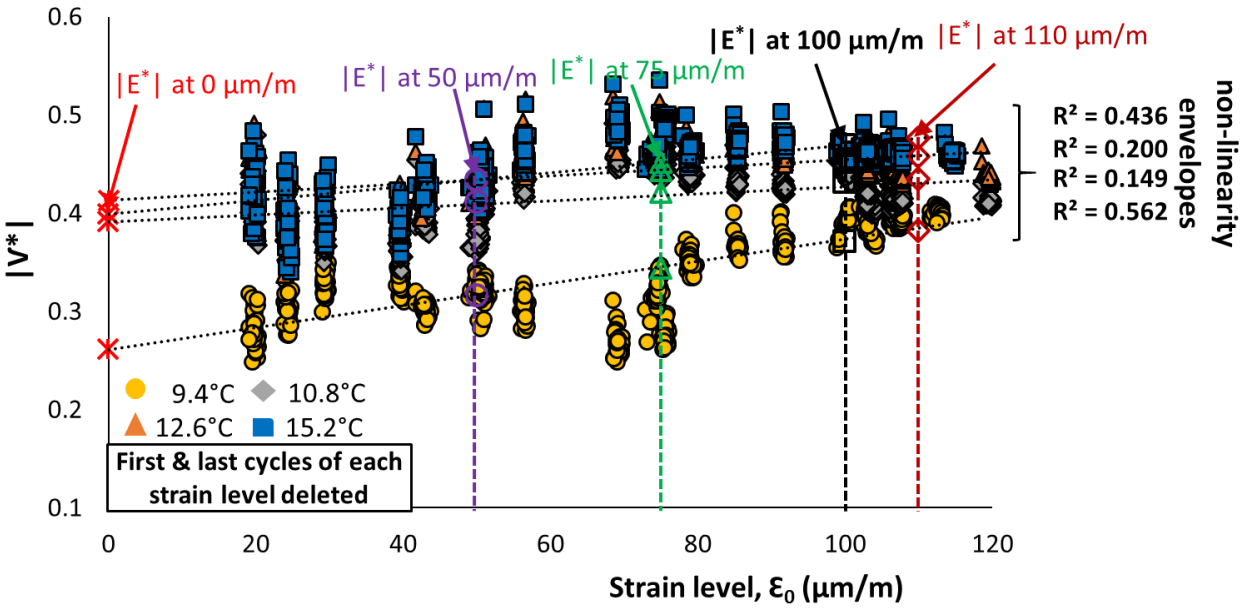
|E*| at 0 µm/m
|E*| at 50 µm/m
|E*| at 75 µm/m
|E*| at 100 µm/m
|E*| at 110 µm/m
R² = 0.436
R² = 0.200
R² = 0.149
R² = 0.562
non-linearity envelopes
9.4°C
10.8°C
12.6°C
15.2°C
First & last cycles of each strain level deleted
|V*|
Strain level, ε0 (µm/m)

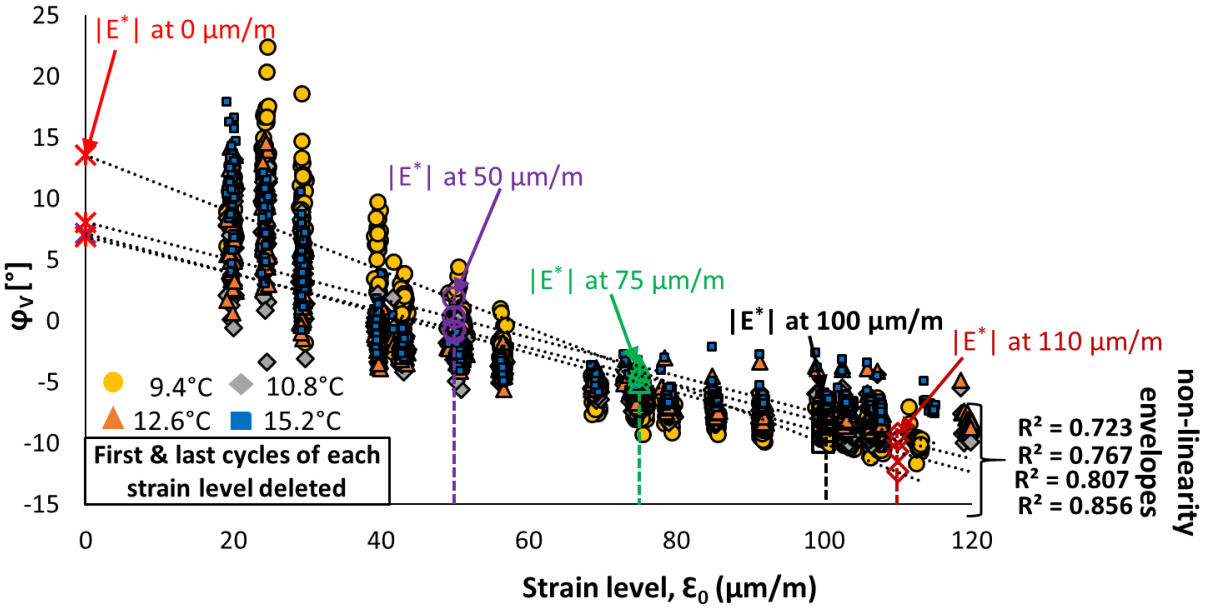

2.1.23. CMT results obtained for Mix PMB - 5: |E*| φ_E, |ν*| and φ_ν against applied strain amplitude at different temperatures.

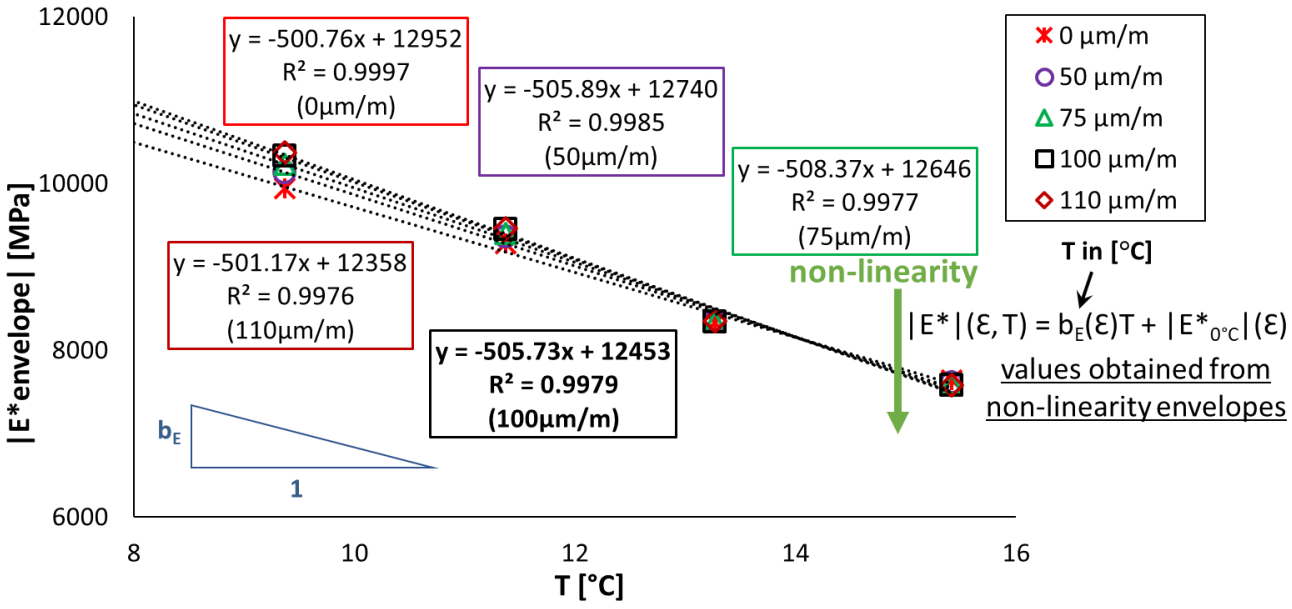

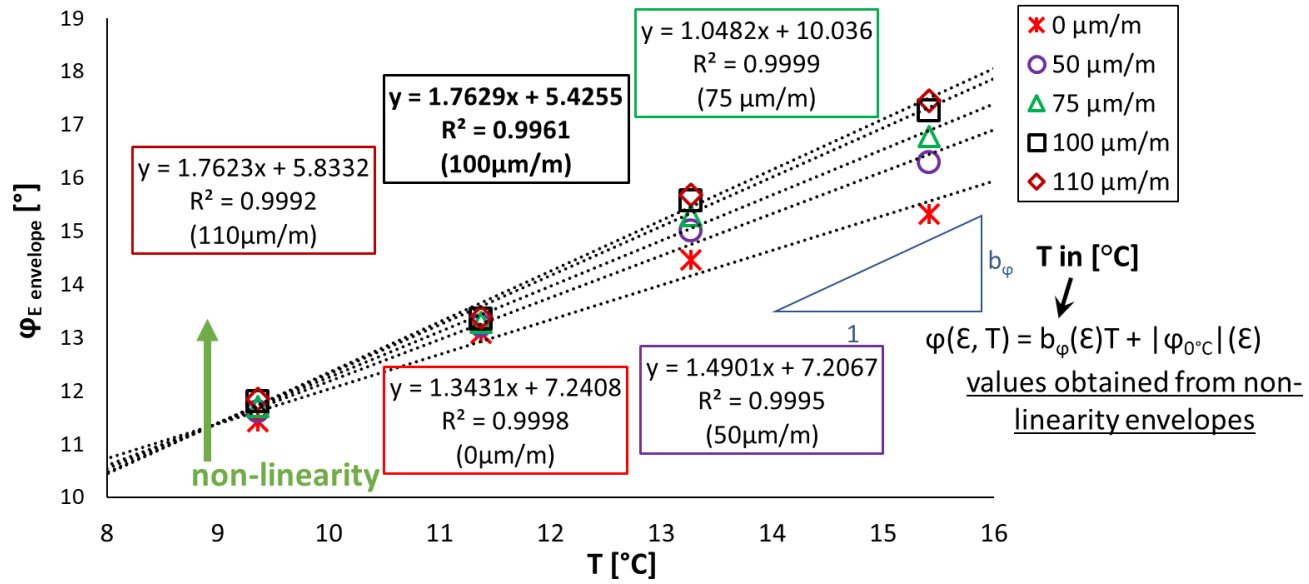
y = 1.7623x + 5.8332
R² = 0.9992
(110µm/m)
y = 1.7629x + 5.4255
R² = 0.9961
(100µm/m)
y = 1.0482x + 10.036
R² = 0.9999
(75 µm/m)
y = 1.3431x + 7.2408
R² = 0.9998
(0µm/m)
y = 1.4901x + 7.2067
R² = 0.9995
(50µm/m)
0 µm/m
50 µm/m
75 µm/m
100 µm/m
110 µm/m
non-linearity
1
bφ
T in [°C]
φ(Ɛ, T) = bφ(Ɛ)T + |φ0°C|(Ɛ)
values obtained from non-linearity envelopes
φE envelope [°]
T [°C]

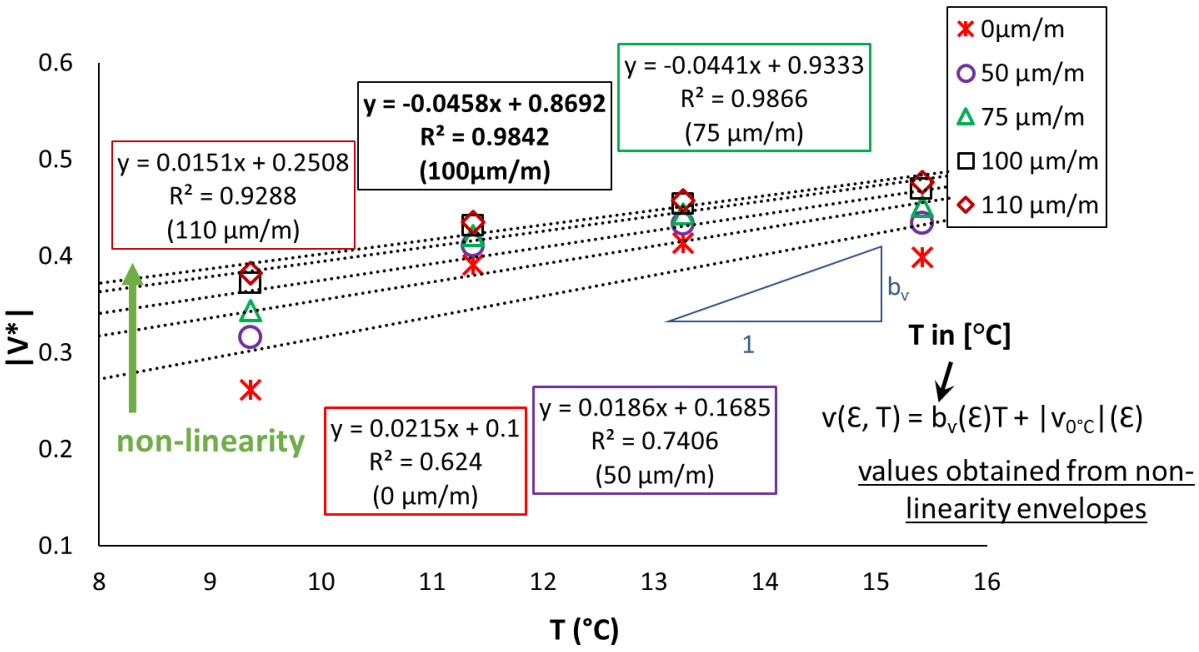
y = 0.0151x + 0.2508
R² = 0.9288
(110 µm/m)
y = -0.0458x + 0.8692
R² = 0.9842
(100µm/m)
y = -0.0441x + 0.9333
R² = 0.9866
(75 µm/m)
y = 0.0215x + 0.1
R² = 0.624
(0 µm/m)
y = 0.0186x + 0.1685
R² = 0.7406
(50 µm/m)
0µm/m
50 µm/m
75 µm/m
100 µm/m
110 µm/m
non-linearity
1
bv
T in [°C]
v(Ɛ, T) = bv(Ɛ)T + |v0°C|(Ɛ)
values obtained from non-linearity envelopes
|V*|
T (°C)

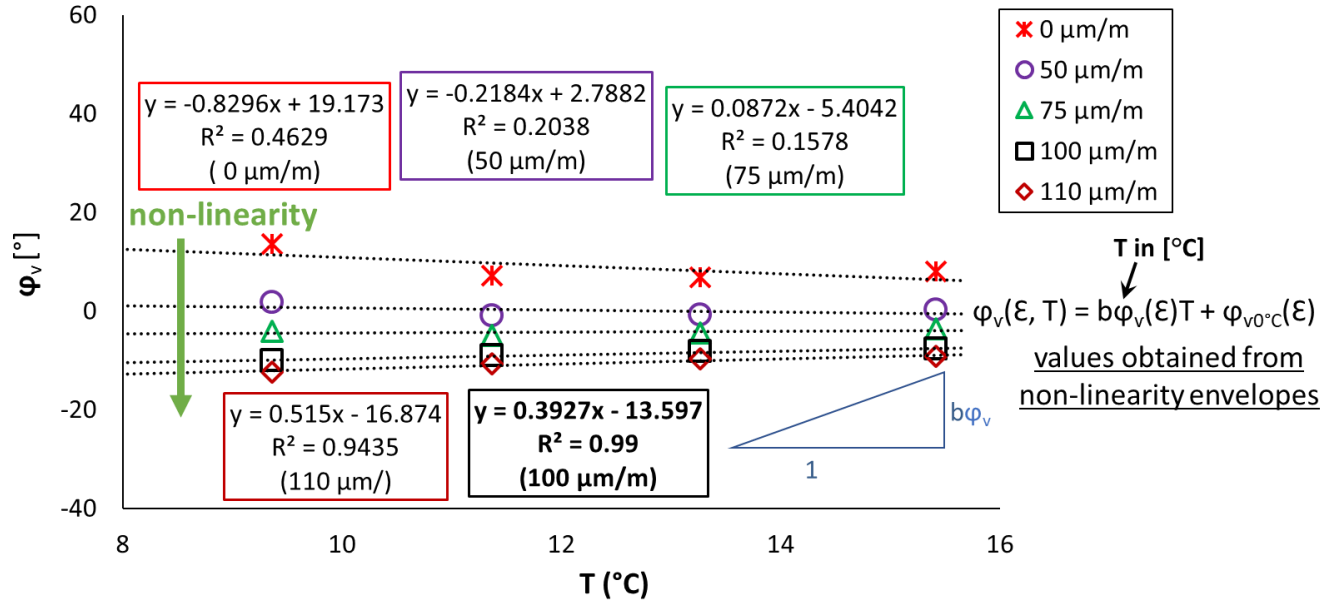

Figure 2.1.24. CMT results obtained for Mix PMB - 5: Regression of estimated values of |E*| φ_E, |ν*| and φ_ν as a function of temperature.

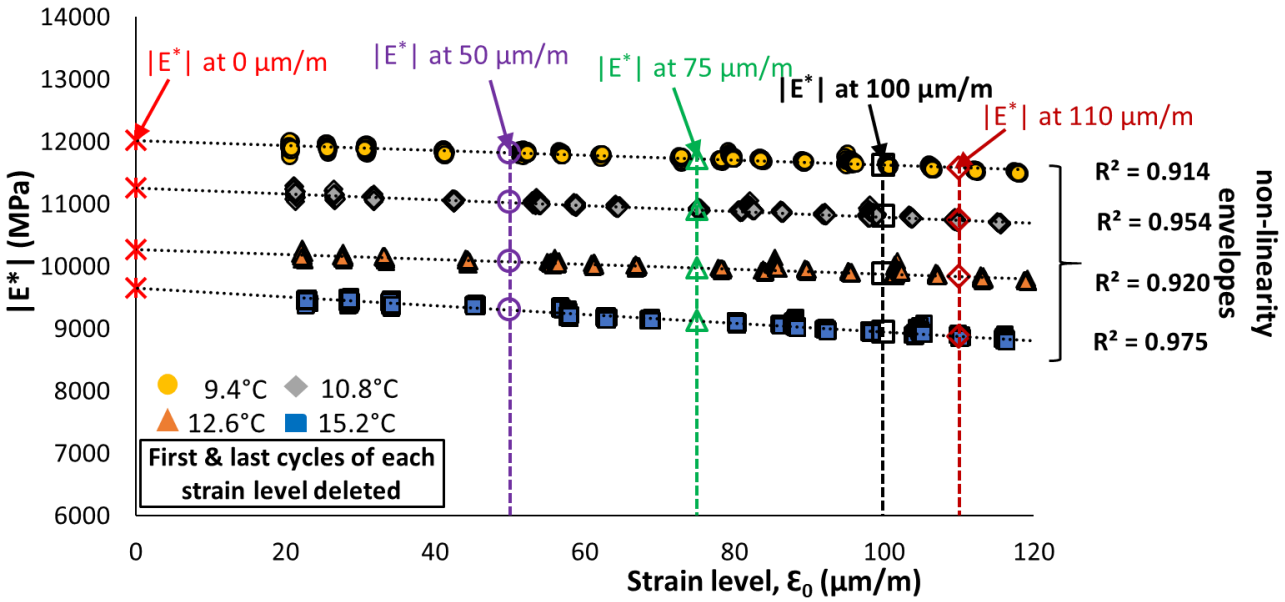

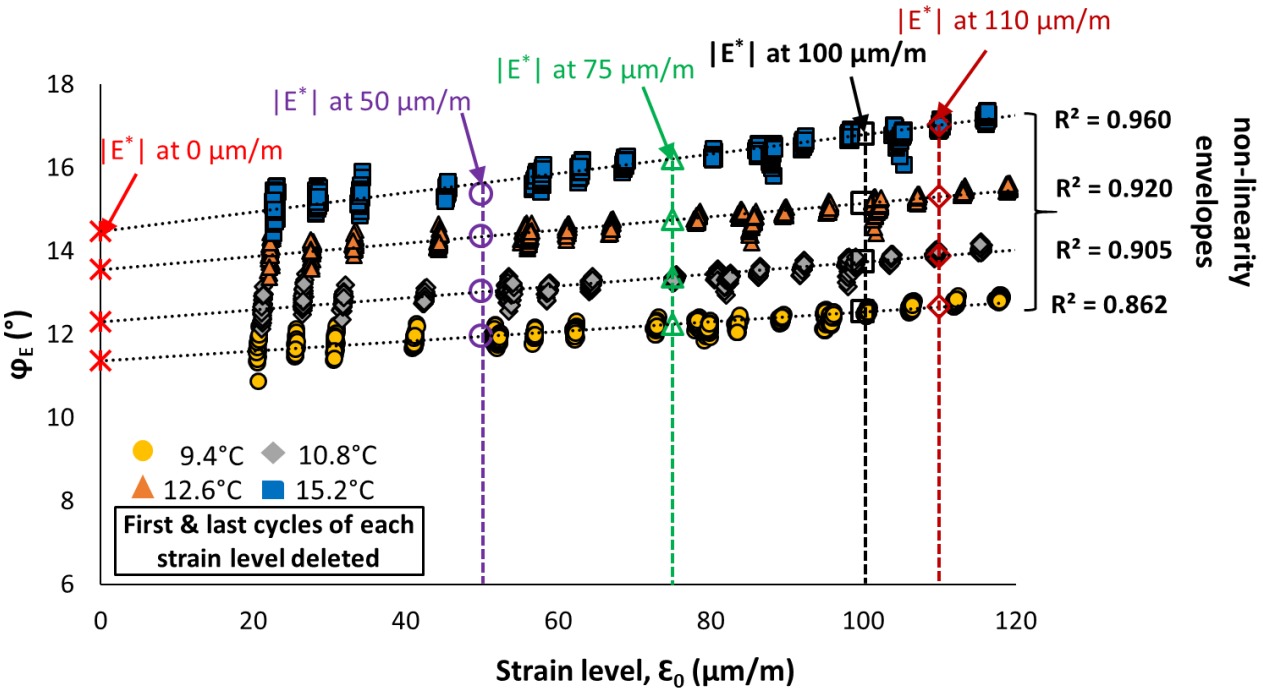
|E*| at 110 µm/m
|E*| at 100 µm/m
|E*| at 75 µm/m
|E*| at 50 µm/m
|E*| at 0 µm/m
R² = 0.960
R² = 0.920
R² = 0.905
R² = 0.862
non-linearity envelopes
φE (°)
9.4°C
10.8°C
12.6°C
15.2°C
First & last cycles of each strain level deleted
Strain level, ε0 (µm/m)

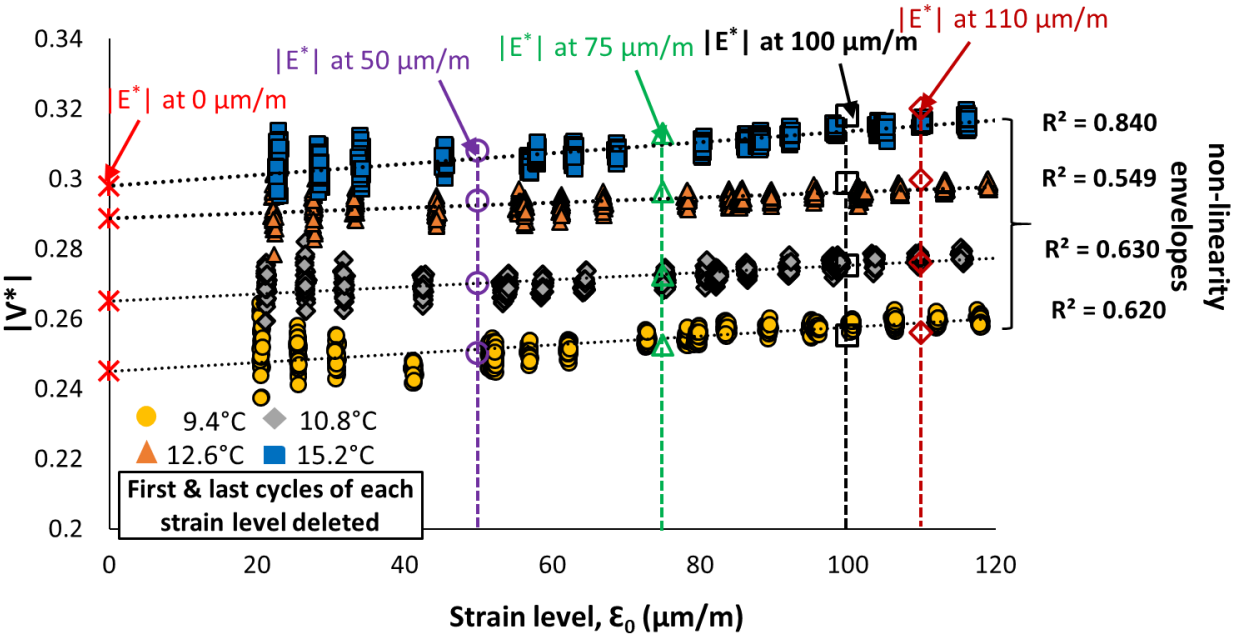
|E*| at 110 µm/m
|E*| at 100 µm/m
|E*| at 75 µm/m
|E*| at 50 µm/m
|E*| at 0 µm/m
R² = 0.840
R² = 0.549
R² = 0.630
R² = 0.620
non-linearity envelopes
|V*|
9.4°C
10.8°C
12.6°C
15.2°C
First & last cycles of each strain level deleted
Strain level, ε0 (µm/m)

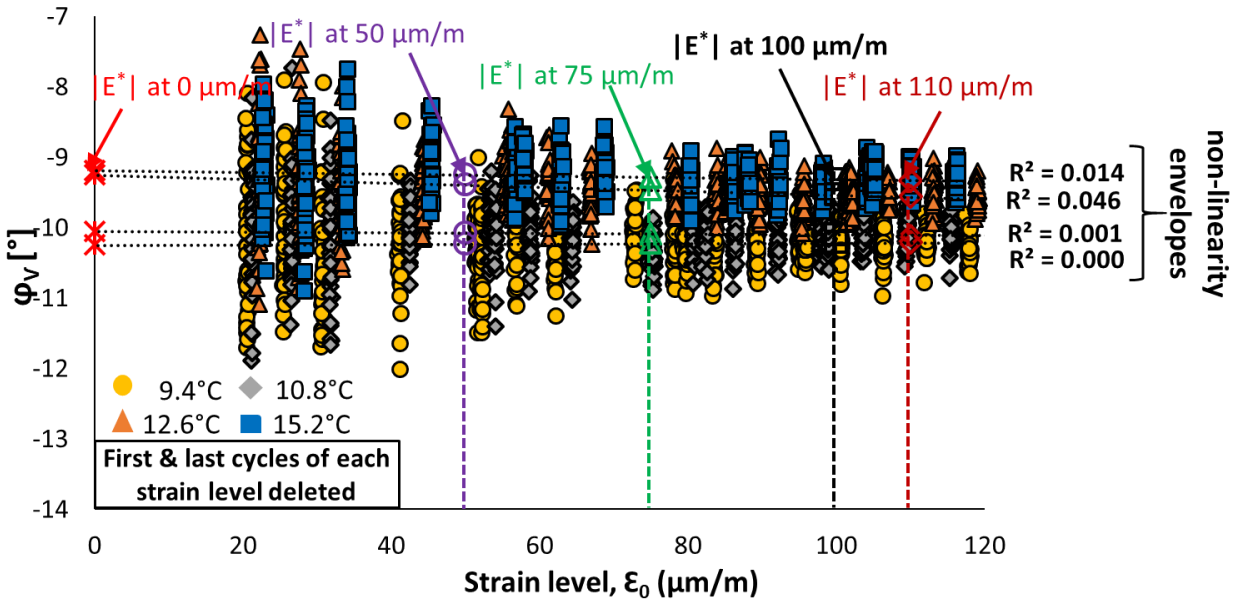

2.1.25. CMT results obtained for Mix PMB - 6: $|E^*|$ φ_E, $|\nu^*|$ and φ_ν against applied strain amplitude at different temperatures.

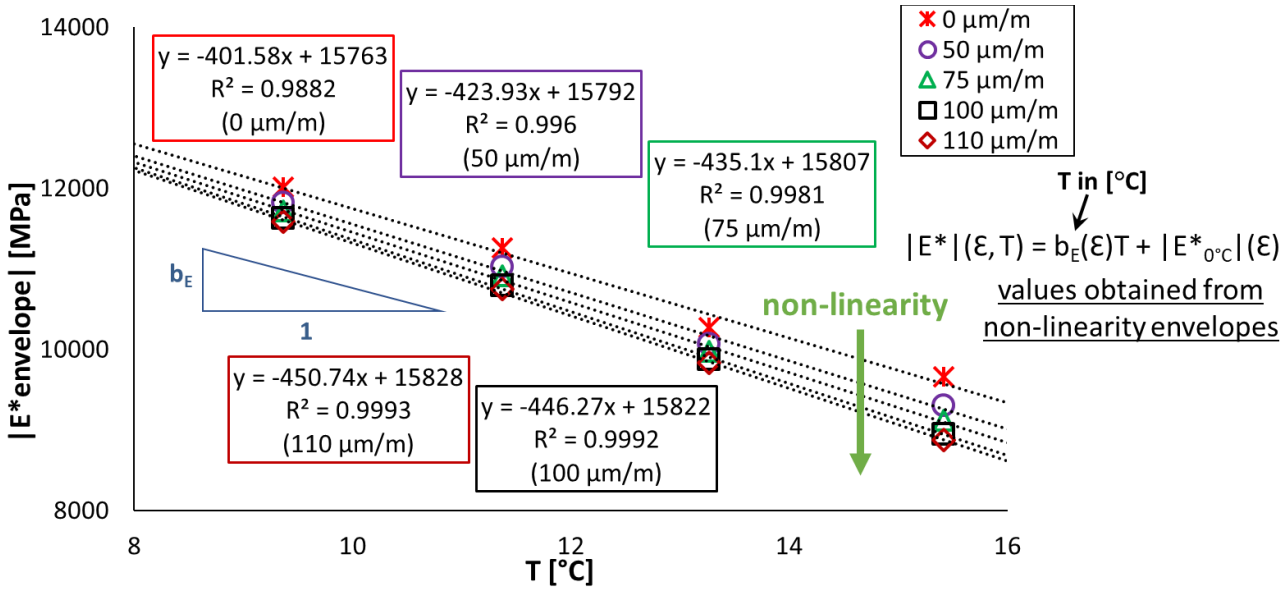

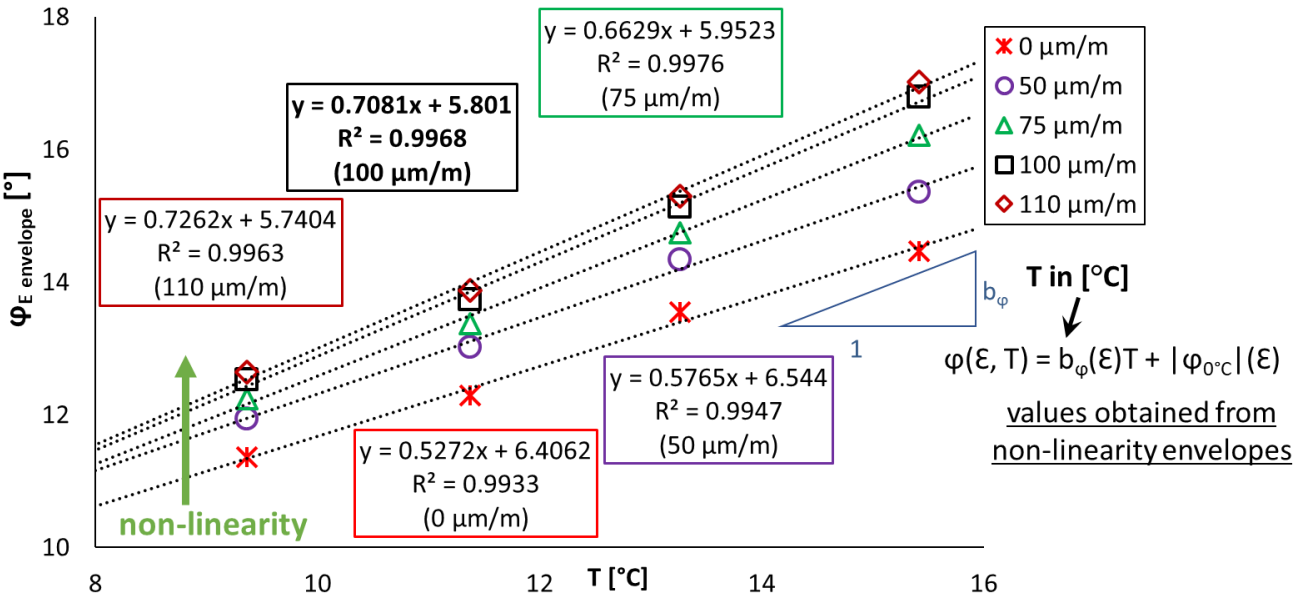
18
16
14
12
10
8
10
12
14
16
φE envelope [°]
T [°C]
y = 0.6629x + 5.9523
R² = 0.9976
(75 µm/m)
y = 0.7081x + 5.801
R² = 0.9968
(100 µm/m)
y = 0.7262x + 5.7404
R² = 0.9963
(110 µm/m)
y = 0.5765x + 6.544
R² = 0.9947
(50 µm/m)
y = 0.5272x + 6.4062
R² = 0.9933
(0 µm/m)
non-linearity
0 µm/m
50 µm/m
75 µm/m
100 µm/m
110 µm/m
bφ
1
T in [°C]
φ(Ɛ, T) = bφ(Ɛ)T + |φ0°C|(Ɛ)
values obtained from
non-linearity envelopes

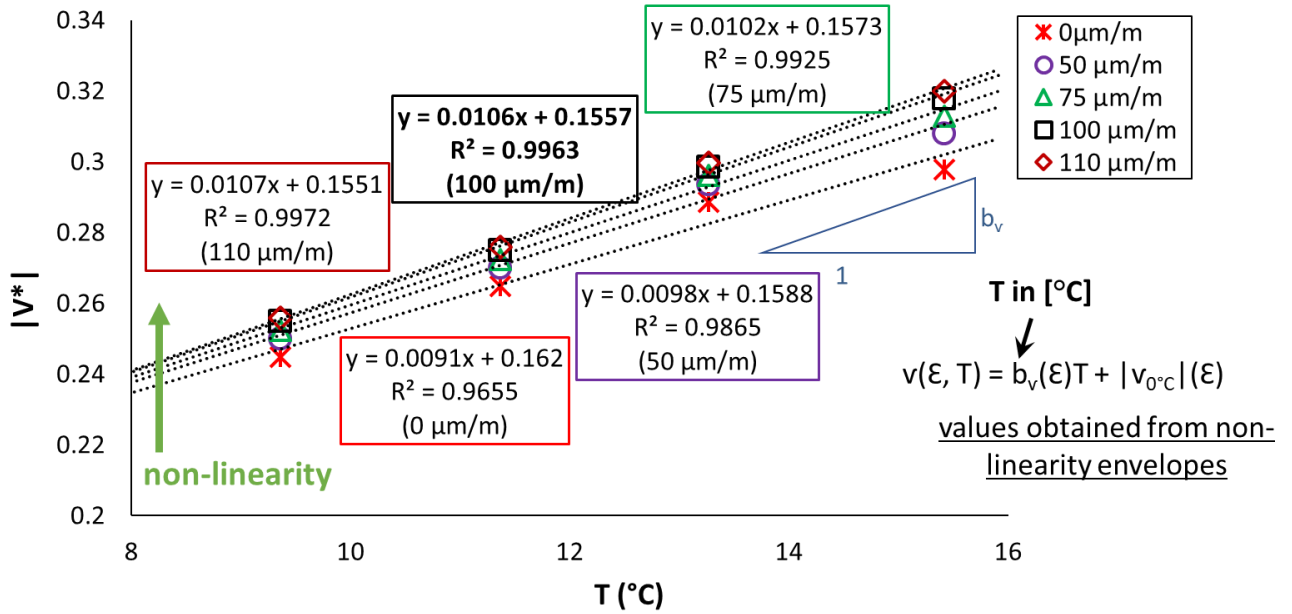
0.34
0.32
0.3
0.28
0.26
0.24
0.22
0.2
8
10
12
14
16
|V*|
T (°C)
y = 0.0102x + 0.1573
R² = 0.9925
(75 µm/m)
y = 0.0106x + 0.1557
R² = 0.9963
(100 µm/m)
y = 0.0107x + 0.1551
R² = 0.9972
(110 µm/m)
y = 0.0098x + 0.1588
R² = 0.9865
(50 µm/m)
y = 0.0091x + 0.162
R² = 0.9655
(0 µm/m)
non-linearity
0µm/m
50 µm/m
75 µm/m
100 µm/m
110 µm/m
bv
1
T in [°C]
v(Ɛ, T) = bv(Ɛ)T + |v0°C|(Ɛ)
values obtained from non-
linearity envelopes

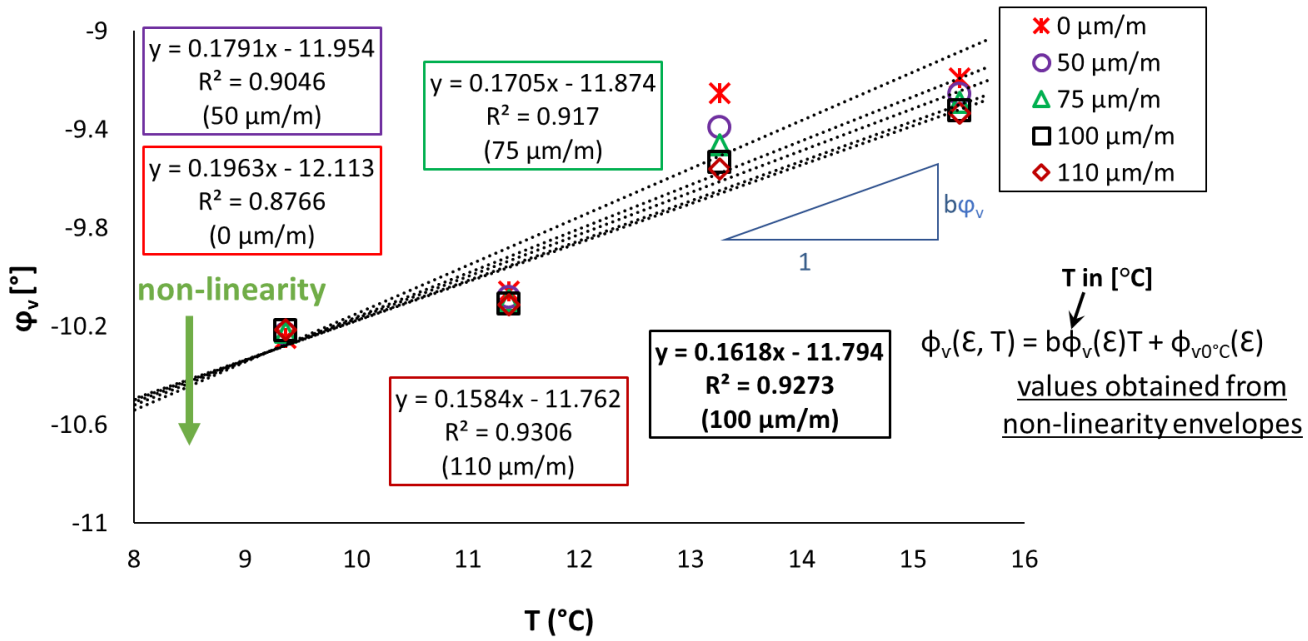

Figure 2.1.26. CMT results obtained for Mix PMB - 6: Regression of estimated values of |E*| φ_E, |v*| and φ_v as a function of temperature.

3. Evolution of 3D mechanical properties (E*eq. and v*eq.) during cyclic loading and rest periods.

3.1. PFRT results

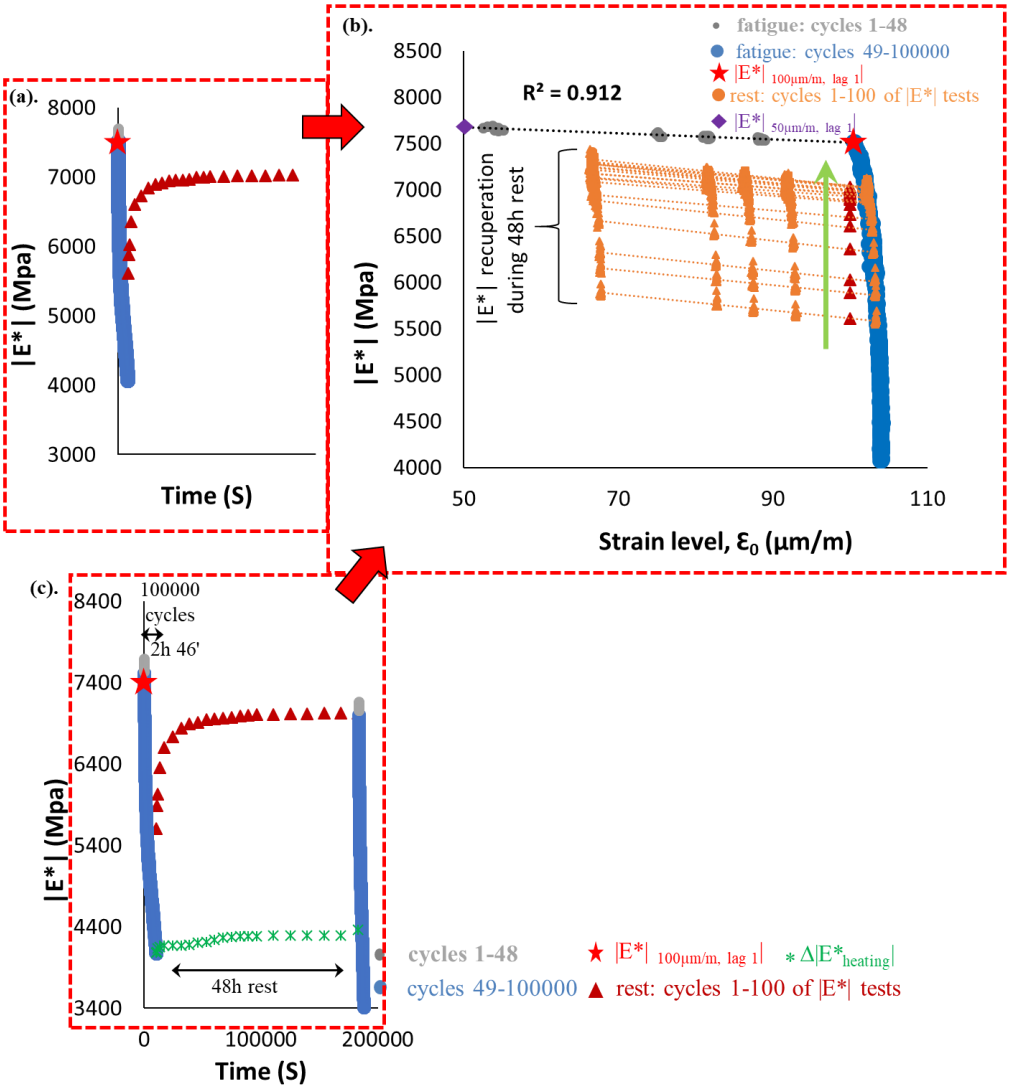

3.1.1. PFRT results obtained for mix 70/100 - 1: (a) |E*| as a function of time during the first fatigue lag and rest period (b) |E*| as a function of applied strain amplitude during the first fatigue lags and the short complex modulus tests performed within its following rest periods; (c) |E*| as a function of time during the five fatigue lags and rest periods [Red stars indicate values of |E*| estimated at 100 µm/m at the beginning of fatigue lag, green asterisk shows values of $\Delta|E^*_{heating}|$ as influence of self-heating and brown triangles indicate values of |E*| estimated at 100 µm/m for each short complex modulus test during rest (all these values were obtained using non-linearity envelopes, as shown in Figure (b) for the first fatigue lag and rest period)].

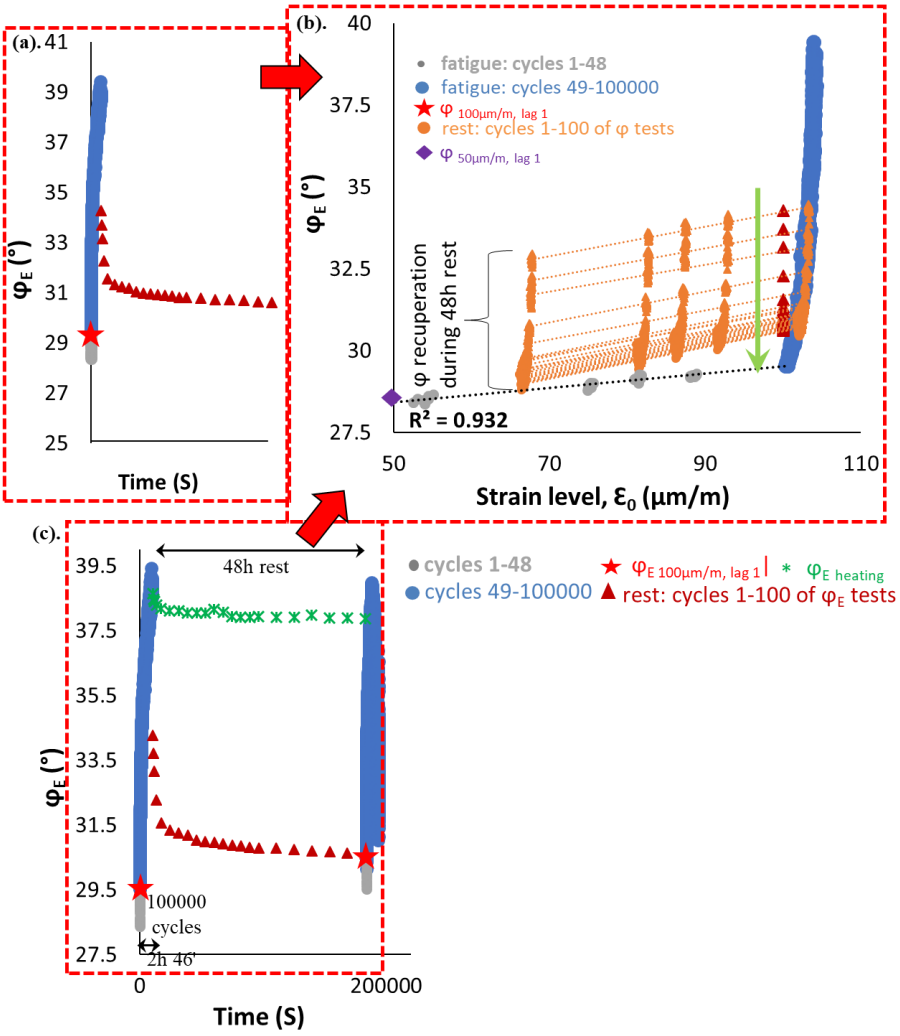

3.1.2. PFRT results obtained for mix 70/100 – 1: (a) φ_E as a function of time during the first fatigue lag and rest period (b) φ_E as a function of applied strain amplitude during the first fatigue lags and the short complex modulus tests performed within its following rest periods; (c) φ_E as a function of time during the five fatigue lags and rest periods (Red stars indicate values of φ_E estimated at 100 µm/m at the beginning of fatigue lag, green asterisk shows values of $\Delta\varphi_{E\ heating}$ as influence of self-heating and brown triangles indicate values of φ_E estimated at 100 µm/m for each short complex modulus test during rest (all these values were obtained using non-linearity envelopes, as shown in (b) for the first fatigue lag and rest period).

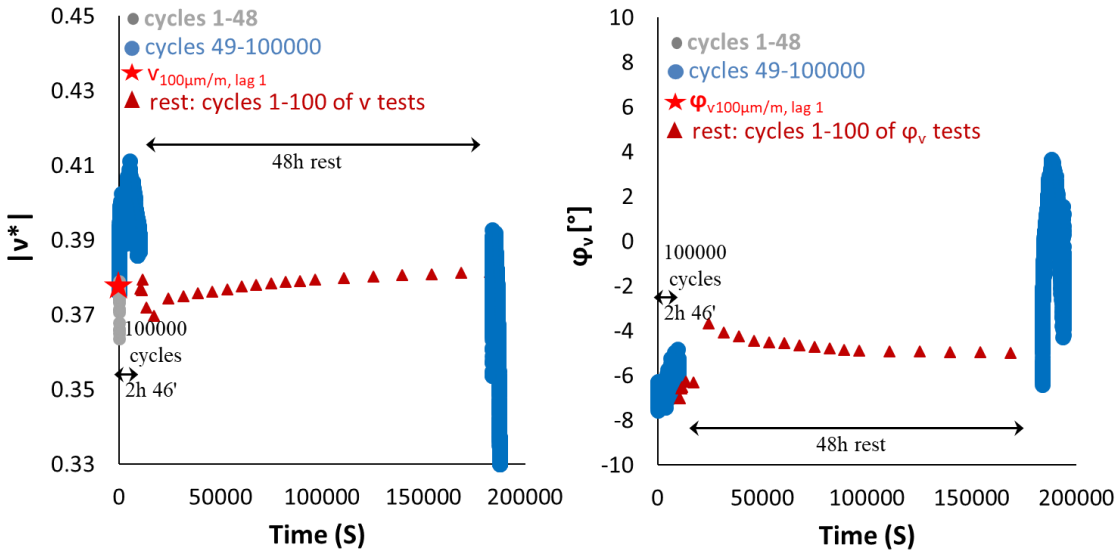

3.1.3. PFRT results obtained for mix 70/100: |v*| and φ_v as a function of time during the first fatigue lags and rest periods (red. stars indicate values of |v*| and φ_v estimated at 100 µm/m at the beginning of fatigue lag, brown triangles indicate values of |v*| and φ_v estimated at 100 µm/m for each short complex modulus test during rest.

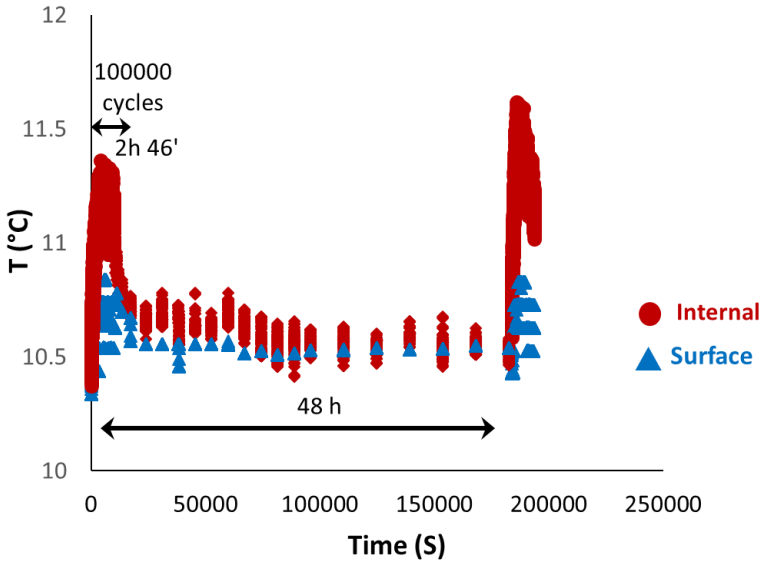

3.1.4. PFRT results obtained for Mix 70/100 – 1: internal and surface temperature evolution during fatigue lags and recovery periods.

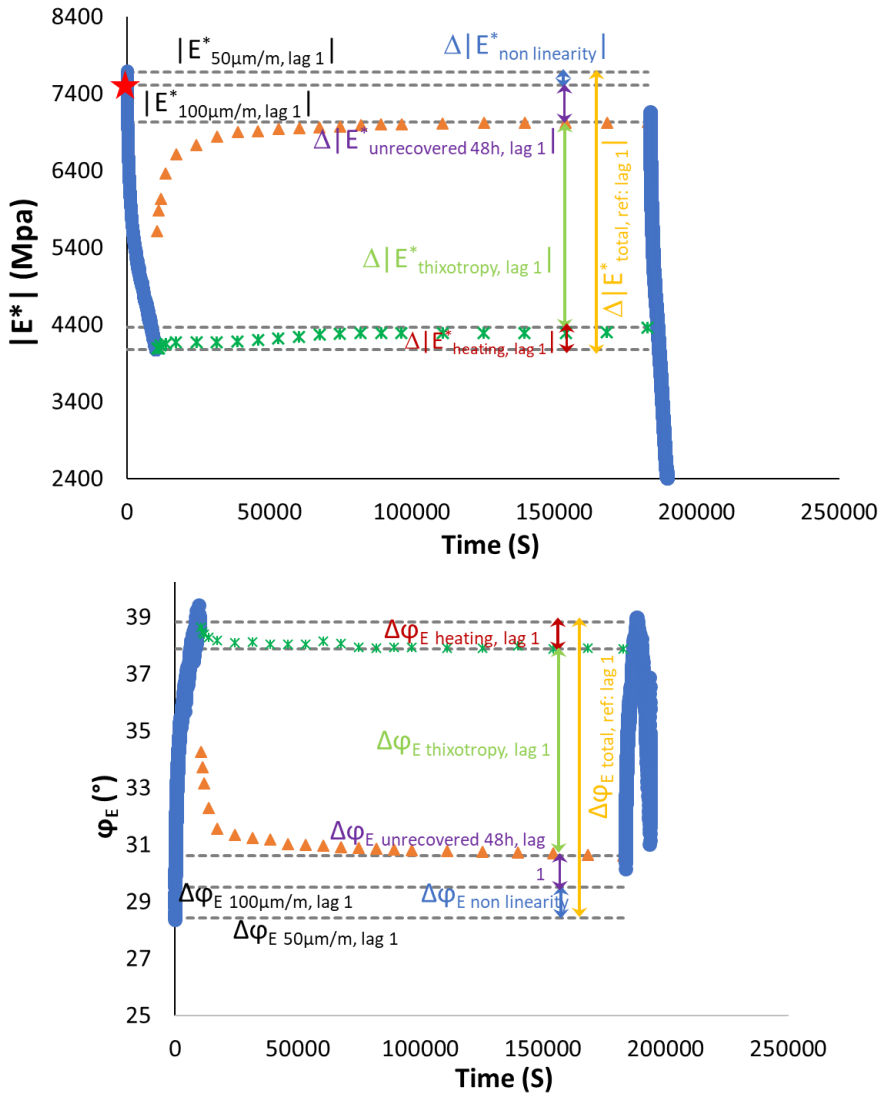

3.1.5. Quantification of different contributions to |E*| and φ_E evolution, for the first two fatigue lags for Mix 70/100 – 1: different envelope line is used for each fatigue lag

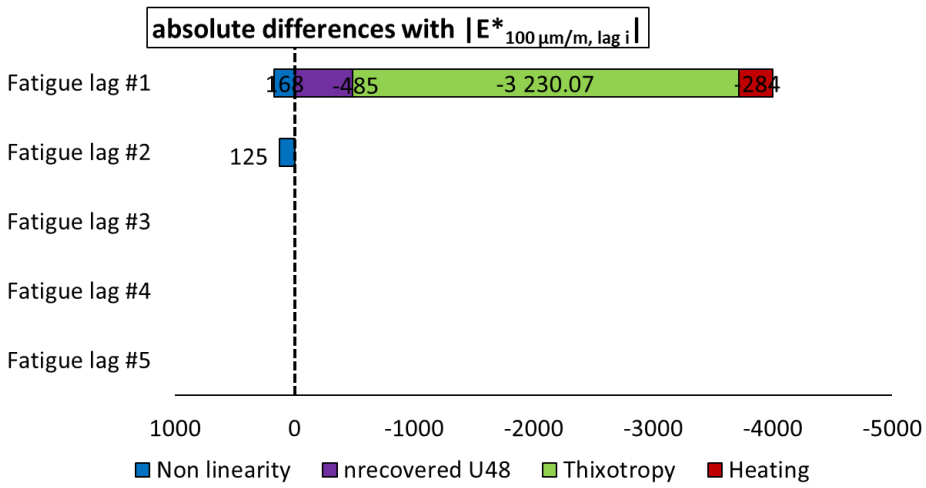

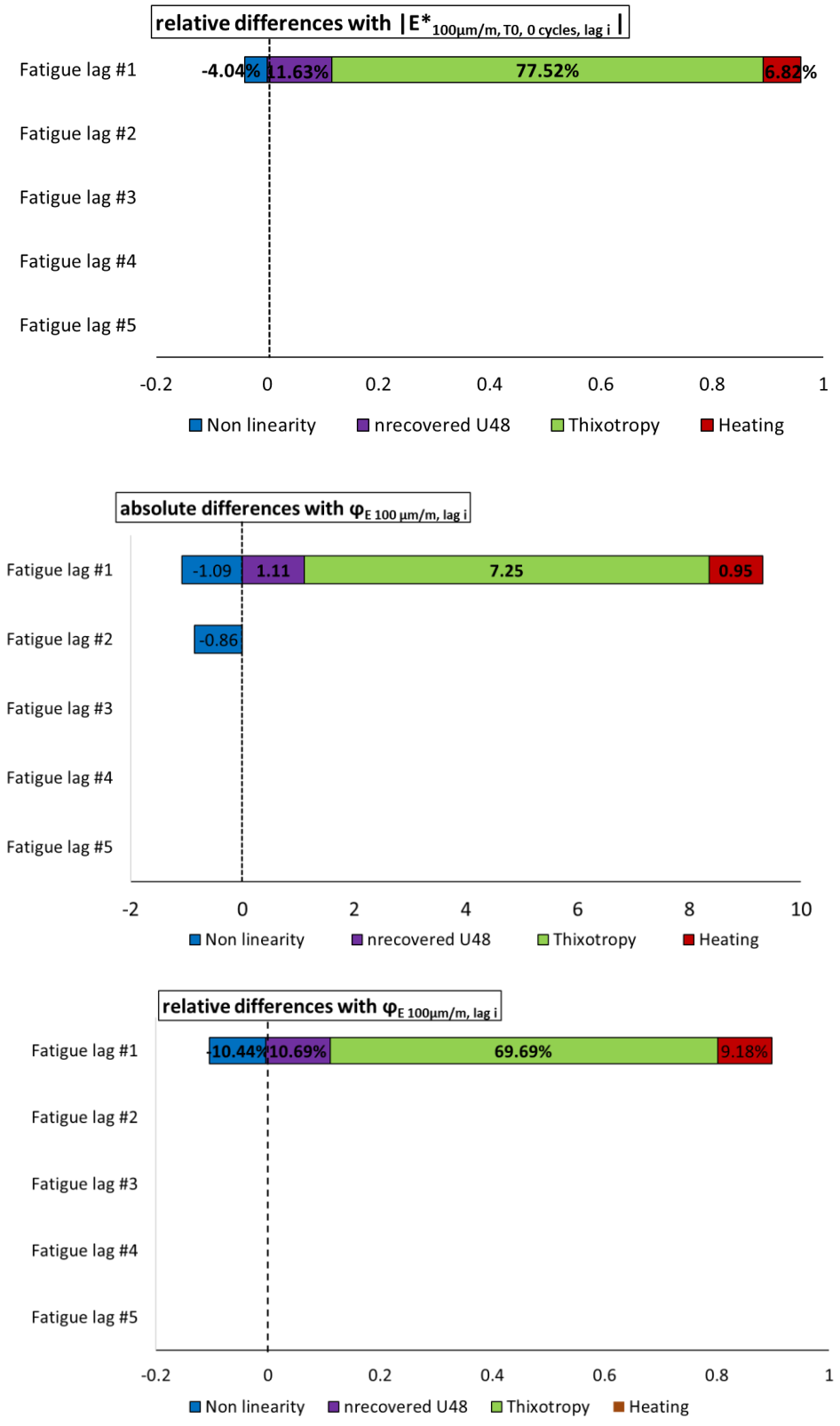

Figure 3.1.6. Quantification of different absolute and relative contributions to |E*| and φ_E evolutions for AZALT 6, calculated using a different envelope line for each fatigue lag.

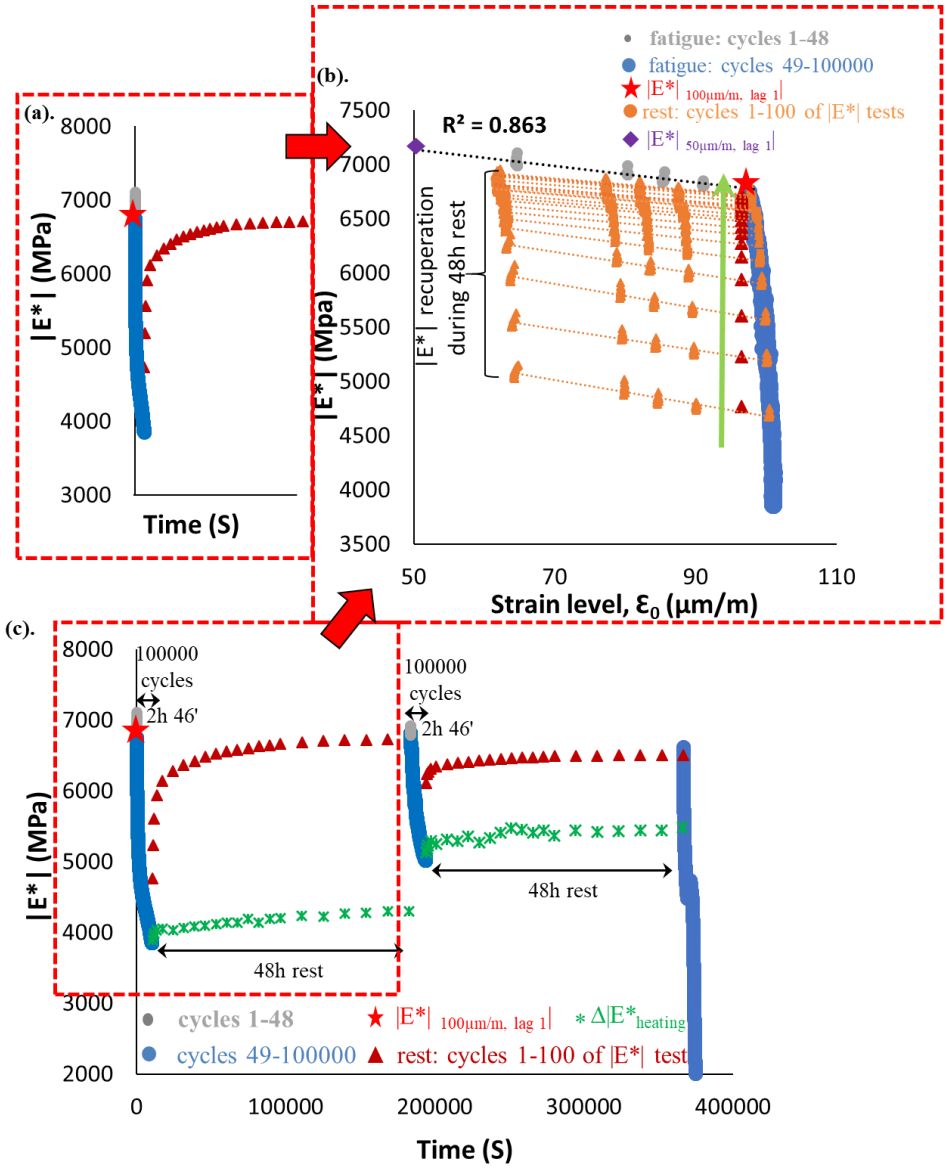

3.1.7. PFRT results obtained for mix 70/100 - 3: (a) |E*| as a function of time during the first fatigue lag and rest period (b) |E*| as a function of applied strain amplitude during the first fatigue lags and the short complex modulus tests performed within its following rest periods; (c) |E*| as a function of time during the two fatigue lags and rest periods [Red stars indicate values of |E*| estimated at 100 µm/m at the beginning of fatigue lag, green asterisk shows values of $\Delta|E^*_{heating}|$ as influence of self-heating and brown triangles indicate values of |E*| estimated at 100 µm/m for each short complex modulus test during rest (all these values were obtained using non-linearity envelopes, as shown in Figure (b) for the first fatigue lag and rest period)].

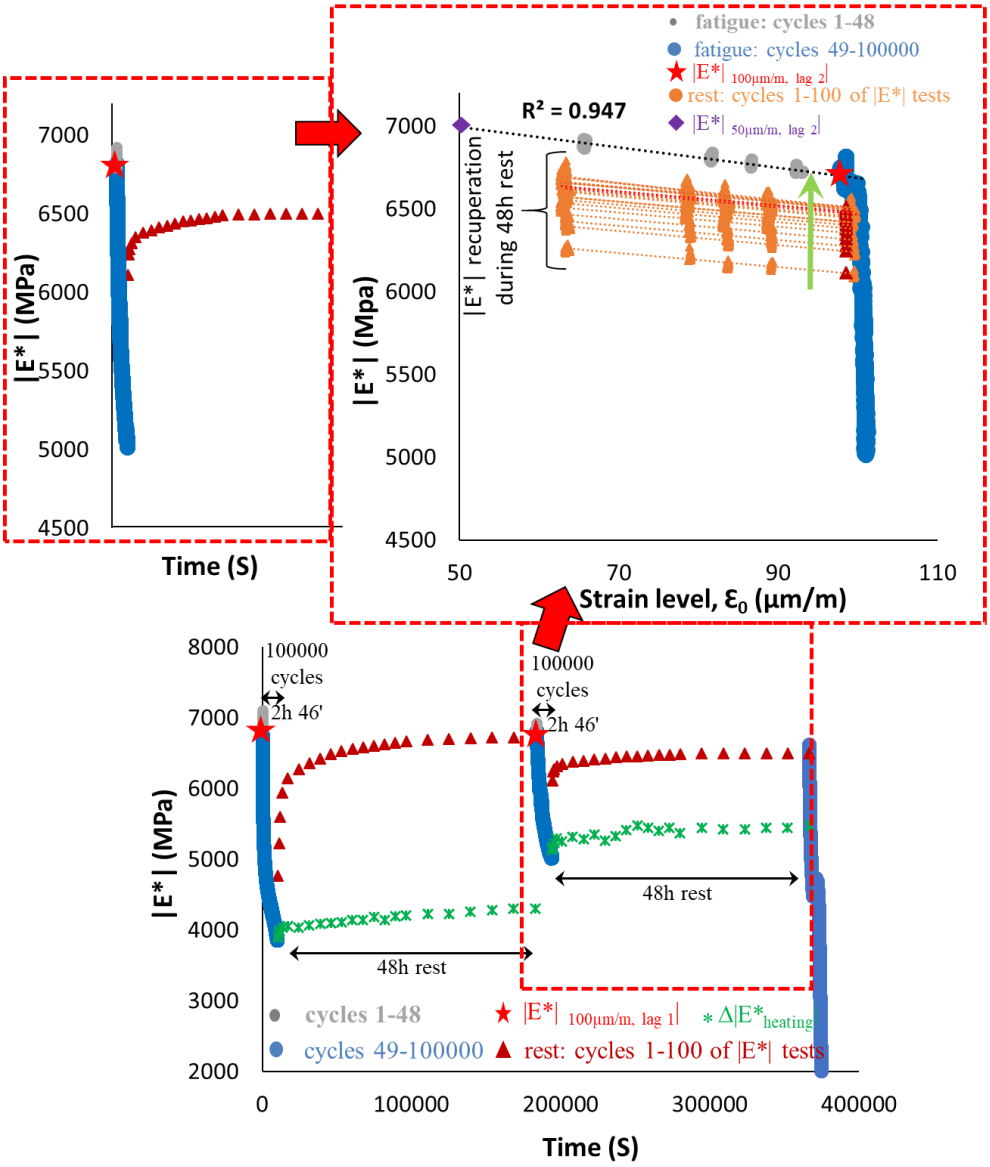

3.1.8. PFRT results obtained for mix 70/100 - 3: (a) |E*| as a function of time during the second fatigue lag and rest period (b) |E*| as a function of applied strain amplitude during the second fatigue lags and the short complex modulus tests performed within its following rest periods; (c) |E*| as a function of time during the two fatigue lags and rest periods [Red stars indicate values of |E*| estimated at 100 µm/m at the beginning of fatigue lag, green asterisk shows values of $\Delta|E^*_{heating}|$ as influence of self-heating and brown triangles indicate values of |E*| estimated at 100 µm/m for each short complex modulus test during rest (all these values were obtained using non-linearity envelopes, as shown in Figure (b) for the first fatigue lag and rest period)].

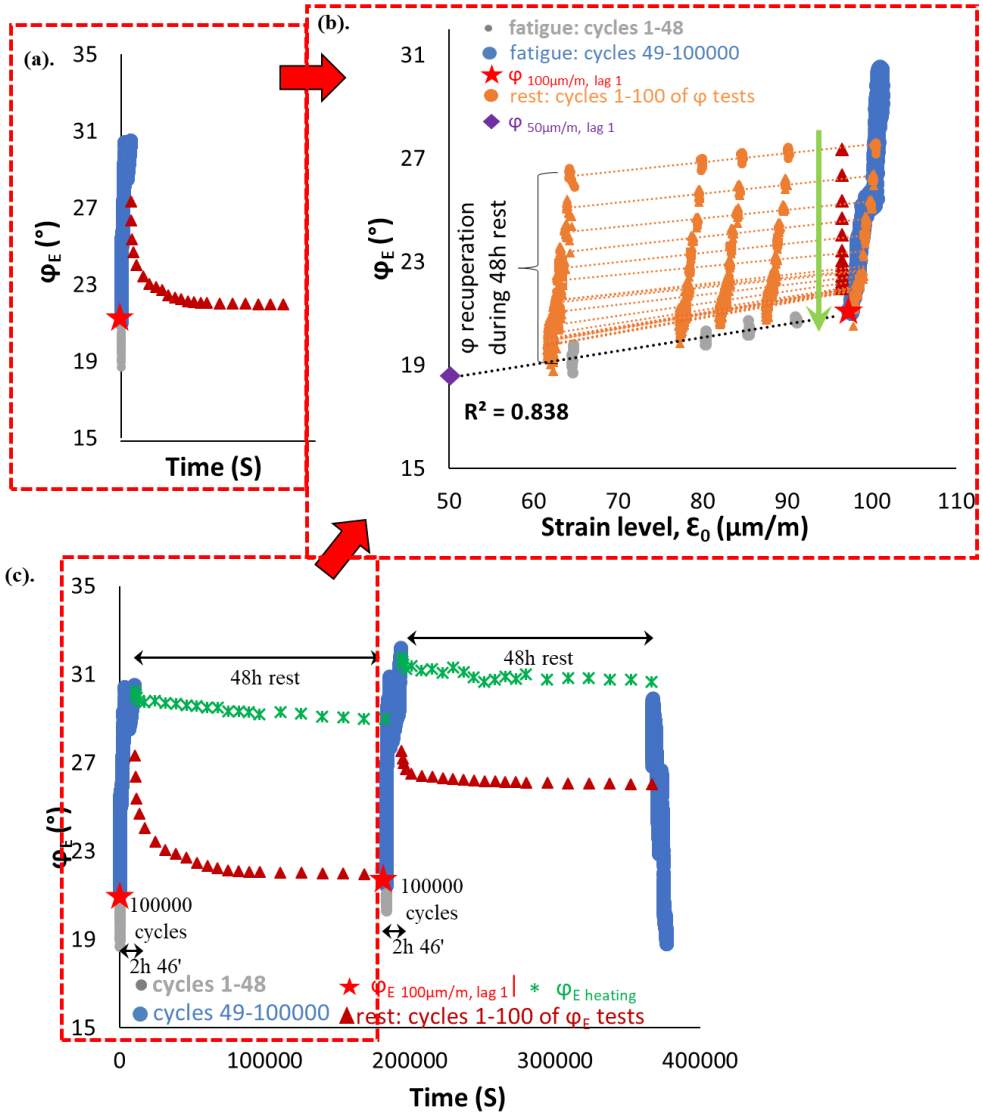

3.1.9. PFRT results obtained for mix 70/100 – 3: (a) φ_E as a function of time during the first fatigue lag and rest period (b) φ_E as a function of applied strain amplitude during the first fatigue lags and the short complex modulus tests performed within its following rest periods; (c) φ_E as a function of time during the two fatigue lags and rest periods (Red stars indicate values of φ_E estimated at 100 µm/m at the beginning of fatigue lag, green asterisk shows values of $\Delta\varphi_{E\ heating}$ as influence of self-heating and brown triangles indicate values of φ_E estimated at 100 µm/m for each short complex modulus test during rest (all these values were obtained using non-linearity envelopes, as shown in (b) for the first fatigue lag and rest period).

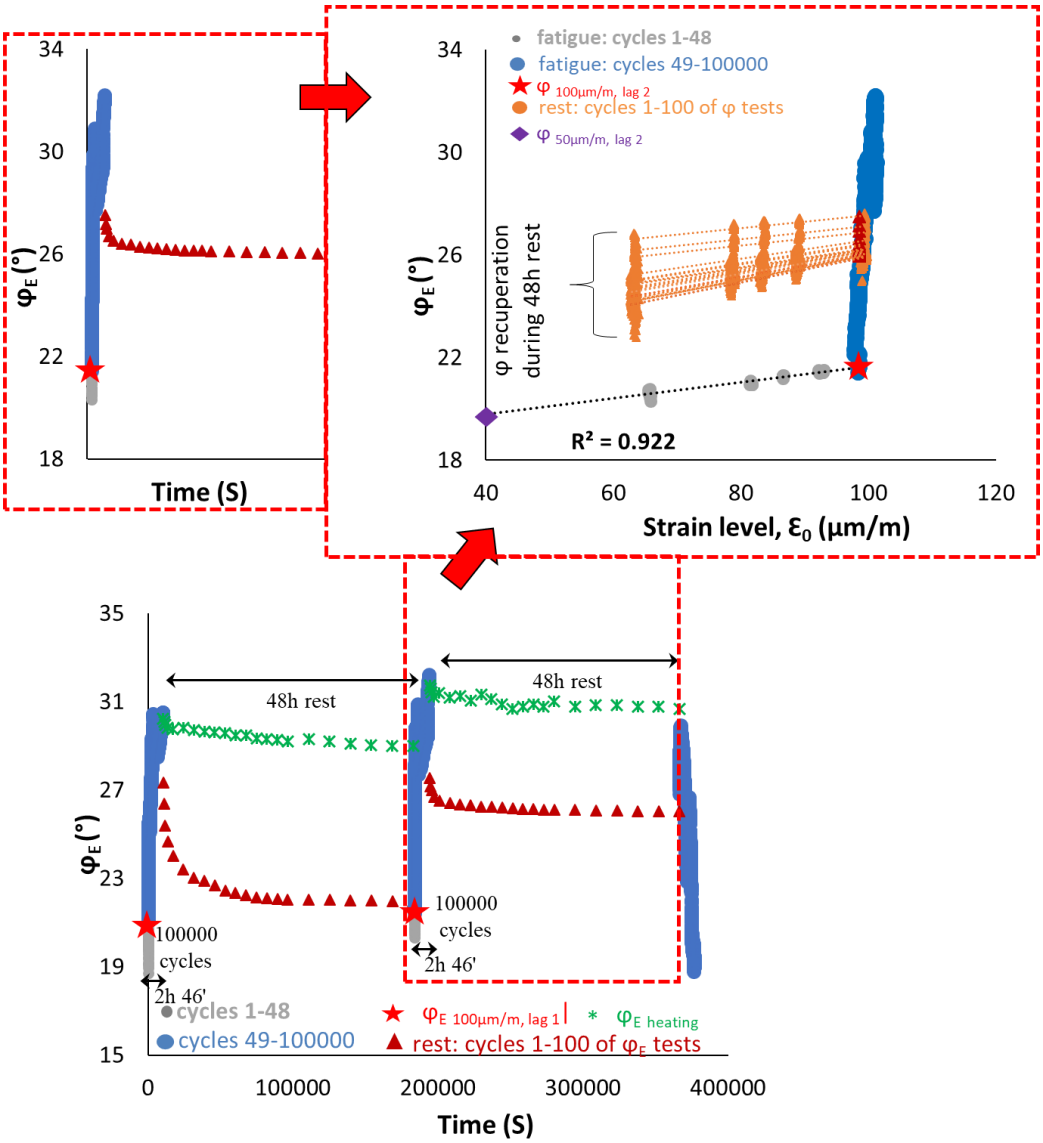

3.1.10. PFRT results obtained for mix 70/100 – 3: (a) φ_E as a function of time during the second fatigue lag and rest period (b) φ_E as a function of applied strain amplitude during the second fatigue lags and the short complex modulus tests performed within its following rest periods; (c) φ_E as a function of time during the two fatigue lags and rest periods (Red stars indicate values of φ_E estimated at 100 µm/m at the beginning of fatigue lag, green asterisk shows values of $\Delta\varphi_{E\ heating}$ as influence of self-heating and brown triangles indicate values of φ_E estimated at 100 µm/m for each short complex modulus test during rest (all these values were obtained using non-linearity envelopes, as shown in (b) for the first fatigue lag and rest period).

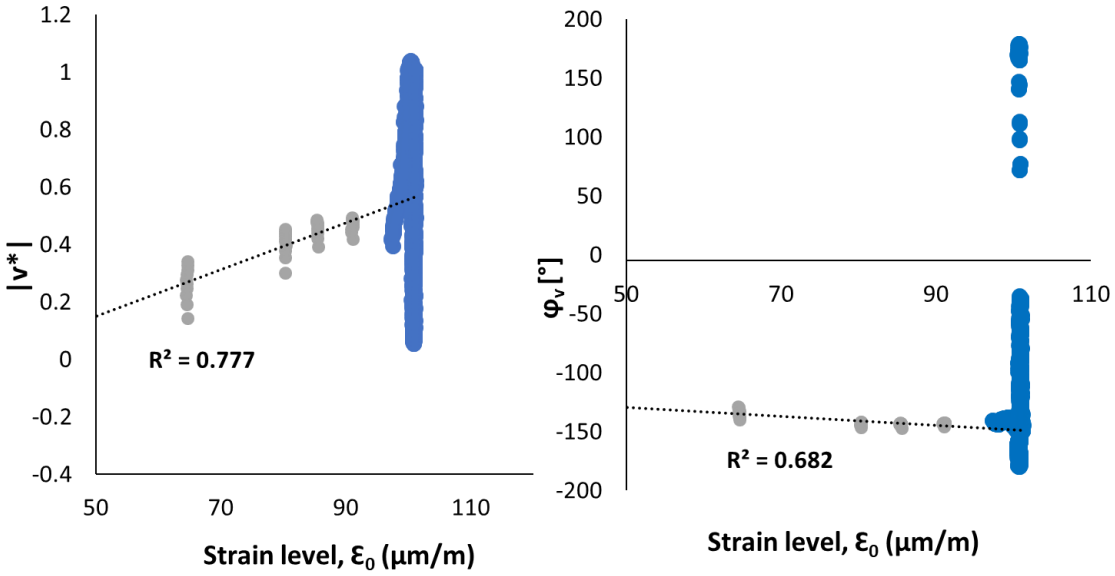

3.1.11. PFRT results obtained for mix 70/100 – 3: |v*| and φ_v as a function of applied strain amplitude during the first fatigue lags.

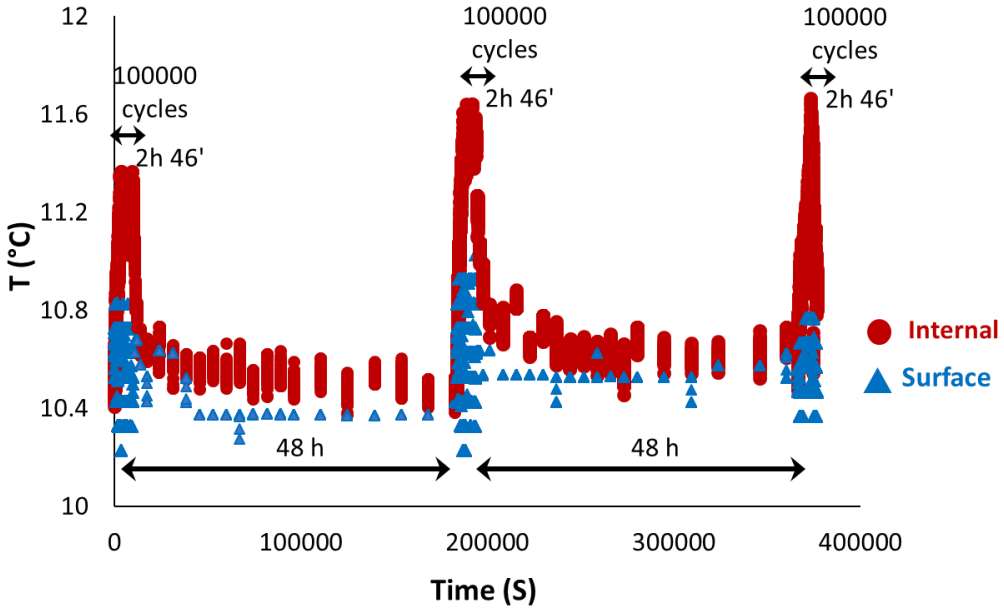

Figure 3.12. PFRT results obtained for mix 70/100 – 3: internal and surface temperature evolution during fatigue lags and recovery periods.

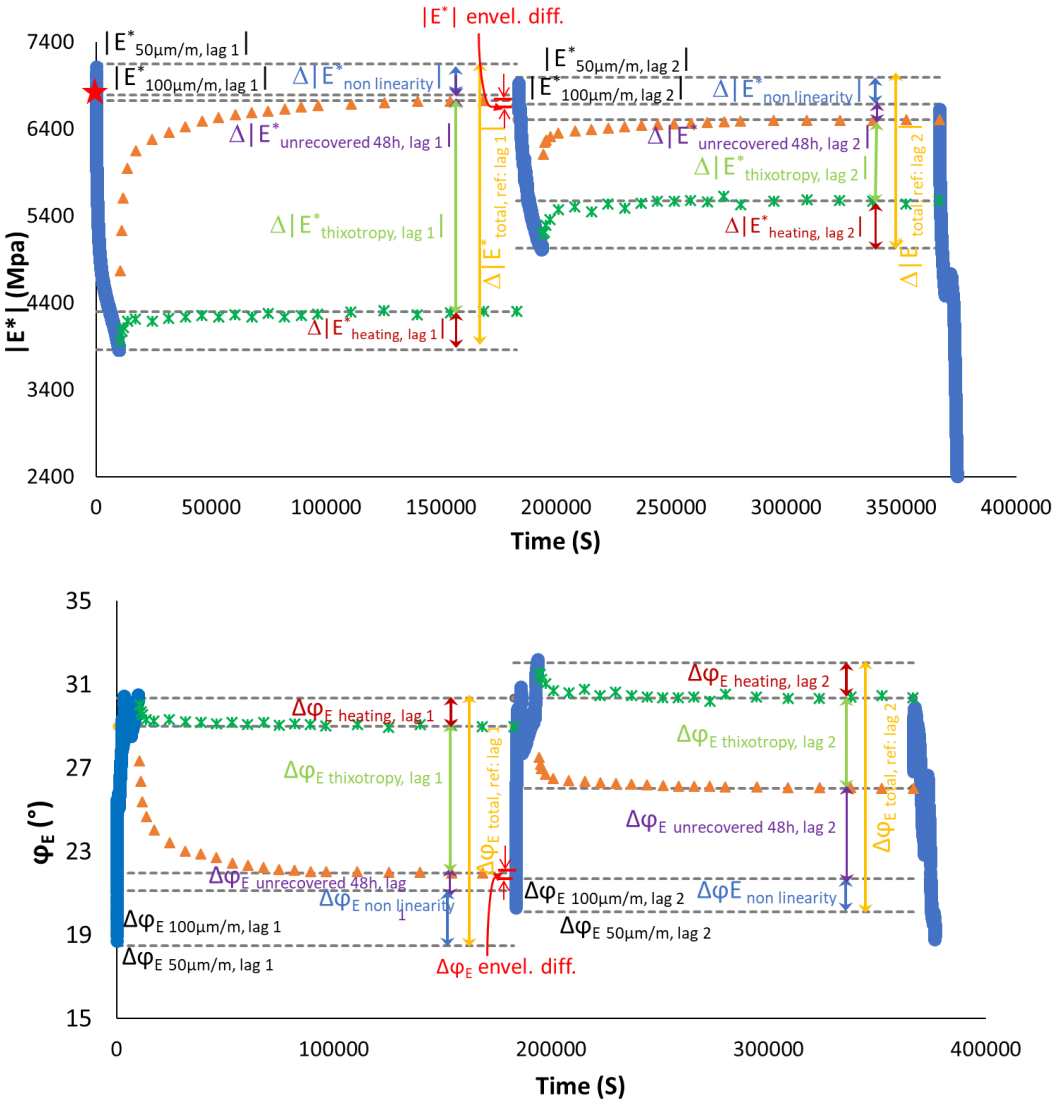

Figure 3.1.13. Quantification of different contributions |E*| and φ_E evolution, for the first two fatigue lags for mix 70/100 - 3: different envelope line is used for each fatigue lag.

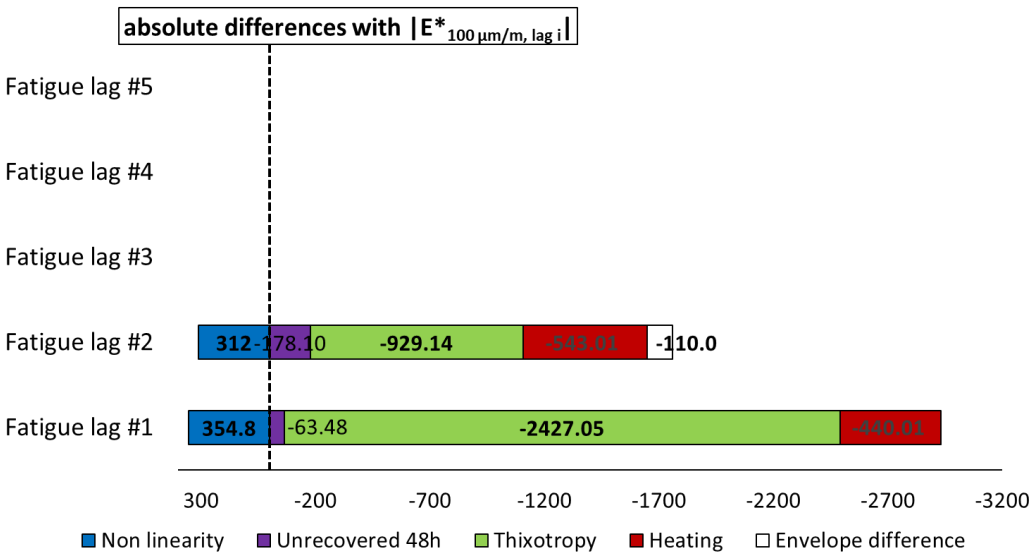

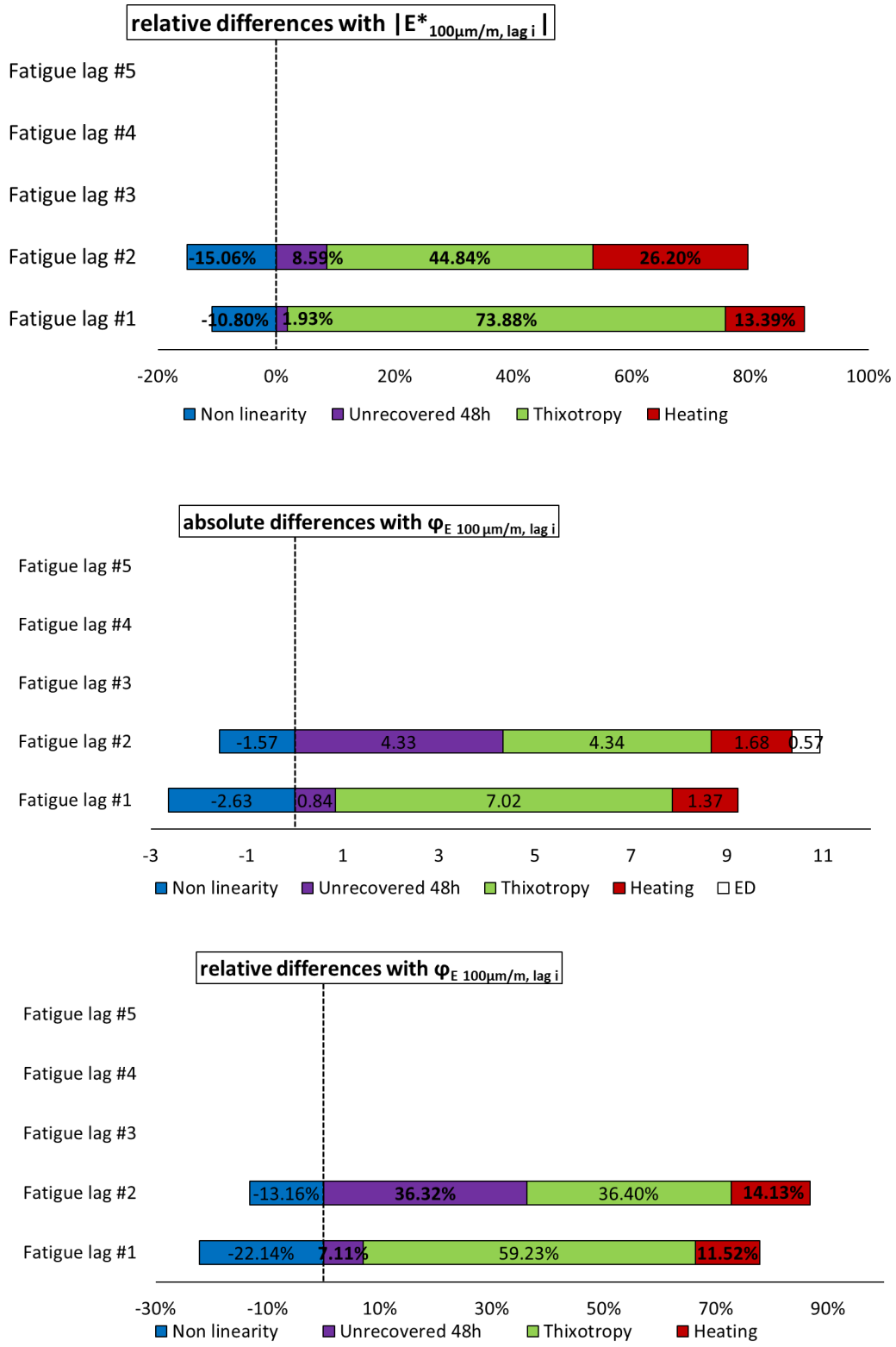

Figure 3.1.14. Quantification of different absolute and relative contributions to |E*| and φ_E evolutions for mix 70/100 - 3, calculated using a different envelope line for each fatigue lag.

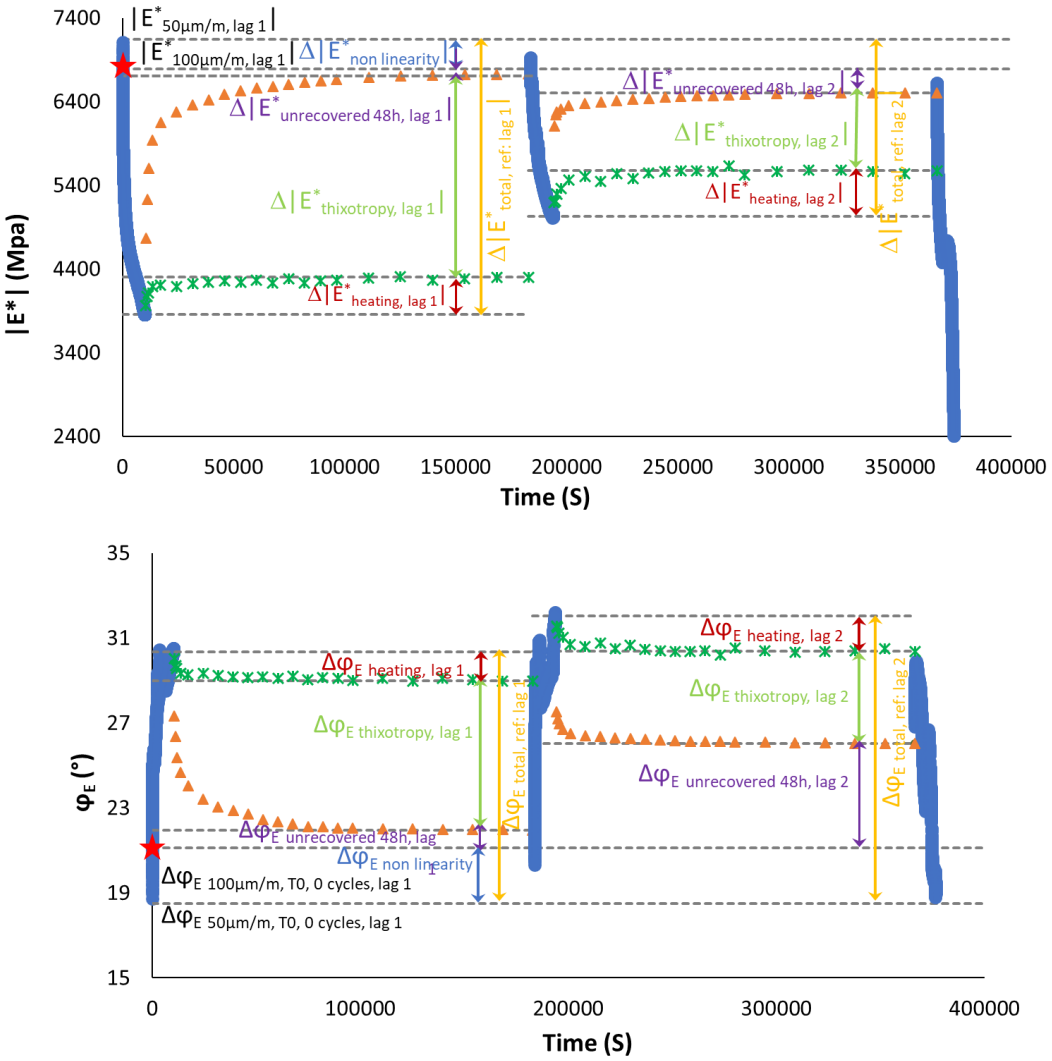

Figure 3.1.15. Quantification of different contributions to |E*| and φ_E evolution during first and second fatigue lags for mix 70/100 - 3: the envelope line of the first fatigue lag is used for all fatigue lags.

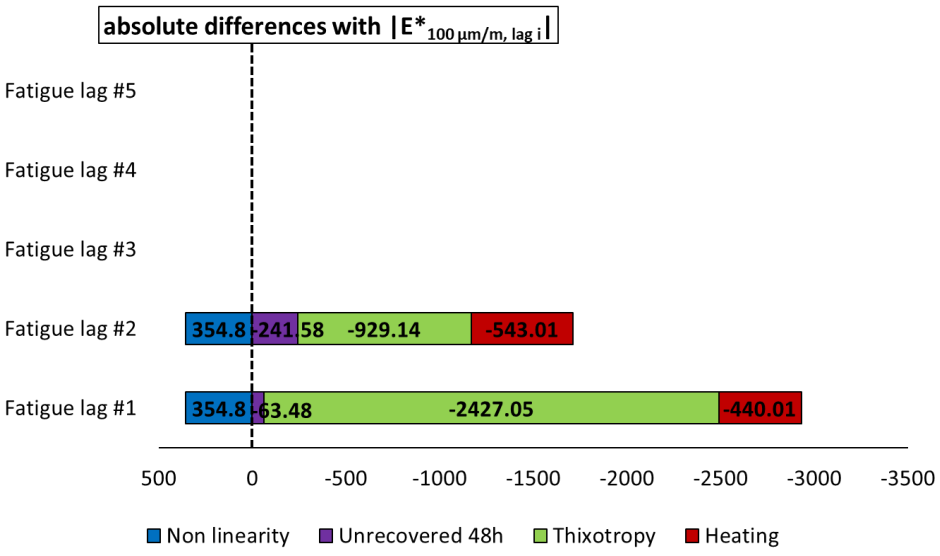

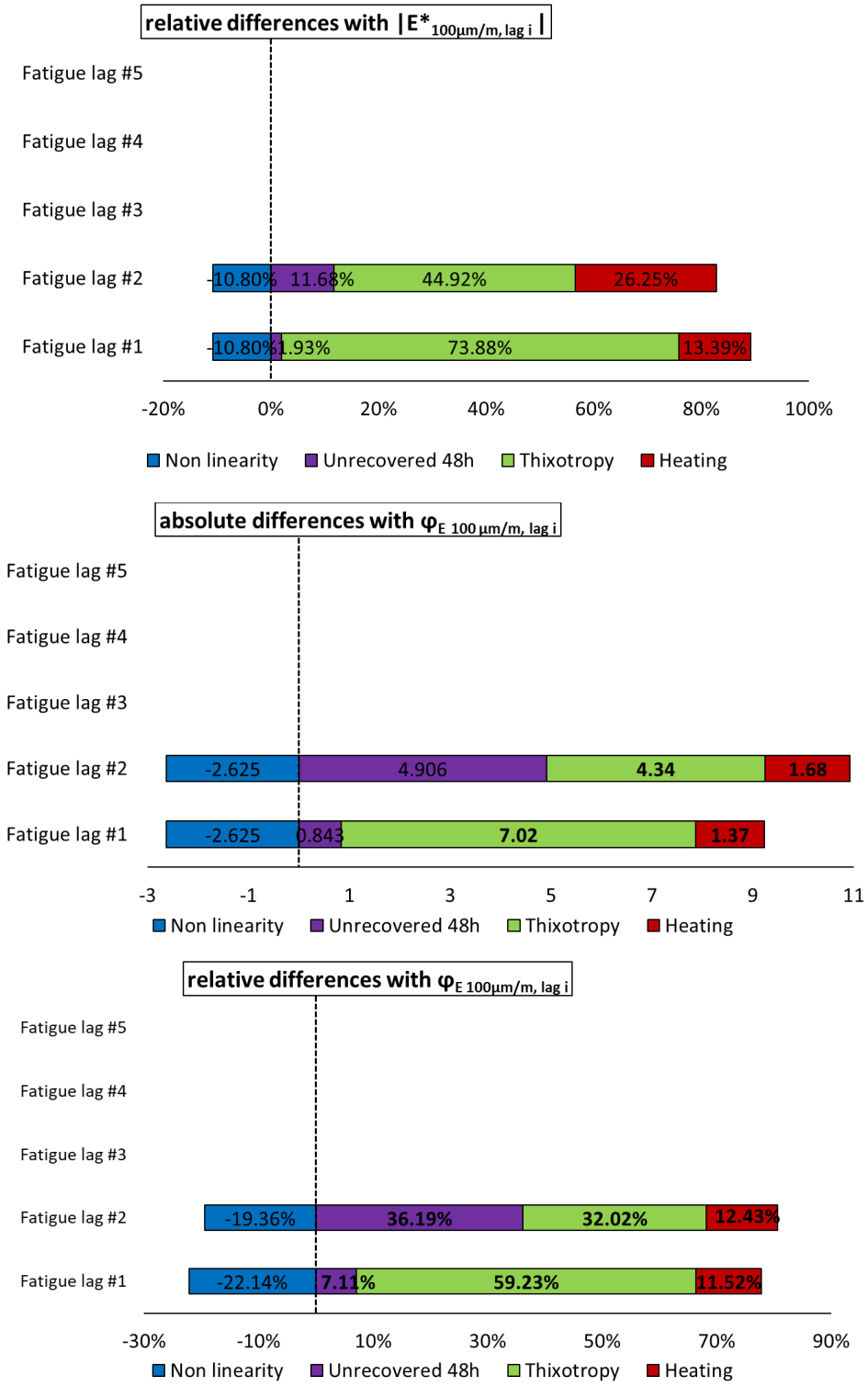

Figure 3.1.16. Quantification of different absolute and relative contributions to |E*| and φ_E evolutions for mix 70/100 - 3, calculated using the envelope line for the first fatigue lag.

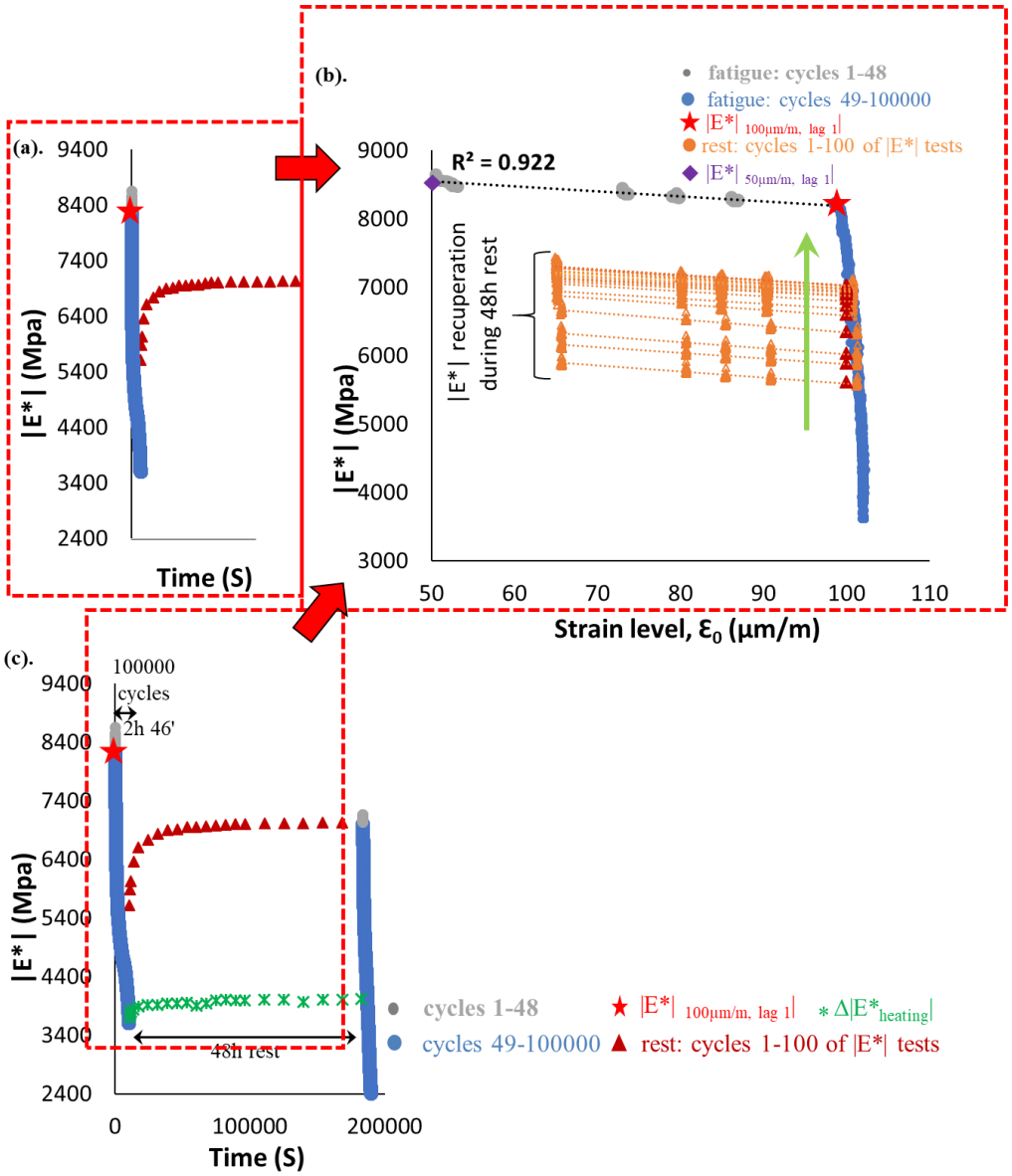

3.1.17. PFRT results obtained for mix 70/100 - 4: (a) |E*| as a function of time during the first fatigue lag and rest period (b) |E*| as a function of applied strain amplitude during the first fatigue lags and the short complex modulus tests performed within its following rest periods; (c) |E*| as a function of time during the two fatigue lags and rest periods [Red stars indicate values of |E*| estimated at 100 µm/m at the beginning of fatigue lag, green asterisk shows values of $\Delta|E^*_{heating}|$ as influence of self-heating and brown triangles indicate values of |E*| estimated at 100 µm/m for each short complex modulus test during rest (all these values were obtained using non-linearity envelopes, as shown in Figure (b) for the first fatigue lag and rest period)].

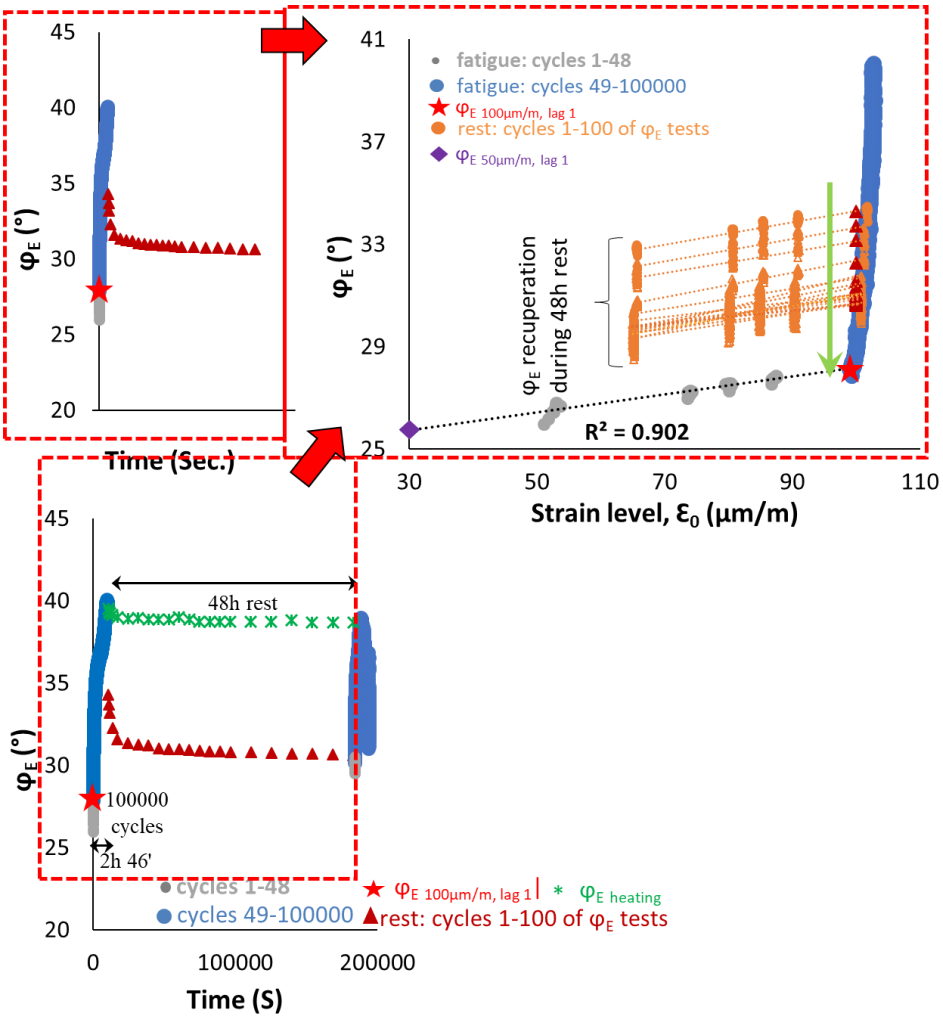

3.1.18. PFRT results obtained for mix 70/100 – 4: (a) φ_E as a function of time during the first fatigue lag and rest period (b) φ_E as a function of applied strain amplitude during the first fatigue lags and the short complex modulus tests performed within its following rest periods; (c) φ_E as a function of time during the two fatigue lags and rest periods (Red stars indicate values of φ_E estimated at 100 µm/m at the beginning of fatigue lag, green asterisk shows values of $\Delta\varphi_{E\ heating}$ as influence of self-heating and brown triangles indicate values of φ_E estimated at 100 µm/m for each short complex modulus test during rest (all these values were obtained using non-linearity envelopes, as shown in (b) for the first fatigue lag and rest period).

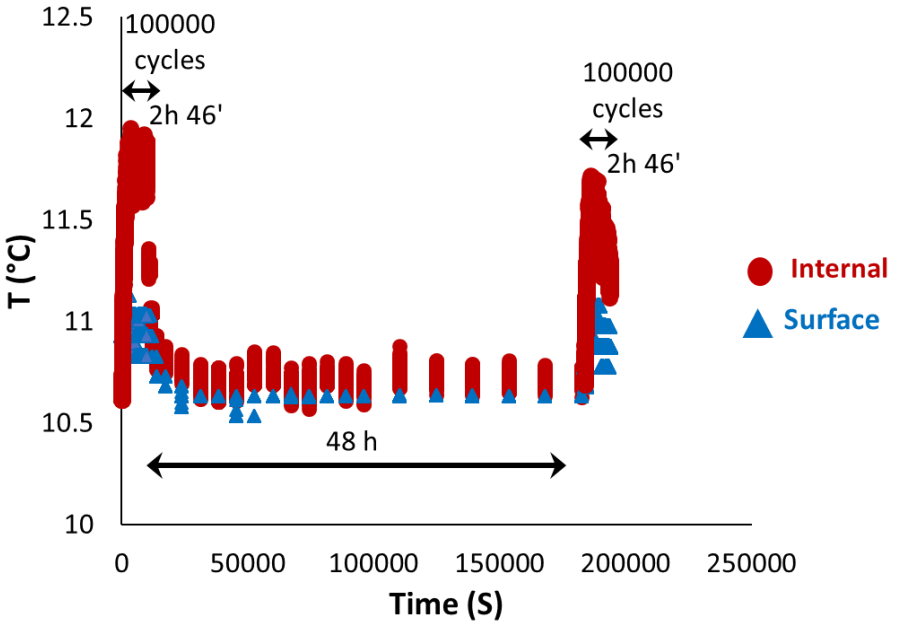

3.1.19. PFRT results obtained for mix 70/100 - 4: internal and surface temperature evolution during fatigue lags and recovery periods.

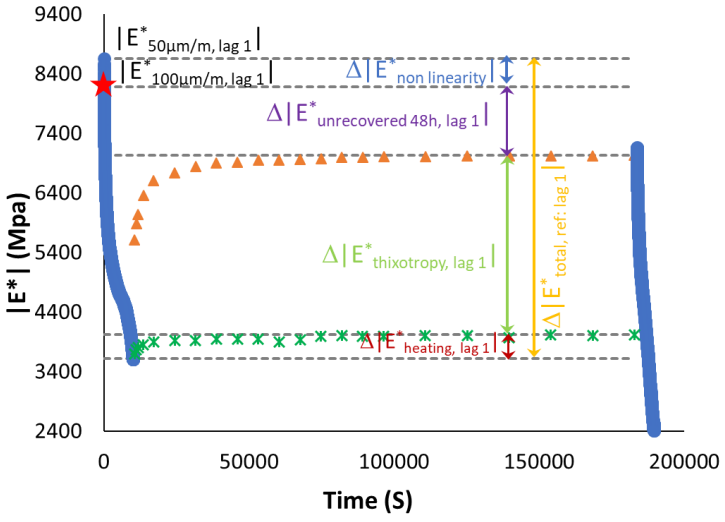

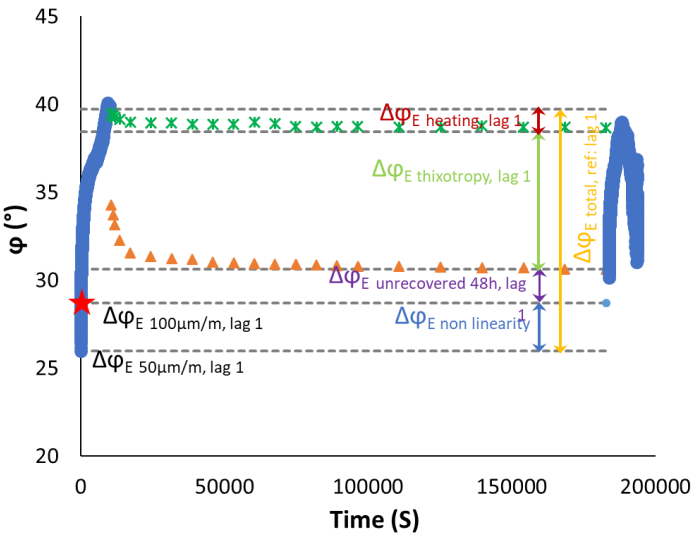

Figure 3.1.20. Quantification of different contributions |E*| and φ_E evolution, for the first two fatigue lags for mix 70/100 - 4: different envelope line is used for each fatigue lag.

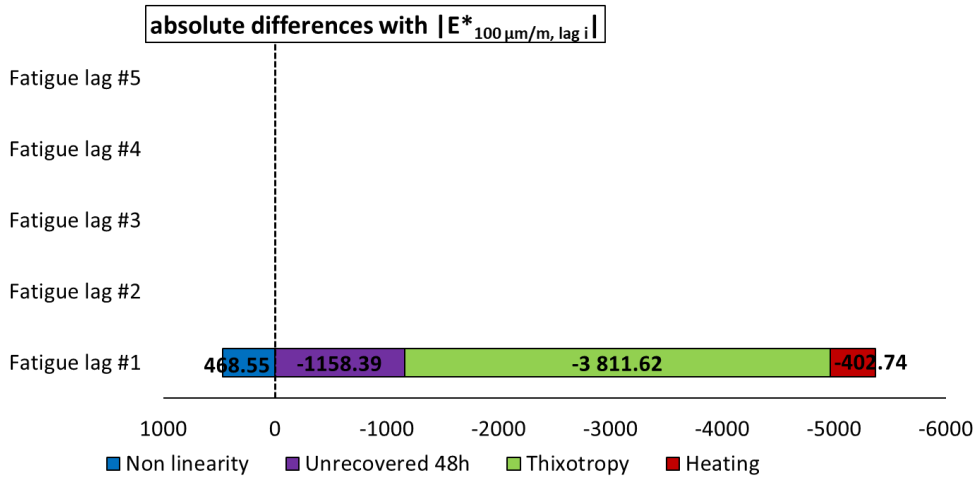

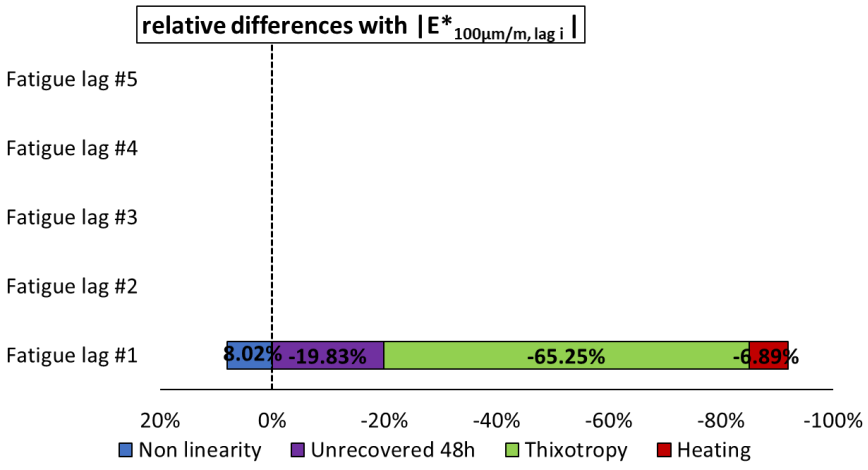

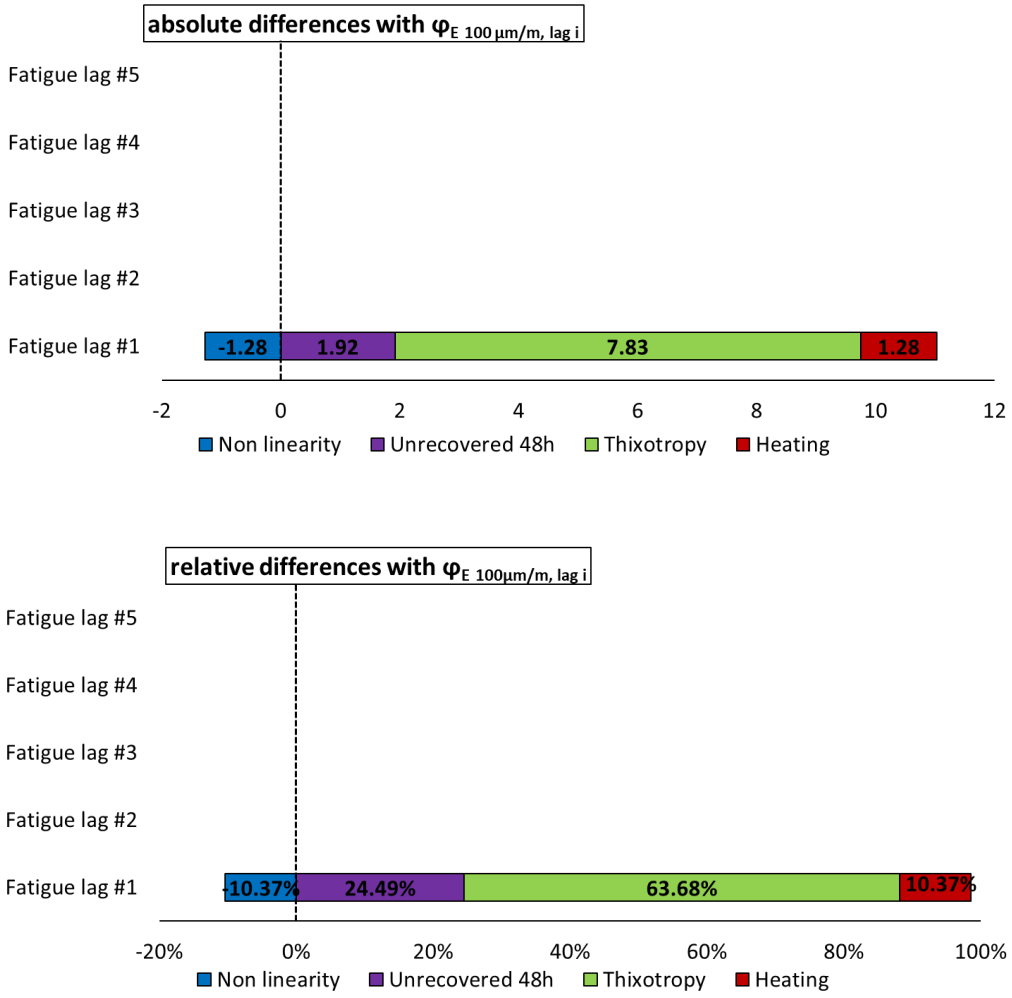

3.1.21. Quantification of different absolute and relative contributions to |E*| and φ_E evolutions for mix 70/100 - 4, calculated using a different envelope line for each fatigue lag.

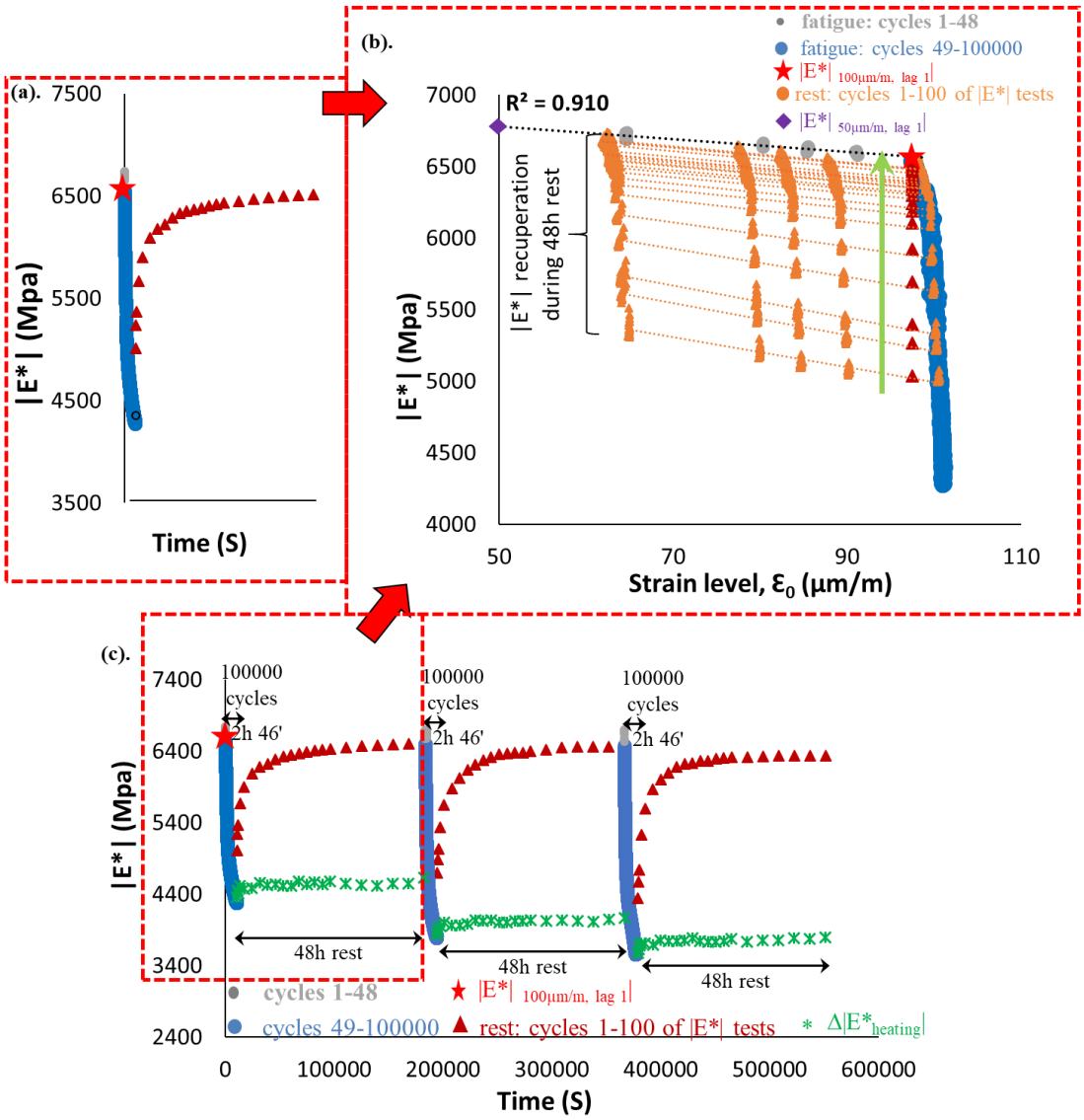

3.1.22. PFRT results obtained for mix 70/100 - 5: (a) |E*| as a function of time during the first fatigue lag and rest period (b) |E*| as a function of applied strain amplitude during the first fatigue lags and the short complex modulus tests performed within its following rest periods; (c) |E*| as a function of time during the three fatigue lags and rest periods [Red stars indicate values of |E*| estimated at 100 µm/m at the beginning of fatigue lag, green asterisk shows values of $\Delta|E^*_{heating}|$ as influence of self-heating and brown triangles indicate values of |E*| estimated at 100 µm/m for each short complex modulus test during rest (all these values were obtained using non-linearity envelopes, as shown in Figure (b) for the first fatigue lag and rest period)].

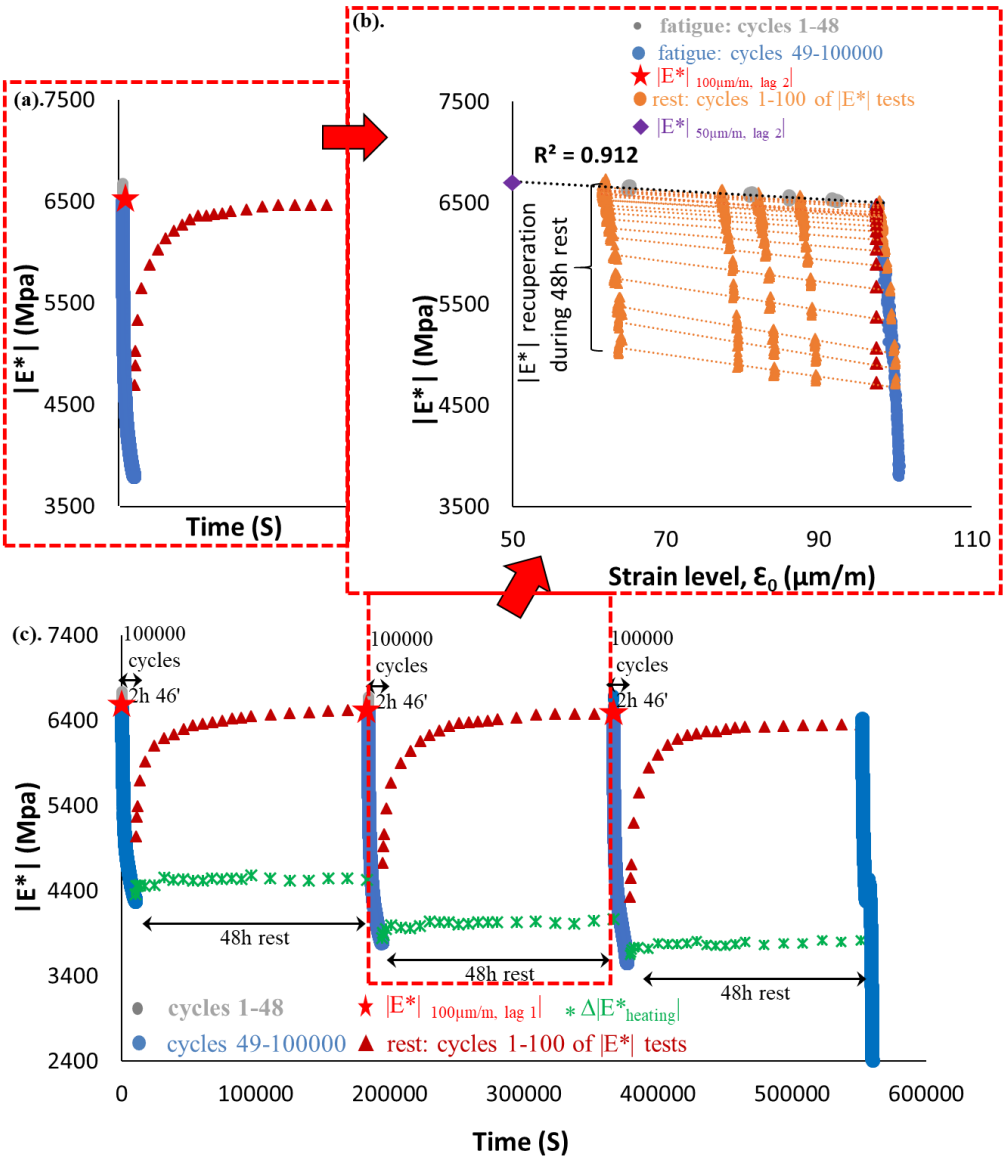

3.1.23. PFRT results obtained for mix 70/100 - 5: (a) |E*| as a function of time during the second fatigue lag and rest period (b) |E*| as a function of applied strain amplitude during the second fatigue lags and the short complex modulus tests performed within its following rest periods; (c) |E*| as a function of time during the three fatigue lags and rest periods [Red stars indicate values of |E*| estimated at 100 µm/m at the beginning of fatigue lag, green asterisk shows values of $\Delta|E^*_{heating}|$ as influence of self-heating and brown triangles indicate values of |E*| estimated at 100 µm/m for each short complex modulus test during rest (all these values were obtained using non-linearity envelopes, as shown in Figure (b) for the first fatigue lag and rest period)].

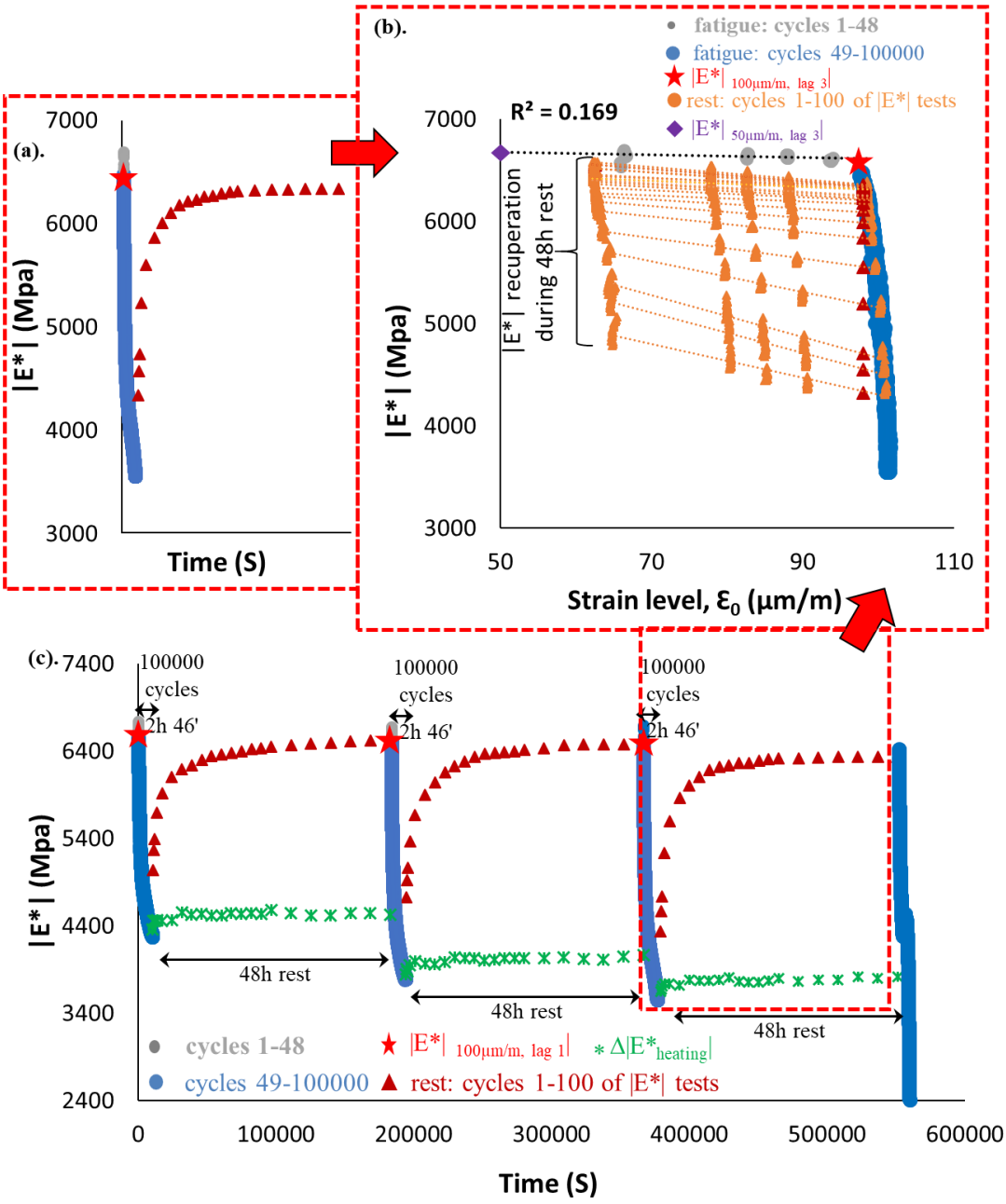

3.1.24. PFRT results obtained for mix 70/100 - 5: (a) |E*| as a function of time during the thirdfatigue lag and rest period (b) |E*| as a function of applied strain amplitude during the third fatigue lags and the short complex modulus tests performed within its following rest periods; (c) |E*| as a function of time during the three fatigue lags and rest periods [Red stars indicate values of |E*| estimated at 100 µm/m at the beginning of fatigue lag, green asterisk shows values of $\Delta|E^*_{heating}|$ as influence of self-heating and brown triangles indicate values of |E*| estimated at 100 µm/m for each short complex modulus test during rest (all these values were obtained using non-linearity envelopes, as shown in Figure (b) for the first fatigue lag and rest period)].

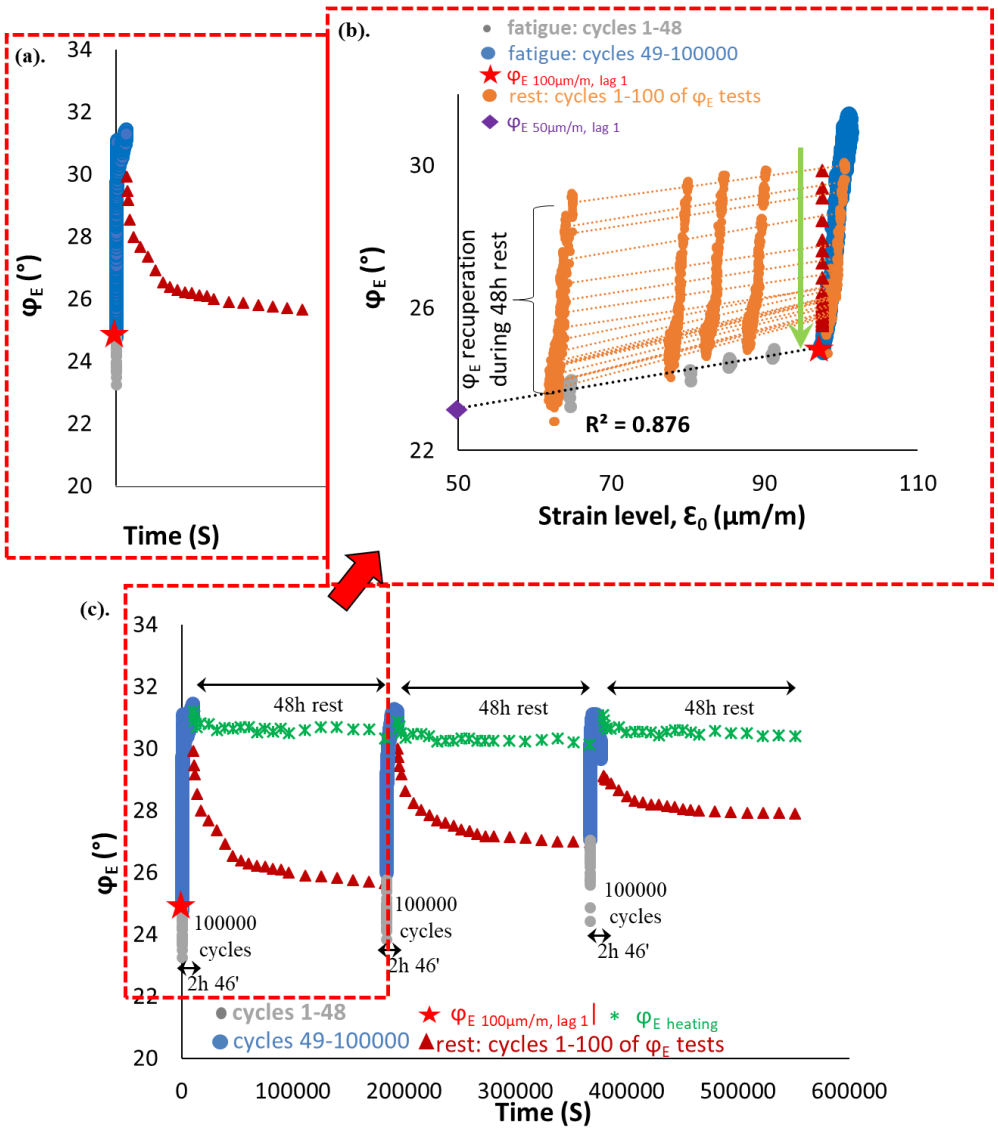

3.1.25. PFRT results obtained for mix 70/100 – 5: (a) φ_E as a function of time during the first fatigue lag and rest period (b) φ_E as a function of applied strain amplitude during the first fatigue lags and the short complex modulus tests performed within its following rest periods; (c) φ_E as a function of time during the three fatigue lags and rest periods (Red stars indicate values of φ_E estimated at 100 µm/m at the beginning of fatigue lag, green asterisk shows values of $\Delta\varphi_{E\ heating}$ as influence of self-heating and brown triangles indicate values of φ_E estimated at 100 µm/m for each short complex modulus test during rest (all these values were obtained using non-linearity envelopes, as shown in (b) for the first fatigue lag and rest period).

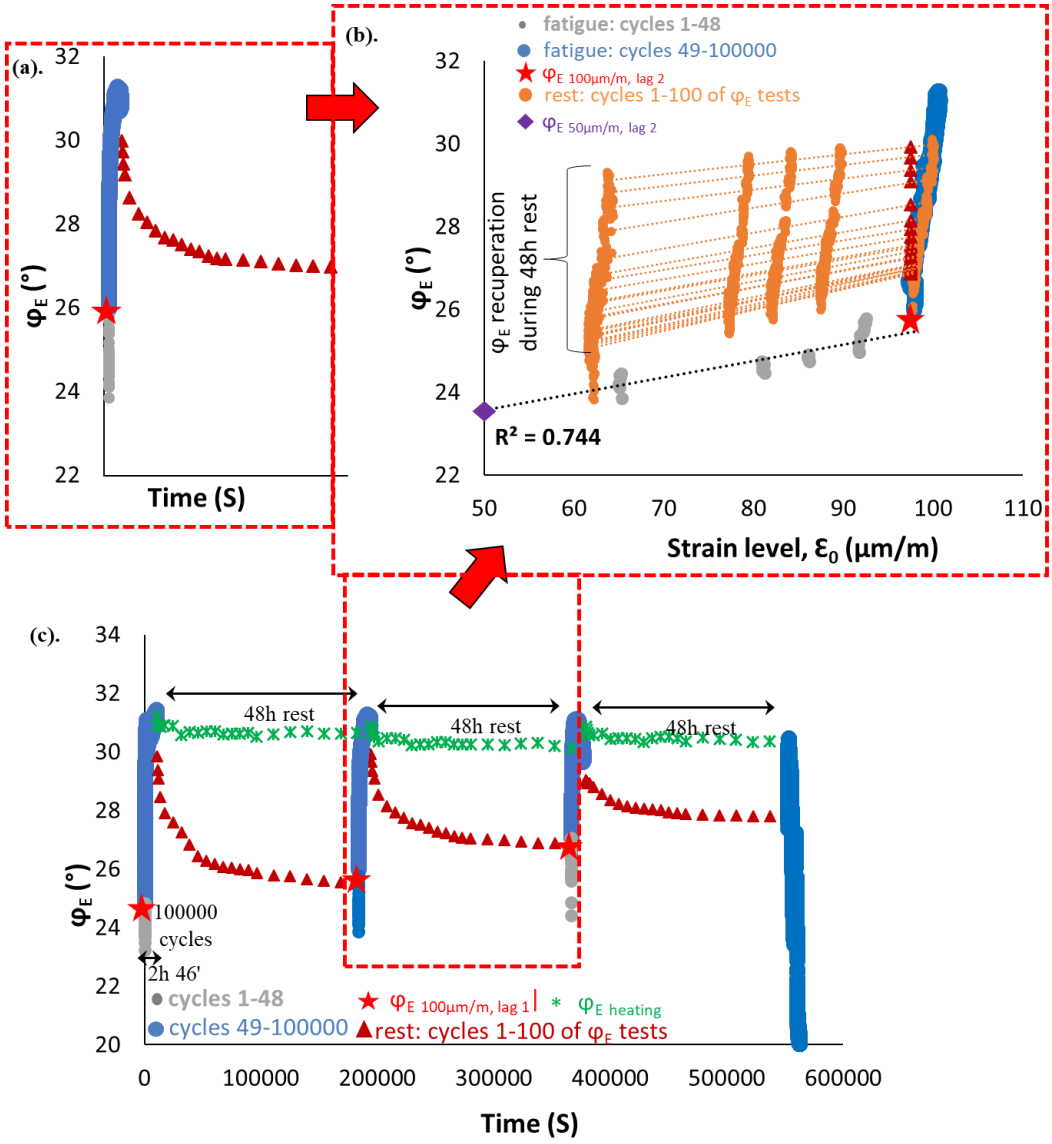

3.1.26. PFRT results obtained for mix 70/100 – 5: (a) φ_E as a function of time during the secondfatigue lag and rest period (b) φ_E as a function of applied strain amplitude during the second fatigue lags and the short complex modulus tests performed within its following rest periods; (c) φ_E as a function of time during the three fatigue lags and rest periods (Red stars indicate values of φ_E estimated at 100 µm/m at the beginning of fatigue lag, green asterisk shows values of $\Delta\varphi_{E\ heating}$ as influence of self-heating and brown triangles indicate values of φ_E estimated at 100 µm/m for each short complex modulus test during rest (all these values were obtained using non-linearity envelopes, as shown in (b) for the first fatigue lag and rest period).

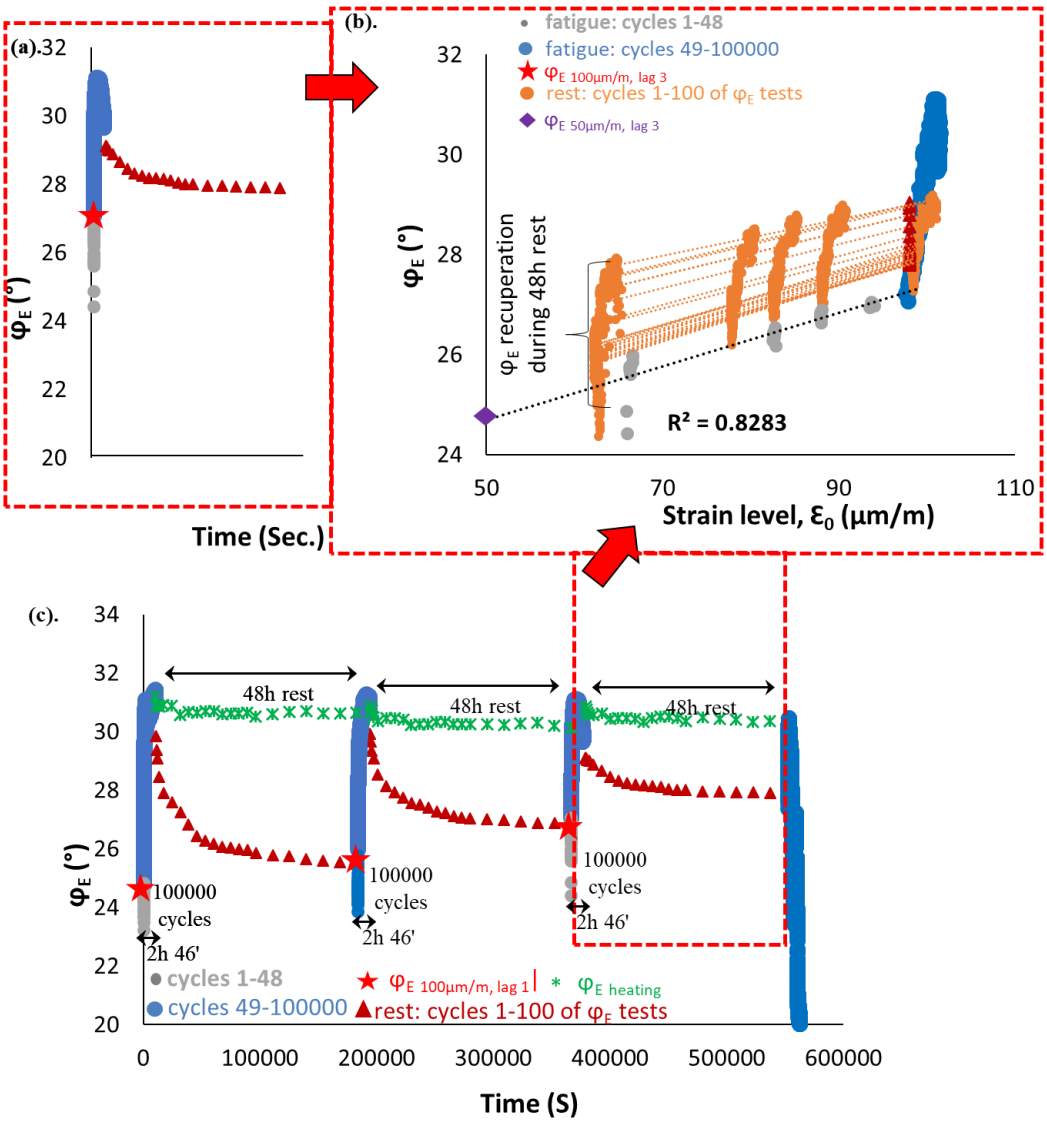

3.1.27. PFRT results obtained for mix 70/100 – 5: (a) φ_E as a function of time during the third fatigue lag and rest period (b) φ_E as a function of applied strain amplitude during the thirdfatigue lags and the short complex modulus tests performed within its following rest periods; (c) φ_E as a function of time during the three fatigue lags and rest periods (Red stars indicate values of φ_E estimated at 100 µm/m at the beginning of fatigue lag, green asterisk shows values of $\Delta\varphi_{E\ heating}$ as influence of self-heating and brown triangles indicate values of φ_E estimated at 100 µm/m for each short complex modulus test during rest (all these values were obtained using non-linearity envelopes, as shown in (b) for the first fatigue lag and rest period).

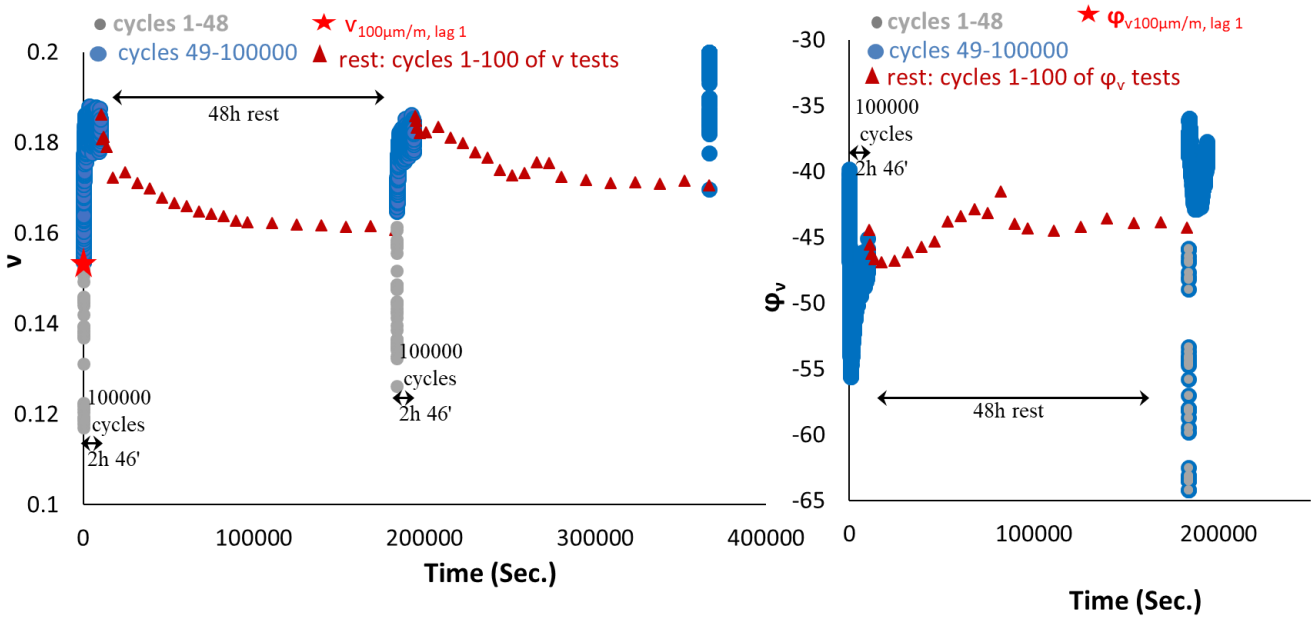

3.1.28. PFRT results obtained for mix 70/100 – 5: |v*| and φ_v as a function of time amplitude during the first fatigue lags.

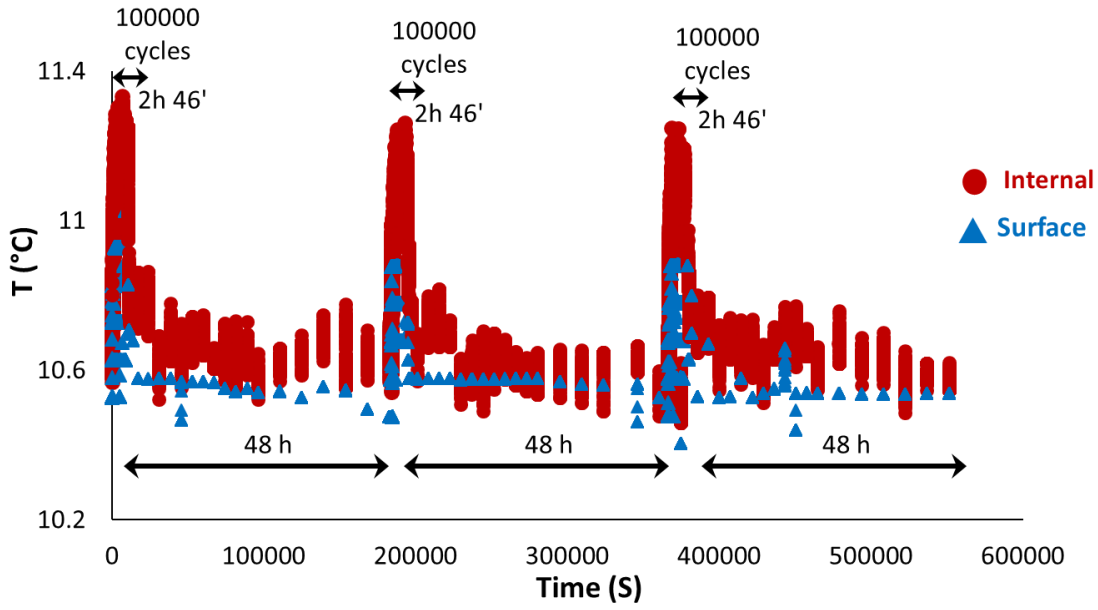

3.1.29. PFRT results obtained for mix 70/100 – 5: internal and surface temperature evolution during fatigue lags and recovery periods.

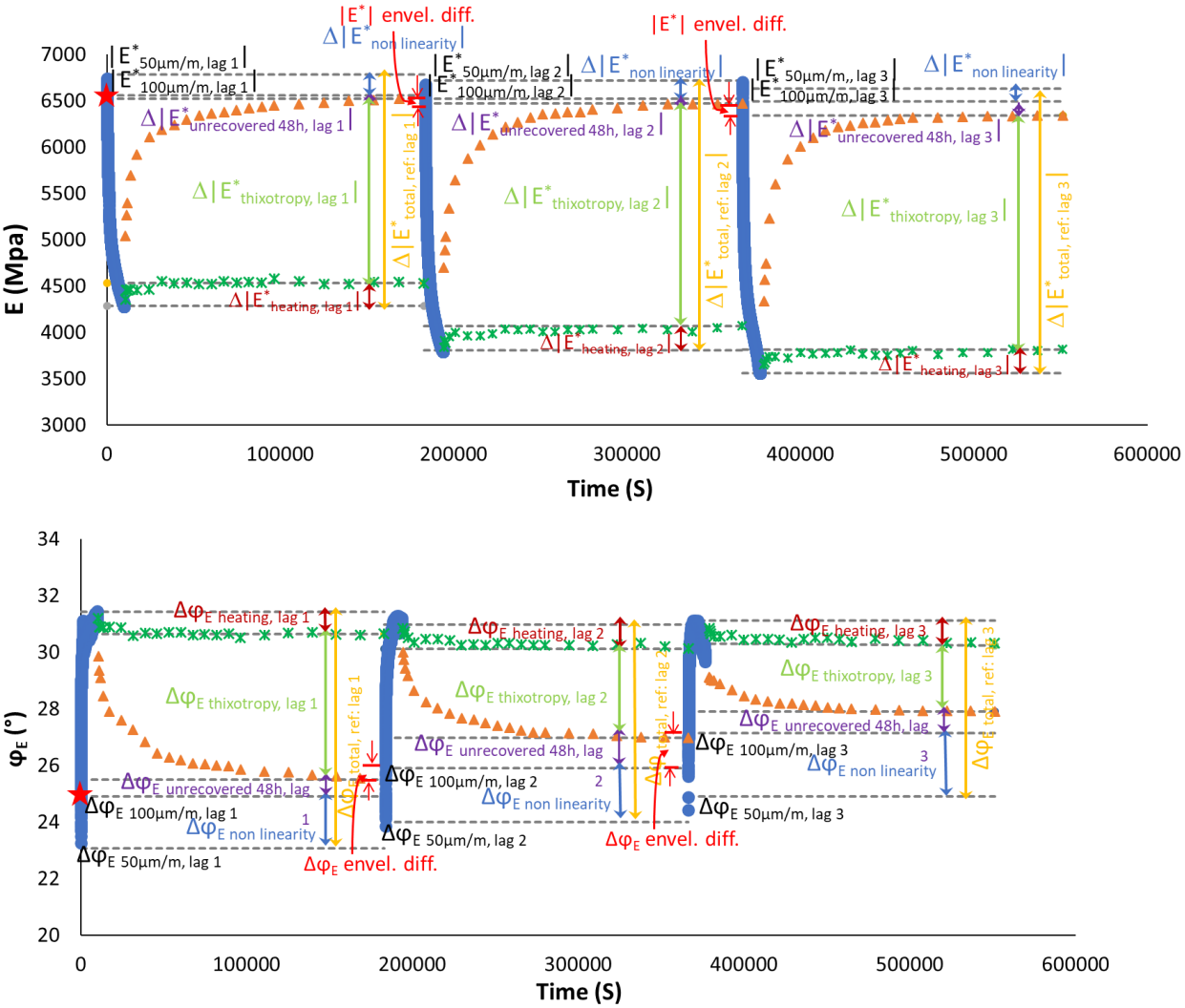

3.1.30. Quantification of different contributions |E*| and φ_E evolution, for the first two fatigue lags for mix 70/100 – 5: different envelope line is used for each fatigue lag.

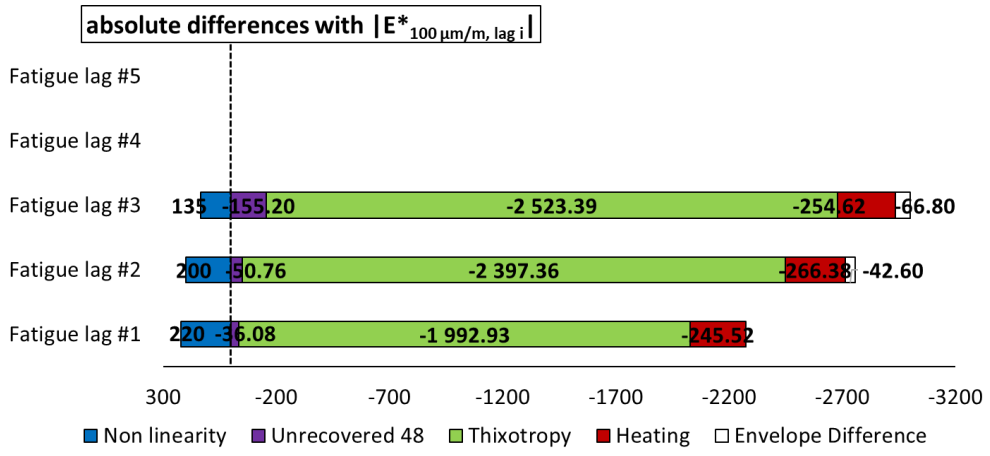

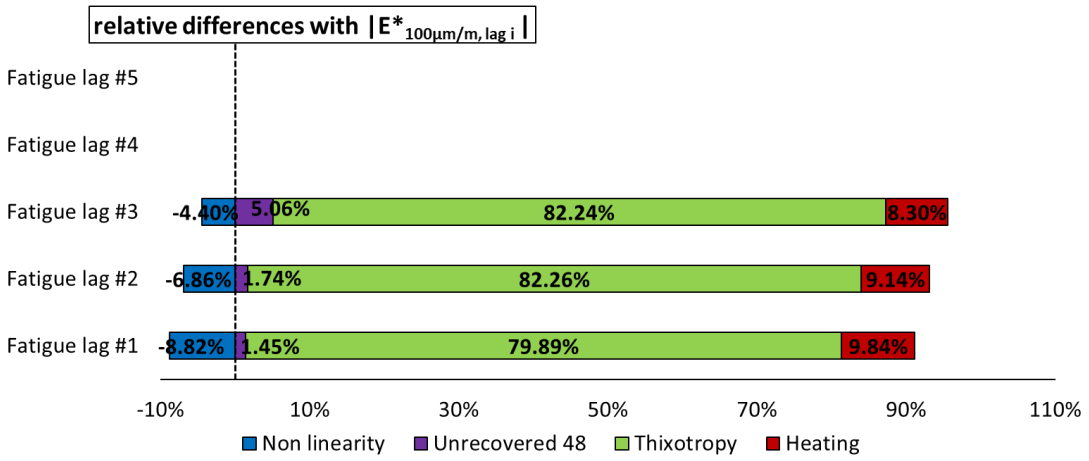

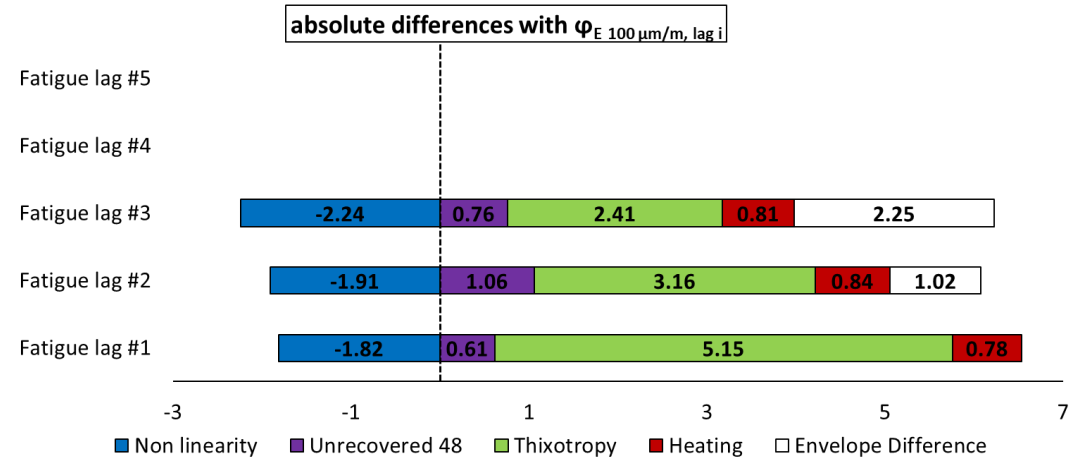

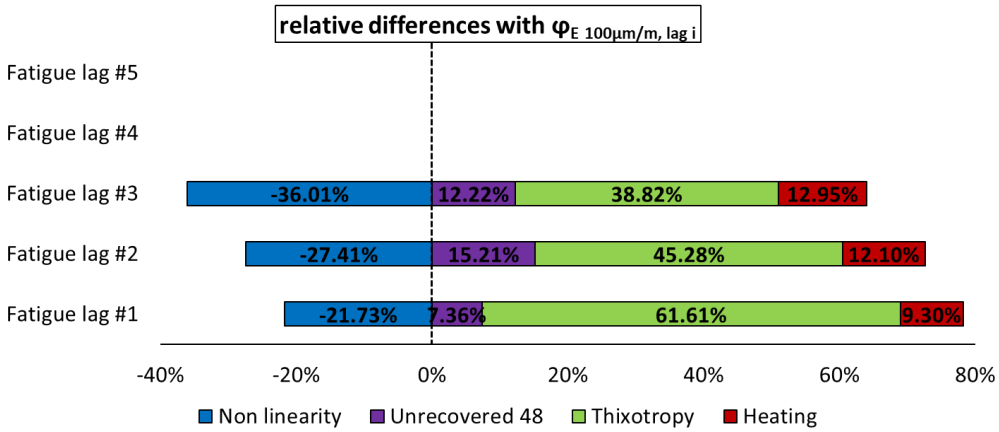

3.1.31. Quantification of different absolute and relative contributions to |E*| and φ_E evolutions for mix 70/100 – 5, calculated using a different envelope line for each fatigue lag.

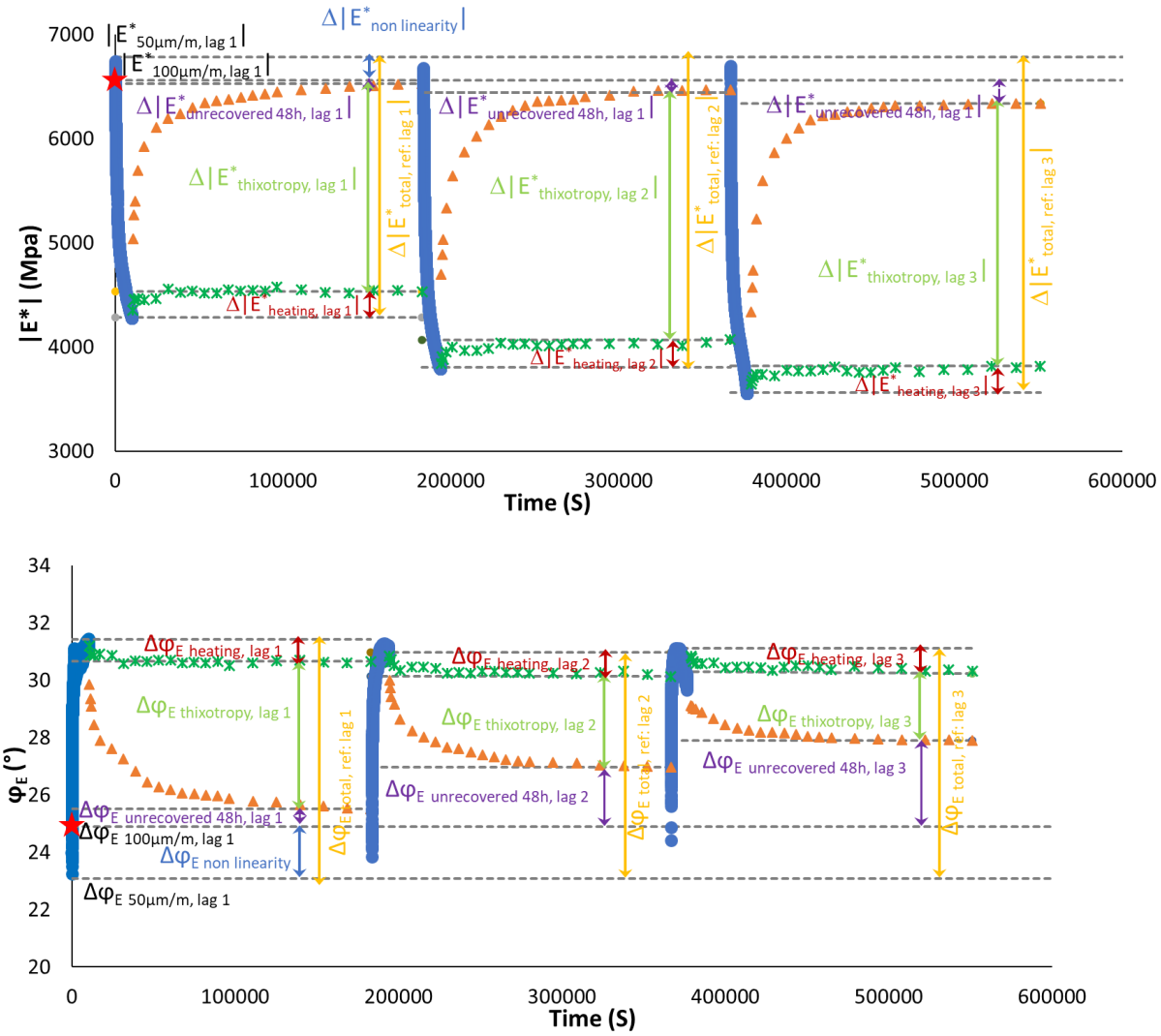

Figure 3.1.32. Quantification of different contributions to |E*| and φ_E evolution during first and second fatigue lags for mix 70/100 – 5: the envelope line of the first fatigue lag is used for all fatigue lags.

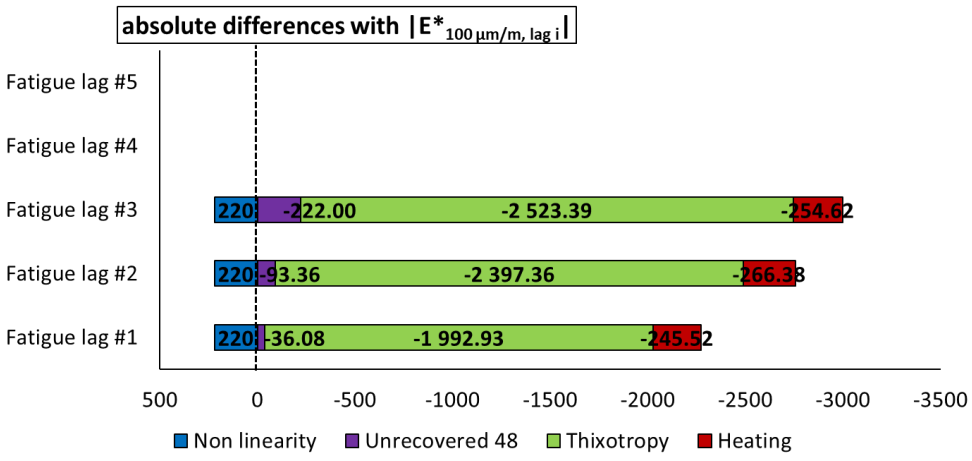

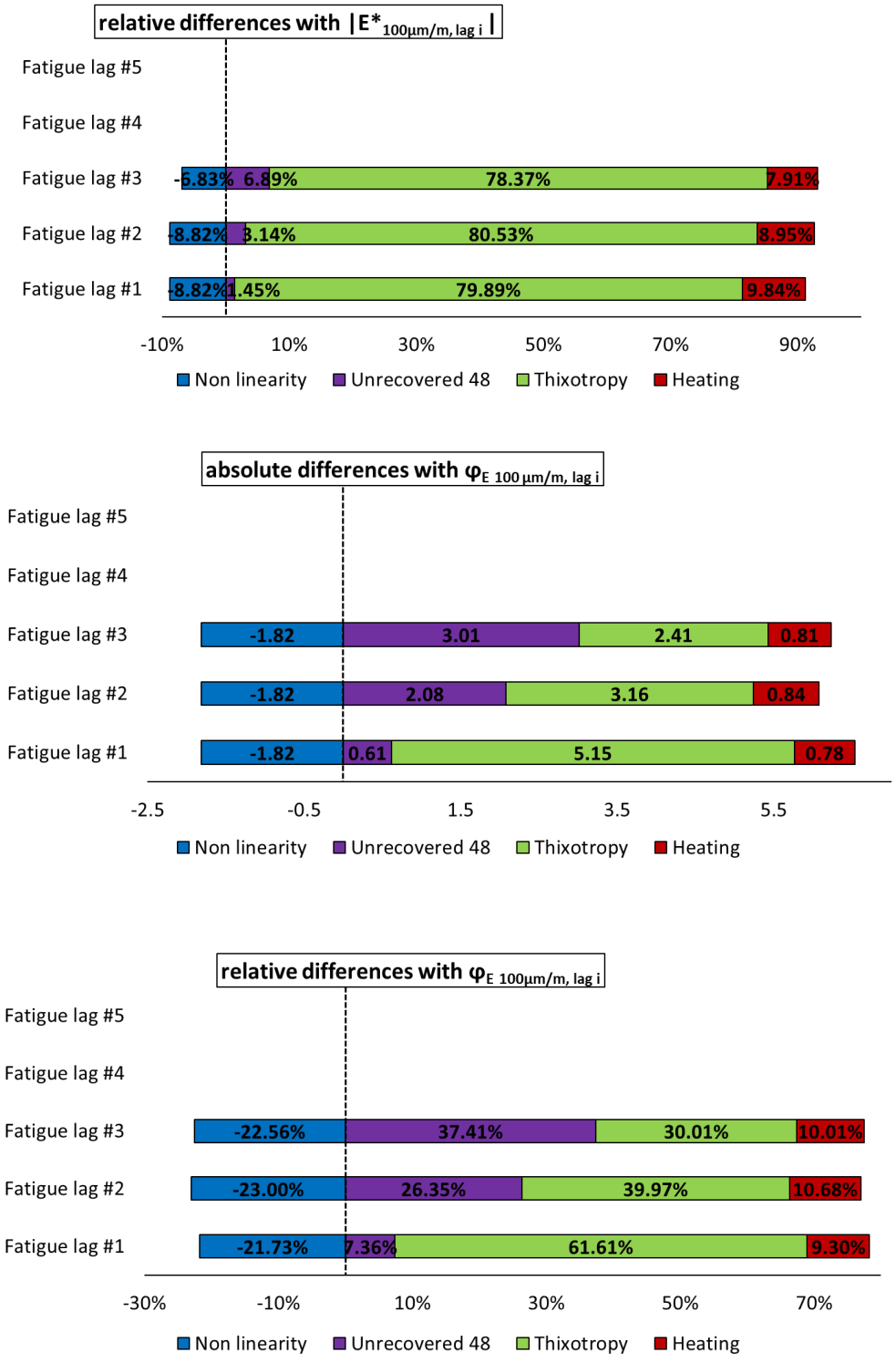

Figure 3.1.33. Quantification of different absolute and relative contributions to |E*| and φ_E evolutions for mix 70/100 – 5, calculated using the envelope line for the first fatigue lag.

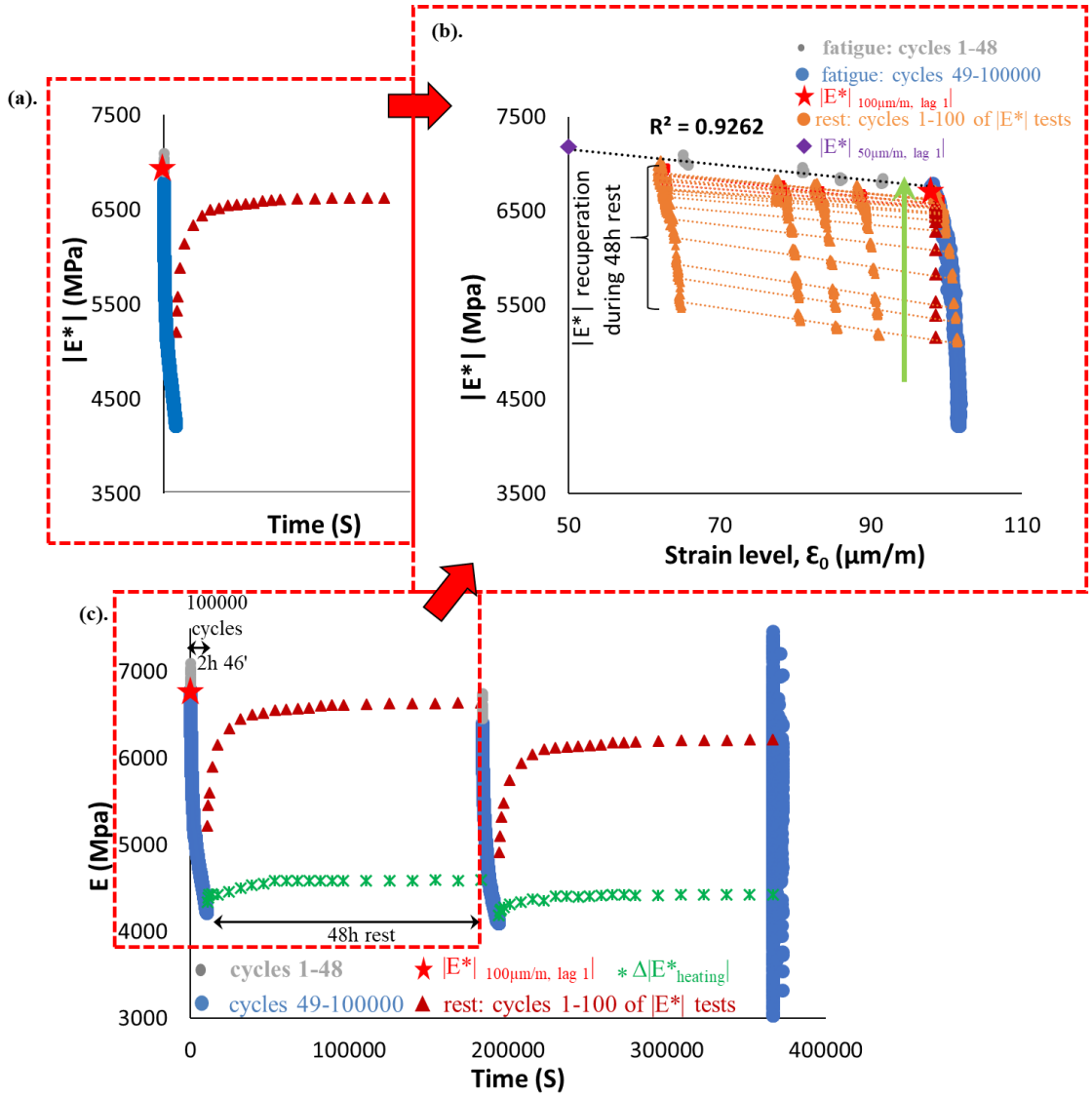

3.1.34. PFRT results obtained for mix 70/100 - 8: (a) |E*| as a function of time during the first fatigue lag and rest period (b) |E*| as a function of applied strain amplitude during the firstfatigue lags and the short complex modulus tests performed within its following rest periods; (c) |E*| as a function of time during the two fatigue lags and rest periods [Red stars indicate values of |E*| estimated at 100 µm/m at the beginning of fatigue lag, green asterisk shows values of $\Delta|E^*_{heating}|$ as influence of self-heating and brown triangles indicate values of |E*| estimated at 100 µm/m for each short complex modulus test during rest (all these values were obtained using non-linearity envelopes, as shown in Figure (b) for the first fatigue lag and rest period)].

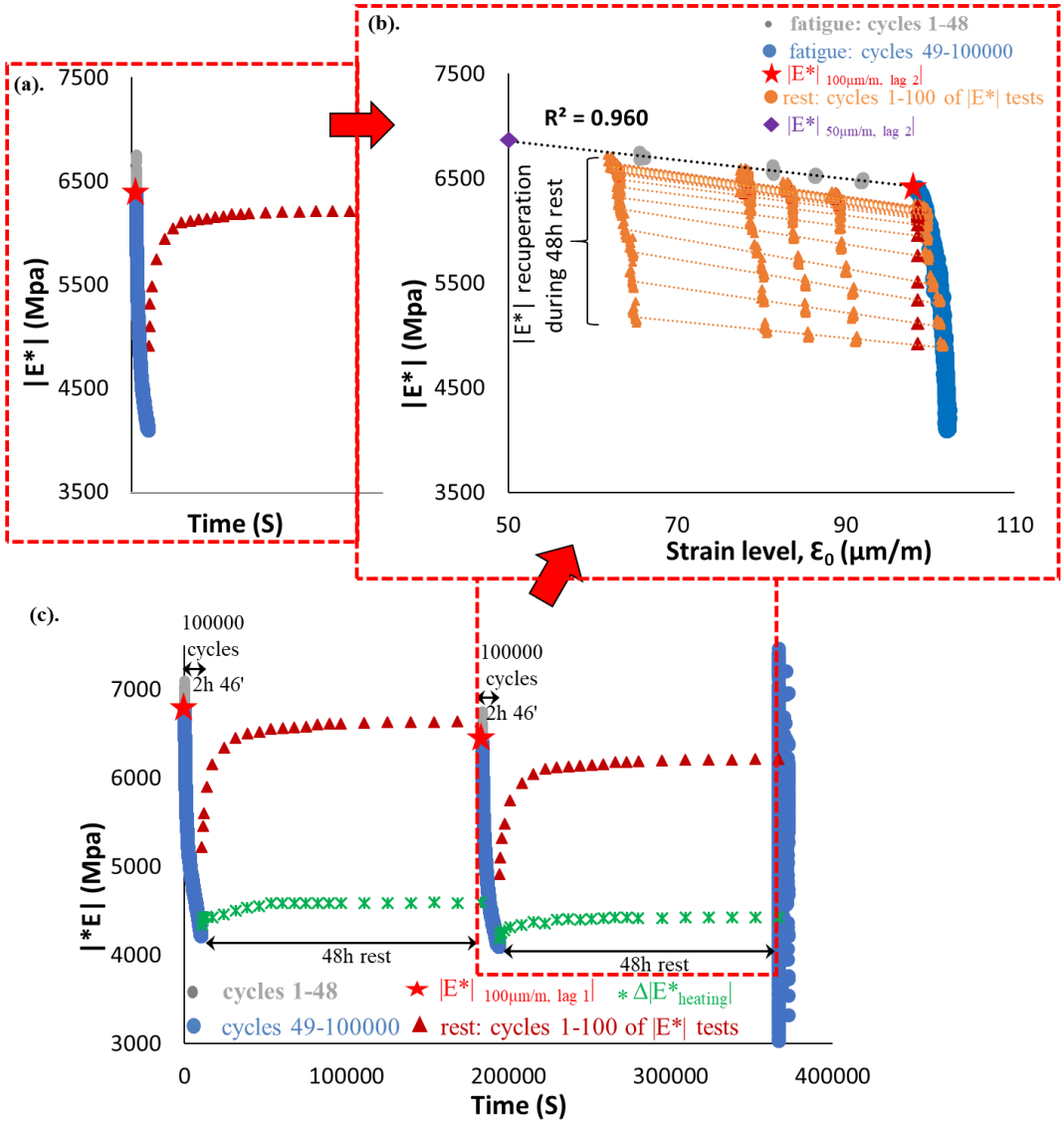

3.1.35. PFRT results obtained for mix 70/100 - 8: (a) |E*| as a function of time during the second fatigue lag and rest period (b) |E*| as a function of applied strain amplitude during the second fatigue lags and the short complex modulus tests performed within its following rest periods; (c) |E*| as a function of time during the two fatigue lags and rest periods [Red stars indicate values of |E*| estimated at 100 µm/m at the beginning of fatigue lag, green asterisk shows values of $\Delta|E^*_{heating}|$ as influence of self-heating and brown triangles indicate values of |E*| estimated at 100 µm/m for each short complex modulus test during rest (all these values were obtained using non-linearity envelopes, as shown in Figure (b) for the first fatigue lag and rest period)].

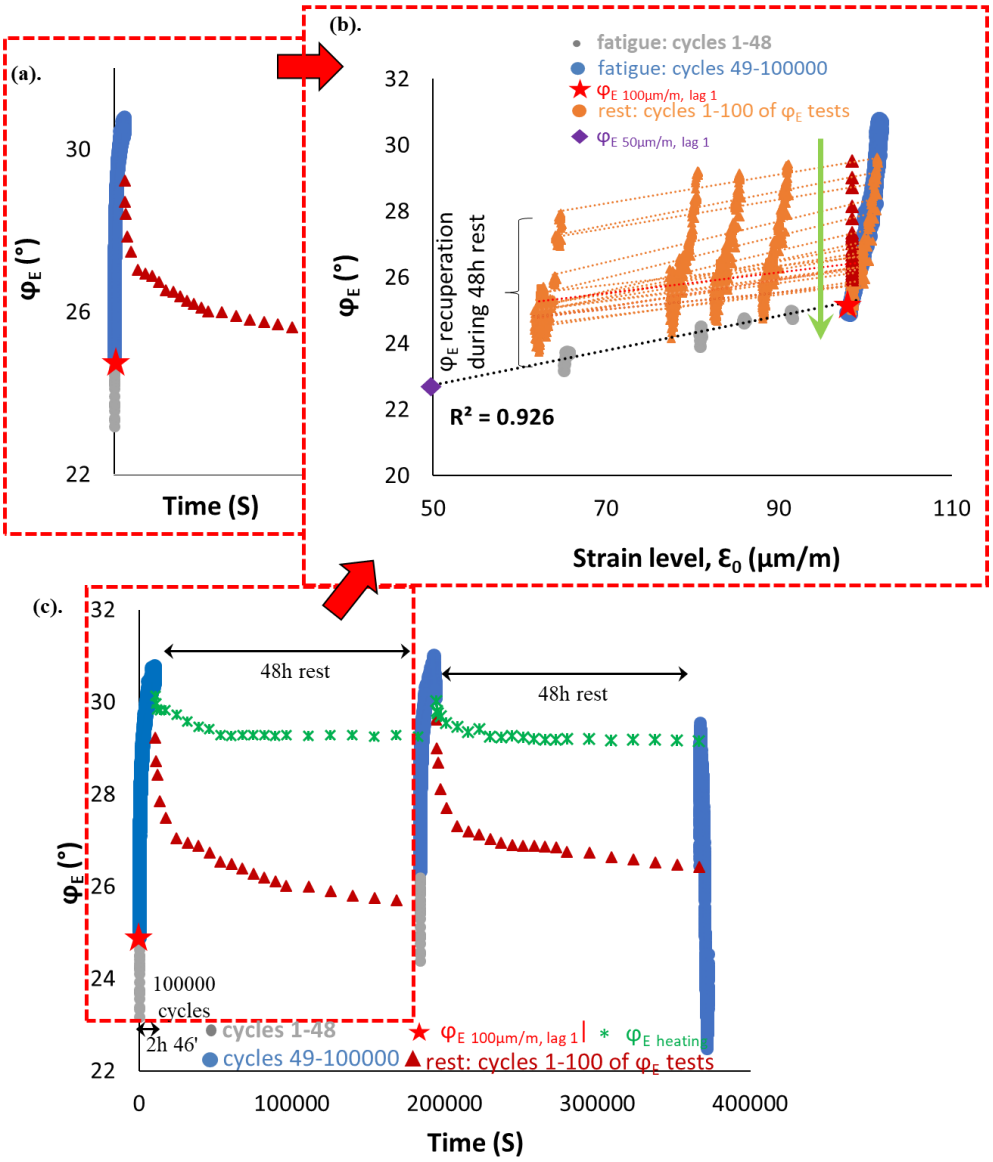

3.1.36. PFRT results obtained for mix 70/100 – 8: (a) φ_E as a function of time during the first fatigue lag and rest period (b) φ_E as a function of applied strain amplitude during the first fatigue lags and the short complex modulus tests performed within its following rest periods; (c) φ_E as a function of time during the two fatigue lags and rest periods (Red stars indicate values of φ_E estimated at 100 µm/m at the beginning of fatigue lag, green asterisk shows values of $\Delta\varphi_{E\ heating}$ as influence of self-heating and brown triangles indicate values of φ_E estimated at 100 µm/m for each short complex modulus test during rest (all these values were obtained using non-linearity envelopes, as shown in (b) for the first fatigue lag and rest period).

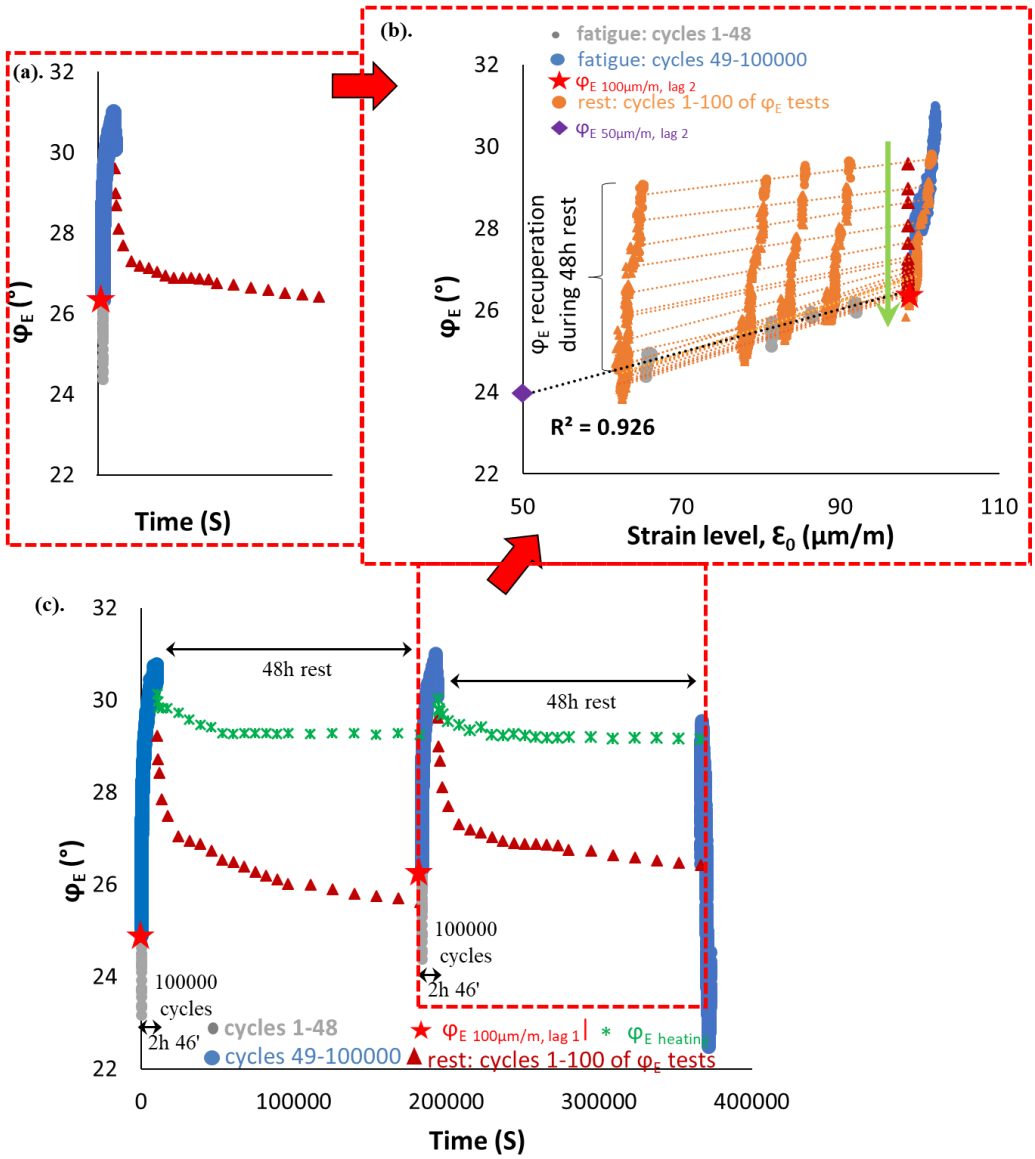

3.1.37. PFRT results obtained for mix 70/100 – 8: (a) φ_E as a function of time during the second fatigue lag and rest period (b) φ_E as a function of applied strain amplitude during the second fatigue lags and the short complex modulus tests performed within its following rest periods; (c) φ_E as a function of time during the two fatigue lags and rest periods (Red stars indicate values of φ_E estimated at 100 µm/m at the beginning of fatigue lag, green asterisk shows values of $\Delta\varphi_{E\ heating}$ as influence of self-heating and brown triangles indicate values of φ_E estimated at 100 µm/m for each short complex modulus test during rest (all these values were obtained using non-linearity envelopes, as shown in (b) for the first fatigue lag and rest period).

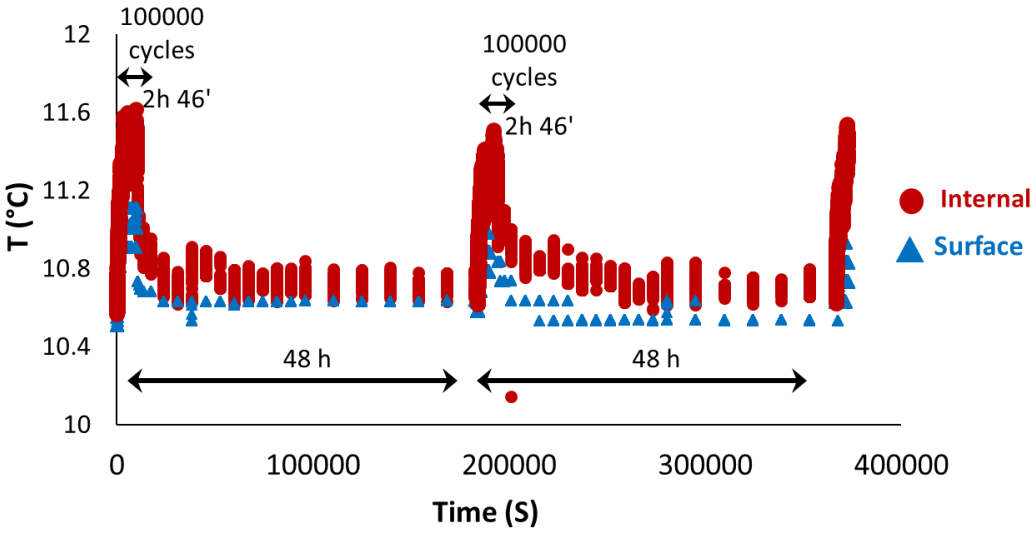

3.1.38. PFRT results obtained for mix 70/100 – 8: internal and surface temperature evolution during fatigue lags and recovery periods

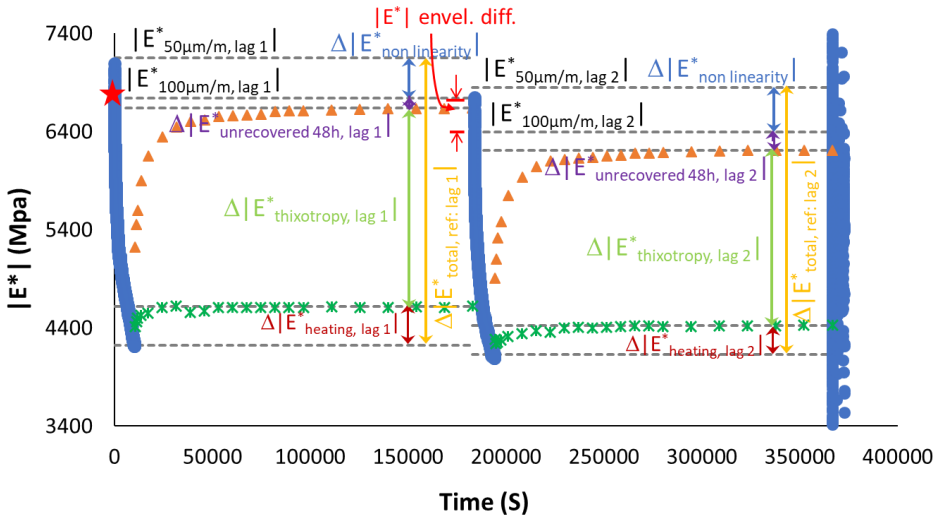

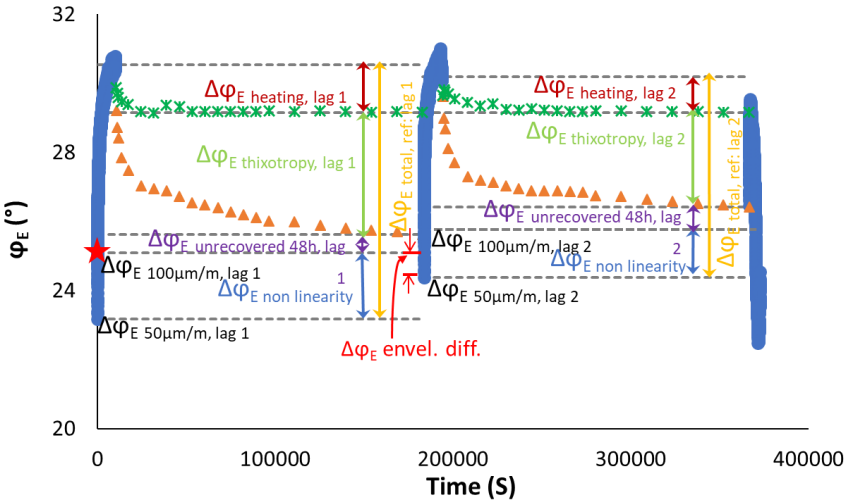

3.1.39. Quantification of different contributions |E*| and φ_E evolution, for the first two fatigue lags for mix 70/100 – 8: different envelope line is used for each fatigue lag.

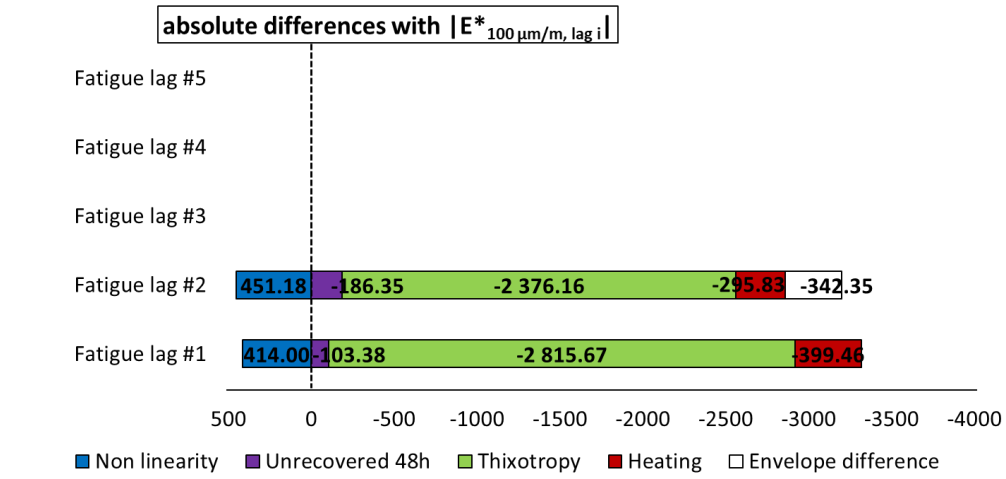

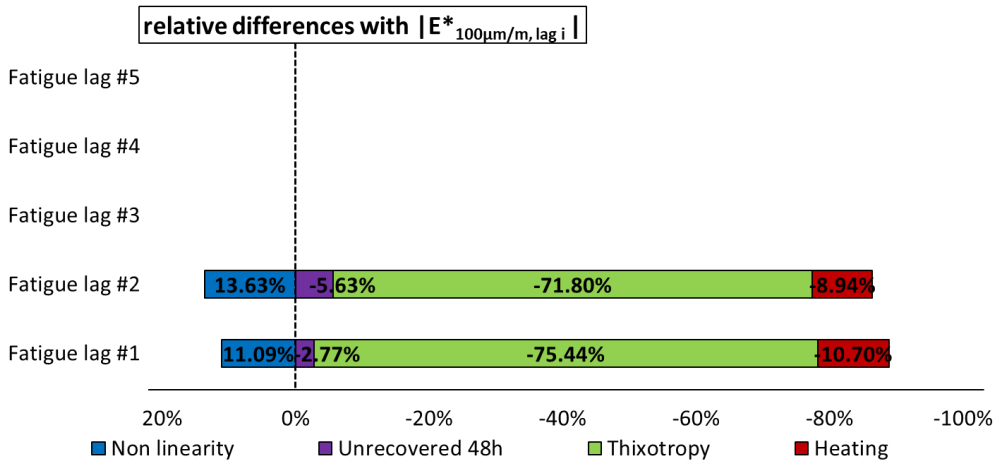

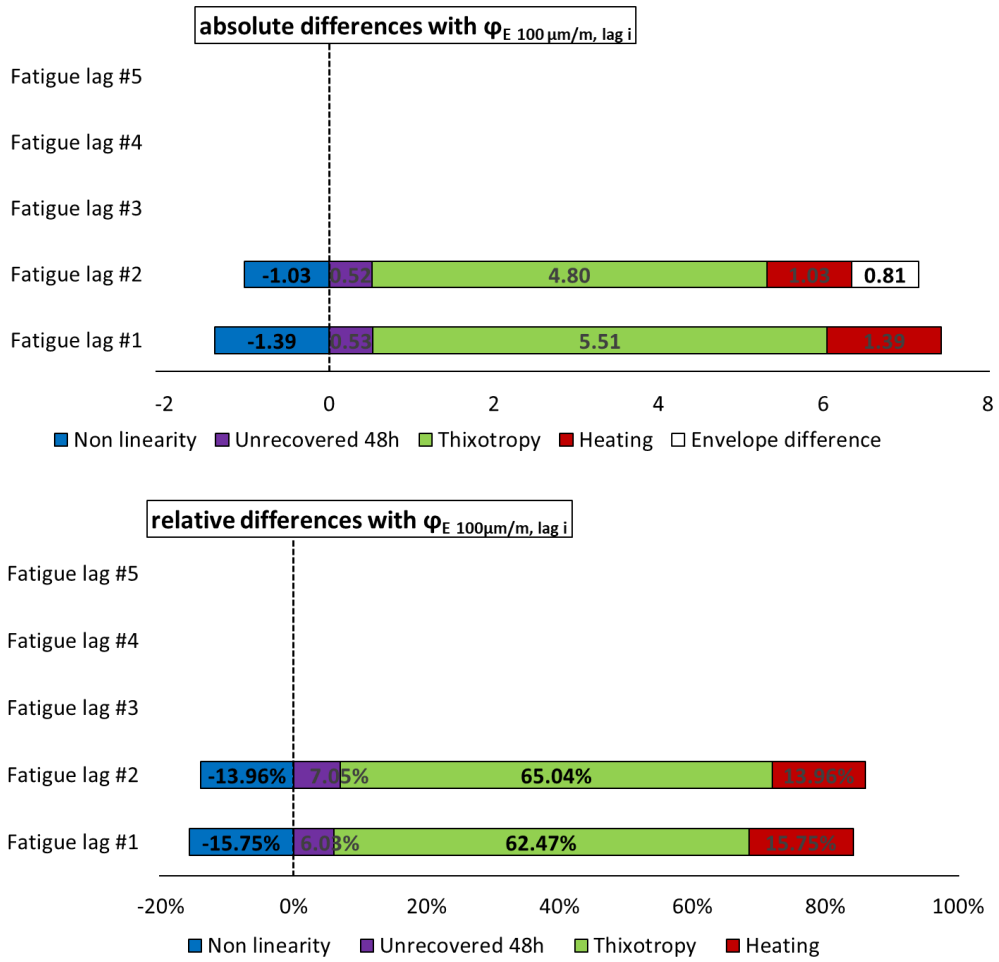

3.1.40. Quantification of different absolute and relative contributions to |E*| and ϕ_E evolutions for mix 70/100 – 8, calculated using a different envelope line for each fatigue lag.

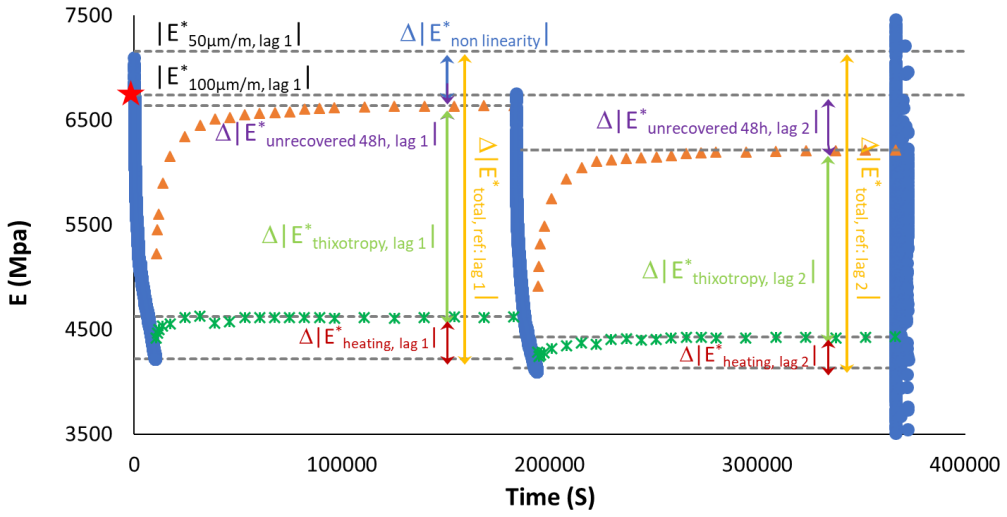

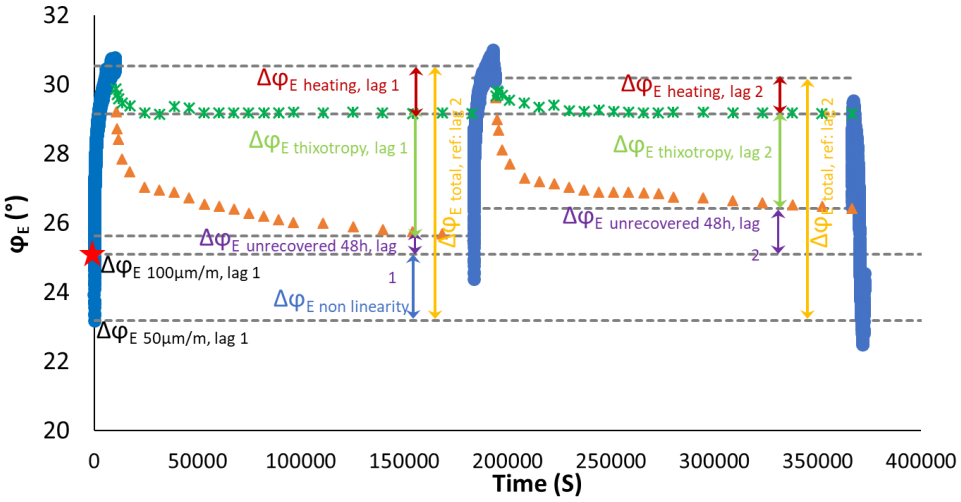

3.1.41. Quantification of different contributions to |E*| and φ_E evolution during first and second fatigue lags for mix 70/100 – 8: the envelope line of the first fatigue lag is used for all fatigue lags.

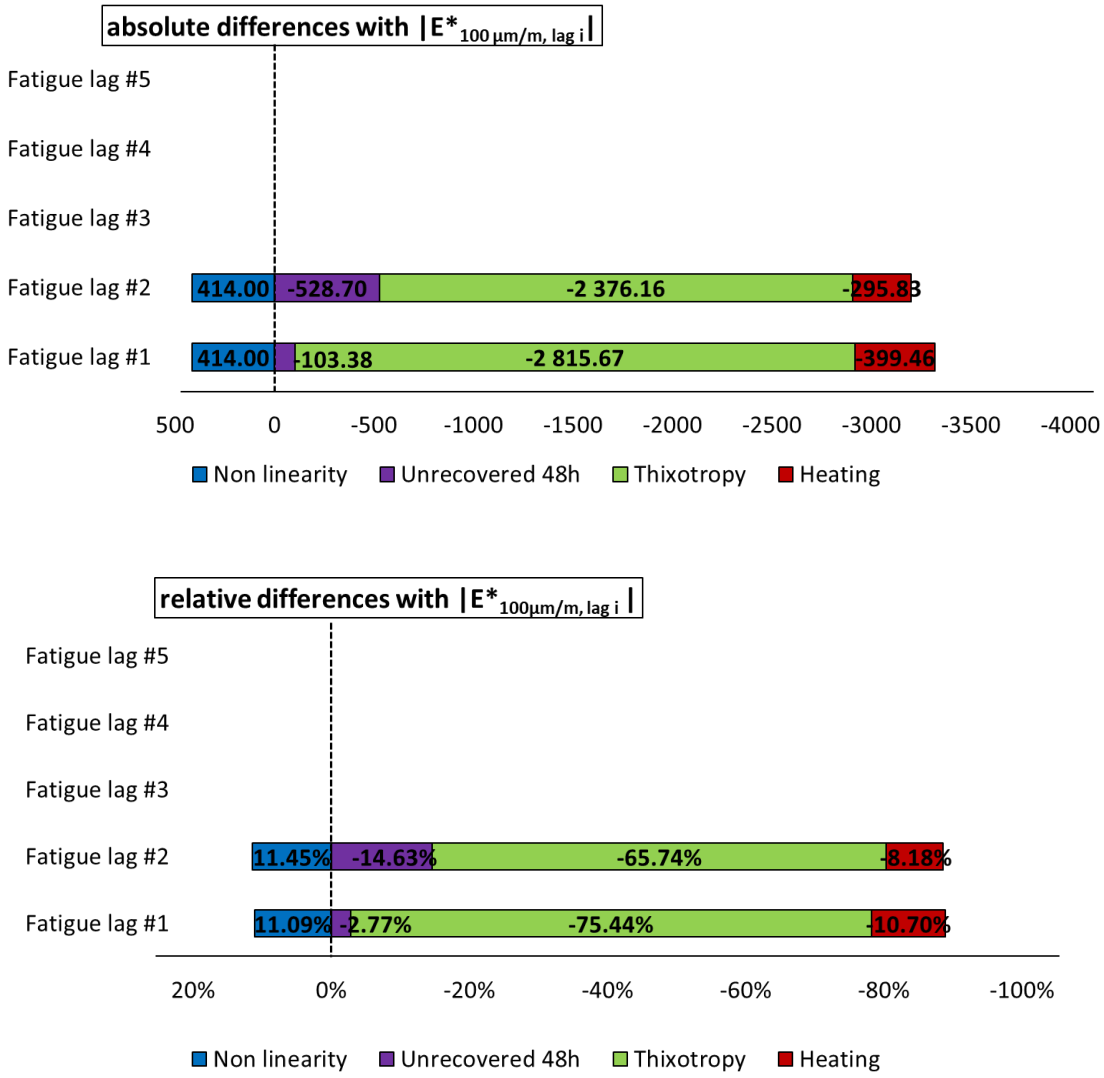

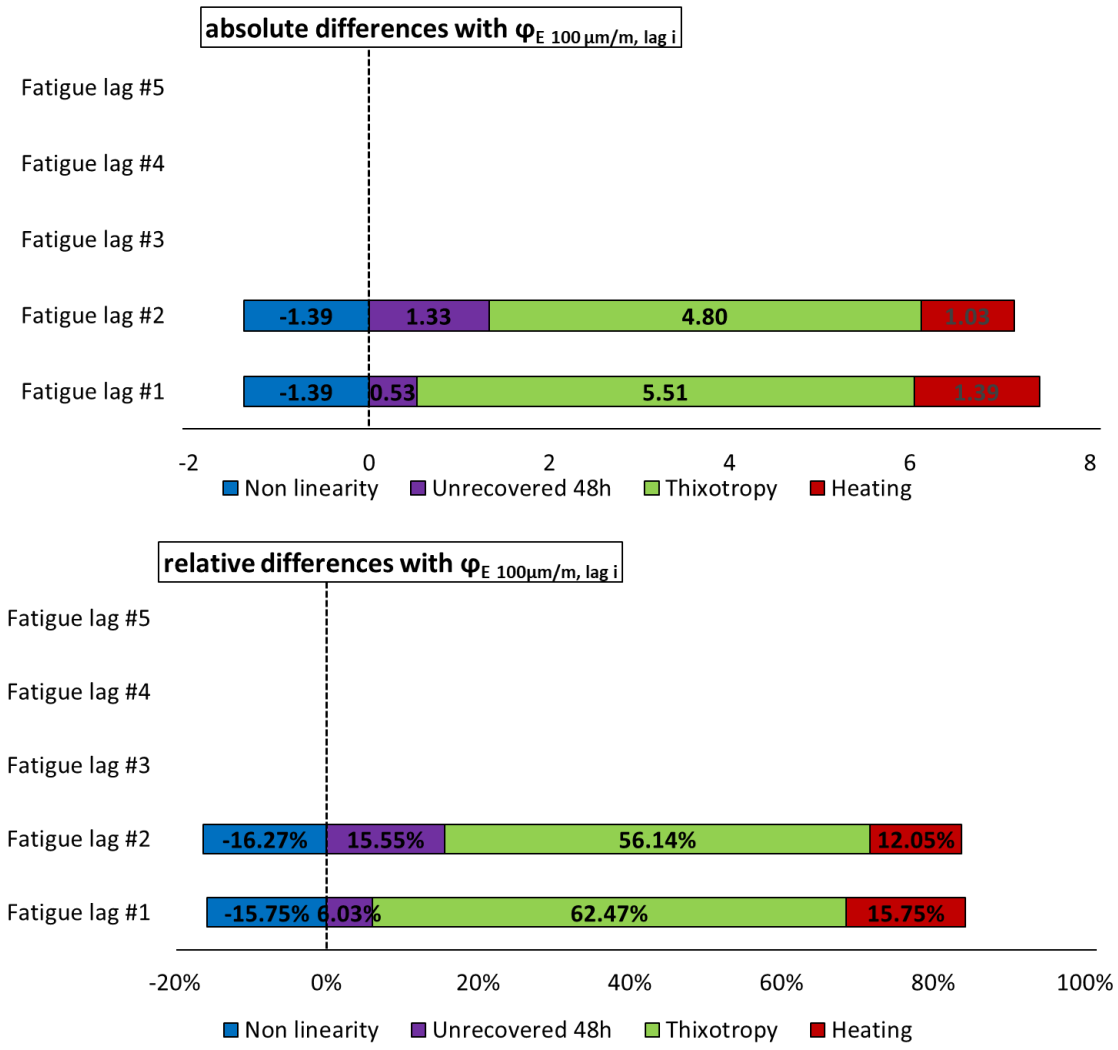

Figure 3.1.42. Quantification of different absolute and relative contributions to |E*| and φ_E evolutions for mix 70/100 – 8, calculated using the envelope line for the first fatigue lag.

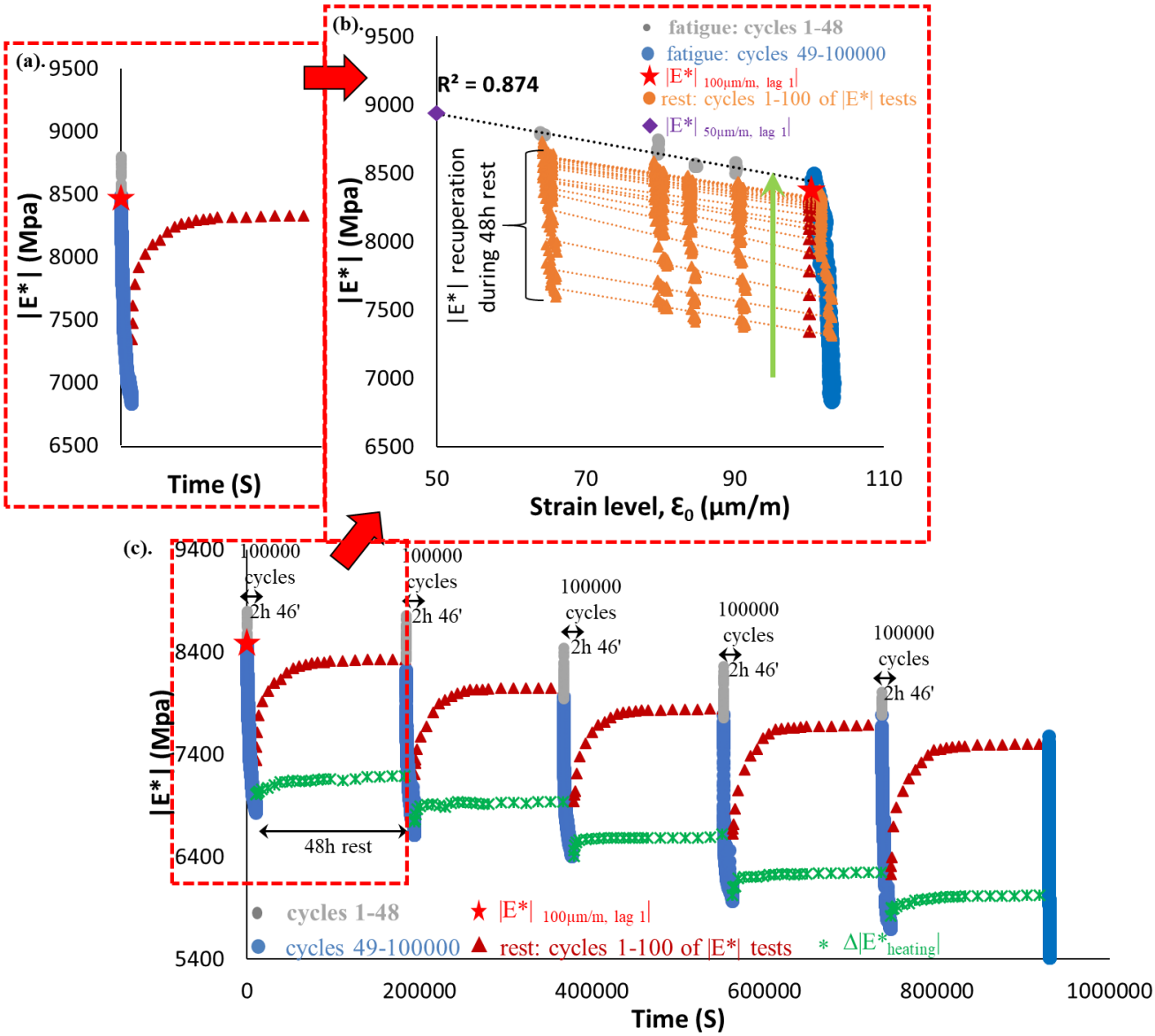

3.1.43. PFRT results obtained for mix 40/60 – 4: (a) |E*| as a function of time during the first fatigue lag and rest period (b) |E*| as a function of applied strain amplitude during the first fatigue lags and the short complex modulus tests performed within its following rest periods; (c) |E*| as a function of time during the five fatigue lags and rest periods [Red stars indicate values of |E*| estimated at 100 µm/m at the beginning of fatigue lag, green asterisk shows values of $\Delta|E^*_{heating}|$ as influence of self-heating and brown triangles indicate values of |E*| estimated at 100 µm/m for each short complex modulus test during rest (all these values were obtained using non-linearity envelopes, as shown in (b) for the first fatigue lag and rest period)].

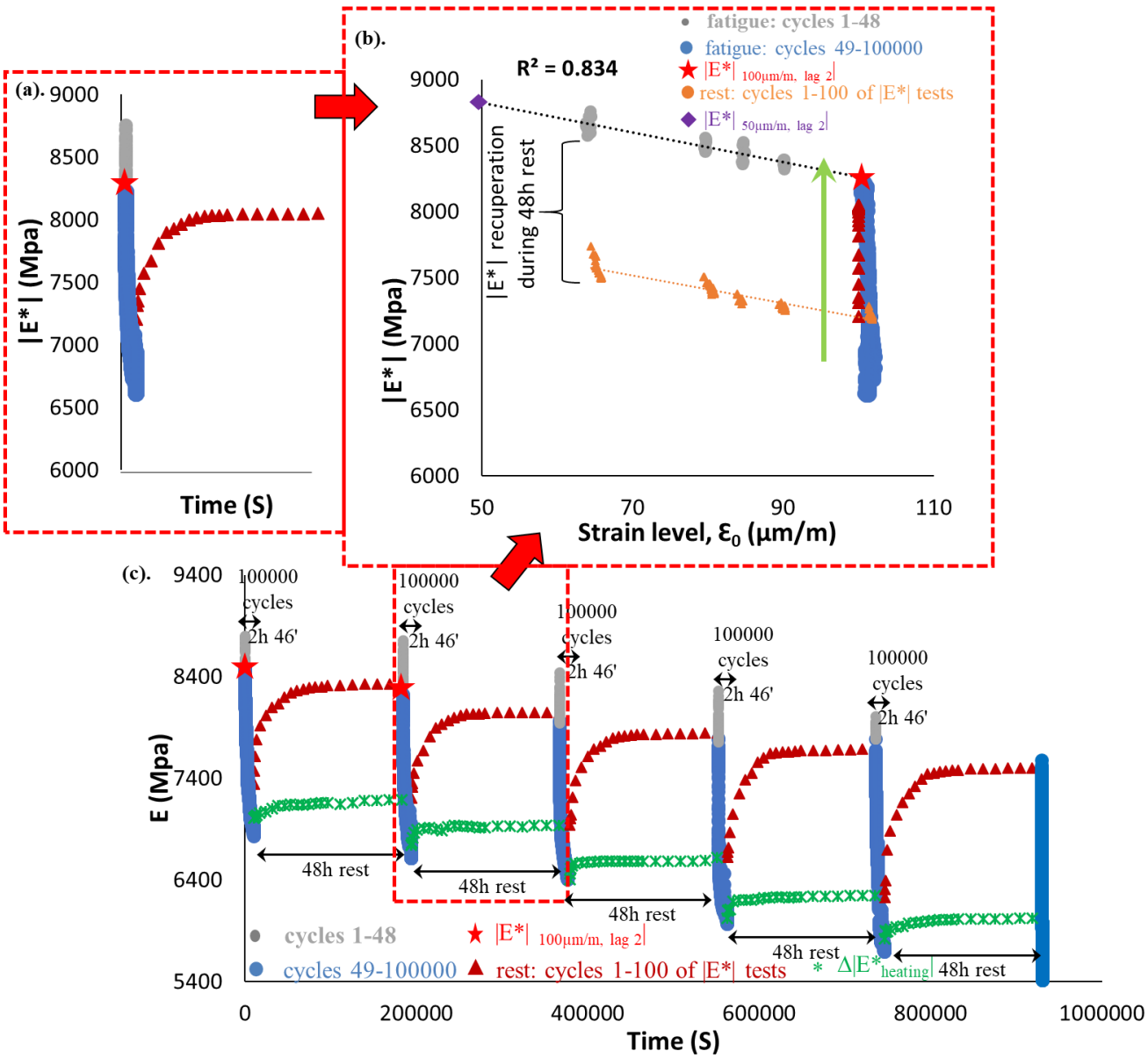

3.1.44. PFRT results obtained for mix 40/60 – 4: (a) |E*| as a function of time during the second fatigue lag and rest period (b) |E*| as a function of applied strain amplitude during the second fatigue lags and the short complex modulus tests performed within its following rest periods; (c) |E*| as a function of time during the five fatigue lags and rest periods [Red stars indicate values of |E*| estimated at 100 µm/m at the beginning of fatigue lag, green asterisk shows values of $\Delta|E^*_{heating}|$ as influence of self-heating and brown triangles indicate values of |E*| estimated at 100 µm/m for each short complex modulus test during rest (all these values were obtained using non-linearity envelopes, as shown in (b) for the first fatigue lag and rest period)].

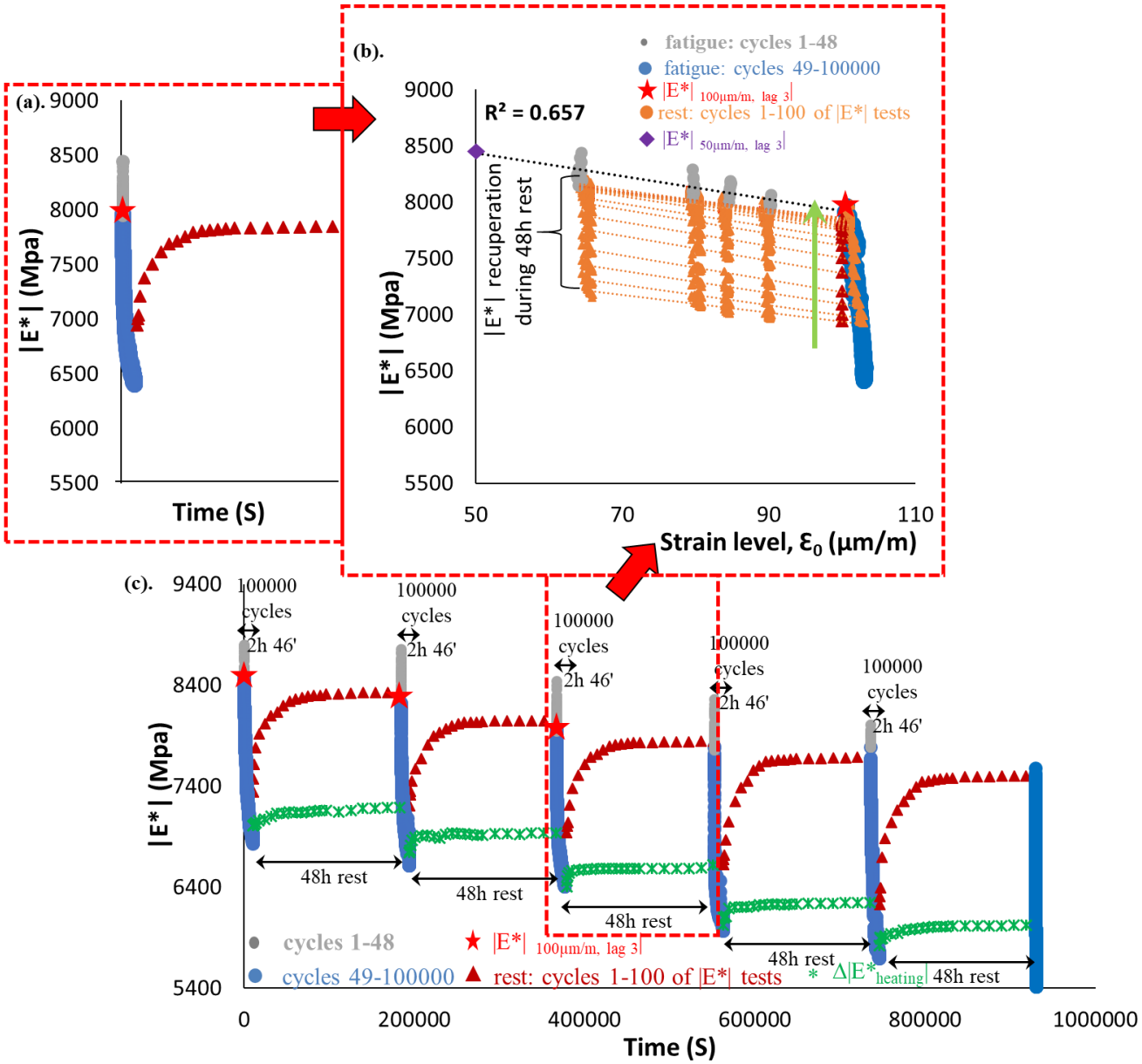

3.1.45. PFRT results obtained for mix 40/60 – 4: (a) |E*| as a function of time during the third fatigue lag and rest period (b) |E*| as a function of applied strain amplitude during the third fatigue lags and the short complex modulus tests performed within its following rest periods; (c) |E*| as a function of time during the five fatigue lags and rest periods [Red stars indicate values of |E*| estimated at 100 µm/m at the beginning of fatigue lag, green asterisk shows values of $\Delta|E^*_{heating}|$ as influence of self-heating and brown triangles indicate values of |E*| estimated at 100 µm/m for each short complex modulus test during rest (all these values were obtained using non-linearity envelopes, as shown in (b) for the first fatigue lag and rest period)].

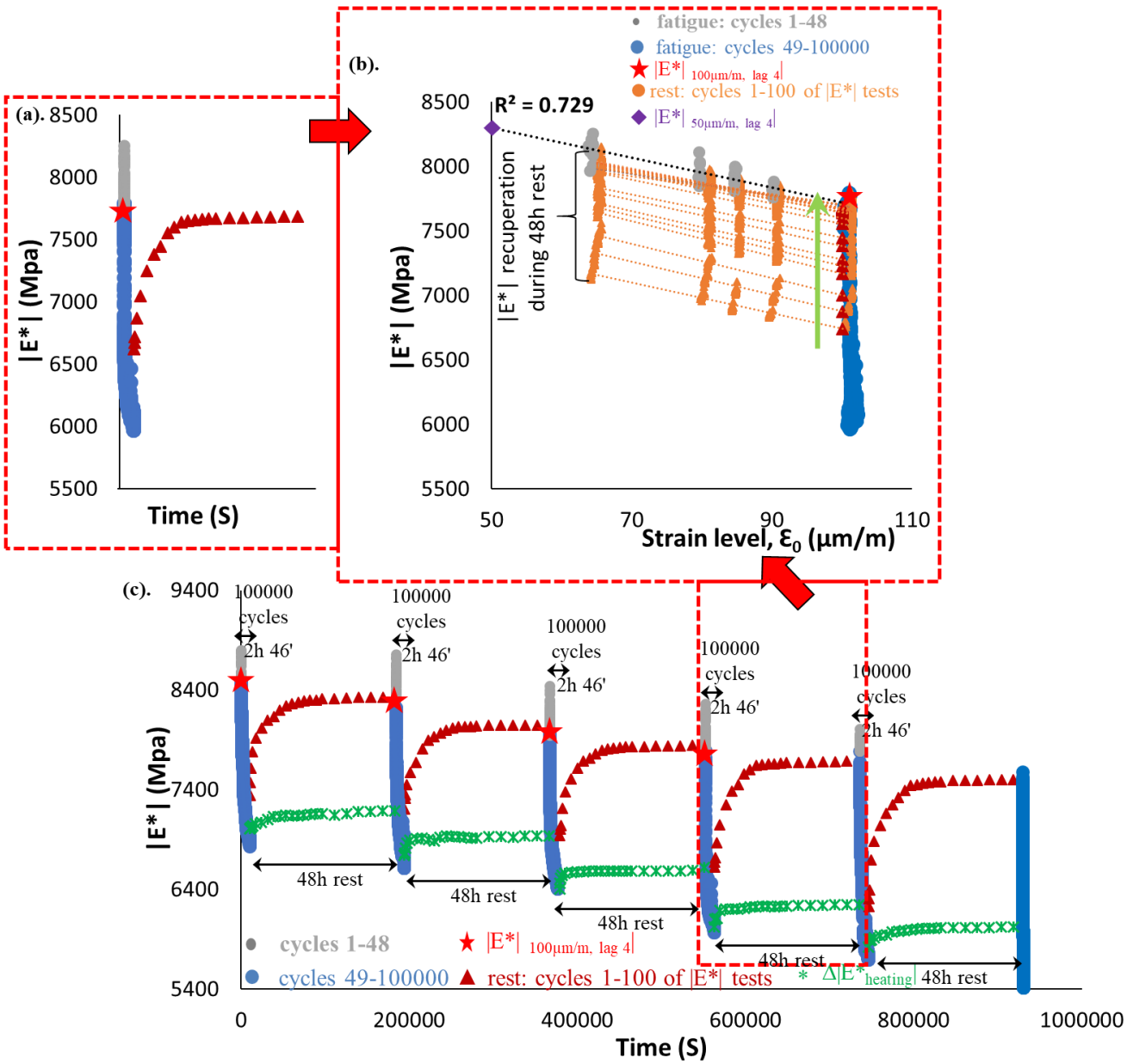

3.1.46. PFRT results obtained for mix 40/60 – 4: (a) |E*| as a function of time during the fourth fatigue lag and rest period (b) |E*| as a function of applied strain amplitude during the fourth fatigue lags and the short complex modulus tests performed within its following rest periods; (c) |E*| as a function of time during the five fatigue lags and rest periods [Red stars indicate values of |E*| estimated at 100 µm/m at the beginning of fatigue lag, green asterisk shows values of $\Delta|E^*_{heating}|$ as influence of self-heating and brown triangles indicate values of |E*| estimated at 100 µm/m for each short complex modulus test during rest (all these values were obtained using non-linearity envelopes, as shown in (b) for the first fatigue lag and rest period)].

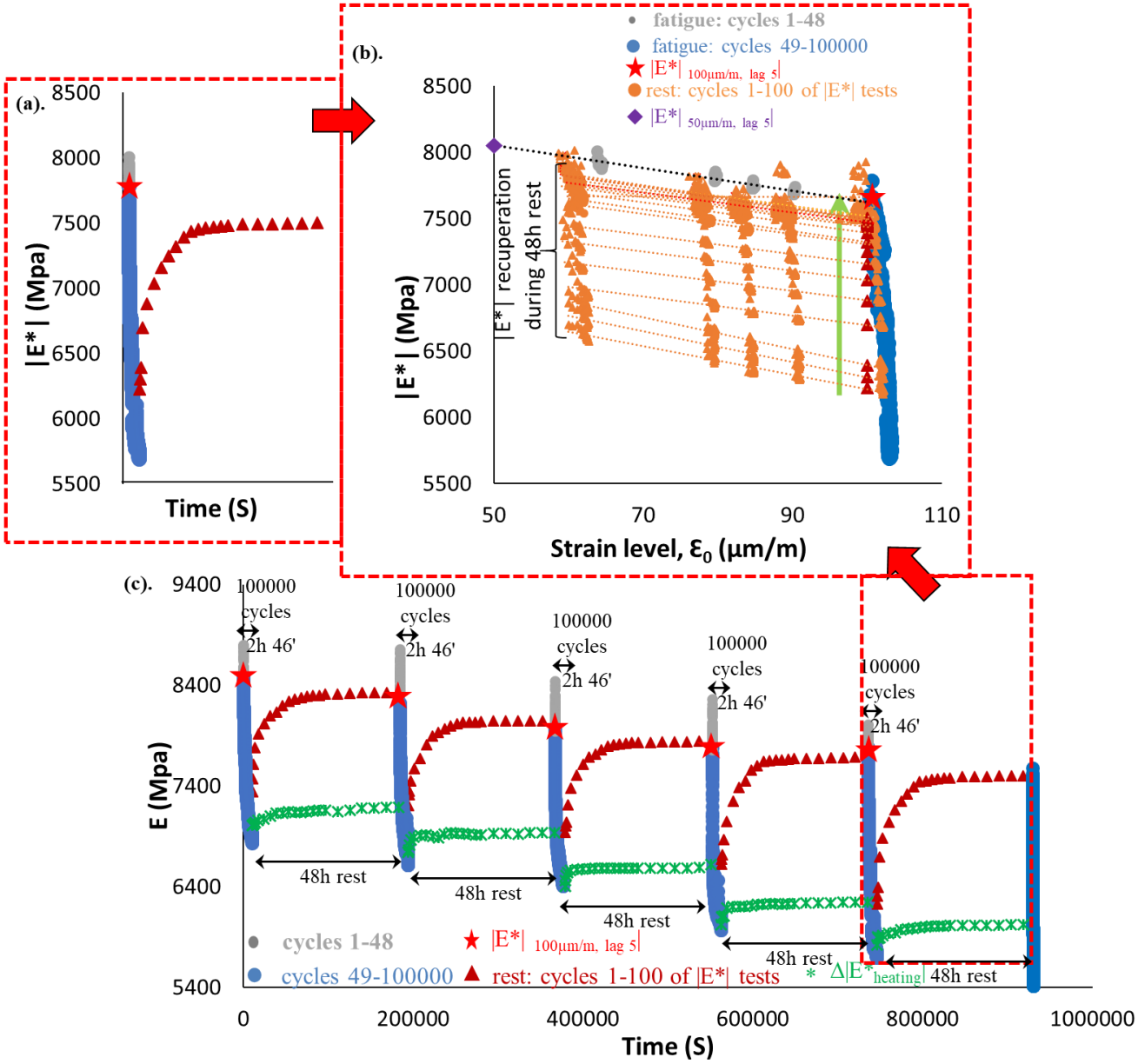

3.1.47. PFRT results obtained for mix 40/60 – 4: (a) |E*| as a function of time during the fifth fatigue lag and rest period (b) |E*| as a function of applied strain amplitude during the fifth fatigue lags and the short complex modulus tests performed within its following rest periods; (c) |E*| as a function of time during the five fatigue lags and rest periods [Red stars indicate values of |E*| estimated at 100 µm/m at the beginning of fatigue lag, green asterisk shows values of $\Delta|E^*_{heating}|$ as influence of self-heating and brown triangles indicate values of |E*| estimated at 100 µm/m for each short complex modulus test during rest (all these values were obtained using non-linearity envelopes, as shown in (b) for the first fatigue lag and rest period)].

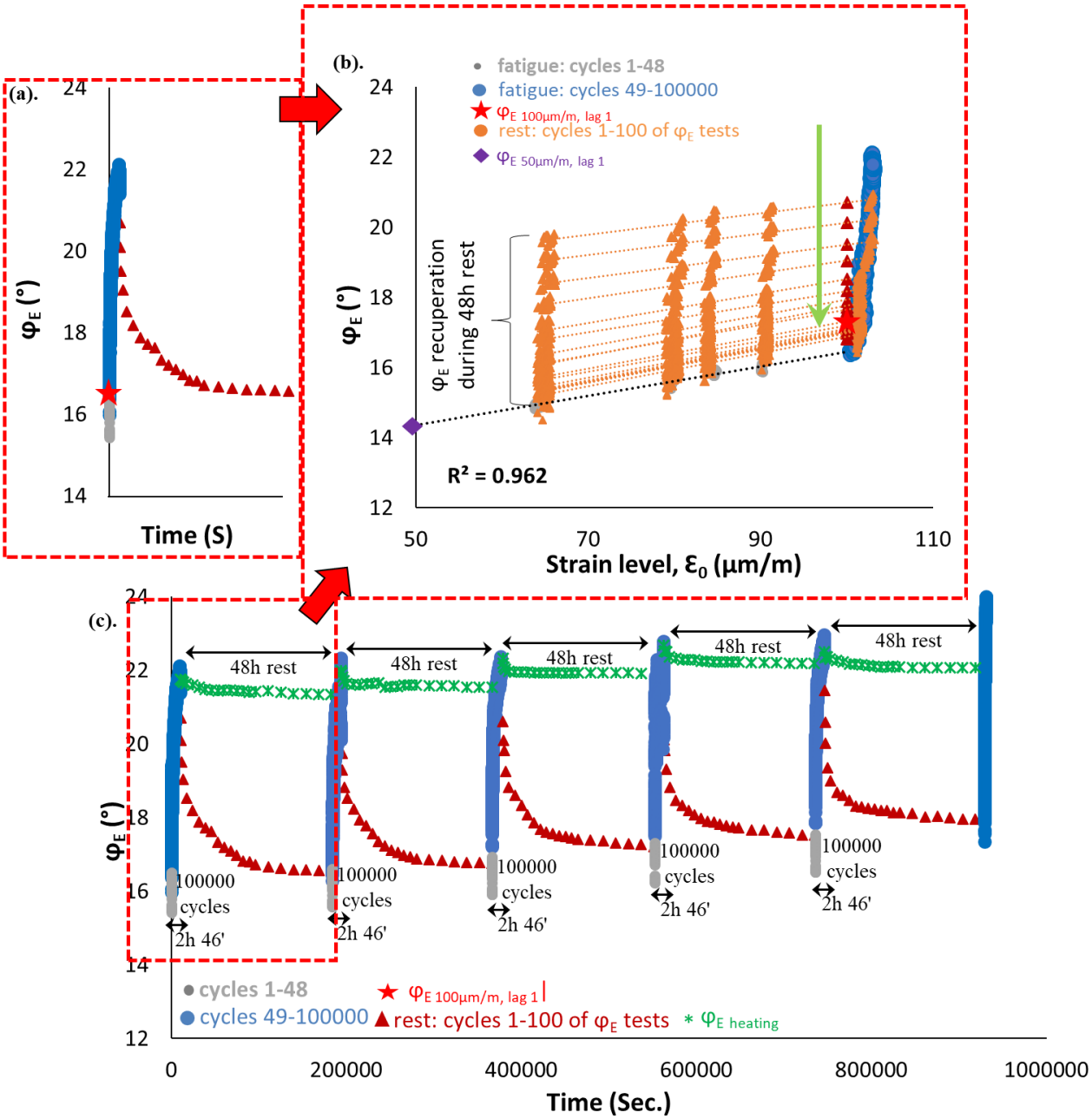

3.1.48. PFRT results obtained for mix 40/60 – 4: (a) φ_E as a function of time during the first fatigue lag and rest period (b) φ_E as a function of applied strain amplitude during the first fatigue lags and the short complex modulus tests performed within its following rest periods; (c) φ_E as a function of time during the five fatigue lags and rest periods (Red stars indicate values of φ_E estimated at 100 µm/m at the beginning of fatigue lag, green asterisk shows values of $\Delta\varphi_{E\ heating}$ as influence of self-heating and brown triangles indicate values of φ_E estimated at 100 µm/m for each short complex modulus test during rest (all these values were obtained using non-linearity envelopes, as shown in (b) for the first fatigue lag and rest period).

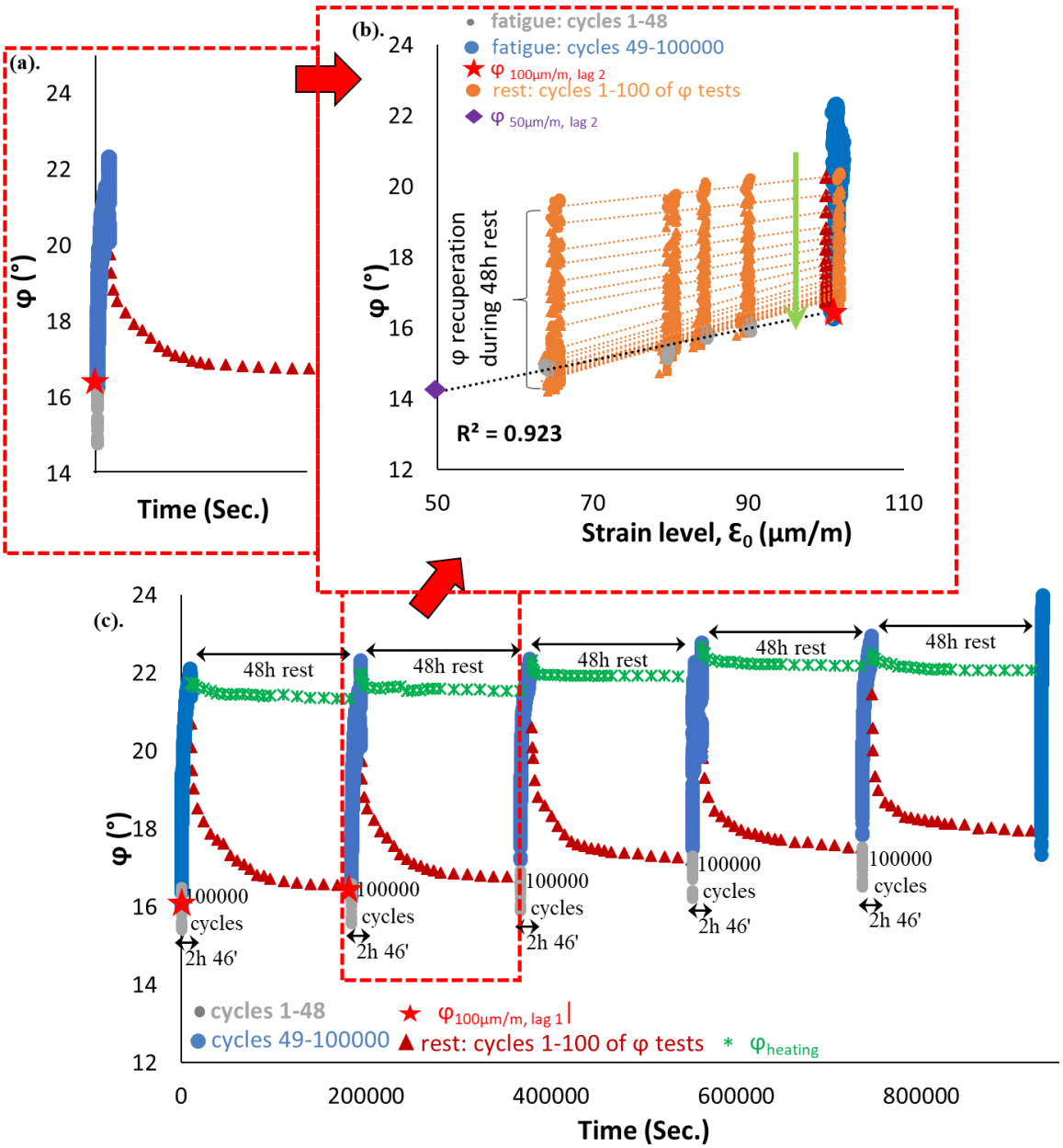

3.1.49. PFRT results obtained for mix 40/60 – 4: (a) φ_E as a function of time during the second fatigue lag and rest period (b) φ_E as a function of applied strain amplitude during the second fatigue lags and the short complex modulus tests performed within its following rest periods; (c) φ_E as a function of time during the five fatigue lags and rest periods (Red stars indicate values of φ_E estimated at 100 µm/m at the beginning of fatigue lag, green asterisk shows values of $\Delta\varphi_{E\ heating}$ as influence of self-heating and brown triangles indicate values of φ_E estimated at 100 µm/m for each short complex modulus test during rest (all these values were obtained using non-linearity envelopes, as shown in (b) for the first fatigue lag and rest period).

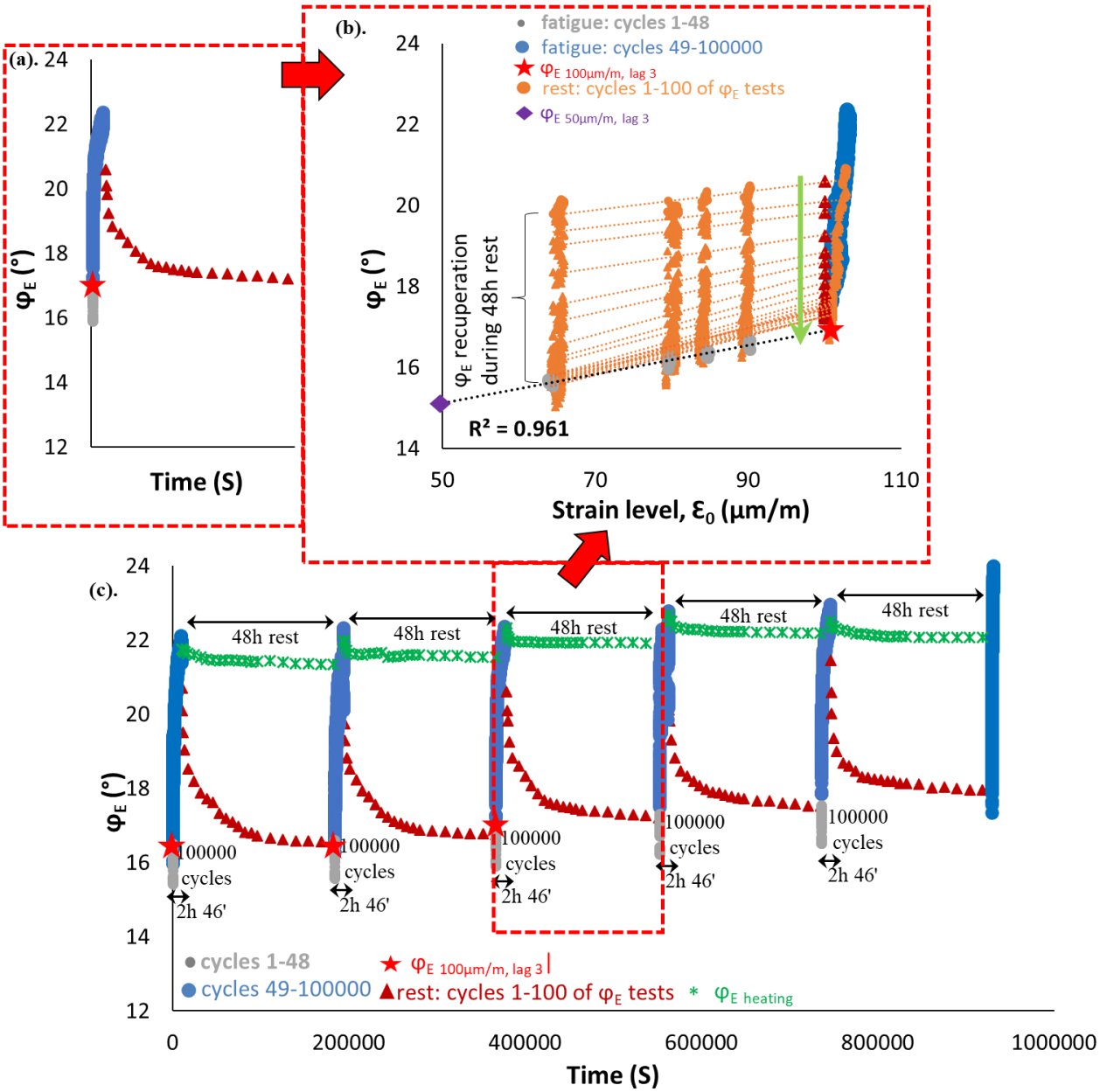

3.1.50. PFRT results obtained for mix 40/60 – 4: (a) φ_E as a function of time during the third fatigue lag and rest period (b) φ_E as a function of applied strain amplitude during the third fatigue lags and the short complex modulus tests performed within its following rest periods; (c) φ_E as a function of time during the five fatigue lags and rest periods (Red stars indicate values of φ_E estimated at 100 µm/m at the beginning of fatigue lag, green asterisk shows values of $\Delta\varphi_{E\ heating}$ as influence of self-heating and brown triangles indicate values of φ_E estimated at 100 µm/m for each short complex modulus test during rest (all these values were obtained using non-linearity envelopes, as shown in (b) for the first fatigue lag and rest period).

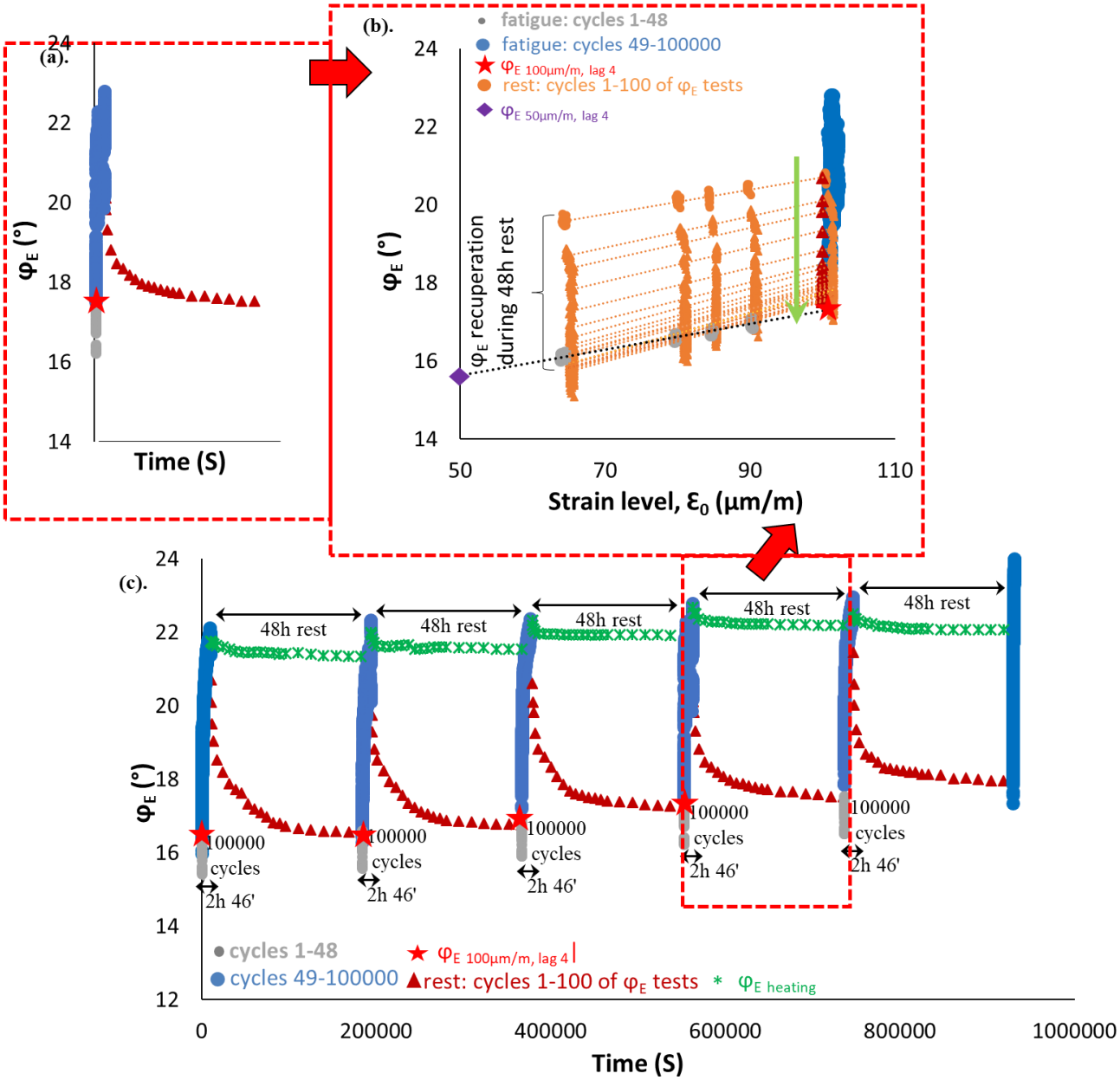

3.1.51. PFRT results obtained for mix 40/60 – 4: (a) φ_E as a function of time during the fourth fatigue lag and rest period (b) φ_E as a function of applied strain amplitude during the fourth fatigue lags and the short complex modulus tests performed within its following rest periods; (c) φ_E as a function of time during the five fatigue lags and rest periods (Red stars indicate values of φ_E estimated at 100 µm/m at the beginning of fatigue lag, green asterisk shows values of $\Delta\varphi_{E\ heating}$ as influence of self-heating and brown triangles indicate values of φ_E estimated at 100 µm/m for each short complex modulus test during rest (all these values were obtained using non-linearity envelopes, as shown in (b) for the first fatigue lag and rest period).

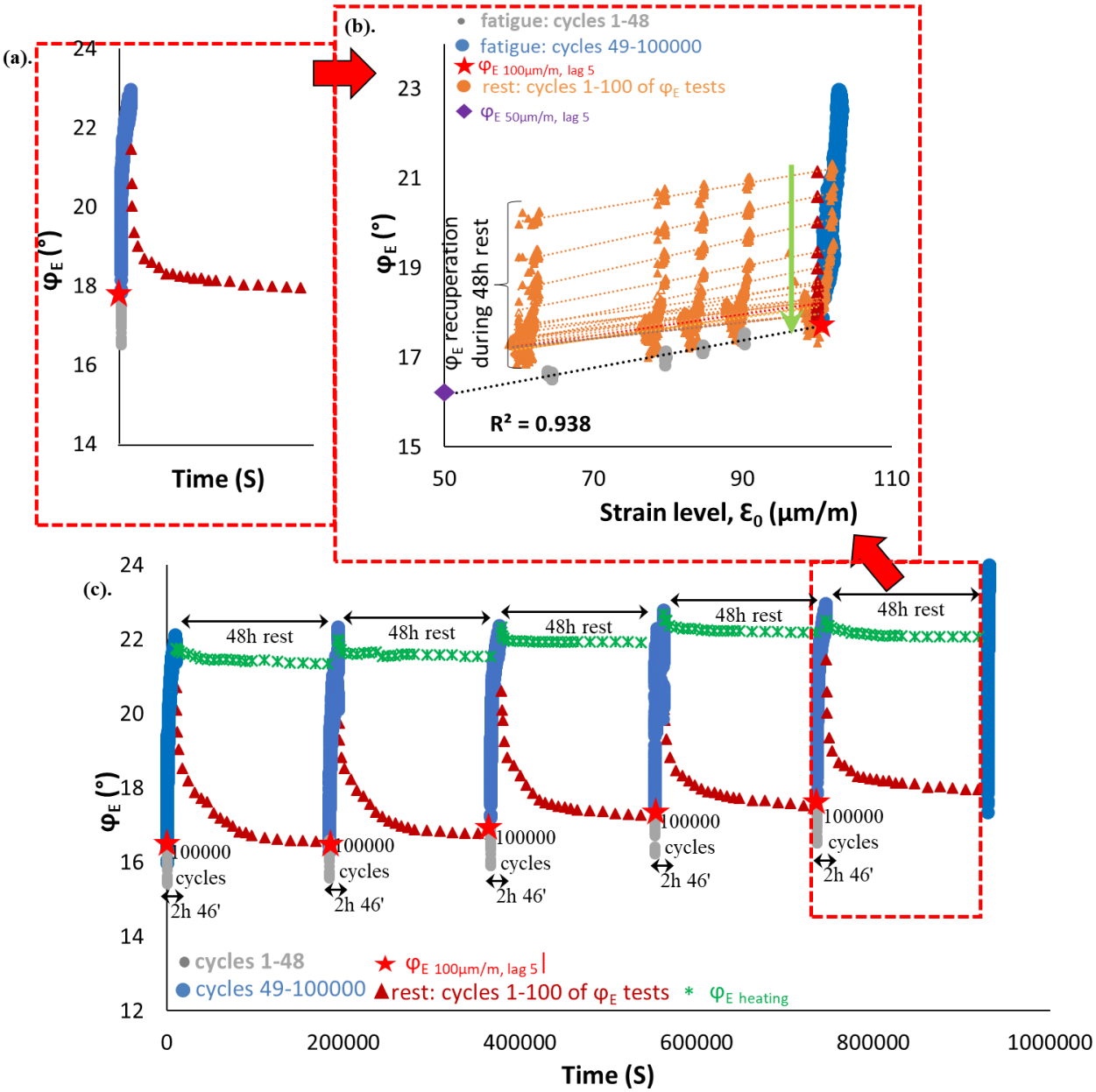

3.1.52. PFRT results obtained for mix 40/60 – 4: (a) φ_E as a function of time during the fifth fatigue lag and rest period (b) φ_E as a function of applied strain amplitude during the fifth fatigue lags and the short complex modulus tests performed within its following rest periods; (c) φ_E as a function of time during the five fatigue lags and rest periods (Red stars indicate values of φ_E estimated at 100 µm/m at the beginning of fatigue lag, green asterisk shows values of $\Delta\varphi_{E\ heating}$ as influence of self-heating and brown triangles indicate values of φ_E estimated at 100 µm/m for each short complex modulus test during rest (all these values were obtained using non-linearity envelopes, as shown in (b) for the first fatigue lag and rest period).

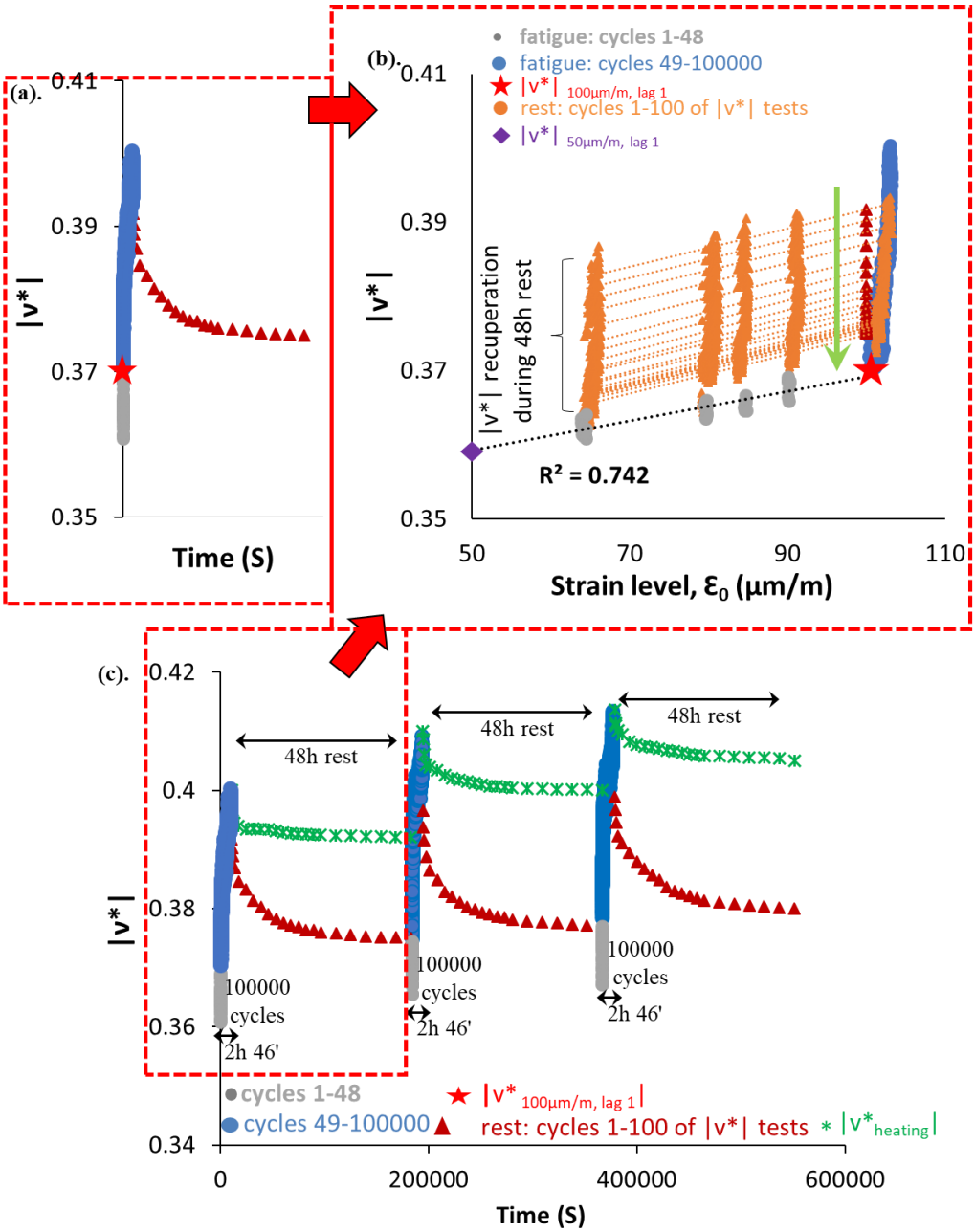

3.1.53. PFRT results obtained for mix 40/60 – 4: (a) |v*| as a function of time during the fifth fatigue lag and rest period (b) |v*| as a function of applied strain amplitude during the fifth fatigue lags and the short complex modulus tests performed within its following rest periods; (c) |v*| as a function of time during the five fatigue lags and rest periods (Red stars indicate values of |v*| estimated at 100 µm/m at the beginning of fatigue lag, green asterisk shows values of $\Delta|v^*|_{heating}$ as influence of self-heating and brown triangles indicate values of |v*| estimated at 100 µm/m for each short complex modulus test during rest (all these values were obtained using non-linearity envelopes, as shown in (b) for the first fatigue lag and rest period).

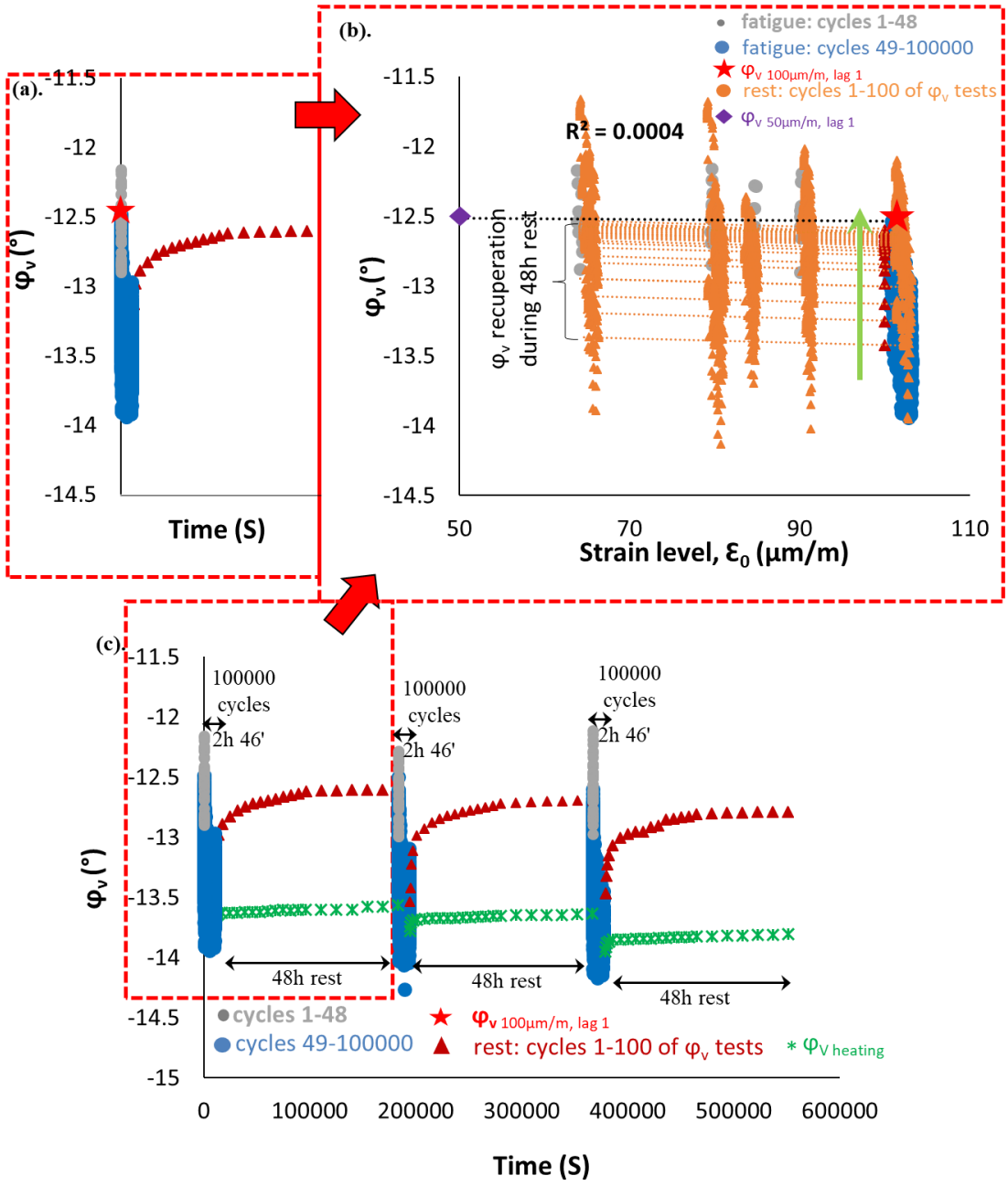

3.1.54. PFRT results obtained for mix 40/60 – 4: (a) φ_v as a function of time during the fifth fatigue lag and rest period (b) |v*| as a function of applied strain amplitude during the fifth fatigue lags and the short complex modulus tests performed within its following rest periods; (c) φ_v as a function of time during the five fatigue lags and rest periods (Red stars indicate values of φ_v estimated at 100 µm/m at the beginning of fatigue lag, green asterisk shows values of $\varphi_{v\ heating}$ as influence of self-heating and brown triangles indicate values of φ_v estimated at 100 µm/m for each short complex modulus test during rest (all these values were obtained using non-linearity envelopes, as shown in (b) for the first fatigue lag and rest period).

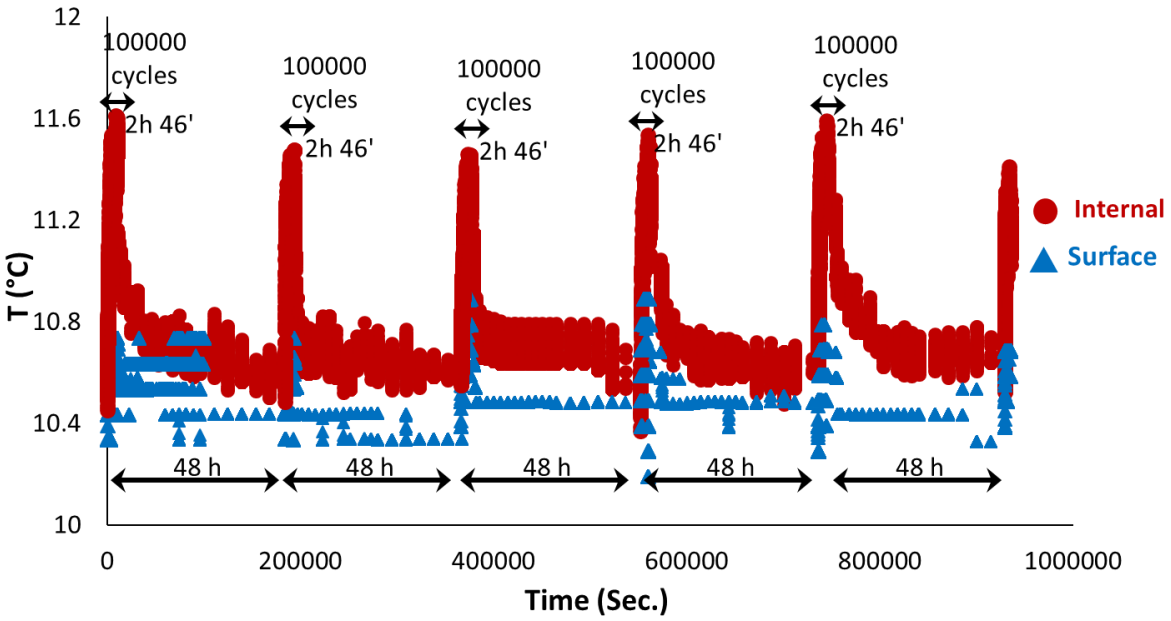

Figure 3.1.55. PFRT results obtained for mix 40/60 – 4: internal and surface temperature evolution during fatigue lags and recovery periods.

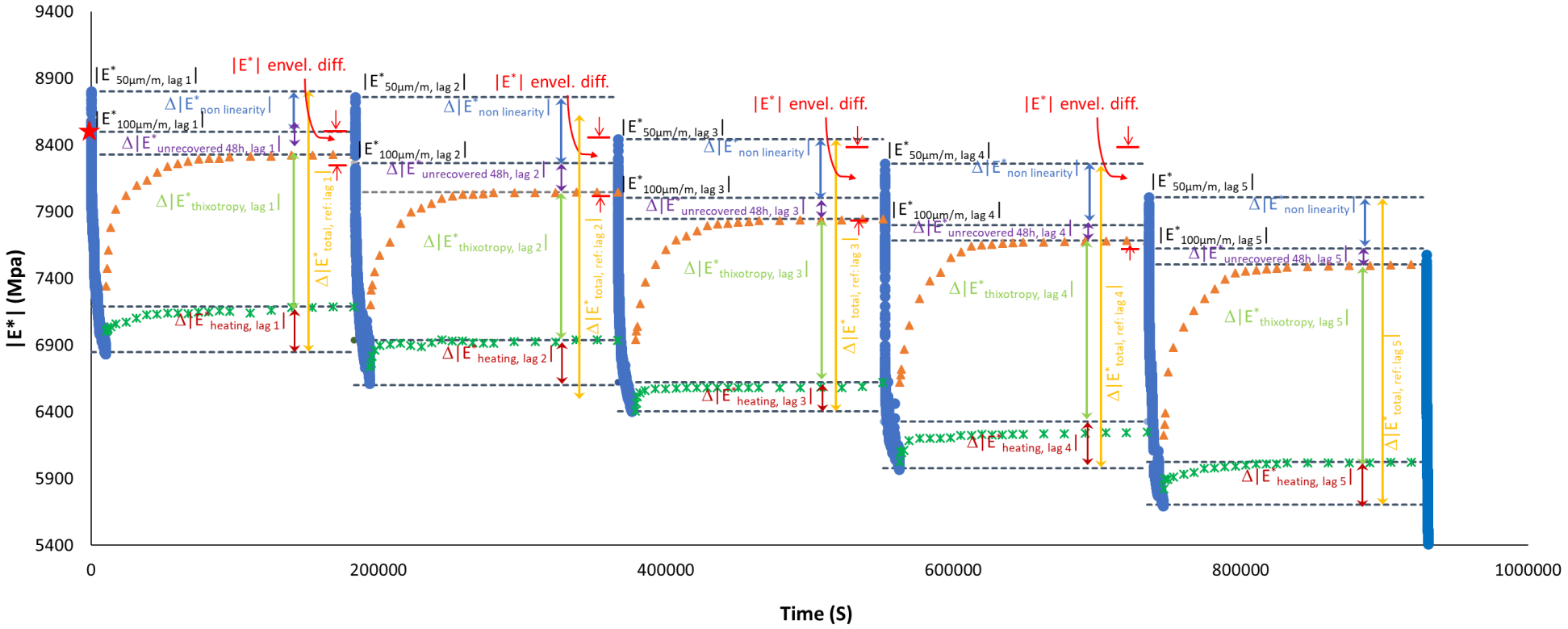
9400
8900
8400
7900
7400
6900
6400
5900
5400
|E*| (Mpa)
0
200000
400000
600000
800000
1000000
Time (S)
|E*50µm/m, lag 1|
|E*100µm/m, lag 1|
Δ|E*non linearity|
Δ|E*unrecovered 48h, lag 1|
Δ|E*thixotropy, lag 1|
Δ|E*heating, lag 1|
|E*| envel. diff.
Δ|E*total, ref: lag 1|
|E*50µm/m, lag 2|
|E*100µm/m, lag 2|
Δ|E*non linearity|
Δ|E*unrecovered 48h, lag 2|
Δ|E*thixotropy, lag 2|
Δ|E*heating, lag 2|
|E*| envel. diff.
Δ|E*total, ref: lag 2|
|E*50µm/m, lag 3|
|E*100µm/m, lag 3|
Δ|E*non linearity|
Δ|E*unrecovered 48h, lag 3|
Δ|E*thixotropy, lag 3|
Δ|E*heating, lag 3|
|E*| envel. diff.
Δ|E*total, ref: lag 3|
|E*50µm/m, lag 4|
|E*100µm/m, lag 4|
Δ|E*non linearity|
Δ|E*unrecovered 48h, lag 4|
Δ|E*thixotropy, lag 4|
Δ|E*heating, lag 4|
|E*| envel. diff.
Δ|E*total, ref: lag 4|
|E*50µm/m, lag 5|
|E*100µm/m, lag 5|
Δ|E*non linearity|
Δ|E*unrecovered 48h, lag 5|
Δ|E*thixotropy, lag 5|
Δ|E*heating, lag 5|
Δ|E*total, ref: lag 5|

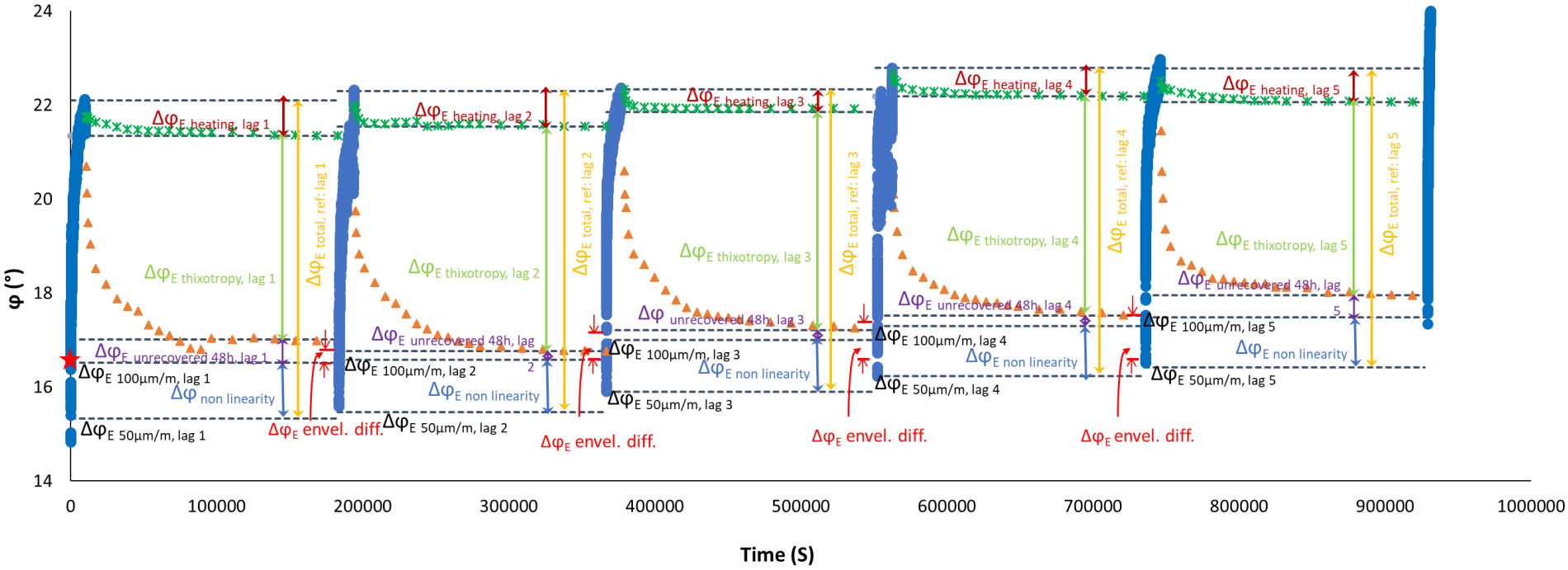
φ (°)
Time (S)
Δφ E heating, lag 1
Δφ E thixotropy, lag 1
Δφ E total, ref: lag 1
Δφ E unrecovered 48h, lag 1
Δφ E 100µm/m, lag 1
Δφ non linearity
Δφ E 50µm/m, lag 1
Δφ E envel. diff.
Δφ E heating, lag 2
Δφ E thixotropy, lag 2
Δφ E total, ref: lag 2
Δφ E unrecovered 48h, lag 2
Δφ E 100µm/m, lag 2
Δφ E non linearity
Δφ E 50µm/m, lag 2
Δφ E envel. diff.
Δφ E heating, lag 3
Δφ E thixotropy, lag 3
Δφ E total, ref: lag 3
Δφ unrecovered 48h, lag 3
Δφ E 100µm/m, lag 3
Δφ E non linearity
Δφ E 50µm/m, lag 3
Δφ E envel. diff.
Δφ E heating, lag 4
Δφ E thixotropy, lag 4
Δφ E total, ref: lag 4
Δφ E unrecovered 48h, lag 4
Δφ E 100µm/m, lag 4
Δφ E non linearity
Δφ E 50µm/m, lag 4
Δφ E envel. diff.
Δφ E heating, lag 5
Δφ E thixotropy, lag 5
Δφ E total, ref: lag 5
Δφ E unrecovered 48h, lag 5
Δφ E 100µm/m, lag 5
Δφ E non linearity
Δφ E 50µm/m, lag 5
24
22
20
18
16
14
0
100000
200000
300000
400000
500000
600000
700000
800000
900000
1000000

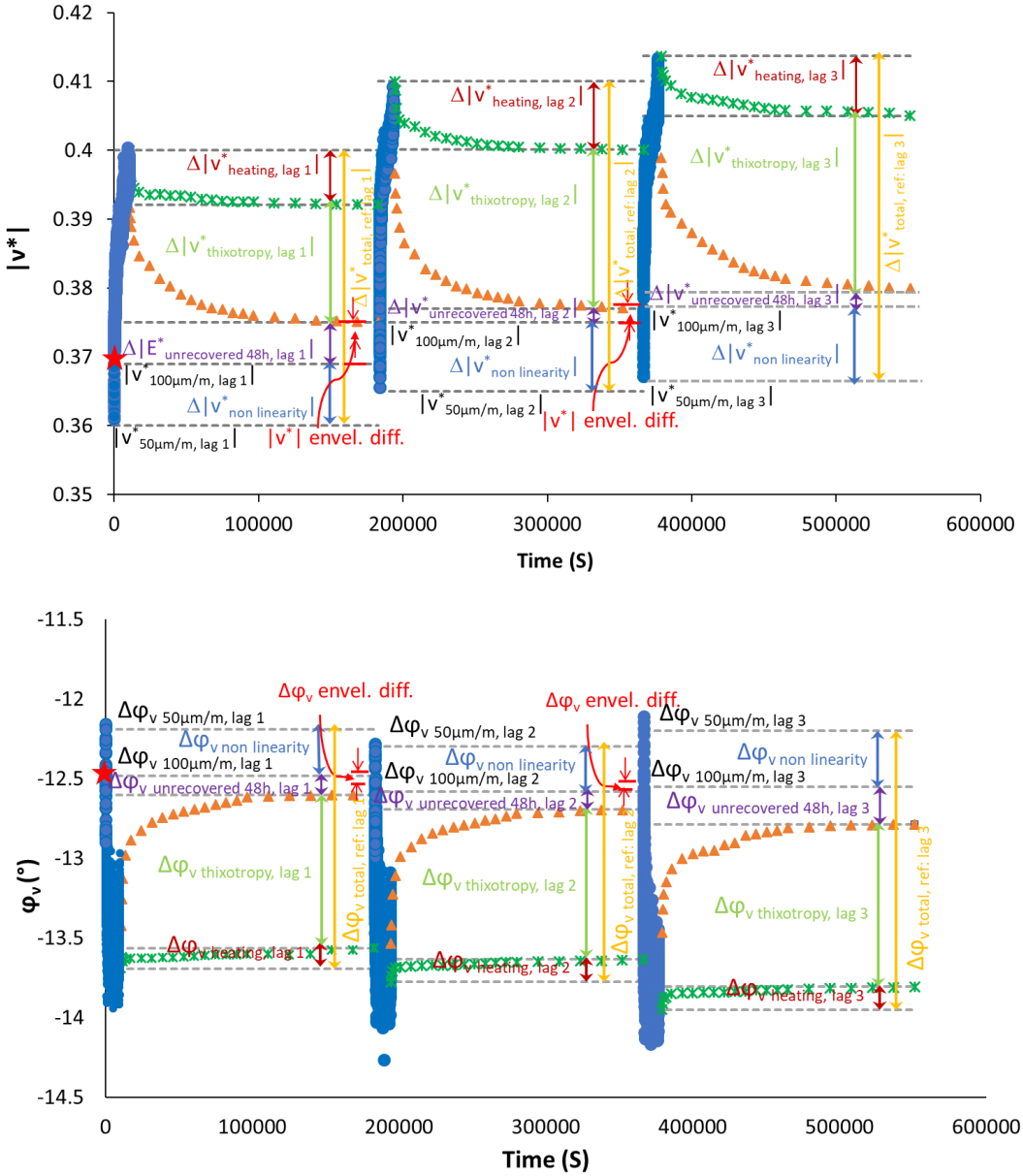

Figure 3.1.56. Quantification of different contributions |E*|, φ_E, |v*| and φ_v evolution, for all fatigue lags for mix 40/60 – 4: different envelope line is used for each fatigue lag.

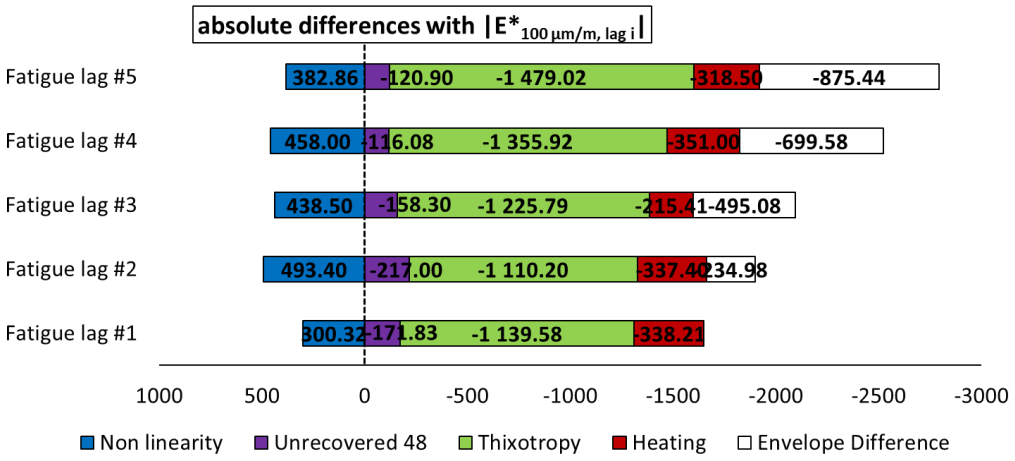
absolute differences with |E*100 µm/m, lag i|
Fatigue lag #5
Fatigue lag #4
Fatigue lag #3
Fatigue lag #2
Fatigue lag #1
382.86
-120.90
-1 479.02
-318.50
-875.44
458.00
-116.08
-1 355.92
-351.00
-699.58
438.50
-158.30
-1 225.79
-215.41
-495.08
493.40
-217.00
-1 110.20
-337.40
-234.98
300.32
-171.83
-1 139.58
-338.21
1000
500
0
-500
-1000
-1500
-2000
-2500
-3000
Non linearity
Unrecovered 48
Thixotropy
Heating
Envelope Difference

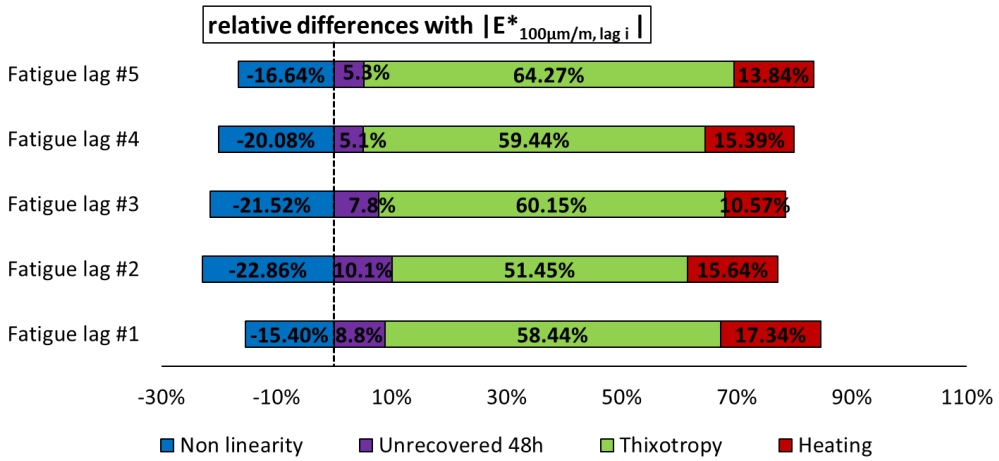
relative differences with |E*100µm/m, lag i|
Fatigue lag #5
Fatigue lag #4
Fatigue lag #3
Fatigue lag #2
Fatigue lag #1
-16.64%
5.3%
64.27%
13.84%
-20.08%
5.1%
59.44%
15.39%
-21.52%
7.8%
60.15%
10.57%
-22.86%
10.1%
51.45%
15.64%
-15.40%
8.8%
58.44%
17.34%
-30%
-10%
10%
30%
50%
70%
90%
110%
Non linearity
Unrecovered 48h
Thixotropy
Heating

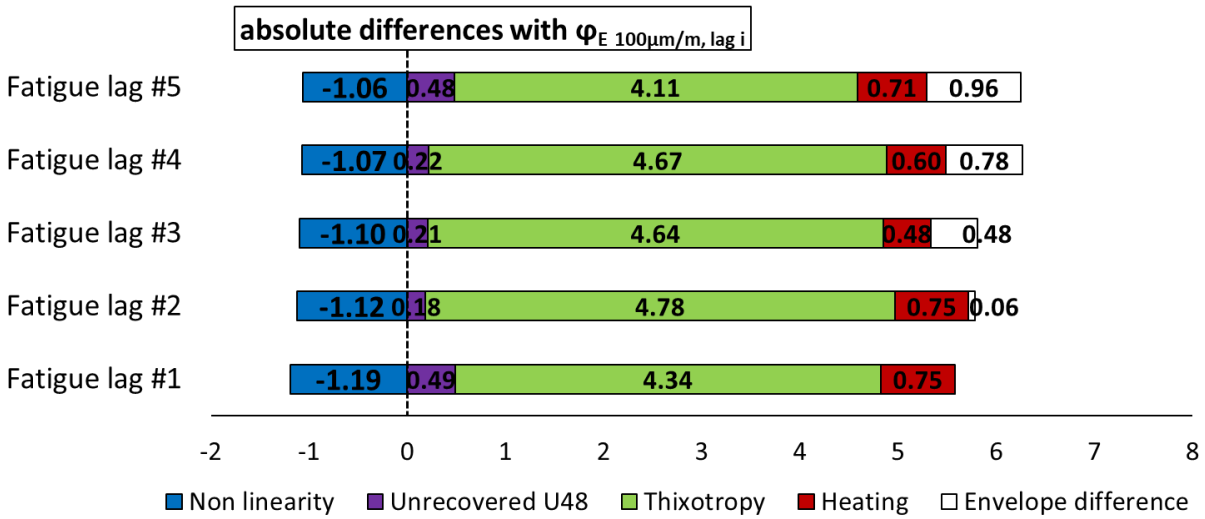
absolute differences with φE 100µm/m, lag i
Fatigue lag #5
Fatigue lag #4
Fatigue lag #3
Fatigue lag #2
Fatigue lag #1
-1.06
0.48
4.11
0.71
0.96
-1.07
0.22
4.67
0.60
0.78
-1.10
0.21
4.64
0.48
0.48
-1.12
0.18
4.78
0.75
0.06
-1.19
0.49
4.34
0.75
-2
-1
0
1
2
3
4
5
6
7
8
Non linearity
Unrecovered U48
Thixotropy
Heating
Envelope difference

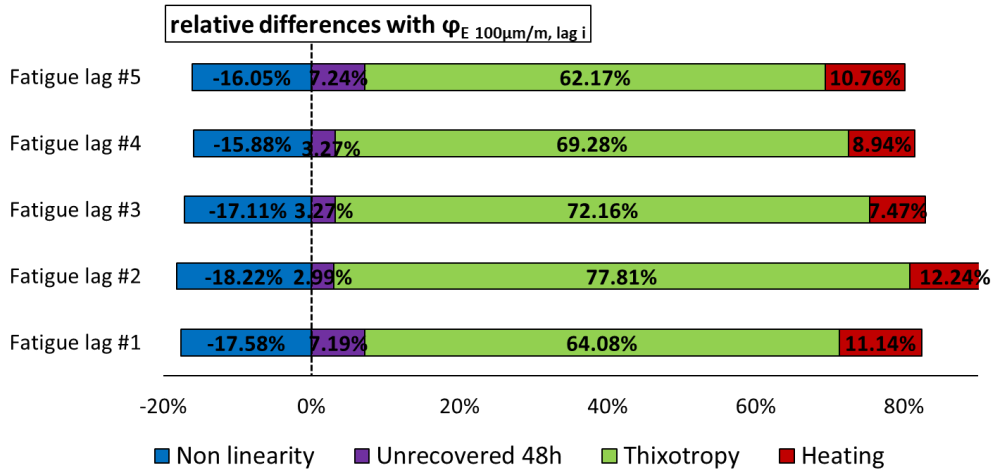
relative differences with φE 100µm/m, lag i
Fatigue lag #5
Fatigue lag #4
Fatigue lag #3
Fatigue lag #2
Fatigue lag #1
-16.05%
7.24%
62.17%
10.76%
-15.88%
3.27%
69.28%
8.94%
-17.11%
3.27%
72.16%
7.47%
-18.22%
2.99%
77.81%
12.24%
-17.58%
7.19%
64.08%
11.14%
-20%
0%
20%
40%
60%
80%
Non linearity
Unrecovered 48h
Thixotropy
Heating

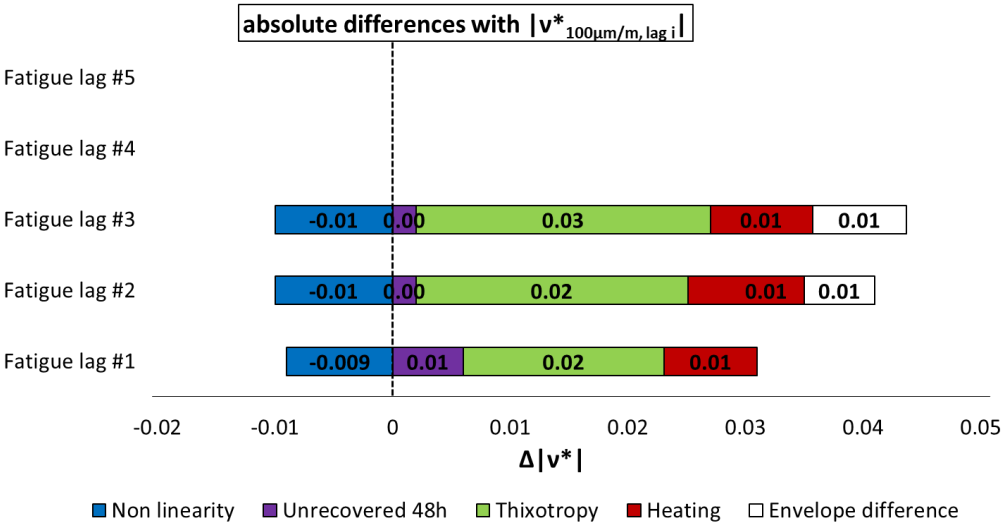
absolute differences with |v*100µm/m, lag i|
Fatigue lag #5
Fatigue lag #4
Fatigue lag #3
Fatigue lag #2
Fatigue lag #1
-0.01
0.00
0.03
0.01
0.01
-0.01
0.00
0.02
0.01
0.01
-0.009
0.01
0.02
0.01
-0.02
-0.01
0
0.01
0.02
0.03
0.04
0.05
Δ|v*|
Non linearity
Unrecovered 48h
Thixotropy
Heating
Envelope difference

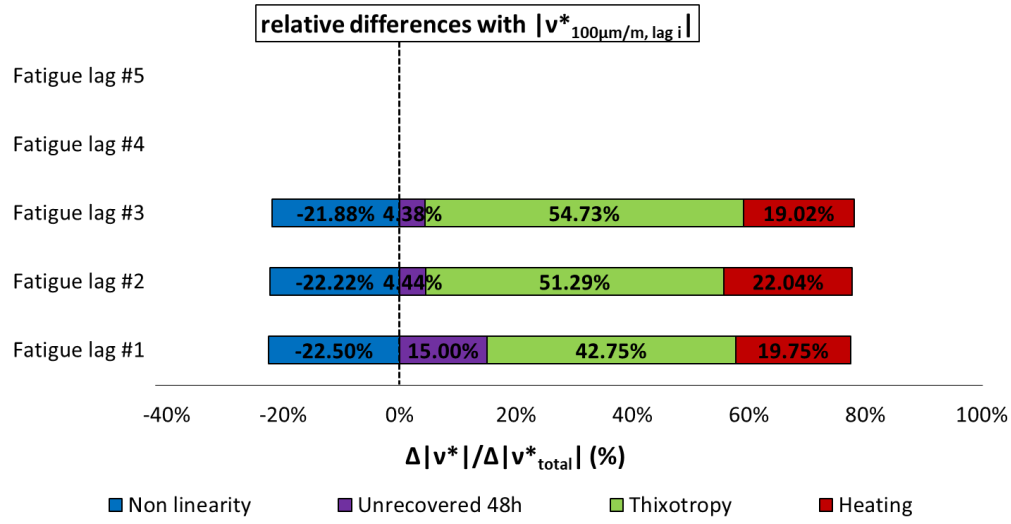
relative differences with |v*100µm/m, lag i|
Fatigue lag #5
Fatigue lag #4
Fatigue lag #3
Fatigue lag #2
Fatigue lag #1
-21.88%
4.38%
54.73%
19.02%
-22.22%
4.44%
51.29%
22.04%
-22.50%
15.00%
42.75%
19.75%
-40%
-20%
0%
20%
40%
60%
80%
100%
Δ|v*|/Δ|v*total| (%)
Non linearity
Unrecovered 48h
Thixotropy
Heating

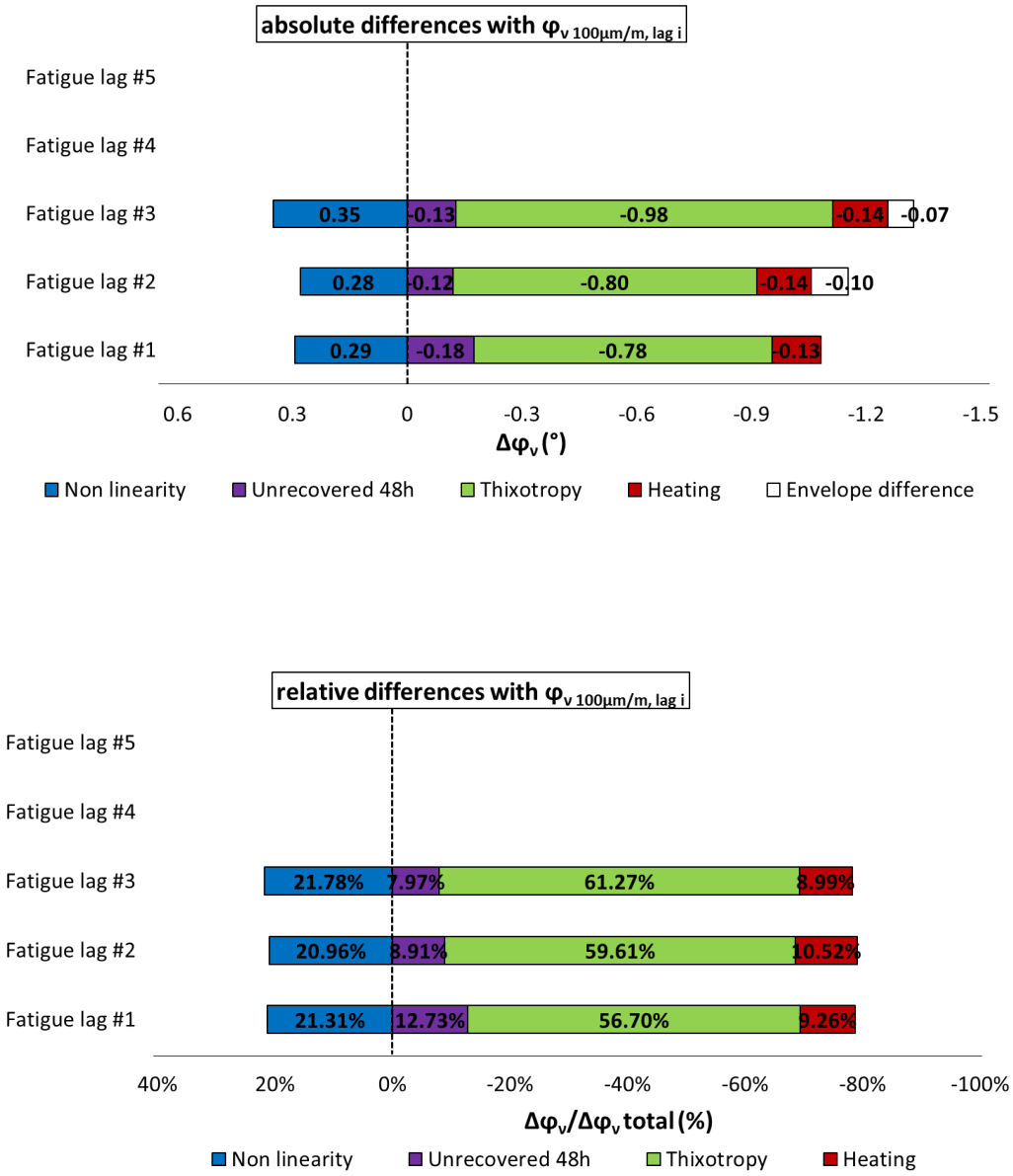

Figure 3.1.57. Quantification of different absolute and relative contributions to |E*|, φ_E, |ν*| and φ_ν evolutions for mix 40/60 – 4, calculated using a different envelope line for each fatigue lag.

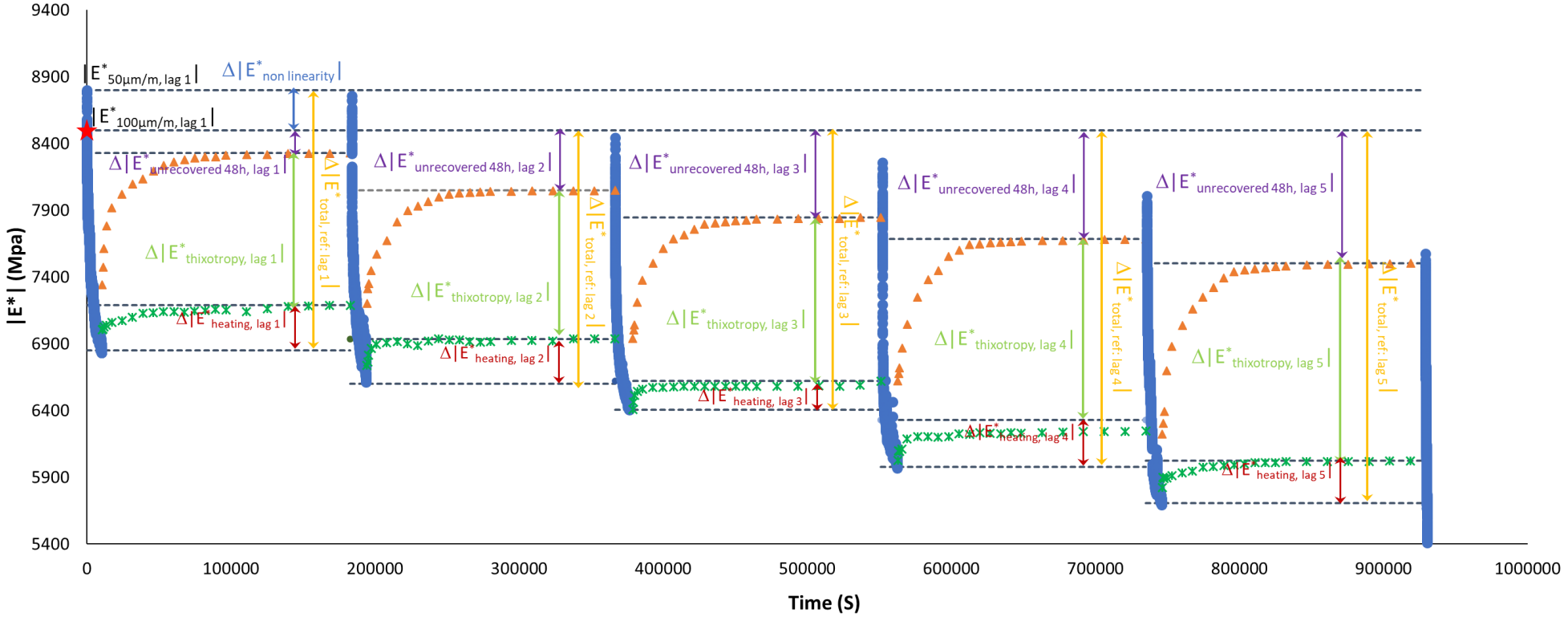
9400
8900
8400
7900
7400
6900
6400
5900
5400
|E*| (Mpa)
0
100000
200000
300000
400000
500000
600000
700000
800000
900000
1000000
Time (S)
|E*50µm/m, lag 1|
|E*100µm/m, lag 1|
Δ|E*non linearity|
Δ|E*unrecovered 48h, lag 1|
Δ|E*thixotropy, lag 1|
Δ|E*heating, lag 1|
Δ|E*total, ref: lag 1|
Δ|E*unrecovered 48h, lag 2|
Δ|E*thixotropy, lag 2|
Δ|E*heating, lag 2|
Δ|E*total, ref: lag 2|
Δ|E*unrecovered 48h, lag 3|
Δ|E*thixotropy, lag 3|
Δ|E*heating, lag 3|
Δ|E*total, ref: lag 3|
Δ|E*unrecovered 48h, lag 4|
Δ|E*thixotropy, lag 4|
Δ|E*heating, lag 4|
Δ|E*total, ref: lag 4|
Δ|E*unrecovered 48h, lag 5|
Δ|E*thixotropy, lag 5|
Δ|E*heating, lag 5|
Δ|E*total, ref: lag 5|

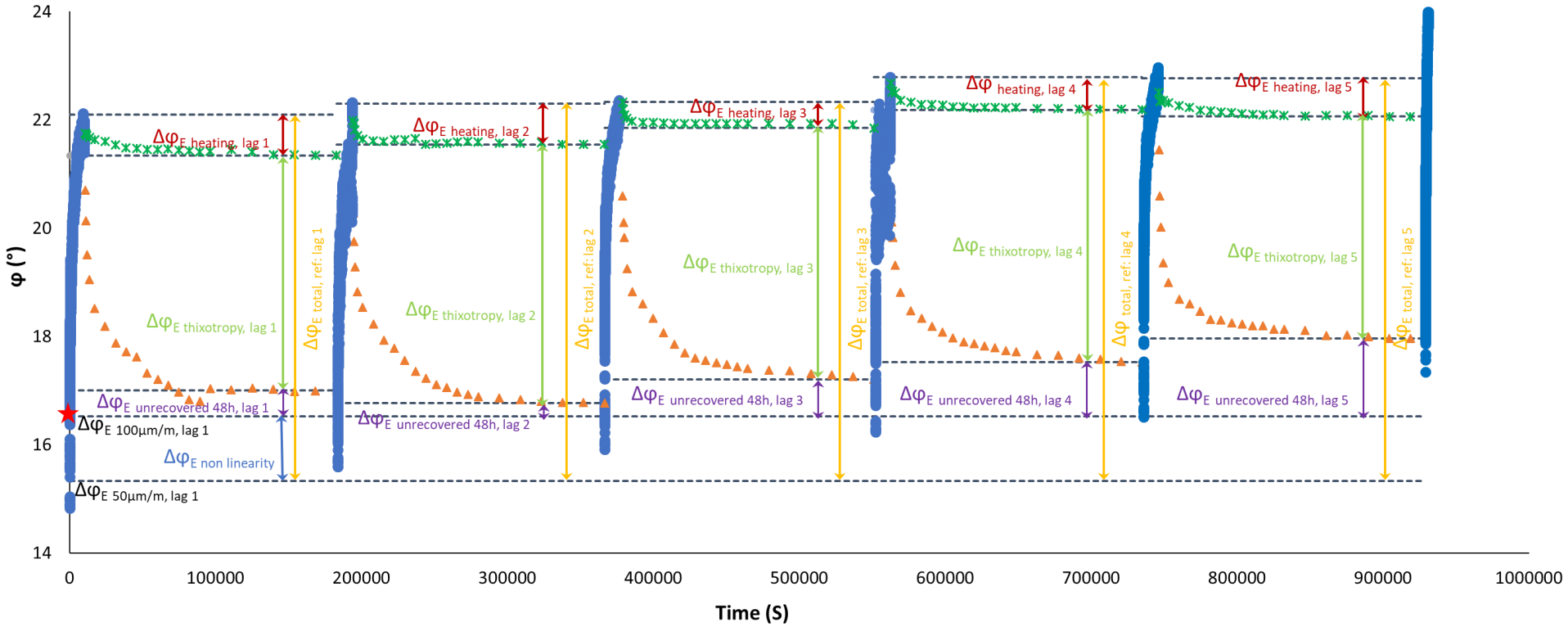
24
22
20
18
16
14
φ (°)
0
100000
200000
300000
400000
500000
600000
700000
800000
900000
1000000
Time (S)
Δφ E heating, lag 1
Δφ E thixotropy, lag 1
Δφ E unrecovered 48h, lag 1
Δφ E 100µm/m, lag 1
Δφ E non linearity
Δφ E 50µm/m, lag 1
Δφ E total, ref: lag 1
Δφ E heating, lag 2
Δφ E thixotropy, lag 2
Δφ E unrecovered 48h, lag 2
Δφ E total, ref: lag 2
Δφ E heating, lag 3
Δφ E thixotropy, lag 3
Δφ E unrecovered 48h, lag 3
Δφ E total, ref: lag 3
Δφ heating, lag 4
Δφ E thixotropy, lag 4
Δφ E unrecovered 48h, lag 4
Δφ total, ref: lag 4
Δφ E heating, lag 5
Δφ E thixotropy, lag 5
Δφ E unrecovered 48h, lag 5
Δφ E total, ref: lag 5

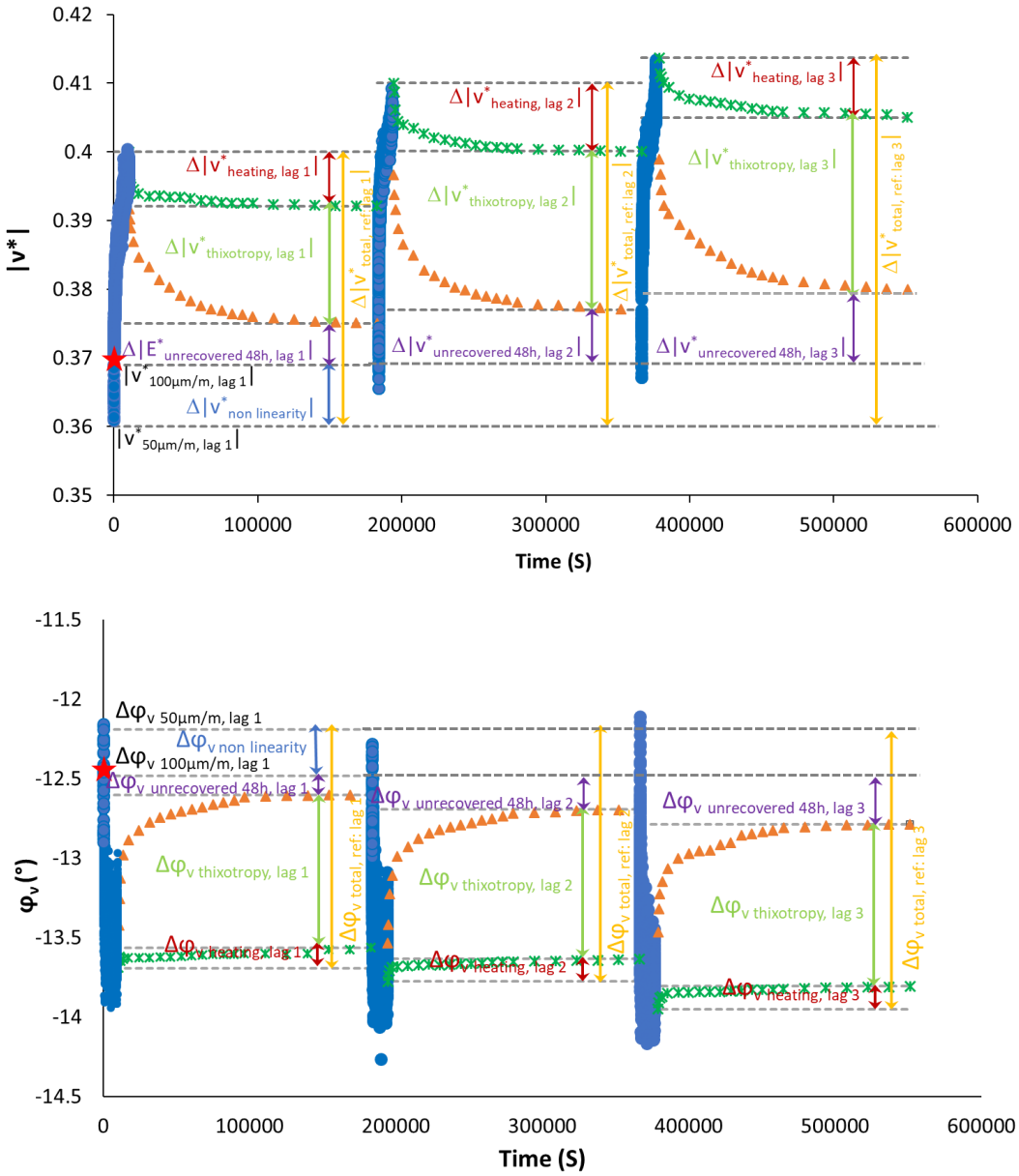

Figure 3.1.58. Quantification of different contributions to |E*|, φ_E, |v*| and φ_v evolution during first and second fatigue lags for mix 40/60 – 4: the envelope line of the first fatigue lag is used for all fatigue lags.

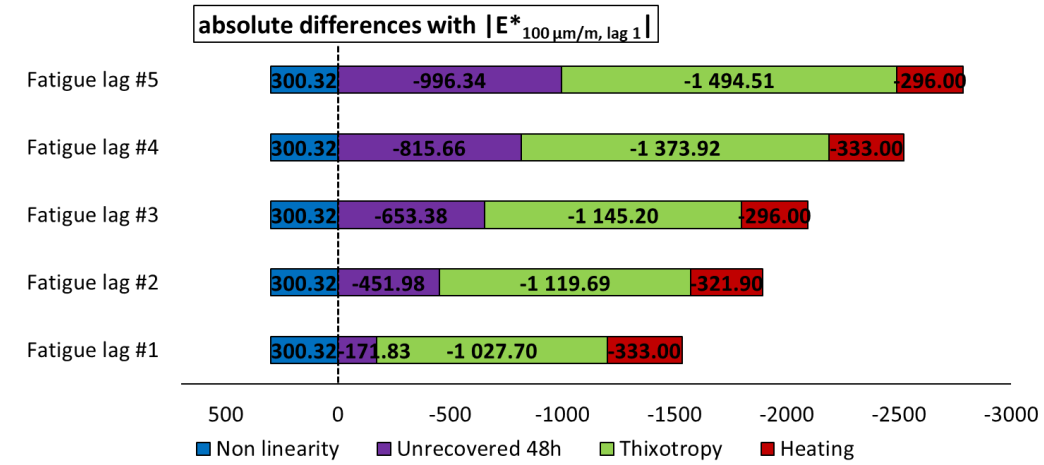
absolute differences with |E*100 µm/m, lag 1|
Fatigue lag #5
Fatigue lag #4
Fatigue lag #3
Fatigue lag #2
Fatigue lag #1
300.32
-996.34
-1 494.51
-296.00
300.32
-815.66
-1 373.92
-333.00
300.32
-653.38
-1 145.20
-296.00
300.32
-451.98
-1 119.69
-321.90
300.32
-171.83
-1 027.70
-333.00
500
0
-500
-1000
-1500
-2000
-2500
-3000
Non linearity
Unrecovered 48h
Thixotropy
Heating

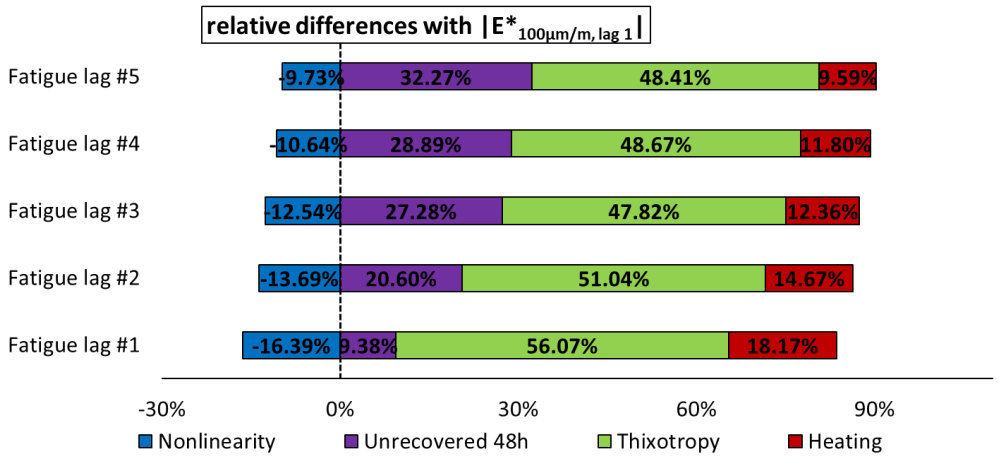
relative differences with |E*100µm/m, lag 1|
Fatigue lag #5
Fatigue lag #4
Fatigue lag #3
Fatigue lag #2
Fatigue lag #1
-9.73%
32.27%
48.41%
9.59%
-10.64%
28.89%
48.67%
11.80%
-12.54%
27.28%
47.82%
12.36%
-13.69%
20.60%
51.04%
14.67%
-16.39%
9.38%
56.07%
18.17%
-30%
0%
30%
60%
90%
Nonlinearity
Unrecovered 48h
Thixotropy
Heating

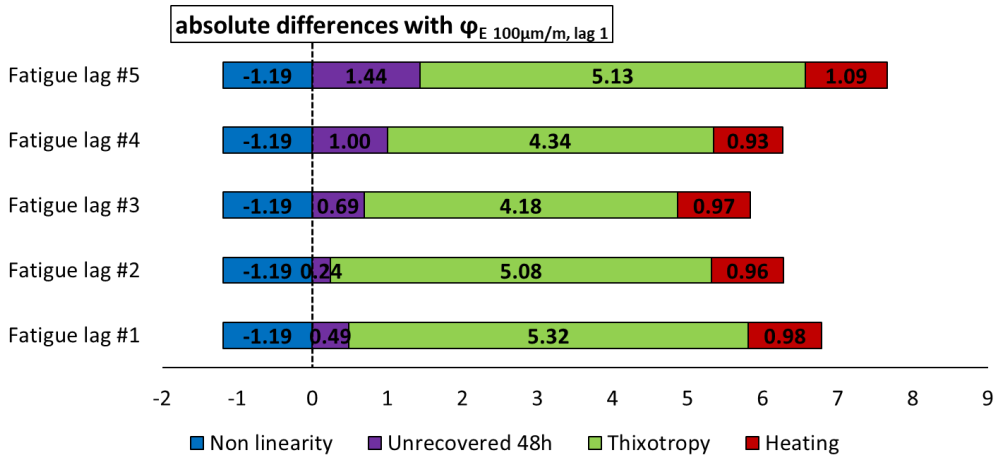
absolute differences with φE 100µm/m, lag 1
Fatigue lag #5
Fatigue lag #4
Fatigue lag #3
Fatigue lag #2
Fatigue lag #1
-1.19
1.44
5.13
1.09
-1.19
1.00
4.34
0.93
-1.19
0.69
4.18
0.97
-1.19
0.24
5.08
0.96
-1.19
0.49
5.32
0.98
-2
-1
0
1
2
3
4
5
6
7
8
9
Non linearity
Unrecovered 48h
Thixotropy
Heating

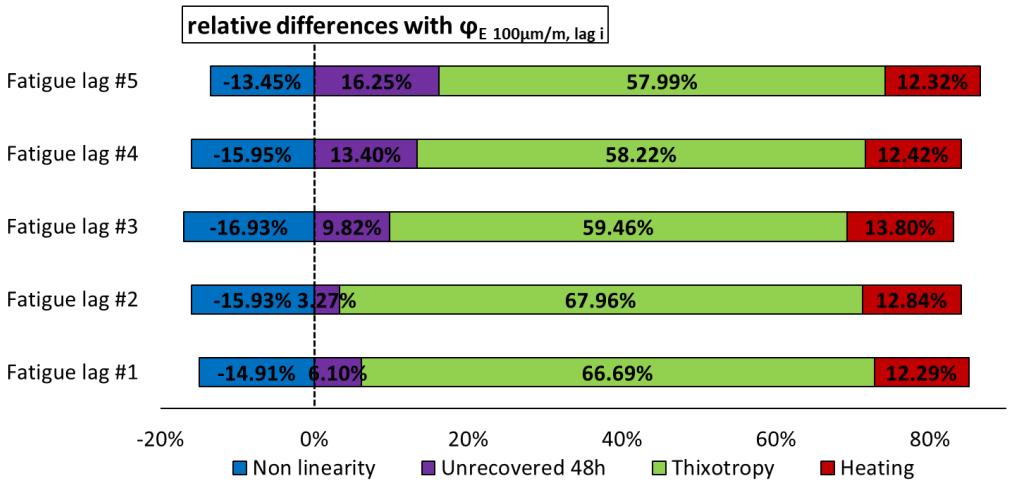
relative differences with φE 100µm/m, lag i
Fatigue lag #5
Fatigue lag #4
Fatigue lag #3
Fatigue lag #2
Fatigue lag #1
-13.45%
16.25%
57.99%
12.32%
-15.95%
13.40%
58.22%
12.42%
-16.93%
9.82%
59.46%
13.80%
-15.93%
3.27%
67.96%
12.84%
-14.91%
6.10%
66.69%
12.29%
-20%
0%
20%
40%
60%
80%
Non linearity
Unrecovered 48h
Thixotropy
Heating

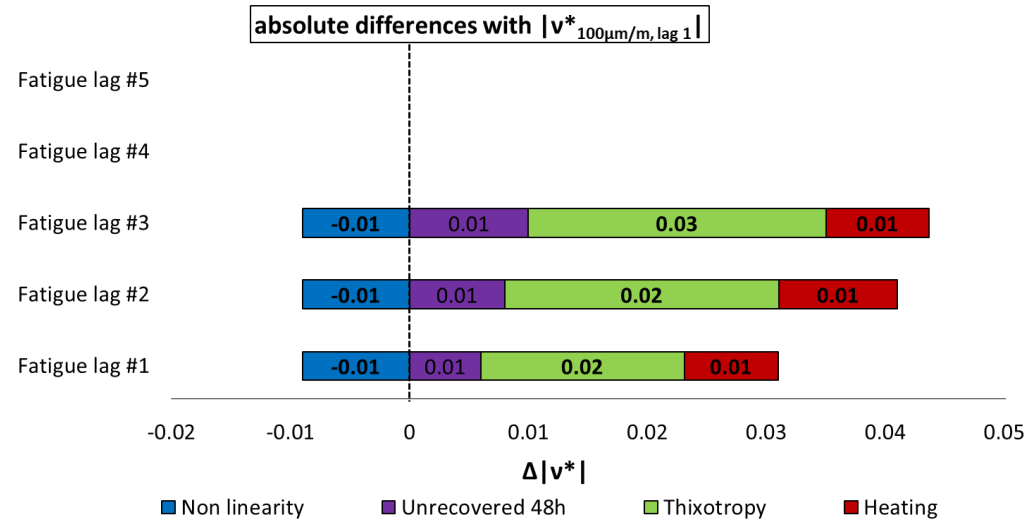
absolute differences with |v*100µm/m, lag 1|
Fatigue lag #5
Fatigue lag #4
Fatigue lag #3
Fatigue lag #2
Fatigue lag #1
-0.01
0.01
0.03
0.01
-0.01
0.01
0.02
0.01
-0.01
0.01
0.02
0.01
-0.02
-0.01
0
0.01
0.02
0.03
0.04
0.05
Δ|v*|
Non linearity
Unrecovered 48h
Thixotropy
Heating

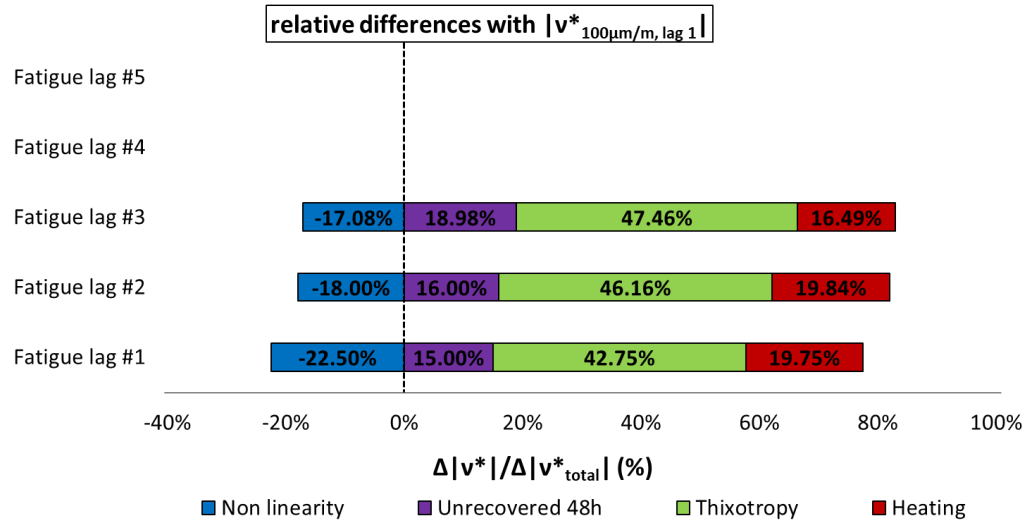
relative differences with |v*100µm/m, lag 1|
Fatigue lag #5
Fatigue lag #4
Fatigue lag #3
Fatigue lag #2
Fatigue lag #1
-17.08%
18.98%
47.46%
16.49%
-18.00%
16.00%
46.16%
19.84%
-22.50%
15.00%
42.75%
19.75%
-40%
-20%
0%
20%
40%
60%
80%
100%
Δ|v*|/Δ|v*total| (%)
Non linearity
Unrecovered 48h
Thixotropy
Heating

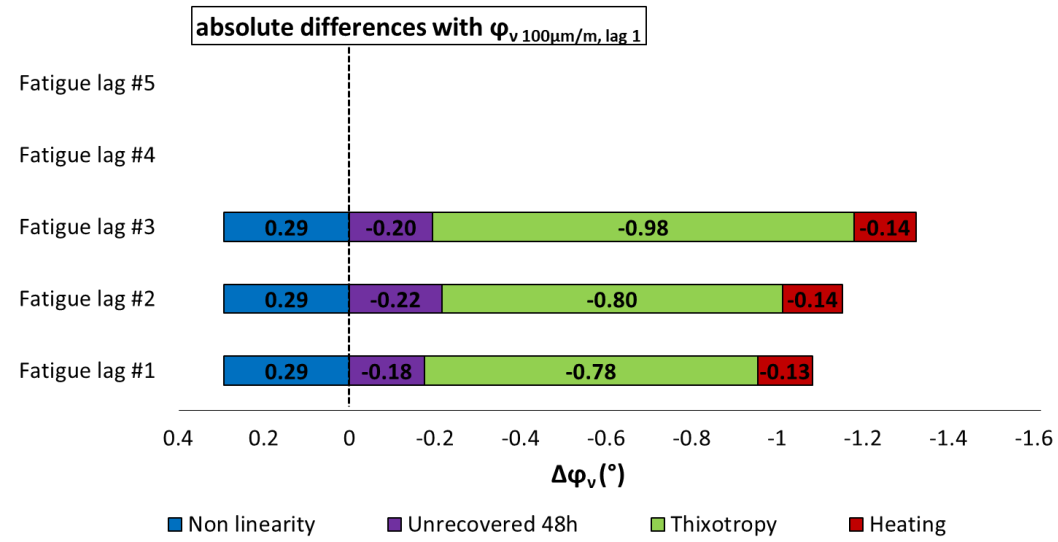

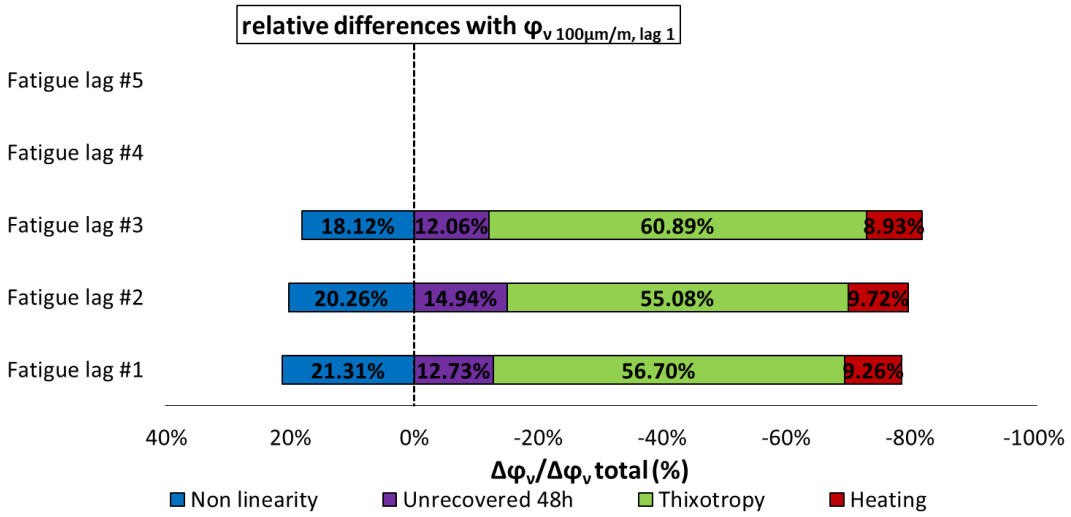

3.1.59. Quantification of different absolute and relative contributions to |E*|, φ_E, |v*| and φ_v evolutions for mix 40/60 – 4, calculated using the envelope line for the first fatigue lag.

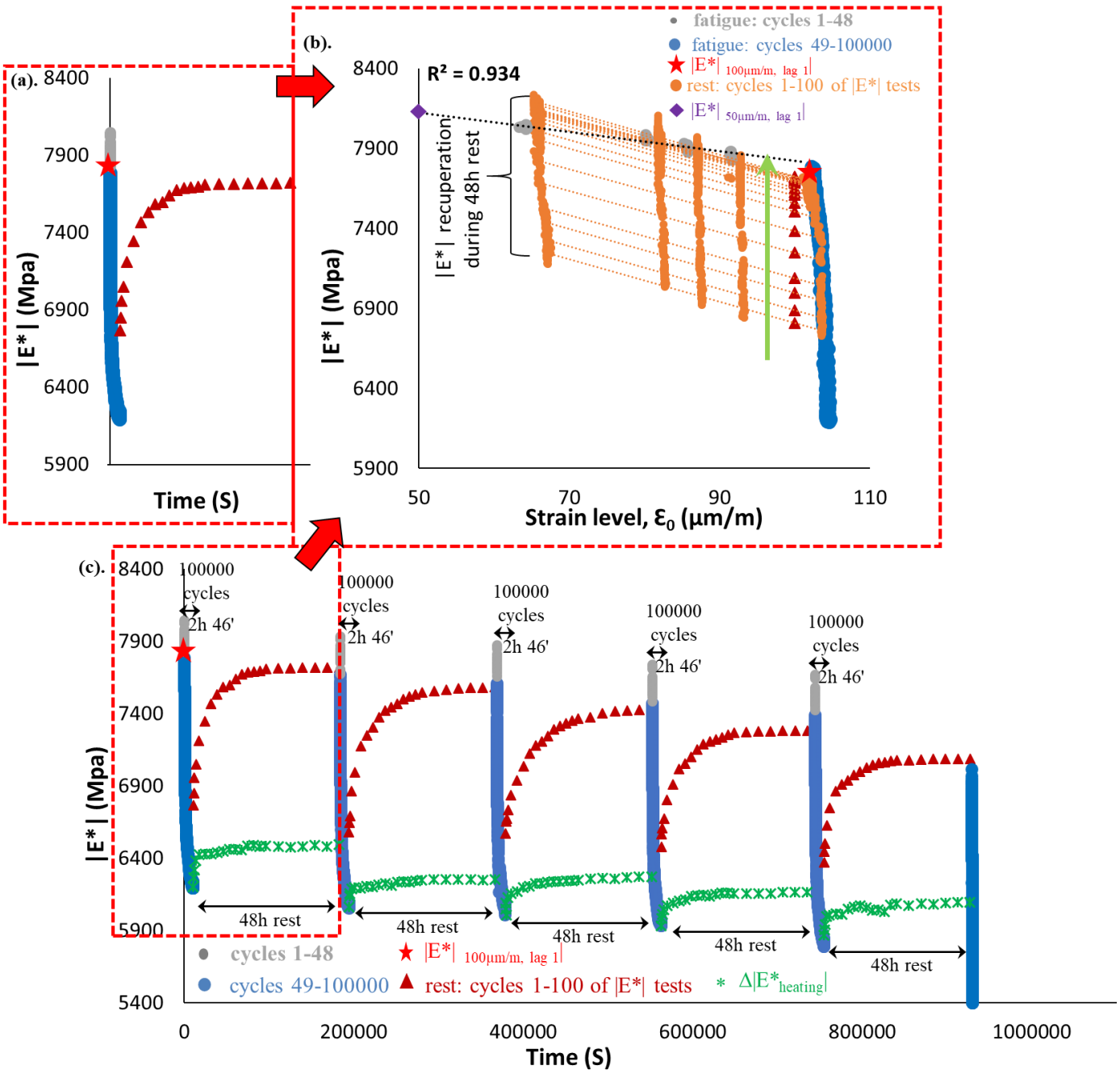

3.1.60. PFRT results obtained for mix 40/60 – 5: (a) |E*| as a function of time during the first fatigue lag and rest period (b) |E*| as a function of applied strain amplitude during the first fatigue lags and the short complex modulus tests performed within its following rest periods; (c) |E*| as a function of time during the five fatigue lags and rest periods [Red stars indicate values of |E*| estimated at 100 µm/m at the beginning of fatigue lag, green asterisk shows values of $\Delta|E^*_{heating}|$ as influence of self-heating and brown triangles indicate values of |E*| estimated at 100 µm/m for each short complex modulus test during rest (all these values were obtained using non-linearity envelopes, as shown in (b) for the first fatigue lag and rest period)].

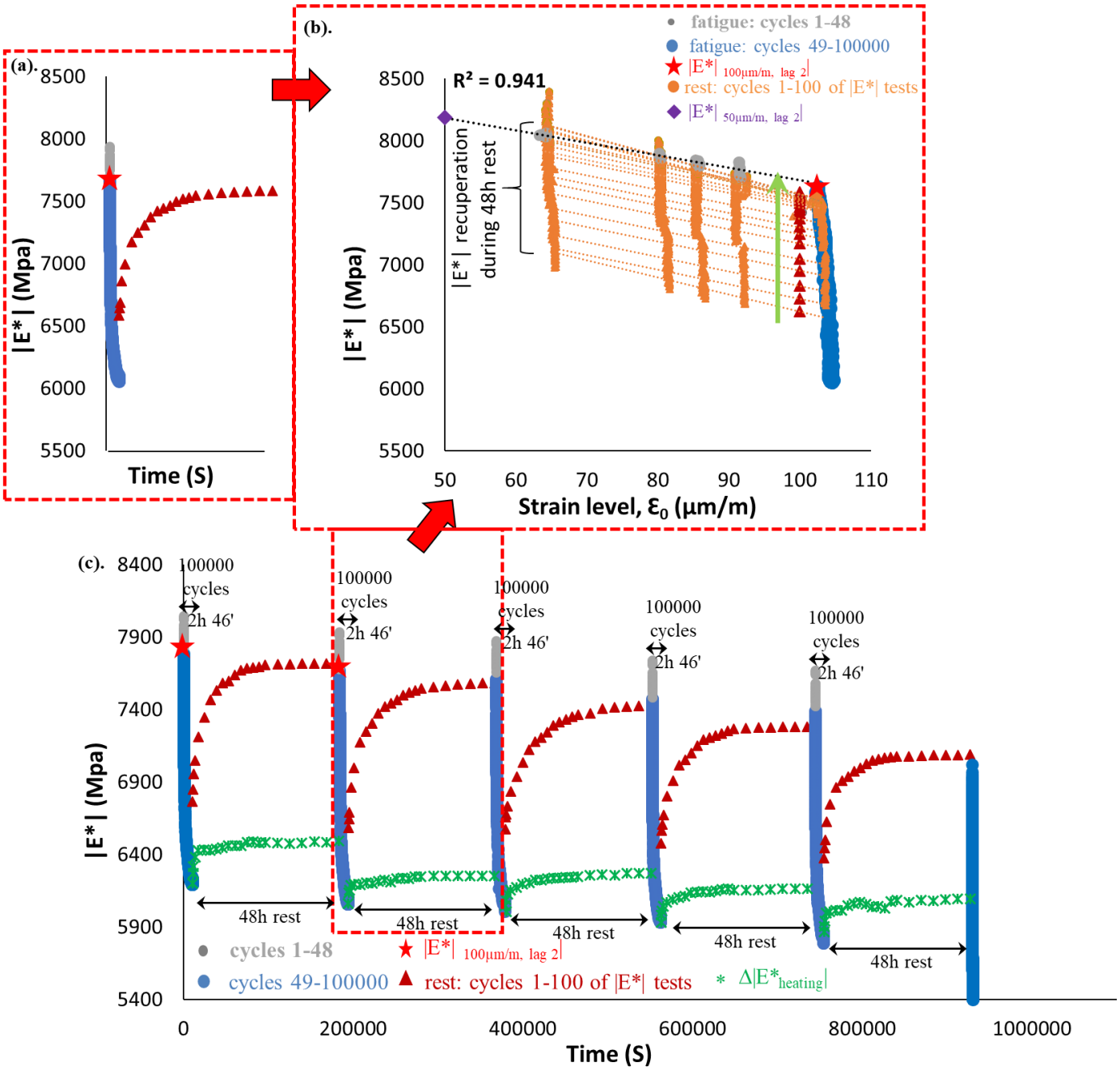

3.1.61. PFRT results obtained for mix 40/60 – 5: (a) |E*| as a function of time during the second fatigue lag and rest period (b) |E*| as a function of applied strain amplitude during the second fatigue lags and the short complex modulus tests performed within its following rest periods; (c) |E*| as a function of time during the five fatigue lags and rest periods [Red stars indicate values of |E*| estimated at 100 µm/m at the beginning of fatigue lag, green asterisk shows values of $\Delta|E^*_{heating}|$ as influence of self-heating and brown triangles indicate values of |E*| estimated at 100 µm/m for each short complex modulus test during rest (all these values were obtained using non-linearity envelopes, as shown in (b) for the first fatigue lag and rest period)].

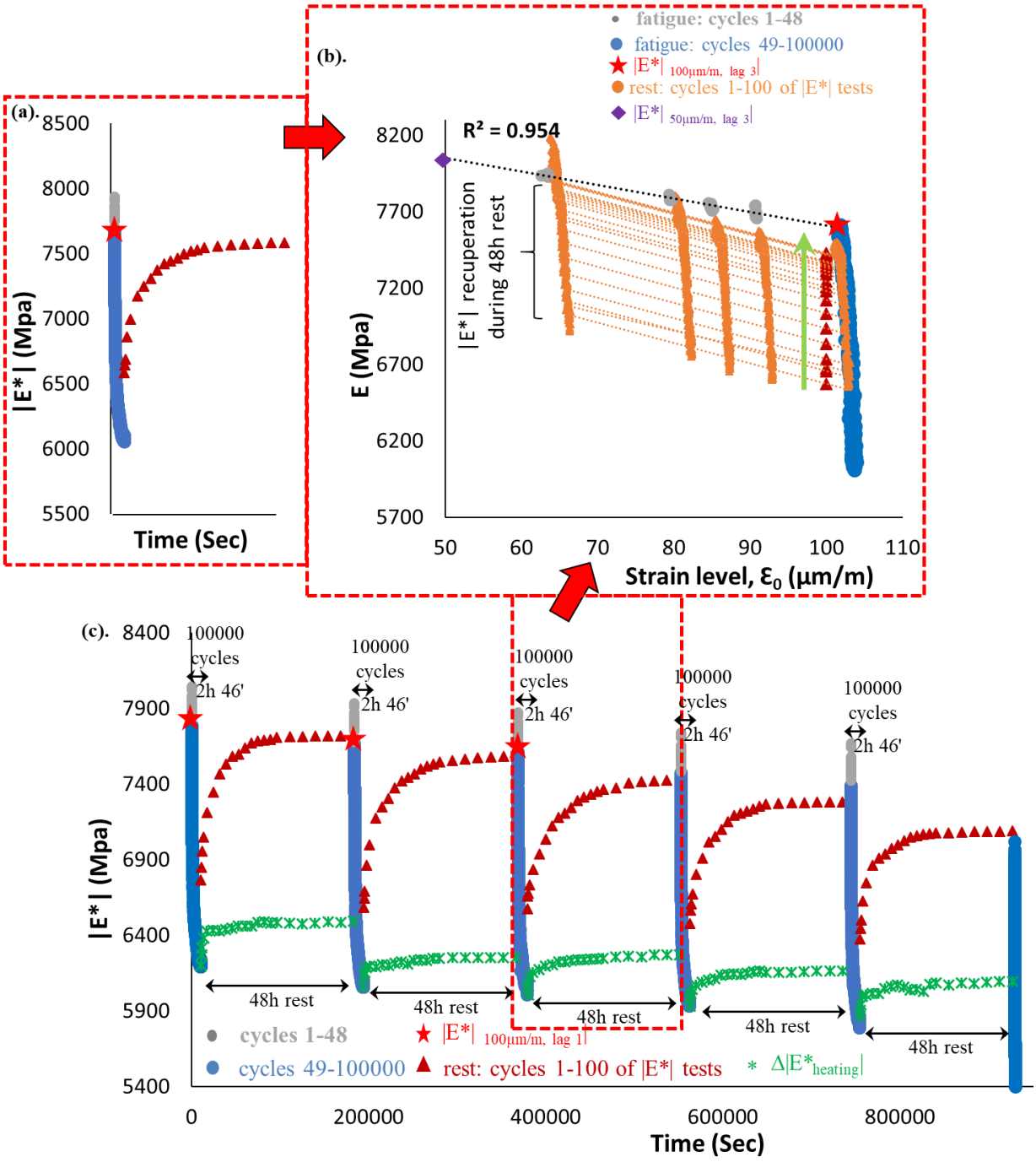

3.1.62. PFRT results obtained for mix 40/60 – 5: (a) |E*| as a function of time during the third fatigue lag and rest period (b) |E*| as a function of applied strain amplitude during the third fatigue lags and the short complex modulus tests performed within its following rest periods; (c) |E*| as a function of time during the five fatigue lags and rest periods [Red stars indicate values of |E*| estimated at 100 µm/m at the beginning of fatigue lag, green asterisk shows values of $\Delta|E^*_{heating}|$ as influence of self-heating and brown triangles indicate values of |E*| estimated at 100 µm/m for each short complex modulus test during rest (all these values were obtained using non-linearity envelopes, as shown in (b) for the first fatigue lag and rest period)].

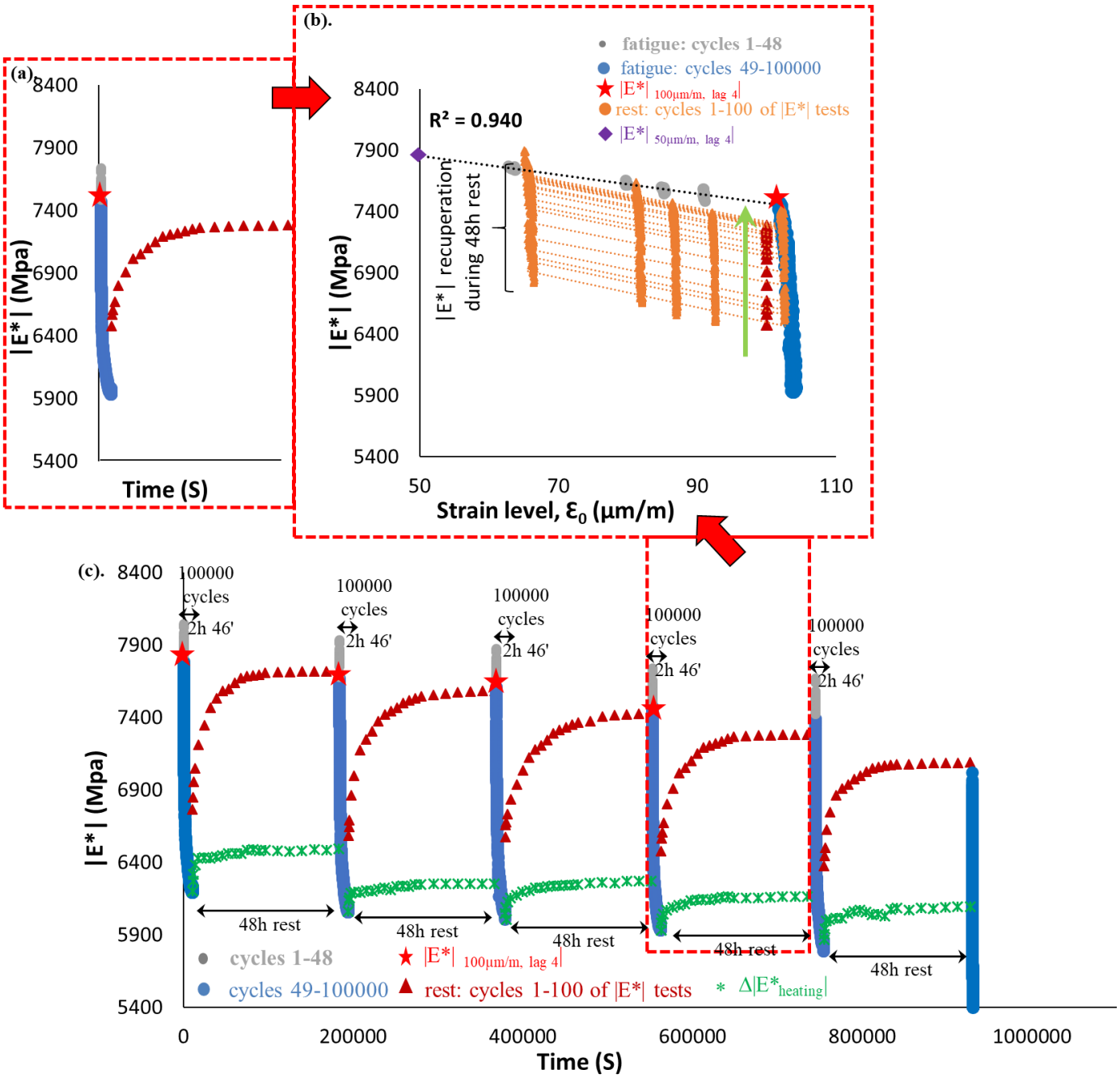

3.1.63. PFRT results obtained for mix 40/60 – 5: (a) |E*| as a function of time during the fourth fatigue lag and rest period (b) |E*| as a function of applied strain amplitude during the fourth fatigue lags and the short complex modulus tests performed within its following rest periods; (c) |E*| as a function of time during the five fatigue lags and rest periods [Red stars indicate values of |E*| estimated at 100 µm/m at the beginning of fatigue lag, green asterisk shows values of $\Delta|E^*_{heating}|$ as influence of self-heating and brown triangles indicate values of |E*| estimated at 100 µm/m for each short complex modulus test during rest (all these values were obtained using non-linearity envelopes, as shown in (b) for the first fatigue lag and rest period)].

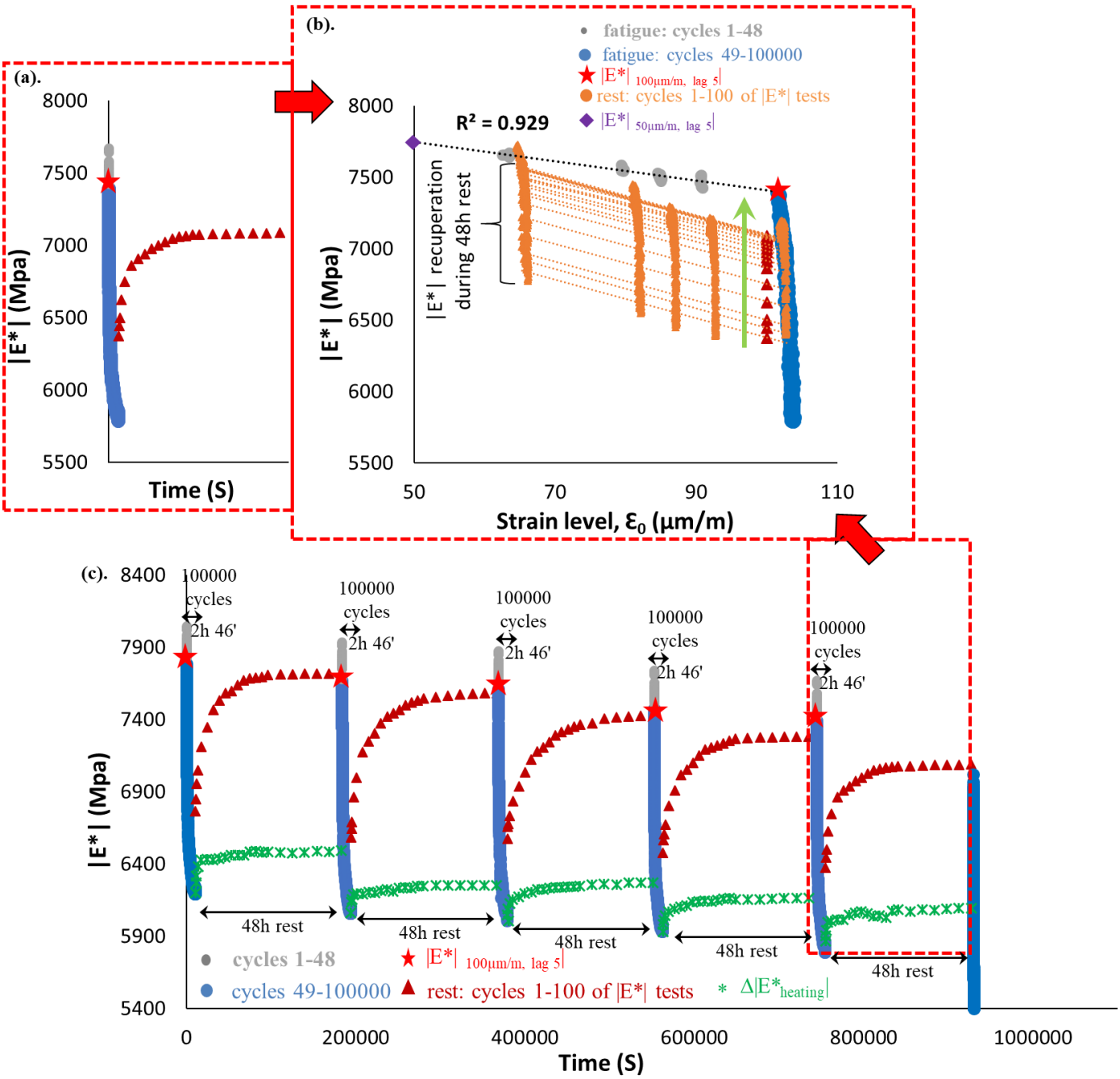

3.1.64. PFRT results obtained for mix 40/60 – 5: (a) |E*| as a function of time during the fifth fatigue lag and rest period (b) |E*| as a function of applied strain amplitude during the fifth fatigue lags and the short complex modulus tests performed within its following rest periods; (c) |E*| as a function of time during the five fatigue lags and rest periods [Red stars indicate values of |E*| estimated at 100 µm/m at the beginning of fatigue lag, green asterisk shows values of $\Delta|E^*_{heating}|$ as influence of self-heating and brown triangles indicate values of |E*| estimated at 100 µm/m for each short complex modulus test during rest (all these values were obtained using non-linearity envelopes, as shown in (b) for the first fatigue lag and rest period)].

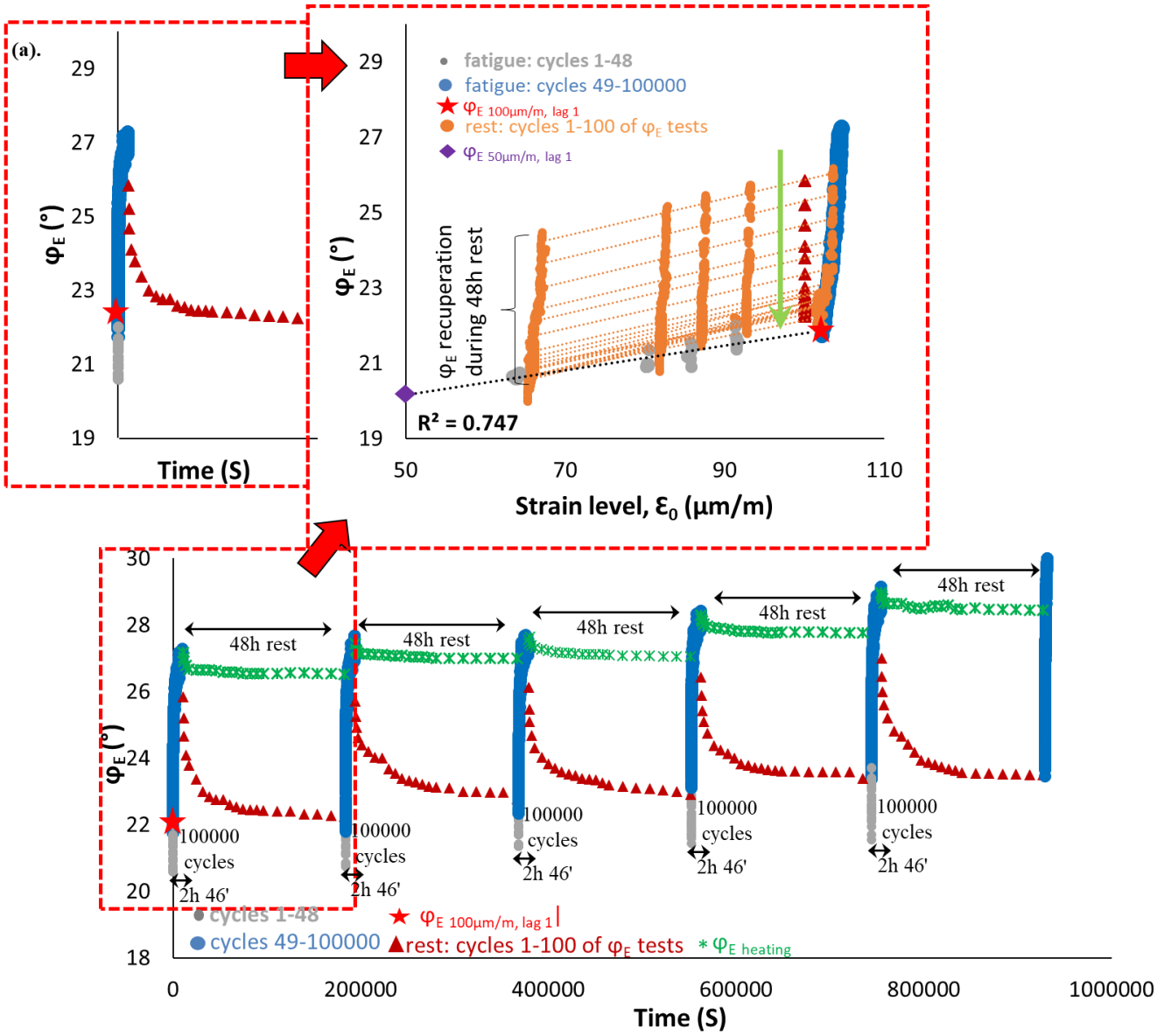

3.1.65. PFRT results obtained for mix 40/60 – 5: (a) φ_E as a function of time during the first fatigue lag and rest period (b) φ_E as a function of applied strain amplitude during the first fatigue lags and the short complex modulus tests performed within its following rest periods; (c) φ_E as a function of time during the five fatigue lags and rest periods (Red stars indicate values of φ_E estimated at 100 µm/m at the beginning of fatigue lag, green asterisk shows values of $\Delta\varphi_{E\ heating}$ as influence of self-heating and brown triangles indicate values of φ_E estimated at 100 µm/m for each short complex modulus test during rest (all these values were obtained using non-linearity envelopes, as shown in (b) for the first fatigue lag and rest period).

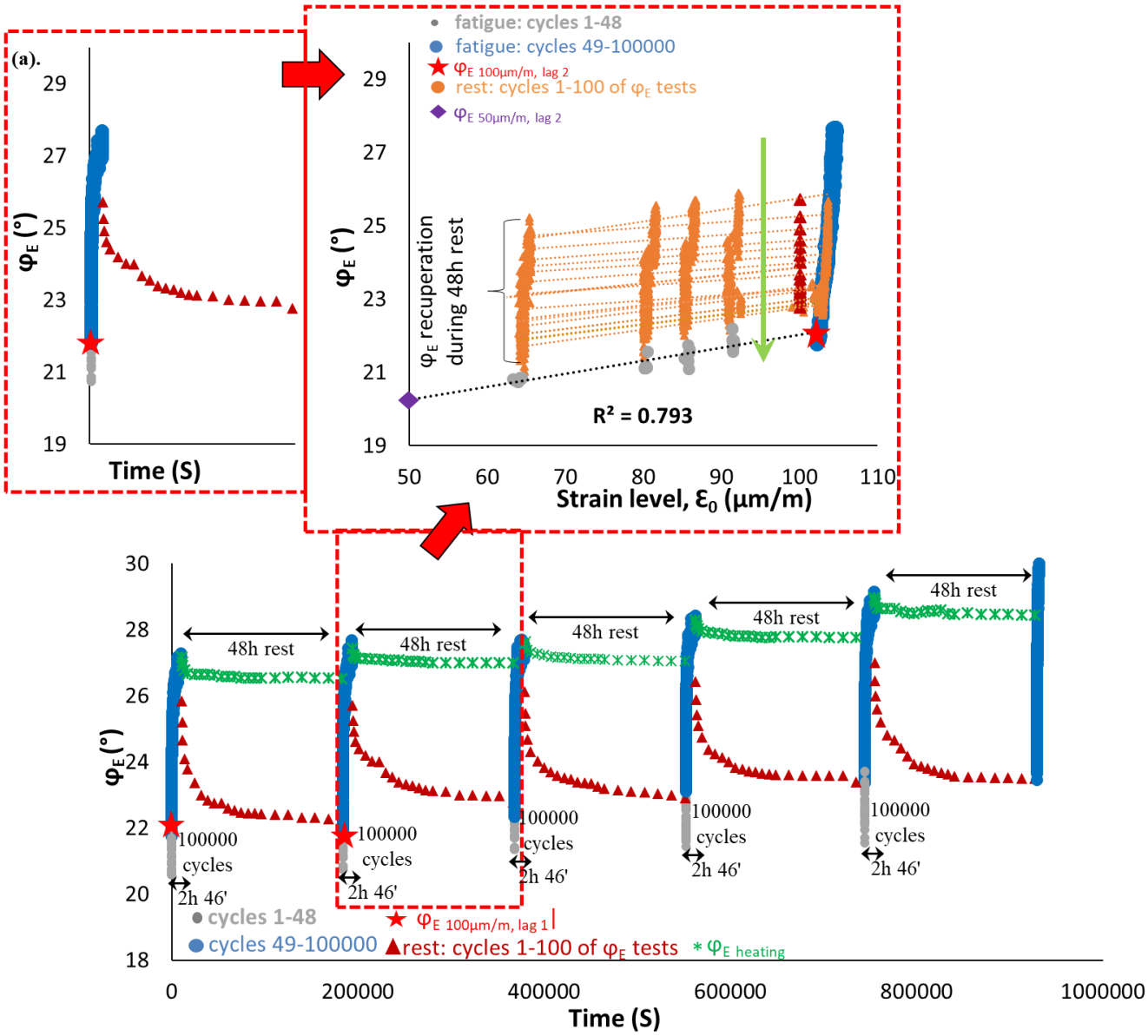

3.1.66. PFRT results obtained for mix 40/60 – 5: (a) φ_E as a function of time during the second fatigue lag and rest period (b) φ_E as a function of applied strain amplitude during the second fatigue lags and the short complex modulus tests performed within its following rest periods; (c) φ_E as a function of time during the five fatigue lags and rest periods (Red stars indicate values of φ_E estimated at 100 µm/m at the beginning of fatigue lag, green asterisk shows values of $\Delta\varphi_{E\ heating}$ as influence of self-heating and brown triangles indicate values of φ_E estimated at 100 µm/m for each short complex modulus test during rest (all these values were obtained using non-linearity envelopes, as shown in (b) for the first fatigue lag and rest period).

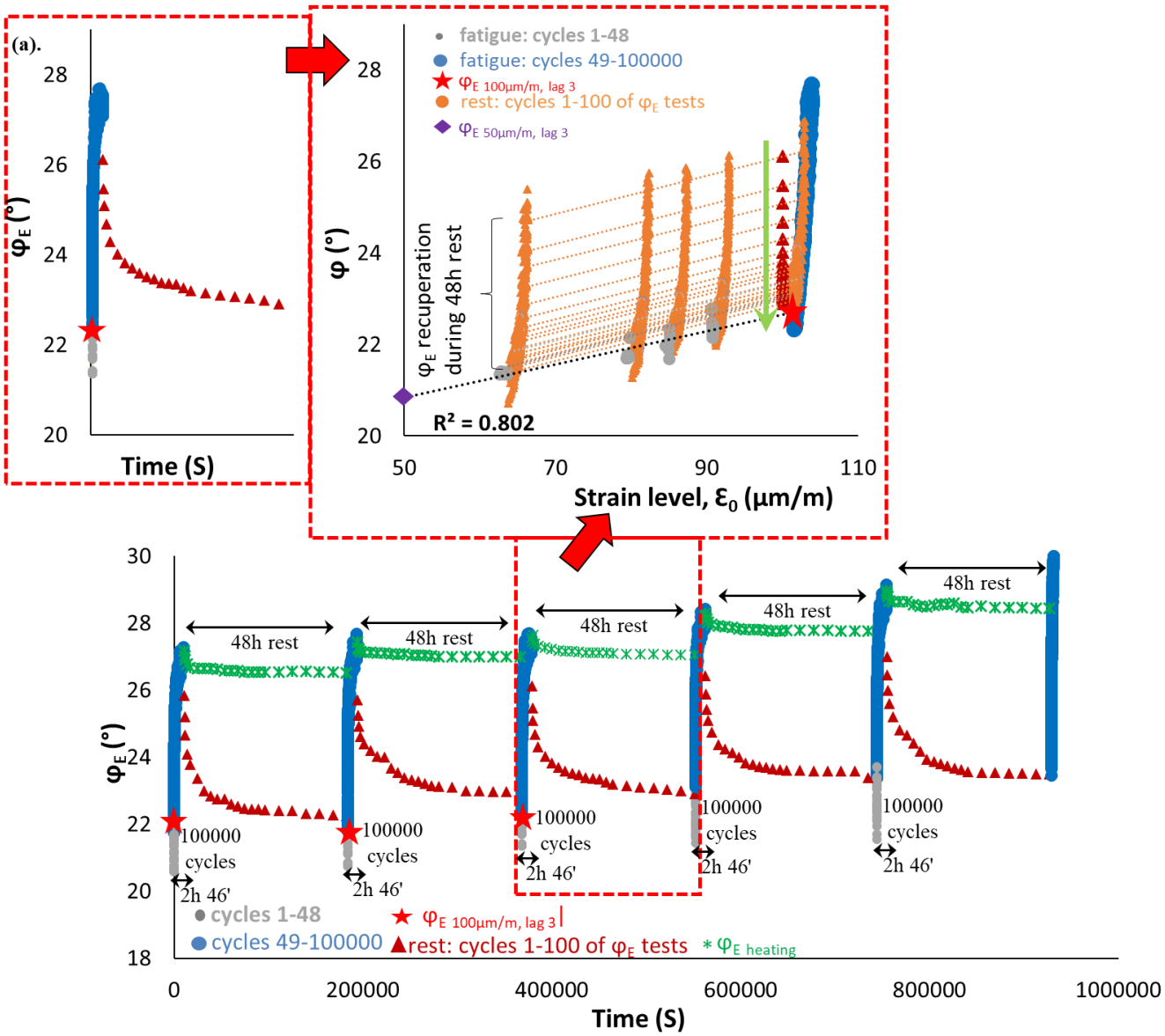

3.1.67. PFRT results obtained for mix 40/60 – 5: (a) φ_E as a function of time during the third fatigue lag and rest period (b) φ_E as a function of applied strain amplitude during the third fatigue lags and the short complex modulus tests performed within its following rest periods; (c) φ_E as a function of time during the five fatigue lags and rest periods (Red stars indicate values of φ_E estimated at 100 µm/m at the beginning of fatigue lag, green asterisk shows values of $\Delta\varphi_{E\ heating}$ as influence of self-heating and brown triangles indicate values of φ_E estimated at 100 µm/m for each short complex modulus test during rest (all these values were obtained using non-linearity envelopes, as shown in (b) for the first fatigue lag and rest period).

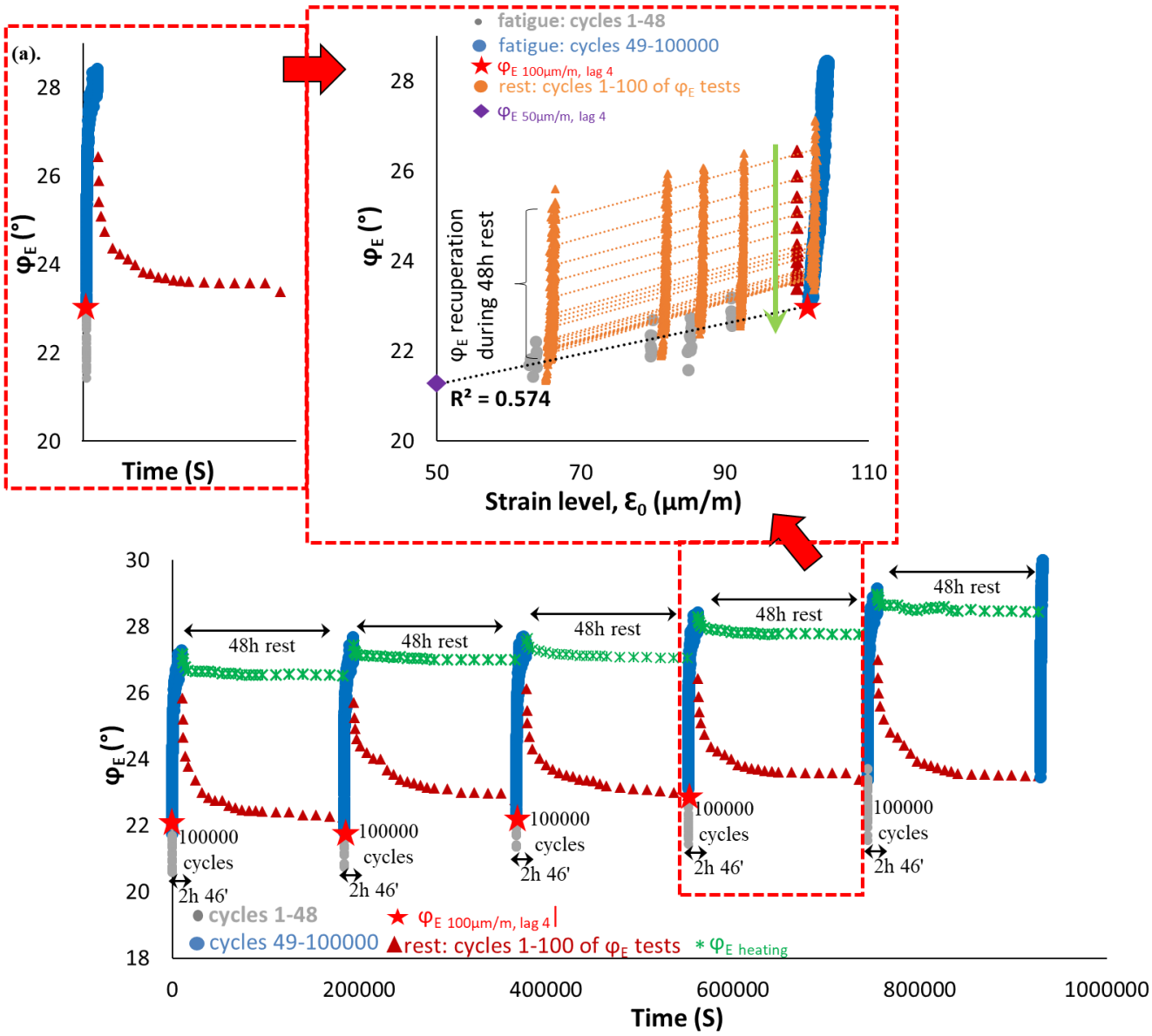

3.1.68. PFRT results obtained for mix 40/60 – 5: (a) φ_E as a function of time during the fourth fatigue lag and rest period (b) φ_E as a function of applied strain amplitude during the fourth fatigue lags and the short complex modulus tests performed within its following rest periods; (c) φ_E as a function of time during the five fatigue lags and rest periods (Red stars indicate values of φ_E estimated at 100 µm/m at the beginning of fatigue lag, green asterisk shows values of $\Delta\varphi_{E\ heating}$ as influence of self-heating and brown triangles indicate values of φ_E estimated at 100 µm/m for each short complex modulus test during rest (all these values were obtained using non-linearity envelopes, as shown in (b) for the first fatigue lag and rest period).

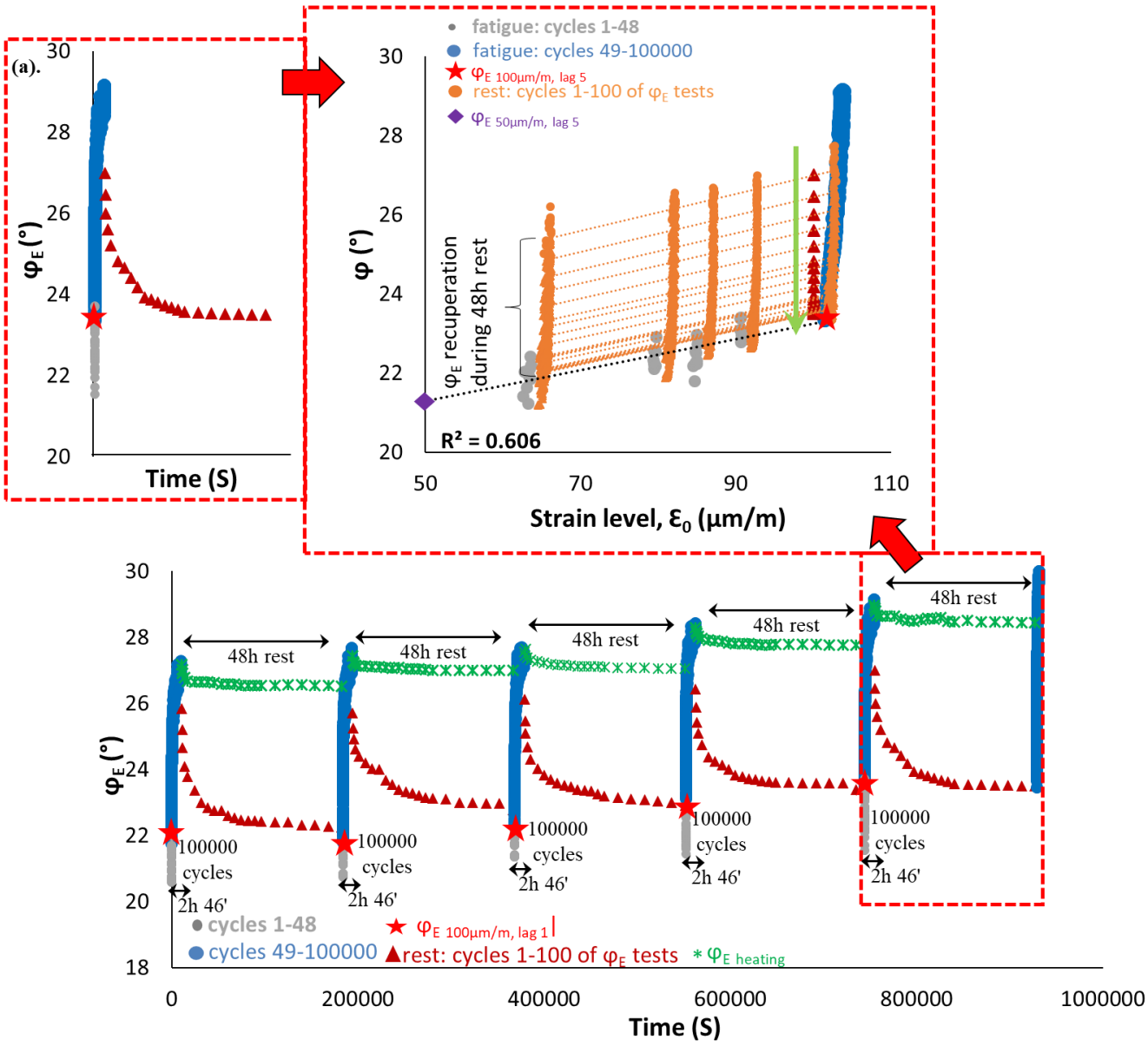

3.1.69. PFRT results obtained for mix 40/60 – 5: (a) φ_E as a function of time during the fifth fatigue lag and rest period (b) φ_E as a function of applied strain amplitude during the fifth fatigue lags and the short complex modulus tests performed within its following rest periods; (c) φ_E as a function of time during the five fatigue lags and rest periods (Red stars indicate values of φ_E estimated at 100 µm/m at the beginning of fatigue lag, green asterisk shows values of $\Delta\varphi_{E\ heating}$ as influence of self-heating and brown triangles indicate values of φ_E estimated at 100 µm/m for each short complex modulus test during rest (all these values were obtained using non-linearity envelopes, as shown in (b) for the first fatigue lag and rest period).

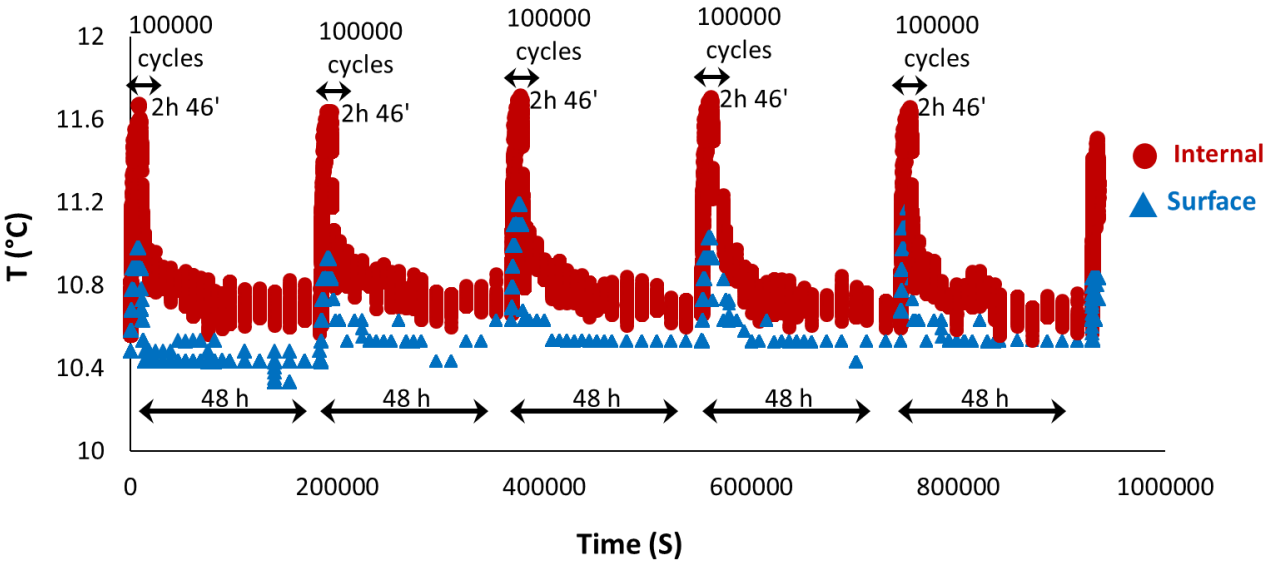

3.1.70. PFRT results obtained for mix 40/60 – 5: internal and surface temperature evolution during fatigue lags and recovery periods.

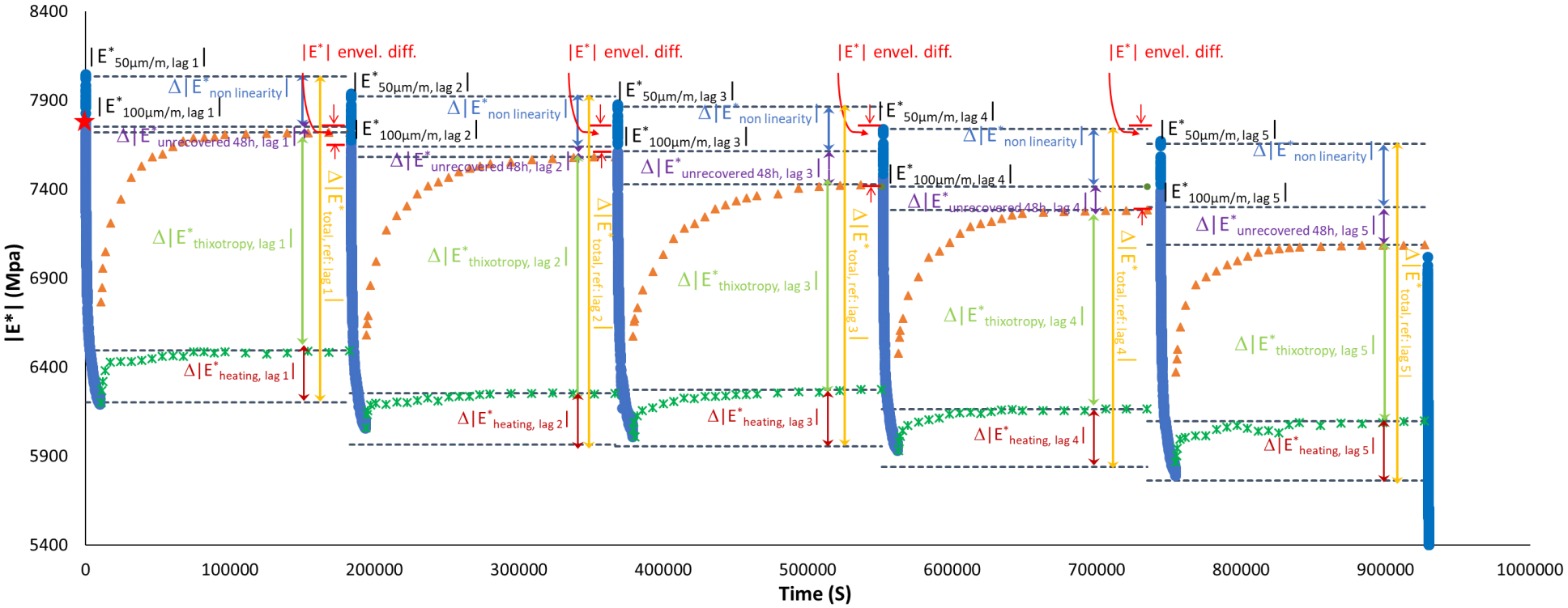
8400
7900
7400
6900
6400
5900
5400
|E*| (Mpa)
0
100000
200000
300000
400000
500000
600000
700000
800000
900000
1000000
Time (S)
|E*| envel. diff.
|E*| envel. diff.
|E*| envel. diff.
|E*| envel. diff.
|E*50µm/m, lag 1|
|E*100µm/m, lag 1|
Δ|E*non linearity|
Δ|E*unrecovered 48h, lag 1|
Δ|E*thixotropy, lag 1|
Δ|E*heating, lag 1|
Δ|E*total, ref: lag 1|
|E*50µm/m, lag 2|
|E*100µm/m, lag 2|
Δ|E*non linearity|
Δ|E*unrecovered 48h, lag 2|
Δ|E*thixotropy, lag 2|
Δ|E*heating, lag 2|
Δ|E*total, ref: lag 2|
|E*50µm/m, lag 3|
|E*100µm/m, lag 3|
Δ|E*non linearity|
Δ|E*unrecovered 48h, lag 3|
Δ|E*thixotropy, lag 3|
Δ|E*heating, lag 3|
Δ|E*total, ref: lag 3|
|E*50µm/m, lag 4|
|E*100µm/m, lag 4|
Δ|E*non linearity|
Δ|E*unrecovered 48h, lag 4|
Δ|E*thixotropy, lag 4|
Δ|E*heating, lag 4|
Δ|E*total, ref: lag 4|
|E*50µm/m, lag 5|
|E*100µm/m, lag 5|
Δ|E*non linearity|
Δ|E*unrecovered 48h, lag 5|
Δ|E*thixotropy, lag 5|
Δ|E*heating, lag 5|
Δ|E*total, ref: lag 5|

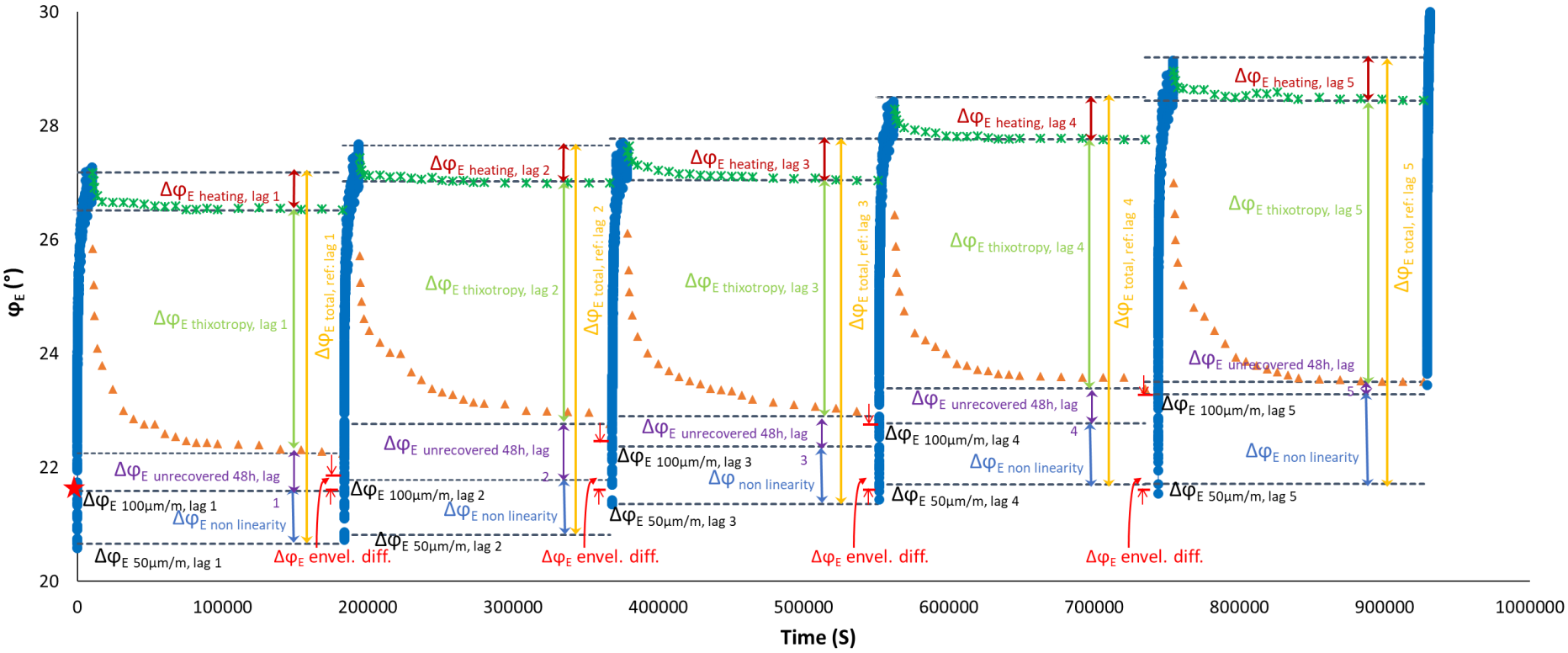

3.1.71. Quantification of different contributions E*| and φ_E evolution, for the five fatigue lags for mix 40/60 – 5: different envelope line is used for each fatigue lag.

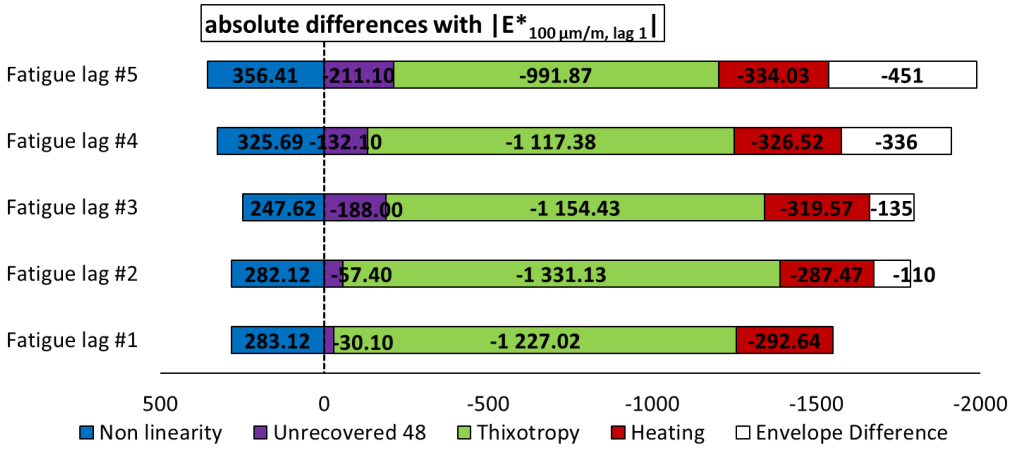
absolute differences with |E*100 µm/m, lag 1|
Fatigue lag #5
Fatigue lag #4
Fatigue lag #3
Fatigue lag #2
Fatigue lag #1
356.41
-211.10
-991.87
-334.03
-451
325.69
-132.10
-1 117.38
-326.52
-336
247.62
-188.00
-1 154.43
-319.57
-135
282.12
-57.40
-1 331.13
-287.47
-110
283.12
-30.10
-1 227.02
-292.64
500
0
-500
-1000
-1500
-2000
Non linearity
Unrecovered 48
Thixotropy
Heating
Envelope Difference

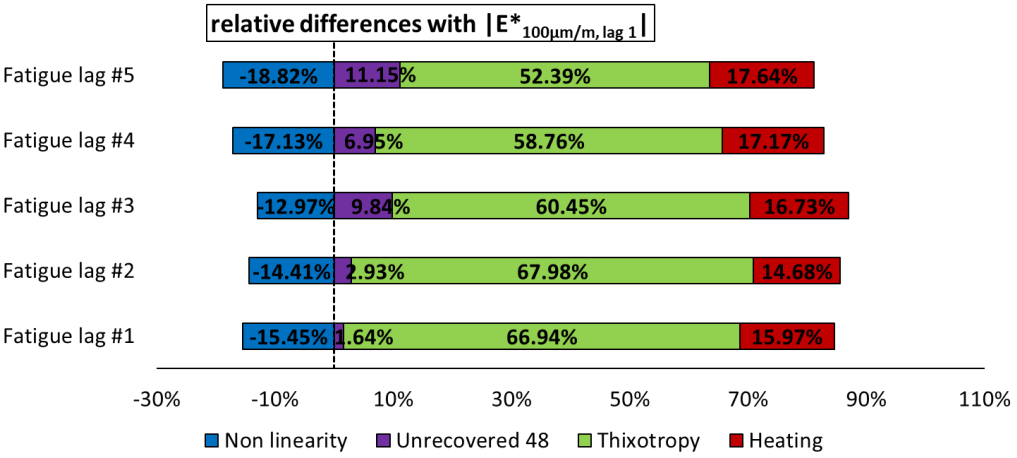
relative differences with |E*100µm/m, lag 1|
Fatigue lag #5
Fatigue lag #4
Fatigue lag #3
Fatigue lag #2
Fatigue lag #1
-18.82%
11.15%
52.39%
17.64%
-17.13%
6.95%
58.76%
17.17%
-12.97%
9.84%
60.45%
16.73%
-14.41%
2.93%
67.98%
14.68%
-15.45%
1.64%
66.94%
15.97%
-30%
-10%
10%
30%
50%
70%
90%
110%
Non linearity
Unrecovered 48
Thixotropy
Heating

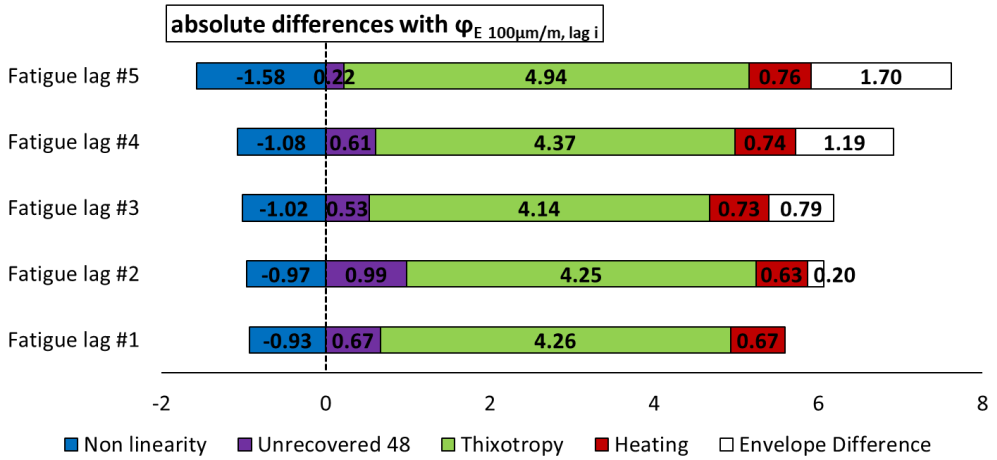
absolute differences with φE 100µm/m, lag i
Fatigue lag #5
Fatigue lag #4
Fatigue lag #3
Fatigue lag #2
Fatigue lag #1
-1.58
0.22
4.94
0.76
1.70
-1.08
0.61
4.37
0.74
1.19
-1.02
0.53
4.14
0.73
0.79
-0.97
0.99
4.25
0.63
0.20
-0.93
0.67
4.26
0.67
-2
0
2
4
6
8
Non linearity
Unrecovered 48
Thixotropy
Heating
Envelope Difference

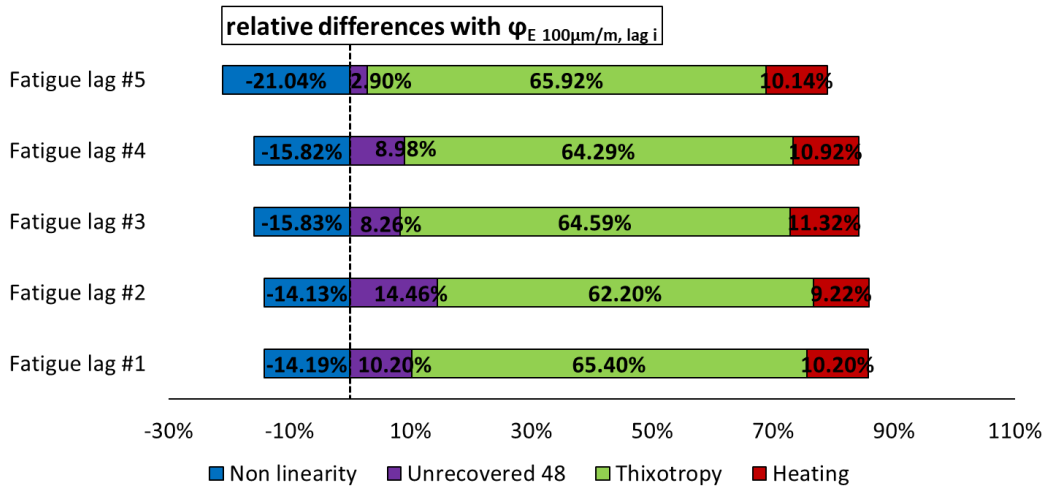

3.1.72. Quantification of different absolute and relative contributions to |E*| and ϕ_E evolutions for mix 40/60 – 5, calculated using a different envelope line for each fatigue lag.

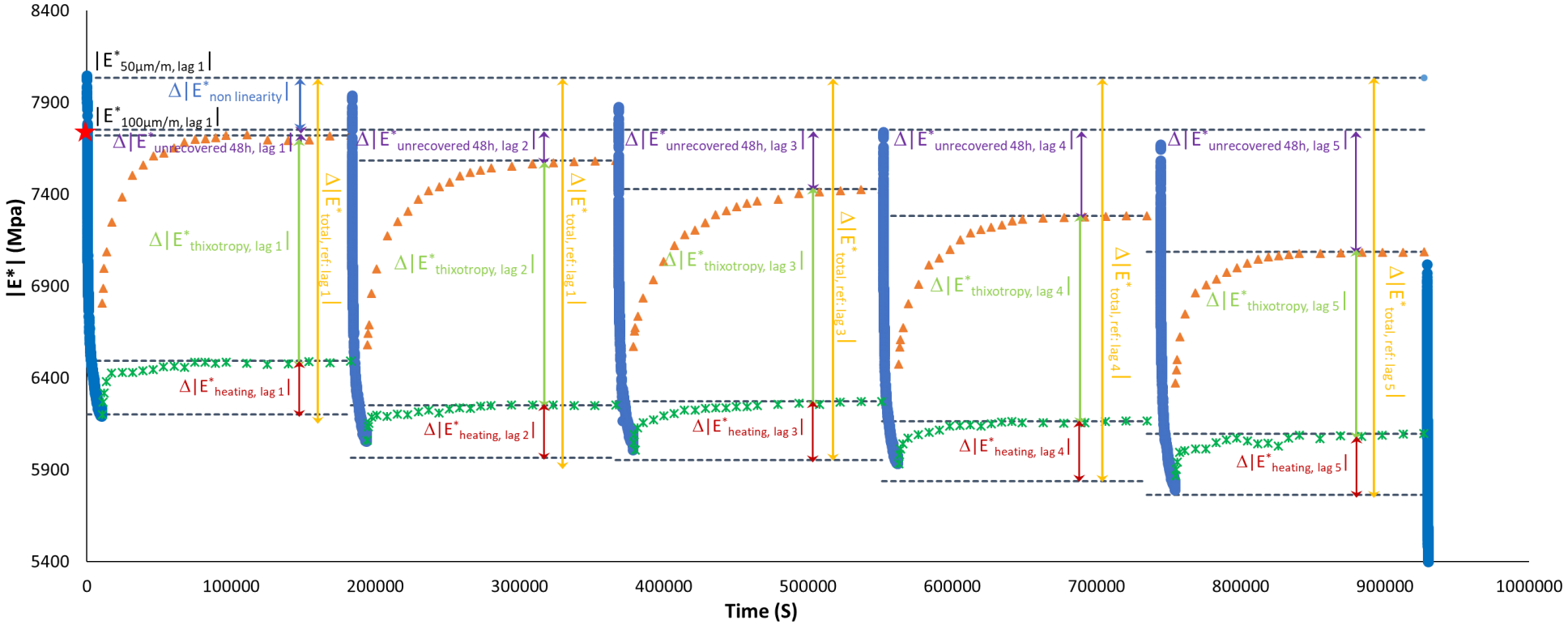
8400
7900
7400
6900
6400
5900
5400
|E*| (Mpa)
0
100000
200000
300000
400000
500000
600000
700000
800000
900000
1000000
Time (S)
|E*50µm/m, lag 1|
|E*100µm/m, lag 1|
Δ|E*non linearity|
Δ|E*unrecovered 48h, lag 1|
Δ|E*thixotropy, lag 1|
Δ|E*heating, lag 1|
Δ|E*total, ref: lag 1|
Δ|E*unrecovered 48h, lag 2|
Δ|E*thixotropy, lag 2|
Δ|E*heating, lag 2|
Δ|E*total, ref: lag 1|
Δ|E*unrecovered 48h, lag 3|
Δ|E*thixotropy, lag 3|
Δ|E*heating, lag 3|
Δ|E*total, ref: lag 3|
Δ|E*unrecovered 48h, lag 4|
Δ|E*thixotropy, lag 4|
Δ|E*heating, lag 4|
Δ|E*total, ref: lag 4|
Δ|E*unrecovered 48h, lag 5|
Δ|E*thixotropy, lag 5|
Δ|E*heating, lag 5|
Δ|E*total, ref: lag 5|

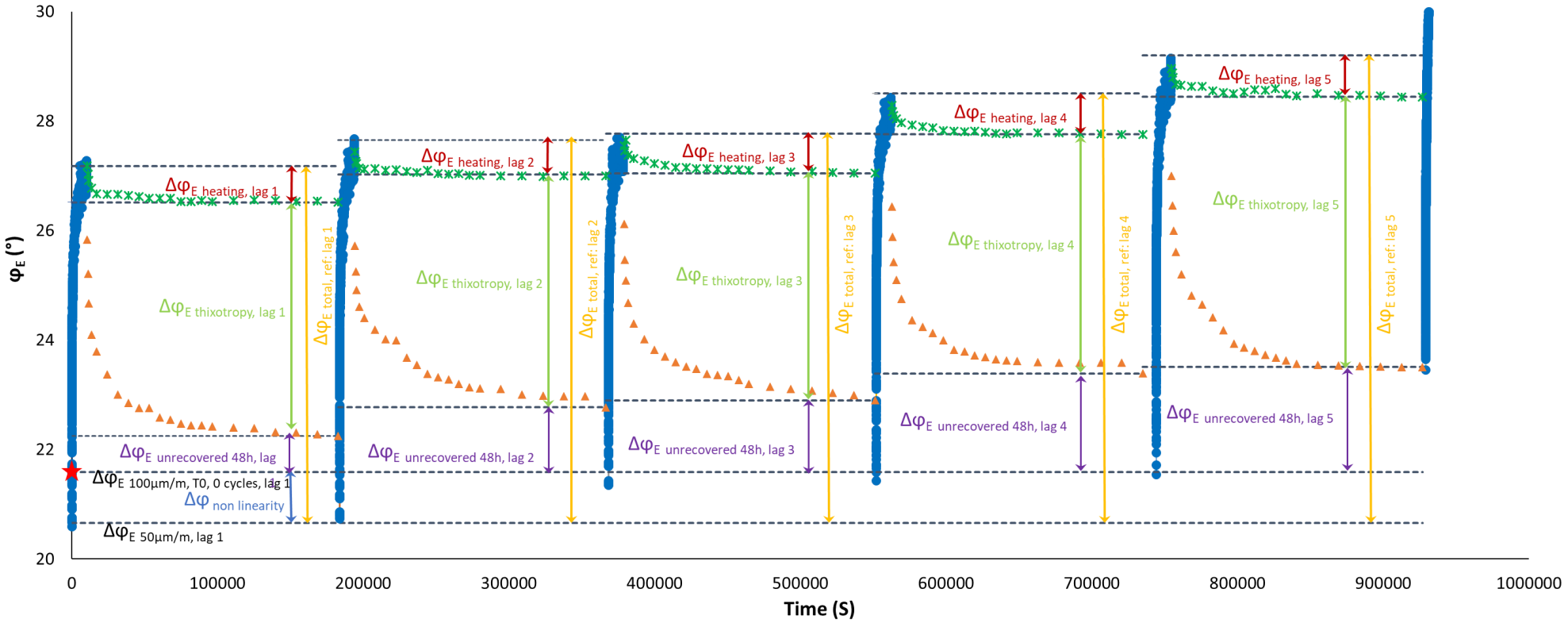

3.1.73. Quantification of different contributions to |E*| and φ_E evolution during five fatigue lags for mix 40/60 – 5: the envelope line of the first fatigue lag is used for all fatigue lags.

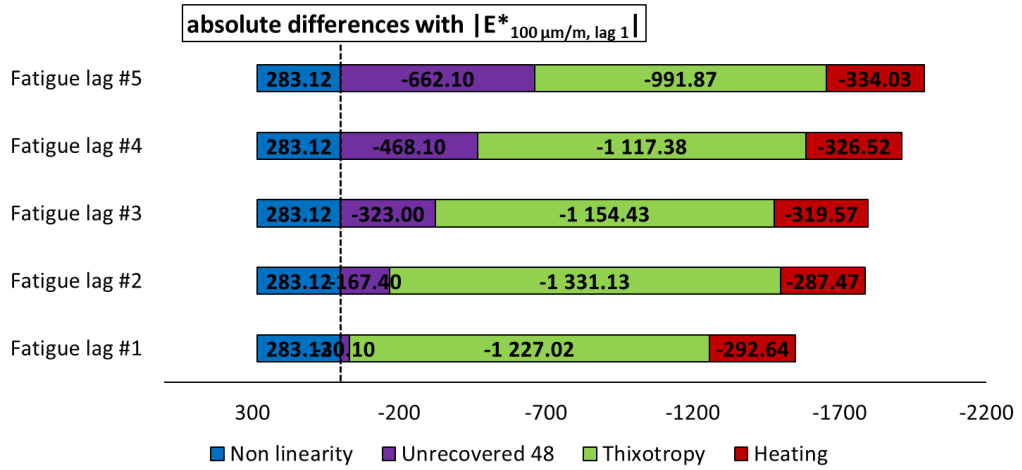
absolute differences with |E*100 µm/m, lag 1|
Fatigue lag #5
283.12
-662.10
-991.87
-334.03
Fatigue lag #4
283.12
-468.10
-1 117.38
-326.52
Fatigue lag #3
283.12
-323.00
-1 154.43
-319.57
Fatigue lag #2
283.12
-167.40
-1 331.13
-287.47
Fatigue lag #1
283.12
-30.10
-1 227.02
-292.64
300
-200
-700
-1200
-1700
-2200
Non linearity
Unrecovered 48
Thixotropy
Heating

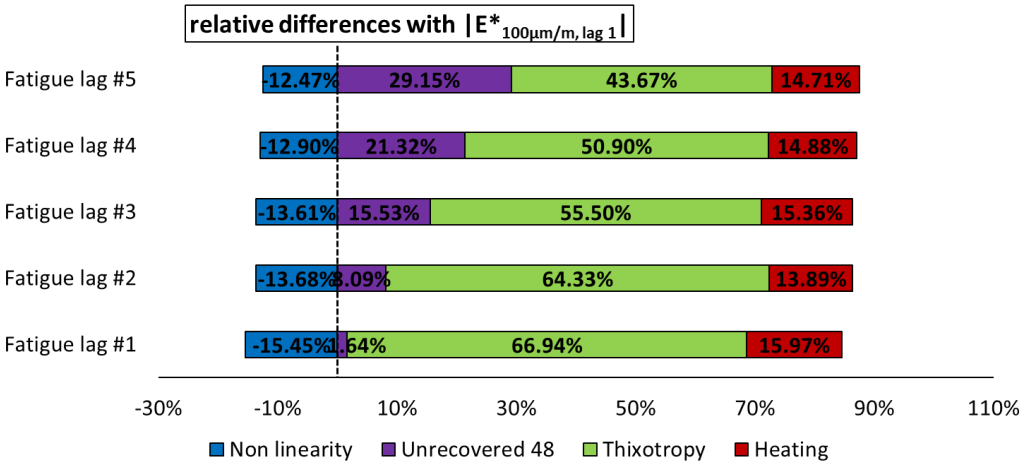
relative differences with |E*100µm/m, lag 1|
Fatigue lag #5
-12.47%
29.15%
43.67%
14.71%
Fatigue lag #4
-12.90%
21.32%
50.90%
14.88%
Fatigue lag #3
-13.61%
15.53%
55.50%
15.36%
Fatigue lag #2
-13.68%
8.09%
64.33%
13.89%
Fatigue lag #1
-15.45%
1.64%
66.94%
15.97%
-30%
-10%
10%
30%
50%
70%
90%
110%
Non linearity
Unrecovered 48
Thixotropy
Heating

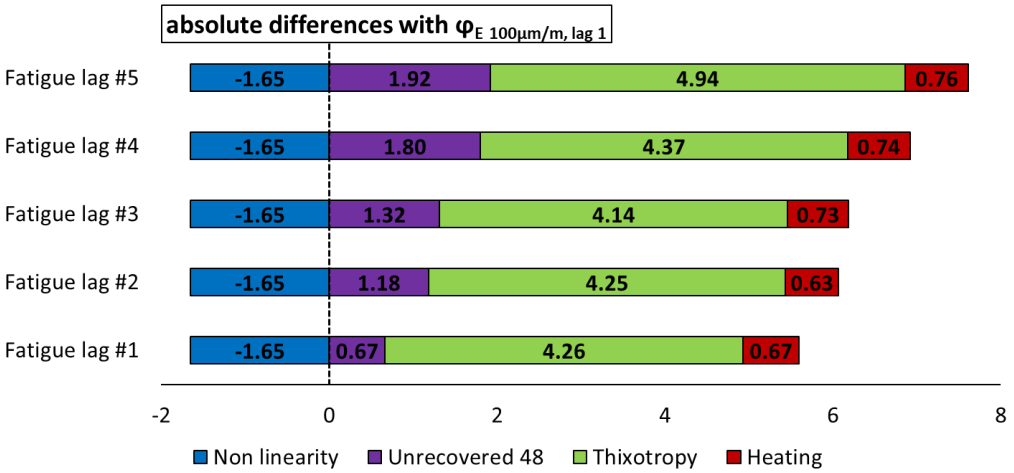
absolute differences with φE 100µm/m, lag 1
Fatigue lag #5
-1.65
1.92
4.94
0.76
Fatigue lag #4
-1.65
1.80
4.37
0.74
Fatigue lag #3
-1.65
1.32
4.14
0.73
Fatigue lag #2
-1.65
1.18
4.25
0.63
Fatigue lag #1
-1.65
0.67
4.26
0.67
-2
0
2
4
6
8
Non linearity
Unrecovered 48
Thixotropy
Heating

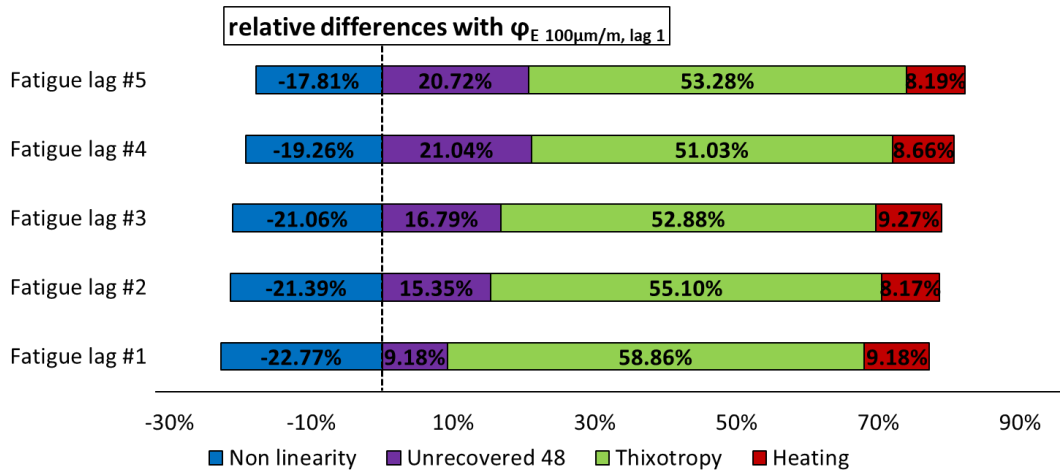

3.1.74. Quantification of different absolute and relative contributions to |E*| and φ_E evolutions for mix 40/60 – 5, calculated using the envelope line for the first fatigue lag.

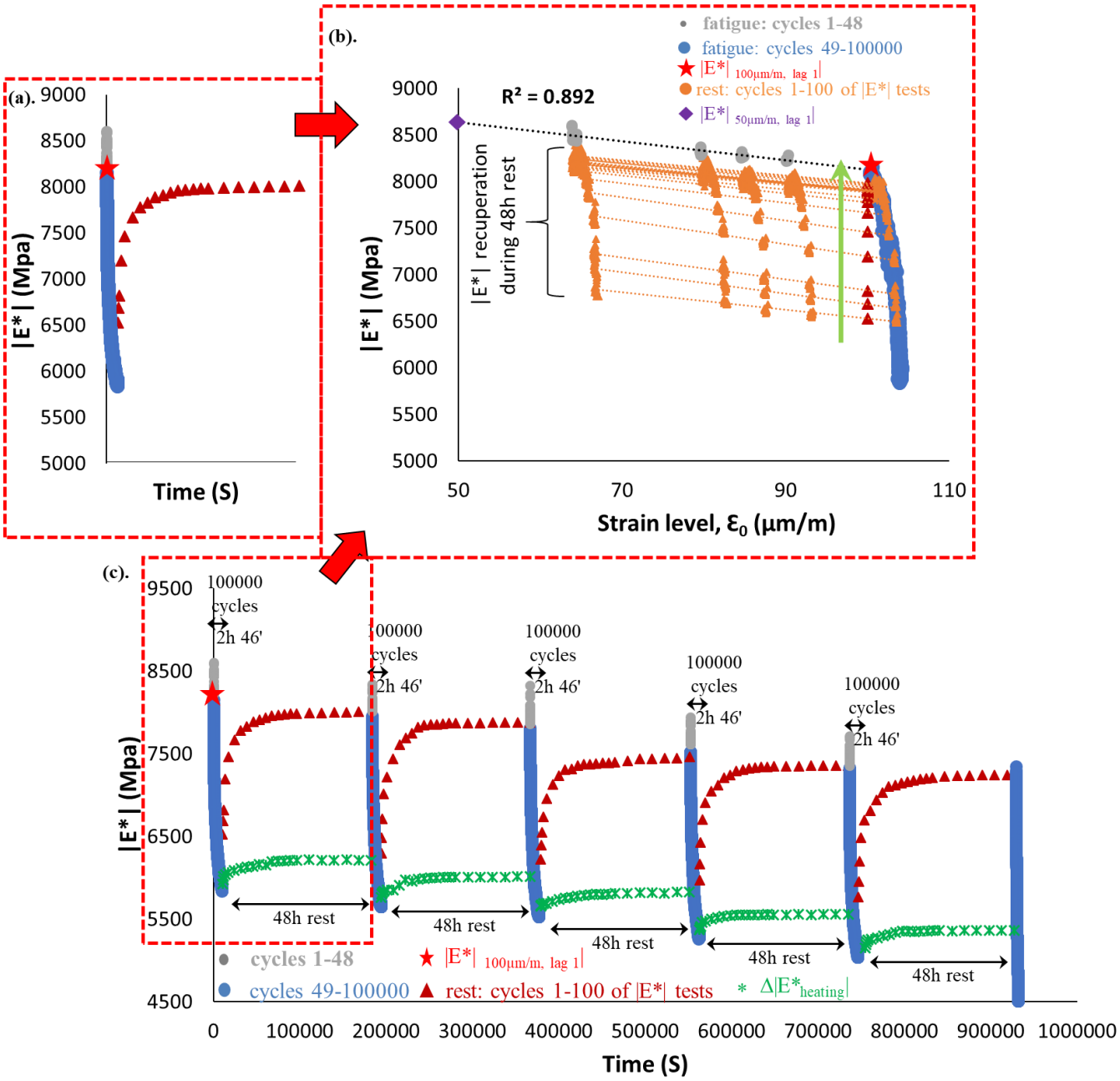

3.1.75. PFRT results obtained for mix 40/60 – 6: (a) |E*| as a function of time during the first fatigue lag and rest period (b) |E*| as a function of applied strain amplitude during the first fatigue lags and the short complex modulus tests performed within its following rest periods; (c) |E*| as a function of time during the five fatigue lags and rest periods [Red stars indicate values of |E*| estimated at 100 µm/m at the beginning of fatigue lag, green asterisk shows values of $\Delta|E^*_{heating}|$ as influence of self-heating and brown triangles indicate values of |E*| estimated at 100 µm/m for each short complex modulus test during rest (all these values were obtained using non-linearity envelopes, as shown in (b) for the first fatigue lag and rest period)].

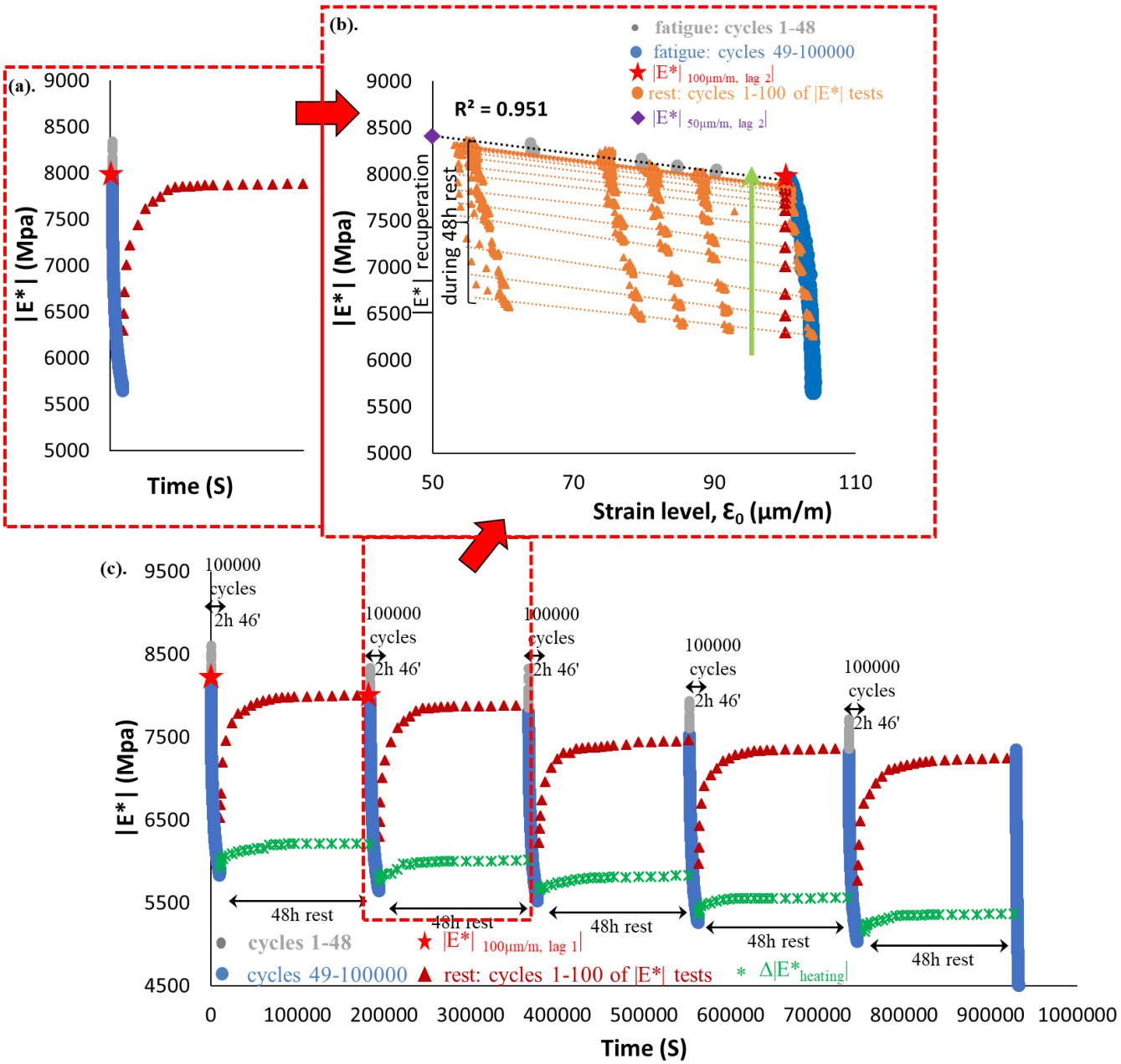

3.1.76. PFRT results obtained for mix 40/60 – 6: (a) |E*| as a function of time during the second fatigue lag and rest period (b) |E*| as a function of applied strain amplitude during the second fatigue lags and the short complex modulus tests performed within its following rest periods; (c) |E*| as a function of time during the five fatigue lags and rest periods [Red stars indicate values of |E*| estimated at 100 µm/m at the beginning of fatigue lag, green asterisk shows values of $\Delta|E^*_{heating}|$ as influence of self-heating and brown triangles indicate values of |E*| estimated at 100 µm/m for each short complex modulus test during rest (all these values were obtained using non-linearity envelopes, as shown in (b) for the first fatigue lag and rest period)].

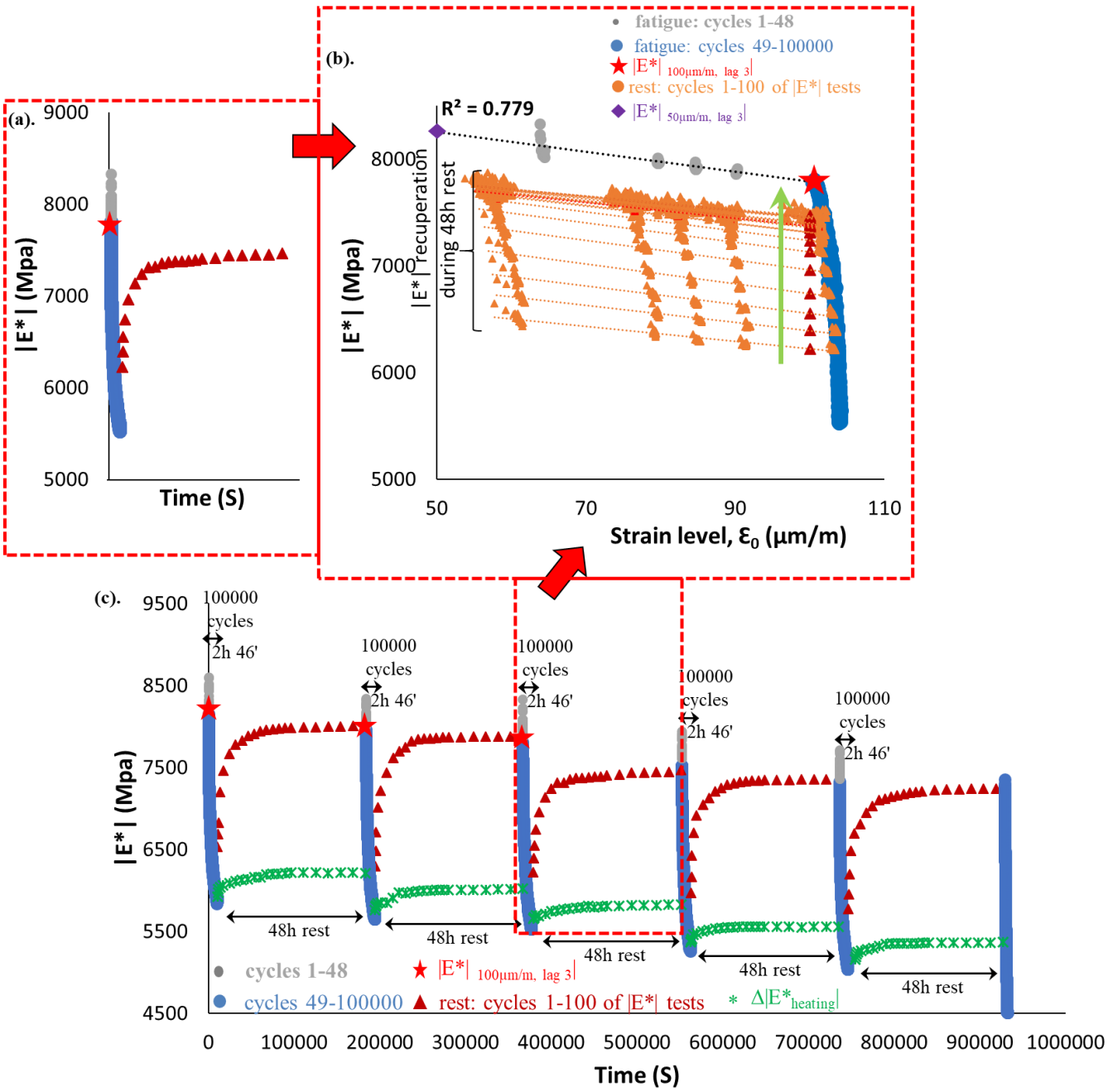

3.1.77. PFRT results obtained for mix 40/60 – 6: (a) |E*| as a function of time during the third fatigue lag and rest period (b) |E*| as a function of applied strain amplitude during the third fatigue lags and the short complex modulus tests performed within its following rest periods; (c) |E*| as a function of time during the five fatigue lags and rest periods [Red stars indicate values of |E*| estimated at 100 µm/m at the beginning of fatigue lag, green asterisk shows values of Δ|E*heating| as influence of self-heating and brown triangles indicate values of |E*| estimated at 100 µm/m for each short complex modulus test during rest (all these values were obtained using non-linearity envelopes, as shown in (b) for the first fatigue lag and rest period)].

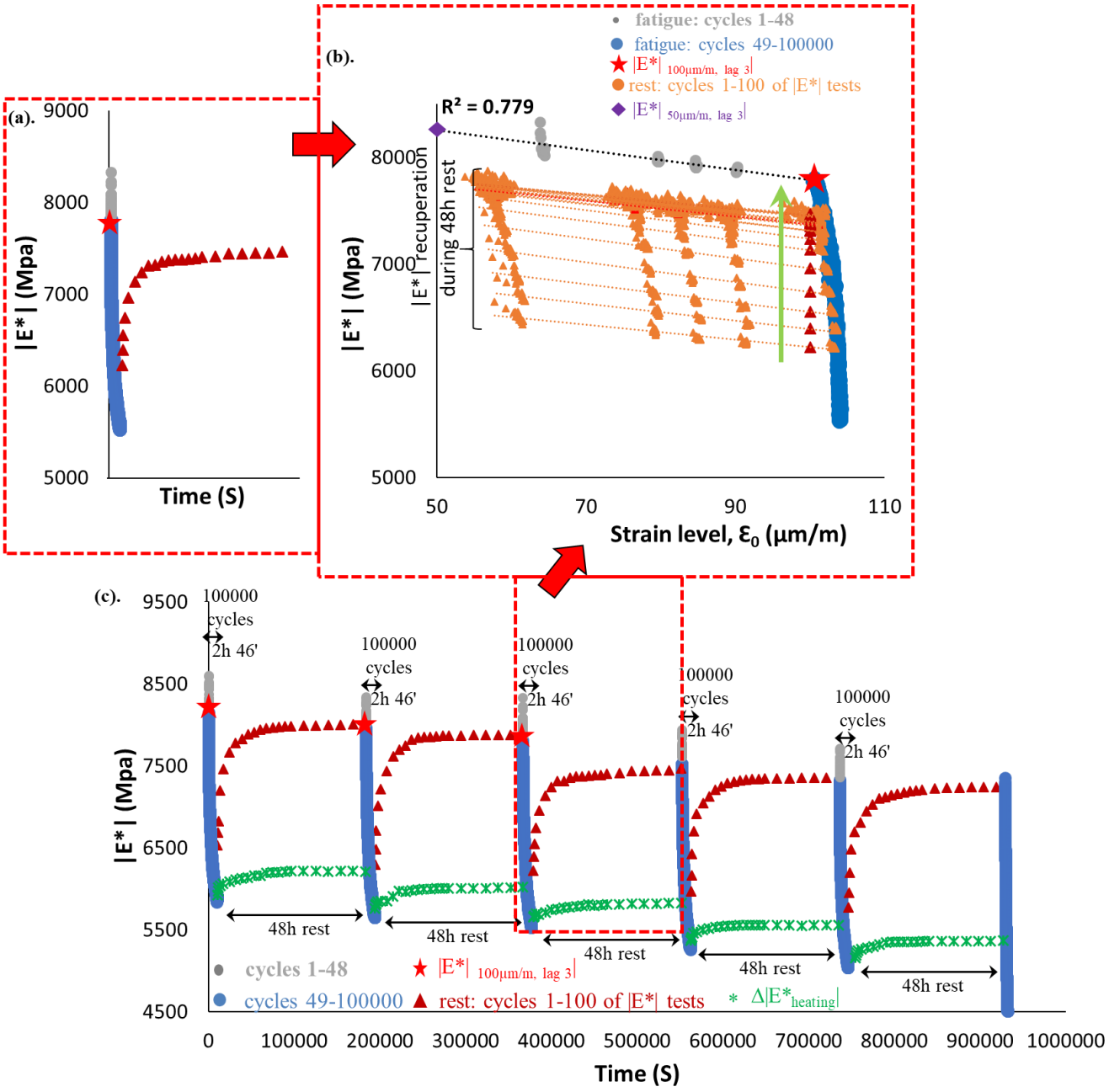

3.1.78. PFRT results obtained for mix 40/60 – 6: (a) |E*| as a function of time during the fourth fatigue lag and rest period (b) |E*| as a function of applied strain amplitude during the fourth fatigue lags and the short complex modulus tests performed within its following rest periods; (c) |E*| as a function of time during the five fatigue lags and rest periods [Red stars indicate values of |E*| estimated at 100 µm/m at the beginning of fatigue lag, green asterisk shows values of $\Delta|E^*_{heating}|$ as influence of self-heating and brown triangles indicate values of |E*| estimated at 100 µm/m for each short complex modulus test during rest (all these values were obtained using non-linearity envelopes, as shown in (b) for the first fatigue lag and rest period)].

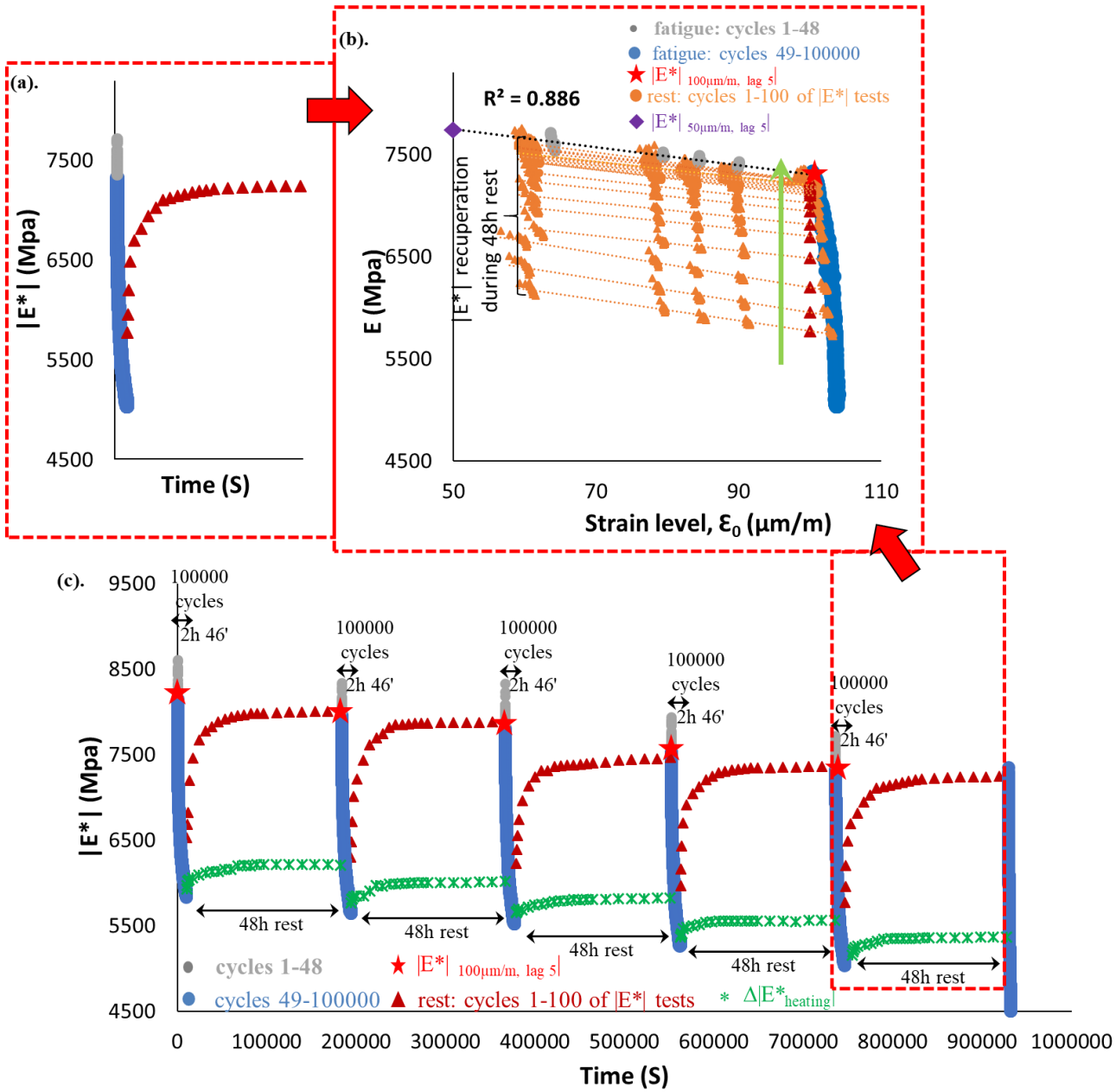

3.1.79. PFRT results obtained for mix 40/60 – 6: (a) |E*| as a function of time during the fifth fatigue lag and rest period (b) |E*| as a function of applied strain amplitude during the fifth fatigue lags and the short complex modulus tests performed within its following rest periods; (c) |E*| as a function of time during the five fatigue lags and rest periods [Red stars indicate values of |E*| estimated at 100 µm/m at the beginning of fatigue lag, green asterisk shows values of $\Delta|E^*_{heating}|$ as influence of self-heating and brown triangles indicate values of |E*| estimated at 100 µm/m for each short complex modulus test during rest (all these values were obtained using non-linearity envelopes, as shown in (b) for the first fatigue lag and rest period)].

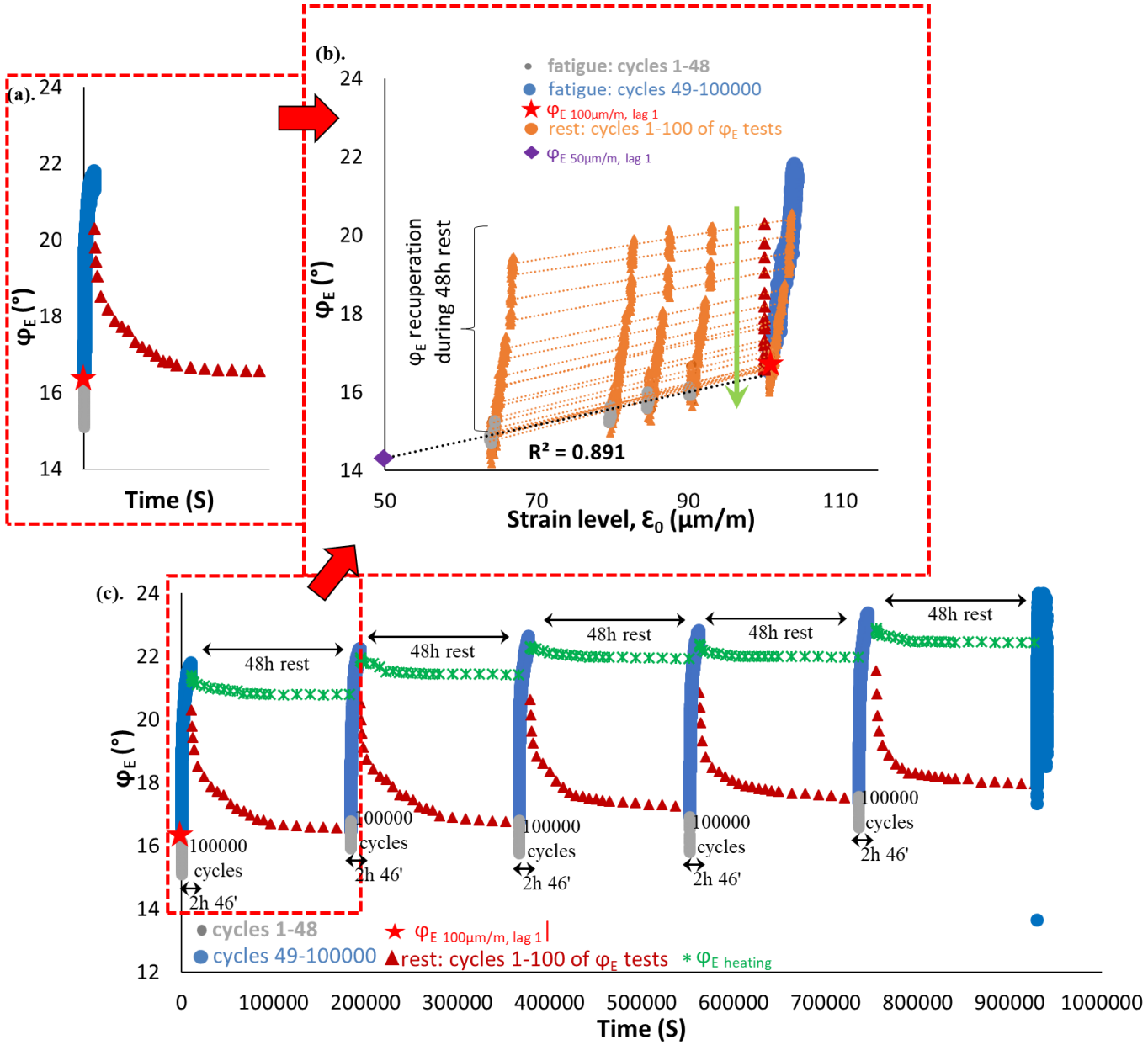

3.1.80. PFRT results obtained for mix 40/60 – 6: (a) φ_E as a function of time during the first fatigue lag and rest period (b) φ_E as a function of applied strain amplitude during the first fatigue lags and the short complex modulus tests performed within its following rest periods; (c) φ_E as a function of time during the five fatigue lags and rest periods (Red stars indicate values of φ_E estimated at 100 µm/m at the beginning of fatigue lag, green asterisk shows values of $\Delta\varphi_{E\ heating}$ as influence of self-heating and brown triangles indicate values of φ_E estimated at 100 µm/m for each short complex modulus test during rest (all these values were obtained using non-linearity envelopes, as shown in (b) for the first fatigue lag and rest period).

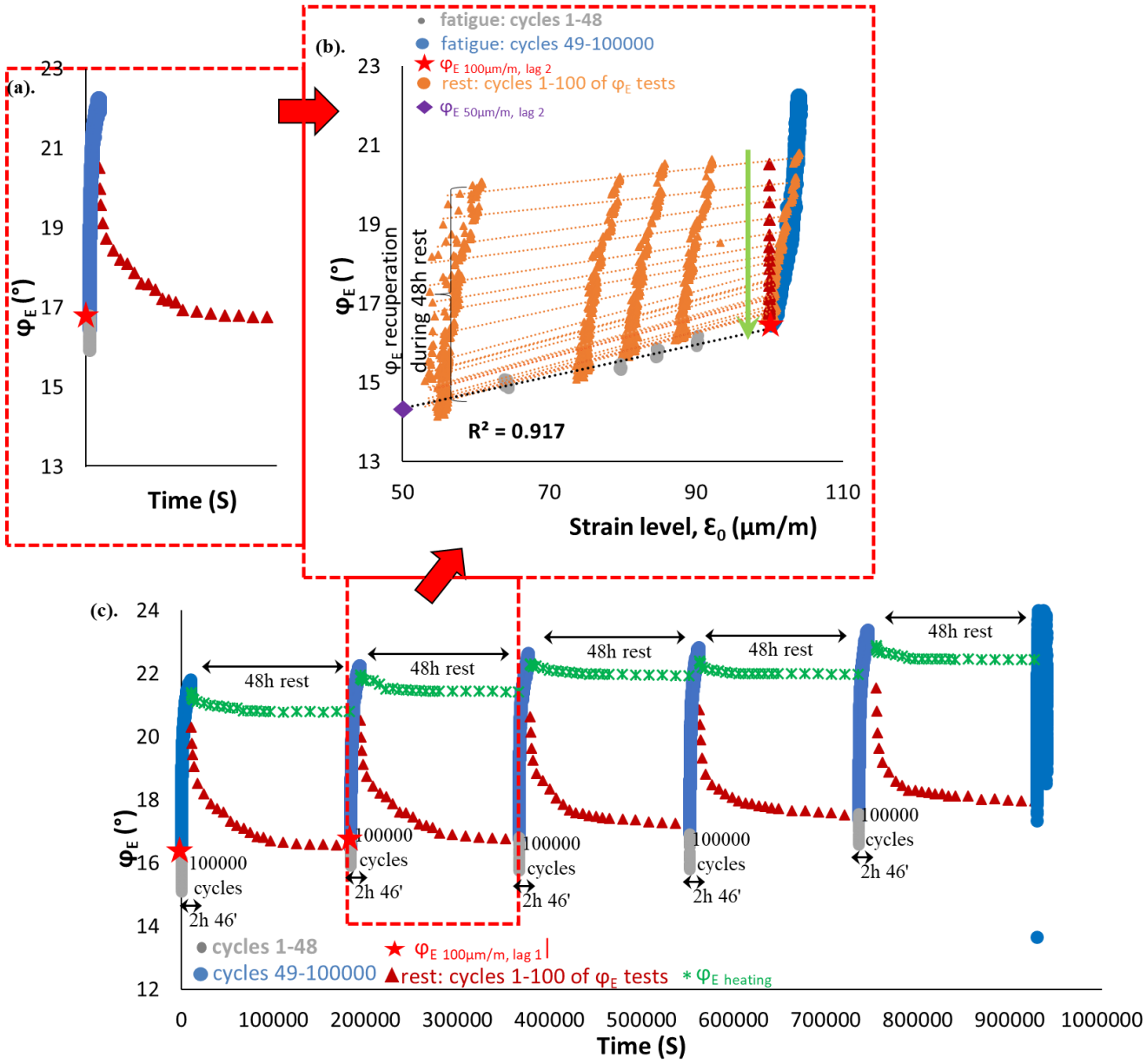

3.1.81. PFRT results obtained for mix 40/60 – 6: (a) φ_E as a function of time during the second fatigue lag and rest period (b) φ_E as a function of applied strain amplitude during the second fatigue lags and the short complex modulus tests performed within its following rest periods; (c) φ_E as a function of time during the five fatigue lags and rest periods (Red stars indicate values of φ_E estimated at 100 µm/m at the beginning of fatigue lag, green asterisk shows values of $\Delta\varphi_{E\ heating}$ as influence of self-heating and brown triangles indicate values of φ_E estimated at 100 µm/m for each short complex modulus test during rest (all these values were obtained using non-linearity envelopes, as shown in (b) for the first fatigue lag and rest period).

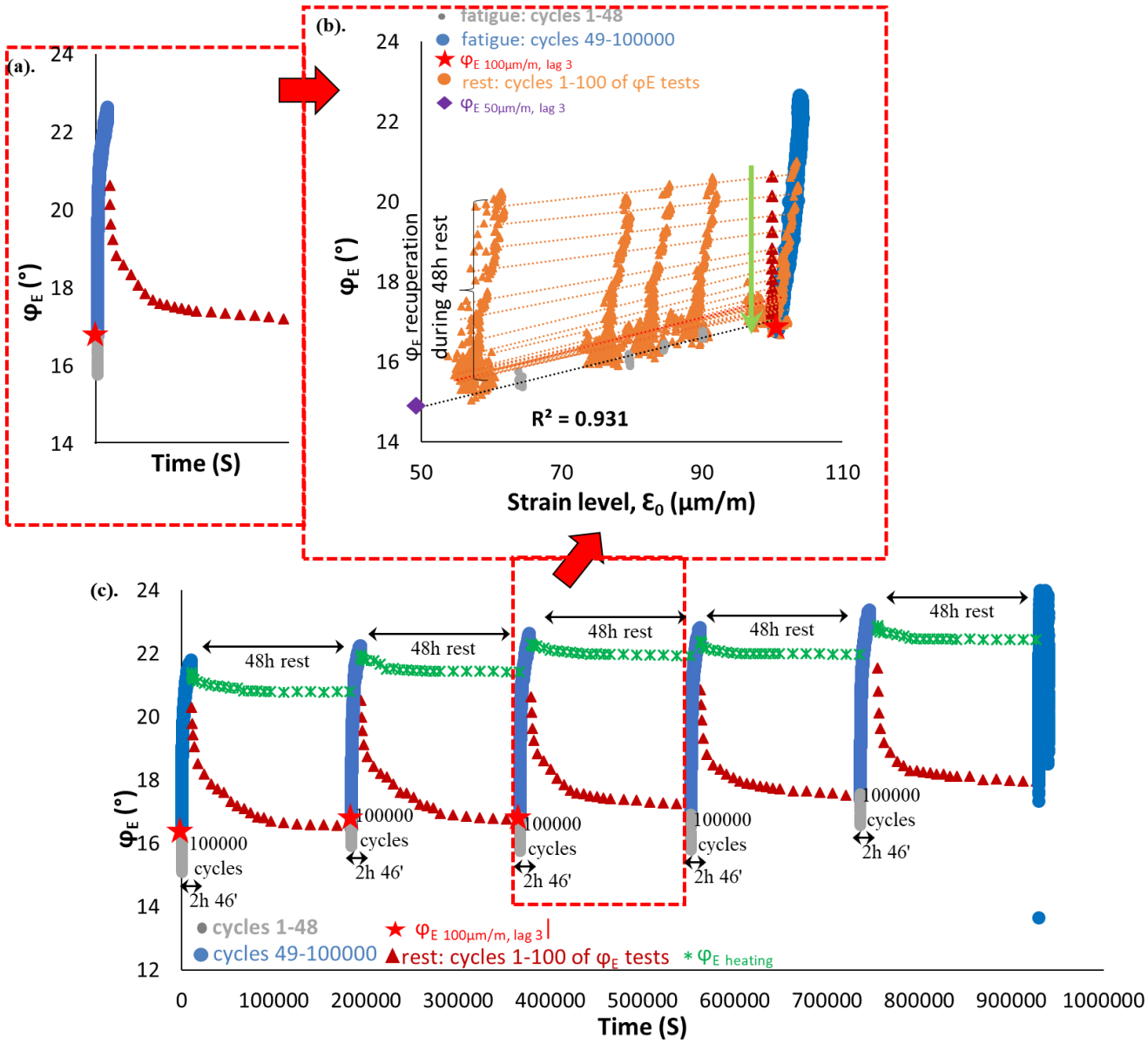

3.1.82. PFRT results obtained for mix 40/60 – 6: (a) φE as a function of time during the third fatigue lag and rest period (b) φE as a function of applied strain amplitude during the third fatigue lags and the short complex modulus tests performed within its following rest periods; (c) φE as a function of time during the five fatigue lags and rest periods (Red stars indicate values of φE estimated at 100 µm/m at the beginning of fatigue lag, green asterisk shows values of ΔφE heating as influence of self-heating and brown triangles indicate values of φE estimated at 100 µm/m for each short complex modulus test during rest (all these values were obtained using non-linearity envelopes, as shown in (b) for the first fatigue lag and rest period).

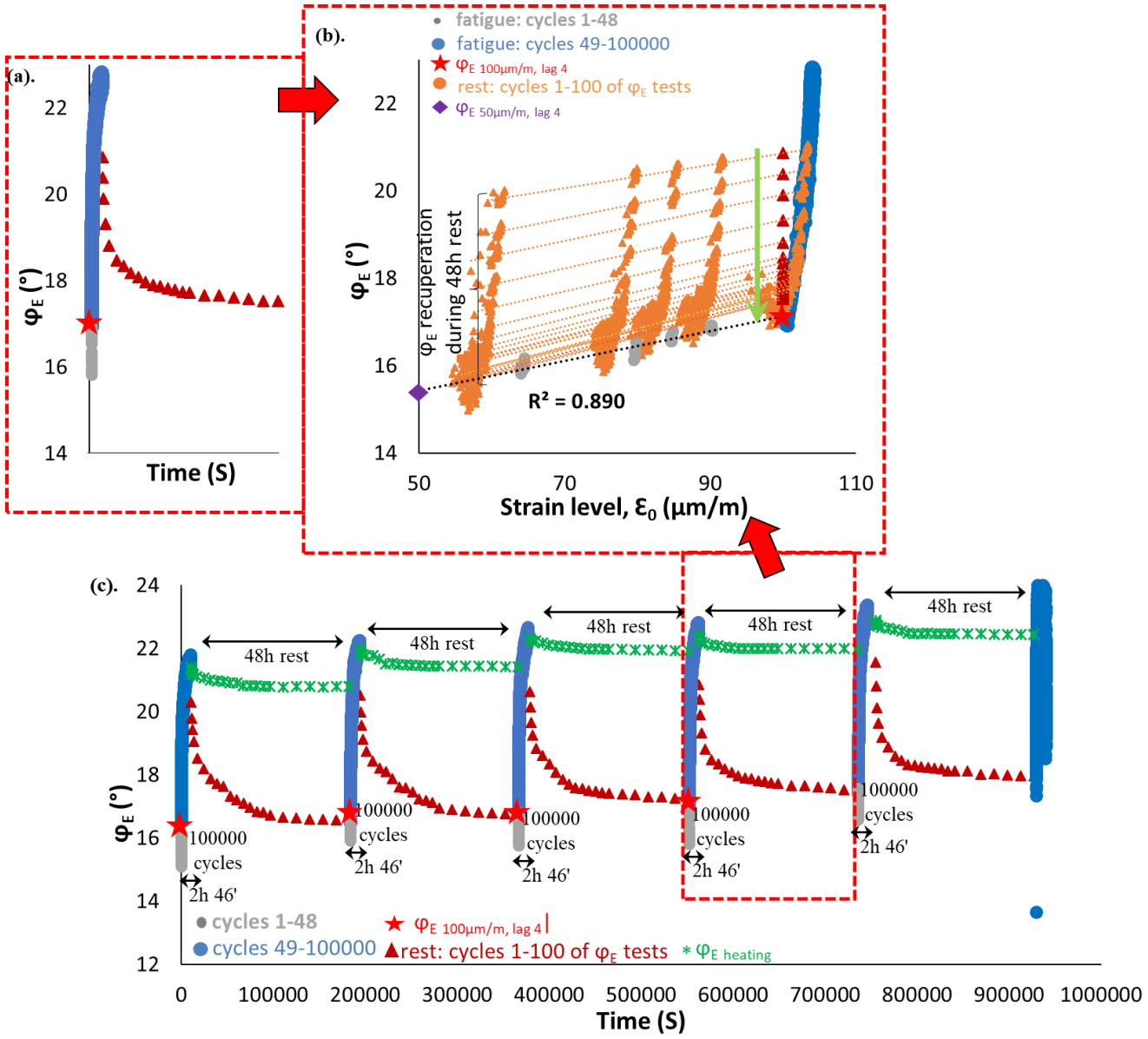

3.1.83. PFRT results obtained for mix 40/60 – 6: (a) φ_E as a function of time during the fourth fatigue lag and rest period (b) φ_E as a function of applied strain amplitude during the fourth fatigue lags and the short complex modulus tests performed within its following rest periods; (c) φ_E as a function of time during the five fatigue lags and rest periods (Red stars indicate values of φ_E estimated at 100 µm/m at the beginning of fatigue lag, green asterisk shows values of $\Delta\varphi_{E\ heating}$ as influence of self-heating and brown triangles indicate values of φ_E estimated at 100 µm/m for each short complex modulus test during rest (all these values were obtained using non-linearity envelopes, as shown in (b) for the first fatigue lag and rest period).

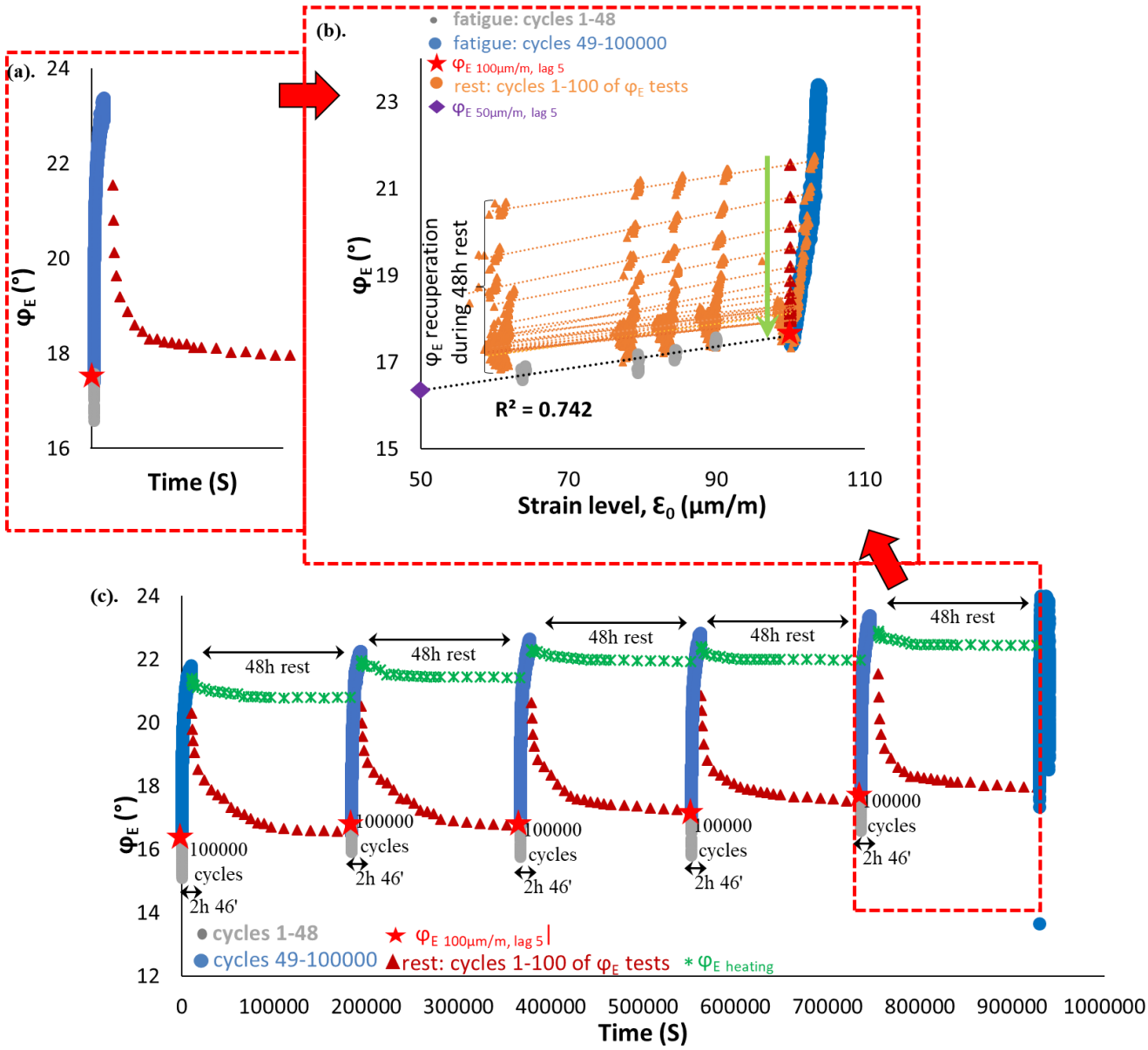

3.1.84. PFRT results obtained for mix 40/60 – 6: (a) φ_E as a function of time during the fifth fatigue lag and rest period (b) φ_E as a function of applied strain amplitude during the fifth fatigue lags and the short complex modulus tests performed within its following rest periods; (c) φ_E as a function of time during the five fatigue lags and rest periods (Red stars indicate values of φ_E estimated at 100 µm/m at the beginning of fatigue lag, green asterisk shows values of $\Delta\varphi_{E\ heating}$ as influence of self-heating and brown triangles indicate values of φ_E estimated at 100 µm/m for each short complex modulus test during rest (all these values were obtained using non-linearity envelopes, as shown in (b) for the first fatigue lag and rest period).

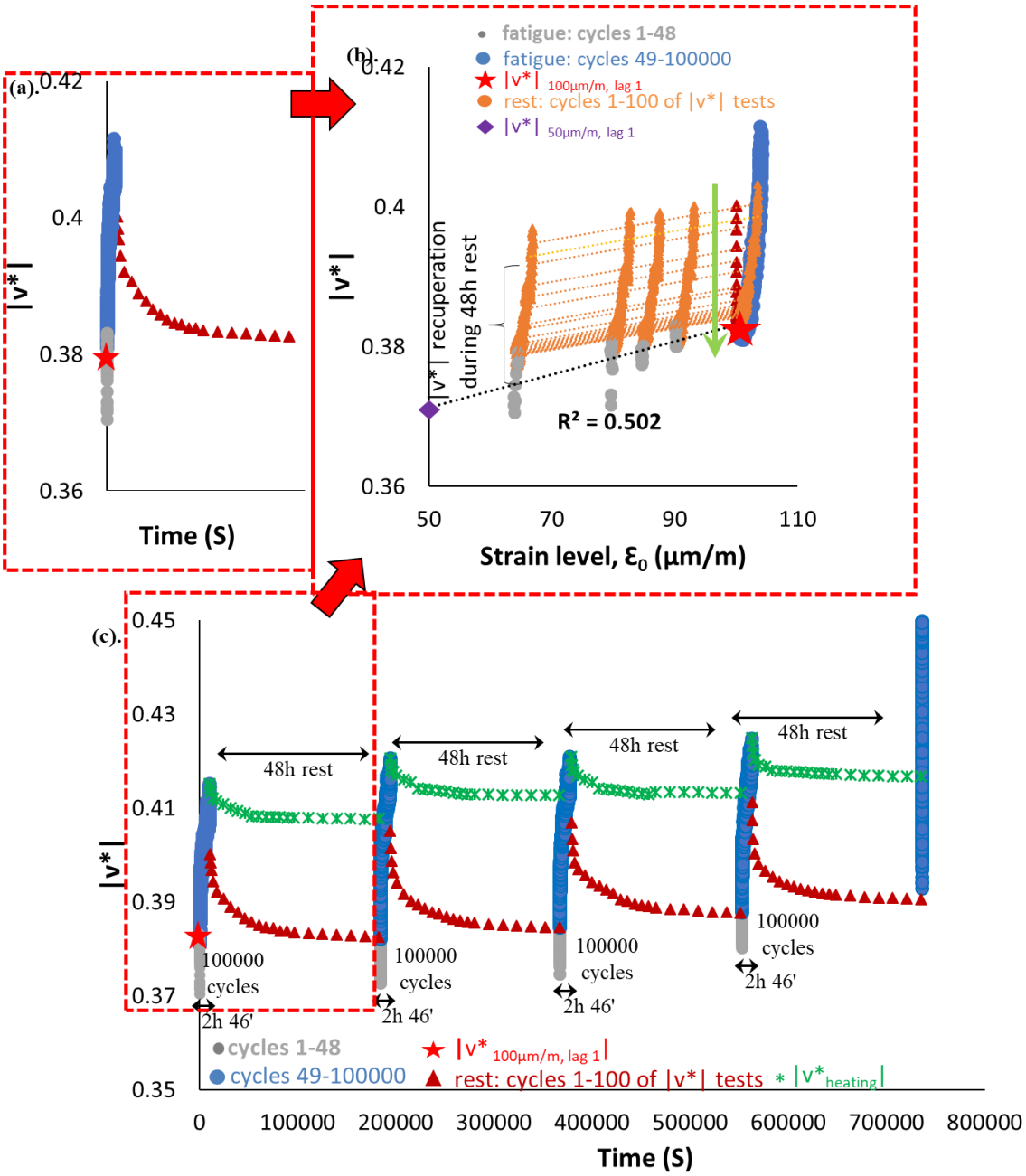

3.1.85. PFRT results obtained for mix 40/60 – 6: (a) |v*| as a function of time during the first fatigue lag and rest period (b) |v*| as a function of applied strain amplitude during the first fatigue lags and the short complex modulus tests performed within its following rest periods; (c) |v*| as a function of time during the five fatigue lags and rest periods [Red stars indicate values of |v*| estimated at 100 µm/m at the beginning of fatigue lag, green asterisk shows values of $\Delta|v^*_{heating}|$ as influence of self-heating and brown triangles indicate values of |v*| estimated at 100 µm/m for each short complex modulus test during rest (all these values were obtained using non-linearity envelopes, as shown in (b) for the first fatigue lag and rest period)].

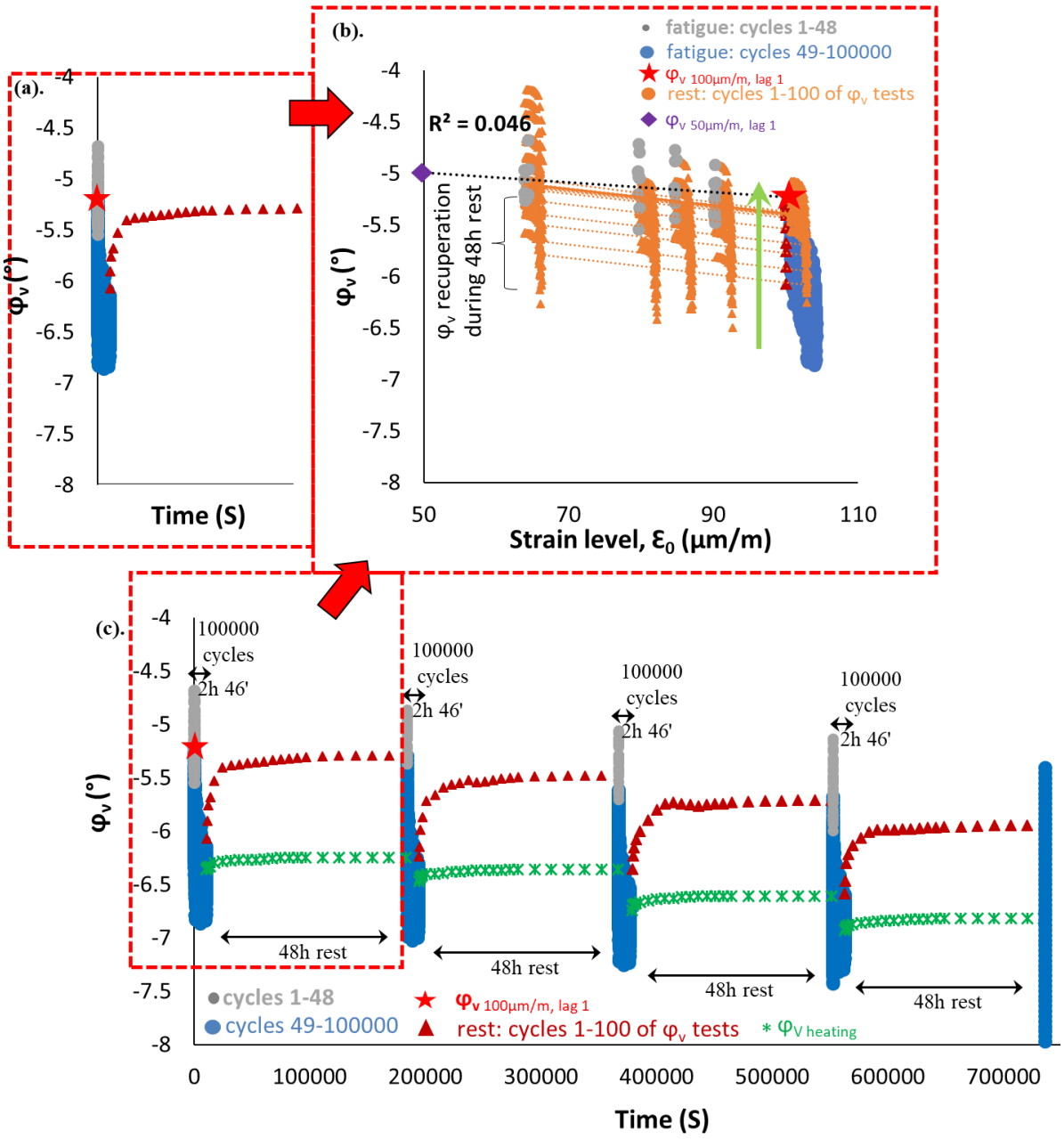

3.1.86. PFRT results obtained for mix 40/60 – 6: (a) φ_V as a function of time during the first fatigue lag and rest period (b) φ_V as a function of applied strain amplitude during the first fatigue lags and the short complex modulus tests performed within its following rest periods; (c) φ_V as a function of time during the five fatigue lags and rest periods (Red stars indicate values of φ_V estimated at 100 µm/m at the beginning of fatigue lag, green asterisk shows values of $\Delta\varphi_{E\ heating}$ as influence of self-heating and brown triangles indicate values of φ_V estimated at 100 µm/m for each short complex modulus test during rest (all these values were obtained using non-linearity envelopes, as shown in (b) for the first fatigue lag and rest period).

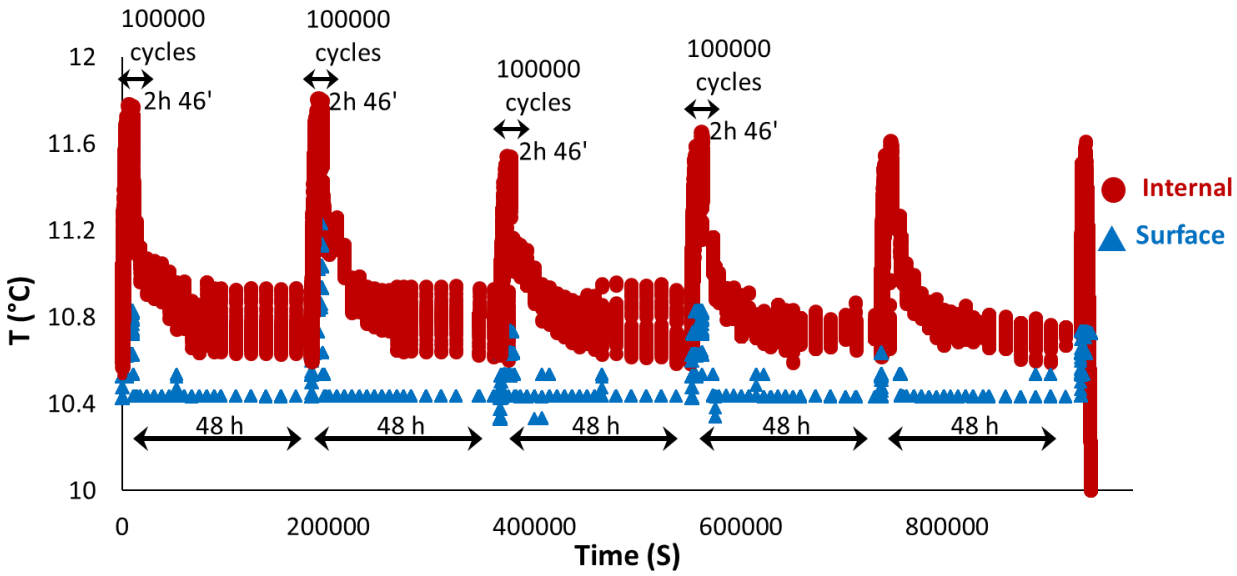

3.1.87. PFRT results obtained for mix 40/60 – 6: internal and surface temperature evolution during fatigue lags and recovery periods.

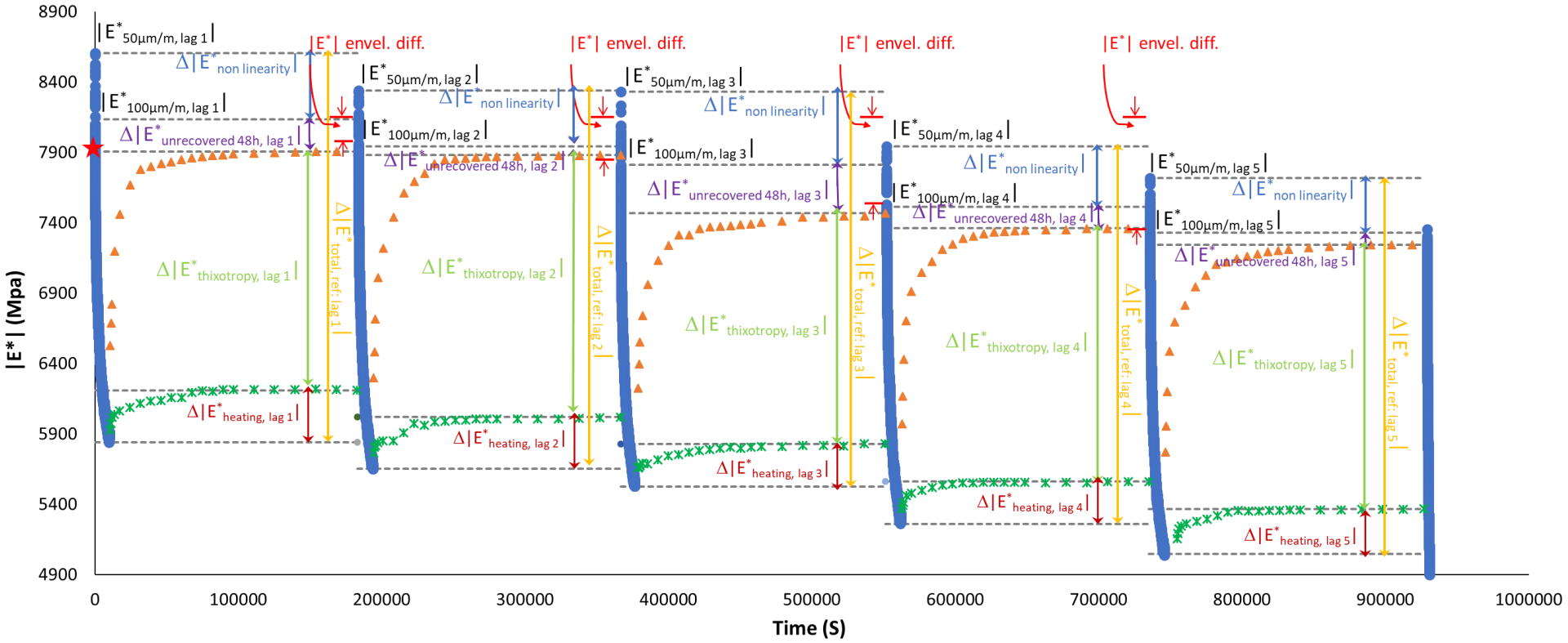
|E*| (Mpa)
Time (S)
8900
8400
7900
7400
6900
6400
5900
5400
4900
0
100000
200000
300000
400000
500000
600000
700000
800000
900000
1000000
|E*50µm/m, lag 1|
|E*100µm/m, lag 1|
Δ|E*non linearity|
Δ|E*unrecovered 48h, lag 1|
Δ|E*thixotropy, lag 1|
Δ|E*heating, lag 1|
Δ|E*total, ref. lag 1|
|E*| envel. diff.
|E*50µm/m, lag 2|
|E*100µm/m, lag 2|
Δ|E*non linearity|
Δ|E*unrecovered 48h, lag 2|
Δ|E*thixotropy, lag 2|
Δ|E*heating, lag 2|
Δ|E*total, ref. lag 2|
|E*| envel. diff.
|E*50µm/m, lag 3|
|E*100µm/m, lag 3|
Δ|E*non linearity|
Δ|E*unrecovered 48h, lag 3|
Δ|E*thixotropy, lag 3|
Δ|E*heating, lag 3|
Δ|E*total, ref. lag 3|
|E*| envel. diff.
|E*50µm/m, lag 4|
|E*100µm/m, lag 4|
Δ|E*non linearity|
Δ|E*unrecovered 48h, lag 4|
Δ|E*thixotropy, lag 4|
Δ|E*heating, lag 4|
Δ|E*total, ref. lag 4|
|E*| envel. diff.
|E*50µm/m, lag 5|
|E*100µm/m, lag 5|
Δ|E*non linearity|
Δ|E*unrecovered 48h, lag 5|
Δ|E*thixotropy, lag 5|
Δ|E*heating, lag 5|
Δ|E*total, ref. lag 5|

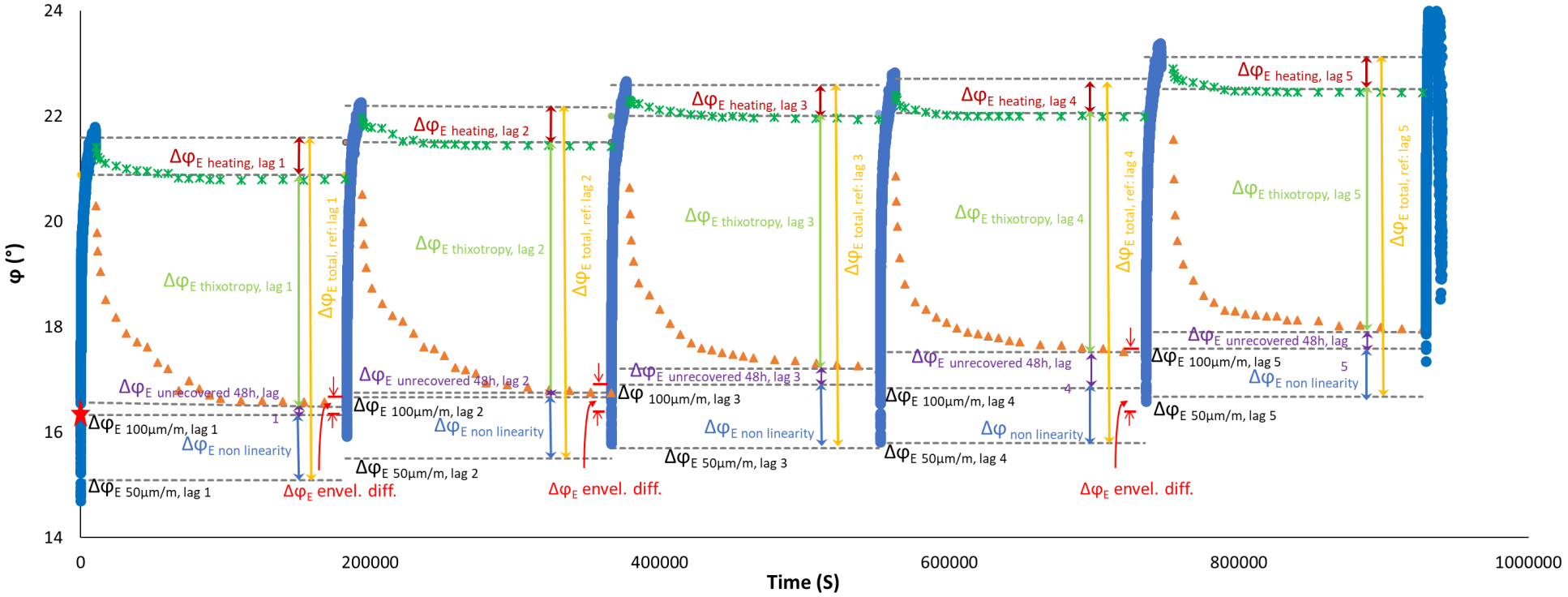
24
22
20
18
16
14
φ (°)
0
200000
400000
600000
800000
1000000
Time (S)
Δφ E heating, lag 1
Δφ E thixotropy, lag 1
Δφ E unrecovered 48h, lag 1
Δφ E 100µm/m, lag 1
Δφ E non linearity 1
Δφ E 50µm/m, lag 1
Δφ E total, ref: lag 1
Δφ E envel. diff.
Δφ E heating, lag 2
Δφ E thixotropy, lag 2
Δφ E unrecovered 48h, lag 2
Δφ E 100µm/m, lag 2
Δφ E non linearity
Δφ E 50µm/m, lag 2
Δφ E total, ref: lag 2
Δφ E envel. diff.
Δφ E heating, lag 3
Δφ E thixotropy, lag 3
Δφ E unrecovered 48h, lag 3
Δφ 100µm/m, lag 3
Δφ E non linearity
Δφ E 50µm/m, lag 3
Δφ E total, ref: lag 3
Δφ E heating, lag 4
Δφ E thixotropy, lag 4
Δφ E unrecovered 48h, lag 4
Δφ E 100µm/m, lag 4
Δφ non linearity
Δφ E 50µm/m, lag 4
Δφ E total, ref: lag 4
Δφ E envel. diff.
Δφ E heating, lag 5
Δφ E thixotropy, lag 5
Δφ E unrecovered 48h, lag 5
Δφ E 100µm/m, lag 5
Δφ E non linearity 5
Δφ E 50µm/m, lag 5
Δφ E total, ref: lag 5

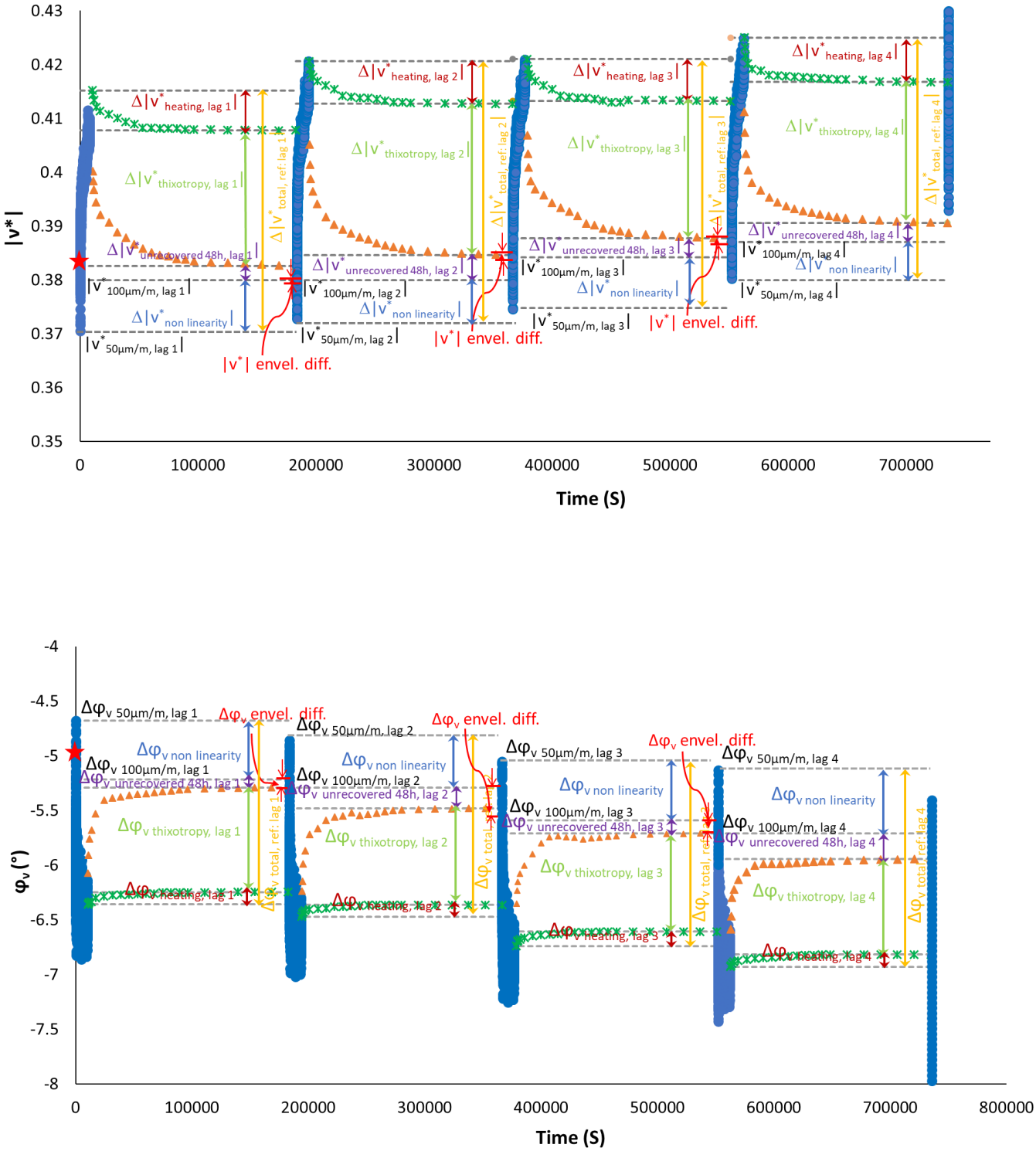

3.1.88. Quantification of different contributions |E*|, φ_E, |v*| and φ_v evolution, for the first two fatigue lags for mix 40/60 – 6: different envelope line is used for each fatigue lag.

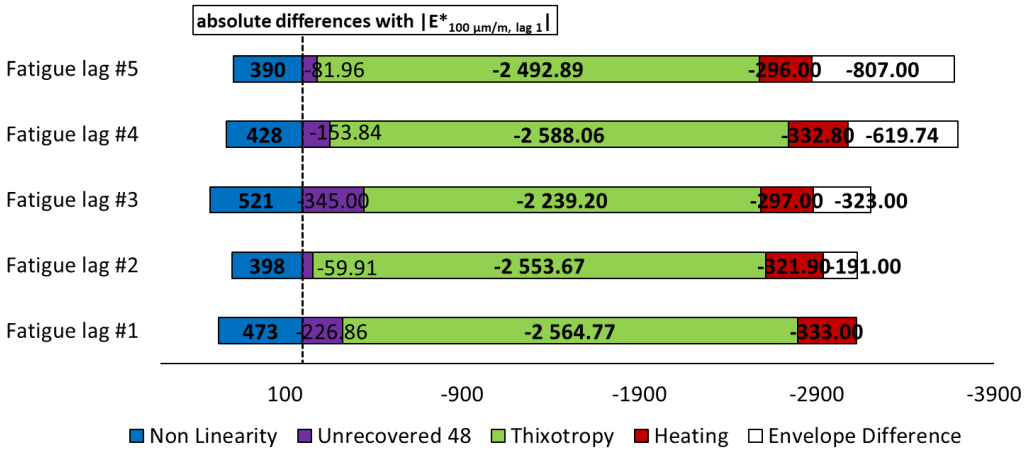
absolute differences with |E*100 µm/m, lag 1|
Fatigue lag #5
Fatigue lag #4
Fatigue lag #3
Fatigue lag #2
Fatigue lag #1
390
-81.96
-2 492.89
-296.00
-807.00
428
-153.84
-2 588.06
-332.80
-619.74
521
-345.00
-2 239.20
-297.00
-323.00
398
-59.91
-2 553.67
-321.90
-191.00
473
-226.86
-2 564.77
-333.00
100
-900
-1900
-2900
-3900
Non Linearity
Unrecovered 48
Thixotropy
Heating
Envelope Difference

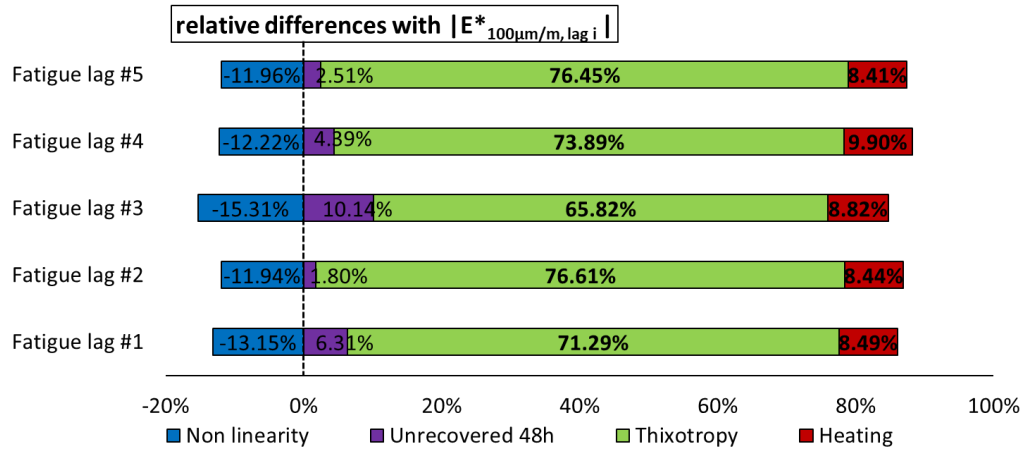
relative differences with |E*100µm/m, lag i|
Fatigue lag #5
Fatigue lag #4
Fatigue lag #3
Fatigue lag #2
Fatigue lag #1
-11.96%
2.51%
76.45%
8.41%
-12.22%
4.39%
73.89%
9.90%
-15.31%
10.14%
65.82%
8.82%
-11.94%
1.80%
76.61%
8.44%
-13.15%
6.31%
71.29%
8.49%
-20%
0%
20%
40%
60%
80%
100%
Non linearity
Unrecovered 48h
Thixotropy
Heating

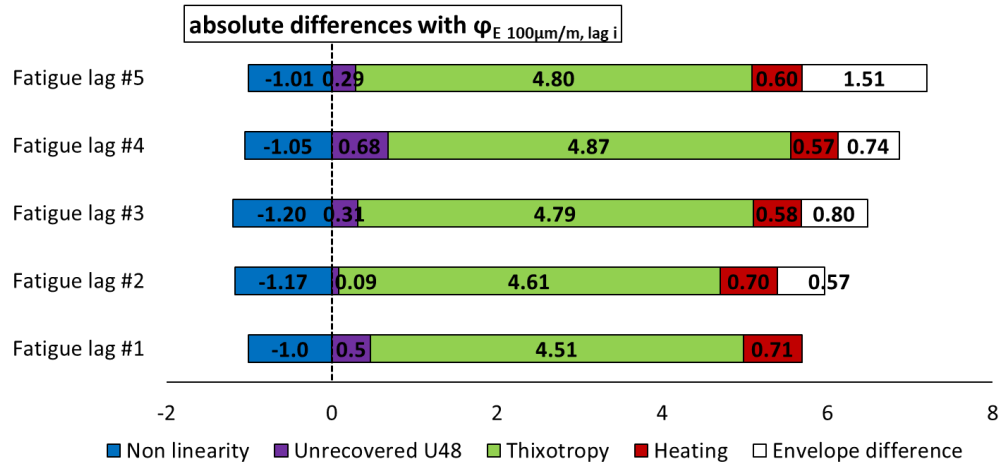
absolute differences with φE 100µm/m, lag i
Fatigue lag #5
Fatigue lag #4
Fatigue lag #3
Fatigue lag #2
Fatigue lag #1
-1.01
0.29
4.80
0.60
1.51
-1.05
0.68
4.87
0.57
0.74
-1.20
0.31
4.79
0.58
0.80
-1.17
0.09
4.61
0.70
0.57
-1.0
0.5
4.51
0.71
-2
0
2
4
6
8
Non linearity
Unrecovered U48
Thixotropy
Heating
Envelope difference

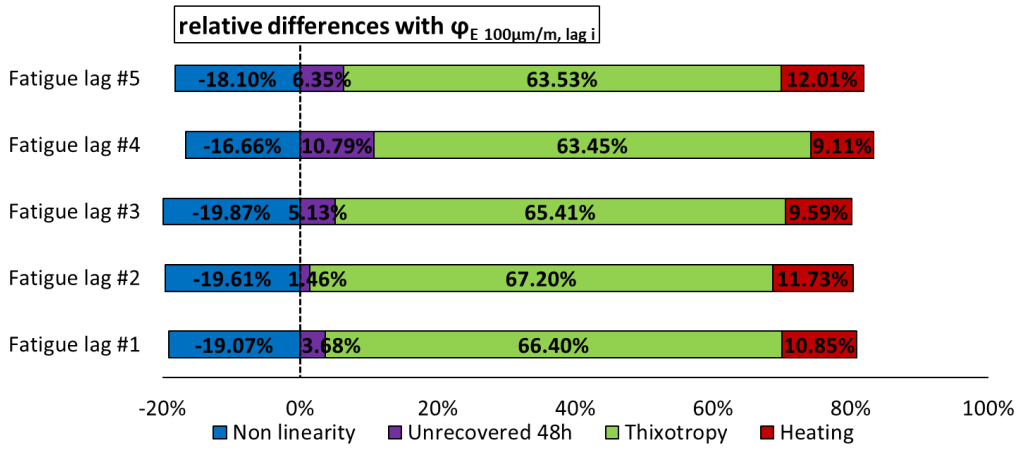
relative differences with $\varphi_{E\ 100\mu m/m,\ lag\ i}$
Fatigue lag #5
Fatigue lag #4
Fatigue lag #3
Fatigue lag #2
Fatigue lag #1
-18.10%
6.35%
63.53%
12.01%
-16.66%
10.79%
63.45%
9.11%
-19.87%
5.13%
65.41%
9.59%
-19.61%
1.46%
67.20%
11.73%
-19.07%
3.68%
66.40%
10.85%
-20%
0%
20%
40%
60%
80%
100%
Non linearity
Unrecovered 48h
Thixotropy
Heating

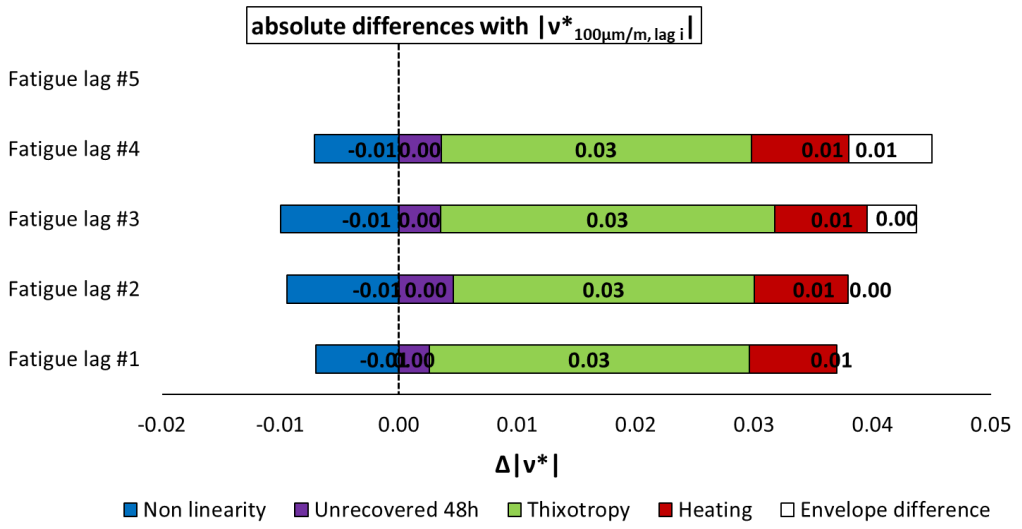
absolute differences with $|v^*_{100\mu m/m,\ lag\ i}|$
Fatigue lag #5
Fatigue lag #4
Fatigue lag #3
Fatigue lag #2
Fatigue lag #1
-0.01
0.00
0.03
0.01
0.01
0.00
0.00
-0.02
-0.01
0.00
0.01
0.02
0.03
0.04
0.05
Δ|v*|
Non linearity
Unrecovered 48h
Thixotropy
Heating
Envelope difference

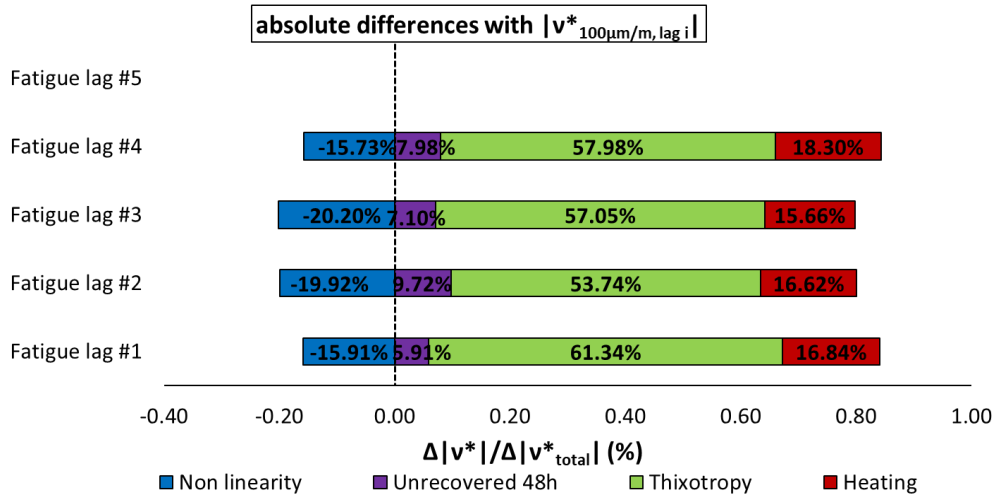
absolute differences with $|v^*_{100\mu m/m,\ lag\ i}|$
Fatigue lag #5
Fatigue lag #4
Fatigue lag #3
Fatigue lag #2
Fatigue lag #1
-15.73%
7.98%
57.98%
18.30%
-20.20%
7.10%
57.05%
15.66%
-19.92%
9.72%
53.74%
16.62%
-15.91%
5.91%
61.34%
16.84%
-0.40
-0.20
0.00
0.20
0.40
0.60
0.80
1.00
Δ|v*|/Δ|v*total| (%)
Non linearity
Unrecovered 48h
Thixotropy
Heating

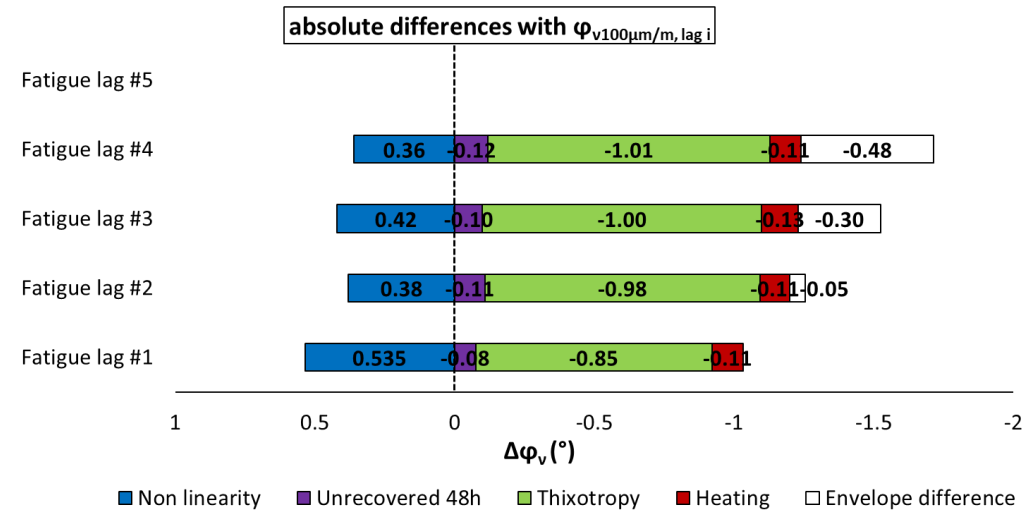

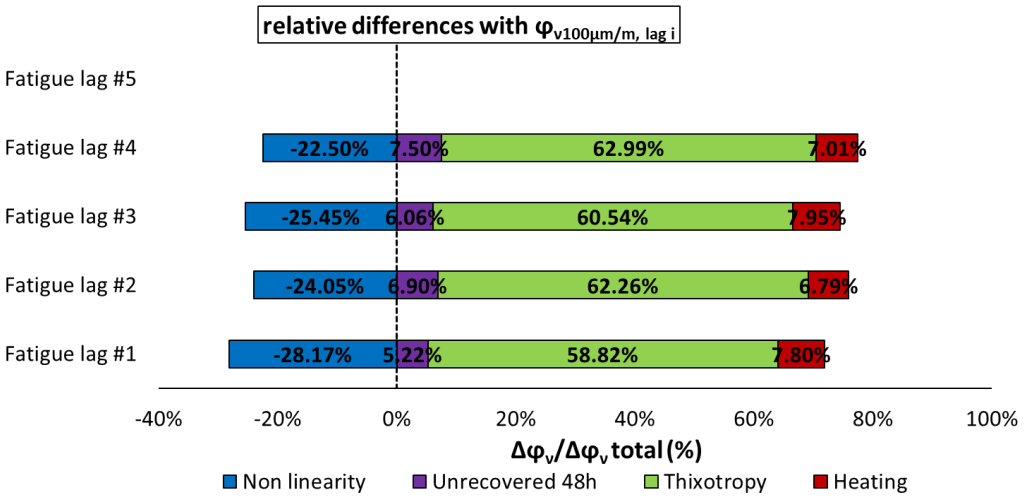

3.1.89. Quantification of different absolute and relative contributions to |E*|, φ_E, |v*| and φ_v evolutions for mix 40/60 – 6, calculated using a different envelope line for each fatigue lag.

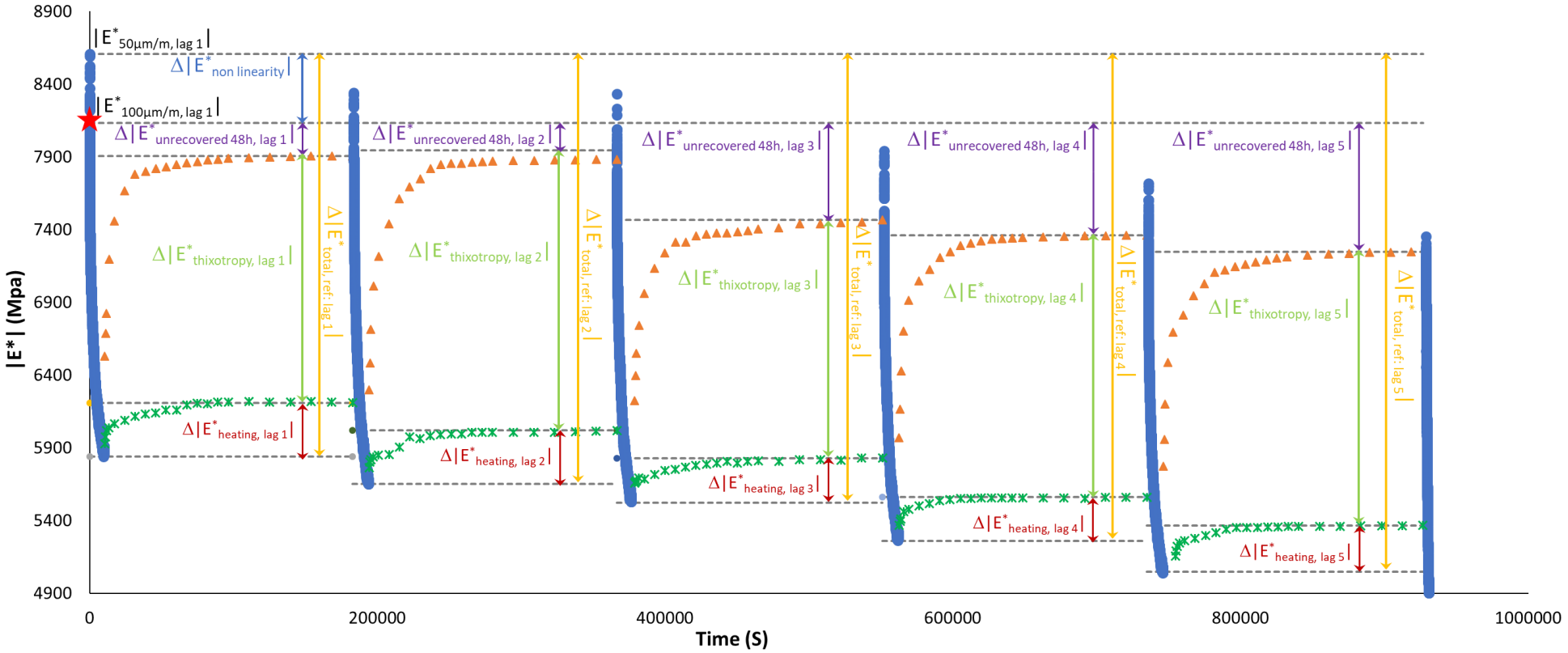
8900
8400
7900
7400
6900
6400
5900
5400
4900
|E*| (Mpa)
0
200000
400000
600000
800000
1000000
Time (S)
|E*50µm/m, lag 1|
|E*100µm/m, lag 1|
Δ|E*non linearity|
Δ|E*unrecovered 48h, lag 1|
Δ|E*thixotropy, lag 1|
Δ|E*heating, lag 1|
Δ|E*total, ref: lag 1|
Δ|E*unrecovered 48h, lag 2|
Δ|E*thixotropy, lag 2|
Δ|E*heating, lag 2|
Δ|E*total, ref: lag 2|
Δ|E*unrecovered 48h, lag 3|
Δ|E*thixotropy, lag 3|
Δ|E*heating, lag 3|
Δ|E*total, ref: lag 3|
Δ|E*unrecovered 48h, lag 4|
Δ|E*thixotropy, lag 4|
Δ|E*heating, lag 4|
Δ|E*total, ref: lag 4|
Δ|E*unrecovered 48h, lag 5|
Δ|E*thixotropy, lag 5|
Δ|E*heating, lag 5|
Δ|E*total, ref: lag 5|

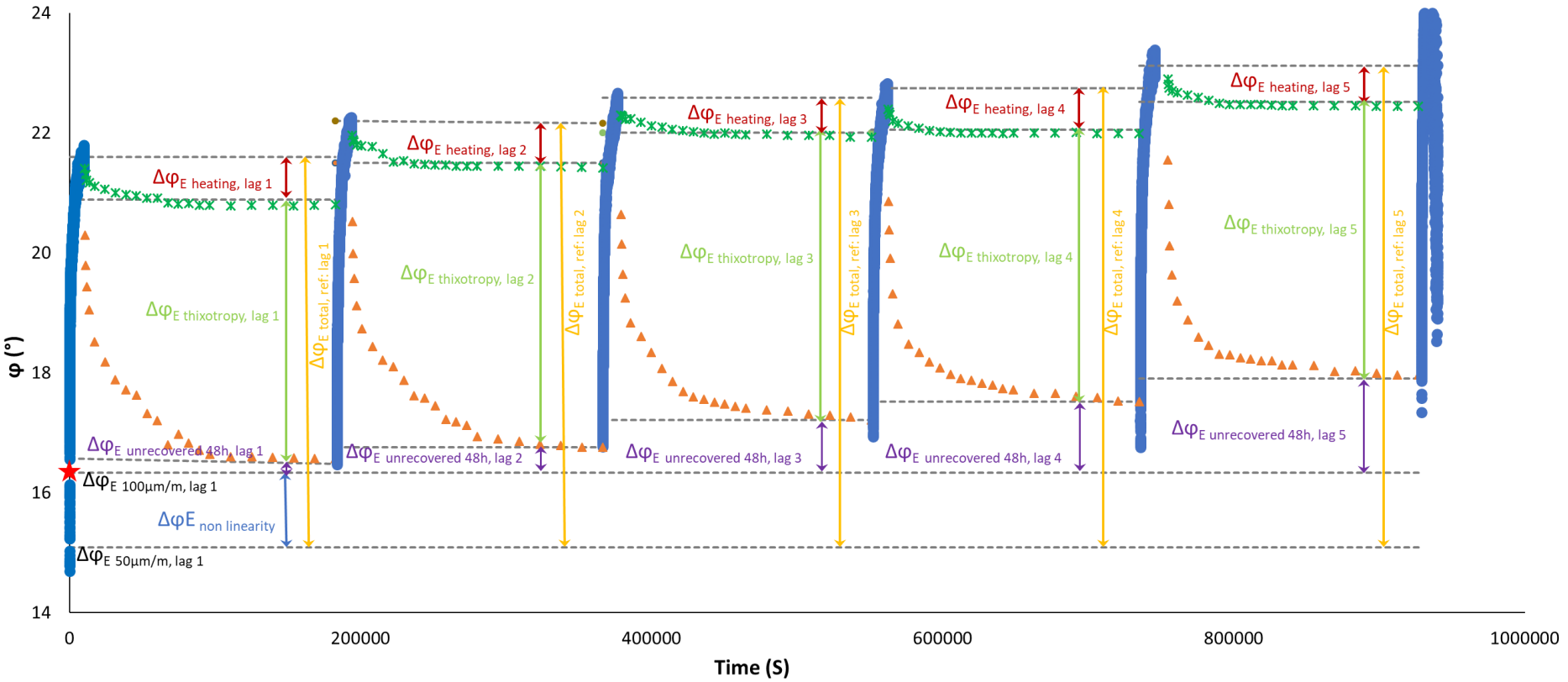
24
22
20
18
16
14
φ (°)
0
200000
400000
600000
800000
1000000
Time (S)
Δφ E heating, lag 1
Δφ E thixotropy, lag 1
Δφ E total, ref: lag 1
Δφ E unrecovered 48h, lag 1
Δφ E 100µm/m, lag 1
ΔφE non linearity
Δφ E 50µm/m, lag 1
Δφ E heating, lag 2
Δφ E thixotropy, lag 2
Δφ E total, ref: lag 2
Δφ E unrecovered 48h, lag 2
Δφ E heating, lag 3
Δφ E thixotropy, lag 3
Δφ E total, ref: lag 3
Δφ E unrecovered 48h, lag 3
Δφ E heating, lag 4
Δφ E thixotropy, lag 4
Δφ E total, ref: lag 4
Δφ E unrecovered 48h, lag 4
Δφ E heating, lag 5
Δφ E thixotropy, lag 5
Δφ E total, ref: lag 5
Δφ E unrecovered 48h, lag 5

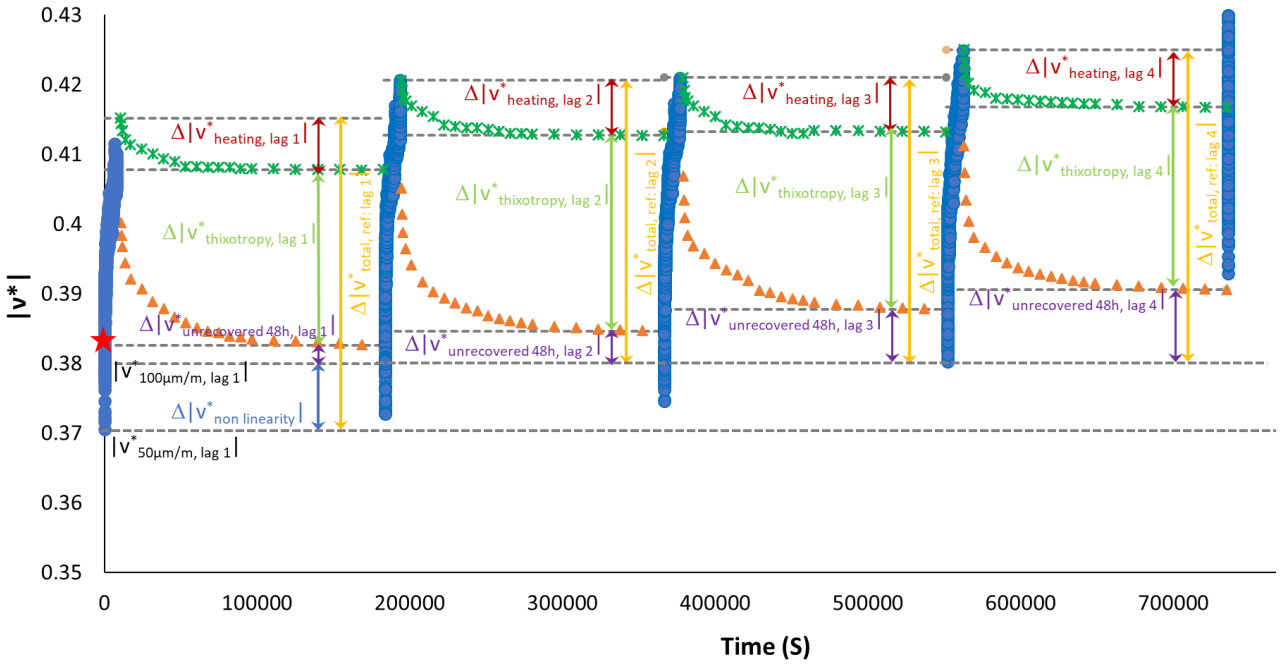

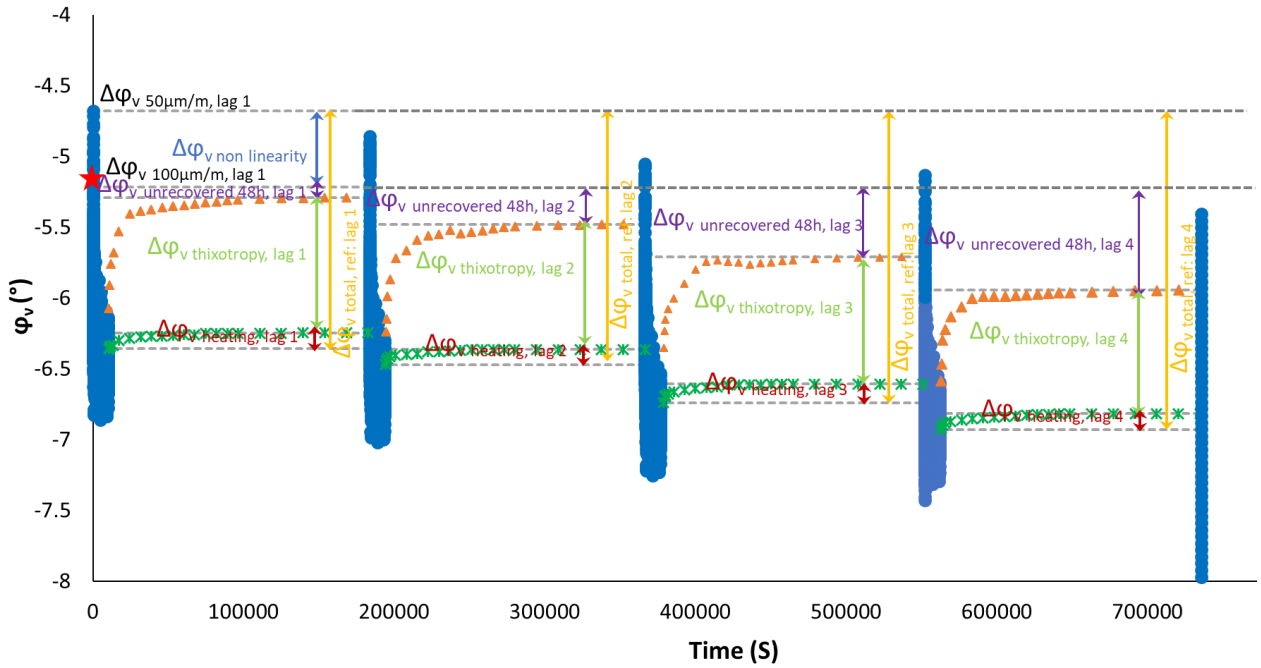

3.1.90. Quantification of different contributions to |E*|, φ_E, |v*| and φ_v evolution during five fatigue lags for mix 40/60 – 6: the envelope line of the first fatigue lag is used for all fatigue lags.

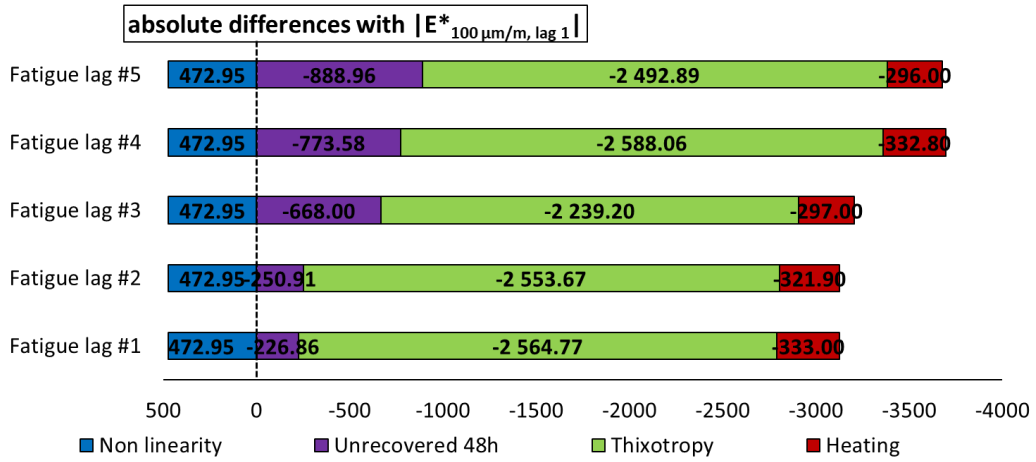
absolute differences with |E*100 µm/m, lag 1|
Fatigue lag #5
Fatigue lag #4
Fatigue lag #3
Fatigue lag #2
Fatigue lag #1
472.95
-888.96
-2 492.89
-296.00
472.95
-773.58
-2 588.06
-332.80
472.95
-668.00
-2 239.20
-297.00
472.95
-250.91
-2 553.67
-321.90
472.95
-226.86
-2 564.77
-333.00
500
0
-500
-1000
-1500
-2000
-2500
-3000
-3500
-4000
Non linearity
Unrecovered 48h
Thixotropy
Heating

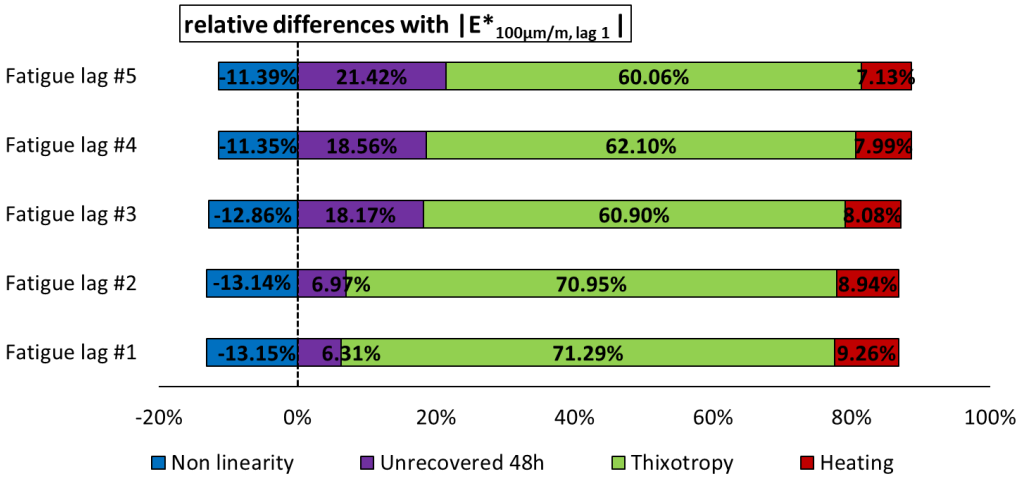
relative differences with |E*100µm/m, lag 1|
Fatigue lag #5
Fatigue lag #4
Fatigue lag #3
Fatigue lag #2
Fatigue lag #1
-11.39%
21.42%
60.06%
7.13%
-11.35%
18.56%
62.10%
7.99%
-12.86%
18.17%
60.90%
8.08%
-13.14%
6.97%
70.95%
8.94%
-13.15%
6.31%
71.29%
9.26%
-20%
0%
20%
40%
60%
80%
100%
Non linearity
Unrecovered 48h
Thixotropy
Heating

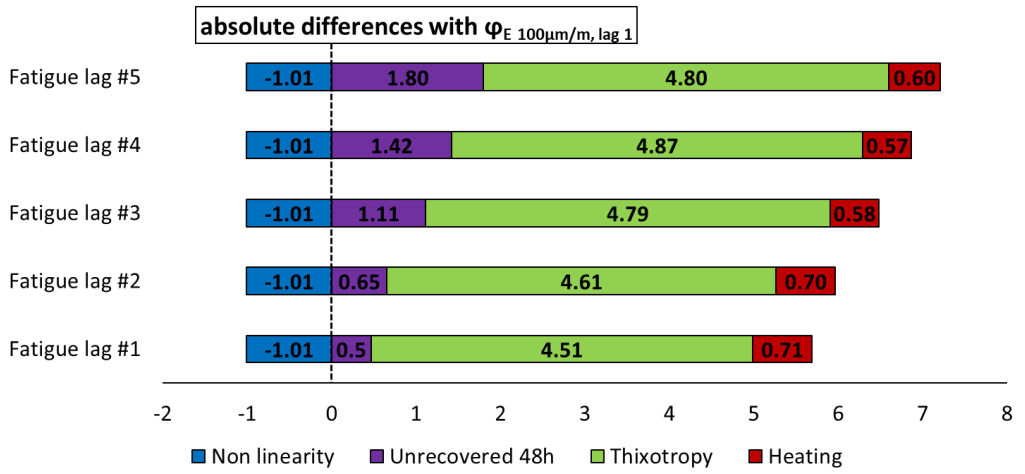
absolute differences with φE 100µm/m, lag 1
Fatigue lag #5
Fatigue lag #4
Fatigue lag #3
Fatigue lag #2
Fatigue lag #1
-1.01
1.80
4.80
0.60
-1.01
1.42
4.87
0.57
-1.01
1.11
4.79
0.58
-1.01
0.65
4.61
0.70
-1.01
0.5
4.51
0.71
-2
-1
0
1
2
3
4
5
6
7
8
Non linearity
Unrecovered 48h
Thixotropy
Heating

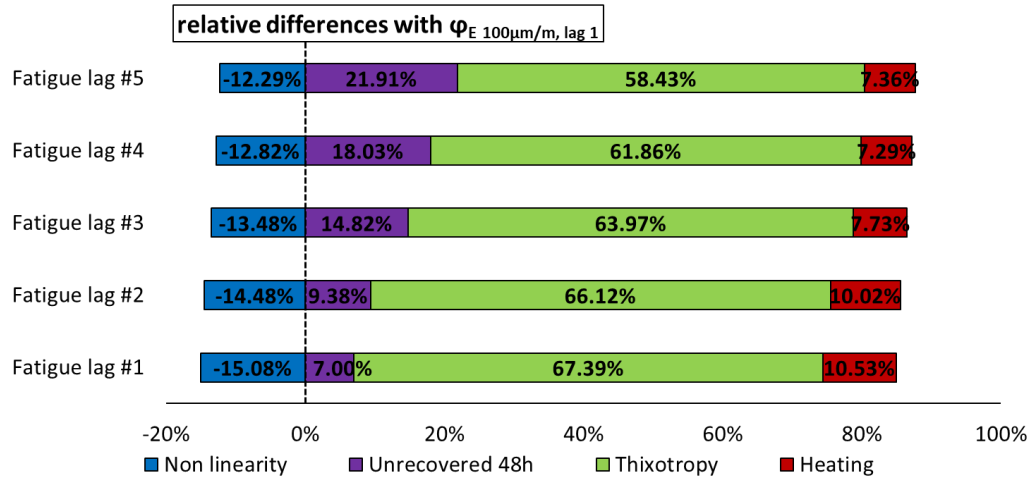
relative differences with φE 100µm/m, lag 1
Fatigue lag #5
Fatigue lag #4
Fatigue lag #3
Fatigue lag #2
Fatigue lag #1
-12.29%
21.91%
58.43%
7.36%
-12.82%
18.03%
61.86%
7.29%
-13.48%
14.82%
63.97%
7.73%
-14.48%
9.38%
66.12%
10.02%
-15.08%
7.00%
67.39%
10.53%
-20%
0%
20%
40%
60%
80%
100%
Non linearity
Unrecovered 48h
Thixotropy
Heating

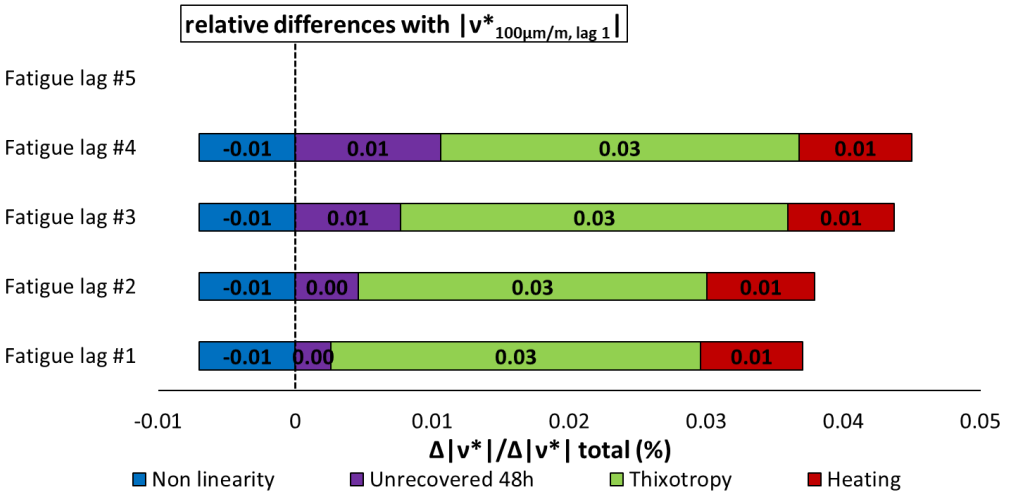
relative differences with |v*100µm/m, lag 1|
Fatigue lag #5
Fatigue lag #4
Fatigue lag #3
Fatigue lag #2
Fatigue lag #1
-0.01
0.01
0.03
0.01
-0.01
0.01
0.03
0.01
-0.01
0.00
0.03
0.01
-0.01
0.00
0.03
0.01
-0.01
0
0.01
0.02
0.03
0.04
0.05
Δ|v*|/Δ|v*| total (%)
Non linearity
Unrecovered 48h
Thixotropy
Heating

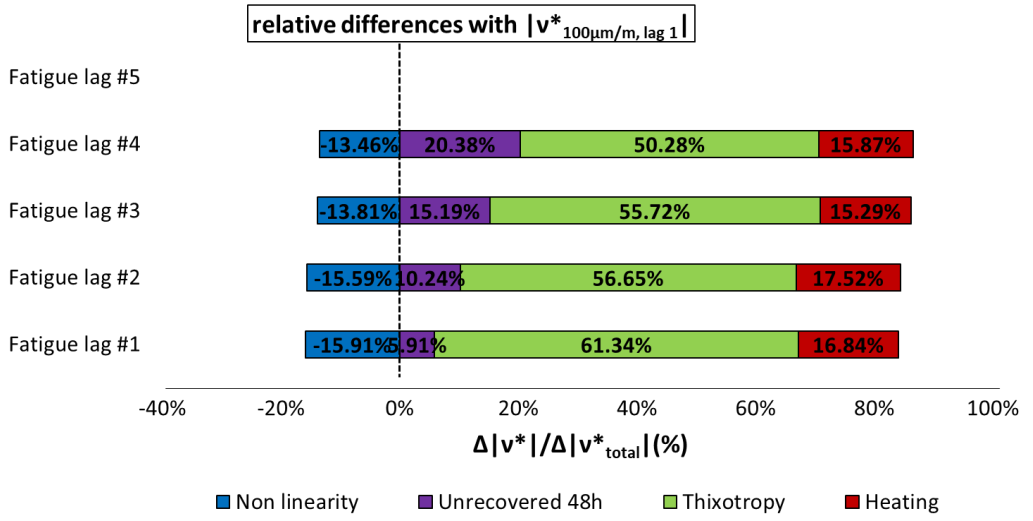
relative differences with |v*100µm/m, lag 1|
Fatigue lag #5
Fatigue lag #4
Fatigue lag #3
Fatigue lag #2
Fatigue lag #1
-13.46%
20.38%
50.28%
15.87%
-13.81%
15.19%
55.72%
15.29%
-15.59%
10.24%
56.65%
17.52%
-15.91%
5.91%
61.34%
16.84%
-40%
-20%
0%
20%
40%
60%
80%
100%
Δ|v*|/Δ|v*total|(%)
Non linearity
Unrecovered 48h
Thixotropy
Heating

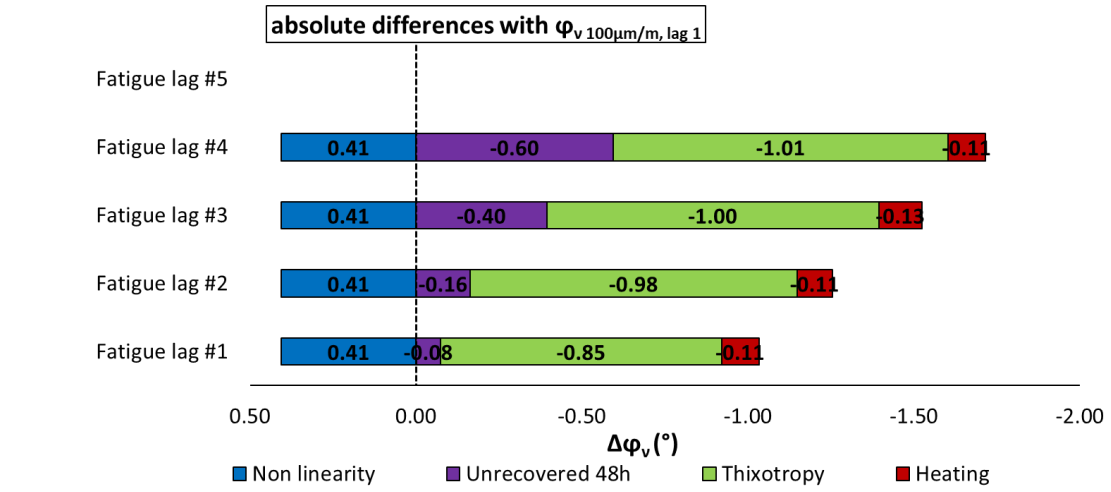

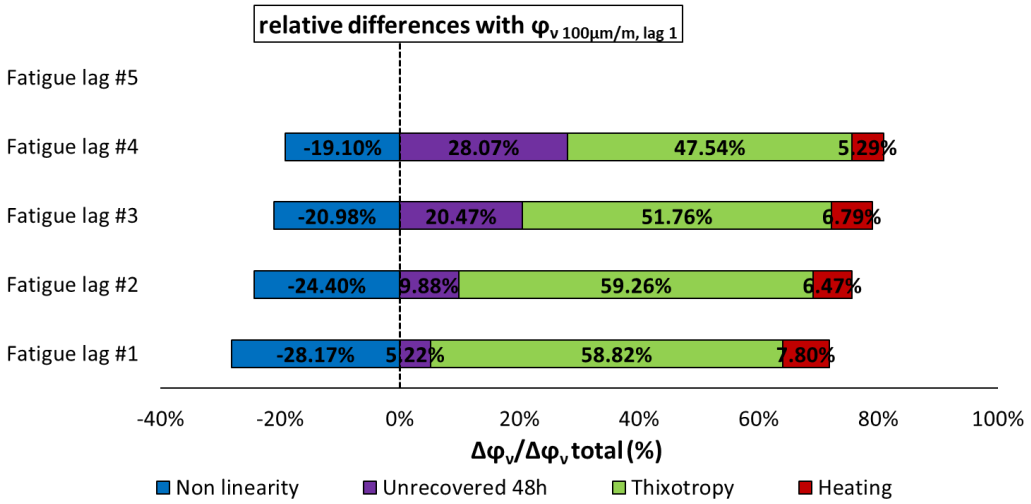

3.1.91. Quantification of different absolute and relative contributions to |E*|, φ_E, |ν*| and φ_ν evolutions for mix 40/60 – 6, calculated using the envelope line for the first fatigue lag.

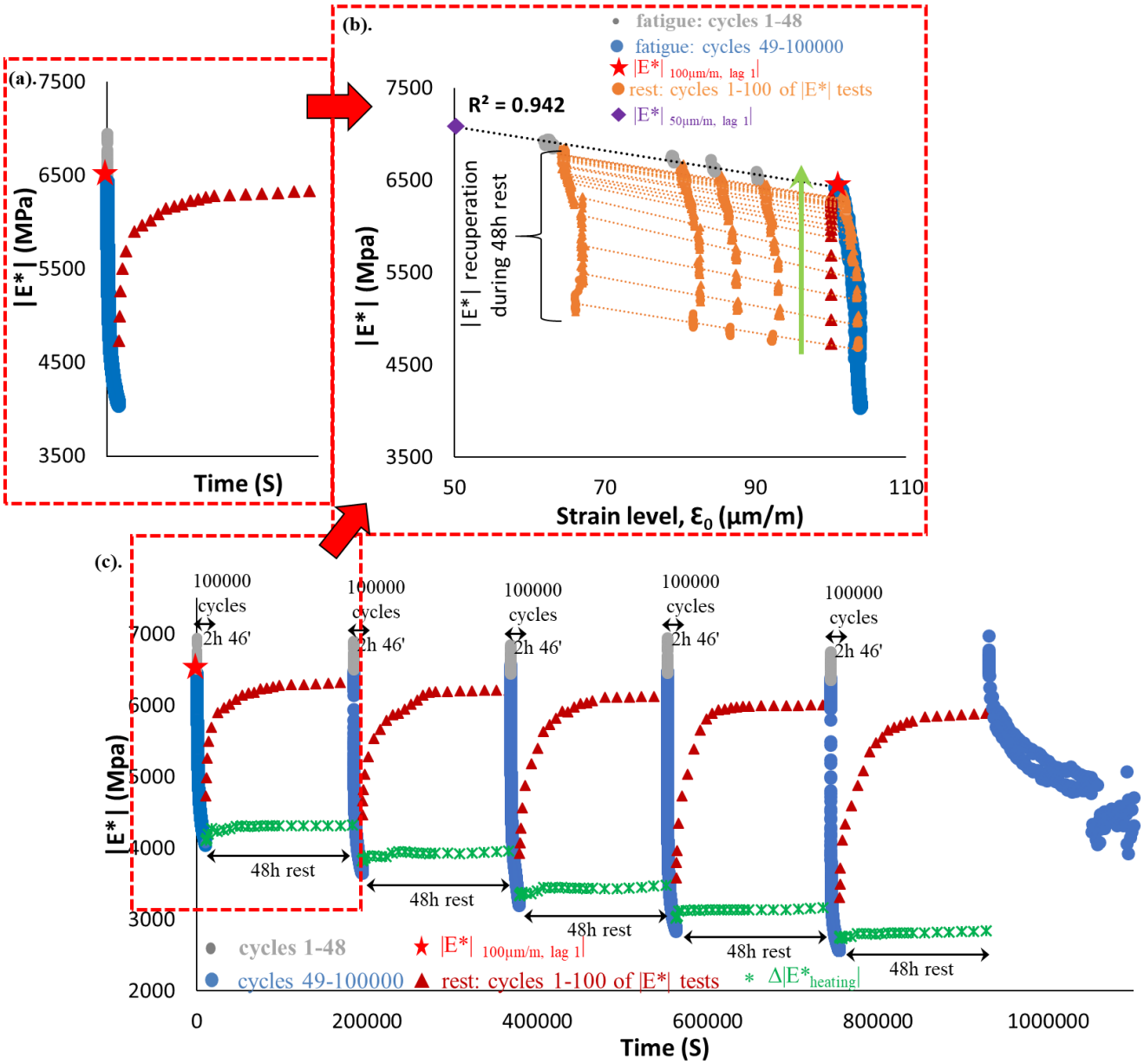

3.1.92. PFRT results obtained for mix 40/60 – 8: (a) |E*| as a function of time during the first fatigue lag and rest period (b) |E*| as a function of applied strain amplitude during the first fatigue lags and the short complex modulus tests performed within its following rest periods; (c) |E*| as a function of time during the five fatigue lags and rest periods [Red stars indicate values of |E*| estimated at 100 µm/m at the beginning of fatigue lag, green asterisk shows values of $\Delta|E^*_{heating}|$ as influence of self-heating and brown triangles indicate values of |E*| estimated at 100 µm/m for each short complex modulus test during rest (all these values were obtained using non-linearity envelopes, as shown in (b) for the first fatigue lag and rest period)].

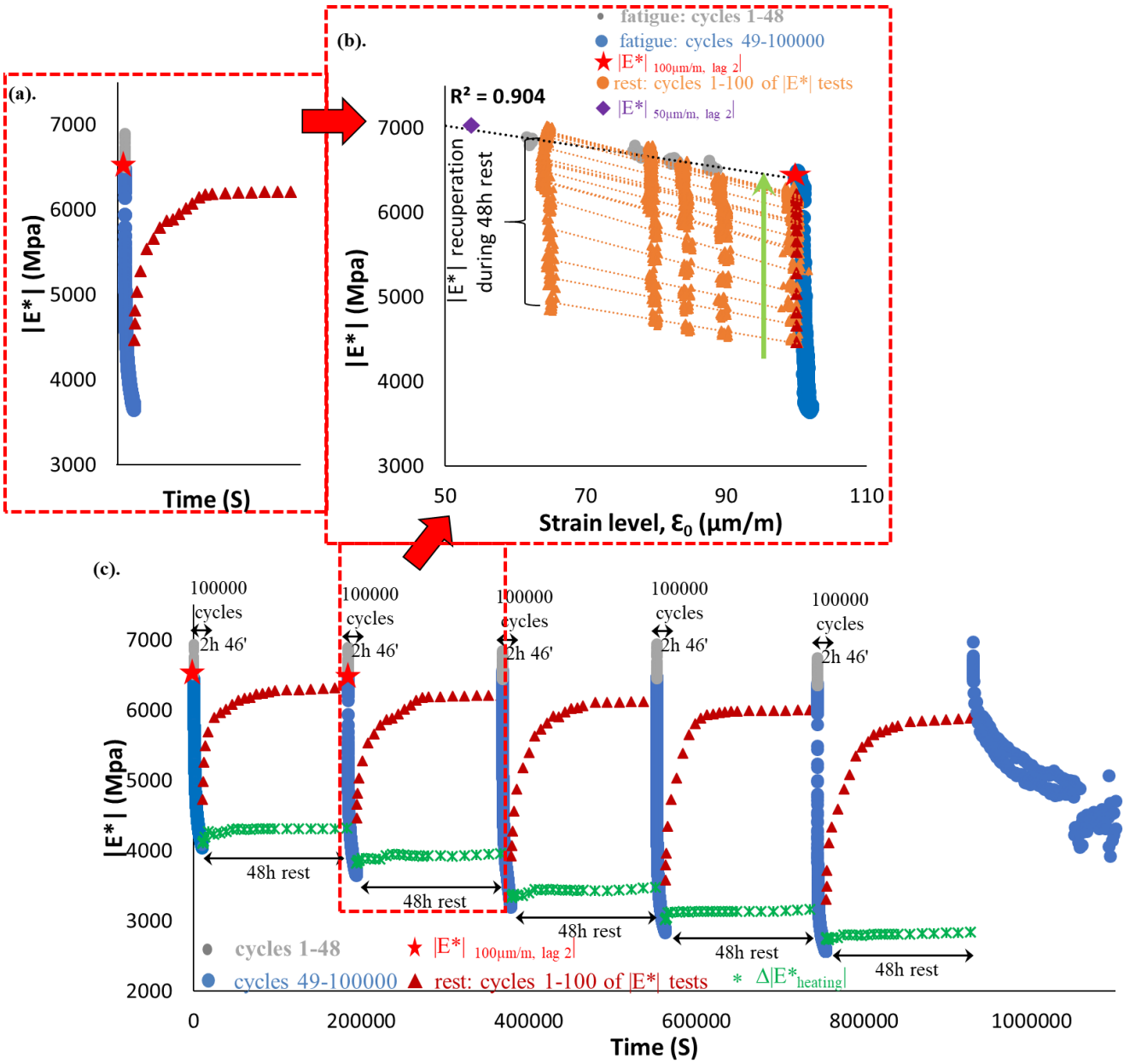

3.1.93. PFRT results obtained for mix 40/60 – 8: (a) |E*| as a function of time during the second fatigue lag and rest period (b) |E*| as a function of applied strain amplitude during the second fatigue lags and the short complex modulus tests performed within its following rest periods; (c) |E*| as a function of time during the five fatigue lags and rest periods [Red stars indicate values of |E*| estimated at 100 µm/m at the beginning of fatigue lag, green asterisk shows values of $\Delta|E^*_{heating}|$ as influence of self-heating and brown triangles indicate values of |E*| estimated at 100 µm/m for each short complex modulus test during rest (all these values were obtained using non-linearity envelopes, as shown in (b) for the first fatigue lag and rest period)].

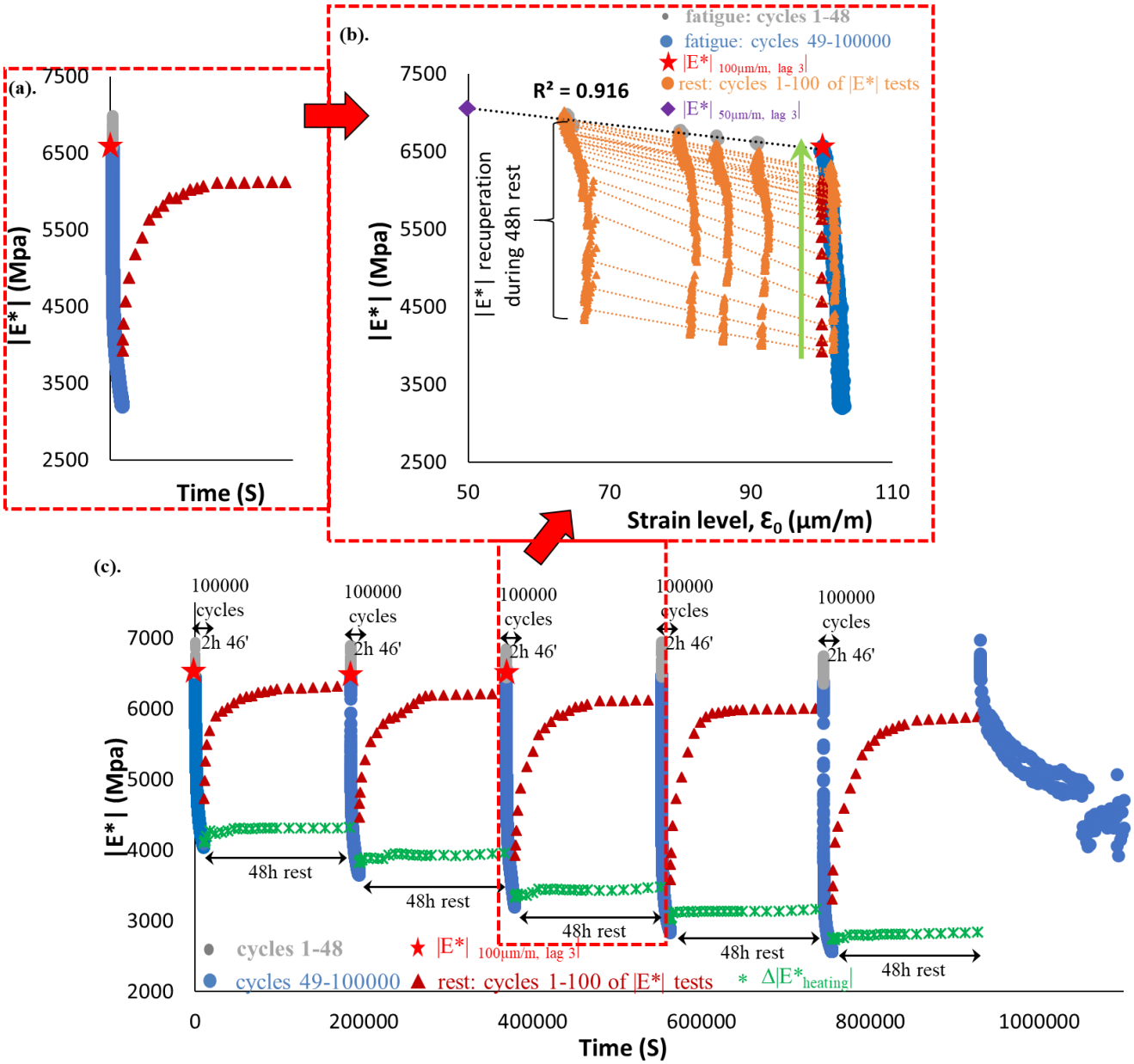

3.1.94. PFRT results obtained for mix 40/60 – 8: (a) |E*| as a function of time during the third fatigue lag and rest period (b) |E*| as a function of applied strain amplitude during the thirdfatigue lags and the short complex modulus tests performed within its following rest periods; (c) |E*| as a function of time during the five fatigue lags and rest periods [Red stars indicate values of |E*| estimated at 100 µm/m at the beginning of fatigue lag, green asterisk shows values of $\Delta|E^*_{heating}|$ as influence of self-heating and brown triangles indicate values of |E*| estimated at 100 µm/m for each short complex modulus test during rest (all these values were obtained using non-linearity envelopes, as shown in (b) for the first fatigue lag and rest period)].

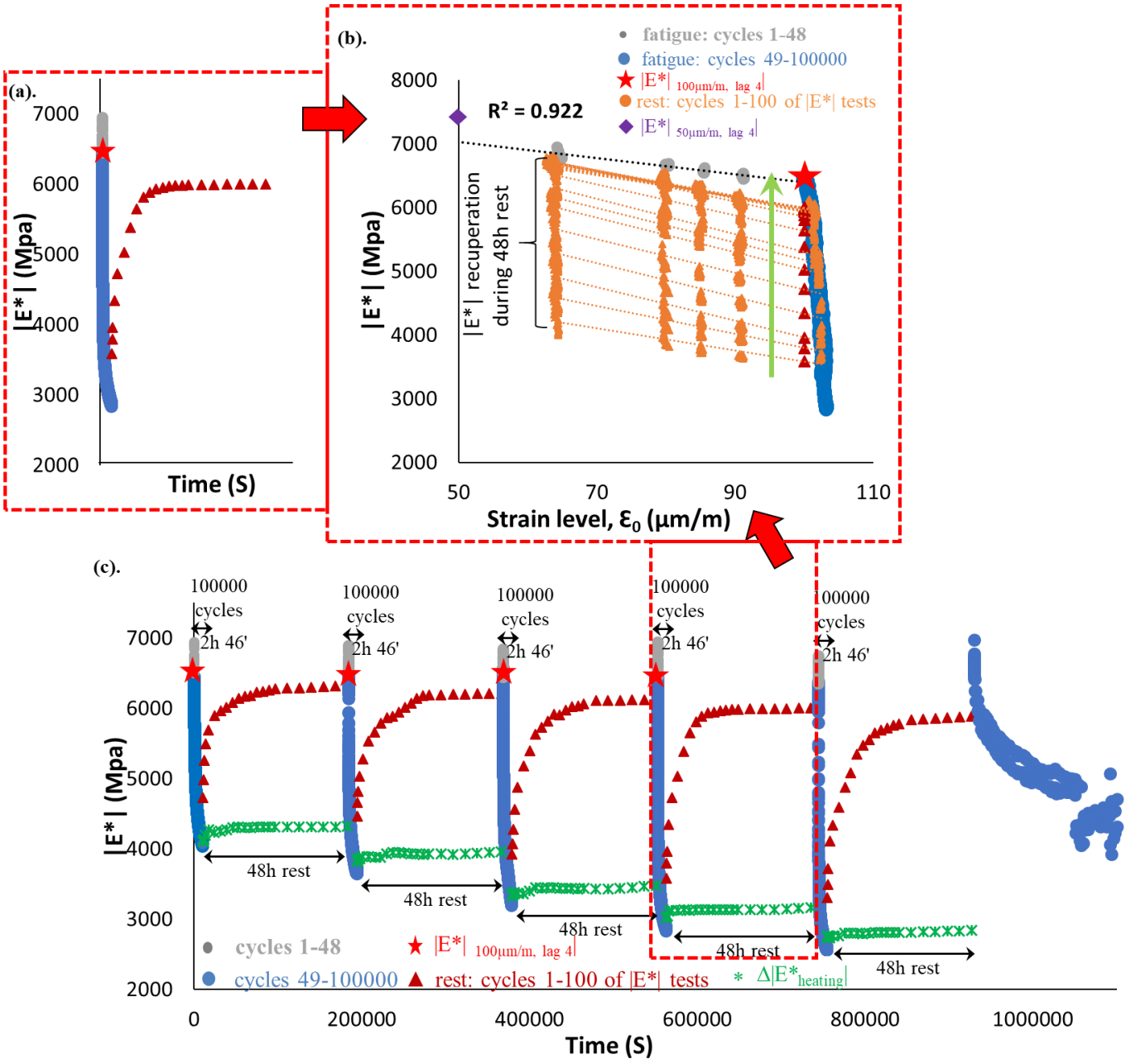

3.1.95. PFRT results obtained for mix 40/60 – 8: (a) |E*| as a function of time during the fourth fatigue lag and rest period (b) |E*| as a function of applied strain amplitude during the fourth fatigue lags and the short complex modulus tests performed within its following rest periods; (c) |E*| as a function of time during the five fatigue lags and rest periods [Red stars indicate values of |E*| estimated at 100 µm/m at the beginning of fatigue lag, green asterisk shows values of $\Delta|E^*_{heating}|$ as influence of self-heating and brown triangles indicate values of |E*| estimated at 100 µm/m for each short complex modulus test during rest (all these values were obtained using non-linearity envelopes, as shown in (b) for the first fatigue lag and rest period)].

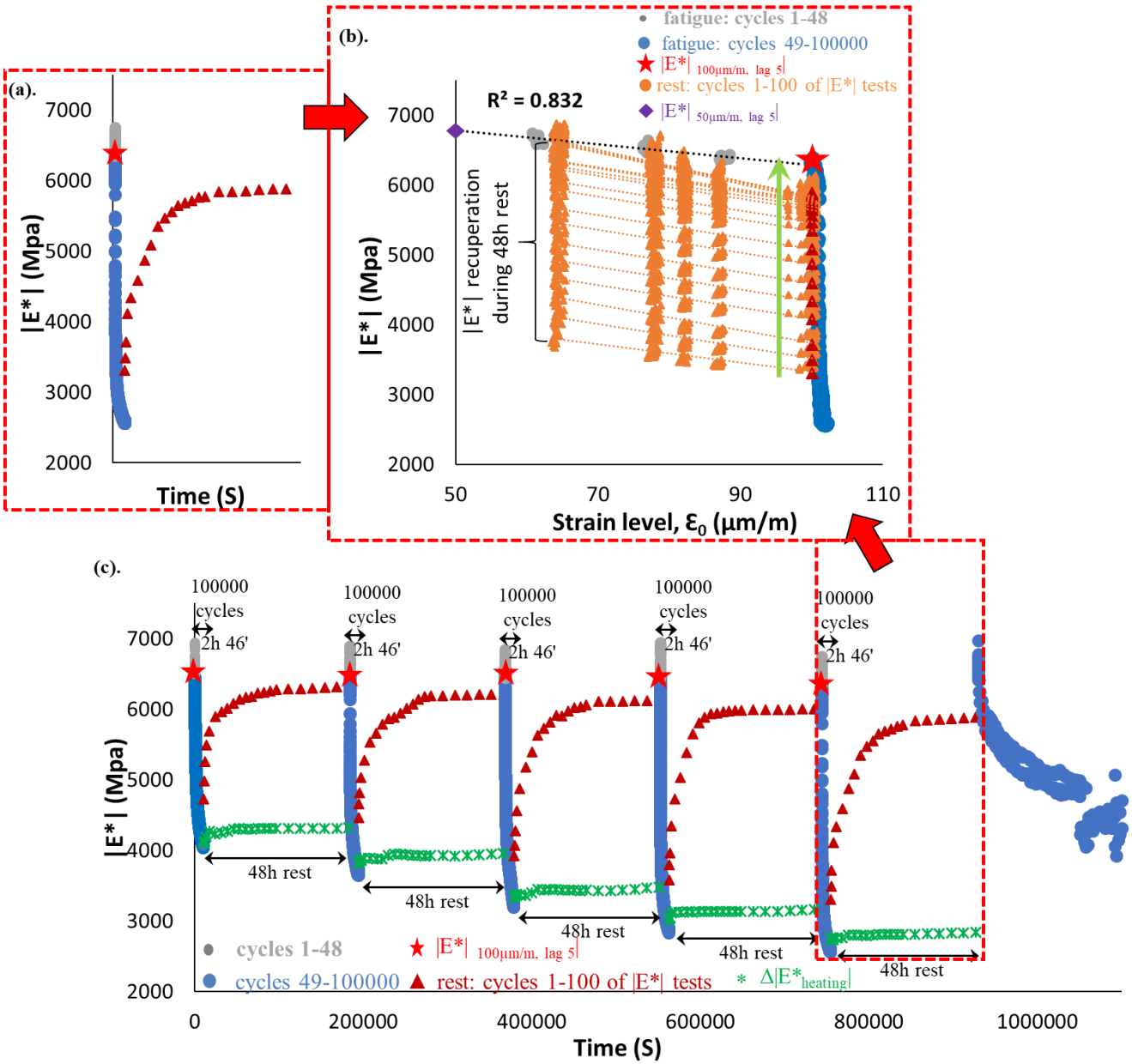

3.1.96. PFRT results obtained for mix 40/60 – 8: (a) |E*| as a function of time during the first fatigue lag and rest period (b) |E*| as a function of applied strain amplitude during the first fatigue lags and the short complex modulus tests performed within its following rest periods; (c) |E*| as a function of time during the five fatigue lags and rest periods [Red stars indicate values of |E*| estimated at 100 µm/m at the beginning of fatigue lag, green asterisk shows values of $\Delta|E^*_{heating}|$ as influence of self-heating and brown triangles indicate values of |E*| estimated at 100 µm/m for each short complex modulus test during rest (all these values were obtained using non-linearity envelopes, as shown in (b) for the first fatigue lag and rest period)].

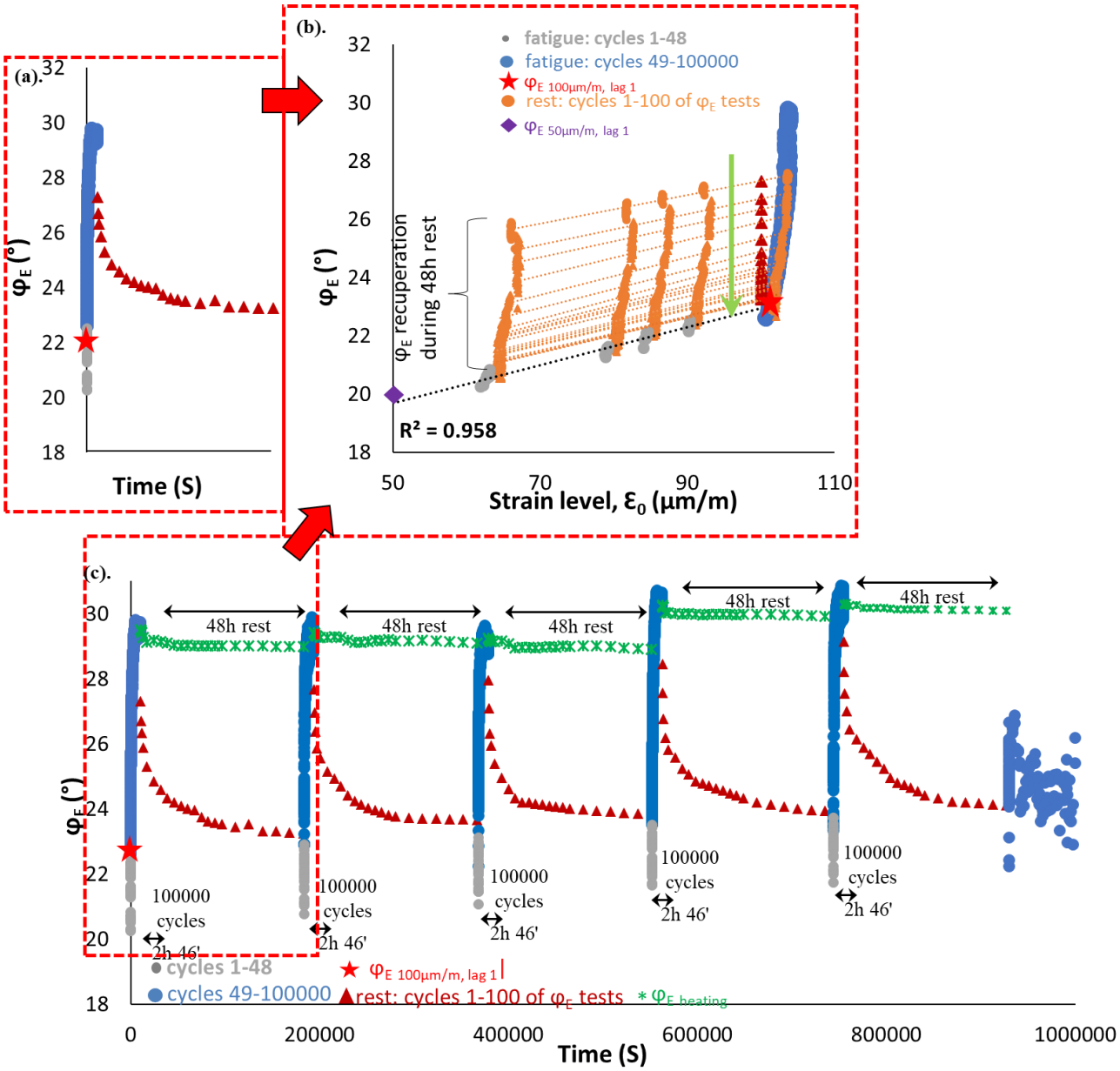

3.1.97. PFRT results obtained for mix 40/60 – 8: (a) φ_E as a function of time during the first fatigue lag and rest period (b) φ_E as a function of applied strain amplitude during the first fatigue lags and the short complex modulus tests performed within its following rest periods; (c) φ_E as a function of time during the five fatigue lags and rest periods (Red stars indicate values of φ_E estimated at 100 μm/m at the beginning of fatigue lag, green asterisk shows values of $\Delta\varphi_{E\ heating}$ as influence of self-heating and brown triangles indicate values of φ_E estimated at 100 μm/m for each short complex modulus test during rest (all these values were obtained using non-linearity envelopes, as shown in (b) for the first fatigue lag and rest period).

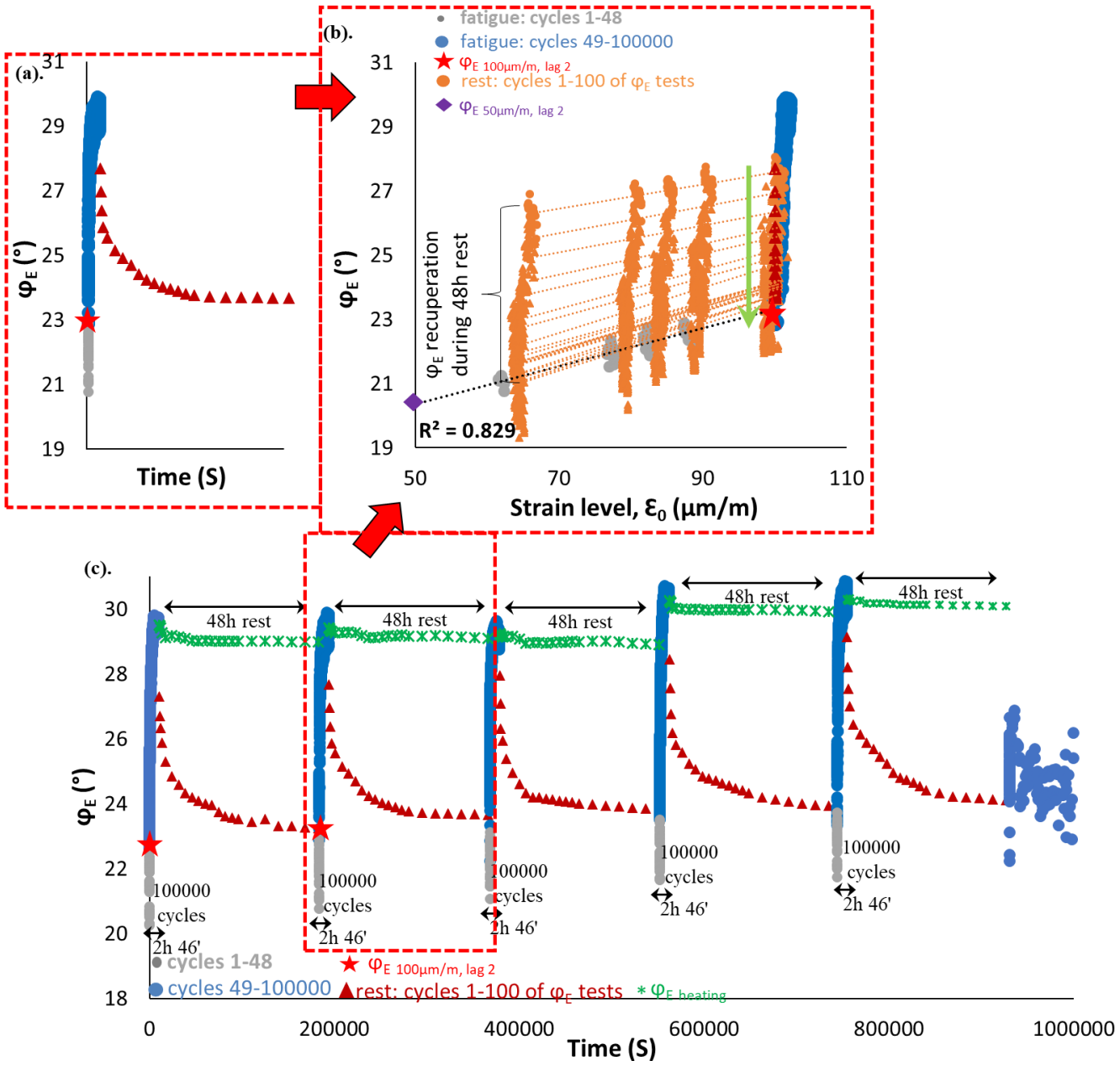

3.1.98. PFRT results obtained for mix 40/60 – 8: (a) φ_E as a function of time during the first fatigue lag and rest period (b) φ_E as a function of applied strain amplitude during the first fatigue lags and the short complex modulus tests performed within its following rest periods; (c) φ_E as a function of time during the five fatigue lags and rest periods (Red stars indicate values of φ_E estimated at 100 µm/m at the beginning of fatigue lag, green asterisk shows values of $\Delta\varphi_{E\ heating}$ as influence of self-heating and brown triangles indicate values of φ_E estimated at 100 µm/m for each short complex modulus test during rest (all these values were obtained using non-linearity envelopes, as shown in (b) for the first fatigue lag and rest period).

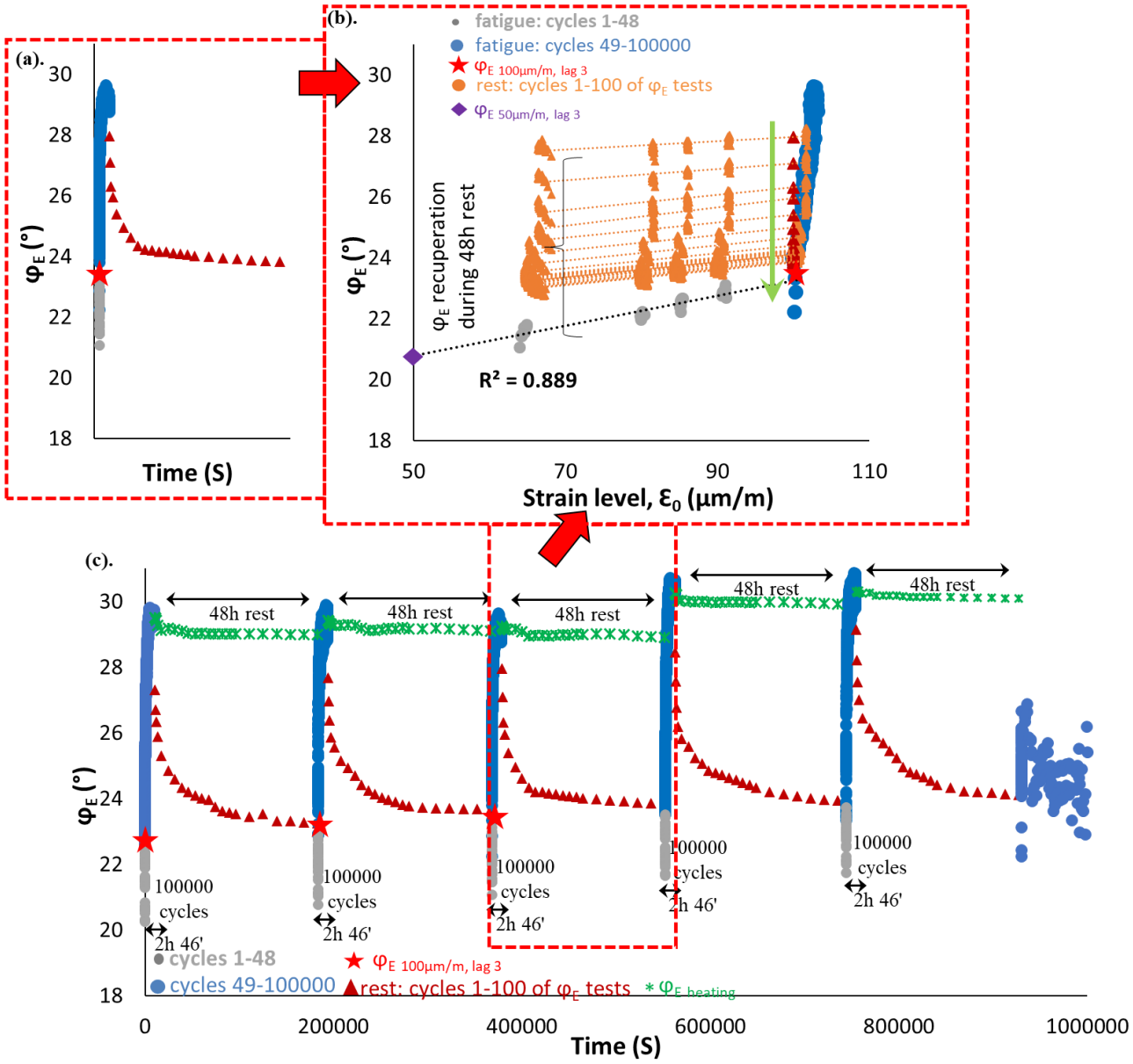

3.1.99. PFRT results obtained for mix 40/60 – 8: (a) φ_E as a function of time during the third fatigue lag and rest period (b) φ_E as a function of applied strain amplitude during the third fatigue lags and the short complex modulus tests performed within its following rest periods; (c) φ_E as a function of time during the five fatigue lags and rest periods (Red stars indicate values of φ_E estimated at 100 µm/m at the beginning of fatigue lag, green asterisk shows values of $\Delta\varphi_{E\ heating}$ as influence of self-heating and brown triangles indicate values of φ_E estimated at 100 µm/m for each short complex modulus test during rest (all these values were obtained using non-linearity envelopes, as shown in (b) for the first fatigue lag and rest period).

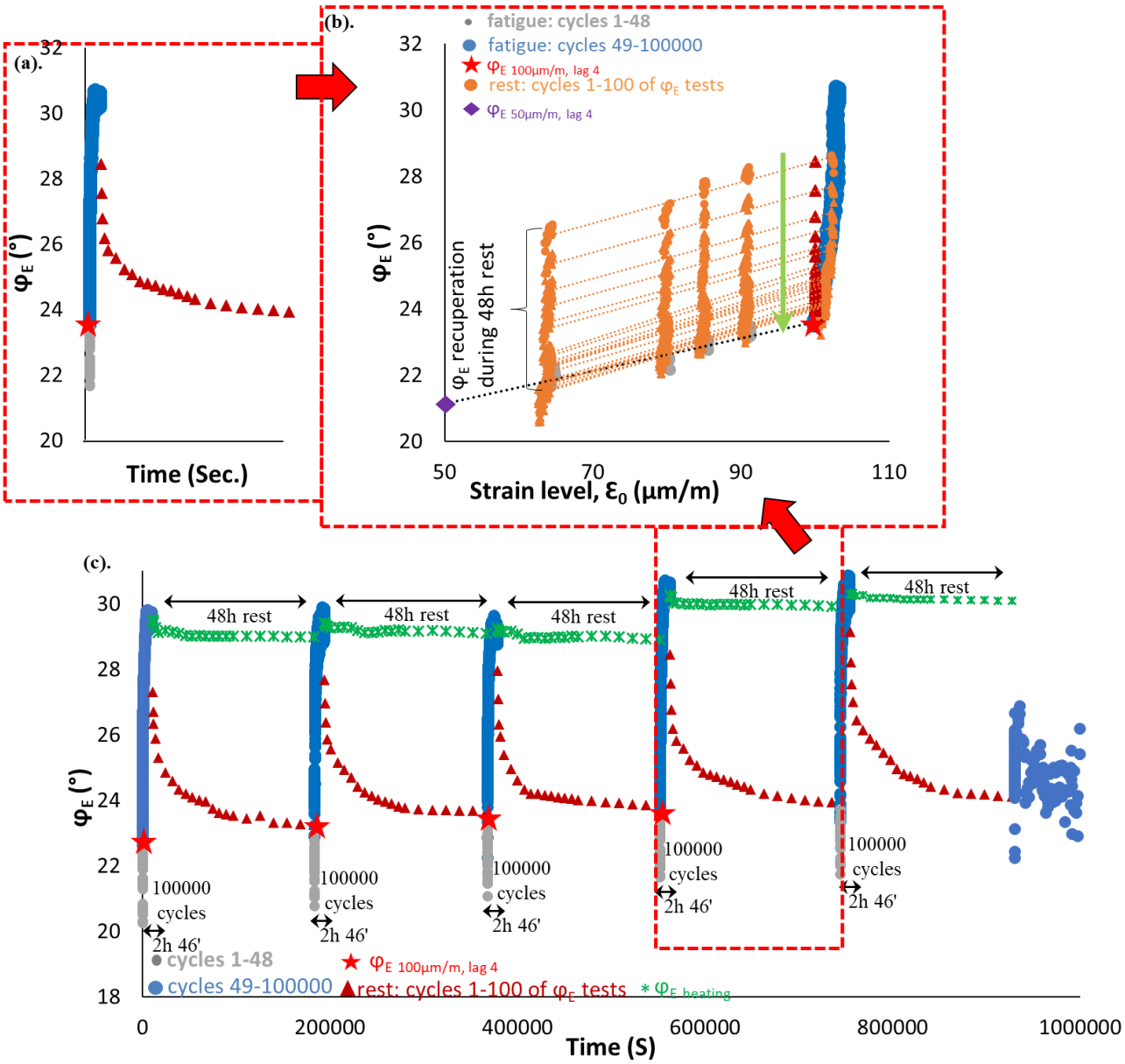

3.1.100. PFRT results obtained for mix 40/60 – 8: (a) φ_E as a function of time during the fourth fatigue lag and rest period (b) φ_E as a function of applied strain amplitude during the fourth fatigue lags and the short complex modulus tests performed within its following rest periods; (c) φ_E as a function of time during the five fatigue lags and rest periods (Red stars indicate values of φ_E estimated at 100 µm/m at the beginning of fatigue lag, green asterisk shows values of $\Delta\varphi_{E\ heating}$ as influence of self-heating and brown triangles indicate values of φ_E estimated at 100 µm/m for each short complex modulus test during rest (all these values were obtained using non-linearity envelopes, as shown in (b) for the first fatigue lag and rest period).

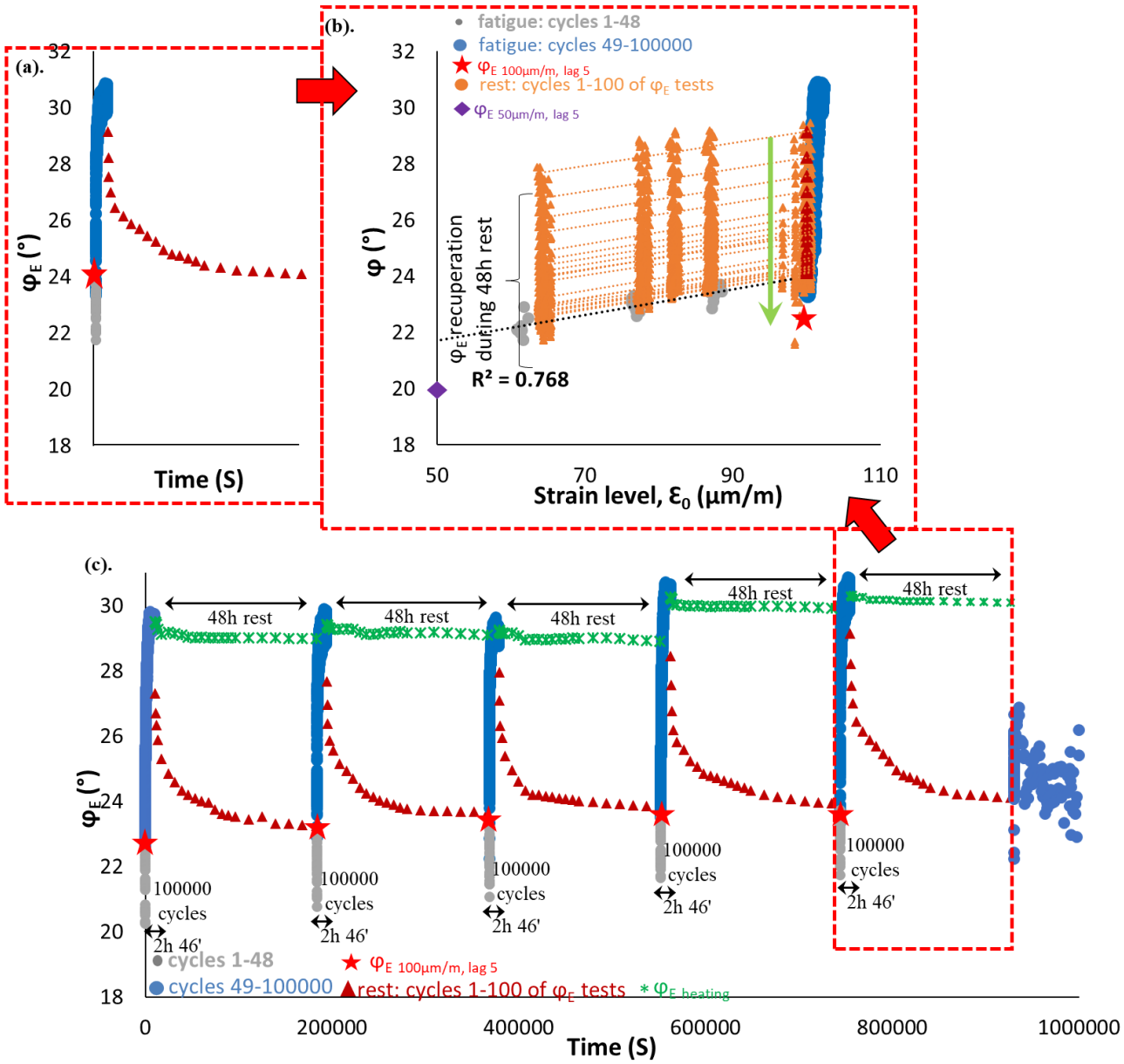

3.1.101. PFRT results obtained for mix 40/60 – 8: (a) φ_E as a function of time during the fifth fatigue lag and rest period (b) φ_E as a function of applied strain amplitude during the fifth fatigue lags and the short complex modulus tests performed within its following rest periods; (c) φ_E as a function of time during the five fatigue lags and rest periods (Red stars indicate values of φ_E estimated at 100 µm/m at the beginning of fatigue lag, green asterisk shows values of $\Delta\varphi_{E\ heating}$ as influence of self-heating and brown triangles indicate values of φ_E estimated at 100 µm/m for each short complex modulus test during rest (all these values were obtained using non-linearity envelopes, as shown in (b) for the first fatigue lag and rest period).

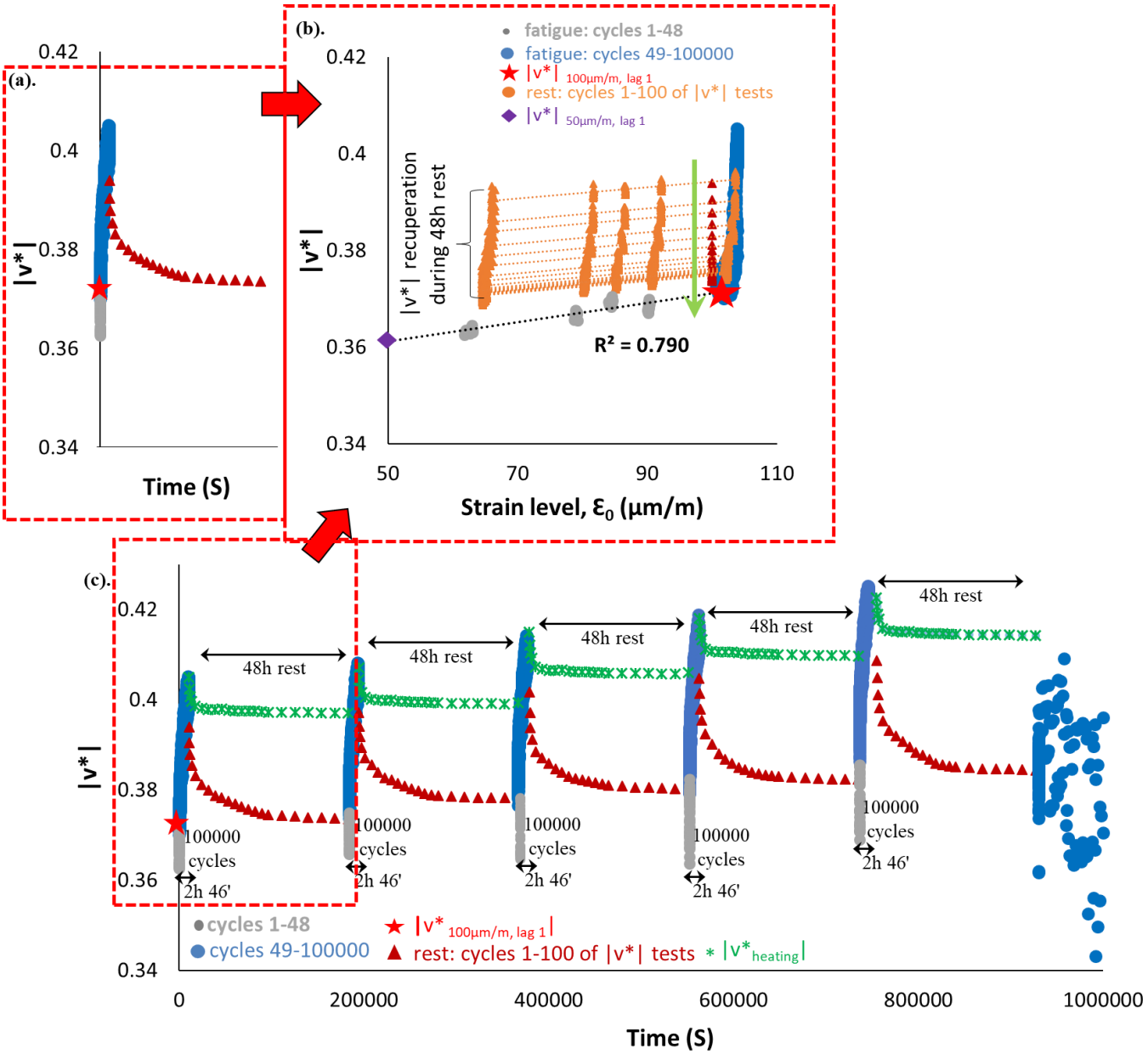

3.1.102. PFRT results obtained for mix 40/60 – 8: (a) |v*| as a function of time during the first fatigue lag and rest period (b) |v*| as a function of applied strain amplitude during the first fatigue lags and the short complex modulus tests performed within its following rest periods; (c) |v*| as a function of time during the five fatigue lags and rest periods [Red stars indicate values of |E*| estimated at 100 µm/m at the beginning of fatigue lag, green asterisk shows values of $\Delta|E^*_{heating}|$ as influence of self-heating and brown triangles indicate values of |v*| estimated at 100 µm/m for each short complex modulus test during rest (all these values were obtained using non-linearity envelopes, as shown in (b) for the first fatigue lag and rest period)].

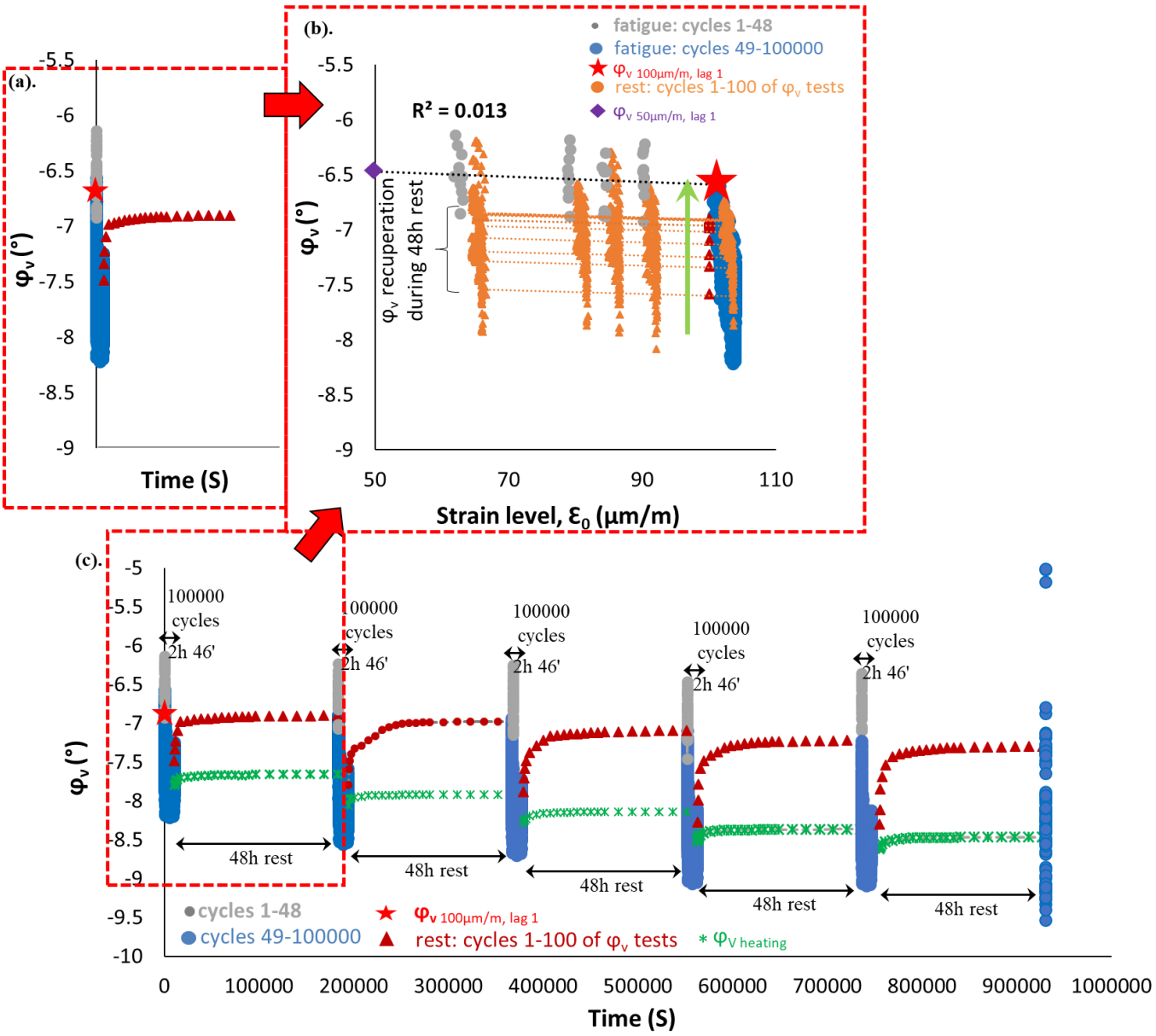

3.1.103. PFRT results obtained for mix 40/60 – 8: (a) φ_E as a function of time during the first fatigue lag and rest period (b) φ_E as a function of applied strain amplitude during the first fatigue lags and the short complex modulus tests performed within its following rest periods; (c) φ_E as a function of time during the five fatigue lags and rest periods (Red stars indicate values of φ_E estimated at 100 µm/m at the beginning of fatigue lag, green asterisk shows values of $\Delta\varphi_{E\ heating}$ as influence of self-heating and brown triangles indicate values of φ_E estimated at 100 µm/m for each short complex modulus test during rest (all these values were obtained using non-linearity envelopes, as shown in (b) for the first fatigue lag and rest period).

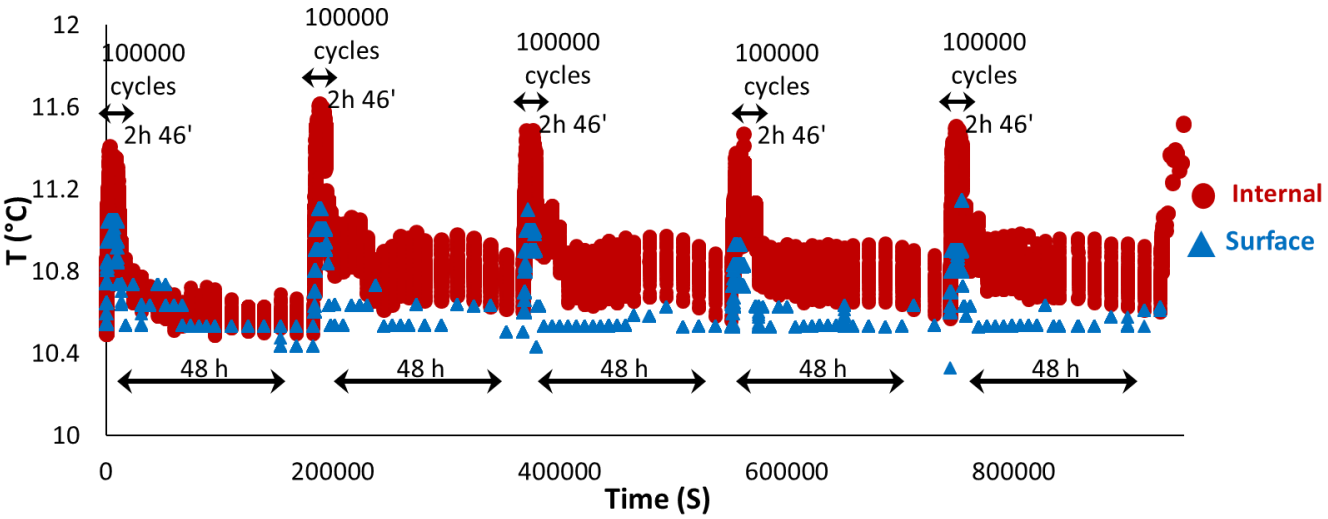

3.1.104. PFRT results obtained for mix 40/60 – 8: internal and surface temperature evolution during fatigue lags and recovery periods.

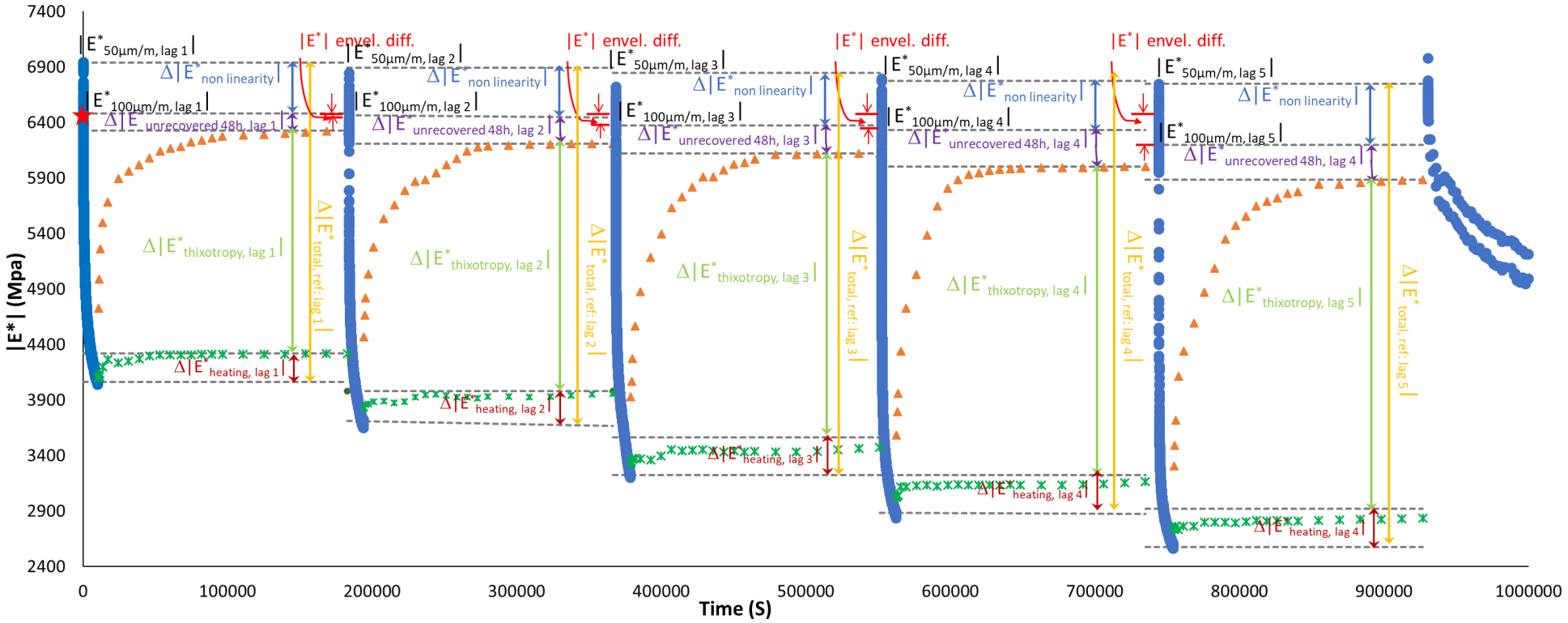
7400
6900
6400
5900
5400
4900
4400
3900
3400
2900
2400
|E*| (Mpa)
0
100000
200000
300000
400000
500000
600000
700000
800000
900000
1000000
Time (S)
|E*| envel. diff.
|E*| envel. diff.
|E*| envel. diff.
|E*| envel. diff.
|E*50µm/m, lag 1|
|E*100µm/m, lag 1|
Δ|E*non linearity|
Δ|E*unrecovered 48h, lag 1|
Δ|E*thixotropy, lag 1|
Δ|E*heating, lag 1|
Δ|E*total, ref: lag 1|
|E*50µm/m, lag 2|
|E*100µm/m, lag 2|
Δ|E*non linearity|
Δ|E*unrecovered 48h, lag 2|
Δ|E*thixotropy, lag 2|
Δ|E*heating, lag 2|
Δ|E*total, ref: lag 2|
|E*50µm/m, lag 3|
|E*100µm/m, lag 3|
Δ|E*non linearity|
Δ|E*unrecovered 48h, lag 3|
Δ|E*thixotropy, lag 3|
Δ|E*heating, lag 3|
Δ|E*total, ref: lag 3|
|E*50µm/m, lag 4|
|E*100µm/m, lag 4|
Δ|E*non linearity|
Δ|E*unrecovered 48h, lag 4|
Δ|E*thixotropy, lag 4|
Δ|E*heating, lag 4|
Δ|E*total, ref: lag 4|
|E*50µm/m, lag 5|
|E*100µm/m, lag 5|
Δ|E*non linearity|
Δ|E*unrecovered 48h, lag 4|
Δ|E*thixotropy, lag 5|
Δ|E*heating, lag 4|
Δ|E*total, ref: lag 5|

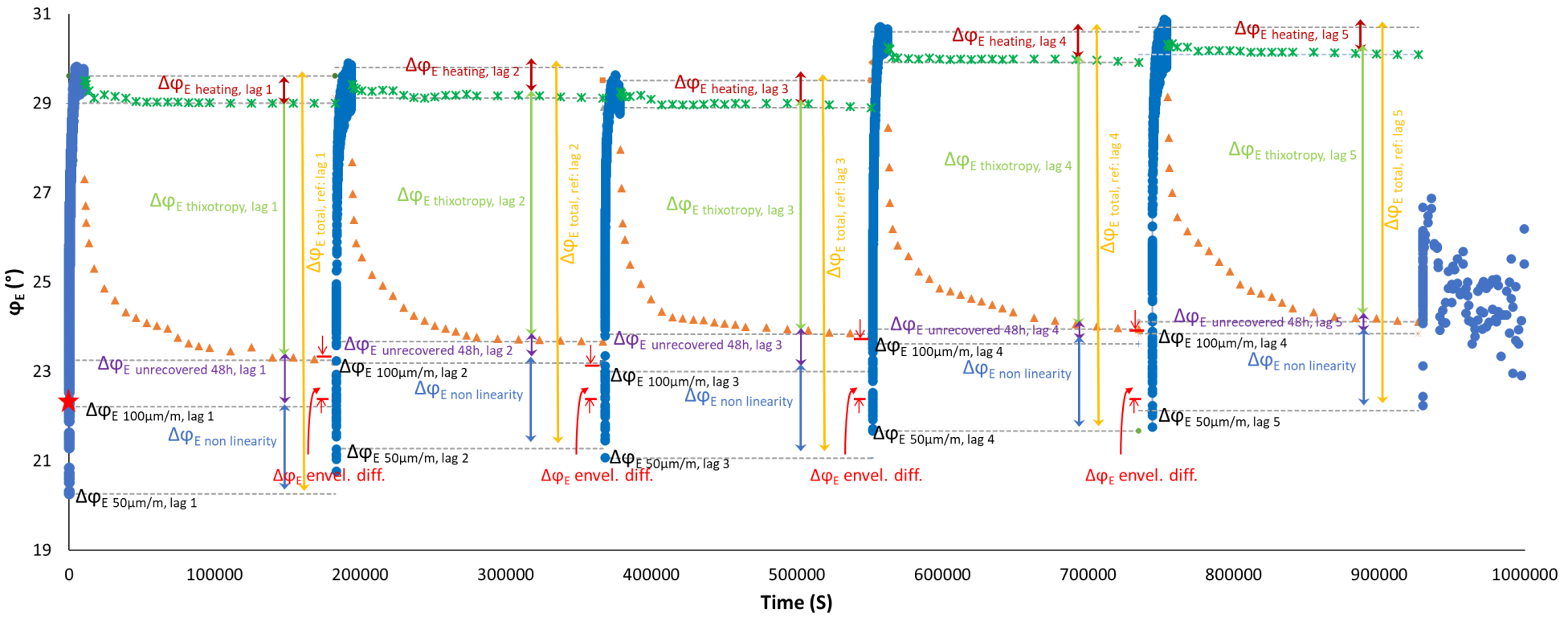
φE (°)
Time (S)
Δφ E heating, lag 1
Δφ E thixotropy, lag 1
Δφ E total, ref: lag 1
Δφ E unrecovered 48h, lag 1
Δφ E 100µm/m, lag 1
Δφ E non linearity
Δφ E 50µm/m, lag 1
Δφ E envel. diff.
Δφ E heating, lag 2
Δφ E thixotropy, lag 2
Δφ E total, ref: lag 2
Δφ E unrecovered 48h, lag 2
Δφ E 100µm/m, lag 2
Δφ E non linearity
Δφ E 50µm/m, lag 2
Δφ E envel. diff.
Δφ E heating, lag 3
Δφ E thixotropy, lag 3
Δφ E total, ref: lag 3
Δφ E unrecovered 48h, lag 3
Δφ E 100µm/m, lag 3
Δφ E non linearity
Δφ E 50µm/m, lag 3
Δφ E envel. diff.
Δφ E heating, lag 4
Δφ E thixotropy, lag 4
Δφ E total, ref: lag 4
Δφ E unrecovered 48h, lag 4
Δφ E 100µm/m, lag 4
Δφ E non linearity
Δφ E 50µm/m, lag 4
Δφ E envel. diff.
Δφ E heating, lag 5
Δφ E thixotropy, lag 5
Δφ E total, ref: lag 5
Δφ E unrecovered 48h, lag 5
Δφ E 100µm/m, lag 4
Δφ E non linearity
Δφ E 50µm/m, lag 5
Δφ E envel. diff.
31
29
27
25
23
21
19
0
100000
200000
300000
400000
500000
600000
700000
800000
900000
1000000

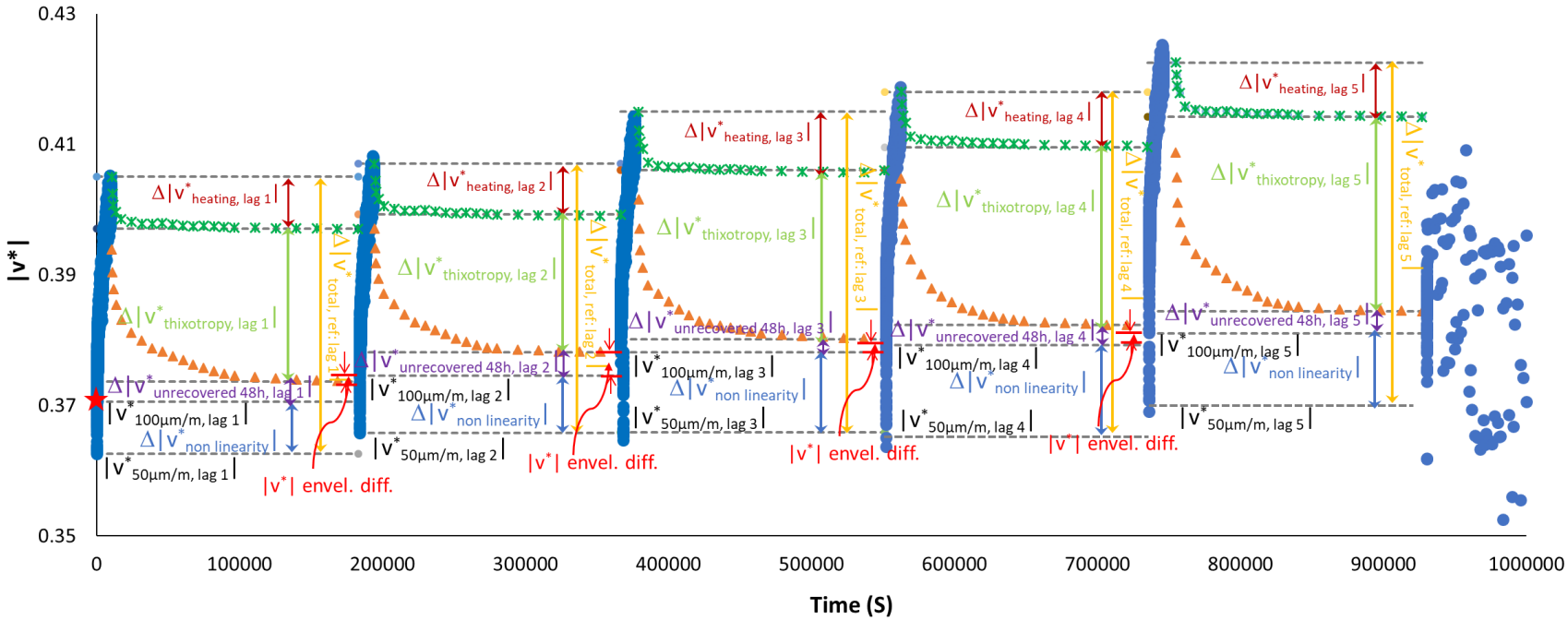
0.43
0.41
0.39
0.37
0.35
|v*|
0
100000
200000
300000
400000
500000
600000
700000
800000
900000
1000000
Time (S)
Δ|v*heating, lag 1|
Δ|v*thixotropy, lag 1|
Δ|v*unrecovered 48h, lag 1|
|v*100µm/m, lag 1|
Δ|v*non linearity|
|v*50µm/m, lag 1|
Δ|v*total, ref: lag 1|
|v*| envel. diff.
Δ|v*heating, lag 2|
Δ|v*thixotropy, lag 2|
Δ|v*unrecovered 48h, lag 2|
|v*100µm/m, lag 2|
Δ|v*non linearity|
|v*50µm/m, lag 2|
Δ|v*total, ref: lag 2|
|v*| envel. diff.
Δ|v*heating, lag 3|
Δ|v*thixotropy, lag 3|
Δ|v*unrecovered 48h, lag 3|
|v*100µm/m, lag 3|
Δ|v*non linearity|
|v*50µm/m, lag 3|
Δ|v*total, ref: lag 3|
|v*| envel. diff.
Δ|v*heating, lag 4|
Δ|v*thixotropy, lag 4|
Δ|v*unrecovered 48h, lag 4|
|v*100µm/m, lag 4|
Δ|v*non linearity|
|v*50µm/m, lag 4|
Δ|v*total, ref: lag 4|
|v*| envel. diff.
Δ|v*heating, lag 5|
Δ|v*thixotropy, lag 5|
Δ|v*unrecovered 48h, lag 5|
|v*100µm/m, lag 5|
Δ|v*non linearity|
|v*50µm/m, lag 5|
Δ|v*total, ref: lag 5|

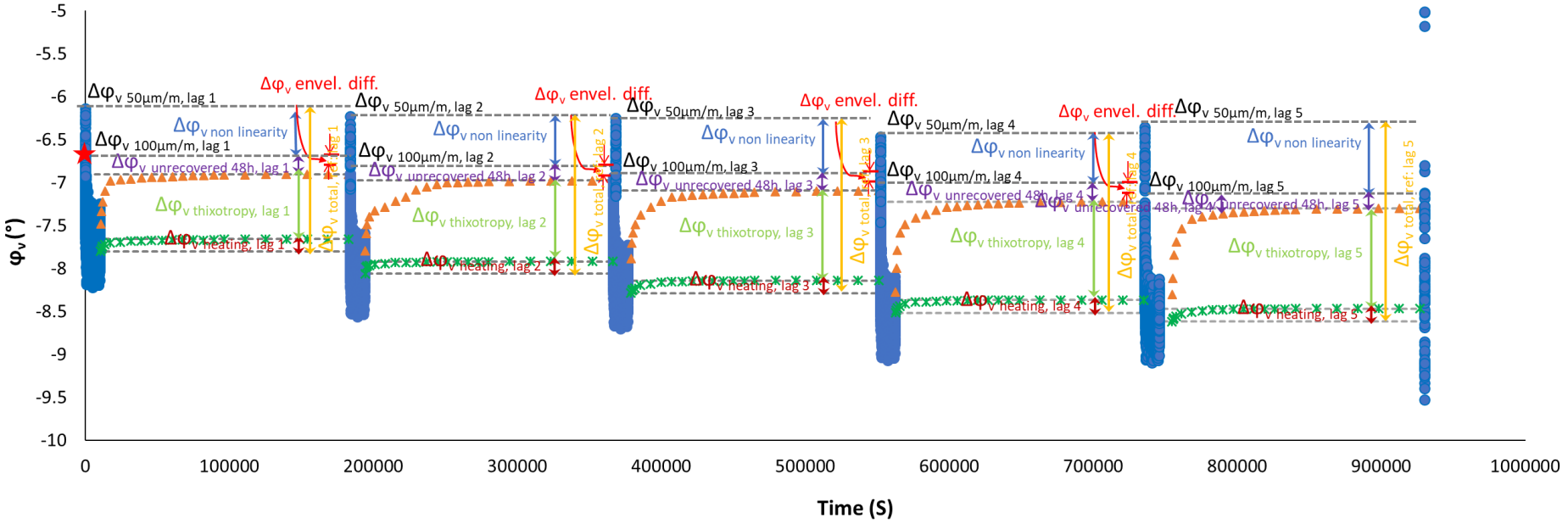

3.1.105. Quantification of different contributions |E*|, φ_E, |ν*| and φ_ν evolution, for the first two fatigue lags for mix 40/60 – 8: different envelope line is used for each fatigue lag.

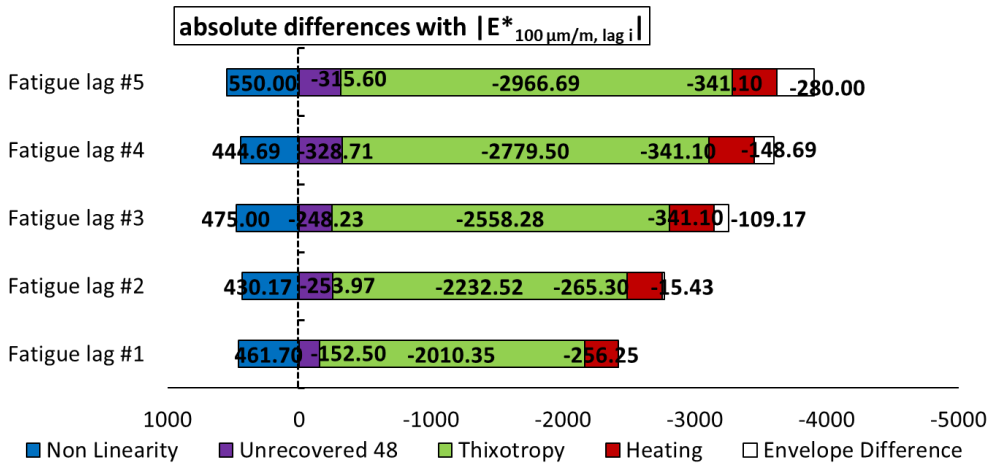
absolute differences with |E*100 µm/m, lag i|
Fatigue lag #5
Fatigue lag #4
Fatigue lag #3
Fatigue lag #2
Fatigue lag #1
550.00
-315.60
-2966.69
-341.10
-280.00
444.69
-328.71
-2779.50
-341.10
-148.69
475.00
-248.23
-2558.28
-341.10
-109.17
430.17
-253.97
-2232.52
-265.30
-15.43
461.70
-152.50
-2010.35
-256.25
1000
0
-1000
-2000
-3000
-4000
-5000
Non Linearity
Unrecovered 48
Thixotropy
Heating
Envelope Difference

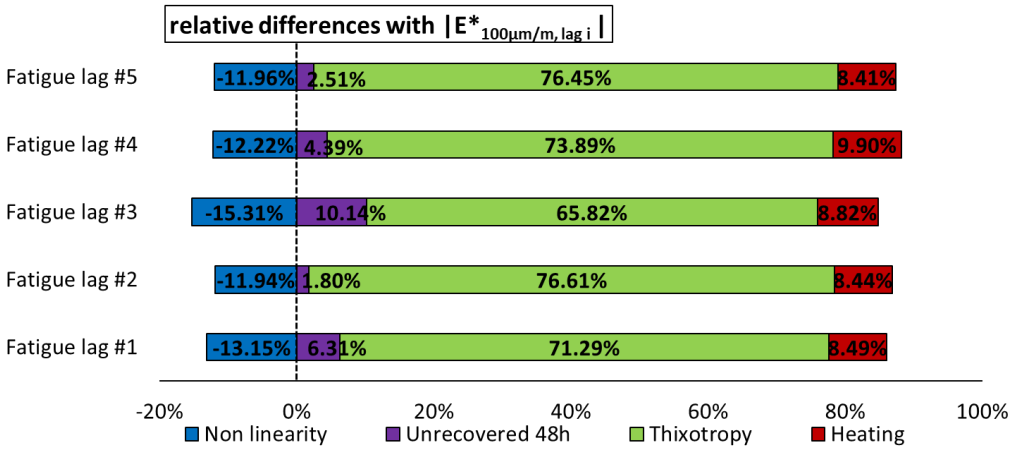
relative differences with |E*100µm/m, lag i|
Fatigue lag #5
Fatigue lag #4
Fatigue lag #3
Fatigue lag #2
Fatigue lag #1
-11.96%
2.51%
76.45%
8.41%
-12.22%
4.39%
73.89%
9.90%
-15.31%
10.14%
65.82%
8.82%
-11.94%
1.80%
76.61%
8.44%
-13.15%
6.31%
71.29%
8.49%
-20%
0%
20%
40%
60%
80%
100%
Non linearity
Unrecovered 48h
Thixotropy
Heating

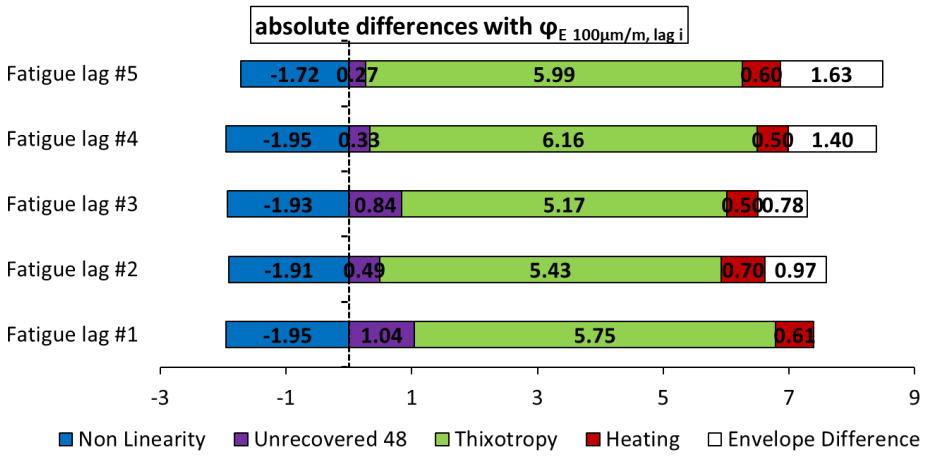
absolute differences with φE 100µm/m, lag i
Fatigue lag #5
Fatigue lag #4
Fatigue lag #3
Fatigue lag #2
Fatigue lag #1
-1.72
0.27
5.99
0.60
1.63
-1.95
0.33
6.16
0.50
1.40
-1.93
0.84
5.17
0.50
0.78
-1.91
0.49
5.43
0.70
0.97
-1.95
1.04
5.75
0.61
-3
-1
1
3
5
7
9
Non Linearity
Unrecovered 48
Thixotropy
Heating
Envelope Difference

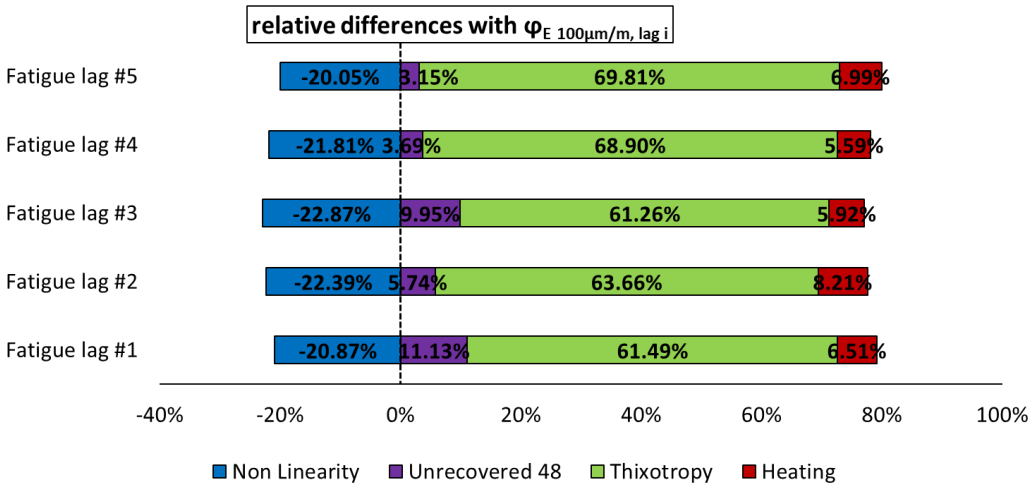
relative differences with φE 100µm/m, lag i
Fatigue lag #5
Fatigue lag #4
Fatigue lag #3
Fatigue lag #2
Fatigue lag #1
-20.05% 3.15% 69.81% 6.99%
-21.81% 3.69% 68.90% 5.59%
-22.87% 9.95% 61.26% 5.92%
-22.39% 5.74% 63.66% 8.21%
-20.87% 11.13% 61.49% 6.51%
-40% -20% 0% 20% 40% 60% 80% 100%
Non Linearity
Unrecovered 48
Thixotropy
Heating

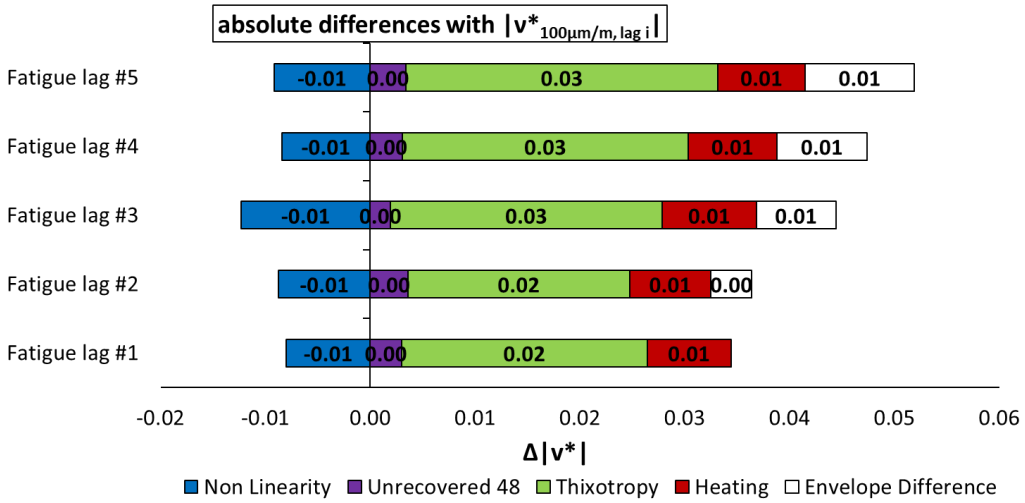
absolute differences with |v*100µm/m, lag i|
Fatigue lag #5
Fatigue lag #4
Fatigue lag #3
Fatigue lag #2
Fatigue lag #1
-0.01 0.00 0.03 0.01 0.01
-0.01 0.00 0.03 0.01 0.01
-0.01 0.00 0.03 0.01 0.01
-0.01 0.00 0.02 0.01 0.00
-0.01 0.00 0.02 0.01
-0.02 -0.01 0.00 0.01 0.02 0.03 0.04 0.05 0.06
Δ|v*|
Non Linearity
Unrecovered 48
Thixotropy
Heating
Envelope Difference

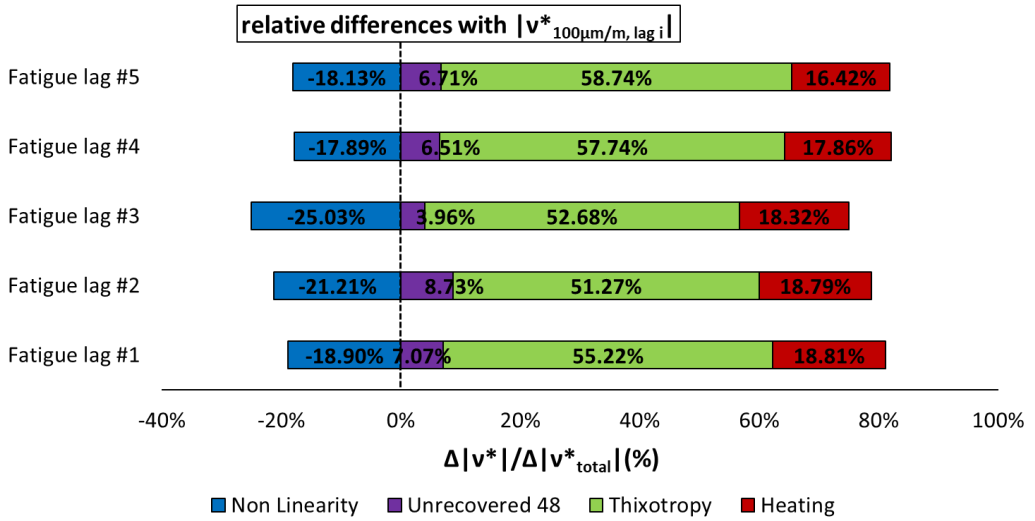
relative differences with |v*100µm/m, lag i|
Fatigue lag #5
Fatigue lag #4
Fatigue lag #3
Fatigue lag #2
Fatigue lag #1
-18.13% 6.71% 58.74% 16.42%
-17.89% 6.51% 57.74% 17.86%
-25.03% 3.96% 52.68% 18.32%
-21.21% 8.73% 51.27% 18.79%
-18.90% 7.07% 55.22% 18.81%
-40% -20% 0% 20% 40% 60% 80% 100%
Δ|v*|/Δ|v*total|(%)
Non Linearity
Unrecovered 48
Thixotropy
Heating

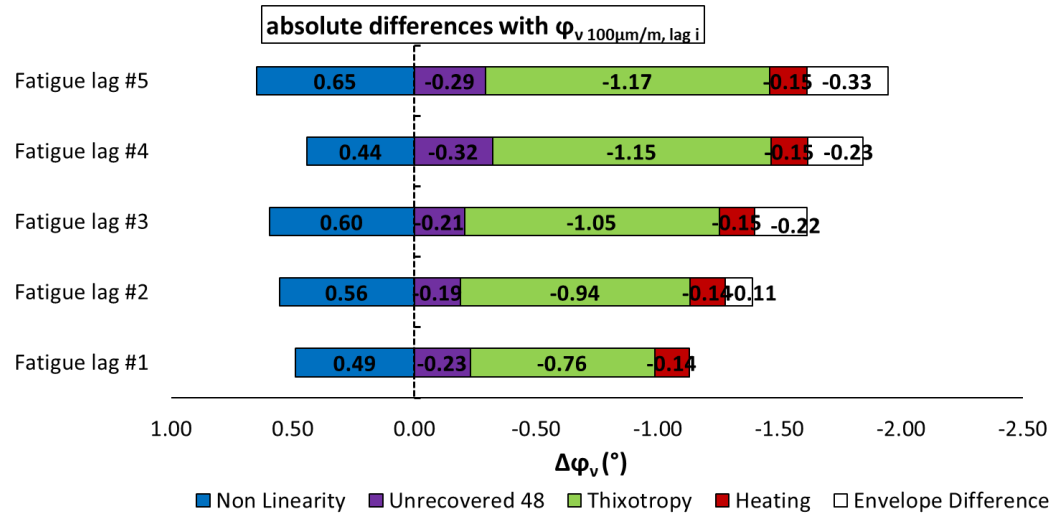

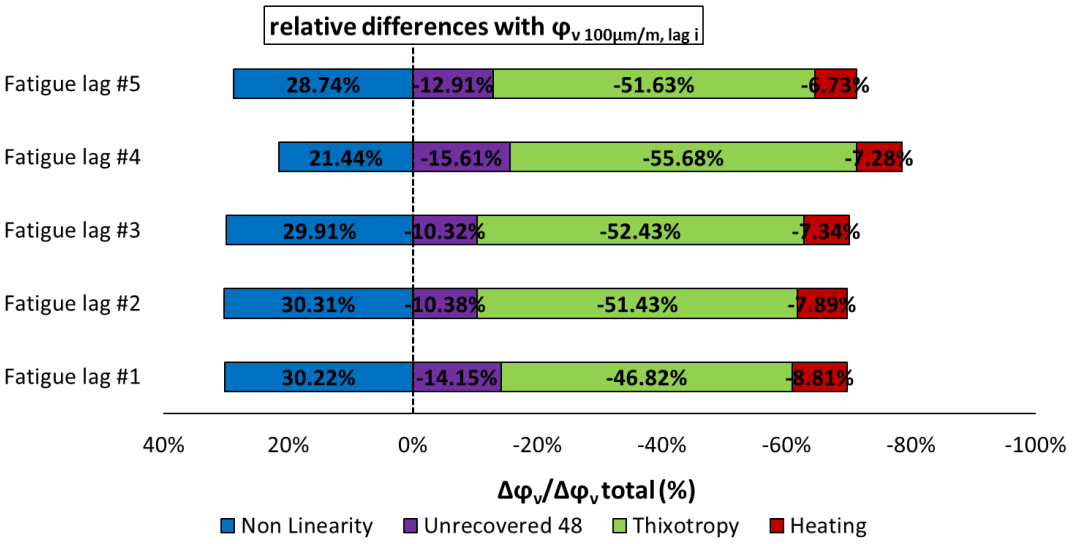

3.1.106. Quantification of different absolute and relative contributions to |E*|, φ_E, |ν*| and φ_ν evolutions for mix 40/60 – 8, calculated using a different envelope line for each fatigue lag.

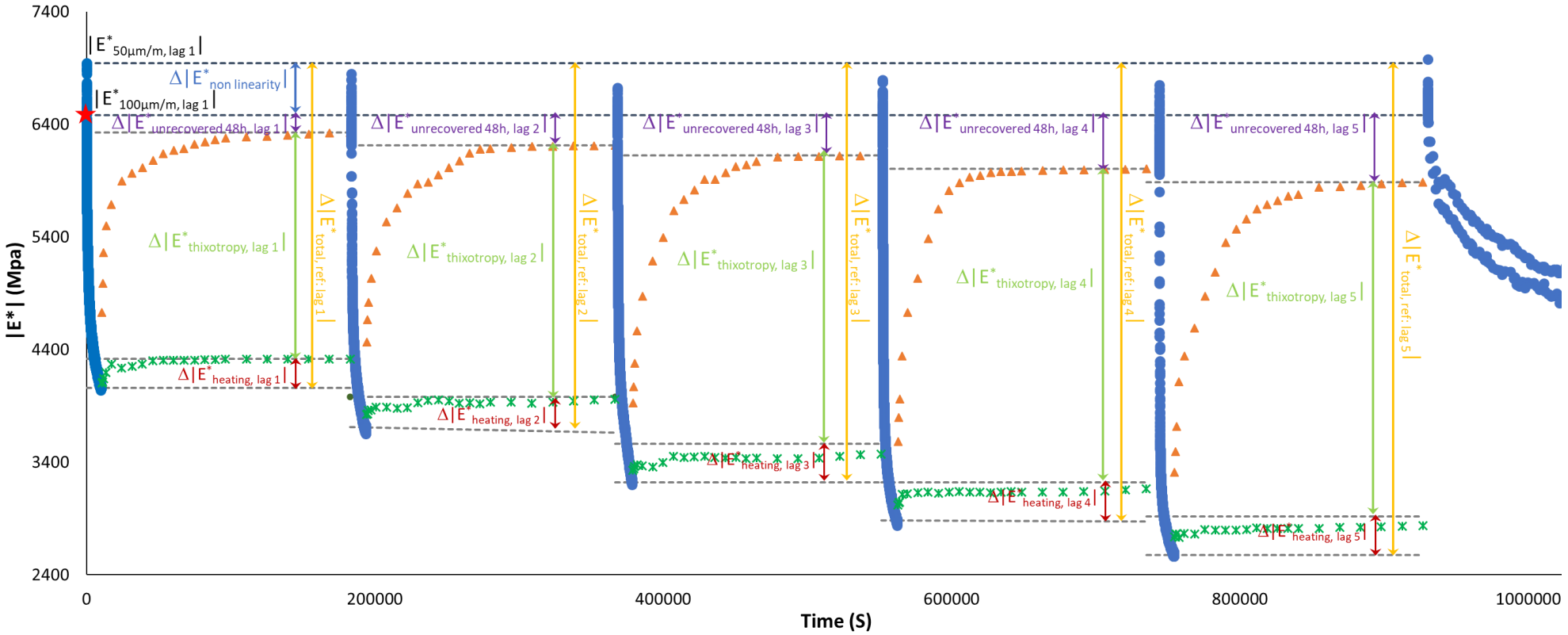
7400
6400
5400
4400
3400
2400
|E*| (Mpa)
0
200000
400000
600000
800000
1000000
Time (S)
|E*50µm/m, lag 1|
|E*100µm/m, lag 1|
Δ|E*non linearity|
Δ|E*unrecovered 48h, lag 1|
Δ|E*thixotropy, lag 1|
Δ|E*total, ref. lag 1|
Δ|E*heating, lag 1|
Δ|E*unrecovered 48h, lag 2|
Δ|E*thixotropy, lag 2|
Δ|E*total, ref. lag 2|
Δ|E*heating, lag 2|
Δ|E*unrecovered 48h, lag 3|
Δ|E*thixotropy, lag 3|
Δ|E*total, ref. lag 3|
Δ|E*heating, lag 3|
Δ|E*unrecovered 48h, lag 4|
Δ|E*thixotropy, lag 4|
Δ|E*total, ref. lag 4|
Δ|E*heating, lag 4|
Δ|E*unrecovered 48h, lag 5|
Δ|E*thixotropy, lag 5|
Δ|E*total, ref. lag 5|
Δ|E*heating, lag 5|

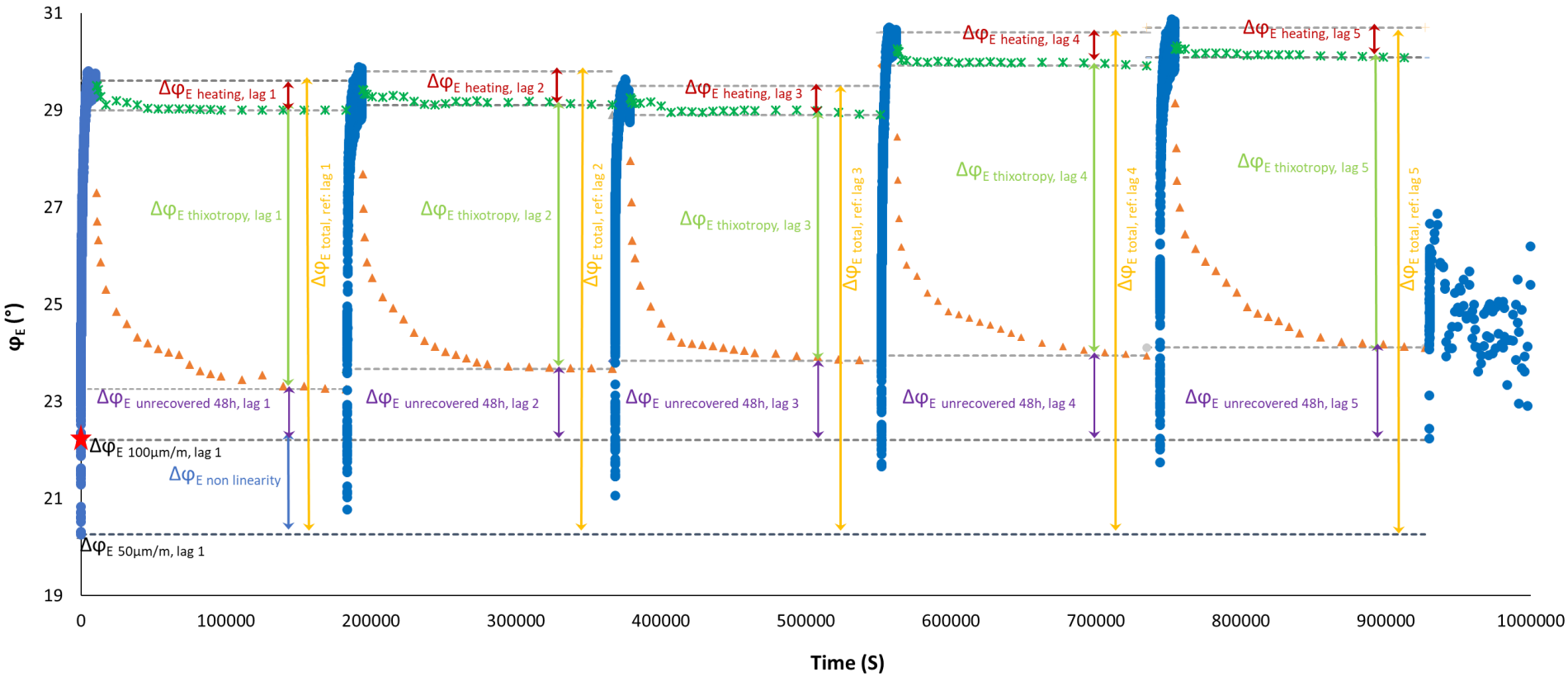
31
29
27
25
23
21
19
φE (°)
0
100000
200000
300000
400000
500000
600000
700000
800000
900000
1000000
Time (S)
Δφ E heating, lag 1
Δφ E heating, lag 2
Δφ E heating, lag 3
Δφ E heating, lag 4
Δφ E heating, lag 5
Δφ E thixotropy, lag 1
Δφ E thixotropy, lag 2
Δφ E thixotropy, lag 3
Δφ E thixotropy, lag 4
Δφ E thixotropy, lag 5
Δφ E total, ref: lag 1
Δφ E total, ref: lag 2
Δφ E total, ref: lag 3
Δφ E total, ref: lag 4
Δφ E total, ref: lag 5
Δφ E unrecovered 48h, lag 1
Δφ E unrecovered 48h, lag 2
Δφ E unrecovered 48h, lag 3
Δφ E unrecovered 48h, lag 4
Δφ E unrecovered 48h, lag 5
Δφ E 100µm/m, lag 1
Δφ E non linearity
Δφ E 50µm/m, lag 1

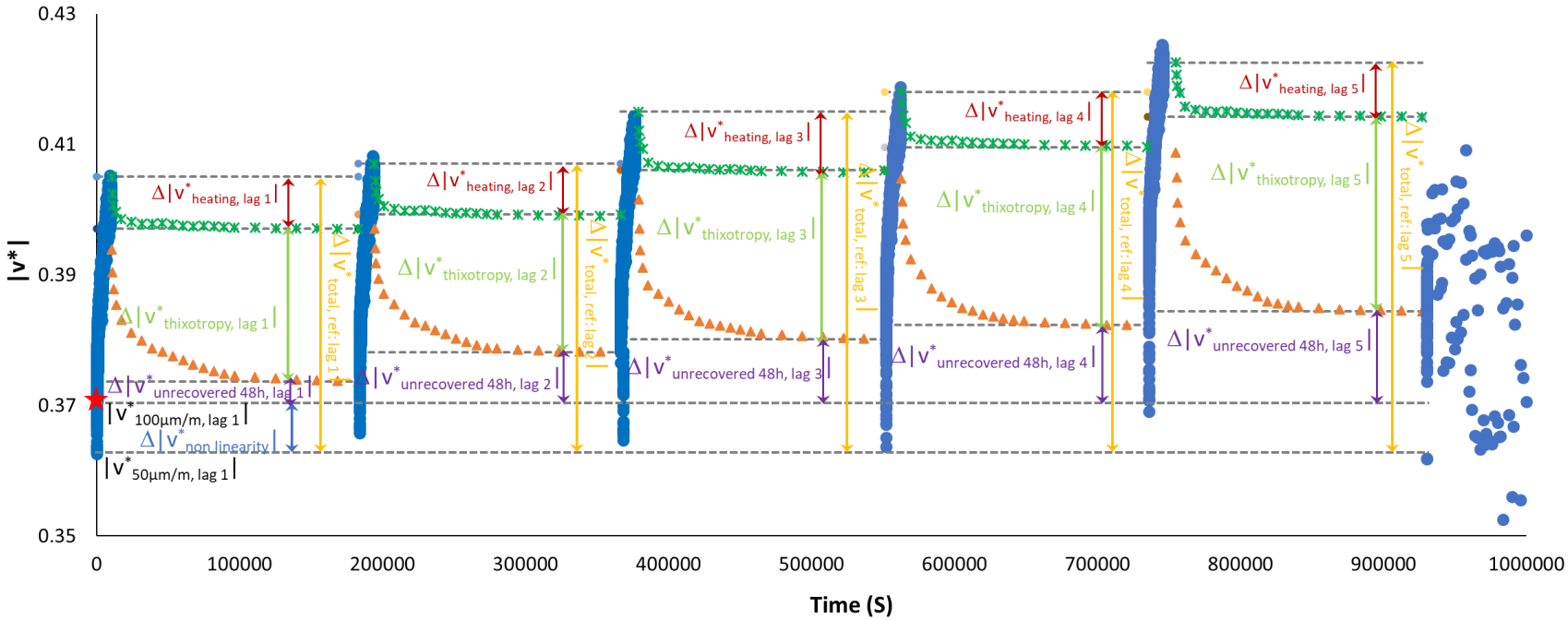
0.43
0.41
0.39
0.37
0.35
|v*|
0
100000
200000
300000
400000
500000
600000
700000
800000
900000
1000000
Time (S)
Δ|v*heating, lag 1|
Δ|v*thixotropy, lag 1|
Δ|v*unrecovered 48h, lag 1|
|v*100µm/m, lag 1|
Δ|v*non linearity|
|v*50µm/m, lag 1|
Δ|v*total, ref: lag 1|
Δ|v*heating, lag 2|
Δ|v*thixotropy, lag 2|
Δ|v*unrecovered 48h, lag 2|
Δ|v*total, ref: lag 2|
Δ|v*heating, lag 3|
Δ|v*thixotropy, lag 3|
Δ|v*unrecovered 48h, lag 3|
Δ|v*total, ref: lag 3|
Δ|v*heating, lag 4|
Δ|v*thixotropy, lag 4|
Δ|v*unrecovered 48h, lag 4|
Δ|v*total, ref: lag 4|
Δ|v*heating, lag 5|
Δ|v*thixotropy, lag 5|
Δ|v*unrecovered 48h, lag 5|
Δ|v*total, ref: lag 5|

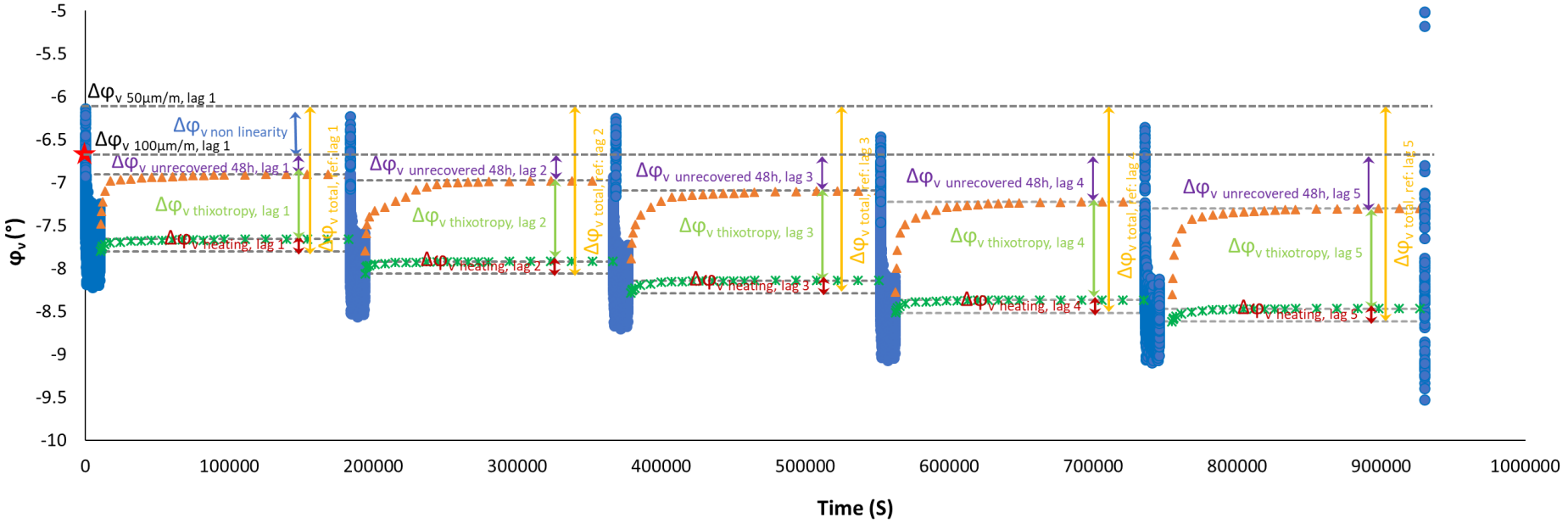

3.1.107. Quantification of different contributions to |E*|, φ_E, |v*| and φ_v evolution during five fatigue lags for mix 40/60 – 8: the envelope line of the first fatigue lag is used for all fatigue lags.

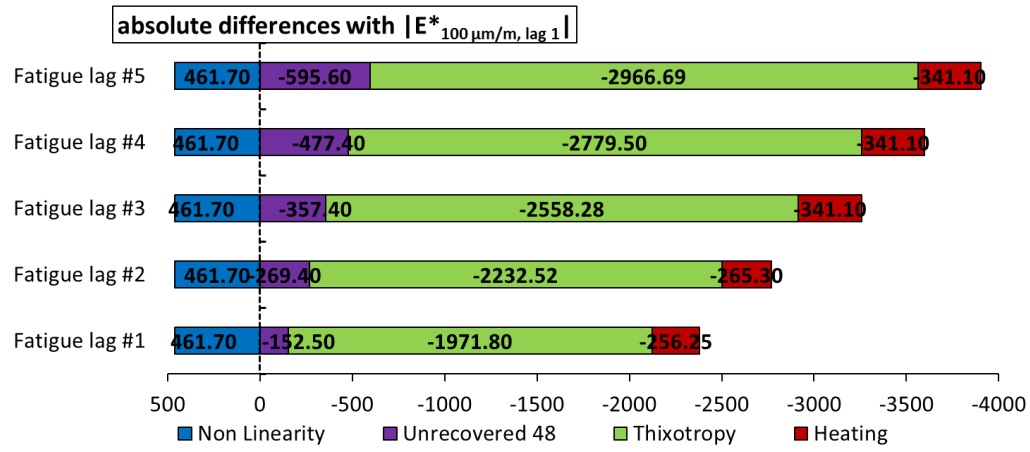
absolute differences with |E*100 µm/m, lag 1|
Fatigue lag #5
Fatigue lag #4
Fatigue lag #3
Fatigue lag #2
Fatigue lag #1
461.70
-595.60
-2966.69
-341.10
461.70
-477.40
-2779.50
-341.10
461.70
-357.40
-2558.28
-341.10
461.70
-269.40
-2232.52
-265.30
461.70
-152.50
-1971.80
-256.25
500
0
-500
-1000
-1500
-2000
-2500
-3000
-3500
-4000
Non Linearity
Unrecovered 48
Thixotropy
Heating

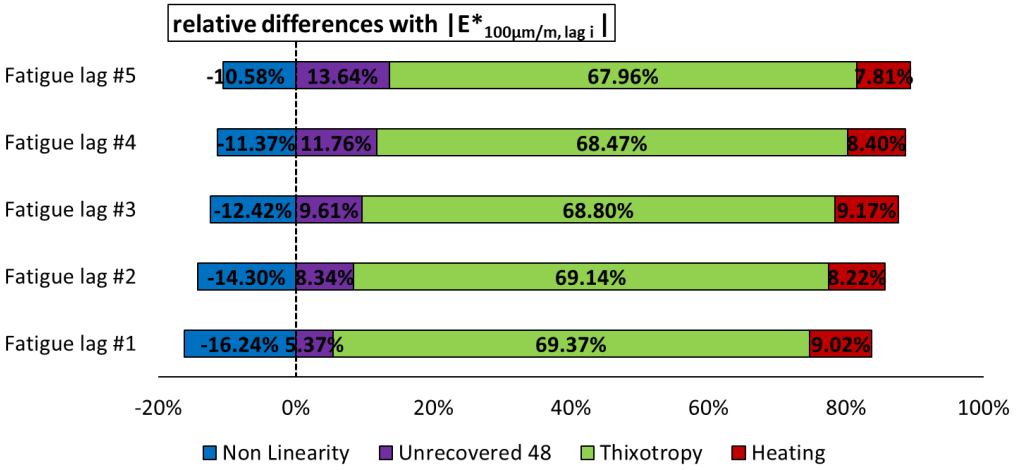
relative differences with |E*100µm/m, lag i|
Fatigue lag #5
Fatigue lag #4
Fatigue lag #3
Fatigue lag #2
Fatigue lag #1
-10.58%
13.64%
67.96%
7.81%
-11.37%
11.76%
68.47%
8.40%
-12.42%
9.61%
68.80%
9.17%
-14.30%
8.34%
69.14%
8.22%
-16.24%
5.37%
69.37%
9.02%
-20%
0%
20%
40%
60%
80%
100%
Non Linearity
Unrecovered 48
Thixotropy
Heating

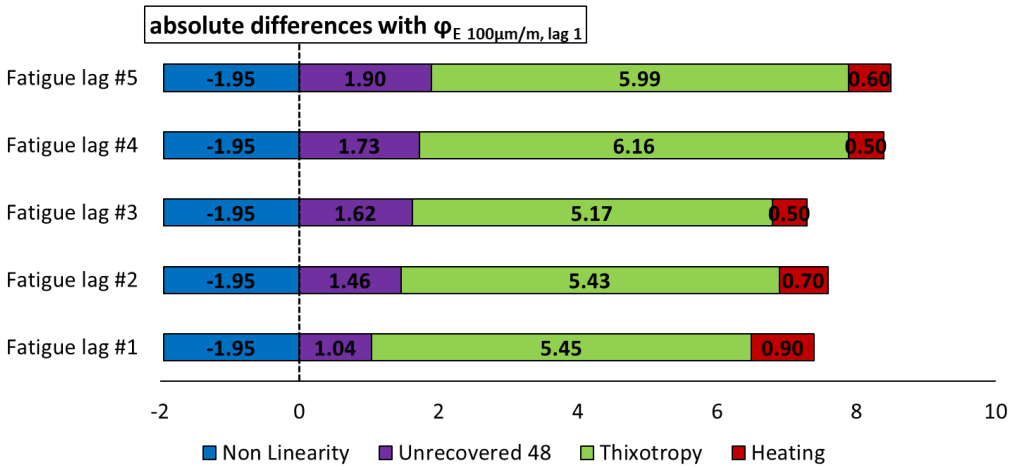
absolute differences with φE 100µm/m, lag 1
Fatigue lag #5
Fatigue lag #4
Fatigue lag #3
Fatigue lag #2
Fatigue lag #1
-1.95
1.90
5.99
0.60
-1.95
1.73
6.16
0.50
-1.95
1.62
5.17
0.50
-1.95
1.46
5.43
0.70
-1.95
1.04
5.45
0.90
-2
0
2
4
6
8
10
Non Linearity
Unrecovered 48
Thixotropy
Heating

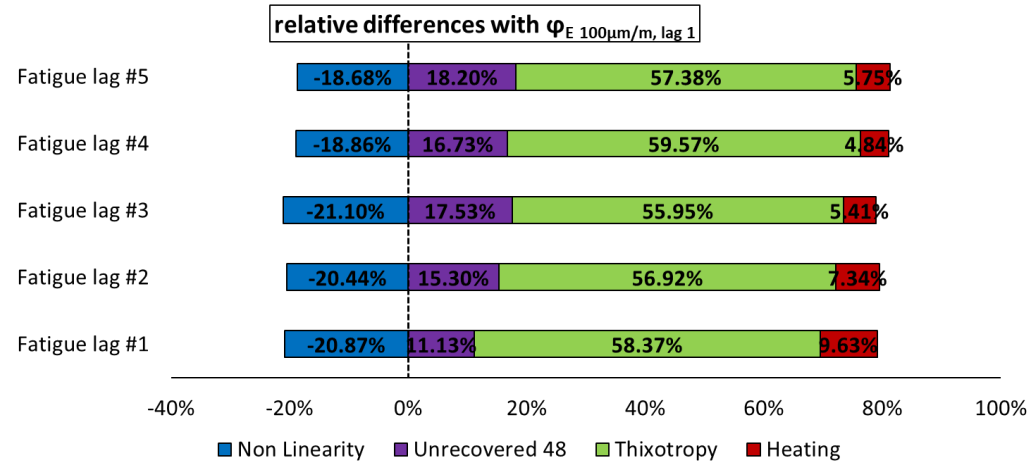
relative differences with $\varphi_{E\ 100\mu m/m,\ lag\ 1}$
Fatigue lag #5
Fatigue lag #4
Fatigue lag #3
Fatigue lag #2
Fatigue lag #1
-18.68%
18.20%
57.38%
5.75%
-18.86%
16.73%
59.57%
4.84%
-21.10%
17.53%
55.95%
5.41%
-20.44%
15.30%
56.92%
7.34%
-20.87%
11.13%
58.37%
9.63%
-40%
-20%
0%
20%
40%
60%
80%
100%
Non Linearity
Unrecovered 48
Thixotropy
Heating

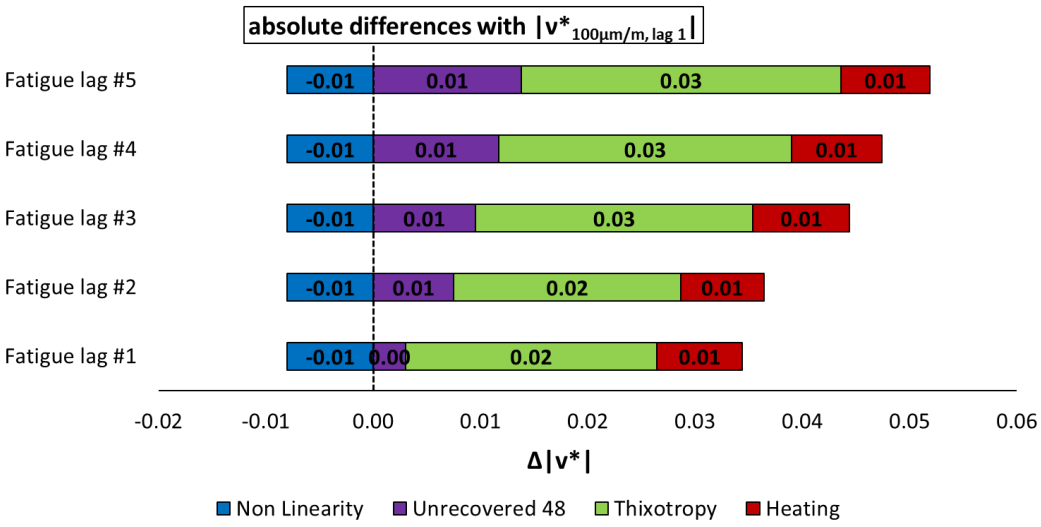
absolute differences with $|v^*_{100\mu m/m,\ lag\ 1}|$
Fatigue lag #5
Fatigue lag #4
Fatigue lag #3
Fatigue lag #2
Fatigue lag #1
-0.01
0.01
0.03
0.01
-0.01
0.01
0.03
0.01
-0.01
0.01
0.03
0.01
-0.01
0.01
0.02
0.01
-0.01
0.00
0.02
0.01
-0.02
-0.01
0.00
0.01
0.02
0.03
0.04
0.05
0.06
Δ|v*|
Non Linearity
Unrecovered 48
Thixotropy
Heating

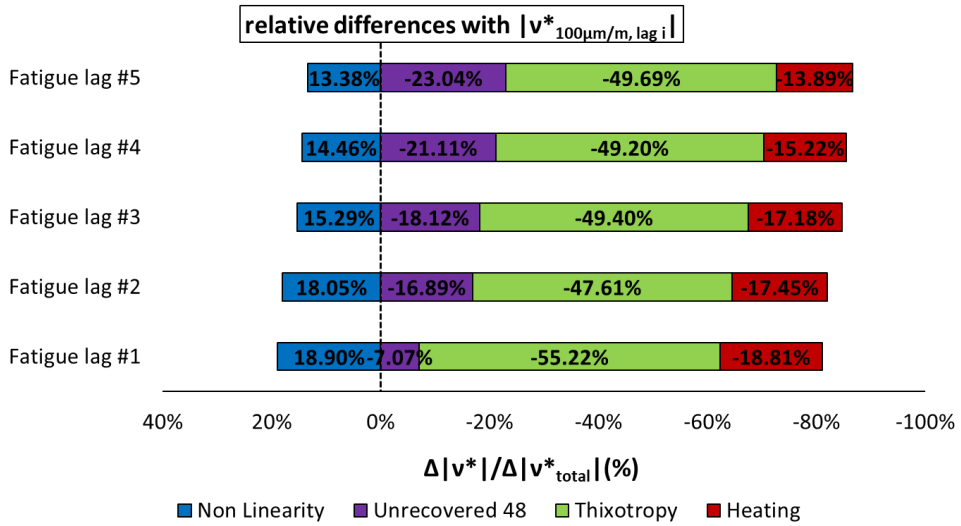
relative differences with $|v^*_{100\mu m/m,\ lag\ i}|$
Fatigue lag #5
Fatigue lag #4
Fatigue lag #3
Fatigue lag #2
Fatigue lag #1
13.38%
-23.04%
-49.69%
-13.89%
14.46%
-21.11%
-49.20%
-15.22%
15.29%
-18.12%
-49.40%
-17.18%
18.05%
-16.89%
-47.61%
-17.45%
18.90%
-7.07%
-55.22%
-18.81%
40%
20%
0%
-20%
-40%
-60%
-80%
-100%
Δ|v*|/Δ|v*total|(%)
Non Linearity
Unrecovered 48
Thixotropy
Heating

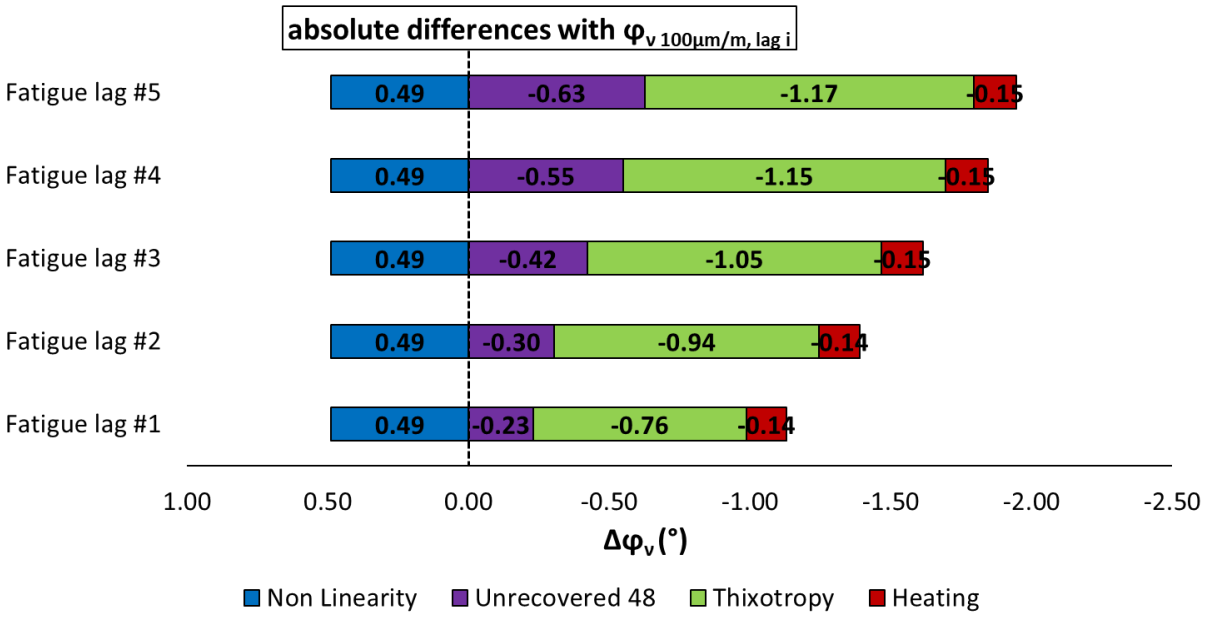

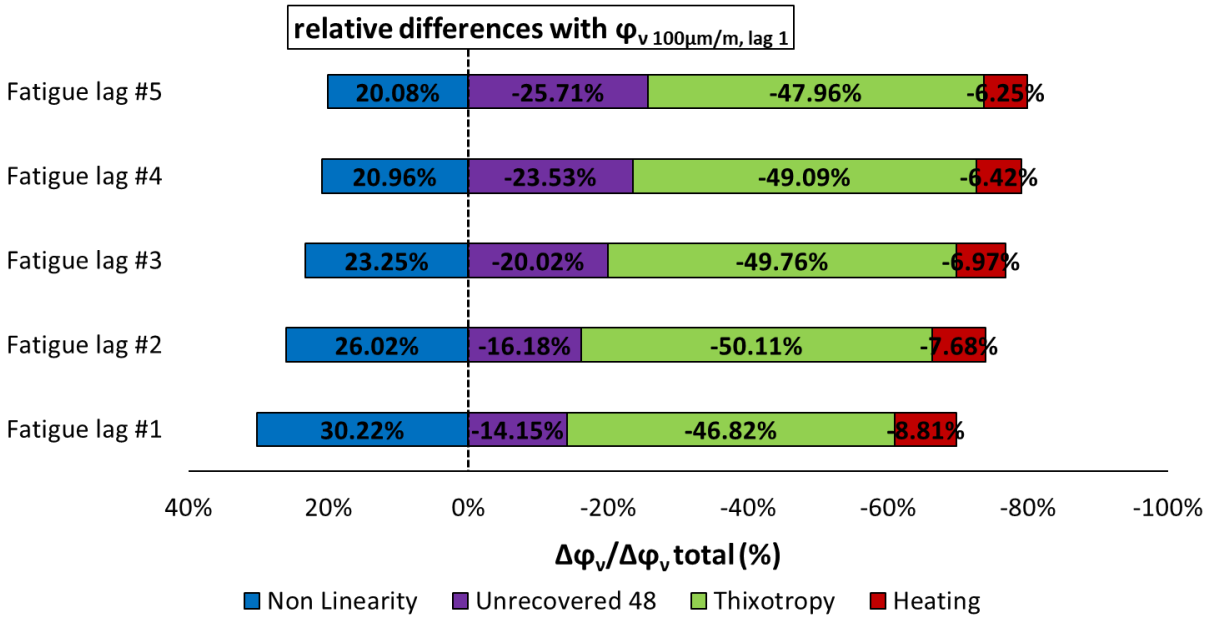

3.1.108. Quantification of different absolute and relative contributions to |E*|, φ_E, |ν*| and φ_ν evolutions for mix 40/60 – 8, calculated using the envelope line for the first fatigue lag.

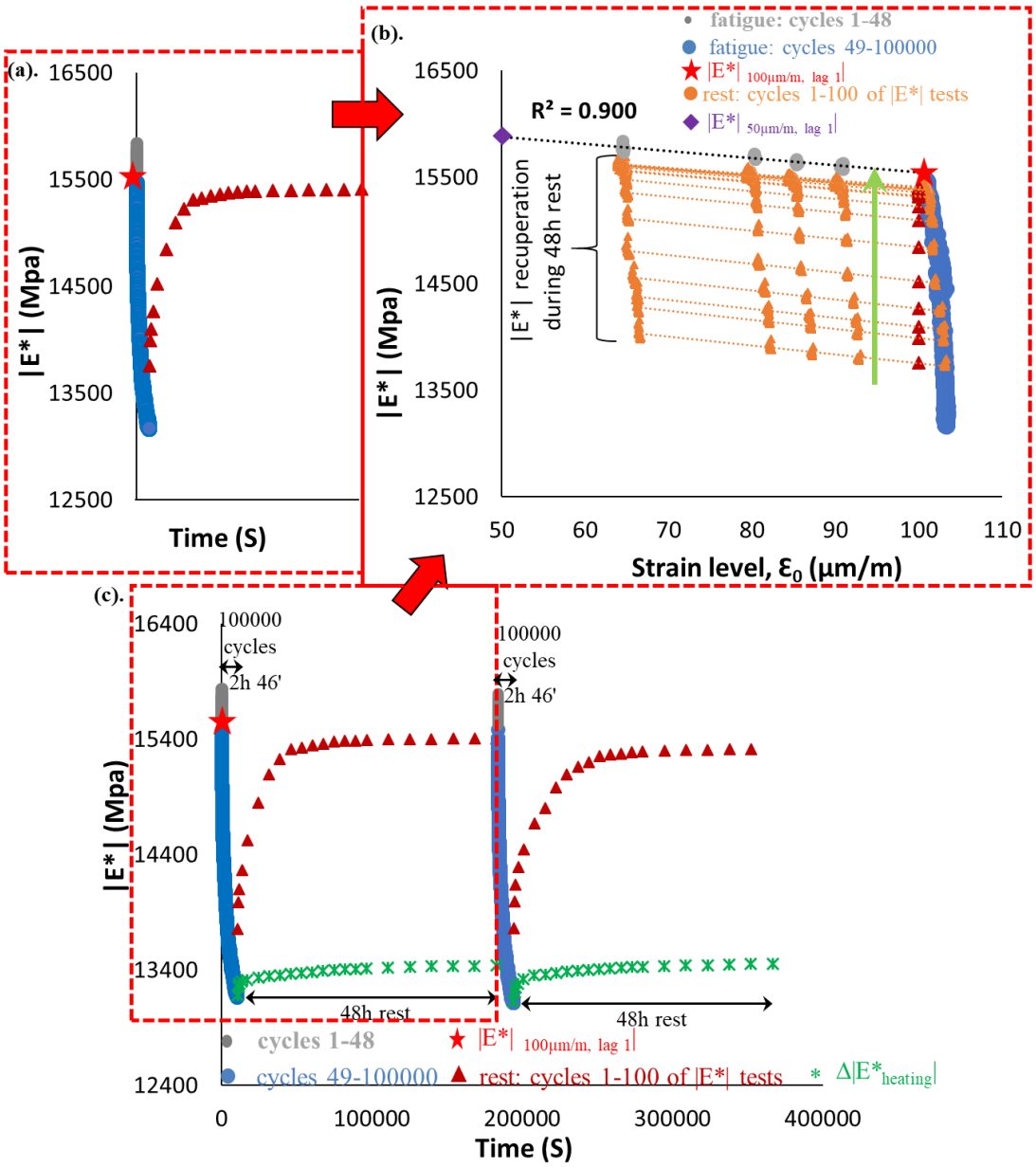

3.1.109. PFRT results obtained for mix PMB - 1: (a) |E*| as a function of time during the first fatigue lag and rest period (b) |E*| as a function of applied strain amplitude during the first fatigue lags and the short complex modulus tests performed within its following rest periods; (c) |E*| as a function of time during the two fatigue lags and rest periods [Red stars indicate values of |E*| estimated at 100 µm/m at the beginning of fatigue lag, green asterisk shows values of $\Delta|E^*_{heating}|$ as influence of self-heating and brown triangles indicate values of |E*| estimated at 100 µm/m for each short complex modulus test during rest (all these values were obtained using non-linearity envelopes, as shown in Figure 5.9(b) for the first fatigue lag and rest period)].

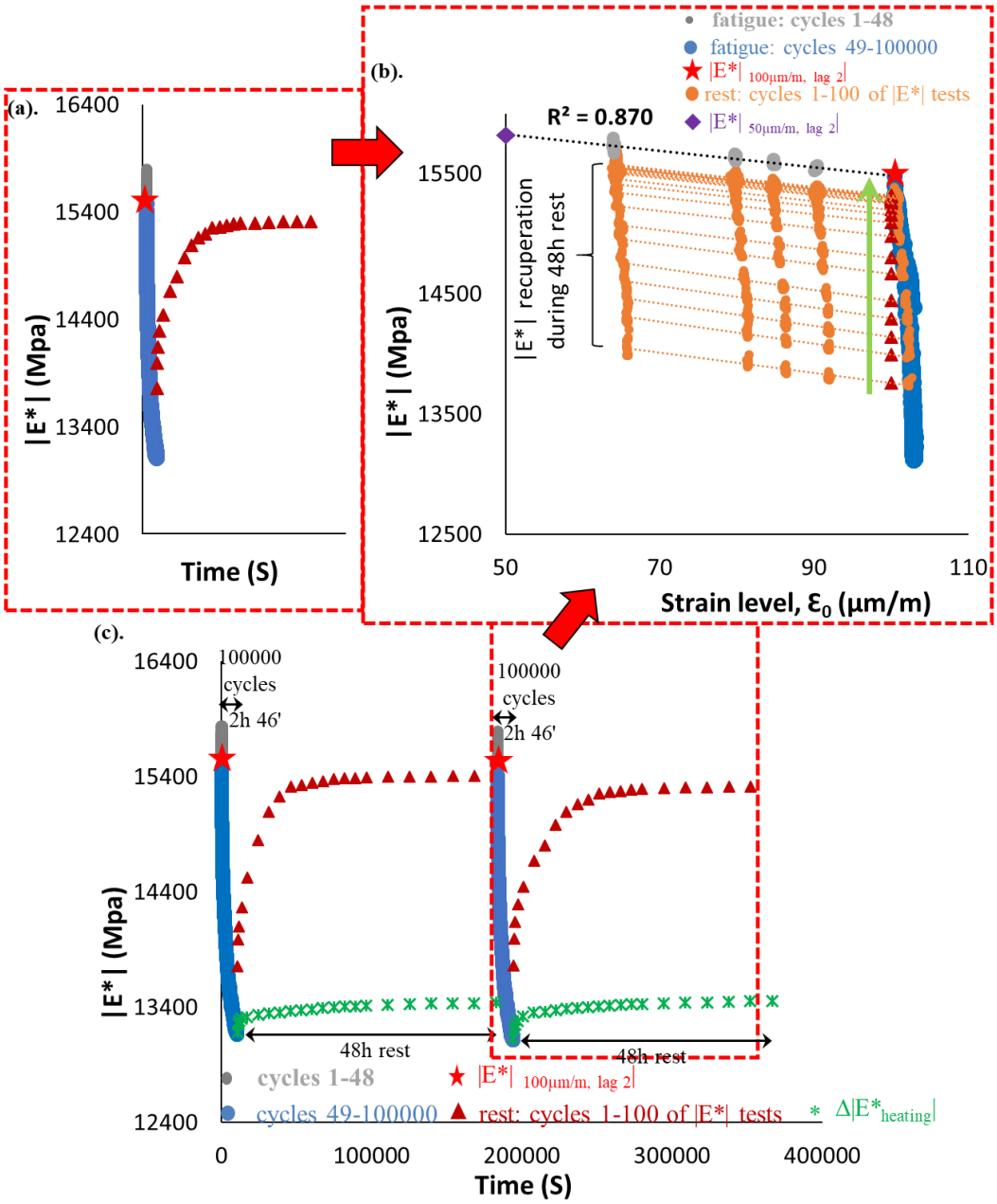

3.1.110. PFRT results obtained for mix PMB - 1: (a) |E*| as a function of time during the second fatigue lag and rest period (b) |E*| as a function of applied strain amplitude during the second fatigue lags and the short complex modulus tests performed within its following rest periods; (c) |E*| as a function of time during the two fatigue lags and rest periods [Red stars indicate values of |E*| estimated at 100 µm/m at the beginning of fatigue lag, green asterisk shows values of $\Delta|E^*_{heating}|$ as influence of self-heating and brown triangles indicate values of |E*| estimated at 100 µm/m for each short complex modulus test during rest (all these values were obtained using non-linearity envelopes, as shown in Figure 5.9(b) for the first fatigue lag and rest period)].

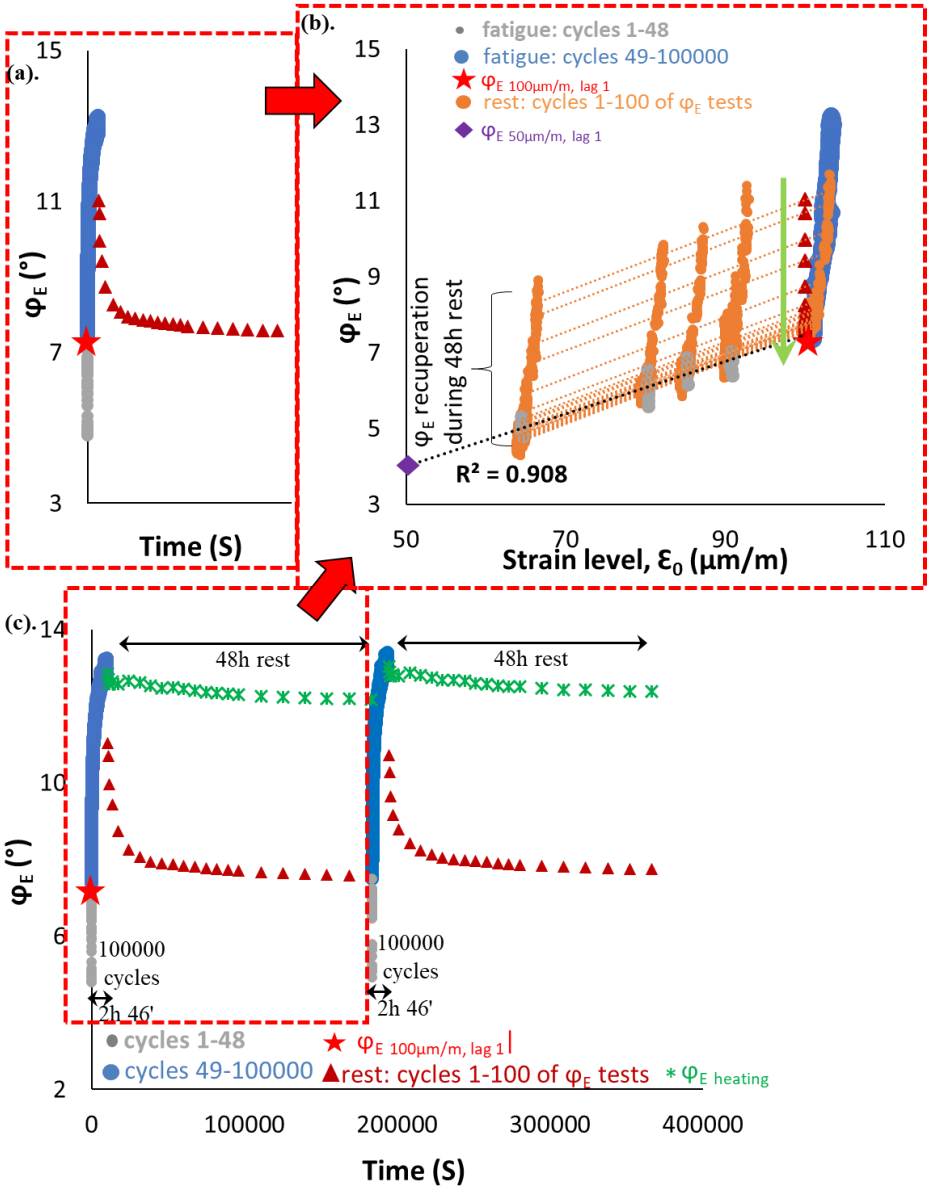

3.1.111. PFRT results obtained for mix PMB - 1: (a) φ_E as a function of time during the first fatigue lag and rest period (b) φ_E as a function of applied strain amplitude during the first fatigue lags and the short complex modulus tests performed within its following rest periods; (c) φ_E as a function of time during the five fatigue lags and rest periods (Red stars indicate values of φ_E estimated at 100 µm/m at the beginning of fatigue lag, green asterisk shows values of $\Delta\varphi_{E\ heating}$ as influence of self-heating and brown triangles indicate values of φ_E estimated at 100 µm/m for each short complex modulus test during rest (all these values were obtained using non-linearity envelopes, as shown in (b) for the first fatigue lag and rest period).

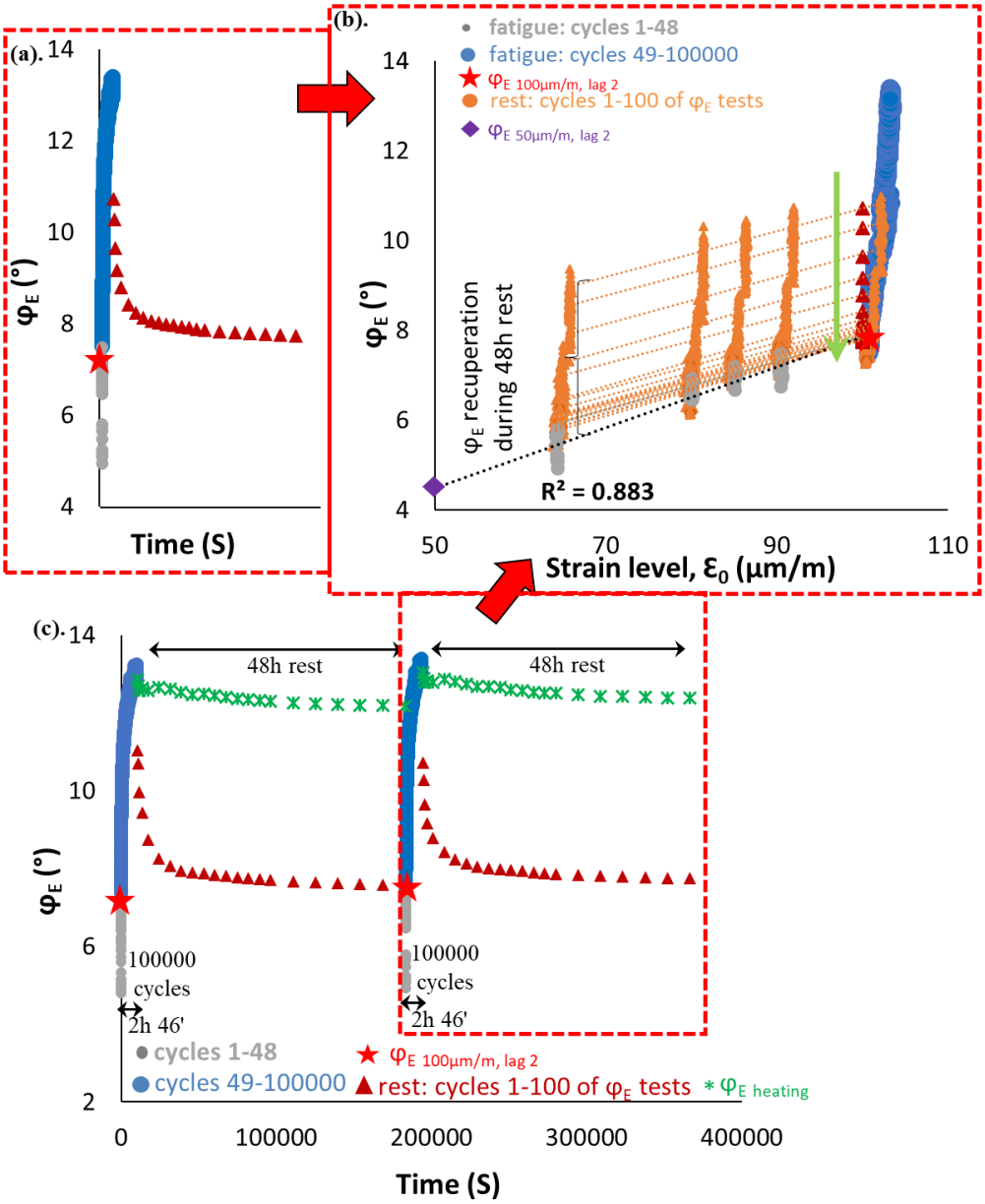

3.1.112. PFRT results obtained for mix PMB - 1: (a) φ_E as a function of time during the second fatigue lag and rest period (b) φ_E as a function of applied strain amplitude during the second fatigue lags and the short complex modulus tests performed within its following rest periods; (c) φ_E as a function of time during the five fatigue lags and rest periods (Red stars indicate values of φ_E estimated at 100 µm/m at the beginning of fatigue lag, green asterisk shows values of $\Delta\varphi_{E\ heating}$ as influence of self-heating and brown triangles indicate values of φ_E estimated at 100 µm/m for each short complex modulus test during rest (all these values were obtained using non-linearity envelopes, as shown in (b) for the first fatigue lag and rest period).

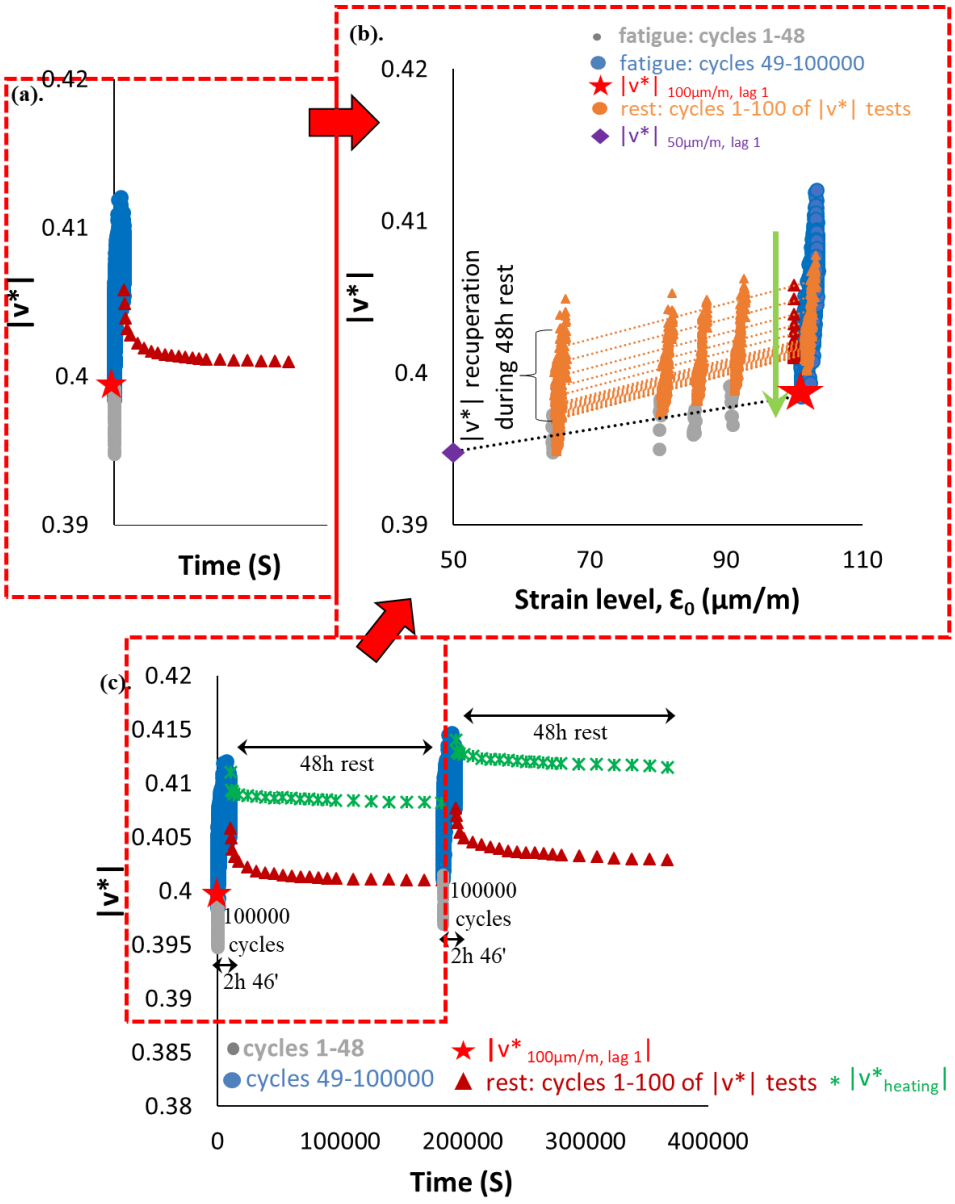

3.1.113. PFRT results obtained for mix PMB - 1: (a) |v*| as a function of time during the first fatigue lag and rest period (b) |v*| as a function of applied strain amplitude during the first fatigue lags and the short complex modulus tests performed within its following rest periods; (c) |v*| as a function of time during the two fatigue lags and rest periods [Red stars indicate values of |E*| estimated at 100 µm/m at the beginning of fatigue lag, green asterisk shows values of $\Delta|v^*_{heating}|$ as influence of self-heating and brown triangles indicate values of |v*| estimated at 100 µm/m for each short complex modulus test during rest (all these values were obtained using non-linearity envelopes, as shown in Figure 5.9(b) for the first fatigue lag and rest period)].

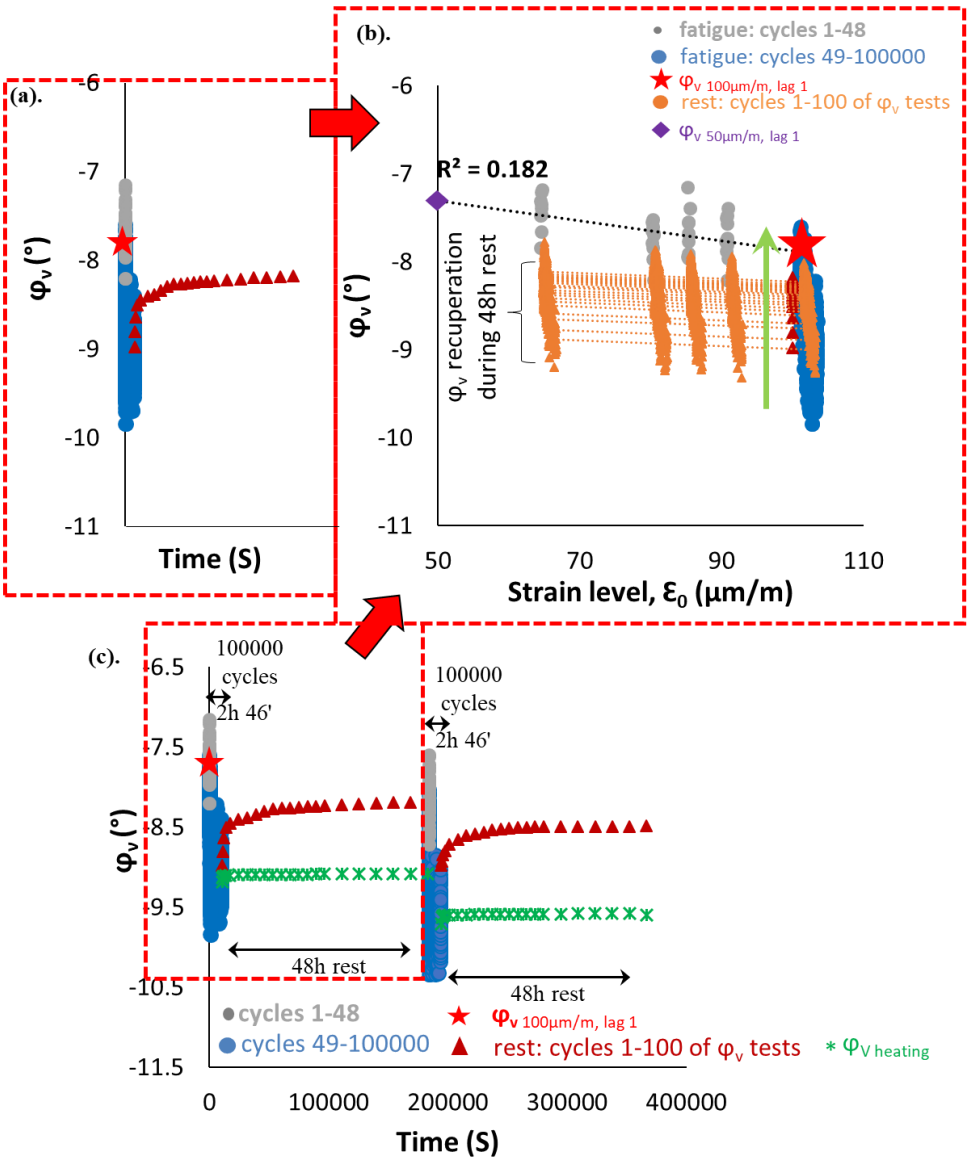

3.1.114. PFRT results obtained for mix PMB - 1: (a) φ_V as a function of time during the first fatigue lag and rest period (b) φ_V as a function of applied strain amplitude during the first fatigue lags and the short complex modulus tests performed within its following rest periods; (c) φ_V as a function of time during the five fatigue lags and rest periods (Red stars indicate values of φ_V estimated at 100 µm/m at the beginning of fatigue lag, green asterisk shows values of $\Delta\varphi_{V\ heating}$ as influence of self-heating and brown triangles indicate values of φ_V estimated at 100 µm/m for each short complex modulus test during rest (all these values were obtained using non-linearity envelopes, as shown in (b) for the first fatigue lag and rest period).

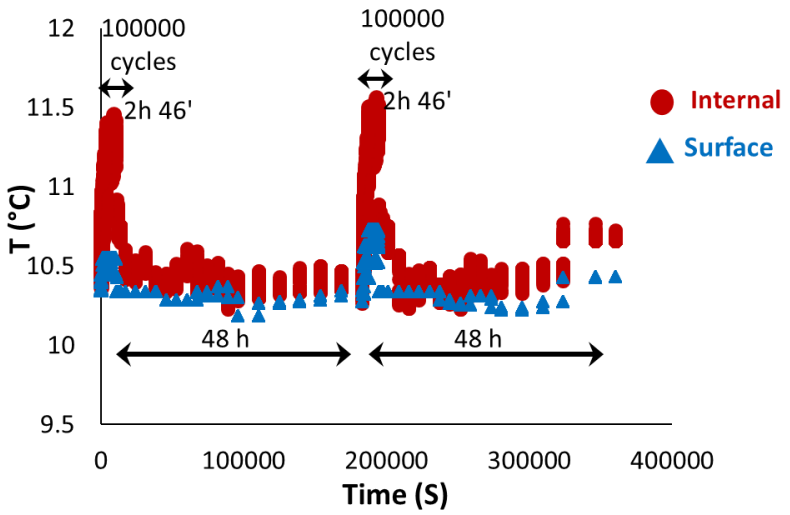

3.1.115. PFRT results obtained for PMB - 1: internal and surface temperature evolution during fatigue lags and recovery periods.

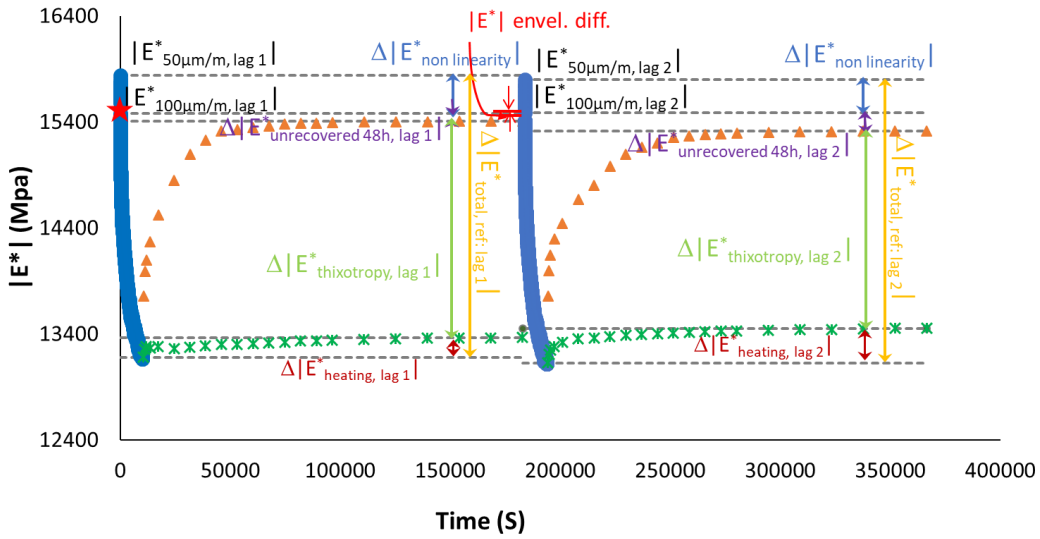

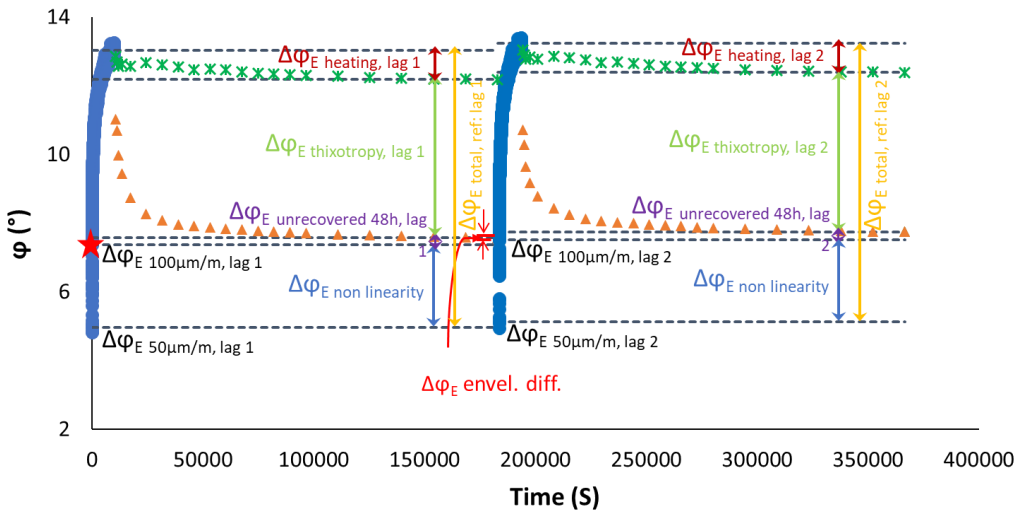

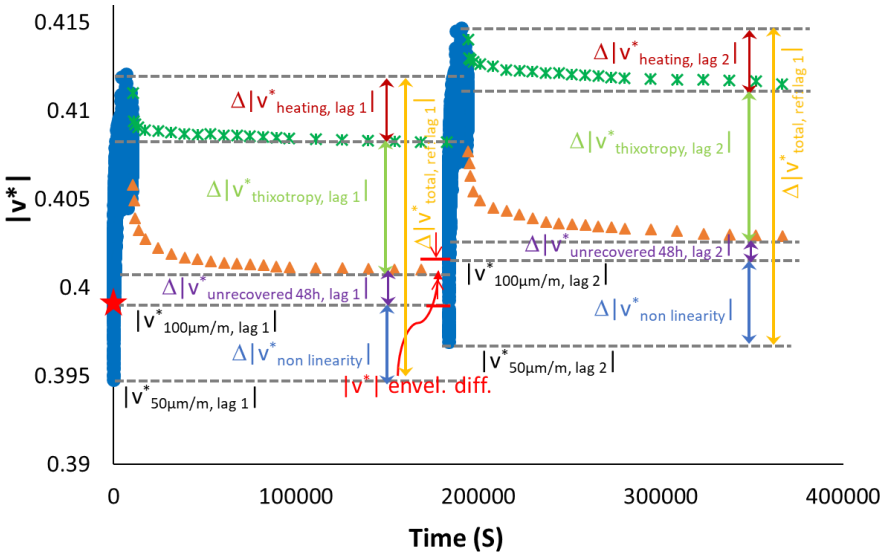

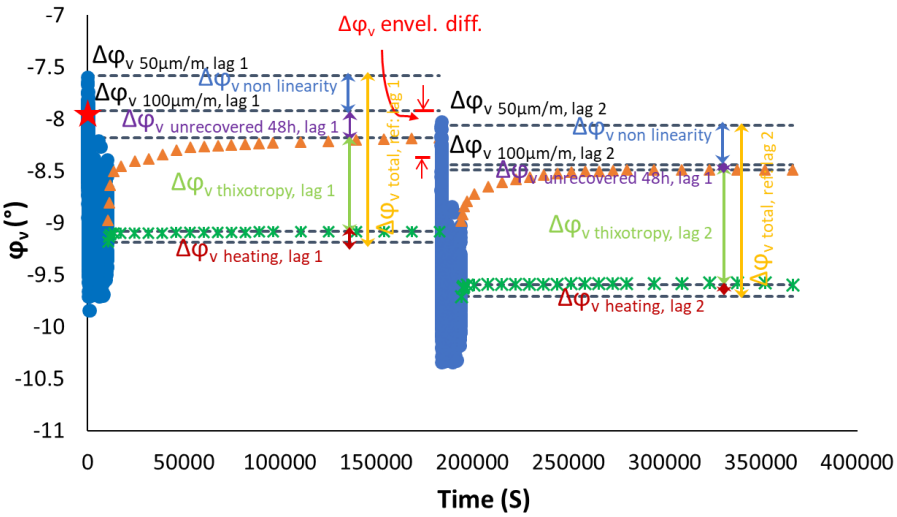

3.1.116. Quantification of different contributions |E*|, φ_E, |v*| and φ_v evolution, for the first two fatigue lags for mix PMB - 1: different envelope line is used for each fatigue lag.

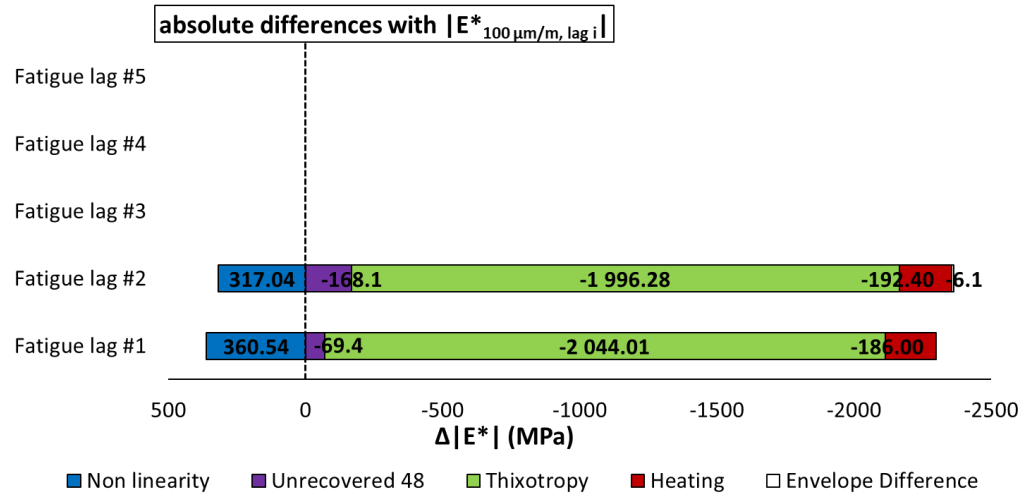
absolute differences with |E*100 µm/m, lag i|
Fatigue lag #5
Fatigue lag #4
Fatigue lag #3
Fatigue lag #2
Fatigue lag #1
317.04
-168.1
-1 996.28
-192.40
-6.1
360.54
-69.4
-2 044.01
-186.00
500
0
-500
-1000
-1500
-2000
-2500
Δ|E*| (MPa)
Non linearity
Unrecovered 48
Thixotropy
Heating
Envelope Difference

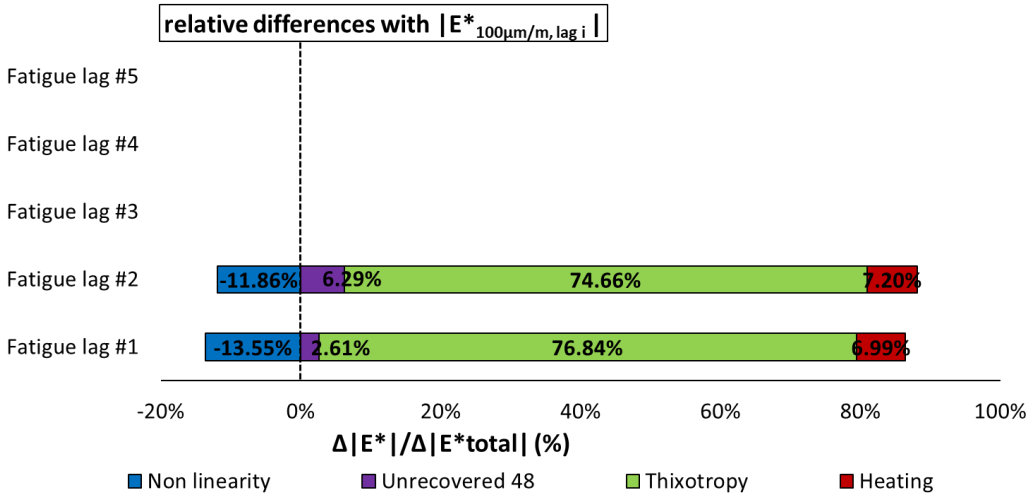
relative differences with |E*100µm/m, lag i|
Fatigue lag #5
Fatigue lag #4
Fatigue lag #3
Fatigue lag #2
Fatigue lag #1
-11.86%
6.29%
74.66%
7.20%
-13.55%
2.61%
76.84%
6.99%
-20%
0%
20%
40%
60%
80%
100%
Δ|E*|/Δ|E*total| (%)
Non linearity
Unrecovered 48
Thixotropy
Heating

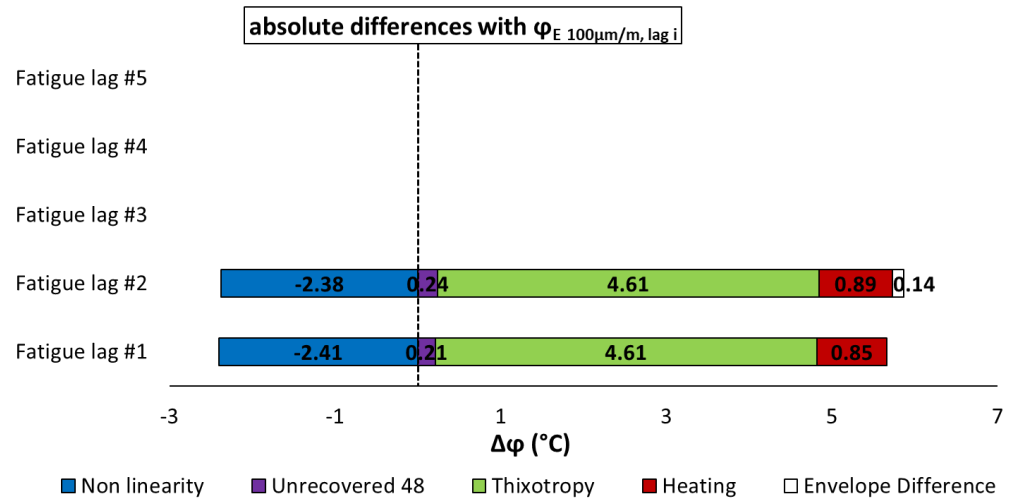
absolute differences with φE 100µm/m, lag i
Fatigue lag #5
Fatigue lag #4
Fatigue lag #3
Fatigue lag #2
Fatigue lag #1
-2.38
0.24
4.61
0.89
0.14
-2.41
0.21
4.61
0.85
-3
-1
1
3
5
7
Δφ (°C)
Non linearity
Unrecovered 48
Thixotropy
Heating
Envelope Difference

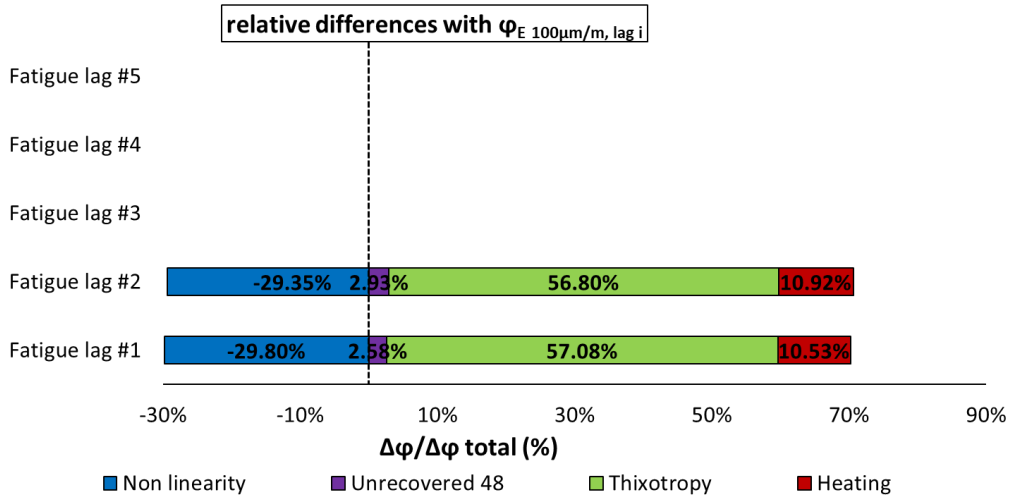
relative differences with φE 100µm/m, lag i
Fatigue lag #5
Fatigue lag #4
Fatigue lag #3
Fatigue lag #2
Fatigue lag #1
-29.35%
2.93%
56.80%
10.92%
-29.80%
2.58%
57.08%
10.53%
-30%
-10%
10%
30%
50%
70%
90%
Δφ/Δφ total (%)
Non linearity
Unrecovered 48
Thixotropy
Heating

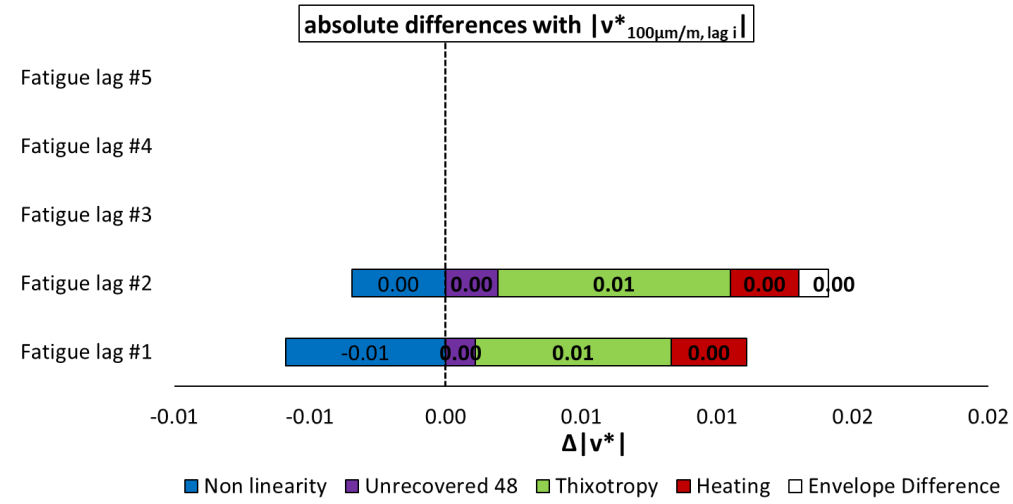
absolute differences with |v*100µm/m, lag i|
Fatigue lag #5
Fatigue lag #4
Fatigue lag #3
Fatigue lag #2
Fatigue lag #1
0.00
0.00
0.01
0.00
0.00
-0.01
0.00
0.01
0.00
-0.01
-0.01
0.00
0.01
0.01
0.02
0.02
Δ|v*|
Non linearity
Unrecovered 48
Thixotropy
Heating
Envelope Difference

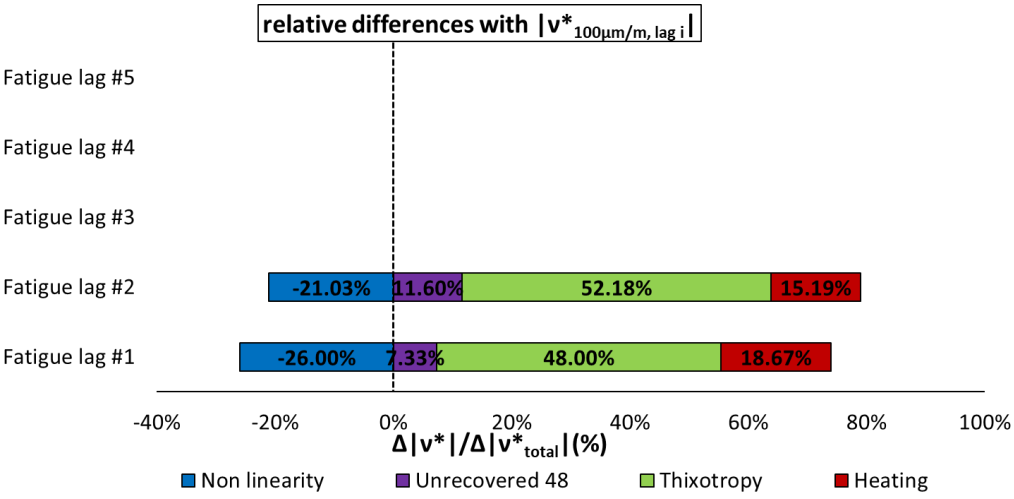
relative differences with |v*100µm/m, lag i|
Fatigue lag #5
Fatigue lag #4
Fatigue lag #3
Fatigue lag #2
Fatigue lag #1
-21.03%
11.60%
52.18%
15.19%
-26.00%
7.33%
48.00%
18.67%
-40%
-20%
0%
20%
40%
60%
80%
100%
Δ|v*|/Δ|v*total|(%)
Non linearity
Unrecovered 48
Thixotropy
Heating

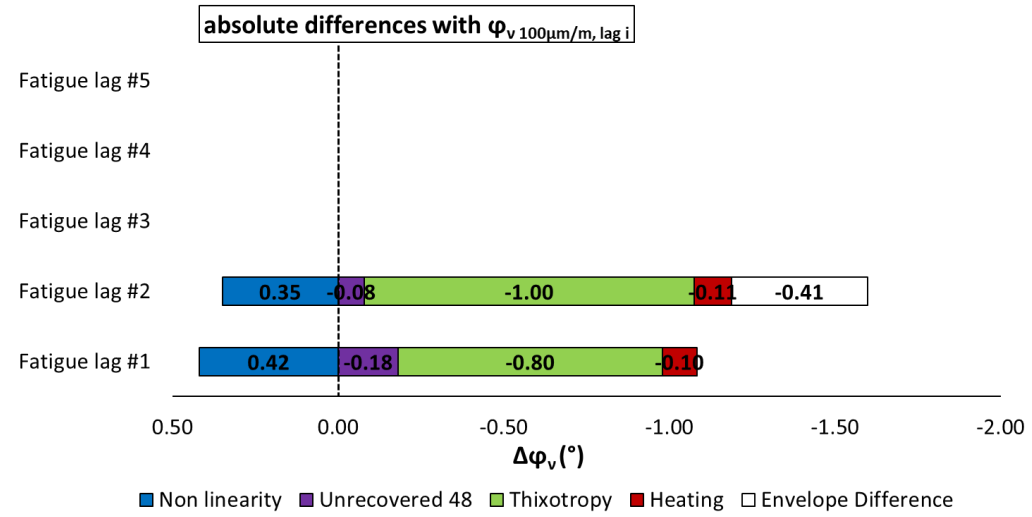

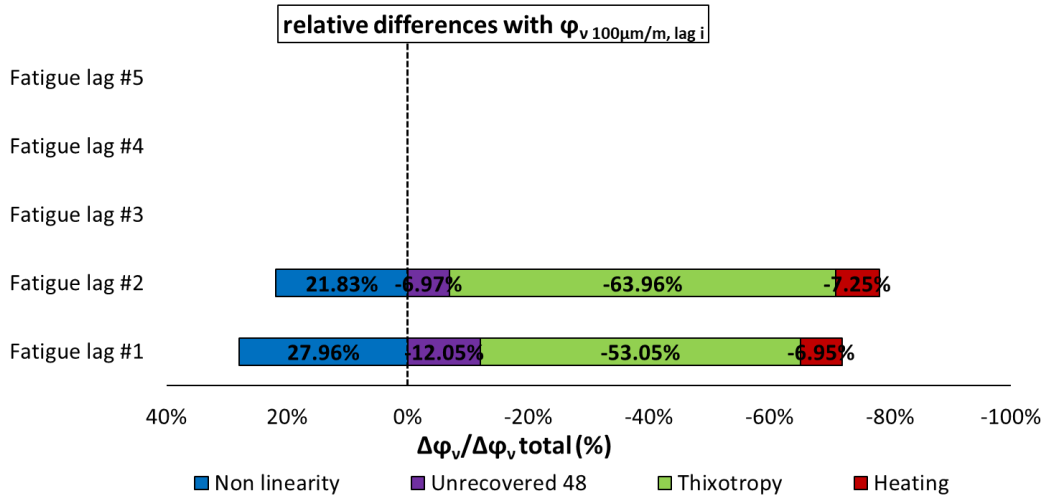

3.1.117. Quantification of different absolute and relative contributions to |E*|, φ_E, |v*| and φ_v evolutions for mix PMB -1, calculated using a different envelope line for each fatigue lag.

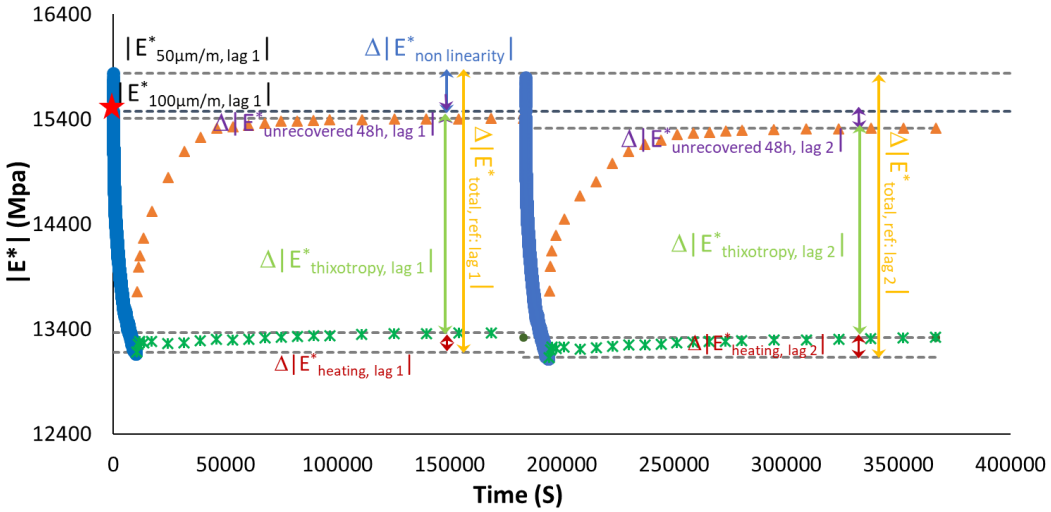

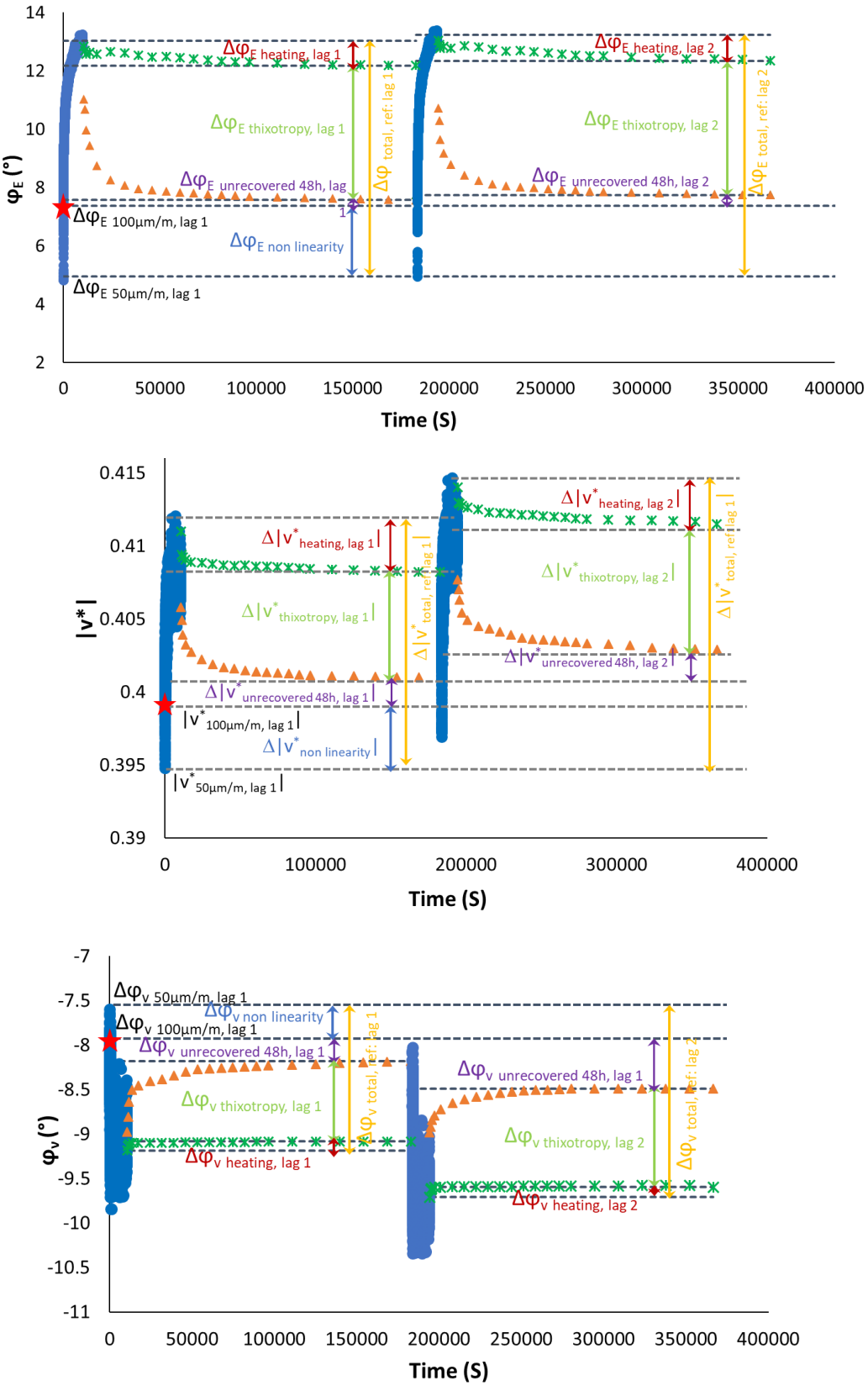

3.1.118. Quantification of different contributions to |E*|, φ_E, |v*| and φ_v evolution during five fatigue lags for mix PMB -1: the envelope line of the first fatigue lag is used for all fatigue lags.

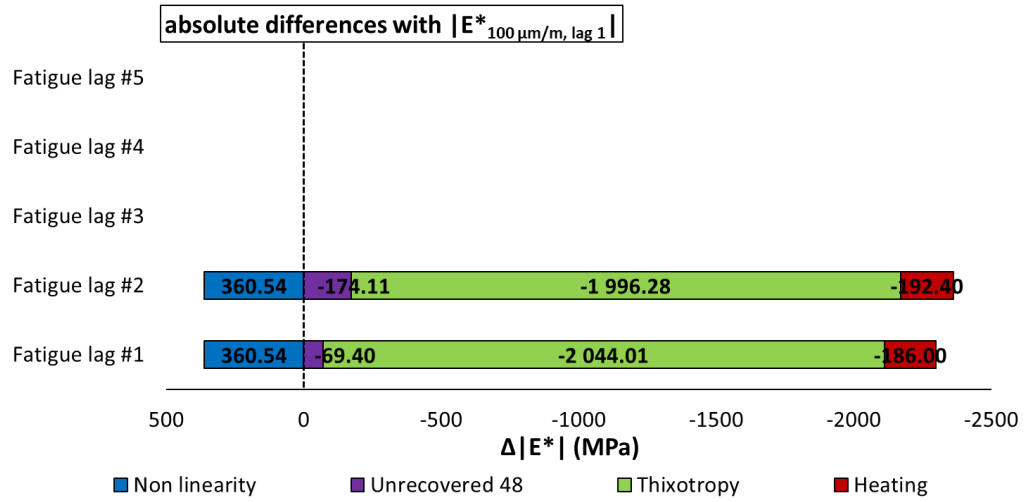
absolute differences with |E*100 µm/m, lag 1|
Fatigue lag #5
Fatigue lag #4
Fatigue lag #3
Fatigue lag #2
Fatigue lag #1
360.54
-174.11
-1 996.28
-192.40
360.54
-69.40
-2 044.01
-186.00
500
0
-500
-1000
-1500
-2000
-2500
Δ|E*| (MPa)
Non linearity
Unrecovered 48
Thixotropy
Heating

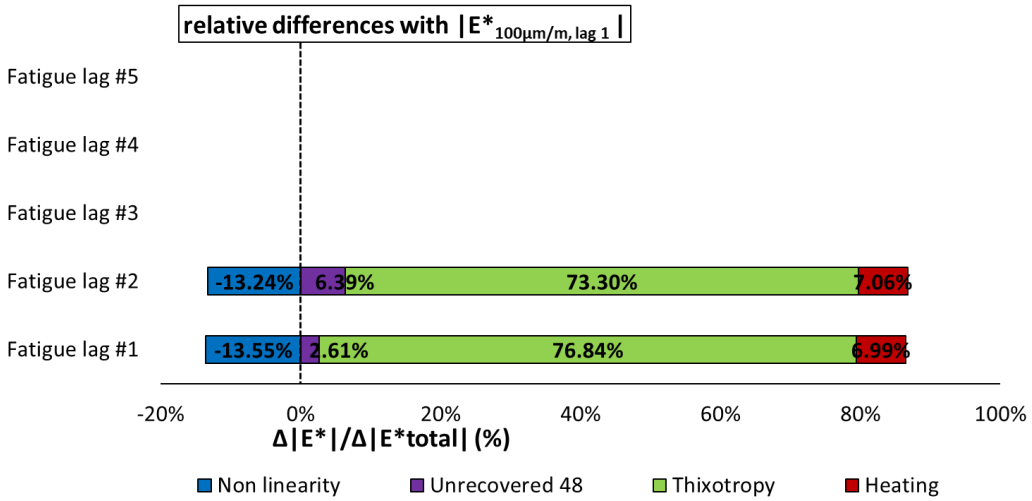
relative differences with |E*100µm/m, lag 1|
Fatigue lag #5
Fatigue lag #4
Fatigue lag #3
Fatigue lag #2
Fatigue lag #1
-13.24%
6.39%
73.30%
7.06%
-13.55%
2.61%
76.84%
6.99%
-20%
0%
20%
40%
60%
80%
100%
Δ|E*|/Δ|E*total| (%)
Non linearity
Unrecovered 48
Thixotropy
Heating

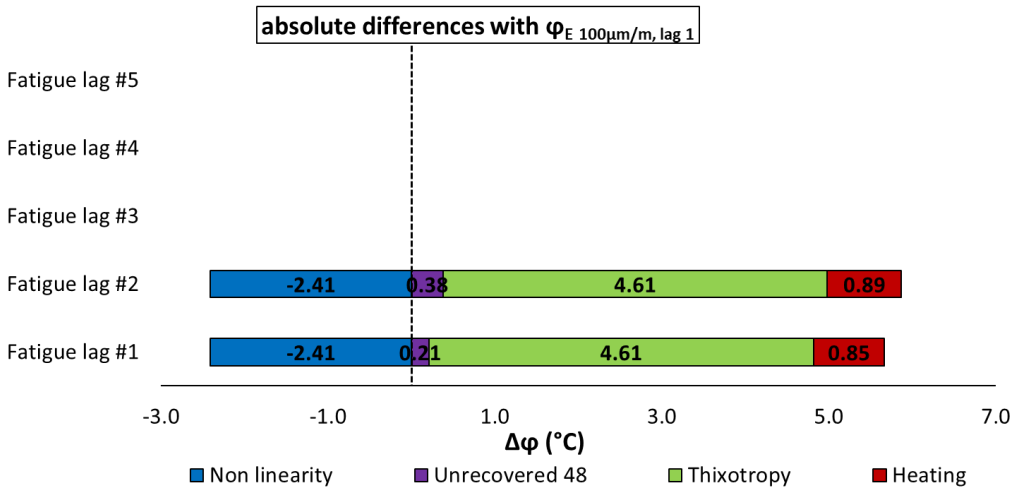
absolute differences with φE 100µm/m, lag 1
Fatigue lag #5
Fatigue lag #4
Fatigue lag #3
Fatigue lag #2
Fatigue lag #1
-2.41
0.38
4.61
0.89
-2.41
0.21
4.61
0.85
-3.0
-1.0
1.0
3.0
5.0
7.0
Δφ (°C)
Non linearity
Unrecovered 48
Thixotropy
Heating

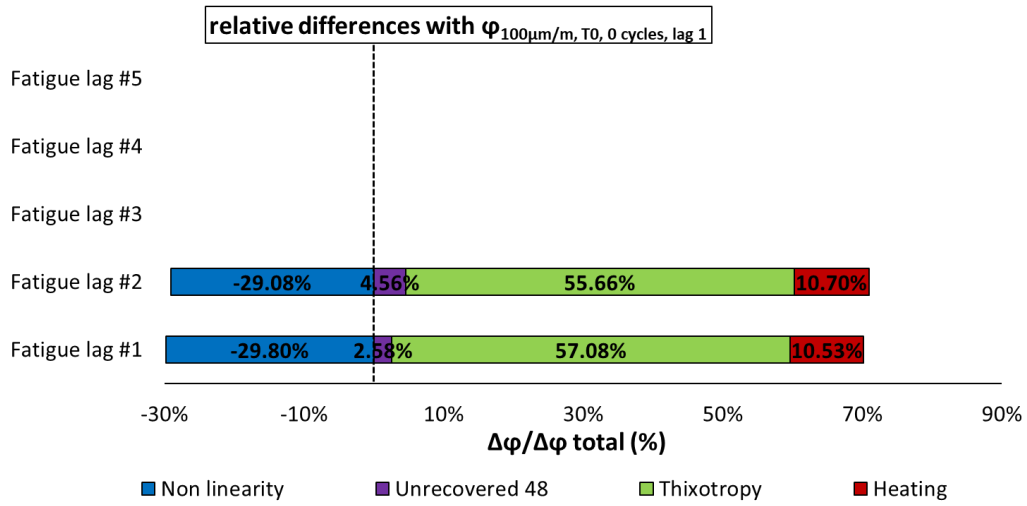
relative differences with φ100µm/m, T0, 0 cycles, lag 1
Fatigue lag #5
Fatigue lag #4
Fatigue lag #3
Fatigue lag #2
Fatigue lag #1
-29.08%
4.56%
55.66%
10.70%
-29.80%
2.58%
57.08%
10.53%
-30%
-10%
10%
30%
50%
70%
90%
Δφ/Δφ total (%)
Non linearity
Unrecovered 48
Thixotropy
Heating

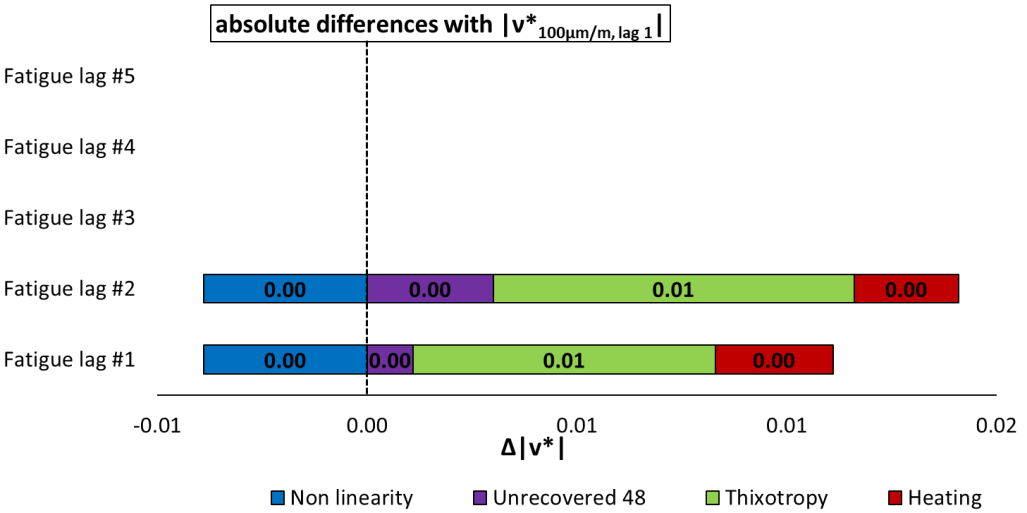
absolute differences with |v*100µm/m, lag 1|
Fatigue lag #5
Fatigue lag #4
Fatigue lag #3
Fatigue lag #2
Fatigue lag #1
0.00
0.00
0.01
0.00
0.00
0.00
0.01
0.00
-0.01
0.00
0.01
0.01
0.02
Δ|v*|
Non linearity
Unrecovered 48
Thixotropy
Heating

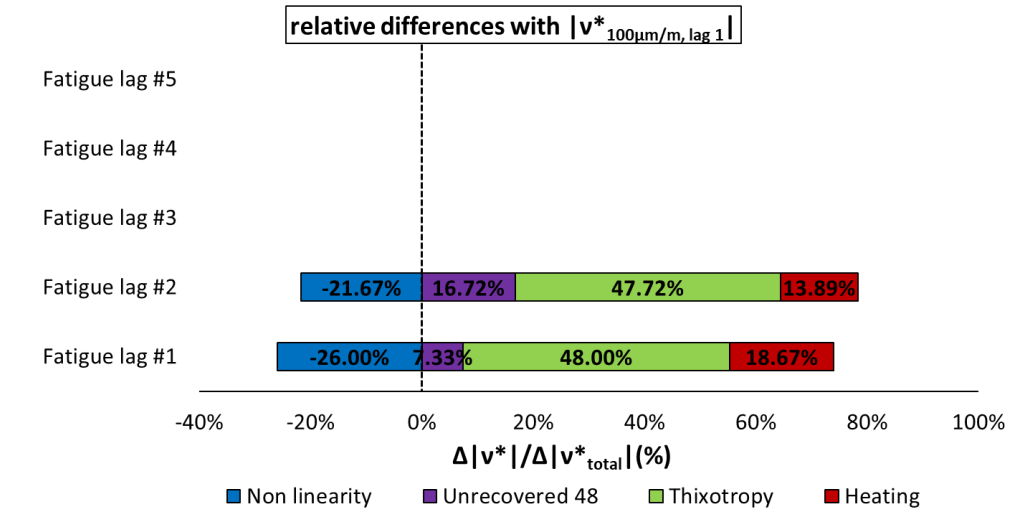
relative differences with |v*100µm/m, lag 1|
Fatigue lag #5
Fatigue lag #4
Fatigue lag #3
Fatigue lag #2
Fatigue lag #1
-21.67%
16.72%
47.72%
13.89%
-26.00%
7.33%
48.00%
18.67%
-40%
-20%
0%
20%
40%
60%
80%
100%
Δ|v*|/Δ|v*total|(%)
Non linearity
Unrecovered 48
Thixotropy
Heating

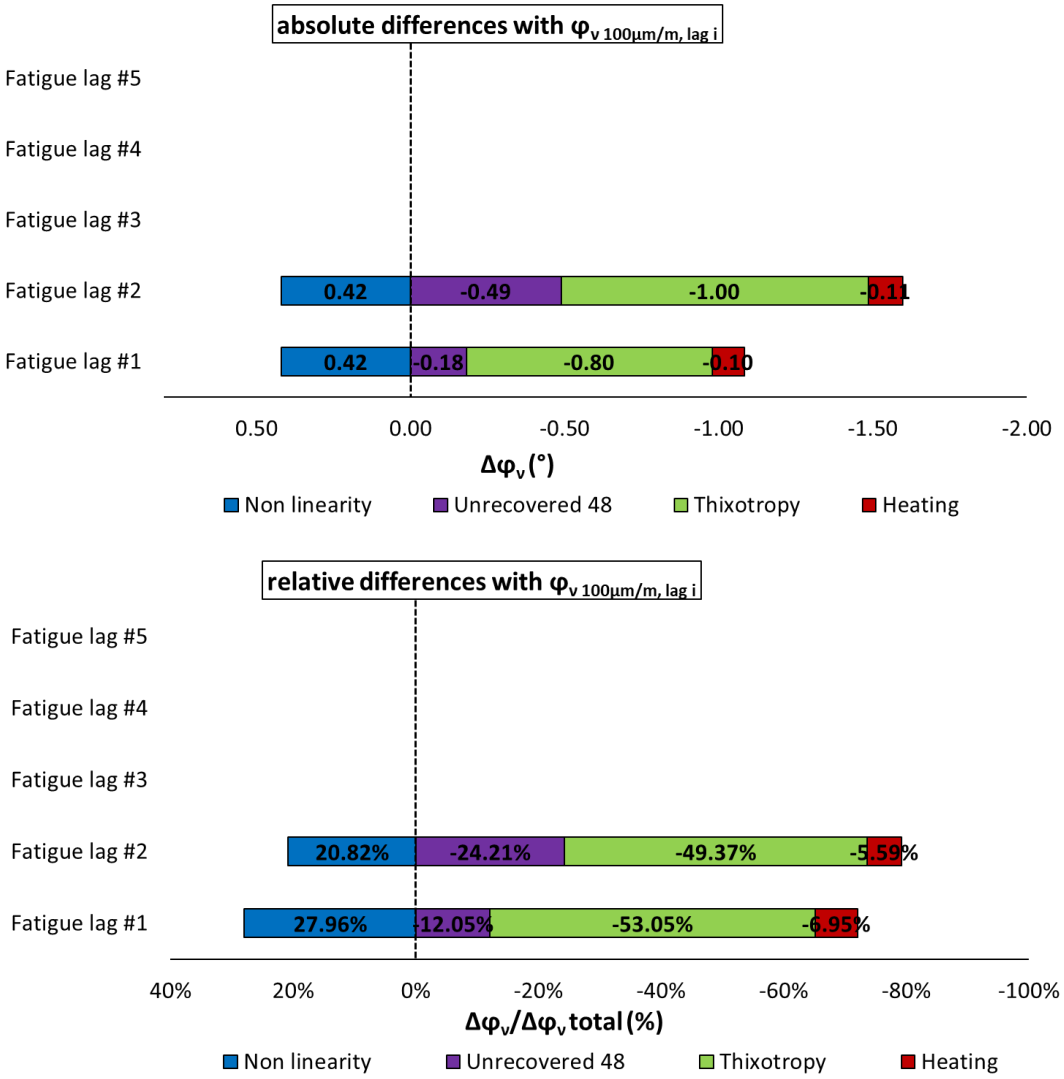

Figure 3.1.119. Quantification of different absolute and relative contributions to |E*|, φ_E, |v*| and φ_v evolutions for mix PMB -1, calculated using the envelope line for the first fatigue lag.

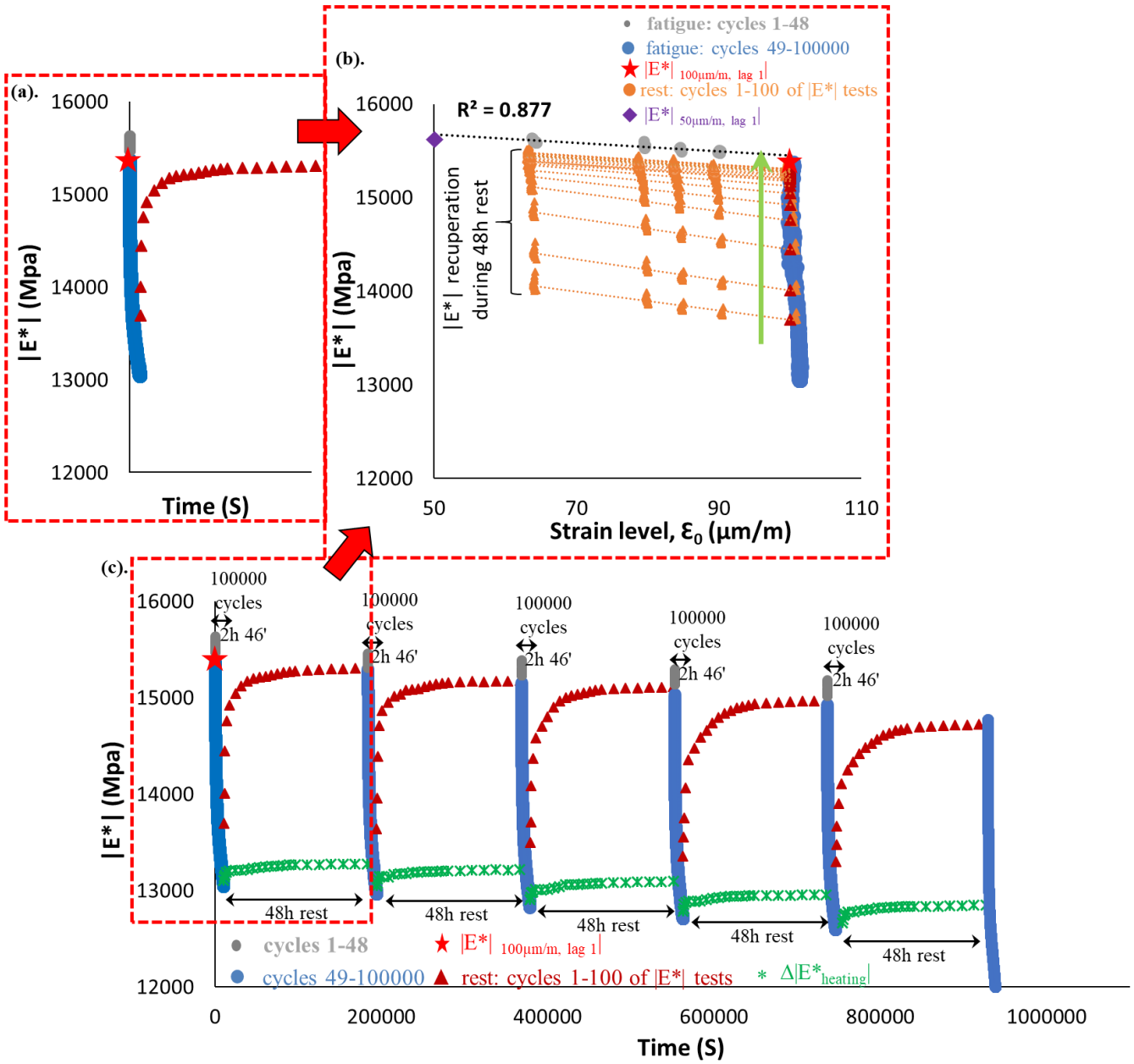

3.1.120. PFRT results obtained for mix PMB - 2: (a) |E*| as a function of time during the first fatigue lag and rest period (b) |E*| as a function of applied strain amplitude during the first fatigue lags and the short complex modulus tests performed within its following rest periods; (c) |E*| as a function of time during the five fatigue lags and rest periods [Red stars indicate values of |E*| estimated at 100 µm/m at the beginning of fatigue lag, green asterisk shows values of $\Delta|E^*_{heating}|$ as influence of self-heating and brown triangles indicate values of |E*| estimated at 100 µm/m for each short complex modulus test during rest (all these values were obtained using non-linearity envelopes, as shown in (b) for the first fatigue lag and rest period)].

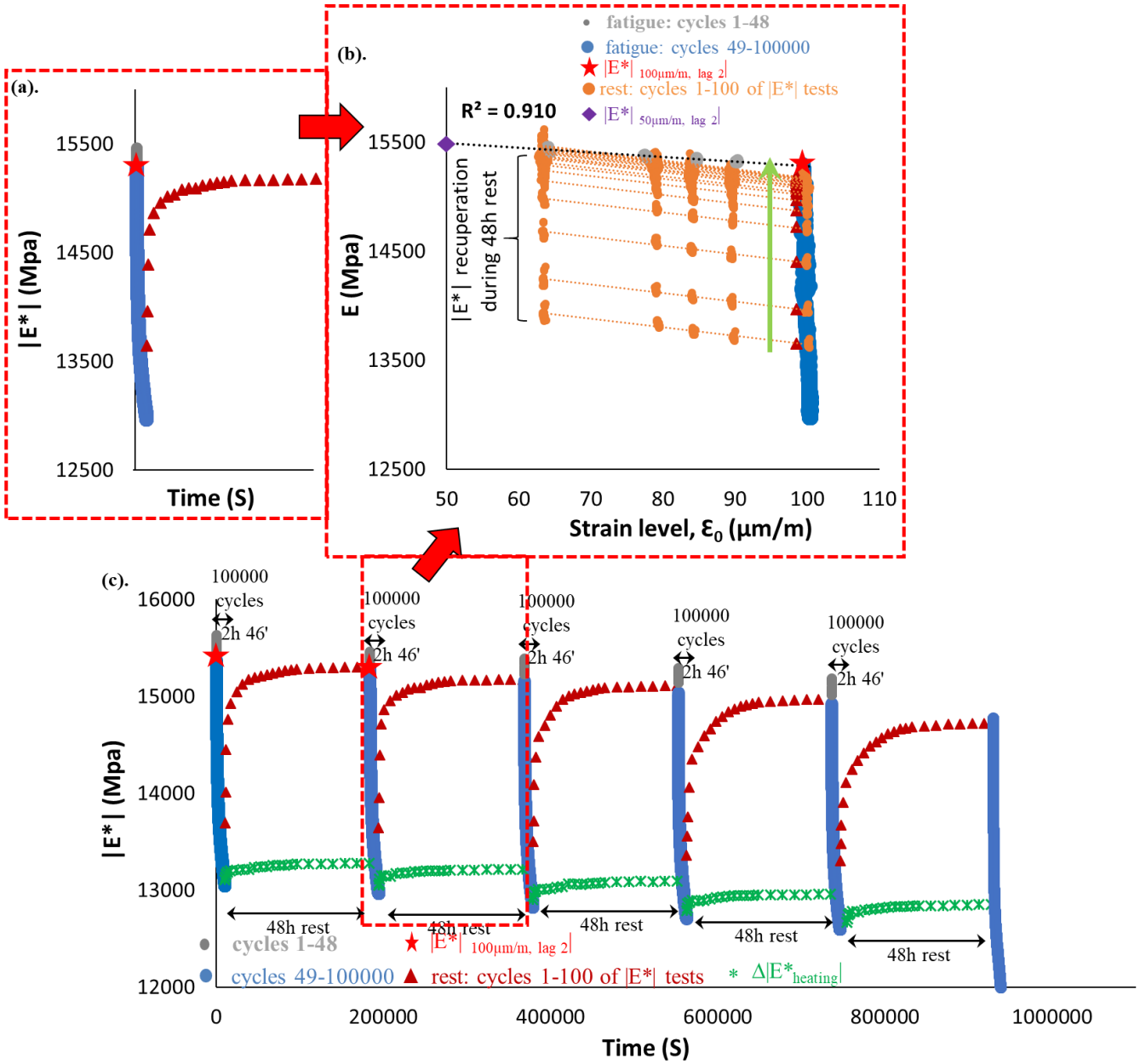

3.1.121. PFRT results obtained for mix PMB - 2: (a) |E*| as a function of time during the second fatigue lag and rest period (b) |E*| as a function of applied strain amplitude during the second fatigue lags and the short complex modulus tests performed within its following rest periods; (c) |E*| as a function of time during the five fatigue lags and rest periods [Red stars indicate values of |E*| estimated at 100 µm/m at the beginning of fatigue lag, green asterisk shows values of $\Delta|E^*_{heating}|$ as influence of self-heating and brown triangles indicate values of |E*| estimated at 100 µm/m for each short complex modulus test during rest (all these values were obtained using non-linearity envelopes, as shown in (b) for the first fatigue lag and rest period)].

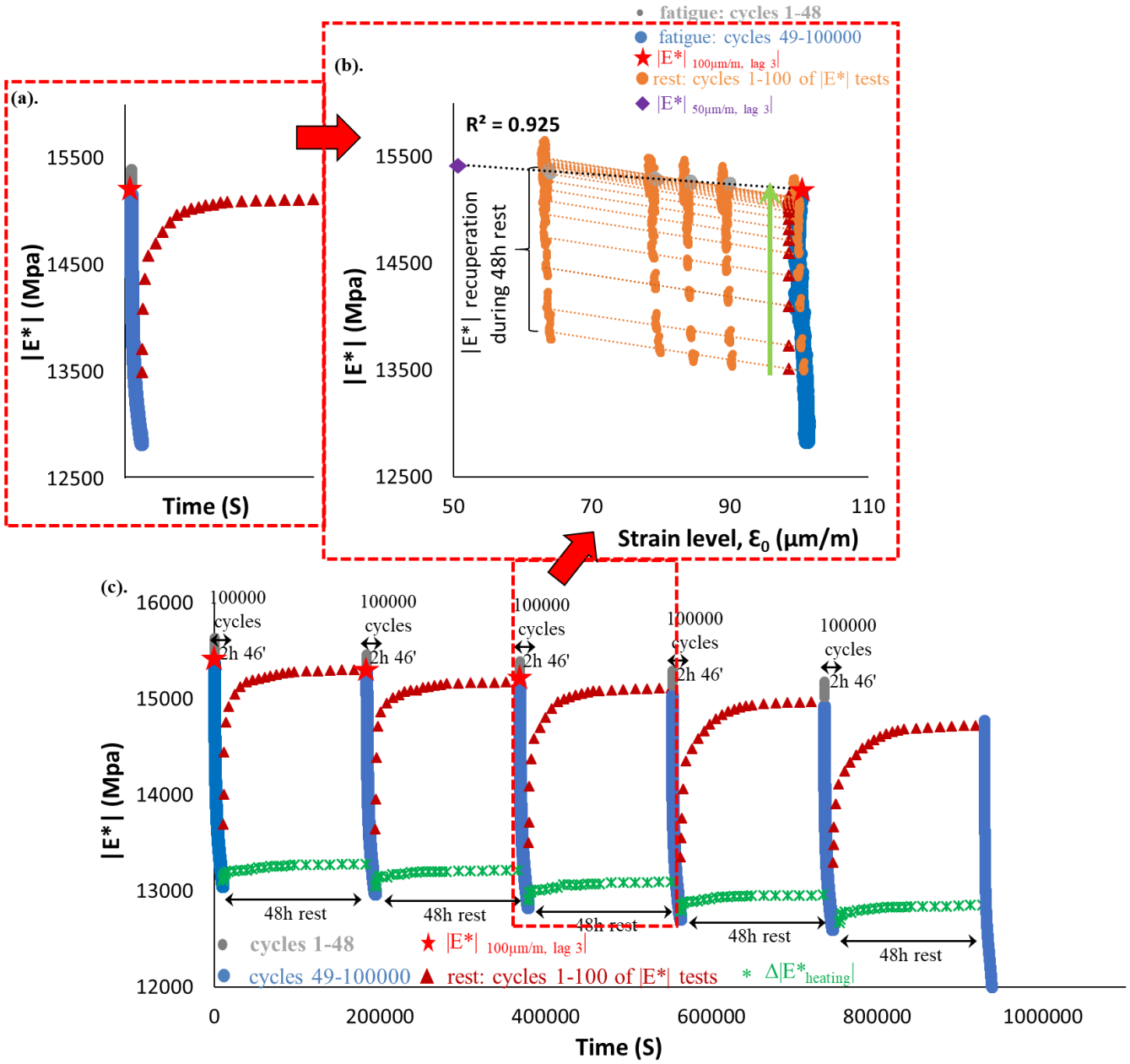

3.1.122. PFRT results obtained for mix PMB - 2: (a) |E*| as a function of time during the third fatigue lag and rest period (b) |E*| as a function of applied strain amplitude during the third fatigue lags and the short complex modulus tests performed within its following rest periods; (c) |E*| as a function of time during the five fatigue lags and rest periods [Red stars indicate values of |E*| estimated at 100 µm/m at the beginning of fatigue lag, green asterisk shows values of $\Delta|E^*_{heating}|$ as influence of self-heating and brown triangles indicate values of |E*| estimated at 100 µm/m for each short complex modulus test during rest (all these values were obtained using non-linearity envelopes, as shown in (b) for the first fatigue lag and rest period)].

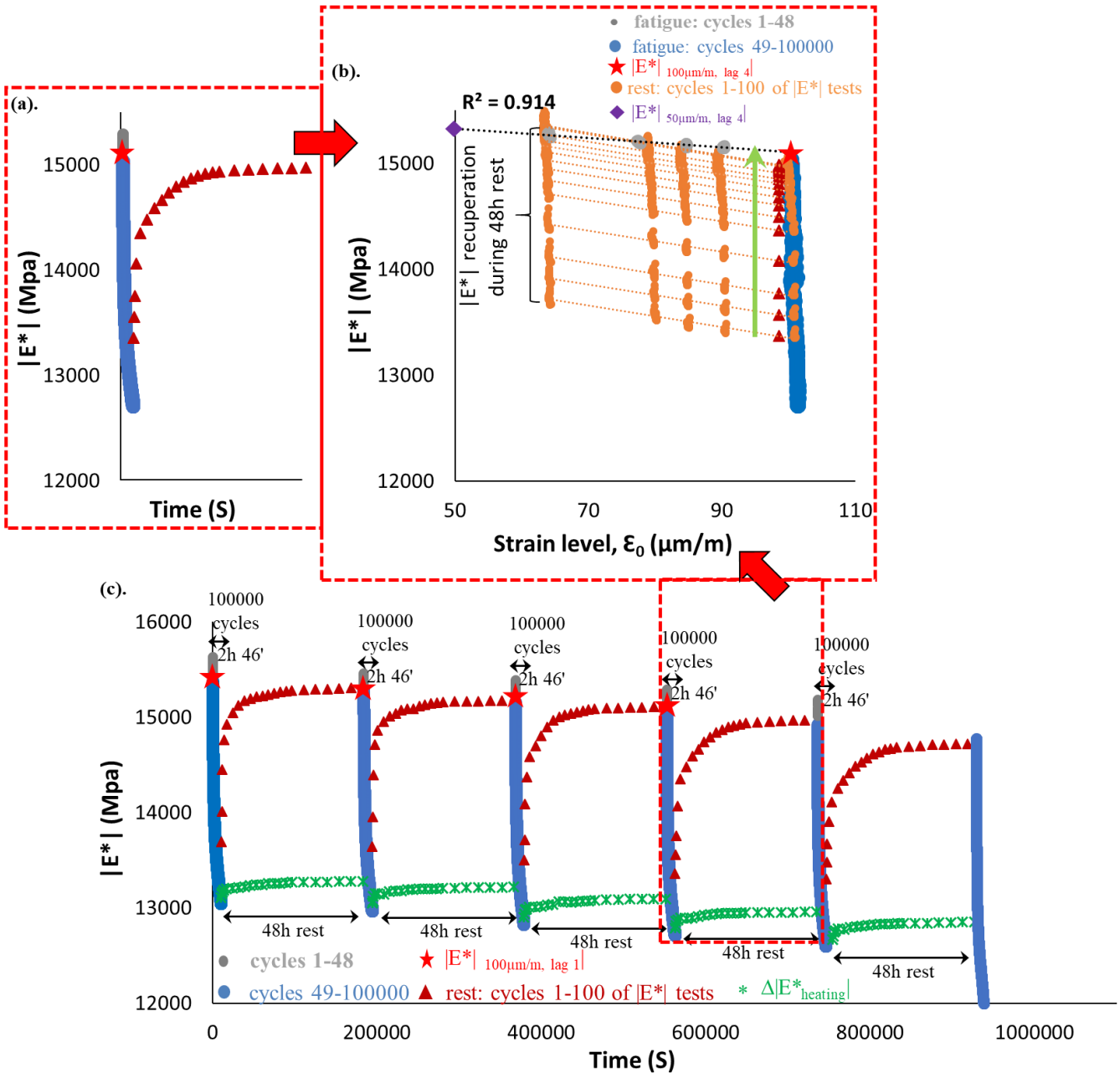

3.1.123. PFRT results obtained for mix PMB - 2: (a) |E*| as a function of time during the fourth fatigue lag and rest period (b) |E*| as a function of applied strain amplitude during the fourth fatigue lags and the short complex modulus tests performed within its following rest periods; (c) |E*| as a function of time during the five fatigue lags and rest periods [Red stars indicate values of |E*| estimated at 100 µm/m at the beginning of fatigue lag, green asterisk shows values of $\Delta|E^*_{heating}|$ as influence of self-heating and brown triangles indicate values of |E*| estimated at 100 µm/m for each short complex modulus test during rest (all these values were obtained using non-linearity envelopes, as shown in (b) for the first fatigue lag and rest period)].

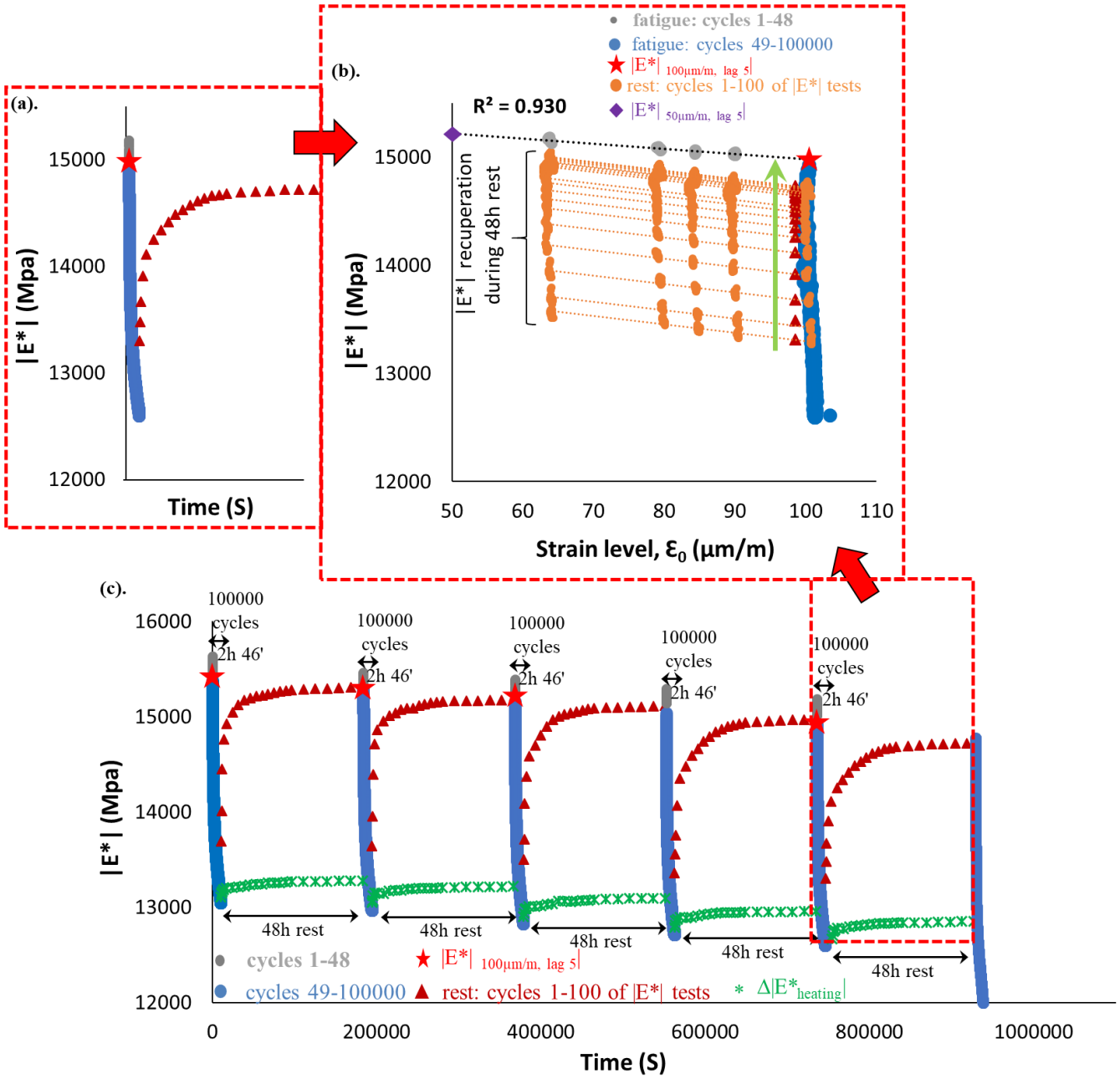

3.1.124. PFRT results obtained for mix PMB - 2: (a) |E*| as a function of time during the fifth fatigue lag and rest period (b) |E*| as a function of applied strain amplitude during the fifth fatigue lags and the short complex modulus tests performed within its following rest periods; (c) |E*| as a function of time during the five fatigue lags and rest periods [Red stars indicate values of |E*| estimated at 100 µm/m at the beginning of fatigue lag, green asterisk shows values of $\Delta|E^*_{heating}|$ as influence of self-heating and brown triangles indicate values of |E*| estimated at 100 µm/m for each short complex modulus test during rest (all these values were obtained using non-linearity envelopes, as shown in (b) for the first fatigue lag and rest period)].

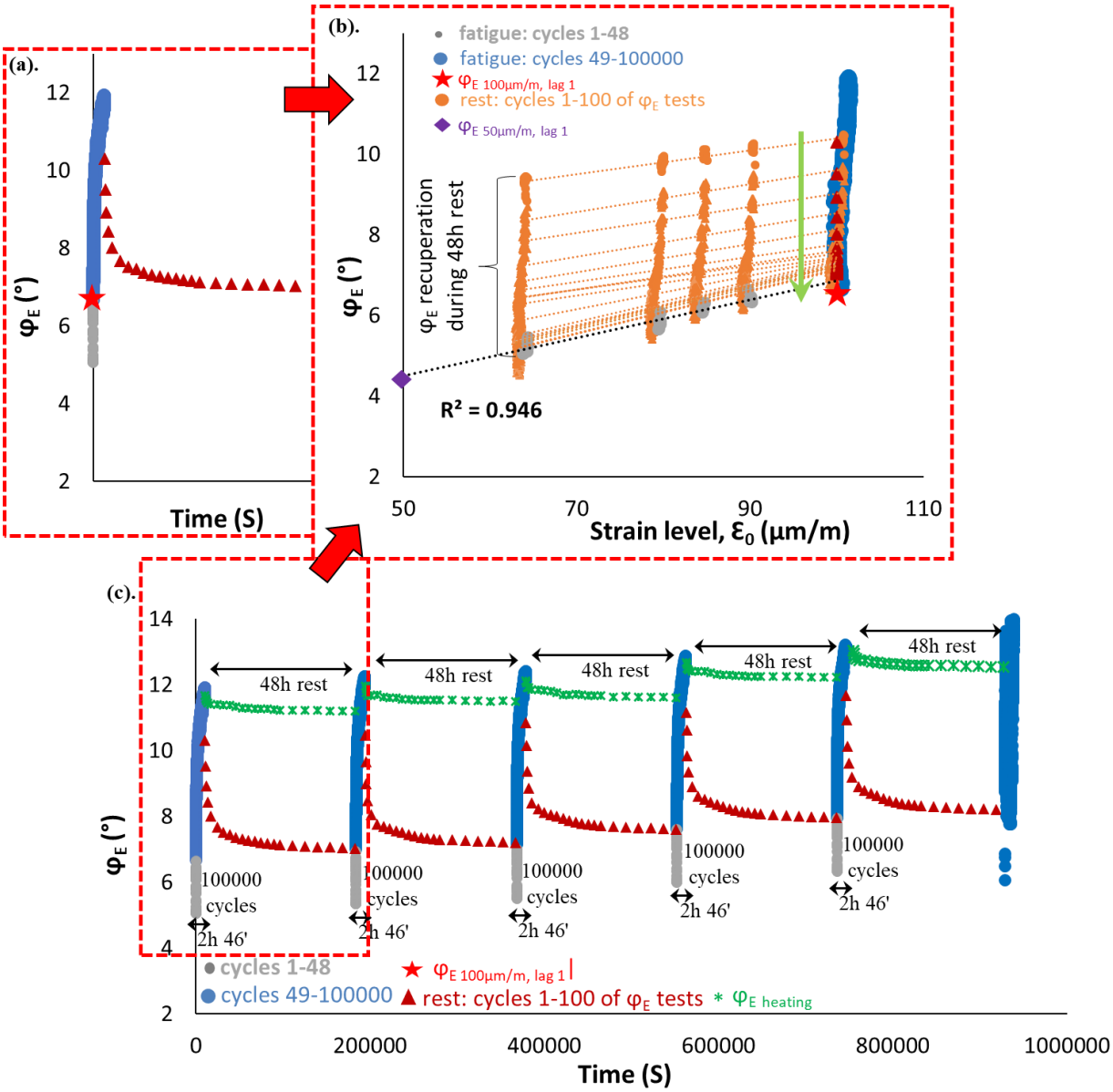

3.1.125. PFRT results obtained for mix PMB – 2: (a) φ_E as a function of time during the first fatigue lag and rest period (b) φ_E as a function of applied strain amplitude during the first fatigue lags and the short complex modulus tests performed within its following rest periods; (c) φ_E as a function of time during the five fatigue lags and rest periods (Red stars indicate values of φ_E estimated at 100 μm/m at the beginning of fatigue lag, green asterisk shows values of $\Delta\varphi_{E\ heating}$ as influence of self-heating and brown triangles indicate values of φ_E estimated at 100 μm/m for each short complex modulus test during rest (all these values were obtained using non-linearity envelopes, as shown in (b) for the first fatigue lag and rest period).

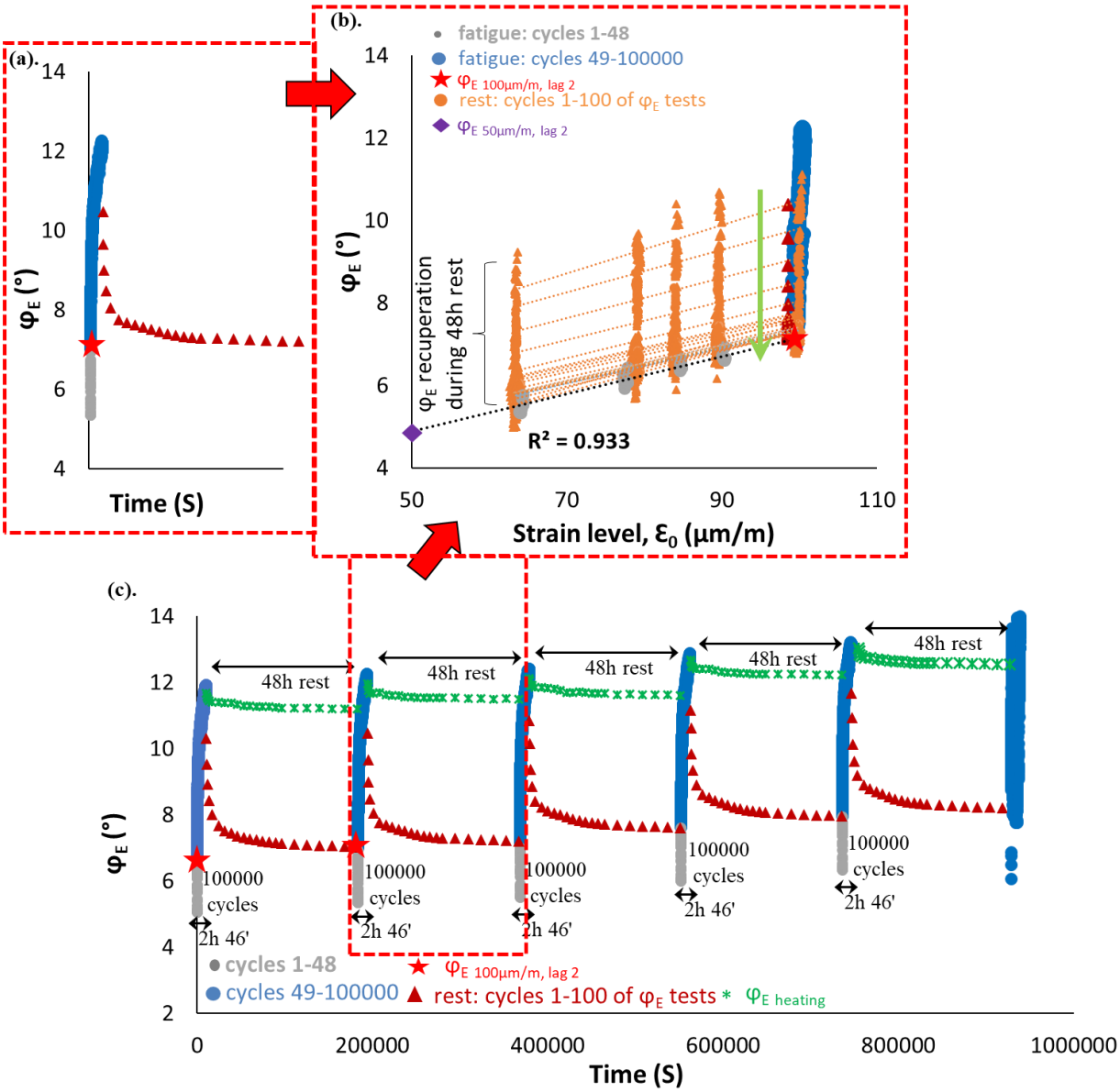

3.1.126. PFRT results obtained for mix PMB – 2: (a) φ_E as a function of time during the second fatigue lag and rest period (b) φ_E as a function of applied strain amplitude during the second fatigue lags and the short complex modulus tests performed within its following rest periods; (c) φ_E as a function of time during the five fatigue lags and rest periods (Red stars indicate values of φ_E estimated at 100 µm/m at the beginning of fatigue lag, green asterisk shows values of $\Delta\varphi_{E\ heating}$ as influence of self-heating and brown triangles indicate values of φ_E estimated at 100 µm/m for each short complex modulus test during rest (all these values were obtained using non-linearity envelopes, as shown in (b) for the first fatigue lag and rest period).

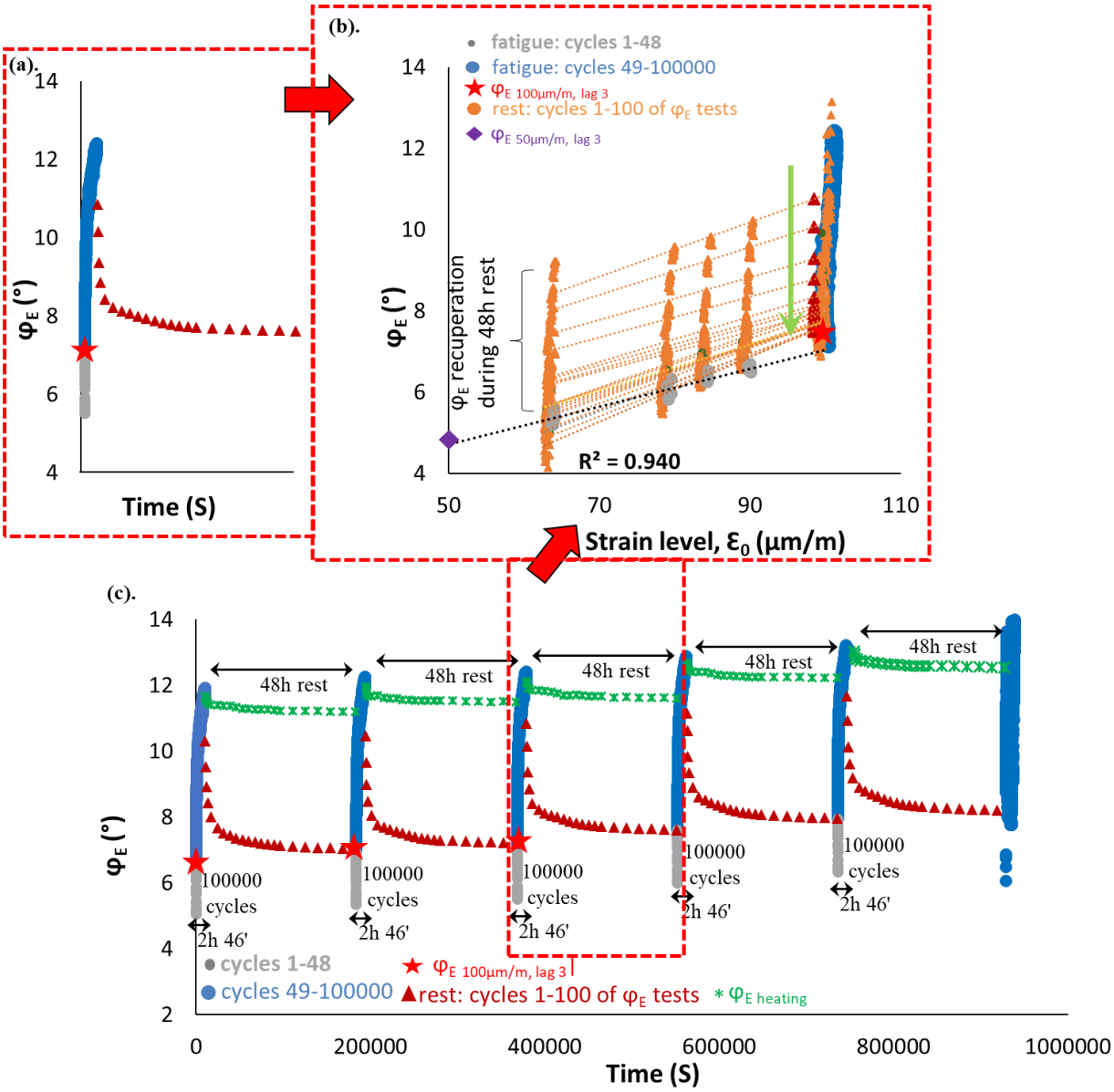

3.1.127. PFRT results obtained for mix PMB – 2: (a) φ_E as a function of time during the third fatigue lag and rest period (b) φ_E as a function of applied strain amplitude during the third fatigue lags and the short complex modulus tests performed within its following rest periods; (c) φ_E as a function of time during the five fatigue lags and rest periods (Red stars indicate values of φ_E estimated at 100 µm/m at the beginning of fatigue lag, green asterisk shows values of $\Delta\varphi_{E\ heating}$ as influence of self-heating and brown triangles indicate values of φ_E estimated at 100 µm/m for each short complex modulus test during rest (all these values were obtained using non-linearity envelopes, as shown in (b) for the first fatigue lag and rest period).

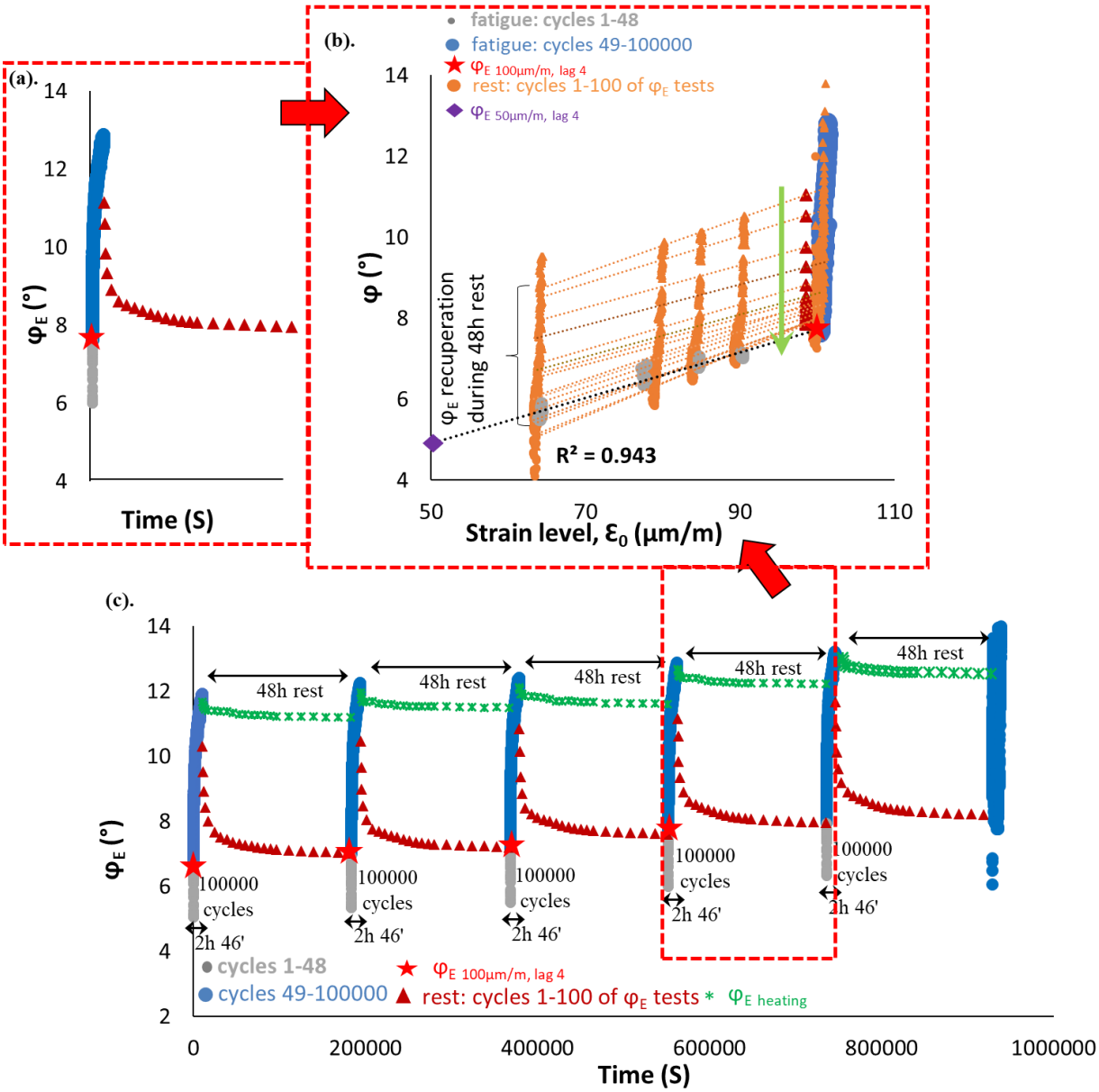

3.1.128. PFRT results obtained for mix PMB – 2: (a) φ_E as a function of time during the fourth fatigue lag and rest period (b) φ_E as a function of applied strain amplitude during the fourth fatigue lags and the short complex modulus tests performed within its following rest periods; (c) φ_E as a function of time during the five fatigue lags and rest periods (Red stars indicate values of φ_E estimated at 100 µm/m at the beginning of fatigue lag, green asterisk shows values of $\Delta\varphi_{E\ heating}$ as influence of self-heating and brown triangles indicate values of φ_E estimated at 100 µm/m for each short complex modulus test during rest (all these values were obtained using non-linearity envelopes, as shown in (b) for the first fatigue lag and rest period).

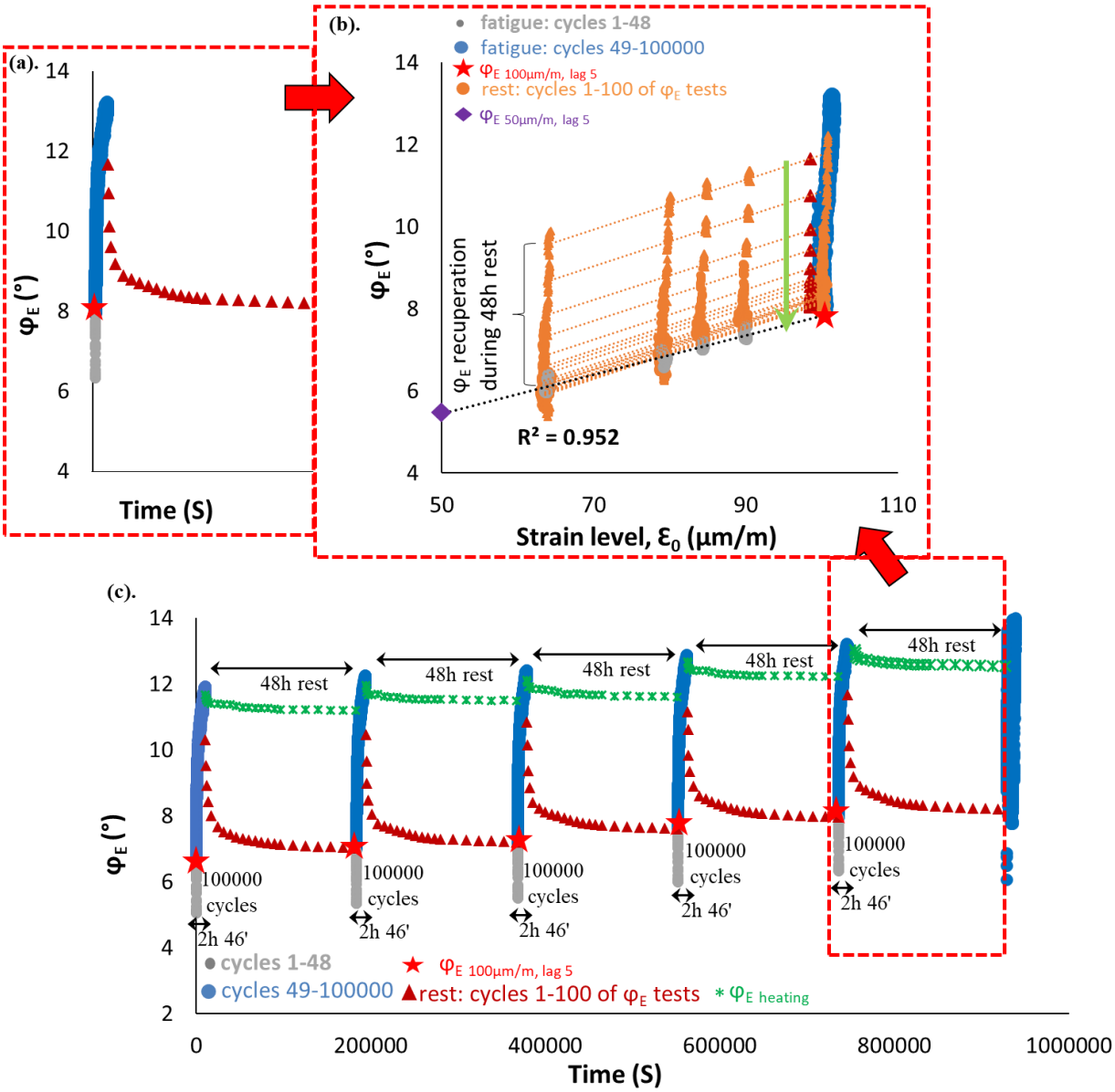

3.1.129. PFRT results obtained for mix PMB – 2: (a) φ_E as a function of time during the fifth fatigue lag and rest period (b) φ_E as a function of applied strain amplitude during the fifth fatigue lags and the short complex modulus tests performed within its following rest periods; (c) φ_E as a function of time during the five fatigue lags and rest periods (Red stars indicate values of φ_E estimated at 100 μm/m at the beginning of fatigue lag, green asterisk shows values of $\Delta\varphi_{E\ heating}$ as influence of self-heating and brown triangles indicate values of φ_E estimated at 100 μm/m for each short complex modulus test during rest (all these values were obtained using non-linearity envelopes, as shown in (b) for the first fatigue lag and rest period).

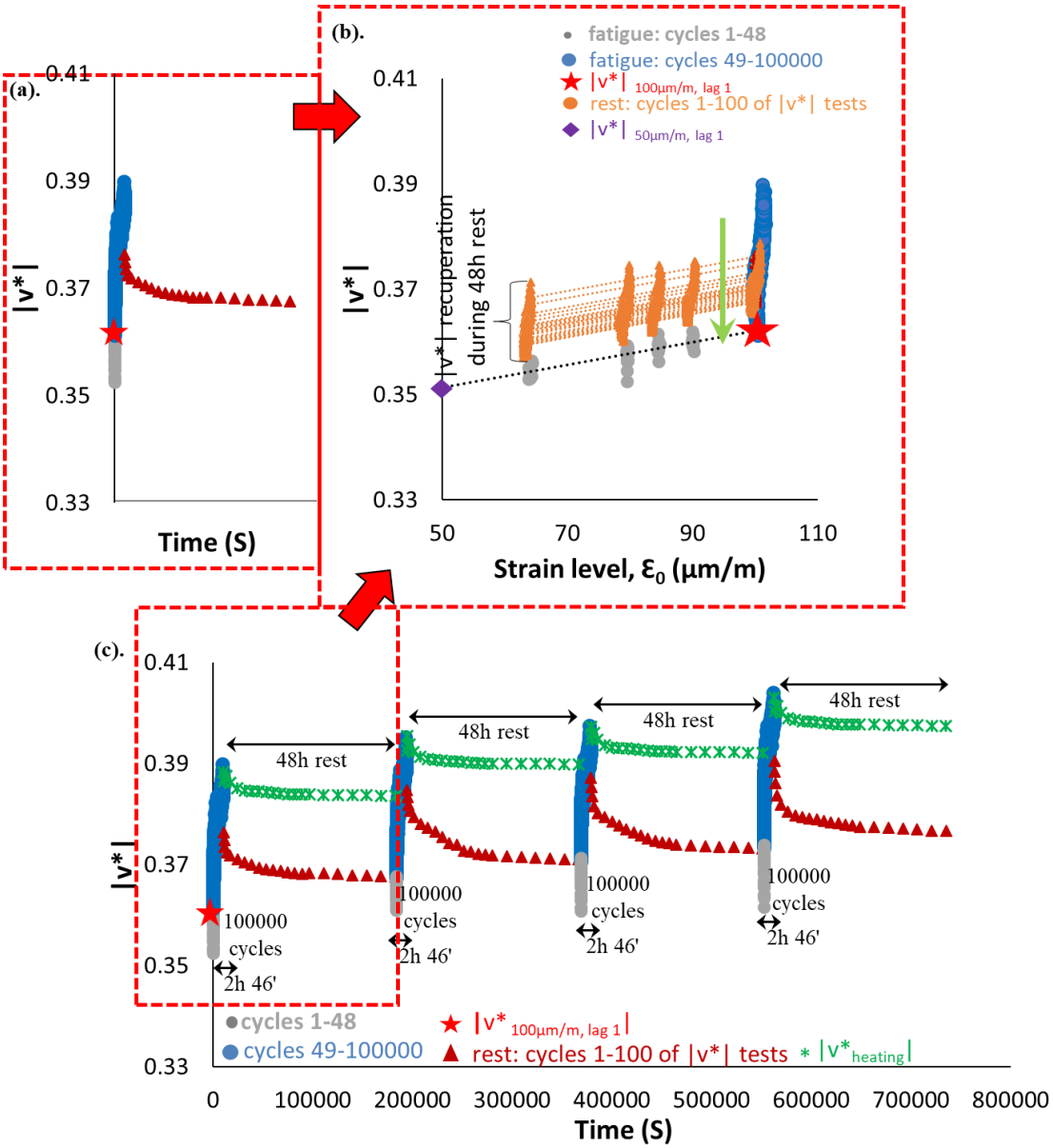

3.1.130. PFRT results obtained for mix PMB - 2: (a) |v*| as a function of time during the first fatigue lag and rest period (b) |v*| as a function of applied strain amplitude during the first fatigue lags and the short complex modulus tests performed within its following rest periods; (c) |v*| as a function of time during the five fatigue lags and rest periods [Red stars indicate values of |E*| estimated at 100 µm/m at the beginning of fatigue lag, green asterisk shows values of $\Delta|v^*_{heating}|$ as influence of self-heating and brown triangles indicate values of |v*| estimated at 100 µm/m for each short complex modulus test during rest (all these values were obtained using non-linearity envelopes, as shown in (b) for the first fatigue lag and rest period)].

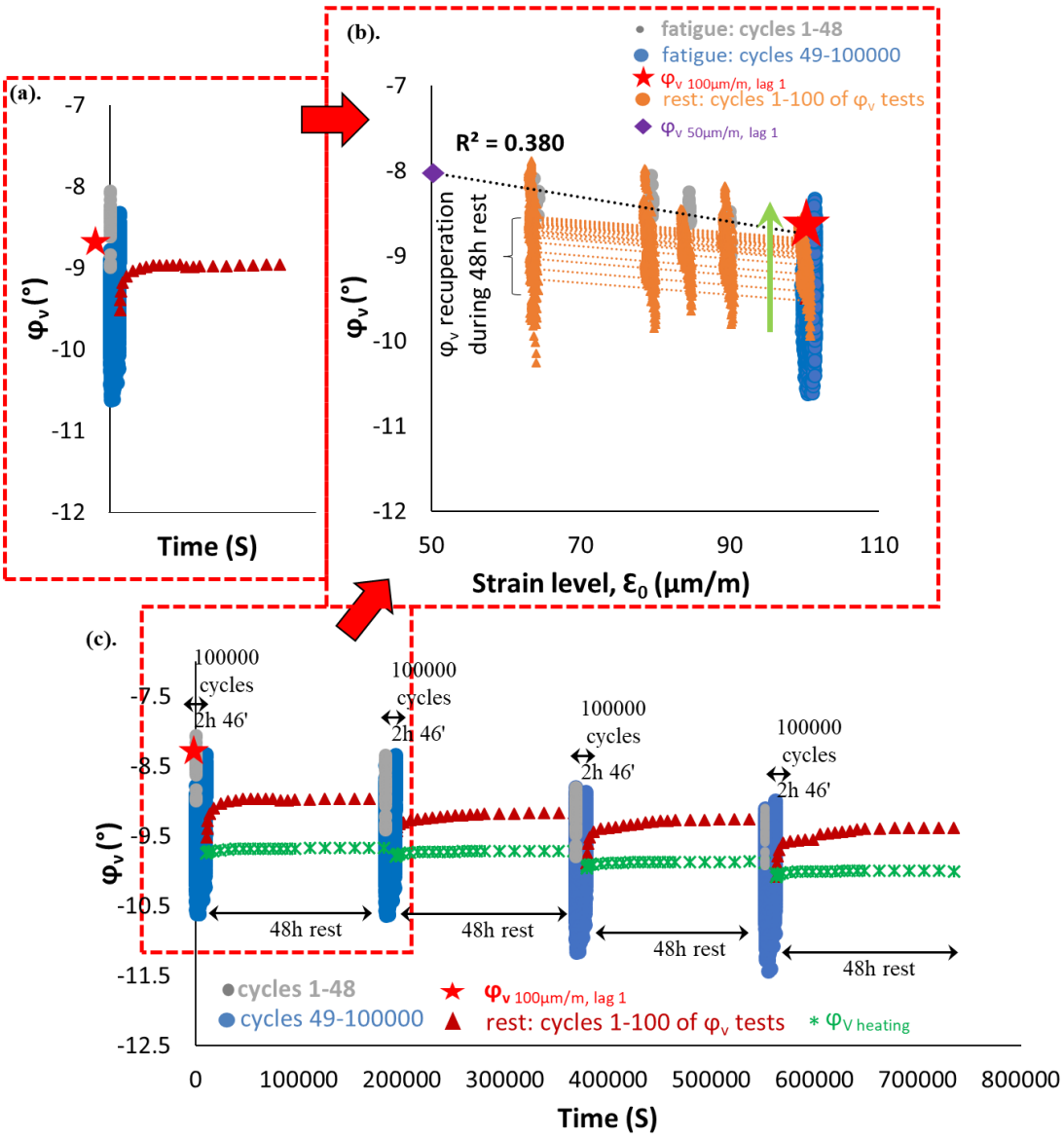

3.1.131. PFRT results obtained for mix PMB – 2: (a) φ_v as a function of time during the first fatigue lag and rest period (b) φ_v as a function of applied strain amplitude during the first fatigue lags and the short complex modulus tests performed within its following rest periods; (c) φ_v as a function of time during the five fatigue lags and rest periods (Red stars indicate values of φ_v estimated at 100 µm/m at the beginning of fatigue lag, green asterisk shows values of $\Delta\varphi_{v\ heating}$ as influence of self-heating and brown triangles indicate values of φ_v estimated at 100 µm/m for each short complex modulus test during rest (all these values were obtained using non-linearity envelopes, as shown in (b) for the first fatigue lag and rest period).

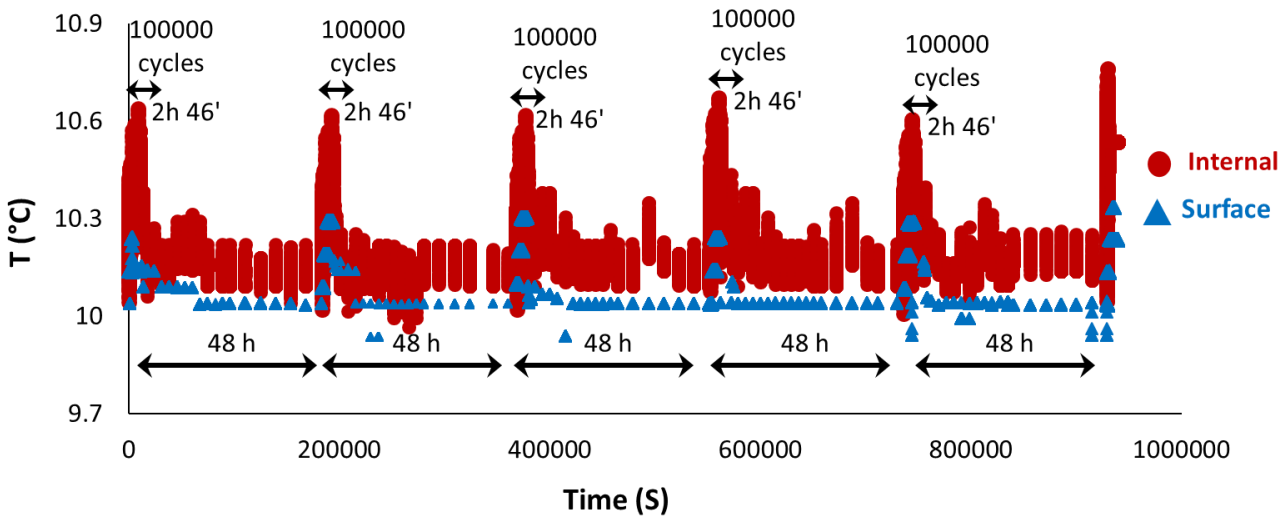

3.1.132. PFRT results obtained for mix PMB – 2: internal and surface temperature evolution during fatigue lags and recovery periods.

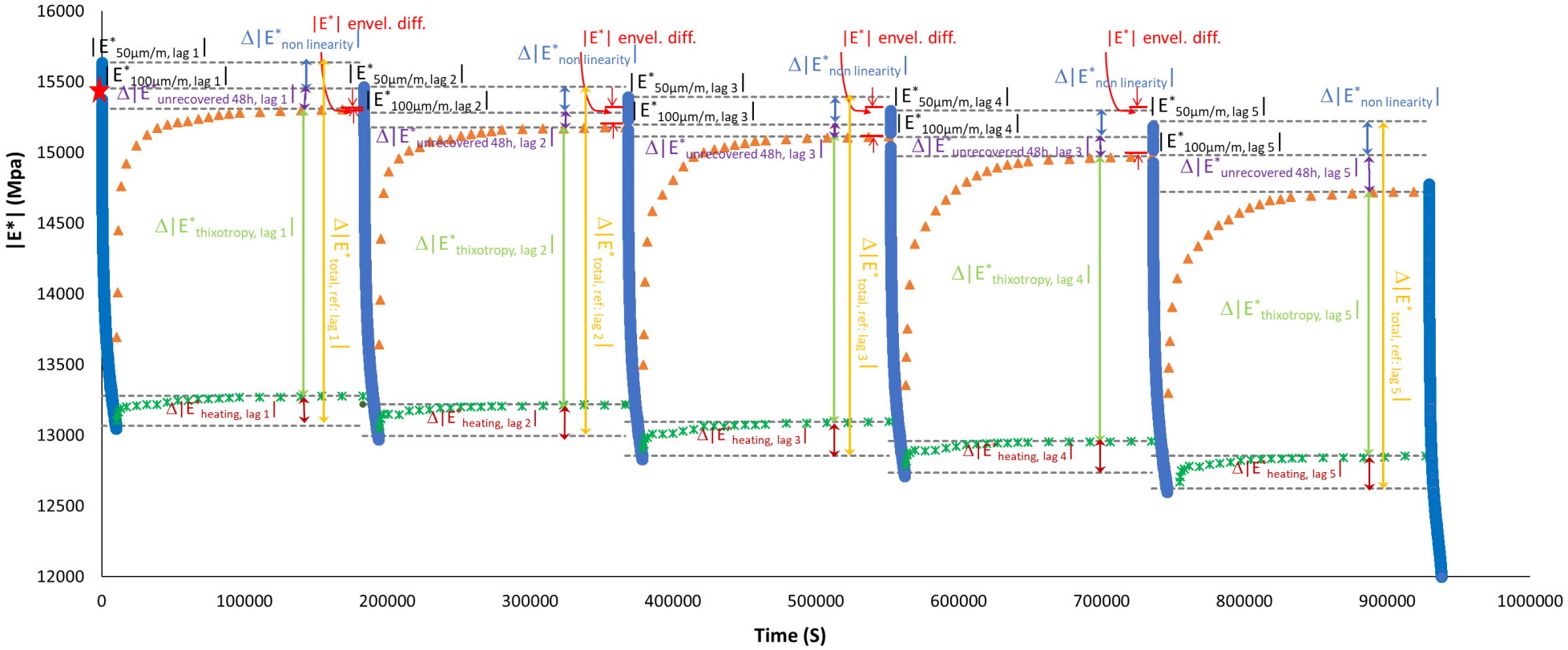
16000
15500
15000
14500
14000
13500
13000
12500
12000
|E*| (Mpa)
0
100000
200000
300000
400000
500000
600000
700000
800000
900000
1000000
Time (S)
|E*50µm/m, lag 1|
|E*100µm/m, lag 1|
Δ|E*non linearity|
|E*| envel. diff.
Δ|E*unrecovered 48h, lag 1|
Δ|E*thixotropy, lag 1|
Δ|E*total, ref: lag 1|
Δ|E*heating, lag 1|
|E*50µm/m, lag 2|
|E*100µm/m, lag 2|
Δ|E*unrecovered 48h, lag 2|
Δ|E*thixotropy, lag 2|
Δ|E*total, ref: lag 2|
Δ|E*heating, lag 2|
|E*50µm/m, lag 3|
|E*100µm/m, lag 3|
Δ|E*unrecovered 48h, lag 3|
Δ|E*thixotropy, lag 4|
Δ|E*total, ref: lag 3|
Δ|E*heating, lag 3|
|E*50µm/m, lag 4|
|E*100µm/m, lag 4|
Δ|E*unrecovered 48h, lag 4|
Δ|E*thixotropy, lag 5|
Δ|E*total, ref: lag 5|
Δ|E*heating, lag 4|
|E*50µm/m, lag 5|
|E*100µm/m, lag 5|
Δ|E*unrecovered 48h, lag 5|
Δ|E*heating, lag 5|

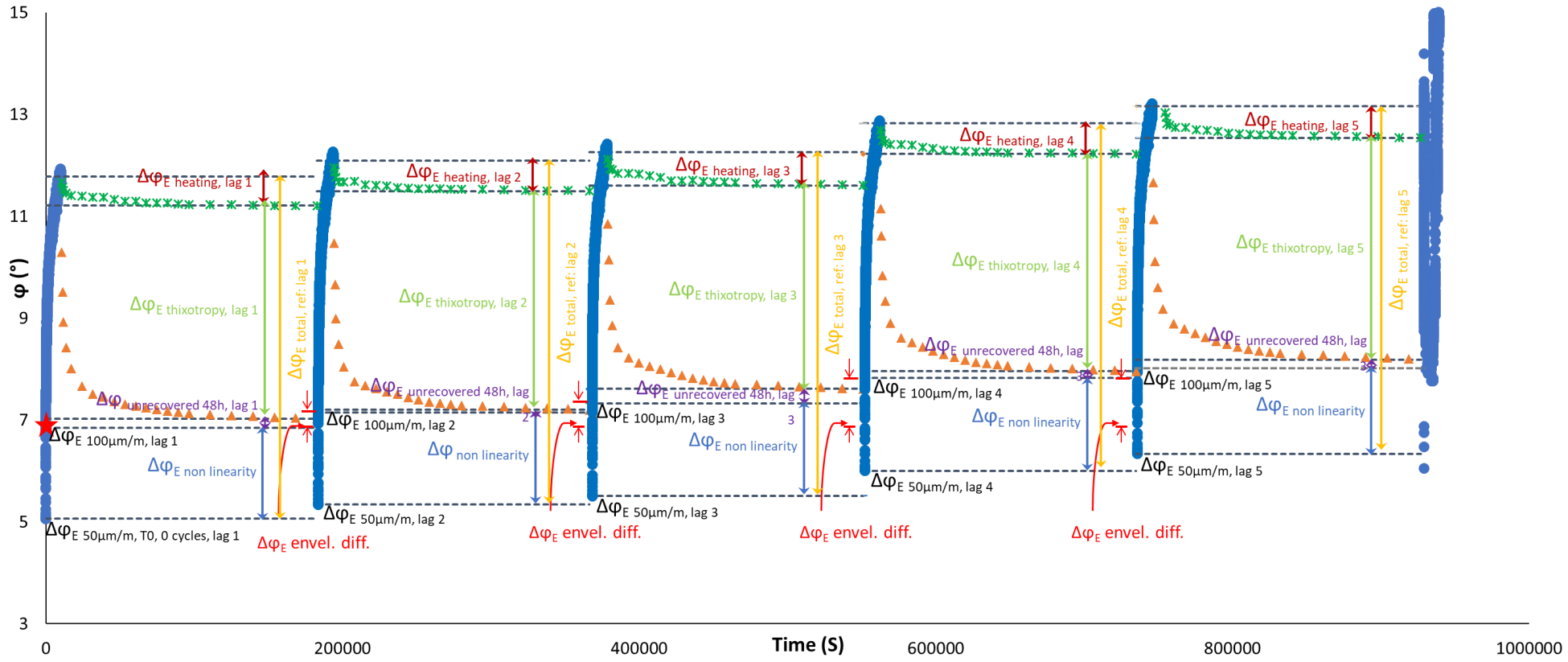

3.1.133. Quantification of different contributions |E*| and φ_E evolution, for the five fatigue lags for mix PMB – 2: different envelope line is used for each fatigue lag.

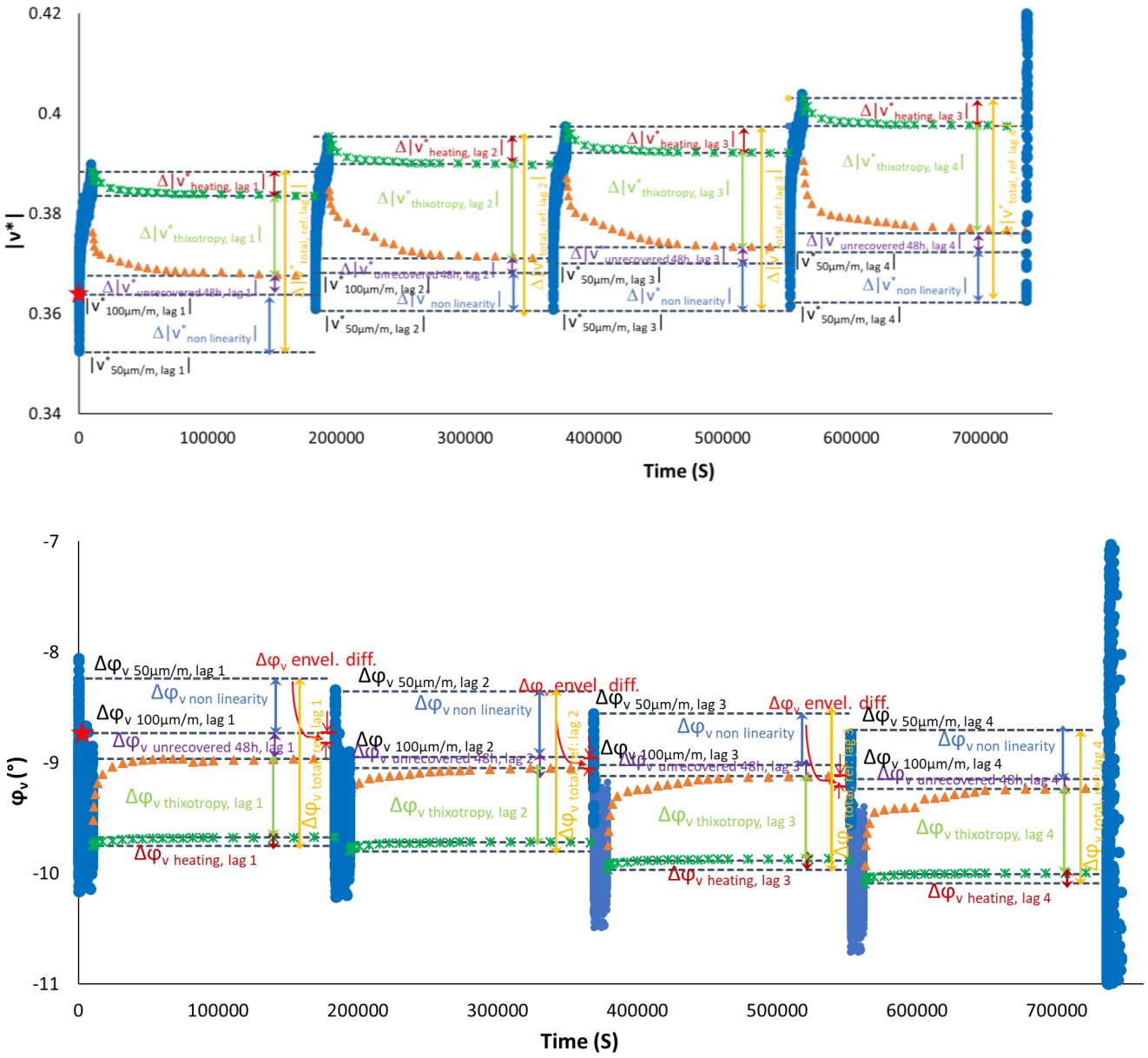

3.1.133. Quantification of different contributions |E*|, φ_E, |v*| and φ_v evolution, for the five fatigue lags for mix PMB – 2: different envelope line is used for each fatigue lag.

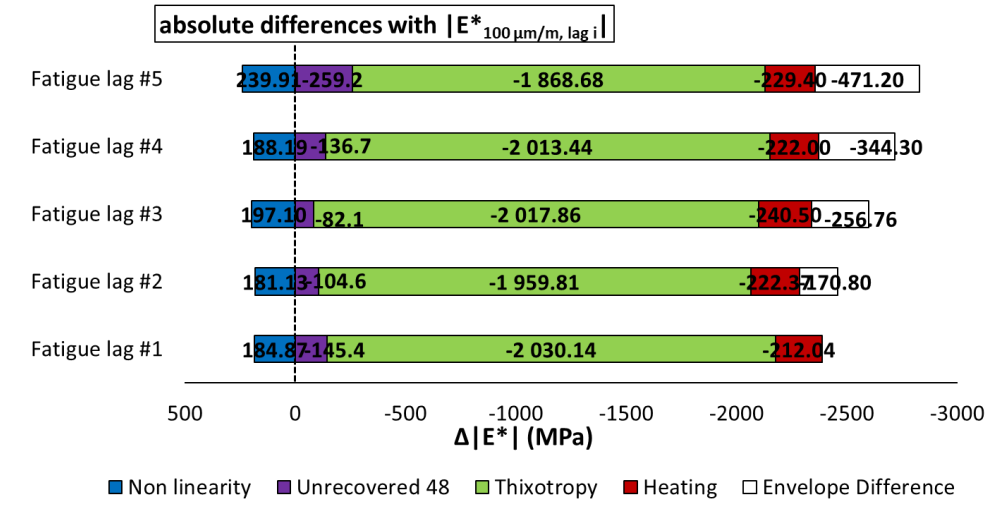
absolute differences with |E*100 µm/m, lag i|
Fatigue lag #5
Fatigue lag #4
Fatigue lag #3
Fatigue lag #2
Fatigue lag #1
-1 868.68
-2 013.44
-2 017.86
-1 959.81
-2 030.14
-471.20
-344.30
-256.76
-170.80
500
0
-500
-1000
-1500
-2000
-2500
-3000
Δ|E*| (MPa)
Non linearity
Unrecovered 48
Thixotropy
Heating
Envelope Difference

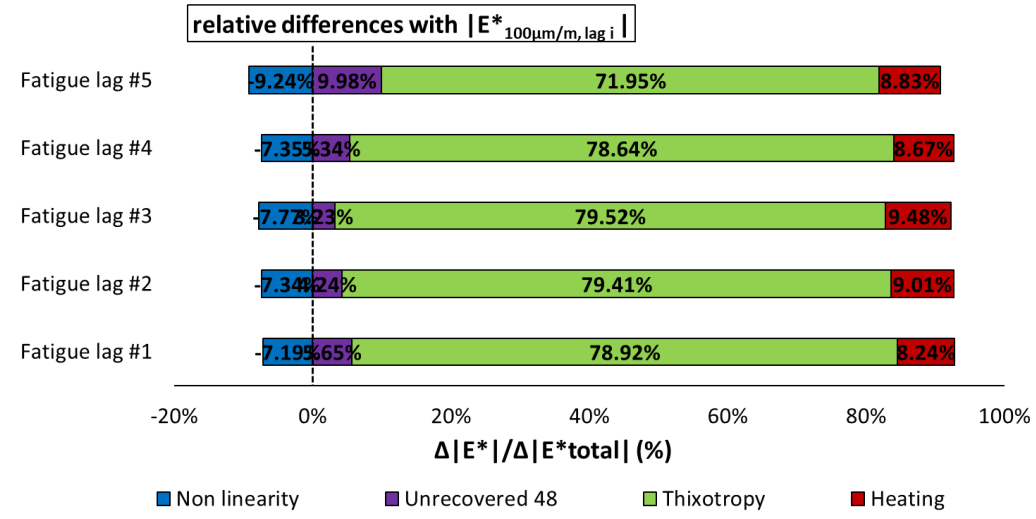
relative differences with |E*100µm/m, lag i|
Fatigue lag #5
Fatigue lag #4
Fatigue lag #3
Fatigue lag #2
Fatigue lag #1
-9.24%
9.98%
71.95%
8.83%
78.64%
8.67%
79.52%
9.48%
79.41%
9.01%
78.92%
8.24%
-20%
0%
20%
40%
60%
80%
100%
Δ|E*|/Δ|E*total| (%)
Non linearity
Unrecovered 48
Thixotropy
Heating

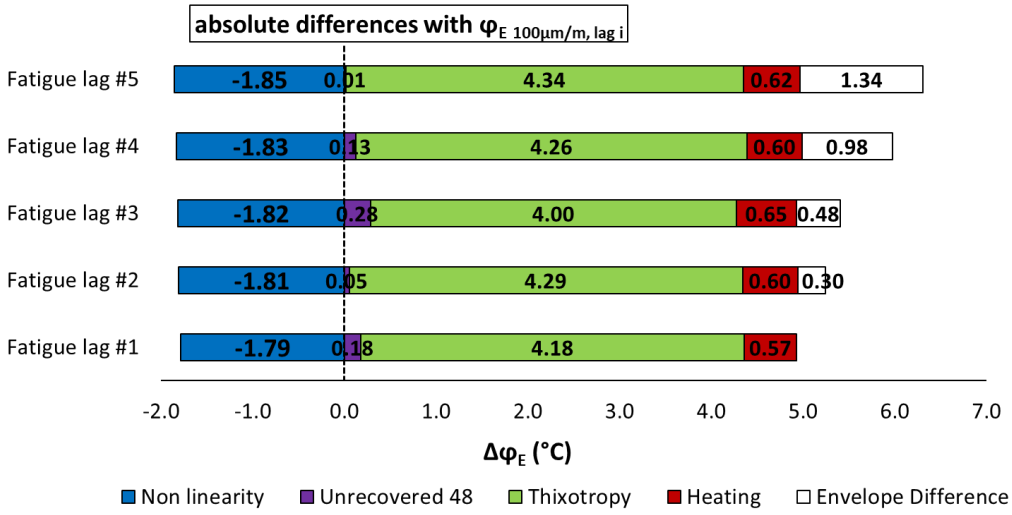
absolute differences with φE 100µm/m, lag i
Fatigue lag #5
Fatigue lag #4
Fatigue lag #3
Fatigue lag #2
Fatigue lag #1
-1.85
0.01
4.34
0.62
1.34
-1.83
0.13
4.26
0.60
0.98
-1.82
0.28
4.00
0.65
0.48
-1.81
0.05
4.29
0.60
0.30
-1.79
0.18
4.18
0.57
-2.0
-1.0
0.0
1.0
2.0
3.0
4.0
5.0
6.0
7.0
Δφ E (°C)
Non linearity
Unrecovered 48
Thixotropy
Heating
Envelope Difference

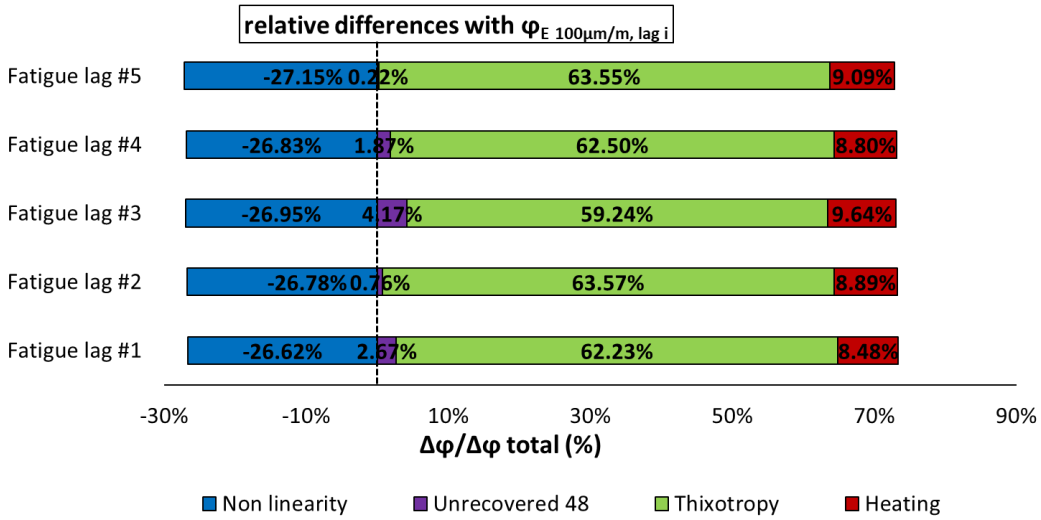
relative differences with $\varphi_{E\ 100\mu m/m,\ lag\ i}$
Fatigue lag #5
Fatigue lag #4
Fatigue lag #3
Fatigue lag #2
Fatigue lag #1
-27.15%
0.22%
63.55%
9.09%
-26.83%
1.87%
62.50%
8.80%
-26.95%
4.17%
59.24%
9.64%
-26.78%
0.76%
63.57%
8.89%
-26.62%
2.67%
62.23%
8.48%
-30%
-10%
10%
30%
50%
70%
90%
Δφ/Δφ total (%)
Non linearity
Unrecovered 48
Thixotropy
Heating

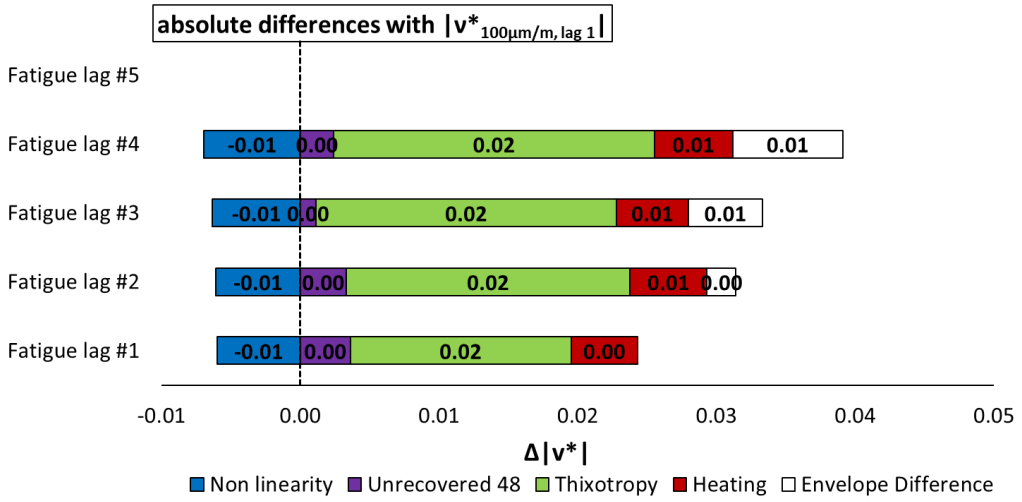
absolute differences with $|v^*_{100\mu m/m,\ lag\ 1}|$
Fatigue lag #5
Fatigue lag #4
Fatigue lag #3
Fatigue lag #2
Fatigue lag #1
-0.01
0.00
0.02
0.01
0.01
-0.01
0.00
0.02
0.01
0.01
-0.01
0.00
0.02
0.01
0.00
-0.01
0.00
0.02
0.00
-0.01
0.00
0.01
0.02
0.03
0.04
0.05
Δ|v*|
Non linearity
Unrecovered 48
Thixotropy
Heating
Envelope Difference

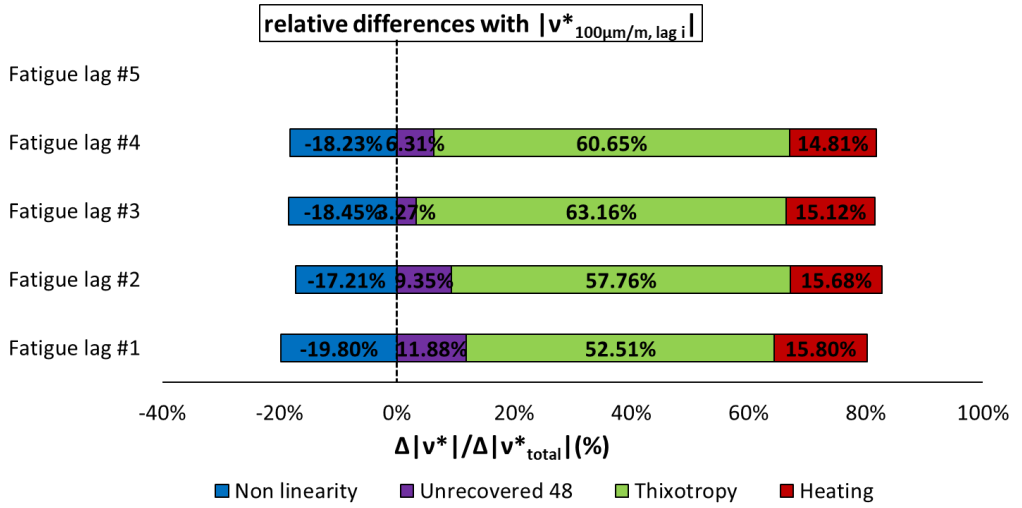
relative differences with $|v^*_{100\mu m/m,\ lag\ i}|$
Fatigue lag #5
Fatigue lag #4
Fatigue lag #3
Fatigue lag #2
Fatigue lag #1
-18.23%
6.31%
60.65%
14.81%
-18.45%
6.27%
63.16%
15.12%
-17.21%
9.35%
57.76%
15.68%
-19.80%
11.88%
52.51%
15.80%
-40%
-20%
0%
20%
40%
60%
80%
100%
Δ|v*|/Δ|v*total|(%)
Non linearity
Unrecovered 48
Thixotropy
Heating

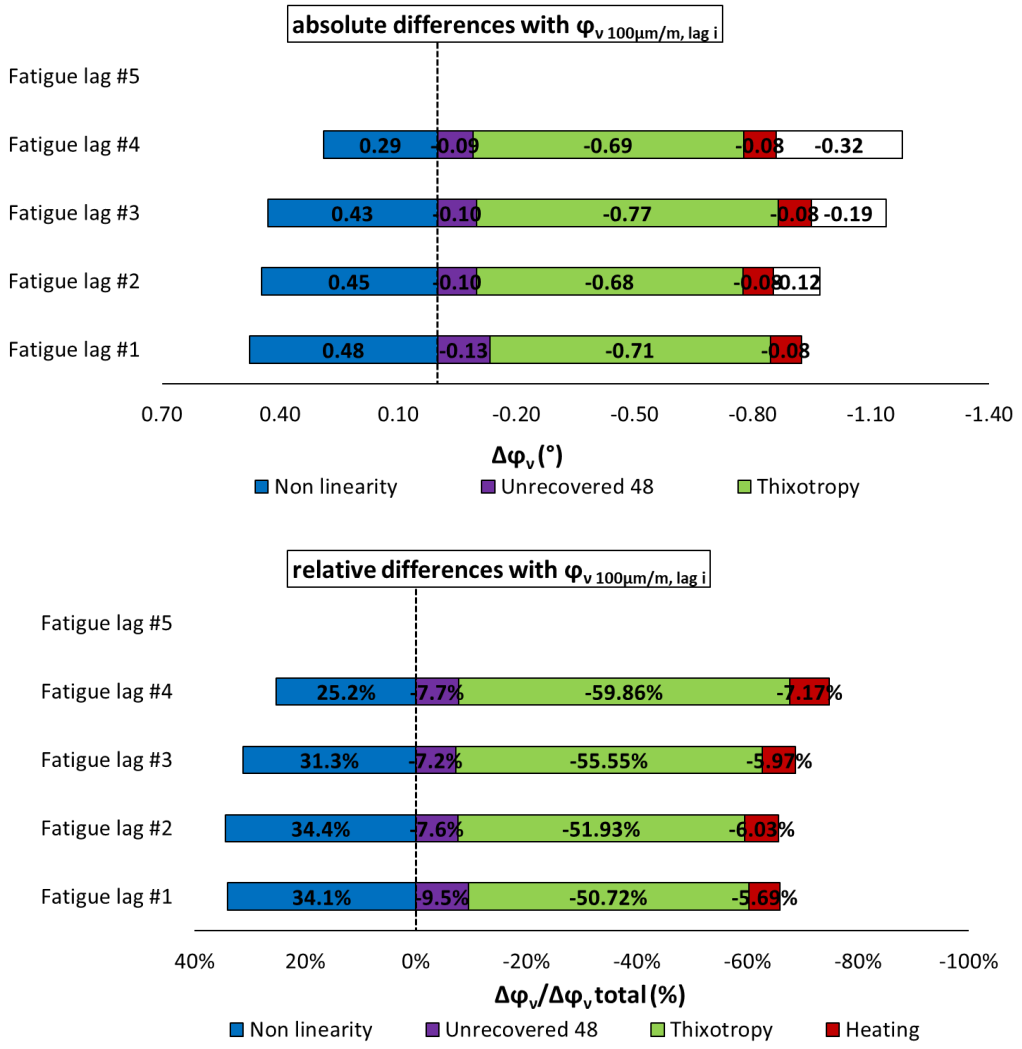

3.1.134. Quantification of different absolute and relative contributions to |E*|, φ_E, |ν*| and φ_ν evolutions for mix PMB – 2, calculated using a different envelope line for each fatigue lag.

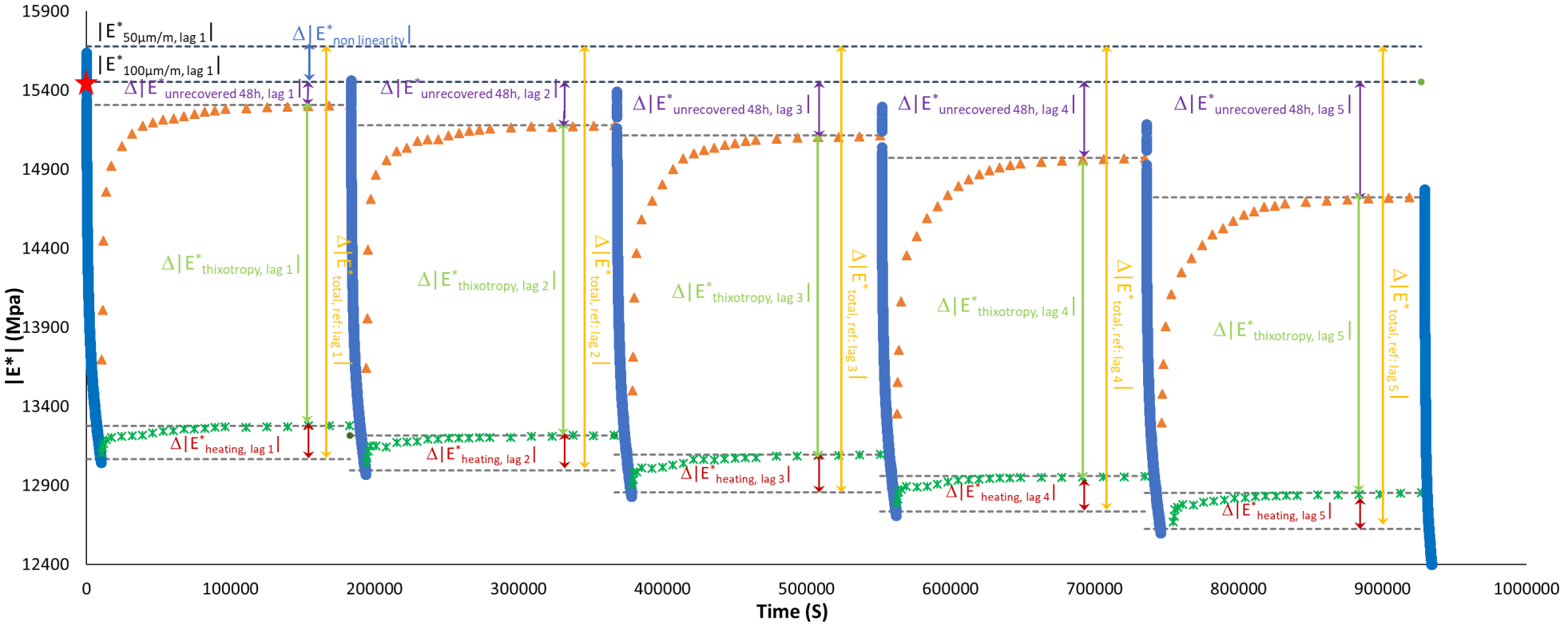
15900
15400
14900
14400
13900
13400
12900
12400
|E*| (Mpa)
0
100000
200000
300000
400000
500000
600000
700000
800000
900000
1000000
Time (S)
|E*50µm/m, lag 1|
|E*100µm/m, lag 1|
Δ|E*non linearity|
Δ|E*unrecovered 48h, lag 1|
Δ|E*unrecovered 48h, lag 2|
Δ|E*unrecovered 48h, lag 3|
Δ|E*unrecovered 48h, lag 4|
Δ|E*unrecovered 48h, lag 5|
Δ|E*thixotropy, lag 1|
Δ|E*thixotropy, lag 2|
Δ|E*thixotropy, lag 3|
Δ|E*thixotropy, lag 4|
Δ|E*thixotropy, lag 5|
Δ|E*total, ref: lag 1|
Δ|E*total, ref: lag 2|
Δ|E*total, ref: lag 3|
Δ|E*total, ref: lag 4|
Δ|E*total, ref: lag 5|
Δ|E*heating, lag 1|
Δ|E*heating, lag 2|
Δ|E*heating, lag 3|
Δ|E*heating, lag 4|
Δ|E*heating, lag 5|

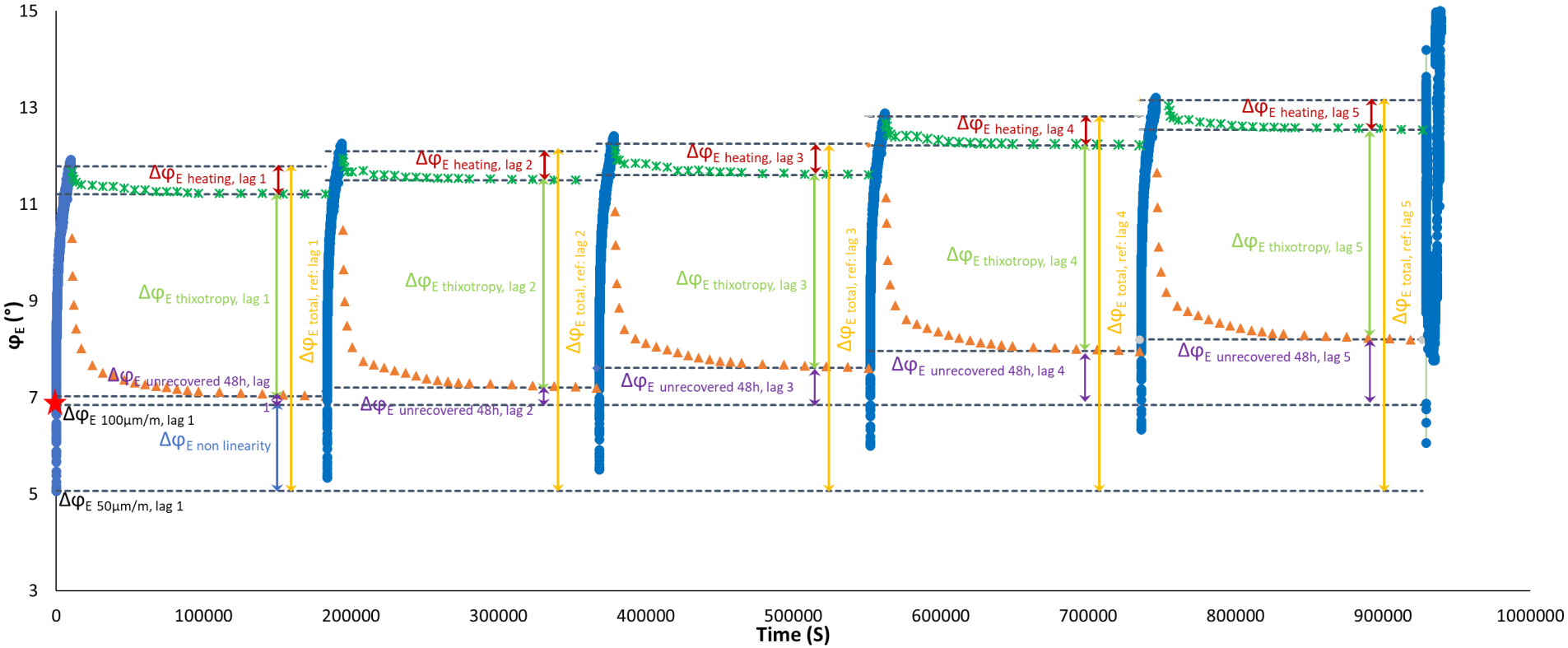
15
13
11
9
7
5
3
φE (°)
0
100000
200000
300000
400000
500000
600000
700000
800000
900000
1000000
Time (S)
Δφ E heating, lag 1
Δφ E thixotropy, lag 1
Δφ E unrecovered 48h, lag 1
Δφ E total, ref: lag 1
Δφ E 100µm/m, lag 1
Δφ E non linearity
Δφ E 50µm/m, lag 1
Δφ E heating, lag 2
Δφ E thixotropy, lag 2
Δφ E unrecovered 48h, lag 2
Δφ E total, ref: lag 2
Δφ E heating, lag 3
Δφ E thixotropy, lag 3
Δφ E unrecovered 48h, lag 3
Δφ E total, ref: lag 3
Δφ E heating, lag 4
Δφ E thixotropy, lag 4
Δφ E unrecovered 48h, lag 4
Δφ E total, ref: lag 4
Δφ E heating, lag 5
Δφ E thixotropy, lag 5
Δφ E unrecovered 48h, lag 5
Δφ E total, ref: lag 5

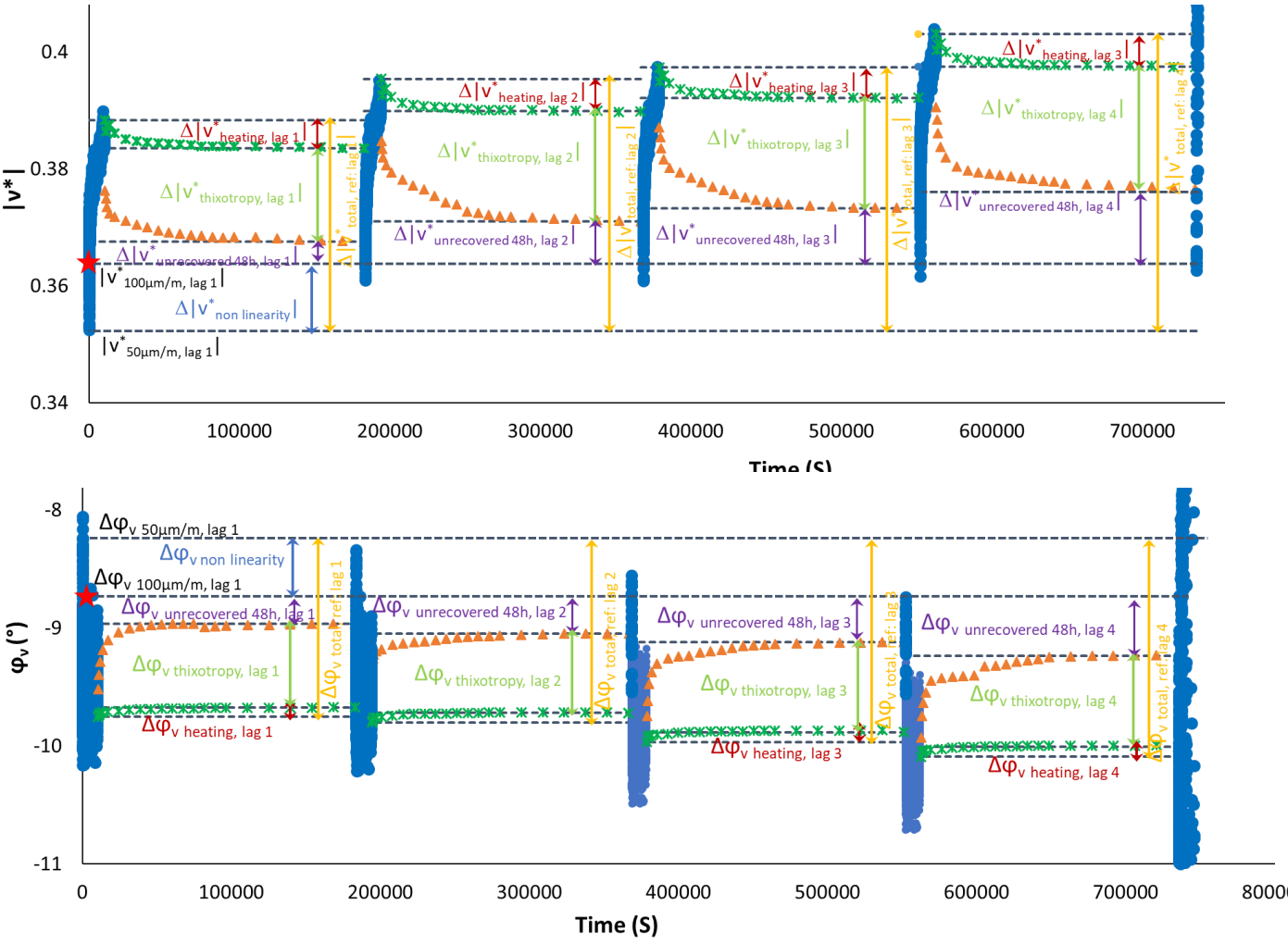

3.1.135. Quantification of different contributions to |E*|, φ_E, |v*| and φ_v evolution during five fatigue lags for mix PMB – 2: the envelope line of the first fatigue lag is used for all fatigue lags.

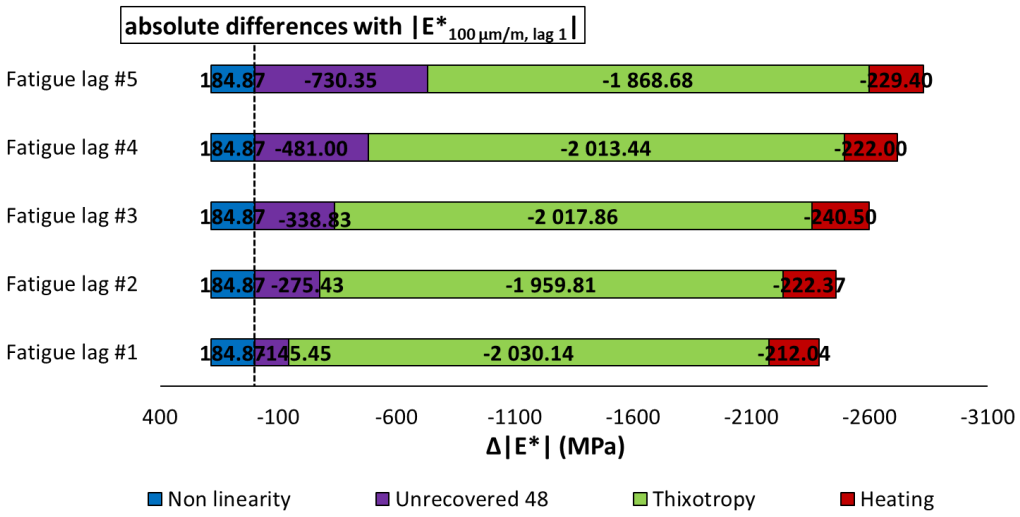

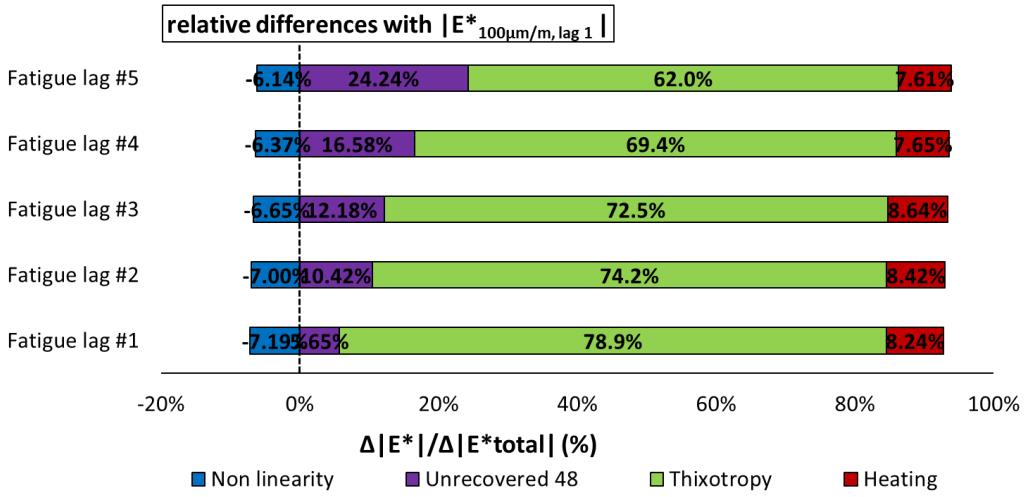
relative differences with |E*100µm/m, lag 1|
Fatigue lag #5
Fatigue lag #4
Fatigue lag #3
Fatigue lag #2
Fatigue lag #1
-6.14%
24.24%
62.0%
7.61%
-6.37%
16.58%
69.4%
7.65%
-6.65%
12.18%
72.5%
8.64%
-7.00%
10.42%
74.2%
8.42%
-7.19%
65%
78.9%
8.24%
-20%
0%
20%
40%
60%
80%
100%
Δ|E*|/Δ|E*total| (%)
Non linearity
Unrecovered 48
Thixotropy
Heating

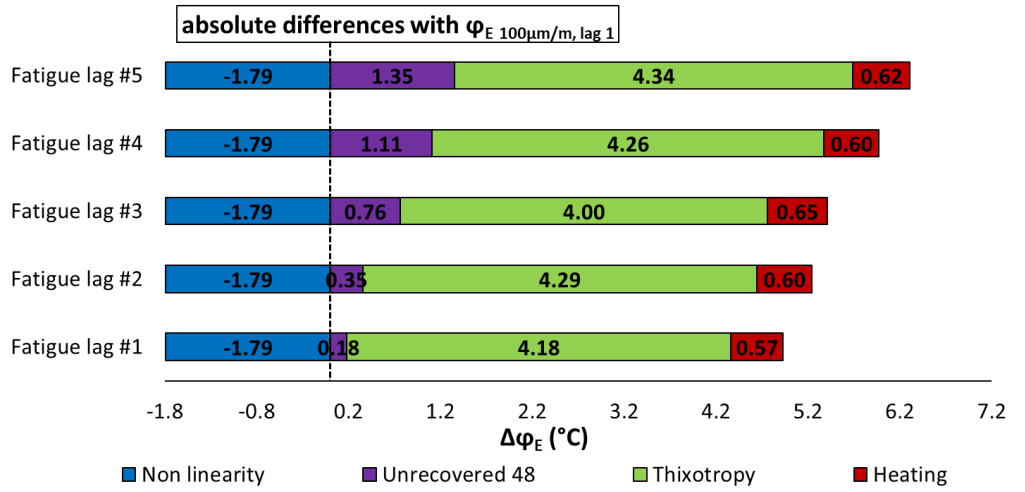
absolute differences with φE 100µm/m, lag 1
Fatigue lag #5
Fatigue lag #4
Fatigue lag #3
Fatigue lag #2
Fatigue lag #1
-1.79
1.35
4.34
0.62
-1.79
1.11
4.26
0.60
-1.79
0.76
4.00
0.65
-1.79
0.35
4.29
0.60
-1.79
0.18
4.18
0.57
-1.8
-0.8
0.2
1.2
2.2
3.2
4.2
5.2
6.2
7.2
ΔφE (°C)
Non linearity
Unrecovered 48
Thixotropy
Heating

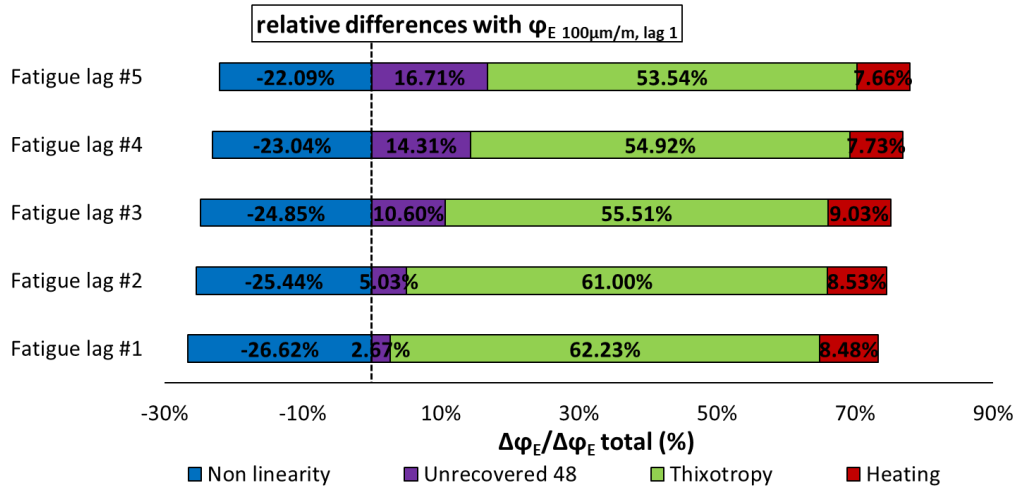
relative differences with φE 100µm/m, lag 1
Fatigue lag #5
Fatigue lag #4
Fatigue lag #3
Fatigue lag #2
Fatigue lag #1
-22.09%
16.71%
53.54%
7.66%
-23.04%
14.31%
54.92%
7.73%
-24.85%
10.60%
55.51%
9.03%
-25.44%
5.03%
61.00%
8.53%
-26.62%
2.67%
62.23%
8.48%
-30%
-10%
10%
30%
50%
70%
90%
ΔφE/ΔφE total (%)
Non linearity
Unrecovered 48
Thixotropy
Heating

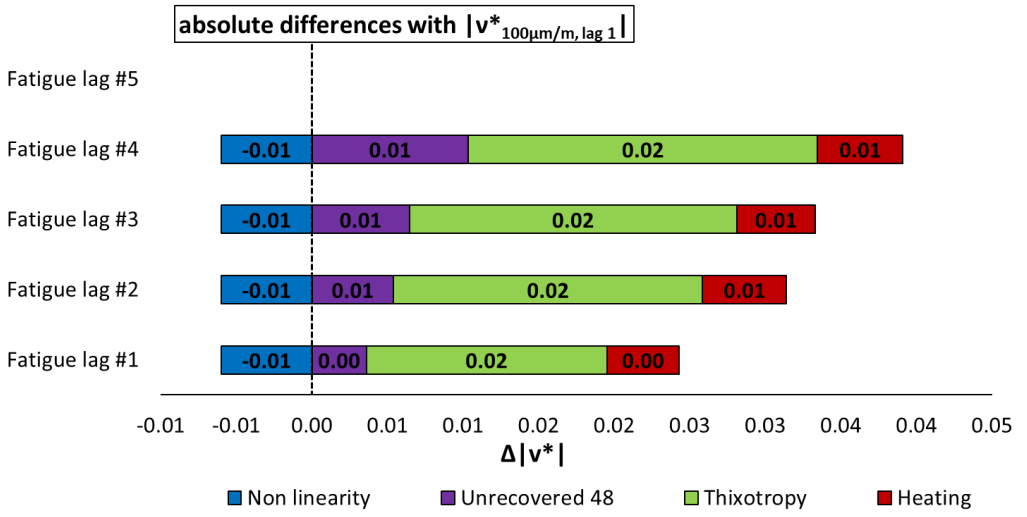
absolute differences with |v*100µm/m, lag 1|
Fatigue lag #5
Fatigue lag #4
Fatigue lag #3
Fatigue lag #2
Fatigue lag #1
-0.01 0.01 0.02 0.01
-0.01 0.01 0.02 0.01
-0.01 0.01 0.02 0.01
-0.01 0.00 0.02 0.00
-0.01 -0.01 0.00 0.01 0.01 0.02 0.02 0.03 0.03 0.04 0.04 0.05
Δ|v*|
Non linearity
Unrecovered 48
Thixotropy
Heating

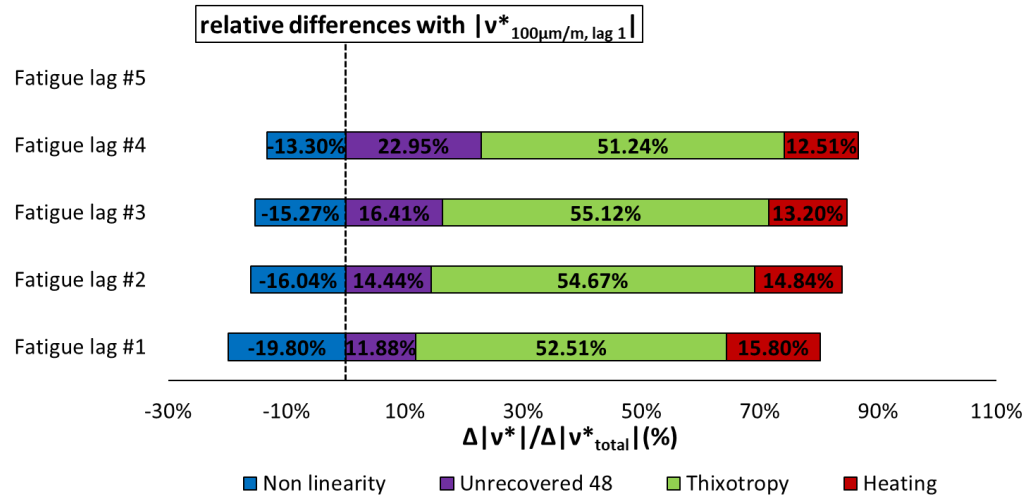
relative differences with |v*100µm/m, lag 1|
Fatigue lag #5
Fatigue lag #4
Fatigue lag #3
Fatigue lag #2
Fatigue lag #1
-13.30% 22.95% 51.24% 12.51%
-15.27% 16.41% 55.12% 13.20%
-16.04% 14.44% 54.67% 14.84%
-19.80% 11.88% 52.51% 15.80%
-30% -10% 10% 30% 50% 70% 90% 110%
Δ|v*|/Δ|v*total|(%)
Non linearity
Unrecovered 48
Thixotropy
Heating

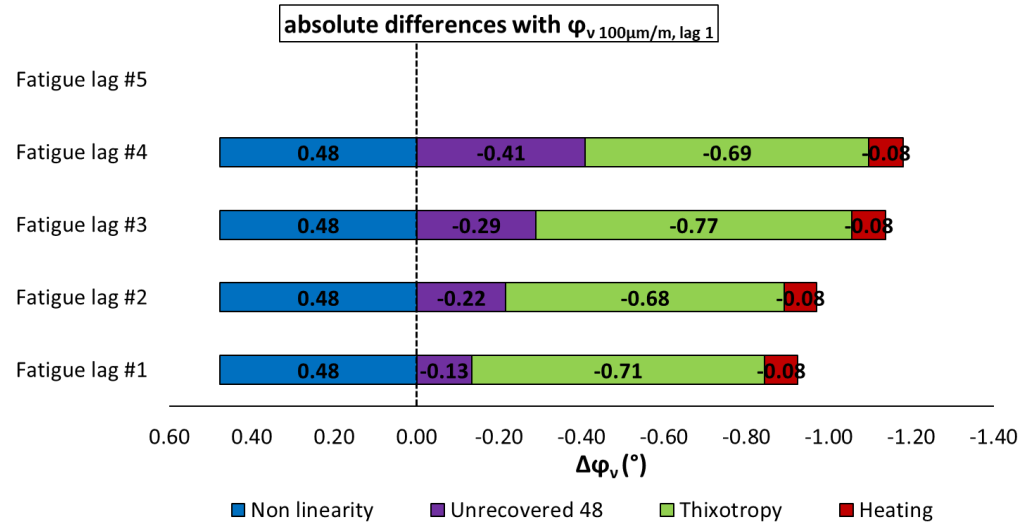
absolute differences with φv 100µm/m, lag 1
Fatigue lag #5
Fatigue lag #4
Fatigue lag #3
Fatigue lag #2
Fatigue lag #1
0.48 -0.41 -0.69 -0.08
0.48 -0.29 -0.77 -0.08
0.48 -0.22 -0.68 -0.08
0.48 -0.13 -0.71 -0.08
0.60 0.40 0.20 0.00 -0.20 -0.40 -0.60 -0.80 -1.00 -1.20 -1.40
Δφv(°)
Non linearity
Unrecovered 48
Thixotropy
Heating

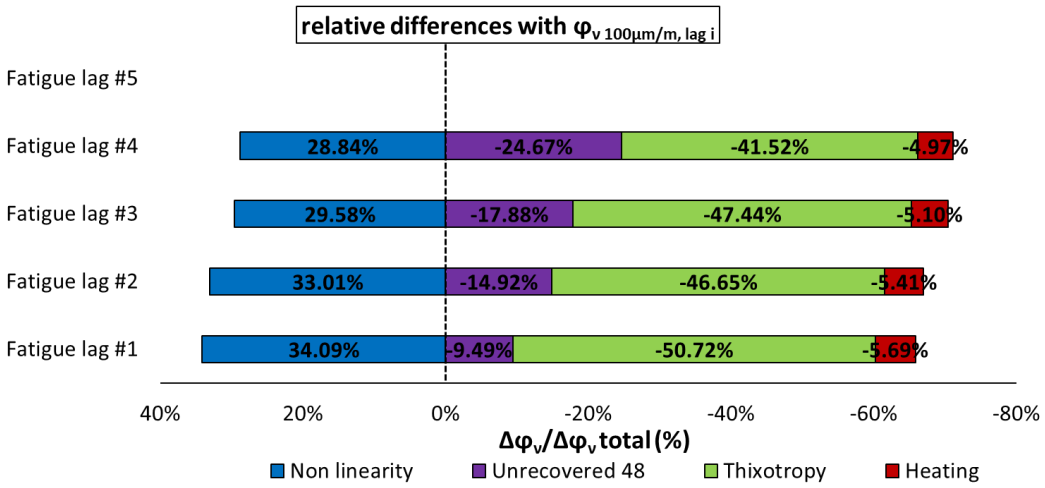

3.1.136. Quantification of different absolute and relative contributions to |E*|, φ_E, |ν*| and φ_ν evolutions for mix PMB – 2, calculated using the envelope line for the first fatigue lag.

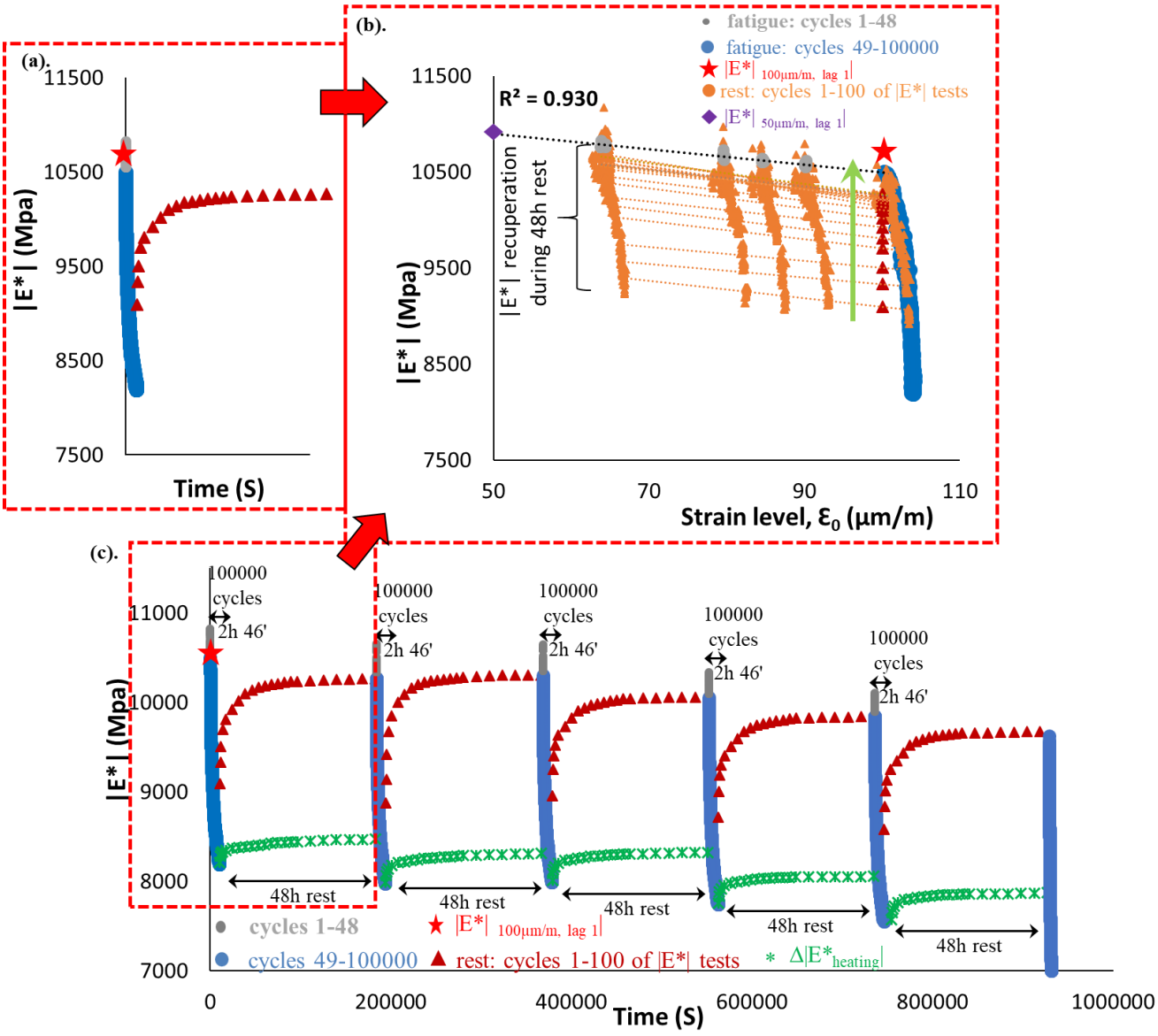

3.1.137. PFRT results obtained for mix PMB – 5: (a) |E*| as a function of time during the first fatigue lag and rest period (b) |E*| as a function of applied strain amplitude during the first fatigue lags and the short complex modulus tests performed within its following rest periods; (c) |E*| as a function of time during the five fatigue lags and rest periods [Red stars indicate values of |E*| estimated at 100 µm/m at the beginning of fatigue lag, green asterisk shows values of $\Delta|E^*_{heating}|$ as influence of self-heating and brown triangles indicate values of |E*| estimated at 100 µm/m for each short complex modulus test during rest (all these values were obtained using non-linearity envelopes, as shown in (b) for the first fatigue lag and rest period)].

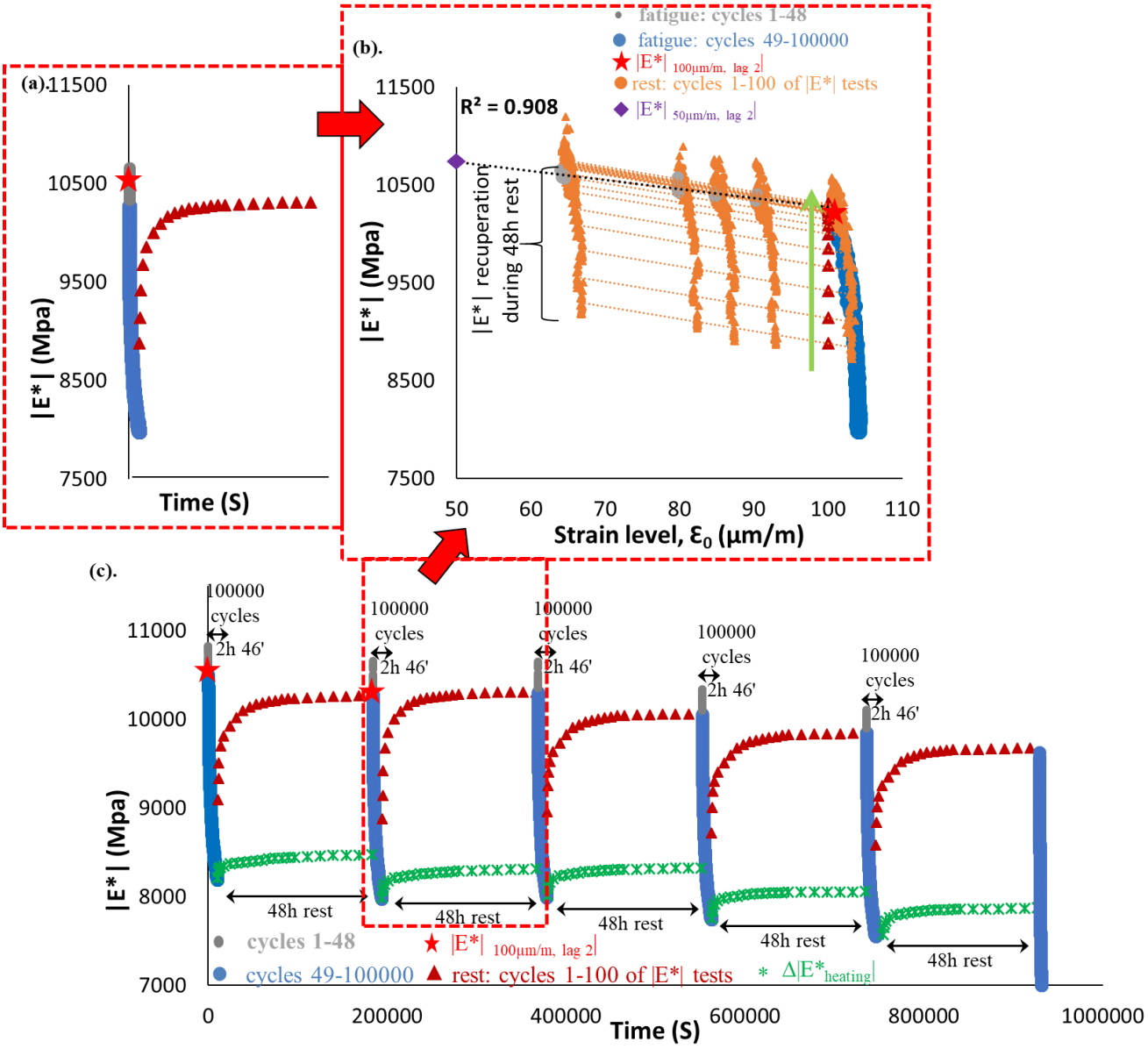

3.1.138. PFRT results obtained for mix PMB – 5: (a) |E*| as a function of time during the second fatigue lag and rest period (b) |E*| as a function of applied strain amplitude during the second fatigue lags and the short complex modulus tests performed within its following rest periods; (c) |E*| as a function of time during the five fatigue lags and rest periods [Red stars indicate values of |E*| estimated at 100 µm/m at the beginning of fatigue lag, green asterisk shows values of $\Delta|E^*_{heating}|$ as influence of self-heating and brown triangles indicate values of |E*| estimated at 100 µm/m for each short complex modulus test during rest (all these values were obtained using non-linearity envelopes, as shown in (b) for the first fatigue lag and rest period)].

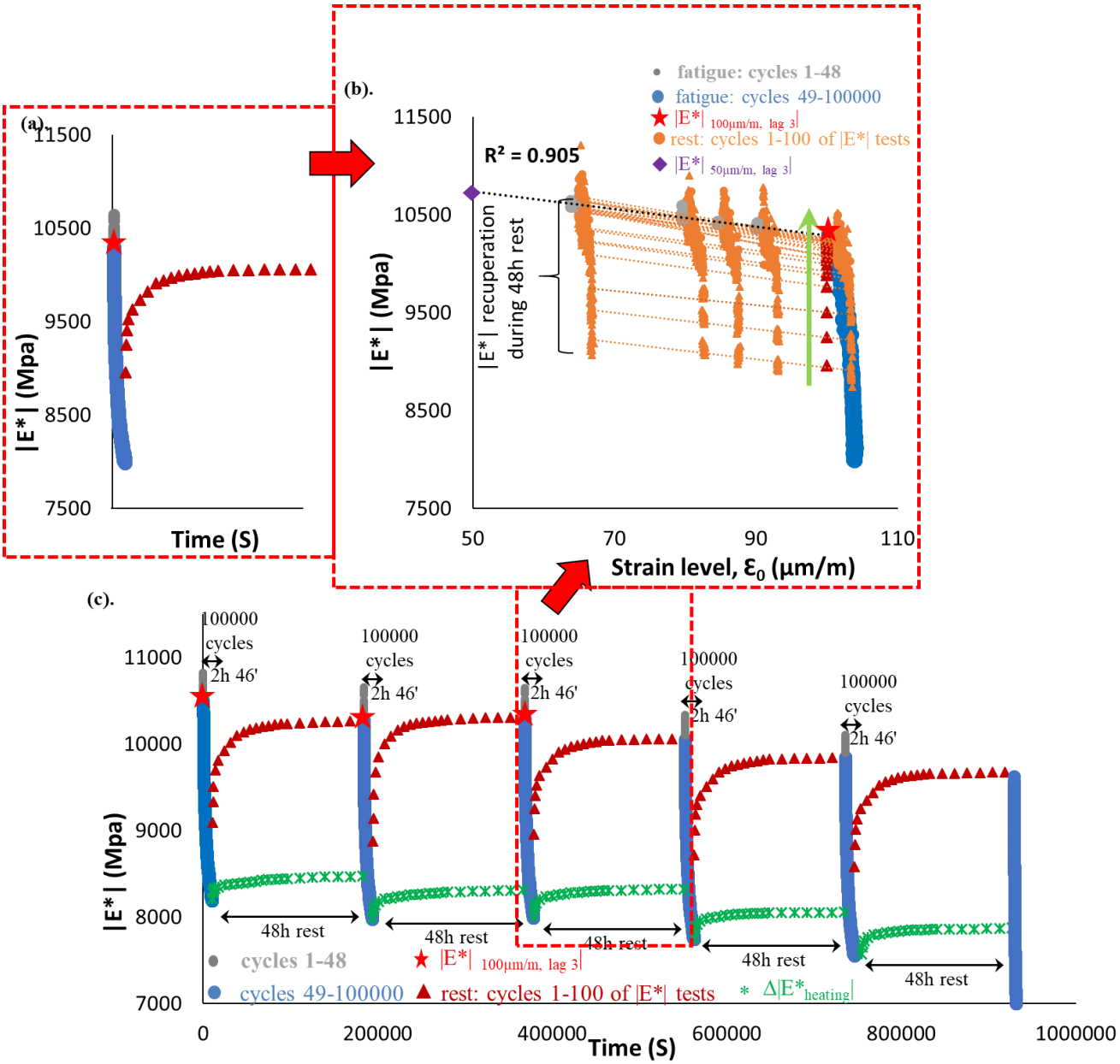

3.1.139. PFRT results obtained for mix PMB – 5: (a) |E*| as a function of time during the third fatigue lag and rest period (b) |E*| as a function of applied strain amplitude during the third fatigue lags and the short complex modulus tests performed within its following rest periods; (c) |E*| as a function of time during the five fatigue lags and rest periods [Red stars indicate values of |E*| estimated at 100 µm/m at the beginning of fatigue lag, green asterisk shows values of $\Delta|E^*_{heating}|$ as influence of self-heating and brown triangles indicate values of |E*| estimated at 100 µm/m for each short complex modulus test during rest (all these values were obtained using non-linearity envelopes, as shown in (b) for the first fatigue lag and rest period)].

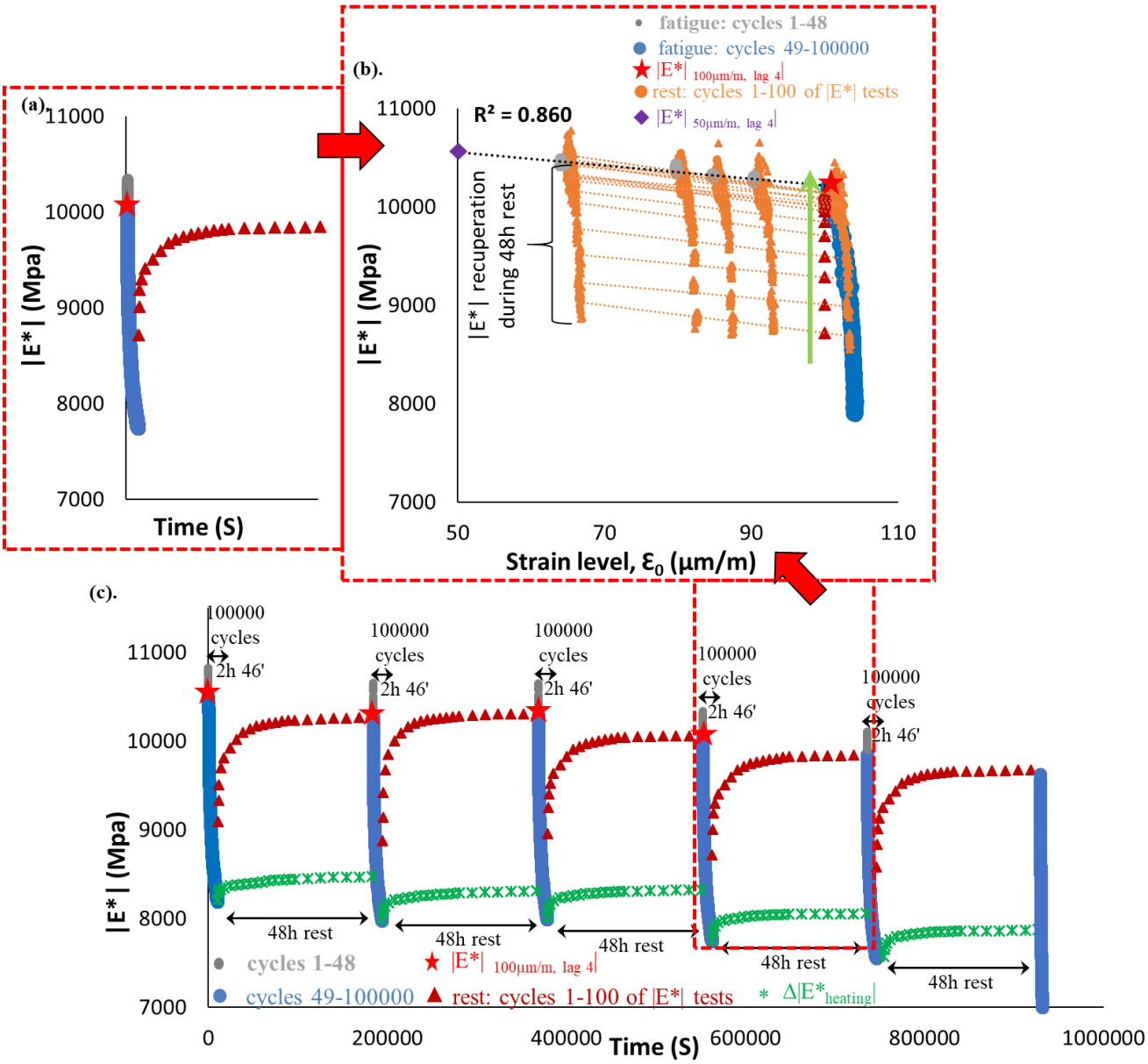

3.1.140. PFRT results obtained for mix PMB – 5: (a) |E*| as a function of time during the fourth fatigue lag and rest period (b) |E*| as a function of applied strain amplitude during the fourth fatigue lags and the short complex modulus tests performed within its following rest periods; (c) |E*| as a function of time during the five fatigue lags and rest periods [Red stars indicate values of |E*| estimated at 100 µm/m at the beginning of fatigue lag, green asterisk shows values of $\Delta|E^*_{heating}|$ as influence of self-heating and brown triangles indicate values of |E*| estimated at 100 µm/m for each short complex modulus test during rest (all these values were obtained using non-linearity envelopes, as shown in (b) for the first fatigue lag and rest period)].

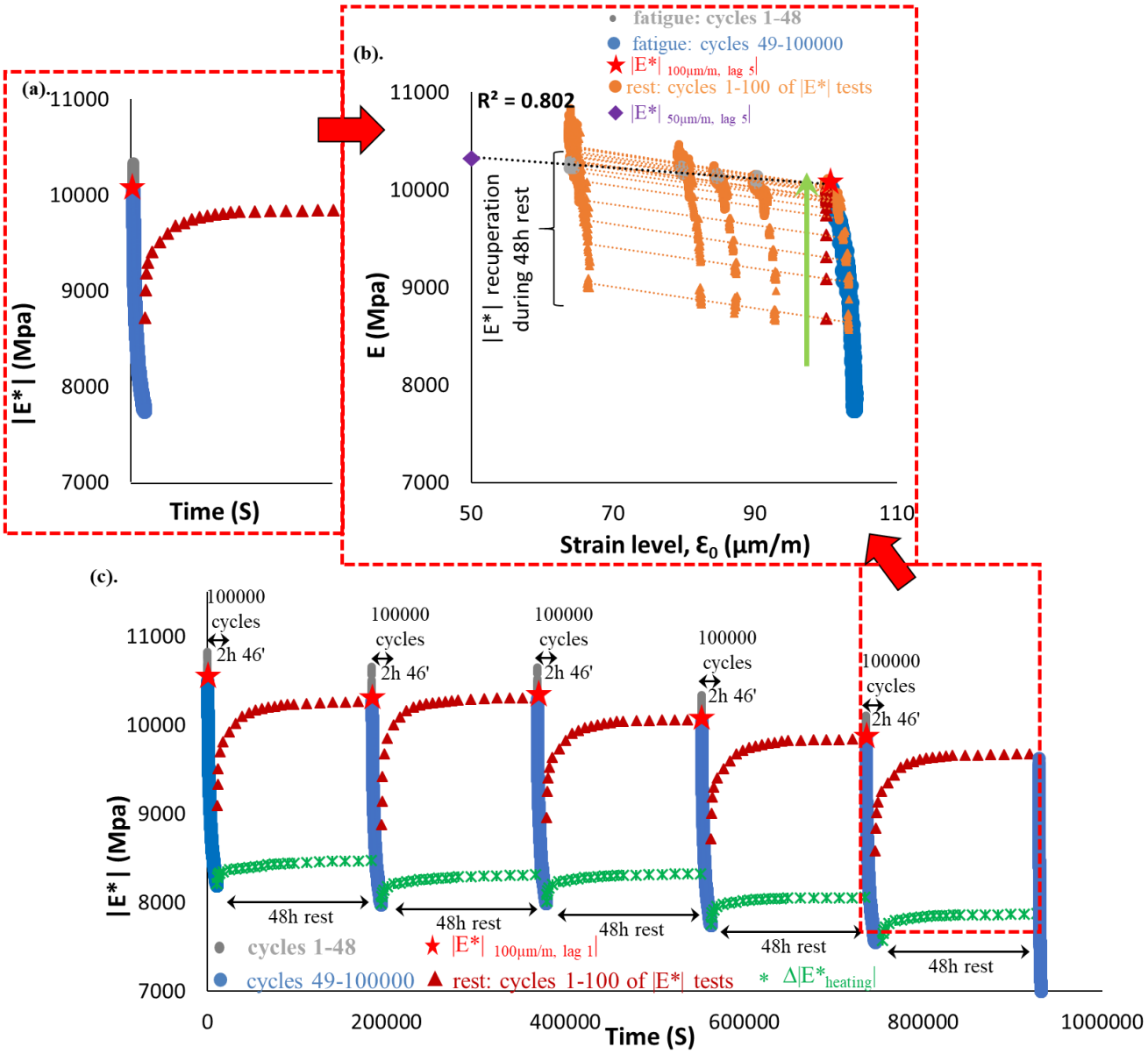

3.1.141. PFRT results obtained for mix PMB – 5: (a) |E*| as a function of time during the fifth fatigue lag and rest period (b) |E*| as a function of applied strain amplitude during the fifth fatigue lags and the short complex modulus tests performed within its following rest periods; (c) |E*| as a function of time during the five fatigue lags and rest periods [Red stars indicate values of |E*| estimated at 100 µm/m at the beginning of fatigue lag, green asterisk shows values of $\Delta|E^*_{heating}|$ as influence of self-heating and brown triangles indicate values of |E*| estimated at 100 µm/m for each short complex modulus test during rest (all these values were obtained using non-linearity envelopes, as shown in (b) for the first fatigue lag and rest period)].

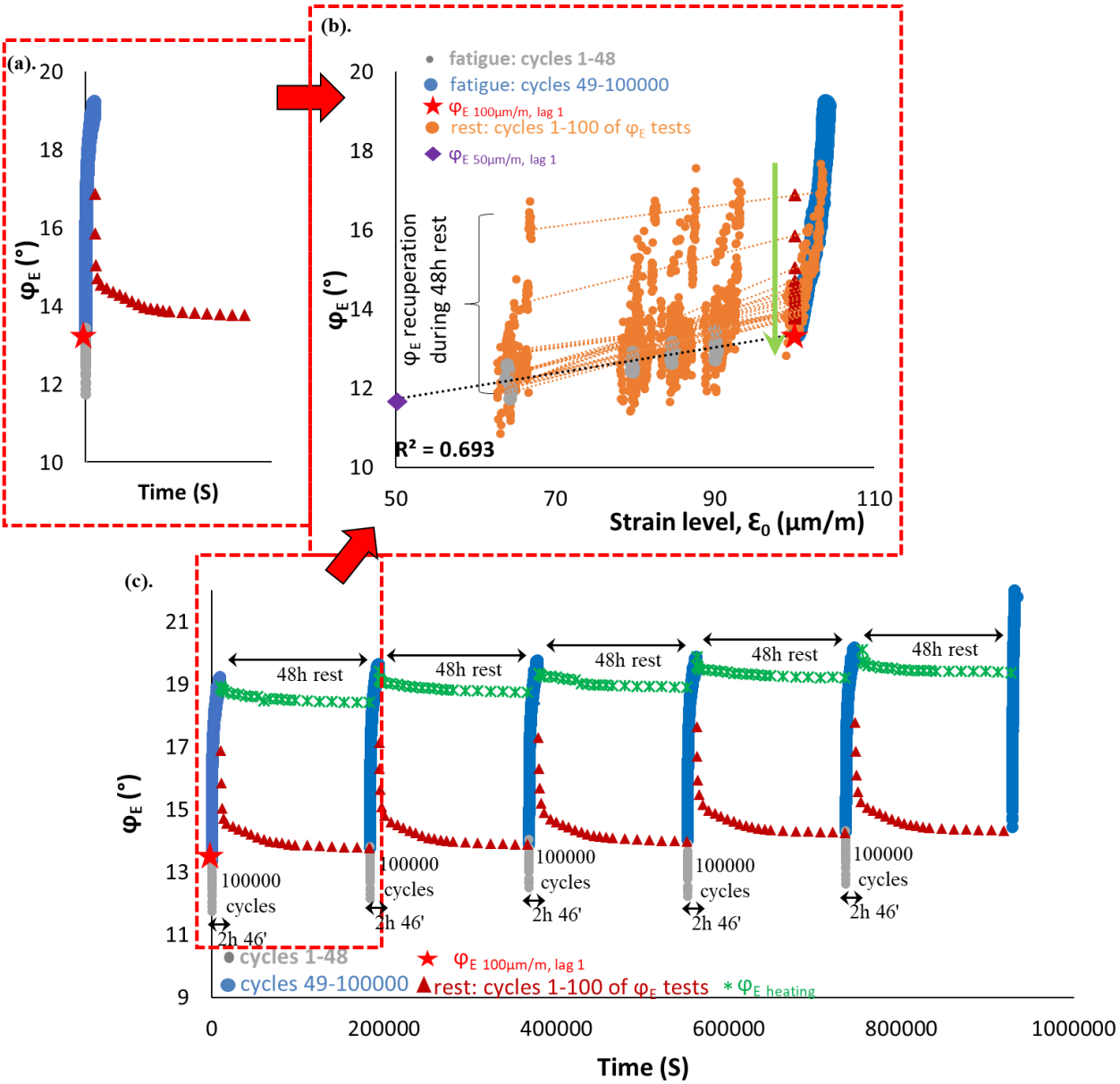

3.1.142. PFRT results obtained for mix PMB – 5: (a) φ_E as a function of time during the first fatigue lag and rest period (b) φ_E as a function of applied strain amplitude during the first fatigue lags and the short complex modulus tests performed within its following rest periods; (c) φ_E as a function of time during the five fatigue lags and rest periods (Red stars indicate values of φ_E estimated at 100 µm/m at the beginning of fatigue lag, green asterisk shows values of $\Delta\varphi_{E\ heating}$ as influence of self-heating and brown triangles indicate values of φ_E estimated at 100 µm/m for each short complex modulus test during rest (all these values were obtained using non-linearity envelopes, as shown in (b) for the first fatigue lag and rest period).

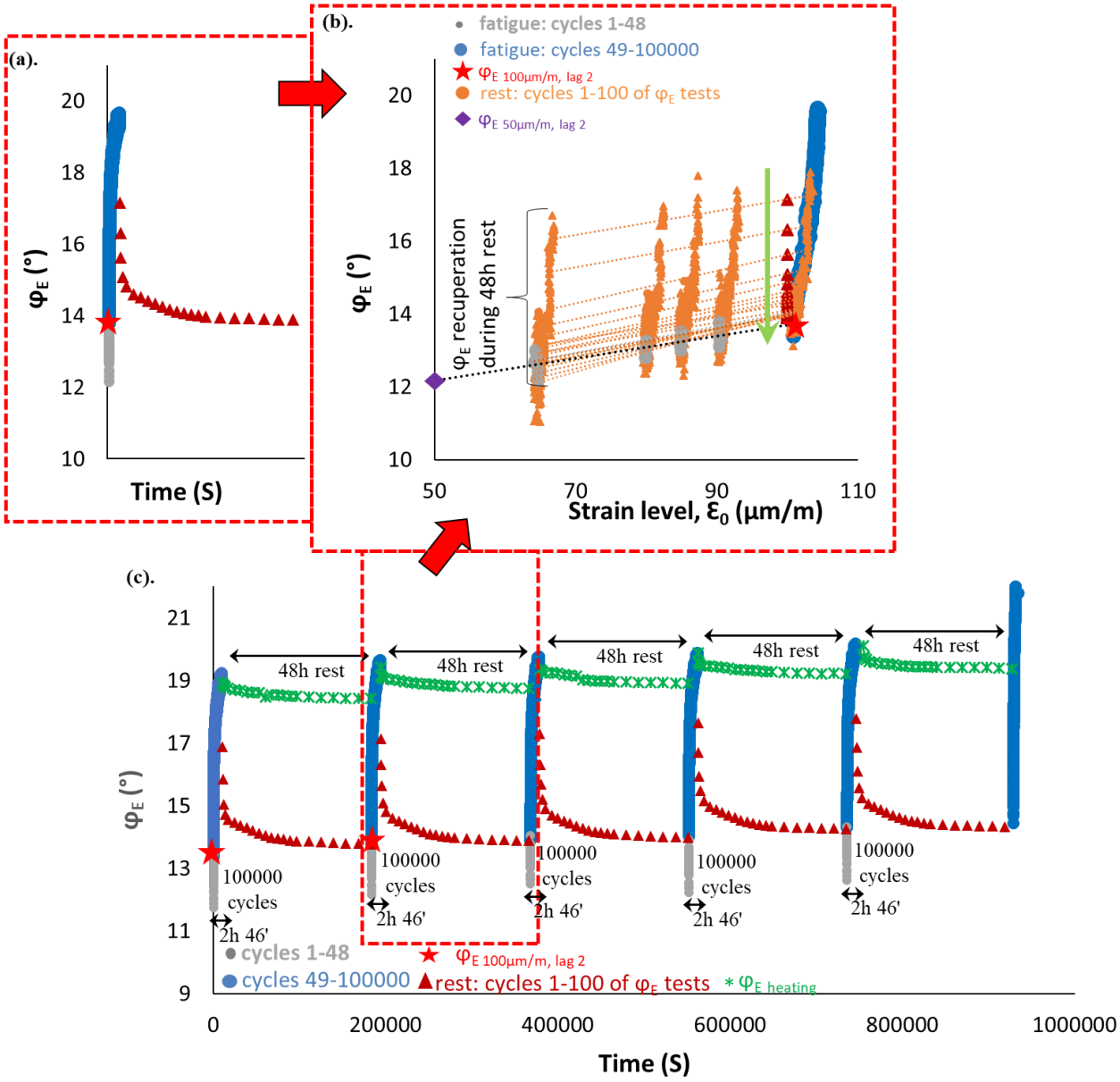

3.1.143. PFRT results obtained for mix PMB – 5: (a) φ_E as a function of time during the second fatigue lag and rest period (b) φ_E as a function of applied strain amplitude during the second fatigue lags and the short complex modulus tests performed within its following rest periods; (c) φ_E as a function of time during the five fatigue lags and rest periods (Red stars indicate values of φ_E estimated at 100 µm/m at the beginning of fatigue lag, green asterisk shows values of $\Delta\varphi_{E\ heating}$ as influence of self-heating and brown triangles indicate values of φ_E estimated at 100 µm/m for each short complex modulus test during rest (all these values were obtained using non-linearity envelopes, as shown in (b) for the first fatigue lag and rest period).

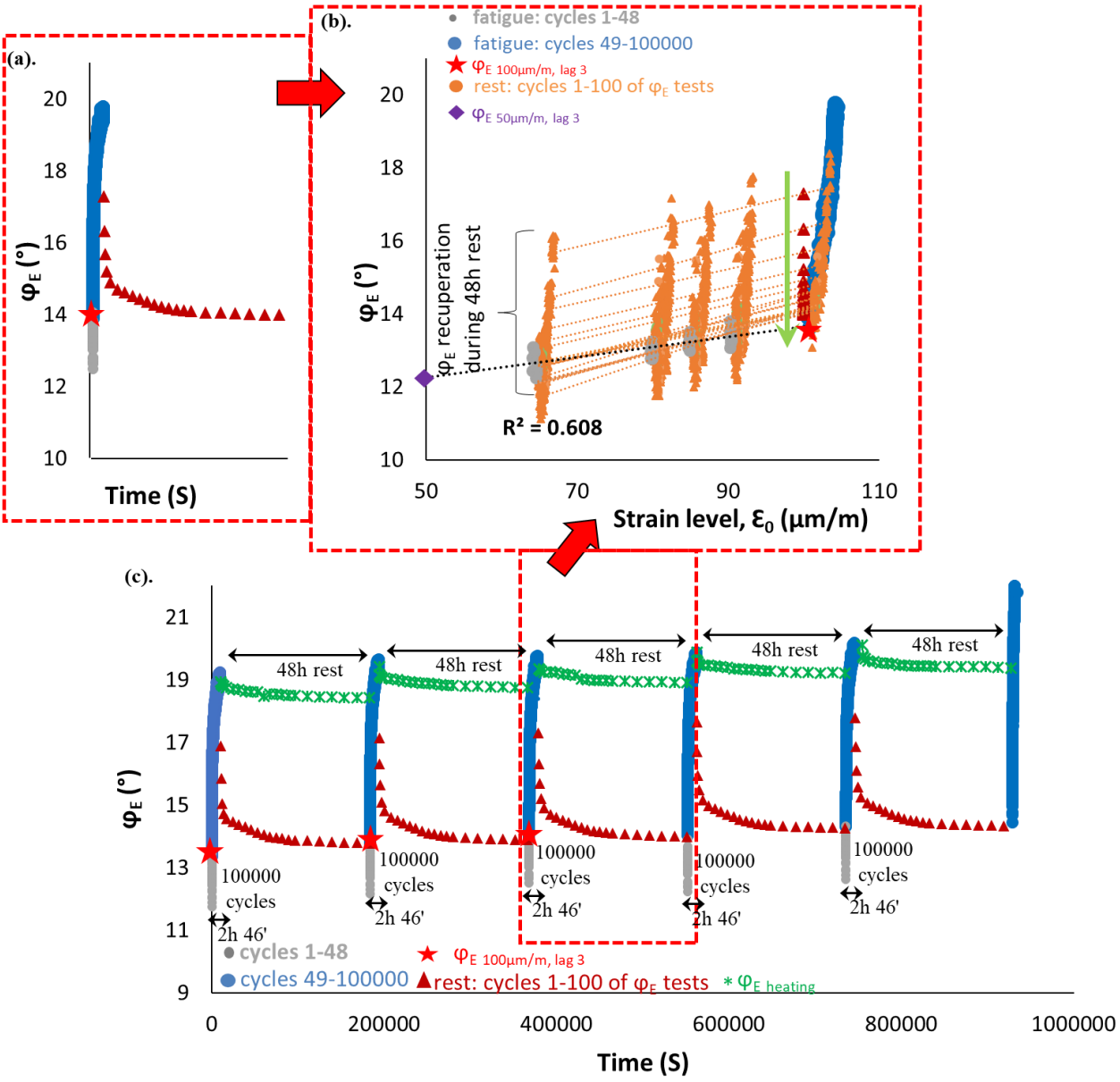

3.1.144. PFRT results obtained for mix PMB – 5: (a) φ_E as a function of time during the third fatigue lag and rest period (b) φ_E as a function of applied strain amplitude during the third fatigue lags and the short complex modulus tests performed within its following rest periods; (c) φ_E as a function of time during the five fatigue lags and rest periods (Red stars indicate values of φ_E estimated at 100 µm/m at the beginning of fatigue lag, green asterisk shows values of $\Delta\varphi_{E\ heating}$ as influence of self-heating and brown triangles indicate values of φ_E estimated at 100 µm/m for each short complex modulus test during rest (all these values were obtained using non-linearity envelopes, as shown in (b) for the first fatigue lag and rest period).

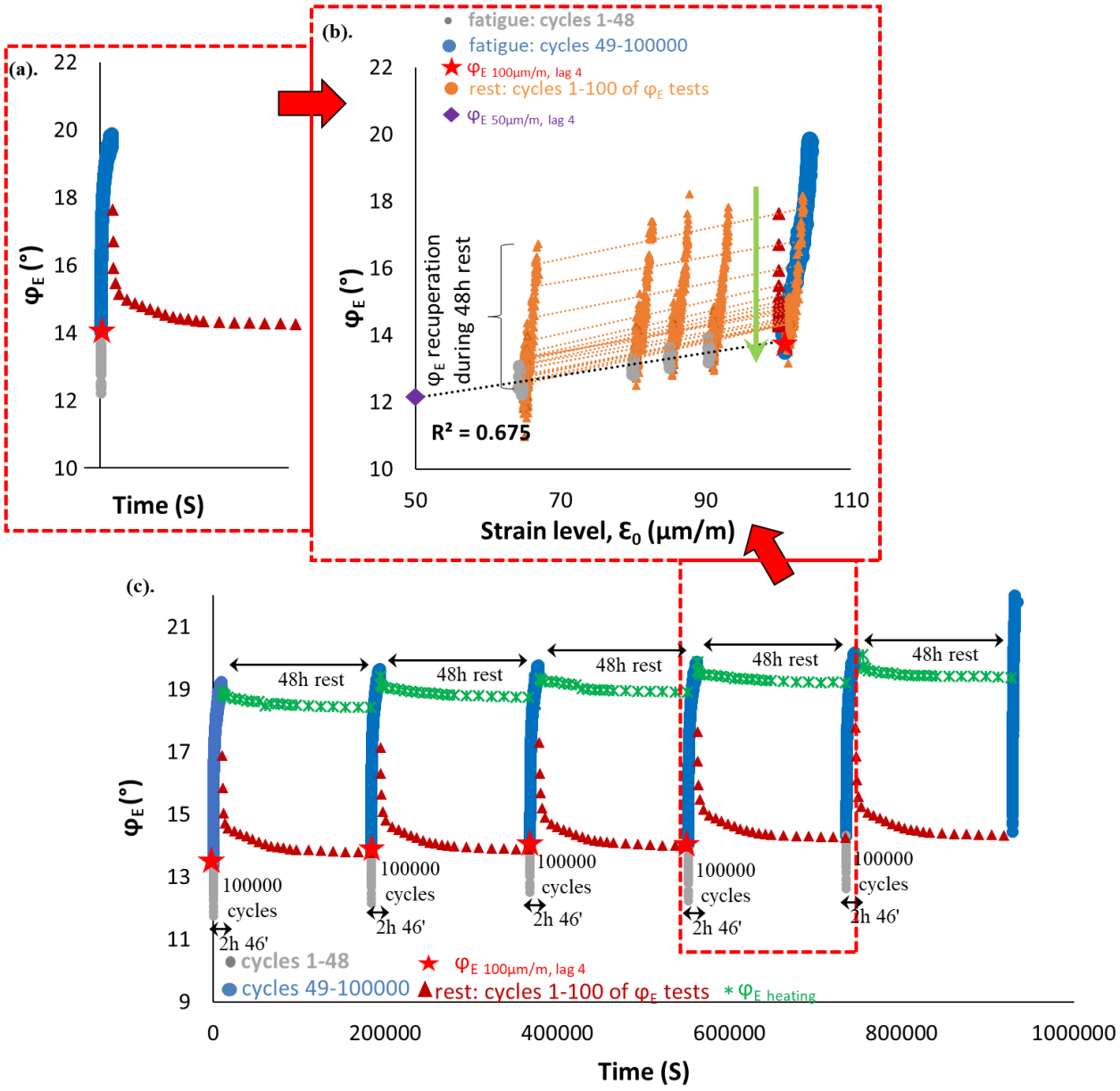

3.1.145. PFRT results obtained for mix PMB – 5: (a) φ_E as a function of time during the fourth fatigue lag and rest period (b) φ_E as a function of applied strain amplitude during the fourth fatigue lags and the short complex modulus tests performed within its following rest periods; (c) φ_E as a function of time during the five fatigue lags and rest periods (Red stars indicate values of φ_E estimated at 100 µm/m at the beginning of fatigue lag, green asterisk shows values of $\Delta\varphi_{E\ heating}$ as influence of self-heating and brown triangles indicate values of φ_E estimated at 100 µm/m for each short complex modulus test during rest (all these values were obtained using non-linearity envelopes, as shown in (b) for the first fatigue lag and rest period).

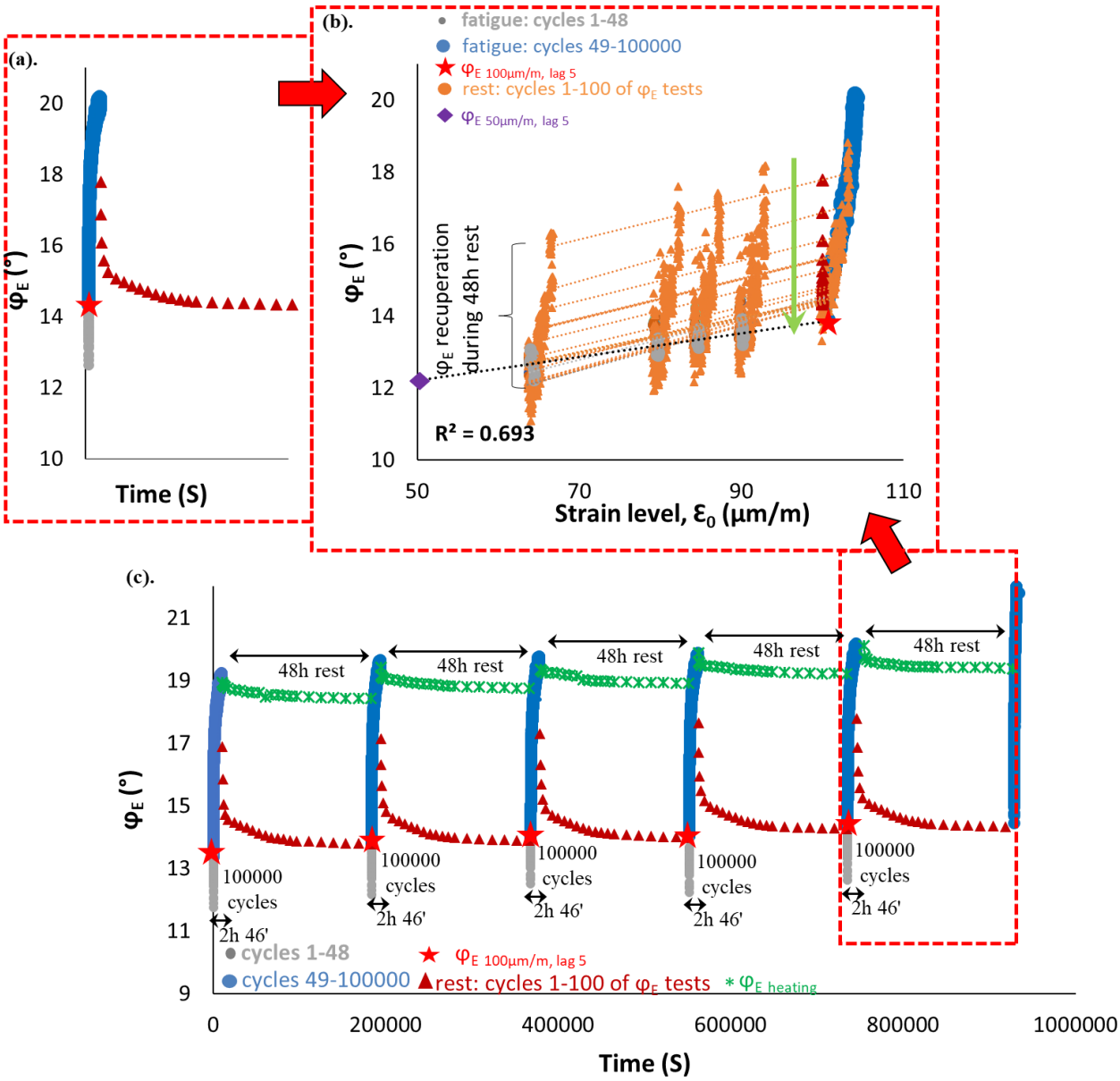

3.1.146. PFRT results obtained for mix PMB – 5: (a) φ_E as a function of time during the fifth fatigue lag and rest period (b) φ_E as a function of applied strain amplitude during the fifth fatigue lags and the short complex modulus tests performed within its following rest periods; (c) φ_E as a function of time during the five fatigue lags and rest periods (Red stars indicate values of φ_E estimated at 100 µm/m at the beginning of fatigue lag, green asterisk shows values of $\Delta\varphi_{E\ heating}$ as influence of self-heating and brown triangles indicate values of φ_E estimated at 100 µm/m for each short complex modulus test during rest (all these values were obtained using non-linearity envelopes, as shown in (b) for the first fatigue lag and rest period).

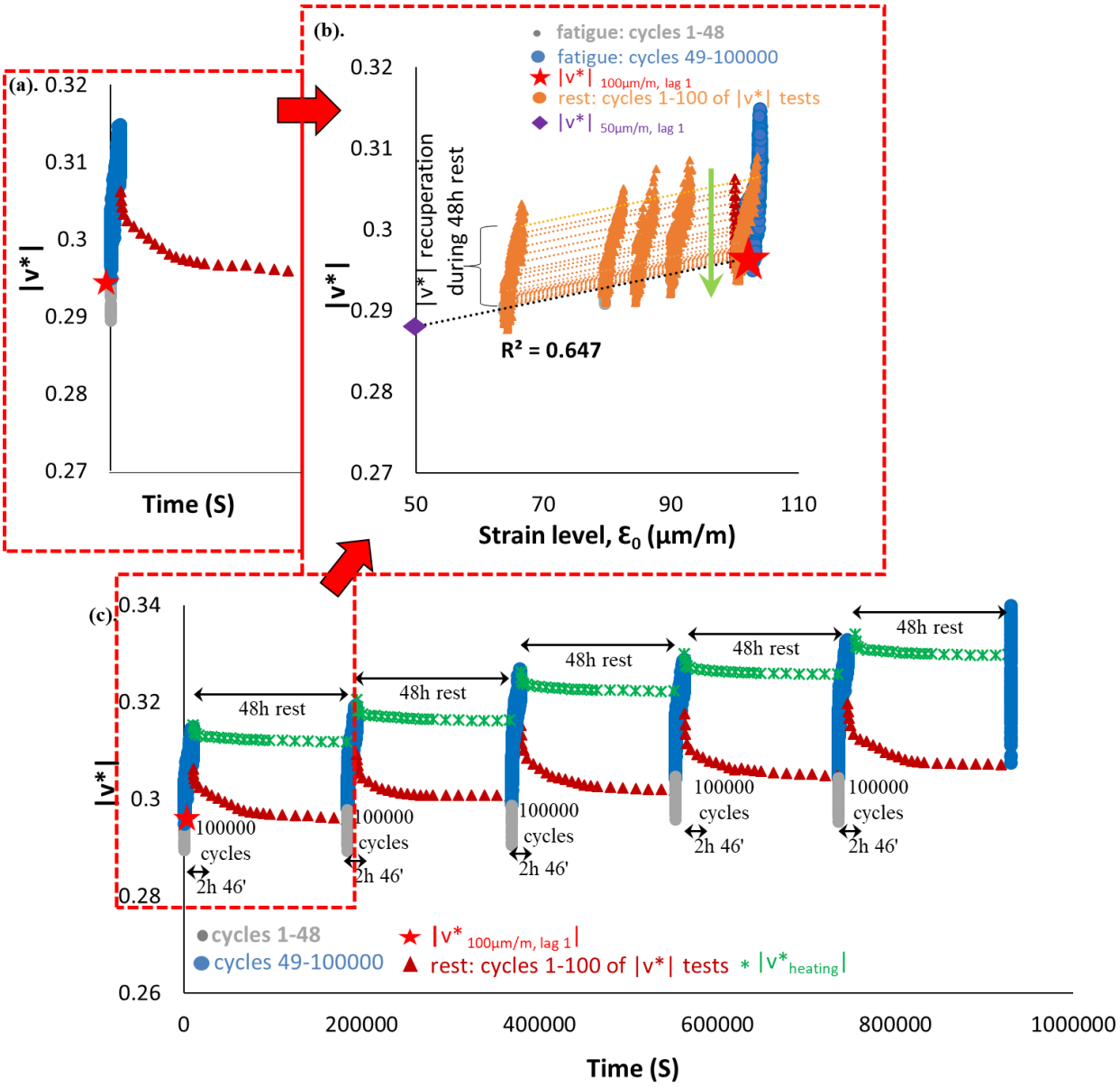

3.1.147. PFRT results obtained for mix PMB – 5: (a) |v*| as a function of time during the first fatigue lag and rest period (b) |v*| as a function of applied strain amplitude during the first fatigue lags and the short complex modulus tests performed within its following rest periods; (c) |v*| as a function of time during the five fatigue lags and rest periods [Red stars indicate values of |v*| estimated at 100 µm/m at the beginning of fatigue lag, green asterisk shows values of $\Delta|v^*_{heating}|$ as influence of self-heating and brown triangles indicate values of |v*| estimated at 100 µm/m for each short complex modulus test during rest (all these values were obtained using non-linearity envelopes, as shown in (b) for the first fatigue lag and rest period)].

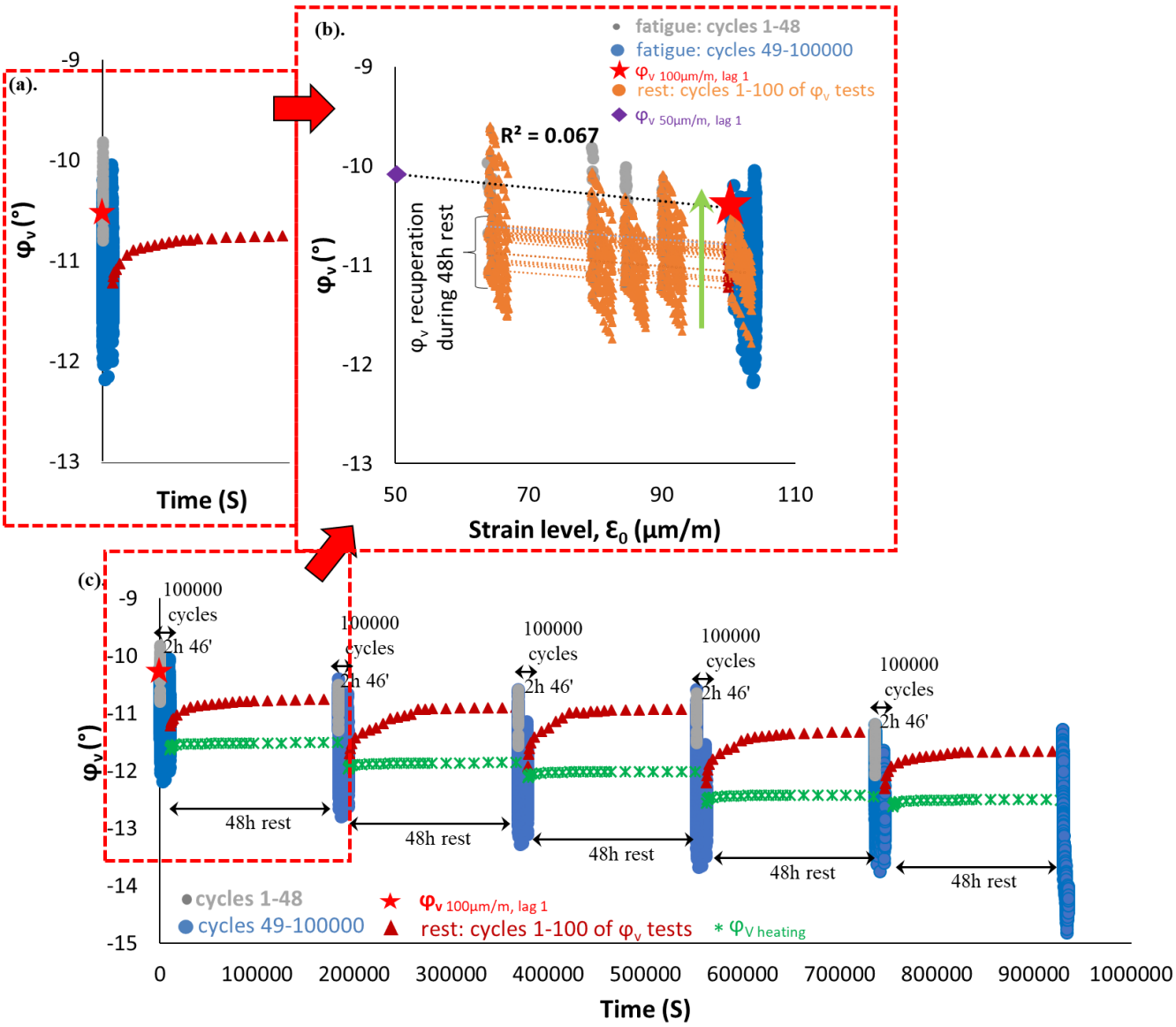

3.1.148. PFRT results obtained for mix PMB – 5: (a) φ_v as a function of time during the first fatigue lag and rest period (b) φ_v as a function of applied strain amplitude during the first fatigue lags and the short complex modulus tests performed within its following rest periods; (c) φ_v as a function of time during the five fatigue lags and rest periods (Red stars indicate values of φ_v estimated at 100 µm/m at the beginning of fatigue lag, green asterisk shows values of $\Delta\varphi_{v\ heating}$ as influence of self-heating and brown triangles indicate values of φ_v estimated at 100 µm/m for each short complex modulus test during rest (all these values were obtained using non-linearity envelopes, as shown in (b) for the first fatigue lag and rest period).

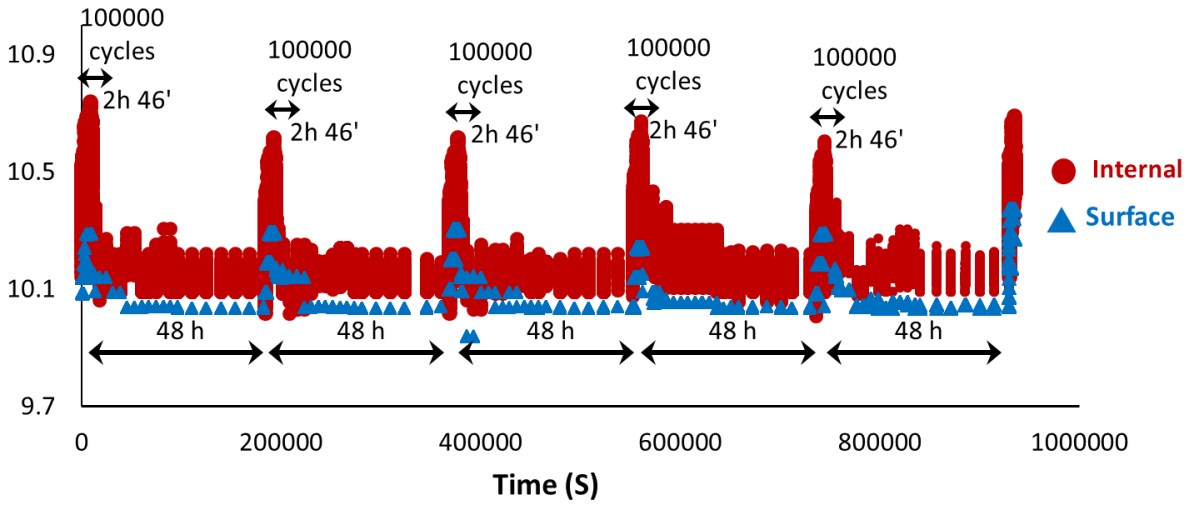

3.1.149. PFRT results obtained for mix PMB – 5: internal and surface temperature evolution during fatigue lags and recovery periods.

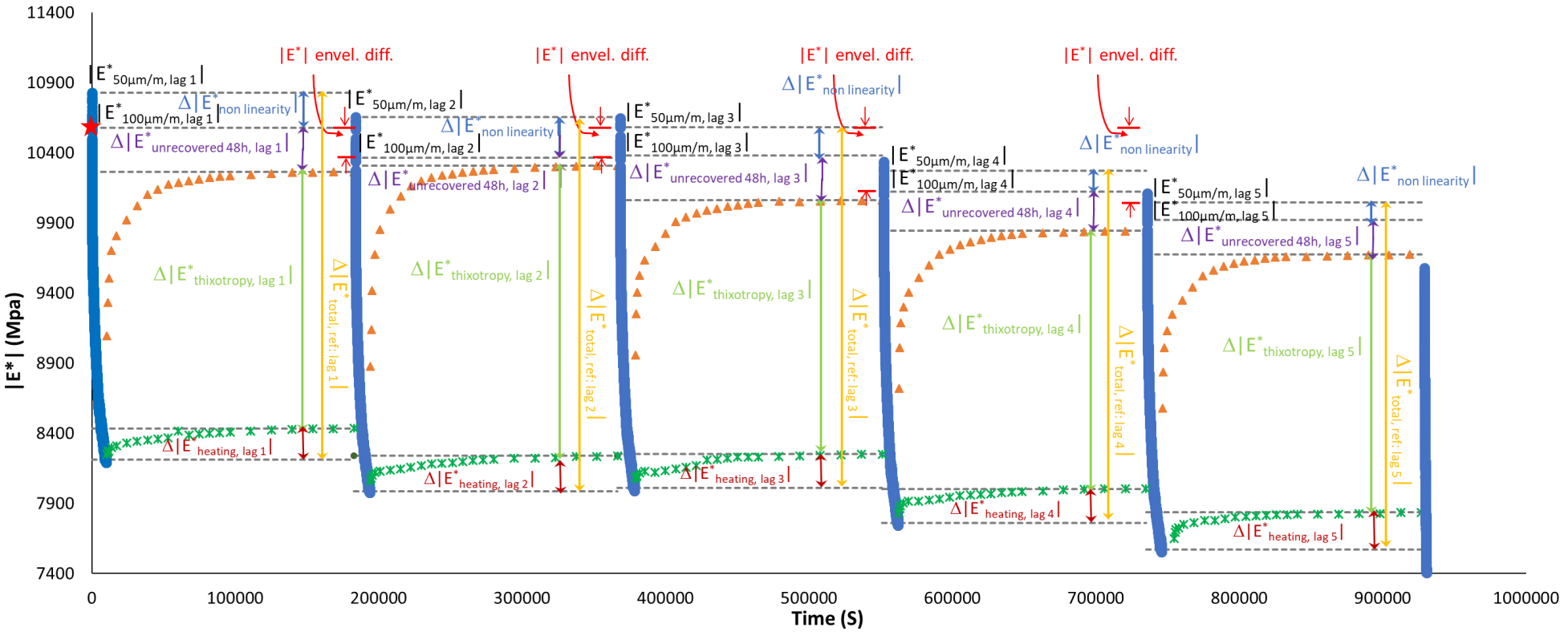
|E*| (Mpa)
Time (S)
11400
10900
10400
9900
9400
8900
8400
7900
7400
0
100000
200000
300000
400000
500000
600000
700000
800000
900000
1000000
|E*| envel. diff.
|E*| envel. diff.
|E*| envel. diff.
|E*| envel. diff.
|E*50µm/m, lag 1|
|E*100µm/m, lag 1|
Δ|E*non linearity|
Δ|E*unrecovered 48h, lag 1|
Δ|E*thixotropy, lag 1|
Δ|E*total, ref: lag 1|
Δ|E*heating, lag 1|
|E*50µm/m, lag 2|
|E*100µm/m, lag 2|
Δ|E*non linearity|
Δ|E*unrecovered 48h, lag 2|
Δ|E*thixotropy, lag 2|
Δ|E*total, ref: lag 2|
Δ|E*heating, lag 2|
|E*50µm/m, lag 3|
|E*100µm/m, lag 3|
Δ|E*non linearity|
Δ|E*unrecovered 48h, lag 3|
Δ|E*thixotropy, lag 3|
Δ|E*total, ref: lag 3|
Δ|E*heating, lag 3|
|E*50µm/m, lag 4|
|E*100µm/m, lag 4|
Δ|E*non linearity|
Δ|E*unrecovered 48h, lag 4|
Δ|E*thixotropy, lag 4|
Δ|E*total, ref: lag 4|
Δ|E*heating, lag 4|
|E*50µm/m, lag 5|
|E*100µm/m, lag 5|
Δ|E*non linearity|
Δ|E*unrecovered 48h, lag 5|
Δ|E*thixotropy, lag 5|
Δ|E*total, ref: lag 5|
Δ|E*heating, lag 5|

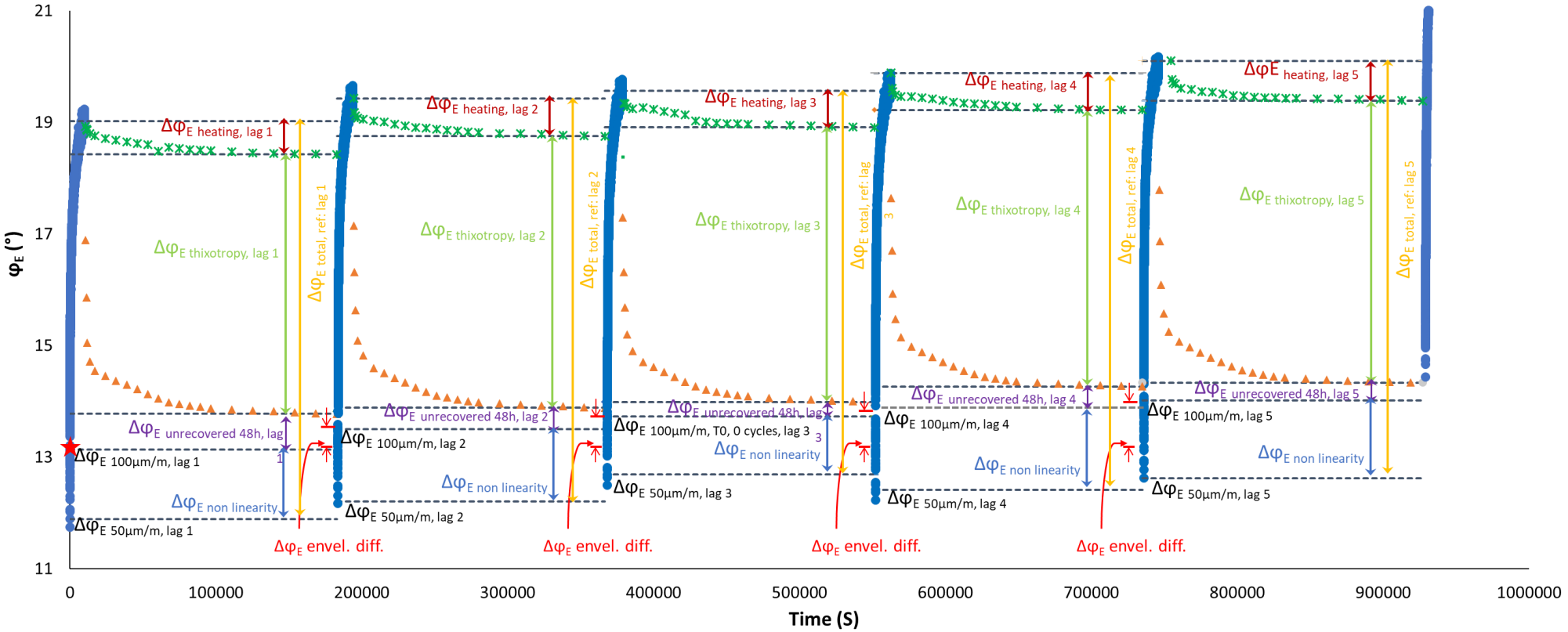

Figure 3.1.150. Quantification of different contributions |E*|, φ_E, |v*| and φ_v evolution, for the five fatigue lags for mix PMB – 5: different envelope line is used for each fatigue lag.

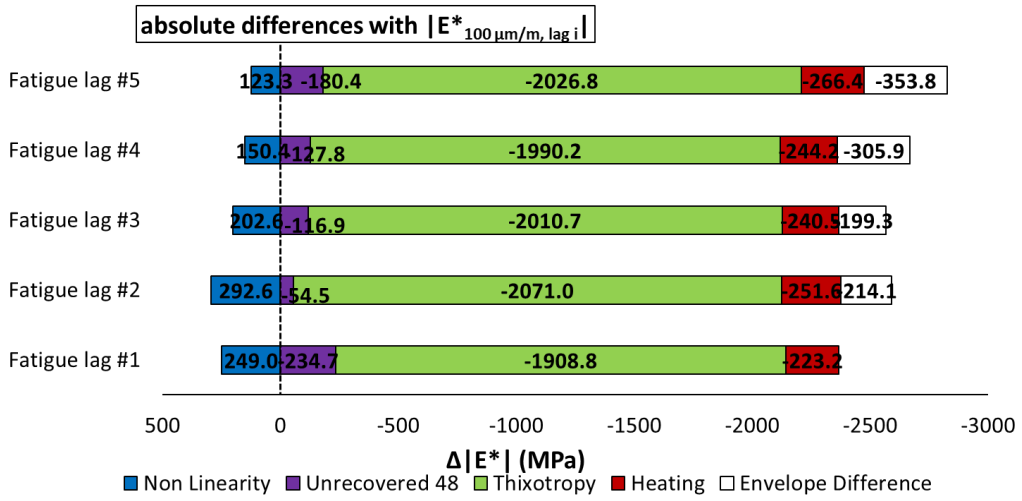
absolute differences with |E*100 µm/m, lag i|
Fatigue lag #5
Fatigue lag #4
Fatigue lag #3
Fatigue lag #2
Fatigue lag #1
123.3 -180.4 -2026.8 -266.4 -353.8
150.4 -127.8 -1990.2 -244.2 -305.9
202.6 -116.9 -2010.7 -240.5 199.3
292.6 -54.5 -2071.0 -251.6 214.1
249.0 -234.7 -1908.8 -223.2
500 0 -500 -1000 -1500 -2000 -2500 -3000
Δ|E*| (MPa)
Non Linearity
Unrecovered 48
Thixotropy
Heating
Envelope Difference

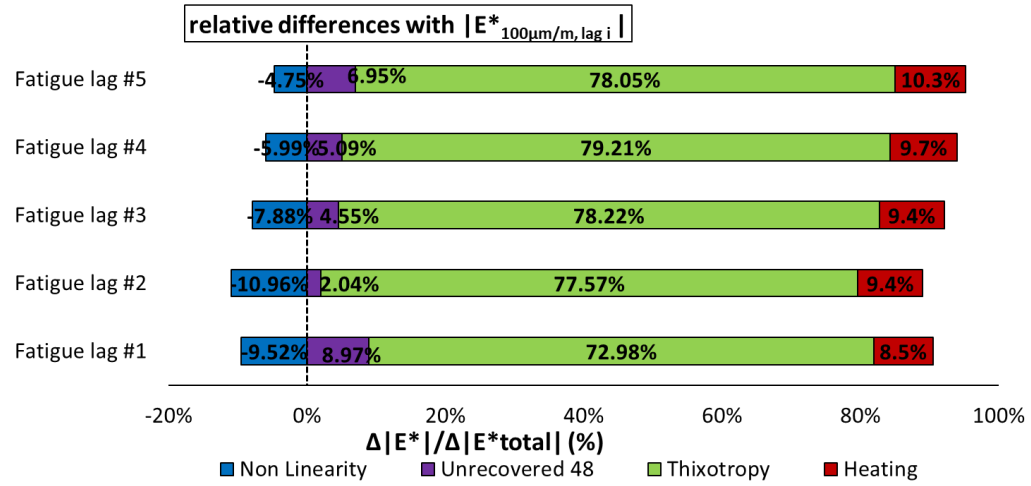
relative differences with |E*100µm/m, lag i|
Fatigue lag #5
Fatigue lag #4
Fatigue lag #3
Fatigue lag #2
Fatigue lag #1
-4.75% 6.95% 78.05% 10.3%
-5.99% 5.09% 79.21% 9.7%
-7.88% 4.55% 78.22% 9.4%
-10.96% 2.04% 77.57% 9.4%
-9.52% 8.97% 72.98% 8.5%
-20% 0% 20% 40% 60% 80% 100%
Δ|E*|/Δ|E*total| (%)
Non Linearity
Unrecovered 48
Thixotropy
Heating

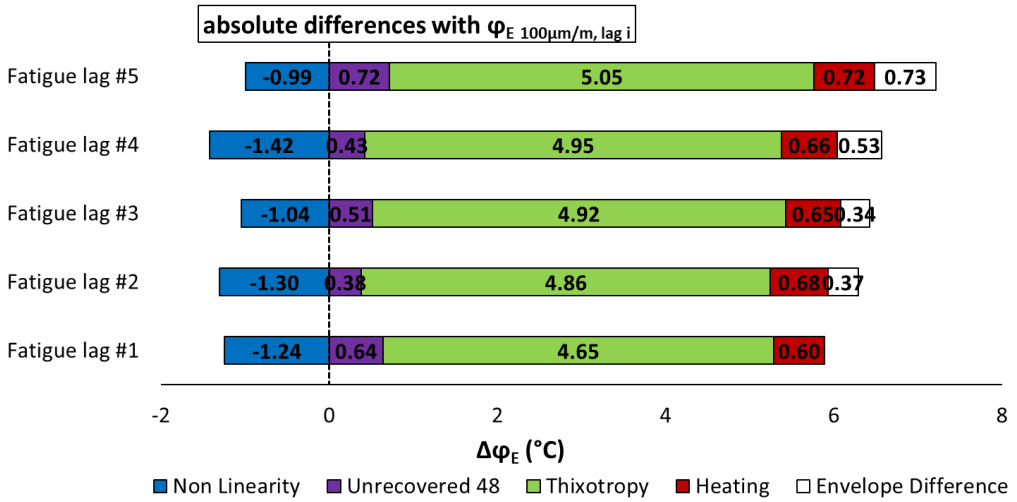
absolute differences with φE 100µm/m, lag i
Fatigue lag #5
Fatigue lag #4
Fatigue lag #3
Fatigue lag #2
Fatigue lag #1
-0.99 0.72 5.05 0.72 0.73
-1.42 0.43 4.95 0.66 0.53
-1.04 0.51 4.92 0.65 0.34
-1.30 0.38 4.86 0.68 0.37
-1.24 0.64 4.65 0.60
-2 0 2 4 6 8
ΔφE (°C)
Non Linearity
Unrecovered 48
Thixotropy
Heating
Envelope Difference

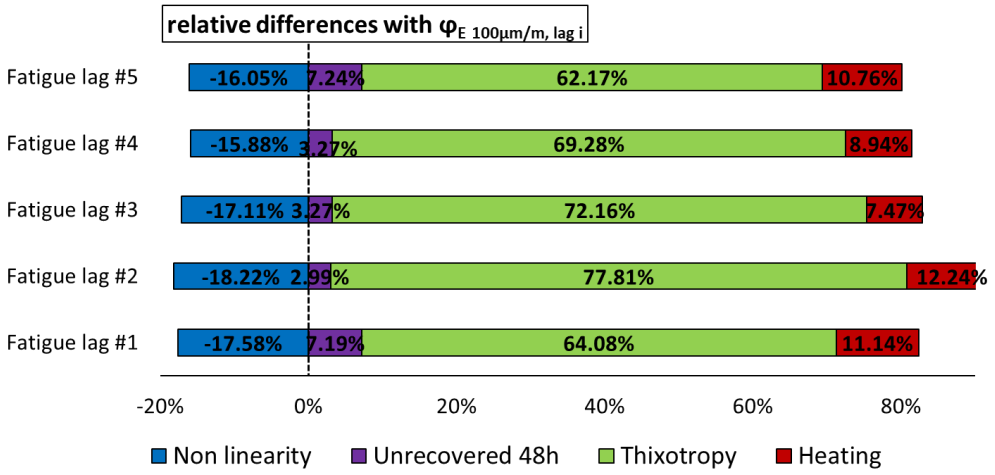
relative differences with φE 100µm/m, lag i
Fatigue lag #5
Fatigue lag #4
Fatigue lag #3
Fatigue lag #2
Fatigue lag #1
-16.05% 7.24% 62.17% 10.76%
-15.88% 3.27% 69.28% 8.94%
-17.11% 3.27% 72.16% 7.47%
-18.22% 2.99% 77.81% 12.24%
-17.58% 7.19% 64.08% 11.14%
-20% 0% 20% 40% 60% 80%
Non linearity
Unrecovered 48h
Thixotropy
Heating

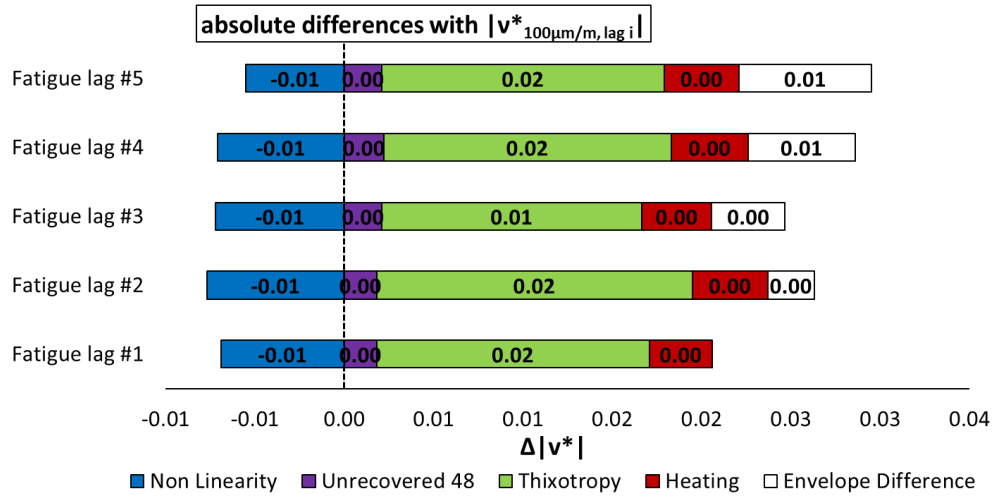
absolute differences with |v*100µm/m, lag i|
Fatigue lag #5
Fatigue lag #4
Fatigue lag #3
Fatigue lag #2
Fatigue lag #1
-0.01 0.00 0.02 0.00 0.01
-0.01 0.00 0.02 0.00 0.01
-0.01 0.00 0.01 0.00 0.00
-0.01 0.00 0.02 0.00 0.00
-0.01 0.00 0.02 0.00
-0.01 -0.01 0.00 0.01 0.01 0.02 0.02 0.03 0.03 0.04
Δ|v*|
Non Linearity
Unrecovered 48
Thixotropy
Heating
Envelope Difference

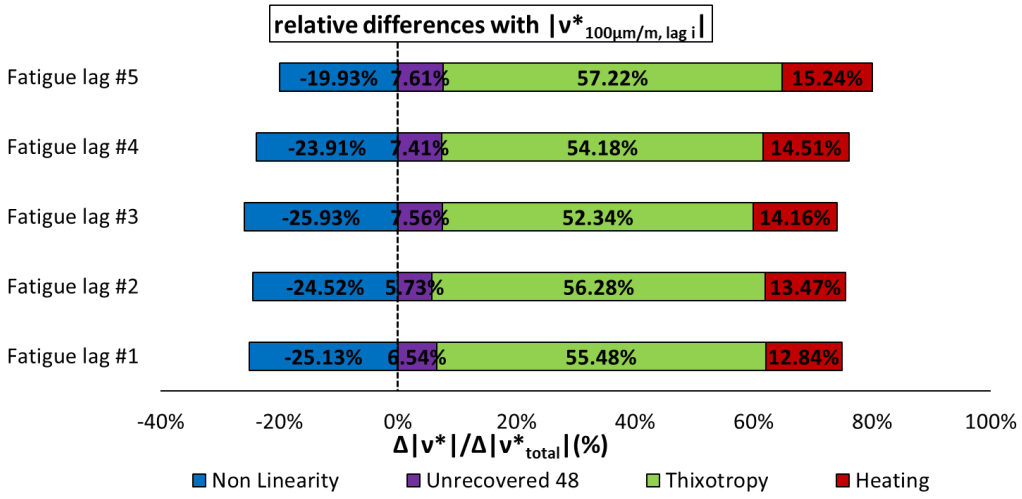
relative differences with |v*100µm/m, lag i|
Fatigue lag #5
Fatigue lag #4
Fatigue lag #3
Fatigue lag #2
Fatigue lag #1
-19.93% 7.61% 57.22% 15.24%
-23.91% 7.41% 54.18% 14.51%
-25.93% 7.56% 52.34% 14.16%
-24.52% 5.73% 56.28% 13.47%
-25.13% 6.54% 55.48% 12.84%
-40% -20% 0% 20% 40% 60% 80% 100%
Δ|v*|/Δ|v*total|(%)
Non Linearity
Unrecovered 48
Thixotropy
Heating

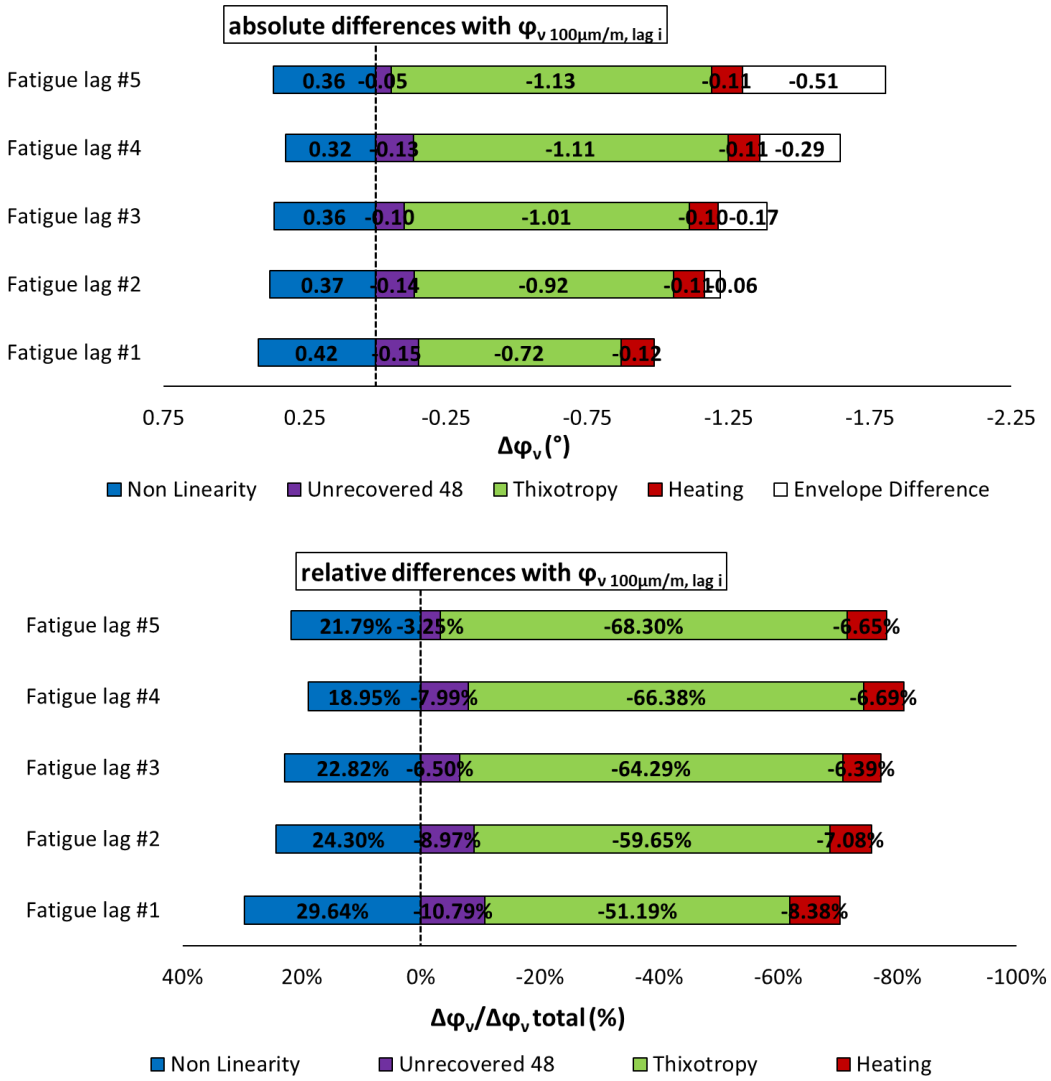

3.1.151. Quantification of different absolute and relative contributions to |E*|, φ_E, |ν*| and φ_v evolutions for mix PMB – 5, calculated using a different envelope line for each fatigue lag.

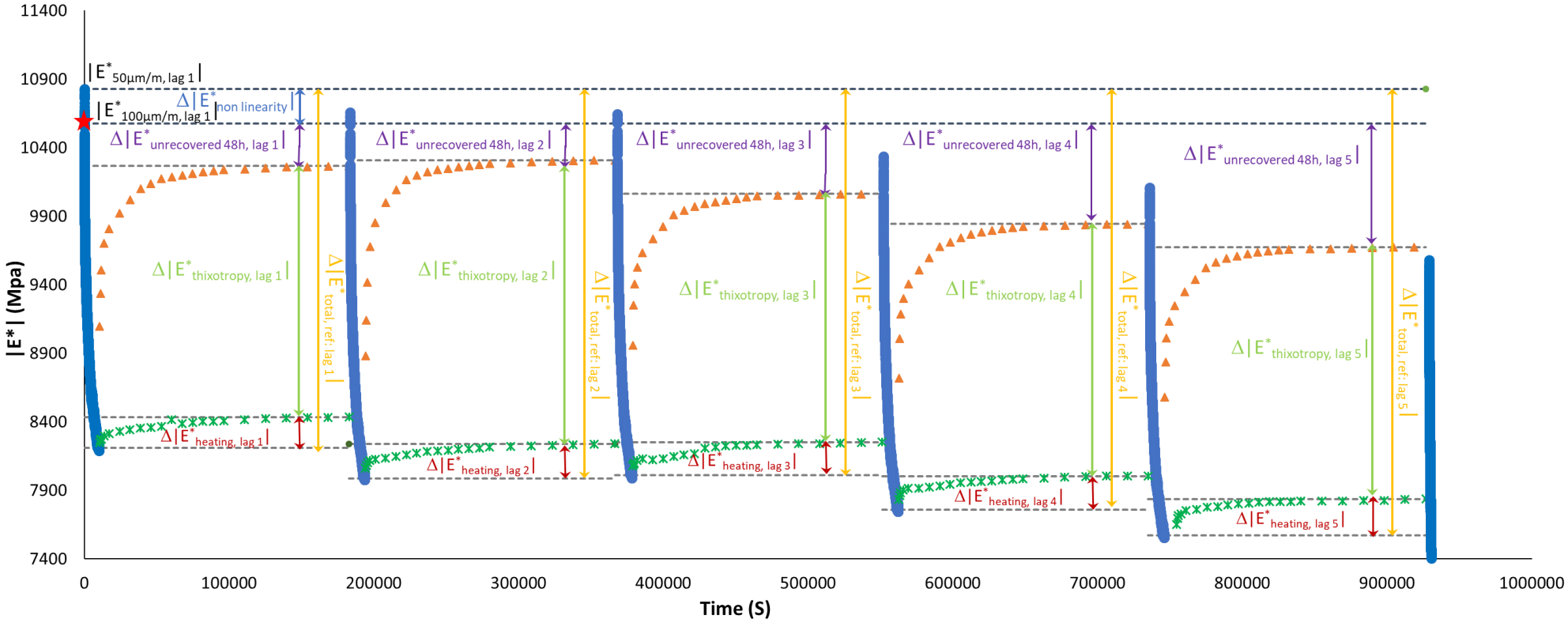
11400
10900
10400
9900
9400
8900
8400
7900
7400
|E*| (Mpa)
0
100000
200000
300000
400000
500000
600000
700000
800000
900000
1000000
Time (S)
|E*50µm/m, lag 1|
|E*100µm/m, lag 1|
Δ|E*non linearity|
Δ|E*unrecovered 48h, lag 1|
Δ|E*unrecovered 48h, lag 2|
Δ|E*unrecovered 48h, lag 3|
Δ|E*unrecovered 48h, lag 4|
Δ|E*unrecovered 48h, lag 5|
Δ|E*thixotropy, lag 1|
Δ|E*thixotropy, lag 2|
Δ|E*thixotropy, lag 3|
Δ|E*thixotropy, lag 4|
Δ|E*thixotropy, lag 5|
Δ|E*total, ref: lag 1|
Δ|E*total, ref: lag 2|
Δ|E*total, ref: lag 3|
Δ|E*total, ref: lag 4|
Δ|E*total, ref: lag 5|
Δ|E*heating, lag 1|
Δ|E*heating, lag 2|
Δ|E*heating, lag 3|
Δ|E*heating, lag 4|
Δ|E*heating, lag 5|

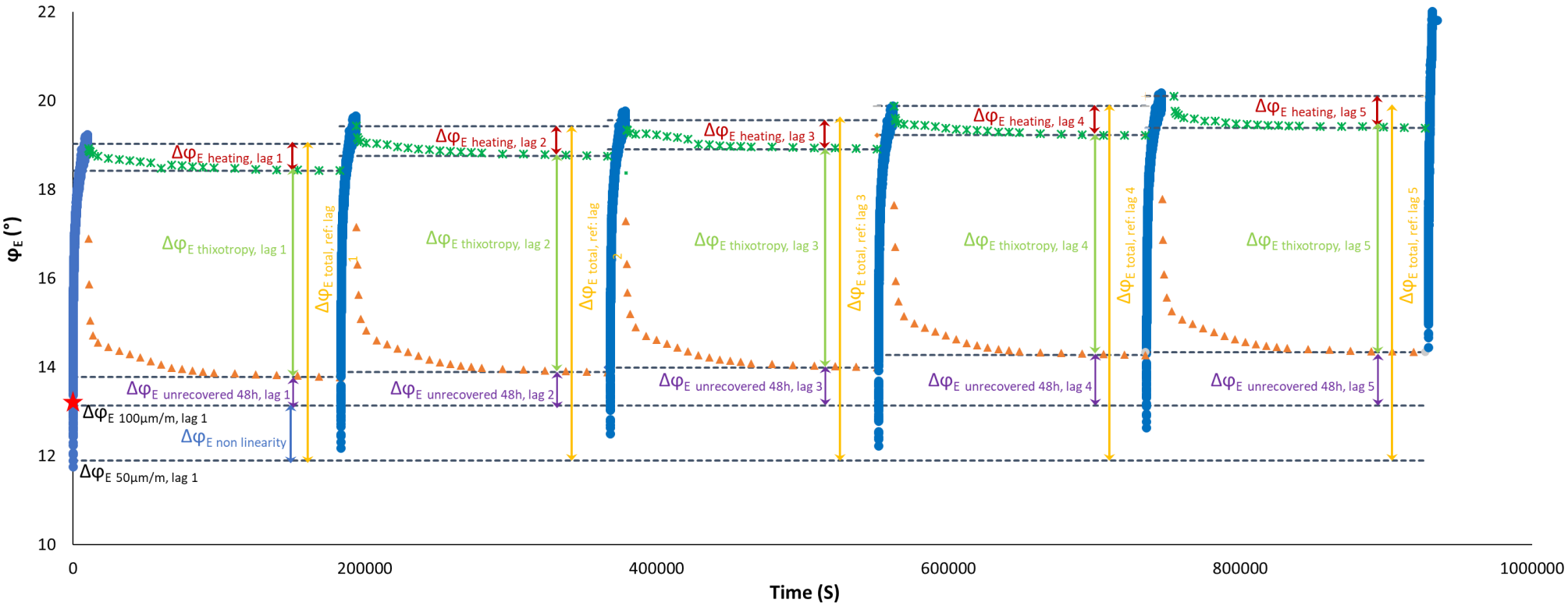

3.1.152. Quantification of different contributions to |E*|, φ_E, |v*| and φ_v evolution during five fatigue lags for mix PMB – 5: the envelope line of the first fatigue lag is used for all fatigue lags.

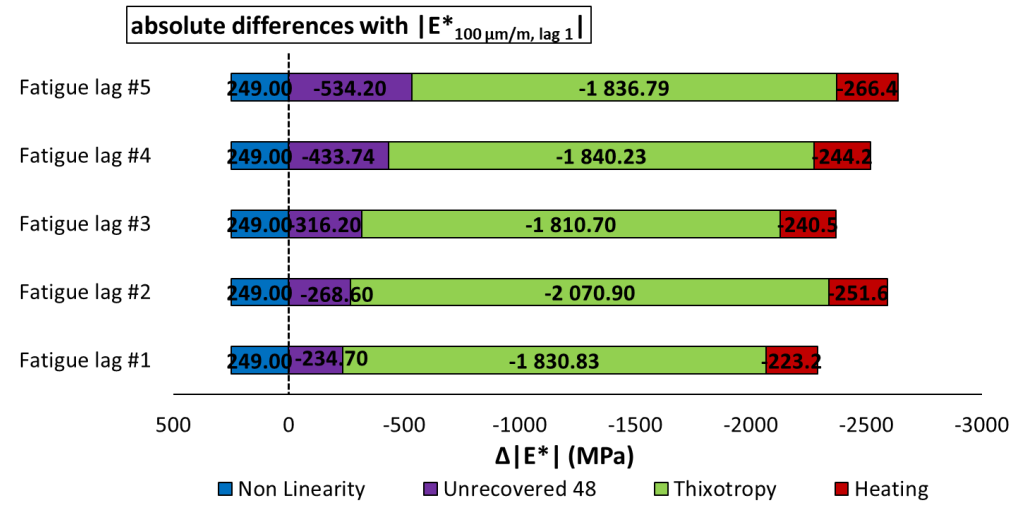
absolute differences with |E*100 µm/m, lag 1|
Fatigue lag #5
Fatigue lag #4
Fatigue lag #3
Fatigue lag #2
Fatigue lag #1
249.00
-534.20
-1 836.79
-266.4
249.00
-433.74
-1 840.23
-244.2
249.00
-316.20
-1 810.70
-240.5
249.00
-268.60
-2 070.90
-251.6
249.00
-234.70
-1 830.83
-223.2
500
0
-500
-1000
-1500
-2000
-2500
-3000
Δ|E*| (MPa)
Non Linearity
Unrecovered 48
Thixotropy
Heating

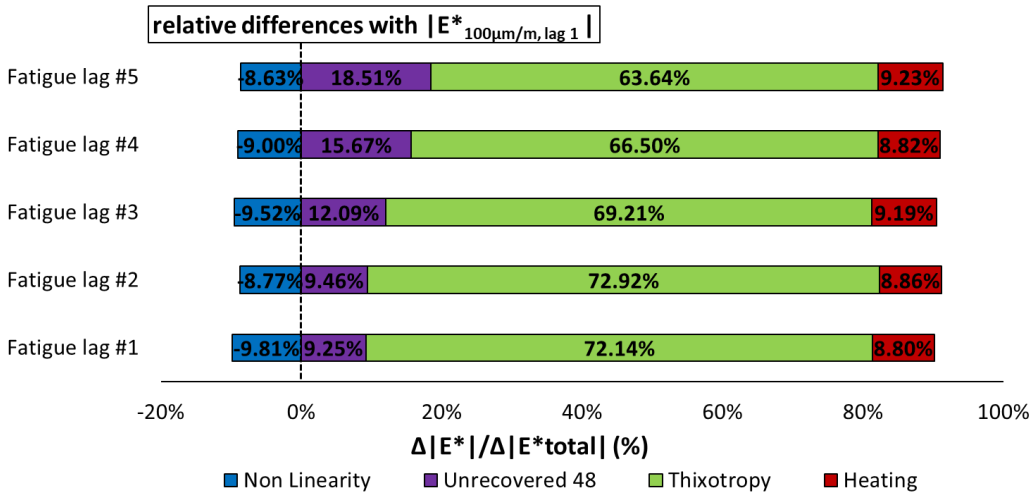
relative differences with |E*100µm/m, lag 1|
Fatigue lag #5
Fatigue lag #4
Fatigue lag #3
Fatigue lag #2
Fatigue lag #1
-8.63%
18.51%
63.64%
9.23%
-9.00%
15.67%
66.50%
8.82%
-9.52%
12.09%
69.21%
9.19%
-8.77%
9.46%
72.92%
8.86%
-9.81%
9.25%
72.14%
8.80%
-20%
0%
20%
40%
60%
80%
100%
Δ|E*|/Δ|E*total| (%)
Non Linearity
Unrecovered 48
Thixotropy
Heating

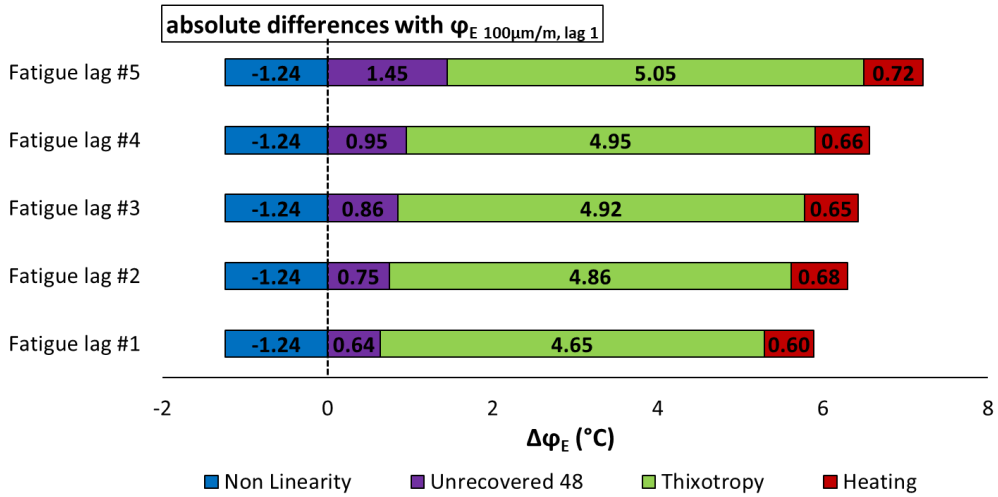
absolute differences with φE 100µm/m, lag 1
Fatigue lag #5
Fatigue lag #4
Fatigue lag #3
Fatigue lag #2
Fatigue lag #1
-1.24
1.45
5.05
0.72
-1.24
0.95
4.95
0.66
-1.24
0.86
4.92
0.65
-1.24
0.75
4.86
0.68
-1.24
0.64
4.65
0.60
-2
0
2
4
6
8
Δφ E (°C)
Non Linearity
Unrecovered 48
Thixotropy
Heating

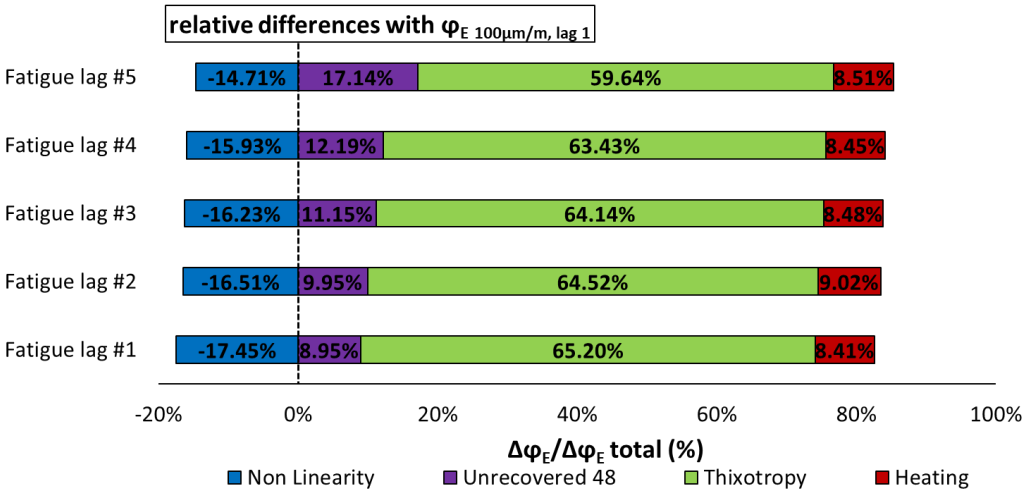
relative differences with $\varphi_{E\ 100\mu m/m,\ lag\ 1}$
Fatigue lag #5
Fatigue lag #4
Fatigue lag #3
Fatigue lag #2
Fatigue lag #1
-14.71%
17.14%
59.64%
8.51%
-15.93%
12.19%
63.43%
8.45%
-16.23%
11.15%
64.14%
8.48%
-16.51%
9.95%
64.52%
9.02%
-17.45%
8.95%
65.20%
8.41%
-20%
0%
20%
40%
60%
80%
100%
$\Delta\varphi_E/\Delta\varphi_E$ total (%)
Non Linearity
Unrecovered 48
Thixotropy
Heating

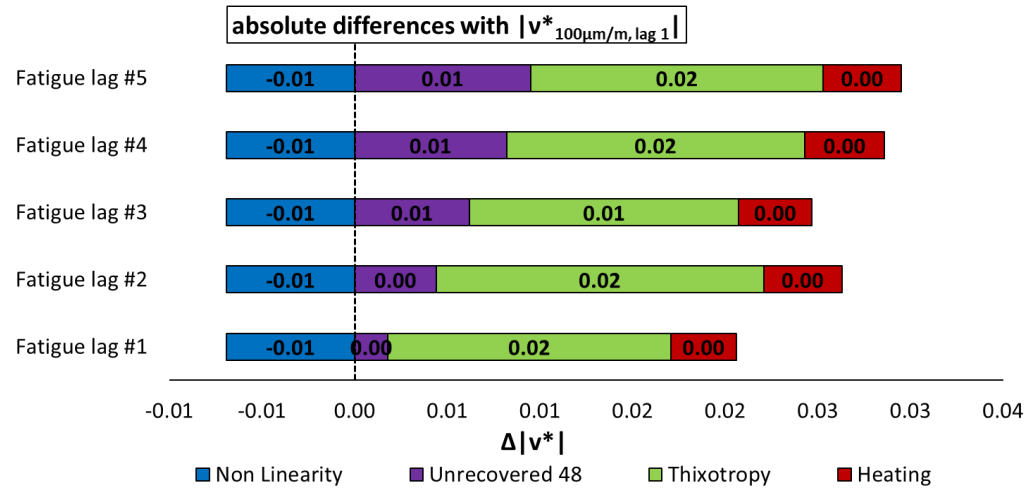
absolute differences with $|v^*_{100\mu m/m,\ lag\ 1}|$
Fatigue lag #5
Fatigue lag #4
Fatigue lag #3
Fatigue lag #2
Fatigue lag #1
-0.01
0.01
0.02
0.00
-0.01
0.01
0.02
0.00
-0.01
0.01
0.01
0.00
-0.01
0.00
0.02
0.00
-0.01
0.00
0.02
0.00
-0.01
-0.01
0.00
0.01
0.01
0.02
0.02
0.03
0.03
0.04
$\Delta|v^*|$
Non Linearity
Unrecovered 48
Thixotropy
Heating

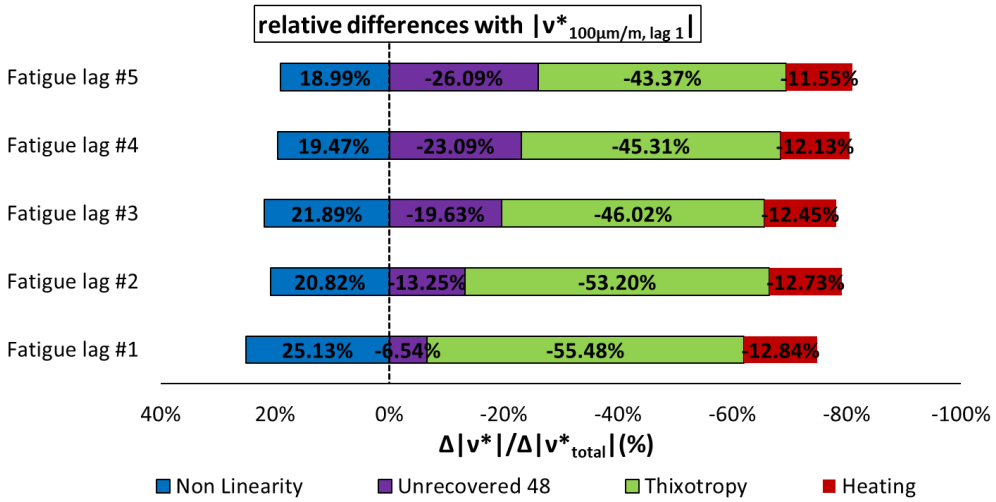
relative differences with $|v^*_{100\mu m/m,\ lag\ 1}|$
Fatigue lag #5
Fatigue lag #4
Fatigue lag #3
Fatigue lag #2
Fatigue lag #1
18.99%
-26.09%
-43.37%
-11.55%
19.47%
-23.09%
-45.31%
-12.13%
21.89%
-19.63%
-46.02%
-12.45%
20.82%
-13.25%
-53.20%
-12.73%
25.13%
-6.54%
-55.48%
-12.84%
40%
20%
0%
-20%
-40%
-60%
-80%
-100%
$\Delta|v^*|/\Delta|v^*_{total}|$ (%)
Non Linearity
Unrecovered 48
Thixotropy
Heating

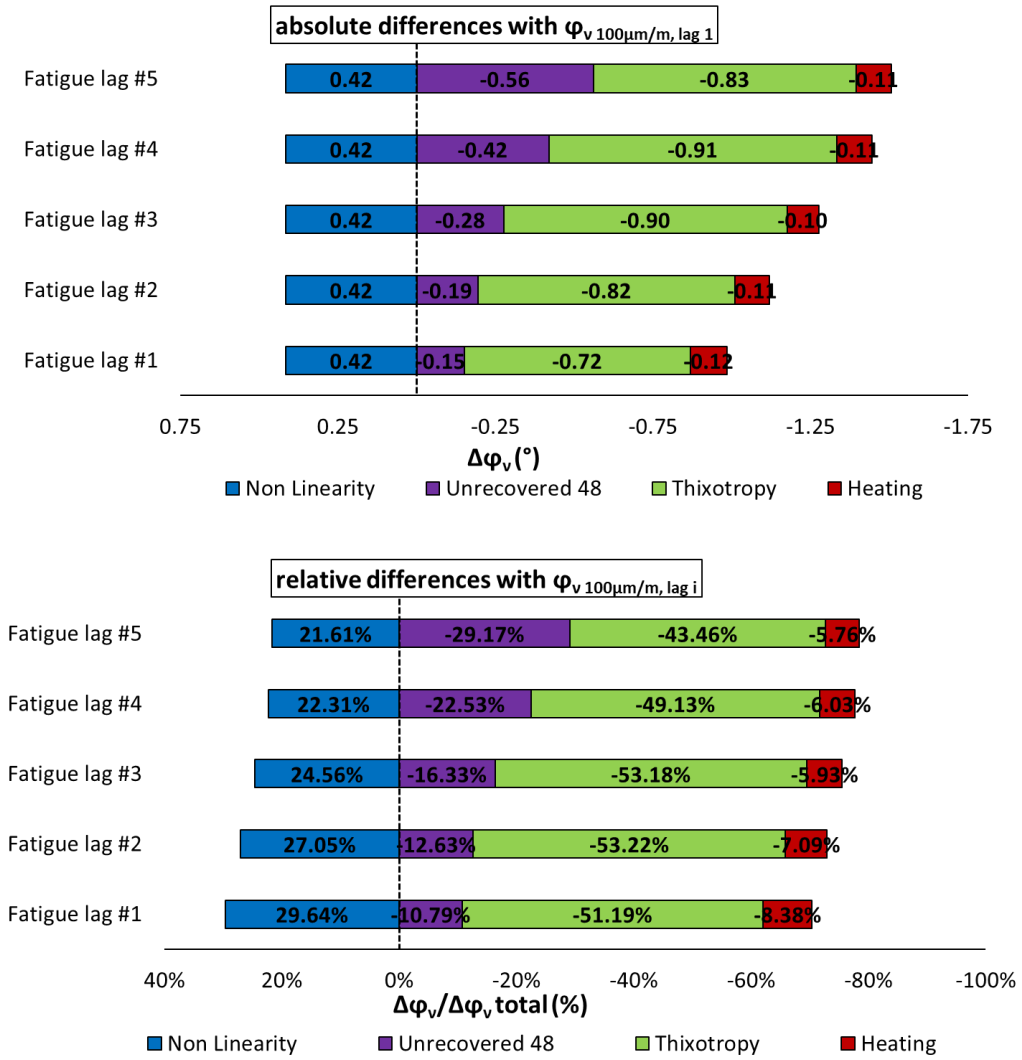

3.1.153. Quantification of different absolute and relative contributions to |E*|, φ_E, |ν*| and φ_ν evolutions for mix PMB – 5, calculated using the envelope line for the first fatigue lag.

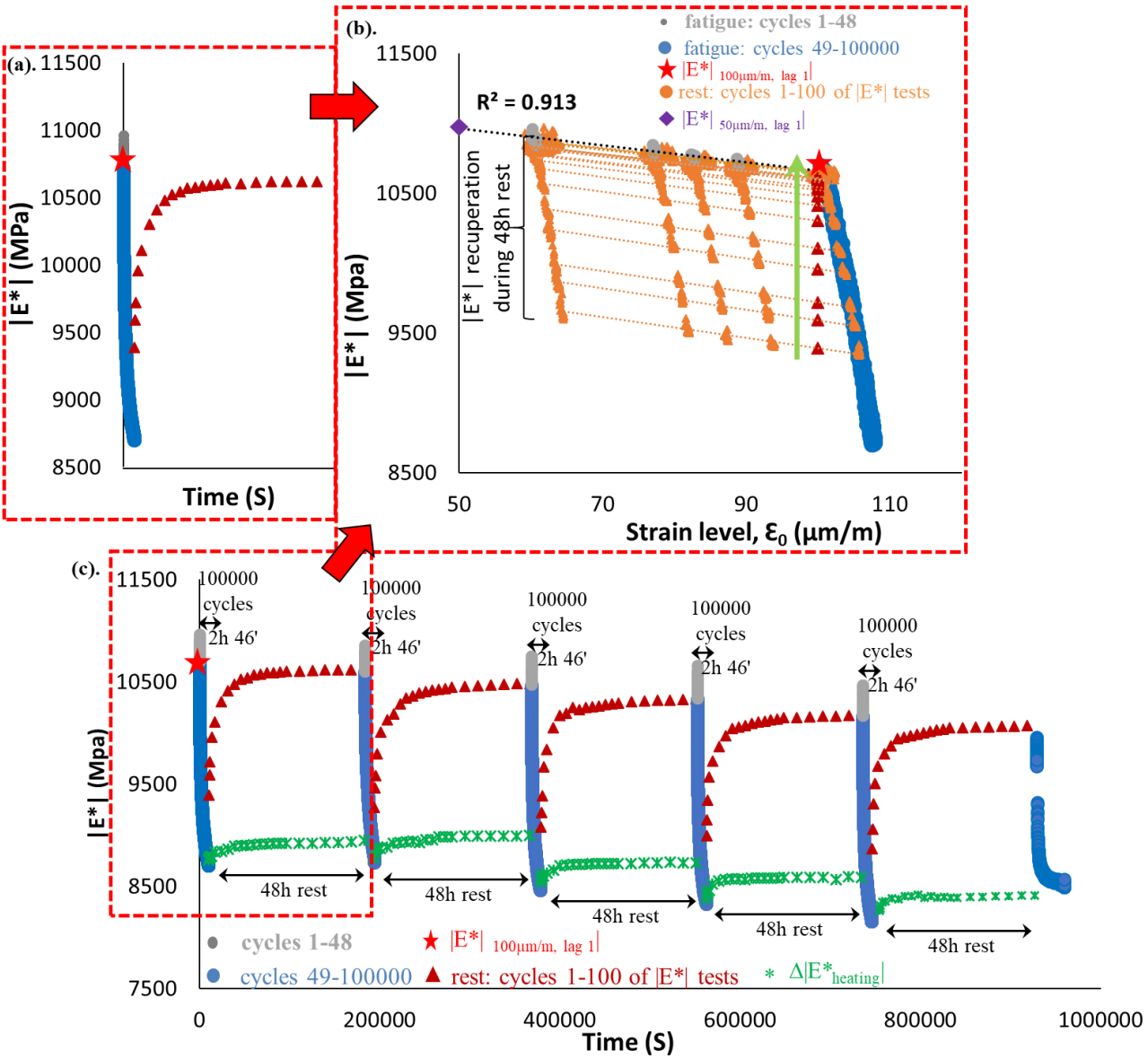

3.1.154. PFRT results obtained for mix PMB – 6: (a) |E*| as a function of time during the first fatigue lag and rest period (b) |E*| as a function of applied strain amplitude during the first fatigue lags and the short complex modulus tests performed within its following rest periods; (c) |E*| as a function of time during the five fatigue lags and rest periods [Red stars indicate values of |E*| estimated at 100 µm/m at the beginning of fatigue lag, green asterisk shows values of $\Delta|E^*_{heating}|$ as influence of self-heating and brown triangles indicate values of |E*| estimated at 100 µm/m for each short complex modulus test during rest (all these values were obtained using non-linearity envelopes, as shown in (b) for the first fatigue lag and rest period)].

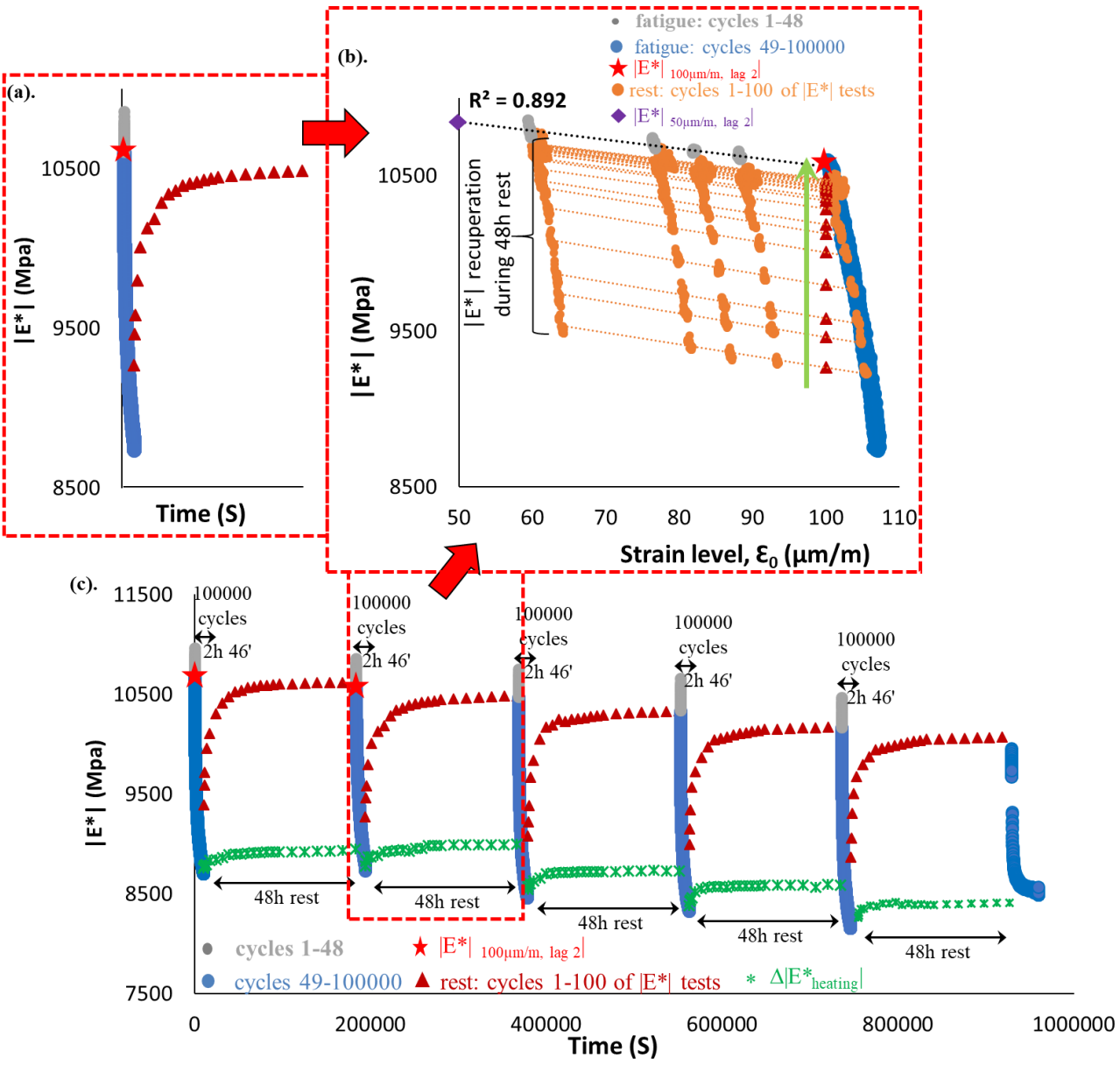

3.1.155. PFRT results obtained for mix PMB – 6: (a) |E*| as a function of time during the second fatigue lag and rest period (b) |E*| as a function of applied strain amplitude during the second fatigue lags and the short complex modulus tests performed within its following rest periods; (c) |E*| as a function of time during the five fatigue lags and rest periods [Red stars indicate values of |E*| estimated at 100 µm/m at the beginning of fatigue lag, green asterisk shows values of $\Delta|E^*_{heating}|$ as influence of self-heating and brown triangles indicate values of |E*| estimated at 100 µm/m for each short complex modulus test during rest (all these values were obtained using non-linearity envelopes, as shown in (b) for the first fatigue lag and rest period)].

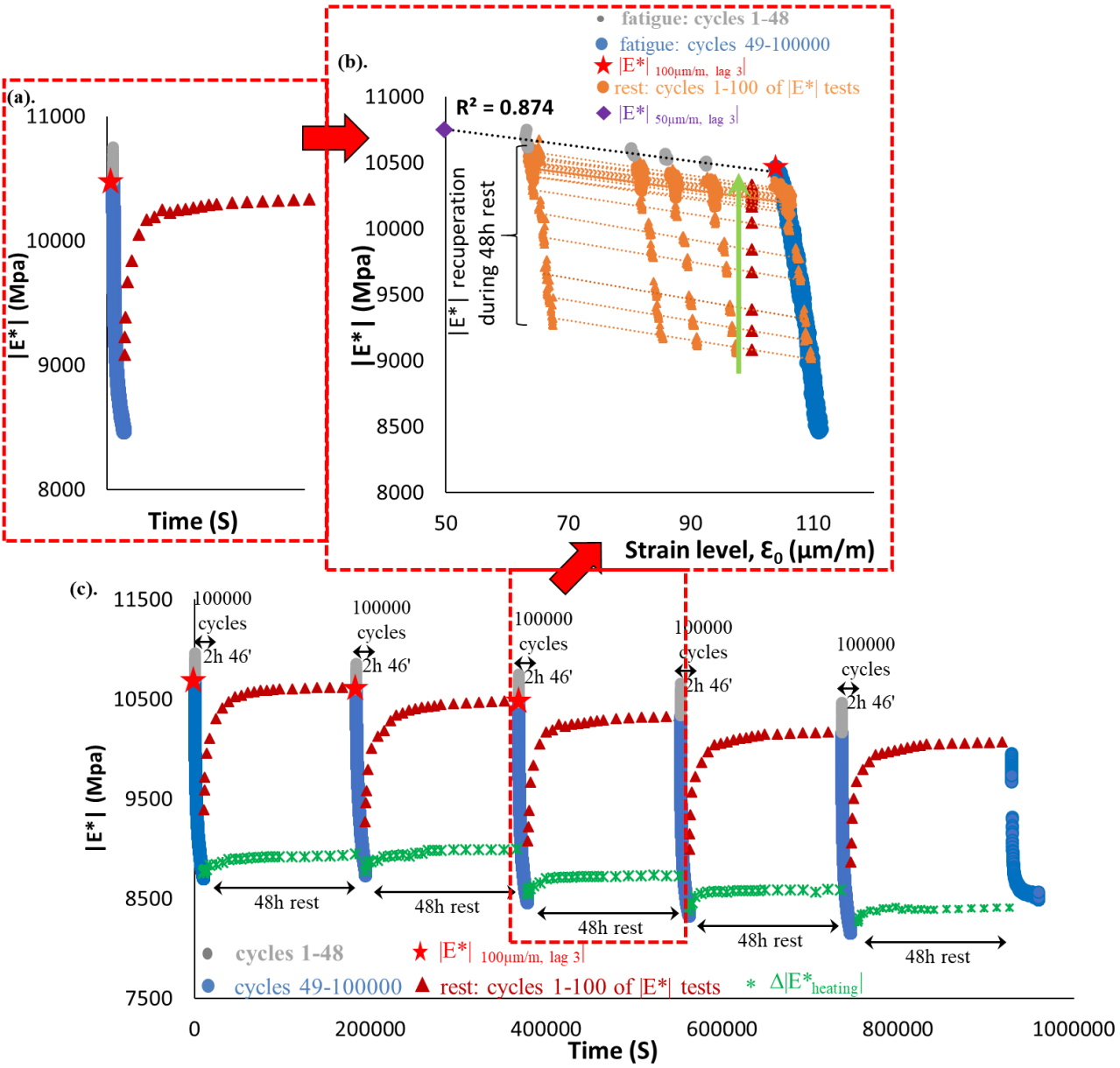

3.1.156. PFRT results obtained for mix PMB – 6: (a) |E*| as a function of time during the third fatigue lag and rest period (b) |E*| as a function of applied strain amplitude during the third fatigue lags and the short complex modulus tests performed within its following rest periods; (c) |E*| as a function of time during the five fatigue lags and rest periods [Red stars indicate values of |E*| estimated at 100 µm/m at the beginning of fatigue lag, green asterisk shows values of $\Delta|E^*_{heating}|$ as influence of self-heating and brown triangles indicate values of |E*| estimated at 100 µm/m for each short complex modulus test during rest (all these values were obtained using non-linearity envelopes, as shown in (b) for the first fatigue lag and rest period)].

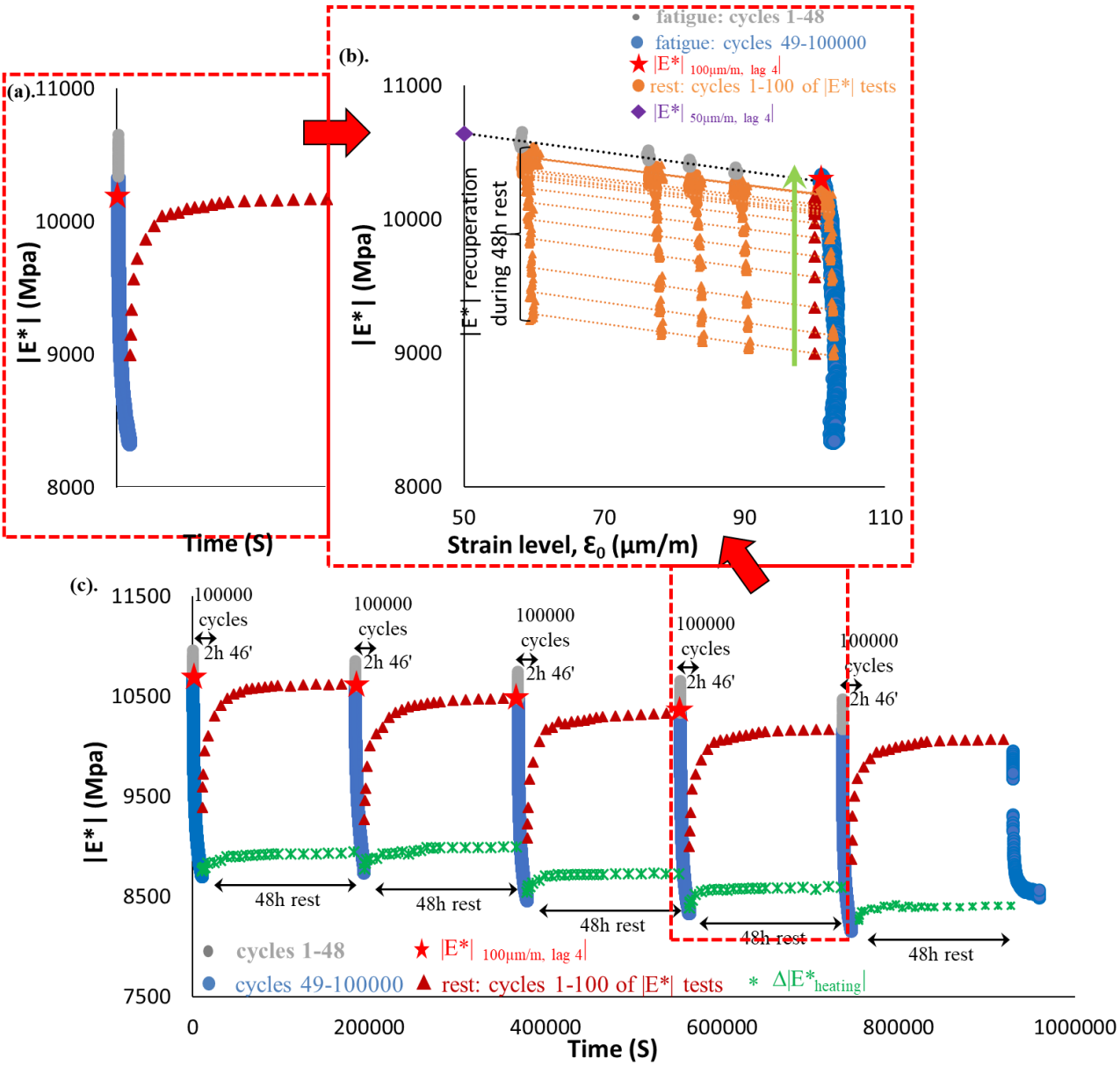

3.1.157. PFRT results obtained for mix PMB – 6: (a) |E*| as a function of time during the fourth fatigue lag and rest period (b) |E*| as a function of applied strain amplitude during the fourth fatigue lags and the short complex modulus tests performed within its following rest periods; (c) |E*| as a function of time during the five fatigue lags and rest periods [Red stars indicate values of |E*| estimated at 100 µm/m at the beginning of fatigue lag, green asterisk shows values of $\Delta|E^*_{heating}|$ as influence of self-heating and brown triangles indicate values of |E*| estimated at 100 µm/m for each short complex modulus test during rest (all these values were obtained using non-linearity envelopes, as shown in (b) for the first fatigue lag and rest period)].

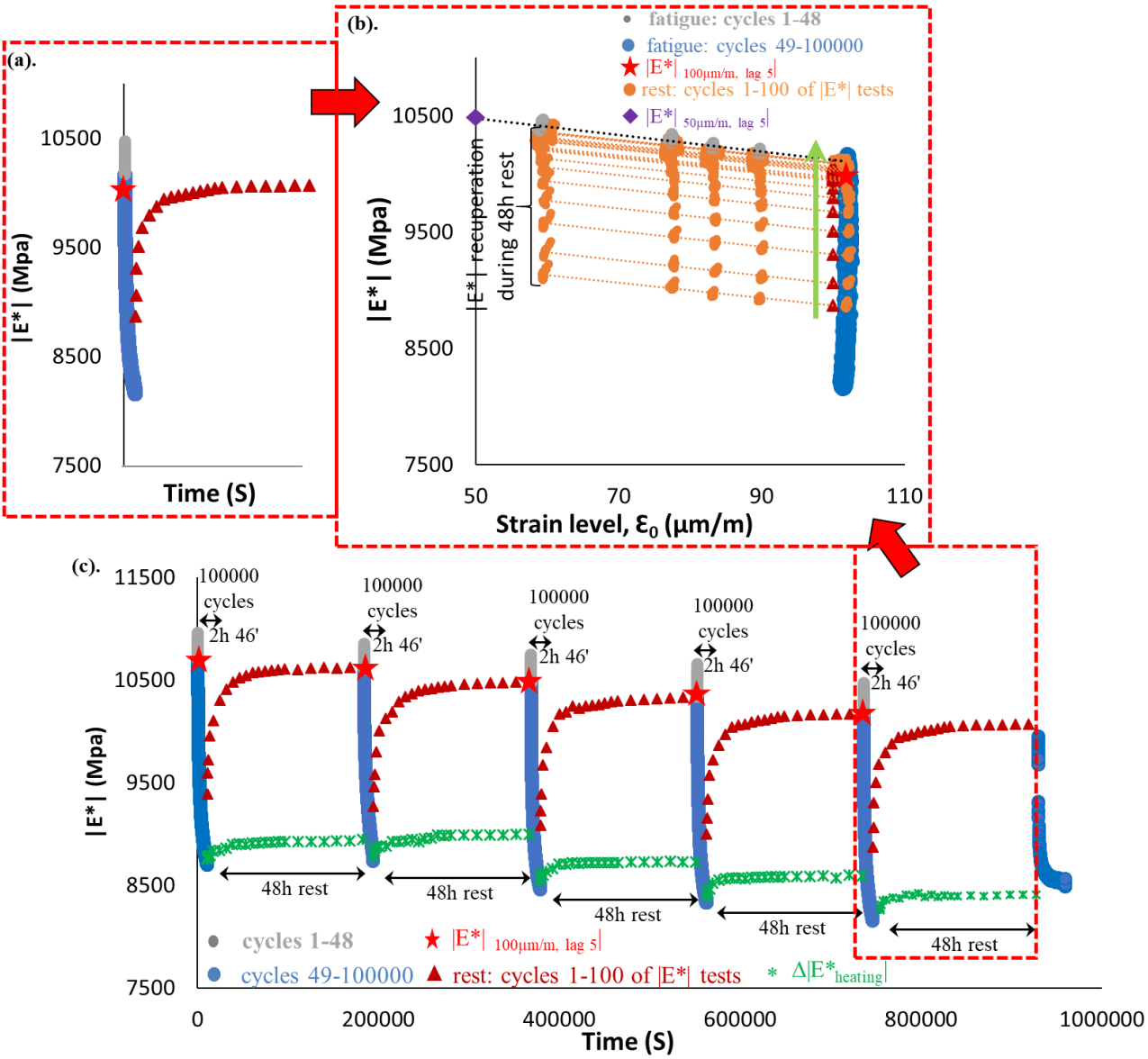

3.1.158. PFRT results obtained for mix PMB – 6: (a) |E*| as a function of time during the fifth fatigue lag and rest period (b) |E*| as a function of applied strain amplitude during the fifth fatigue lags and the short complex modulus tests performed within its following rest periods; (c) |E*| as a function of time during the five fatigue lags and rest periods [Red stars indicate values of |E*| estimated at 100 µm/m at the beginning of fatigue lag, green asterisk shows values of $\Delta|E^*_{heating}|$ as influence of self-heating and brown triangles indicate values of |E*| estimated at 100 µm/m for each short complex modulus test during rest (all these values were obtained using non-linearity envelopes, as shown in (b) for the first fatigue lag and rest period)].

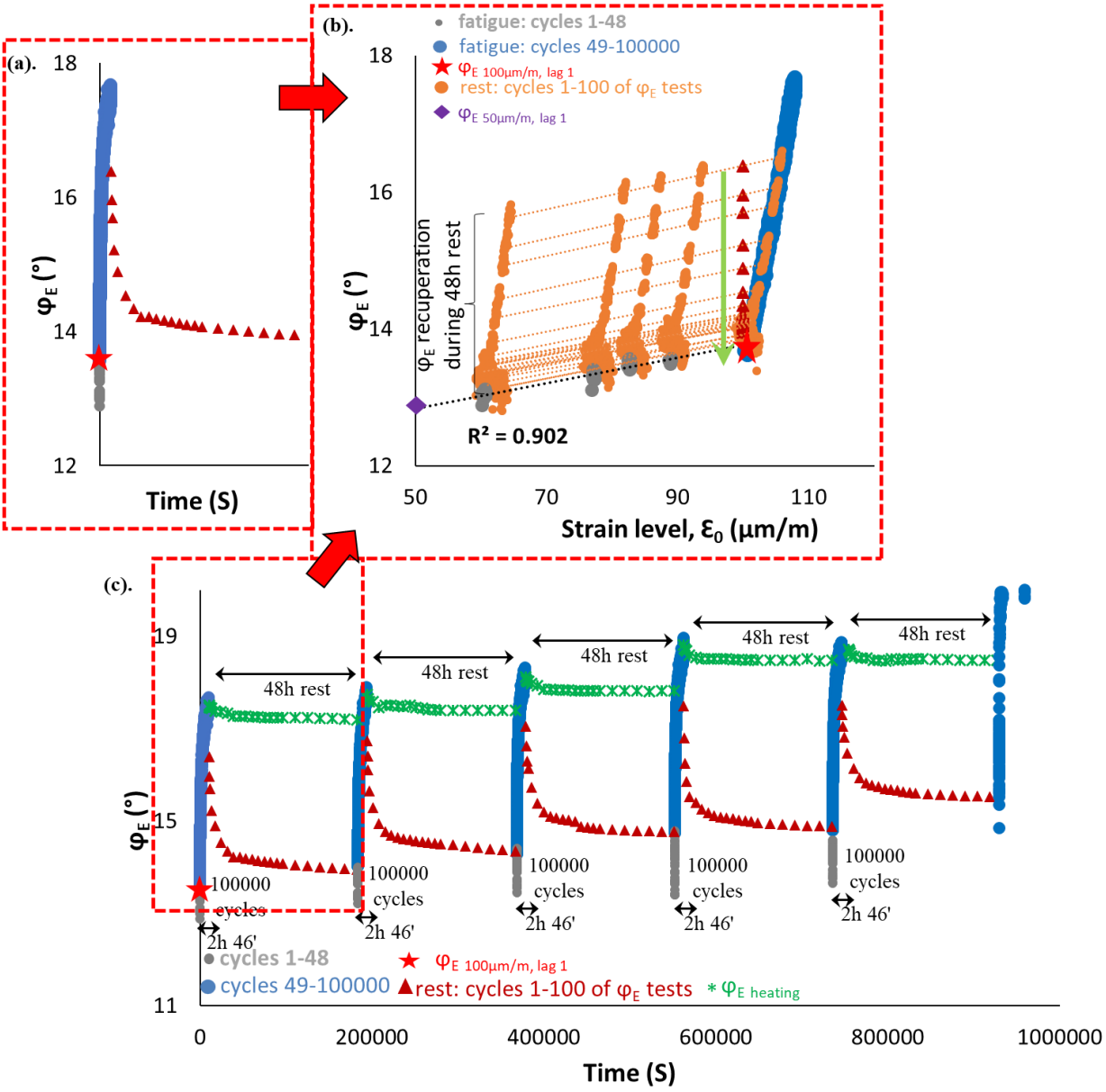

3.1.159. PFRT results obtained for mix PMB – 6: (a) φ_E as a function of time during the first fatigue lag and rest period (b) φ_E as a function of applied strain amplitude during the first fatigue lags and the short complex modulus tests performed within its following rest periods; (c) φ_E as a function of time during the five fatigue lags and rest periods (Red stars indicate values of φ_E estimated at 100 µm/m at the beginning of fatigue lag, green asterisk shows values of $\Delta\varphi_{E\ heating}$ as influence of self-heating and brown triangles indicate values of φ_E estimated at 100 µm/m for each short complex modulus test during rest (all these values were obtained using non-linearity envelopes, as shown in (b) for the first fatigue lag and rest period).

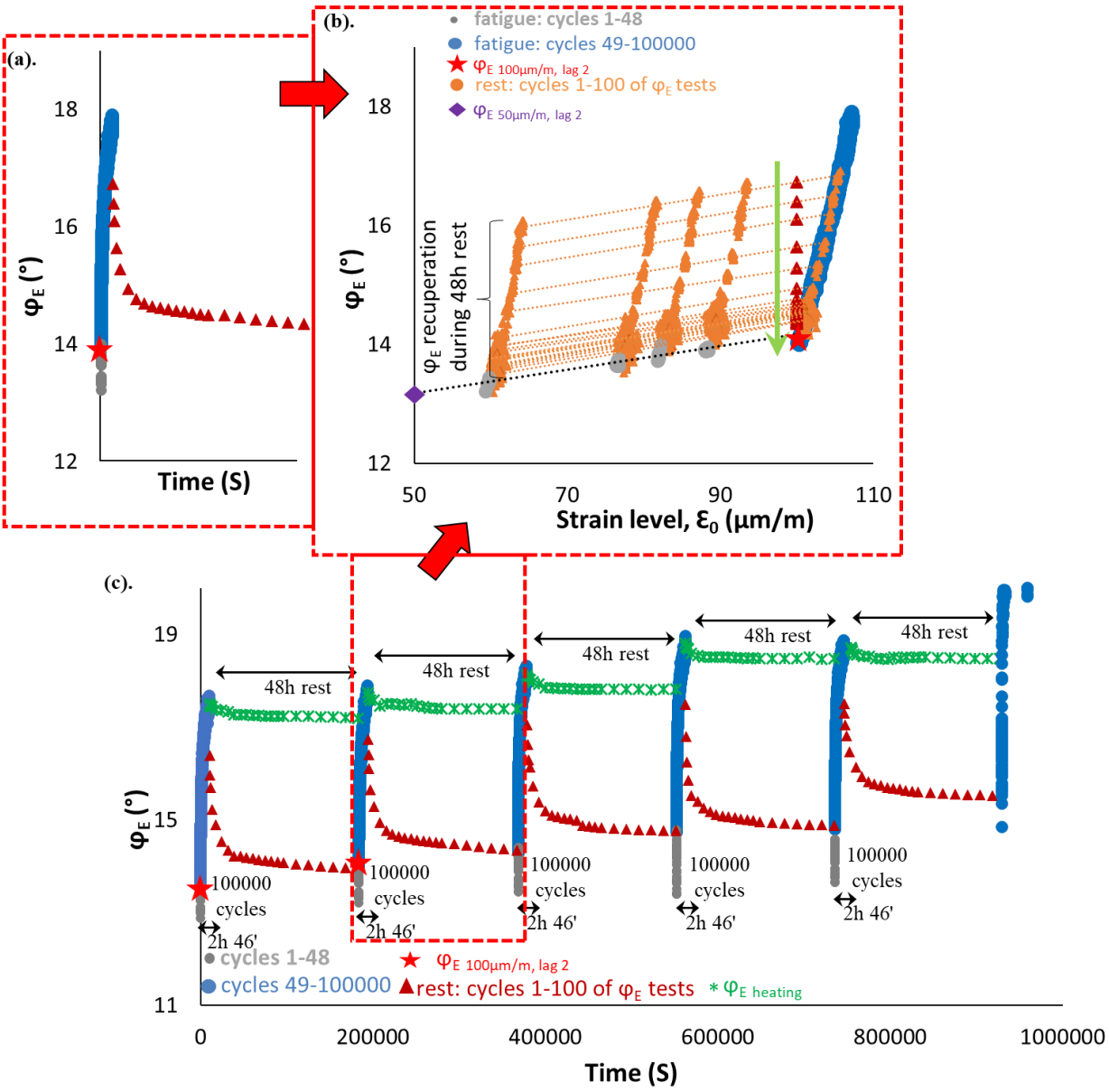

3.1.160. PFRT results obtained for mix PMB – 6: (a) φ_E as a function of time during the second fatigue lag and rest period (b) φ_E as a function of applied strain amplitude during the first fatigue lags and the short complex modulus tests performed within its following rest periods; (c) φ_E as a function of time during the five fatigue lags and rest periods (Red stars indicate values of φ_E estimated at 100 µm/m at the beginning of fatigue lag, green asterisk shows values of $\Delta\varphi_{E\ heating}$ as influence of self-heating and brown triangles indicate values of φ_E estimated at 100 µm/m for each short complex modulus test during rest (all these values were obtained using non-linearity envelopes, as shown in (b) for the first fatigue lag and rest period).

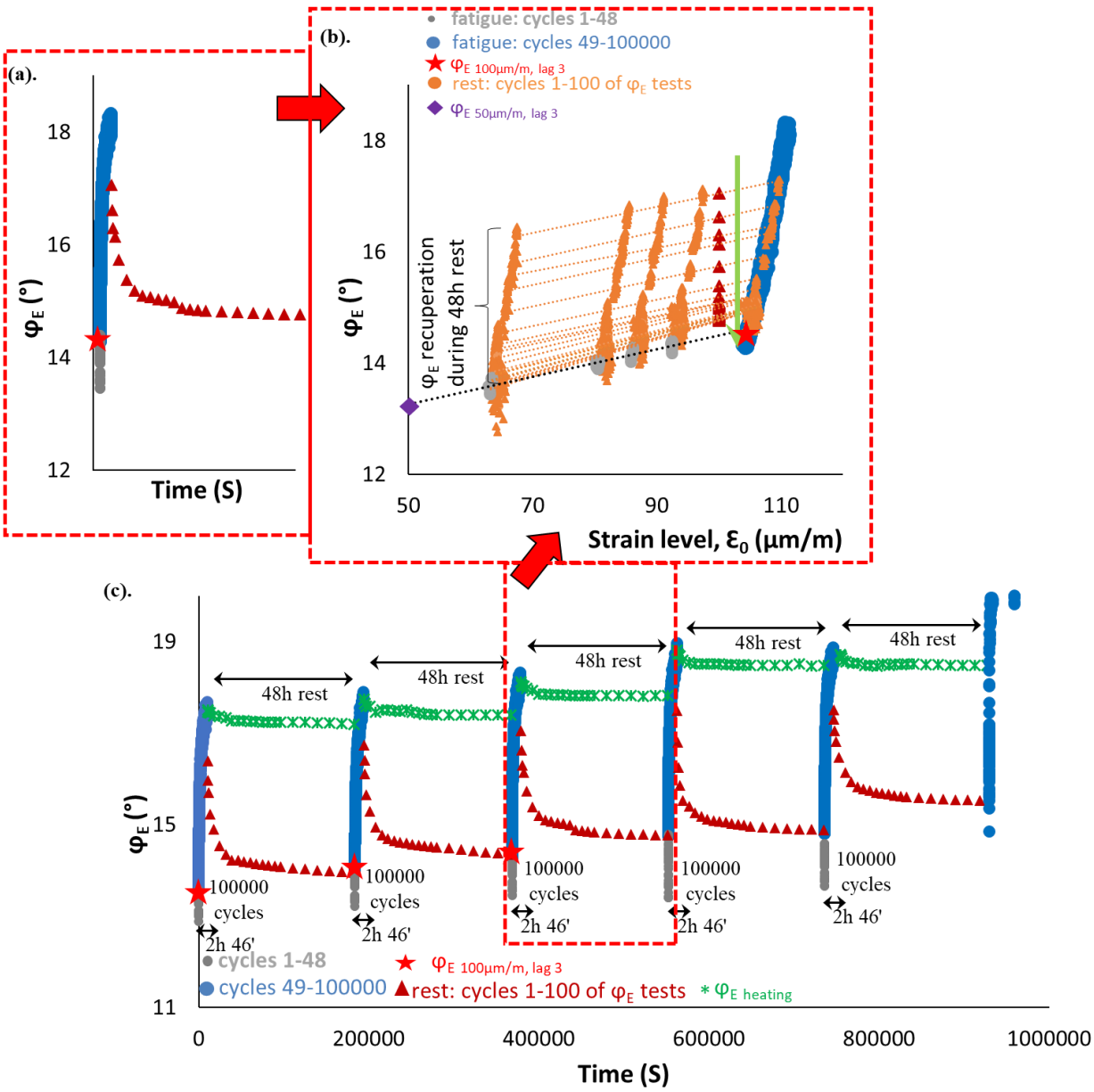

3.1.161. PFRT results obtained for mix PMB – 6: (a) φ_E as a function of time during the third fatigue lag and rest period (b) φ_E as a function of applied strain amplitude during the third fatigue lags and the short complex modulus tests performed within its following rest periods; (c) φ_E as a function of time during the five fatigue lags and rest periods (Red stars indicate values of φ_E estimated at 100 µm/m at the beginning of fatigue lag, green asterisk shows values of $\Delta\varphi_{E\ heating}$ as influence of self-heating and brown triangles indicate values of φ_E estimated at 100 µm/m for each short complex modulus test during rest (all these values were obtained using non-linearity envelopes, as shown in (b) for the first fatigue lag and rest period).

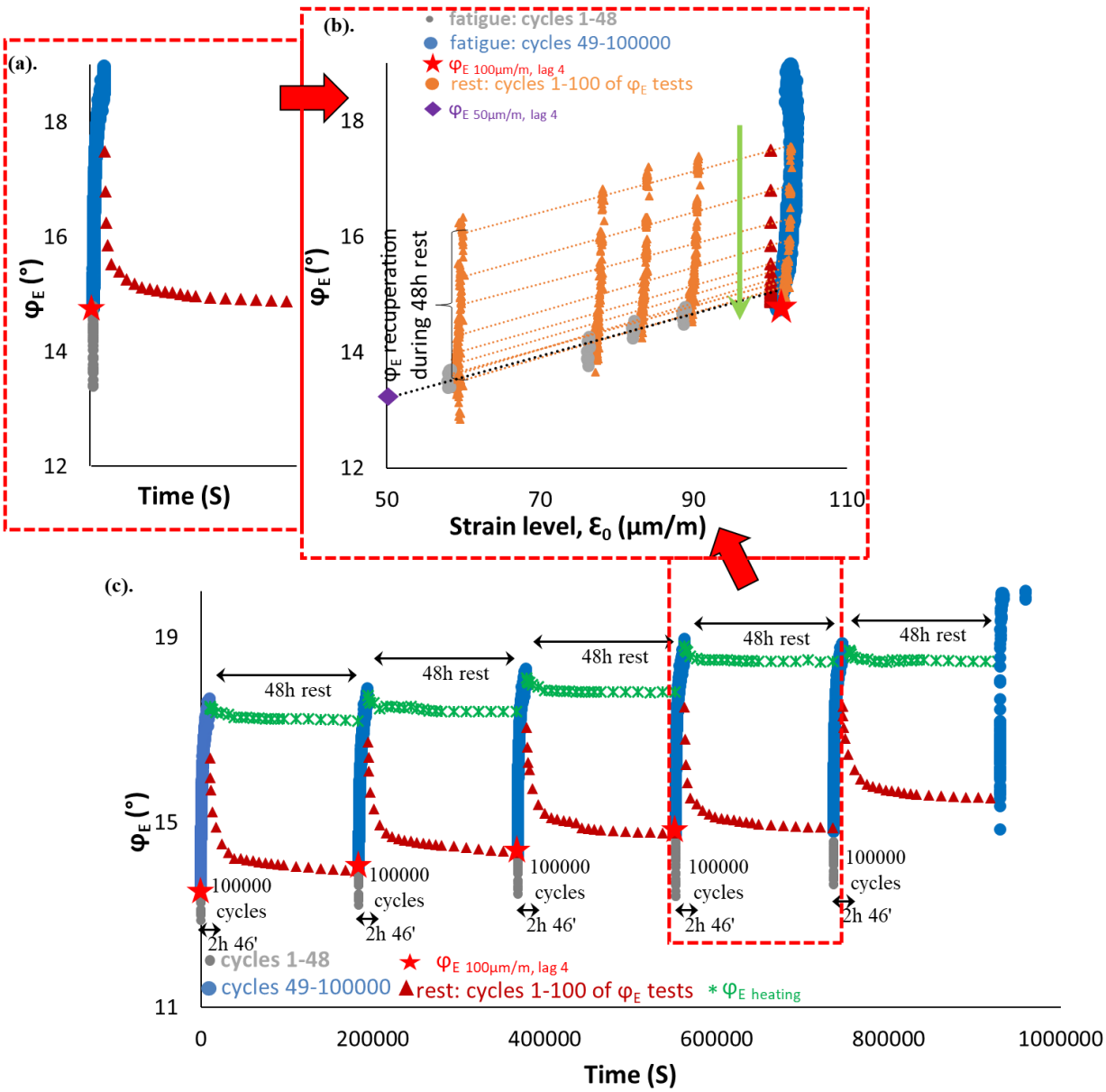

3.1.162. PFRT results obtained for mix PMB – 6: (a) φ_E as a function of time during the fourth fatigue lag and rest period (b) φ_E as a function of applied strain amplitude during the fourth fatigue lags and the short complex modulus tests performed within its following rest periods; (c) φ_E as a function of time during the five fatigue lags and rest periods (Red stars indicate values of φ_E estimated at 100 µm/m at the beginning of fatigue lag, green asterisk shows values of $\Delta\varphi_{E\ heating}$ as influence of self-heating and brown triangles indicate values of φ_E estimated at 100 µm/m for each short complex modulus test during rest (all these values were obtained using non-linearity envelopes, as shown in (b) for the first fatigue lag and rest period).

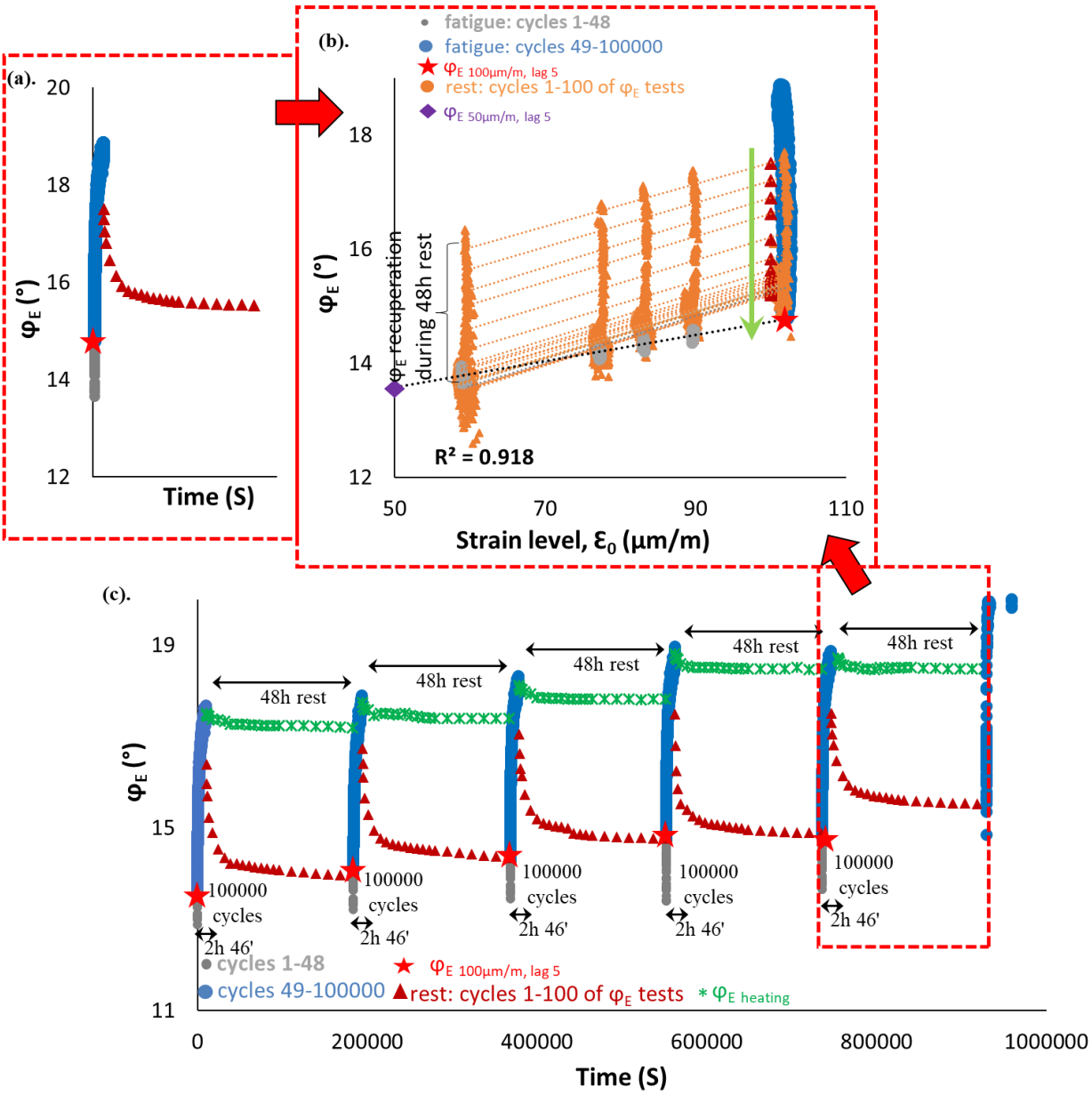

3.1.163. PFRT results obtained for mix PMB – 6: (a) φ_E as a function of time during the fifth fatigue lag and rest period (b) φ_E as a function of applied strain amplitude during the fifth fatigue lags and the short complex modulus tests performed within its following rest periods; (c) φ_E as a function of time during the five fatigue lags and rest periods (Red stars indicate values of φ_E estimated at 100 µm/m at the beginning of fatigue lag, green asterisk shows values of $\Delta\varphi_{E\ heating}$ as influence of self-heating and brown triangles indicate values of φ_E estimated at 100 µm/m for each short complex modulus test during rest (all these values were obtained using non-linearity envelopes, as shown in (b) for the first fatigue lag and rest period).

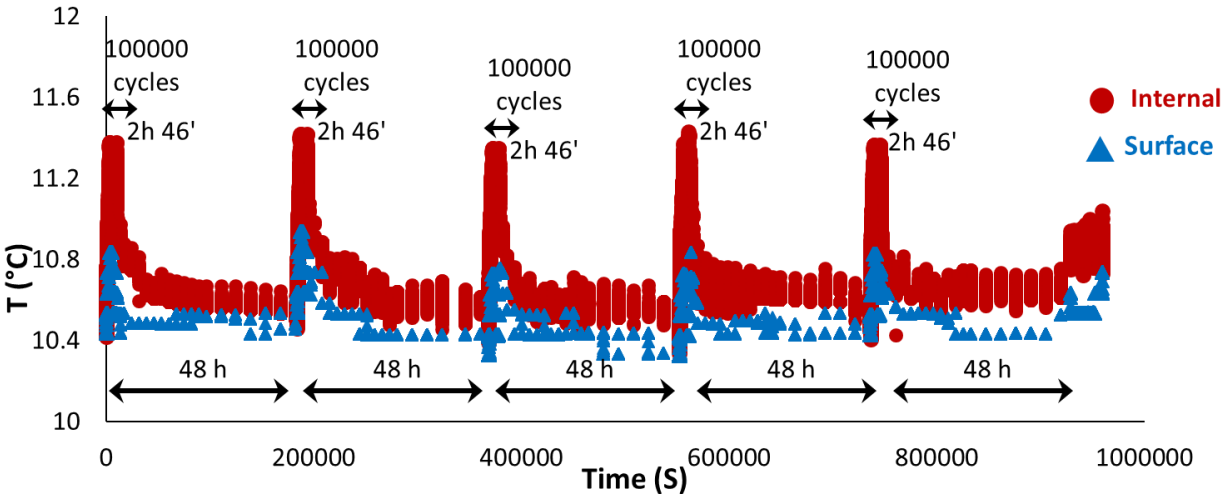

3.1.164. PFRT results obtained for mix PMB – 6: internal and surface temperature evolution during fatigue lags and recovery periods.

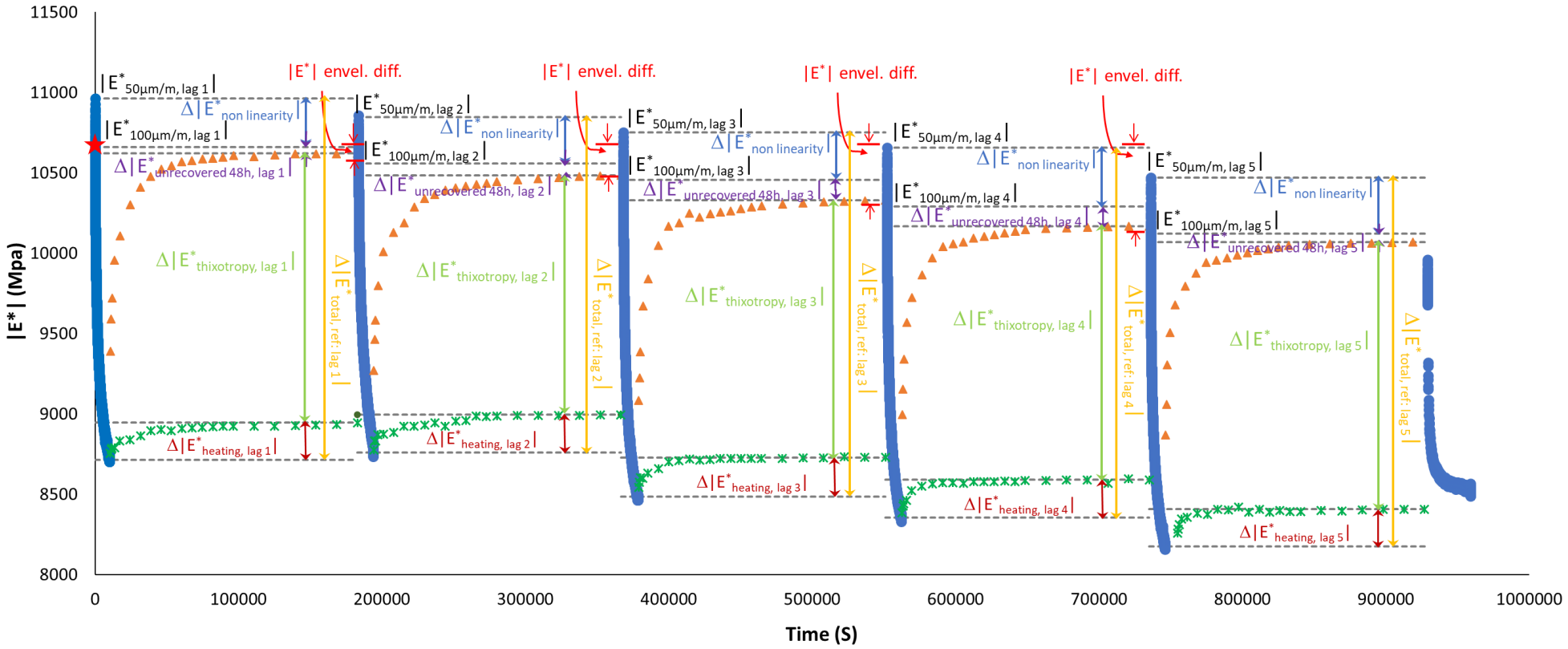
11500
11000
10500
10000
9500
9000
8500
8000
|E*| (Mpa)
0
100000
200000
300000
400000
500000
600000
700000
800000
900000
1000000
Time (S)
|E*| envel. diff.
|E*| envel. diff.
|E*| envel. diff.
|E*| envel. diff.
|E*50µm/m, lag 1|
|E*100µm/m, lag 1|
Δ|E*non linearity|
Δ|E*unrecovered 48h, lag 1|
Δ|E*thixotropy, lag 1|
Δ|E*total, ref: lag 1|
Δ|E*heating, lag 1|
|E*50µm/m, lag 2|
|E*100µm/m, lag 2|
Δ|E*non linearity|
Δ|E*unrecovered 48h, lag 2|
Δ|E*thixotropy, lag 2|
Δ|E*total, ref: lag 2|
Δ|E*heating, lag 2|
|E*50µm/m, lag 3|
|E*100µm/m, lag 3|
Δ|E*non linearity|
Δ|E*unrecovered 48h, lag 3|
Δ|E*thixotropy, lag 3|
Δ|E*total, ref: lag 3|
Δ|E*heating, lag 3|
|E*50µm/m, lag 4|
|E*100µm/m, lag 4|
Δ|E*non linearity|
Δ|E*unrecovered 48h, lag 4|
Δ|E*thixotropy, lag 4|
Δ|E*total, ref: lag 4|
Δ|E*heating, lag 4|
|E*50µm/m, lag 5|
|E*100µm/m, lag 5|
Δ|E*non linearity|
Δ|E*unrecovered 48h, lag 5|
Δ|E*thixotropy, lag 5|
Δ|E*total, ref: lag 5|
Δ|E*heating, lag 5|

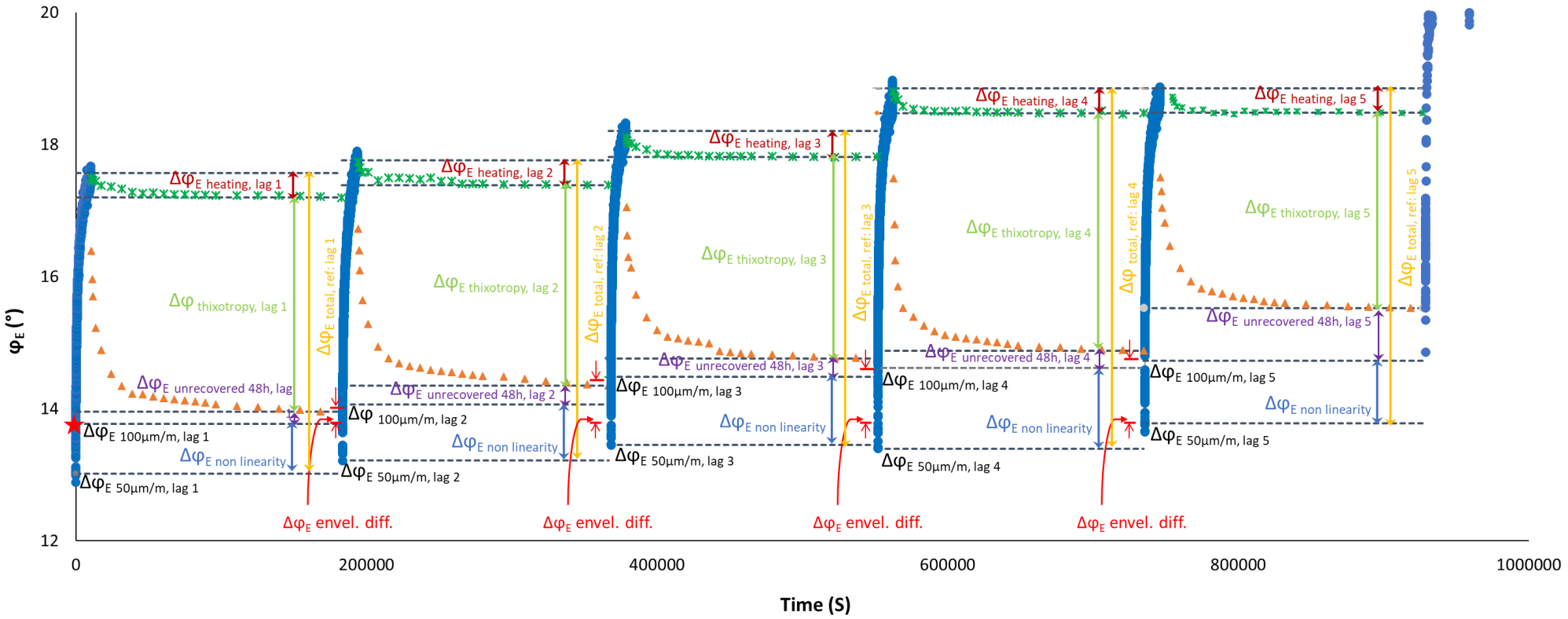

3.1.165. Quantification of different contributions to |E*|, φ_E, |v*| and φ_v evolution during five fatigue lags for mix PMB – 6: the envelope line of the first fatigue lag is used for all fatigue lags.

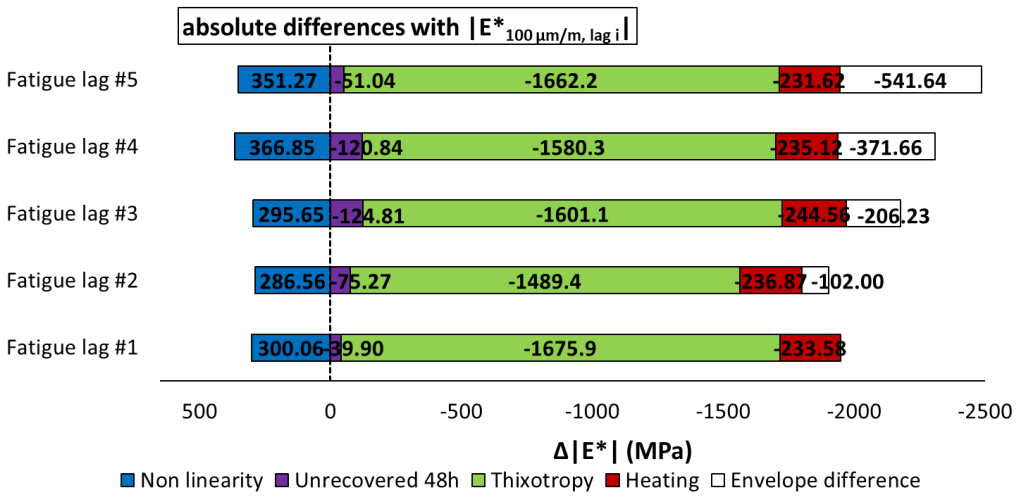
absolute differences with |E*100 µm/m, lag i|
Fatigue lag #5
Fatigue lag #4
Fatigue lag #3
Fatigue lag #2
Fatigue lag #1
351.27
-51.04
-1662.2
-231.62
-541.64
366.85
-120.84
-1580.3
-235.12
-371.66
295.65
-124.81
-1601.1
-244.56
-206.23
286.56
-75.27
-1489.4
-236.87
-102.00
300.06
-99.90
-1675.9
-233.58
500
0
-500
-1000
-1500
-2000
-2500
Δ|E*| (MPa)
Non linearity
Unrecovered 48h
Thixotropy
Heating
Envelope difference

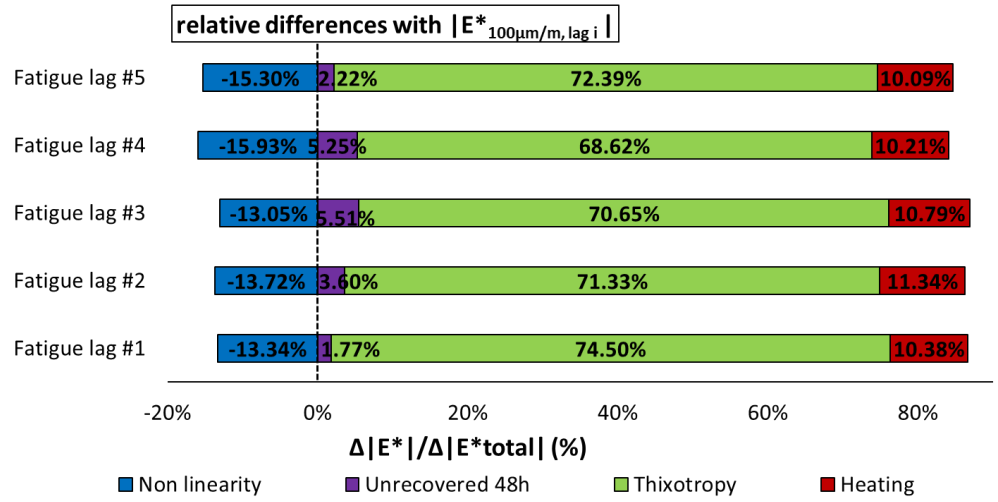
relative differences with |E*100µm/m, lag i|
Fatigue lag #5
Fatigue lag #4
Fatigue lag #3
Fatigue lag #2
Fatigue lag #1
-15.30%
2.22%
72.39%
10.09%
-15.93%
5.25%
68.62%
10.21%
-13.05%
5.51%
70.65%
10.79%
-13.72%
3.60%
71.33%
11.34%
-13.34%
1.77%
74.50%
10.38%
-20%
0%
20%
40%
60%
80%
Δ|E*|/Δ|E*total| (%)
Non linearity
Unrecovered 48h
Thixotropy
Heating

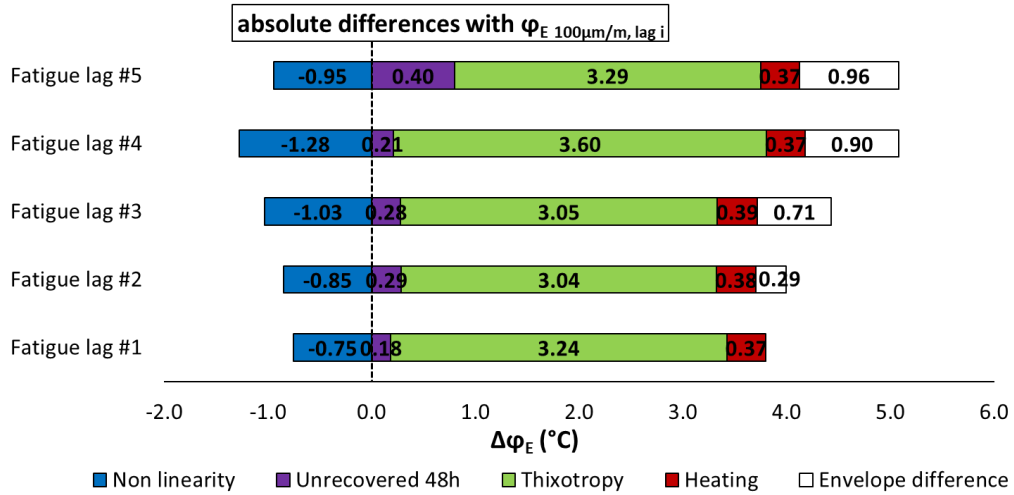
absolute differences with φE 100µm/m, lag i
Fatigue lag #5
Fatigue lag #4
Fatigue lag #3
Fatigue lag #2
Fatigue lag #1
-0.95
0.40
3.29
0.37
0.96
-1.28
0.21
3.60
0.37
0.90
-1.03
0.28
3.05
0.39
0.71
-0.85
0.29
3.04
0.38
0.29
-0.75
0.18
3.24
0.37
-2.0
-1.0
0.0
1.0
2.0
3.0
4.0
5.0
6.0
Δφ E (°C)
Non linearity
Unrecovered 48h
Thixotropy
Heating
Envelope difference

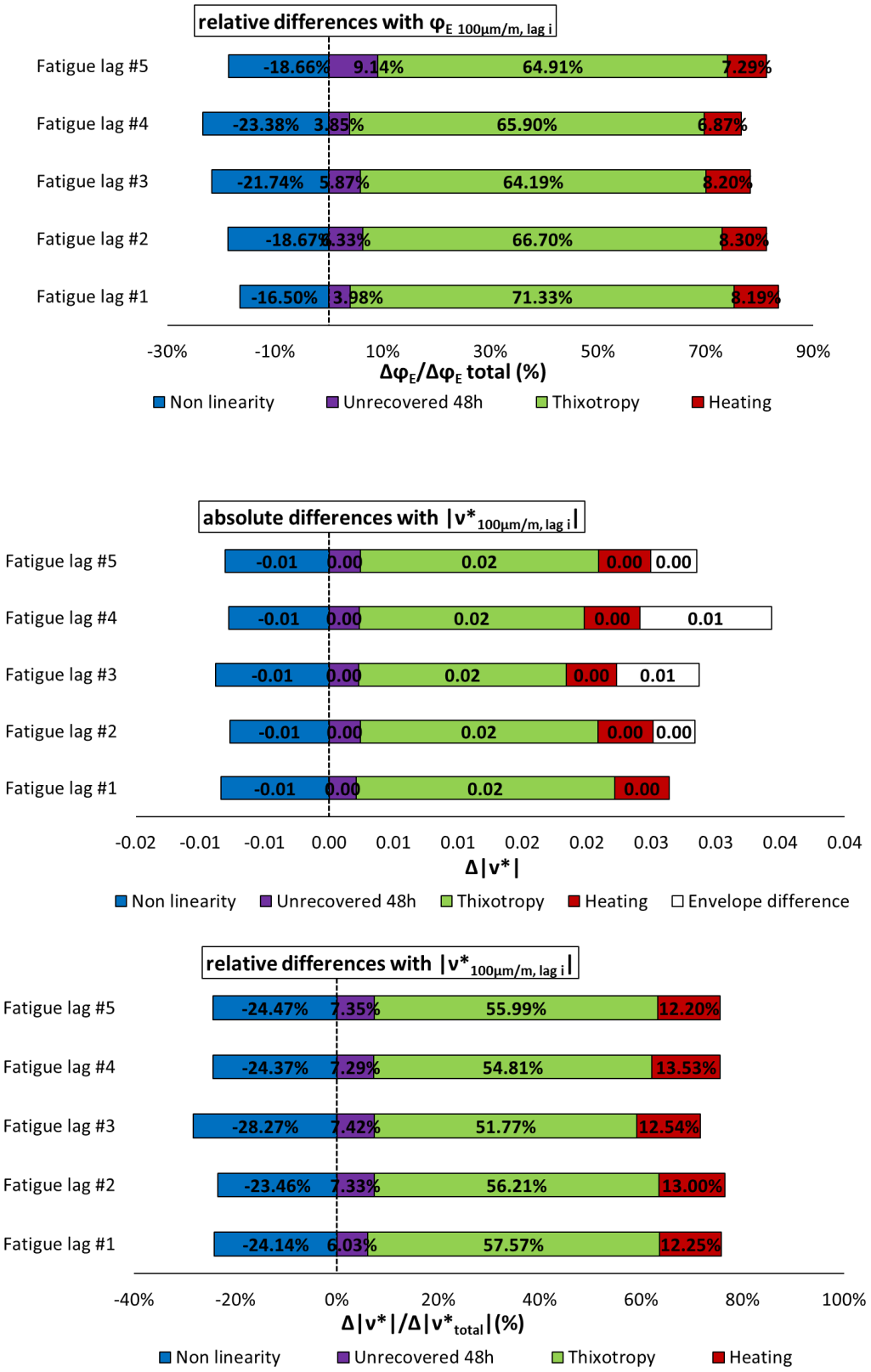

3.1.167. Quantification of different absolute and relative contributions to |E*|, φ_E, |v*| and φ_v evolutions for mix PMB – 6 calculated using a different envelope line for each fatigue lag.

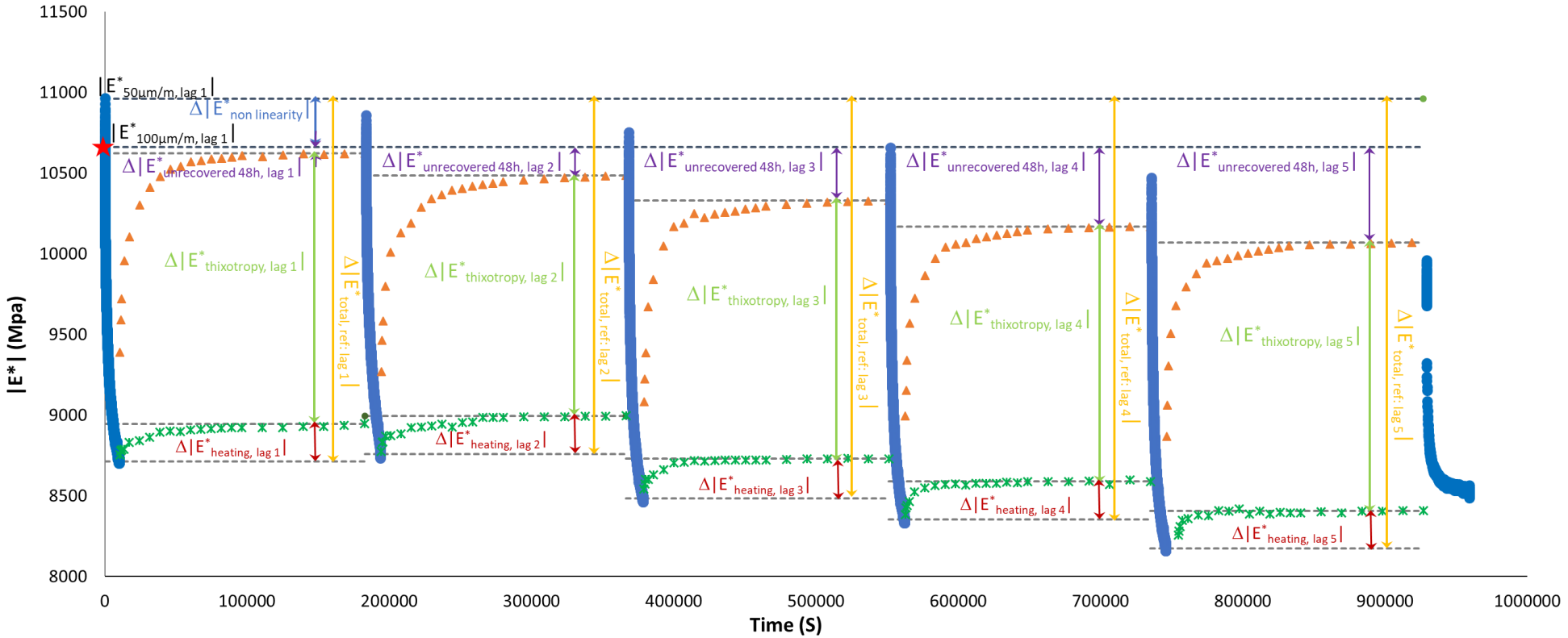
11500
11000
10500
10000
9500
9000
8500
8000
|E*| (Mpa)
0
100000
200000
300000
400000
500000
600000
700000
800000
900000
1000000
Time (S)
|E*50µm/m, lag 1|
|E*100µm/m, lag 1|
Δ|E*non linearity|
Δ|E*unrecovered 48h, lag 1|
Δ|E*thixotropy, lag 1|
Δ|E*heating, lag 1|
Δ|E*total, ref: lag 1|
Δ|E*unrecovered 48h, lag 2|
Δ|E*thixotropy, lag 2|
Δ|E*heating, lag 2|
Δ|E*total, ref: lag 2|
Δ|E*unrecovered 48h, lag 3|
Δ|E*thixotropy, lag 3|
Δ|E*heating, lag 3|
Δ|E*total, ref: lag 3|
Δ|E*unrecovered 48h, lag 4|
Δ|E*thixotropy, lag 4|
Δ|E*heating, lag 4|
Δ|E*total, ref: lag 4|
Δ|E*unrecovered 48h, lag 5|
Δ|E*thixotropy, lag 5|
Δ|E*heating, lag 5|
Δ|E*total, ref: lag 5|

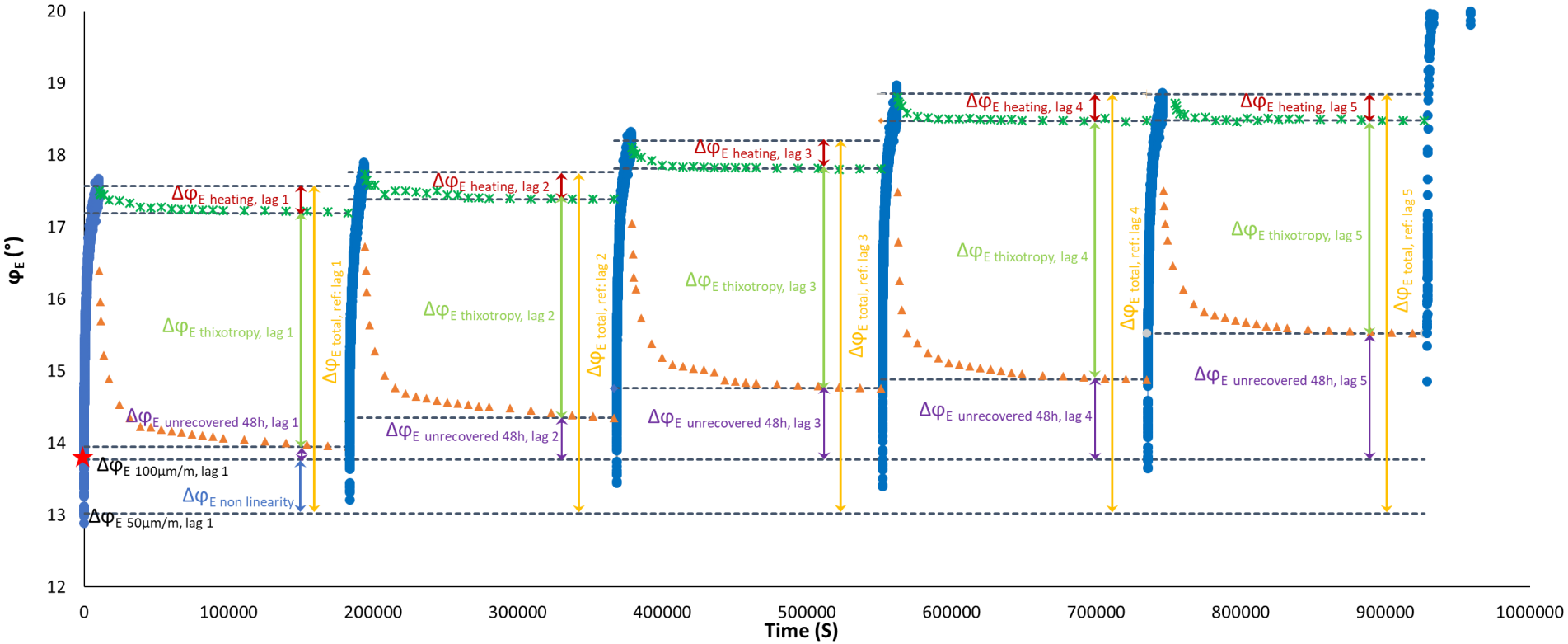

3.1.168. Quantification of different contributions to |E*|, ϕ_E and |v*| evolution during five fatigue lags for mix PMB – 6: the envelope line of the first fatigue lag is used for all fatigue lag

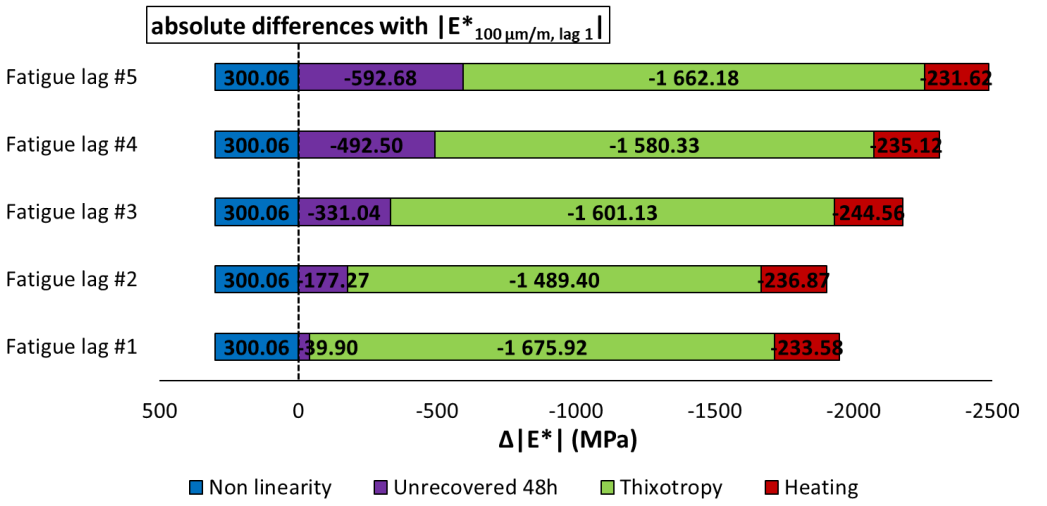
absolute differences with |E*100 µm/m, lag 1|
Fatigue lag #5
Fatigue lag #4
Fatigue lag #3
Fatigue lag #2
Fatigue lag #1
300.06
-592.68
-1 662.18
-231.62
300.06
-492.50
-1 580.33
-235.12
300.06
-331.04
-1 601.13
-244.56
300.06
-177.27
-1 489.40
-236.87
300.06
-39.90
-1 675.92
-233.58
500
0
-500
-1000
-1500
-2000
-2500
Δ|E*| (MPa)
Non linearity
Unrecovered 48h
Thixotropy
Heating

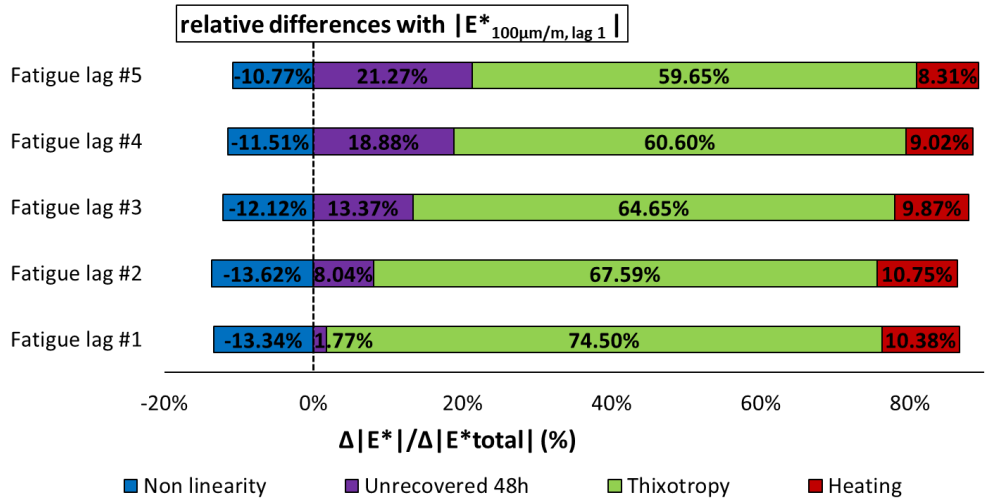
relative differences with |E*100µm/m, lag 1|
Fatigue lag #5
Fatigue lag #4
Fatigue lag #3
Fatigue lag #2
Fatigue lag #1
-10.77%
21.27%
59.65%
8.31%
-11.51%
18.88%
60.60%
9.02%
-12.12%
13.37%
64.65%
9.87%
-13.62%
8.04%
67.59%
10.75%
-13.34%
1.77%
74.50%
10.38%
-20%
0%
20%
40%
60%
80%
Δ|E*|/Δ|E*total| (%)
Non linearity
Unrecovered 48h
Thixotropy
Heating

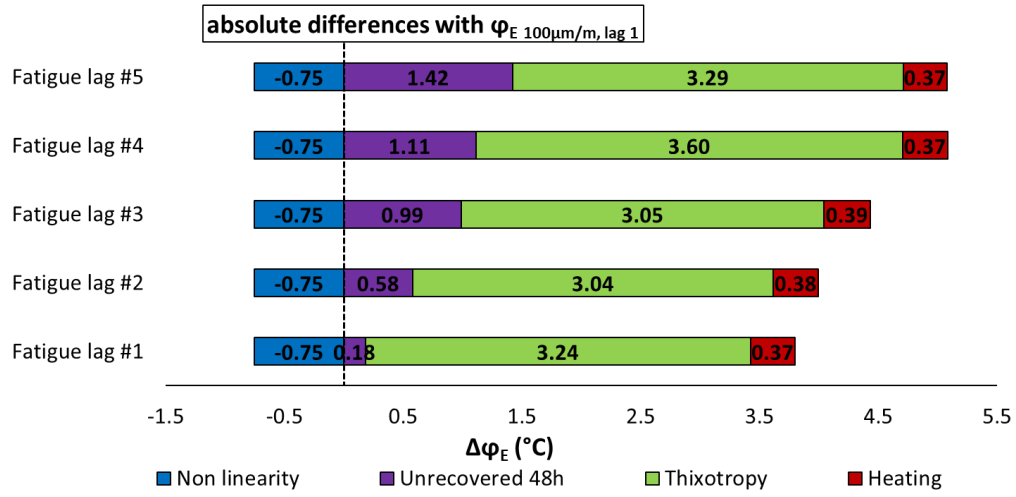
absolute differences with φE 100µm/m, lag 1
Fatigue lag #5
Fatigue lag #4
Fatigue lag #3
Fatigue lag #2
Fatigue lag #1
-0.75
1.42
3.29
0.37
-0.75
1.11
3.60
0.37
-0.75
0.99
3.05
0.39
-0.75
0.58
3.04
0.38
-0.75
0.18
3.24
0.37
-1.5
-0.5
0.5
1.5
2.5
3.5
4.5
5.5
Δφ E (°C)
Non linearity
Unrecovered 48h
Thixotropy
Heating

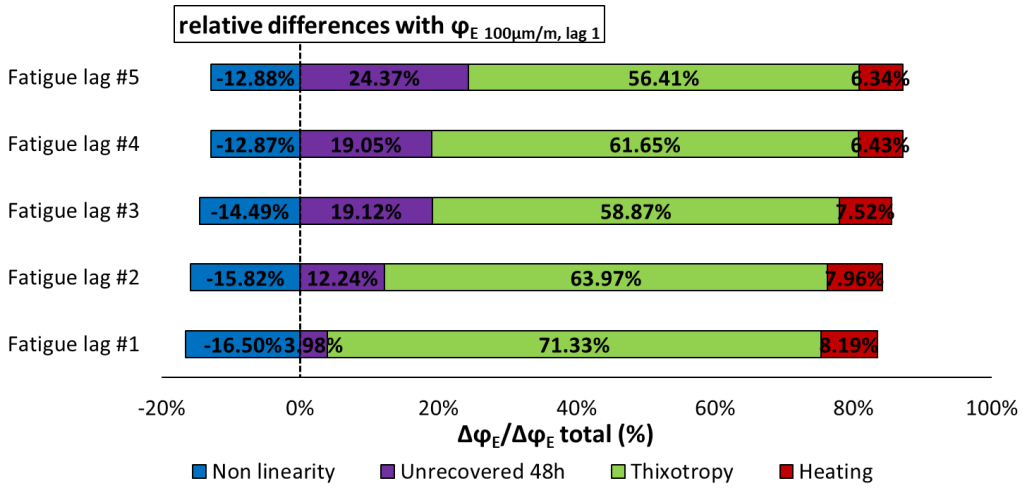
relative differences with $\varphi_{E\ 100\mu m/m,\ lag\ 1}$
Fatigue lag #5
-12.88%
24.37%
56.41%
6.34%
Fatigue lag #4
-12.87%
19.05%
61.65%
6.43%
Fatigue lag #3
-14.49%
19.12%
58.87%
7.52%
Fatigue lag #2
-15.82%
12.24%
63.97%
7.96%
Fatigue lag #1
-16.50%
3.98%
71.33%
8.19%
-20%
0%
20%
40%
60%
80%
100%
$\Delta\varphi_E/\Delta\varphi_E$ total (%)
Non linearity
Unrecovered 48h
Thixotropy
Heating

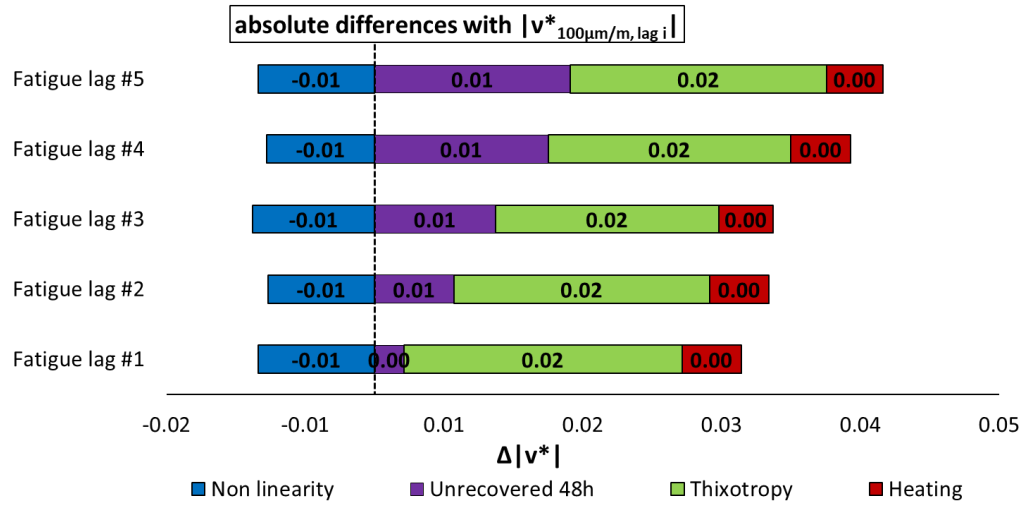
absolute differences with $|v^*_{100\mu m/m,\ lag\ i}|$
Fatigue lag #5
-0.01
0.01
0.02
0.00
Fatigue lag #4
-0.01
0.01
0.02
0.00
Fatigue lag #3
-0.01
0.01
0.02
0.00
Fatigue lag #2
-0.01
0.01
0.02
0.00
Fatigue lag #1
-0.01
0.00
0.02
0.00
-0.02
-0.01
0.01
0.02
0.03
0.04
0.05
$\Delta|v^*|$
Non linearity
Unrecovered 48h
Thixotropy
Heating

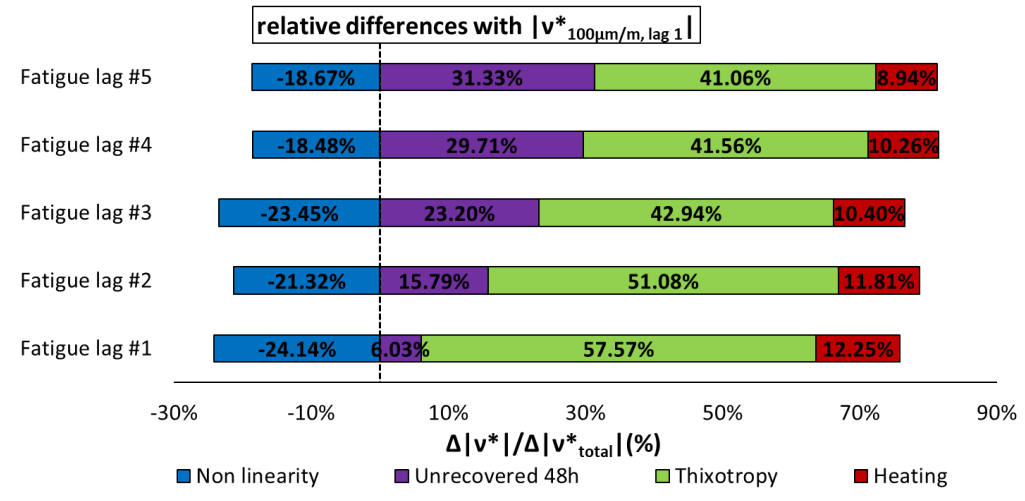
relative differences with $|v^*_{100\mu m/m,\ lag\ 1}|$
Fatigue lag #5
-18.67%
31.33%
41.06%
8.94%
Fatigue lag #4
-18.48%
29.71%
41.56%
10.26%
Fatigue lag #3
-23.45%
23.20%
42.94%
10.40%
Fatigue lag #2
-21.32%
15.79%
51.08%
11.81%
Fatigue lag #1
-24.14%
6.03%
57.57%
12.25%
-30%
-10%
10%
30%
50%
70%
90%
$\Delta|v^*|/\Delta|v^*_{total}|$(%)
Non linearity
Unrecovered 48h
Thixotropy
Heating

3.1.169. Quantification of different absolute and relative contributions to |E*|, φ_E, |v*| and φ_v evolutions for mix PMB – 6, calculated using the envelope line for the first fatigue lag.

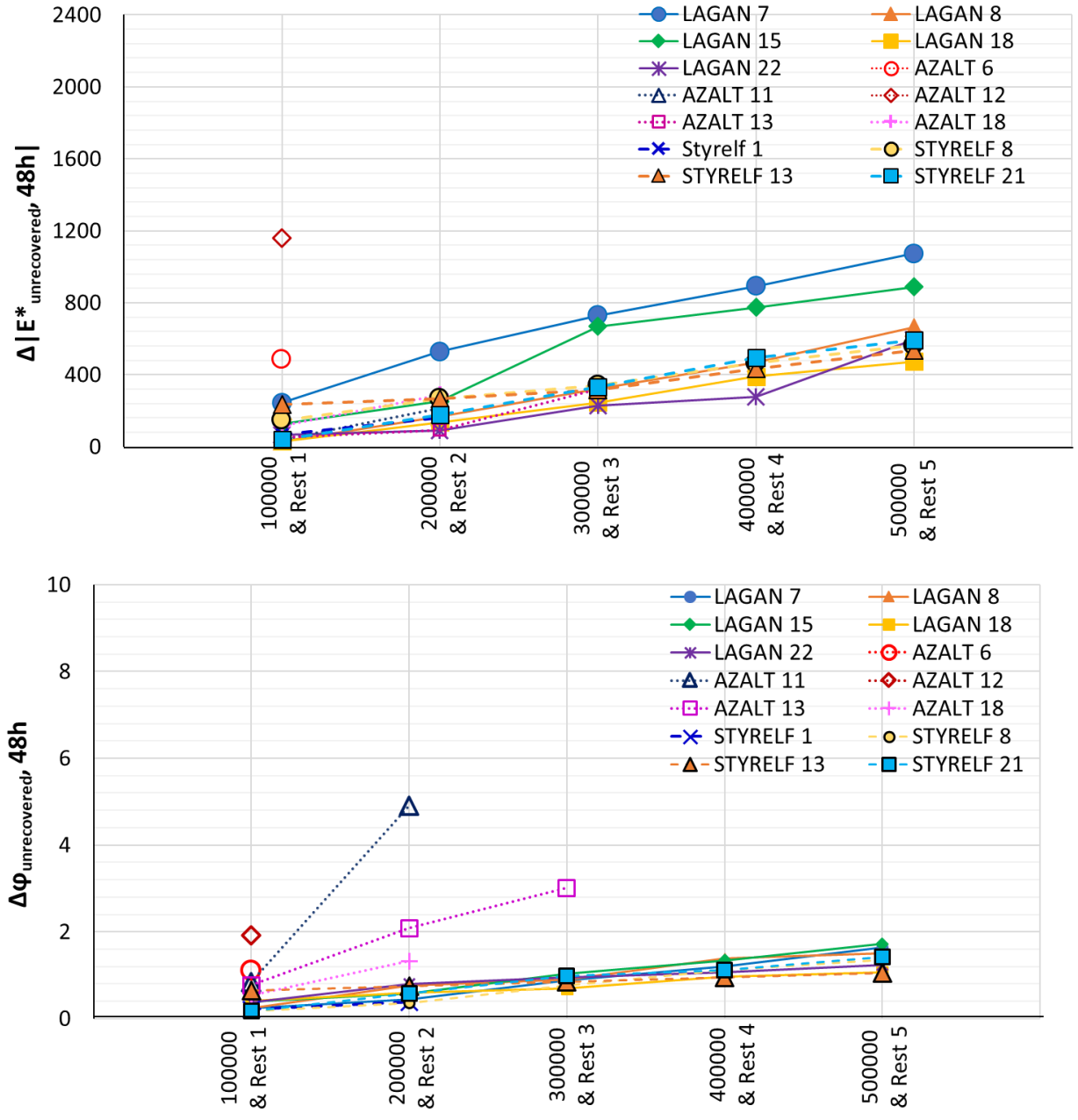

3.2.9. Comparing the relative contributions of unrecovered variations of |E*| and φ_E with respect to the total variation of |E*| and φ_E for each fatigue and rest lag for all the tested samples, calculated using the envelope line for the first fatigue lag

3.4.Analysis of rate of variation of mechanical properties during loading and recovery.

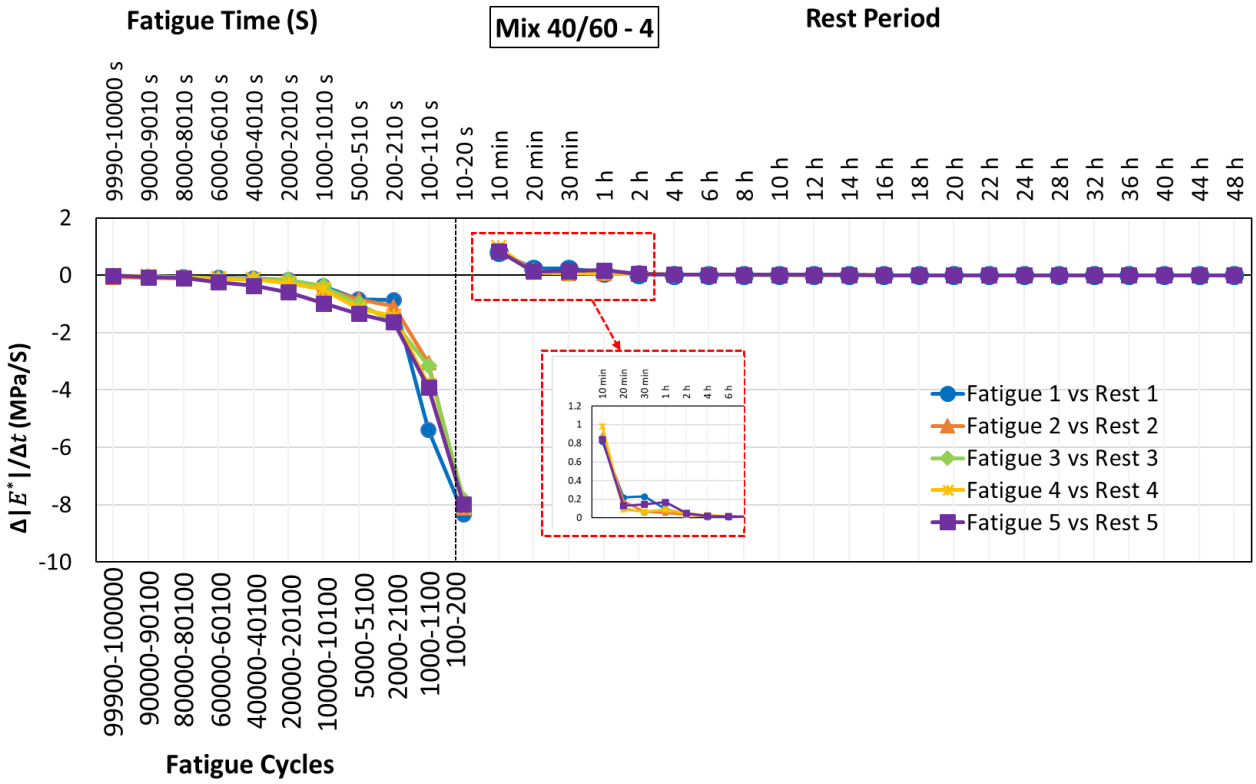

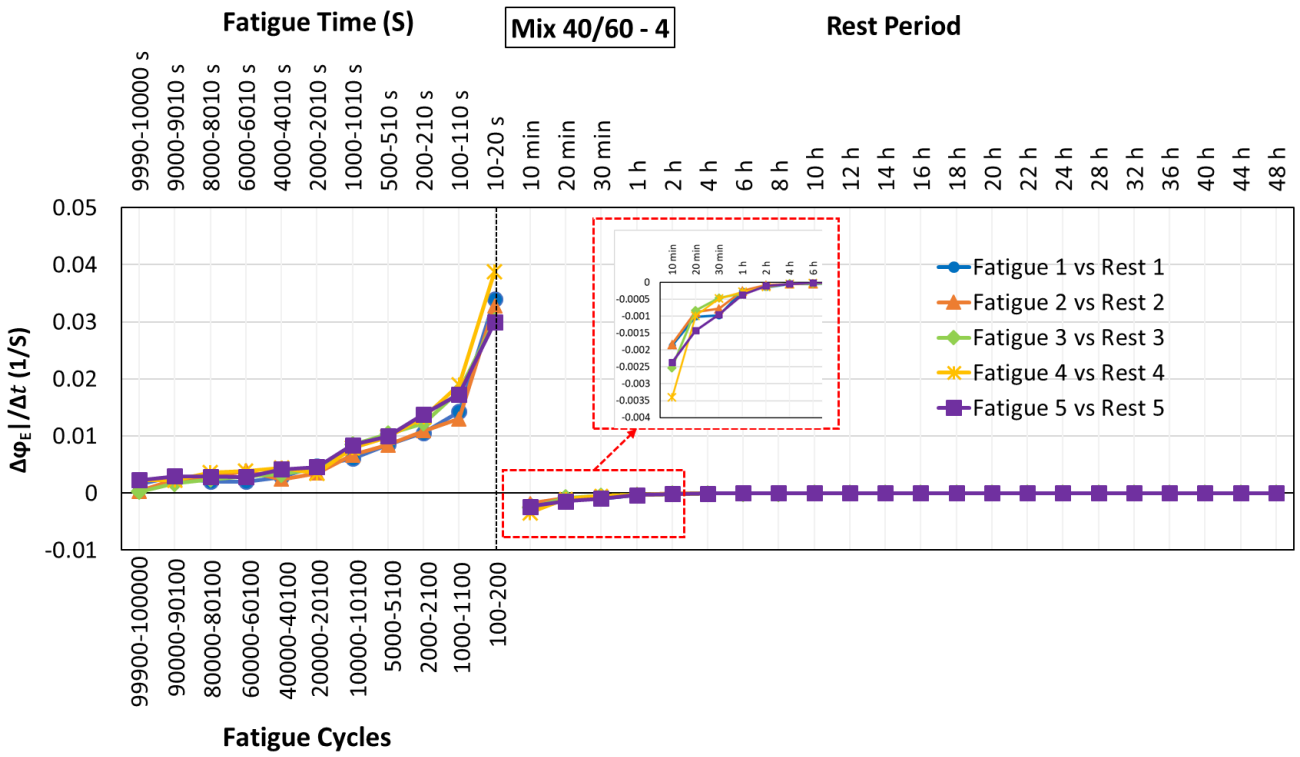
Fatigue Time (S)
Mix 40/60 - 4
Rest Period
9990-10000 s
9000-9010 s
8000-8010 s
6000-6010 s
4000-4010 s
2000-2010 s
1000-1010 s
500-510 s
200-210 s
100-110 s
10-20 s
10 min
20 min
30 min
1 h
2 h
4 h
6 h
8 h
10 h
12 h
14 h
16 h
18 h
20 h
22 h
24 h
28 h
32 h
36 h
40 h
44 h
48 h
0.05
0.04
0.03
0.02
0.01
0
-0.01
Δφ_E|/Δt (1/S)
Fatigue 1 vs Rest 1
Fatigue 2 vs Rest 2
Fatigue 3 vs Rest 3
Fatigue 4 vs Rest 4
Fatigue 5 vs Rest 5
99900-100000
90000-90100
80000-80100
60000-60100
40000-40100
20000-20100
10000-10100
5000-5100
2000-2100
1000-1100
100-200
Fatigue Cycles

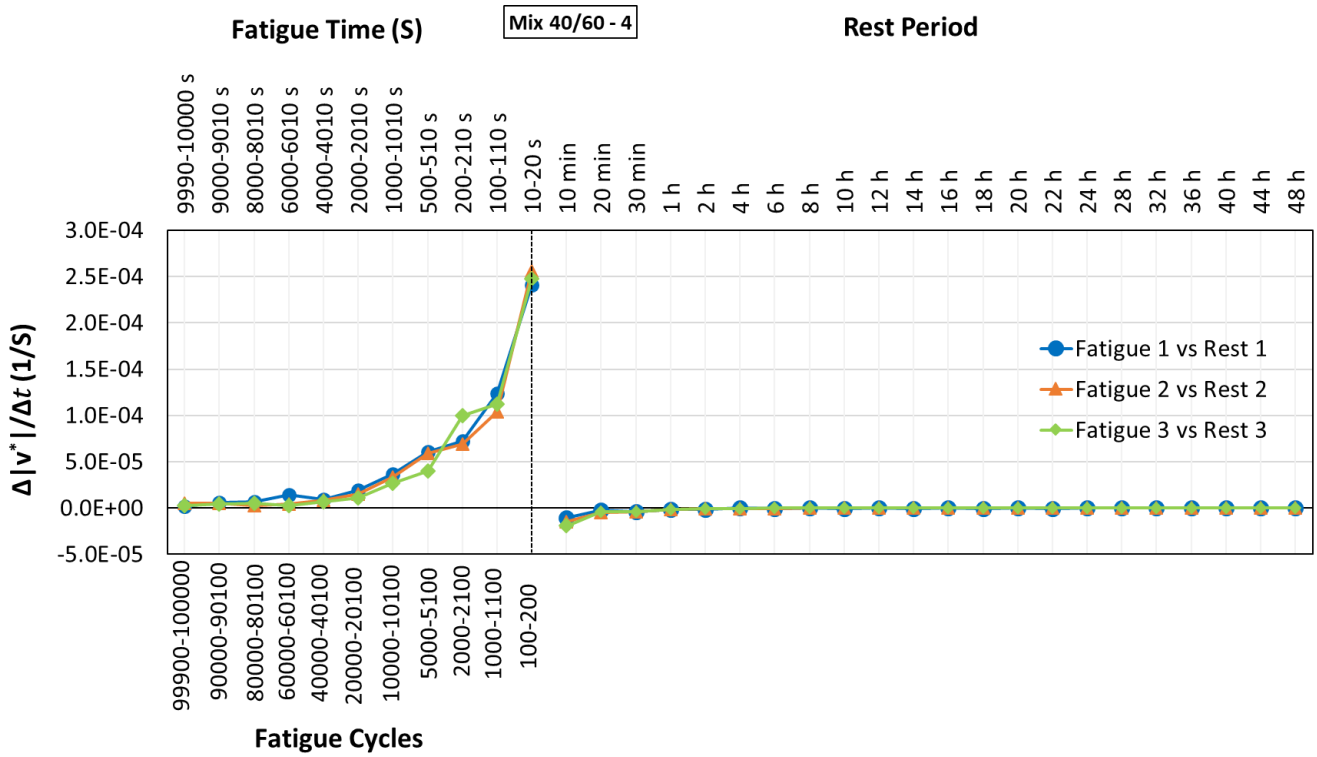
Fatigue Time (S)
Mix 40/60 - 4
Rest Period
9990-10000 s
9000-9010 s
8000-8010 s
6000-6010 s
4000-4010 s
2000-2010 s
1000-1010 s
500-510 s
200-210 s
100-110 s
10-20 s
10 min
20 min
30 min
1 h
2 h
4 h
6 h
8 h
10 h
12 h
14 h
16 h
18 h
20 h
22 h
24 h
28 h
32 h
36 h
40 h
44 h
48 h
3.0E-04
2.5E-04
2.0E-04
1.5E-04
1.0E-04
5.0E-05
0.0E+00
-5.0E-05
Δ|v*|/Δt (1/S)
Fatigue 1 vs Rest 1
Fatigue 2 vs Rest 2
Fatigue 3 vs Rest 3
99900-100000
90000-90100
80000-80100
60000-60100
40000-40100
20000-20100
10000-10100
5000-5100
2000-2100
1000-1100
100-200
Fatigue Cycles

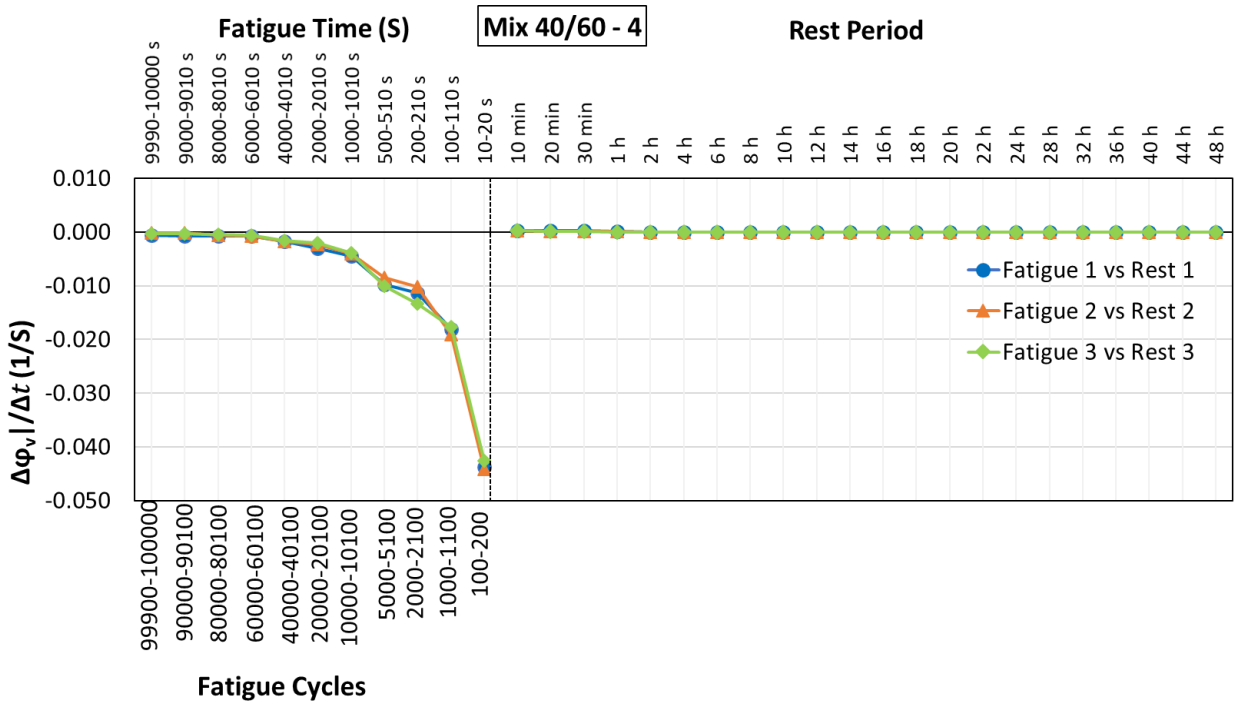

3.3.1. Rate of variation during loading and recovery for for |E*|, φ_E, |v*| and φ_v for each fatigue and rest lag for mix 40/60 - 4.

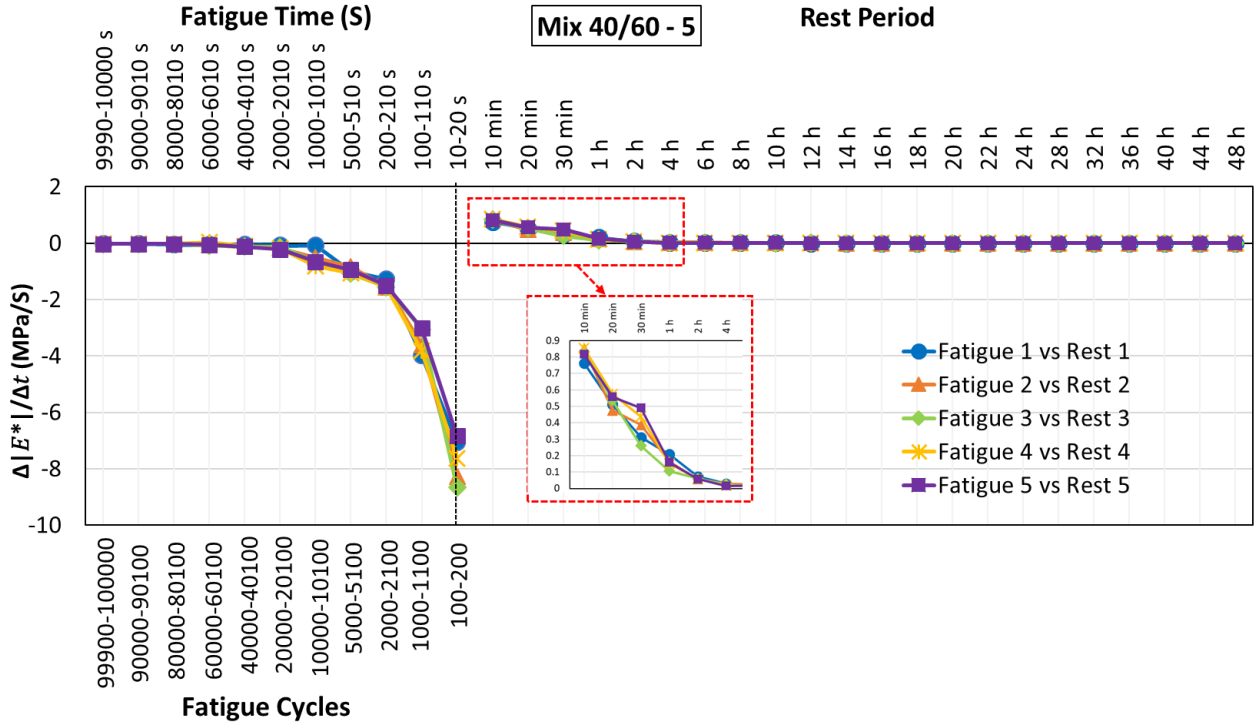

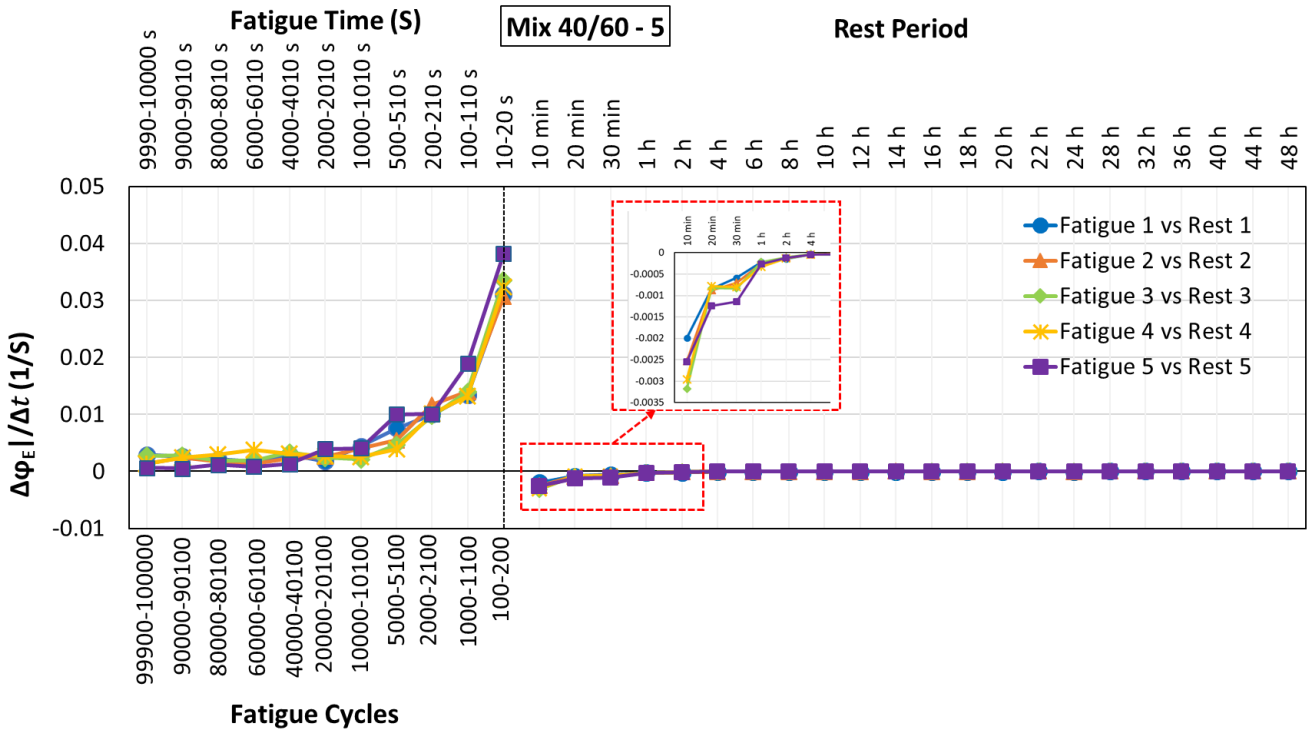

3.3.2. Rate of variation during loading and recovery for |E*| and φ_E for each fatigue and rest lag for mix 40/60 - 5

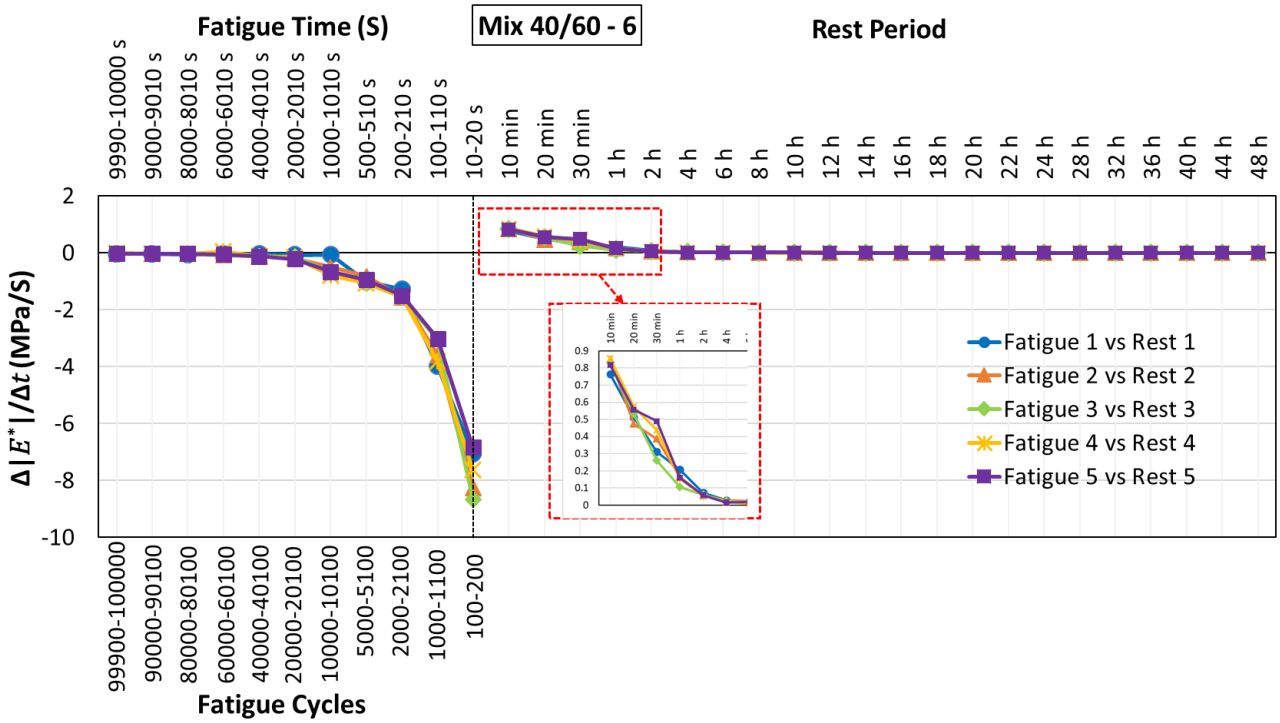

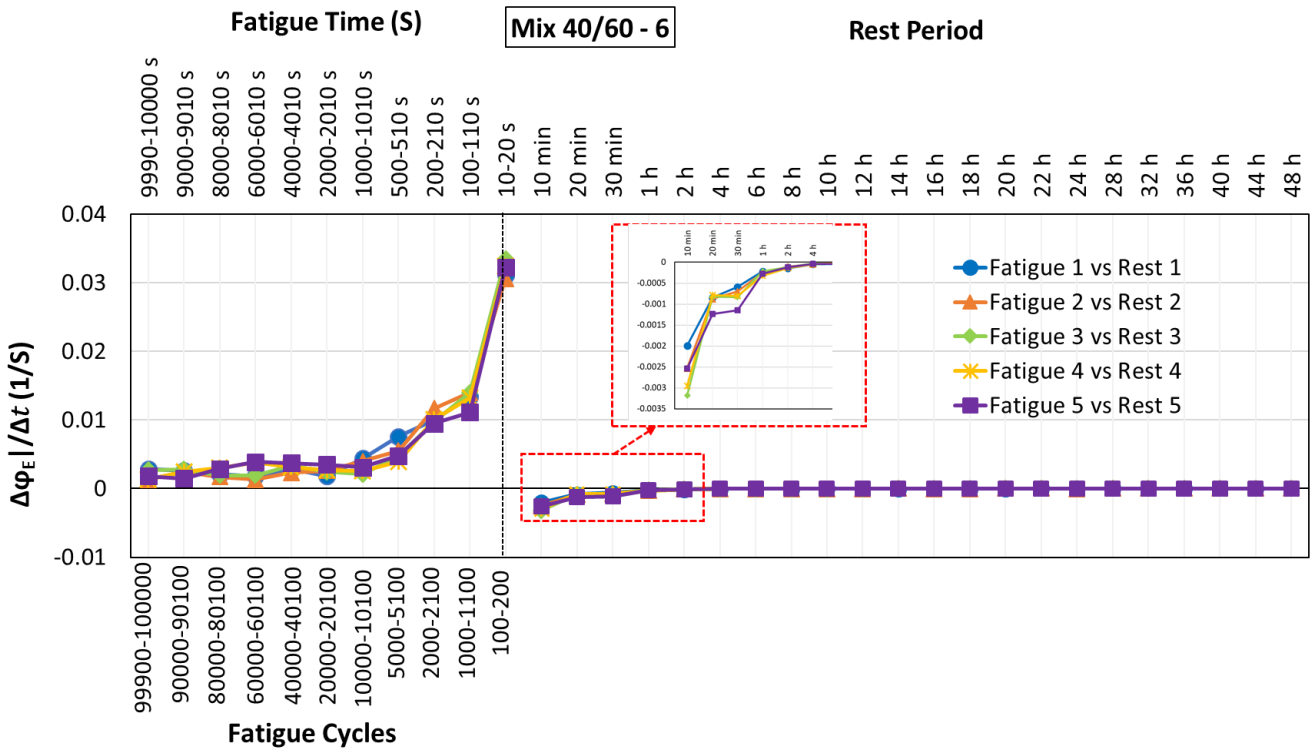
Fatigue Time (S)
Mix 40/60 - 6
Rest Period
9990-10000 s
9000-9010 s
8000-8010 s
6000-6010 s
4000-4010 s
2000-2010 s
1000-1010 s
500-510 s
200-210 s
100-110 s
10-20 s
10 min
20 min
30 min
1 h
2 h
4 h
6 h
8 h
10 h
12 h
14 h
16 h
18 h
20 h
22 h
24 h
28 h
32 h
36 h
40 h
44 h
48 h
0.04
0.03
0.02
0.01
0
-0.01
Δφε|/Δt (1/S)
Fatigue 1 vs Rest 1
Fatigue 2 vs Rest 2
Fatigue 3 vs Rest 3
Fatigue 4 vs Rest 4
Fatigue 5 vs Rest 5
99900-100000
90000-90100
80000-80100
60000-60100
40000-40100
20000-20100
10000-10100
5000-5100
2000-2100
1000-1100
100-200
Fatigue Cycles

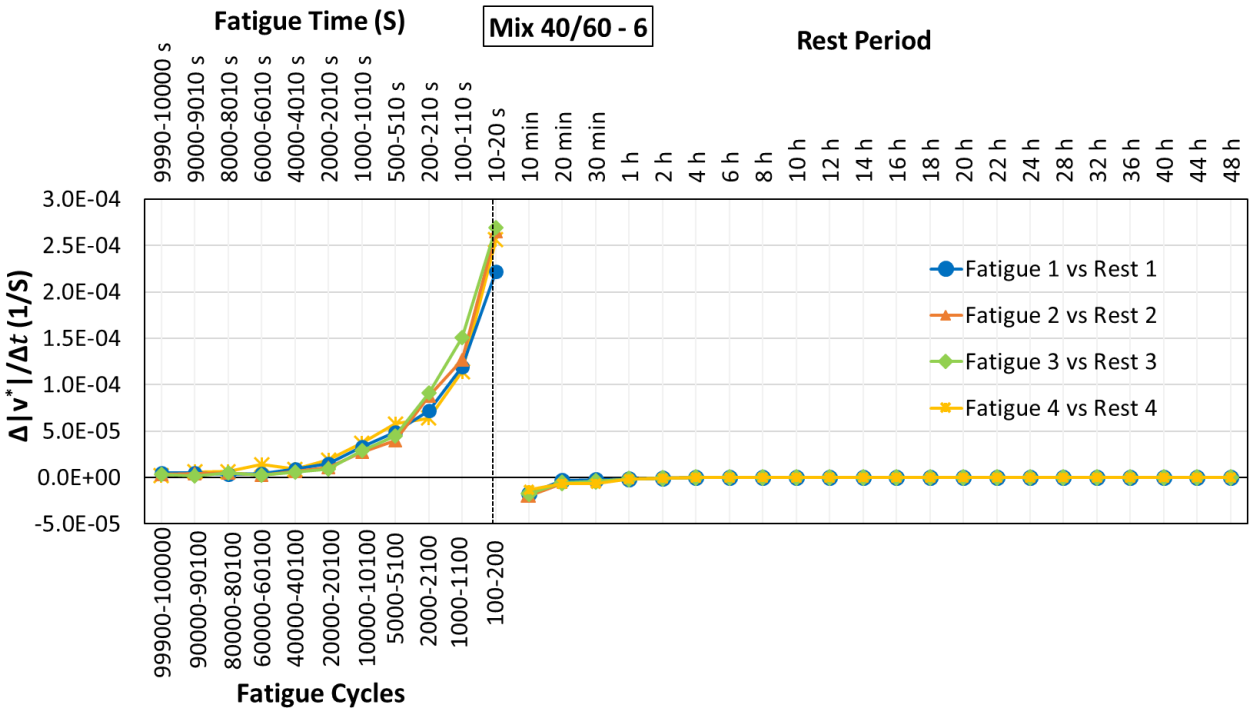
Fatigue Time (S)
Mix 40/60 - 6
Rest Period
9990-10000 s
9000-9010 s
8000-8010 s
6000-6010 s
4000-4010 s
2000-2010 s
1000-1010 s
500-510 s
200-210 s
100-110 s
10-20 s
10 min
20 min
30 min
1 h
2 h
4 h
6 h
8 h
10 h
12 h
14 h
16 h
18 h
20 h
22 h
24 h
28 h
32 h
36 h
40 h
44 h
48 h
3.0E-04
2.5E-04
2.0E-04
1.5E-04
1.0E-04
5.0E-05
0.0E+00
-5.0E-05
Δ|v*|/Δt (1/S)
Fatigue 1 vs Rest 1
Fatigue 2 vs Rest 2
Fatigue 3 vs Rest 3
Fatigue 4 vs Rest 4
99900-100000
90000-90100
80000-80100
60000-60100
40000-40100
20000-20100
10000-10100
5000-5100
2000-2100
1000-1100
100-200
Fatigue Cycles

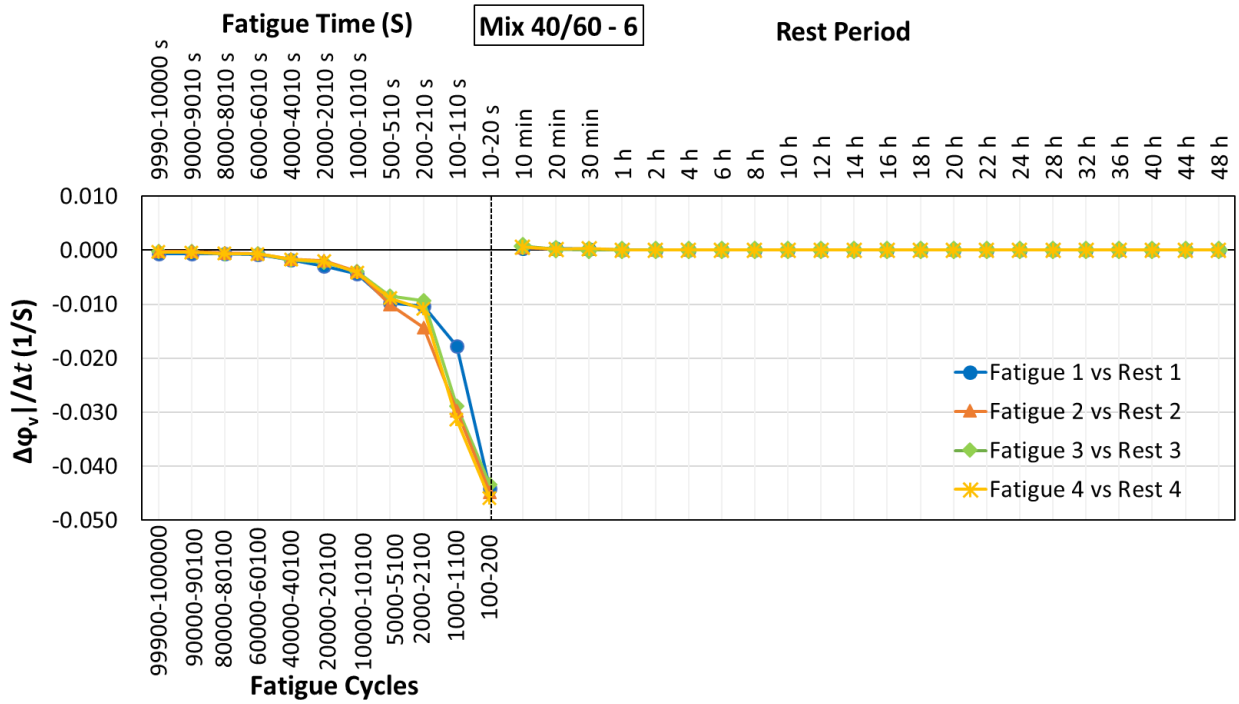

3.3.3. Rate of variation during loading and recovery for |E*|, φ_E, |v*| and φ_v for each fatigue and rest lag for mix 40/60 - 6.

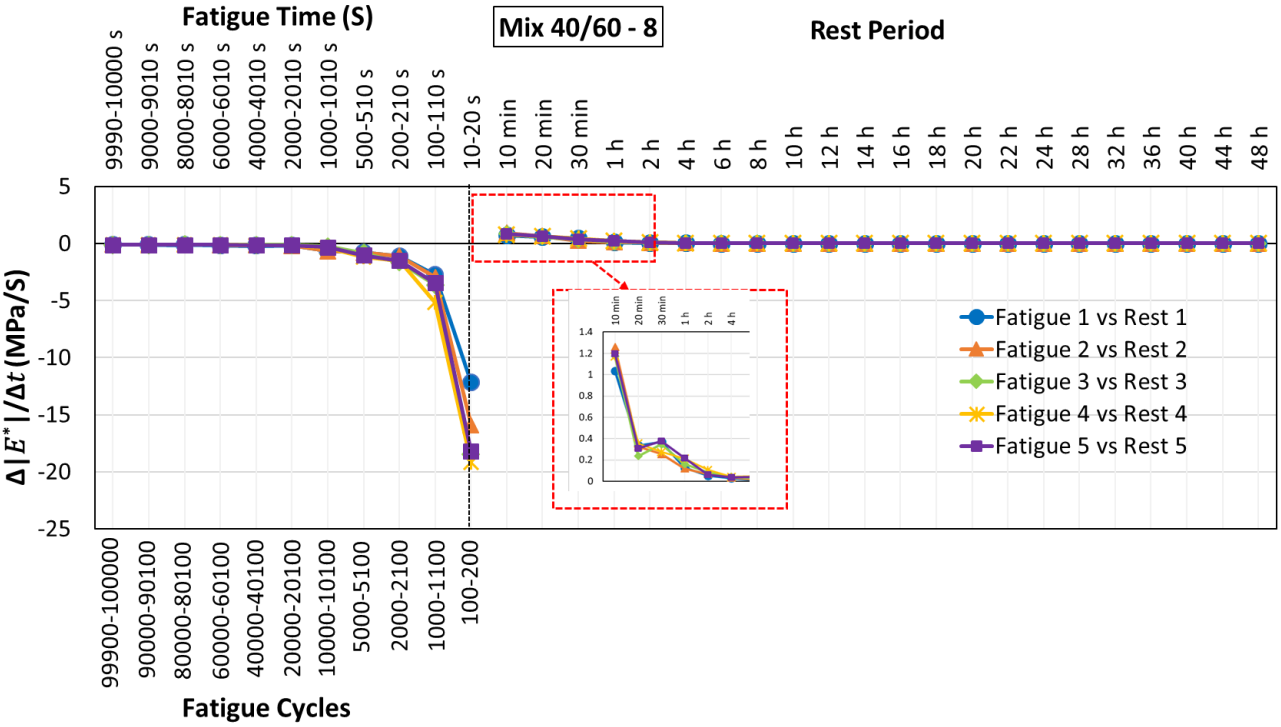

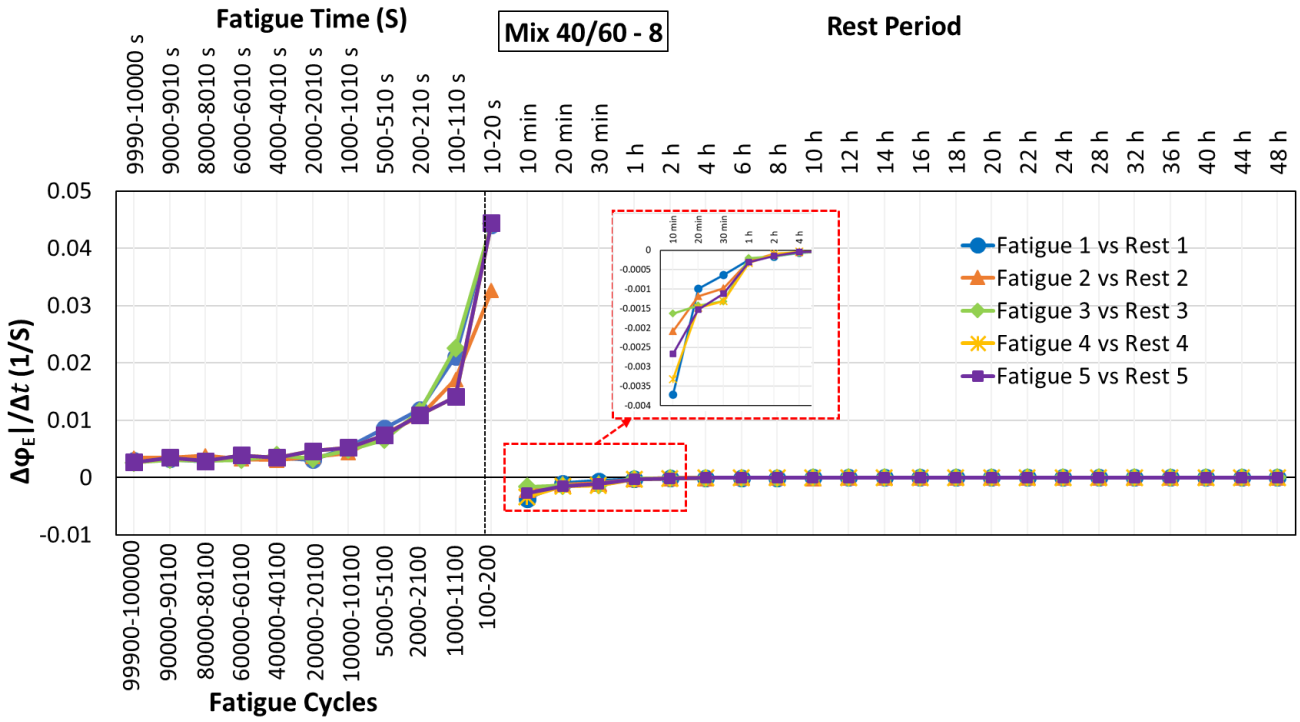
Fatigue Time (S)
Mix 40/60 - 8
Rest Period
9990-10000 s
9000-9010 s
8000-8010 s
6000-6010 s
4000-4010 s
2000-2010 s
1000-1010 s
500-510 s
200-210 s
100-110 s
10-20 s
10 min
20 min
30 min
1 h
2 h
4 h
6 h
8 h
10 h
12 h
14 h
16 h
18 h
20 h
22 h
24 h
28 h
32 h
36 h
40 h
44 h
48 h
0.05
0.04
0.03
0.02
0.01
0
-0.01
Δφ_E|/Δt (1/S)
Fatigue 1 vs Rest 1
Fatigue 2 vs Rest 2
Fatigue 3 vs Rest 3
Fatigue 4 vs Rest 4
Fatigue 5 vs Rest 5
99900-100000
90000-90100
80000-80100
60000-60100
40000-40100
20000-20100
10000-10100
5000-5100
2000-2100
1000-1100
100-200
Fatigue Cycles

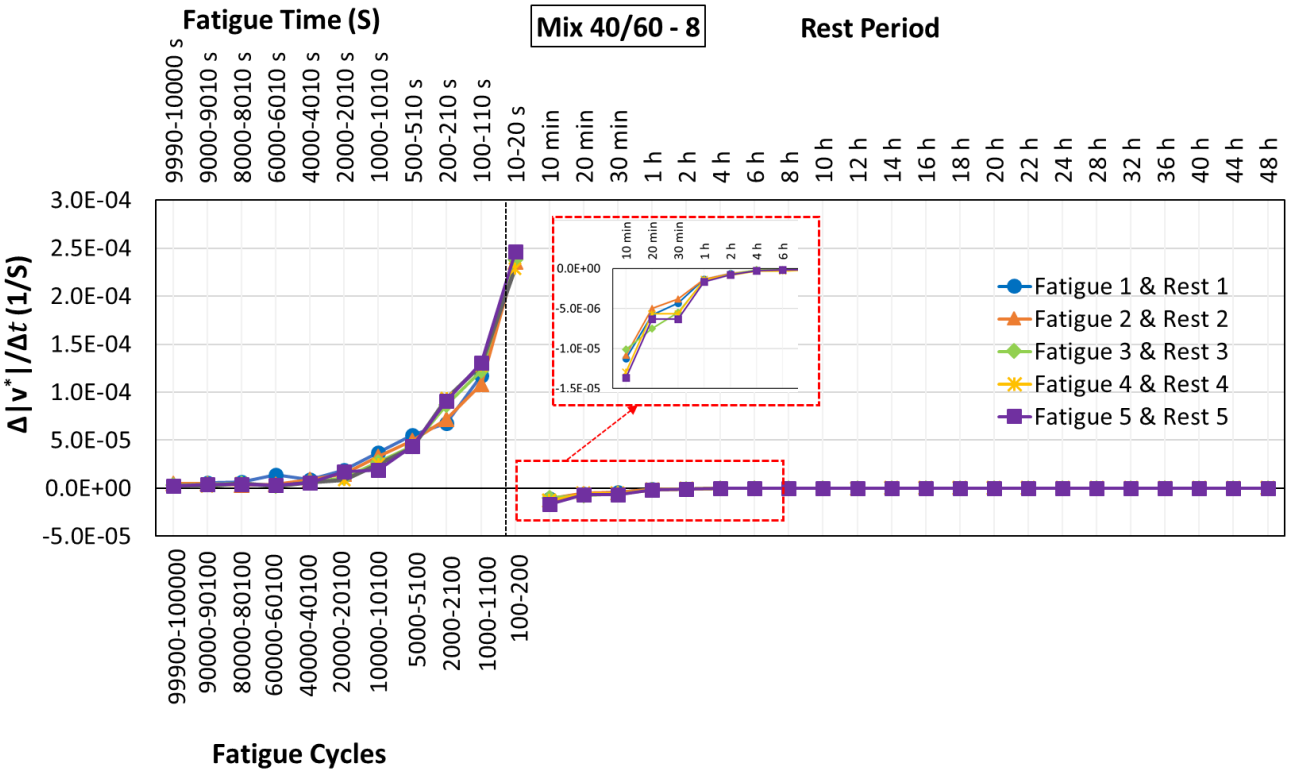
Fatigue Time (S)
Mix 40/60 - 8
Rest Period
9990-10000 s
9000-9010 s
8000-8010 s
6000-6010 s
4000-4010 s
2000-2010 s
1000-1010 s
500-510 s
200-210 s
100-110 s
10-20 s
10 min
20 min
30 min
1 h
2 h
4 h
6 h
8 h
10 h
12 h
14 h
16 h
18 h
20 h
22 h
24 h
28 h
32 h
36 h
40 h
44 h
48 h
3.0E-04
2.5E-04
2.0E-04
1.5E-04
1.0E-04
5.0E-05
0.0E+00
-5.0E-05
Δ|v*|/Δt (1/S)
Fatigue 1 & Rest 1
Fatigue 2 & Rest 2
Fatigue 3 & Rest 3
Fatigue 4 & Rest 4
Fatigue 5 & Rest 5
99900-100000
90000-90100
80000-80100
60000-60100
40000-40100
20000-20100
10000-10100
5000-5100
2000-2100
1000-1100
100-200
Fatigue Cycles

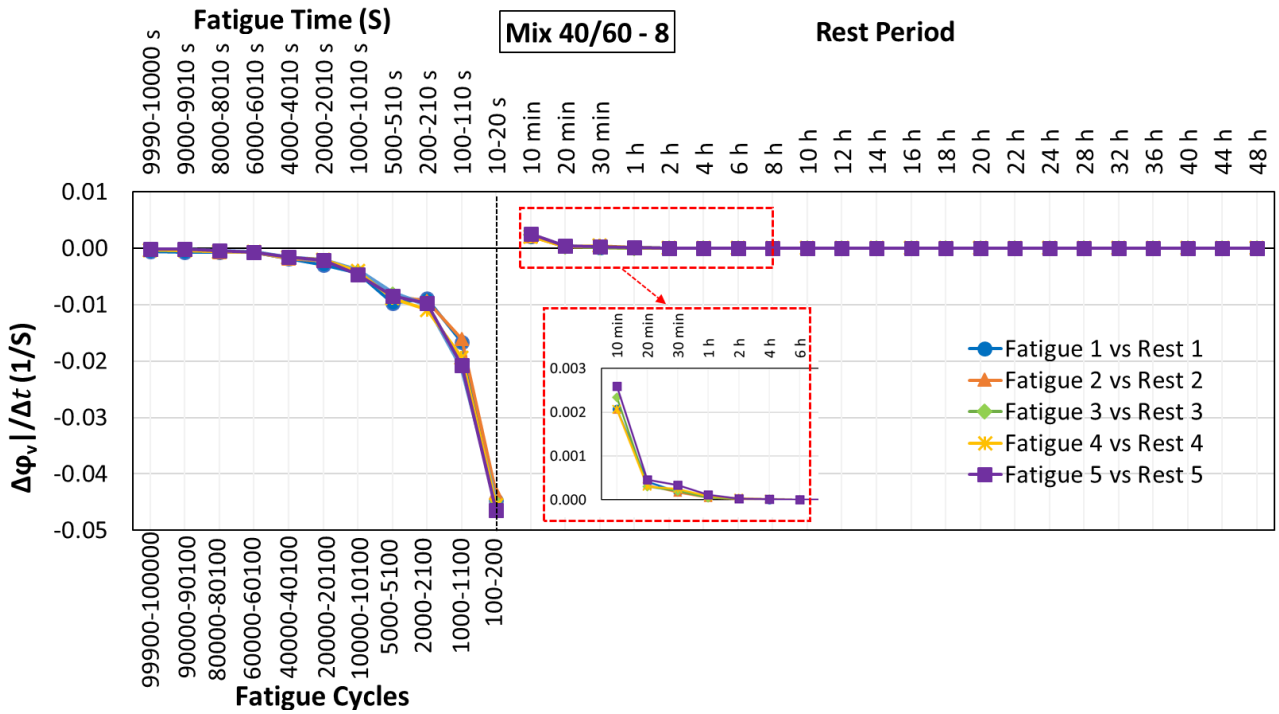

3.3.4. Rate of variation during loading and recovery for |E*|, φ_E, |ν*| and φ_v for each fatigue and rest lag for mix 40/60 - 8.

02

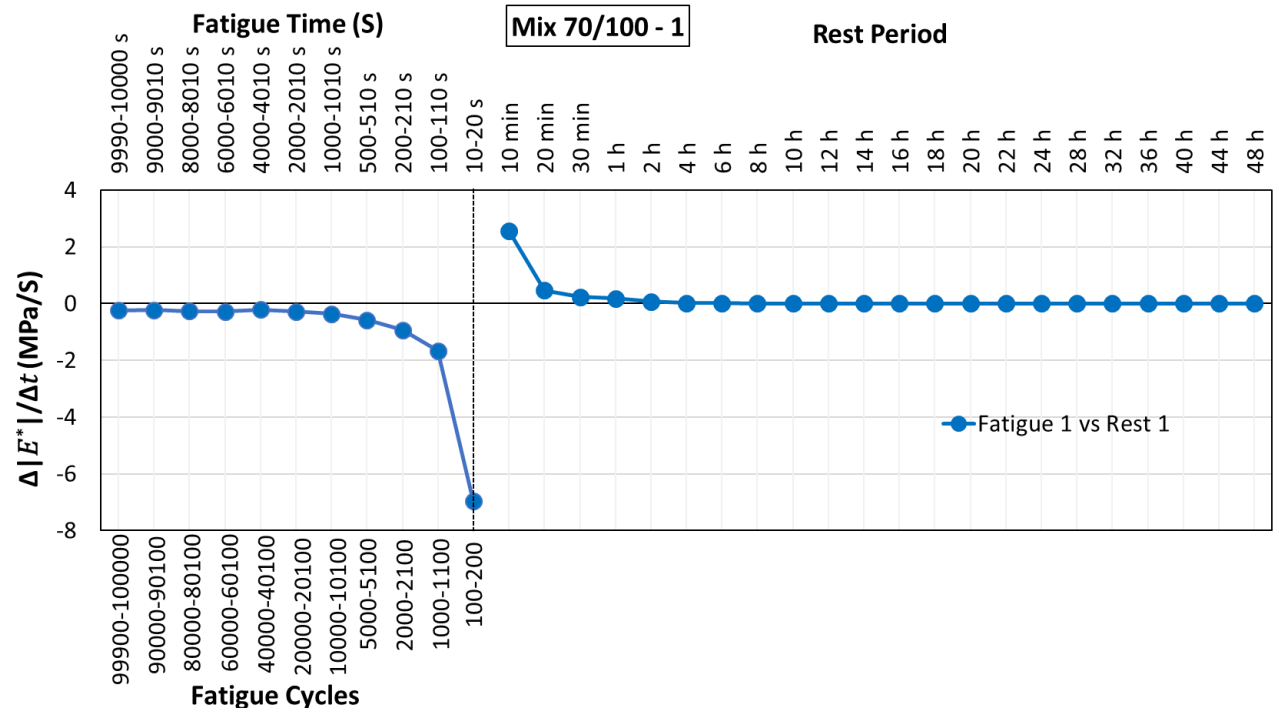

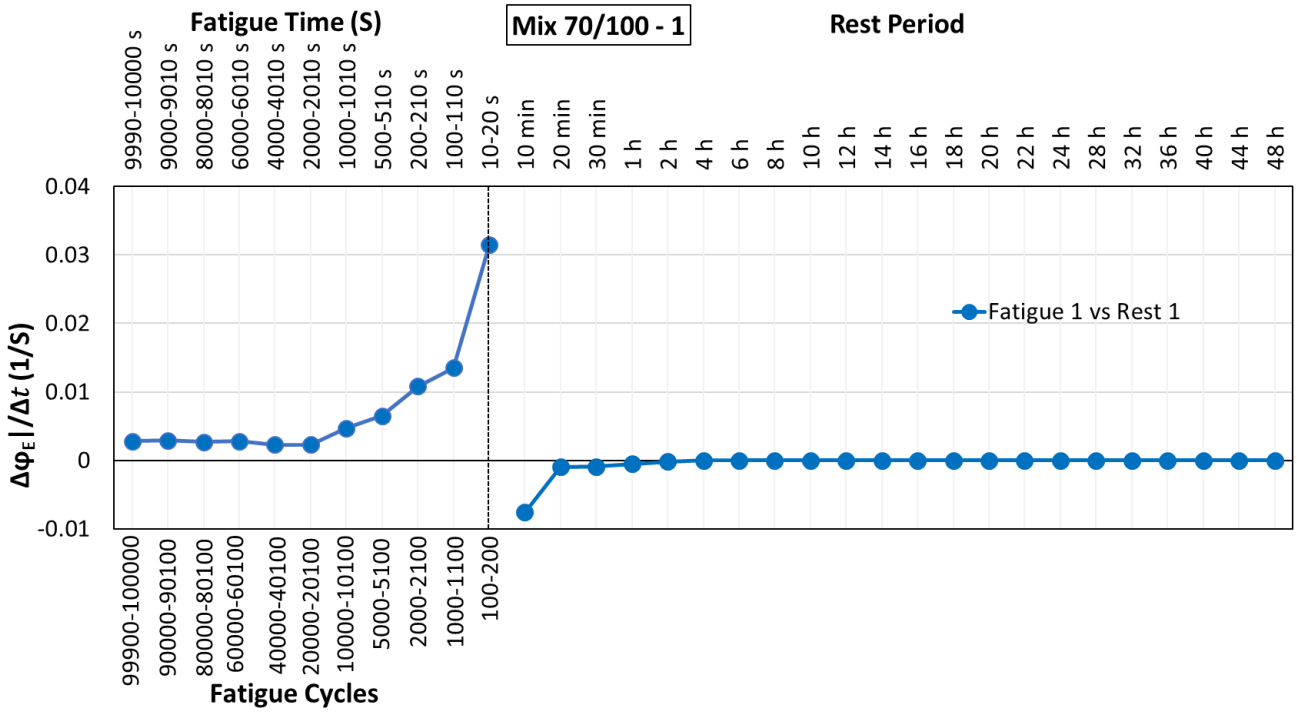

3.3.5. Rate of variation during loading and recovery for |E*| and φ_E for each fatigue and rest lag for mix 70/100 - 1.

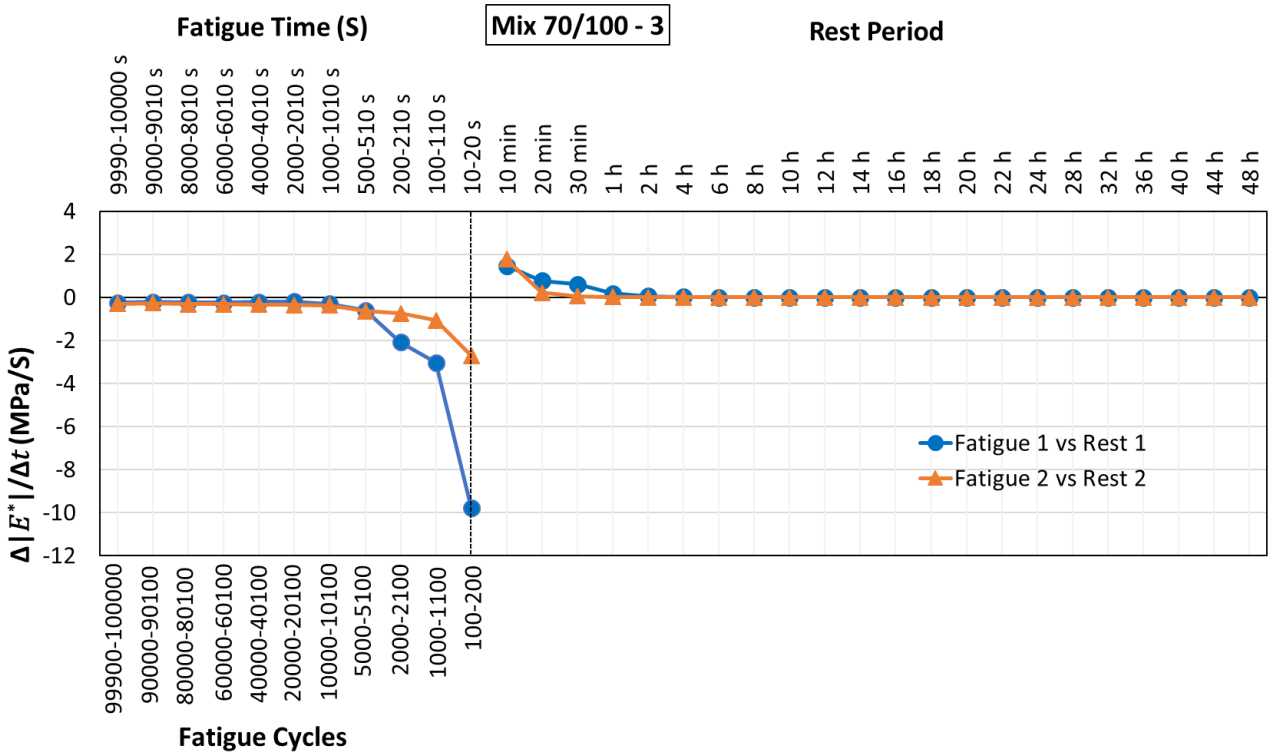

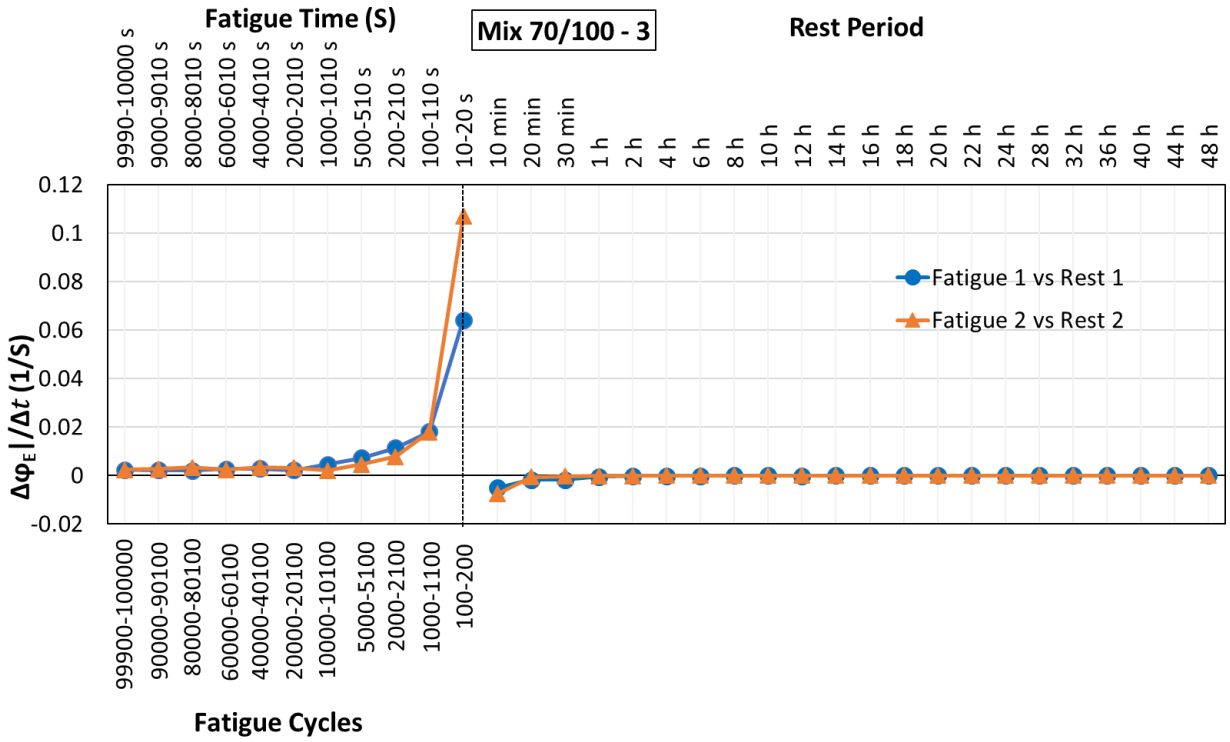

3.3.6. Rate of variation during loading and recovery for |E*| and φ_E for each fatigue and rest lag for mix 70/100 - 3.

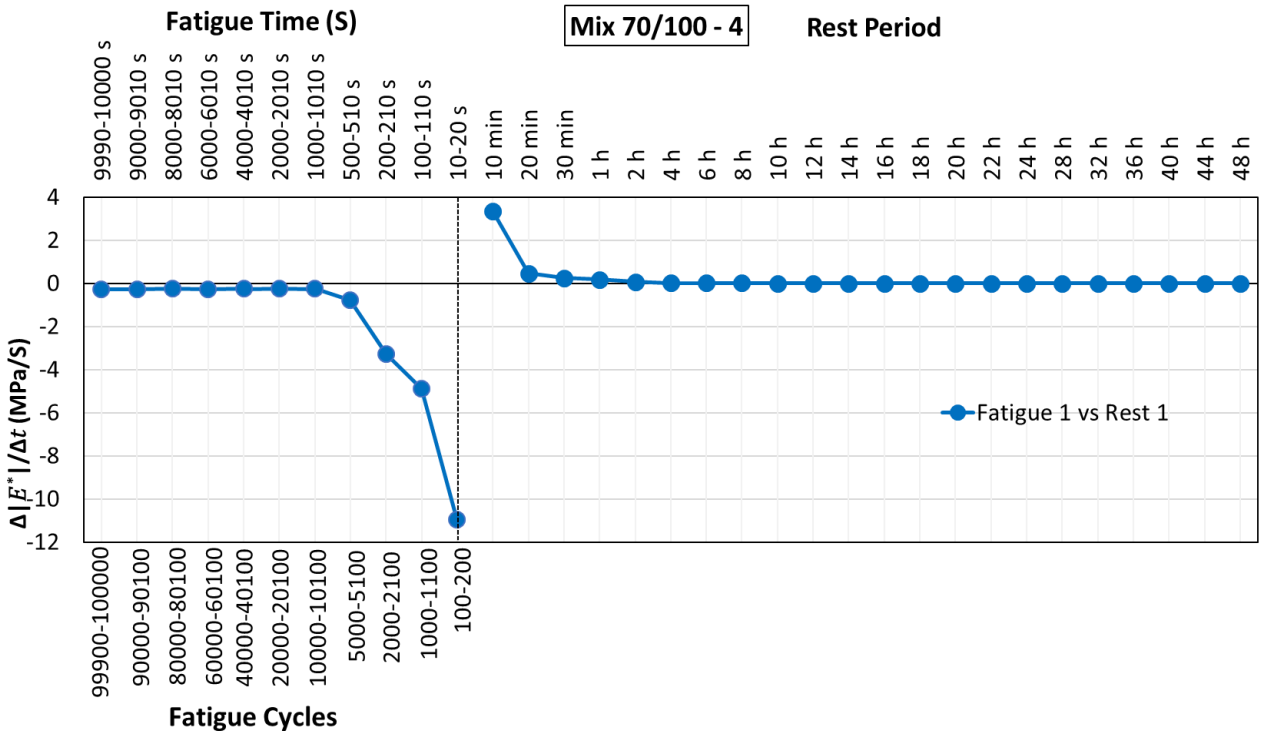

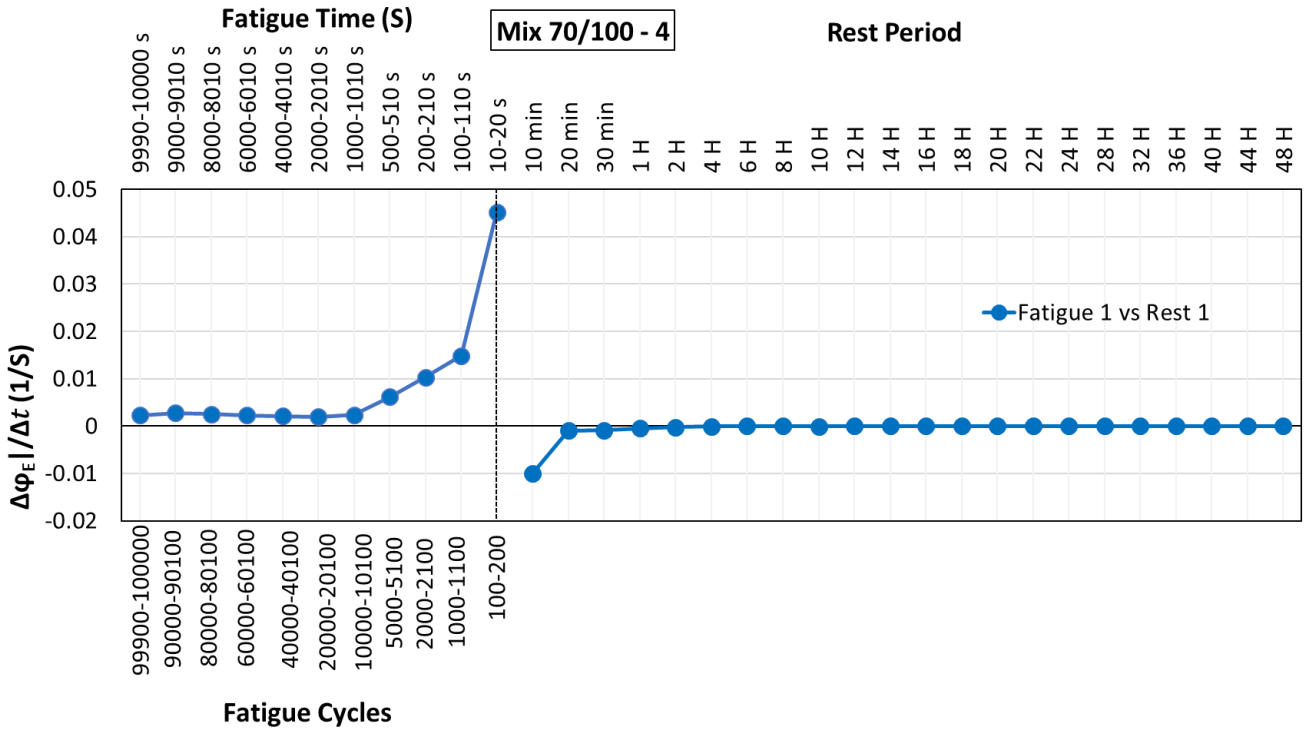

3.3.7. Rate of variation during loading and recovery for |E*| and φ_E for each fatigue and rest lag for mix 70/100 - 4.

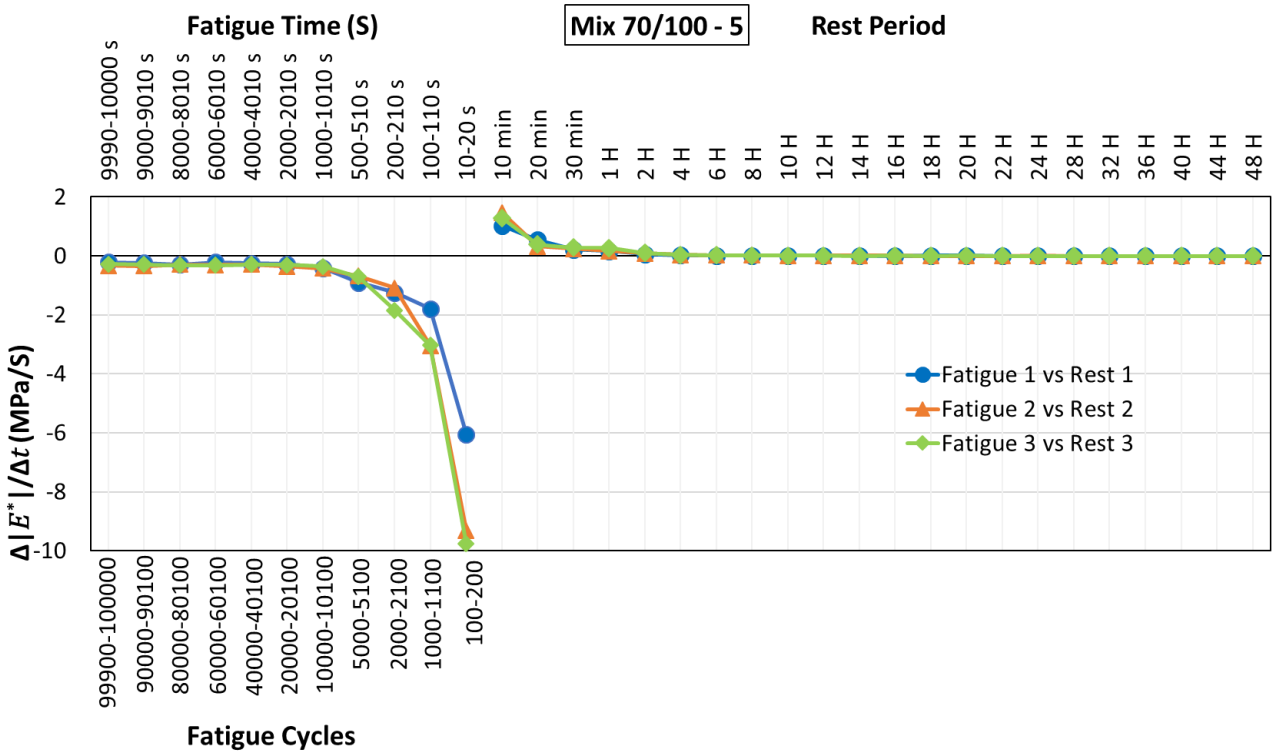

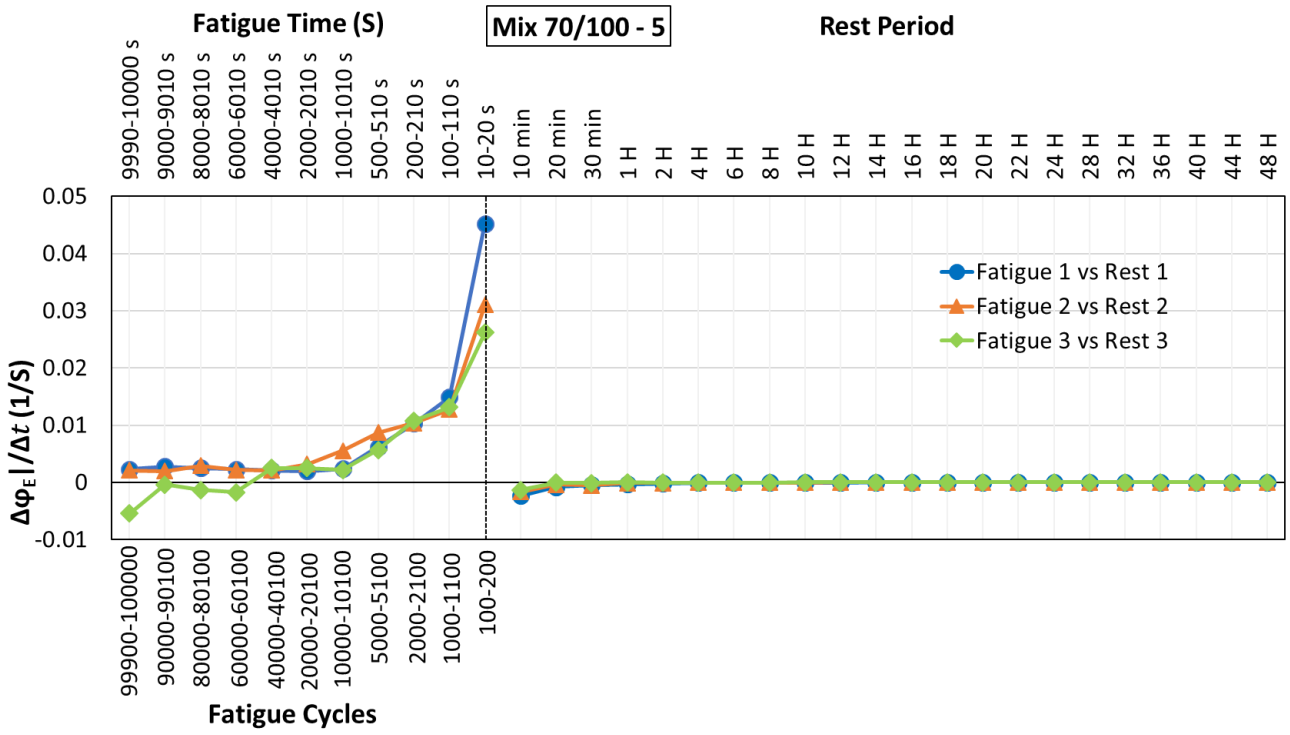

3.3.8. Rate of variation during loading and recovery for |E*| and φ_E for each fatigue and rest lag for mix 70/100 - 5.

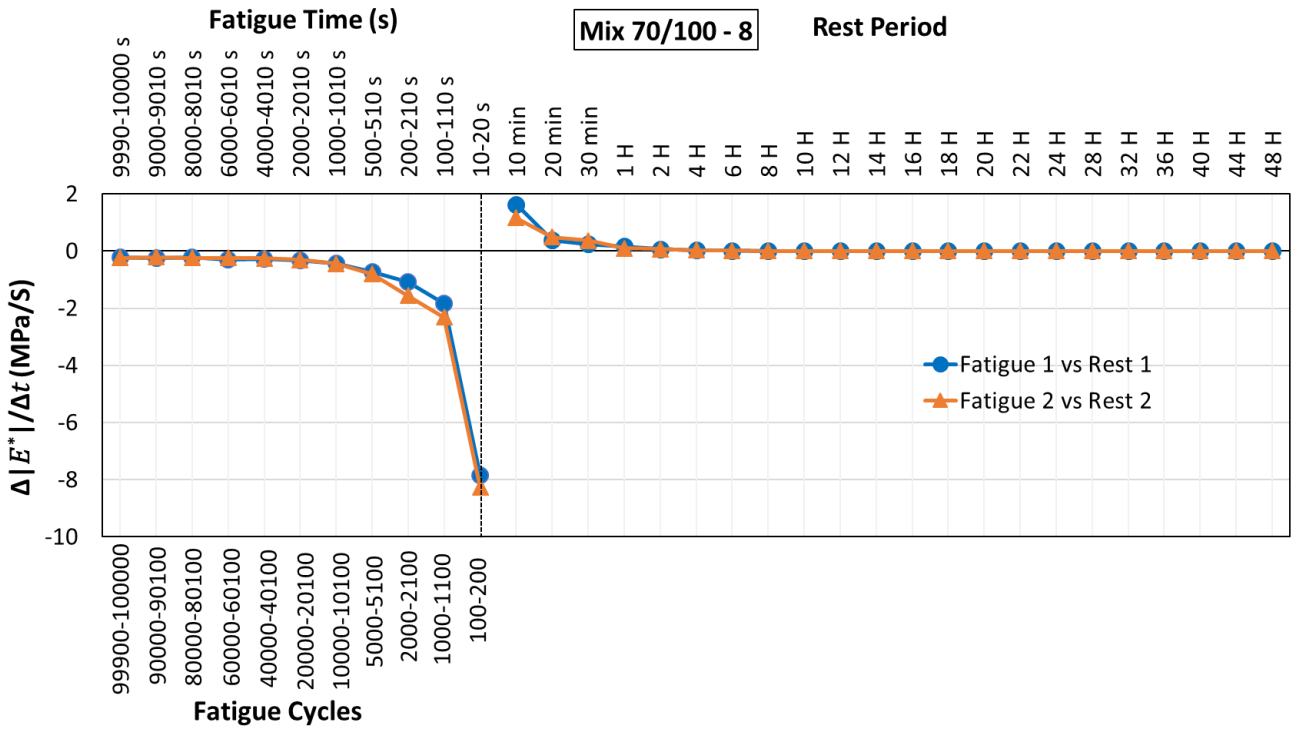

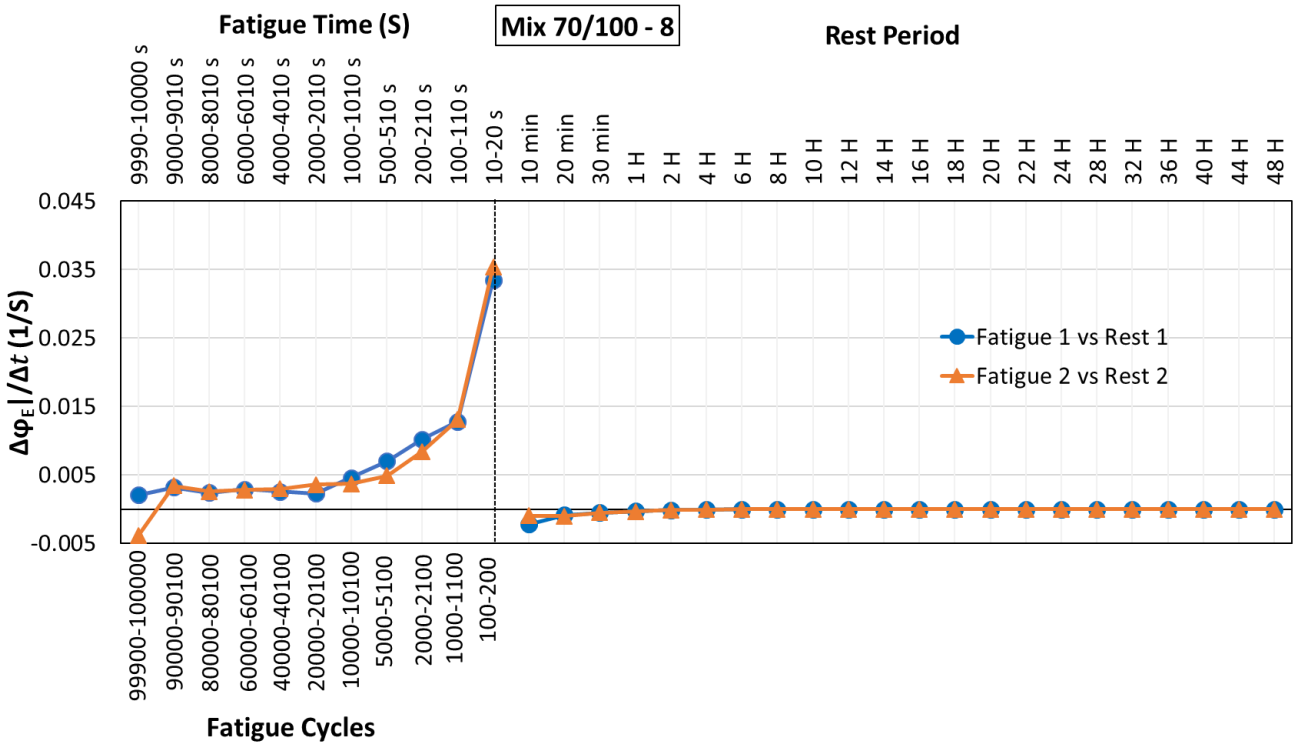

3.3.9. Rate of variation during loading and recovery for |E*| and φ_E for each fatigue and rest lag for mix 70/100 – 8.

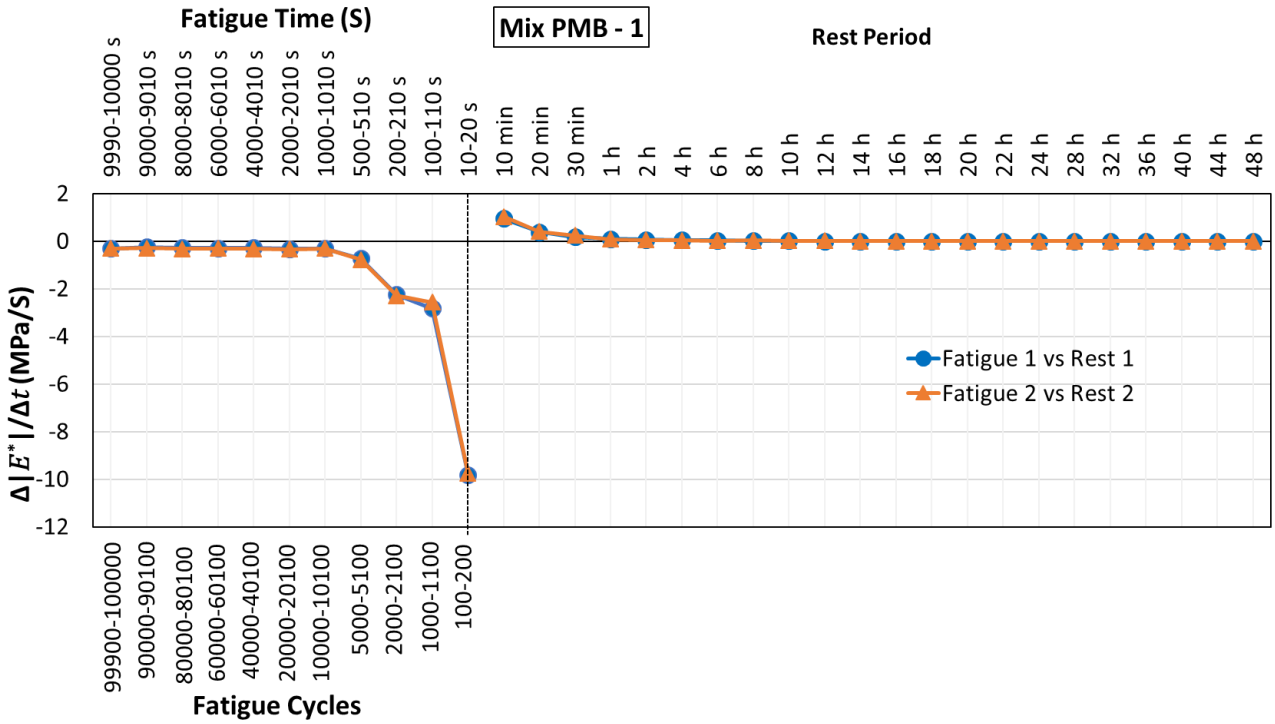

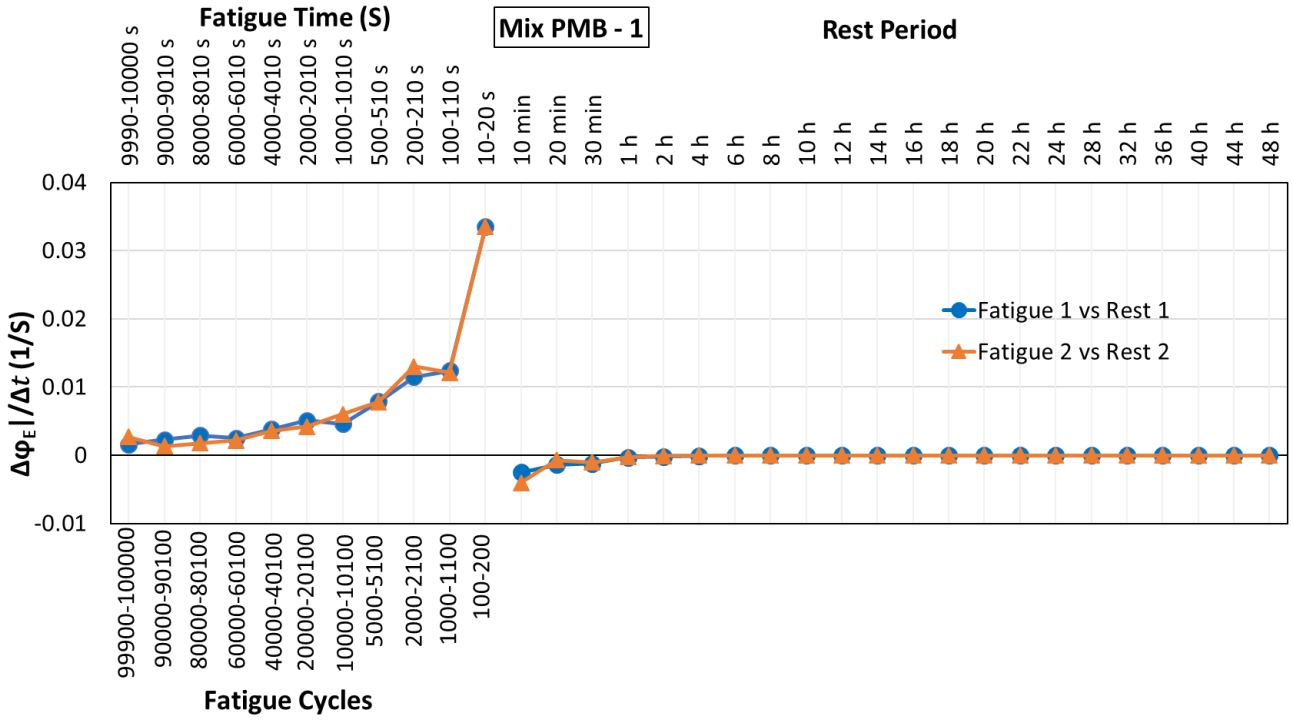
Fatigue Time (S)
Mix PMB - 1
Rest Period
9990-10000 s
9000-9010 s
8000-8010 s
6000-6010 s
4000-4010 s
2000-2010 s
1000-1010 s
500-510 s
200-210 s
100-110 s
10-20 s
10 min
20 min
30 min
1 h
2 h
4 h
6 h
8 h
10 h
12 h
14 h
16 h
18 h
20 h
22 h
24 h
28 h
32 h
36 h
40 h
44 h
48 h
0.04
0.03
0.02
0.01
0
-0.01
Δφ_E|/Δt (1/S)
Fatigue 1 vs Rest 1
Fatigue 2 vs Rest 2
99900-100000
90000-90100
80000-80100
60000-60100
40000-40100
20000-20100
10000-10100
5000-5100
2000-2100
1000-1100
100-200
Fatigue Cycles

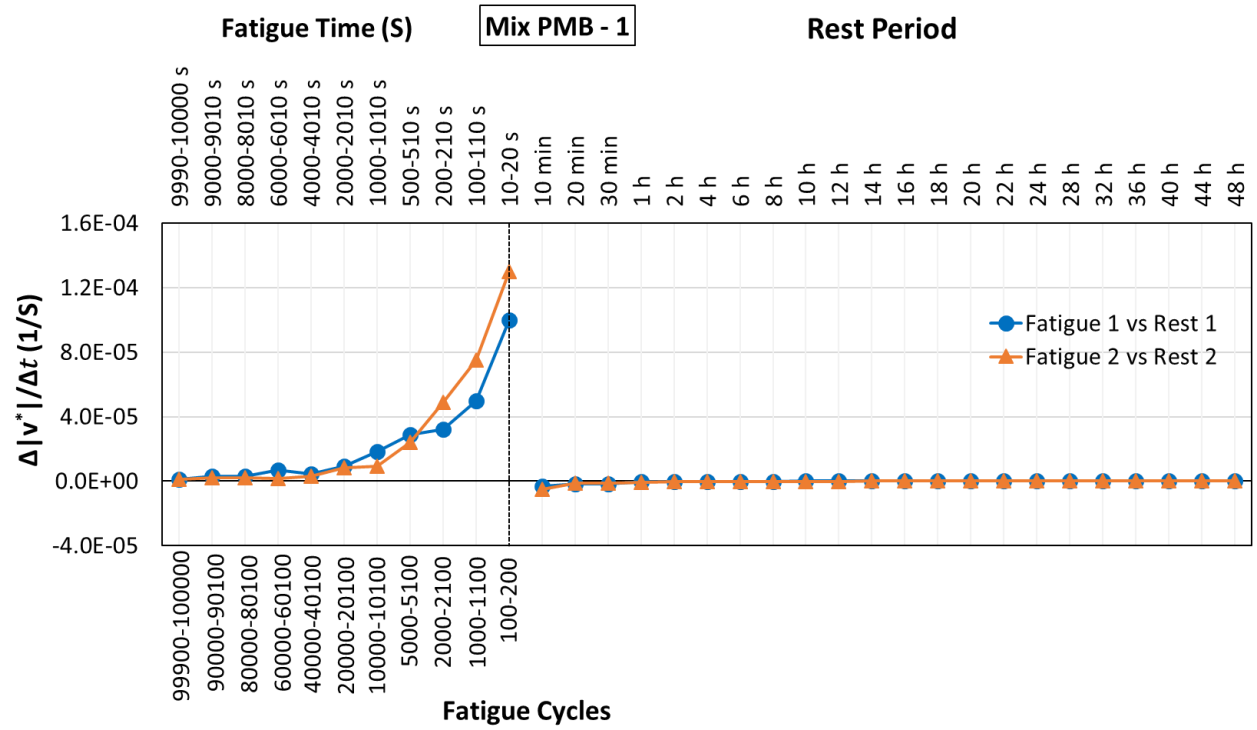
Fatigue Time (S)
Mix PMB - 1
Rest Period
9990-10000 s
9000-9010 s
8000-8010 s
6000-6010 s
4000-4010 s
2000-2010 s
1000-1010 s
500-510 s
200-210 s
100-110 s
10-20 s
10 min
20 min
30 min
1 h
2 h
4 h
6 h
8 h
10 h
12 h
14 h
16 h
18 h
20 h
22 h
24 h
28 h
32 h
36 h
40 h
44 h
48 h
1.6E-04
1.2E-04
8.0E-05
4.0E-05
0.0E+00
-4.0E-05
Δ|v*|/Δt (1/S)
Fatigue 1 vs Rest 1
Fatigue 2 vs Rest 2
99900-100000
90000-90100
80000-80100
60000-60100
40000-40100
20000-20100
10000-10100
5000-5100
2000-2100
1000-1100
100-200
Fatigue Cycles

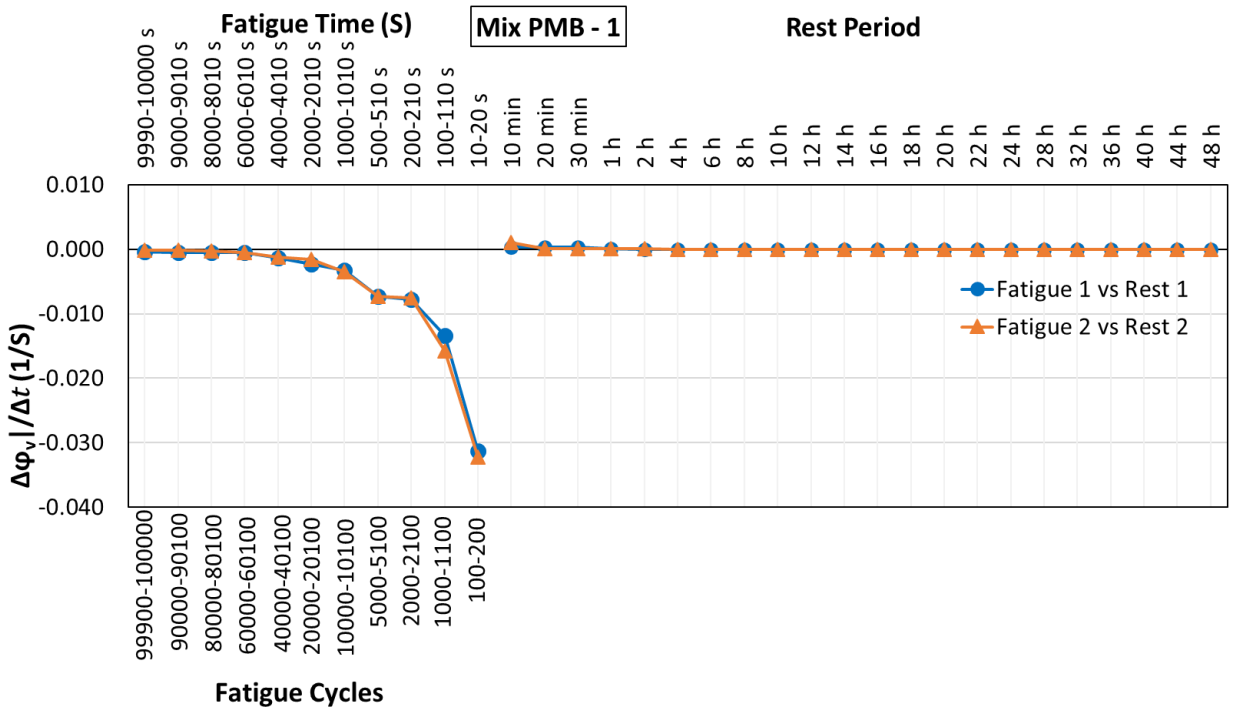

3.3.10. Rate of variation during loading and recovery for |E*|, φ_E, |v*| and φ_v for each fatigue and rest lag for mix PMB – 1.

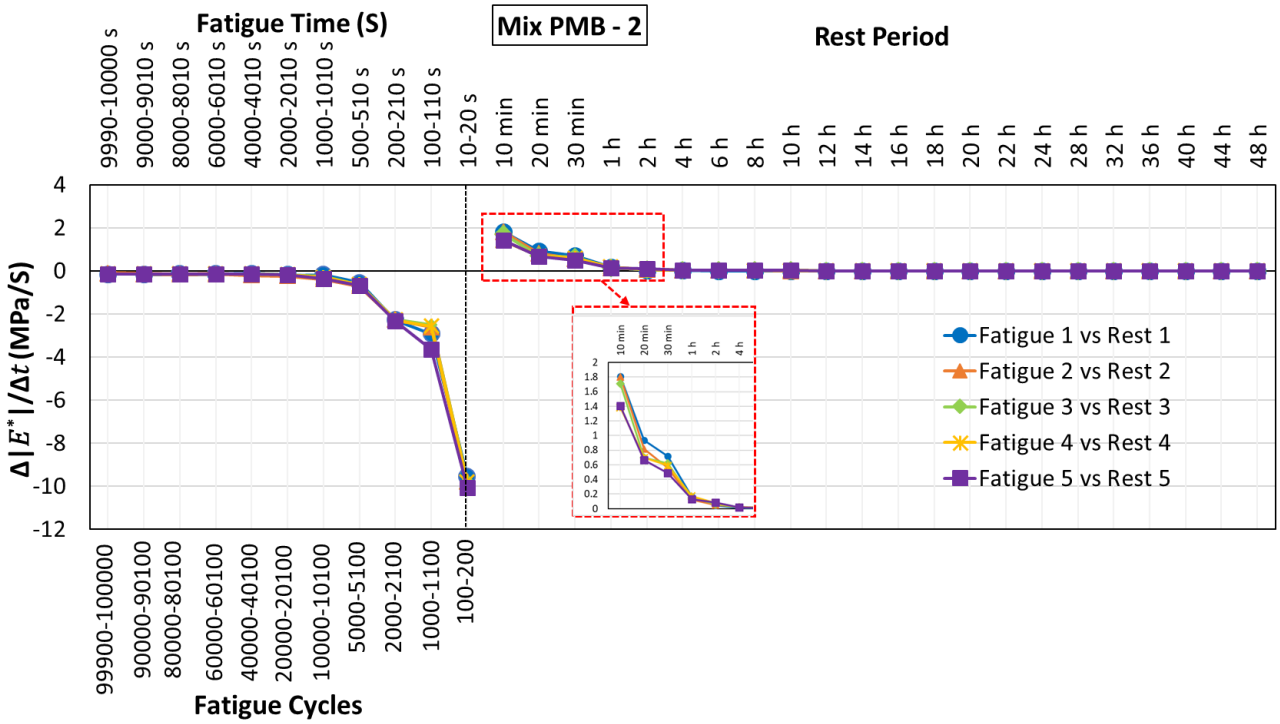

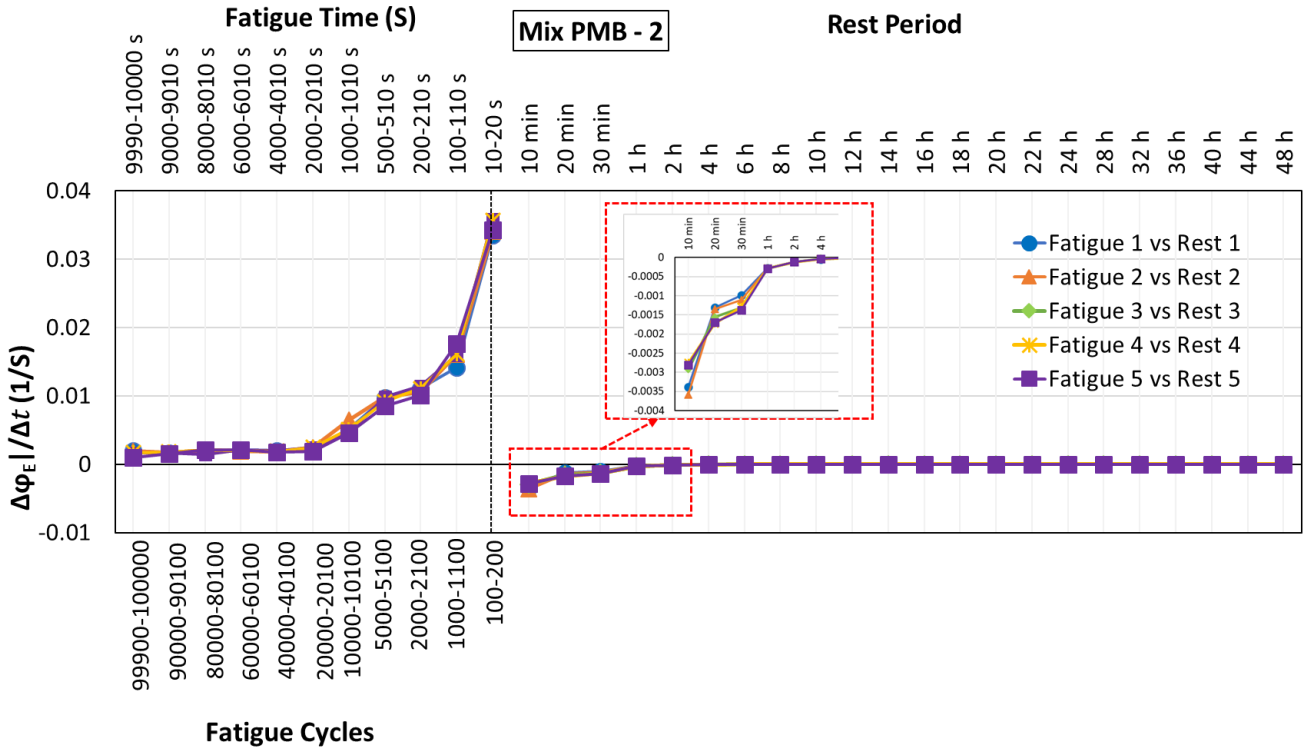
Fatigue Time (S)
Mix PMB - 2
Rest Period
9990-10000 s
9000-9010 s
8000-8010 s
6000-6010 s
4000-4010 s
2000-2010 s
1000-1010 s
500-510 s
200-210 s
100-110 s
10-20 s
10 min
20 min
30 min
1 h
2 h
4 h
6 h
8 h
10 h
12 h
14 h
16 h
18 h
20 h
22 h
24 h
28 h
32 h
36 h
40 h
44 h
48 h
0.04
0.03
0.02
0.01
0
-0.01
Δφ_E|/Δt (1/S)
Fatigue 1 vs Rest 1
Fatigue 2 vs Rest 2
Fatigue 3 vs Rest 3
Fatigue 4 vs Rest 4
Fatigue 5 vs Rest 5
99900-100000
90000-90100
80000-80100
60000-60100
40000-40100
20000-20100
10000-10100
5000-5100
2000-2100
1000-1100
100-200
Fatigue Cycles

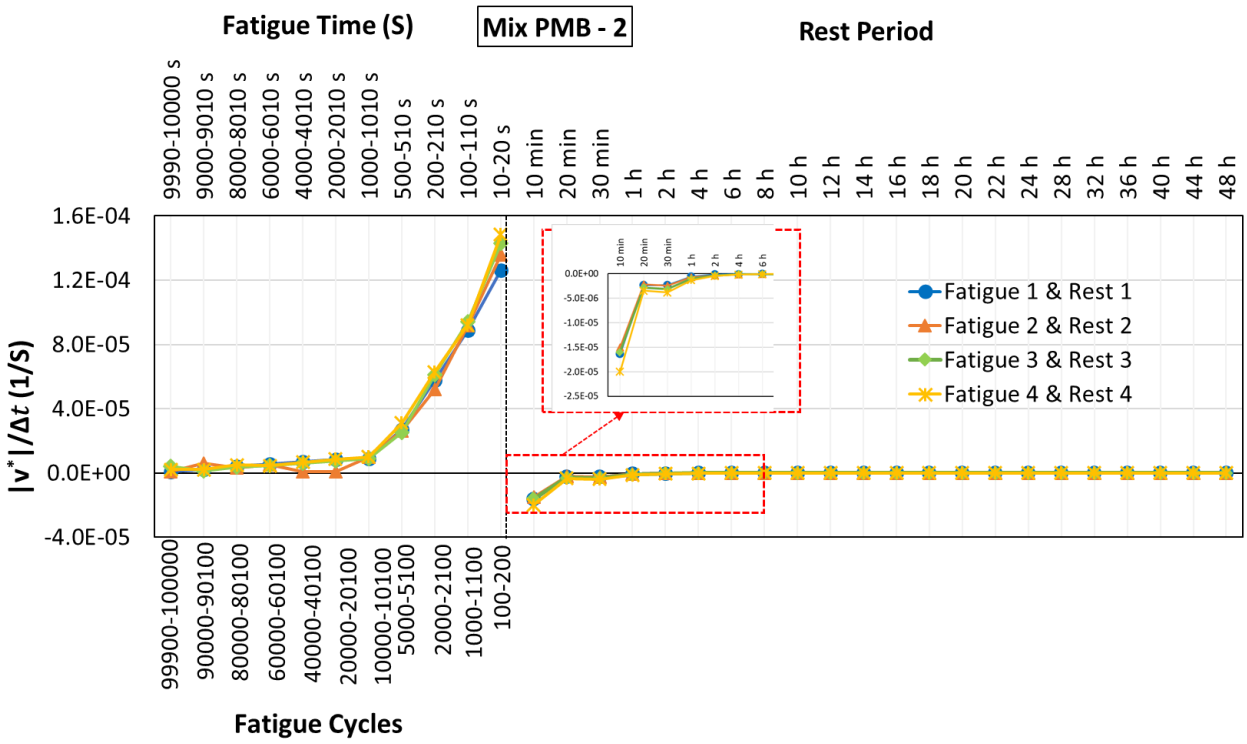
Fatigue Time (S)
Mix PMB - 2
Rest Period
9990-10000 s
9000-9010 s
8000-8010 s
6000-6010 s
4000-4010 s
2000-2010 s
1000-1010 s
500-510 s
200-210 s
100-110 s
10-20 s
10 min
20 min
30 min
1 h
2 h
4 h
6 h
8 h
10 h
12 h
14 h
16 h
18 h
20 h
22 h
24 h
28 h
32 h
36 h
40 h
44 h
48 h
1.6E-04
1.2E-04
8.0E-05
4.0E-05
0.0E+00
-4.0E-05
|v*|/Δt (1/S)
Fatigue 1 & Rest 1
Fatigue 2 & Rest 2
Fatigue 3 & Rest 3
Fatigue 4 & Rest 4
99900-100000
90000-90100
80000-80100
60000-60100
40000-40100
20000-20100
10000-10100
5000-5100
2000-2100
1000-1100
100-200
Fatigue Cycles

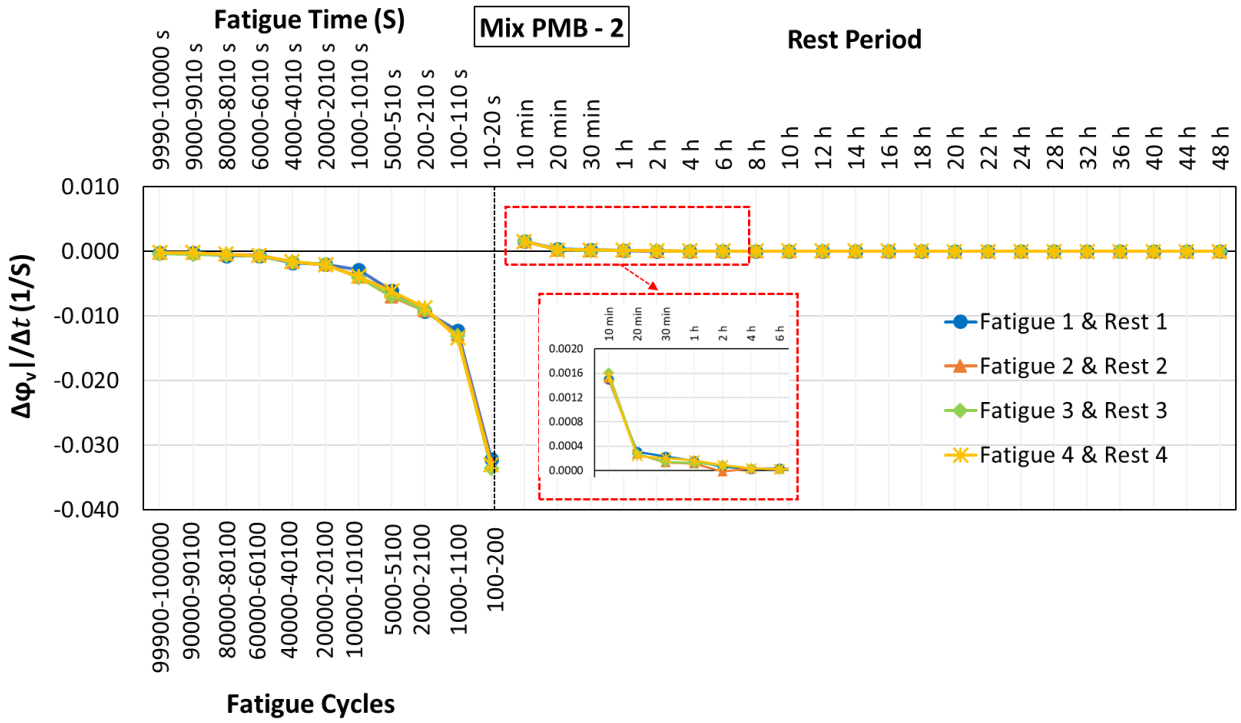

3.3.11. Rate of variation during loading and recovery for |E*|, φ_E, |v*| and φ_v for each fatigue and rest lag for mix PMB – 2.

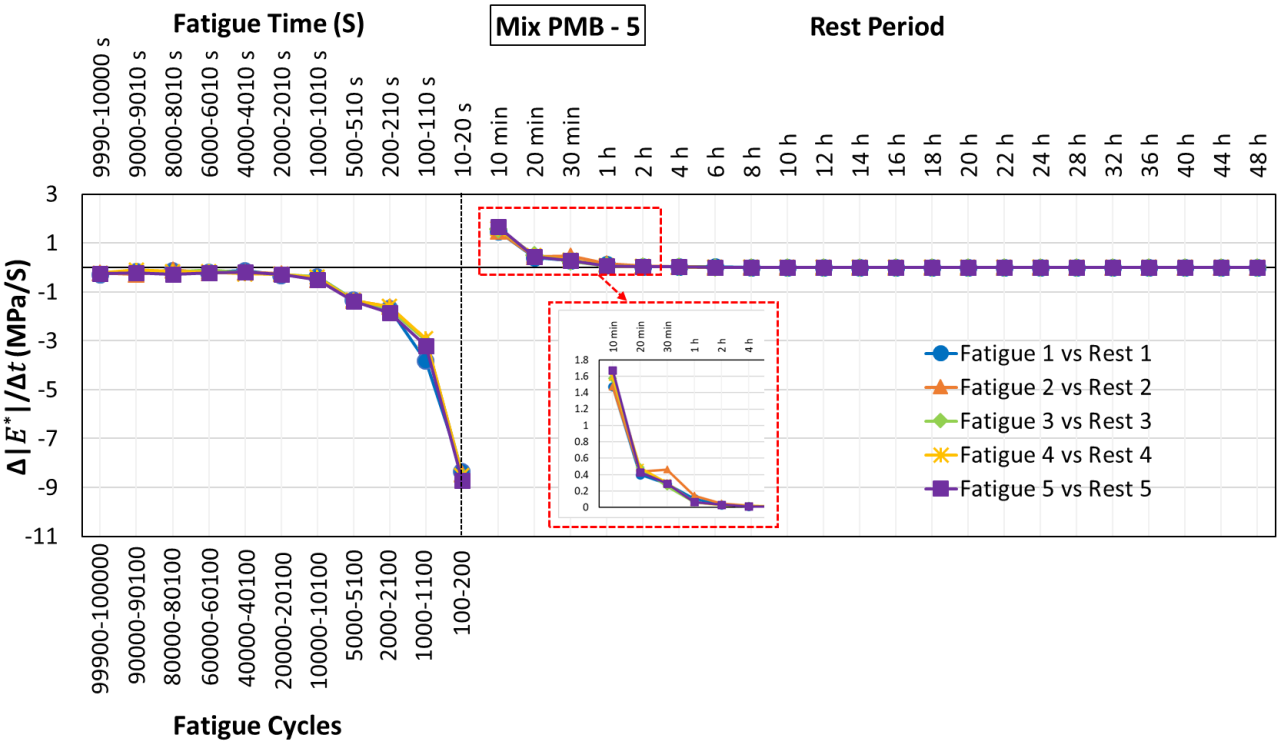

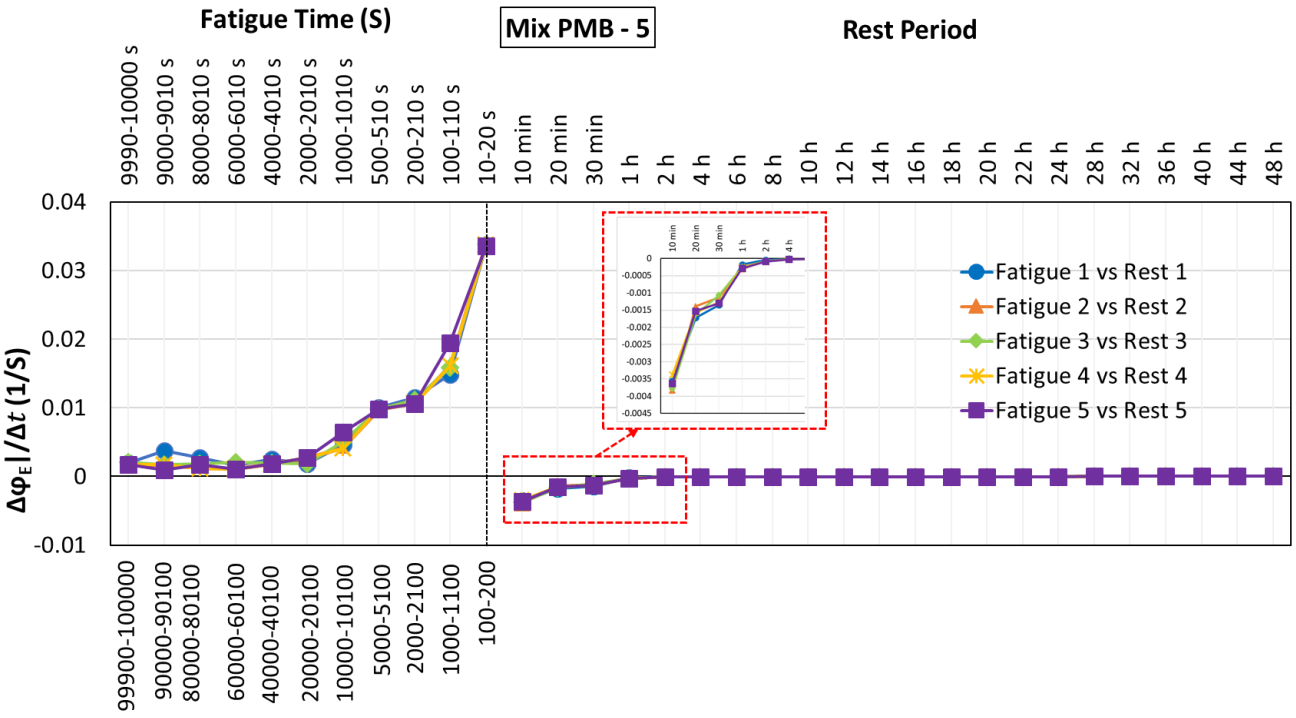
Fatigue Time (S)
Mix PMB - 5
Rest Period
9990-10000 s
9000-9010 s
8000-8010 s
6000-6010 s
4000-4010 s
2000-2010 s
1000-1010 s
500-510 s
200-210 s
100-110 s
10-20 s
10 min
20 min
30 min
1 h
2 h
4 h
6 h
8 h
10 h
12 h
14 h
16 h
18 h
20 h
22 h
24 h
28 h
32 h
36 h
40 h
44 h
48 h
0.04
0.03
0.02
0.01
0
-0.01
Δφ_E|/Δt (1/S)
Fatigue 1 vs Rest 1
Fatigue 2 vs Rest 2
Fatigue 3 vs Rest 3
Fatigue 4 vs Rest 4
Fatigue 5 vs Rest 5
99900-100000
90000-90100
80000-80100
60000-60100
40000-40100
20000-20100
10000-10100
5000-5100
2000-2100
1000-1100
100-200
Fatigue Cycles

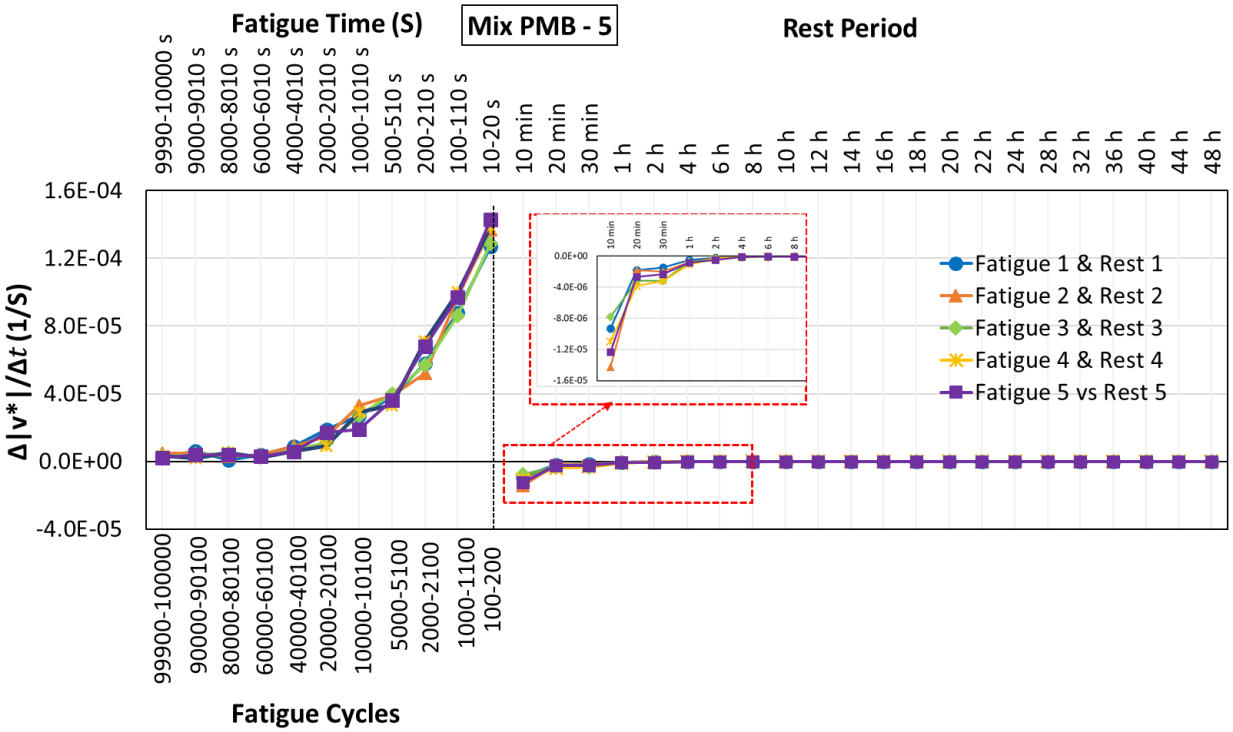
Fatigue Time (S)
Mix PMB - 5
Rest Period
9990-10000 s
9000-9010 s
8000-8010 s
6000-6010 s
4000-4010 s
2000-2010 s
1000-1010 s
500-510 s
200-210 s
100-110 s
10-20 s
10 min
20 min
30 min
1 h
2 h
4 h
6 h
8 h
10 h
12 h
14 h
16 h
18 h
20 h
22 h
24 h
28 h
32 h
36 h
40 h
44 h
48 h
1.6E-04
1.2E-04
8.0E-05
4.0E-05
0.0E+00
-4.0E-05
Δ|v*|/Δt (1/S)
Fatigue 1 & Rest 1
Fatigue 2 & Rest 2
Fatigue 3 & Rest 3
Fatigue 4 & Rest 4
Fatigue 5 vs Rest 5
99900-100000
90000-90100
80000-80100
60000-60100
40000-40100
20000-20100
10000-10100
5000-5100
2000-2100
1000-1100
100-200
Fatigue Cycles

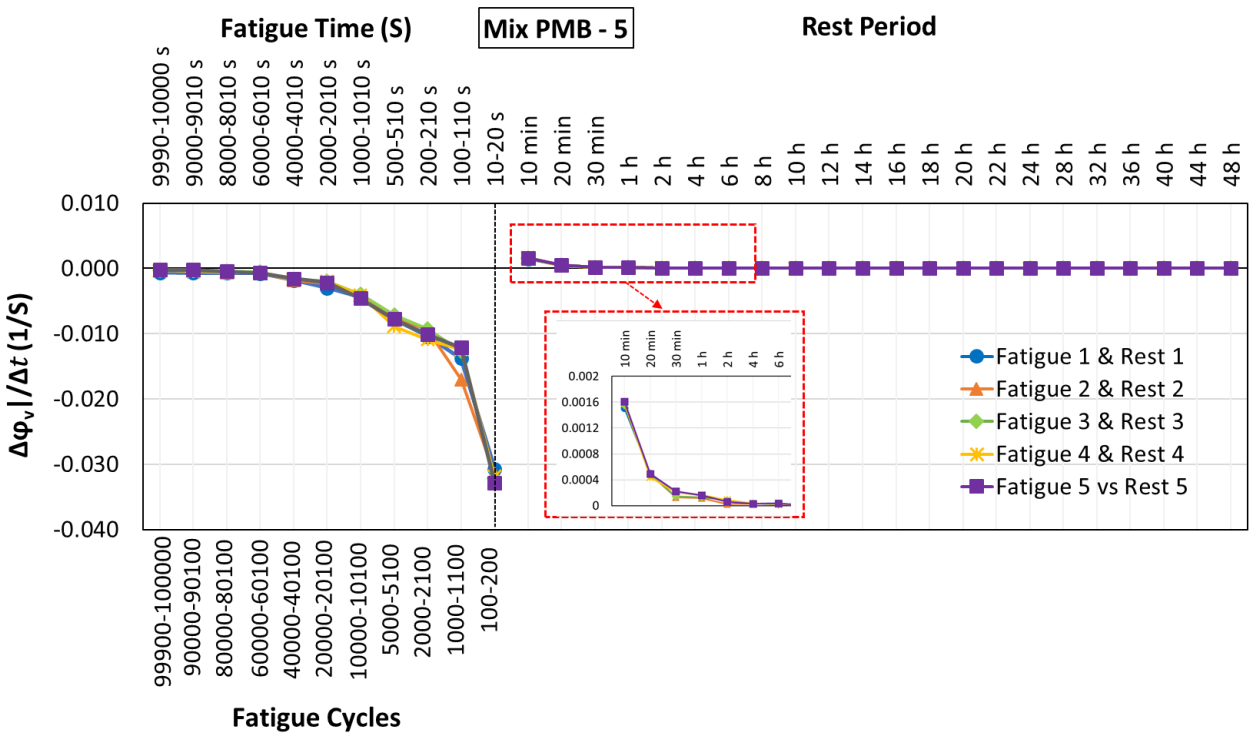

3.3.12. Rate of variation during loading and recovery for |E*|, φ_E, |v*| and φ_v for each fatigue and rest lag for mix PMB – 5.

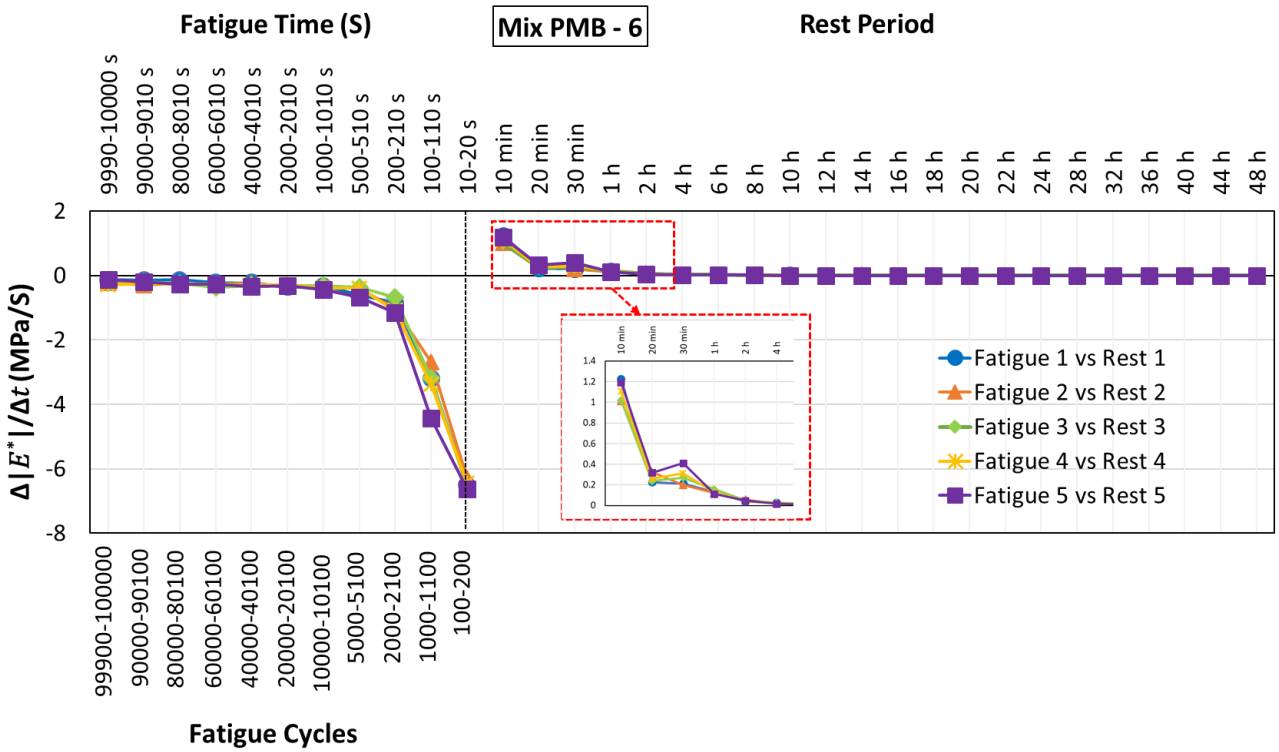

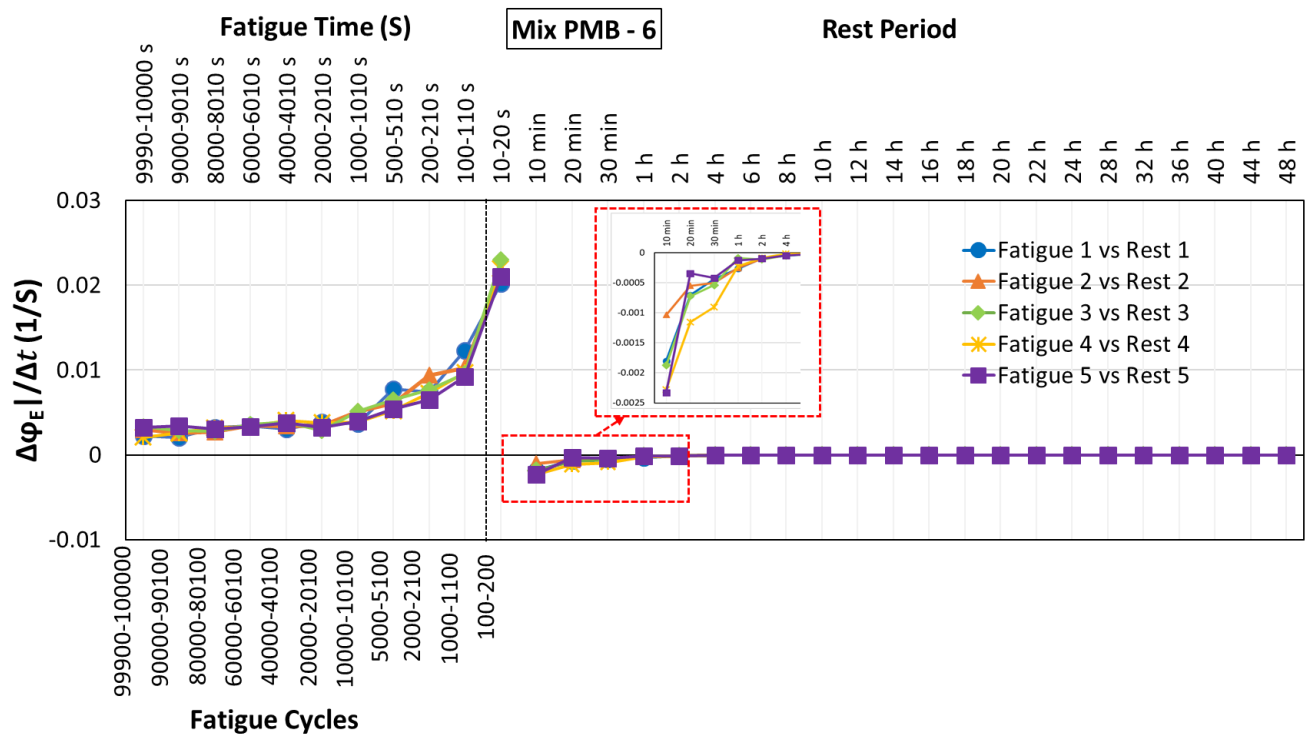
Fatigue Time (S)
Mix PMB - 6
Rest Period
9990-10000 s
9000-9010 s
8000-8010 s
6000-6010 s
4000-4010 s
2000-2010 s
1000-1010 s
500-510 s
200-210 s
100-110 s
10-20 s
10 min
20 min
30 min
1 h
2 h
4 h
6 h
8 h
10 h
12 h
14 h
16 h
18 h
20 h
22 h
24 h
28 h
32 h
36 h
40 h
44 h
48 h
0.03
0.02
0.01
0
-0.01
Δφ_E|/Δt (1/S)
Fatigue 1 vs Rest 1
Fatigue 2 vs Rest 2
Fatigue 3 vs Rest 3
Fatigue 4 vs Rest 4
Fatigue 5 vs Rest 5
99900-100000
90000-90100
80000-80100
60000-60100
40000-40100
20000-20100
10000-10100
5000-5100
2000-2100
1000-1100
100-200
Fatigue Cycles

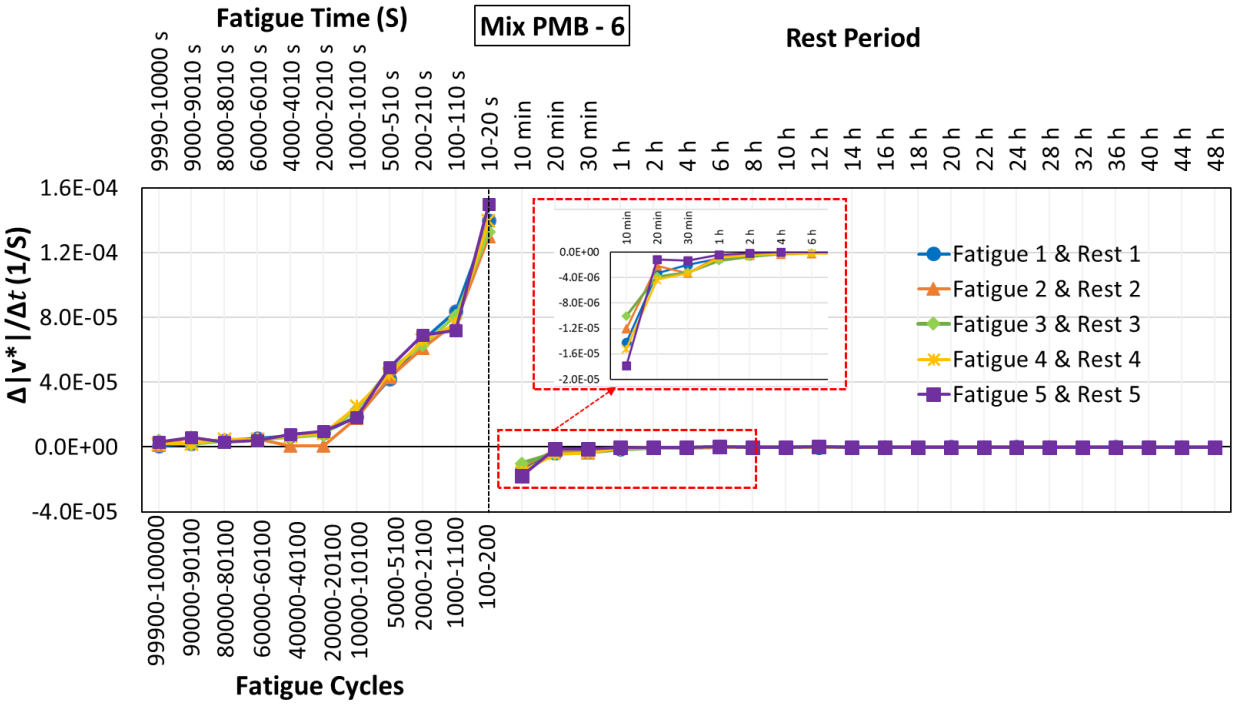
Fatigue Time (S)
Mix PMB - 6
Rest Period
9990-10000 s
9000-9010 s
8000-8010 s
6000-6010 s
4000-4010 s
2000-2010 s
1000-1010 s
500-510 s
200-210 s
100-110 s
10-20 s
10 min
20 min
30 min
1 h
2 h
4 h
6 h
8 h
10 h
12 h
14 h
16 h
18 h
20 h
22 h
24 h
28 h
32 h
36 h
40 h
44 h
48 h
1.6E-04
1.2E-04
8.0E-05
4.0E-05
0.0E+00
-4.0E-05
Δ|v*|/Δt (1/S)
Fatigue 1 & Rest 1
Fatigue 2 & Rest 2
Fatigue 3 & Rest 3
Fatigue 4 & Rest 4
Fatigue 5 & Rest 5
99900-100000
90000-90100
80000-80100
60000-60100
40000-40100
20000-20100
10000-10100
5000-5100
2000-2100
1000-1100
100-200
Fatigue Cycles

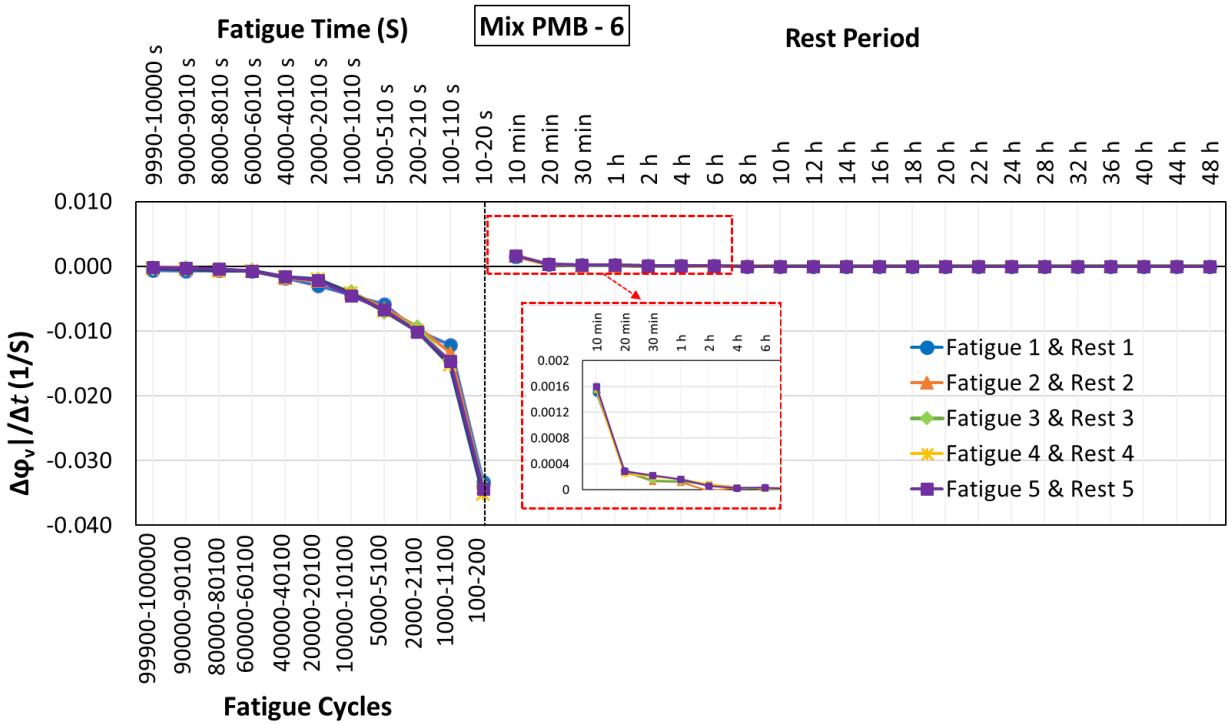

3.3.13. Rate of variation during loading and recovery for |E*|, φ_E, |v*| and φ_v for each fatigue and rest lag for mix PMB – 6.

3.4. Analysis of energy dissipation

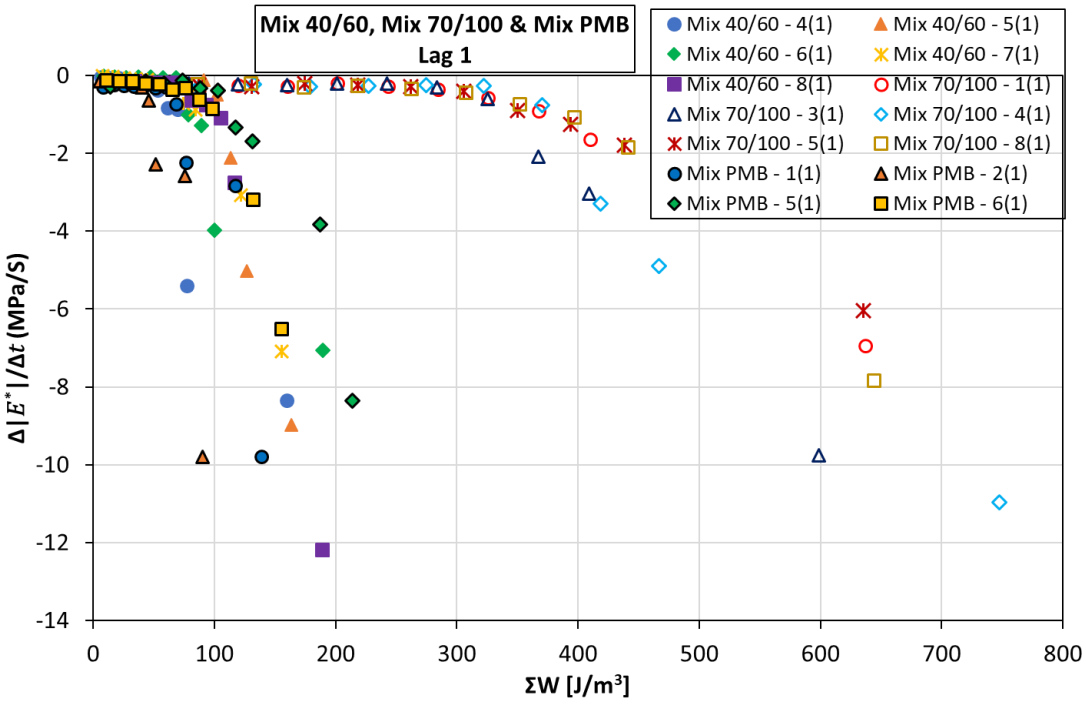

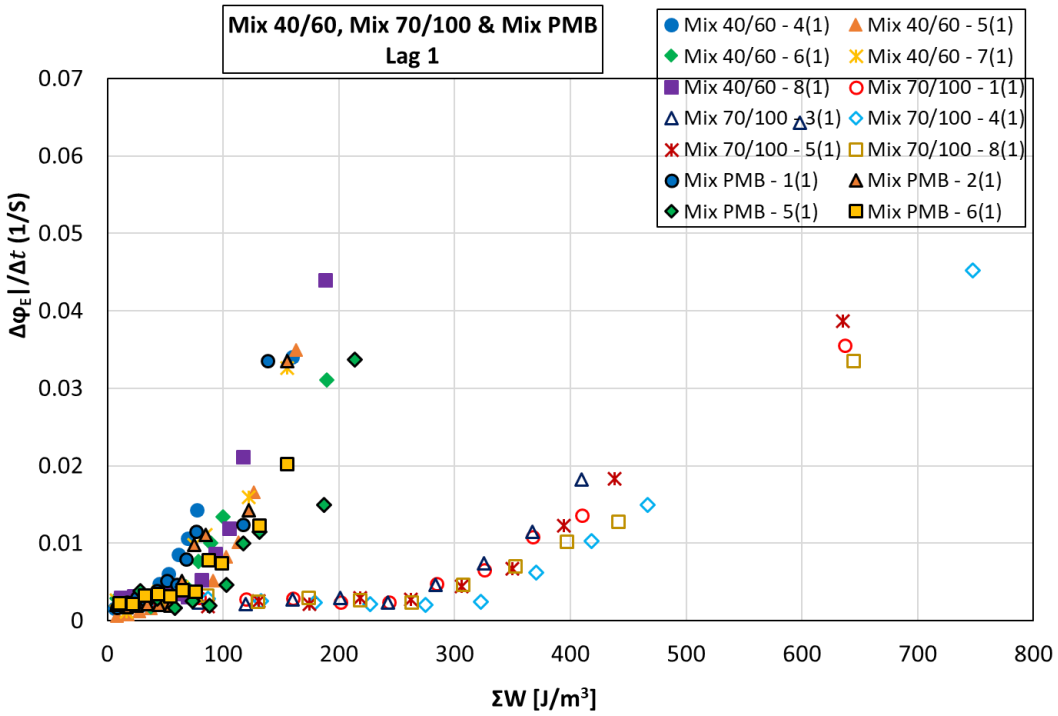

3.4.1. Rate of variation during loading and energy dissipation for |E*| and φ_E for fatigue and rest lag 1 for mix 70/100, mix 40/60 and mix PMB.

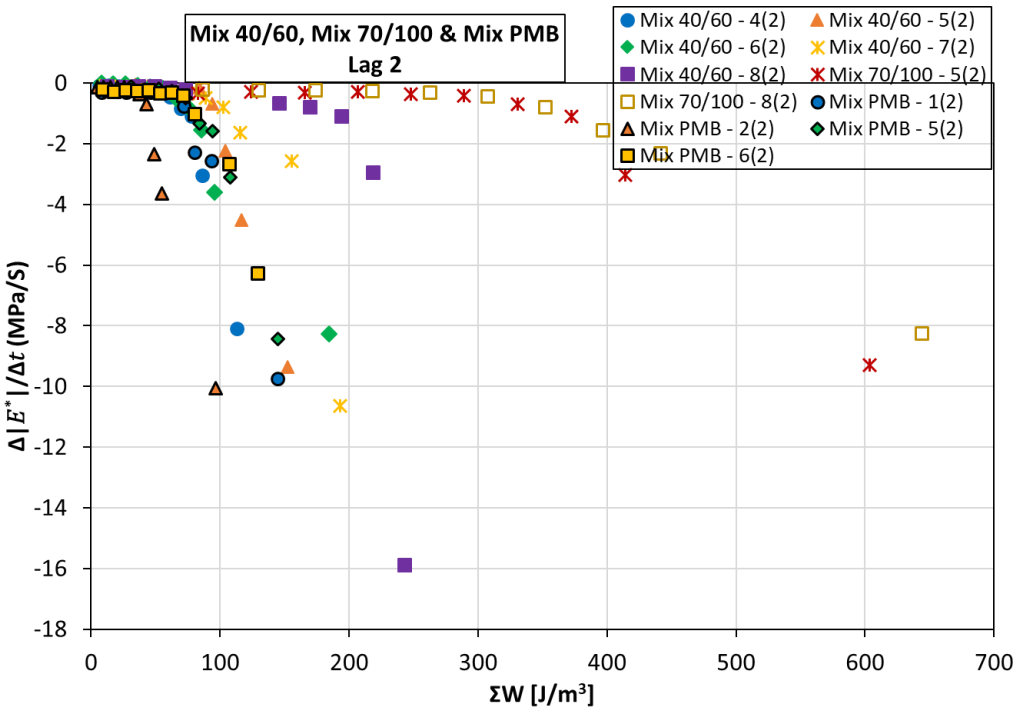

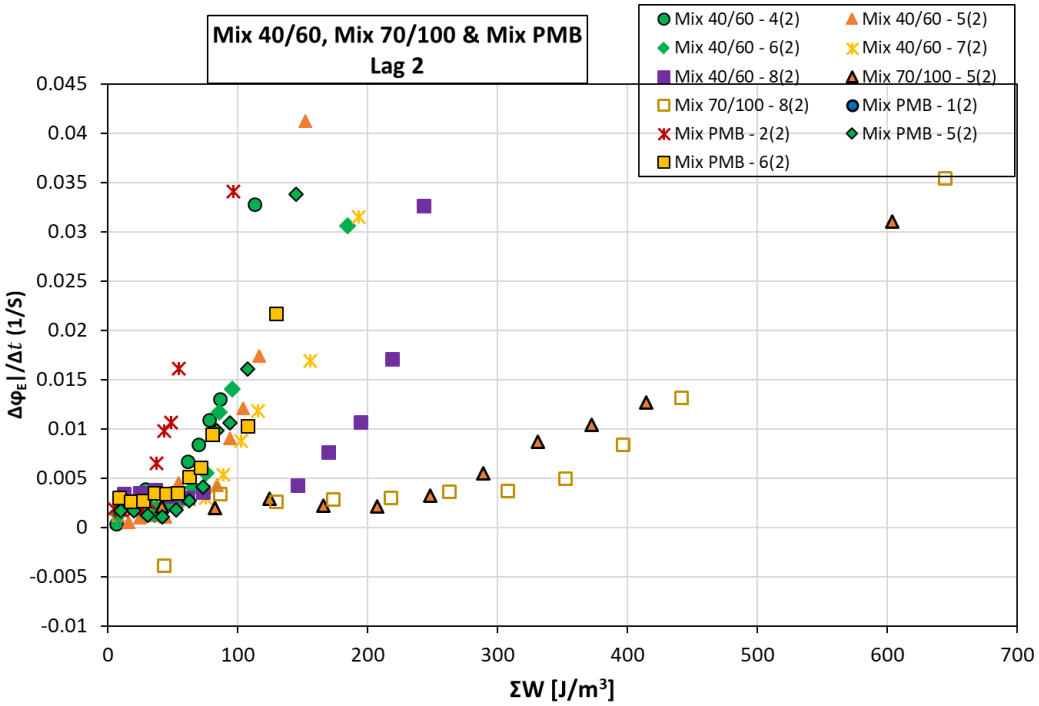

3.4.2. Rate of variation during loading and energy dissipation for |E*| and φ_E for fatigue and rest lag 2 for mix 70/100, mix 40/60 and mix PMB.

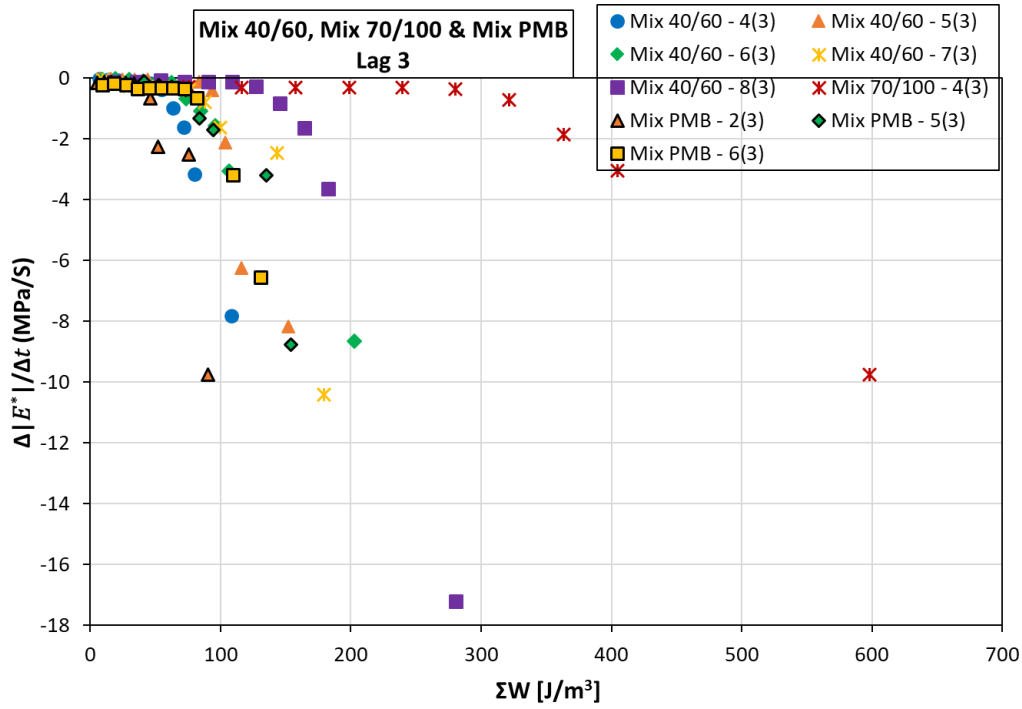

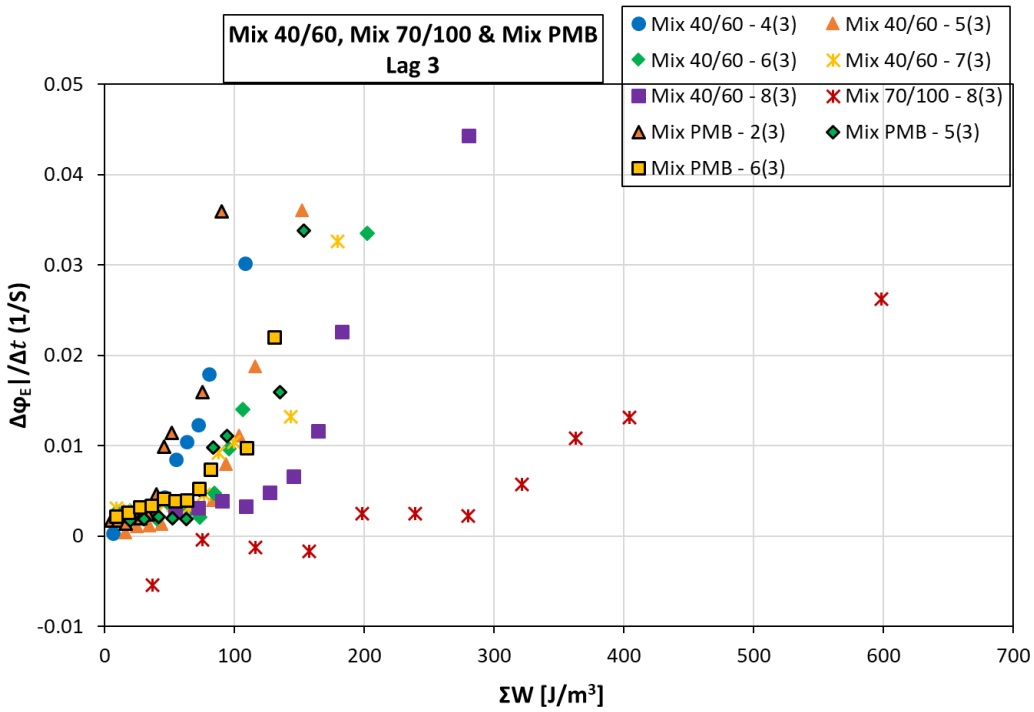

3.4.3. Rate of variation during loading and energy dissipation for |E*| and φ_E for fatigue and rest lag 3 for mix 70/100, mix 40/60 and mix PMB.

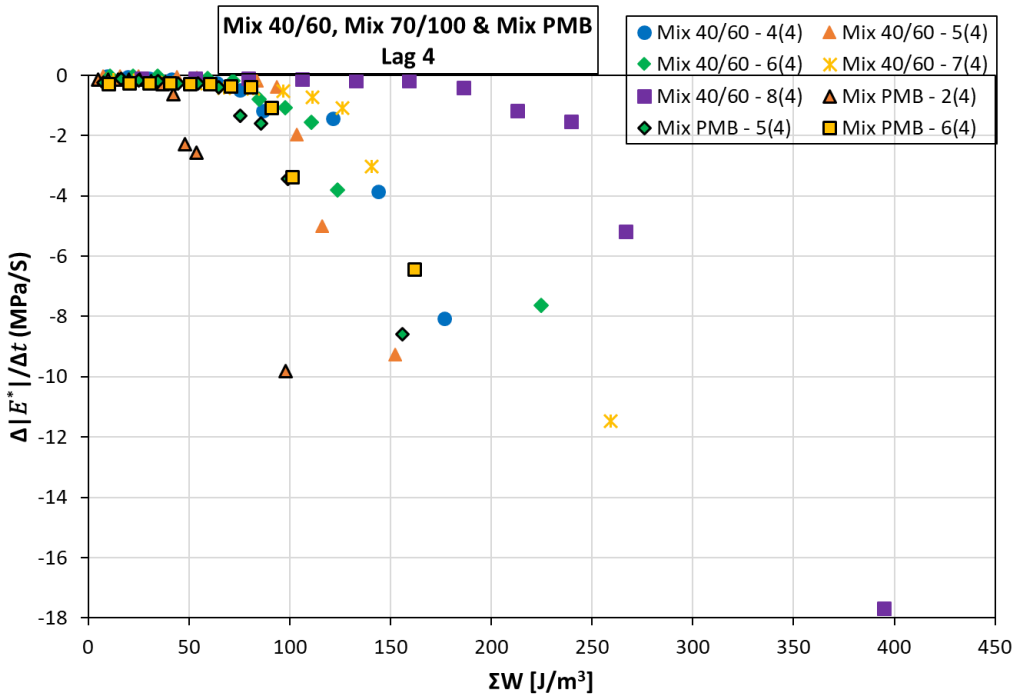

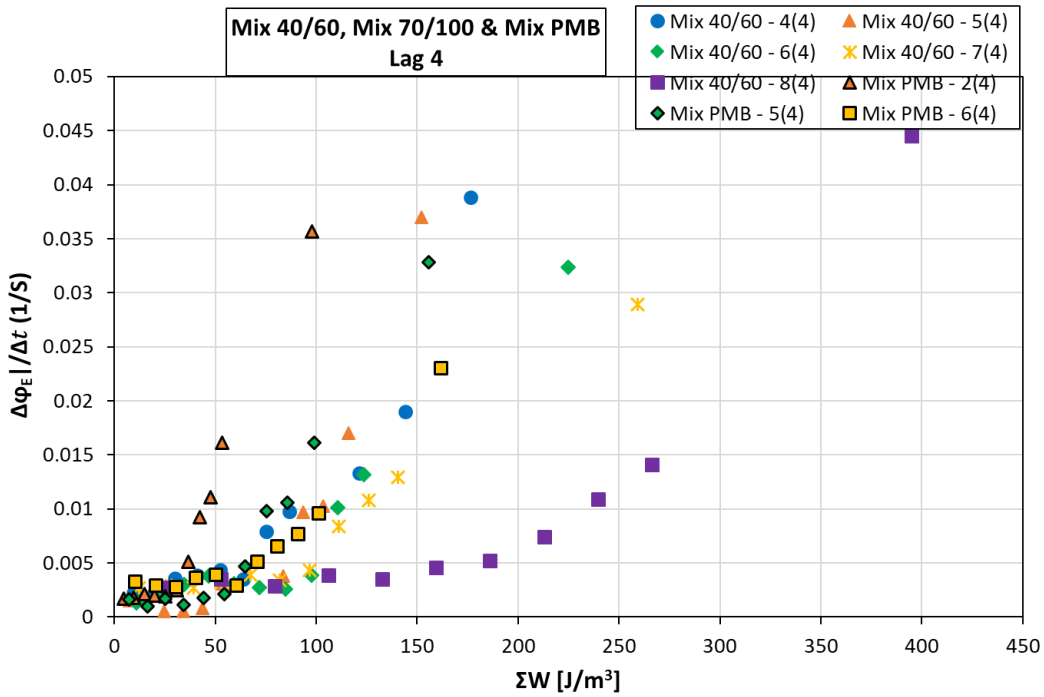

3.4.4. Rate of variation during loading and energy dissipation for |E*| and φ_E for fatigue and rest lag 4 for mix 70/100, mix 40/60 and mix PMB.

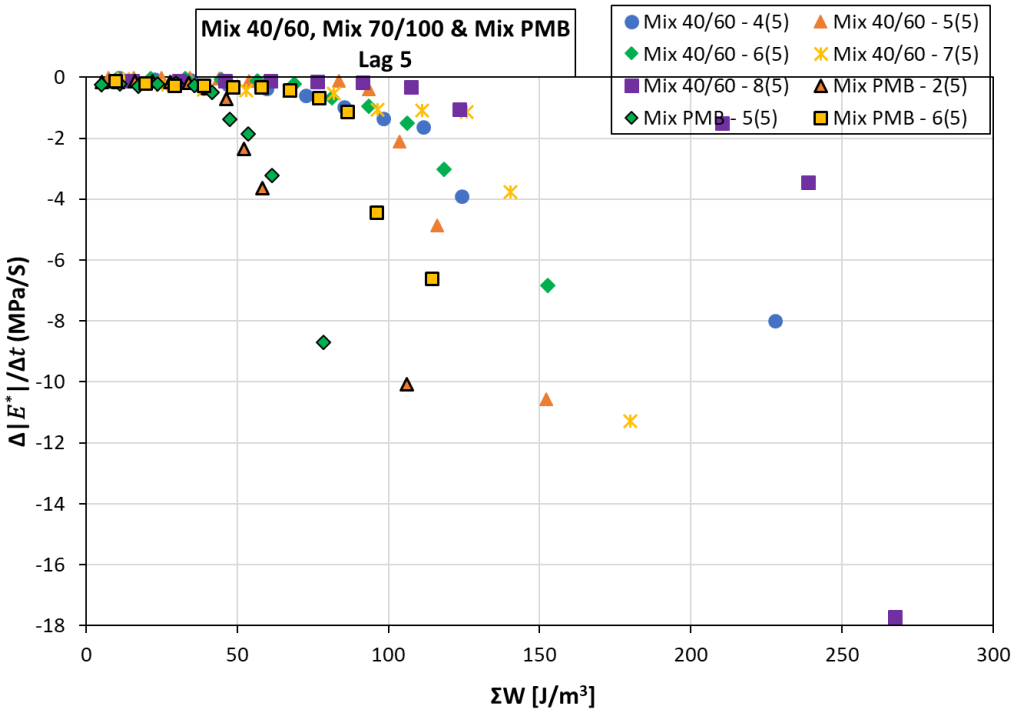

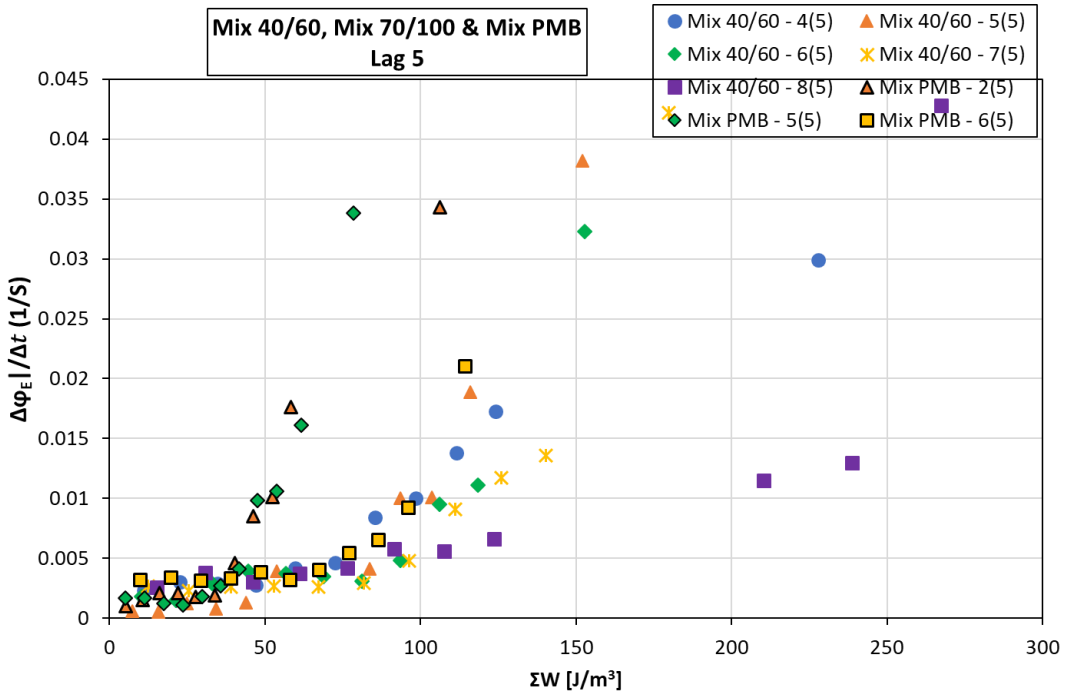

3.4.5. Rate of variation during loading and energy dissipation for |E*| and φ_E for fatigue and rest lag 5 for mix 70/100, mix 40/60 and mix PMB.

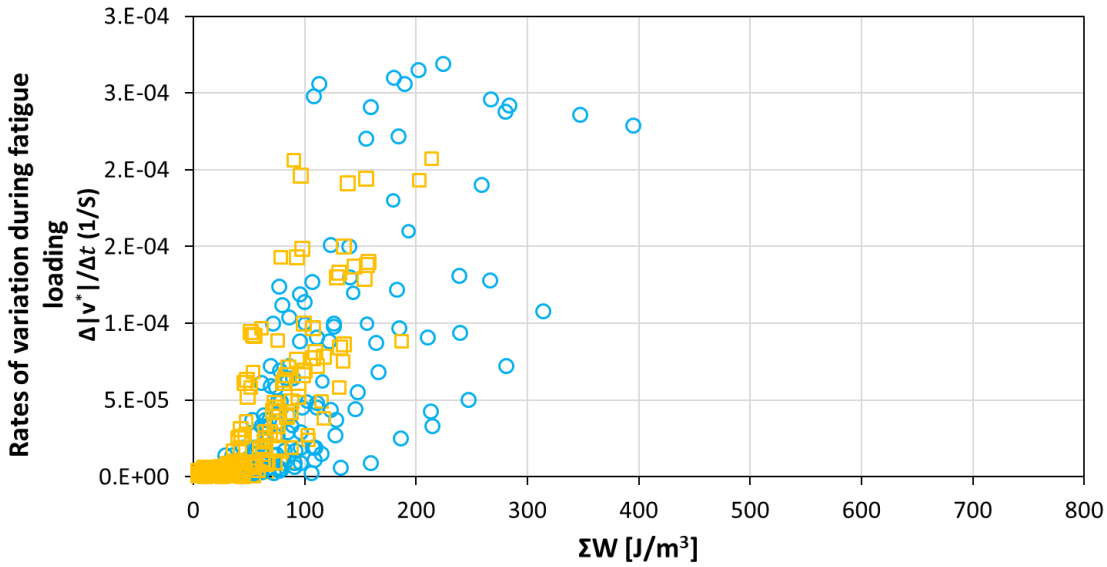

3.4.6. Rate of variation during loading and energy dissipation for |v*| and φ_v of all fatigue and rest lags for mix 70/100, mix 40/60 and mix PMB.